STUDIES IN MECHANICAL ENGINEERING

Volume 1	Analysis, Synthesis and Design of Hydraulic Servosystems and Pipelines (Viersma)
Volume 2	Interordering: A New Method of Component Orientation (Den Hamer)
Volume 3	Combustion Systems of High-Speed Piston I. C. Engines (Kowalewicz)
Volume 4	Mechanical Conveyors for Bulk Solids (Colijn)
Volume 5	Railway Traction (Andrews)
Volume 6	Pumps and Pumping (Ionel)
Volume 7	Fundamentals of Hydraulic Power Transmission (Kröell Dulay, Editor)
Volume 8	Dependability of Mechanical Systems (Bílý)
Volume 9	Cold-Pressing Technology (Iliescu)
Volume 10	Vibration Testing of Machines and their Maintenance (Lipovszky, Sólyomvári and Varga)
Volume 11	Hovercraft Technology, Economics and Applications (Amyot, Editor)

STUDIES IN MECHANICAL ENGINEERING, 11

Hovercraft Technology, Economics and Applications

Edited by

JOSEPH R. AMYOT

Division of Mechanical Engineering, National Research Council of Canada, Ottawa, Ontaria, Canada

Elsevier
Amsterdam – Oxford – New York – Tokyo 1989

ELSEVIER SCIENCE PUBLISHERS B.V.
Sara Burgerhartstraat 25
P.O. Box 211, 1000 AE Amsterdam, The Netherlands

Distributors for the United States and Canada:
ELSEVIER SCIENCE PUBLISHING COMPANY INC.
655 Avenue of the Americas
New York, N.Y. 10010, U.S.A.

ISBN 0-444-88152-2 (Vol. 11)
ISBN 0-444-41872-5 (Series)

© Elsevier Science Publishers B.V., 1989

Al rights reserved. No part of this publication may be reproduced, stored in a retrieval system or transmitted in any form or by any means, electronic, mechanical, photocopying, recording or otherwise, without the prior written permission of the publisher, Elsevier Science Publishers B.V./ Physical Sciences & Engineering Division, P.O. Box 1991, 1000 BZ Amsterdam, The Netherlands.

Special regulations for readers in the USA – This publication has been registered with the Copyright Clearance Center Inc. (CCC), Salem, Massachusetts. Information can be obtained from the CCC about conditions under which photocopies of parts of this publication may be made in the USA. All other copyright questions, including photocopying outside of the USA, should be referred to the copyright owner, Elsevier Science Publishers B.V., unless otherwise specified.

No responsibility is assumed by the Publisher for any injury and/or damage to persons or property as a matter of products liability, negligence or otherwise, or from any use or operation of any methods, products, instructions or ideas contained in the material herein.

Printed in The Netherlands.

PREFACE

The air-cushion vehicle concept can be traced back to Emmanuel Swedenborg's man-powered air-cushion platform in 1716. However, the practical form of today's hovercraft is generally recognized to have originated with Christopher Cockerell's annular jet principle in 1955. Since then, many types of land, marine and amphibious air-cushion vehicles have been developed. Whereas some are supported exclusively by a cushion of air, others are assisted by alternative forms of support, such as planing seals in surface-effect ships and wheels, or tracks, in air-cushion-assisted land vehicles. This volume deals mainly with those hovercraft which are supported essentially by an air cushion, but which may include some solid contact with the land or water surface for propulsion and guidance purposes; surface-effect ships are excluded.

The hovercraft is rarely able to compete economically with conventional modes of transportation in their traditional environments. But its amphibious versatility, marine speed and low footprint pressure have given it a role in specialized applications. Among them are search and rescue, emergency medical services, military and arctic operations, icebreaking, patrol, law enforcement, ferries, and recreational activities such as racing. To meet these demands, the hovercraft has undergone considerable development since its inception. Therefore, an examination of its status is appropriate at this time.

The objective of this book is to provide a tutorial-style review of the analysis, design, operation, economics and applications of hovercraft. Twenty-three authors with appropriately diverse expertise were recruited for this broad mandate. A short biography and identification of the contributed section(s) of each are appended.

The topics are covered from first principles to the state-of-the-art, with proper reference to the literature. The overall present-ation is intended not to exceed the final year level of undergraduate engineering. Furthermore, Chapter 4 on homebuilt hovercraft and the introduction and summary sections of all chapters are meant to be within the high school graduation level in the

Mathematics and physics stream. Thereby, it is possible to obtain a qualitative grasp of the material covered without having to read all the technical portions.

Of the seventeen chapters, the emphasis of the first nine is more on the overall technology, economics and applications of hovercraft than on the detailed analytical, experimental and research aspects dealt with in the following six chapters. In varying degrees, the first group of chapters will appeal to managers, decision-support staff, operators, technologists, undergraduate students, hobbyists, and anyone entering the hovercraft field or seeking an introduction to it. Chapters 10 to 15 will be of greatest interest to design engineers, researchers and graduate students. As the personal perspective of a pioneer who has been active in this field since its inception in the late fifties, Chapter 16 should be of interest to all. The final Chapter, on safety, will be useful to anyone involved in the production or operation of hovercraft. Thus, this volume can serve as an up-to-date reference on several important aspects of hovercraft for a wide range of readers.

Chapter 1 gives a historical background of the air cushion principle, describes the major elements and general characteristics of hovercraft, describes their capabilities and limitations, and places them in perspective relative to other craft.

The fundamentals of practical hovercraft design for reliability, ruggedness and low cost are explored in Chapter 2. The main constituent systems of hovercraft, namely the lift, propulsion and control systems, and the structure (or hull), are treated.

Because of their relatively low cost, so-called light hovercraft are affordable by many individuals and small organizations. However, they are limited to a maximum of perhaps up to six passengers, but usually less, or an equivalently light load. The next two chapters are devoted to light hovercraft. Chapter 3 deals mainly with commercially-built craft, examining the evolution, status and prospects of the light hovercraft industry from development and marketing perspectives. It discusses recreational and other applications and surveys promotional organizations such as hovercraft clubs and manufacturing associations. Chapter 4 is a layman's practical guide describing how a one- or two-seater can be designed, built, transported to a destination and driven safely.

The distinction between *light* and *heavy*, or *small* and *large*, hovercraft is somewhat arbitrary. Given the full spectrum of possible sizes, a *medium* classification covering a maximum capacity of perhaps up to two dozen passengers, or an equivalent load, could be defined. The performance and economics of large craft and some of the larger medium-sized ones is the subject of Chapter 5. A craft's performance depends on the efficiency with which it can

be operated. Operational efficiency is discussed as a function of reliability, supportability and ease of manning. The production costs of commercial and military hovercraft are examined. As specific examples, the performance and economics of two large commercial craft from British Hovercraft Corporation are presented: (1) SR.N4 Mk3, Britain's premier fast ferry, and (2) AP.1-88, a modern passenger/utility craft.

The icebreaking ability of hovercraft is an important discovery for the task of keeping shipping channels open in freezing conditions. One method consists of a self-propelled hovercraft with certain desired characteristics operated at specified velocities over ice-covered water. Another method, a concept developed in Canada since 1971, is an *Air Cushion Icebreaking Bow* (ACIB) attached to the front of a conventional icebreaker. The theory and practice of air cushion icebreaking is presented in Chapter 6.

A twenty year operating record has firmly proven the concept of arctic hovercraft. Chapter 7 reviews this record and, considering recent advances, concludes that hovercraft should be regarded as one of the most promising vehicles for future arctic offshore transportation.

The Canadian Coast Guard has been operating a highly successful search and rescue hovercraft unit at the mouth of the Fraser River on the Pacific coast, near Vancouver, for over fifteen years. Meanwhile, the Maryland Natural Resources Police has begun a hovercraft operation at the mouth of the Potomac River on the Atlantic coast, near Washington, D.C. Its mandate includes patrol, law enforcement, emergency medical services and icebreaking, in addition to search and rescue. These coastal operations are described in Chapter 8.

The use of hovercraft on rivers and various soil conditions is examined in Chapter 9, Inland Applications. Whereas the discussion proceeds from the Canadian experience, it can be extrapolated to similar situations elsewhere. Following a discussion of economics and design aspects of hovercraft ferries, examples of cable ferries are presented. Large air-cushion platforms for drilling, pile driving, etc. are described. Various types of hovercraft for off-road transportation, where wheels or tracks may be inadequate, are reviewed.

The design of composite materials to satisfy the required properties of hovercraft skirts are studied in Chapter 10. Fabrication methods involving the vulcanization of several elastomer types and formulations bonded to fabric substrates by adhesives are investigated. Test results are examined to determine various properties, including tensile strength, flexural fatigue, hardness, abrasion resistance, hysteresis and resilience. The study concludes with recommendations for the design of skirt materials.

Chapter 11 establishes the relationship between lift airflow and overland drag for a variety of terrains. Included in the diverse soil and vegetation

conditions are: concrete, crushed rock, firm snow, short grass, medium grass and long reedy grass. A method of measuring terrain porosity is described, leading to test data and a tabulation of terrain factors. Some test results are presented to determine drag as a function of vehicle speed and lift air-flow. The empirical methods and relationships presented in this chapter can be used with other design considerations to determine the lift-air and propulsive power requirements of low-speed segmented-skirt hovercraft operating over a range of specified terrains.

The mechanical properties of skirt materials that affect hovercraft dynamics are discussed in Chapter 12. Stiffness, damping and hysteresis are represented by various conceptual models. The effects of these properties on pitch and heave dynamics are examined with the aid of analytical and experimental results. The choice of skirt material is shown to be an important design decision concerning the stability of some craft.

An analysis of the heave dynamics of skirts of the bag and finger type is presented in Chapter 13 with a view to providing insights into the factors that affect static and dynamic stability, and responsiveness or ride comfort. A measure or index of skirt responsiveness is proposed. It is shown that the effect of both skirt and cushion on the craft dynamics can be expressed through a single scalar gain which has a simple physical interpretation. Analytical and experimental results pertaining to static stiffness and to static *tuck-under* instability arising from surface contact are presented.

The heave dynamics of hovercraft can be improved by means of vent-valve control. Chapter 14 presents extensive computer simulation and and physical experimentation results to show the heave-dynamics improvements possible by controlling vent valves. A few heave-dynamics performance indices are defined, based on vent-valve action and heave position, velocity and acceleration. It is demonstrated that a control law can be more effective when utilizing both velocity and acceleration feedback than either one individually. Passive control is generally less effective but can be satisfactory for some applications.

Chapter 15 looks at some interactions of lift air with a hovercraft's environment. The aerodynamic drag is affected by the amount of lift air interacting with the atmosphere surrounding a moving craft. On the other hand, the lift-air requirements of hovercraft operating over water are influenced by the relationship between water-surface deflection and lift airflow. These phenomena are examined by means of computer studies and physical experiments.

A personal perspective on the development of hovercraft is presented in Chapter 16 by William R. Bertelsen, an innovative pioneer who has been active in this field since its inception in the late fifties. He demonstrated the first controllable man-carrying hovercraft at the First Symposium on Ground

Effect Phenomena, Princeton University, October 1959. It is on display in the Permanent Collection of the National Air and Space Museum, Smithsonian Institute. His fascinating experience with various ideas, eventually leading to the tilting fan concept, is described. Explanations for the slow growth of the hovercraft industry and means of revitalizing it are presented.

Hovercraft are sufficiently different from other forms of transport that their special design and operational characteristics must be fully understood and recognized when attempting to develop safety requirements and when trying to operate them safely. Therefore, safety considerations pertinent to the production and operation of hovercraft are discussed in Chapter 17.

As shown by the biographies in Appendix B, this book was written by highly qualified authors. Each author's contribution(s), down to the section level, can be determined from the two tables in Appendix A.

My sincere acknowledgement is extended to all who have had a direct impact on this work. Foremost are the numerous contributors to air cushion technology. Most of them are referred to in these pages. I am grateful to the authors who stuck with this project from beginning to end, and to those who stepped into the breach when two of the original authors dropped out. Some were unable to adhere to the schedule, so I am grateful as well to the Publisher for his patience in accommodating delays. Special thanks go to the Division of Mechanical Engineering, National Research Council of Canada, for its wholehearted support of this project. I was continually impressed by the expeditiousness and expertise of the Stenographic Services staff, under the management of Mrs. H.S. Cuccaro. Finally, thanks to Morlene, my wife, for her unwavering support throughout all my endeavours, including this one; editing such a book turned out to be far more demanding than originally expected.

This work is dedicated to the persons of vision and perseverance in the development and application of air cushion technology; the authors of this book are included.

Joseph R. Amyot

Chapter 1

INTRODUCTION

Hovercraft began serious practical development in England when Christopher Cockerell, who was later knighted for his achievement, began experimenting with the hovercraft concept in 1955. These early experiments led to the design, construction, and test of the SR.N1 by Saunders-Roe (subsequently British Hovercraft Corporation, now Westland Aerospace) in 1959. Development in the United States began during the same time period with the work of Melvin Beardsley who also experimented with the annular jet principle of hovercraft or ground effect machines (GEM) as they were known in the United States.

The use of an air cushion to provide support and to reduce drag of vehicles has taken many forms. Mantle (ref. 1) provides a definitive description of the many types of craft that use the air cushion principle. As stated in the Preface, historical traces can be found back to Emmanuel Swedenborg's man-powered air cushion platform in 1716. Other historical research includes the first patent for air lubrication issued in England to another Swedish engineer, Gustav Lavalle, in 1882. Lavalle was not successful with his experiments, however, and it was not until after 1916, when Von Tomamhul built a torpedo boat for the Austrian Navy using fans to pump air beneath the hull to form a lubricating air cushion, that various forms of air cushion craft began to evolve. In 1925, a patent was issued to V.F. Casey for the use of the energy saving recirculation principle in hovercraft design. This principle was revived in the 1960s in the United States and Canada but was quickly overshadowed by the development of hovercraft skirts.

In 1927, K.E. Tsiolkovski, a noted Russian scientist, developed what today might be called the hovertrain. This idea proposed to run trains supported by a thin air cushion layer along a track.

In 1929, D.K. Warner won the boat races on Lake Compounce, Connecticut, by the use of the trapped air cushion or captured air bubble principle on his sidehull craft with planing bow and stern seals. This craft was the genesis of the surface effect ship (SES) of today. In 1935, Toivio Karrio, a Finnish engineer, developed both a plenum air cushion craft and the first ram wing craft.

All of these and other beginnings formed the basis for the various forms of air cushion supported craft that have appeared on the modern scene. This book is devoted primarily to the one particular form pioneered by Sir Christopher Cockerell, namely the hovercraft or air cushion craft that obtains essentially all its support from the air cushion. Because many of the developments and improvements have occurred through the development of these other forms of air cushion craft, reference will be made, as appropriate, to these other developments in presenting the state of the art.

1.1 GENERAL DESCRIPTION

Throughout the developmental history of the various forms of air cushion support, different and sometimes conflicting names have been used to describe the different forms (see Reference 1 for a more complete description of the various names). For this volume, the word *hovercraft*, or the expression *air cushion vehicle (ACV)*, will be used to describe the fully amphibious form. The reader should be aware, however, that other authors may vary in their descriptive names. Figure 1.1 shows a family tree that provides some reference point for the various types of air cushion craft. The *roots* of this tree are the various forms of lifting or support mechanism. To the left, the form of lift is hydrostatic, as in a displacement hull. As speed increases, hydrodynamic lift come into play. At higher speeds still, full hydrostatic or hydrodynamic lifting mechanisms become inefficient, due to high power consumption, and the principle of a low resistance air cushion comes into being. Because this air *cushion* is self-generated (by onboard fans), this can be called an aerostatic lifting mechanism. As speed is increased further, aerostatic lift is either augmented by, or even supplanted by, aerodynamic lift and the craft takes on a different shape. In this context the aerostatic air cushion craft is what will be referred to here as the hovercraft. One can see from Figure 1.1 how, by combining the various lifting mechanisms of hydrostatic, hydrodynamic, aerostatic, and aerodynamic forces, the various forms of evolving craft have emerged. When one form of craft is more efficient than another for a given application, the choice depends on such technical considerations as size, speed and seakeeping, such operational considerations as mission suitability, cost, and payload capability, and other factors. Some of these various considerations and factors will be the subject of other chapters in this book.

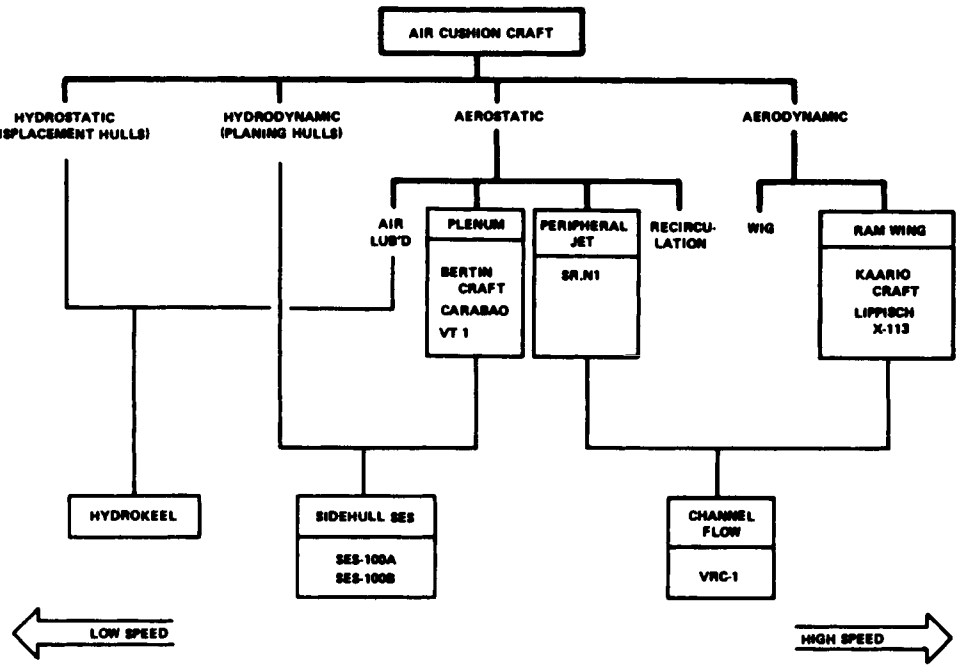

Fig. 1.1 Air cushion craft family tree.

The basic forms of hovercraft are the plenum and the peripheral jet that have, over the years, merged into one common form that may be described as a *modified plenum*. All of today's hovercraft are derivatives of the plenum and peripheral jet forms of aerostatic air cushion craft shown in Figure 1.1. Figure 1.2 shows the two basic forms most commonly used today. Chapters 2 and 10 provide more details on these skirt forms.

At this point, it is appropriate to highlight an essential feature of the hovercraft that is both an advantage and a disadvantage. As can be seen from Figure 1.2, the presence of an air cushion and flexible skirt provides the hovercraft with its true amphibious capability whereby it can traverse all surfaces (land, water, ice, mud, etc.). This is its unique advantage. The continuous leakage of air beneath the skirt, however, is a power drain that contributes to its high cost compared to other forms of transportation. This is its disadvantage. Typically, the lift power is approximately one-third of the total power. As discussed in Chapter 5, Section 5.3, power is a prime factor in determining the cost of a hovercraft. The most efficient skirt system devised to date is the peripheral jet form (Fig. 1.2(d)) but was found impractical and costly; hence, the migration toward the modified skirted plenum (Fig. 1.2(e)). Some early attempts were made in the late fifties and early sixties to develop recirculation lift systems to minimize the power drain. In

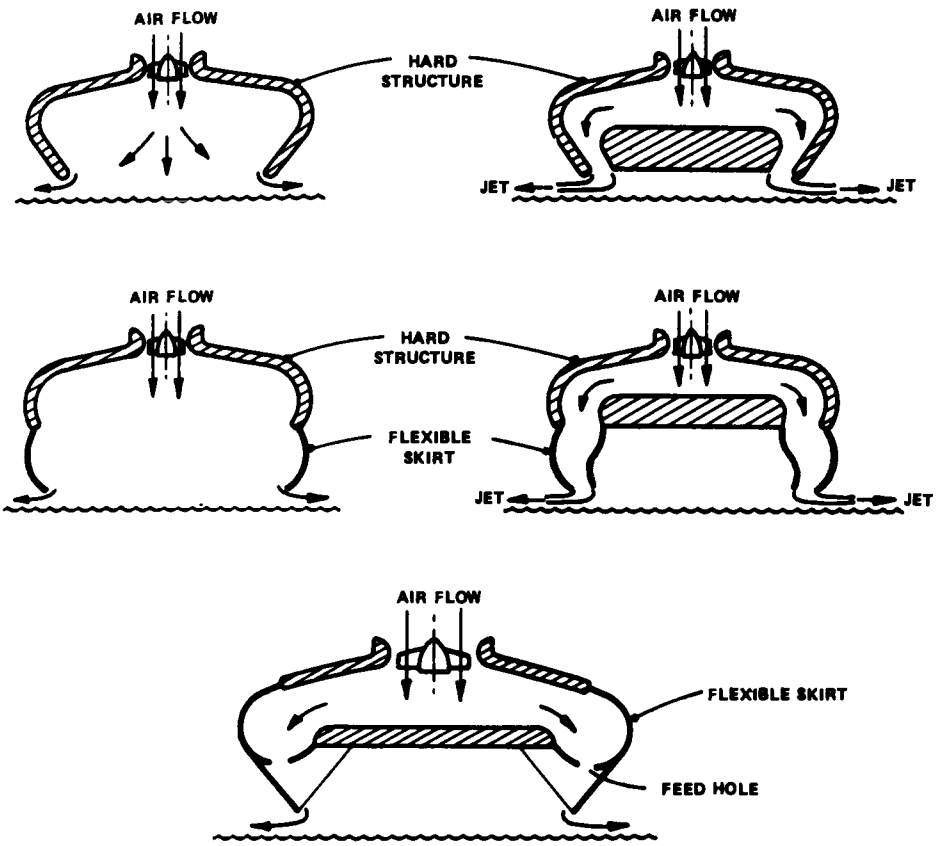

Fig. 1.2 Plenum and peripheral-jet basic forms: (a) simple plenum; (b) simple peripheral jet; (c) skirted plenum; (d) skirted peripheral jet; (e) modified plenum (skirted).

the case of the Canadair Ltd. work, an attempt was made to recirculate the air at the bottom of the skirt but these efforts were unsuccessful. It is hoped that an innovative solution to this basic characteristic of the hovercraft is yet to be discovered. The automobile uses a *zero leakage skirt system*, called the tire, for part of its suspension, which received significant development from the crude tires of 1903 to the long-life, smooth-running tires of today. What will the highly developed form of the hovercraft (and its skirt system) look like tomorrow?

Simply stated, the hovercraft is a craft that sustains itself above the surface by the generation of a pressurized cushion of air in the manner shown in Figure 1.2. It is capable of hovering in this manner and, by various means of propulsion, gets underway to serve as a transportation vehicle.

While theoretically the hovercraft skirt is not a fundamental requirement

of the concept, in practice the skirt is required for any useful application. Without a skirt (Fig. 1.2(a) and (b)), the clearance between the hard structure of the hovercraft and the surface over which it is to operate is small, i.e., a few centimetres, for any reasonable power expenditure. This is adequate if the device is to be an air-lubricated machine operating over relatively flat surfaces, e.g., moving a heavy object over a factory floor; but not at all adequate if the craft is to operate as a transportation device over rough terrain or in waves. The addition of the flexible skirt (Fig. 1.2(c) and (d)) provides two essential features that make the hovercraft a practical transportation vehicle. The first is that, for the same power expenditure as the skirtless machine, the skirted hovercraft's hard structure can ride much higher over the surface. This is because the lift power is proportional to the escaping air-jet height, not the height of the cushion or hard structure. The second advantageous feature of the skirt is that because the hard structure is much higher, i.e., perhaps a metre or more, it can traverse rough terrain with the flexible skirt undulating with the surface while the hard structure rides relatively smoothly. To provide some visualization of typical hovercraft, Figure 1.3 shows a skirted hovercraft hovering over water. The pressurized air exits from the cushion at some velocity V_e through an air gap, or hovergap, h. The craft is supported by the cushion of air acting against the hard structure with pressure P_c. For most of today's hovercraft, the cushion pressure varies from about 0.14 N/cm^2 to 0.84 N/cm^2 (0.20 - 1.2 psi) depending on the size and planned use for the vehicle, i.e., high-speed or low-speed transport. Hovergaps are typically 2.5 to 15 cm (1 - 6 in) and skirt heights are typically 1 to 3 m (3 - 10 ft). Statically, at hover over water, the water depression h_{SH}

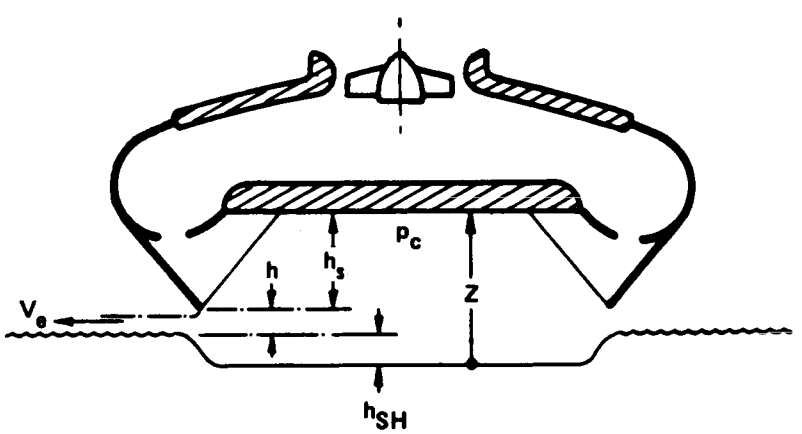

Fig. 1.3 Hovercraft hovering over water.

would then vary between 0.15 m and 0.50 m (6 - 18 in) such that the static hard clearance would typically vary from 1.5 m to 3.5 m (4.5 - 12 ft). As the hovercraft moves forward at speed, e.g., at typical cruise speeds of 15.4 m/s to 41.15 m/s (30 - 80 knots), the dynamics of the craft affect what the water depression becomes and what waves (or obstacles overland) can be negotiated. This will be discussed later in this chapter and in Chapter 2.

The hovercraft is unique among other means of transportation in that it can influence and control to some extent its support mechanism (air) as it passes through it. The ability to be relatively free of the surface, yet to interface with it, opens up a wide range of vehicle arrangements that have led to an equally wide range of vehicle types over the last twenty-eight years. Once this unique characteristic is recognized, then many options become available to the designer in the choice and design of many of the hovercraft's systems. Many of these features are expanded upon further in the chapters that follow, but it is helpful to encapsulate the key features such that the reader can keep the hovercraft's advantages in focus and perhaps even help stimulate its development.

These key features can be grouped under the following general headings: a) low resistance, b) low footprint pressure, c) flexible skirts, d) self-generated air cushion, and e) flexibility of propulsion mechanisms. These key features, individually and in combination, provide for a great flexibility in design that makes the hovercraft a useful member of the transportation family for industrial use, commercial transportation and military applications. These features are described in the following sections.

1.1.1 Resistance

A key feature of the hovercraft, and one that Sir Christopher Cockerell was searching for, is its low resistance brought about by riding on a *cushion of air*. This relative freedom of the surface over which it operates gives, not only its low resistance to all forms of terrain and water surface, but also its unique amphibiousness that allows it to operate over many different surfaces in a continuum mode of operation. This is a feature that cannot be matched by any other surface-constrained vehicle and only indirectly by air vehicles (balloons, airships and aircraft). Most marine vehicles reach a hydrodynamic limit of resistance at speed, first through the wave drag phenomenon and then through frictional resistance of the vehicle body in water. The low resistance of the air cushion allows the hovercraft to operate efficiently, i.e., with low power expenditure, over a wide range of speeds, depending on size and configuration. The craft speeds most commonly associated with hovercraft are as previously stated, 15.4 to 41.15 m/s (30 - 80 knots), which provides a wide design choice for the potential user.

1.1.2 Footprint Pressure

As a corollary to the low resistance of the air cushion, there is the feature of a low cushion pressure which equates directly to a low footprint pressure on the surface. The effect of this low pressure (0.14 - 0.84 N/cm^2) has advantages in reducing resistance over water, as is discussed in Chapter 2. The low footprint pressure is also of significance when operating over unprepared and sensitive terrain. To place this footprint pressure into perspective, consider the requirements for operating over the ecologically sensitive terrain, such as the tundra and bogs, of the Arctic. From the work done by the University of Alaska (ref. 2) the maximum contact pressure to avoid ecological damage should be no more than 2.4 N/cm^2 (3.5 psi) for operation on tundra, and no more than 0.52 N/cm^2 (0.75 psi) for operation over bog. It is seen that the hovercraft is very compatible with these limiting values of footprint pressure. Similar favorable comparisons can be made with snow, mud and sand. By contrast, the footprint pressure of a conventional automobile tire or track is some ten times these values.

1.1.3 Skirts

The hovercraft skirt is a key feature that elevates the machine from a low-clearance, air-lubricated device to a functional transportation vehicle. Chapter 2 describes the various types of skirt systems that have been developed for use on hovercraft, but they are all flexible extensions of the vehicle itself and serve several functions. These functions are:

(a) To contain the cushion and raise the hard structure above the localized obstacles. (See Figure 1.3.)

(b) To serve as a low-stiffness extension that complies as the hovercraft's hard structure moves forward over obstacles or waves. (See Chapter 2 on drag.)

(c) By different geometrical arrangements, to contribute to the stiffness and damping of the air cushion beneath the hovercraft. In this sense, the skirt is part of the suspension system of the hovercraft. (See Chaper 2 on seakeeping and motion.)

(d) By different design variants, to contribute to the control and maneuverability of the hovercraft. Skirt lifting and cushion shifting are mechanical adaptations of hovercraft skirts that show how the skirt can be integrated into the hovercraft design to serve other functions in addition to containing the air. (See Chapter 2 on hovercraft control.)

(e) By different geometrical arrangements and compartmentation, to be the major contributor to the stability of the hovercraft, especially in the pitch, heave and roll modes. (See Chapter 2 on stability.)

Thus, the hovercraft skirt is an important part and is influential in determining the practicality and, to some extent, the profitability of the

craft's operation. Chapter 5, Section 5.3.7, shows that skirt maintenance can be a large contributor to the operating cost of hovercraft. Early automobiles suffered from tire wear that limited their usefulness but, with later developments in material and design, today's tires boast 80,500 to 161,000 km (50,000 - 100,000 mile) lifetimes. Hovercraft skirts have not yet reached such values but 24,150 km (15,000 mile) lifetimes, i.e., 500 hours at 15.4 m/s (30 knots), are not unusual. Again, different geometrical and design variants produce such items as replaceable fingers to lower maintenance costs and make the hovercraft a practical transportation vehicle.

Some of the basic geometric forms that have been employed on hovercraft are shown in Figure 1.4. The terminology of bag, finger, loop, segment, jupes and pericells has all grown from the various designers and developers of hovercraft

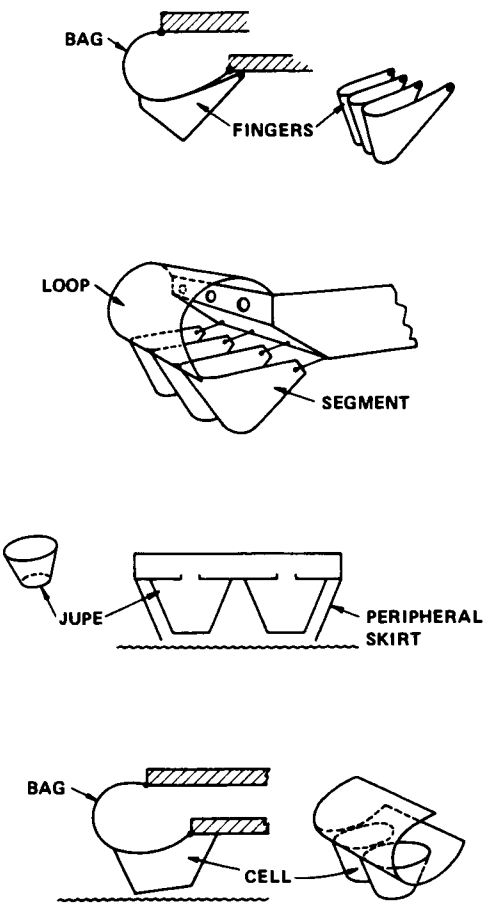

Fig. 1.4 Hovercraft skirts: (a) bag-finger; (b) loop-segment; (c) jupe; (d) pericell.

skirts. Chapter 2 provides expanded details on the more common types of skirt systems that have been developed.

1.1.4 Air Cushion

At the heart of the hovercraft lies the key feature of a self-generated pressurized air flow that serves many functions unique to the hovercraft (and its close relative, the surface effect ship). The driving force is the lift fan system that generates pressurized air at a cushion pressure p_c and cushion flow Q.

The basic functions that this on-board generated pressurized air serves are:

(a) To provide the *lifting mechanism* for the hovercraft at a cushion pressure p_c sufficient to lift the craft, i.e., when (craft weight) = (cushion pressure) × (planform area of craft). The airflow Q varies quite markedly depending of vehicle size, dynamic considerations involving craft stiffness and damping, control requirements and other needs. Airflows of 140 to 700 m^3/s (5,000 - 25,000 ft^3/s) are not uncommon. Typically, the lift power (= p_cQ) is approximately one-third of the total onboard power of the hovercraft. Chapter 2 provides more description, but generally lift power varies from 3 kW/tonne (4 HP/ton) for low-speed hoverbarges to approximately 22 kW/tonne (30 HP/ton) for high-speed hovercraft. the reader should be aware that simplistic measures, such as kW/tonne, should be used with caution because they depend on both size and speed (see Chapter 2).

(b) To provide a basic mechanism for *ride control*. As the hovercraft experiences motion while it travels over (say) waves, the very existence of the supporting pressurized air provides a relief mechanism from the unwanted forces or motions, such as pitching, heaving or rolling in waves. By various implementations of valving, vanes and similar devices, the cushion air can be vented, or otherwise worked upon, to create pressure relief from the forcing functions. This integration of the support medium (air) with the vehicle itself it fundamental to the hovercraft and can be exploited by the designer.

(c) To provide a mechanism for *directional control* by venting the air overboard through such devices as *puff ports* or *bow thrusters* to generate thrust in any direction (Fig. 1.5). Other forms of venting can be used in the air cushion itself to aid banking into turns by rolling the craft on its cushion.

As mentioned earlier, an essential part of a hovercraft is the on-board generation of pressurized air as a *lifting mechanism*. To date, this has been accomplished by some form of rotating fan system which has both an advantage and a disadvantage in most commonly used systems. The disadvantage has been that the fan systems (the fans themselves plus the ducting) consume large

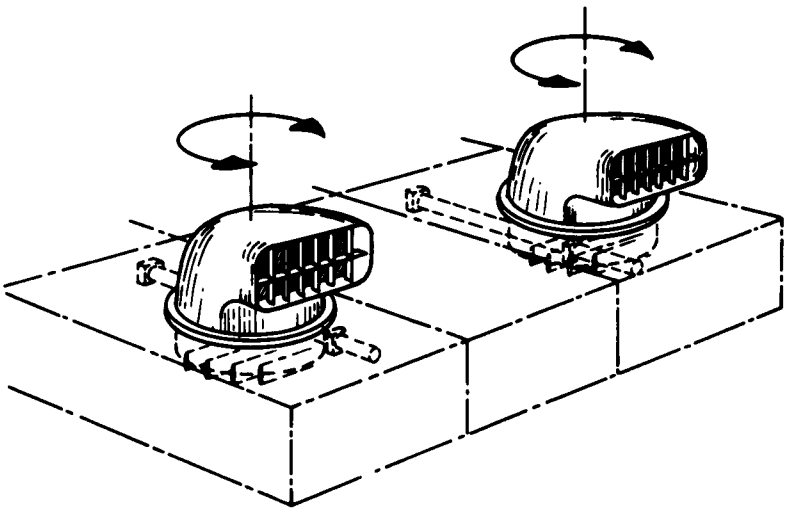

Fig. 1.5 Puff ports or thrusters.

amounts of space and weight that limit the disposable load (payload plus fuel) to between 40 and 50 percent of the craft's total weight. This might be compared to the aircraft at 50 - 70 percent, for example. However, the advantage is that, to within reasonable limits, the lift fan system can be placed anywhere in the craft to satisfy the designer's needs. This gives flexibility of craft layout for design optimization, taking the mission requirements into account. Such flexibility is difficult to achieve in other vehicles. This particular feature of the hovercraft has yet to be developed to its fullest because the development of fan systems has not been fully explored. Figure 1.6 shows some of the possible concepts of generating the hovercraft's pressurized air. They include axial fans, centrifugal fans, mixed-flow fans, cross-flow fans, and air ejectors. Most development to date has concentrated on axial-flow, centrifugal and mixed-flow fans. The cross-flow fan offered much in the way of space and weight saving but fell short on efficiency.

Many other innovations for lift fan systems have been used in hovercraft that are in operation, but they all center on the above basic functions of providing: (a) the lifting mechanism, and (b) aid in ride control.

1.1.5 Propulsion Mechanisms

Because the hovercraft is essentially free of the surface over which it operates, the choice of the means of propulsion is quite wide. In theory, this can include air propellers, marine propellers, wheels, paddle rollers, tracks, water jets and more. In many of the choices, however, the use of some of these schemes would compromise some other key feature of the hovercraft. For

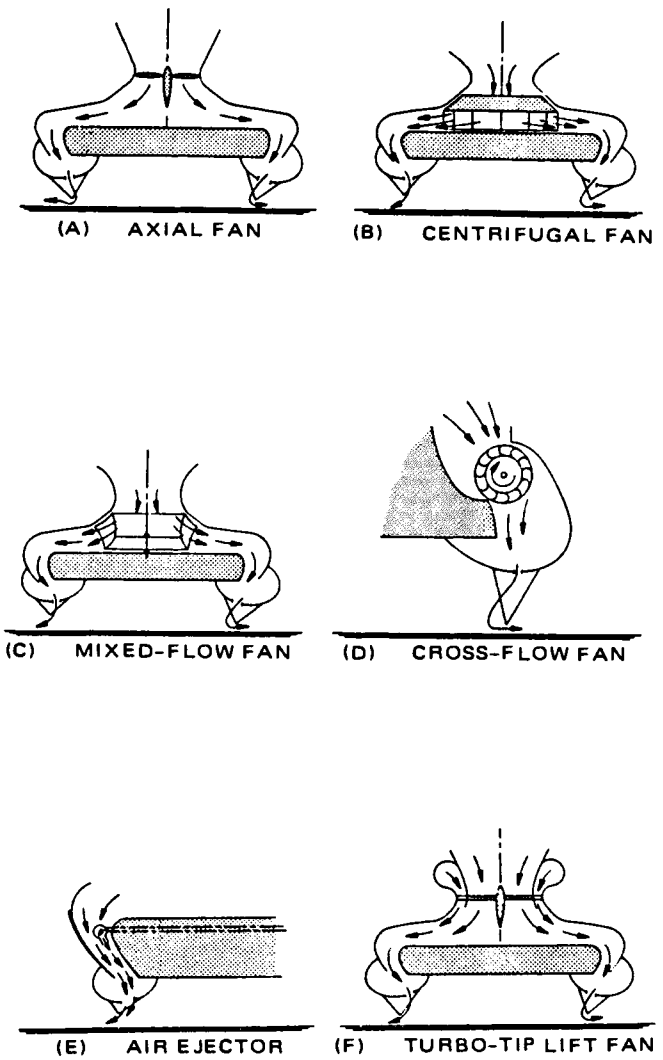

Fig. 1.6 Means of generating the air cushion: (a) axial fan; (b) centrifugal fan; (c) mixed-flow fan; (d) cross-flow fan; (e) air ejector; (f) turbo-tip lift fan.

example, the use of wheels would compromise the true amphibious feature. Most variations have been tried, including use of the basic ingredient of the hovercraft, pressurized air. Figure 1.7 shows such a technique that has been applied to early small British and Swedish craft.

As will be discussed in Chapter 2, the majority of hovercraft have maintained the key feature of being amphibious and have used the high-efficiency air propeller for propulsion. It is important to realize that such is not an automatic design choice when considering new designs for new applications of

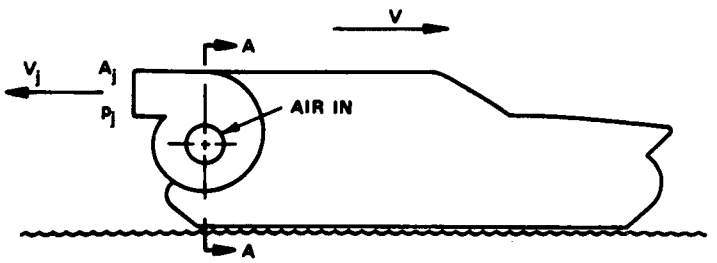

Fig. 1.7 Pressurized air propulsion.

hovercraft.

One feature that results from the low-resistance air cushion is that the hovercraft will usually require some auxillary means of propulsion if it is to be able to climb slopes or gradients greater than approximately 5 - 10 percent. Some small recreational hovercraft have improved their slope-climbing ability by means of auxiliary-propulsion soft roller tires at the stern. No commercial or military hovercraft have incorporated such capability into their hardware design to date. Some design studies have been conducted to integrate surface traction systems into the hovercraft to overcome the low slope-climbing capability inherent in the generic hovercraft concept. One such study (ref. 3) was conducted for the Defense Advanced Research Projects Agency (DARPA) in its studies of the usefulness of hovercraft in the Arctic. It was determined that large-diameter (4.25 - 6.0 m) low-pressure tires, when added to hovercraft of 100 to 700 tonnes gross weight, could augment the climbing ability to approximately 20 - 25 percent gradient. Unfortunately, such wheeled systems typically increase the craft's weight by 15 - 20 percent.

In addition to flexibility of propulsion mechanisms because of the existence of the air cushion, there is the ability to add drag devices by innovative means. Some early British and Japanese hovercraft have used either extendable rods or extendable wheels below the air cushion. These devices are not for propulsion but for braking and steering. In the case of the Japanese hovercraft (Mitsui MV-PP1, circa 1967), the rods were extended into the water on one side or the other to create drag such that the hovercraft would turn quickly in the direction of the drag force. This provided much smaller turn radii than would otherwise be attainable by the low-resistance air cushion. Similar techniques for use overland were tried in England with the Hovercraft Development Limited HD-2 and Vickers-Armstrong VA-1 and VA-2 (all circa 1967/8) where differential braking on lowered wheels (or undercarriage) provided a braking and turning capability not possible with the cushion alone. Many of these early techniques have fallen by the wayside for various technical and lack of

development reasons, especially for the larger-size classes of hovercraft in use today.

A further capability of the hovercraft is its ability to integrate the propulsion system with the lift system (in like manner to the helicopter). It is usually found in practical applications that a hovercraft travels slowly when it is about to encounter high obstacles. This situation requires high lift power and low propulsion power. Conversely, when traveling at speed (with high propulsion power) it normally operates over relatively low obstacle heights (with correspondingly lower lift power). The improvement in thrust efficiency at speed and the power recovery features of most lift systems at speed all serve to help this power balance. Accordingly, it is inherent in most hovercraft designs to trade the power from propulsion to lift from a common, constant power source on board as the need arises. This feature can be accomplished by mechanical means (gears and pitch changes) or by more novel means. One such novel scheme is the gimbal fan developed by Bertelsen (ref. 4). As discussed later in this chapter, it integrates propulsion, lift and control with one device on a small hovercraft.

Based on these examples, it is seen that the hovercraft concept includes the feature of flexibility of choice or propulsion. The basic functions of the propulsive mechanism are:

(a) By suitable thrust generation, to *propel the craft* at the desired speeds required for practical operation.

(b) By generation of sufficient thrust margin, to provide the necessary *acceleration and deceleration* to ensure that the craft is maneuverable and safe to operate. (See Chapter 2 for determination of thrust margins.)

(c) With suitable use of thrust vectoring (thrust and pitch change mechanisms), to provide the necessary *directional control* for the hovercraft. The addition of various auxiliary devices such as puff ports, bow thrusters, extension rods, wheels, etc. serve to increase the flexibility of directional control depending on vehicle size, speed and mission.

(d) By integration with the lift system, to provide an *energy saving* mechanism for an otherwise high power consuming vehicle.

(e) By exploitation of such novel schemes as the gimbal fan, to combine propulsion, lift and control so as to give the hovercraft *flexibility of design layout* that can have many ramifications on simplicity and cost.

As can be seen from this discussion, propulsion is a relatively unexplored area in hovercraft development that could well change the look of the hovercraft of the future. Furthermore, based on the foregoing fundamental look at the key features of hovercraft, it is seen that many design variants can be produced. Table 1.1 summarizes these features and serves as a focal point for

Table 1.1. Technical features of hovercraft.

Key feature	Impact on hovercraft characteristics
Low resistance	High speed for less power Amphibious Highly maneuverable
Low footprint pressure	Ecologically safe on most surfaces
Flexible skirts	Cushion containment over high obstacles Low resistance over obstacles Part of suspension system Aids control and maneuverability Contributes to craft stability
Self-generated air cushion	On-board lift mechanism Contributes to ride control and good seakeeping Directional control Energy saving (by integration) Flexibility of design layout
Propulsion mechanism	Propels the craft Acceleration and Deceleration Gradient climbing Directional control Energy saving (by integration) Flexibility of design layout

the various design variants that are discussed throughout the book. It serves also to highlight whether the feature being discussed is well developed or at the early stages of its development. It is now appropriate to show selected hovercraft to illustrate how different designers and builders around the world have taken the above generic features and produced operational hardware.

1.2 SELECTED HOVERCRAFT

It is not intended to provide a catalogue of all the hovercraft that have been built around the world over the last twenty-eight years since Sir Christopher Cockerell's brainchild, the SR.N1, took to the water in 1959. Such cataloguing is more eloquently done by Jane's (ref. 5). It is more appropriate for present purposes to show examples of hovercraft that illustrate the level of development in some of the major areas. There have been many hovercraft and surface effect ships (SES) built and operated around the world, and approximately eighteen countries have been involved in their design and construction. Air cushion craft are operating in approximately twenty-seven countries at this time.

Table 1.2 provides an approximate account of the major number of air cushion craft either built or planned to be built by the year AD 2000. To provide some perspective on the development, both hovercraft and surface effect ships (SES) are included because their development has been concurrent and mutually beneficial. Early prototypes such as SR.N1, Britten-Norman craft, SAAB

Table 1.2. Numbers of air cushion craft.

Country	Built to date(1)		Additional planned(2) (By AD 2000)	
	Hovercraft	SES	Hovercraft	SES
Australia	---	---	10	---
Canada	5	---	5	---
PRC	7	11	---	---
Finland	16	---	1	---
France	3	1	---	2
Japan	27	---	---	---
Korea	2	7	1	---
Netherlands	---	---	---	4
New Zealand	1	---	2	---
Norway	---	1	---	---
Romania	---	1	---	---
Spain	1	---	6	---
Sweden	---	---	---	1
Switzerland	---	---	1	---
Taiwan	1	---	2	---
UK	108	100	20	10
USA	89	10	117	21
USSR	70(3)	114(3)	Note (4)	Note (4)
Total	330	245	185	38

NOTES

(1) Eliminated from this table are early prototypes, craft no longer in operation and recreational hovercraft.

(2) Approximate projections based on today's known plans.

(3) USSR existing military craft restricted to published data.

(4) USSR military projections are classified and not included.

vehicles, etc. have been excluded from this table in an attempt to focus attention on operational vehicles. Such early prototypes might increase the count by 20 to 30 craft. Sports and recreational hovercraft are treated separately in Chapters 3 and 4.

By this approximate account, there have been some 575 air cushion craft (330 hovercraft; 245 SES) built to date with approximately 80 percent operational in 1987. Table 1.2 does not include a correct account of the USSR military hovercraft or SES for the reasons noted. It is known, however, that the USSR is the world's largest operator and producer of military air cushion craft (ref. 6). It is now believed to have the largest force of air cushion craft in the world, made up of the Aist, Lebed, Tsaplya, Uteknok and Gus classes. According to ref. 6, two new classes have been added to the Baltic Fleet.

These are the Pelikan and Pomornik classes (see later), the first units of which entered the Fleet in 1985. There are reports of yet another USSR craft of a different type under construction. The USSR air cushion craft estimate in Table 1.2 has been taken from Jane's (ref. 5), which is believed to understate the actual number of Soviet hovercraft.

With a certain amount of trepidation, an approximate projection has been made into the future based on known and published projections from each country. Also, it should be noted that not accounting for the Soviet plans distorts (underestimates) the projection somewhat. While the projection of another 223 air cushion craft (185 hovercraft; 38 SES) may appear modest, it might be noted that since individual builder's projections have usually been conservative in the past, this projection is to be considered conservative. It is reasonable to assume therefore (with the above cautionary notes in mind) that, by AD 2000, there will be approximately 800 operational air cushion craft (allowing for some retirements of vehicles) of which more than 500 would be hovercraft. Table 1.3 provides a further breakdown of the types into commerical and military vehicles. To date, the development has centered on commercial applications, but Table 1.3 shows a trend toward military applications. Two explanations are suggested for this trend: a) the economics of commercial air cushion craft have not been as profitable as originally projected (see Chapter 5 for a more detailed look at hovercraft economics), and b) the military value of a high-speed amphibious vehicle is gradually being recognized. The current building of hovercraft by the US and USSR for amphibious warfare is a strong contributor in Tables 1.2 and 1.3 to this trend. It is quite likely that, if sufficient numbers of hovercraft would appear in the military inventory of amphibious warfare craft, the application to other missions (e.g., mine countermeasures, among others) would accelerate the build plans. Also, as experience would be gained by industry on building in such large production quantities, a sufficient *learning curve* (see Chapter 5) would be generated. Such a learning curve would then allow the hovercraft to be produced at sufficiently economic prices that the commercial applications would increase correspondingly. An interesting article by Meredith (ref. 7) points both to the success of such commercial operations as the SR.N4 (27 million passengers transported to date across the English Channel) and to the concerns of profitability in the future.

Clearly, compared to the numbers of automobiles, ships and aircraft being produced each year, the hovercraft is not enjoying a large part of the transportation market today. One of the purposes of this book is to provide sufficient technical and economic data to guide the hovercraft designers along lines that will produce practical, profitable and useful vehicles for their planned applications.

Table 1.3. Commercial and military air cushion craft. Numbers are subject to the limitations noted in Table 1.2.

Type	Built to date		Additional planned (By AD 2000)	
	Hovercraft	SES	Hovercraft	SES
Commercial	214	235	94	18
Military	116	10	91	20
Total	330	245	185	38

1.2.1 The First Hovercraft

The first selected hovercraft to illustrate the technological development is the SR.N1 which, as stated earlier, was the first practical hovercraft based on the pioneering work of Christopher Cockerell. Figure 1.8 shows the SR.N1 operating in its skirted configuration and not in the original unskirted form used for its historic first crossing of the English Channel on 25 July 1959 (a date selected by Cockerell to be 50 years after the epic flight by Louis Bleriot, also from Calais to Dover). On that first trip, the SR.N1 had an initial all-up weight (AUW) of 38.7 kN (8,700 lb) and an end-of-trip weight of 36.92 kN (8,300 lb), the average over-water speed was 7.10 m/s (13.8 knots) and an air speed of 11.83 m/s (23 knots). The trip time was approximately 1.8 hours. The hovergap (no skirt) averaged 24.13 cm (9.5 inches). The installed power (Alvis Leonides engine) of 336 kW (450 HP) was used to produce an air-jet thrust of 3.02 kN (680 lb) generated by the deck-mounted nozzles (see Figure 1.8). The cushion pressure of the SR.N1 was 0.081 N/cm^2 (0.118 psi) which is very low by today's standards for an economical hovercraft. It is interesting to note that this first hovercraft used an axial-flow fan (seen in the white vertical duct of Figure 1.8) to maximize the lift system efficiency.

In subsequent testing of the SR.N1, after it was realized that skirtless hovercraft do not function well in waves (SR.N1 experienced 1.22m (4 ft) waves on the first trip), skirts were added. Hovercraft skirts were first introduced by Hovercraft Development Ltd (HDL) which still functions today as a patent holder on such items. These first skirts (shown in Figure 1.8) were of a 1.22 m (4 ft) skirt height and were of the peripheral jet form shown in Figure 1.2(d). More detailed descriptions of the SR.N1 and its first voyage can be found in the papers by R. Stanton-Jones, at that time Chief Designer of Saunders-Roe (now Westland Aerospace, formerly British Hovercraft Corporation) co-builder of the SR.N1 (ref. 8) with Sir Christopher Cockerell (ref. 9).

As development of the hovercraft continued, new skirt forms evolved (see Chapter 2) along the lines shown in Figure 1.2, centrifugal fans came into

Fig. 1.8 The first hovercraft: SR.N1.

vogue because of their ruggedness and quietness, air propellers appeared on the scene and other features were integrated, all of which changed the basic look of hovercraft. The British Hovercraft Corporation's (BHC's) SR.N4 epitomizes many of the features of the hovercraft development discussed above and today represents the world's largest commercial hovercraft.

1.2.2 The Largest Commercial Hovercraft

The first SR.N4 (SR.N4 Mk 1, Mountbatten) was a 193 tonne passenger/car ferry. It entered commercial service with British Rail Hovercraft Ltd. in August 1968 on the Dover to Boulogne route. Its calm water speed was 36 m/s (70 knots). It had an average speed of 20.6 to 25.7 m/s (40 - 50 knots) in waves 3.05 m (10 ft) in height and was capable of operating in seas of up to 3.7 m (12 ft) wave height at a speed of 10.3 m/s (20 knots). The SR.N4 Mk 1 had an overall length of 39.68 m (130.17 ft), overall beam of 23.77 m (78 ft) and a skirt height of 2.44 m (8 ft). Its payload was designed basically for 254 passengers and 30 cars but could be varied to 174 passengers and 34 cars or an all-passenger version of 609 passengers.

British Rail took delivery of a second SR.N4 Mk 1 in July 1969. Hoverlloyd Ltd. started service on the Ramsgate/Calais route in April 1969 with two of the Mountbatten class. Hoverlloyd introduced a third SR.N4, Mk 1 (the fourth to be built) on the Ramsgate/Calais route in the summer of 1972. The success of

these operations was such that Hoverlloyd had the SR.N4, Mk 1 modified to an increased capacity SR.N4, Mk 2 that re-entered commercial service in January 1973. The craft weight was increased to 203 tonnes; the payload, to 282 passengers and 37 cars. The skirt was also modified to the now-standard *tapered skirt*, with a skirt height at the bow of 3.05 m (10 ft). The two remaining Hoverlloyd SR.N4 hovercraft were also modified to the SR.N4, Mk 2 configuration in January 1974. Figure 1.9 shows the SR.N4, Mk 2 named the Swift.

Several key features of hovercraft can be seen in the SR.N4, Mk 2 (Figure 1.9). The flexible deep skirt of the modified plenum or bag-finger type (Figure 2(e)) allows the hovercraft to travel at speed over waves. Because of the dynamics of the cushion/wave interaction, the 2.44 to 3.05 m (8 - 10 ft) skirt height allows passage over 3.05 to 3.7 m (10 - 12 ft) waves without significant hard-structure impact.

Fig. 1.9 BHC Hovercraft: SR.N4 Mk 2.

The propulsion system is integrated with the lift system for power saving. Power is supplied by four 2,536 kW (3,400 HP) Rolls-Royce Marine Protens free-turbine, turboshaft engines. Each engine is mechanically connected by suitable gearbox and shafting to a propeller/fan unit. Each of the four propeller/fan units is identical.

The gear ratios between the engine, fan and propeller are fixed, such that the power sharing between propeller and fan can be altered simply by changing propeller pitch. Power can be varied to the lift system fan unit from zero to 1,566 kW (2,100 HP). Hence, by changing propeller pitch, the hovercraft can be converted from operating in the boating mode (zero lift power) to hovering on full cushion. A typical cruising-power division per propeller/fan unit would be 1,492 kW (2,000 HP) to the propeller and 858 kW (1,150 HP) to the lift fan. the remaining power from the 2,563 kW (3,400 HP) engine would be for transmission losses and auxiliary drive requirements. The propellers, made by Hawker-Siddeley Dynamics, are 4-bladed, variable reverse-pitch 5.79 m (19 ft) diameter propellers. The lift fans (made by BHC) are 12-bladed centrifugal fans 3.5 m (11.5 ft) in diameter. The propeller/fan units are modeled after the systems used in earlier BHC hovercraft (see later). They are used in multiples as needed (in this case, four per craft) and placed appropriately around the passenger/car payload to allow a drive-through capability without compromising the technical design. This valuable feature for a car ferry has been used to advantage on several later hovercraft.

The propulsion system on the SR.N4 has also been made part of the directional control system. Each propeller pylon can be rotated to give different combinations of forward, reverse and side thrust. This makes the craft highly maneuverable and controllable despite the inertia of a 203 tonne machine sitting on a low-resistance air cushion.

The success of the SR.N4 Mk 1 and 2 series brought about the upgrading of the Mk 3 version, or Super 4. On 6 April 1978, BHC launched the first SR.N4 Mk 3 (Super 4) and later it entered commercial service for Seaspeed on the Dover/Boulogne/Calais route. The Super 4 shown in Figure 1.10 is actually one of the earlier SR.N4 Mk 1 hovercraft, the Princess Anne, modified. The all-up weight was increased to 305 tonnes with the addition of a 16.76 m (55 ft) section amidships. The propeller pylons were raised to accommodate larger 6.4 m (21 ft) diameter air propellers.

This stretched SR.N4, the largest hovercraft in commercial service today, can carry 416 passengers and 60 cars over coastal routes up to 240 km (150 miles). Its overall length and beam are respectively 56.4 m (185 ft) and 23.2 m (76 ft). The average skirt length of the tapered skirt is 2.75 m (9 ft). Westland Aerospace (formerly BHC) reports that the Super 4 has a 70 percent greater earning capacity than the earlier Mk 1 and 2 versions but costs only 15 percent more to operate. It is also reported that, due to the increased length-to-beam ratio (2.43:1 compared to 1.67:1) and the increased cushion area (approximately 38 percent greater), the ride comfort measured in vertical acceleration imparted to the passengers is "a three-fold improvement over the Mk 2 series." The SR.N4 Mk 3 (Super 4) also has 2,834 kW (3,800 HP) of power

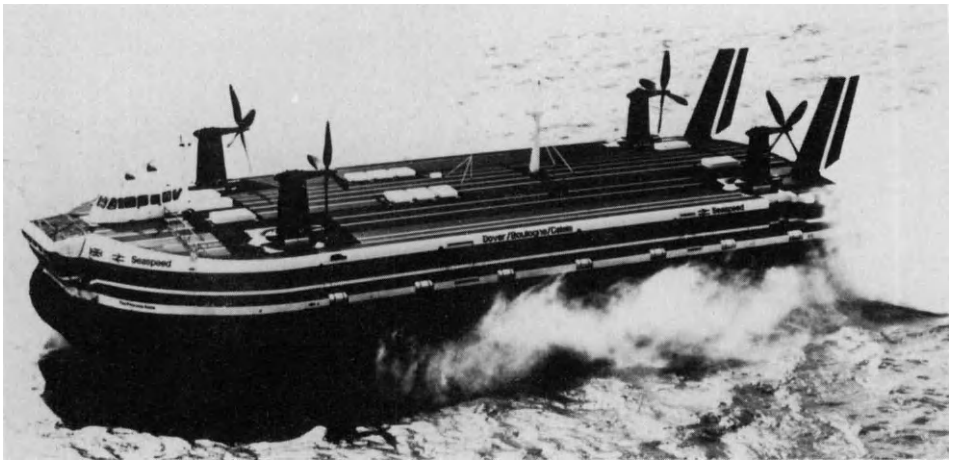

Fig. 1.10 BHC Hovercraft: SR.N4 Mk 3 (Super 4).

to each of the propeller/fan units, which is an increase of approximately 8.5 percent.

1.2.3 The Largest Military Hovercraft

Another example of a large hovercraft is, as mentioned earlier, a Soviet military hovercraft, called the Pomornik by NATO (ref. 10). The Pomornik is shown in Figure 1.11. It has an estimated displacement (all-up weight) of 350 tonnes, which if correct would make it approximately 45 tonnes larger than the commercial SR.N4 Mk 3 (Super 4), with approximately the same dimensions. These are the two largest hovercraft built to date. According to International Defense Review (IDR) (ref. 10), the Pomornik built at one of the Leningrad shipyards is 56 m (186.67 ft) long, 22 m (73.3 ft) wide and draws 0.5 m (1.67 ft) off cushion. No estimate is available on skirt height. Estimates of the hovercraft's top speed have been made at 25.7 to 30.8 m/s (50 - 60 knots). The three 4-bladed ducted propellers are approximately 5.2 m (17 ft) in diameter. There are four fans to provide lift. The type of fan has not been identified although most of the Pomornik's predecessors, i.e., the Gus, the Lebed and the Aist hovercraft, used axial-flow fans.

Furthermore, IDR notes that the Pomornik has bow and stern ramps and is thought to be capable of transporting four PT-76 amphibious light tanks (each 14 tonnes weight) and a detachment of naval infantry. While it is not the intent of this book to analyze mission suites that can be placed on board hovercraft, it is noted that the Pomornik is equipped with air defense weapons for use during an amphibious landing; these are two six-barrelled Gatling-type 30 mm cannons, mounted forward of the lift fans, and two surface-to-air

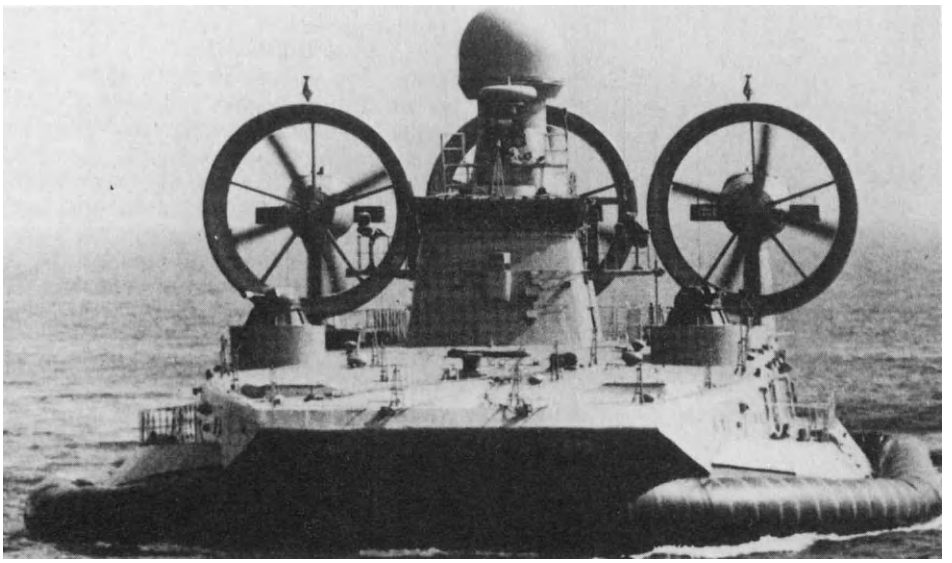

Fig. 1.11 Soviet amphibious assault hovercraft: Pomornik.

(SA-N-8) missile launchers on either side of the bridge.

1.2.4 Early British Hovercraft

Between the 4 tonne SR.N1 in 1959 and the 350 tonne Pomornik in 1985, a large number of many different types of hovercraft have been built (see Tables 1.2 and 1.3). Some selected examples to illustrate where the development has progressed is provided for reference. Figure 1.12 shows some of the British air cushion craft that have seen extensive development for both commercial and military uses. Figure 1.12(a) shows the SR.N5, which was the first commercially successful hovercraft and has operated on commercial routes around the world. It was constructed in 1963 and launched on 11 April 1964. It has a nominal gross weight of 7 tonnes and carries 20 passengers. Its maximum calm water speed is 33.9 m/s (66 knots). It has been manufactured under licence in the United States by Bell Aerospace (now Textron Marine Systems) (circa 1965-67) and designated the SK-5, and in Japan by Mitsubishi and designated the SR.N5(M). In the case of the Bell construction, significant changes were made to the craft to make it suitable for military missions in Vietnam. The SR.N5 is now out of production and has been replaced by the SR.N6 (Fig. 1.12(b)) which first entered trials on 29 March 1965. The SR.N6 in its early form was a 9 tonne craft carrying 38 passengers. It has a maximum calm water speed of 30.9 m/s (60 knots). The SR.N6 has seen commercial and military successes in many countries around the world and is now on its *Mk 8* variation. For example,

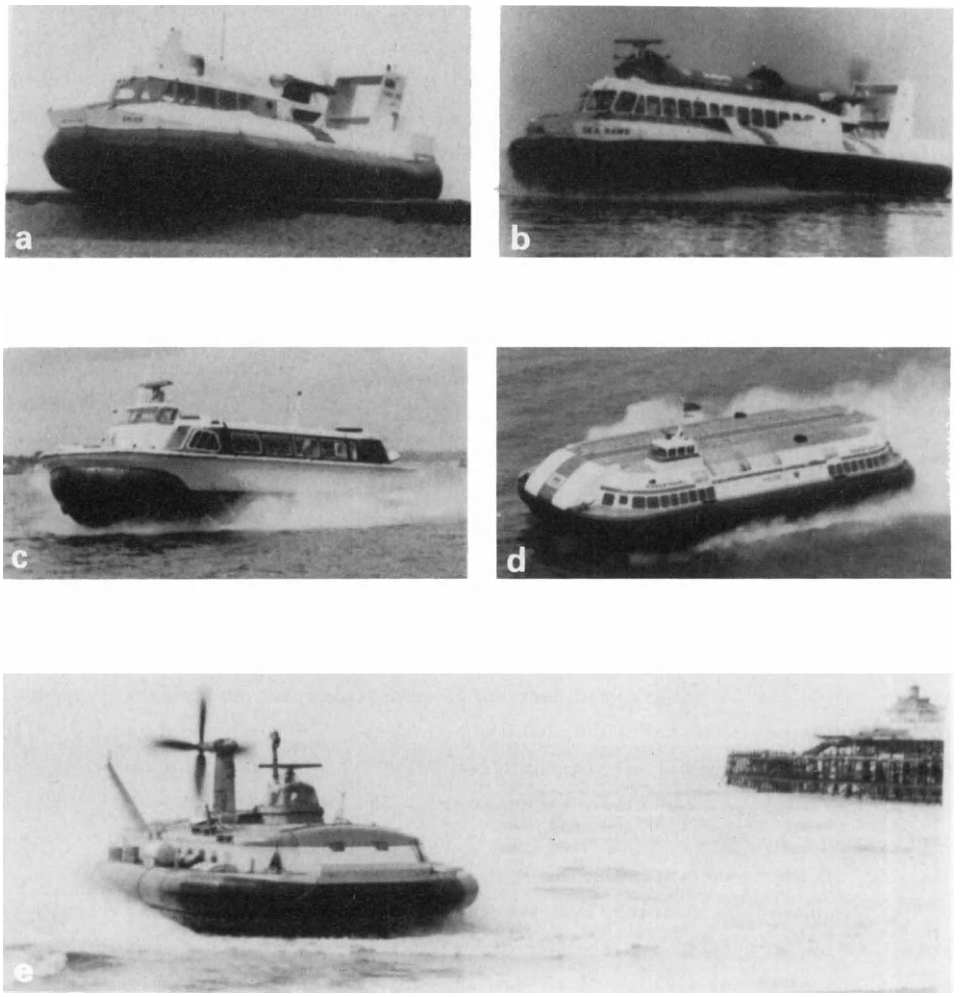

Fig. 1.12 Early British air cushion craft: (a) hovercraft SR.N5 by BHC; (b) hovercraft SR.N6 by BHC; (c) surface effect ship HM.2 by Hovermarine; (d) hovercraft VT-1 by Vosper-Thornycroft; (e) hovercraft BH.7 by BHC.

in 1973, BHC developed a twin propeller version for improved control, lower noise and general purpose use (shown to the public on 25 September 1973). The SR.N6 Mk 8, developed as a military variant for logistics missions, has returned to the single propeller. Other variants have been produced including stretches, deeper skirts, tapered skirts, etc. to make it suitable for various commercial and military missions. The SR.N6 and its predecessor, the SR.N5, embody most of the features discussed earlier. To date there have been over

fifty-four of the SR.N5/SR.N6 series hovercraft built; they clearly form the foundation of the numbers shown in Table 1.2 for the United Kingdom. Wheeler (ref. 11) provides a comprehensive description of the development and chronological history of the SR.N5 and SR.N6 series of hovercraft.

Figure 1.12(c) is a photograph of the HM.2, an SES, built by Hovermarine in England. It is included because it embodies many of the features of British hovercraft and large numbers (over 100) have been built and operated in over 30 countries of the world. The company, while developing a successful product, has suffered several setbacks in its long history. It began in the 1960s with the Denny sidewall craft and gradually developed the sidehull SES craft containing many features expected to be successful in a hovercraft. The craft is relatively inexpensive (see Chapter 5, Section 5.3.2) in terms of both acquisition and operating cost. The original company, Hovermarine Ltd., was established in 1965 and has gone through four ownerships, including U.S. ownership (as part of Technical Transport Inc. (TTI) in 1969). After another change of ownership in 1972, Vosper bought the company in 1980 and formed Vosper Hovermarine which went into liquidation in February 1986. On 21 July 1986 the company was again purchased by U.S. interests as Hovermarine International. Despite these management and name changes, the Hovermarine craft continue to serve the commercial transportation needs worldwide. The HM.2 has several *Mark* versions depending on the needs of the customer. In its version, it has an all-up weight of 21 tonnes and carries 65 passengers at a calm-water speed of 18 m/s (35 knots). It has a GRP (Glass Reinforced Plastics) construction hull; the skirts are simple loop-segment (see Fig. 1.4(b)); lift fans are of the centrifugal type powered by diesel engines. The propulsion is a direct-drive marine propeller/diesel engine combination. Many of the simple and rugged features of the hovercraft have been incorporated into this craft.

As discussed in Section 1.1, it is not axiomatic that the hovercraft be propelled by air propulsion mechanisms or that it be completely amphibious. A unique approach was incorporated in the Vosper-Thornycroft hovercraft VT-1 shown in Figure 1.12(d) in that, while the craft and skirt system was of the amphibious form discussed, the propulsion system was a conventional inclined shaft, water-propeller propulsion system. Three such craft were built, two of which operated commercially between Sweden and Denmark in 1972, carrying over 310,000 passengers more than 98,000 km (61,000 miles). The craft was operated successfully, but the service was discontinued. The operation's demise can be attributed to non-technical reasons and directly related to stiff price competition from state-owned and state-operated ferries and hydrofoils. The VT-1, because of its cushion and water propulsion system, has an aesthetically pleasing external profile, as seen in the photograph. This particular design was chosen on the assumption that, for the speed range of 15 to 20 m/s (30 - 40

knots), the quietness and high efficiency of the marine propeller would give the craft an economic advantage. The VT-1 was an 87 tonne hovercraft capable of carrying 146 passengers and 10 cars cruising at 18 to 19.5 m/s (35 - 38 knots). It could operate in 3 to 3.7 m (10 - 12 ft) seas. Propulsion and lift power was supplied by two Avco Lycoming TF 25 marine gas turbine at 1,417 kW (1,900 HP) each. Each engine was directly coupled to four 1.5 m (5 ft) diameter centrifugal lift fans through a transfer gearbox and then to the inclined water propeller through a V-drive gearbox. The skirt system was a loop-segment type (see Figure 1.4(b)) with a skirt height of 1.68 m (5.5 ft). The KaMeWa propellers were 3-bladed with controllable pitch and a diameter of 0.64 m (2.1 ft). The VT-1 conducted amphibious landings by nudging up to the beach with the inclined propeller shaft protected by skegs.

In 1973, Vosper-Thornycroft made the decision to convert the VT-1 to the VT-2, a fully amphibious hovercraft propelled by ducted air propellers. A VT-2-001 hovercraft is shown in Figure 1.13 approaching a beach. The angle of the propeller shafts is the result of the conversion whereby the gearbox for the inclined marine propeller was used for the ducted air propeller. This particular hovercraft was used in 1977 and 1978 by the Royal Navy during the Whiskey Galore exercises of amphibious landings around England and Scotland. It was also used in mine-countermeasure trials of hovercraft, a mission which appears to be well-suited for the hovercraft because of various features of the air cushion, as discussed below in conjunction with the BH.7 hovercraft.

1.2.5 British and American Military Applications

Returning to Figure 1.12, photograph (e) shows the British Hovercraft

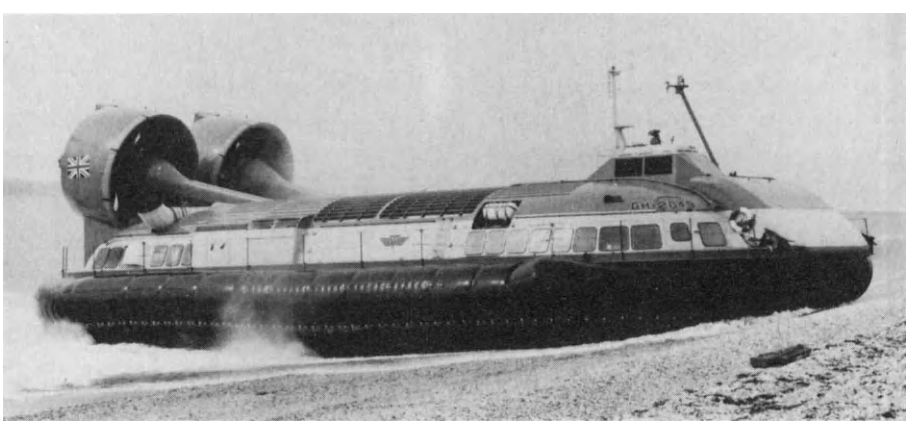

Fig. 1.13 Vosper-Thornycroft's VT-2-001 hovercraft approaching beach.

Corporation's BH.7 on a demonstration run up the beach at Brighton, England, at the 1974 International Hovercraft and Hydrofoil Conference and Exhibition. The BH.7 was the first hovercraft built in quantities designed specifically for military missions. The first military hovercraft was the SR.N3 (1963). As will be discussed, the BH.7 has shown, in many military operations for two Navies, some of the key features of a hovercraft that offer several advantages. The first of seven BH.7 craft was launched on 31 October 1969. This prototype, designated BH.7 Mk 2, has been in service with the Royal Navy since 1970 conducting various missions including fishery protection, anti-submarine warfare (ASW) and mine countermeasures (MCM). The remaining six craft are in operation with the Iranian Navy (two Mk 4s and three Mk 5As). The BH.7 Mk 4 is used in a logistic support role; the BH.7 Mk 5A is used for coastal defense, combat and logistics missions.

The BH.7 Mk 5A is shown in Figure 1.14. Its all-up weight is 61 tonnes. The overall length is 23.4 m (76.75 ft); overall beam is 13.9 m (45.5 in); skirt height is 1.68 m (5.5 ft). The integrated lift and propulsion system is

Fig. 1.14 BH.7 Mk5A military hovercraft.

powered by a Rolls-Royce Marine Proteus gas turbine with 3,170 kW (4,250 HP). Its calm-water speed is 30.9 m/s (60 knots) and it is capable of carrying up to 14 tonnes of military equipment. The diameter of its single propeller is 6.4 m (21 ft). The Mk 2 and Mk 4 versions have less power and a smaller-diameter propeller. The combat system installed on the Mk 5A, shown in Figure 1.14, includes medium range ship-to-ship missiles, such as Exocet.

A military mission for which the hovercraft appears well suited is mine-countermeasures (MCM) because of the particular feature of the insulating air cushion. The following features summarize some of the more evident characteristics in support of this application.

(i) Control. The hovercraft, with its combination of aerodynamic controls, skirt lifting, etc., is adept at maintaining track and thus not prone to drift (when close to mines). Its maneuverability provides a rapid response to the mine warfare officer's commands.

(ii) Sonar *visibility*. A conventional ship masks a sonar's capability in the stern arc because of the presence of propellers. On the other hand, since the hovercraft has no part in the water, its dipping sonar has no blind area.

(iii) Self-noise. The air cushion provides sound insulation such that very little self-noise (from propulsors, etc.) is transmitted into the water. This enhances the sonar's capability to detect. Also, unlike a conventional displacement hull, the self-generated noise remains low even at high forward speed. As new high-speed sonars become available, the advantages of the hovercraft should become even more evident. Figure 1.15 is an artist's rendering of the BH.7 in an MCM role, with a dipping sonar (like the Plessey 193M sonar transducer) sweeping the ocean floor for a bottom-laying mine. It is planned to use a larger BH.7, the BH.7 Mk 20, for such missions. The mine neutralization device is shown moving in for the kill (Fig. 1.15).

(iv) Low footprint pressure. It has been found over many years of testing that the low footprint pressure of the hovercraft air cushion is particularly advantageous in mine hunting. The low footprint pressure results in a low underwater pressure signature providing invulnerability to acoustic mines. The separation of the metal structure from the surface by the air cushion also provides invulnerability to magnetic mines. This insulating feature of the air cushion has been proven many times in explosion trials such as with the Vickers-Armstrong VA.3 hovercraft in 1967 and 1968, the SR.N3 in 1974, and the amphibious landing craft JEFF(A) most recently in the United States. A photograph demonstrating one of these JEFF(A) tests in 1983 is shown in Figure 1.16. A more complete description of the application of hovercraft in mine countermeasures may be found in references 12 and 13.

In addition to the use of hovercraft in the MCM role, the amphibious char-

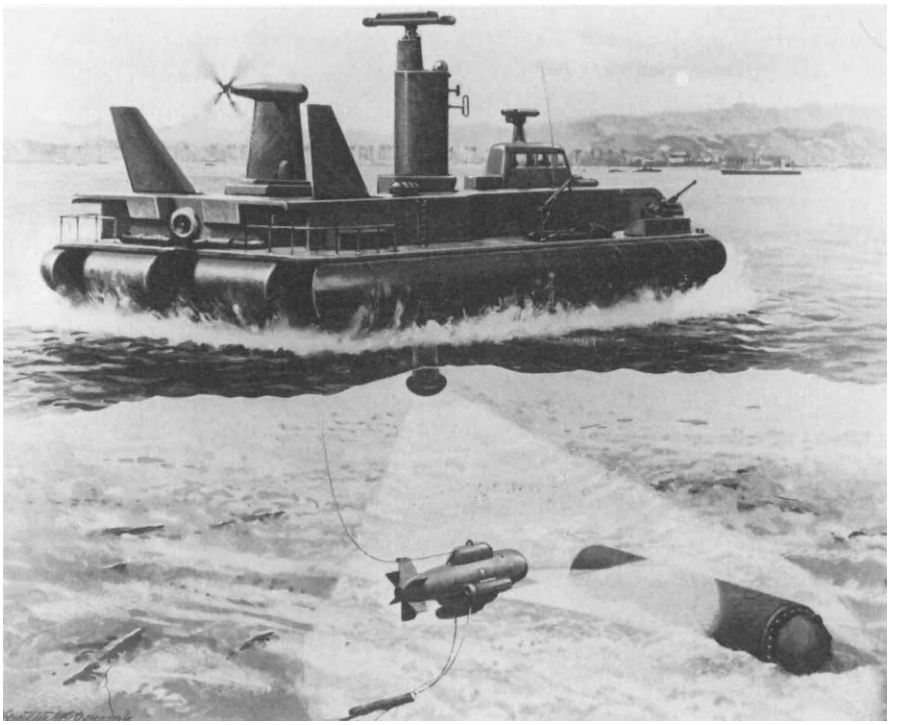

Fig. 1.15 BH.7 hovercraft in minehunting role.

acteristic of the hovercraft is ideal for use in amphibious warfare. The ability to transport troops and military equipment from over-the-horizon to beyond-the-beach without the vulnerability of having to stop at the shoreline is an obvious military advantage. Also, the ability to select which part of the coastline to effect an amphibious strike is again a military advantage that can be achieved with a vehicle that can operate independently of the surface. The problem of amphibious warfare, especially the problem of amphibious landing, has plagued all would-be invaders of foreign soils for centuries. A discussion of amphibious warfare in more recent times, and in particular the application of the hovercraft in this mission, is provided by Piersall and Kenefick (ref. 14). While the use of the hovercraft for such a mission may seem natural, its implementation has taken a long and arduous route. The United States Marine Corps (USMC) recognized the problem early and participated in the development of hovercraft from the beginning (1959). Slafkosky (ref. 15) provides a succinct summary of USMC activities in bringing along improved vehicles for amphibious warfare and describes the genesis of the current hovercraft program, i.e., the Landing Craft, Air Cushion (LCAC) program.

While there was some earlier interest by the USMC in the use of the hover-

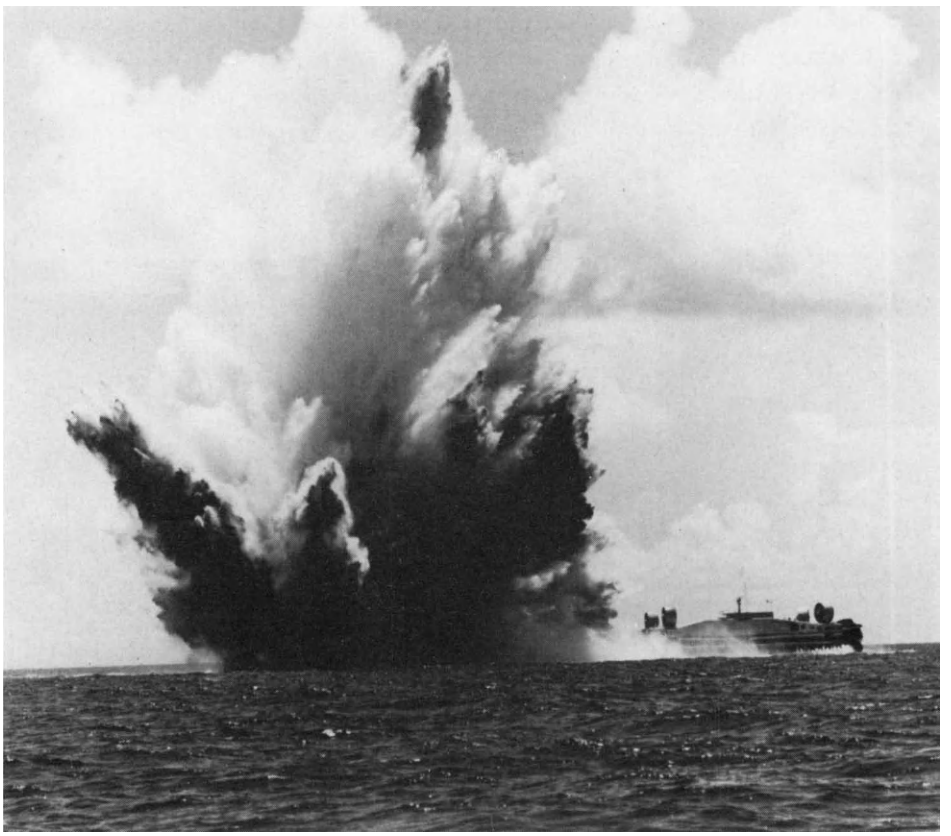

Fig. 1.16 JEFF(A) undergoing underwater shock tests.

craft (ref. 16), it began officially on 27 March 1961 (ref. 17). That was when the Commandant requested the Chief of Naval Research to begin investigations of *Ground Effect machines (GEM)*, an early American name for hovercraft, in all applications concerned with amphibious assault. This program developed through many phases (ref. 15), finally culminating in the delivery of the first LCAC to an operational squadron in December 1984 - a span of twenty-four years! While there have been sporadic introductions of the hovercraft into other miliary operations (e.g., use in the British Army in 1968), the USMC program with its underway production of 90 LCAC craft represents a major commitment of the hovercraft to the *natural* mission of amphibious operations. While the period of twenty-four years may seem long, it is not unusual. Mantle (ref. 18) shows that twenty-two years is an average time to introduce new vehicles into the *system*. Hopefully, understanding the technology, economics and applicability

of the hovercraft to missions (military or commercial) can aid in reducing such gestation periods.

The immediate forerunners to the LCAC craft were the JEFF(A) and JEFF(B) craft shown in Figure 1.17 operating off Panama City, Florida, in 1978. These craft (JEFF(A) built by Aerojet Corporation; JEFF(B), by Bell Aerospace) were designed to evaluate various hovercraft concepts before selecting the final configuration for the LCAC. The JEFF(A), in the foreground of Figure 1.17, had

Fig. 1.17 JEFF(A) and JEFF(B) operating in Florida.

separate lift and propulsion systems; a "pericell" skirt (see Chapter 2) and four rotatory ducted propellers for propulsion and control. The JEFF(B), in the background of Figure 1.17, had integrated lift and propulsion, a bag-finger skirt, two unducted propellers for propulsion, and two bow thrusters for control. There were other minor differences between the craft but the key differences were as described. After extensive evaluation, a selection was made and a contract given to Bell on 5 June 1981 for the first of the LCAC craft. Figure 1.18 shows the first LCAC craft, LCAC-1, which was delivered to the U.S. Navy in Panama City, Florida, in December 1984. As of January 1987, six Bell LCACs were delivered to the operational unit of the Amphibious Force, Pacific Fleet assigned to Assault Craft Unit five at Camp Pendleton, California. More were in production at the (now) Textron Marine Systems facilities in New Orleans, Louisiana. On 24 September 1985, a second source production line was begun at the Gulfport Marine facilities of the Lockheed Shipbuilding Company in Gulfport, Mississippi. Two LCACs (LCAC-18 and LCAC-21) were under construction with delivery planned in 1988. As shown earlier in Table 1.2, the U.S. Navy

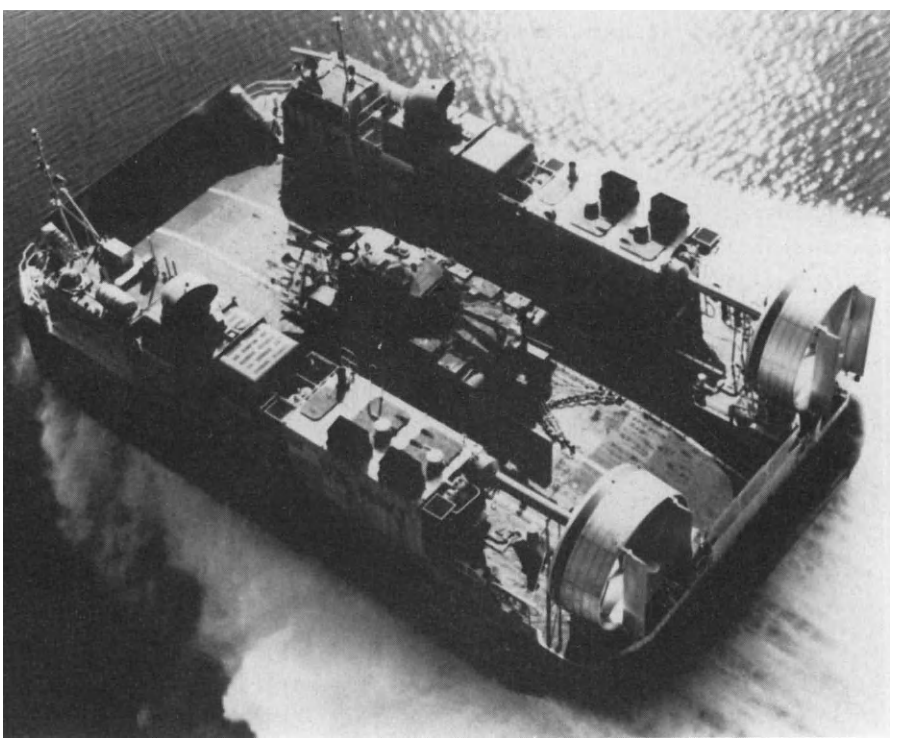

Fig. 1.18 LCAC-1 transporting M-1 tank.

plans to produce 90 such craft with 45 craft planned for deployment at Camp Pendleton and 45 more at a similar facility under construction at the Naval Amphibious Base at Little Creek, Virginia.

The LCAC has a gross weight of 149 tonnes and can carry a payload of 54 tonnes. It is specially designed to carry the M-1 tank shown in Figure 1.18. Its overall length is 26.43 m (86.75 ft), its beam is 14.32 m (45 ft) and its skirt length is 1.52 m (5 ft). The installed power is delivered by six 2,088 kW (2,800 HP) Avco Lycoming gas turbines, driving four 1.52 m (5 ft) diameter double-entry centrifugal fans for lift, and two four-bladed 3.5 m (11.75 ft) diameter, Hamilton-Standard variable pitch, ducted propellers. The double-entry fans provide air to the cushion and to the bow thrusters shown pointing aft in a thrust mode atop the port and starboard side structure in Figure 1.18.

In addition to the U.S. Navy and USMC interests in the hovercraft, another major interest has occurred with the U.S. Army who also has need for transporting equipment across the shoreline. Prior to 1979, the U.S. Army was having to handle its lighterage and logistics over the shore (LOTS) mission with a combination of wheeled amphibians, displacement boats and helicopters. With varied terrain such as mud, ice, snow, water, sand, etc. the Army was faced with similar problems to the U.S. Navy and the Marine Corps. Such vehicles as LCU, LCM, LARC-5, LARC-15 are used in various combinations to transport the equipment. Most of these vehicles are low-cost, compact and easily transportable on existing shipping. Unfortunately, most hovercraft do not meet these requirements, but in seeking a low-cost easily transportable hovercraft for commercial use, Bell Aerospace Canada Textron in 1972-1975, working in conjunction with the Department of Industry, Trade and Commerce of the Government of Canada, built and delivered the Voyageur and the Viking shown in Figure 1.19.

These craft had emphasized low-cost in their design and construction. The crew compartment was an existing truck cab, the lift system was the same as the SK-5 and the hull structure was made up of standard modules. The Voyageur in particular met the needs of the U.S. Army for the LOTS mission. In September 1979, the U.S. Army Mobility Equipment R&D Command (MERADCOM) gave a contract to Bell for the first four of twelve modified Voyageurs, lengthened by 3.35 m (11 ft) to accommodate additional Milvan containers. The twelve production craft were delivered during 1981 - 1983 to the newly-formed U.S. Army 331st Transportation Company at Fort Story, Virginia. The LACV-30, as the craft is called, was designed with simplicity and low-cost as driving factors. The LACV-30, shown in Figure 1.20, is made up of fifteen easily-assembled modules. These include structural modules, power modules, skirts, the truck cabin and other sections. The displacement is 52.17 tonnes. The overall length is 23.3 m (76.5 ft), the overall beam is 11.2 m (36.67 ft) and the skirt height is 1.21

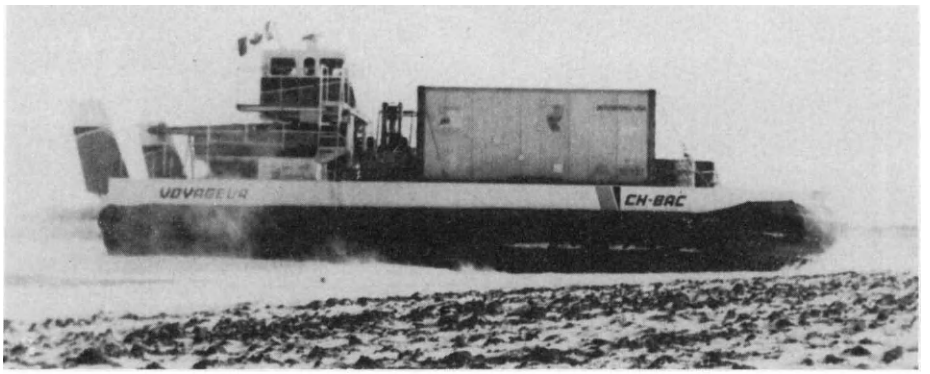

Fig. 1.19 Bell Aerospace Canada Textron hovercraft: (a) Voyageur; (b) Viking.

m (4 ft). The propulsion and lift systems are integrated, modelled after the SK-5, and powered by two Pratt and Whitney ST6 Twin-Pac gas turbines, each engine rated at 1,343 kW (1,800 HP). Two three-bladed Hamilton-Standard reversible-pitch propellers provide the thrust; two 2.13 m (7 ft) diameter centrifugal fans are used for lift.

The U.S. Army ordered twelve additional LACV-30 craft for 1987 and are examining other low-cost hovercraft for logistics operations (LAMP-H). It is encouraging to see awareness of the need to integrate *low-cost* into the

Fig. 1.20 United States Army LACV-30.

requirements of such vehicles that heretofore had tended to be dominated by *high performance*.

1.2.6 Emphasis on Low Cost

In Chapter 5, the costs of hovercraft are discussed in some detail in terms of both acquisition and operating costs. It is shown that historically hovercraft have been expensive and fragile vehicles. Expensive because they have emphasized high performance (high power) and light weight (to maximize payload) and thus have tended to be constructed with aerospace-like techniques. The use of gas turbines and their high fuel consumption has also contributed to their high cost. It is explained in Chapter 5 that costs must be reduced if hovercraft are to penetrate much further into the market, whether military or commercial. In recent years there has been an encouraging trend towards seeking ways to lower the cost of hovercraft. The above-cited examples of the U.S. Army LACV-30 built by Bell and the planned Army's LAMP-H are good examples of how this can be accomplished. Another operating example of where this low cost feature has been *designed-in* is the British Hovercraft Corporation's AP.1-88 hovercraft. The AP.1-88 was designed specifically with low cost in mind. Six craft have been built to date, three in the so-called *prototype*, or 80-seat version, and three in the *production*, or 101-seat version.

Figure 1.21 shows the AP.1-88 in its production version. The AP.1-88 was designed to have the performance of the highly successful SR.N6 (see Figure 1.12) but at a much lower acquisition cost and with more payload, a lower operating cost and much quieter operation. This was accomplished by incorporating the following features: a) all-welded aluminum structure (built by boat-building techniques), b) use of diesel engines, c) use of powder couplings and toothed belt drives, and d) use of standard robust parts throughout. All other parts were either equal to or modelled after well-proven components used on earlier BHC craft.

Low cost is a key feature that must be incorporated into hovercraft design and the AP.1-88 embodies much of what needs to be done to achieve it. Therefore, a pictorial cutaway is shown in Figure 1.22. As an example of cost reduction, the use of all-welded marine aluminum, instead of the previous rivetted aluminum structure, approximately halves the hull-construction cost in terms of manhour per Newton (pound). Because cost is such an important parameter to control in hovercraft design, the reader is referred to Chapter 5, Sections 5.3.2, 5.3.3 and 5.4.2, where a discussion of the AP.1-88 costs is expanded further.

The AP.1-88, in its production configuration, has a maximum all-up weight of 38.6 tonnes and can carry 101 passengers at speeds of 25.72 m/s (50 knots). Its overall length is 23.85 m (78.17 ft), overall beam is 10 m (32.83 ft), and skirt height (average) is 1.37 m (4.5 ft). Propulsion is supplied by two 12-cylinder Deutz Diesel engines, each 319 kW (428 HP), driving two 2.74 m (8 ft)

Fig. 1.21 Production version of AP.1-88.

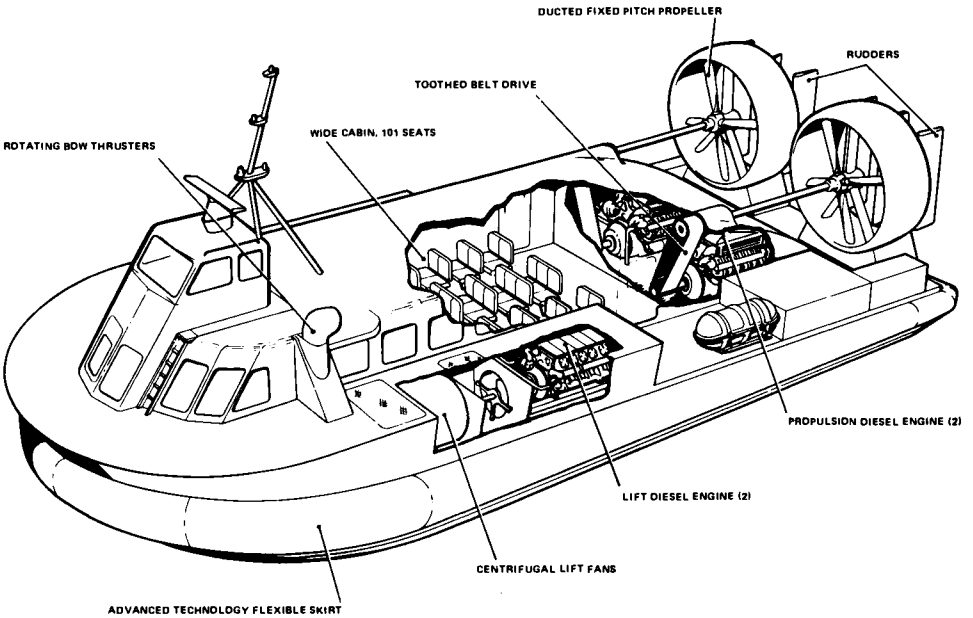

Fig. 1.22 Cutaway view of AP.1-88.

diameter, four-bladed Hoffman fixed-pitch ducted propellers. Lift is supplied by two 12-cylinder Deutz Diesel engines, each 319 kW (428 HP) driving six 0.84 m (2.75 ft) diameter double-entry centrifugal fans.

The first two (prototype) AP.1-88 hovercraft (named *Tenacity* and *Resolution*) operated between Ryde, Isle of Wight, and Southsea, England in 1983. In 1985, the Resolution was chartered to the U.S. Navy at Panama City for use as a trainer for the LCAC (see earlier). Two of the larger production craft entered commercial service in 1984 between Copenhagen's Kastrup airport and Malmo. The first prototype AP.1-88/100 was also leased by Hoverwest Ferry Services in May-October 1986 for Expo 86 operating between Victoria and Vancouver, Canada. Mant (ref. 19) provides many of the details of the AP.1-88 and its operational experience. Westland Aerospace foresees such a craft being used not only in successful commercial operations, but also in several military missions such as patrol, amphibious assault and logistics.

1.2.7 Soviet Military Hovercraft

While the costs of Soviet hovercraft are not known, it appears from their designs that similar techniques to those discussed earlier with respect to the AP.1-88 are incorporated. Simple boatbuilding practice and robustness are emphasized in many of their designs. Table 1.2 showed that the Soviets are operating and building large numbers of hovercraft; hence, it is appropriate to

show some examples of the Soviet hovercraft technology. The Pomornik, the world's largest military hovercraft, has already been discussed and shown (see Figure 1.11). Soviet technology dates back to the early days of hovercraft when the small river craft Raduga appeared in 1960. Trillo (ref. 5) provides an excellent compilation of most of the known Soviet air cushion craft and, as Table 1.2 summarizes, most of the development has centered on the SES type for riverine passenger use. The first production hovercraft for Soviet military use was the Gus (launched 1969) which was modelled after the commercial Skate (launched 1968). The Gus, of which more than thirty were built and entered into the Soviet inventory throughout the period 1969-1979, was used for reverine patrol, amphibious assault and rapid strike missions carrying one platoon at 25.72 m/s (50 knots).

The successor to this early military amphibious hovercraft was the Lebed which was launched in 1973 and entered production in the period 1976-1977. It is believed that more than 18 Lebed hovercraft are now operational. The Lebed is designed for amphibious assault and LOTS missions.

The Lebed (shown in Figure 1.23), unlike the U.S. LCAC, is designed and equipped specifically for the initial assault wave, whereas the LCAC is specifically designed for the follow-on landing of equipment. In terms of overall size, the Lebed is slightly smaller than the LCAC, with a length of 25 m (82 ft) and a beam of 11 m (36 ft). There is some disagreement on the type of skirt system but it is believed to be of the loop and segment type (see Figure

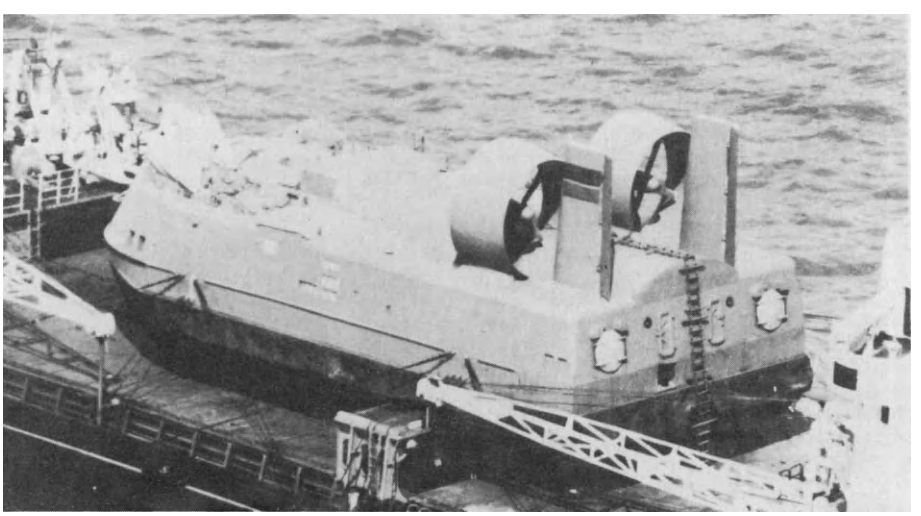

Fig. 1.23 Soviet amphibious assault hovercraft: LEBED.

1.4 and Chapter 2) similar to that used on the JEFF(A). The influence of aerospace technology is seen in that the structure is of rivetted marine aluminum and the power is supplied by marine gas turbines. The lift and propulsion system is integrated with power supplied by two AI-20 marine gas turbines, each rated at 3,096 kW (4,150 HP), driving two 3.6 m (11.83 ft), four-bladed variable-pitch ducted propellers and two variable-pitch axial fans. For control the Lebed has aerodynamic rudders, differential propeller pitch and *puff ports*, making it a highly maneuverable hovercraft. Like the LCAC craft that are carried to the theatre of operations by amphibious ships (LSD, LPD), the Lebed is also carried in the Soviet LPD (Ivan Rogov class) ship. Two Lebed craft (or three of the earlier Gus hovercraft) can be carried in the well deck of the Soviet LPD ship. In Figure 1.23, the Lebed is being carried as a deck cargo.

A second example of Soviet military hovercraft is the Aist (see Figure 1.24) which, until the recent appearance of the Pomornik, was the world's largest military hovercraft. Designed by the same group which designed the Gus, namely the Soviet Navy High-Speed Ship Design Bureau, the Aist is a more rugged craft built to shipyard standards of all-welded marine aluminum. It is estimated to be 260-270 tonnes all-up weight and has an overall length of 46 m (150.9 ft), overall beam of 17.5 m (57.4 ft) and a skirt height of 2.5 m (8.17 ft).

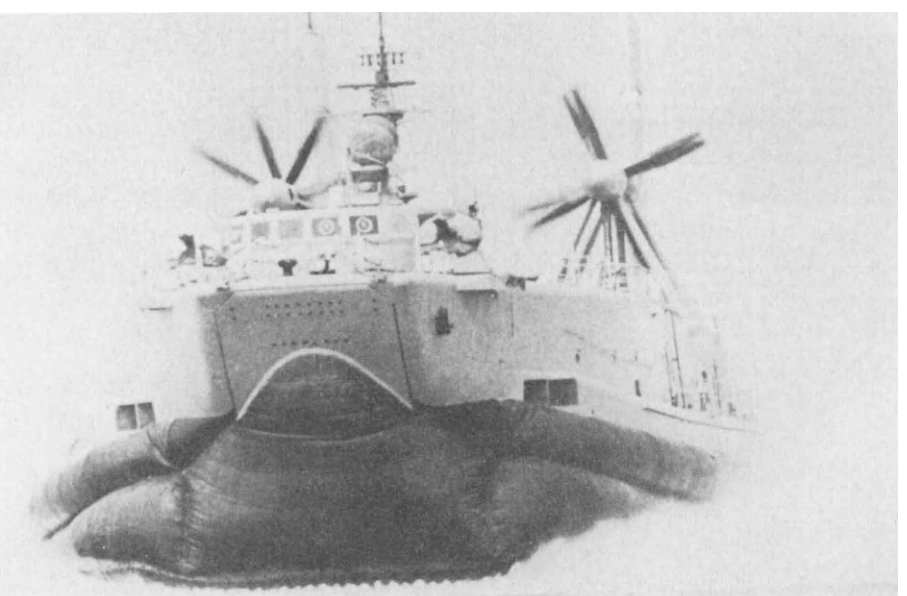

Fig. 1.24 Soviet amphibious landing craft: Aist.

Its maximum speed in calm water is estimated to be 30.9 to 33.4 m/s (60 - 65 knots). The lift and propulsion systems are integrated with power supplied by two NK-12MV marine gas turbines, each rated at approximately 7,500 kW (10,000 HP). Each engine drives two 3.65 m (12 ft) diameter variable-pitch axial fans for lift and two pylon-mounted propellers arranged in *pusher-tractor* combination for thrust augmentation (see Figure 1.24). Each propeller is a four-bladed variable reverse-pitch unit of approximately 5.99 m (19.67 ft) diameter. The skirt system is similar to the BHC bag-finger type except that it has a double bag.

1.2.8 Japanese and French Hovercraft

Two innovations, one in craft control and the other in skirt design, have appeared respectively in the work by Japanese and French hovercraft designers. The craft control innovation was implemented in the Japanese craft, Mitsui MV-PP15, shown in Figure 1.25(a). The skirt design innovation appeared in the French craft, SEDAM N.300, shown in (b) of the same figure.

The Mitsui MV-PP15, launched in 1972 and of which four were built, is a 56 tonne all-up weight craft with overall length of 26.4 m (86.67 ft), overall beam of 13.9 m (45.58 ft), and an average skirt height of 1.8 m (5.92 ft). The skirt design is a tapered, loop and segment type. The MV-PP15 carries 155 passengers over inland waterways at speeds of about 18.3 m/s (60 knots). The integrated lift and propulsion system is powered by a pair of Avco Lycoming TF 25 gas turbines, each with a rated power of 1,641 kW (2,200 HP). Each engine drives a 2.3 m (7.5 ft) diameter centrifugal fan for lift and 3.2 m (10.5 ft) diameter four-bladed variable-pitch propeller for propulsion. The unique feature of this craft is the use (as originally installed on the craft) of two retractable wheels located aft inside the cushion. These wheels could be extended downward into the water to prevent drift when turning and assist braking at high speeds. On land, the wheels assisted in maneuvering and helped to reduce skirt wear. This unique feature, not used on today's hovercraft, is a forgotten technology that may have application in future designs.

The SEDAM N.300 represents the early French successes in originating and developing the *jupe* skirt system (see Figure 1.4 and Chaper 2). The jupe was introduced by the late Jean Bertin and used on the N.300, which first hovered in December 1967 and entered commercial service along the Cote d'Azur in 1970. Two craft were built and operated on many routes in the mid-1970s. An interesting account of the history of the development of the N.300 and of French air cushion craft in general, was given by Bertin to the Isle of Wight branch of the Royal Aeronautical Society in 1970 (ref. 20). The jupe skirt was quite different from the *bag-finger* modified plenum skirts used on the majority of earlier hovercraft. It had a high degree of stability and tolerance to imbalance of deck loading. The jupe was also the genesis of such skirt systems

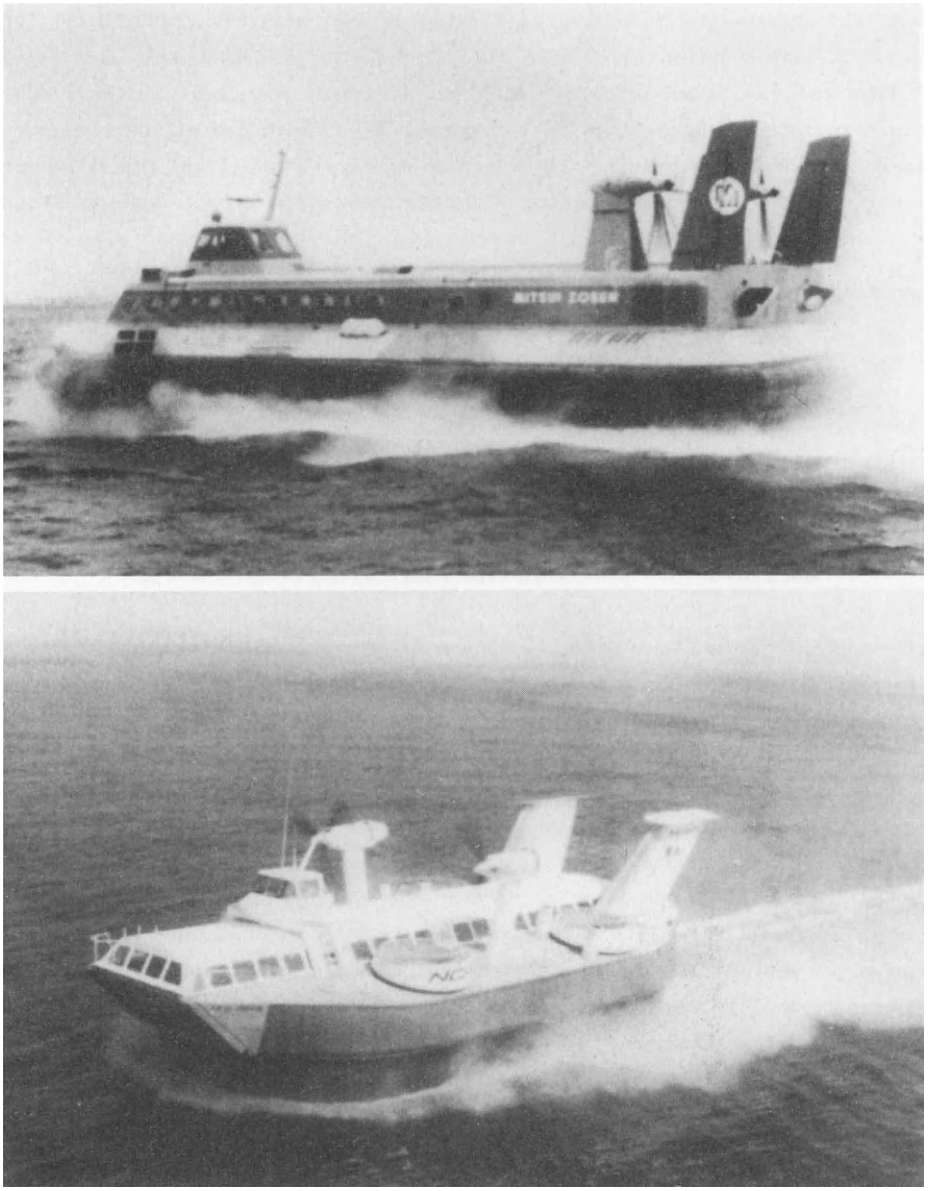

Fig. 1.25 Japanese (MV-PP15) and French (N.300) hovercraft.

as the pericell skirt systems used on the AALC JEFF(A).

The N.300, of which two commercial craft were built, has an all-up weight of 27 tonnes and is capable of carrying either 13 tonnes of freight or up to 120 passengers. Its overall length is 24 m (78.75 ft), overall beam is 10.5 m

(34.42 ft), and skirt height is 2 m (6.58 ft). Total installed power is provided by two Turbomeca Turmo III N3 gas turbines for a total of 2,238 kW (3,000 HP). Each engine drives a three-bladed Ratier-Figeac 3.6 m (11.83 ft) diameter variable reverse-pitch propeller and two eleven-bladed 1.9 m (6.25 ft) diameter axial lift fans. This hovercraft has a unique skirt system made up of eight individual cones, or jupes (see Figure 1.4), surrounded by a single-sheet wrap-around skirt. Each jupe has a skirt height of 2 m (6.58 ft) and a hemline diameter of 3.09 m (10.17 ft). The N.300 craft were built in 1967 and entered passenger service in 1970 along the Cote d'Azur.

A larger passenger craft, the N.500, with an all-up weight of 260 tonnes and capbable of carrying 200 passengers and 60 cars entered service on 5 July 1978 for Seaspeed on the Boulogne-Dover cross-channel route. The N.500 used the same unique jupe skirt system as the earlier Bertin designs. Reference 21 provides details of the full-size operating N.500 but not many photographs available show the unique skirt system. A photograph (Fig. 1.26) of the N.500, taken at Pauillac, France, during tests in 1977, clearly shows the conical jupes. In the case of the N.500 the wrap-around skirt (as used on the N.300) is excluded. There are 48 identical jupes, each 4 m (13.13 ft) in diameter, arranged around the cushion area in a continuous double ring. Fan air is fed directly into the central cushion area and to the skirts in groups. This provides a stable and stiff cushion system. The N.500 has an overall length of 50 m (164.08 ft), an overall beam of 23 m (75.13 ft) and a skirt height of 3.6

Fig. 1.26 Manned model of the N.500 Arctic.

m (11.79 ft). The lift and propulsion systems are not integrated. The lift system is powered by two Avco-Lycoming TF40 marine gas turines, each 2,387 kW (3,200 HP). Each lift engine drives a 4 m (13.13 ft) 13-bladed axial-flow fan through reduction gearing. Propulsion is by three TF40 engines, each driving a 6.3 m (20.67 ft) diameter, four-bladed variable reversible-pitch propeller.

1.2.9 Hovercraft in the Arctic

A key feature of the hovercraft discussed earlier was the low footprint pressure of the air cushion and how this feature had an advantage in operating over the ecologically sensitive tundra (with contact pressure limits of 2.4 N/cm^2 (3.5 psi)) without causing damage. The amphibious nature of the cushion also provides the ability to travel over ice flows, snow and, in some cases, ice pressure ridges.

It is not surprising, therefore, that the hovercraft has operated extensively in the cold regions of Northern Europe, Scandinavia, Canada, Alaska and in the Baltic. In 1970, ARPA (now DARPA, Defense Advanced Research Projects Agency) initiated a major effort to develop and demonstrate the necessary technology for acquiring and operating Arctic-based hovercraft for military missions. This effort included a major study of the Arctic environment, materials research, obstacle detection systems, navigation, life support systems, hovercraft technology and vehicle designs. A comprehensive description of this effort can be found in reference 22.

Two relatively recent experiences of operating hovercraft for commercial purposes in the Arctic are those obtained with the JEFF(A), discussed earlier as a forerunner to the LCAC program, and the Polar Utility Craft, PUC-22 LARUS. The JEFF(A) was leased from the U.S. Navy by RMI, Inc. (now Wheeler Systems, Inc.) for a time charter program to Sohio Alaska Petroleum Company. The purpose of the program was to provide hovercraft design data and to provide logistic support for offshore drilling operations in the Beaufort Sea. This undertaking began in June 1983, with the first Arctic operation occurring on 7 December 1983 with a 77.3 km (41.7 nautical miles) run to Mukluk Island from Milne Point, Harrison Bay. Eggington and Edwards (ref. 23) provide a concise description of this operation. Figure 1.27 shows the JEFF(A) operating near Mukluk Island in 1984. Based on these operations, reference 23 reports the following effects on the JEFF(A) hovercraft: a) temperature effects on electronic gear, b) need for improved low-temperature ductibility for "O" rings, gaskets and other seals, c) increased skirt damage due to stiffening of the (otherwise) flexible skirt, d) reduced material strengths in bolts and fasteners due to low temperatures, and e) higher gas turbine power levels due to low temperatures.

Because the JEFF(A) was not originally designed for operation in the Arctic, it is encouraging to note that, other than the normal winterization

Fig. 1.27 JEFF(A) operating in the Arctic.

design requirements necessary for any vehicle, there were no fundamental limitations and many decided advantages to using a hovercraft. No general set of requirements has been drawn up for an Arctic hovercraft but reference 22 does provide some guielines. For example, while ice pressure ridges can go as high as 6.1 m (20 ft), it is recommended that 2.4 m (8 ft) skirt heights be used. Temperature varies widely from summer to winter and with geographical location in the Arctic. The reader is referred to Arctic maps for temperatures, surface winds, etc. for any particular route application being planned. A point of reference is that temperatures to -50°C are not uncommon in such regions.

The second example of Arctic hovercraft use is Wartsila's PUC-22, LARUS. The LARUS craft has an outward resemblance to the JEFF(A), except that it is smaller, diesel-powered and specifically designed for Arctic operations. The LARUS was built by the Wartsila Helsinki Shipyard and delivered to the Finnish Board of Roads and Waterways in December 1981. It has a maximum all-up weight of 100 tonnes and can carry 22 tonnes of payload and 50 passengers. Alternative load-outs are 16 cars or 2 trucks. The overall length of the LARUS is 33 m (108.25 ft), overall beam is 14.7 m (48.25 ft) and skirt depth is 1 m (3.25 ft). The skirt is of the bag and finger type. Figure 1.28 shows the LARUS operating over ice. The design speed is 12.86 m/s (25 knots). The lift and propulsion systems are integrated and powered by four high-speed marine diesels, each rated at 650 kW (870 HP). Each diesel drives either one or two centrifugal fans through a main gearbox and a four-bladed pylon-mounted ducted rotatory CP propeller, through bevel gears and a vertical shaft. The cushion

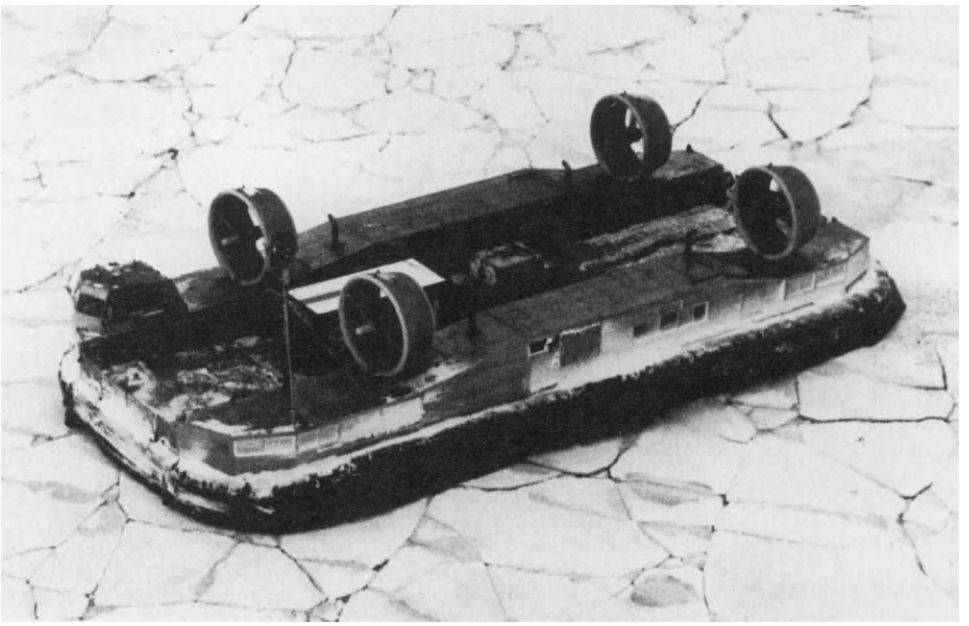

Fig. 1.28 Wartsila LARUS hovercraft.

pressure of the LARUS is 0.245 N/cm^2 (0.36 psi) which again is quite compatible with Arctic terrain limits. This particular hovercraft was designed for Arctic conditions. In 1982-1985, it operated in the Gulf of Bothnia between Oulumsalo and the island of Hailuoto in Finland. Temperatures were typically -30°C. In March 1985, LARUS was refurbished for operation in the Beaufort Sea in Canada. Other than specific customer requirements, the major change was in refurbishment for operation to -50°C in the Canadian Arctic. The operation of LARUS in the Canadian cold weather regions was successful and terminated in November 1986. Makinen and Wainwright (ref. 24) summarize the main LARUS features that they consider essential for Arctic use: a) use of diesel engines for simplicity and proven cold weather operation, b) design for relatively low speed (12.86 m/s) to keep skirt design simple, c) design of simple controls for improved reliability, and d) all-welded aluminum hull structure for low cost and robustness.

1.2.10 Some Other Applications

The hovercraft principle as discussed has been applied to fairly high speed vehicles, of the order of 15-40 m/s (30-80 knots), designed for transporting passengers or military payloads. Several examples of the application of the hovercraft principle have been described to illustrate how practical vehicles have evolved. There is another avenue of development of hovercraft that has

application and economic value in other areas. This avenue includes *heavy lift applications* and *off-road transporters*.

An example of a hover transporter is shown in Figure 1.29. This transporter (HL-104) built by Hoverlift Systems, Ltd. in Alberta, Canada is used as a year-round ferry across the Fort Nelson River. In the summer months, the route is made up largely of water and marshes and in the winter the route is ice covered. This application is particularly suitable for the hovercraft. The uniqueness of this application is that there is no conventional on-board propulsion power plant and the motive force is provided by cables (shown in the photograph) and on-board winches. This means of propulsion allows for sure passage over the Fort Nelson River with its fast flowing currents. The HL-105 is also very economical. Built in 1978, it was delivered to the British Columbia Ministry of Transportation, Communications and Highways in January 1979. The HL-105 is 20.19m (66.25 ft) long, 14.82m (48.58 ft) wide, and it has a skirt height of 0.91m (3 ft). The lift power is provided by two General Motors Detroit Diesel 12V71 engines. The propulsion is achieved by bull-wheel

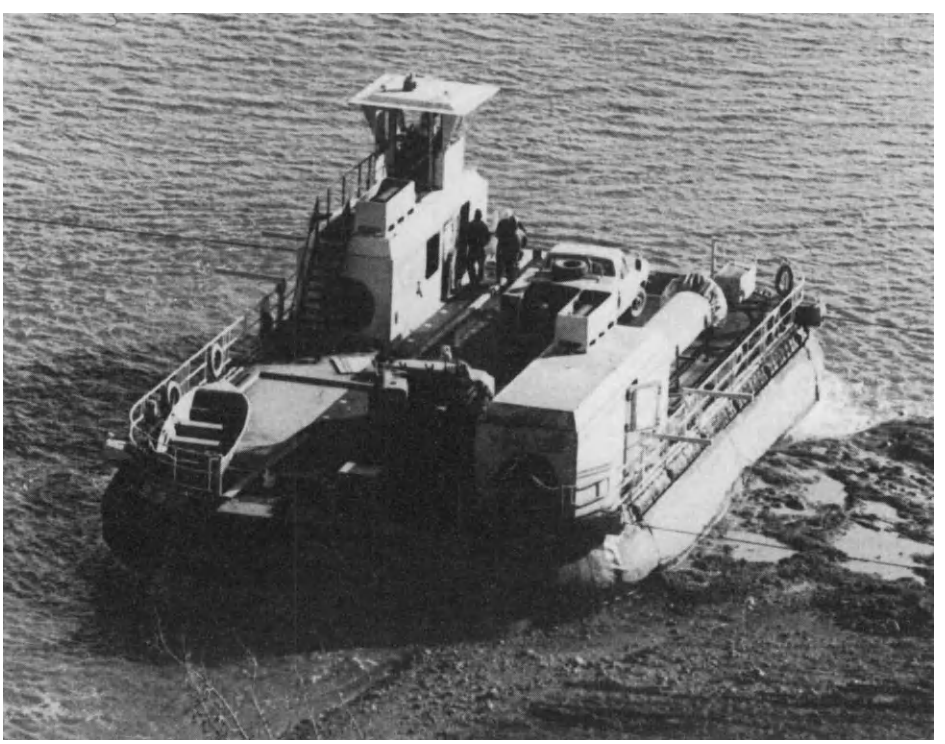

Fig. 1.29 HL-104 hover transporter.

winch drive off the shafts of the lift engines and onto the cables. The payload capacity is 75 tonnes.

Another example of heavy lift transporter that also does not use the usual propulsion system is the ACT-100 shown in Figure 1.30, (upper photograph). The ACT-100 was designed and built in Edmonton, Alberta, Canada, by Arctic Engineers and Constructors of Texas in 1971. It was evaluated by the Canadian Ministry of Transport in Tuktoyaktuk, Northwest Territories in November 1972 and on the Mackenzie River in the summer of 1973 as a cushion ferry. The means of moving forward is either by towing or by tug. Its normal gross weight is 250 tonnes and it has a payload capability of 100 tonnes. The lift power is provided by two 485 kW (640 HP) diesel engines driving two 1.37m (4.5 ft) diameter centrifugal fans that generate 6.89 kPa (1 psi) cushion pressure. This cushion pressure is well within the limits discussed earlier (see Section 1.1) for operation over the ecologically sensitive tundra.

The line drawings and lower photograph in Figure 1.30 show another form of hovercraft used as off-road transporter and sometimes referred to as *hover platform*. The particular hover trailer shown is one designed by Mackley-Ace, Ltd., of Southampton, England for Hover Trailers International Ltd., based on the first hover-trailer developed by Vickers-Armstrong in the early 1960s. The world's largest hover transporter is the 750 tonne gross weight Sea Pearl designed and built by MackAce Hoversystems in 1974 and used in the Persian Gulf to transport heavy items such as liquid natural gas plant components. The payload capability is 250 tonnes. It is 54.9m (180 ft) long, 24.4m (80 ft) wide, and has a skirt height of 1.2m (4 ft). The lift system is powered by two 664 kW (890 HP) diesel engines each driving a 1.39m (4.58 ft) diameter centrifugal fan. The cushion pressure is 6.89 kPa (1 psi) as for the other hover platforms.

Many other examples exist where the hovercraft principle has been used to move heavy objects. These include moving storage tanks with wrap-around skirt systems (tanks up to 700 tonnes in weight have been moved in this manner), aircraft recovery systems, industrial pallets, ice-breaking equipment, and many other applications too numerous to mention.

1.3 GENERAL CHARACTERISTICS

While there is clearly a wide range of types of hovercraft, as illustrated in Section 1.2, there are certain trends and general sizing relationships that can be used to guide the designer and applications engineer. It should be noted that sometimes these trends are the results of fundamental laws and sometimes the result of design compromises driven by such realities as engine power limits, weights, pressure limits (e.g. footprint pressure limits on tundra) and other parameters. Some of these overall sizing relationships are provided in the following sections.

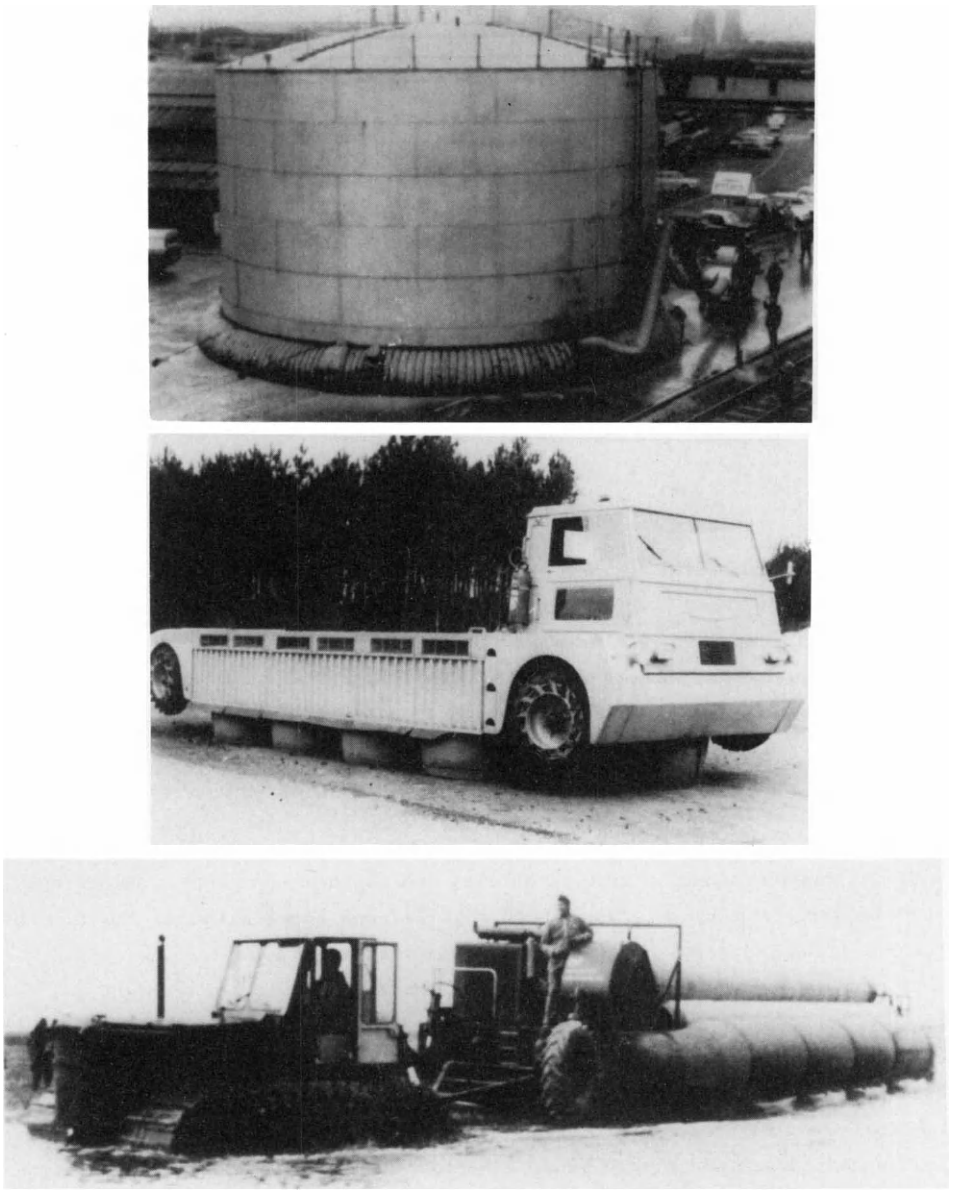

Fig. 1.30 Some heavy lift applications using the hovercraft principle.

1.3.1 Overall Sizing

Useful indicators of the size of hovercraft are length, beam, cushion pressure, power and disposable load, among others. Some of the key sizing parameters, based on a large data base of hovercraft, are summarized in Subsections

(i) to (vi) below:

(i) Length, beam and weight. The hovercraft, hovering at rest, must satisfy the simple equation:

$$W = P_c S \tag{1.1}$$

where W is the total weight of the hovercraft, P_c is the cushion pressure and S is the cushion area. The cushion area is usually smaller than the projected or planform area because of the geometry of the skirts. While the cushion area can be of any shape, it is convenient to express it as if it were rectangular, such that:

$$S = L B \tag{1.2}$$

where the cushion length L and cushion beam B are *effective* lengths so as to correctly compute the actual cushion area S. Typically, L and B are of the order of 80 percent of the overall length (LOA) and beam (BOA) of the hovercraft.

From these simple relationships, we can express the weight of the hovercraft as:

$$W = L^3(P_c/L)/(L/B) \tag{1.3}$$

This relationship states that, provided the *cushion density* P_c/L and the length/beam ratio L/B remain constant, the weight varies with the length cubed. Some authors prefer to express the cushion density in terms of the cushion area such that the relationship can be written as:

$$W = (P_c/S^{1/2})S^{3/2} \tag{1.4}$$

Unfortunately, this form eliminates the length-beam ratio (L/B) which has important ramifications on drag, stability and structural design. Accordingly, the form expressed by equation (1.3) will be used here, although the form of equation (1.4) is useful to reduce some data scatter.

Figure 1.31 shows the trend of cushion length L versus craft weight W. The data is bounded by an upper curve labelled *low density craft* and a lower curve labelled *high density craft.* Whereas there are no fundamental restrictions or numerical limits on *high* and *low* cushion density, practical considerations of platform size, fan pressure capabilities, etc., have tended to set practical bounds. Performance and stability considerations have set bounds on the length/beam ratio at (1.5 - 7.5) with the majority of hovercraft being in the range of (1.5 - 2.5). Cushion densities range from $P_c/L = 79.5\ N/m^3$ ($0.50\ lb/ft^3$) to $317.9\ N/m^3$ ($2.0\ lb/ft^3$). These *typical values* are compatible with the statistical relationships shown in Figure 1.31 and are expressed by:

$$L = 6\ W^{1/3} \tag{1.5}$$

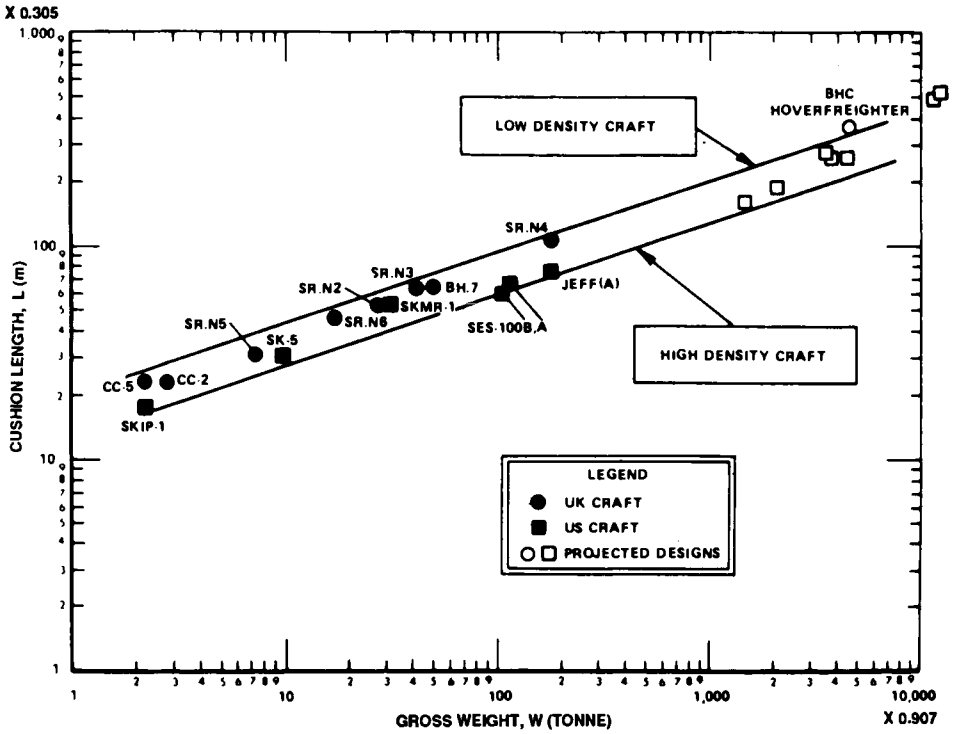

Fig. 1.31 Length of air cushion craft.

for low density craft, and

$$L = 3.75\ W^{1/3} \tag{1.6}$$

for high density craft, where W is the craft weight (in tonnes) and L is the cushion length (in meters).

The data base that is governed by these relationships covers craft from many countries and spans a time frame from 1965 to the present day. There has been a tendency to develop low cushion density craft for commercial operations and high cushion density craft for military operations. Because surface effect ships (SES) are also supported mainly by the air cushion, the relationship given by equation (1.1) also applies to these ships in a reasonably accurate manner. The data points of SES are included in Figure 1.31 as squares; the hovercraft are shown as circles.

(ii) Cushion pressure. The cushion pressure P_c is an important parameter in the design and sizing of hovercraft. In addition to its impact on the size of the craft, the cushion pressure contributes to the performance stability and seakeeping of the craft. Cushion pressure also contributes to skirt design and structural loading. This important parameter can be expressed in terms of the

craft characteristics discussed earlier by the relationship:

$$P_c = W^{1/3}(P_c/L)^{2/3}/(L/B)^{1/3} \tag{1.7}$$

In similar fashion to the cushion length L, the cushion pressure varies as the cube root of the hovercraft weight W provided the cushion density and length/beam ratio remain constant. Figure 1.32 shows the data base that supports this relationship such that the following expressions can be written:

$$P_c = 0.0478\ W^{1/3} \tag{1.8}$$

for low density craft, and

$$P_c = 0.0908\ W^{1/3} \tag{1.9}$$

for high density craft, where the units of P_c and W are kPa and tonne, respectively.

(iii) Cushion Flow and Air Gap. Determination of the amount of cushion air flow from the cushion is not an easy matter. The cushion flow Q is the result of several considerations: leakage through the structure, flow into the cushion, diverted flow for bow thrusters or puff ports, cooling system air,

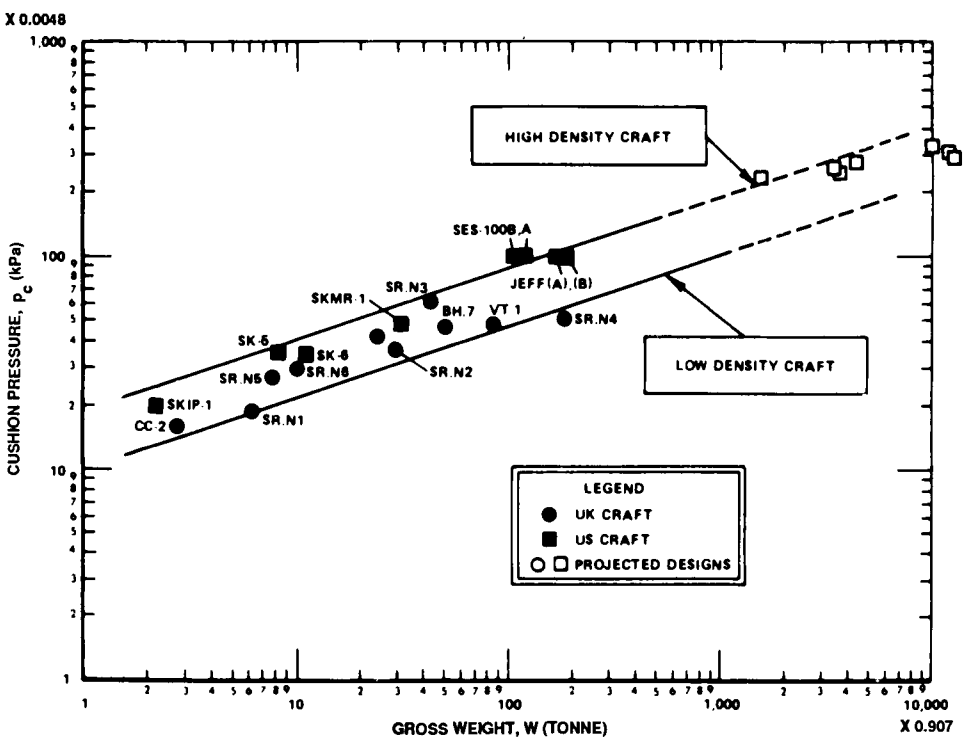

Fig. 1.32 Cushion pressure of air cushion craft.

lift augmentation by blowing on aerodynamic rudders, and *wave pumping* requirements for rough water operation.

A simplistic treatment that can provide a guide to the amount of lift air or cushion flow required for the operation of hovercraft over relatively smooth surfaces is provided by the equation:

$$Q = A_e V_e \tag{1.10}$$

where V_e is the velocity of the escaping air beneath the skirt as shown in Figure 1.3. Applying the same effective cushion length and beam arguments used earlier for the gap area A_e, this relationship can be written:

$$Q = 2(L+B)h(2P_c/\rho)^{1/2} \tag{1.11}$$

where h is the nominal air gap between the skirt hemline and the surface (see Figure 1.3) and ρ is the cushion air density.

After some algebraic manipulation, the cushion flow Q can be expressed in terms of known craft parameters as:

$$Q = 2\ L^{5/2}(h/L)\ (2P_c/\rho L)^{1/2}(1+L/B)/(L/B) \tag{1.12}$$

which states that the cushion flow Q is proportional to the hemline length or effective cushion length L to the 5/2 power. This strong function of the cushion length is a driving reason for the introduction of the surface effect ship (SES) to the air cushion craft family; the smaller cushion reduces the lift power requirements. In addition to the parameters L/B and P_c/L already discussed, the new nominal air gap parameter h/L has now been introduced as a sizing parameter. Figure 1.33 shows the *typical* air gaps that have been employed in hovercraft design. In early designs, higher gaps were used to prevent wear of the skirt hemline when moving over surfaces of varied texture. As skirt technology progessed both in design and materials, lower air gaps became possible; the following represents a statistical average:

$$h/L = 0.014\ W^{-1/3} \tag{1.13}$$

where W is the hovercraft weight in tonnes.

Mantle (ref. 1) provides further discussion of the effects of skirt movement, coefficients of discharge and wave pumping flow. These effects must be analyzed if any particular design is to be pursued. Equation (1.13) in conjunction with equation (1.12) provides a general sizing for the hovercraft cushion flow.

(iv) Lift power. The lift power P_L for a hovercraft can be written:

$$P_L = P_c Q \tag{1.14}$$

Using the scaling relationships developed earlier, one would expect the lift power to be proportional to $W^{5/6}$. Statistical data of existing hovercraft shown in Figure 1.34 indicate a trend close to this expected variation in that

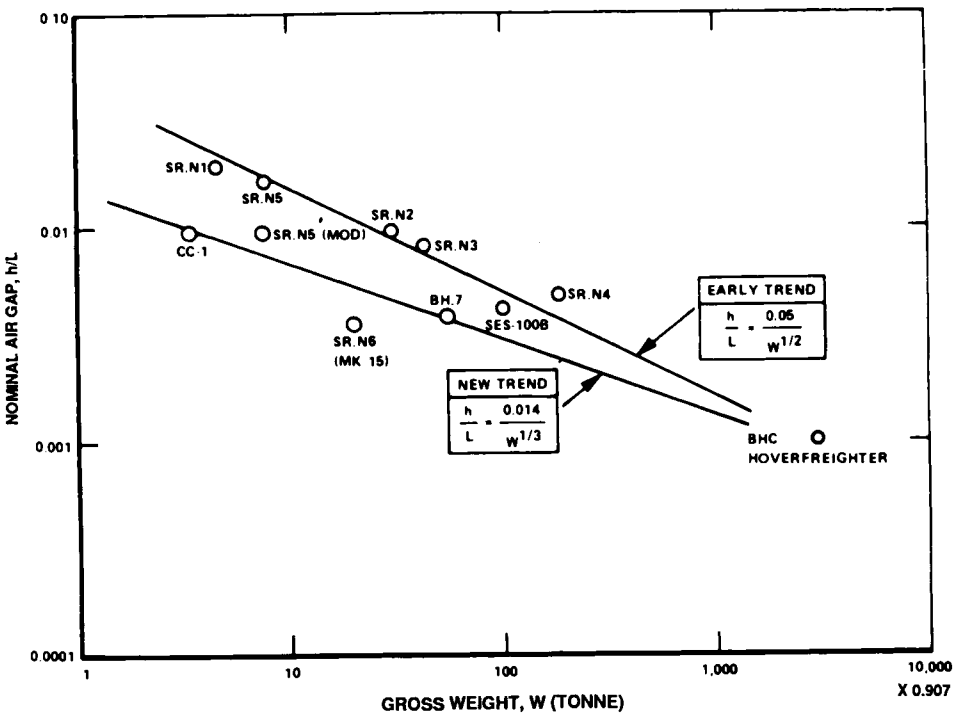

Fig. 1.33 Nominal air gap.

the variation is proportional to $W^{7/8}$. The same figure also shows statistical data on the low speed *heavy lift applications* and *off-road transporter* form of hovercraft discussed earlier. Here the requirements for wave pumping and high gap clearance are not required, and the lift power requirements are correspondingly less. The small data base supports the expectation of lower power requirement for lift. In this case, the lift power is seen to be proportional to $W^{2/3}$.

(v) Propulsion power. While propulsion power is not a derivable parameter in the same way as the other characteristics, it is useful to display the statistical data base on total power of hovercraft. This provides an overall measure of the power requirements when considering the design of such craft. Propulsion power is then given by the difference between total power and lift power.

In Chapter 5, reference is made to the fact that hovercraft cost is a strong function of installed total power P and (empty) weight of the craft. Figure 1.37 shows a rather surprising statistic over a wide variety of hovercraft types (and surface effect ships) that the total installed power P can be

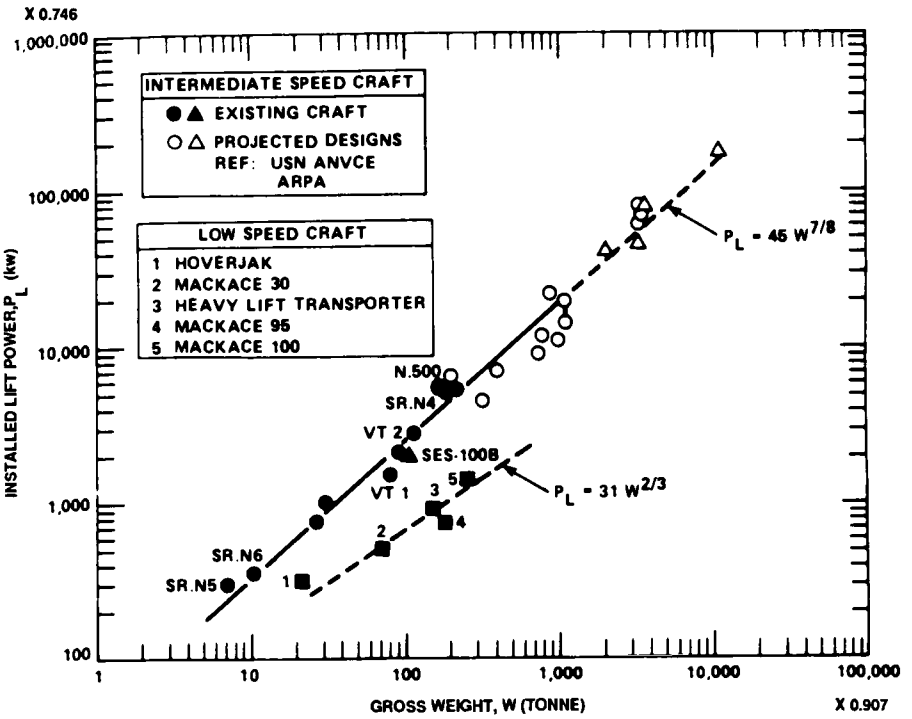

Fig. 1.34 Air cushion craft lift power.

provided from the simple relationship:

$$P = 113\ W^{7/8} \tag{1.15}$$

where the units of P and W are kW and tonne, respectively.
This relationship (for hovercraft) covers a wide range of craft size, cushion pressure, speed and other sizing parameters.

(vi) Cushion height. The selection of the cushion height h_s of a hovercraft (see Figure 1.3) depends on several factors that involve a knowledge of the dynamics of the vehicle as well as the degree of desired performance throughout its typical operating scenario. Considerations of obstacle, wave and surf clearances all enter into the selection process. It is useful to examine two simple considerations that give a reasonable or *first-cut* measure of skirt height. The first relates to the performance of the hovercraft in waves and the second relates to its static stability while hovering on its cushion of air.

No reliable methodology exists for the prediction of skirt height to achieve some desired performance and dynamic stability characteristics. Much of the design data rests with empirical data derived from operational experi-

ence and model tests. The performance of the hovercraft in waves, based on actual craft performance, is shown in Figure 1.35.

The performance of hovercraft in rough seas is dependent on craft size, skirt geometry (and mass distribution), and other parameters. An attempt has been made in Figure 1.35 to remove some of the variations by normalizing rough water speed V to the calm water speed V_c. The size effect is further normalized by expressing the skirt height (or cushion height) h_c to the significant wave height h_w. The data shown covers a wide selection of hovercraft (and an SES) using full-scale operational data, model data and design study results. Some of the variation in the data is due to the difficulty of determining the sea conditions from the published data, e.g., the effect of wind speed, steepness of the waves, craft heading relative to the waves, and other factors. Also, the dynamic motion of the craft and whether it was designed to either contour or platform the waves further affect the resistance of the skirt, and thus the speed loss. Another key factor that is buried in the data is the operator's tendency to lower the craft speed to meet seakeeping or ride quality limits. In anticipation that the designer will strive to attain the highest possible speed, especially in military craft, it can be assured that the upper

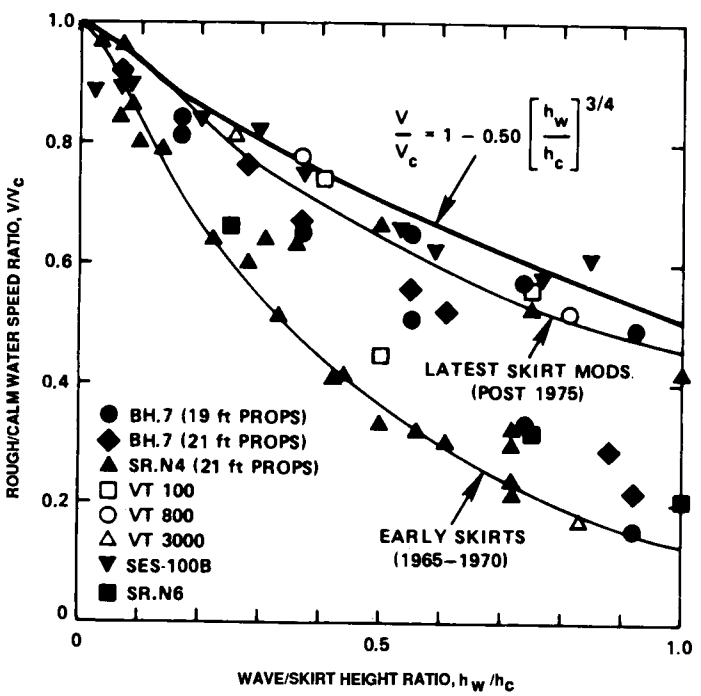

Fig. 1.35 Speed in rough seas.

ramps of data (in Figure 1.35) are fairly representative of modern day hovercraft operation in rough seas. The speed performance in rough seas can then be expressed by the equation:

$$V/V_c = 1 - 0.50(h_w/h_c)^{3/4} \tag{1.16}$$

where V is speed in rough seas, V_c is speed in calm seas, h_w is significant wave height, and h_c is skirt height.

This simple relationship that holds true for a wide variety of craft shows the strong dependency of speed on skirt height. One can expect the craft speed in rough seas to degrade to approximately 50% of its calm water speed as the skirt height approaches the significant wave height. This relationship assumes that the power setting is approximately constant throughout the range of data considered.

The second consideration in skirt height is the static stability of the craft while *on-cushion*. Because the beam B is typically smaller than length L, the governing static roll stability criterion would be the cushion height to beam ratio h_c/B or, equivalently, skirt height to beam ratio h_s/B. This simple parameter can be related to the static stability characteristics of the cushion from a simple analysis.

The rolling moment for a simple compartmented cushion can be shown to be (ref. 1):

$$M_\phi = -(LB/8)(BP_c)(B\phi/h) \tag{1.17}$$

where M_ϕ is rolling moment, ϕ is roll angle, and h is the air gap beneath the skirt. It is usual to express this rolling moment in normalized form through the craft weight W (= $P_c LB$) and beam B, such that:

$$M_\phi/WB = -B\phi/8h) \tag{1.18}$$

If a cushion center of pressure (C.P.) shift per degree is defined as:

$$K_\phi = -B/(8h) \tag{1.19}$$

then by simple rearrangement of the rolling moment equation, the following relationship of skirt height h_s to craft beam B can be derived:

$$h_s/B = (8K_\phi)^{-1}(h_s/L)/(h/L) \tag{1.20}$$

The values of the roll stiffness K_ϕ in terms of C.P. shift per degree vary widely. Trillo (ref. 25) reports that static stability curves of typical British and French hovercraft show variations from 0.20 to 2.0 depending on the roll angle and the skirt design. Similar characteristics have been built into the US craft and, as shown in Figure 1.36, values of the static stability parameter h_s/B of between 0.10 and 0.20 give good roll stiffness for today's hovercraft. Here, *good* must be interpreted as reflecting handling qualities with today's skirt designs and should not be regarded as limiting. For exam-

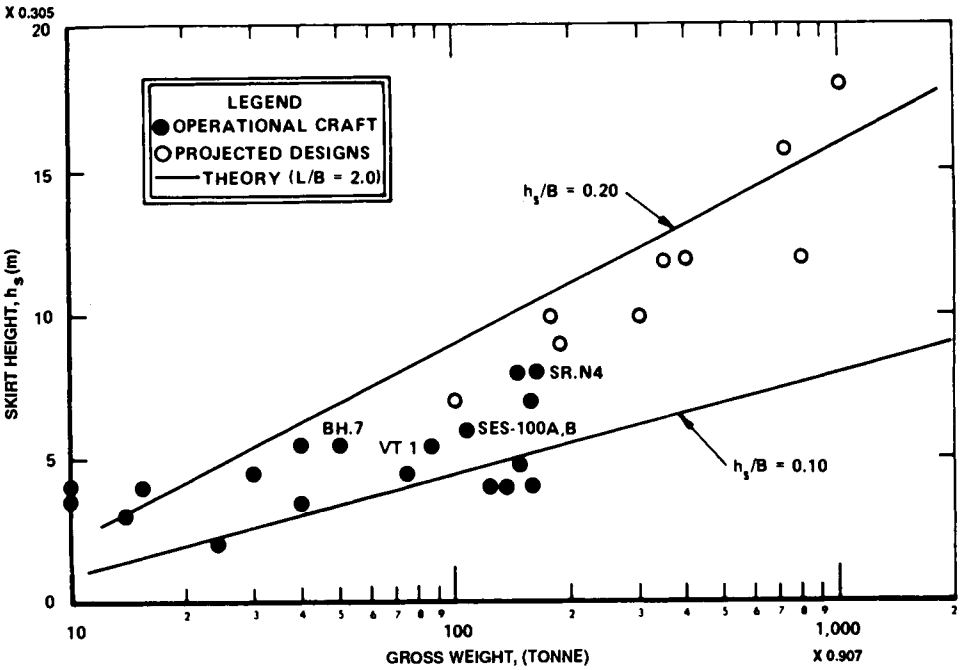

Fig. 1.36 Skirt height of hovercraft.

ple, some of the skirt development pursued in the Arctic Surface Effect Vehicle (SEV) Program (ref. 22) provided data whereby skirt systems could be built with h_s/B values greater than 0.20. While there are clearly many considerations that enter the selection of cushion or skirt height, equations (1.16) and (1.20) provide a good first approximation in determining the overall sizing.

1.3.2 Weight Trends

Weight trends of the many hovercraft, including both operational and projected designs, provide a good basis for parametric design and for costing (see Chapter 5). It is important to understand the two ways in which weight trends are presented here:

(1) Weight trends as a function of no more than one or two major craft parameters such as gross weight and cushion density. This set of information is useful in determining the state-of-the-art at a fairly top level (system and subsystem) so that an appreciation can be obtained in the event that another design *of the same family* can be rapidly determined.

(2) Weight trends of more detailed parameters at a lower level in the system, subsystem or component hierarchy. This set of weight information is useful in the *detective* process of determining the key driving parameters in

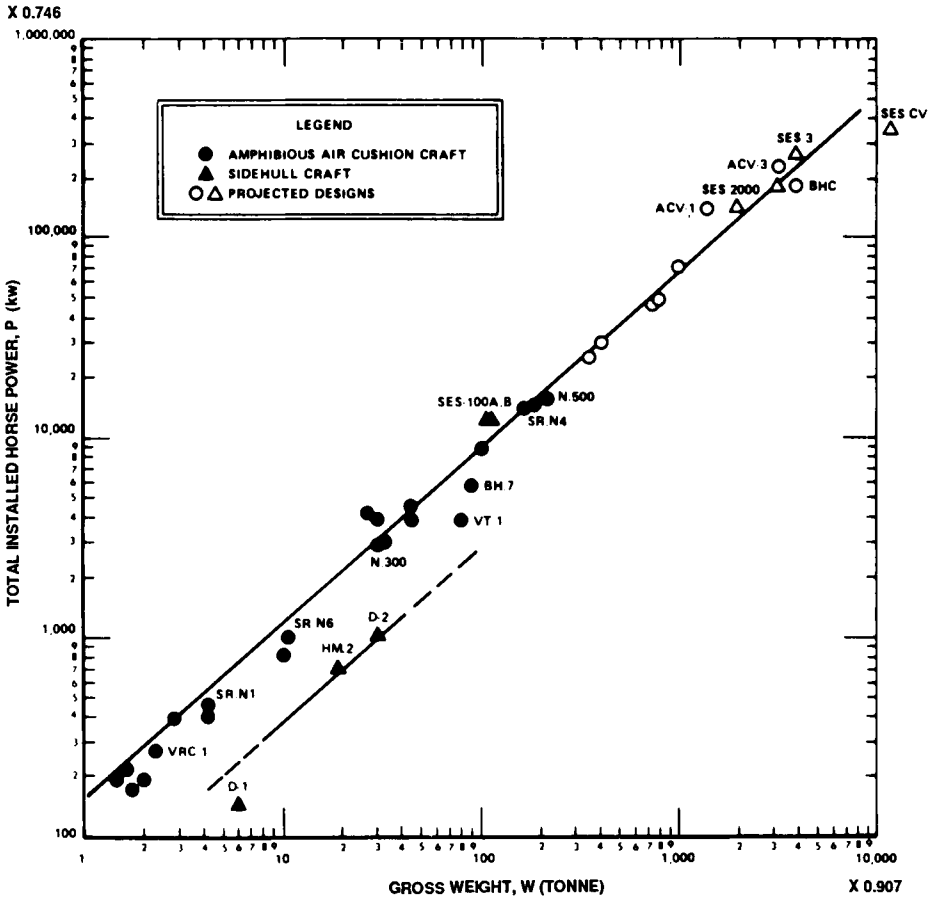

Fig. 1.37 Air cushion craft total power.

a particular system, so that *departures from the state-of-the-art* can be projected and a new family weight trend generated. As might be expected, this set of data is much more difficult to obtain, requiring much more data than that which is readily available.

The following sets of weight trends are presented as a starting point in a technology base that is still young. One problem in collecting weight data is that of ensuring that the same definition of weight groups is being followed. Some effort has been expended here in expressing all the weights in the terminology of the US Navy Ship Work Breakdown Structure (SWBS), as described in ref. 26. While the details of the general SWBS for ship use are provided in this reference and the details as specifically generated for hovercraft are provided in ref. 1, Figure 1.38 provides a ready pictorial overview of the weight breakdown. A summary of data for each of the weight groups is provided

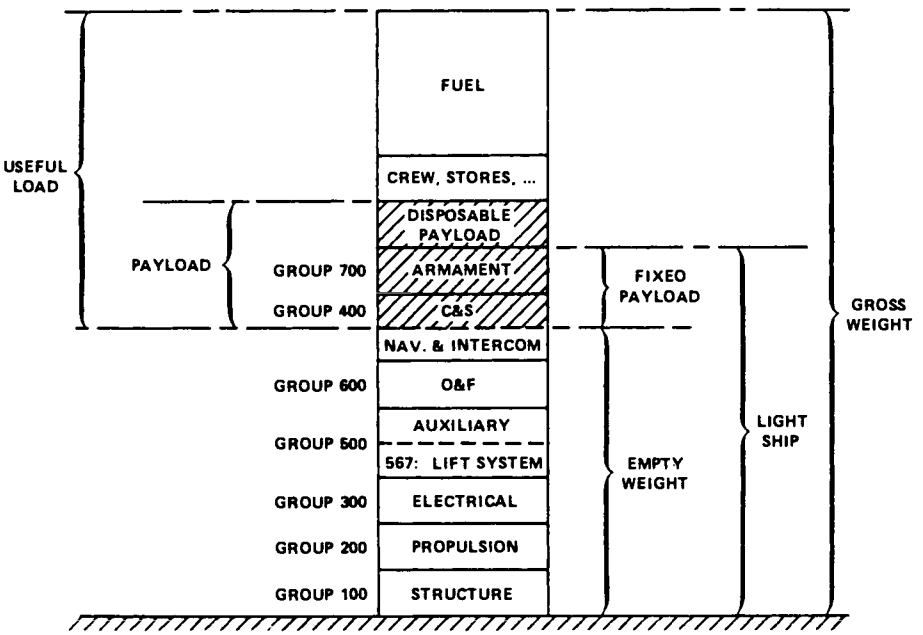

Fig. 1.38 Identification of weight items.

in subsections (i) to (viii). These sets of data and the weight equations derived from them are used for early design work and form a basis for the cost estimating realtionships (CER) provided in Chapter 5.

(i) Structural weight (group 100). The structural weight of a wide range of air cushion craft (hovercraft and SES) is shown in Figure 1.39, adapted from ref. 1. The data base (mostly projected designs for the larger displacements) is gradually expanding such that trend lines can be drawn. The structural weight can be shown to be the sum of two terms involving the gross weight W. The effect of cushion density:

$$D_c = P_c/S^{1/2} \tag{1.21}$$

where S is the footprint area, is quite marked for low values ($D_c < 1.0$) but diminishes for high values ($1.0 < D_c < 2.0$).

While not completely collapsible in terms of gross weight W and cushion density D_c, the following equation closely approximates the available data:

$$W_1/W = \begin{cases} 0.28/W^{1/3} + 0.216(W/D_c)^{1/3} & , D_c \simeq 80 \text{ N/m}^3 \\ 0.24 + 0.038(W/D_c)^{1/3} & , D_c \simeq 159 \text{ N/m}^3 \\ 0.21 + 0.043(W/D_c)^{1/3} & , D_c \simeq 318 \text{ N/m}^3 \end{cases} \tag{1.22}$$

Obviously much more work needs to be done in the area of accurate structural

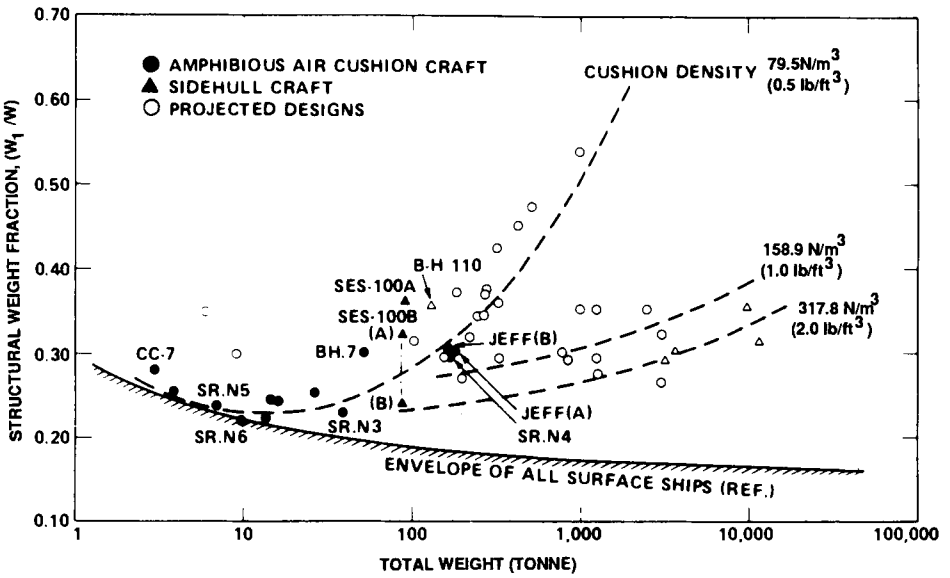

Fig. 1.39 Structural weight fraction.

weight prediction. The absence of speed in these equations is disturbing but the current data base shows no discernible trends (see Chapter 2).

(ii) Propulsion system weight (group 200). There are considerable variations in the propulsion system weights of hovercraft due to variations in powerplants, transmissions, propulsors and design speeds. Expressing the propulsion system weight as a fraction of the craft weight and relating this to the key parameters that drive the design, a sense of the importance of each parameter can be gained, as follows:

$$W_2/W = (W_2/P)(P/WV)V \qquad (1.23)$$

The propulsion system weight is shown to be a function of three key parameters. The first is the *specific propulsion system weight* W_2/P that depends on the type of engine (diesel, marine gas turbine, etc.), the type of transmission, and finally the type of propulsor (air propeller, water propeller, waterjet). The second key parameter is the *transport efficiency* WV/P of the craft that expresses the ratio of the work done by the craft in moving the craft of weight W at a speed V to the total power P required to do the work. The third key parameter is the design maximum speed V of the hovercraft. Because of the variation in these key parameters for the many craft built it should not be surprising to see some scatter in the available data. Figure 1.40 shows the data for several hovercraft (ACV) and SES. Other marine vehicles (ships) are also shown for comparison purposes.

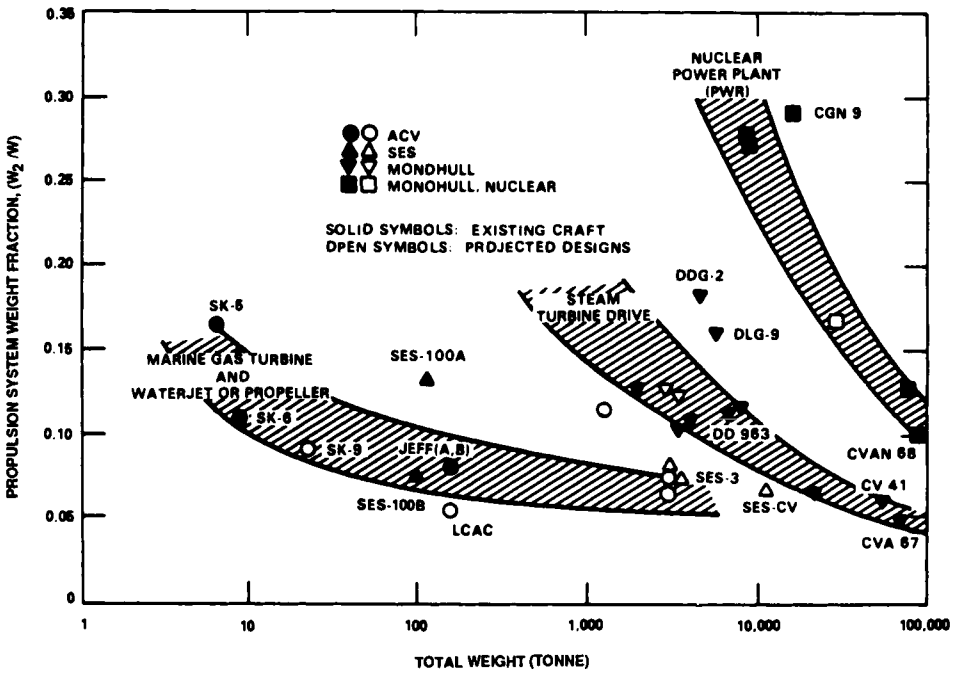

Fig. 1.40 Propulsion system weight.

For future designs of hovercraft, it is important to examine the detailed make-up of the propulsion system weight W_2/W to determine what improvements are possible. Reference 1 provides detailed data on specific engine system weights, transmission system weights and propulsor weights that all contribute to this driving parameter. The same reference also provides information on state-of-the-art improvements in weight from pre-1970 to the present, with projections to the year 2000. These effects all contribute to the determination of the important parameter W_2/P.

The efficiency of the craft expressed as the ratio of a measure of work done to power input, WV/P, is also a key parameter that depends on the fundamental design characteristics of the craft. Some indications of the determining features in this parameter are provided in Chapter 2 and in the literature.

(iii) Electrical system weight (group 300). The available data on the weights of the electrical systems in hovercraft and SES is shown in Figure 1.41. The electrical power requirements and choice of generating equipment on-board air cushion craft has not been sufficiently uniform to establish any definite trends. Most of today's craft use 60 Hz equipment, but some designs are projected to use 400 Hz together with conversion equipment. While these differences in the data base have caused some scatter, the overall trend can be represented by:

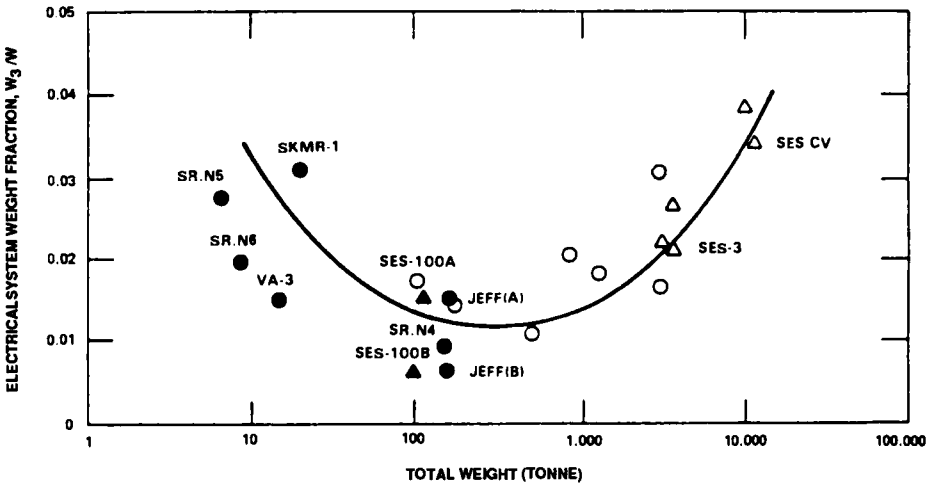

Fig. 1.41 Electrical system weight.

$$W_3/W = 0.00034\ W^{1/2} + 0.10\ W^{-1/2} \qquad (1.24)$$

(iv) Command and surveillance system weight (group 400). The command and surveillance system is made up of the craft's navigational system, communication system and, if a military craft, the fire control system. The data base covers commercial hovercraft, military test craft and projected designs for fully-operational military craft. Commercial data is rarely in the SWBS format, difficult to convert, and therefore not shown. For those craft which are designed for military use, the command and surveillance systems are similar to those of conventioinal ships and, as Figure 1.42 shows, their data tend to *collect* around the conventional ship data. Using this data, the trend line is given by:

$$W_4/W = 15/W^{3/4} \qquad (1.25)$$

(v) Auxiliary systems weight (group 500). The auxiliary systems on a hovercraft are, as on most vehicles, a collection of subsystems such as pneumatic, hydraulic, air conditioning, steering, etc. They also include, at least according to the 1973 issue of the US Navy SWBS (ref. 26), the lift system (of weight W_{LS}) which is made up of the lift engines (if separate from the propulsion engines), lift fans, ducting, ride control elements, and the skirt system.

To provide better insight into the auxiliary system W_S make-up, the available data has been separated into the lift system weight W_{LS} and the total auxiliary system weight less the lift system weight ($W_S - W_{LS}$). Figure 1.43 shows this latter data for both air cushion craft (hovercraft and SES) and, for

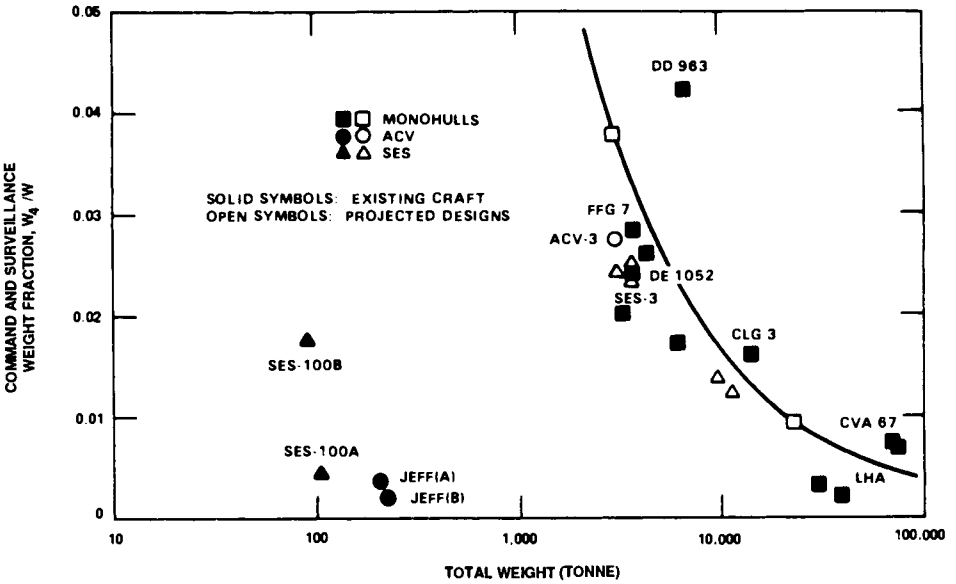

Fig. 1.42 Command and surveillance system weight.

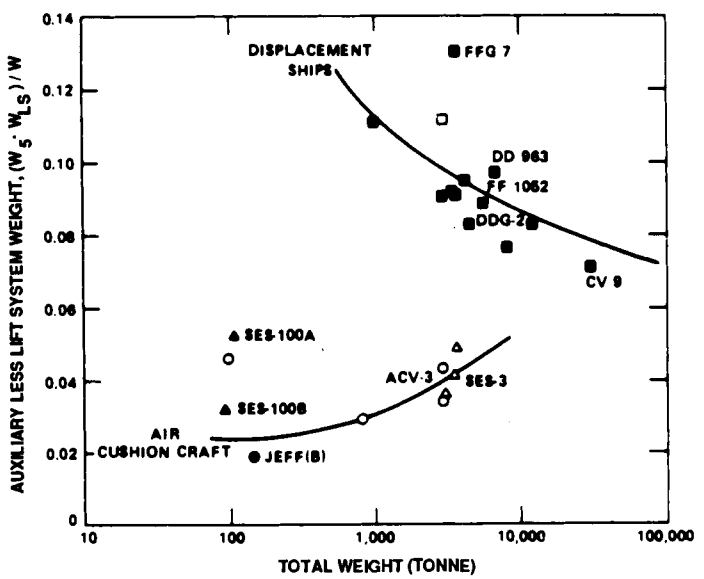

Fig. 1.43 Auxiliary less lift system weight.

comparative purposes, conventional displacement ships. Although there is

considerable scatter because of the many varied types and requirements for auxiliary systems, some general trends can be seen. For the air cushion craft data the trend can be expressed by:

$$(W_S - W_{LS})/W = 0.0024\ W^{1/3} + 0.06\ W^{-1/3} \tag{1.26}$$

The lift system weight W_{LS} can be separated from the available data into the weight of the skirt W_{SK} and the remaining components (engines, lift fans, controls and ducting). Figure 1.44 shows the weight of the total lift system W_{LS} (upper curve) and the skirt system W_{SK} (lower curve). Part of the scatter in the total lift system weight is due to the different functions being performed by the lift system (e.g. ride control) and part is due to the differing power levels of the various designs. As might be expected, the SES data is generally lower than the hovercraft for the same total weight. Another difference is the variations in skirt designs (see earlier) which results in differences in skirt weights. Based on this data, the following trend lines can be derived:

$$W_{LS}/W = 0.0044 + 0.08\ W^{-1/3} \tag{1.27}$$

$$W_{SK}/W = 0.014 + 0.08\ W^{-1/3} \tag{1.28}$$

These results would then infer that the weight of the remaining part of the lift system (engines, lift fans, ducting, etc.) can be written as:

$$(W_{LS} - W_{SK})/W = 0.03 \tag{1.29}$$

As a larger data base becomes available (subject to proprietary or classification release) a better trend can be determined.

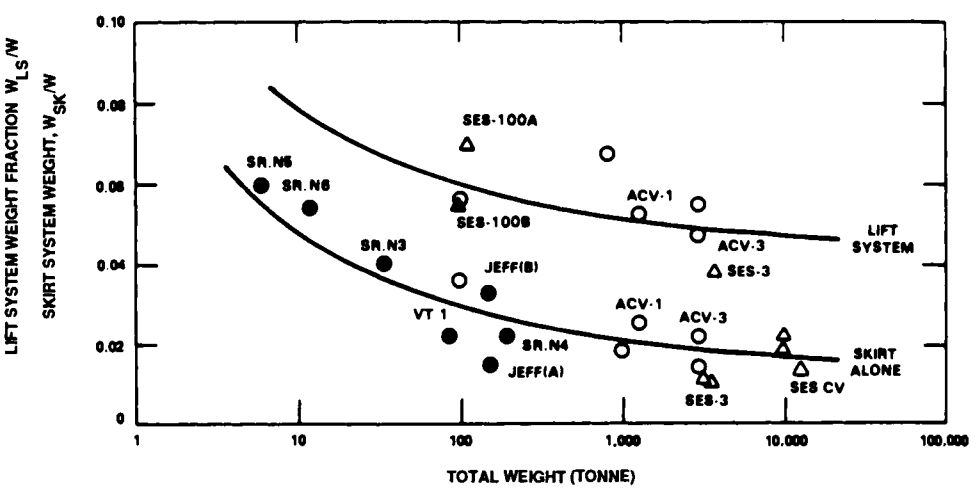

Fig. 1.44 Lift system and skirt system weight.

(vi) Outfit and furnishings weight (group 600). Data can be prepared for the weight of the outfit and furnishing (O&F) systems either as a function of manning (M) which is a key determining factor of craft size (as in conventional ships), or as a function of craft weight. Figure 1.45 shows the limited amount of data for air cushion craft and also for conventional displacement ships. It is seen that, as hovercraft and SES designs are projected into larger sizes, the O&F weights (and the manning) approach conventional ship proportions. For smaller sizes (say 50 to 200 tonnes) the data base applies to either prototypes (and therefore typical O&F weights) or special missions with limited O&F requirements.

The smaller sized craft are also *less than one room* operation craft calling for less O&F systems. Thus, it is more likely that the data shown is a collection of separate *families* of craft, each with its own trend curve having the general shape characterizing the conventional displacement ships.

In the absence of better data the equations for conventional displacement ships and air cushion craft are provided so that the reader will have at his

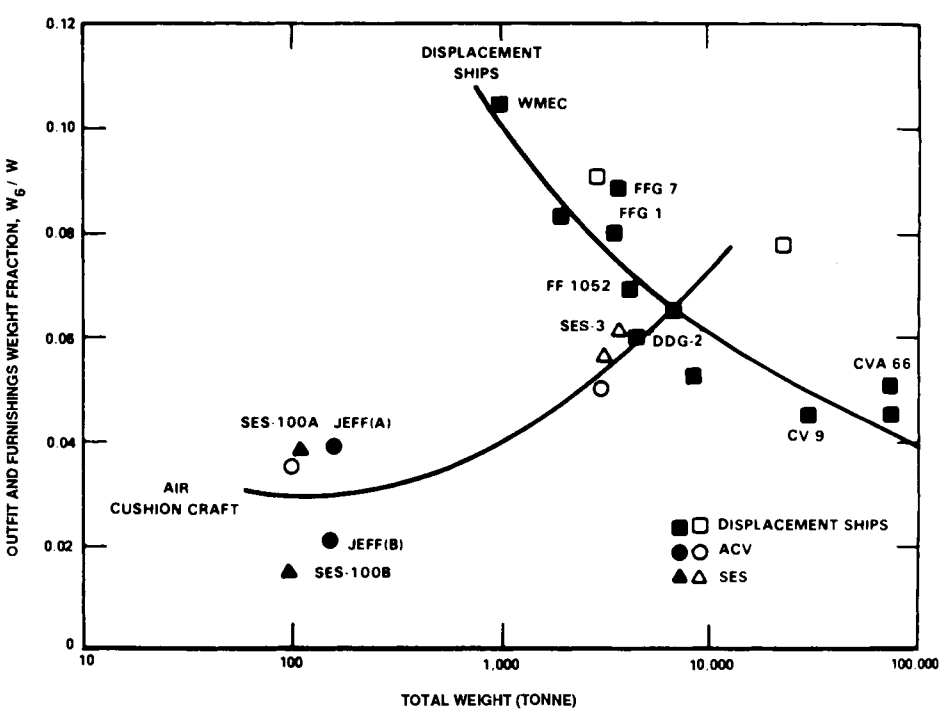

Fig. 1.45 Outfit and furnishings system weight.

disposal the data base to guide his thinking for new craft design. For displacement ships:

$$W_6/W = 0.01 + 0.50\ W^{-1/4} \tag{1.30}$$

For air cushion craft (tentative):

$$W_6/W = 0.003\ W^{1/3} + 0.07\ W^{-1/3} \tag{1.31}$$

(vii) Armament system weight (group 700). The armament group is made up of that part of the weapon system that is fixed to the craft, e.g., missile launchers, installed guns and torpedo tubes. Figure 1.38 shows schematically how the craft payload is divided into fixed and disposable payloads. With this convention, a missile launcher would be part of the fixed payload (and therefore in Group 700); the missiles would be part of the disposable payload.

For a given missile system there is usually a choice of launcher system; some lightweight and others integrated with the craft sturcutre. It is normal practice to use lightweight launchers and canisters on weight-limited craft. However, comparing the data from (actual) displacement ships and (projected) air cushion craft, no discernible difference was seen (Figure 1.46). Therefore, within early design accuracy, the weight of the armament systems is driven more by the make-up of the armament than the type of platform. The trend line can be represented by:

$$W_7/W = 0.50\ W^{-1/3} \tag{1.32}$$

(viii) Empty weight. The sum of all the above system weights (groups 100 to 700) is the *light ship weight*, as shown in Figure 1.38. The *empty weight* W_E is then obtained by subtracting those items which are designated as fixed *payload*. Figure 1.47 collects this aggregate of weights for a wide range of craft sizes. For reference purposes, the empty weights of conventional ships are also shown. These results merge as hovercraft grow to displacement ship sizes. The empty weight trend for air cushion craft (hovercraft and SES) is given by:

$$W_E/W = 0.25\ W^{0.10} + 0.50\ W^{-0.25} \tag{1.33}$$

From the above data, it can be seen that the empty weight of hovercraft is typically 50 to 60 percent of the craft's gross weight. Correspondingly, the amount left for the payload (fixed and disposable) and the fuel is 50 to 40 percent of the craft weight.

1.4 RELATED DEVELOPMENTS

As discussed earlier in this chapter, hovercraft are family members of several types of air cushion supported craft (see Figure 1.1). Other developments include the surface effect ship (SES) and wing-in-ground-effect (WIG) vehicles.

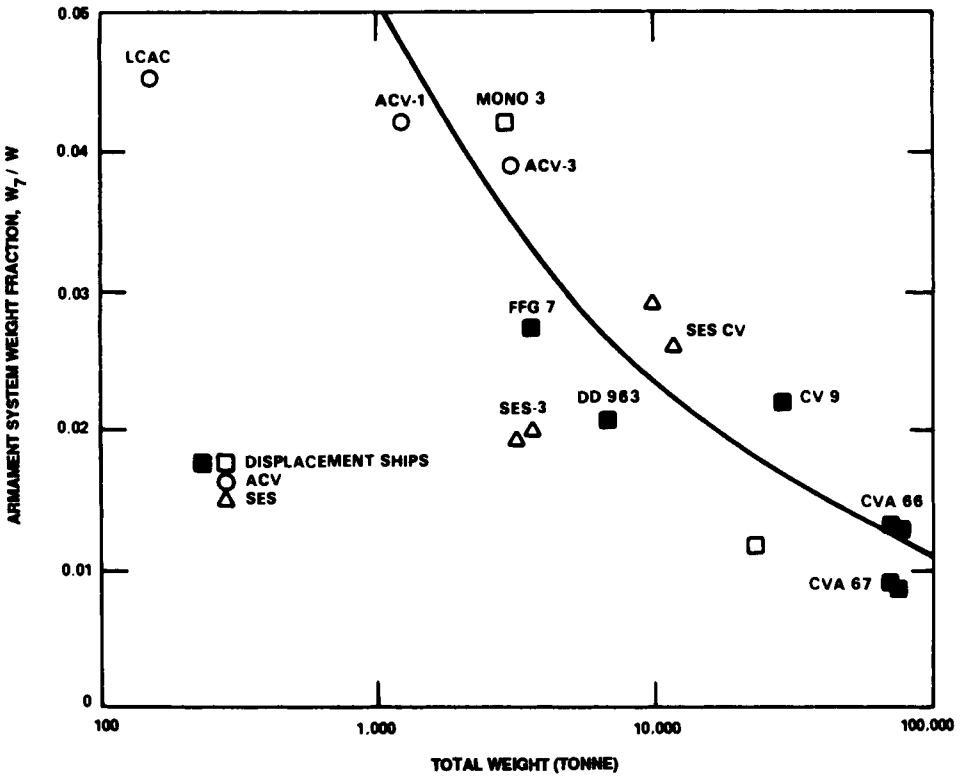

Fig. 1.46 Armament system weight.

At various places throughout this book reference is made to these other developments as necessary to provide a supporting data base. Because of the nature of evolving technology, the *boundaries* separating these various members of the air cushion craft family can become less well-defined.

In order to understand these *boundaries* a little better, it is convenient to invoke the principles of dimensional analysis to determine the governing parameters. Reference 27 is recommended reading for the understanding of dimensional analysis. Classical treatments on the dynamics of bodies moving through water and air have established the importance of such non-dimensional numbers as *Froude Number* F_N, *Reynolds Number* R_N and *Cavitation Number* J. For those craft that interface with water and air at relatively high speed, Mantle (ref. 1) showed that a *Pressure Number* k proved useful in the non-dimensional treatment of the performance of such craft. The four key non-dimensional numbers of concern to the hovercraft designer can be summarized as:

Froude Number F_N = (Hydrodynamic forces)/(Gravity forces)

$$= V/(gL)^{1/2} \qquad (1.34)$$

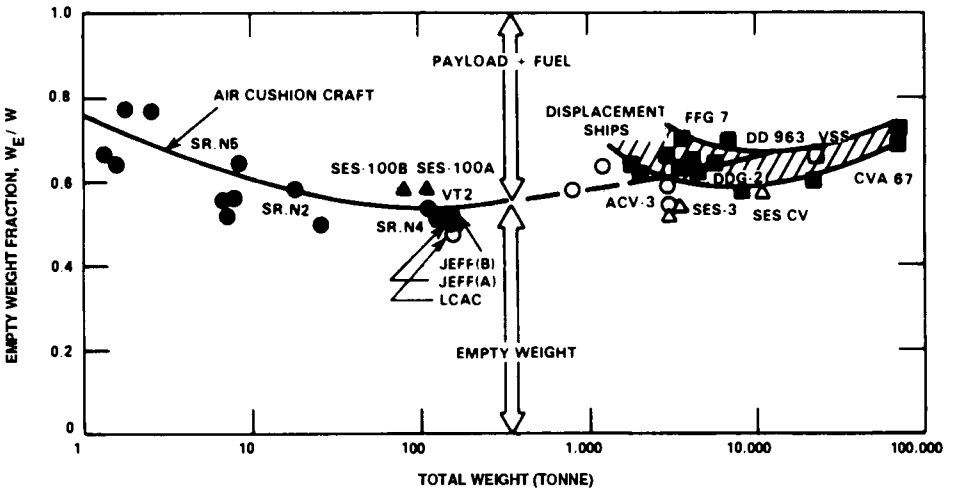

Fig. 1.47 Empty weight trend.

Cavitation Number J = (Hydrostatic forces)/(Hydrodynamic forces)

$$= P_{amb}/(\rho V^2/2) \tag{1.35}$$

Pressure Number k = (Aerodynamic forces)/(Aerostatic forces)

$$= (\rho V^2/2)/P_c \tag{1.36}$$

Reynolds Number R_N = (Dynamic forces)/(Frictional forces)

$$= \rho VL/\mu \tag{1.37}$$

Each of the above non-dimensional numbers play a role in determining the level of importance of the various forces acting on the craft and serve to define *boundaries* of best operation. The craft and *medium of operation* parameters all impact on this characterization. Craft speed V and size, through length L and cushion pressure P_c, characterize the craft. Fluid density ρ, kinematic viscosity μ and cavity bubble pressure P_{amb} characterize its medium of operation.

The Pressure Number k aids in the approximate determination of the *boundaries* and thus relates hovercraft to its cousins, the surface effect ship (SES) and wing-in-ground effect vehicles (WIG), and provides guidelines in determining their most efficient areas of operation. For low values of Pressure Number ($k < 0.10$), the aerodynamic forces on a hovercraft are minimal and the hydrodynamic forces dominate. The hovercraft is then appropriately shaped in recognition of this dominance. At high values of the Pressure Number ($k > 1$), the aerodynamic forces dominate and the craft takes on a significantly different geometric form. This is the region where the WIG vehicle is most efficient.

Figure 1.48 shows a carpet plot for the range of Pressure Number, Froude Number and Cushion Density D_c (see eqn. (1.21)) of interest to hovercraft and related vehicles. The several operational craft displayed on this figure indicate where most of today's craft operate. Note that most air cushion craft are designed to operate in a region of $0.20 < k < 0.60$ and at a cruise speed of some 2 to 3 times hump speed (on a Froude scale). Hump speed is where self-induced hydrodynamic wave resistance is a maximum. The best regions of operation for hovercraft and SES are less well-defined. All else being equal, the hovercraft is more efficient at higher speeds (higher values of k) than the SES. Some early SES prototypes, such as the SES-100B shown in Figure 1.48,

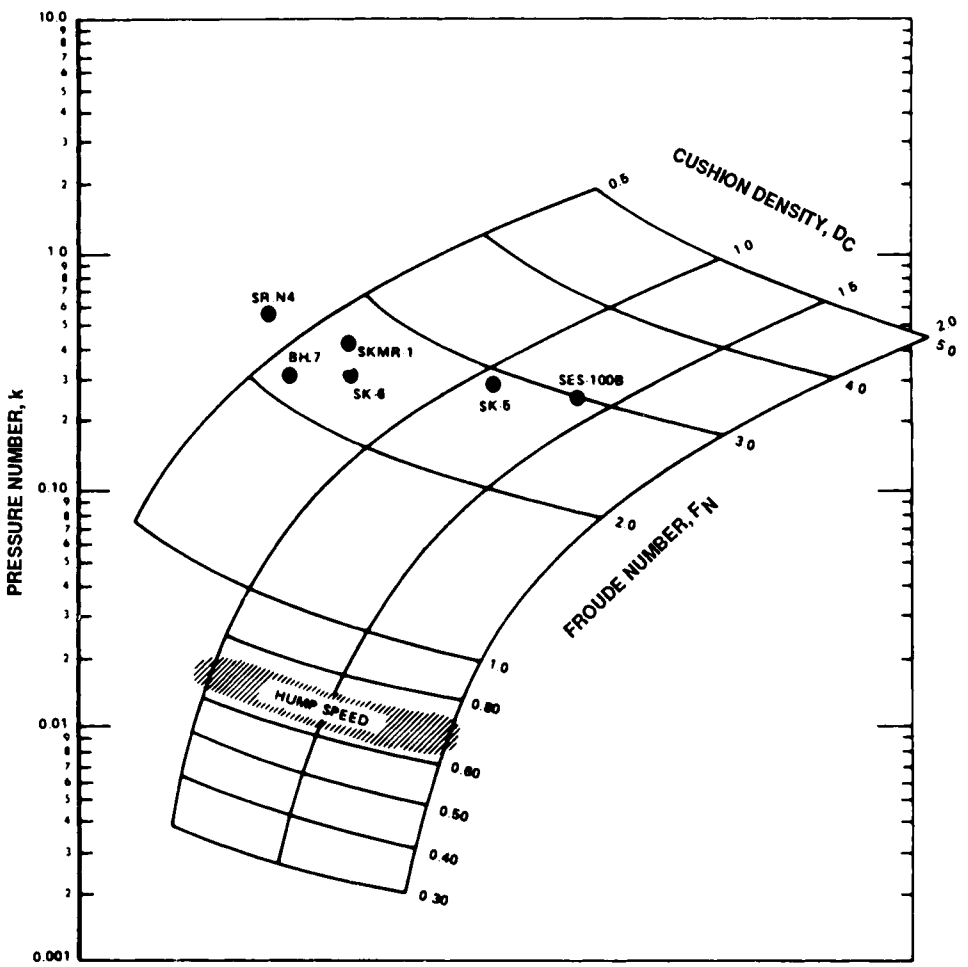

Fig. 1.48 Speed domains of air cushion craft.

were deliberately designed for much higher speeds for the determination of high speed effects on craft design.

Figure 1.49 provides further indication of where related developments in SES, hovercraft and WIG might best be pursued. The data, taken from ref. 28, is for the three types of craft. Curve A is for an air cushion hull model (SES) and was designed to be most efficient in the hydrodynamic mode (high F_N; low k). The middle set of data (0.02 < k < 0.60) is from hovercraft tests done for various air gap values. The set of data on the right is from various WIG designs (k > 0.60). One can see where each of the various basic types of craft using air cushion support in one form or another have their region of maximum *transport efficiency* WV/P. Curve B represents a concept of a craft that operates efficiently on its hydrodynamic hull at low speeds, passes through the hovercraft mode at intermediate speeds and finally leaves the confines of the

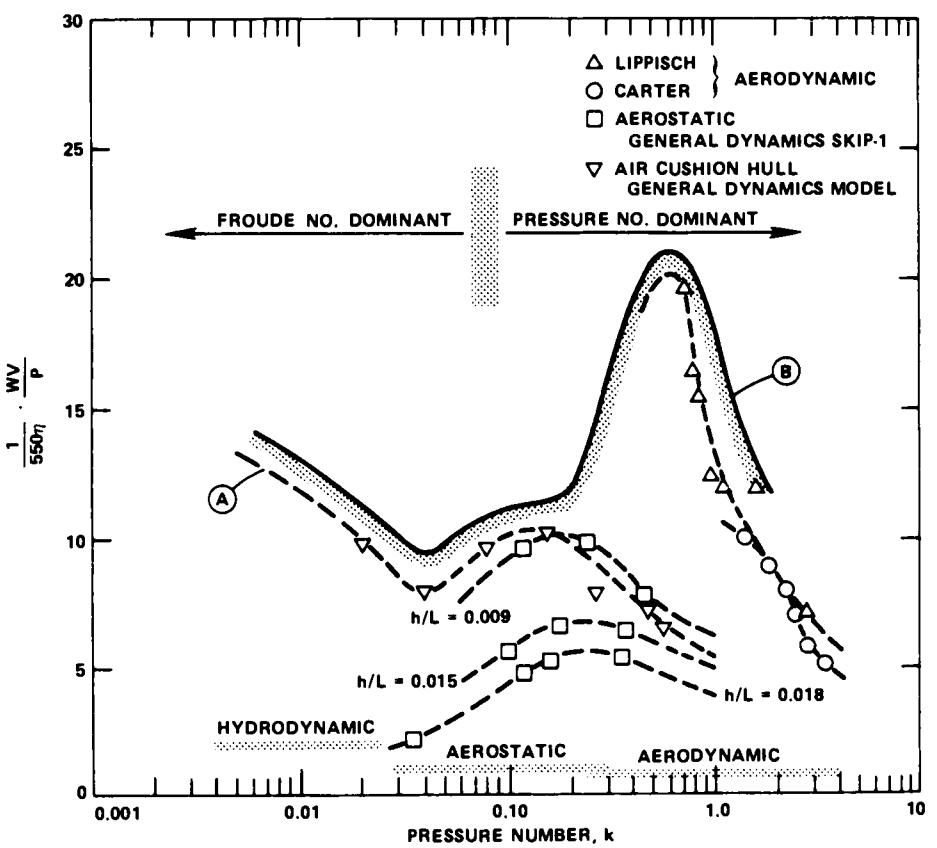

Fig. 1.49 Efficient speeds for air cushion craft.

water surface and operates in a WIG mode at high speeds. These curves may be used as a backdrop in comparing the various craft as they are built to determine their areas of most efficient operation.

1.5 SUMMARY

This introductory chapter has summarized the history of the development of hovercraft and their application in the field of transportation (military and commercial). It has also provided parameters that describe the basic characteristics of hovercraft. The history has been traced from the early work in the Seventeenth Century, but more specifically from modern operational vehicles stemming from Sir Christopher Cockerell's pioneering efforts in England, circa 1955.

Hovercraft have evolved under a series of names through a family tree that has branches named: air cushion vehicle (ACV), ground effect machines (GEM), surface effect ships (SES), wing-in-ground effect (WIG) vehicles and others. The various interrelationships and their developments have been traced and explained and related to the hovercraft: an amphibious vehicle supported on a cushion of air, as treated throughout this book.

The hovercraft is shown to be a vehicle ranging in size from small recreational vehicles up to several hundred tonnes and carrying a variety of payloads at speeds of 30 m/s (60 knots) or more. The largest commercial hovercraft in the world is the British SR.N4 MK3 (Super 4) with an all-up weight of 305 tonnes, and capable of carrying 416 passengers and 60 cars over coastal routes up to 240 km (150 nautical miles) at sustained calm water speeds up to 30 m/s (60 knots). The largest military hovercraft in the world is the Soviet Pomornik with an all-up weight of 350 tonnes and capable of carrying up to four 14-tonne light tanks. The speed estimated for this hovercraft is also 30 m/s (60 knots).

This chapter summarized many other types of hovercraft that have developed around the world, specifically: England, USA, Canada, France, Japan, Finland and the USSR. Tables were provided showing the numbers of hovercraft developed to date and expectations through the beginning of the next century (AD 2000).

As a backdrop for the detailed design chapters to follow, parametric relationships have been provided to describe some of the important overall sizing characteristics. Parametric relationships have been provided for weight, length, beam, cushion pressure, power and other important design parameters. A surprising uniformity of results was found from a data base comprising many vehicles from several countries over a time span of some thirty years. Finally, using the principles of dimensional analysis, regions for the most efficient operation of hovercraft have been described to provide guidance for future design.

1.6 REFERENCES

1. P.J. Mantle, Air Cushion Development, U.S. Government Printing Office, Stock Number 008-047-00291-2, Report Number DTNSRDC 80/012, January, 1980.
2. G.R. Bert, Travel on Thawed Tundra, University of Alaska Note 7005, September 1970.
3. Surface Traction Systems - Arctic Surface Effect Vehicle Program, Bell Aerospace Company Report 7416-950001, February 1973.
4. W.R. Bertelsen, The Gimbal Fan Air Cushion Vehicle, AIAA/SNAME Advanced Marine Vehicles Conference, AIAA Paper 78-734, April 17-19, 1978.
5. R.L. Trillo (Ed.), Jane's High Speed Marine Craft and Air Cushion Vehicles, 19th Edition, (formerly Jane's Surface Skimmers), Jane's Publishing Co., London, England, 1986.
6. Soviet Military Power, U.S. Government Printing Office, March 1986.
7. D. Meredith, Meeting the Channel Tunnel Challenge, Fifth International High-Speed Surface Craft Conference, Southampton, England, 7-8 May 1986.
8. R. Stanton-Jones, The Development of the Saunders-Roe Hovercraft SR.N1," Paper Number 13, Symposium on Ground Effect Phenomena, Princeton, 21-23 October 1959.
9. C. Cockerell, Some Remarks on the English Channel Crossing of the Hovercraft on July 25, 1959, Paper Number 14, Symposium on Ground Effect Phenomena at Princeton, 21-23 October 1959.
10. International Defense Review article, September 1986, p 1203.
11. R. Wheeler, A Decade of Development - The SR.N6 Family of Hovercraft - International Hovering Craft, Hydrofoil & Advanced Transit Systems Conference, Brighton, England, 13-16 May 1974.
12. R.L. Wheeler, The BH.7 Mk 20 Amphibious Hovercraft in the Mine Countermeasures Role, BHC Paper (1985).
13. D.J. Hardy and J.H. Martin, Coastal Mine Countermeasures Hovercraft - Outlook and Future Trends, European Naval Forecast Technical Marketing Society Conference, April 1985.
14. C. Piersall and R. Kenefick, US Navy and Marine Corps Amphibious, Naval Engineers Journal, Special Edition: Modern Ships and Craft, Vol 97, No. 2, February 1985.
15. A.L. Slafkosky, "Ship-To-Shore Surfaceborne Mobility, Naval Engineers Journal, Special Edition: Modern Ships and Craft, Vol 97, No. 2, February 1985.
16. J.L. Wosser, and A.J. Van Tuyl, A GEM for Amphibious Support" SAE International Congress January 1961.
17. Letter from Commandant, USMC to Chief of Naval Research, A/4E/bj/2 entitled "Research Program in Ground Effect Machines (GEM)," dated 27 March 1961.
18. P.J. Mantle, Introducing New Vehicles, Naval Engineers Journal, Special Edition: Modern Ships and Craft, Vol 97, No. 2, February 1985.
19. M.D. Mant, Operational Experience with the AP.1-88, AIAA Paper No. 862390, AIAA 8th Advanced Marine Systems Conference, San Diego, California, 22-24 September 1986.
20. J. Bertin, French Marine Air Cushion Vehicles, The Aeronautical Journal of the Royal Aeronautical Society, Vol 74, No. 717, September 1970, pp. 726-735.
21. R. McLeary, (Ed.) Jane's Surface Skimmers, 13th Edition, Jane's Publishing Co., London, England 1980.

22. Arctic Surface Effect Vehicle Program, Vol I: Program Review and History of Related Developments, NSRDC Report 4594, June 1975 and Vol. II: Technology Summary and Design Development, NSRDC Report 4595, David Taylor Naval Ship Research and Development Center, August 1975.

23. W. Eggington and J. Edwards, Arctic Operations with JEFF(A), Naval Engineers Journal, Special Edition: Modern Ships and Craft, Vol 97, No. 2, February 1985.

24. E. Makinen and J. Wainwright, First Winter's Experience with the Air Cushion Vehicle "LARUS" in the Beaufort Sea, Paper No. AIAA-2380, AIAA 8th Advanced Marine Systems Conference, San Diego, California, September 22-24, 1986.

25. R.L. Trillo, Marine Hovercraft Technology, Leonard Hill Publishers, London, England, (1971).

26. Ship Work Breakdown Structure (SWBS), United States Naval Ship Systems Command Report NAVSHIPS 0900-039-9010, March 1973.

27. E. Buckingham, Model Experiments and the Forms of Empirical Equations, American Society of Mechanical Engineers, 1915.

28. P.J. Mantle, Some Design Aspects of Air Cushion Craft, Annals of the New York Academy of Sciences, Vol. 154, Article 2, November 1968, pp 924-952.

Chapter 2

DESIGN FUNDAMENTALS

The basic concepts of hovercraft design are described in Chapter 1. Here, we present some of the design fundamentals that have bene employed to produce special and operational craft from these concepts. The main sub-systems treated are: structure, lift (fan and skirt systems), propulsion and control.

2.1 HULL STRUCTURE

The form of the hull structure for hovercraft is usually box-like. The shape of the box varies from craft to craft. It may take the form of a closed box or an open box. The variations usually depend on choice of materials (metal or GRP), method of construction (rivetted, welded, bonded) and other factors. To gain some insight into the structural form of hovercraft, consider the closed box form used in the SR.N4. Further, consider an idealized box structure to represent the actual box structure, as shown in Figure 2.1. Assume that this idealized box is acted upon by shear forces, end loads and bending moments as in an actual craft. This idealized structure, although simplified, is representative of the closed structures, used in existing operational craft such as the SR.N4. For example, as shown in Figure 2.1(b), the SR.N4 main bending strength comes from a longitudinal box formed by the buoyancy tank as its bottom member, two longitudinal deep-beam shear webs, and the center portion of the roof. Passenger decks and outer skins are secondary structures.

Returning to the idealized structure (shown in Figure 2.1(a)), the main bending is taken by two deep beams running fore and aft on either side of the centerline. This torsional box is completed by two webs at top and bottom. The dimensions of this idealized structure can be thought of as effective

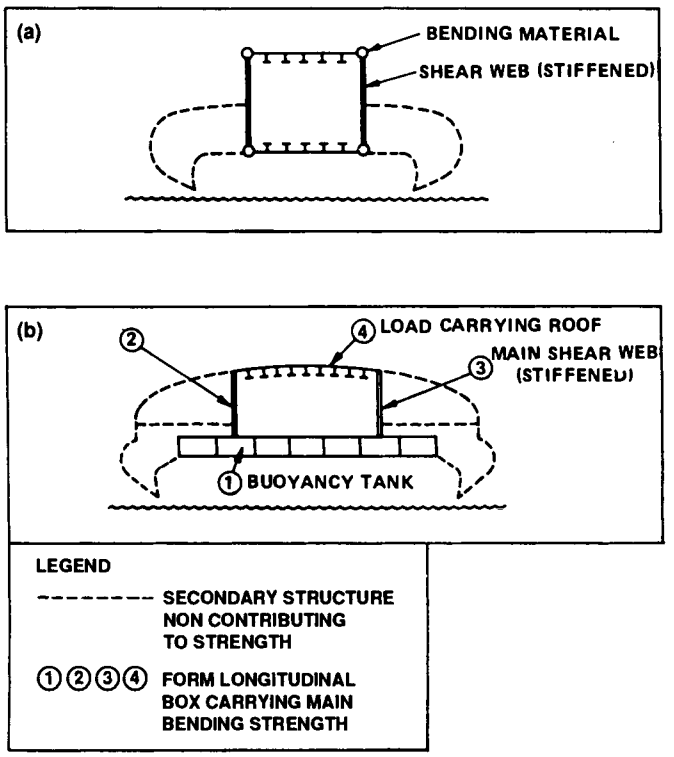

Fig. 2.1 (a) Idealized hovercraft structure; (b) actual SR.N4 structure.

values of the actual length L, beam B and structural depth H of an actual craft. By subjecting this idealized structure to the shear forces, axial loads and bending moment due to loads nW, it is possible to derive the following simplified form of the structural weight fraction as follows:

$$W_1/W = F(t,E,\ldots)/P_c + (n/\sigma)W^{1/3}\, G(L/B,H/L,\ldots) \qquad (2.1)$$

where F( ) and G( ) denote *function of*. In this form, it is seen that the structural weight comprises two basic terms. The first term reflects the contribution to the weight due to the area of the craft structure, while the second term is determined by the loading conditions and stress levels in the structure. Because it can be shown that speed affects the load factor n on the craft (ref. 1), it is anticipated that any speed effects on the structural weight would appear through the second term.

The first term, determined by F(t,E,...), includes the local properties of the panels and stiffeners and reflects the buckling criteria effect on the type of construction and minimum gauge thickness for structural members. The second term, governed by the geometric function G(L/B, H/L,...), reflects some of the

overall sizing of the design, e.g., deeper beams with higher H/L are more efficient than narrower beams within limits. This second term also reflects the load factor n mentioned earlier and the average stress level J in the structure.

The form of the structural weight equation (2.1) provides a basis for exploring avenues for lowering the structural weight other than simply making the craft more dense (higher cushion density). Raising the cushion density has adverse effects on hydrodynamic resistance, fan power and stability characteristics.

As shown in Chapter 1, the available data on hovercraft supports the above theoretical prediction for structural weight, and trend lines were drawn based on the equation:

$$W_1/W = AW^{-1/3} + BW^{1/3}[(P_c/S)^{1/2}]^{-1/3} \qquad (2.2)$$

where A and B are given constants.

While many hovercraft designs of varying structural concepts have been built, no breakthrough has occurred to significantly reduce structural weight much below 30% of the craft weight. It will be the gradual development of a combination of design refinements that will bring the structural weight down. Improvement in the knowledge of loads acting on the craft may allow the load factor n to be reduced. The use of higher strength-to-weight ratio materials and more efficient structural methods (e.g. sandwich construction) will also help reduce weight. By efficient design, the average stress level σ can be kept uniformly high throughout the structure and again reduce the weight. The challenge to the hovercraft designer is to accomplish these improvements without increasing the complexity and cost of the structure. Chapter 5 shows some of the effects on cost of invoking some of these structural design changes.

Until recently, builders of hovercraft have struggled to implement lightweight, high strength designs using aeronautical techniques of construction. This has resulted in combinations of rivetted and welded construction, complex structural members such as sandwich construction, unique section beams and other weight saving devices. The prototype for the current US Navy's LCAC, namely the JEFF(B), is one such example. Figure 2.2 shows the mid-ship section and its structural details.

Over the last few years, the high cost of complex structures has prompted a re-evaluation into the use of simplified construction techniques centered around all-welded marine aluminum hulls with increased use of standard sections. There are penalties, however, in terms of *lost* payload due to heavier structures. In some cases, the use of complex structures has not always resulted in significant enough reductions in structural weight (and thus increased payload capacity) to offset the associated cost increases (see Chapter 5).

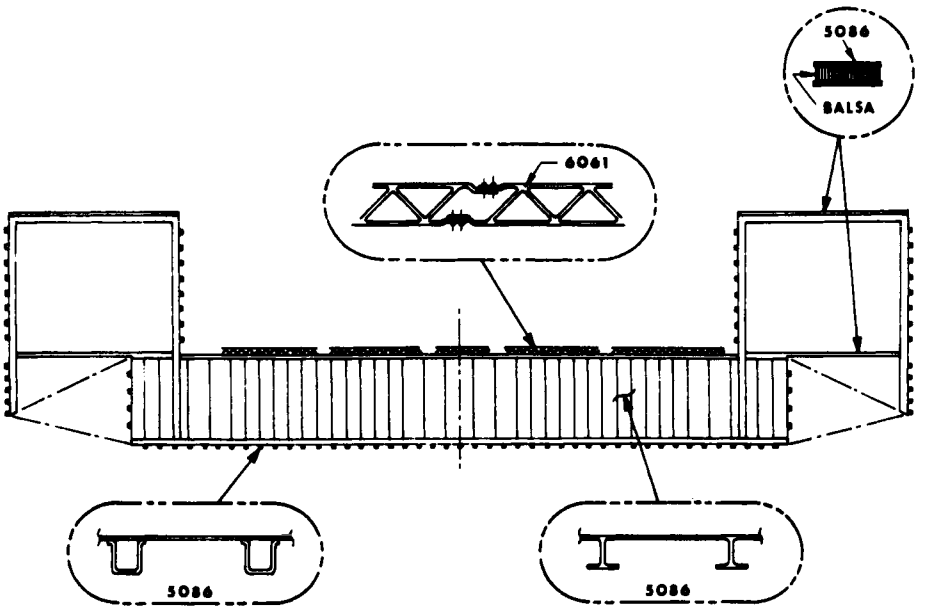

Fig. 2.2 JEFF(B) hovercraft mid-ship section.

Table 2.1 summarizes the structural weight fractions (W_1/W), materials and construction methods of several representative hovercraft and SES. While the sample base is not complete, it is seen that despite the varied (and complex) use of materials and construction methods, the variation in structural weight is not radically different (30-32% of craft gross weight). It should also be noted that speed and size effects are not apparent from these representative craft. Craft size variations in the data are 5:1 and design speed variations are almost 3:1 with only 10-20% variation in structural weight. More complete details of the craft materials thickness methods of construction (except for the AP-1.88) may be found in Ref. 1.

The AP-1.88 introduced in 1983 was specifically designed to be of much lower cost and more robust than earlier hovercraft. Figure 2.3 shows some of its simplified construction techniques. The hull is constructed from marine grade aluminum alloy, plate N8 and sections HE30; plating thicknesses are generally in the 2-3 mm range with some increased thicknesses in areas of high stress. Some of the ramifications of this simpler construction methodology appear in both a lowering of the acquisition cost and in the operating costs of the hovercraft, as discussed in Chapter 5.

2.2 LIFT SYSTEM

The lift system of a hovercraft is made up of the air intake, lift fan(s) and engine(s), diffuser, ducting, controls and a skirt system. In particular

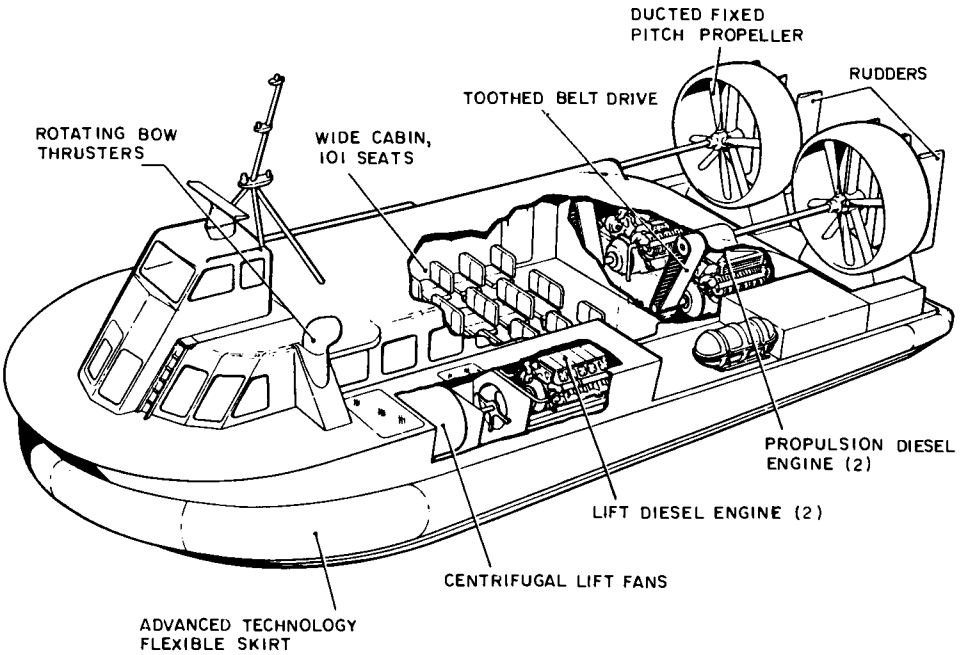

Fig. 2.3 Hull structure of AP-1.88 hovercraft.

Table 2.1: Structural weight of air cushion craft.

Craft	Structural material	Type of construction	W_1/W (%)
<u>Hovercraft</u>			
BH.7	N8, GRP	Rivetted Al. and extensive GRP	30
JEFF(A)	5086	All welded corrugated sheet	30
JEFF(B)	5086, 6061 Balsa wood	Welded, rivetted Balsa & truss	31
SR.N4	N8	All rivetted	30
VT.1	NS6	All rivetted	30
AP-1.88	N8	All welded	32
<u>SES</u>			
SES-100A	5086	Welded with mechanically fastened GRP panels	31
SES-100B	5456	All welded	33
BH.110	5086, 6061	All welded	36

designs there may be different geometric arrangements and the lift system may be integrated with other systems such as propulsion or control. The two key parts of the lift system are the fan and the skirt, and the following sections describe the design fundamentals of these parts of the lift system.

2.2.1 Lift fans

The lift fan is a key component of the lift system on any hovercraft and most lift fans provide three basic functions, namely: a) to generate sufficient cushion pressure P_c to support the craft, b) to provide sufficient air flow Q to meet performance requirements, i.e. reduce drag and satisfy wave pumping requirements, and c) to provide the correct rate of change of cushion pressure with respect to cushion flow (fan slope) to meet dynamic stability requirements.

In addition to the above basic requirements, the lift fan may be called upon to provide sufficient air flow for control purposes and engine filtration. Figure 2.4 shows a typical *tree* of functions that the lift fan system must supply. Each branch of this *tree* has a pressure drop (or rise), flow and efficiency associated with it. A network analysis is required either by computer, analysis or *cut and try* to determine the branch conditions that provide a net momentum and energy balance.

Various fan types can be used in hovercraft design. While specific designs may vary, they are always some variant of one of four basic types: axial, centrifugal, mixed flow, and tangential or crossflow. Figure 2.5 shows these various types of hovercraft fans. The SR.N1 used an axial flow fan. This fan, with its large intake and constant diameter duct beneath the fan (see Figure 1.8), dominated the configuration. Axial flow fans are usually selected because they offer the greatest efficiency for a given size. In the intervening years since the SR.N1, research and development has continued on other fan types including the centrifugal fan (most commonly used), mixed flow fans (to regain more efficiency) and finally, to a much lesser extent, crossflow fans. These crossflow fans were an attempt to reduce the space allocation for fans to the minimum by laying the fans in rolling-pin fashion along the edges of the craft, directing air immediately into the peripheral ducts. This would leave a larger part of the craft free to carry payload and other systems. Because the centrifugal fan has received the most development, it will be used to illustrate some of the key points facing the designer. The same characteristics discussed for the centrifugal fan apply, though in different degrees, to the other fan types shown in Figure 2.5.

Figure 2.6 shows the pressure distribution through a typical hovercraft lift system. The total pressure rise H_f that must be developed by the fan in order to produce the required cushion pressure P_c to support the hovercraft can be written:

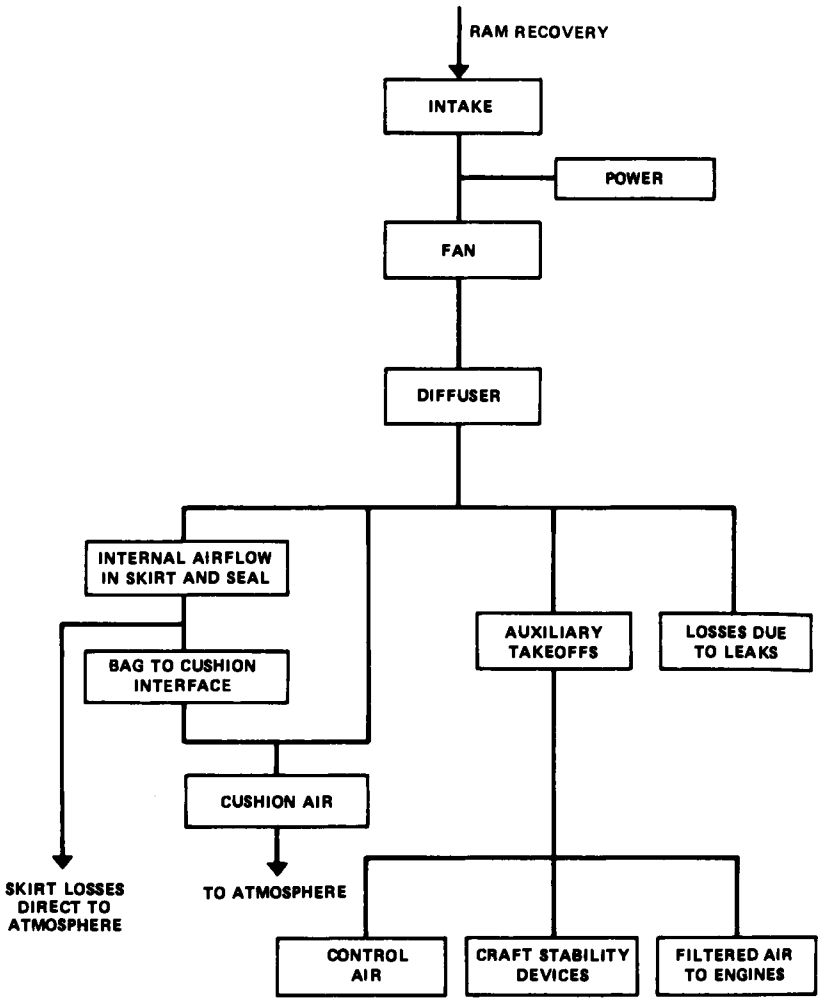

Fig. 2.4 Typical lift fan system.

$$H_f = P_c + (P_b - P_c) + K_3q_3 + K_2q_2 + K_1q_1 - \epsilon q_o \qquad (2.3)$$

Hence, the fan must produce a static pressure equal to the cushion pressure P_c plus the increased static pressure in the skirt bag $(P_b - P_c)$, if there is one, which may be from 10 to 50 percent, depending on the skirt geometry. In addition, the fan must produce sufficient dynamic head to overcome the dump loss K_3q_3 from the diffuser exit into the bag, where $q_3 (= 1/2\ \rho V_3^2)$ is the dynamic pressure to the undiffused velocity head. The factor K_3 depends on the geometry; it could be as high as 1.0 for a sudden expansion from the hard structure into the peripheral bag (or loop). The remaining dynamic head losses

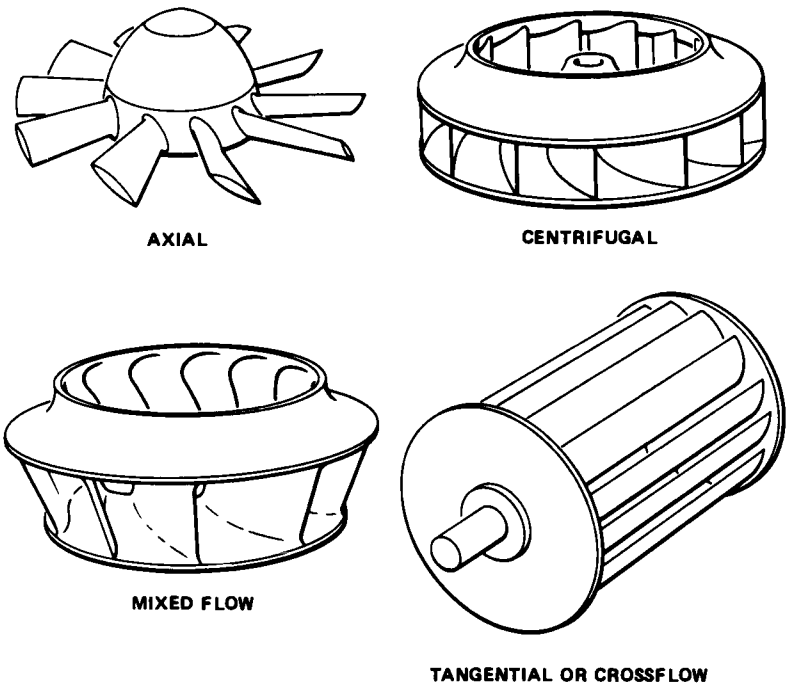

Fig. 2.5 Types of lift fans.

are: a) K_2q_2, which is the pressure loss due to the undiffused velocity head existing from the fan impeller into the diffuser, and b) K_1q_1, which is the intake loss into the fan. These latter two losses can be quite large in practical installations where clean fan intake and exits are disturbed by gearbox and shafting protrusions into the intake area and primary structure scantlings in the fan exit area. Some relief to the pressure rise requirements is available from the ram recovery ϵq_o, where ϵ is the intake ram recovery factor and $q_o (= 1/2\ \rho V^2)$ is the dynamic head of the oncoming free stream.

The basic equations for any lift fan system are:

$$P_c = W/S \tag{2.4}$$

where W is the craft's total weight and S is the cushion area, and

$$Q = V_e\ h\ C \tag{2.5}$$

where V_e is the velocity of the existing air beneath the skirt with gap height h and peripheral length C.

The total fan efficiency is given by:

$$\eta_t = H_f Q/P_L \tag{2.6}$$

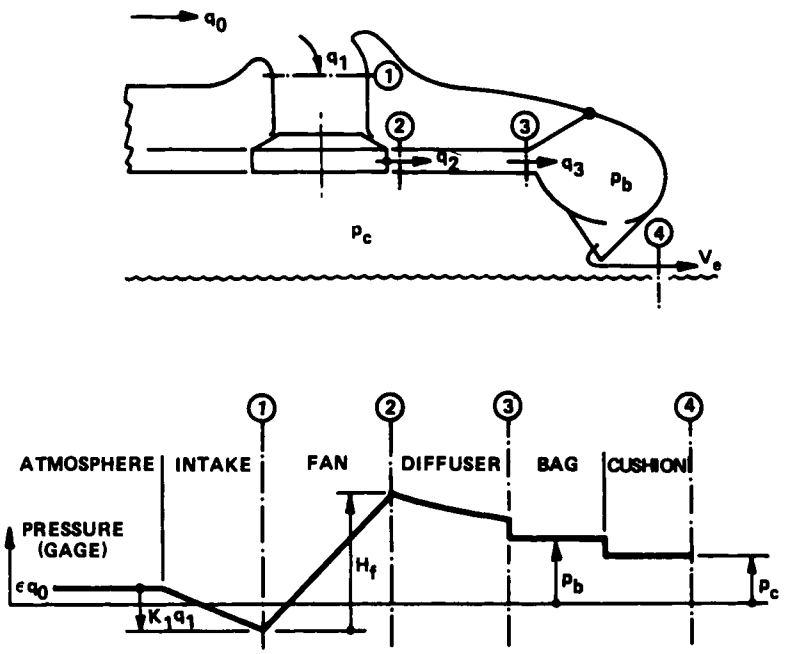

Fig. 2.6 Typical pressure distribution through lift system.

where P_L is the power supplied to the lift fan. The fan static efficiency is given by

$$\eta_s = Q(H_f - q_2)/P_L \tag{2.7}$$

Clearly, to provide the best system in terms of maintaining an even distribution of pressure around the craft periphery, it is necessary to minimize the fan exit velocity (and thus q_2); hence, it is important to maximize the static efficiency η_s of the system.

To provide some indication of the magnitude of the changes in pressure and flow through a hovercraft lift fan system, Table 2.2 has been prepared for the SR.N4. The numbers have been rounded and can be taken as typical of current hovercraft with lift fan systems similar to the SR.N4. For the SR.N4, approximately 35 percent of the lift power is absorbed by the cushion. The intake, fan plenum, and bag-to-cushion interface losses vary between 10 and 17 percent or an average of 14 percent. If lift system efficiency η_L is defined as:

$$\eta_L = \text{(Fan total efficiency)(Cushion pressure)/(Total fan pressure)} \tag{2.8}$$

then it is seen that an efficiency of the lift system of the order of 35 to 40 percent is not atypical. Much development work into mixed flow fans (such as radial fans) has been undertaken to improve these efficiencies without having

Table 2.2 SR.N4 Power Distribution.

Component	Pressure drop or loss Δp (%)	Flow Q (%)	Power $Q\Delta p$ (%)
Intake	12.4	100	12.4
Fan Impeller	15.0	100	15.0
Plenum chamber or ducts	12.0	86	10.3
Bag/cushion interface	20.0	86	17.2
Hinge leaks	2.0	86	1.7
Engine air	64.0	14	9.0
Cushion	40.0	86	34.4
			100.0

Note: (a) $\Sigma\Delta p$ is not 100 percent because of parallel paths.
(b) ΣQ is not 100 percent because of series paths.
(c) Control and stability power takeoff is assumed to be intermittent or negligible.

to *give up* valuable payload space within the hovercraft. Recent information on the radial fan may be found in ref. 2. To provide a better understanding in selecting a fan or fans for a hovercraft, it is best to express the pressure and flow characteristics in non-dimensional form which, from the standard theory of turbo machines, can be written for the pressure coefficient ψ as:

$$\psi = P/\rho n^2 D^2 \tag{2.9}$$

where P is the pressure rise across the fan, ρ is air density, n is the fan's rotational speed, and D is the maximum diameter of the fan. The units are selected such that ψ is non-dimensional. The flow coefficient ϕ is given as:

$$\phi = Q/nD^3 \tag{2.10}$$

The performance of a fan can be completely described by these non-dimensional pressure and flow coefficients. They apply across fan types (axial, centrifugal, ...) and they also allow scaling performance within a given type of fan, such as performance at rotational speeds or diameters other than the design point.

Two other important lift fan design parameters are the specific speed N_s and specific diameter D_s, both of which are non-dimensional; they are defined:

$$N_s = \phi^{1/2}/\psi^{3/4} = nQ^{1/2}/(P/\rho)^{3/4} \tag{2.11}$$

and

$$D_s = \psi^{1/4}/\phi^{1/2} = D(P/\rho)^{1/4}/Q^{1/2} \tag{2.12}$$

or, alternatively, in terms of the pressure H across the fan:

$$N_s = nQ^{1/2}/(gH)^{3/4} \tag{2.13}$$

and

$$D_s = D(gH)^{1/4}/Q^{1/2} \tag{2.14}$$

The significance of this particular form of non-dimensionalization is that the specific speed N_s and specific diameter D_s are the required speed and diameter of a fan to deliver unit pressure and unit flow; that is,

$$\psi = (N_s D_s^{\ 3})^{-2} \tag{2.15}$$

and

$$\phi = (N_s D_s^3)^{-1} \tag{2.16}$$

The various intricacies of blade shaping, fan proportions and other geometric properties of fans can be found in Eck (ref. 3). Most of today's design methods for hovercraft fans have as their basis the work of Osborne (ref. 4), and Shipway (ref. 5) for centrifugal fans and Wallis (ref. 6) and Shipway (ref. 7) for axial fans. It is fortunate that designs for maximum efficiency of axial, centrifugal and mixed flow fans can be represented by single curves of specific diameter D_s and maximum efficiency η_t when plotted against specific speed N_s. In 1955, Cordier (ref. 8) compiled specific speed and specific diameter data of high efficiency fans and showed that the data exhibited very little scatter over a wide range of specific speeds for all fan types. His fan sizing relationship is shown in Figure 2.7. In 1960, Balje (refs. 9 and 10) derived a theoretical prediction for the same information that Cordier derived empirically. Although more complete analysis is available in the Balje and Cordier work, Mantle (ref. 1) shows that a good representation of the fan data can be obtained from the empirical relationships:

$$D_s = 0.90 + 2/N_s \tag{2.17}$$

and

$$\eta_t = 0.85 - 0.02\ N_s \tag{2.18}$$

From such representations as Figure 2.7 it can be shown that the three main types of fans can be grouped according to their specific speed ranges, as follows: a) centrifugal fans, $N_s < 3$, b) mixed flow fans, $2 < N_s < 4$, and c) axial flow fans, $N_s > 3$.

Typical pressure-flow characteristics of centrifugal, mixed flow and axial flow fans are shown in Figure 2.8. The curves are drawn for ratios of pressure, flow and efficiency at some selected design point which, for the example shown, is the maximum efficiency point. Although it is difficult to generalize, there are certain characteristics inherent in each fan type that have influenced their use in hovercraft. For operation at other than the design

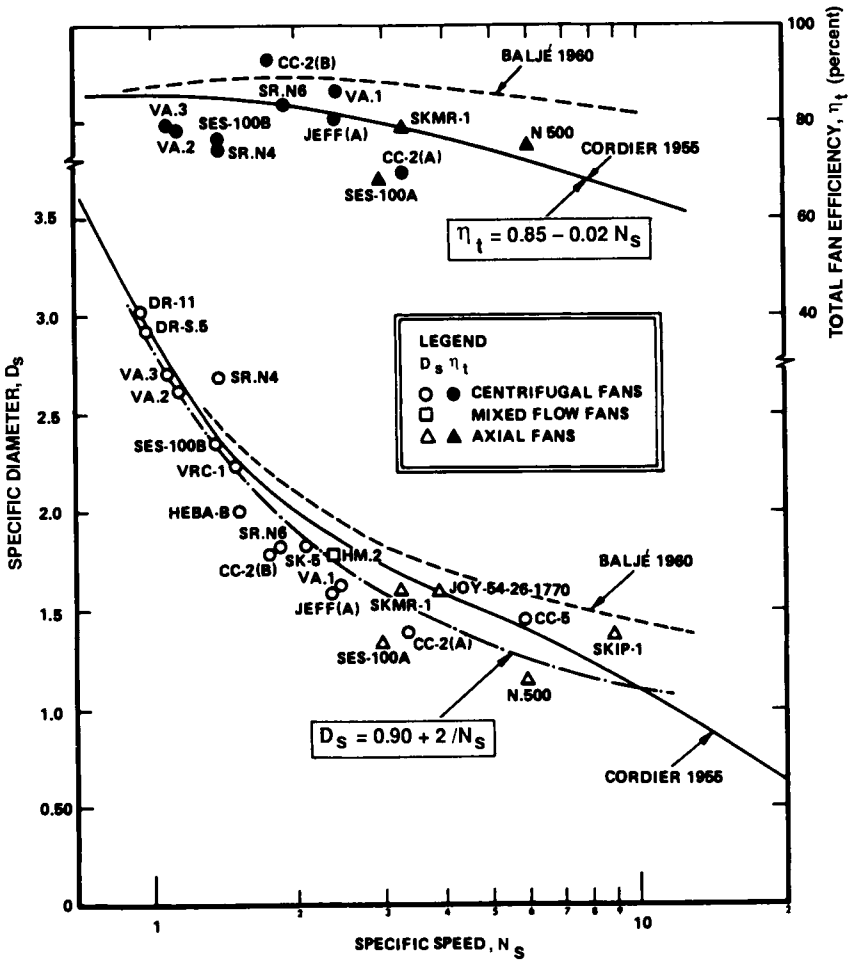

Fig. 2.7 Generalized fan sizing.

point, which is a frequent occurrence (e.g., in rough seas), then the flatter the characteristic is (i.e., low pressure-flow slope) the better. This has strongly influenced the choice of centrifugal fans, especially when coupled with their simpler, more rugged construction feature. Also, the centrifugal fan has a generally monotonic pressure-flow characteristic with no regions of stall near zero flow, which are inherent in high flow axial or mixed flow fans. It is possible to achieve a stall-free axial fan, but only in special applications with narrow operating limits. The steep slope and high cut-off pressure of axial fans provide a great deal of hovercraft heave stability not attainable with centrifugal fans. The steep slope of the pressure-flow curve of axial fans, however, generally leads to degraded ride quality in sea state operation. The properties of axial fans are well understood, based on years of aircraft

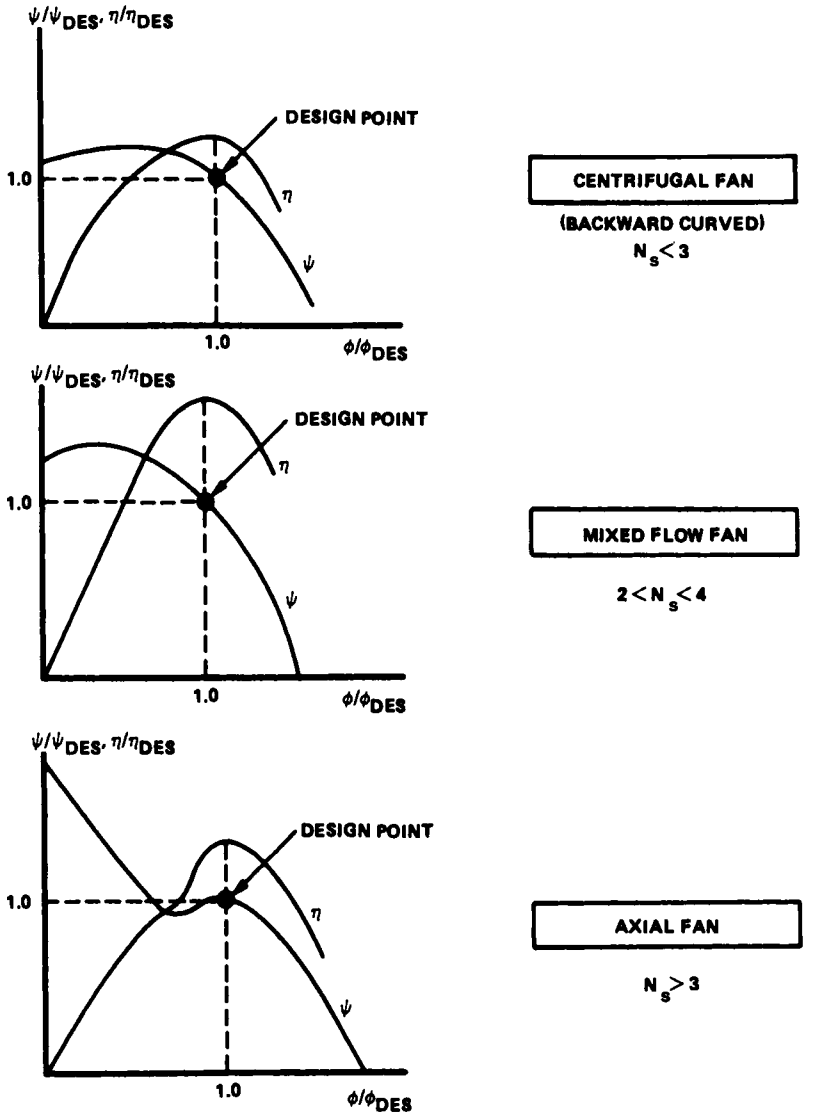

Fig. 2.8 Typical pressure-flow and efficiency curves.

propeller development and their performance predictions are analytical and predictable. On the other hand, centrifugal fans are less predictable, and their performance prediction methods contain several empirical factors that are not always controllable.

In addition to the type of lift fan that can be used in hovercraft design, there is the consideration of incorporating such fans into either a passive or active lift fan system. Such a consideration is necessary if the craft is to

be operated under conditions of rapid changes in pressure and flow demands such as when operating in rough seas.

(i) Passive lift fan systems. A passive lift fan system is defined as that system where the fan is a simple, rotating, air-moving device and does not include any pitch change mechanism or other means of controlling pressure and flow variations in the cushion. Most hovercraft (and SES) built to date are of this type and discussion of pressure-flow characteristics is restricted to quasi-steady conditions. Except in special operating conditions, it has been found that such an assumption is entirely satisfactory. Usually the weight and inertia of the fan are sufficient to maintain constant speed of rotation such that the designer does not have to contend with variations in a given pressure-flow curve due to dynamic conditions. At high frequency variations, however, such assumptions are incorrect and the dynamics of the motion (including fan inertia) must be included.

Of the passive lift fan systems, the centrifugal fan has seen the most application. The design of such fans has, by and large, been based on the fan technology developed at either Dowty-Rotol and Airscrew-Weyroc in England or Buffalo Forge Company in the United States. Airscrew-Weyroc developed a fan series which they characterized as *high efficiency backward airfoil* or HEBA series (ref. 11). The HEBA fans were developed in two basic forms: the HEBA-A, a narrow-width fan suitable for high pressure, and HEBA-B, a wide-width fan suitable for low pressure. The actual pressure levels are unimportant here because the Airscrew HEBA fans were developed for industrial use and fabricated from mild steel. The HEBA-B fan geometry, however, was found to give the best pressure-flow characteristic for air cushion craft and has formed the basis for most of the designs in use today. The HEBA-B fan has been used in such craft as the Britten-Norman hovercraft CC-1 and C-2 in 1962, the British Hovercraft Corporation (now Westland) series of hovercraft, SR.N5, SR.N6, SR.N4, BH.7 and AP.1-88, and many other British and US hovercraft and SES.

The HEBA-B fan is characterized by a blade section that has a flat undersurface and an airfoil-like cambered upper surface. Buffalo Forge Company (ref. 12) found that a reflex to the upper surface trailing edge provides a more aerodynamically stable characteristic around zero flow. This was incorporated into the SES-100B and later craft designs. A typical pressure-flow curve for a HEBA-B type hovercraft lift fan is shown in Figure 2.9. The specific data shown is for the JEFF(B) fan, which was the *prototype* for the US Navy - Marine Corps Amphibious Landing Craft, Air Cushion (LCAC) currently in production. The first LCAC *rolled-out* from the prime source facilities at Bell-Halter, New Orleans on 2 May 1984. The second source production craft, to make-up the ninety (90) hovercraft planned, is scheduled for the Lockheed facilities (now owned by Avondale Shipyards) in Gulfport, Mississippi, in the

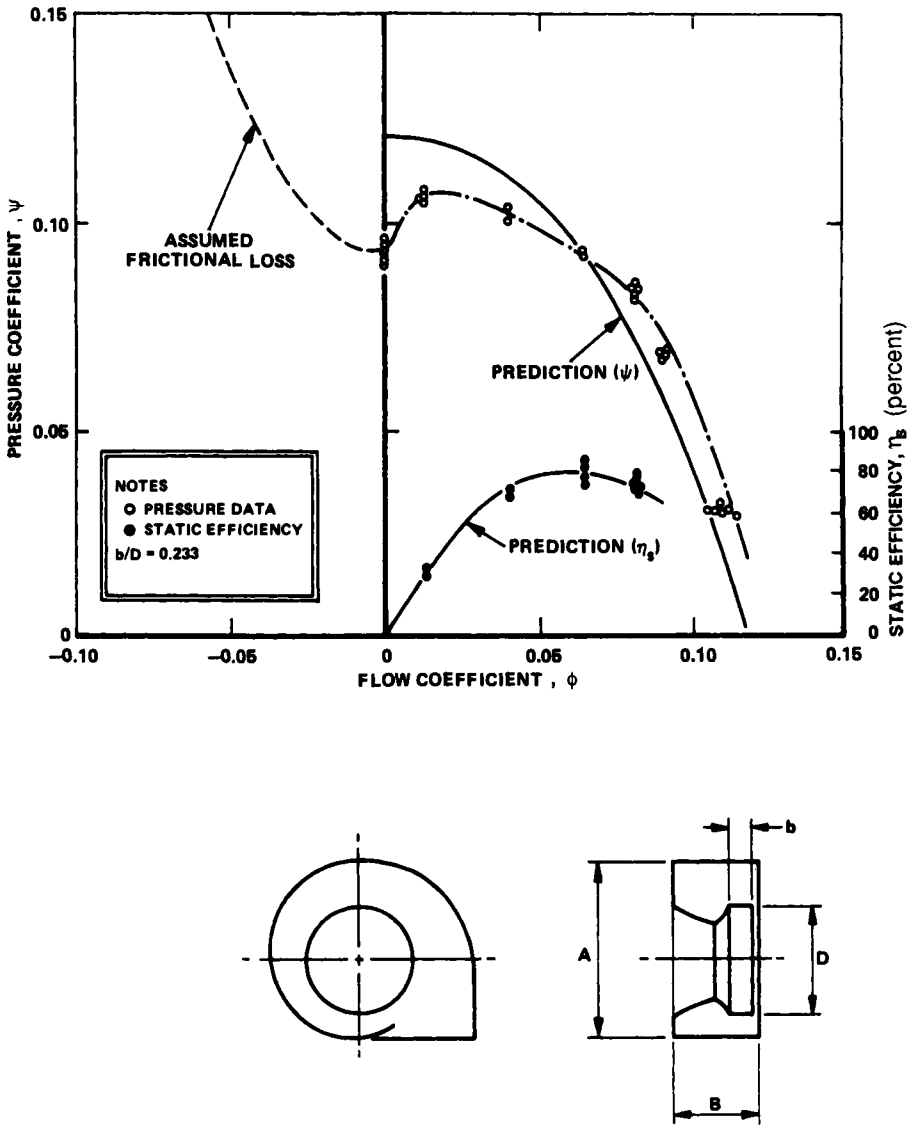

Fig. 2.9 Typical HEBA-B fan performance.

summer of 1988. All these craft use variants of the HEBA-B and Buffalo Forge Company lift fans. Figure 2.10 shows the general configuration of these fans.

A parameter of importance in centrifugal fan design is the ratio of blade depth to fan diameter b/D which, as Csaky (refs. 13 and 14) points out, is 0.17 for HEBA-A fans and 0.23 for HEBA-B fans. Also, the volute volume parameter U/bD^2, where $U = \pi/4\ A^{2B}$, is an important parameter in determining fan performance. It is found that increasing U/bD^2 provides a flatter pressure-flow

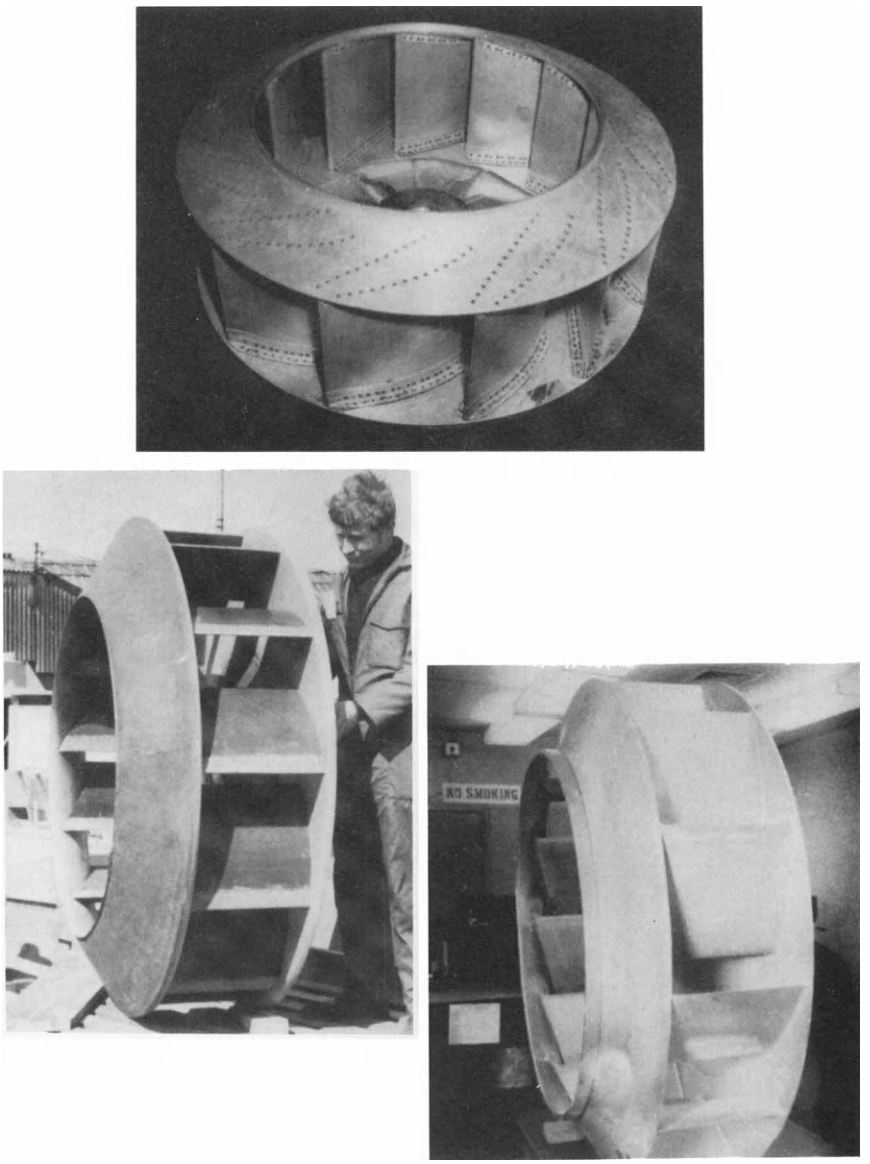

Fig. 2.10 Some centrifugal fans.

curve, but at the expense of a large (space consuming) fan installation. Figure 2.11 shows the effect of these design parameters on the performance of HEBA-B fans. Typically, the volute in which the actual fan must operate to

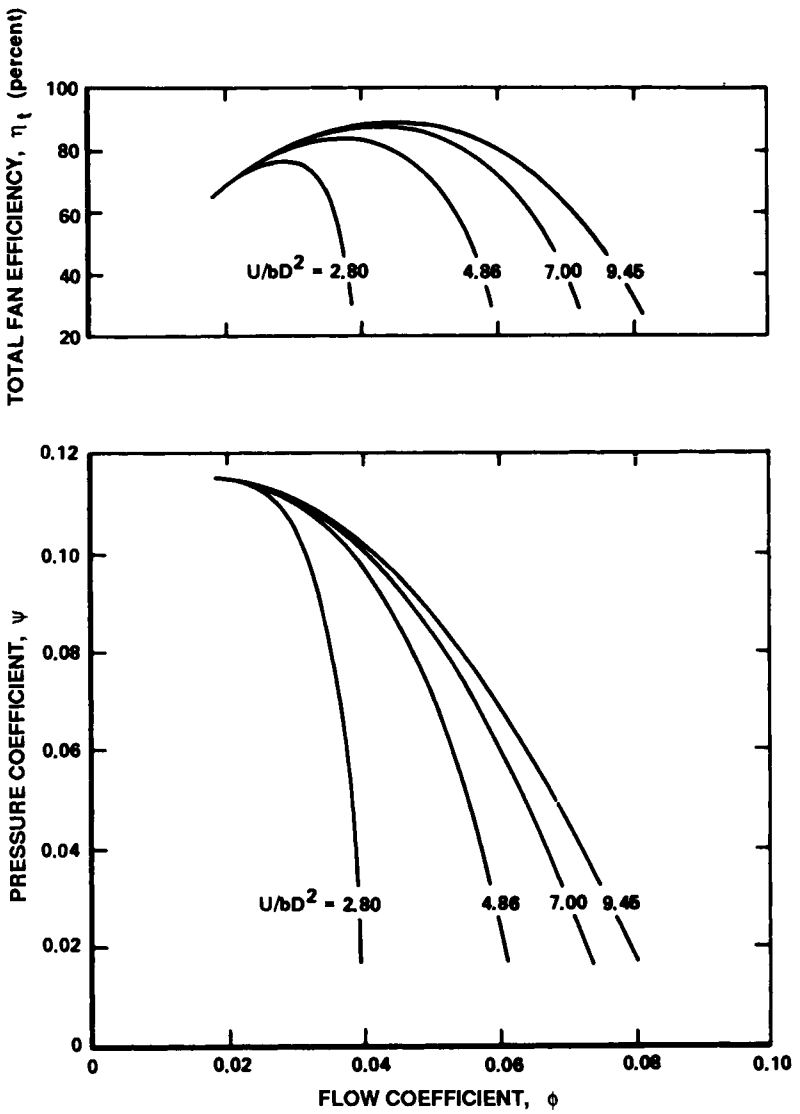

Fig. 2.11 HEBA-B fan performance characteristics.

produce the desired performance would have proportions of volute height A approximately 60 to 80 percent larger than the fan diameter D. The volute width B would be some 80 percent of the fan diameter. While not a precise rule, it is frequently found that varying design parameters to flatten the curve around the design point increases the tendency to stall near the zero flow point. For hovercraft designed to operate in extreme sea conditions,

where wave pumping can cause large variations in flow and even reverse flow through the fan, a characteristic curve such as that shown in Figure 2.9 can occur.

Although not elaborated upon here, the stall characteristics near zero flow are more pronounced in axial flow fans (see Figure 2.8). In such instances, it is required that the design point on the pressure flow curve be at sufficiently high values of the flow coefficient ϕ so that the design flow range about the design point does not include the stall region. Axial flow fans have been employed in such hovercraft as the SR.N1, SKMR-1 and SKIP-1. French hovercraft have also favored axial flow fans. The Bertin Craft N.300 and N.500 are such examples.

(ii) Active lift fan systems. As discussed above, current operational hovercraft concentrated on passive lift fan systems with emphasis on simplicity and ruggedness. The designs have tended to maximize efficiency influenced by the need to maintain a flat pressure-flow curve over a wide operating range and the avoidance of stall near zero flow. Additionally, the need to ensure proper heave stability, which requires a steep slope or large cutoff pressure to design point pressure ratio has also influenced the final design. Such requirements (often conflicting) have led to the development of active lift fan systems to control the pressure and flow delivery at the various operating points in the design envelope. Techniques for controlling the pressure and flow have been investigated over the years for use in turbomachinery. Such devices as mechanical flaps on blades, jet flaps, discharge guide vanes and variable camber have all been tried with varying degrees of success. Mantle (ref. 1) provides a description of the various techniques developed in the US Navy SES program for the dynamic control of pressure and flow. These techniques included variable pitch blades, variable inlet guide vanes (VIGV), vent valves from the cushion, and other techniques. Design parameters and test results are provided in ref. 1.

While a significant amount of research and development has been expended in determining reliable active lift fan system design, not much beyond simple venting has been incorporated into operational craft. Venting the cushion (to reduce pressure increases and thus craft vertical accelerations) is wasteful in terms of power loss but is still the simplest solution to date. Two developments on other than venting are of interest in that they can be applied to hovercraft design to avoid the power-consuming disadvantage of venting, especially in heavy seas (not so much on land). The first is the Hamilton Standard approach for use on axial flow fans (ref. 15); the second is the Aerojet Liquid Rocket Company's approach for centrifugal fans (ref. 16).

A set of predicted pressure-flow characteristics for the Hamilton Standard controllable-pitch axial fan system is shown in Figure 2.12. The curves are

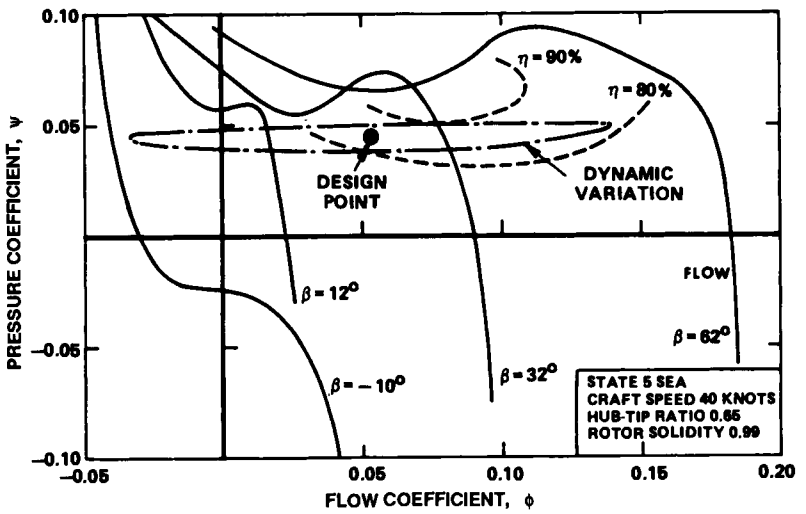

Fig. 2.12 Hamilton standard active axial fan scheme.

shown for a 2.13m (7.0 ft) diameter, variable pitch, axial flow fan operating at 2183 rpm with a tip speed of 243 m/s (800 ft/s). Each pressure-flow characteristic curve shown is for a particular pitch setting (blade pitch at 3/4 radius point) from reverse to forward positions. Envelopes of total fan efficiency are also shown. In the steady state condition, the design point represents a cushion pressure of 175 N/cm^2 (250 psi) at 118 m^3/s (4170 ft^3/s) requiring 1790 kW (2400 HP). The dotted line represents a dynamic simulation where the pitch change is modulated to maintain (as near as possible) a constant cushion pressure. The dotted line would indicate achieving the desired flat pressure-flow characteristic while at the same time maintaining a high fan efficiency (and low lift power installed) at the design point and, furthermore, avoiding stall. It is seen that this also allows operation into the negative flow region. Reference 15 predicts heave acceleration levels below 0.10g if such a design were installed in a large hovercraft operating in sea states 4 to 6. The hysteresis curve shown in Figure 2.12 collapses to a single curve at higher speeds and lower sea state operating conditions.

The second development of active lift fan systems is by Aerojet Liquid Rocket Company. It is referred to as a variable geometry centrifugal fan design where, by means of valving, the flow of the fan is modulated to achieve the desired flat pressure-flow curve. Figure 2.13 shows the results of model tests in early 1974 using this type of valving. An isometric view of a fan based on these model tests is shown in Figure 2.14. The fan shown was designed for use in a 3000 tonne Surface Effect Ship (SES) (ref. 16). This particular

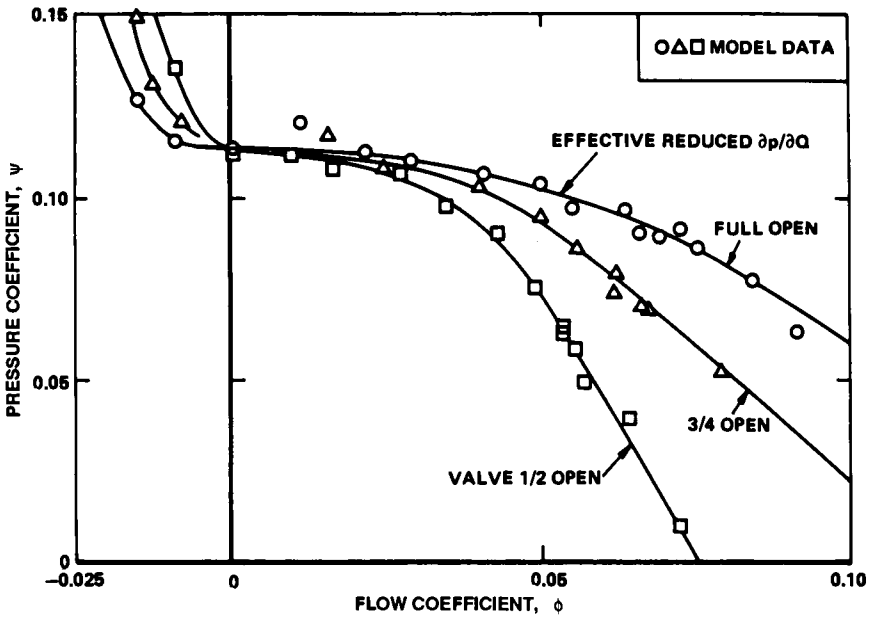

Fig. 2.13 Aerojet active centrifugal fan scheme.

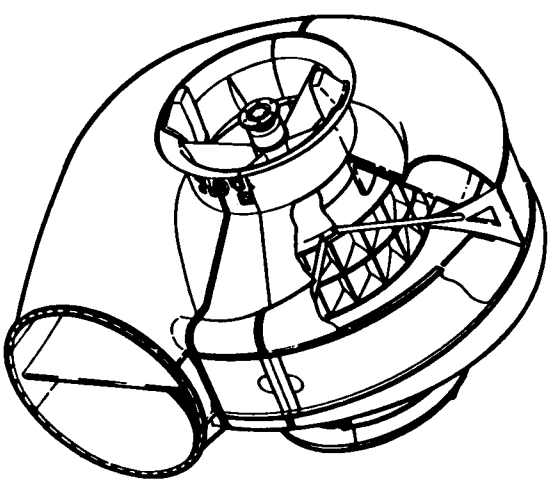

Fig. 2.14 Variable geometry centrifugal fan.

design would be one of six fans envisaged for such an SES. These variable geometry centrifugal fan systems would have 2.18 m (7.16 ft) diameter rotors installed in 4.63 m (15.25 ft) diameter housings or volutes, and incorporate the variable geometry feature (valve) shown on the intake to the fan housing in Figure 2.14. These particular fans incorporate double axial inlet design, airfoil shaped radial blades, constant velocity housings and a simple circular discharge. More details are provided in refs. 1 and 16.

While these developments offer benefits to hovercraft designed to operate in rough seas, none of these efficient means have as yet gone beyond the laboratory or prototype stage. The demands for low cost and ruggedness of operation have continued to result in either passive lift fan systems or simple venting systems.

2.2.2 Effect of Lift Fan Design on Heave Dynamics

The above sections have described the basic characteristics of each type of lift fans used in hovercraft. Reference was made to the impact of some of the design choices on the ride quality and heave response of a hovercraft operating in waves. While the dynamic stability characteristics of hovercraft operating at sea is a complex subject receiving much treatment in the literature, the basic characteristics can be described in simple form as guidance to the fan designer.

Consider a hovercraft operating over simple, regular seas where wave height h_w is given by:

$$h_w = A \cos (Kx - \omega t) \tag{2.19}$$

where A is the wave amplitude and the wave frequency in distance is $K = 2\pi/\lambda$ and in time is $\omega = 2\pi V/\lambda$; λ is the sea wavelength, V is the hovercraft forward speed, and x is the distance along the craft; therefore, $0 < x < L$, where L is the hovercraft cushion length. For small heave perturbations H about an equilibrium air gap h, a simple analysis yields the following equation:

$$\frac{d^2H}{dt^2} + 2\zeta\omega_n \frac{d}{dt}(H-h_w) + \omega_n^2(H-h_w) = 0 \tag{2.20}$$

where ω_n is the natural frequency in heave and ζ is the damping ratio. The cushion stiffness K_h and heave natural frequency ω_n of the hovercraft are given by:

$$K_h = S \frac{\partial P_c}{\partial h} \tag{2.21}$$

and

$$\omega_n = \left[(g/P_c) \frac{\partial P_c}{\partial h}\right]^{1/2} \tag{2.22}$$

where S is the cushion area and P_c is the cushion pressure. Mantle (refs. 17 and 18) showed that the solution to the heave motion of hovercraft in waves

could be expressed by:

$$H = MFA \cos(\phi - \omega t) \tag{2.23}$$

where M is the magnification ratio:

$$M = \{[1 - (\omega/\omega_n)^2]^2 + [2\zeta\omega/\omega_n]^2\}^{-1/2} \tag{2.24}$$

The function $F(L/\lambda)$ is that function which *converts* the moving waveform beneath the hovercraft to a piston-like forcing function that excites the heave motion. This function can be written:

$$F(L/\lambda) = \text{abs}[(\pi L/\lambda)^{-1}\sin(\pi L/\lambda)] \tag{2.25}$$

It has the property that it normalizes test data over a wide range of wave and craft geometries, such that $0.417 < L/\lambda < 1.668$ and $0.005 < A/\lambda < 0.020$. Mantle further showed that the damping ratio of a hovercraft operating in waves is given by:

$$\zeta = (\rho H/2P_c)^{1/2} F(t/h)/(Ch/S) \tag{2.26}$$

The function F(t/h) applies to peripheral jet hovercraft with a similar functional relationship as for plenum hovercraft. The key elements of each of these relationships relate to how the craft parameters of cushion pressure P_c, air gap Ch/S, craft size relative to sea state L/λ and other craft parameters influence the dynamic response of the hovercraft. It has been found (ref. 1) that data from small models heaving over water waves and over hard sinusoidal surfaces tend to collapse to a common non-dimensional base through use of the normalizing function $F(L/\lambda)$ and the natural frequency ω_n, respectively given by eqns. 2.25 and 2.22. Figure 2.15 shows this comparison of simple theory and model tests.

The influence of the lift fan characteristic on these craft dynamic response parameters can be seen from the small perturbation relationship for the cushion pressure:

$$P_c = P_o + (Q - Q_o)\frac{\partial P_c}{\partial Q} \tag{2.27}$$

where P_o, Q_o are the design operating point values of pressure and flow. This is shown diagrammatically in Figure 2.15. In this figure, the cushion slope $\partial P_c/\partial Q$ is less than the individual fan slope for the case of multiple fan installations operating in parallel. The lift fan slope discussed in the earlier sections is now seen to have a direct influence on the heave dynamics of the hovercraft. While not shown here, a similar relationship exists in both pitch and roll motions (see Chapter 1).

Breslin (ref. 19) expanded on the above analysis by including the effect of the lift fan slope and showed that the cushion stiffness K_h of eqn. (2.21) would now become:

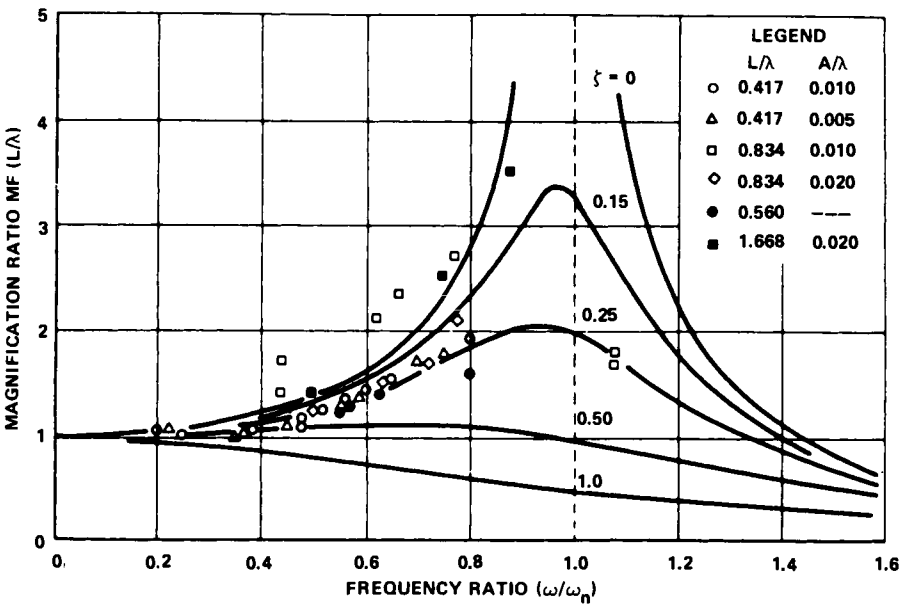

Fig. 2.15 Normalized heave response over waves.

$$K_h = S(Q/h)\frac{\partial P_c}{\partial Q}\left[1 + (Q/P_c)\frac{\partial P_c}{\partial Q}\right]^{-1} \tag{2.28}$$

and that the natural frequency in heave ω_n would be given by:

$$\omega_n = \left\{(g/h)(Q/P_c)\frac{\partial P_c}{\partial Q}\left[1 + (Q/P_c)\frac{\partial P_c}{\partial Q}\right]^{-1}\right\}^{1/2} \tag{2.29}$$

Although Breslin was specifically analyzing the case of an SES, it can be taken that, to a first order, the results apply equally well to hovercraft.

An analysis of the problems of scaling from model scale to full scale with these relationships is treated in ref. 1, as are the problems of incorporating the effects of skirt stiffness or compliance. While all these factors are real and must be considered in any particular design, the above relationships are valid and provide the fan designer guidelines in any systems engineering approach to the design of lift fan systems.

2.2.3 Skirt Systems

In Chapter 1, a description was provided of the basic types of skirt systems that have been used in hovercraft design (see Figure 1.4). Hovercraft skirts were originally developed to be flexible appendages to give obstacle (wave) clearance with low lift power expenditure. Indeed, because of the high

power requirements for anything other than small air gaps h, the skirt had to be invented and developed to avoid an early demise of hovercraft. The skirt has now become an integral part of the suspension system of the hovercraft, with its own characteristics of stiffness and damping that contribute to the hovercraft's response, like the lift fan system. Additionally, some skirt designs have also contributed to the control of the hovercraft in all modes. An example is that, by tucking its skirt underneath in a controlled manner, a hovercraft can be made to bank into a turn and thereby improve its maneuverability. Bag-finger, loop-segment, jupe and pericell are the main types of skirt systems used in hovercraft. Some of the key design features are summarized here.

(i) Bag-finger. This type of skirt system has seen the most use in hovercraft design. It was pioneered by British Hovercraft Corporation following earlier finger developments in England by Vickers and the loop-segment concept developed by Hovercraft Development Limited (HDL). Crewe (ref. 20) and Wheeler (ref. 21) provide a historical summary of the bag-finger skirt development. This particular form of skirt system has been used successfully on the early BHC hovercraft SR.N5, SR.N6 and SR.N4. It has been used also on the BH.7 and most recently the AP.1-88 hovercraft. In the United States, the bag-finger skirt system was used on the JEFF(B) prototype and is now in use on the production versions of LCAC.

Figure 2.16 shows the development history since skirts were first used on the SR.N1, in 1960, up to the introduction of the bag-finger skirt on the SR.N5, in 1966. Then, development and improvement of various features of the bag-finger skirt continued through to the present day. The finger, as it was first introduced, was a simple version of the peripheral jet, replacing the original holding chains (shown as dotted lines in Figure 2.16), with a simple piece of material. This change is important in that it marked the conversion of a peripheral jet craft into a form of plenum craft. It also separated the main bag from the lower edges that wore away during operation. The fingers could then be replaced, after wear, without having to replace or repair the main bag.

In 1967, the skirt design was modified to give a more free supporting shape to the bags and the fingers were lengthened to become approximately 50 percent of the cushion depth. This decreased the stiffness of the fingers, lowered the drag and provided a softer ride. In the late 1970s, the SR.N4 hovercraft was *stretched* by 50 percent to increased the craft weight from 200 to 300 tonnes. A major design change in skirt technology was required to accomplish this configuration and weight change. This change resulted in the introduction of the *fully responsive* skirt. This is a deep fingered (greater than 70 percent), low pressure ratio and low drag skirt. These improvements are shown in Figure 2.17 that traces the design changes from 1964 through to the fully-

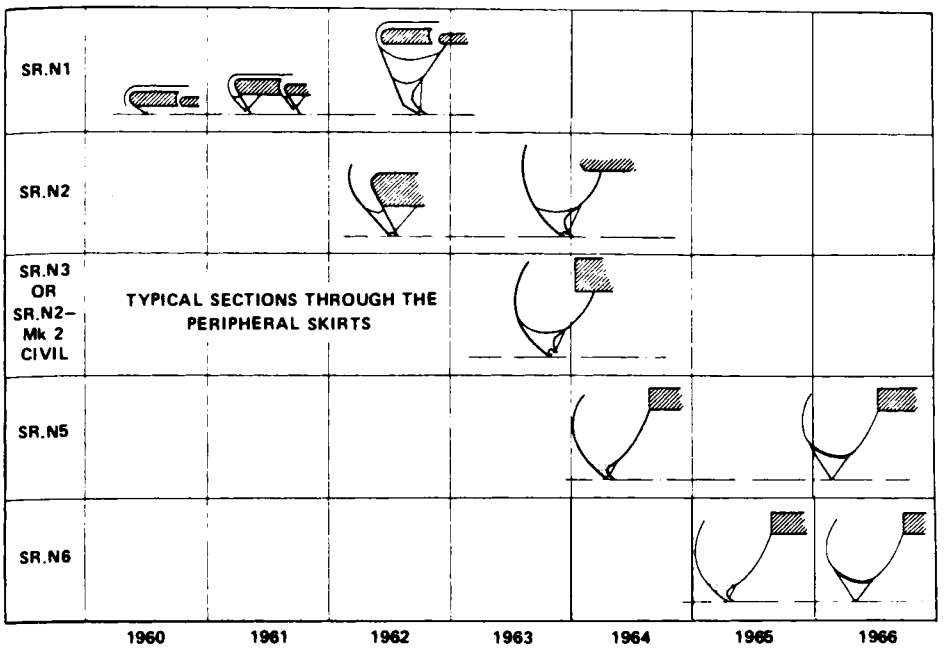

Fig. 2.16 Development of bag-finger skirt, 1960-66.

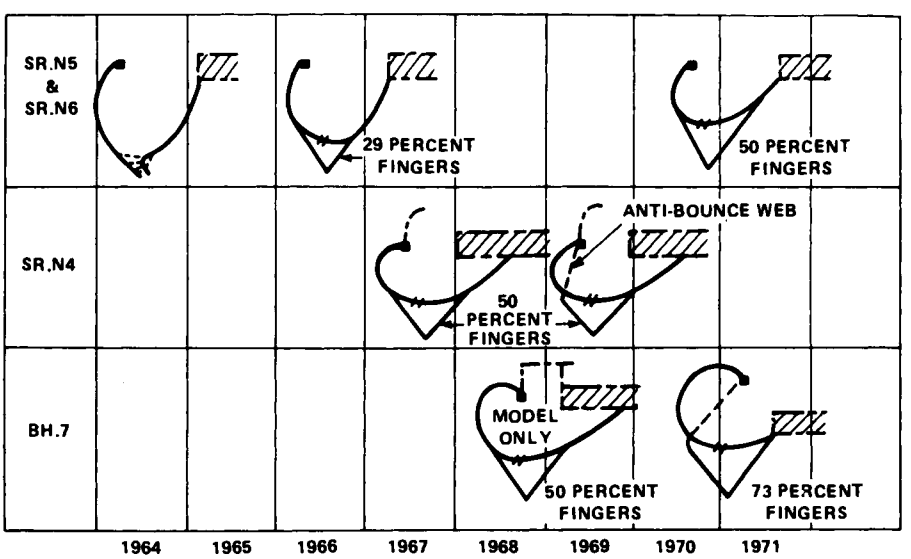

Fig. 2.17 Developments in figure length.

responsive or deep-finger skirts in 1970, used first on the BH.7 hovercraft. It was found that this change resulted in a halving of the specific power requirements over earlier hovercraft. This contributed to the AP.1-88 hovercraft's having one-third the acquisition and operating cost of its earlier counterpart, the SR.N6.

The BH.7 skirt system that is representative of the current form of bag-finger skirt system is shown in Figure 2.18. This figure is useful in that it is representative of most of today's bag-finger skirt systems and provides the nomenclature used to describe their various parts. It shows the bags and it also shows how the cushion is compartmented through use of longi

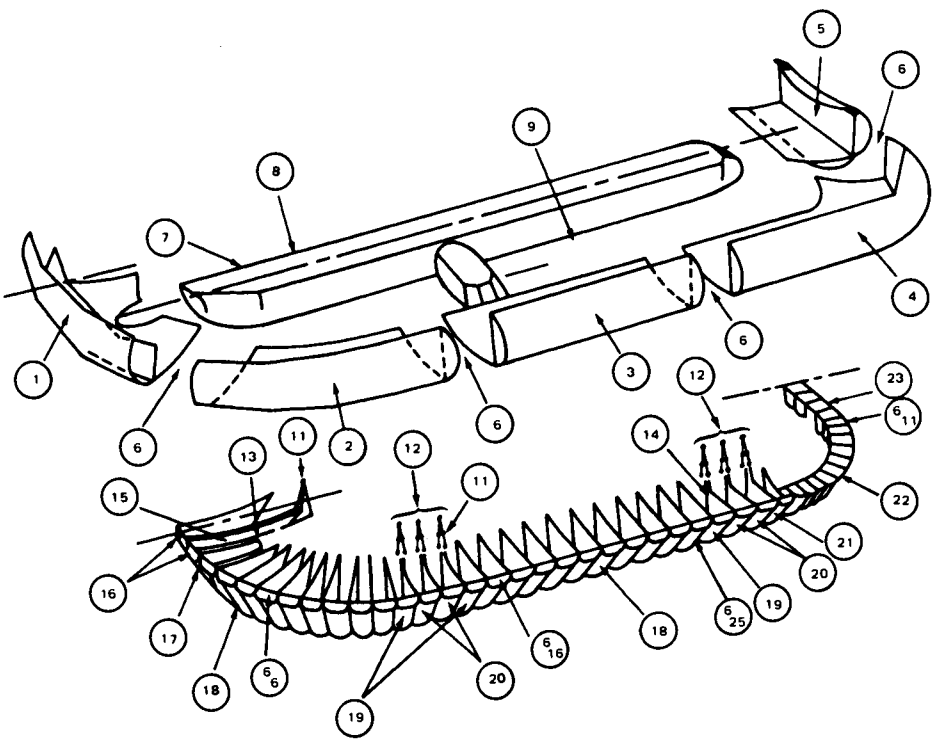

1. BOW SEGMENT
2. FORWARD CORNER SEGMENT
3. SIDE SEGMENT
4. AFT CORNER SEGMENT
5. REAR SEGMENT
6. BREAKDOWN JOINTS (SUBSCRIPT DENOTES FINGERNUMBER)
7. HINGES ON SKIRTS
8. HINGE RING
9. KEEL
10. STABILITY TRUNK
11. BONIO'S
12. SKIRT LIFTS
13. FINGER BAG ATTACHMENT FLAP WITH STANDARD FINGERS
14. FINGER BAG ATTACHMENT FLAP WITH SKIRT LIFT FINGERS
15. BOW FINGER ATTACHMENT FLAP
16. BOW FINGERS
17. NEW STANDARD BOW FINGER
18. BASIC FINGER
19. HANDED SKIRT LIFT FINGERS
20. STANDARD SKIRT LIFT FINGERS
21. NEW STANDARD SKIRT LIFT FINGERS (AFT)
22. TAPERED CONE
23. REAR CONE

Fig. 2.18 BH.7 Mk 2 bag-finger skirt system.

tudinal and transverse stability keels. Compartmentation is a logical way of dividing the cushion into *pads* of separate cushions to provide stability in pitch and roll. Figure 2.19 shows the various compartmentation methods developed since the early days. The fingers that are attached to the bags are usually removable for repair or replacement. The shape of a typical finger is shown in Figure 2.20.

In designing the bag-finger skirt, it is necessary to analyze the forces working on the skirt. Some of the basic forces and dimensions are shown in Figure 2.21. For simplicity, it is convenient to consider the two-dimensional section of the bag-finger. Most analyses are based on a two-dimensional treatment although some digital computation techniques have been used to design the skirt system in three-dimensions.

In the treatment of the bag, the hoop tension T per unit width is given by the simple relationship:

$$T = P_b R_1 \tag{2.30}$$

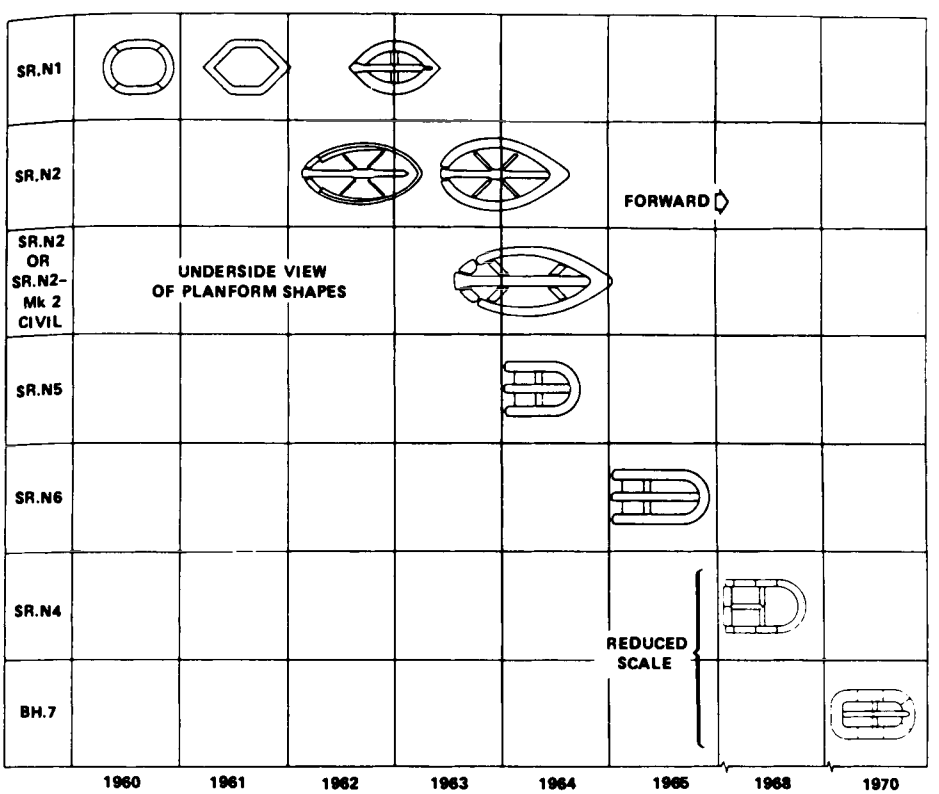

Fig. 2.19 Compartmentation development.

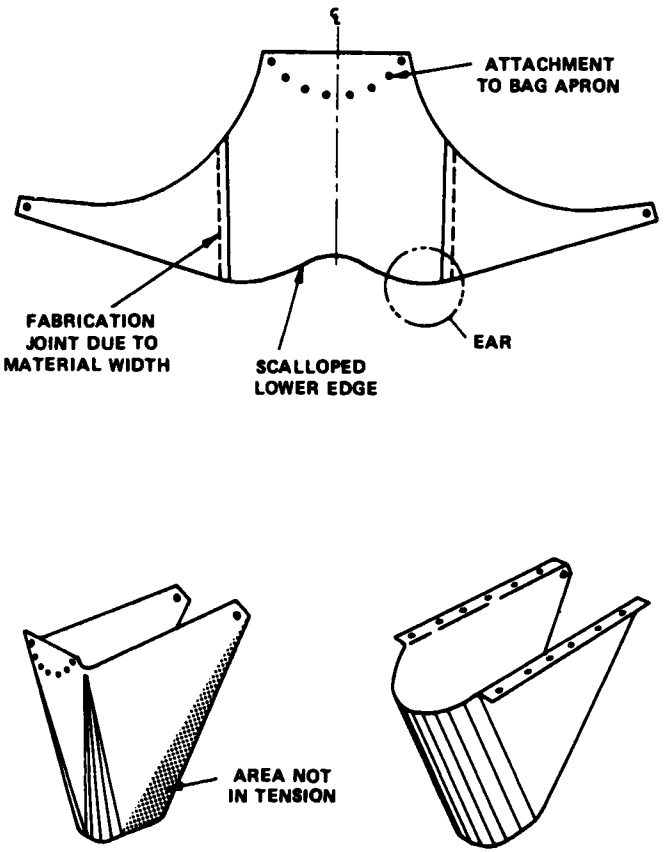

Fig. 2.20 Typical finger and attachment.

where P_b is the bag pressure and R_1 is the local radius. Also from Figure 2.21, for no discontinuity within the bag, the tension per unit width is given by:

$$T = (P_b - P_c)\ R_2 \tag{2.31}$$

Hence, the bag shape can be determined from eqns. (2.30) and (2.31) to yield the relationship:

$$R_1/R_2 = [(P_b/P_c - 1]/(P_b/P_c) \tag{2.32}$$

Typically, the pressure ratio P_b/P_c from bag to cushion varies in hovercraft design between the limits:

$$1.10 < P_b/P_c < 1.8 \tag{2.33}$$

The tendency is toward the lower values for improved dynamic response of the hovercraft when operating in waves. While not developed here, it can be shown

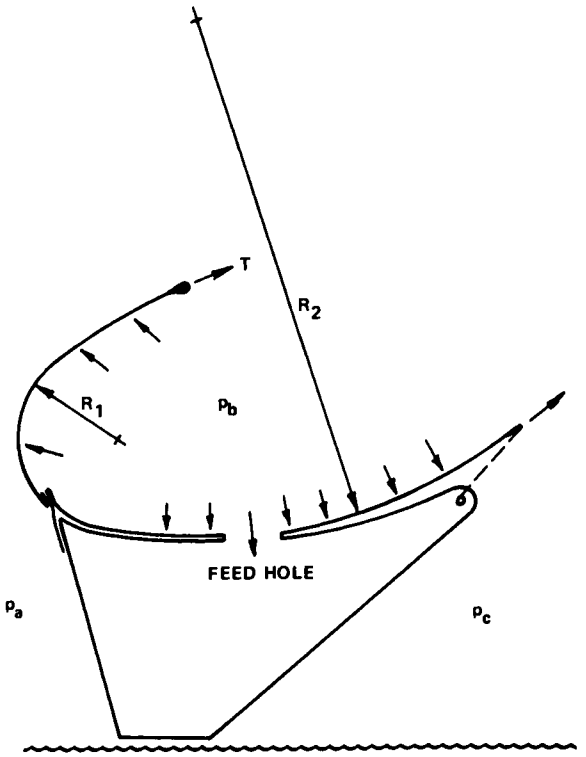

Fig. 2.21 Two-dimensional bag-finger.

that the motion of the finger can also be determined with reasonable accuracy, at least in the two-dimensional treatment. A recent analysis of the static forces and geometry of bag-finger skirts is provided by Xie and Hua (ref. 22). Bag-finger skirts are analysed extensively in Chapter 13.

The dynamic forces acting on the finger are more complex and Hogben (ref. 23) showed early in the design of hovercraft that the acceleration n of the lower edge of a finger following a sinusoidal waveform is given by:

$$n = 2\pi^2(h_w/\lambda^2)[V+(g\lambda/2\pi)^{1/2}]^2 \qquad (2.34)$$

where g is acceleration due to gravity, h_w is the wave height, λ is the wave length, and V is the craft's forward speed. For the simple case of sinusoial motion, on a hovercraft traveling at 31 m/s (60 knots) in 2m (6 ft) waves of wavelength 62m (120 ft) the lower finger edges would experience accelerations of 3g. This simple calculation does not include the snapback action, due to cushion pressure, which can occur after the finger has moved up by wave action; in this case, even higher accelerations can occur. Values of 100g have been measured in the snapback motion. Such accelerations and forces contribute

significantly to the wear of fingers. A more detailed treatment of the bag-finger skirt geometries, the dynamic characteristics of skirt *bounce* and finger oscillation may be found in ref. 1 and Chapter 13, but the essential features of the bag-finger skirt are as described here.

(ii) Loop-segment skirt. The loop-segment (see Chapter 1, Fig. 1.4) was developed by Hovercraft Development Limited (HDL) in England. It is similar to the bag-finger skirt except that the bag is replaced by an open loop. This means that the pressure ratio $P_b/P_c \approx 1$ and provides for much softer ride than the bag-finger skirt. Instead of compartmentation for stability, the loop-segment relies on cushion area change to provide for shifts in the cushion center of pressure. This form of skirt was developed by HDL in the period 1961-1965. An advantage of this design is that, as a softer spring, the fingers create a slightly lower rough-water drag. Also, because there is virtually no pressure drop from the loop into the fingers and cushion, the lift system efficiency is higher. A disadvantage is that it is more susceptible to tuck-under than the bag-finger and thus potentially more hazardous from the viewpoint of dynamic stability in pitch and roll. The stability is regained for the loop-segment skirt by having a higher hinge line than the equivalent bag-finger skirt. The loop-segment skirt was employed successfully on such hovercraft as the VT.1 and the VT.2.

(iii) Jupe skirt. The principle of separately-fed multiple-plenum systems originated with the late Jean Bertin in France, in 1957. The concept, from Bertin's patents, is that craft stability can be achieved by means of several slightly conical skirt forms. The basic features of the jupe skirt are shown in Figure 2.22. The half cone angle varies with the design but is usually no greater than 5-10 degrees. For best performance and stability of shape, the jupe proportions are:

$$0.25 < h_s/D < 0.80 \tag{2.35}$$

where h_s is the jupe height and D is the major diameter of the jupe. If the jupe is inclined at an angle α, then Bertin (ref. 24) shows that the values of the half-cone angle β yield a basically very simple system. However, it appears to suffer, in its original form, by the inefficient use of available cushion area, and, through the use of multiple cushions, by an associated increase in hemline length. Bertin solved this problem by adding a wrap-around skirt (see Figure 2.22). It was found that the relative position of the height of the jupes and the height of the wrap-around skirt had a marked effect on the heave stiffness of the hovercraft. If the jupes were longer than the wrap-around skirt, the heave stiffness was high, and if the jupes were shorter than the wrap-around or peripheral skirt then the heave stiffness was low. Accordingly, Bertin introduced a height adjustor by way of a pressurized bag (see Figure 2.22) that could be used by the operator to set the degree of stiffness

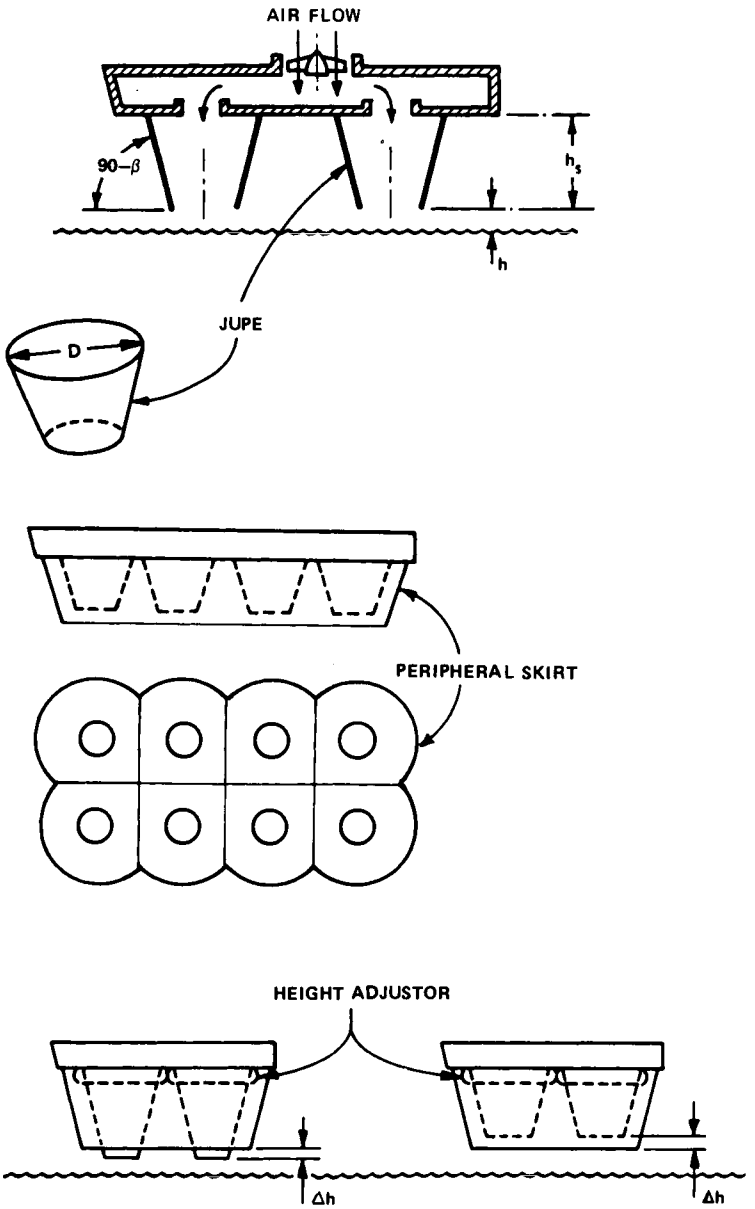

Fig. 2.22 Some jupe skirt characteristics.

desired in the cushion. This skirt system has been used successfully on the SEDAM hovercraft N.300 and the later N.500.

(iv) Pericell skirt system. The pericell skirt system is a combination of the bag-finger and the jupe. It has been used successfully on the LCAC proto-

type JEFF(A) and the SES-100A air cushion craft. As shown in Chapter 1, Figure 1.4, the pericell skirt is made up of a series of jupes attached to a peripheral bag. Figure 2.23 shows the geometry as it was applied to the JEFF(A). The pericell skirt tends to be stiffer than the bag-finger skirt. Different geometric proportions yield quite different stability characteristics. Figure 2.24 shows the results of a *deep pericell* developed specifically to provide

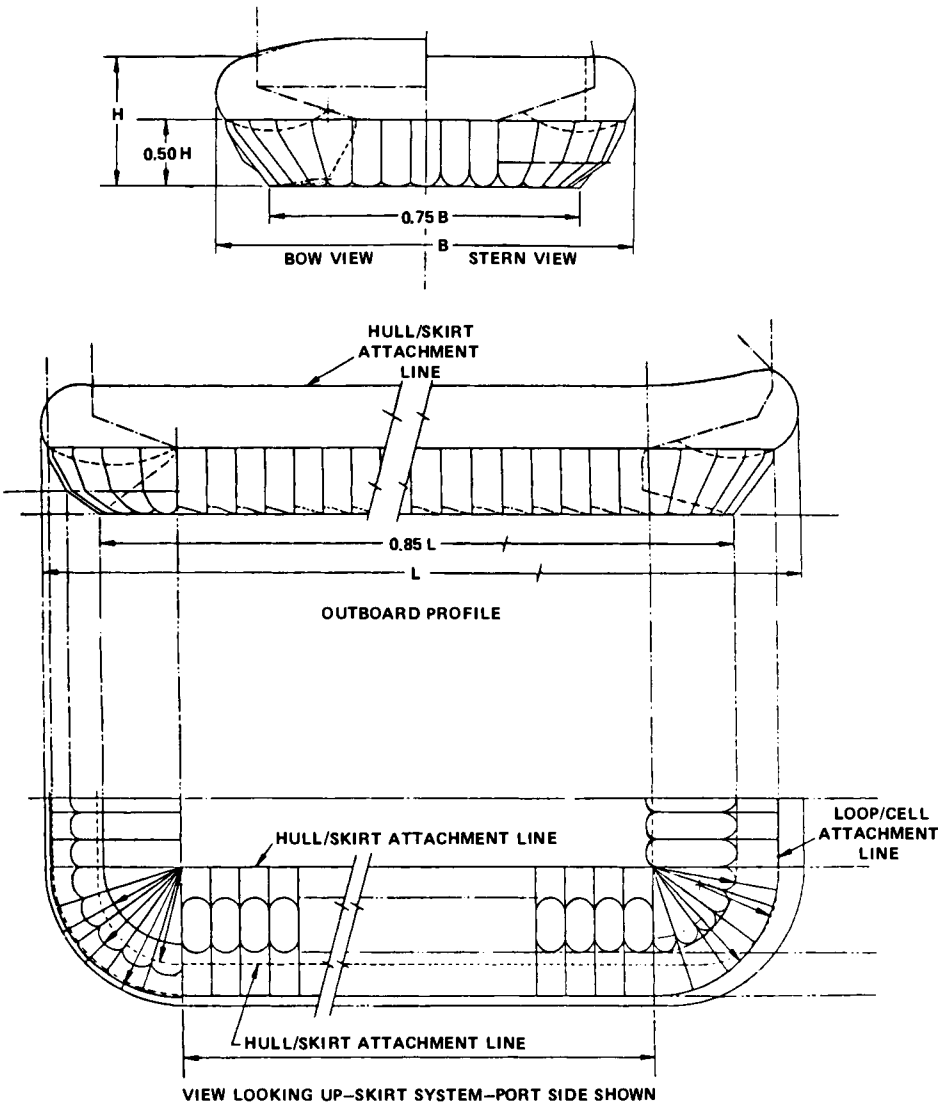

Fig. 2.23 JEFF(A) pericell skirt system.

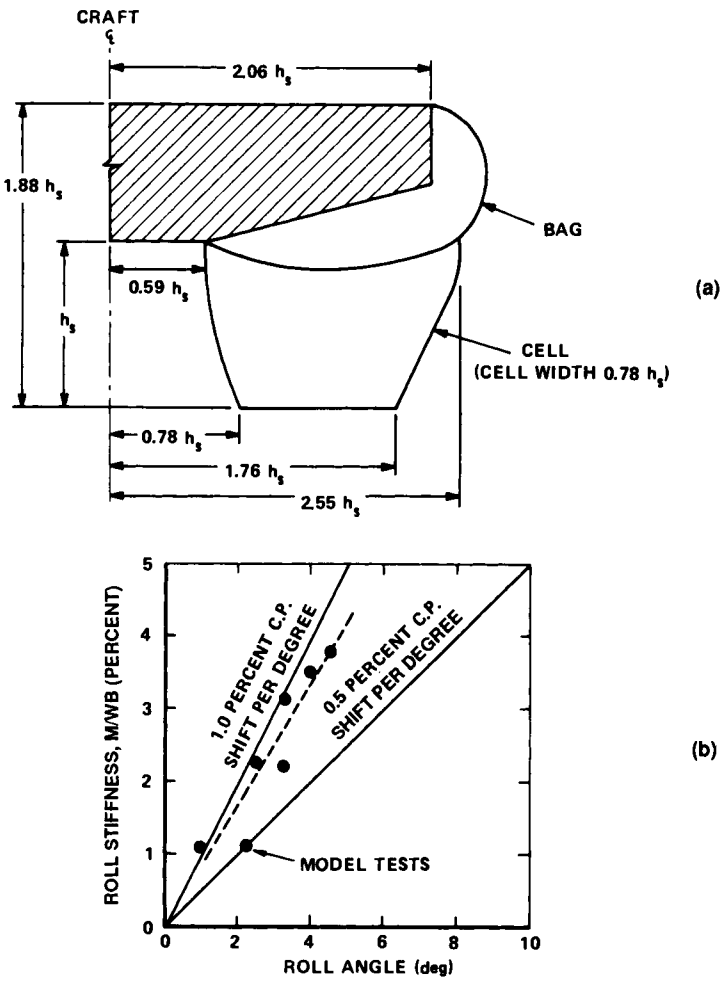

Fig. 2.24 Deep pericell skirt: (a) geometry; (b) roll stiffness characteristics.

higher obstacle clearance than normal for a given size of hovercraft. Specific descriptions of this skirt form as applied to different craft found in ref. 1. Zheng and Ma (ref. 25) provide a recent analysis of the forces and geometrical characteristics of the pericell skirt system.

2.3 PROPULSION SYSTEM

The propulsion system in hovercraft has taken several different forms since the early development years, from the original air jet propulsion to the air propellers used in most of today's hovercraft. Other means of propulsion

include water propulsion, track and wheel, and other novel forms depending on the particular application.

The propulsion system is made up of a power source (engine), some form of transmission, and a propulsor of one form or another. Regardless of the type of propulsion system used or the selection of hardware (e.g. gas turbines or diesels, and fixed pitch propellers or other propulsors), the propulsion system must be capable of performing the following functions: a) provide sufficient thrust to overcome hump drag D_H, b) have sufficient thrust to provide a predetermined acceleration capability, c) generate sufficient thrust to reach and sustain cruise speed, d) provide sufficient thrust, efficiency and fuel economy to meet some specified range or endurance, e) if integrated with the control system, provide adequate thrust forces to give the hovercraft control and maneuverability, and f) if required, provide sufficient thrust for a grade climbing capability. Each of the above requirements depends on several factors, such as environmental (sea state, terrain) and operational (noise level, reliability, etc.) constraints, and design constraints, such as space and weight limitations for the propulsion system.

2.3.1 Thrust and Drag

Complete derivations of the thrust and drag characteristics of hovercraft are provided in the literature. See for example, Elsley and Devereux (ref. 26) and Mantle (ref. 1) for detailed treatments, including the basic equations and data on thrust and drag from both theory and practice. However, there are some governing equations pertaining to the design of hovercraft that are useful to summarize for design purposes.

While the detailed shape of the thrust and drag curves for any particular hovercraft vary, Figure 2.25 shows the typical drag curves, including the characteristic *humps* at low speeds. The monotonically decreasing thrust curve is also typical of a conventional air screw or propeller. In the literature, discussions on *hump drag* usually refer to the *primary hump* that occurs in the vicinity of a Froude Number value of 0.60, analogous to the planing speed of conventional planing monohulls. *Secondary hump* (shown to the left of the primary hump in Figure 2.25) and *tertiary hump* (not shown) occur at successively lower speeds. Such humps are predicted by theory and are experienced in practice more at the primary hump than at the higher order humps. Because of the shape of the thrust curve and the relative magnitude of the primary hump, the *getting over hump* expression usually refers to the primary hump. This particular phenomenon in the shape of the drag curve is caused by the resistance of the standing wave ahead of the water depression caused by the cushion pressure. As the water depression generated by the cushion pressure moves forward and gains momentum through action of the hovercraft's propulsion system, the standing wave first builds up and then, as the water depression

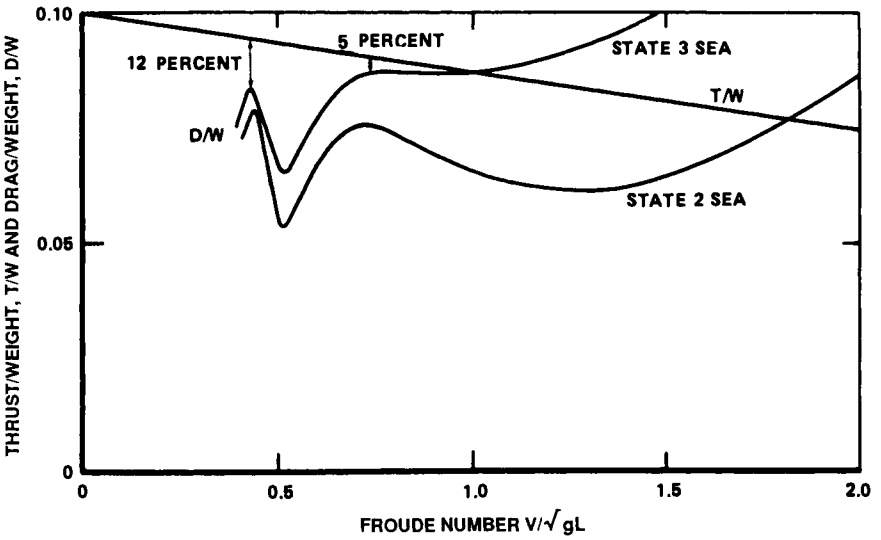

Fig. 2.25 Typical thrust and drag curves of high density hovercraft (P_c/L = 1.3).

approaches planing speed, the standing wave reaches a maximum and then falls away. This point in the drag curve is referred to as *hump speed* , V_H. While the actual speed of any particular hovercraft will vary due to craft geometry, cushion density, and other factors (such as shallow water effects), it can usually be assumed that $0.50 < V_H < 1.0$.

As mentioned earlier, detailed treatments of thrust and drag predictions for hovercraft may be found in the literature. It will be useful, however, to summarize certain *rules of thumb* that have developed from over thirty years of hovercraft design and operation. Before proceeding, let us consider the five main contributors to hovercraft drag: momentum drag, wave drag, skirt drag, spray drag and aerodynamic drag. Each of these contributors or components vary with different environmental and craft parameters.

(i) Momentum drag D_M. This drag is due to the rate of change of momentum required to accelerate the cushion airflow Q to the craft's velocity V. Thus,

$$D_M = f(Q,V) \tag{2.36}$$

where f( ) signifies *function of*.

(ii) Wave drag D_W. The wave resistance of the moving water depression beneath the hovercraft has been discussed and several analyses have been provided for its prediction. Barratt (ref. 27), Newman and Poole (ref. 28) and Doctors (ref. 29) have provided the particular treatments applicable to hovercraft design. Figure 2.26 shows how the wave drag varies as a function of key

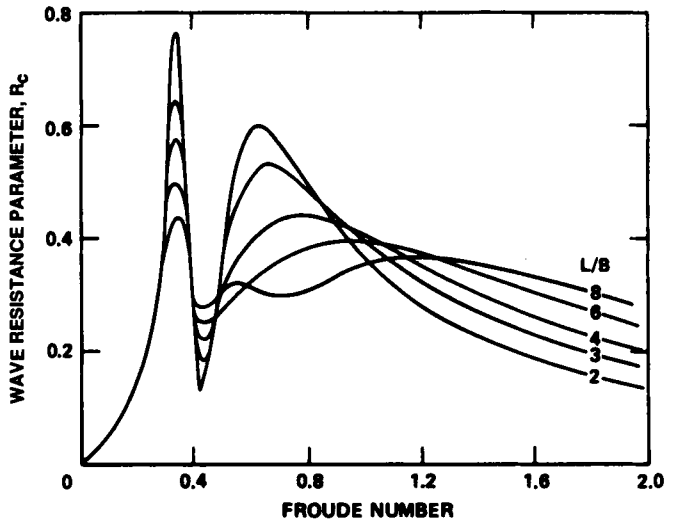

(a)

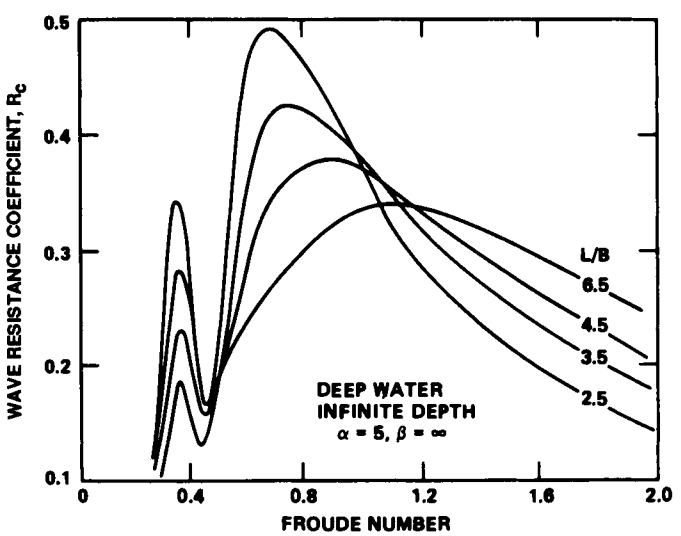

(b)

Fig. 2.26 Wave resistance coefficient, $R_c = (D_W/W)/[(4/\rho_w g)(P/L)]$, where D_w = wave drag of air cushion; (a) Newman and Poole theory (unshaped); (b) Doctors theory (shaped).

parameters. From such treatments, the wave drag D_W is a complex function:

$$D_W = f(W, P_c/L, L/B, F_N) \tag{2.37}$$

with additional effects due to the shape of the cushion and water depth. Using Barratt's theory, Mantle (ref. 1) showed how the speed at which the wave drag

is a maximum (primary hump speed V_H) varies with cushion density P_c/L, craft size L and cushion length/beam ratio L/B. Early model experiments confirmed Barratt's theory. Figure 2.27 shows these results.

(iii) Skirt drag D_{SK}. Various treatments have been put forward to account for the drag of skirts in rough water, over ice and over rough terrain. The paucity of reliable data from controlled experiments has left a legacy of not very predictable levels of skirt drag (see ref. 1 for the various available theories and data). Generally, skirt drag D_{SK} is a function of the following parameters:

$$D_{SK} = f(P_c/L,\ h/L,\ L/B,\ h_w/L,\ V) \tag{2.38}$$

In addition, the various geometrical complexities of skirt geometry (e.g., finger length and pericell configuration) play an important role in skirt drag.

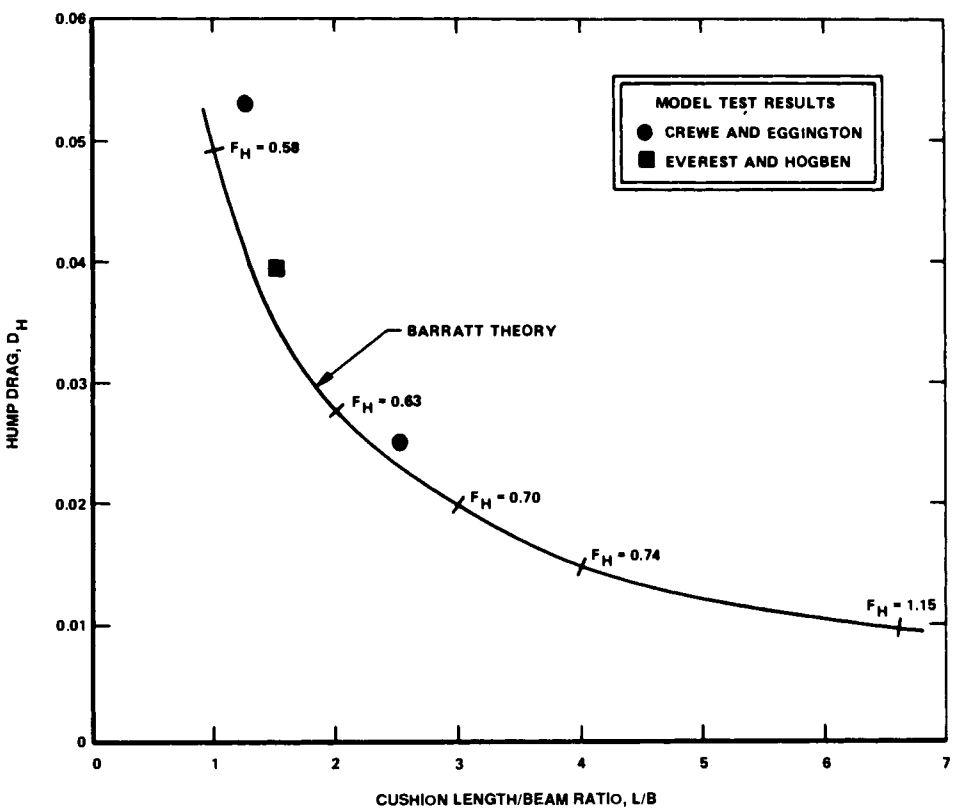

Fig. 2.27 Normalized deep water hump drag, $D_{WH}(L/B^{1/2}/[(P_c/L)^2L^3]$, where D_{WH} is the deep water hump drag; F_{NH} is the Froude Number at hump speed.

(iv) Spray drag D_s. This component of drag is highly dependent on skirt geometry (e.g., use of spray skirt aprons) and operational techniques. It is difficult to predict, so that most treatments resort to additive *spray factor* margins in the total drag prediction.

(v) Aerodynamic drag D_{aero}. The aerodynamic drag of a hovercraft is easily predicted as a function of its shape S and velocity V:

$$D_{aero} = f(S, V) \tag{2.39}$$

The addition of the above drag components results in the drag curves shown in Figure 2.25. For the purposes of addressing the needs of a propulsion system design, some *rules of thumb* are summarized below in two general areas of concern: a) up-to-hump speed, and (b) above hump speed.

2.3.2 Up–To–Hump Speed Design Rules

While the analysis of the drag curves up to the primary hump speed is somewhat cumbersome, there are some basic needs of the propulsion system designer that can be easily satisfied. In setting the thrust requirements for the propulsion system, the following questions must be answered:

a) What thrust margin is required to *get over* hump in the design sea state?

b) How fast is it required to accelerate past hump speed?

The answer to the first will determine the *minimum*, or *go - no go*, level of thrust required. The answer to the second question will determine the *maximum* value of thrust level, depending on the need to have either a sluggish craft or a *hot rod* craft as it accelerates past hump speed. Economics and operational maneuverability limits influence this answer.

The answer to question a) is still the subject of empirical treatment. Figure 2.28 shows the results of many hovercraft designs and operational craft in terms of rough water drag increments in different sea states. Today's hovercraft tend to congregate around the upper line, such that the following expression can be written:

$$D_{rough}/D_{calm})_{hump} = 1 + K\, h_w\, W^{-1/3} \tag{2.40}$$

where D_{rough} and D_{calm} are the hump drags in rough and calm waters, respectively, h_w is the significant wave height, and W is the craft displacement (tonne). The factor K represents the area of uncertainty but good practice indicates that K = 1.40 applies to a hovercraft with good handling qualities as it accelerates past hump speed. If the thrust margin over drag at hump speed is expressed by:

$$n = [(T-D_{calm}/W)]_{hump} \tag{2.41}$$

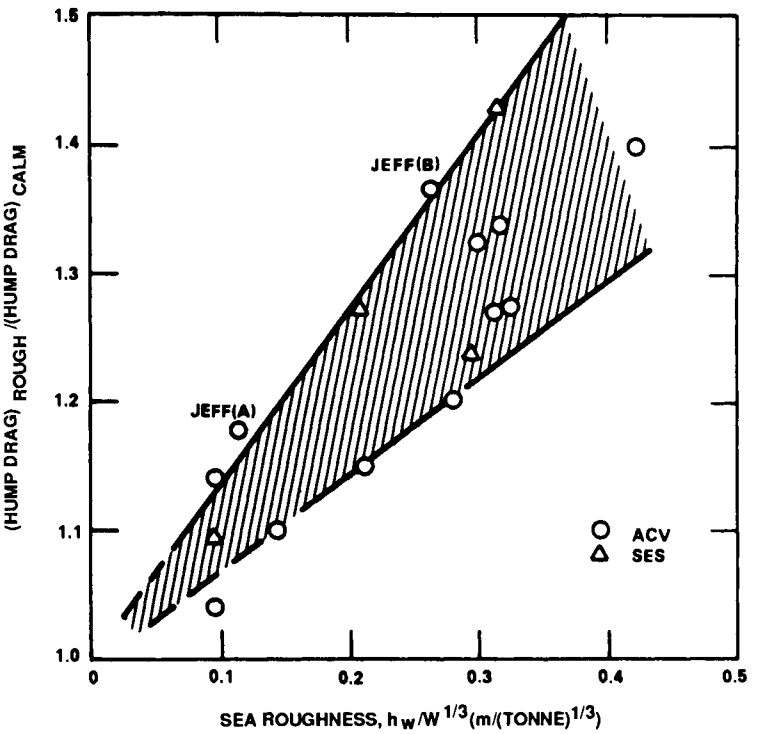

Fig. 2.28 Hump drag in rough water.

then, by combining equations (2.40) and (2.41), the following governing equation for the thrust margin can be derived:

$$n = K[D_{calm}/W]_{hump}[h_w/W^{1/3}]_{limit} \tag{2.42}$$

This relationship expresses the thrust margin n in terms of known design parameters of the hovercraft, the limiting sea state in which it is constrained to operate, and the empirical factor K to account for rough water effects. The prediction of the calm water drag D_{calm} is provided in the literature as described earlier.

The answer to question b) can be determined from the solution to Newton's Second Law of Motion which, in this context, can be written:

$$T-D = (W/g)\frac{dV}{dt} \tag{2.43}$$

By transposing and expressing this relationship in terms of the time t_H required to accelerate to hump speed V_H, we obtain the simple relationship:

$$t_H = (1/g) \int_0^{V_H} [W/(T-D)]dV \tag{2.44}$$

This result can be expressed in non-dimensional form:

$$\tau = \int_0^1 [W/(T-D)]dv \tag{2.45a}$$

where

$$\tau = gt_H/V_H \tag{2.45b}$$

and

$$v = V/V_H \tag{2.45c}$$

Because of the complex shape of the drag curve below hump speed (see Figure 2.26), the integrand in equation (2.45a) is not amenable to analytical integration. Using numerical integration techniques, Mantle (Ref. 1) analyzed many hovercraft, including both design studies and operational craft. He determined general trends of those craft which were deemed to have good handling qualities while accelerating to hump speed. The results are shown in Figure 2.29. A cross-plot of Figure 2.29 expresses the results in terms of acceleration times, thrust margins and size of craft. This is shown in Figure 2.30.

The characterization of the acceleration time t_H depends on the size of hovercraft. For $W \leq 200$ tonnes, Figure 2.30 provides the numerical values of the thrust margins and acceleration times. For $W > 200$ tonnes, a good approximation is provided by:

$$n = 0.05 - 0.0014\ \tau \tag{2.46}$$

An example, taken from these results, illustrates the importance of the thrust level selection for a hovercraft. From Figure 2.29, for a 150 tonne hovercraft with a thrust margin $(T-D)/W = 0.04$, the nomdimensional time τ to accelerate to hump speed is 15 seconds. If the thrust margin is cut in half to 0.02, the nondimensional time to accelerate is 20 seconds. Given such tools, the designer can select an appropriate propulsion system.

2.3.3 Above Hump Speed Design Rules

Above the hump speed V_H, the shape of the drag curve becomes more amenable to analysis. The design criteria are different and are based on the following two main requirements: a) to maintain efficient cruise, and b) to achieve some desired maximum speed (in a given sea state or other environmental condition). Usually, except in special cases of sport hovercraft and other uses, the governing requirement is the most efficient cruise speed.

From classifical aerodynamics, the range R (km) of any fuel-consuming device can be determined from the Breguet equation:

$$R = (602/sfc)(WV/P)\ell n(W_i/W) \tag{2.47}$$

where sfc is the specific fuel consumption of the engine(s), WV/P is the transport efficiency expressed as a function of craft weight W, craft speed V, and total onboard power P, W_i is craft weight at start of cruise, and W is weight

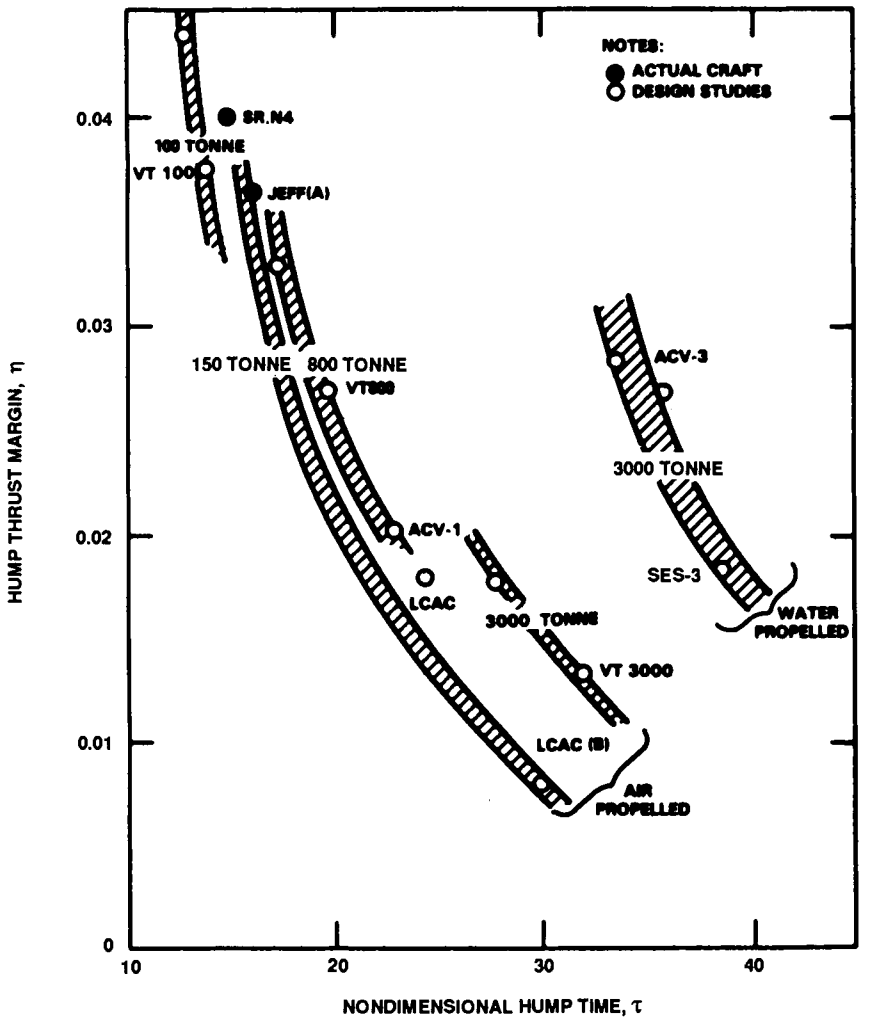

Fig. 2.29 Thrust margin and hump time.

at end of cruise (= W_i less fuel consumed). In terms of the parameters important to hovercraft, this equation can be rewritten:

$$R = (602\ \eta_p/sfc)(L/D)_{eff}\ell n(W_i/W) \tag{2.48}$$

where the effective lift/drag ratio $(L/D)_{eff}$ can be expressed in terms of the hovercraft parameters, as follows:

$$(L/D)_{eff} = W/[D+(\eta_p/\eta_L)(P_cQ/V)] \tag{2.49}$$

where W is craft displacement, D is drag at cruise speed, η_p and η_L are effic-

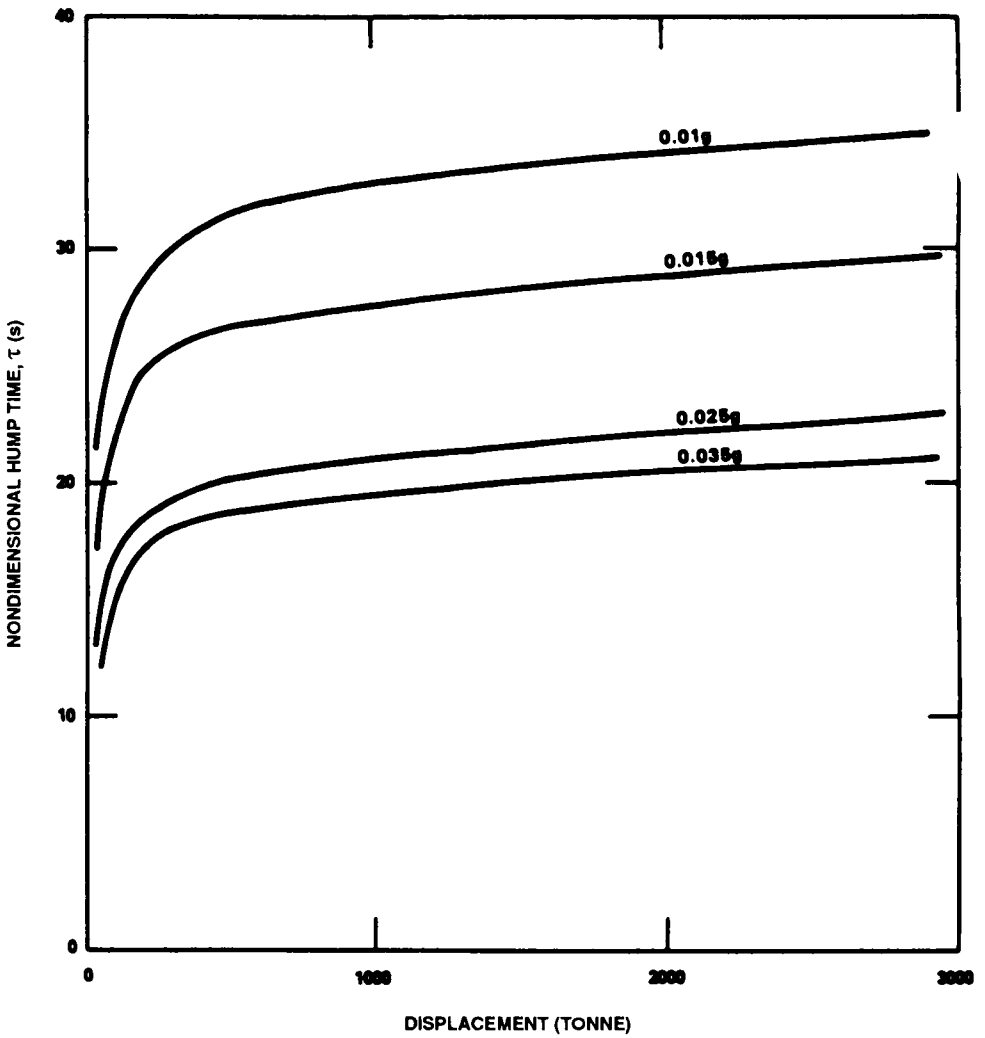

Fig. 2.30 Hump time and displacement for air propelled ACV's accelerating over calm, deep water.

iencies of propulsion and lift systems, P_c and Q are cushion pressure and flow at cruise speed, and V is cruise speed.

Above hump speed, certain simplifying assumptions can be made as to the variation of drag with speed. For example, the wave drag (shown in Figure 2.26) reduces to an analytical function of speed:

$$D_w = C/F_N^2, \; F_N > 1 \qquad (2.50)$$

where C is a constant. By means of such analytical expressions for the various

drag components contributing to the total drag of hovercraft, Mantle (ref. 1) derived expressions for the effective lift/drag ratio L/D_{eff} and made comparisons with results of operational hovercraft operating at different hovergaps h/L. Figure 2.31 shows these results plotted against the nondimensional speed parameter k. As the hovergap h/L is reduced to very low values, a simple result appears for the lift/drag ratio; specifically, for h/L = 0:

$$(L/D)_{eff} = k/(C_{Do}k + \kappa) \tag{2.51a}$$

where C_{Do} is the aerodynamic profile drag of the hovercraft, k is the nondimensional speed given by

$$k = 0.5\ \rho V^2/P_c \tag{2.51b}$$

and κ is the *induced drag* factor given by

$$\kappa = 1.2(\rho/\rho_w)/(L/B)^{1/2} \tag{2.51c}$$

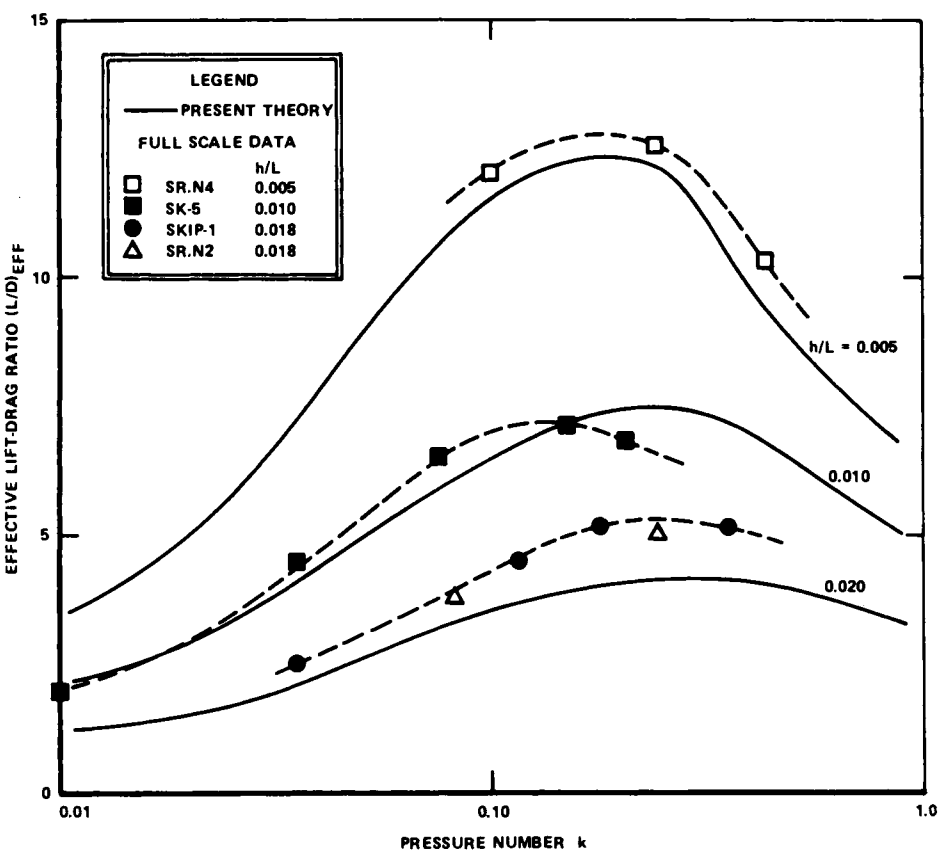

Fig. 2.31 Typical effective lift/drag ratio.

where ρ and ρ_w are the densities of air and water respectively. The speed for best range is then given by:

$$k = \kappa/C_{Do} \tag{2.52}$$

which can be rewritten in dimensional terms:

$$V_{cruise} = (2/\rho_w)^{1/2}\{1.2/[C_{Do}(L/B)^{1/2}]\}^{1/2}P_c^{\ 1/2} \tag{2.53}$$

This simple result for the cruise speed of a hovercraft shows the relative importance of the aerodynamic resistance C_{Do}, the craft geometry L/B and the cushion pressure P_c. While equation (2.53) was derived for the special case of zero air gap (h/L = 0), the general conclusions and relative importance of the craft parameters remain the same for nonzero air gaps. Only gradual changes in the magnitude of the speed are required as the additional factors of air gap and drag components are incorporated in the expression for the effective lift/drag ratio $(L/D)_{eff}$.

Now that the general characteristics of the thrust requirements of a hovercraft have been outlined, it is appropriate to outline what thrust mechanisms are available and how best to apply some design rules in hovercraft propulsion. Because of the extensive treatments in the literature on various means of propulsion schemes concentration on only two schemes will be presented here. These are: a) air jet propulsion, and b) air screw or propeller propulsion. Water jets and water screws, wheels, tracks and other mechanisms have all been used to varying degrees of success on hovercraft. The air jet was the first form of hovercraft propulsion used (on the SR.N1). It has the advantage of being simple and quiet, but the disadvantage of low efficiency. The air propeller, on the other hand, is more complex and far from quiet, but enjoys the highest propulsive efficiency of the hovercraft propulsors.

2.3.4 Air–Jet Propulsion

The essential elements of an air jet propelled hovercraft are shown in Figure 2.32. The thrust produced by such a propulsion system is given by:

$$T = \rho Q\ (V_j - V) \tag{2.54}$$

where Q is now the flow required for propulsion and would normally be additive to the flow required for lift. The jet velocity V_j is determined by the pressure P_j produced by the propulsive fan (say) through the relationship:

$$V_j = (2\ P_j/\rho)^{1/2} \tag{2.55}$$

The propulsive efficiency η_p is given by:

$$\eta_p = \eta_F[2(V_j/V)-1]/[(V_j/V)^2-\epsilon] \tag{2.56}$$

where η_F is the fan efficiency, and ϵ is ram recovery at the propulsive fan

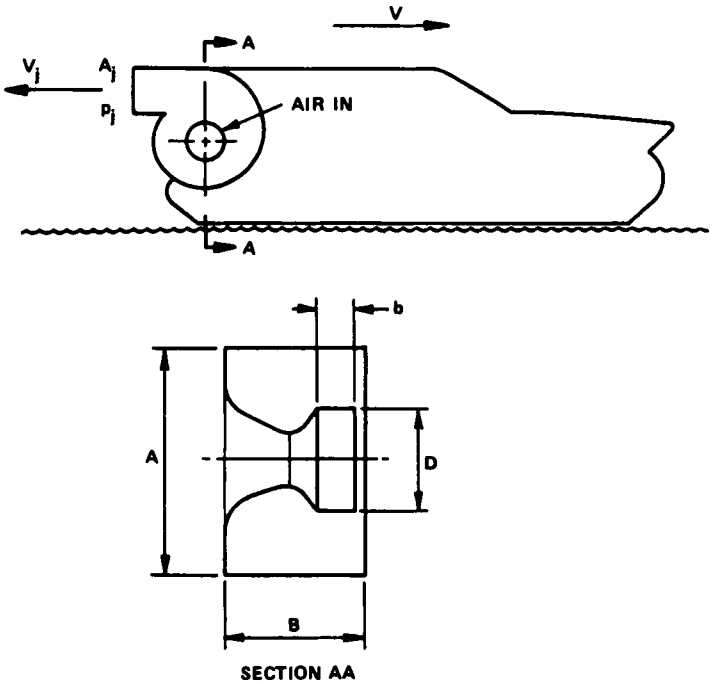

Fig. 2.32 Air jet propulsion elements, with volute parameter = U/bD^2 and $U = (\pi/4)A^2B$.

inlet. In the ideal case with no losses, such that $\eta_F = \epsilon = 1.0$, equation 2.56 reduces to the momentum disc theory result:

$$\eta_{pi} = 2/[1+(V_j/V)] \tag{2.57}$$

The use of jet velocity ratio V_j/V proves to be cumbersome in most analyses; it is more convenient to use a thrust coefficient defined by:

$$C_T = T/(0.5\rho V^2 A_\beta) \tag{2.58}$$

where T is thrust and A_β is propeller (or thruster) disc area. The thrust coefficient is related to the jet velocity ratio by:

$$C_T = 2(V_j/V)[(V_j/V)-1] \tag{2.59}$$

To provide some indication of the design parameters when considering propelling a hovercraft by air jet propulsion, some calculations are provided for a typical hovercraft. The ideal efficiency η_{pi} and a typical actual efficiency η_p, computed for an assumed total fan efficiency of 85 percent and an intake ram recovery of 50 percent, are shown as a function of the jet velocity ratio in Figure 2.33. The relationship between thrust coefficient C_T and jet velocity

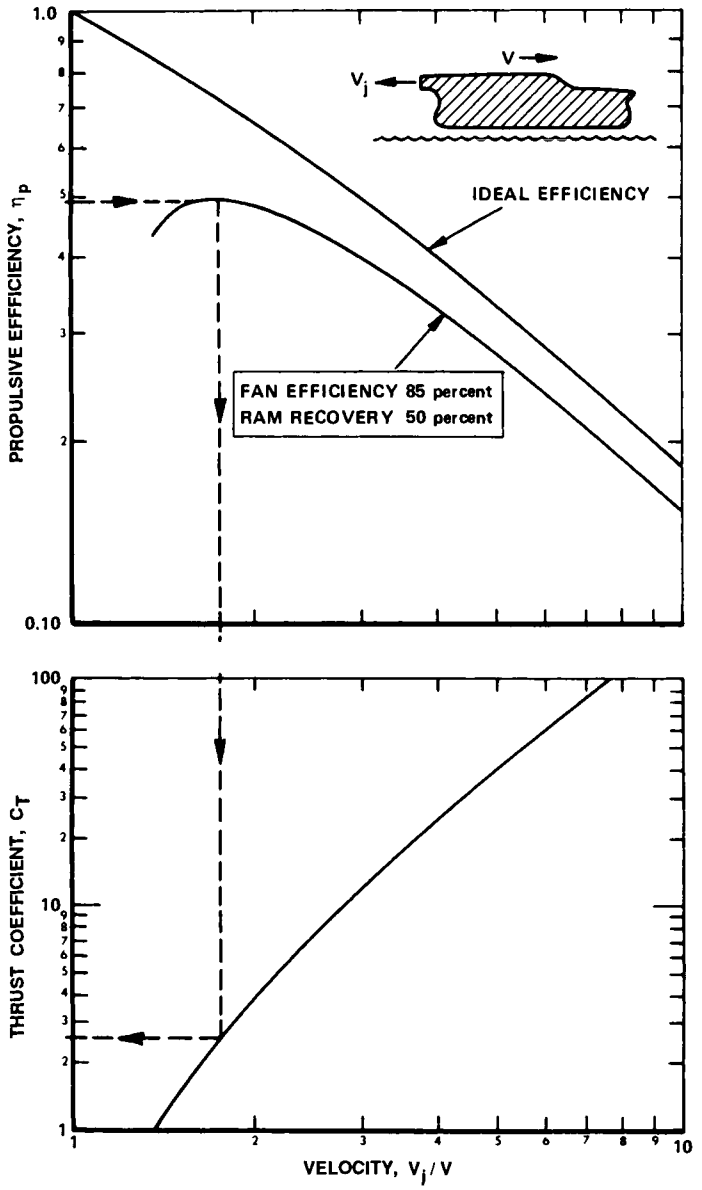

Fig. 2.33 Fan air jet propulsion thrust efficiency.

ratio V_j/V is also shown. It is seen that, even with high fan efficiencies, it is difficult to obtain much more than 50 percent propulsion efficiency. For $\epsilon = 0$, the propulsive efficiency drops to 42 percent; for $\epsilon = 1.0$, that is for full ram recovery, the propulsive efficiency approaches 56 percent for the case of an 85 percent efficient fan. This maximum efficiency occurs for a jet velo-

city ratio $V_j/V = 1.75$ or, following the dashed line, for a thrust coefficient $C_T = 2.6$. A free or shrouded propeller for the same thrust coefficient would have a propulsive efficiency of approximately 60 percent. For hovercraft speeds of 25 to 30 m/s (50 to 60 knots), jet velocities of 45 to 60 m/s (150 to 200 ft/s) will thus provide the maximum efficiency. For comparison, the jet velocity of the Britten-Norman hovercraft CC-5 was approximately 53 m/s (175 ft/s). A key advantage of low velocity air-jet propulsion (other than safety) is the low noise level that is generated. The disadvantage is the space requirement of the fan(s) to produce sufficient thrust.

An indication of the fan sizing to produce the necessary thrust can be obtained by consideration of the total pressure rise across the fan and equating it to the various key design parameters The total pressure rise can be expressed as the total pressure in the jet less any ram recovery at the fan intake, that is:

$$P_F = P_j - \epsilon\rho V^2/2 \tag{2.60}$$

By means of equations (2.55) and (2.60), the jet velocity ratio can be expressed as:

$$V_j/V = \left[2\psi(nD/V)^2 + \epsilon\right]^{1/2} \tag{2.61}$$

The jet velocity is thus seen to be a function of the fan pressure coefficient ψ, the fan intake recovery ϵ and the advance ratio $J = V/nD$, where n is the number of revolutions per second and D is the diameter of the fan. Figure 2.34 shows this relationship for the specific case $\epsilon = 0.50$.

In the discussion of lift fans in Section 2.2.1, Figure 2.11 specifically shows how the pressure coefficient ψ depends on the fan and volute geometries of HEBA fans. Figures 2.11 and 2.34 thus provide the governing design parameters that relate from geometry to produce a desired air-jet thrust.

2.3.5 Air–Screw Propulsion

The most common form of propulsion for the hovercraft has been the air screw or air propeller. It is the most efficient, although noisier and more complicated than the air jet discussed earlier. At the equilibrium forward speed (V) of the hovercraft, the thrust coefficient of the propeller(s) must be of sufficient magnitude to equal the drag coefficient through the relation:

$$C_T = (S/A)C_D \tag{2.62}$$

where S is cushion area, A is total disc area of all propellers, and C_D is the hovercraft drag coefficient. From simple momentum theory, the maximum ideal efficiency of the free propeller is

$$\eta = 2/\left[1 + (1+C_T)^{1/2}\right] \tag{2.63}$$

and, for the shrouded propeller,

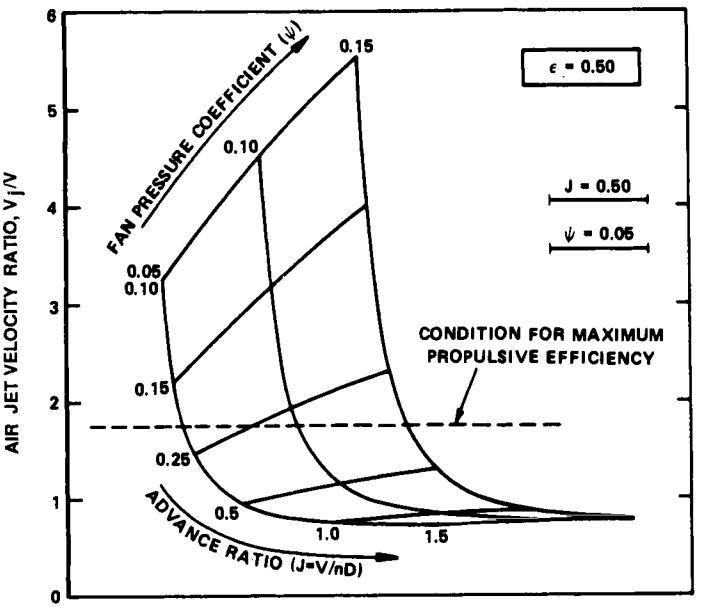

Fig. 2.34 Jet velocity ratio and fan parameters.

$$\eta = 4/[3 + (1+2C_T)^{1/2}] \tag{2.64}$$

The methods of calculating the real fluid effects due to thickness, camber and solidity of propellers are well documented. The standard references by Hamilton-Standard on free (unshrouded) propellers (ref. 30) and shrouded propellers (ref. 31) cover a range of design parameters, including solidity, number of blades, lift coefficients and others. Sheets and Mantle (refs. 32 and 33) compiled the Hamilton-Standard propeller data as a function of the thrust coefficient C_T. They showed that the data could be contained within a ± 2.5 percent bandwidth envelope covering all the design parameters discussed. This compilation is shown for free propellers in Figure 2.35 and for shrouded propellers in Figure 2.36. It can be seen from the two sets of data that the free propeller efficiency is approximately 82 percent of the maximum ideal efficiency predicted by the simple momentum theory and that the shrouded propeller efficiency is approximately 85 percent of the maximum ideal efficiency. It is also seen that the various representative hovercraft propellers shown follow the general trend of the Hamilton-Standard data. A more complete set of detailed characteristics of the hovercraft propellers may be found in Reference 1. There, Mantle provides specific data on lift coefficients, blade geometries, and many other pertinent parameters, and includes a discussion on structural characteristics. However, the general trend of the propeller thrust is as shown in Figures 2.35 and 2.36.

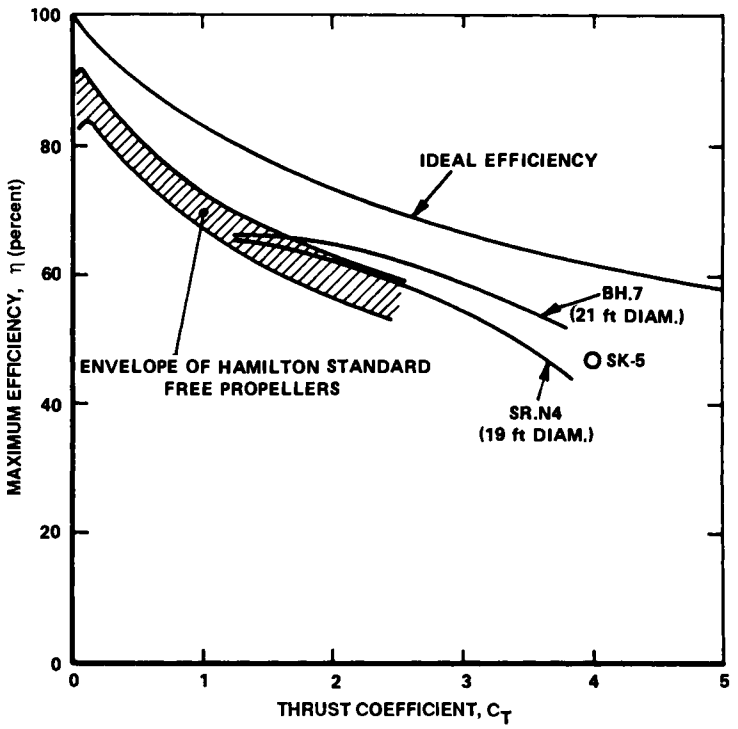

Fig. 2.35 Free propeller thrust efficiency.

2.4 CONTROL SYSTEM

The related requirements of stability and control of a hovercraft frequently become intermingled and design decisions are often made according to operator handling needs. As such, it is difficult to give specific criteria for control systems of hovercraft. Difficulty in the control of hovercraft has been associated with directional control, specifically in the control of the craft in both the lateral and yaw modes of operation. The difficulties arise mainly because of the hovercraft's unique necessity to combine relative freedom from the surface over which it operates with the ability to maneuver in a confined space, such as in a harbor or port.

A distinction should be made between *trim* and *control*, although the same device is often used for both. The distinction is determined by whether the setting is small or large or whether the setting is fixed or variable. For example, the adjustment of skirt lifters would provide a roll (or pitch) trim and a continuous movement of the skirt lifters would provide roll (or pitch) control. The subject of thrust and lift *engine controls*, although an

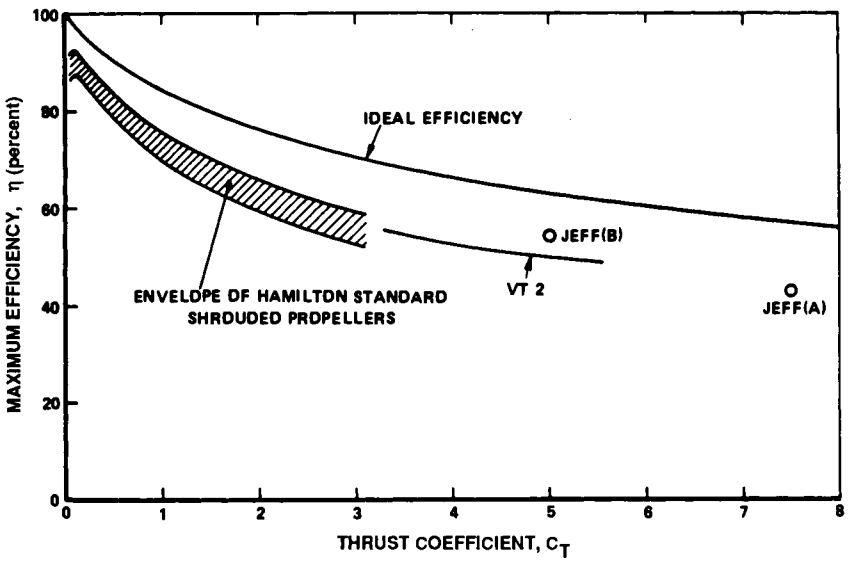

Fig. 2.36 Shrouded propeller thrust efficiency.

important design topic for hovercraft, is not discussed here under the heading of control systems.

Control systems, as used on most hovercraft to date have taken the form of one of the following: a) aft-installed fins with rudders for yaw control, b) differential thrust for yaw control, c) swiveling bow thrusters (as on the LCAC) for yaw, sideforce and craft speed control, d) multiple, swiveling free propellers (as on the SR.N4) for side force, yaw and speed control, e) swiveling ducted propellers (as on the AALC JEFF(A)) for yaw, side force and speed control, f) puff ports for low-speed side force and yaw control (as on the SR.N5, SK.5 and SR.N6 series of hovercraft), g) propulsive thrust from the lift system, with rudders installed in the outlet jet (as on the CC-5 and CC-7) for yaw control, and reverse thrust *buckets* for braking, h) skirt lift for roll, yaw and side force control (as on the SR.N5 and SR.N6), and i) surface contact devices, such as retractable rods for turning (as on the MITSUI MV-PP05). Some of the important features of the control systems used in hovercraft are described in the following sections.

2.4.1 Aerodynamic Control Surfaces

The primary use of aerodynamic control surfaces in hovercraft has been to provide directional control through the generation of yaw moments. However, they are not widely used because they are not very efficient at low speeds and

large yaw angles typical of hovercraft operation. On the other hand, mounting the aerodynamic control surfaces (fins or rudders) in the slipstream of an air jet or propeller improves their effectiveness considerably. The use of engine bleed or cushion air bleed is another mechanism to improve the effectiveness of aerodynamic surfaces.

As already stated, there are many variations of aerodynamic controls that can be applied to hovercraft, but they have not been pursued vigorously for the 15 - 25 m/s (30 - 50 knots) speed range. For higher speed hovercraft, say 25 - 60 m/s (50 - 120 knots) which encroaches on the wing-in-ground-effect (WIG) craft realm, aerodynamic control becomes a much more effective control mechanism. One such scheme used to advantage on the MARAD VRC-1 is dorsal fin control. Figure 2.37 shows the VRC-1 operating at high speed (approximately 35 m/s, (70 knots)) over the Rogers Dry Lake Bed, Edwards Air Force Base, in 1964. The dorsal fin is mounted mid-ship above the craft's C.G. and is activated through steering control of the pilot's wheel. Such a control mechanism, provides the necessary side force with minimal banking, thus alleviating the ground proximity problem and the need for skirt lifting.

2.4.2 Thrust Producing Devices

This blanket title includes air propellers, control ports and air jets. Such devices have the advantage of being relatively independent of wind speed and yaw angle. They are normally integrated with the propulsion system or lift fan system of the hovercraft, thus providing an opportunity to reduce the number of systems required and leave more space and weight for the payload. Typical early examples of hovercraft illustrate the basic features of propeller control. Figure 2.38 shows these basic schemes.

In the case of the VA.3, twin propellers mounted side by side on the after portions of the hovercraft provided a yawing moment by means of differential propeller pitch and thus differential thrust. Although such a control system arrangement is very effective and positive, it has the disadvantage that decreasing the thrust on one side tends to reduce the craft's speed. Also, with this arrangement, there is no mechanism for producing a side force. In contrast, the SR.N3 arrangement with fore and aft swiveling, pylon mounted propellers eliminates the two problems of speed loss and lack of side force. Variations of these arrangements have been used in later hovercraft. Figure 2.39 shows some of the main types in use today in one form or another.

2.4.3 Multiple Propeller Control

The free and ducted propeller has been the most widely used thrust and control mechanism on hovercraft for the reasons cited. The disadvantage is the noise level, but in the absence of more efficient means, it will still provide the main directional control mechanism for the foreseeable future. Some of the

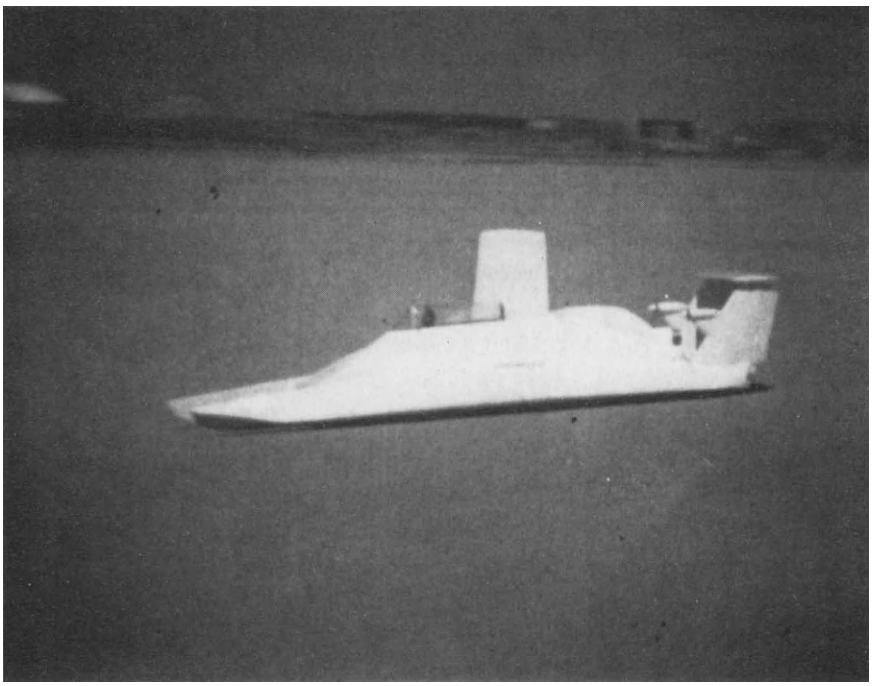

Fig. 2.37 VRC-1 with dorsal fin control

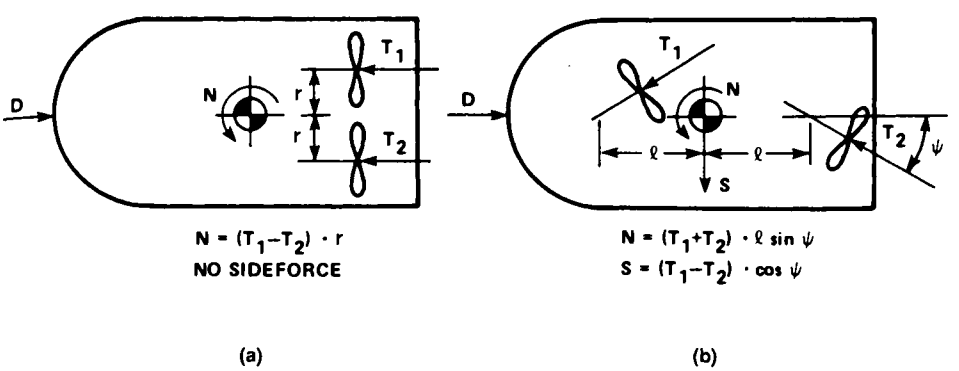

Fig. 2.38 Thrust vectoring: (a) side by side propellers (VA-3); (b) tandem propellers (SR.N3).

design considerations for multiple propeller installations, when used in tandem and at high angles of yaw, follow.

(i) Tandem operation. The SR.N4 (see Chapter 1) is a good example of the use of tandem installations. The practical limitations of increasing the pro-

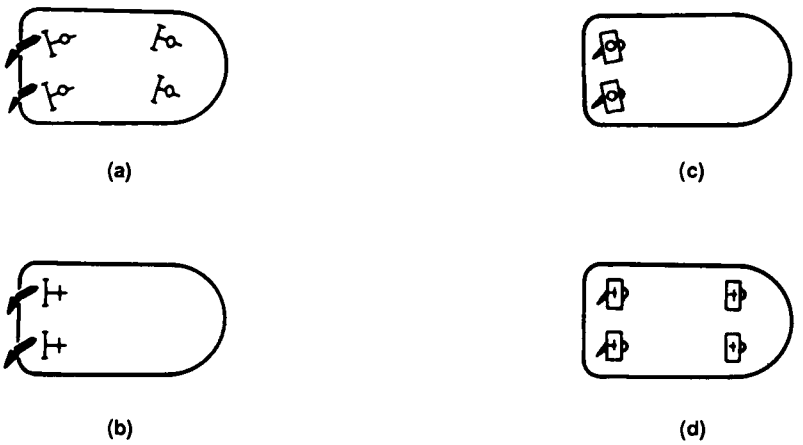

Fig. 2.39 Free propeller and ducted fan (propeller) arrangements: (a) four swivelling propulsors, free propellers and all-moving vertical fins; (b) two side by side nonswivelling propulsors, free propellers and all-moving vertical fins; (c) two side by side swivelling propulsors with ducted fans; (d) four nonswivelling propulsors with ducted fans.

peller disc area to maximize propeller efficiency at cruise speed, coupled with the practical limitations of single installations of large diameter propellers, prompts consideration of tandem installations. This is of practical importance when it is realized that propellers have approached 8 - 10 m (25 - 30 ft) in diameter on various hovercraft to date. The physical dimensions of hovercraft (the beam of the SR.N4 is 24 m (78 ft), for example) illustrate the practical installation problem of such large propellers. The Super 4 uses 4 6.4 m (21 ft) diameter propellers in tandem operation as a partial solution in offsetting the problem of large propellers. The problem of tandem propeller installations, however, is the influence of one propeller on another due to the small area available on the hovercraft. Some results of Shank (ref. 34) and Trebble (ref. 35), presented in Fig. 2.40, show the impact of tandem operation on the thrust efficiency of the propellers. It can be seen that, for a typical thrust coefficient $T_c = 1.0$, the overall propeller efficiency of the front and aft propellers would be 66 % and 52 %, respectively. Some improvement can be made in actual installations by operating the aft propellers at blade angles approximately 5 to 10 degrees higher than the forward propellers.

(ii) Operation at high yaw angles. In maneuvering and in crosswind operation, hovercraft propellers will encounter yaw angles of no more than 10 degrees, nominally, but with variations of up to 5 degrees. Propellers operating at such yaw angles will experience lift and drag forces that can be quite significant, especially in the case of ducted or shrouded propellers because of

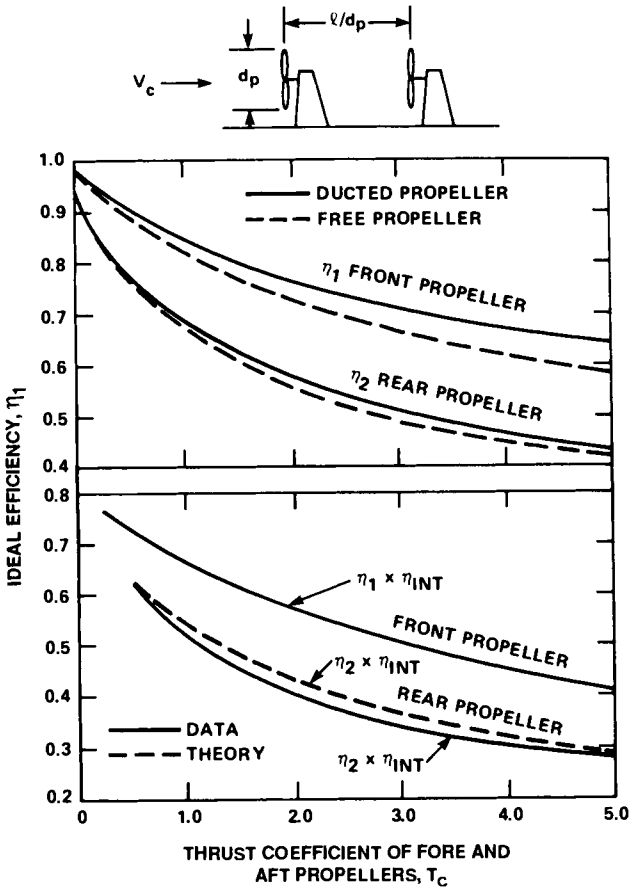

Fig. 2.40 Efficiency of tandem propellers.

the aerodynamic forces acting on the ducts. Some experimental results regarding the thrust T and normal force N acting on free and shrouded propellers are shown in Figures 2.41 and 2.42. The effective thrust T_{eff} and side force S available for control of the hovercraft can be determined from such results by the equations:

$$T_{eff} = T \cos \alpha - N \sin \alpha \tag{2.65}$$

and

$$S = T \sin \alpha + N \cos \alpha \tag{2.66}$$

where α is the yaw angle. Figure 2.43 is the result of applying these equations to the data of Figures 2.41 and 2.42.

2.4.4 Puff Ports and Bow Thrusters

A distinction should be made between the various schemes of vectoring

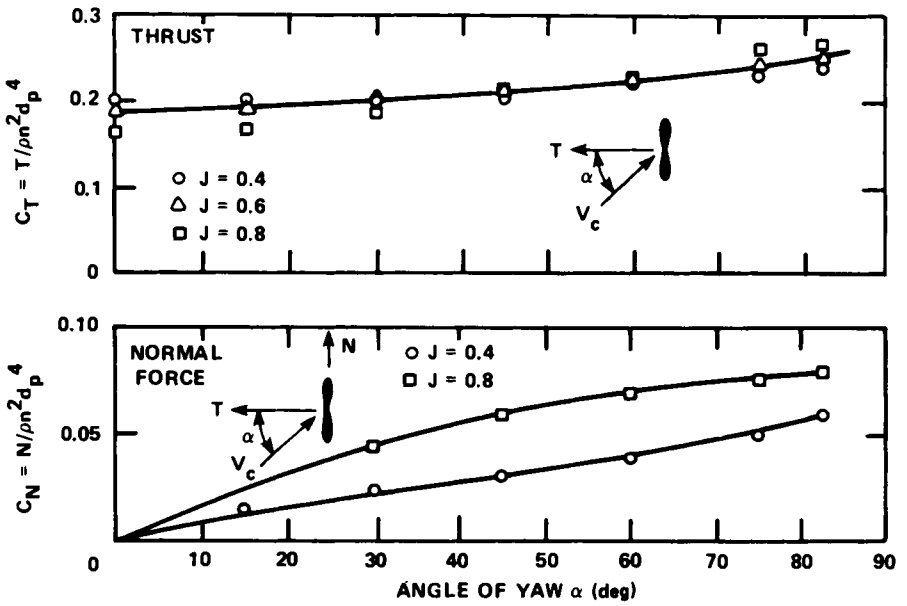

Fig. 2.41 Thrust and normal force on free propeller.

thrust from the lift system. Puff ports were the original schemes used on the early SR.N5 and SR.N6 craft. Puff ports were used to provide side force and could be used independently or in combination to provide both lateral and rotational motion control. The forces were usually quite low, resulting in acceleration levels of approximately 0.01g. As such, puff port control is normally used for low speed maneuvering such as docking.

Bow thrusters or air jet thrusters, on the other hand, are high velocity air ejectors (see earlier discussion on air jets) where the control is directly coupled to the lift fan system, i.e., upstream of the low velocity plenum chamber where puff ports are used. Bow thrusters are used on the LCAC hovercraft with a high degree of success in controlling the craft directionally and in braking.

2.4.5 Lift Vectoring Devices

Lift vectoring devices for hovercraft control can be divided into two general categories: a) those which modify the pressure distribution in the cushion, thereby changing the C.P. position, and b) those which physically move the cushion to displace the C.P. Both mechanisms result in a change in the C.P. and hence cause a shift in the lift force moment about the craft's C.G., with a resulting control of the motion. Both these basic types may be used to provide rolling and pitching moments and hence side and thrust forces. If surface contact occurs through such action, the yaw mode may be affected.

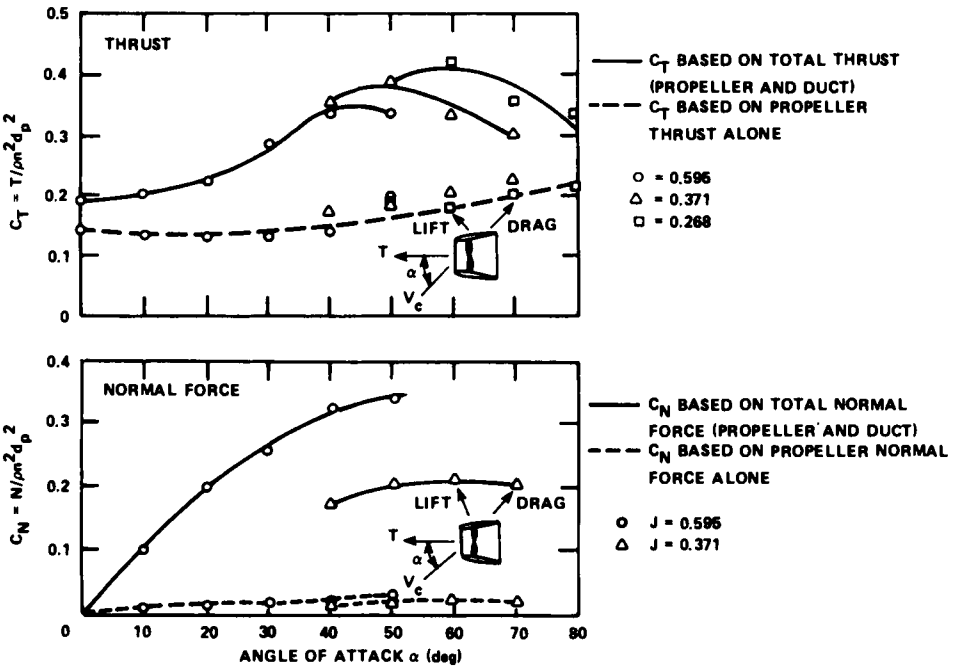

Fig. 2.42 Thrust and normal force on shrouded propeller.

Some possible schemes for changing the pressure distribution are shown in Figure 2.44. Variations of the valving and porting to modify the cushion pressure distribution have been used on various hovercraft, from the early SR.N1 to today's craft. Finally, there are various methods of skirt lifting and cushion shifting. It is important to note that the force produced by skirt lifters is a component of cushion lift caused by rolling (or pitching) the hovercraft and not by the reaction to the escaping air, i.e. the force acts towards the part of the craft where the skirt is lifted. Although the use of asymmetrical skirt contact produced by roll control is not generally acceptable as a means of yaw control because of the associated water resistance, it may be of use in selected operational circumstances. Figures 2.45 and 2.46 show some of the basic schemes used on hovercraft today. These schemes have been used in various mechanical variations on such hovercraft as the SR.N5, SR.N6, VT.1 and others. On the HD.2 and VT.1, the skirt hemline was moved horizontally by means of jacks and cables. Other design variations of these simple control mechanisms can be envisaged for a particular hovercraft under consideration.

2.5 SUMMARY

The fundamentals of hovercraft design were presented in this Chapter.

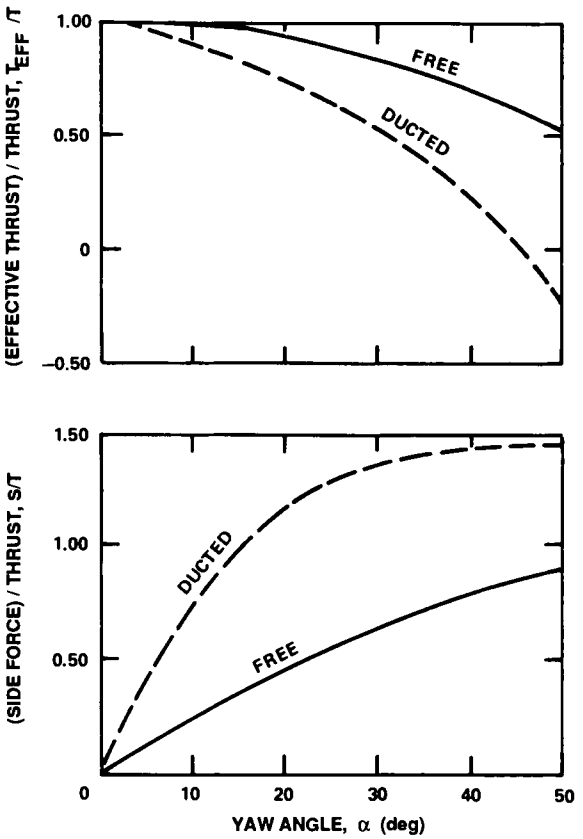

Fig. 2.43 Typcial propeller forces in yaw.

These fundamentals cover the key design parameters of the main subsystems: the hull structure, the lift system (fan systems and skirts), the propulsion system, and the control system. Included in the propulsion system was the description of the thrust requirements, or drag characteristics of the hovercraft, as well as description of the various thrust producing mechanisms. The emphasis was on providing the design tools for overall design and sizing of hovercraft and their main systems. Detailed design techniques for specific components were appropriately not covered, but were left for the detailed design stage of any particular hovercraft. This chapter provided the overall design sizing equations for a range of hovercraft types and established the groundwork for the necessary detailed treatments of particular and specific subsystems.

It was seen that the key characteristics of overall size and cushion density have a major impact on the structural weight. The influence of various structural concepts (rivetted, welded, composites, etc.) was shown, based on

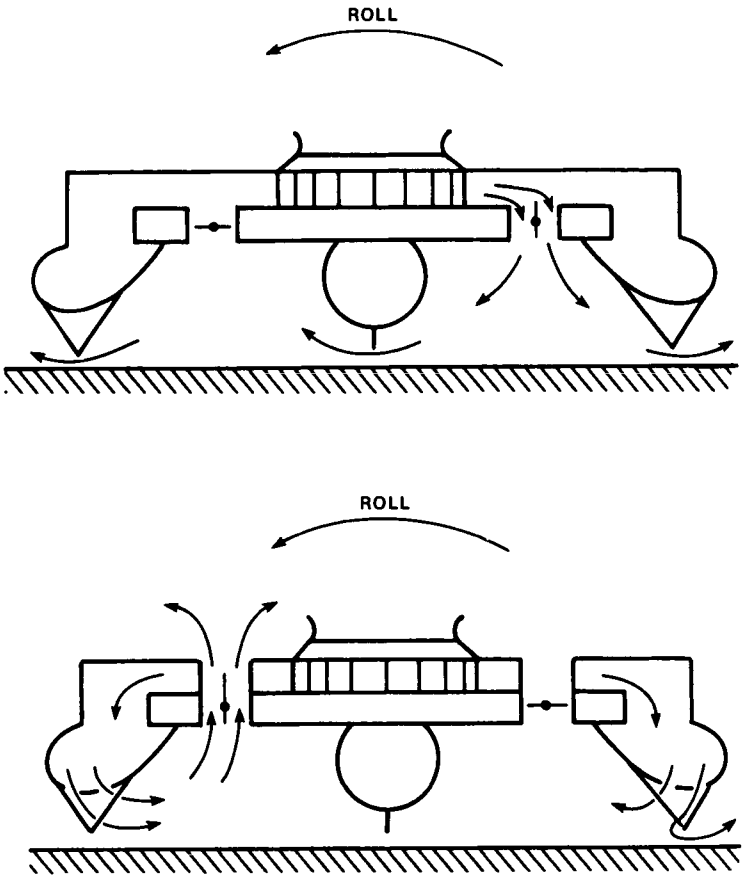

Fig. 2.44 Cushion valving control.

many actual hovercraft. Conclusions were drawn that, while it is possible to reduce structural weight somewhat with the use of complex structures, the designer must be careful that the associated cost increases of such design choices are worth the modest reductions in structural weight. The structural weight design fundamentals provided in this Chapter can be balanced with the cost formulas provided in Chapter 5.

The lift system design fundamentals covered all the fan systems (passive and active centrifugal and axial fan systems) used to-date in operational hovercraft together with descriptions of less used fan systems (mixed flow and cross-flow). Equations were provided for fan sizing that included lift efficiency, pressure and flow characteristics, and volumetric requirements in the form of fan diameter and volute dimensions. In all cases, theory and actual fan data were compared to provide a confidence level in the equations to be

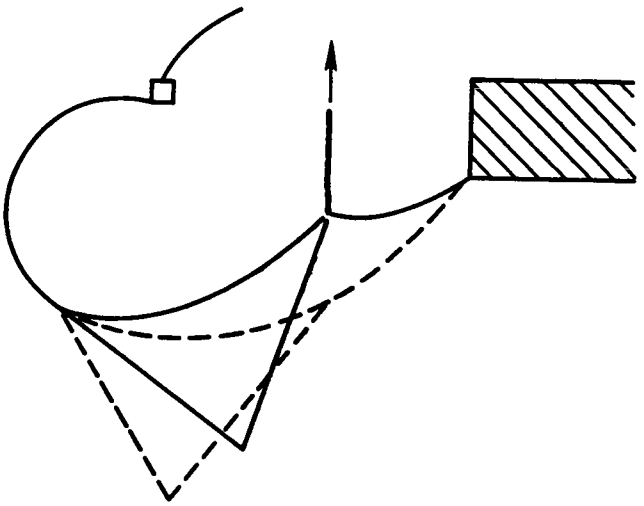

Fig. 2.45 Skirt lift.

used for design purposes. A variety of skirt systems have been used throughout the history of the development of hovercraft from the early 1960's to the present day. These skirt systems include bag and finger, loop and segment, pericell and jupe. All these systems were described together with overall design parameters for sizing purposes.

The performance characteristics of a hovercraft require an understanding of both its drag and thrust mechanisms. Thus, design equations and data for all the main components of thrust and drag were given. Momentum drag, wave drag, skirt drag, spray drag and aerodynamic drag were treated and appropriate equations for overall sizing were presented. The determination of the required acceleration performance of a hovercraft from a standing (hover) position to accelerating past hump speed was also examined.

The various mechanisms for producing thrust (air-screw and air-jet) were described in their various forms. Equations were provided to size these thrust producers in terms of thrust efficiency, diameter and other design parameters. Many references were cited for more detailed design information.

Finally, the subject of control of a hovercraft operating on cushion was treated. Maneuvering at speed, pitch and roll control methods, and some overall sizing design fundamentals were provided.

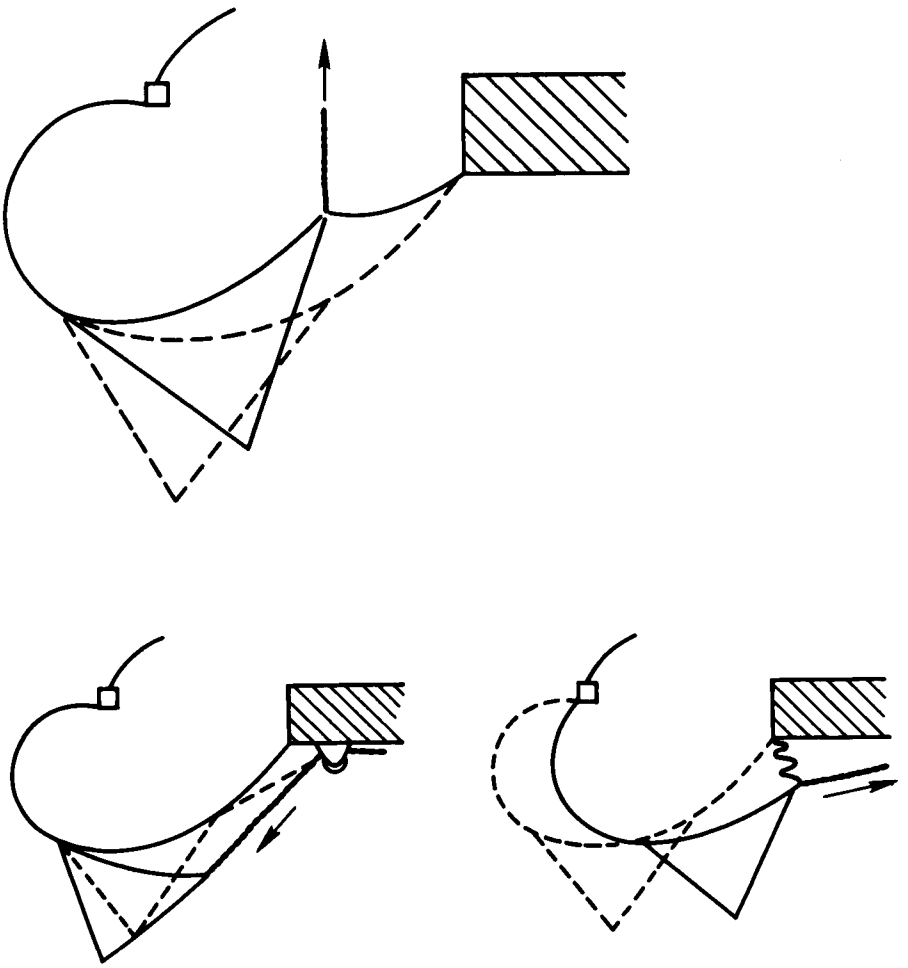

Fig. 2.46 Cushion shift.

2.6 REFERENCES

1. P.J. Mantle, Air Cushion Craft Development, U.S. Government Printing Office, Stock Number 008-047-00291-2, Report Number DTNSRDC 80/012, January 1980.
2. E.A. Butler, The Surface Effect Ship, Naval Engineers Journal, Special Edition: Modern Ships and Craft, Vol. 97, No. 2, February 1985.
3. B. Eck, Ventilatoren, Springer-Verlag, Berlin, Germany, 1962.
4. W. C. Osborne, Fans, Pergammon Press, London, England, 1966.
5. J.C. Shipway, Estimation of Head-Flow Curves for Centrifugal Fans, National Physical Laboratory Report, Hovercraft Report 5, October 1968.

6. R.A. Wallis, Axial Flow Fans, Newnes Academic Press, London, England, 1961.

7. J.C. Shipway, Aerodynamic Design of Axial Lift fans, National Physical Laboratory Report, Hovercraft Report 4, July 1968.

8. O. Cordier, Ahnligkeitsbedingungen Fur Stromungsmaschinen, VDI Berichts, Vol. 3, 1955, pp 85-88.

9. O.E. Balje, A. Study on Design Criteria and Matching of Turbomachines, Part A: Similarity Relations and Design Criteria of Turbines, American Society of Mechanical Engineers Paper 60-WA-230, 1960.

10. O.E. Balje, A Study on Design Criteria and Matching of Turbomachines, Part B: Compressor and Pump Performance and Matching of Turbo-components, American Society of Mechanical Engineers Paper 60-WA-231, 1960.

11. Performance Curves for Airscrew Standard HEBA-A and HEBA-B Fan Ranges, Airscrew-Weyroc Ltd., Webridge, Surrey, England, (not dated).

12. Fan Engineering (5th Edition), published by Buffalo Forge Co., Buffalo, New York, 1966.

13. T.G. Csaky, A Synthesis of Fan Design for Air Cushion Vehicles, Phase I, NSRDC Report 3599, October 1972.

14. T. G. Csaky, Some Aspects of Optimum Design of Lift Fans, Paper No. 76/9 Sixth Canadian Symposium on Air Cushion Technology, London, Ontario, Canada, 12-14 June 1972.

15. G. Rosen and G.R. Ketley, Powering Systems for Advanced Surface Vehicles, First International Hovering Craft, Hydrofoil and Advanced Transit Systems Exhibition and Conference, Brighton, England, May 13-16, 1974.

16. G.D. McGhee, 3KSES Design Development and Construction, Hovering Craft and Hydrofoil, Vol. 17, No. 3, December 1977.

17. P.J. Mantle, On the Dynamic Heave Motion of Single Peripheral Jet GEMs Over an Undulating Surface, Vehicle Research Corporation, Paper No. 9, May 1962.

18. P.J. Mantle, Some Design Aspects of Air Cushion Craft, Annals of the New York Academy of Sciences, Vol. 154, Article 2, November 22, 1968, pp 924-952.

19. J. Breslin, The Dependence of Surface Effect Ship Heave Response on Model Scaling Parameters as Deduced from a Simplified Linear Analysis, Surface Effect Vehicles Summer Study Report for Institute of Defense Analysis, October 1968.

20. P.R. Crewe, The BHC Contribution to Hovercraft Development, Hovercraft Conference, Adelaide, Australia, November 15, 1968.

21. R.L. Wheeler, The Amphibious Hovercraft, Diamond Jubilee International Meeting, SNAME Paper 23, New York, June 18-21, 1968.

22. Y.N. Xie and Y. Hua, Calculation of the Static Forces Acting on ACV Bag-Finger Skirts, Paper presented at 1985 Joint International Conference on Air Cushion Technology, Rockville, Maryland, September 24-26, 1985.

23. N. Hogben, Hovering Craft Over Water, Advanced Hydroscience No. 2, Academic Press, New York, 1967.

24. J. Bertin, French Marine Air Cushion Vehicles, The Aeronautical Journal of the Royal Aeronautical Society, Vol. 74, No. 717, September 1970, pp 726-735.

25. N. Zheng and T. Ma, Aerodynamic Characteristics of Bag-Cone Skirt, Paper presented at 1975 Joint International Conference on Air Cushion Technology Rockville, Maryland, September 24-26, 1985.

26. G.H. Elsley and A. J. Devereux, Hovercraft Design and Construction, published by Cornell Maritime Press, Inc., 1968.

27. M. J. Barratt, The Wave Drag of Hovercraft, Journal of Fluid Mechanics, Vol. 22, Part 1, 1965, pp 39-47.

28. J.N. Newman and F.A.P. Poole, The Wave Resistance of a Waving Pressure Distribution in a Canal, DTMB Report No. 1619, March 1962.

29. L.J. Doctors, The Wave Resistance of an Air Cushion Vehicle, University of Michigan, December 1970.

30. Generalized Method of Propeller Performance Estimation, Hamilton-Standard Handbook, PDB 6101, (not dated).

31. Generalized Method of Shrouded Propeller Performance Estimation, Hamilton-Standard Handbook, PDB 6220, (not dated).

32. H.E. Sheets and P.J. Mantle, Air Cushion Craft Propulsion, American Institute of Aeronautics and Astronautics/U.S. Navy Second Marine Systems and ASW Conference, AIAA Paper 66-731, August 8-10, 1966.

33. H.E. Sheets and P.J. Mantle, Air Cushion Craft Propulsion, Journal of Aircraft, Vol. 4, No. 3, May-June 1967, pp. 237-244.

34. S.R. Shank, Jr., Performance Prediction of Tandem Air Propeller Arrangements for Large Surface Effect Vehicles, NSRDC Report, December 1973, pp. 27-664.

35. W.J.G. Trebble, Investigation of the Mutual Interference of Propellers Mounted in Tandem, Royal Aircraft Establishment Technical Report 68282 (AD 857118), December 1968.

Chapter 3

LIGHT HOVERCRAFT

3.1 INTRODUCTION

Sir Christopher Cockerell described the hovercraft as "a very expensive motorcar tire with a permanent puncture!" The continuous flow of air through a fan into a skirt keeps the craft hovering, while air flowing through the craft generates propulsion. Size and payload capacity are used to qualify light hovercraft. Many organizations and agencies world-wide have specific definitions. The 1962 United Kingdom Air Registration Board's *Green Book* suggested that a light hovercraft is a vehicle under 9.8 kN empty weight, with a maximum power of 59.7 kW (80 HP) and a two-person capacity. Pinder, a former British light-hovercraft manufacturer, considered small hovercraft to be self-propelled amphibious vehicles under 10 meters in length and supported wholly on an air cushion. The Hoverclub of Great Britain's *Light Hovercraft Handbook* (ref. 1) defines light hovercraft to be vehicles with a maximum unladen (empty) weight of less than 9.8 kN (1,000 kg mass). For our purposes, we shall assume a light hovercraft to be any vehicle which is wholly-supported on a cushion of air and has a carrying capacity (payload) not exceeding approximately 9.8 kN.

While the world's first working hovercraft was a model, the second was a man-carrying light hovercraft built by the Westland Aircraft Company's Saunders-Roe division and called Saunders-Roe Number One (SR.N1). In the morning of July 25, 1959, the SR.N1 captured the world's attention by crossing the English Channel from Calais, France, to Dover, England (ref. 2). This feat had been rivalled 50 years earlier by Bleriot's amazing airplane flight along the same route on July 25, 1909. Whereas Bleriot's crossing was covered only by newspapers, many people saw the four-man crew of the SR.N1 on television making this historic crossing.

This unique mechanical curiosity, called a *hovercraft* by Cockerell, had excited the attention and imagination of hobbyists and mechanically-minded enthusiasts everywhere. Cockerell's hovercraft had all the appearance of a safe and inexpensive new type of flying machine. The media thought this was interesting and gave it much attention. Consequently, many people became involved. These enthusiasts began experimenting by building hovercraft for themselves. The British media's promotional contribution was most significant in the initial evolution of the hovercraft. However, it is interesting that hovercraft remained relatively unknown in the United States. This lack of American awareness exists even today and must be overcome before any significant market penetration can take place.

It was not long before numerous publications began appearing in the United Kingdom. *Flight International Magazine* started publishing a supplement called *Air Cushion Vehicles* (ref. 3). This superb magazine remained a classic until it folded in 1971 due to limited circulation. *Air Cushion Vehicles* published *Homebuilt Hovercraft* (ref. 4), a fine series of articles, by G.H. Williams, which became very popular as "a plain man's guide to ACV design and construction." There were other publications, too: *The History of Air Cushion Vehicles* by Leslie Hayward (ref. 5), *Jane's Surface Skimmer Systems*, now Jane's High-Speed Marine Craft and Air Cushion Vehicles (ref. 6), *Hovering Craft and Hydrofoil*, now *Combat Craft* (ref. 7), *HOVERcraft* by Angela Croome (ref. 8), *Hovercraft World* (ref. 9), and *Slipstream* (ref. 10). References 6 and 7 are presently in publication.

Therefore, it is not surprising that hobbyists began to build man-carrying models. Many saw the hovercraft as an inexpensive airplane. Experimenters who managed to construct a craft that could hover began thinking of manufacturing it as a business. Remarkably, this became a world-wide phenomenon and occurred in university laboratories, backyards and basements. It was relatively easy to construct machines that would hover. However, they were a long way from being workable vehicles and even further from being capable of forming the basis of a light hovercraft manufacturing business. Most entrepreneurial enthusiasts were not prepared for the long haul and soon fizzled out. Until 1964, light hovercraft were still quite crude, despite major technical improvements documented in the general and scientific literature. What happened next in terms of development, starting with the world's first hovercraft race in Canberra, Australia, March 14, 1964, was nothing short of amazing!

3.2 EVOLUTION

The evolution of small hovercraft has been influenced considerably by local environments. Machines developed in different countries tend to have regional characteristics, and there have been advancements in many countries. However, since more information is readily available from the United Kingdom and North

America, we will concentrate on developments in these two regions up to 1987, but starting with the world's first hovercraft race which took place in Australia in 1964.

3.2.1 World's First Hovercraft Race

Canberra, the picturesque capital of Australia, was about to celebrate the opening of its new Lake Burley Griffin. As part of the Canberra Day celebrations on March 14, 1964, the Canberra Branch of the Royal Aeronautical Society planned and promoted a commemorative hovercraft race. As N.F. Lamb, Chairman of the Canberra Branch of the Royal Aeronautical Society put it, "The hovercraft was chosen as a project because success is possible in this field by one man's personal efforts at a very limited cost" (ref. 11). There were twelve entries all from Australia. Eleven arrived; they are shown in Figs. 3.1-3.11. Ten participated and five finished the race. This meeting was compared to the Rheims Air Meet of 1909. Both were attended by enthusiasts with primitive machines, heralding competitive development in aviation and hovercraft operation, respectively.

Criteria for an ingenuity prize included: structure, ease of maintenance, materials, propulsion, engine configuration, safety, buoyancy, aerodynamics, stability, control, air ducting, and maneuverability. It was awarded to a team of Royal Australian Air Force technicians who had adapted a helicopter tail-rotor, making reverse-thrust possible (Fig. 3.1).

There were also prizes for the formula efficiency race. A formula was devised to assign handicaps based on: a) comparative times to complete a prescribed course of 2.41 km (1.5 miles), b) total installed power, and c) hoverheight. The objective was to give all entrants a chance to win. An American kit-built hovercraft, the Dobson Air Dart seen in Fig. 3.2, won first prize. Another version appears in Fig. 3.12. The second and third prizes were won by the machines in Figs. 3.3 and 3.4, respectively.

The first and second prizes for the slalom, or maneuverability, event were awarded to the craft shown in Figs. 3.4 and 3.3, respectively. The delta-shaped entry of Fig. 3.6 won a special trophy for the highest recorded speed, i.e., an average of 48 km/h (30 mph) over 7.3 km (4.5 miles) and a top speed of over 73 km/h (45 mph). However, by virtue of its greater reliability, the Dobson Air Dart was able to win the formula event with a lower speed.

The craft of Fig. 3.2 was based on the plenum-chamber principle, whereas all others were peripheral-jet machines. The vehicles of Figs. 3.3 to 3.10 were driven by their entrants, but the other three were not. The eleven entries which arrived at the race site are now described in greater detail.

(i) Figure 3.1. Driven jointly by J.K. Murray and L. Gillies, this vehicle was entered by the Amberley Hovercraft Group of the Royal Australian Air Force. With a 5.57 m^2 (60 ft^2) surface area and 2.67 kN (600 lb) gross weight, it

employed a pair of 2.42 kW (3.25 HP) two-cycle lift engines and a similar thrust engine to produce hoverheight and speed capabilities rated at 15.2 cm (6 in) and 64.4 km/h (40 mph), respectively. The hoverheight was site-tested at 1.02 cm (0.4 in). The ingenuity prize was awarded to this machine's entrants

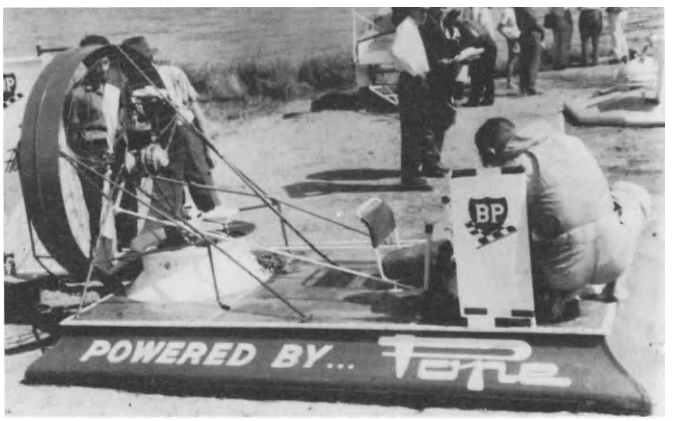

Fig. 3.1 Entry in world's first hovercraft race. Powered by three lawn-mower engines, two for lift and one for thrust. Thrust engine drove a variable-pitch helicopter tail-rotor. Prize winner for ingenuity.

Fig. 3.2 Entry in world's first hovercraft race. Dobson Air Dart with a single 6.7 kW (9 HP) lift and thrust engine. First prize winner of formula efficiency race. (See. Fig. 3.12 for another version of the Air Dart.)

because of its variable-pitch thrust propeller, which had been adapted from a helicopter tail-rotor.

(ii) Figure 3.2. The entrant and driver were respectively G.L. Cottee and A. Hawkins. This craft, called Dobson Air Dart, was assembled in Australia from a kit supplied by F. Dobson of the United States. A later version is shown in Fig. 3.12. With a 3.34 m^2 (36 ft^2) surface area and 0.76 kN (170 lb) gross weight, it employed a single 6.7 kW (9 HP) lift and thrust engine to produce hoverheight and speed capabilities of 10.2 cm (4 in) and 48.3 km/h (30 mph), respectively. On site, the hoverheight was tested at 5.33 cm (2.1 in). This entry placed first in the formula (efficiency) race.

(iii) Figure 3.3. The entrants were W. Seige and K.M. McLeod. With a 7.9 m^2 (85 ft^2) surface area and 2.67 kN (600 lb) gross weight, this vehicle employed two 2.61 kW (3.5 HP) two-cycle lift engines to produce a hoverheight capability of 7.62 cm (3 in). A similar engine was used for thrust. The hoverheight was site-tested at 10.7 cm (4.2 in). This entry placed second in both the formula and maneuverability races, and was highly commended for its ingenuity.

(iv) Figure 3.4. The entrant was A.L. Ellis. With a 743 m^2 (80 ft^2) surface area and 1.42 kN (320 lb) gross weight, this machine was powered by three lawn-mower engines, i.e., two for lift, each driving a contra-rotating fan, and one for thrust, adding up to a total power of 9.32 kW (12.5 HP). Its hoverheight and speed capabilities were rated at 15.2 cm (6 in) and 32.2 km/h

Fig. 3.3 Entry in world's first hovercraft race. Powered by three Victa lawn-mower engines. This entry's hoverheight of 10.67 cm (4.2 in) was the highest. Second prize winner of both the formula efficiency race and the maneuverability event.

(20 mph), respectively. The hoverheight was site-tested at 7.6 cm (3 in). This entry placed first and third respectively in the maneuverability and formula races.

(v) Figure 3.5. The entrant was D. Reece. With a 9.48 m^2 (102 ft^2) surface area and 1.37 kN (308 lb) gross weight, this craft was powered by three

Fig. 3.4 Entry in world's first hovercraft race. Powered by three lawn-mower engines, two for lift and one for thrust. Contra-rotating lift fans and swiveling thrust-engine arrangement.

Fig. 3.5 Entry in world's first hovercraft race. Two lawn-mower engines for lift and one for thrust. Most dependable, it operated all day with little maintenance or breakdown.

two-cycle lawn-mower engines, i.e., a pair of 1.5 kW (2 HP) engines for lift and a 2.61 kW (3.5 HP) engine for propulsion. Its hoverheight and speed capabilities were rated at 7.62 cm (3 in) and 32.2 km/h (20 mph), respectively. On site, the hoverheight was tested at 2.67 cm (1.05 in).

(vi) Figure 3.6. The entrant was A.W. Powell. With a 5.57 m^2 (60 ft^2) surface area and 2.22 kN (500 lb) gross weight, this vehicle employed a 7.46 kW (10 HP) engine for lift and a 19.39 kW (26 HP) motorcycle engine for the thrust propeller. Its hoverheight and speed capabilities were rated at 5.08 cm (2 in) and 48.3 km/h (30 mph), respectively. The hoverheight was site-tested at 5.46 cm (2.15 in). Whereas its average speed during the race was as rated above, a speed in excess of 72.3 km/h (45 mph) was reached at the end of the final leg. This entry was awarded a special trophy for best time.

(vii) Figure 3.7. The entrant was B. Kensington. With a 5.57 m^2 (60 ft^2) surface area and 2.58 kN (580 lb) gross weight, this was a triple-pod craft with conical fabric lift-chambers. Each pod was lifted by a 1.5 kW (2 HP) two-cycle lawn-mower engine and propulsion was supplied by a retractable outboard motor. Although rated a 2.54 cm (1 in), the hoverheight was site-tested at 7.87 cm (3.1 in). It was the only vehicle to use a flexible skirt successfully.

(viii) Figure 3.8. The entrant was N.C. Hyett. With a 3.72 m^2 (40 ft^2) surface area and 1.17 kN (263 lb) gross weight, this machine employed a 2.24 kW (3 HP) four-cycle lawn-mower engine for lift and a couple of 3.73 kW (5 HP) two-cycle engines for propulsion. Its hoverheight and speed capabilities were

Fig. 3.6 Entry in world's first hovercraft race. Lift power supplied by a 7.46 kW (10 HP) engine. Thrust provided by a motorcycle engine driving a propeller. This delta-shaped craft was awarded a trophy for reaching the highest speed of 73 km/h (45 mph).

rated at 7.62 cm (3 in) and 80.5 km/h (50 mph), respectively. It was, however, unable to compete due to a malfunction of its lift motor.

(ix) Figure 3.9. The entrant was F. Greenham. With a 5.02 m^2 (54 ft^2) surface area and 1.96 kN (440 lb) gross weight, this craft was powered by a 2.98 kW (4 HP) two-cycle engine for lift and a similar one for propulsion. Its

Fig. 3.7 Entry in world's first hovercraft race. Triple-pod craft with jupe skirts, the only craft with a flexible skirt. Each pod lifted by a 98 cc lawn-mower engine. Propulsion supplied by an outboard motor.

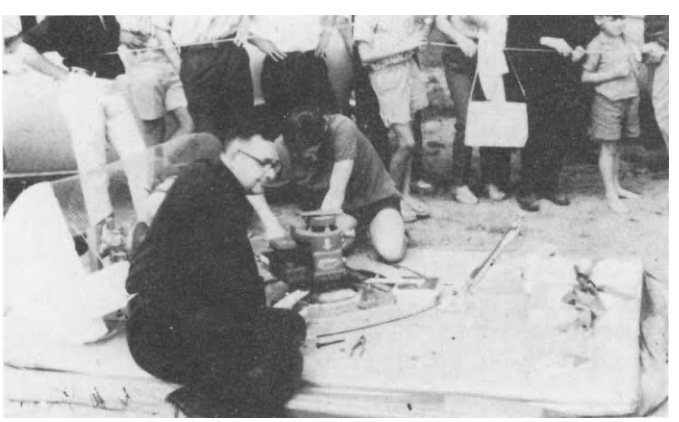

Fig. 3.8 Entry in world's first hovercraft race. Powered by three lawn-mower engines.

rated hoverheight was 7.62 cm (3 in). This vehicle's buoyancy was considered inadequate, since it sank while being towed to make way for another event.

(x) Figure 3.10. The entrant was R. Murray. With a 7.43 m^2 (80 ft^2) surface area and 1.78 kN (400 lb) gross weight, this vehicle was powered by three 1.5 kW (2 HP) two-cycle engines, i.e., two for lift and one for thrust. Its

Fig. 3.9 Entry in world's first hovercraft race. Tractor-propeller design with lawn-mower engines for lift and thrust.

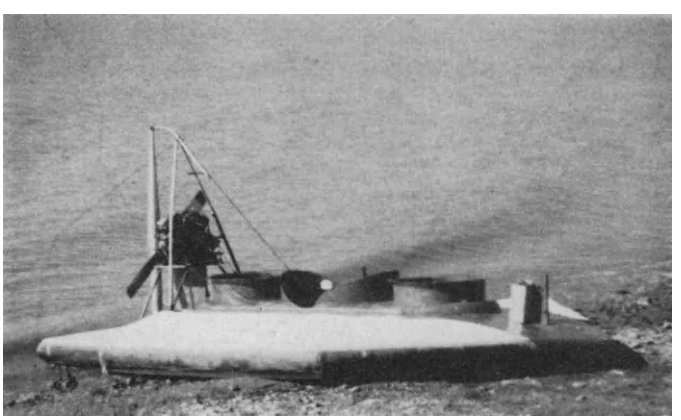

Fig. 3.10 Entry in world's first hovercraft race. Two lawn-mower engines for lift and one for thrust.

hoverheight and speed capabilities were rated at 5.08 cm (2 in) and 32.2 km/h (20 mph), respectively. The hoverheight was site-tested at 4.7 cm (1.85 in).

(xi) Figure 3.11. Australian Air Cushion Vehicle Development (now, Neoteric Engineering Affiliates Pty. Ltd.) was the entrant. The driver was C.J. Fitzgerald. With its 10.22 m^2 (110 ft^2) surface area and 5.12 kN (1,150 lb) gross weight, this craft was lifted by means of an 11.9 kW (16 HP)

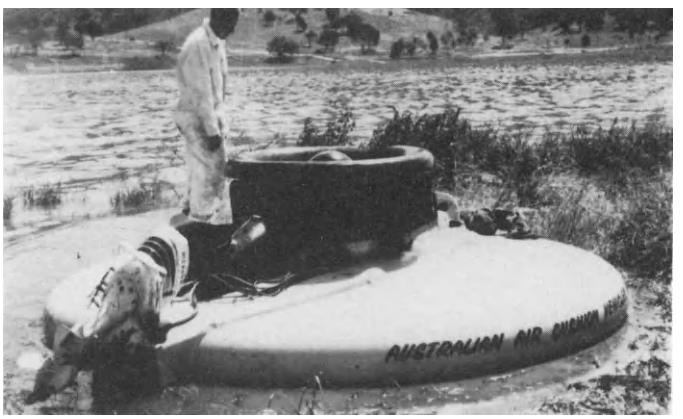

Fig. 3.11 Entry in world's first hovercraft race. Powered by a motorcycle engine for lift and a retractable outboard engine for thrust. Failed to compete due to damage in the lift-fan transmission.

Fig. 3.12 Dobson Air Dart in California during the mid-sixties.

motorcycle engine and propelled by a 29.8 kW (40 HP) retractable outboard motor. Rated at a hoverheight and speed of 10.2 cm (4 in) and 48.3 km/h (30 mph), respectively, it was unable to compete due to lift-transmission trouble.

The event was a remarkable success, considering the following circumstances: a) Australia was remote from the technical developments occurring in Europe, b) the participants had to work on a tight schedule, largely isolated from one another and with little technical support or assistance, and c) some of them had to transport their machines over long distances to the race site. It was well-summarized by N.F. Lamb: "The trials were an outstanding success. They illustrated the ingenuity of the individual to allocate sufficient time and a little money to have a worthwhile hobby and make a first class machine. The ACV Races have helped sustain a personal interest in aeronautics, which is extremely difficult, considering the high cost of aeroplanes" (ref. 11).

Of the participants, D. Reece returned to his native England to develop light hovercraft and C. Fitzgerald eventually emigrated to the United States, where he founded the Hoverclub of America and established Neoteric USA, Inc., a manufacturer of light hovercraft.

3.2.2 United Kingdom

In the early sixties, the United Kingdom had an active group of light-hovercraft experimenters. Outstanding among these was a mechanical engineer, Jeff Harding. In January, 1965, he proposed that individuals should form an organization and arrange a race meeting where they would have the opportunity to meet, discuss, compare ideas, and compete. On June 18, 1966, Europe's first amateur hovercraft rally took place at Apethorpe Hall, Northants. Lord Brassey, owner of Apethorpe Hall, was very interested in hovercraft and had recently purchased one. The task of organizing the rally was undertaken by Jeff Hatton. Twelve craft were at the rally, although not all of them competed. This was the beginning of the British Hoverclub movement. One of the participants was Dan Reece who had been in the Canberra race. His craft won the Lord Brassey challenge cup. Reece went on to become the designer for Lord Brassey's new company, Hover Air Ltd., established in August, 1966. Although the company eventually failed, it produced about one hundred Hoverhawk craft which were sold world-wide. The Hoverhawk was a two-seater, with three engines and a bag skirt (Fig. 3.13).

John Player and Sons, a tobacco company, sponsored the Hoverclub during the early years, but dropped out in 1969. Thereafter, the British Hoverclub became self-sufficient. British craft demonstrated some improvement throughout the sixties. Hovercraft enthusiasts benefitted from corporate technology, which was forming the basis of this new industry. Britain's public press continued enthusiastically to promote this new invention and its technology. England had

the advantage of being a small country where enthusiasts lived within easy driving distance of each other and could meet frequently to compare and exchange ideas about their new machines. However, there were relatively few suitable hovercraft operating areas. Most waterways and canals had incredibly low speed limits, such as 5 km/h (3 mph), and were overrun by fishermen. Although coastal regions were suitable for cruising craft, the salt water was hazardous. Club members were forced to seek out suitable private estates and regional government lands for rally activities. The race courses in such areas were usually half water and half land; the land being grass, sand, gravel, and mud. Courses contained sharp turns and banks to negotiate, trees to dodge, ridges and ledges to jump, and even railroad tracks to cross. Many locations were subsequently developed into a national circuit. The better courses happened to be located on the grounds of stately homes. Regulations, safety rules, points scoring, and classification were developed as courses were established. Some members became marshalls and announcers. Regular meets, get-togethers, rallies, hover-ins, and especially competitive trials set the stage for development in the following decade. No other country was so well-equipped for the subsequent evolution of the sport.

In the seventies, craft changed from underpowered, bag-skirted, propeller-driven vehicles to light-weight, high-powered racing machines with segmented skirts and ducted fans. Racing meets took place regularly in locations where the majority of members could participate, and several really proficient drivers evolved. Club members were quick to adopt any new idea that proved itself in competition. An evolutionary process took place, in which the best machines were selected and copied. The process involved a large number of

Fig. 3.13 Hoverhawk built by Hover Air Ltd.

machines and a gestation period of about 15 years. Machines that consistently won were soon duplicated and successful ideas were emulated by other members. No light hovercraft company could have afforded such an approach to product development. The resources required to match those of hundreds of members experimenting with different ideas and evaluating them in regular competition would have been too great. Thus, it was (and remains) beneficial for manufacturers to participate in club activities.

3.2.3 North America

The environment also influenced hovercraft development in North America. In contrast with their British counterparts, enthusiasts were scattered across vast distances. Since both the United States and Canada abounded in ideal hovercraft operating terrain, enthusiasts were not as prone to get together to share selected sites.

Communications were sporadic, usually duplicating those of British publications. An Indiana enthusiast, Jan Eglen, published a newsletter called *The Kestral*, and formed the *National Association of Air Cushion Vehicle Enthusiasts*. The newsletter and association prospered until Eglen resigned in about 1973. Another enthusiast, Rod McKeighan, transferred the club to Michigan and changed its name to the *American Hovercraft Association*. In 1975, at the time of Christopher Fitzgerald's arrival in the United States, this association was in disarray. Therefore, in January of the following year, he established and organized the *Hoverclub of America, Inc.* in Indiana. It has since become the largest club of its kind, with membership fluctuating between 600 and 1000. This club has promoted national rallies. Because distances are great, its national rallies do not attract large attendances as compared to England. Usually 30-35 machines and approximately 150 members participate. Unlike its British counterpart, the American club has not been very successful at developing competitive activities. Whereas races and cruises are usually included in the national event, they are not yet part of any planned racing system. Also, the wide variety of craft designs makes it difficult to establish competitive standards. Although handicap races were successful for a few years, they produced little incentive to improve machines.

In North America, there seems to be two types of light hovercraft enthusiasts. Some are interested in sport; the others in profit. The latter group may be in the majority. As a result, during the late sixties and early seventies, many attempts were made at commercialization. Several companies individually produced about 3,000 units, and these machines were sold through dealers. Unfortunately, usually in desperation to sell units, manufacturers drifted away from their initial attempts to qualify dealers. When, in addition, hovercraft products fell short of customer expectations, many manufacturers were driven out of business. Such were the fates of Air Cycle, MHV

Spectra (Fig. 3.14), Skimair, Canahover HoverRover (Figs. 3.15 and 3.16), Eglen Hoverbug (Fig. 3.17), Cushionflight (Fig. 3.18), Chinook, and Windcraft Hurricane (Fig. 3.19).

Nevertheless, some small American companies have survived through low overhead, minimal production, and subsidies. This method of operation has a

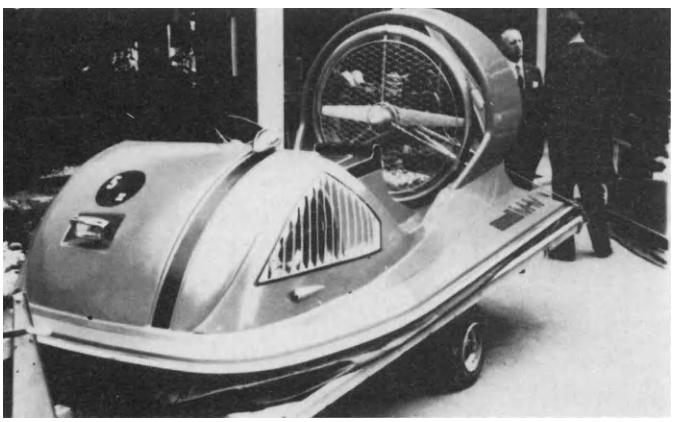

Fig. 3.14 The MHV Spectra built in Canada during the late sixties. The craft had twin 2-cycle engines and bag skirt. Twin Multi-Wing lift fans were arranged, one on each side of the craft, behind the front inlet louvers.

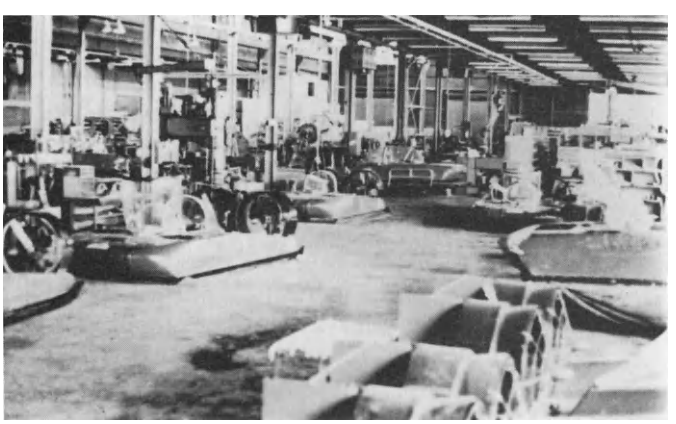

Fig. 3.15 Canahover HoverRover production plant in Ottawa, Canada, 1970.

similar counterpart in the United Kingdom, where individual vendors (usually club members) act as suppliers of machines and parts. This is, in effect, a cottage industry. When sales are few, the enterprise hibernates, and it reappears as demand improves. In other words, such a system is market-driven and not dealer-dependent. The successful vendors are keenly aware of the need to

Fig. 3.16 Canahover HoverRover design from Ottawa, Ontario, used three 9 kW (12 HP) engines: one for lift, driving two centrifugal fans; two for thrust, driving two-bladed aluminum propellers.

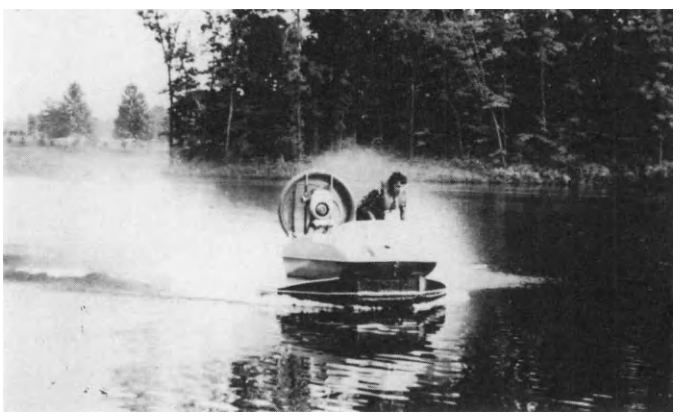

Fig. 3.17 The Eglen Hoverbug was manufactured in Terre Haute, Indiana. This machine had two engines and a molded thermoplastic body and hull.

survive while their products are developed and accepted in the market. Some typical examples of survivors are Air Vehicles Limited and Griffon in the United Kingdom and Hover Systems Inc. in the United States. A few more successful American companies are described below.

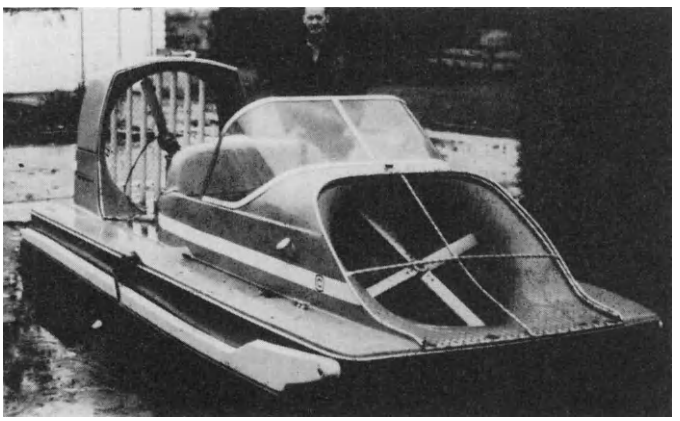

Fig. 3.18 The Cushionflight of California used a 1600 cc Volkswagen engine to power a forward-mounted lift fan. This fan was driven via a timing belt and cable drive. A similar system drove a variable-pitch thrust propeller. A servo-motor control system was used to retract the brush skirt.

Fig. 3.19 The Windcraft Hurricane of Toledo, Ohio, was powered by a single air-cooled snowmobile engine coupled to a multi-bladed fiberglass fan via a tooth-belt reduction drive.

(i) Universal Hovercraft. Early in 1976, Robert Windt formed *Universal Hovercraft* in Cordova, Illinois. This mail-order business backs onto the Mississippi River, an ideal location for testing craft. Windt has amassed more hovercraft operating time than anyone else in the United States. His philosophy is not unlike Sir Christopher Cockerell's i.e., hovercraft should be fun, enjoyable, and must go faster than any comparable boat. He has limited his sales to plans, propellers and fans, and has survived for more than twelve years. In conjunction with his many customers, Windt tests lots of ideas and he has successfully developed a large following for his machines. Approximately 90% of all homebuilt hovercraft in the Hoverclub of America are his designs.

The Windt designs have common features. They are constructed from wood, have two-bladed wooden propellers for thrust and four-bladed wooden fans for lift, are fitted with bag skirts, use lawn-mower or small industrial engines for lift, and automotive or snowmobile engines for thrust. The faster craft are arrowhead-shaped and have pointed noses. The more common configurations are rectangular with chisel-shaped fronts. In single-engine machines, the engine is always in the rear. He has developed a clever auto-lift system that uses two Salisbury belt-driven clutches. As engine speed increases, sheaves on the engine shaft open while sheaves on the driven lift-fan shaft close. This changes the drive ratio. The lift-fan speed remains practically unchanged while the thrust-propeller speed increases. Several designs have servo-operated arrangements controlled from the cockpit. At speeds around 100 km/h (62 mph), very little lift power is required from the engine because of fan-intake ram air, so power to the lift fan can be reduced. For control, two or more vertical rudders and one horizontal elevator are mounted in the propeller slip-stream. To sum up, Windt's craft are popular because: (a) the machines are fast and their performance is impressive, (b) they are not complicated to build, (c) most construction materials are available in cities and towns throughout North America, and (d) a range of machines is available, varying from 3 m (10 ft) to 8 m (26 ft) in length, and capable of carrying one to twelve passengers.

In July, 1979, Robert Windt and a crew of four drove his 8 m UH-26S craft (Fig. 3.20) on the Mississippi River from Cordova, Illinois, to New Orleans, Louisiana, and back, a distance of 4,410 km (2,740 miles). Then on June 30, 1985, following two previous reconnaissance trips by hovercraft in 1979 and 1984 and two attempts in 1984 and 1985 with his UH-19P craft (Fig. 3.21), Windt and Michael Kiester set the boat-speed record from New Orleans to St. Louis. The 1,653 km (1,027 miles) distance was covered in 21 hours and 47 minutes, for an average speed of 75.9 km/h (47 mph). The previous record of 23 hours and 34 minutes was set by a 175 kW (235 HP) bass boat. Windt estimated that he could significantly reduce this time by running faster during daylight, thus reducing

the time of having to run at the slower speed of 56 km/h (35 mph) during darkness.

(ii) Neoteric USA. In 1975, two years after registration of Neoteric Engineering Affiliates Pty. Limited in Australia, Neoteric USA was incorporated in Indiana and based in Terre Haute. Since the Australian do-it-yourself plans for Neova hovercraft were more complicated than competitor's designs sold in the United States, Neoteric developed and marketed kits to improve the competitiveness of the Neova design. The company handbuilds five distinctive models.

Fig. 3.20 Windt 8m UH-26S craft. A 5.8 litre V-8 engine drives the thrust propeller via Poly-V belts and the axial-flow lift fan through a novel variable-ratio transmission system called AutoLift.

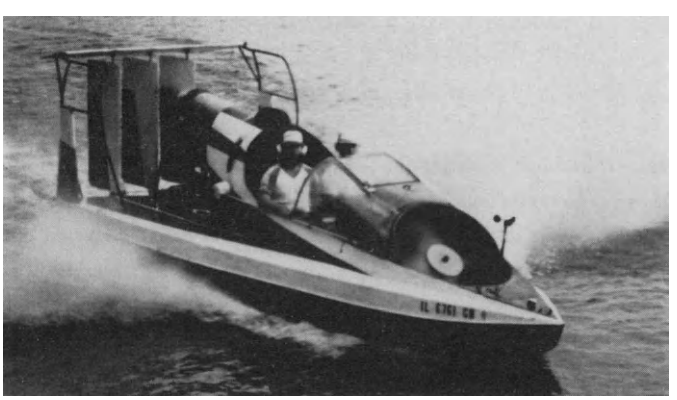

Fig. 3.21 Windt UH-19P craft. A 2.8 litre V-6 engine drives both the lift fan and thrust propeller.

The Neova I shown in Fig. 3.22 was used for hunting in a tidal mangrove swamp. Some of Neotric's machines have been used in television advertisements in Canada (Fig. 3.23), Brazil and Germany. The Neoteric Explorer model (Fig. 3.24) is used by Disney to promote the Skyleidoscope air and water show. Twelve of its Racer models, dressed as dragons and driven by human lizards, appear daily at Disney World's EPCOT Center in Orlando, Florida. These dragon

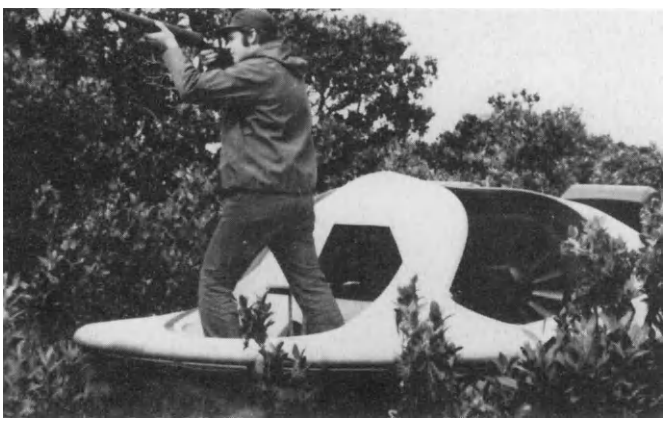

Fig. 3.22 Neoteric Neova I. A 1600 cc engine drives twin axial fans for lift and thrust. Features thrust reversers and jupe skirts.

Fig. 3.23 Neoteric Neova II. Equipped with a 1600 cc engine, thrust reversers and jupe skirts.

hovercraft take part in a 15-minute choreographed performance, called Skyleidoscope, on Disney's EPCOT Lake and have run successfully since October 1985 (Fig. 3.25). An undressed Neoteric Racer at Hoverally '85 is shown in the foreground of Fig. 3.26. A larger Neoteric model, the Neova 6, is shown in Fig. 3.27.

Fig. 3.24 Neoteric Explorer. Equipped with a bag skirt. Powered by an air-cooled two-cycle 41 kW (55 HP) thrust engine and a 6 kW (8 HP) lift engine.

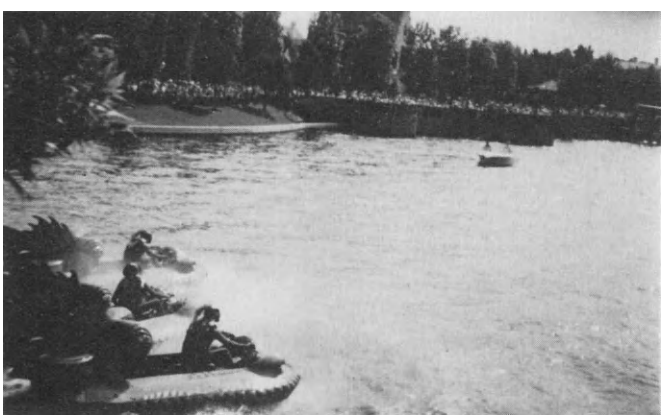

Fig. 3.25 Neoteric Racer model. Dressed as a dragon and driven by human lizards at Disney World's EPCOT Center. Equipped with a segmented skirt and thrust reversers. Powered by a 41 kW (55 HP) two-cycle engine for a combined thrust and lift fan-system.

(iii) Other Manufacturers. Because of increasing exposure and improving performance, several British craft designs have found recent success in the United States. During the mid-eighties, three designs, i.e., Sunrider, Bill Baker's Special (Hoverstar) and Kip McCollum's Pee Wit (Scat), formed the bases of new American companies. American Hovercraft Industries, Inc., in Orlando, Florida, began making and selling the Sunrider; Hovertechnics, Inc.,

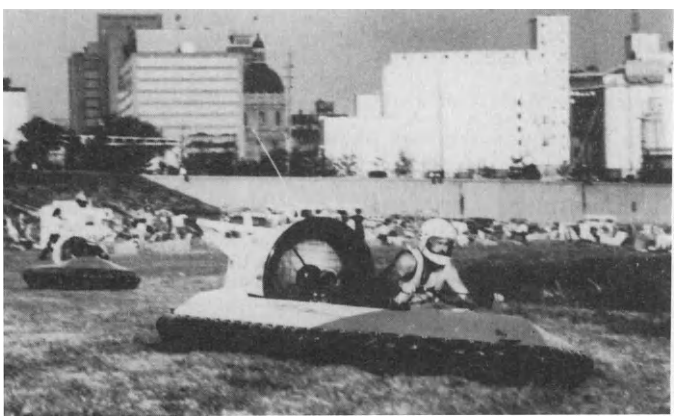

Fig. 3.26 Neoteric Racer, in foreground, at Hoverally '85, Indianapolis, Indiana.

Fig. 3.27 Neoteric Neova 6. Twin 0.914 m (3 ft) axial fans are driven by a 5.1 litre V-8 engine. This 2.59 m (8.5 ft) by 5.94 m (19.5 ft) craft has thrust reversers, jupe and segmented skirts, and a 0.304 m (1 ft) hoverheight.

in Benton Harbor, Michigan, is doing the same with the Hoverstar; Scat Hovercraft, Inc., Miami, Florida, is producing and marketing the Scat. These companies seem to be reasonably well-capitalized. For example, a few months after incorporation, Scat went public and raised a working capital of 3.25 million dollars.

These new companies are also aiming at the dealer market. If they screen their dealers and select qualified representatives who can develop a market, then they stand a chance of success. Recent products are much improved over those of the past decade and offer better value and customer satisfaction.

3.3 TECHNICAL TRENDS

3.3.1 Engines

One of the first questions interested people ask is: "What kind of an engine does it have?" Engines are a natural fascination for anyone with a mechanical bent. The availability of suitable light-weight engines has contributed much to the development of small hovercraft. Early designers used engines which were readily available in their respective countries. England had a wide variety of small, light-weight, two-cycle engines. A few builders used aluminum-block car engines. American builders used chain-saw, lawn-mower, snowmobile, and air- and liquid-cooled automobile engines.

The power-to-weight ratio of an automobile engine is such that a fairly large machine is required just to carry the engine. They also take up a lot of space. The snowmobile engines of the seventies were relatively new. Their maximum power outputs were around 23 kW (30 HP), but they were unreliable. They proved particularly uncooperative when it came to operating in the hovercraft's environment of spray and dust.

Early designers and builders put an inordinate effort into adapting engines and trying to persuade transmission and fan systems to stay together. Persons living where the choice of engines was limited were forced to put more effort into engine installation. During the late sixties, the United Kingdom was probably best equipped with small, light-weight, two-cycle engines. Therefore, having to spend less time with unworkable engine installations, its builders and designers who were able to concentrate more on operating and testing hovercraft. This is one reason why small hovercraft evolved more rapidly in the United Kingdom during that period.

The seventies were the golden years of the snowmobile in America. In 1971, North American sales soared to almost 500,000 units. Engine manufacturers, mostly in Japan, were busily developing snowmobile engines with power-to-mass ratios of around 1.67 kW/kg. Reliability, dependability and ease of starting were improved with the introduction of capacitor discharge ignitions, better materials and manufacturing tolerances, and high-performance resonance-exhaust systems. These engines began to find their way into hovercraft toward the end

of the decade. About this time, trail bikes began to increase in popularity. Their engines and those of go-karts were also adapted for use in some hovercraft.

Practically all small hovercraft in England today use two-cycle, high performance engines for lift and thrust, because of their low cost, compact size, and high power-to-weight ratio. The fact that these engines run at about twice the speed normally required by fans has not been a handicap. If they would run at close to fan speeds, then direct coupling would be popular. Since this is not the case, a reduction transmission is required. Thus, the engine tends to be placed lower, resulting in a lower craft center of gravity and slightly less fan-intake blockage. The major disadvantages of these engines are their temperamental nature, high fuel-consumption, noise and vibration, and poor availability in some countries. Automobile engines and air-cooled diesel engines are commonly used in the 1,000 kg capacity craft sizes.

3.3.2 Fans and Propellers

(i) Lift. As in the case of engines, fans and propellers also seem to fascinate hovercraft enthusiasts. It is not uncommon for fans or propellers to be the first items purchased by a would-be builder; they represent a starting point. In the early days, a lot of theory dealt with fans and propellers; but now with 20 years hindsight, what works best is known and most builders use commercially available fans. Some of the heavier light hovercraft use centrifugal fans for lift. These are similar to fans found on home-heating and air-conditioning units. However, the axial-flow fan is a very common type of fan, which can be found practically everywhere for cooling, venting, and circulating air. It is good for the movement of large volumes of air at low pressures, whereas the centrifugal fan offers lower air-flows but at higher pressures. As light hovercraft rarely operate with cushion pressures above 958 Pa (20 lb/ft^2), or 96 mm of water, they happen to fit comfortably within the axial flow fan's capability. Such a fan is usually more than two-bladed. Wooden fans usually have four blades, and the Multi-Wing brand of plastic fan has a minimum of three. This Multi-Wing is found in most light hovercraft. It is available in diameters up to 1 m (3.28 ft) and is light. For example, a 0.6 m (2 ft) fan with 9 polyamide plastic blades has a 2.7 kg (6 lb) mass. Blades can be individually replaced and their pitch-angle settings are adjustable from 20 degrees to 45 degrees. The maximum recommended tip speed is 121 m/s (397 ft/s), but this is frequently exceeded in British and European machines. Such fans give best performance when operated with stationary blades and slight back-pressure. They are reasonably priced at about one-sixth of the engine cost. Generally, lift fans are mounted directly to vertical-shaft lift motors. Lift-fan installations are operated without stationary blades. When one fan is used to supply both lift and thrust (an integrated system), stationary blades

are often employed. For most applications, one-third of a machine's total air-flow is sufficient for lift.

(ii) Thrust. All amphibious light hovercraft are propelled by either fans or propellers. The quantity of static thrust available to accelerate a craft is important. One measure of performance is thrust efficiency, i.e., the ratio of thrust per unit of power. Air devices are notoriously inefficient when compared with tracked vehicles or even water propellers. The highest efficiency static-thrust air devices are helicopter rotors, which are capable of generating up to 72 N/kW (12 lb/HP). Next on the efficiency scale are propellers at 35.9-47.8 N/kW (6-8 lb/HP). The ducted axial-flow fan's efficiency is around 24.4-36.6 N/kW (4-6 lb/HP). The dominating parameter is diameter; the larger the diameter, the higher the static thrust efficiency. Safety considerations dictate that a propeller must be enclosed. A properly constructed wire cage is heavy and does nothing for the appearance of the machine; therefore, designers prefer to enclose propellers in ducts. A duct improves the propeller efficiency, acts as safety enclosure, and reduces propeller tip-generated noise. Ducts are, unfortunately, difficult and expensive to manufacture accurately and with light weight. Ducted-propeller thrust units are employed on most of the heavier light hovercraft. Whereas open and ducted propellers dominate the American do-it-yourself market, ducted thrust fans are found on almost every small hovercraft in England and Europe and also on all current production machines. The ducted fans' universal popularity has much to do with safety. Ducted fans are easily enclosed, offer a low thrust line, require less supporting-structure and transmission weight, and can incorporate thrust reversers. Furthermore, ducted fans lower the visual profile of small craft, thereby tending to make them more aesthetically appealing. Their true cost, however, must include their loss of static-thrust efficiency over that of propellers. At speed, the thrust efficiency of ducted fans can approach, or exceed, the efficiency of propellers. For the range of practical hovercraft speeds, both efficiencies are more likely to be equal at the top end. At low speeds, propellers offer higher thrust and, consequently, superior acceleration.

3.3.3 Power Transmissions

Many types of power transmission are employed in light hovercraft, but the most universal is the toothed timing belt. A more refined version is the HTD belt, which can be found on most of the larger commerically-made light hovercraft. Pulleys and sprockets are mostly aluminum, but Delrin and other plastics are also in use. Some homebuilders in the United States use wooden sheaves and poly-V belts. Modern HTD belt drives are virtually trouble-free and need little attention. Practically all machines are now direct-drive, except for the heaviest models, in which various types of clutches can be

found. A few small craft use centrifugal clutches and some use rubber torsion-couplings. Sprocket ratios are selected so as to ensure that fan and engine power curves are properly matched.

3.3.4 Controls

Larger light hovercraft sometimes employ skirt-shift controls. Such controls move the inner skirt attachments to change the air cushion's center of pressure and cause the machine to roll or pitch. Alternatively, water or fuel is pumped into fluid tanks fitted in the bow and stern to change longitudinal trim. Such complications are unnecessary on smaller machines. If a machine is operating at the proper angle, i.e., horizontally or slightly nose-up, it is said to be correctly trimmed. Drivers and passengers in small machines have to move about to adjust trim as required. This method, called kinesthetic control, is extremely important on small racing machines. The driver must constantly shift his/her weight about to assist the machine in operation while accelerating, decelerating, or banking into turns, to prevent it from nose-diving into water or becoming airborne. All hovercraft are fitted with vertical rudder blades, which are mounted in the fan, or propeller, slip-stream and controlled through a steering wheel, joystick, or bicycle-style handlebar. Some machines have horizontal elevators for longitudinal trim. These are especially useful for machines in which the driver cannot readily move about. Some machines utilize thrust reverse-buckets for control, braking, and backing up. Hovercraft throttles provide an important means of control.

When the lift engine is separate, precise control over the air cushion is possible. Such control helps to reduce dust and spray, minimize skirt drag, or adjust the skirt drag for braking. Also hovering without moving is possible. Separate lift is handy when trying to move a machine around inside a workshop. Plow-in tendencies while traveling can often be offset by a correct application of lift throttle. Reducing the thrust throttle setting is one means of slowing, but emergency stops are achieved by throttling the engine(s) and setting the machine down on under-hull skids. A full-power 180-degree turn using maximum thrust is also a common means of braking.

3.3.5 Skirts

Skirts have had a profound effect on the practicality of hovercraft. They are, in essence, the base technology of hovercraft. Most of today's skirt know-how was invented and developed in England over a few years during the mid-sixties. Not much development has occurred since then. In the United States, the majority of homebuilt hovercraft uses the nonflow bag skirt. This is perhaps the simplest of skirts and one of the most rugged. However, it has a tendency to bounce, which is especially serious over smooth hard surfaces such as blacktop and ice. A few machines employ the jupe skirt system. The Ameri-

can companies which manufacture English designs use segmented (finger) skirts. With a few exceptions, European and British machines use segmented skirts made with 140 g/m^2 (4 oz/yd^2) pack cloth or 200 g/m^2 (6 oz/yd^2) neoprene-coated nylon. Bag and jupe skirts use 540 g/m^2 (16 oz/yd^2) neoprene-coated nylon. Neoprene-coated nylon cloth has demonstrated its superiority to most other fabrics as a suitable skirt material. Small British craft started out using bag skirts in the late sixties, but ended up using mostly the segmented type in the eighties.

3.3.6 Structures

The selection of building materials for hovercraft followed a natural course. The first builders began using wood, which is still popular today. The majority of American homebuilt craft are wooden. Some early builders used fabric-covered structures, fiberglass (usually requiring expensive molds), and aluminum. Nothing radical has taken place in the use of materials. Several machines, especially the larger passenger-carrying craft, are aluminum; others are composite fiberglass with a foam-sandwich construction. Most wooden construction employs ribs and longitudinal stringers covered with thin plywood. Curved parts and joints use fiberglass-covered foam. Moldings are used where compound-curve sections are needed, such as for intake bellmouths and ducts.

Making light hovercraft structures strong enough is not difficult. Over the years, there have been few examples of structural failures, probably due to the nature of the craft. With its large area, internal ducts and encasing body, it happens to be strong torsionally. Point loadings are few and not subject to fatigue since the structure's motion is well-damped by the air cushion. It can be concluded that it is difficult to make a hovercraft structure light enough to compromise its strength. Long before this would happen, other problems would appear, such as local failure where someone stepped on the structure.

Some machines, notably by Pindair Ltd., have used inflatable boat principles. These structures are sensible for small hovercraft because they can absorb point impacts, which are an important concern. However, there are difficulties in keeping them inflated, distributing point loads, and keeping their specific weight and cost down. It is also quite a challenge to make them look appealing; they tend to have a bulbous appearance.

Structural stiffness in small hovercraft is not critical because the structure is supported evenly by the cushion pressure. However, flimsy structures face difficulties in distributing point loads, just as inflated constructions do. Tolerances and dimensional accuracies need not be high. The crudest hovercraft seem to work. Proper craftsmanship and design are not critical to their successful operation. However, the cost of small hovercraft is relatively high because of their large surface area and volume, requiring large quantities of materials.

Because they can operate over water, hovercraft are more like boats than airplanes; only their low weights are in common with the latter. However, hovercraft must combine features from both the boat and the airplane. Their cost will probably always exceed that of an equivalent boat, but should be less than that of an equivalent aircraft. The hovercraft's bulkiness will always limit its eventual market penetration. Hovercraft are relatively costly, they take up a lot of storage space at home, and transportation can be a problem, e.g., they may not fit in the back of a pickup truck. For these reasons, their potential market penetration is limited as compared to more compact vehicles.

Most mass-produced small hovercraft are constructed from inexpensive chopmat fiberglass. The hull is constructed on a mold and sandwiched between a urethane core and a fiberglass body. It is usually constructed in two pieces which are then bonded, or mechanically fastened together, with engine mounts, controls, landing skids, and handling points reinforced by additional glass material. Some wooden craft are built to look like their glass-molded production counterparts. Plywood sheets are fastened together and sealed with epoxy, microspheres and glass cloth tape. American machines built from wood usually employ a set of lateral ribs tied together with longitudinal stringers. The floor and upper deck are covered with 3 mm (0.12 in) or 4 mm (0.16 in) plywood. The corners are glass-taped, and the entire box-like structure is painted inside with epoxy and outside with exterior paint, or coated in polyester and glass cloth.

Esthetic design has taken a long time to achieve importance, and there is still room for improvement. Craft usually look like a pin cushion sliding along the water. Integrating bulky components into a sleek form is a challenge! Comparable products, i.e., snowmobiles and small boats, have set extremely high styling standards. Hovercraft should achieve greater acceptance with compact features, styling appeal, and a low, streamlined profile.

3.4 ORGANIZATIONS

3.4.1 Clubs and Federations

The hoverclub movement, which began in England, has spread throughout the world. Some addresses are listed below:

Hoverclub of America Inc.
P.O. Box 216
Clinton, IN 47842-0216
USA

Hoverclub of Japan
Masahiro Mino
Col. Ind. Tech., Nihon Univ.
2-11-1 Shin-Ei Narashino-shi
Chuba-Ken, Japan 275

Hoverclub of Great Britain
12 Mount Pleasant
Bishops Itchington
Leamington Spa
Warwickshire CV33 0QE England

Skeertuigklub Van Suid-Africa
Mariasstraat 5
Somerset West 7130, South Africa

Hovercraft Club of New Zealand
162 Carnoustie Dr.
Manurewa, New Zealand

Fédération Française des Clubs d'Aéroglisseurs-Secrétariat
12, rue Béranger-92100 Boulogne
Billancourt, France

Hoverclub of Victoria
16A Rennison St., Mordialloc
Victoria 3195, Australia

World Hovercraft Federation & Hoverclub von Deutschland
Lechfeldstr. 2
8905 Mering Bayern, West Germany

Hoverclub of Uppsala P.O. Box 1436
S-75144 Uppsala, Sweden

As each club forms, the members usually adopt many of the rules and regulations developed by the Hoverclub of Great Britain. These rules and standards are contained in one or more of the following publications, which are available from the Hoverclub of Great Britain Information Officer: (1) Light Hovercraft Handbook, (2) Design, (3) Construction and Safety Requirements, (4) Light Hovercraft Competition Rules, (5) A Guide to Model Hovercraft, and (6) Insurance.

Competition between hoverclubs of various countries has existed from the outset. To help organize and establish international standards, a world federation is emerging from the present European Hovercraft Federation. An international Federation has been in existence for some time, but it has been dormant. Now, with Europeans entering the sport in a big way, the Federation has begun moving into prominence. In 1986, the American club joined the World Federation at the invitation of its President, Franz Berndt, Sr., who is planning to establish a world series. An annual international meet is to be held in participating host countries. One of the Federation's objectives will be to select an annual world champion driver.

3.4.2 Manufacturers' Associations

With the increased cost of product liability insurance, especially in the United States, a need exists for a manufacturers' association. This association could influence and monitor developments within the industry and assume an advocacy role. American manufacturers are now considering the formation of such an association. A similar organization was incorporated in England some years back, but is presently inactive.

3.4.3 Racing Classifications

The system of craft classification adopted by the World Federation of Hoverclubs is as follows:

Formula Junior - 12 to 16 years of age, and under 250 cc engine capacity
Formula 3 - Under 250 cc total engine capacity
Formula 2 - Under 500 cc total engine capacity
Formula 1 - Over 500 cc total engine capacity

The European Federation uses another formula, called:

Formula S - Single duct, maximum diameter 800 mm.

International craft numbers indicate the country which the driver represents:

1 - 199	Great Britain	400 - 499	Belgium
200 - 299	France	500 - 599	Sweden
300 - 399	Germany	900 - 999	Italy

Craft racing numbers within Britain indicate the final position of the driver in the previous year's racing. British numbers are also divided as follows:

Formula 1, 1 - 49; Formula 2, 51-99; Formula 3, 101-199.
New drivers must qualify before racing in national championship events. Novices must complete five novice races to qualify for Formula 3 and must complete fifteen Formula 3 races to qualify for Formulas 1 and 2.

The point scoring system for all races is: 20 for winner, 17 for second, 15 for third, 14 for fourth, reducing by one point per place for all qualifying finishers. If there are four national meets per year, points are added to determine the national champion. If there are five, six, or seven meets, the score from one meet can be dropped; if there are eight or more meets, scores from any two meets can be deleted, usually the lowest.

3.5 FUTURE

The hovercraft industry is a wide-open area for research and potential breakthroughs. Tremendous opportunities exist for improvements in marketing and manufacturing concepts, power plants, skirts, structures, dynamics, and performance.

Some problems are inherent to all hovercraft and require urgent attention. Plow-in, dust, noise, spray, maintenance, and dependability are problems in need of solutions. Power plants, power-to-weight ratio, dependability and cost should gradually improve. With the manufacturers' market for hovercraft engines expanding, their research and development budgets should increase, and engines specifically developed for hovercraft should appear. Materials used in hovercraft construction should improve in strength, stiffness, durability, ease of repair, but most importantly reduce in cost. Hovercraft control, maintenance, esthetics, and creature comforts should improve as the industry puts more effort into product development.

Hovercraft tend to be more expensive than equivalent vehicles. However, as market demand increases, economy of scale effects should work to improve manufacturers' margins and lower unit retail prices. Lowering labour and material costs will be essential to reducing unit prices. When an annual market develops for more than 2,000 of any one hovercraft model, capital-intensive stretch-formed aluminum hulls and vacuum-preimpregnated glass cloth oven-curing techniques could find applications as labour-saving alternatives, and perhaps even thermoplastics.

Technically, light hovercraft should continue to improve as they have over the past decade. The present speed limit is the airborne speed barrier, at which the forward-speed dynamic air-pressure exceeds the static cushion pressure and the hovercraft begins to fly. Many racing machines are experiencing problems in this area.

Small hovercraft have the potential for becoming primary transport vehicles in many undeveloped areas. They can be constructed on site; only the engines and a few essential components need be imported. Furthermore, their extreme

versatility suggests world-wide applications. Requiring no road or special track, they could become an important mode of transportation. Some existing and potential applications include: racing, touring, cruising, exploring, nature study, commercial rides, search and rescue, ice fishing, hunting, crop and water-weed spraying, transportation, surveying, water-taxi service, flood control, environmental projects, advertising, public entertainment, speed records, training, hiring-out, do-it-yourself projects, educational projects, studies in the military, police, civil and scientific spheres, animal husbandry, and farming. As the number of light hovercraft increases, new applications will be found, based on their unique capabilities. Because hovercraft are not as limited as snowmobiles geographically, their sales as racing units, cruising craft, machines for hunting, and commercial applications should eventually exceed snowmobile sales. Light hovercraft should become a significant new vehicle in the marine industry. They are a truly new and novel type of boat. Their concept represents one of the few breakthroughs in marine transportation since the hydrofoil. Their future as a viable transportation vehicle for sport, recreation, and commerce should be assured.

However, if the market should remain small, the industry would remain labour-intensive rather than capital-intensive. When the automobile, motorcycle, snowmobile, and aircraft industries began, large numbers of individuals and companies entered manufacturing and selling. As these industries matured, a few companies captured a major share of the market. The light hovercraft industry could be expected to do likewise. But it is likely that there would always be room for backyard and small-business types. If individual-model production runs would remain small, manufacturing would probably take place close to the end user.

Small hovercraft make spectacular and safe racing vehicles. Their future should be guaranteed for this type of entertainment. Great things can be expected. They are inexpensive when compared to modern wheeled racing machines and natural tracks for hovercraft races exist in practically every city in the world. A first-class race needs little more than some water and adjacent land, ice, or snow. But before world racing can become a reality, commercial sponsorship is necessary. The rate of growth of this sport will depend upon sponsorship. Whereas the potential is enormous, insurance difficulties and a lack of public awareness are barriers to be overcome before this sport can achieve international renown.

3.6 SUMMARY

This chapter has studied the evolution of light hovercraft, particularly in the United Kingdom and North America, from the time of the first one, the SR.N1 built by Saunders-Roe of Britain in 1959, to the present. The world's first

hovercraft race, held in Canberra, Australia, March 4, 1964, was described in some detail as a turning point giving impetus to hovercraft development. Technical information and photographs of entries were given, since these hovercraft can be thought of as having provided a foundation for subsequent developments. Current practice in the design and use of light hovercraft components, including engines, fans, propellers, power transmissions, controls, skirts and structures, was examined. Hovercraft clubs and federations, manufacturers' associations and racing classifications were surveyed. Possible directions for the future development of light hovercraft were presented.

3.7 REFERENCES

1. The Hoverclub of Great Britain Ltd., Light Hovercraft Handbook, reprinted 1983.
2. The British Petroleum Company Limited, The Story of HOVERCRAFT, p. 14, Portsoken Press, England.
3. Air Cushion Vehicles, (out of print periodical), Iliffe-Transport Publications Limited, London, England.
4. G.H. Williams, Homebuilt Hovercraft, Air Cushion Vehicles, Vol. 5 (30), Iliffe Transport Publications Limited, London, England.
5. L. Hayward, The History of Air Cushion Vehicles, Kalerghi-McLeavy Publications, London, England, 1963.
6. R. McLeavy (Ed.), Jane's Surface Skimmer Systems, now Jane's High-Speed Marine Craft and Air Cushion Vehicles Yearbook, Jane's Publishing Company Limited, London, England (annual).
7. Hovering Craft & Hydrofoils, Kalerghi Publications, now Combat Craft, Capstan Publishing Company, London, England.
8. A. Croome, HOVERcraft, Brockhampton Press, Leicester, England, 1960.
9. B. Arkel, Hovercraft World (out of print periodical).
10. C.J. Richards (Ed.), Slipstream, Hovermail Collector's Club, Southsea, England.
11. N. Tanswell, World's First Hovercraft Races, Air Cushion Vehicles, Vol. 4 (22) (April, 1984) 49-52.

Chapter 4

HOMEBUILT HOVERCRAFT

4.1 INTRODUCTION

There are many things an ACV (air cushion vehicle) can do, and many other things it cannot do. A light ACV is like any other vehicle, it has definite capabilities, and limitations. It can move over smooth land, soft land, water, thin or thick ice, and some snow conditions. But it cannot go over very rough land, long grass and other vegetation, loose pebbles, or up and down steep slopes. Moving slowly, it can be steered quite accurately by a practiced pilot. Moving fast, it needs a lot of room to manoeuver, owing to its lack of ground friction. It can go where other vehicles cannot; but if it breaks down there, rescue is difficult. Its operation must therefore be approached with considerable caution.

An air cushion vehicle is not a *magic carpet*. It is just what its name implies – a vehicle which rides on a cushion of air. It is large for its carrying capacity, so that its *footprint* is large and very light, and air is pumped under it by a fan driven by a small gasoline engine. The *air cushion* is retained under it by a rubberized fabric curtain all round it, called the *skirt*. There are various kinds of skirts, and their design is very subtle, and based on considerable experiment and development. Another fan (or sometimes the same one) drives the machine along, just as does the propeller of an aeroplane. The design of these propellers is an expert's job. They must be efficient, strong, and as quiet as possible, none of which is easy. The machinery is mounted on a light but strong hull, on which the pilot sits, and which must have enough built-in buoyancy to float if the engine fails.

If one wishes to build and drive an ACV it is better to build a simple basic machine first, have fun and learn on it, and then go on to a more advanced

version, than to try to start with an advanced one and get frustrated. The first step is to write down in detail just what is required regarding size, power, ground over which it has to operate, cost limitations, etc. Kits of parts or detailed drawings and instructions can be purchased to build reliable, simple, well-proved designs. Alternatively, one can work carefully through this chapter to design and build one's own. But whichever way is chosen, get an expert to check the designs before buying any materials. He may save a lot of frustration and expense by sharing a little of his experience. And get him to check the craft before testing it. This could save the craft and the pilot's neck.

4.2 BASIC DESIGN

Simplicity, lightness, quietness and safety are marks of an excellent design. Complication, overweight, and noisiness are to be avoided. First, to get the possibilities and outlines settled, a few simple sums are in order.

(a) What is the load? This means the pilot, plus a motorcycle helmet, a life jacket, and a few pounds for luck – 890 N (200 lb). If you want a two-seater, add 890 N (200 lb) for the passenger. Do not think of more than two people at this stage.

(b) For a craft of this kind, experience has shown that the cushion pressure (air pressure under the craft, supporting it) should be not more than 5 cm (2 in) of water gauge – about 500 Pa (10 lb/ft^2). As a very rough first guess the craft might weigh 1330 N (300 lb), for a single seat type, so the total weight would be 2220 N (500 lb). Since cushion pressure = (total weight)/(footprint area), it follows that the footprint area is 4.5 m^2 (50 ft^2).

(c) The width of the craft should be between 1/2 and 2/3 of its length, so we come up with a planform of about 2.75 m × 1.70 m (9 ft × 5½ ft). The hard-hull structure will be a little bigger than this; so, as a first guess, 3.0 m × 1.8 m (10 ft × 6 ft) would give a small margin.

(d) The obstacle clearance of the craft will be about 7% of its length, in this case about 21 cm (8 in).

(e) The static thrust of the propulsion system should be about 150 N per 1000 N (15 lbs per 100 lbs) of total craft weight, including crew; so the present 2220 N (500 lb) craft will need approximately 330 N (75-80 lb) of thrust. The thrust fans available will generate something like 36 N/kW (5 lb/HP); approximately 11 kW (16 HP) will be needed for thrust from 75-90 cm (30-36 in) diameter fan in a duct.

(f) A lift power of about 3-4 kW (4-5 HP) is required for a craft of this size, so, if we combine the two functions in one engine, 15 kW (20 HP) is actually needed. It would be very wise to install an 18-22 kW (25-30 HP) engine, and have some power in hand.

From these quick sums the size and shape of the craft begin to emerge, and the more detailed design process can begin. It is probably best to consider thrust, control, lift, skirt, and hull separately. The hull will be considered last since its only function is to support the other systems and the crew. It is just as important as the other systems, but its design obviously must depend on their requirements, so the other systems are designed first.

4.3 THE U–TUBE MANOMETER

At this point it is important to introduce a basic tool of aerodynamics, the *U-tube manometer*. This is used to measure air pressures of up to 100 cm (40 in) of water, and the hovercraft builder would be completely lost without it. A U-tube manometer is a very simple pressure gauge, which in its most elementary form consists of a glass tube bent into a U shape and half-filled with colored water (Fig. 4.1). When there is a pressure difference

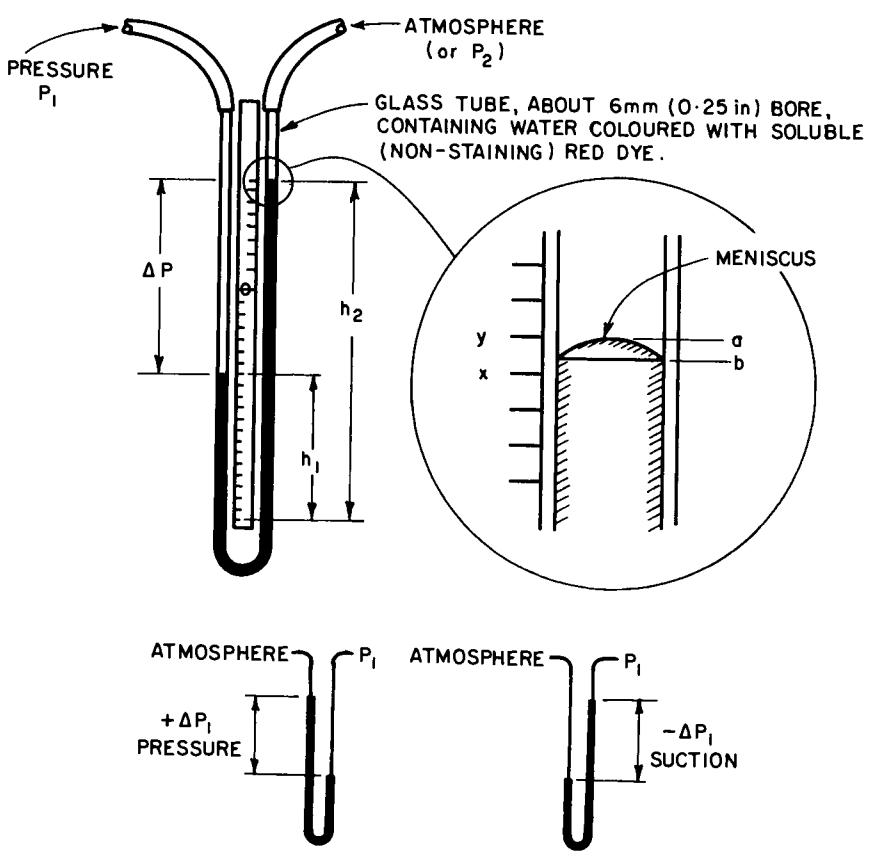

Fig. 4.1 U-tube manometer.

between the two arms of the U, this pressure difference is equal to the difference in height of the liquid in the two arms, and is stated as *so many centimeters (inches) of water*. Often one arm is left open to atmosphere and the pressure in the other arm is a *gauge pressure* (as distinct from *absolute pressure*) and is *so many centimeters (inches) of water above (or below) atmosphere*. The distinction between pressure (+pressure) and suction (-pressure) is most important, and must be stated carefully to avoid confusion.

Referring to Fig. 4.1, always measure to the same point on the meniscus of the surface of the liquid in both columns. For example, in the enlarged view at the right, if we measure at the top of the meniscus, the reading is y (opposite aq). If we measure at the bottom of the meniscus, the reading is x+(y-x)/2 (opposite b).

In the manometer shown on the left, either we can measure both arms from a zero near the bottom of the scale, so that the pressure difference $\Delta P = h_2 - h_1$ length units of water; or we can measure ΔP directly. Note that P_1 is at a higher pressure than P_2. The lower figures show the difference between positive pressure and suction (negative pressure) relative to atmosphere.

4.4 SKIRT

The first hovercraft retained the cushion of presurized air under the hull simply by pointing a peripheral air-jet curtain inwards to feed it, but only a very small hover height could be obtained unless excessive airflow was used. A rubberized fabric *curtain* was therefore put down under the hull to surround the cushion of lift air, while at the same time any solid obstacles on the ground could push through this curtain without harm. A number of types of curtain *skirt* evolved, and a few are now firmly established. The simplest is the *bag* skirt, while a version of the *HDL* skirt is also suitable for light craft. The *BHC* skirt is more suited to larger machines, and the French Bertin *Jupe* skirt is also not particularly suited to light craft. In this Chapter we shall deal only with the simple *bag* skirt.

4.4.1 Skirt Material

The skirt material has to be light, flexible, non-porous (to water and air), of high tensile strength, and reasonably abrasion-resistant. For use in Canada, it has to retain these properties at low temperature, otherwise the craft is out of action for at least half the year. For this reason, the PVC-proofed fabrics often used for skirts on British vehicles are useless for Canadian applications. These requirements are usually met by a nylon fabric coated oin both sides with a synthetic rubber such as hypalon, in thickness varying from 0.05 mm (0.020 in) down to 0.01 mm (.004 in) for a very light craft for use over smooth soft terrain or water. For a limited amount of experimenting in warm weather it is possible to get by with 0.01 mm (.004 in)

builder's plastic sheeting, or even plastic garbage bag material, secured with contact cement and office staples, but this won't hang together for more than an hour or so's running, and goes stiff if the temperature gets much below +10°C. It is worth remembering for a quick cheap first shot, to get a hands-on understanding of skirt technology.

4.4.2 Bag Skirt Design and Construction

A bag skirt, such as shown in Fig. 4.2 is the simplest skirt to design and build, and is very stable in roll and pitch. However, this stability is likely to result in a rather *hard* ride if the terrain is bumpy, or if the water has a short chop on it, and a torn bag has the additional disadvantage that it usually loses its inflation completely. Nevertheless, a bag is the starting point for most builders. There are more advanced types than the bag, but it is better to start with this, and progress to more complicated types later.

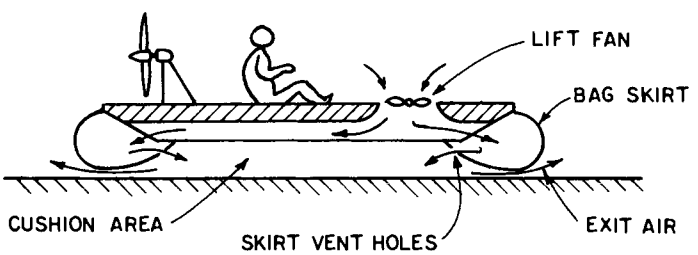

Fig. 4.2 General diagram of a simple bag skirt.

It is possible to have only a small air feed to the bag, with no exit holes at all, but even a slight tear will deflate the bag in a quick and dangerous manner. It is therefore much better to use the so-called *full flow* system, where all the lift air is blown into the bag. Vent holes on the inner walls of the bag then let this air into the cushion area (with a slight pressure drop in passing through the vent holes) after which the air escapes between the bag bottom and ground. The problem is how to design and build the skirt so that when inflated it will assume the desired shape in a strong and stable manner. We set about solving it as follows.

We begin by deciding on the clearance we want under the hull, while hovering. This should not be too small, otherwise rough ground will defeat us, and not too large, or the craft will become unstable and tend to over-balance. A height of about 7% of the length is a good compromise, so for our estimated 3 m (10 ft) length we shall arrive at about 21 cm (9 in) of clearance. In a diagram like Fig. 4.3 or Fig. 4.4, we can draw the outer curve of the skirt as a semicircle of radius r, coming from the hull outer edge A to the ground at B (vertically below A). The hull depth is likely to be about 30 cm (12 in) for this kind of craft.

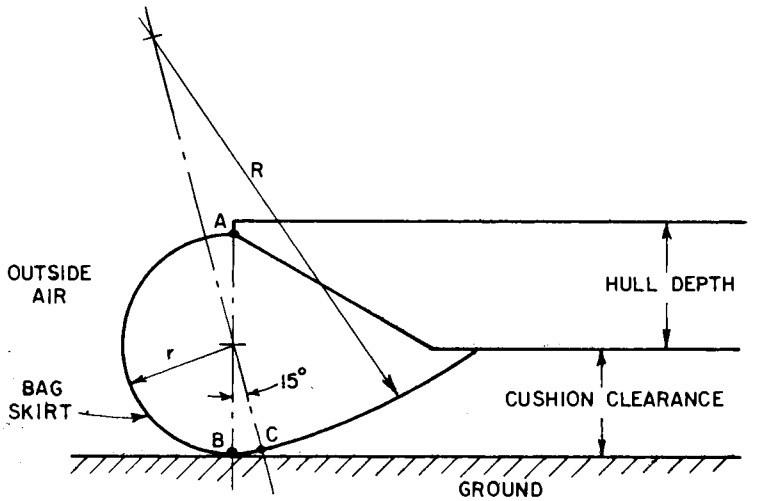

Fig. 4.3 Geometry of a simple bag skirt.

The skirt inner radius R is determined from Table 4.1. This table has been calculated so that for a given pressure ratio between bag and cushion, the skirt will assume the shape shown when it is inflated. The larger this pressure ratio (i.e. the higher the bag pressure) the stiffer the bag will be, like a well pumped-up tire, and the *harder* the ride. A reasonable value to try is about 1.3:1, which means that the bag pressure is 1.3 times the cushion pressure. Here, we are talking about *gauge pressures*, as read on a U-tube manometer, open to the air on its second limb. They are pressures above atmospheric.

Measure both bag and cushion pressures separately. Do not try to connect a U-tube between bag and cushion. In the present case, with 5 cm (2 in) of water gauge pressure in the cushion, we shall need 1.3 × 5 = 6.5 cm (2.6 in) of water gauge in the bag, with the 1.5 cm (0.6 in) being the loss through the vent holes. Assuming a further 1.0 cm (0.4 in) water gauge pressure loss in getting the air from the fan into the bag, this will mean that the lift air fan has to produce the required flow at 7.5 cm (3.0 in) water gauge pressure. If, for

Table 4.1. Determination of bag-skirt inner radius.

Bag/cushion pressure ratio	Ratio of skirt radii, R/r
1.2	6.0
1.3	4.5
1.4	3.5
1.5	3.0

example, we choose the 1.3 pressure ratio, then the inner radius is given by R = 4.5 r. We can now draw the skirt section, and notice that the two curves join at 15° inside the vertical line AB. The point A can be moved up to 5 cm (2 in) outside this, but never inside this line, as this will make the bag an unstable structure.

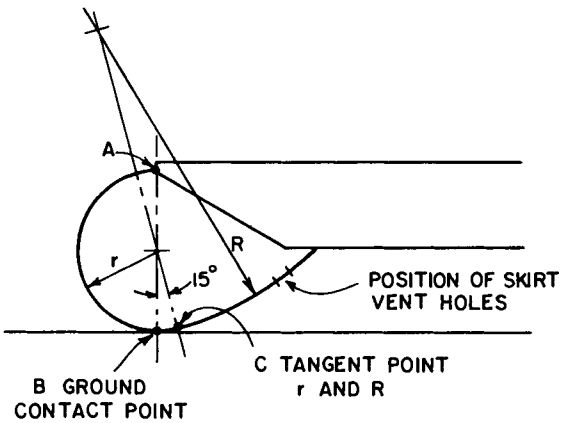

Fig. 4.4 Section of a simple bag skirt with vent holes.

The peripheral line through B, the *ground contact point*, is approximately the boundary of the cushion area, and defines the footprint area we estimated in our first rough calculations. We have now drawn the cross-section of the skirt along the sides and stern of the craft. However, the bow needs to be a little different, because here the bag is pushed back by the ground or water hitting it as the craft moves forward. This means that while the back end of the hull can be cut off square, and have the same skirt section, the bow must be shaped differently to produce a different skirt geometry (Fig. 4.5).

The simplest way to set this out is to make a full-size or quarter-size model, and set out skirt templates on it. This will also give the shape of the pieces to be cut to form the stern corners of the bag. The hull shape is made, and set upside-down on a floor or board. Templates to the skirt section already designed are fixed onto the hull along the sides and stern, with extra ones at the stern corners, as shown in Fig. 4.6. The stern corner sections are drawn in position to give a smooth transition round the corner. A simple *mitred* corner would lead to a weak and wrinkled fabric structure.

(i) Bow sections. The bow is a little more complicated, as seen in Fig 4.7. The lower view is a side view, in which the side section of the already-designed skirt bag is laid in, to show how it relates to the shape of the bow section. The bow of the hull has been raised somewhat, to allow the craft to rise over waves or obstacles instead of nosing into them. Now, on the

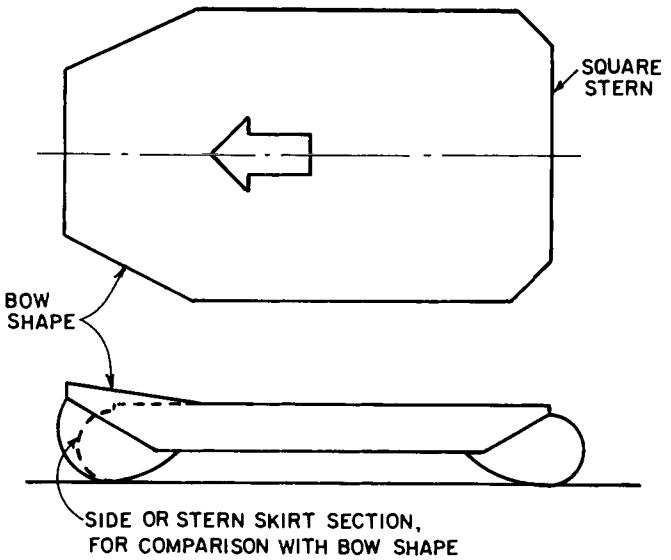

Fig. 4.5 Bow and skirt shapes.

hull model we have made, with the bow part in position, more skirt section templates are put in place at I, II, and III, with the last of the existing side sections at IV. The pair of views in Fig. 4.7 show the way to approach it. The upper view is a view from above, showing the upper edge of the bow of the hull (the gunwale) and the lower corner (chine), with the skirt also shown.

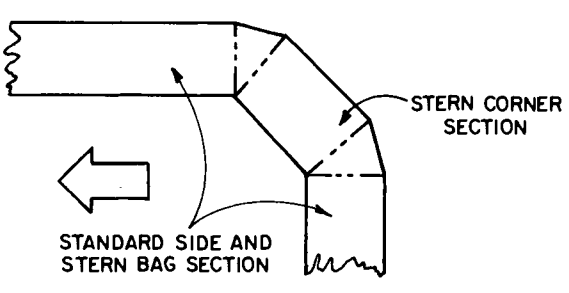

Fig. 4.6 Stern corner.

The section at e is drawn in very much the same way as the side section, except that the outer face is made as a circular arc with its centre at bow deck level, and its centre vertically above the ground contact point. This will define the length of the hull at the bow. When this section has been drawn, as in Fig. 4.8, and set up in cardboard on the model, the blank cards for sections III, II and I are set up, and cut to shapes which will transform smoothly from e to IV. This can be checked by bending a thin strip of wood or

wire round the surfaces along a horizontal plane, such as XX or YY, and seeing that makes a smooth curve (Fig. 4.7).

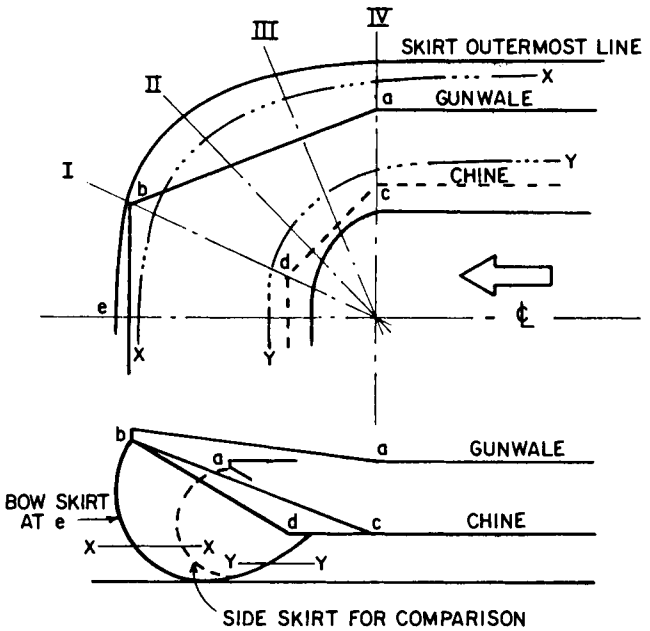

Fig. 4.7 Bow corner.

These sections define the cross-sectional shape of the skirt. The shape of the pieces of skirt material is now found by laying pieces of brown paper over the sections, to form the skirt surface, and cutting them to fit, with adequate allowance round the edges for seams and attachment tongues. The extent of the pieces will depend on the width of skirt material available, there being as few joints as possible, and the shading in Fig. 4.9(a) suggests the extent of the separate pieces. However, it is essential to note that the weave of the material must run horizontal and vertical in every piece when installed as shown by the arrows in Fig. 4.9(b).

(ii) Joints. The joints are very critical. If they are not substantial enough, they will come apart; if they are too substantial they will act as stiff ribs in a thin membrane, and the fabric will tear away from these stiff elements. For the bag skirt, the joints should be plain lap joints, made with contact cement, machine-sewn with strong preferably-synthetic thread, and covered with a cap strip on the inside of the bag (Fig. 4.10(a)). At the bottom stern corners, it is very helpful to reinforce the joints around the bottom with pop rivets as shown, put in from the inside, and using steel washers on the outside and inside (Fig. 4.10(a) and (b)). Washer dimensions

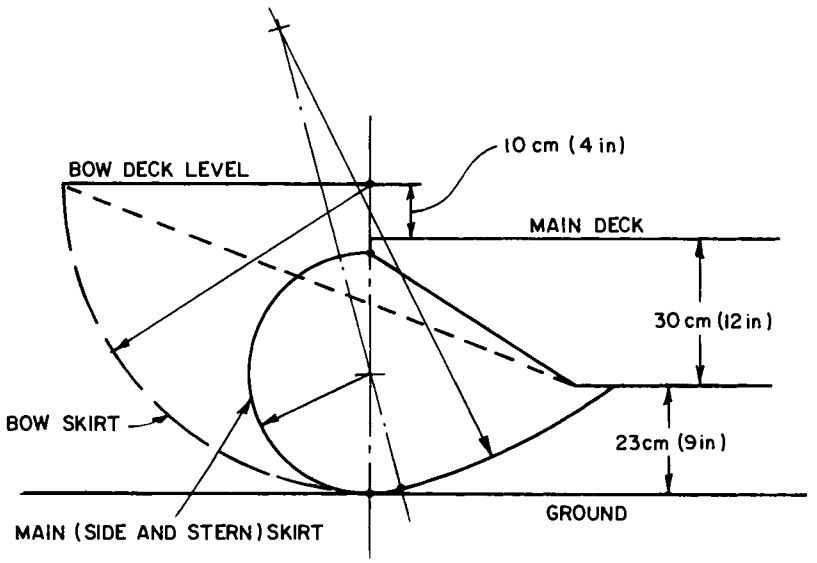

Fig. 4.8 Bow and stern (or side) skirt sections.

should be appropriately 0.3 cm (0.125 in) for the inside diameter and 0.95 cm (0.375 in) for the outside diameter.

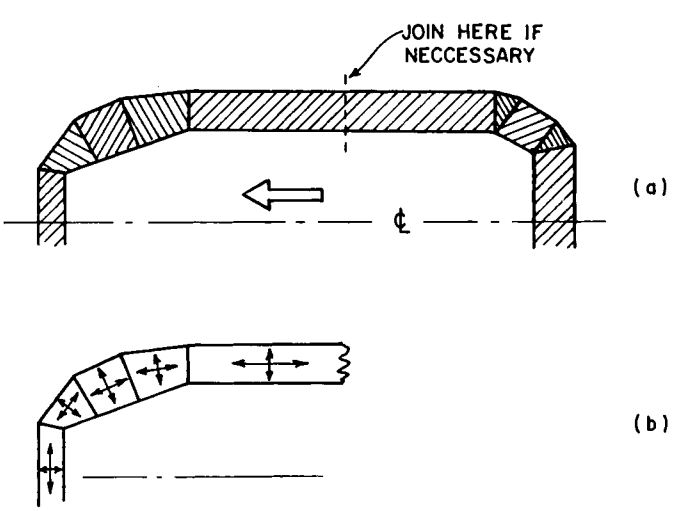

Fig. 4.9 Skirt layout: (a) make-up of skirt from separate pieces of material; (b) weave of material.

(iii) Skirt attachment. Attaching the skirt to the hull is fairly simple. The tongue of material left on the skirt is doubled over a 6 mm (0.25 in) diameter polypropylene rope, called the *bolt rope*, clamped onto the gunwale of the hull by wood or aluminum strips, and held in place by wood or sheet metal screws. Note that the edge of the clamping strip must be nicely rounded or chamfered, as shown, to avoid wearing through the skirt fabric. Half-round moulding may be conveniently used, with the rounded side next to the skirt.

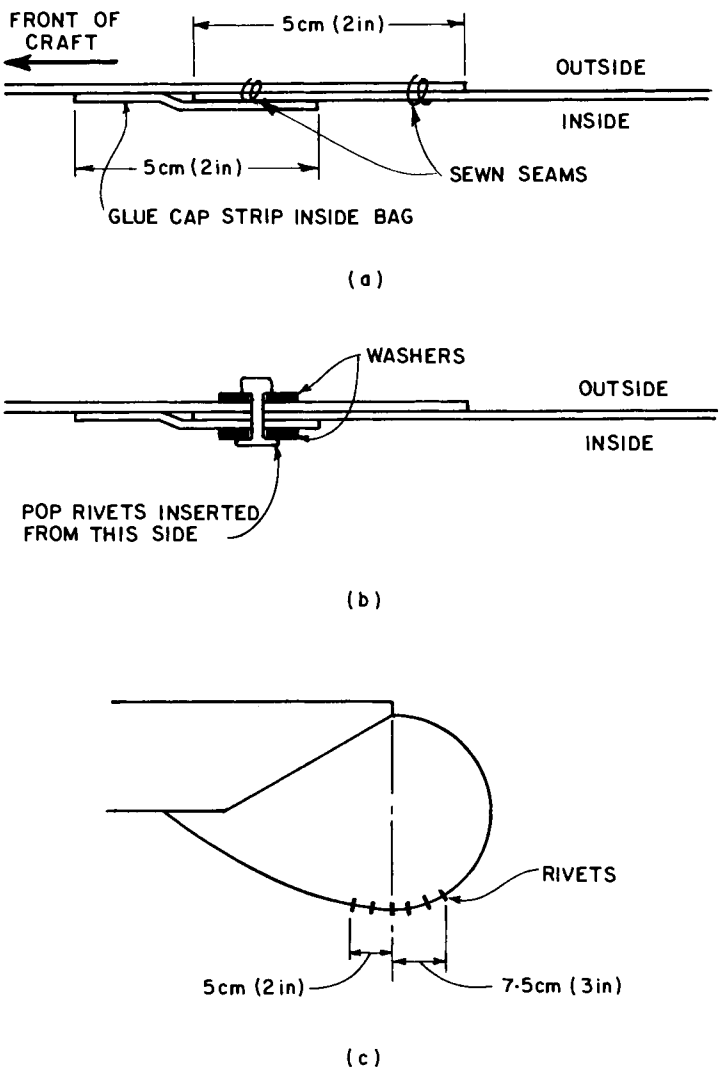

Fig. 4.10 Skirt joints: (a) seams for all joints; (b) installation of rivets at rear corner joints only; (c) location of rivets at rear corner joints.

(iv) Vent holes. The air feed into the bag will be dealt with in Section 4.5, which deals with the lift system, but the bag skirt design involves the air vent holes from the skirt into the cushion space. It is the pressure loss through these holes which controls the bag/cushion pressure ratio used at the beginning of this section. The holes are cut in the inner face of the bag, high up near the hull underside so that they are well away from snagging and tearing on rough ground or vegetation, and they are on the front end and sides. They are not put at the stern, as forward motion over water could then scoop water into the bag through them (Figs. 4.2 and 4.4).

The holes are 13 cm (5.25 in) in diameter (i.e., area = 0.013 m^2 (0.15 ft^2) per hole), and the number of holes is calculated from the formula:

$$N = \frac{Q}{K(P_b - P_c)^{1/2}} \qquad (4.1)$$

where N = number of 13 cm (5.25 in) diameter holes

Q = lift airflow, m^3/s (ft^3/s)

P_b = bag pressure, cm H_2O (in H_2O)

P_c = cushion pressure, cm H_2O (in H_2O)

K = constant, 0.126 (7.0)

If in the present example we needed a lift airflow of 8 m^3/s (100 ft^3/s), with a bag pressure of 6.6 cm (2.6 in) H_2O and a cushion pressure of 5.08 cm (2.0 in) H_2O, we should therefore need, by substitution in eq. (4.1), 18 holes.

It would be wise to cut about six of the 18 holes, and check the bag and cushion pressures with the craft hovering, and full designed load on board. Probably the bag pressure will be too high, so more holes are cut, one or two at a time, until the pressures should settle to the required values, hopefully at about 18 holes. Plot a graph of pressures against number of holes as you go, to get warning of the correct moment to stop cutting.

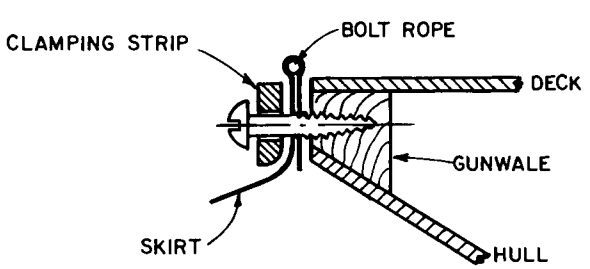

Fig. 4.11 Attachment of skirt to hull.

(v) Skirt drain holes. If the craft is left floating on the water with the lift engine shut down, the bag skirt will get water in it through the skirt vent holes. To blow this out when we start up again, we need drain holes in

the skirt, but they must not let too much air escape. A row of from 5 to 10 holes, 5 cms (2 in) diameter, is therefore cut in the bottom of the skirt at the stern, and is covered by a flap on the outer surface, as shown in Fig. 4.12. The flap is normally kept shut by the water or ground sliding past below it. This allows a small leak, and drains water in a reasonable time without too much loss of air from the bag. Try first with 5 holes. Draining can be speeded up by cutting more holes, but not so many as to lose too much lift air or to reduce the bag pressure significantly.

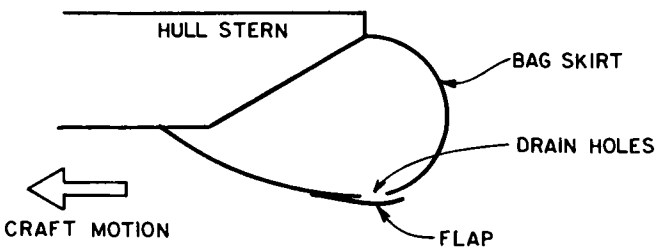

Fig. 4.12 Drain holes in skirt at stern.

(vi) Skirt buzz. A bag skirt may vibrate, particularly when hovering over hard smooth ground or smooth water. This can be a minor annoyance, or it can be severe enough to wear the skirt and even hammer the craft to such an extent that things begin to crack and fall off. The buzzing usually stops as soon as the machine gets onto rougher ground, or grass. This buzz can be cured by taping or glueing small packets of sand onto the skirt in appropriate places. The explanation is that the vibration is like that of a violin string which can be damped by placing a small mass at an antinode (place of maximum motion) to absorb the energy of vibration. The masses (small packets of sand) are commonly called *buzz-dingers*. The positioning of the packets is shown in Fig. 4.13. It is usually sufficient to fit them along the two sides of the craft, but, if the skirt still buzzes, they may be added at the ends as well. The distances A and B of the upper and lower rows of dingers from the attachment point of the skirt to the gunwale are given by:

$$A = w/5 \tag{4.2}$$

and

$$B = w/4 \tag{4.3}$$

where w is the skirt width, as shown. Each buzz-dinger is a flat envelope of skirt material, filled with approximtely 60 gm (20 oz) of sand, and glued to the skirt surface. Seven dingers in each row should be adequate for a 3 m × 1.8 m (10 ft × 6 ft) craft.

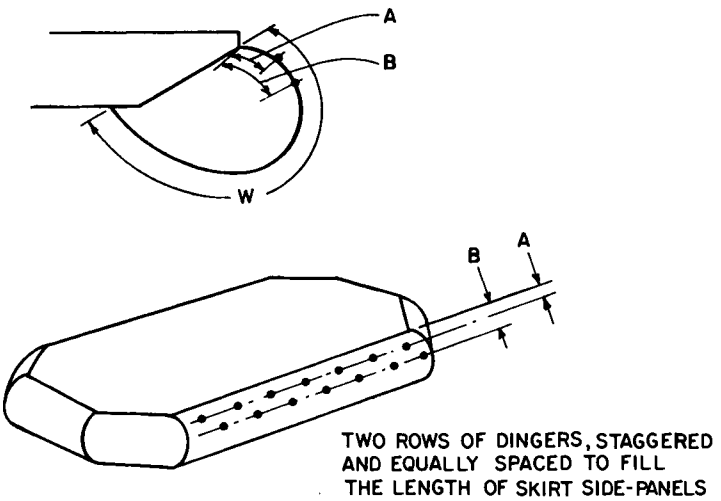

Fig. 4.13 Buzz-dinger array.

4.5 LIFT SYSTEM

The lift system includes the engine, blower and ducting that supply the air to the skirt and cushion. There are many ways of supplying lift air and, like all engineering, a successful design lies in selecting the best compromise for the purpose in hand. Mechanically, the simplest system is to have one engine driving one fan which supplies both lift and thrust air. However, the efficiency is rather low, control gets rather complicated and, if the engine fails, the craft is dead. One engine can also be used to drive separate lift and thrust fans, but this is difficult mechanically and has the same disadvantage in the event of failure.

Two separate engines for lift and thrust raise the price and weight somewhat, but give better control, better efficiency, and more reliablity. Surprising as it may seem, tilting the craft will provide a little thrust from the lift system alone, and get the craft to shore when over water. If the lift engine fails, the thrust system will push the craft to the shore, slowly but surely.

The lift fan itself can be either an axial flow or a centrifugal flow type; both have been used successfully. However, for a light small craft such as we are considering here, the choice is almost inevitably an axial fan running as slowly as possible with a step-down belt drive from a small two-stroke engine. We are forced into this choice owing to the large size and weight of a centrifugal fan to produce the same airflow. Just as important as the fan is the design of the air duct configuration required to feed the bag.

4.5.1 Lift Airflow

The first thing is to get some idea of the amount of lift airflow required to hover the craft. We will continue to use as an example the 2220 N (500 lb) craft, 3 m × 1.6 m (10 ft × 6 ft), with a cushion pressure of 5 cm (2 in) H_2O and a bag pressure of 6.5 cm (2.6 in) H_2O. There are many ways of arriving at the required lift airflow, varying all the way from *borrow a fan and see if it lifts* to the somewhat involved calculations used on large vehicles. We will take a fairly simple-minded but soundly-based approach, using a simple equation with constants derived from the more complicated methods. The lift airflow required for reasonable performance over water and land is given by:

$$Q = \frac{KLW}{S_c(p_c)^{1/2}} \tag{4.4}$$

where Q = lift airflow, m^3/s (ft^3/s)
L = skirt footprint perimeter, m (ft)
W = total weight, N (lb)
S_c = footprint area, m^2 (ft^2)
p_c = cushion pressure, cm (in) H_2O
K = constant, 0.0272 (0.444)

So, by substitution in eq. (4.4), the required lift airflow for our example is $Q = 2.36\ m^3/s$ ($83.72\ ft^3/s$). If we suck this in through a 48.2 cm (19 in) diameter lift fan, which will have approximately 0.163 m^2 (1.75 ft^2) area, allowing for fan hub, etc., the air speed will be about 15 m/s (48 ft/s), which will cause no problems. The fan tip speed will be 80 m/s (270 ft/s), resulting in a tolerably quiet fan.

4.5.2 Lift Power

The required fan power is given by:

$$H = KP_fQ \tag{4.5}$$

where H = fan power, kW (HP)
P_f = fan pressure rise, Pa (in H_2O)
Q = fan airflow, m^3/s (ft^3/s)
K = constant, 0.00167 (0.016)

Allowing for 7.6 cm (3 in) H_2O at fan exit to produce 6.6 cm (2.6 in) H_2O in the bag and 5 cm (2 in) H_2O in the cushion, and allowing a 0.6 deficiency in fan ducting (which is included in the K factor above) the required fan power is by substitution in eq (4.5), H = 2.9 kW, say 3 kW (4 HP). If the fan tip speed is 80 m/s (270 ft/s), on a 48.25 cm (19 in) fan, this means a fan speed of 3200 RPM. To produce 3 kW (4 HP), many small engines will run at more than 3200 RPM, so they will need a step-down belt drive. This is not complicated, but the belt does put a side-load on the motor shaft, which will rapidly wreck the crankshaft bearings if they are not meant to stand it. Most lawnmower motors

have the cutter mounted straight on the crankshaft, and therefore have fairly flimsy bearings. So, if you use one, you must put an extra bearing beyond it and a flexible coupling between the crankshaft and the jackshaft on which the drive pulley is mounted. However, if the engine is meant to take a belt drive, no extra bearing is needed. And it is strongly advisable to get a two-stroke engine, which will use oil-fuel mixture. The propulsion engine will be more powerful, and almost certainly run at higher speed. It will be a snowmobile engine, definitely two-stroke, so that the two of them will use the same fuel.

It is possible but highly undesirable, to avoid the complication of a belt drive by fitting a fast-running fine-pitch fan directly onto the crankshaft, and running it at engine speed. However, the noise of such a high tip-speed fan will damage the driver's hearing, and will annoy the community so much that

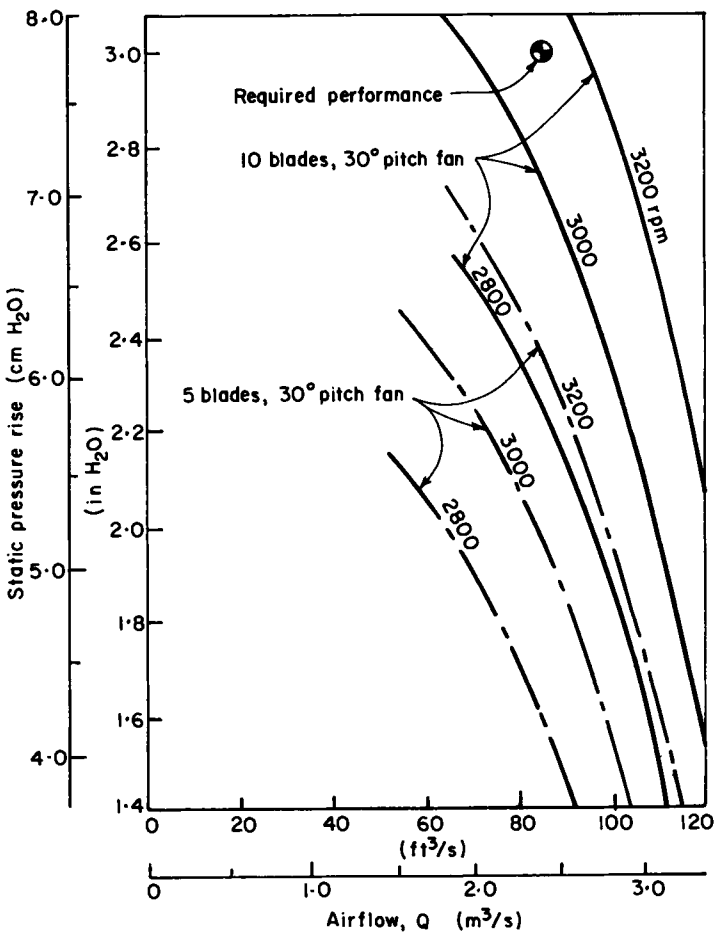

Fig. 4.14 Specimen lift-fan performance curves, for a 50 cm (19 in) diameter fan.

the running of ACVs will be banned.

4.5.3 Fan Selection and Installation

How to choose a fan? Any light fan which satisfies the pressure rise and airflow requirements will do. For example, there is a range of axial fans, called *Multiwing* fans (Sheldon Fan Co., Cambridge, Ontario, Canada), which are particularly suitable for light ACVs. They consist of metal hubs into which varying numbers of a range of plastic blades of different pitch angles can be fitted. These fans are light, and can even be turned down on a lathe to fit various duct sizes. A specimen set of performance curves for fans of this type is shown in Fig. 4.14.

Continuing with our example, we should probably use a fan with twelve 30-degree blades running at 3000 RPM, or ten 35° blades running at 3000 RPM. A few graphs like Fig. 4.14 plotted from the manufacturer's catalogue, would soon put us on the right track.

Now any rotating machinery is a bomb which doesn't need an explosive charge. If a fan blade breaks, or is broken by sucked-in debris, the fan can explode and the flying pieces can kill. So do not give it a chance! The inlet to any fan MUST be covered by a tough wire guard, of about 5 cm (2 in) mesh, which will keep hands, caps, spanners, lumps of mud or ice, etc., out of the fan. The fan MUST also be enclosed in a strong cylindrical duct, to catch the bits if it does burst. Finally, a *bellmouth inlet* is required in order to organize the air into the fan so that the blades can work efficiently.

The lift system can be organized in an installation something like Fig. 4.15. The top bearing A is self-aligning and free to slide in its housing. The bottom bearing B is a self-aligning thrust bearing, fixed in its housing. It takes the fan's weight and the lift, which acts upwards when the fan is running. The duct length L_D and bellmouth radius R_B can be calculated in terms of the fan diameter D_F by:

$$L_D = D_F/3 \tag{4.6}$$

and

$$R_B = D_F/4 \tag{4.7}$$

Thus, given D_F = 48.25 cm (19 in) in our example, we obtain L_D = 16 cm (6.1 in) and R_B = 12 cm (4.75 in) from eqs. (4.6) and (4.7), respectively.

Note that the belt is on top of the unit, where it can be seen, inspected, and got at easily. But it is underneath the screen, which will catch it if it flies off. Do not run the engine, even for a quick test, without the screen on and bolted down!

4.5.4 Ducting

Having guided the air into and through the fan, it now has to be ducted

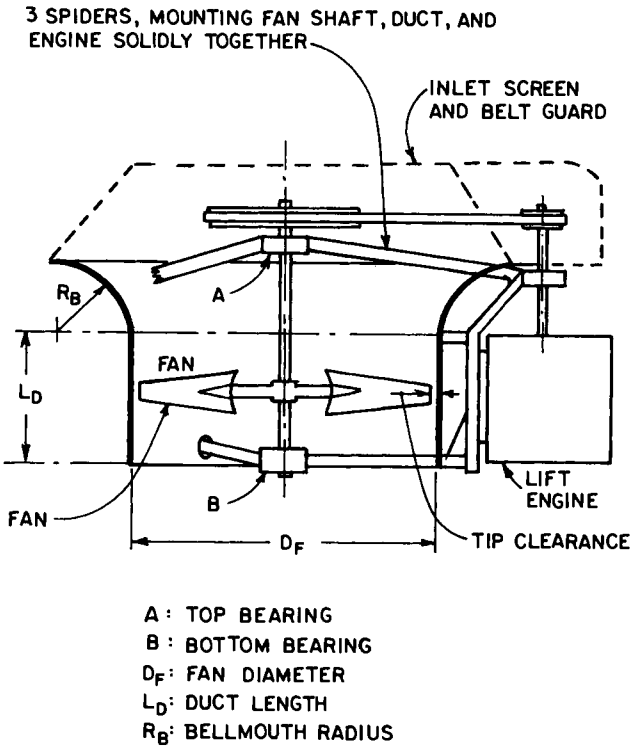

Fig. 4.15 Lift-fan installation.

into the skirt with as little loss as possible. This points out one of the disadvantages of the bag skirt. It does impose quite a pressure loss on the air before reaching the cushion, where the required pressure is fixed by the size and weight of the craft. The fan therefore has to produce that much extra pressure, so the ducting must be carefully designed to cut down the extra pressure required to the minimum possible.

The pressure loss of air moving along a duct and round corners is proportional to the energy of movement, i.e., the *kinetic energy* or *dynamic head*, which is itself proportional to the square of the speed of the air. Therefore, to cut down the loss, the speed must be kept down by using the biggest ducts possible. Pressure is also lost by changing the air direction; so, the smallest possible number of bends is also a requirement. Finally, the loss in those bends can be minimised by putting vanes in them to keep the air organized and filling the duct as it goes round, instead of crowding to the outside of the bends and speeding up in the process.

A good solution to this complex problem can be obtained by ducting of the form shown in Fig. 4.16. Sets of *turning vanes* are set in the duct at A, B, C, and D, to get the air from the fan down into the skirt. Although very simple, these vanes cut down the loss of dynamic head from about 100% at each bend to something like 15%. They are shown in more detail in Fig. 4.17. This assembly is best placed at the front end of the craft, since the largest airflow and the highest pressure are needed at the bow skirt, to stiffen it and prevent nosing-in when traversing waves or land obstacles.

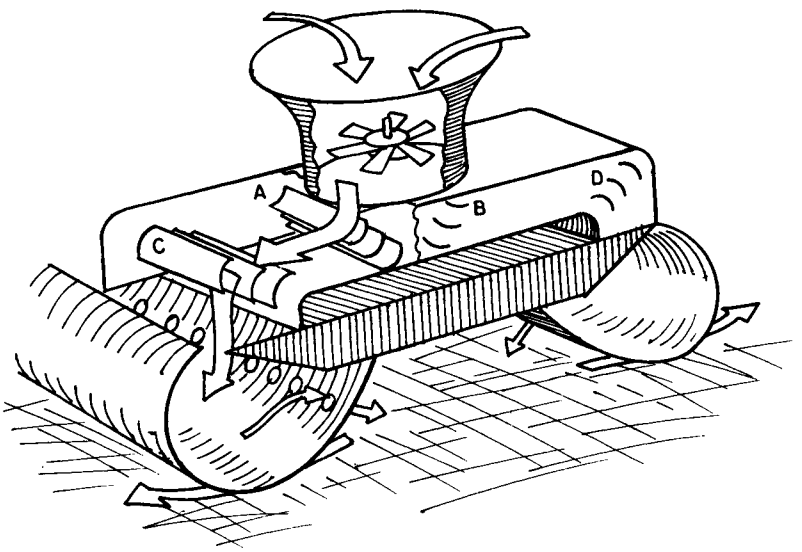

Fig. 4.16 Lift-air ducting.

4.6 THRUST SYSTEM

Much of what was said about the lift system also applies to the thrust system, which almost always uses a large axial flow fan or propeller in a duct at the rear of the craft. Some machines have been driven by centrifugal fans, which make control with reverse thrust an easy proposition. But the efficiency of these units is very low in terms of thrust per horsepower, so we will only consider the axial fan or propeller. Furthermore, since putting a proper duct round a propeller increases safety and makes it as effective as an unducted propeller of twice the area, we will consider only the ducted type.

The fans used are axial-flow multi-bladed fans of the same general type as for the lift system, but rather larger, say 76-92 cm (30-36 in) diameter for the kind of craft we are using as our example. We shall start by finding out how much thrust we shall need, and then which fan and motor are necessary to produce it.

4.6.1 Thrust Requirements

The starting point is the total weight of the craft and pilot, which we decided would be about 2220 N (500 lb). There are three critical values: a) the thrust to get through *hump speed* and plane over water, b) the thrust needed to get the craft over the worst ground we are likely to traverse, and c) the thrust to get up the steepest slope we want to climb.

(i) On water. The over-water case is about the most definite, so we will look at that first. When an ACV moves slowly on water, it behaves just like an ordinary boat, and displaces water under it to equal its own weight. It moves forward making the usual pattern of bow waves until it is running fast enough to climb out of the displacement hollow, at *hump speed*, and start planing. The wave pattern then almost vanishes and the craft accelerates rapidly. A large proportion of the low-speed drag is caused by the energy put into making the waves. Once the wave pattern vanishes, this wave-making drag also disappears. The result is a pronounced *hump* in the graph of drag vs speed, whence the name *hump speed*. This hump speed depends on the length of the

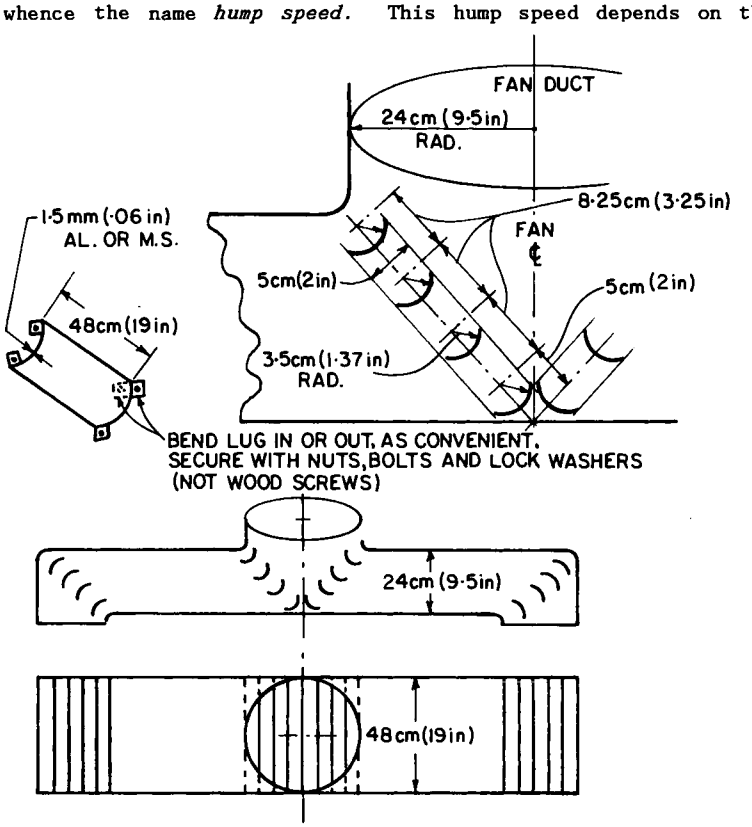

Fig. 4.17 Turning vanes in lift-air duct. Drawn for 48 cm (19 in) diameter fan. For other sizes, scale in proportion.

craft, and is given by:

$$V_H = K(\ell)^{1/2} \tag{4.8}$$

where V_H = hump speed, m/s (ft/s)

ℓ = hull length, m (ft)

K = constant, 1.70 (3.24)

Then the wave-making drag at hump speed is given by:

$$D_H = \frac{FAM^2}{S_c \ell} \tag{4.9a}$$

where D_H = hump-wave drag, N (lb)

M = craft mass, kg (lb)

S_c = cushion footprint area, m^2 (ft^2)

ℓ = hull length, m (ft)

A = constant, 0.03 (0.049)

The factor F depends on the state of the water, as follows:

$$F = \begin{cases} 1, \text{ smooth deep water} \\ 2, \text{ rough deep water, waves = skirt height} \\ 3, \text{ shallow water, 0.61 m (2 ft) deep or less} \end{cases} \tag{4.9b}$$

In order to be able to accelerate readily through hump speed into the planing mode, it is usually recommended that the thrust should be about 1½ times the hump wave-drag.

For the craft of our example, eq. (4.8) yields a hump speed of 3 m/s (10.3 ft/s), or 10.8 km/h (6.71 mph). Using eq. (4.9) and F = 2, for rough water, the hump wave-drag is D_H = 190 N (40.8 lb). So, for the over-water requirement, a thrust of 190 × 1.5 = 280 N (62 lb) should be aimed at.

(ii) On flat land. Over land, the vehicle behaves in a frictional manner, with coefficients of friction varying from 1% or less over smooth ice or glazed snow, to 5% for short grass, and up to 30% for long grass and scrub; they can reach 20% over rough ground. This means that, at the sort of lift airflows we have built in, the drag of the craft over these types of terrain will be so many percent of the total weight, moving at low speeds of up to 6.44 km/h (4 mph), or so. The very high values through tall grass and scrub are really due to the effort required to push aside the vegetation, and are greatly reduced on second or third passes along the same trail.

If we take 10% as a figure which will allow us to operate over quite a wide range of terrain, we need to install at least 10% × 2220 N = 222 N (50 lb) for operation over flat land. This will allows us to get up a good speed over smooth flat open ground. But we should remember that this sort of operation could lead to severe skirt wear, which seems to increase as the square, or even the cubic power, of speed. The worst surface for wear is hard ground such as asphalt or concrete, which can destroy a skirt in half an hour of operation at 32 km/h (20 mph).

(iii) On sloped land. We must also consider the thrust to get the craft up a slope. This thrust is needed to overcome the component of the weight acting down the slope, which is equal to the total weight multiplied by the sine of the slope angle. However, in practice, most slopes are climbed by taking a run at them. So this case should be easily covered by 280 N (62 lb) already proposed for operation on water.

(iv) On land and water. Given that the thrust requirements on water and land are 280 N (62 lb) and 222 N (50 lb), respectively, we should have quite a capable vehicle if we can generate 280-300 N (62-67 lb) of thrust.

4.6.2 Thrust Fan and Motor

The next step is to look at the performance of a thrust fan. As was explained above, a guard round the fan is essential for safety, and a duct increases the effective fan diameter, so it is assumed that these two functions will be combined in a correctly shaped duct.

The curves of Fig. 4.18 make it very clear that the best conversion of engine power into fan thrust is obtained by using the largest possible fan, to get the lowest loading of power and thrust per square unit of fan disc area. It is also well established that fan tip speeds should be kept below 120 m/s (400 ft/s) to produce a tolerably quiet fan, as well as to reduce stress

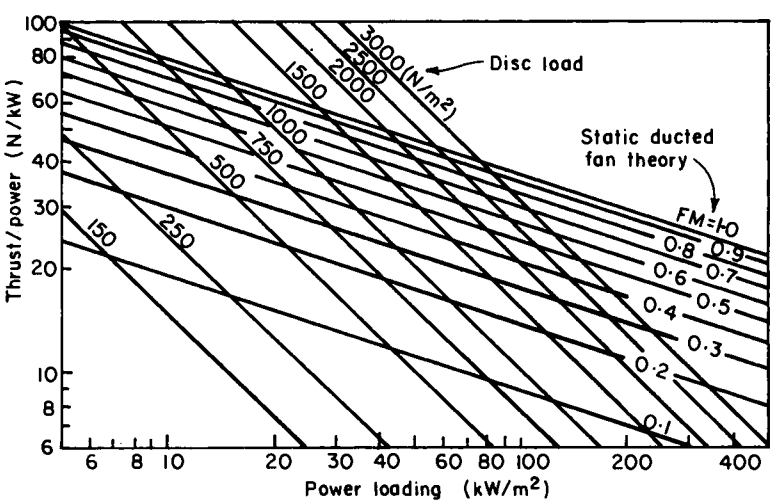

Fig. 4.18 Static ducted-fan performance map. The ducted-fan area is equal to the jet area. For unducted propellers, use (area) = 1/2 (propeller disc area).

levels. On the other hand, there are strong reasons why the size (and weight) of the fan should not be too large. The sheer unwieldiness of a very large propeller on the back of a light craft is obvious; because the propeller is placed high up, the craft becomes top-heavy. Also the necessarily high thrust line will tend to push the nose down when full thrust is applied. Finally, the gyroscopic forces of the large rotor could become quite difficult to control.

If we look at Fig. 4.18 and try a 76 cm (30 in) diameter fan for 290 N (65 lb) of thrust, as a first estimate the area is 0.456 m^2 (4.9 ft^2); hence, the disc loading is 290/0.456 = 636 N/m^2 (13.26 lb/ft^2). Assuming a Figure of Merit (FM) of 0.60 (a sort of efficiency), the fan will give about 53 N/kW (9 lb/HP) of thrust so that 5.5 kW (7.3 HP) will be required to produce 290 N (65 lb) of thrust. A 6-8 kW (8-10 HP) snowmobile or go-cart motor should be suitable, and a V-belt drive will easily transmit this power. A toothed timing belt is even better, but the shaft alignment is very critical if the timing belt is not to drift towards a pulley rim and either tear itself to pieces, jump the pulley, or even force the rim off.

Returning to the fan, Fig. 4.19 shows a typical curve for the same type of fan as was discussed in the section on lift systems. Thus, a fan speed of about 1600 RPM will be needed to develop 290 N (65 lb) of thrust. This is equivalent to a tip speed of 64 m/s (210 ft/s), which should result in a reasonably quiet fan.

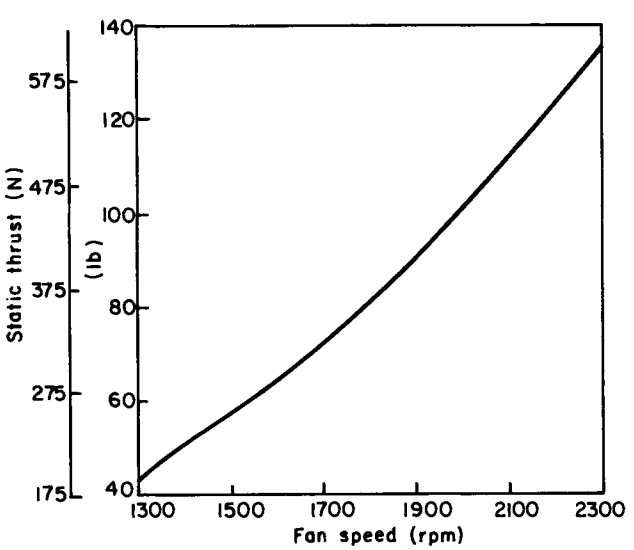

Fig. 4.19 Typical speed-thrust curve for a 76 cm (30 in) diameter axial fan with 10 blades at 45° pitch angle. Refer to the manufacturer's specifications for any specific fan.

The 6-8 kW (8-20 HP) engine will probably run at about 5000 RPM to give the 5.5 kW (7.3 HP) we need, so a 3.125:1 step-down in the belt drive will be required. This should present no problems, except that aluminum pulleys must be used. The weight of steel pulleys would be excessive when we are scraping to get rid of every bit of surplus weight. The actual engine speed must be checked from the maker's curve of power vs speed to determine the correct engine speed for the required power.

4.6.3 Thrust Fan Duct

The design of the duct to surround the fan is very simple, as shown in Fig. 4.20. The essential features are: (a) a moderate inlet radius R_T, (b) a short length of parallel duct L_T, and (c) a small fan tip clearance ϵ_T added to the fan diameter D_F. Since the craft speed is not excessive, the shape of the outside of the duct is not important, and weight should not be wasted to provide a streamlined exterior. For a fan of diameter D_F = 76.2 cm (30 in), the duct diamensions should be approximately R_T = 15.2 cm (6 in), L_T = 19 cm (7.5 in) and $D_F + \epsilon_T$ = 77 cm (30.3 in).

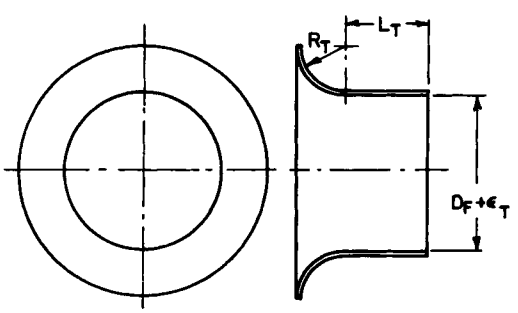

Fig. 4.20 Thrust-fan duct.

With the small running clearance, which is essential for good fan performance, the duct must be mounted very firmly onto the engine/fan mounting. A suitable system is shown in Fig. 4.21. Steel or aluminum tubes make very good struts, with the ends squeezed flat for attachment lugs. There is an appreciable distance between the propeller-shaft bearings. The front bearing and large pulley stand well ahead of the duct to avoid interfering with the airflow, and they permit the erection of a rigid cone of struts to hold the duct firmly. The propeller shaft can be shimmed up on top of the main pillar in order to adjust the drive-belt tension; the duct moves up and down with it. The inlet screen is shaped to cover the drive belts, pulleys and fan intake.

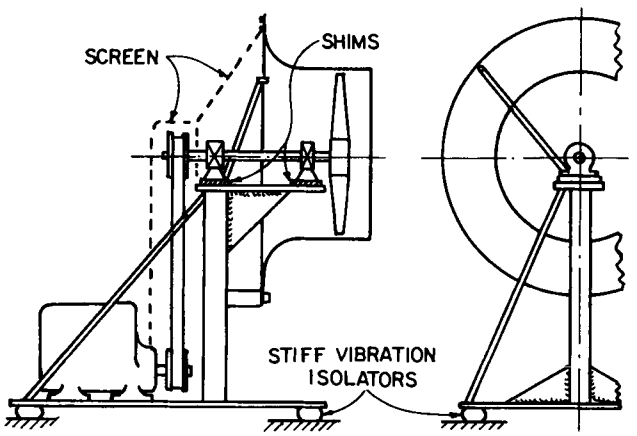

Fig. 4.21 Thrust-system installation.

4.7 COMBINED LIFT/THRUST SYSTEM

As was remarked at the beginning of the section on Lift Systems, the very simplest system, mechanically speaking, uses a single engine and axial fan to provide both lift and thrust. A diagram of such a system is shown in Fig. 4.22. The single axial fan sucks its air in through the bellmouth, which must be large enough to accommodate both lift and thrust airflows. However, in the lower part of the duct, immediately aft of the fan, a splitter separates the air flow. A set of turning-vanes below the splitter directs the lift air down into the bag skirt. While on the face of it the splitter should divide the duct area in the ratio of designed lift/thrust airflow, the practical aspects of airflow distribution are such that the splitter should be made adjustable, to be locked firmly in place after tuning the finished craft to optimum performance.

It is also essential to provide a thrust-reverser, so that engine speed and lift airflow may be held at full level while thrust is reduced or even reversed to permit manoeuvering or static hovering while maintaining a firm cushion. A pair of simple bucket-type reversers, as discussed in Section 4.8, Controls, would do this.

A further point to be remembered is that the fan must be carefully chosen to do double duty. Ideally, the lift fan should possess high static pressure and low velocity, while the thrust airstream needs high velocity and low static pressure. It is not easy to attain a suitable compromise in a single fan. The relatively high back-pressure imposed by the cushion has an awkward tendency to stall the fan, particularly at lift-off, when the lift-flow is almost zero,

since the exit gap under the skirt has not yet been established. Considerable experimentation with fan blading may be necessary. However, the lightness and simplicity of the single engine and fan installation is an attractive goal for those with an adequate understanding of fan and duct aerodynamics.

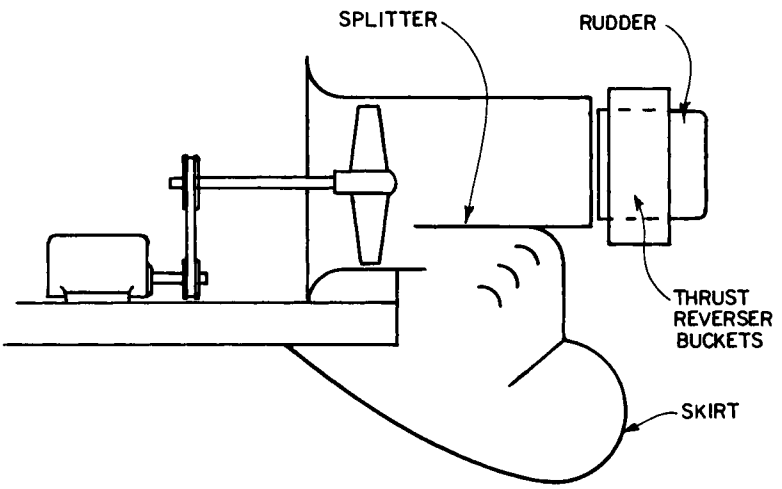

Fig. 4.22 Combined lift/thrust system.

4.8 CONTROLS

Most light ACVs are controlled by the lift and thrust engines and a rudder. Very light machines also use movement of the driver's weight as a control aid, and an increasing number of machines have simple thrust reversers. The driver's input is usually by push/pull knobs, or quadrant levers as second choice, for the throttles, and a steering wheel, tiller bar or joystick for the rudder. The thrust engine control is sometimes implemented as a twist grip or trigger type on the tiller or stick.

The controls should be simple and natural to operate, simple and reliable to install and maintain, and light in weight. It is wise to spring-load the thrust throttle so that it closes automatically when released, in case the driver is thrown overboard. In normal operation the lift throttle is adjusted and secured, such as by locking a push/pull type. The thrust throttle is likely to need continuous adjustment, and is therefore held in the hand continuously. A pedal could also be used for the thrust throttle.

The rudder is also likely to need continuous input, so that either the rudder and thrust throttle are in one hand (e.g., tiller bar with twist grip) or one hand rests on each (e.g., steering wheel and quadrant lever). Natural throttle movements (e.g., push for *go* and pull for *stop*) and steering movements, etc., are important. The engine controls should be placed sensibly.

For example, it would be pointless to have the ignition key (with electric start), choke and throttle placed far apart, making it difficult to start the machine. Connections from the operator-manipulated devices to the controlled components need to be strong, well anchored and reliable. Bowden or similar cable, push/pull rods, torque tubes, or pulley/cable systems may be used appropriately.

The rudder assembly is placed directly in the slipstream of the thrust fan, close up against the thrust duct. In the lightest craft, a single rudder may be used; but, two to four smaller rudders acting together provide a much larger turning moment with less thrust-loss and muscular effort on the controls. This is because a *venetian blind* of vanes turns the jet of thrust air more efficiently than a single *barn door* (Fig. 4.23). Any rudder needs to be

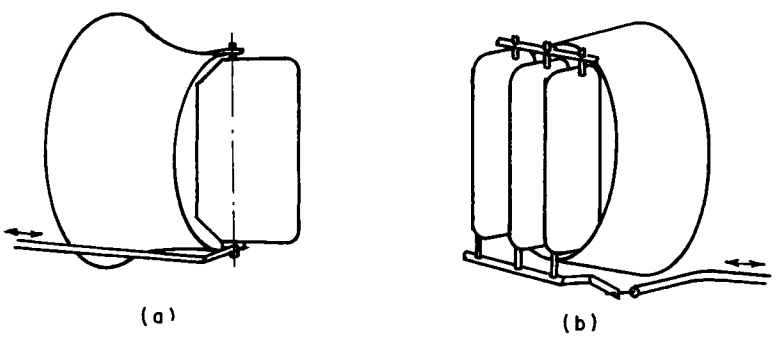

Fig. 4.23 Rudder: (a) single vane; (b) multiple vanes.

mounted very firmly, in good bearings, as the blast of turbulent air from the fan hits it with considerable force, and can rattle it to pieces if it is not rigidly made and secured. The position of the pivots is also critical, to avoid heavy loads on the driver's control. As a general guide, one can try pivotting the rudder 1/3 back from its leading edge, but a range of positions around this should be tried. It is most awkward to have a rudder which needs constant heavy force, and it is disconcerting to have one which is light up to a certain position beyond which it whips hard over, leaving the craft in a spin while the driver rubs his knuckles.

The air from a thrust fan moves in a spiral, unless de-swirl vanes are fitted behind it, so that the air does not meet the rudder in a straight axial direction. This swirl accounts for the peculiar steering characteristics which have mystified some builders. It might be an improvement to bend the rudder's leading edge one way at the top, the other way at the bottom, to pick up the swirling air cleanly. However, try a simple rudder first, and work up to refinements later.

There are several types of thrust reversers. Perhaps the simplest to visualize is a pair of *buckets* which swing into the jet behind the thrust duct when a lever is pulled (Fig. 4.24). These catch a portion of the jet and throw it forward, thus giving a resultant thrust which is either reduced, zero or actually reversed. Clearly, if the driver is allowed to operate either bucket independently, he has a very powerful added steering mechanism. The use of these various controls is dealt with in the section on driving technique (Section 4.11).

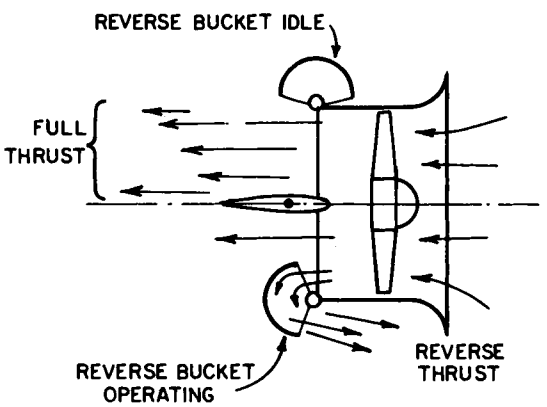

Fig. 4.24 Reverse-thrust bucket system, viewed from above.

4.9 HULL

The hull has many functions. It is: a) a frame which supports all the other components, b) an airtight top for the air cushion cavity, c) a raft which floats, d) a boat which, if the lift engine fails, can drop into the water at cruising speed without going under or cartwheeling, and e) a sled which can do the same thing on ground. It is required to perform these functions with as little weight as possible. There are many ways of constructing a hull. At one extreme, a stiff spine girder is used, with the engine(s), driver and fans mounted on it; then a light structure is built out from the spine. Alternatively, a rigid girder outer-frame supports the skirt, while the driver, engines, fans, etc., are located on a structure which is attached to the outer frame. At the other extreme, an inflated boat is used, and the various components sit in it with a minimum of stiffening members. In any case, there is a problem of anchoring a number of heavy concentrated loads and forces to a light structure. Some feeling for light aircraft construction can be useful here. The design process has a number of distinct steps which we will examine.

4.9.1 Layout of Components

Knowing the weight and size of the various components and the overall size of craft, the position of each unit has to be decided such that the combined centre of gravity (CG) will be on the centre of lift, i.e., the geometrical centre of the skirt footprint. This is done by taking moments about some convenient datum, for example the hull stern.

An example is shown in Fig. 4.25 using approximate numbers for the light single-seat machine we have been considering. Taking moments about the stern datum, we have:

$(223\times2.14)+(890\times1.83)+(668\times1.53)+(223\times1.37)+(400\times.61) \simeq (2403\times1.53)$

i.e., $3678 \simeq 3677$

This distribution is therefore satisfactory, but must be rechecked and modified, if necessary, when actual weights become available.

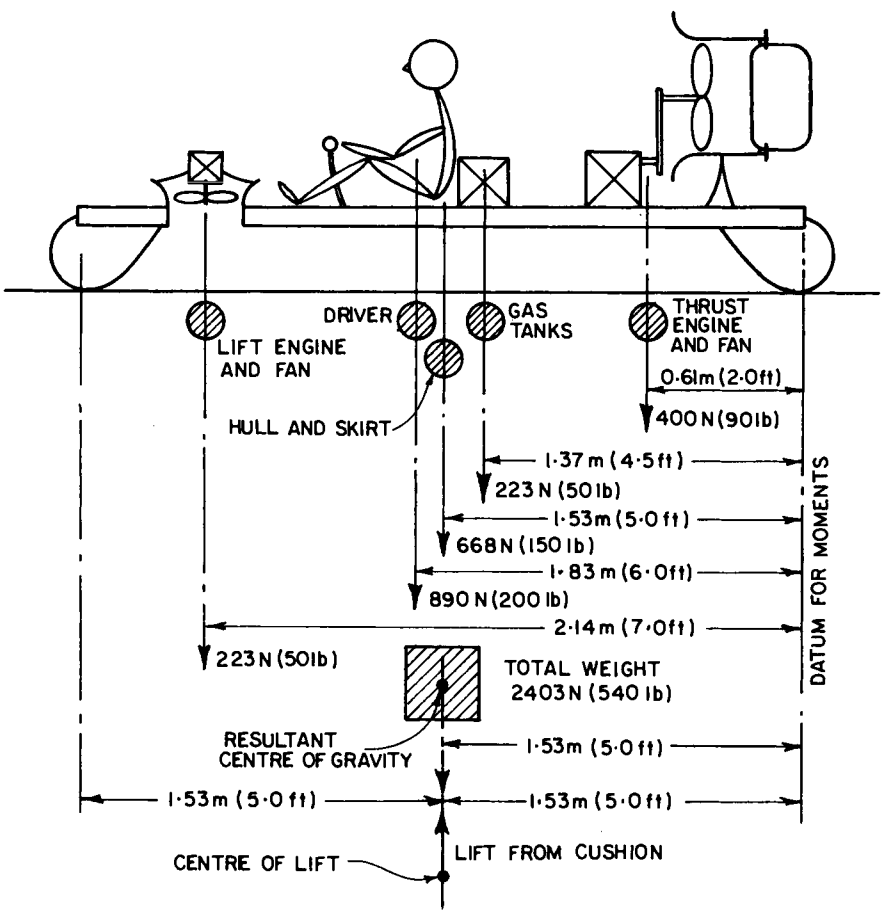

Fig. 4.25 Layout of components. Zero pitch-moment example.

The driver and gas tanks are placed as near as possible to the CG, so that variations in their weight will have the least possible effect on the trim of the vehicle. Since the thrust duct is high, and the main drag on the vehicle is at ground level, due to skirt/terrain interaction, the thrust will exert a nose-down moment on the craft. It is often useful to trim the craft to be slightly tail-heavy so as to reduce this effect. From Fig. 4.26, it is seen that the nose-down moment M_y is given by:

$$M_y = Th \tag{4.10}$$

where T is the thrust force and h is its elevation above ground. At constant speed, thrust is equal to drag. It is quite useful to displace the CG of the vehicle aft so as to leave a nose-up out-of-balance moment equal to $M_y/2$, in the previous calculation. Otherwise, when attempting to accelerate it at full thrust, the nose is apt to dig in and reduce the craft's acceleration.

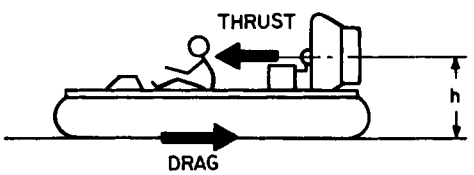

Fig. 4.26 Thrust and drag forces.

The *component* whose shape, CG, and dimensions are least known is usually the driver. The size and shape of an average adult driver are shown in Fig. 4.27. Different schools of thought place the driver riding high, as in a motorcycle, or sitting low as in a racing car. The latter position keeps the craft CG low, increasing stability, and reducing aerodynamic drag and pressure losses at the thrust fan intake.

It is highly desirable to have at least a standard automobile lap-belt, with quick release, for over-land use. Over water, it is usually not used. In any case, a motorcycle helmet is of paramount importance. A strong roll-bar behind the pilot's head is highly recommended. Nobody wants to get thrown out of a hovercraft over land for want of a seat belt, or trapped under an overturned craft on land or underwater for lack of a roll-bar or belt quick-release, respectively. Needless to say, all the items of equipment, i.e., engines, gas tanks, battery, driver's seat, etc., must be firmly anchored to the main frame of the hull. It would not be safe to have these heavy objects flying loose if the hull should hit a rock or stump and stop suddenly.

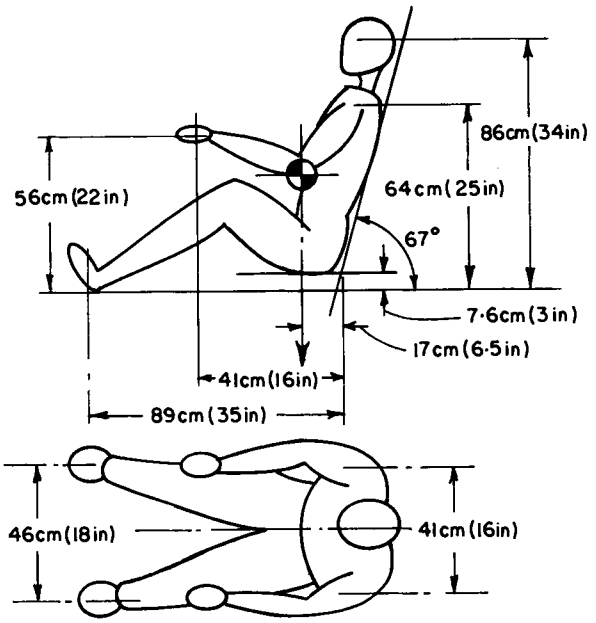

Fig. 4.27 Typical dimensions for a 1.83 m (6 ft) driver.

4.9.2 Hull Shape

The bottom of the hull should be flat, with protruding landing pads or skids, so that it is not punctured by odd stones, etc., when sitting on the ground (Fig. 4.28(a)). The sides, bow and stern should be sloping gently such that, in the event of loss of lift and in whatever direction it is moving, the craft will ride up over water or ground instead of digging in. The bow is often given a raised form, as shown in Fig. 4.28(b), to enable the craft to rise over waves easily, or enter the water safely from a sloping ramp.

4.9.3 Hull Structure

As was remarked earlier, there are many ways of building the hull. An increasing number of builders in Britain are forming groups to build moulds for fibreglass hulls. Larger (6-10 seat) vehicles are often built of rivetted aluminum, and small commercial craft are built successfully on the inflatable-boat principle. However, most amateur craft are built of 3 mm (1/8 in) plywood, with fibreglass tape reinforcement at joints, and 2.5 cm × 2.5 cm (1 in × 1 in) framework added to distribute concentrated loads. Engine mounts are usually of thin-walled steel tubing, with carefully-fabricated plugged ends

and attachments. Welding has to be done well, to withstand continuous vibration and avoid ruining the properties of the tubing by overheating. Glueing should be done with the best waterproof glue obtainable, and the plywood should be of the exterior grade. Even an *overland-only* craft is going to get wet at times.

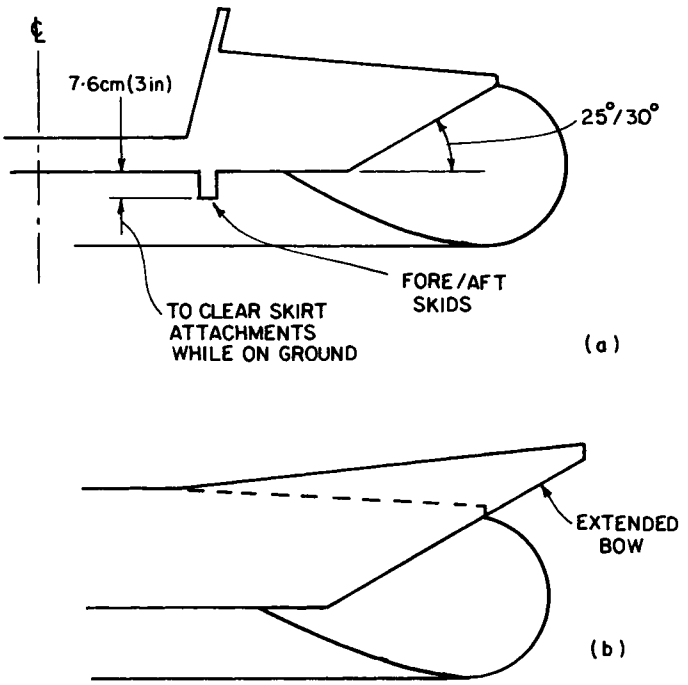

Fig. 4.28 Hull shape: (a) typical cross-section; (b) typical bow section.

In order to combine the various requirements set out above, a typical hull might have a cross-section as shown in Fig. 4.29. The floatation boxes are airtight compartments, whose enclosed volume of air will give a buoyancy of 9800 N/m^3 (62 lb/ft^3) of water displaced when immersed. The machine's buoyancy should be sufficient to support 150% of its total loaded weight. The use of foam blocks to achieve this is not wise, since most foams will absorb water in time. In a known case, a 2220 N (500 lb) machine gained an extra 1780 N (400 lb) of weight in this way in two years. If you must use foam blocks, they should be sealed in plastic bags and inspected periodically for bag punctures. However, sealed tanks formed by hull members, or filled with inflated bags are far better. Even sealed tanks can leak and take in water, so they should have inspection covers which can be opened occasionally, to ventilate against *dry rot* and check for leaks. All in all, inflated air bags inside the hull or lashed onto the deck are an excellent way of providing buoyancy.

The bow of an over water craft has to deal with wave impacts. Any air-feed holes in this region should be small (less than 7.5 cm (3 in) diameter) so that the skirt cannot get pushed back through them. If the lift fan blows straight down into the cushion, its duct should be sloped back, as shown in Fig. 30, so that water cannot easily get forced up into the fan during a rough landing.

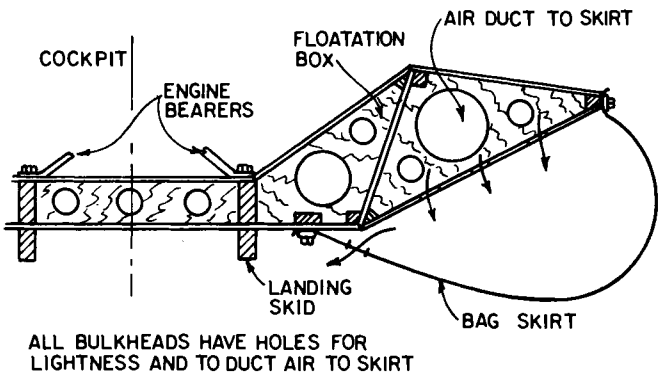

Fig. 4.29 Typical hull cross-section.

4.10 TRAILER

Unless the machine can be operated straight out of your back door, a trailer is probably essential. It can be very simple, but must be fully road-worthy. Also, it may require a licence. An approach is to buy the

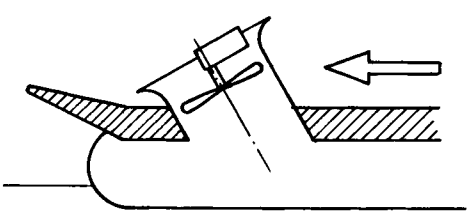

Fig. 4.30 Lift fan mounted at angle to avoid water ingestion.

required hardware from an auto-parts store and mount a flat plywood deck on it. Walls 0.305 m (1 ft) high round the sides and front end will help to prevent the craft from sliding off while it is being hovered off and on. The space inside the walls needs to be a few inches wider than the inflated skirt. However, the legal maximum vehicle-width should be checked and adhered to.

To get the craft on and off, it may be necessary to tilt the trailer deck in which case the tilting point should be chosen carefully to give stability. A detachable or slide-out ramp at the tail end will be needed also. Strong tie-down points are required to hold the craft securely during emergency stops or turns.

4.11 DRIVING

The hovercraft is not a magic carpet which can go anywhere. It has limits, which are quite severe with a small craft, but they are different from those of other vehicles. It can go over smooth land and water, but not over very rough land or water. It can go over moderatley rough land, with occasional potholes, much faster than a wheeled vehicle, without shaking the driver's teeth out. But loose gravel or pebbles, or long grass, soak up all the lift air and bring it abruptly to a halt. It has too little thrust to climb steep hills, except short slopes which it can take a run at. It is very difficult to manage in a cross-slope or cross-wind, and may need to be *crabbed* along at up to 45° or so to its direction of motion in order to keep on course. You need to start a turn well in advance, as it is slow to answer to the controls. Always *think 50 metres (50 yards) ahead*!

It has no brakes! It is much easier to start than stop, so slow down far ahead of your intended stopping point. And most of all, beware of running down-wind! It is difficult to stop, and you have very little control. *Tack* across-wind, like in a sailing boat, if you have to go down-wind. Snow, too, has its problems. If it is soft and deep, you may dig a hole and stay there; if hard and glazed, you may set a new land-speed record before encountering trees or boulders! Now, how do you learn to drive?

4.11.1 Hovering

Find a really flat level piece of ground, preferably with very short grass or asphalt but without loose dust or sand. Tow the craft to the middle of the site after having set the lift engine to hover it. Do not let fingers, bits of rope, a hat, scarf, etc., get near the fans. With the craft on the ground and the lift engine ticking over, embark with helmet on and strap yourself in. Advance the lift throttle slowly and notice the rpm at which the craft begins to stir; then, at which it lifts off properly. Lower the rpm and let it settle back gently. Try this a few times, and then set it at hover.

Have someone verify that the skirt is developed properly all round, and not vibrating. While remaining properly seated, have someone check that the craft is level when hovering. If not, adjust the centre of gravity by adding some ballast until it is level. Note the weight and position of the ballast accurately, and secure it here upon completion of this test.

Now, lean far to one side. The craft will roll that way, and probably begin to drift in that direction due to lift air escaping on the opposite side. This is worth remembering; if the thrust engine fails over water you can get to shore this way!

4.11.2 Beginning to Move

Again, put the machine in the middle of a large flat space, and have everyone else get well clear. Check that the lift engine tank contains at least as much fuel as the thrust engine tank. If the thrust engine runs out and stops, no great harm is done. But if the lift engine fails while the craft is at full speed, the craft can stop abruptly, overturn, or have its skirt and hull damaged. Once you are strapped in, with helmet on and both engines idling, look round carefully. This *looking round* is a most important habit, and particularly necessary even before starting either engine. Helpers have a habit of fussing round the thrust fan, behind your back, just when you want to start it. Look round first!

Bring the machine up gently to hover; notice that even low thrust will edge the machine forward. At full lift rpm, it moves easily. At low lift rpm, it moves along with difficulty. Reducing lift is a way of braking, but it wears out the skirt and reduces stability, in the sense that the craft can pitch forward and dig in. Therefore, it is dangerous to reduce lift when moving fast, whether on water or land!

Try the rudder, at low thrust rpm it is fairly useless, so give a burst of thrust to see how it immediately becomes effective. Then try full rudder at low thrust, and slowly increase thrust a little so that you turn round in a full circle. Do this both to the left and right. You may find one way easier than the other, due to the fan exit swirl hitting the rudder unevenly. Remember this. In an emergency, a 270° turn one way may be quicker than a 90° turn the other way. You will find that the craft changes course slowly, although it points in a new direction quickly. Also, once it is yawing, it needs a touch of opposite rudder to stop the yawing. A lot of practise at low speed is needed to become proficient at this.

4.11.3 Stopping

We have already seen that lowering the lift rpm will drag the skirt and slow the craft down, but at the expense of skirt wear and some loss of stability. Never do this when moving fast, whether over land or water. Decide

early where you want to stop, reduce thrust well ahead, slow down, and then reduce lift and settle gently. If there is a wind (or a slope) and you have enough room, go round to down-wind of the stopping place and approach it up-wind (or uphill). Come in slowly, reduce speed to a crawl, lower the craft onto the ground, and switch off.

If you must stop in a hurry, the 180° spin is the answer. Try it slowly, at first. Moving slowly forward, while on full lift, put on hard rudder and give a blast of throttle. At about 120°, as you spin round, put on full opposite rudder to stop the spin, with another blast of throttle. This should leave you heading at 180° and moving backwards on the original course. Now keep the rudder central and give full thrust until you come to a standstill. Try this gently and slowly over smooth ground, with plenty of room, and do not reduce lift power. It is an emergency procedure which should be practised.

4.11.4 Slopes or Wind

Going up a hill is easy. Going across a slope is more difficult. Coming down a hill is not at all easy until you know how. The same applies to up-wind, cross-wind, and down-wind, respectively.

Try it on a gentle hill. Start on the flat ground at the bottom, going at a smart walking pace towards the hill, and keep on up it. If you lose speed and slide backwards, there is no problem. Keep headed up the slope and slide slowly backwards down to the bottom. If you want to stop on the slope, reduce lift to set the craft down first, and cut the thrust afterwards; otherwise, you will slide back while the lift is decaying, which may take 10 seconds or so. To run across the slope, point up it and then use the rudder momentarily to head a bit in the intended direction. You will then crab sideways across the hill-side, adjusting heading and thrust to keep on course.

Downhill is the difficut direction. If the hill is gentle and the ground not too abrasive, go down forwards at low lift, dropping completely onto the ground if the speed begins to build up. If the hill is steeper, do a 180° turn at the top and go down backwards using thrust as a brake. Again, if speed builds up, drop the craft on its skids with the thrust still on.

Running down-wind can be quite hazardous, especially over water. You only have control when you have a fair thrust on, and the speed then rises alarmingly. Any attempt at turning is likely to drop the nose in and roll the craft at high speed. Any attempt to reduce lift and drag the skirt will create instability and make the roll inevitable. A down-wind course should therefore be run as a series of cross-wind *tacks*. If the wind is really strong, the turn from one tack to the next should be 270°, sweeping through the up-wind direction; not 90°, sweeping through the down-wind direction.

4.11.5 Over Water

On water, the seat belt is often not used, but a life jacket is necessary. If the water is cold, an exposure suit is strongly advisable. A person can live only for a few minutes in near-freezing water. Snowmobile suits, incidentally, are death traps in water. They are not waterproof, and the thick lining absorbs many pounds of water in a few moments, dragging the wearer down. A yachtsman's *exposure suit* is the answer in cold weather.

As explained earlier in Section 4.6, a craft can be driven below or above hump speed, i.e., approximately 7 km/h (5 mph). Below hump is used only in restricted spaces or in coming alongside moorings or ramps. It usually generates a lot of spray, which erodes the fans and wastes power. If the craft has proper thrust installed, it should accelerate through hump, lose its spray and wake, and surge forward without difficulty. It may perhaps help if the driver moves forward in his seat in the process.

When starting on the water, the craft is first gradually lifted, with a little thrust to keep the spray away from the bow, until all the water is drained out of the skirt. Then the lift is throttled back and full thrust applied. When at full thrust, full lift is given; the craft pops up, and is away with a minimum of spray. Otherwise, if lift is opened up first, the craft sits surrounded by spray, which soaks the driver and erodes the fan, until thrust builds up enough to get it moving. Pointing the craft into the wind helps to give the driver a clear view.

When making a turn over water, the speed drops. Therefore, above hump speed, make only gentle turns; otherwise, the craft may fall below hump speed, drop into the water with a splash, and experience a sudden deceleration. If this is done in a turn, it can cause the leading outer-corner to dig into the water and perhaps even cause an overturn. This is almost inevitable if lift air is reduced, softening the cushion. Furthermore, turns are very flat and skidding, needing a lot of room. Because a hovercraft can skid sideways or backwards, a flashing yellow light is required on top of it. This warns other mariners that port and starboard lights do not necessarily give any clue as to the craft's course.

To get into or out of the water, it is essential to have a gently-sloping beach or ramp. The craft cannot be expected to climb up a step or a steep bank. When starting from a beach, provided the beach and water are clear of obstructions, boats, or swimmers, go down the beach sufficiently fast for the craft to be over hump speed when it reaches the water, giving an excellent spray-free start.

4.11.6 Over Snow and Ice

If the ice surface is smooth, the drag on the skirt is small and high speeds can be reached. However, manoeuvering power is minimal, and stopping or obstacle avoidance requires a great distance. Coming off ice onto water at high speed leads to a sudden increase in drag, which can cause a nose-in, with potentially disastrous consequences.

Snow with a glazed surface will usually support the craft, just like ice. However, fluffy or damp snow is difficult to traverse. It blows up in a cloud, and the craft can easily dig itself a hole from which it has difficulty escaping. The blowing snow can erode the propeller badly. A start in such conditions should be made as when over water. Full thrust is applied first; then the lift throttle is opened quickly, so that the vehicle immediately moves forward, instead of digging itself in.

For safety in harsh climatic or terrain conditions, vehicles should operate in pairs. A trip plan should be left with a person who will be responsible to verify that the machines and crews have arrived safely. Furthermore, at freezing temperatures over water, the spray builds up as ice on the craft. The craft weight can increase to the point at which it will no longer hover; also, engine and rudder controls can freeze. A carefully-driven hovercraft is a unique vehicle which can be great fun. However, driven carelessly or without proper planning, it can be annoying, frightening, or even fatal to its occupant(s) or bystanders.

4.12 SUMMARY

This chapter has described the design, construction, and operation of a light home-built hovercraft. It has been written from a severely practical point of view, with a minimum of mathematical treatment. The theoretical basis of the aerodynamics involved is discussed elsewhere in this book. In this chapter, the design process was laid out in sequence, starting from the specification of requirements, and proceeding through the design of a simple bag-skirt, the lift and thrust systems, the controls, and the hull. There followed a short course of instruction on the driving of a light hovercraft, a technique which has been likened to sailing a dinghy in a gusty wind, without a keel. The hovercraft is not an all-terrain vehicle, but it can traverse many otherwise-difficult areas of land, water, snow and ice, particularly those which are too soft or fragile to support other vehicles, or a person on foot. In the hands of a good driver, it can be controlled well. The construction and operation of such vehicles has been shown to form excellent projects for high-school students. It involves a good combination of workshop skills with applied physics and mathematics, and culminates in exciting sporting possibilities.

4.13 REFERENCES

1. R.L. Trillo, Marine Hovercraft Technology, Leonard Hill Books Ltd., London, U.K., 1971.

2. P.J. Mantle, Air Cushion Craft Development, Report No. DTNSRDC-80/012 (4727 Revised), David W. Taylor Naval Ship Research and Development Center, Bethesda, Maryland 20084, U.S.A, January 1980.

3. H.S. Fowler, Overland and Amphibious ACV Design Data Relating to Performance, Mechanical Engineering Report ME-245, National Research Council of Canada, Ottawa, Canada, April 1979.

4. H.S. Fowler, On the Lift-Air Requirements of ACVs, and Its Relation to the Terrain and Operational Mode, Mechanical Engineering Report ME-246, National Research Council of Canada, Ottawa, Canada, May 1979.

5. H.S. Fowler, Thrust Systems for Light Air Cushion Vehicles, Report LTR-ENG-21, National Research Council of Canada, Ottawa, Canada, December 1973.

Chapter 5

LARGE HOVERCRAFT PERFORMANCE AND ECONOMICS

5.1 INTRODUCTION

Performance and economics are important factors in the consideration of large hovercraft for civilian and military transportation applications. They are treated in this chapter by examining the applicability of operational efficiency concepts, general trends and statistical data related to production costs, and the performance of two successful craft produced by British Hovercraft Corporation (BHC).

Section 5.2 explains how supportability engineering requires a balanced application of maintainability, reliability and manning considerations. The applicability of this concept to the operational efficiency of hovercraft is examined.

A key ingredient in determining the commercial or military acceptability of a hovercraft is its cost of production. *Cost* means different things to different people. A few governing cost equations are provided in Section 5.3 to place all terms into context. Then, trends and data on costs of actual hovercraft are presented.

Two of BHC's most successful hovercraft are described in Section 5.4, including hull and component structure, flexible structure, mechanical design, systems, and accommodation and passenger services. Their performance (speed versus sea state, crossing times, etc.) and operating experience (hours or miles run, cars or passengers carried, etc.) are presented. Also discussed, as an example of the versatility of hovercraft, are the special requirements of a Canadian Coast Guard application and how they were satisfied with the AP.1-88 craft.

5.2 OPERATIONAL EFFICIENCY

The designers must strike an operational/cost balance between reliability

and supportibility. This requires: a) an understanding of what reliability is and what it costs to acquire more of it, b) what supportability is, how it affects ship design and what it costs, and c) last but not least, how the human element, the crew, fits the equation and what it costs to obtain and keep it.

If reliability is the probability that a system will perform satisfactorily for a continuous period of time before allowing a failure to occur, supportability measures the ability to keep a ship in satisfactory condition by maintaining the ship material condition and treating it as a consumer of goods and services. These goods and services are consumed by the personnel assigned to the ship as its crew, that must have the skills and facilities to achieve the required reliability. Having come full circle, we will now delve into the mysteries of reliability in detail.

5.2.1 Reliability

From a parochial perspective, increasing inherent reliability of shipboard equipment will alleviate most of the problems that arise during the deployment of a naval ship. Reliable equipment on board reduces the need for skilled maintainers on board and minimizes the spare parts stockage requirements. Reliable equipment is a function of the following: 1) proper engineering during the design process, 2) selection of reliable components subjected to parts-control screening and quality workmanship during fabrication, 3) intensive testing in a simulated operational environment of both a prototype and a sample from the production lot, 4) proper installation and checkout onboard the ship, 5) proper feedback reporting on equipment problems/casualties, and 6) preventive maintenance programs that are used. The probability that all six of these activities will occur is so low that fallback positions from the ideal are to be expected.

As has been emphasized at the highest levels, material readiness has one of the highest priorities of the Navy today. It is important to understand the elements that contribute to achieving high levels of readiness beyond the aspect of inherent reliability just addressed. A key factor lies in the ability to repair equipment at the organizational level. The obvious prerequisite for this is the availability of properly trained land motivated personnel. If the equipment were designed for ease of maintenance, the need for highly skilled individuals on board would be reduced. Thus, simplicity is a key to low *mean time to repair* (MTTR) values.

A second consideration in ship readiness is the selection of spare parts for onboard stockage. The use of a methodology similar to TIGER/FLSIP to identify the appropriate range and depth of component spares is needed to avoid the typical case of *too many of the wrong parts and not enough of the needed ones* (ref. 1). If a replacement for the filed component has not been stocked on board, ready access to an intermediate or depot level is essential. The

parameters that quantify these delays are: i) *administrative delay time* (ADT), the time required to obtain a needed part that is spared onboard, and ii) *logistic delay time* (LDT), the time to obtain a part from offship. ADT is usually a matter of hours; LTD is often a matter of days.

To illustrate the relationships among the various factors that affect readiness, a hypothetical example is presented. Consider an equipment that is mission-essential and has demonstrated a *mean time between failures* (MTBF) of 1,000 hours and MTTR of 10 hours. The ship is deployed for a 60-day mission during which the equipment is required to operate continuously. The inherent reliability and availability for this item can be readily calculated, assuming unlimited access to spare parts without delay times and trained personnel availability without delay. The values are 0.237 for reliability at 60 days and 0.99 for average availability during the mission.

It is crucial to understand the distinction between these two parameters. Reliability is the probability that the system or equipment will operate continuously (without interruption) for the mission duration. Average availability is simply the ratio of *uptime* (time during which the system or equipment is operating satisfactorily) to total mission time. That is why reliability of a single item in series (without redundancy) is unaffected by sparing, while availability of this item is drastically altered by redundancy policy.

In addition to onboard sparing, two other obvious ways of improving performance are redundancy and reliability improvement. The latter can increase the MTBF of the equipment by 25% without an intensive application of resources. Typically there are several modes (causes) of failure for a given equipment or system. Associated with each mode is an MTBF. If an improvement program succeeds in minimizing a seemingly dominant mode, the other modes are still present to be potential sources of failure during the mission. This is called *competing risk*. Thus, for the example discussed, the MTBF might be increased from 1,000 hours to 1,250 hours.

Figures 5.1 and 5.2 illustrate the impact on reliability and availability of onboard spares stockage, redundancy, and MTBF improvement. The conditions which apply to curves a, b, c and d of these figures are specified in Table 5.1. As noted above, reliability of a single unit is unaffected by sparing since continuous, uninterrupted performance is required. In the example, increasing the MTBF by 25% increased the reliability by 33% to 0.32.

Redundancy has a major impact on reliability while onboard sparing alone can improve availability, as seen in Figures 5.1 and 5.2. The effect of administrative and logistic delay time on availability, Figure 5.3, reinforces the requirement for having the necessary spares onboard. The option of reducing MTTR from 10 hours to 1 hour by such means as modularity and built-in test equipment improves availability by only 1 percent in this example. This is due

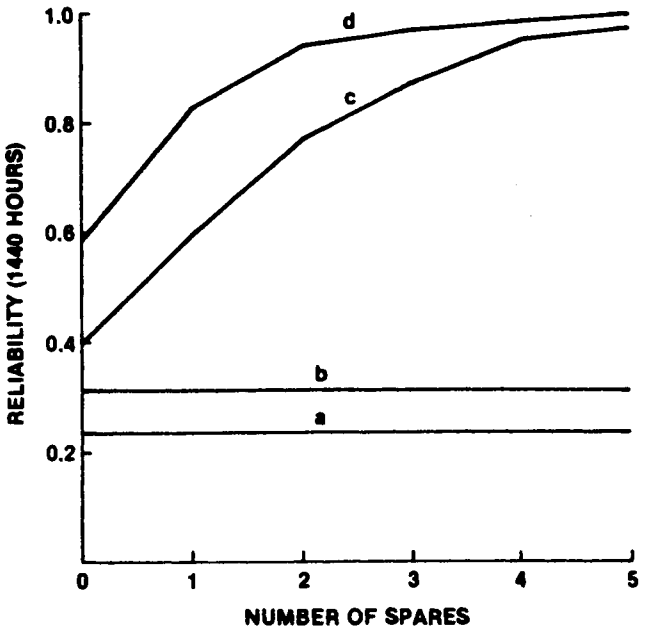

Fig. 5.1 Reliability as a function of onboard spares.

to the large spread between the MTBR and MTTR values (1000 hours compared with 10 hours). When the MTBF is small and MTTR large, a significant impact can be seen, but this is generally not the case.

From the considerations that have been addressed, it is clear that there are alternative ways of achieving high levels of reliability and availability. A *reliability improvement program* (RIP) can be implemented using the *test, analyze and fix* approach of MIL-STD-1635. This may entail internal redundancy or upgrading of components. This cost has to be traded off against the cost of onboard sparing or redundancy. On the other hand, the RIP approach can do no better than the state-of-the-art which may still produce an inadequate solution to satisfy mission requirements.

As far as resolving conflicts in resource allocation between availability and reliability is concerned, careful consideration to the system utilization is necessary. For example, during Condition I (General Quarters), a radar system must operate continuously without interruption, so reliability is the appropriate figure of merit. During cruise or transit, short downtimes may be tolerable, so availability is the correct measure. A single combined measure of performance called PAR is often used in the U.S. Naval Sea Systems Command to represent a mission; it is the probability of being available to enter an engagement and being reliable during the engagement. The program manager

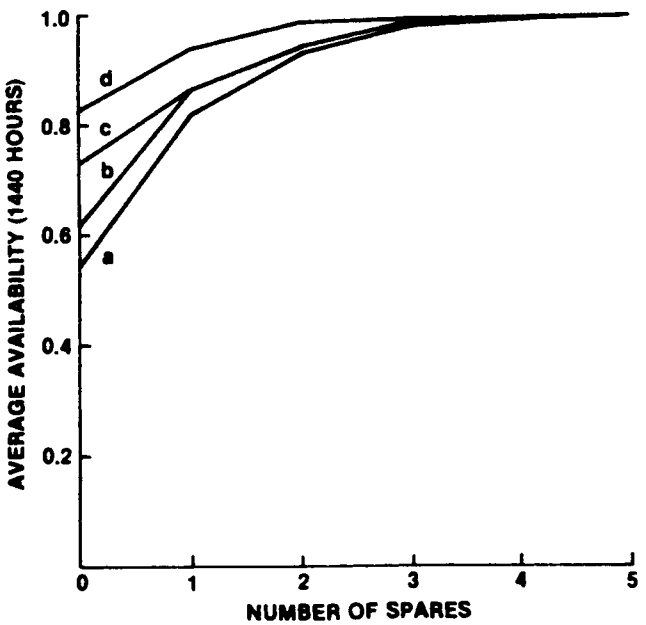

Fig. 5.2 Availability as a function of onboard spares.

should always take an analytical approach to resource allocation for material readiness in order to balance the potential impact of sparing, redundancy, and reliability/maintainability improvement programs.

Table 5.1. Conditions applicable to the curves a, b, c and d of Figures 5.1 and 5.2.

Curve	MTBF(hrs)	MTTR (hrs)	Number Installed	Number Required	Type of Redundancy
a	1000	10	1	1	none
b	1250	10	1	1	none
c	1000	10	2	1	active
d	1000	10	2	1	standby

5.2.2 Supportability

Logistic support analysis (LSA) is the process whereby all elements relevant to the design, operation and maintenance of a component, equipment, subsystem or system are critically examined from first concept to last usage. During the process a maintenance or ownership concept is developed which is in consonance with Navy policy of the time. This maintenance concept establishes the work which will be done aboard ship by the organizational (O) level on a tender by the intermediate (I) level, or ashore by the depot (D) level. Consideration is given to such factors as: a) failure rates, b) MTBF, c) repair times, MTTR, d) *mean logistics delay time* (MLDT), e) personnel.

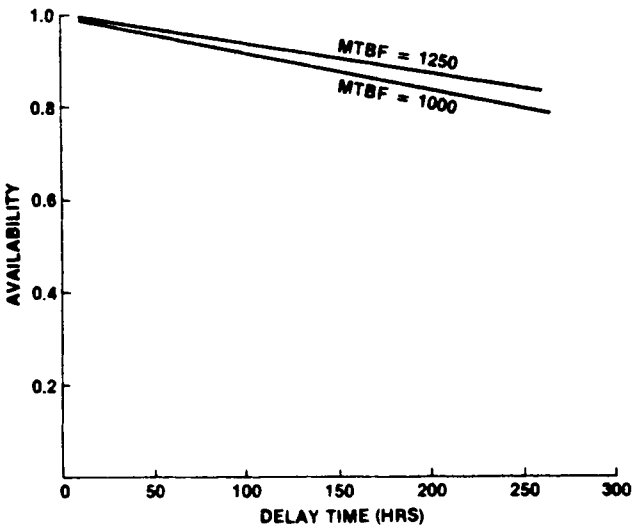

Fig. 5.3 Availability as a function of administrative/logistics delay time, with MTTR = 10.

The starting point is the range of reliability allowed by the system availability requirement. Systems that are highly reliable may take a long time to repair without adversely affecting availability, while systems that have relatively low reliability must be quickly repaired before their availability is adversely affected. Table 5.2 illustrates acceptable availability for systems A_1 and A_3 where system downtime is 1% of system operating time; whereas the 8 percent downtime of A_2 is unacceptable. While this time is nice in theory a judgment must be made regarding acceptability in practice. The range of values that create the mean in MTBF is significant in that a narrow range creates confidence that the equipment will last approximately that same number of hours while a wide range indicates that equipment failure may be either imminent or a long time in the future. The latter case is worrisome while the former produces confidence.

All of this theory is nice, but how it relates to the real world fraught with the dangers of combat is another story. The ability to meet a theoretical availability is worthless if a system fails when it is called upon to perform its part of the mission. Let us look more closely, then, at our theoretically acceptable values of availability for systems A_1 and A_3. The data for A_1 tells us that we may expect the system to operate for 10,000 hours between failures but that we may also expect to be without its use for 100 hours while it is being repaired. The data for A_3 tells us that we may expect 1000 hours of operation between failures and that we must do without it for only 10 hours.

Table 5.2. Availability A of three systems, where:

$$A = \frac{\text{Uptime}}{\text{Downtime}} = \frac{\text{MTBF}}{\text{MTBF} + (\text{MTTR} + \text{MLDT})}$$

MTBF = mean time between failures
MTTR = mean time to repair
MLDT = mean logistic delay time

System	Availability, A		
	Computation	Value	Conclusion
A_1	$\frac{10000}{1000 + (100)}$	.990	Acceptable
A_2	$\frac{1000}{1000 + (80)}$	.926	Unacceptable
A_3	$\frac{1000}{1000 + (10)}$	.990	Acceptable

Given a choice between two systems with these characteristics we must make a decision regarding which one will be installed in our ship. However, this information alone is not sufficient. We must know the range of the mean in each case. For the 10,000 hour MTBF system, the range is from 1000 hours to 19,000 hours, while the 1000 hour MTBF system ranges from 900 to 1100 hours. Predicting when the 10,000 hour system will fail is almost an impossibility, whereas predicting when the 1000 hour system will fail is comparatively a certainty. With a system which has a predictable failure rate, the LSA process in conjunction with an *engineered operating cycle* (EOC) can help to decide if a system should be repaired before a deployment or at what time during a deployment it may be feasible to take the system down for repairs. The repairs, in this case, are the replacement of those parts which were predicted to fail between 900 and 1100 hours of operation. Since the repair will take only 10 hours rather than 100 hours, the time out from our ability to support the mission is significantly less.

Even in a protracted deployment, the downtime for the system can be scheduled to minimize the effect on mission readiness by having it coincide with a replenishment cycle. The decision that we make may have an impact on the stowage of spare parts (ref. 2), the cost of spare parts, the number of personnel aboard ship, the skills those personnel are required to have and the shop facilities that the ship will require. Additionally, we must consider the effect on the intermediate and depot level facilities.

If the part (lowest replaceable assembly) to be replaced every 1000 hours is a large pump or motor, we will probably be required to keep three spares onboard for each one in service. If we will repair the unit aboard our ship, we may need only one unit for each one in service plus three sets of spare

parts. If the parts to be replaced are expensive electronic circuit boards, we must consider the cost of procuring and owning three of each board instead of the possible cost of an expensive onboard repair facility and the equally expensive services of a highly trained technician to repair them.

For the system with the 10,000 hour MTBF, the average requirement for spare parts is approximately 417 days. Thus, we would not normally have these parts onboard ship. However, the fictional equipment has a range of 1000 to 19,000 hours, so we will jog the system and require at least two spares in case two failures occur consecutively at the low end of the spectrum. Normal practice is to let equipment run to failure (refs. 2 and 3). Failure is not necessarily catastrophic. Failure may be the inability of the equipment to function at full capacity. When the equipment performance is degraded sufficiently, we decide it is time to do something about it.

The easiest example to understand is operation of a ship in a warm salt water environment. We start with a clean hull, with fresh anti-fouling paint. The moment that the hull hits the water, the hull's performance degradation begins. As each minute passes, its performance potential decreases steadily. Failure occurs when the ship can no longer perform its mission due to a loss of speed and/or range. It is not practical to stop in mid-ocean and clean the hull while the rest of the group sails on without us. But it is practical to perform maintenance on other equipment which will restore its performance, thereby upgrading total ship system performance. Normal practice for some equipment is to run to failure, but failure might occur in mid-deployment. By developing an EOC, we increase the likelihood that the failure point will occur when the ship is not deployed and thereby keep the ship available to perform its mission. Thus, we maintain it before deployment, not knowing positively whether or not it needs maintenance, since we are sure that it can still operate for some time, but confident that it will not perform through another full deployment.

An additional benefit of an EOC is a reduction in the frequency of failures since we usually repair/refurbish before failure. When we acquire sufficient experience with a particular system or equipment in a particular environment, we may introduce *reliability centered maintenance* (RCM). RCM may let us omit some of the repair/refurbishment cycles because we have learned through experience that they are not necessary. We may or may not substitute preventive maintenance for the old repair/refurbishment actions dictated by our experience. Indeed, it has been reported at various times that some *preventive maintenance* (PM) requirements have been found through trial and error not only to require an excessive amount of PM, but have actually caused increases in corrective maintenance (CM) through the excessive application of PM. These factors affecting equipment performance must all be considered for each design.

They form the initial maintenance concept and establish the supportability design criteria, which result in a ship specification. During the detailed design and construction phase, the ship-builder utilizes these requirements and guidance during his LSA process to perform engineering/cost trade-offs. Going overboard on any given reliability/availability criteria will increase cost unfavorably and deny him monetary rewards which should be part of the design and construction contract. But this is where the weak spot is. The ship acquisition program manager is not inclined to discuss contract incentive clauses with the technical community, such as paying higher prices for equipment which requires less preventive maintenance. Without such clauses, cost-benefit design changes will never be initiated or adopted. Since a ship will be operational for at least thirty years, consideration must be given at the outset to the relationships of reliability, supportability and the manning required to achieve the reliability, mantainability and availability objectives at the least possible cost.

5.2.3 Manning

The Navy has long realized that its most expensive commodity is manpower itself. About 1960, the Navy concluded that it needed better manpower allocation methods and it was also felt that a greater design effort was required to optimize the man-machine combination. By 1967, a *Design Work Study* policy was defined, including the following statement. "Naval Ship Engineering Center assists in the development of designated ship contract or modernizations by coordinating the use of Design Work Study techniques to systematically determine the optimum efficient and effective combination of ship, systems and manning for operation and maintenance." Since its inception, the application of the Navy's Design Work Study Techniques to shipboard manning has resulted in greater accuracy and efficiency in developing ships' crews. This technique has proved its worth in improving accuracy in skill assignments, as a guide and as a justification for sizing crews to minimum requirements.

While most people involved in national defense have long recognized, in a general way, that a properly trained crew is essential to both the ship's support and its reliability, the rapidly increasing technological complexity of shipboard hardware is continuing to place a serious strain on the Navy, due to the decreasing availability if trained personnel. Thus it has become essential, not merely important, to develop a crew composition which is: a) efficiently designed to the ship's requirements, b) properly trained to function effectively, and c) of the minimum skill levels required.

Indeed, even this is no longer enough if we are to make the ship both reliable and supportable. A Navy Personnel Research and Development Center projection of skills and their shortfalls predicted alarming losses of critical skills among the petty officers of the Fleet. But to satisfy essential

supportability requirements, the ship's crew must include personnel with the skills needed to carry out the ship's mission, including operation and maintenance of the ship and all its hardware.

How can we satisfy the need for more and more highly trained crewmen given that their actual numbers in the Navy are decreasing each year? The responsibility for husbanding these scarce resources and for employing them as sparingly as possible falls on personnel in three functional areas. To lessen the impact of the problems, the following personnel should increase their efforts as follows:

1) Design engineers: to design and select the simplest, most reliable and most easily maintained hardware. Also to aid standardization by selecting hardware which is already in the fleet, where practicable.
2) Manpower developers: to carefully assign personnel who are capable of operating and maintaining the hardware, but not *over trained* for the work.
3) Training personnel: to ensure that training courses cover the actual shipboard equipment and impart *hands-on* training.

Where equipment reliability is of a high order, potential corrective maintenance actions can be changed into preventive maintenance actions by scheduling repairs and replacements. Some of these actions require intermediate level maintenance which can be accomplished in port or on a tender. In any case, such scheduling represents an opportunity to place some personnel, who possess scarce skills, aboard tenders, where they can be used to greater advantage than is possible when they are part of a ship's complement.

Because of examples of equipment failure through lack of attention or improper maintenance, the U.S. Fleet has been criticized for having too many sailors considered to be incapable of absorbing advanced training. The inability to meet entrance requirements for U.S. Navy A, B, or C schools is greatest among sailors who had not completed their high school education before entering the Navy. Due to shortages of trained personnel, untrained sailors such as these must frequently be assigned responsibility for equipment operation and maintenance. However, to an increasing extent the Fleet is finding solutions to this problem by breaking down the A, B or C school training into short courses which cover more limited areas of maintenance or one specific hardware system.

5.2.4 Systems Analysis Example

A U.S. Navy study was conducted on the reliability, availability, supportability and manning of several subsystems of a given class of craft involving gas turbines (GT) and diesel engines, among other components. In this example, we examine the choice between GTs or diesel engines. it is shown that the wrong choice can be made if the problem is examined from too narrow a perspective.

Gas turbine engines have moved to the fore as favored propulsion plants and as prime movers for ship service generators. They eliminate all of the problems inherent in steam plants and appear glamorous due to their origin in the aerospace industry. They are also very reliable. On the other hand, diesel engines were mainly used ashore, except when installed as emergency diesel-generators or main surface propulsion. Their popularity in long haul trucking and with the railroads was due to their reliability and fuel efficiency. Furthermore, they emit a foul odour and are not considered glamorous.

An interesting situation is illustrated by the Navy's experience with these two principal engine types for propulsion. Diesel engines have been found to require a significant amount of preventive maintenance (PM) and corrective maintenance (CM). For a typical example, the total weekly PM and CM averaged 22 man hours by the ship's force. The mean time between forced shutdowns (same as MTBF) was 2500 operating hours (OH) (upper 90 percent confidence limit = 3940 hours; lower 90% confidence limit = 1670 hours) (ref. 4). Although the ship's mean time between corrective maintenance was 435 operating hours, the crew was able to perform the CM in nearly all instances (even after forced shutdowns, unless a rare casualty such as a broken crankshaft had occurred). Thus the ship was repairable and could complete its mission without being diverted to a tender or port.

On the other hand, the popularity of gas turbines can be attributed to a number of factors, among which are good reliability and very little shipboard maintenance. A study generated tabulations of experience with the LM 2500 GTs over a 3-year period taken across a range of ships. Total shipboard maintenance averaged approximately 8 man-hours per engine per week (36% of our diesel example). This maintenance consisted of work done on GT peripheral equipment as well as *changeout* time for the engine itself. Not that major repairs to a gas turbine cannot be made while the ship is underway. The ship must return to port or to a tender for either onboard repairs or engine changeout.

If forced to repair at sea, under combat, a loss of one of four engines (two GTs per shaft) reduces the ship's top speed and therefore its combat capability. A loss of two out of four engines could jeopardize the ship's mission. However, the MTBF for the GTs of the DD 963 Class, based on a two year period, was 1000 operating hours (OH) while the average time between engine changeouts was about 5730 OH. This represents a time spread between changeouts of 76 OH to 6170 OH. Gas turbines are normally run to failure.

For DD 963 Class ships which have four propulsion GTs, two on each shaft, it is sufficient to have one LM 2500 GT operating on each shaft during Condition III, Wartime Cruise. However, for Condition I, Battle Stations, it may be necessary to operate all four engines. If the mean time between removal of any of the four engines would be approximately 1433 hours (60 days), offship

assistance would be required to accomplish the engine replacement. The superior reliability of the gas turbine is offset by the inability of the crew to return it to duty while at sea.

Another consideration regarding repairability at sea or ashore is the availability or lack thereof of trained personnel to perform repairs. A study of gas turbine technician availability versus engineman availability from 1981 to 1987, conducted by Naval Sea Systems Command, yielded the following graphs:

a) Figure 5.4, GSM E-4 grade. For the years 1985 through 1987, an availability of 740 GSM3 petty officers was predicted against a requirement of 600. (GSM: Gas Turbine Mechanic).
b) Figure 5.5, GSM E-5 grade. An availability of GSM2 petty officers of 530 was predicted against a requirement of 470.
c) Figure 5.6, GSM E-6 grade. An availability of GSM1 petty officers of 90 was predicted against a Fleet requirement of 290.

Since E-5 petty officers would fill E-6 grade shortages and E-4s would fill the resultant E-5 shortages, there would barely be enough GSMs overall to meet Fleet requirements. This did not take into account expanding Fleet requirements resulting from planned craft acquisitions. Similar shortages were also predicted for all GSE pay grades, except E-4 and E-5.

However, Figure 5.7, EN E-4, projected an availability of 2455 enginemen, EN3 petty officers, against a Fleet requirement of 2186 for 1985 through 1987.

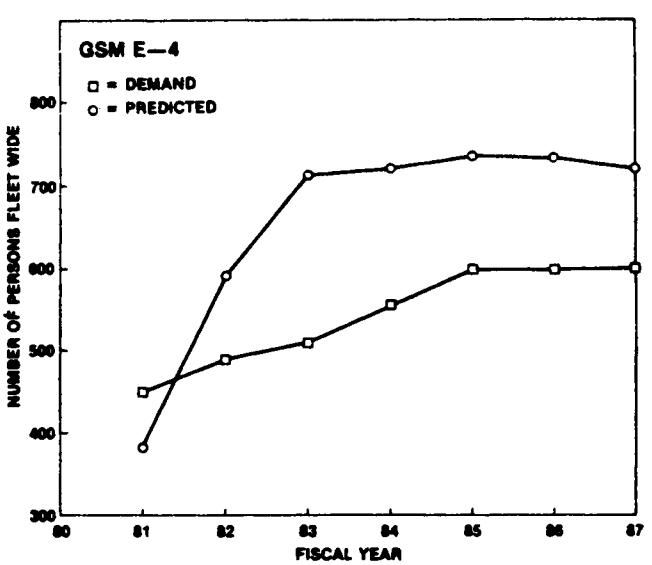

Fig. 5.4 U.S. Navy manpower estimates (1981-1987) for gas turbine mechanic grade GSM E-4.

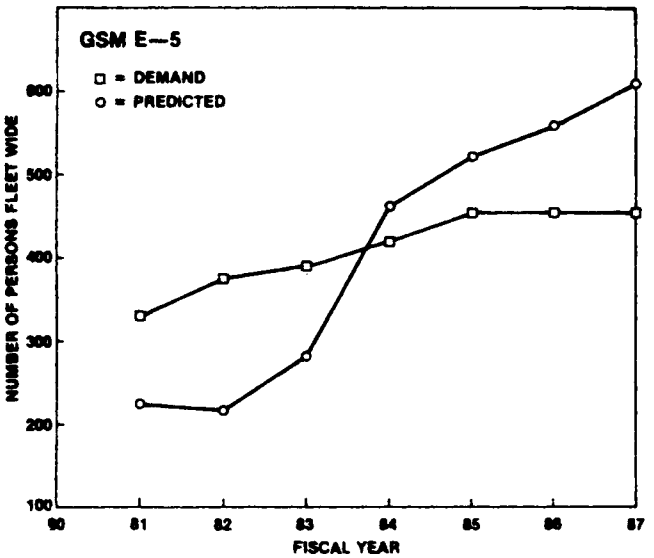

Fig. 5.5 U.S. Navy manpower estimates (1981-1987) for gas turbine mechanic grade GSM E-5.

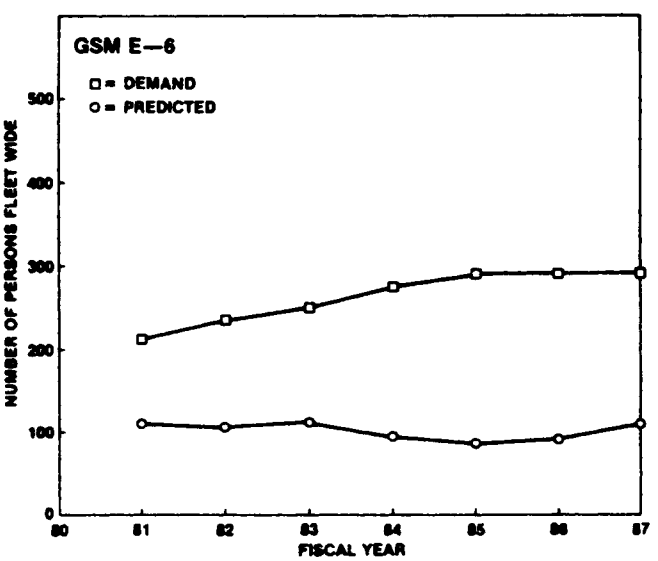

Fig. 5.6 U.S. Navy manpower estimates (1981-1987) for gas turbine mechanic grade GSM E-6.

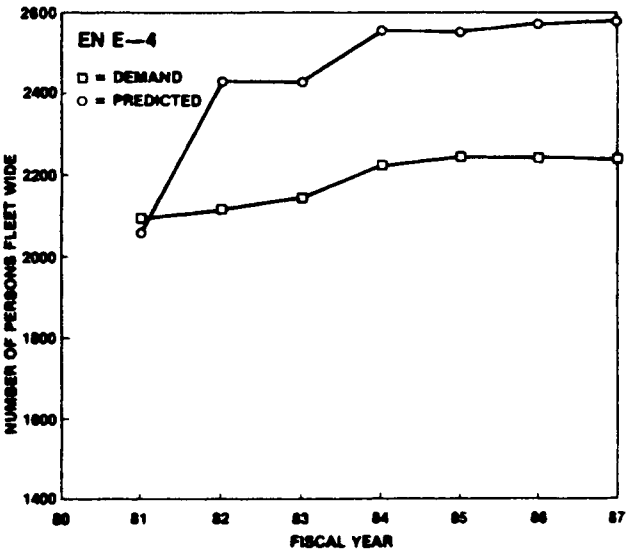

Fig. 5.7 U.S. Navy manpower estimates (1981-1987) for engineman GRADE EN E-4.

Except for a temporary shortage of about 25 EN1 petty officers, Ffgures 5.8 and 5.9 display sufficient numbers of EN1, EN2, and EN3 petty officers through 1987. Thus, while new ships entering the Fleet reduce the available enginemen to a point of shortage for certain grades, assignments of personnel of the next lower grade would be expected to eliminate the shortages.

The overall effect is unmistakeable. The continuing proliferation of gas turbines in the Fleet would result in a serious lack of personnel qualified to maintain them. However, under the available skill projections, the new ships expected to enter the fleet in the next six years, if propelled by diesel engines, would cause some shortages in diesel maintenance personnel, although less severe than the gas turbine specialist shortage.

5.3 HOVERCRAFT COSTS

A key ingredient in the determination of the commercial and military acceptability of a hovercraft is its cost. *Cost* means different things to different people depending on their vantage point and experience. In the following sections, *cost* will be put into context with fundamental relationships and supporting data. The detailed make-up of the costs of a hovercraft, as for any other vehicle, varies quite markedly with the builder, the standards to which the craft is built, and the efficiency of production as well as many other factors. Despite this variation in detail there still remain fundamental and governing relationships that can be expressed quantitatively. These are

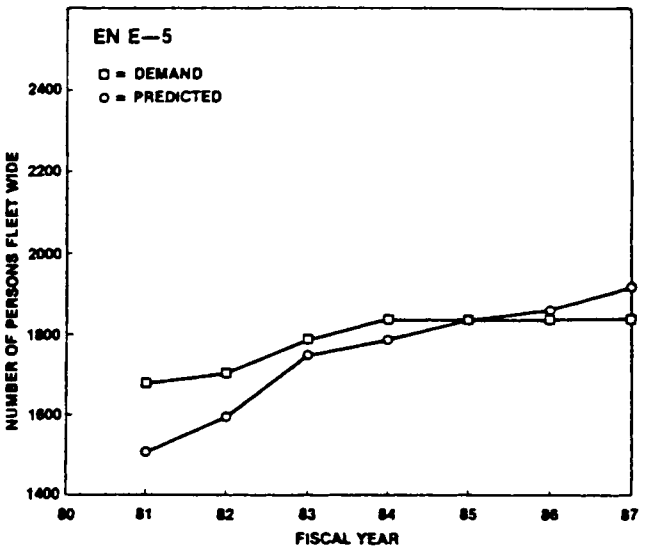

Fig. 5.8 U.S. Navy manpower estimates (1981-1987) for engineman grade EN E-5.

presented here such that the reader can use the equations and data to place a given vehicle into context with others and to determine *cost drivers* in any particular design.

The cost analysis of a hovercraft starts with its initial development

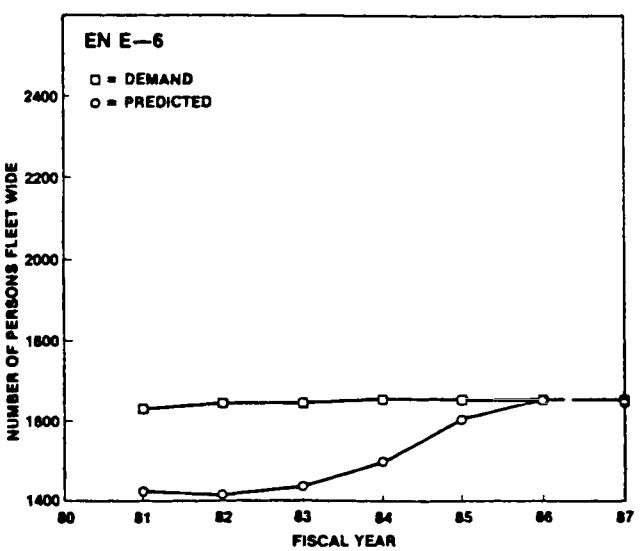

Fig. 5.9 U.S. navy manpower estimates (1981-1987) for engineman grade EN E-6.

costs, followed by the cost of investment in the craft itself, its operating cost over some specified lifetime, and finally its residual or scrap value. This is typically referred to as its *life cycle cost*. While the following sections will cover all aspects of these elements of life cycle cost, concentration will be given to the investment or acquisition cost and the operating cost as these are usually of prime consideration in the purchase of any particular vehicle.

5.3.1 Governing Cost Equations

The governing cost equation that relates all elements of cost, called the *life cycle cost*(LCC) equation, is simply:

$$LCC = C_{RD} + C_{INV} + C_{OP} - C_{RES} \tag{5.1}$$

where C_{RD} is the research and development cost, C_{INV} is the investment cost of the hovercraft and associated equipment, facilities, initial spares, etc., C_{OP} is the operating cost of the hovercraft including such items as crew costs, fuel, replenishment spares, etc., and C_{RES} is the residual or scrap value of the hovercraft at the end of its useful life.

Figure 5.10 displays this life cycle cost showing the main elements. These elements apply in varying degrees to all hovercraft whether military, commercial, or recreational. Most of the cost elements shown are self-explanatory but some may require further elaboration.

(i) Research and development costs, C_{RD}. In the case of military vehicles these costs would be funded under a contract separate from the *investment* or acquisition cost. In the case of commercial vehicles this is usually taken out of the profit. In either case, the true cost of the hovercraft must include any research and development, early design work, and testing, unless the hovercraft in question is simply a carbon copy of some other hovercraft.

(ii) Investment cost, C_{INV}. This covers the cost of acquisition of the craft itself, plus any other costs essential to its initial acquisition. These additional cost elements would include any new facilities required, associated systems such as special fueling arrangements, the initial set of spares, and finally, in the case of military hovercraft, the initial set of expendable ordnance or weapon system. In many instances the cost of the weapon system can be equal to or greater than the basic cost of the hovercraft itself.

(iii) Operations and support cost, C_{OPS}. This encompasses all costs involved in the actual operation of the craft in service after investment has been made in its acquisition. These cost elements include the cost of personnel (pay, allowances, subsistence, etc.), the energy or fuel costs, operational costs such as janitorial supplies, medical material, etc., and maintenance costs such as depot and in-the-field maintenance costs (tools, rework, etc.). The operations and support cost also includes costs of replenishment spares and

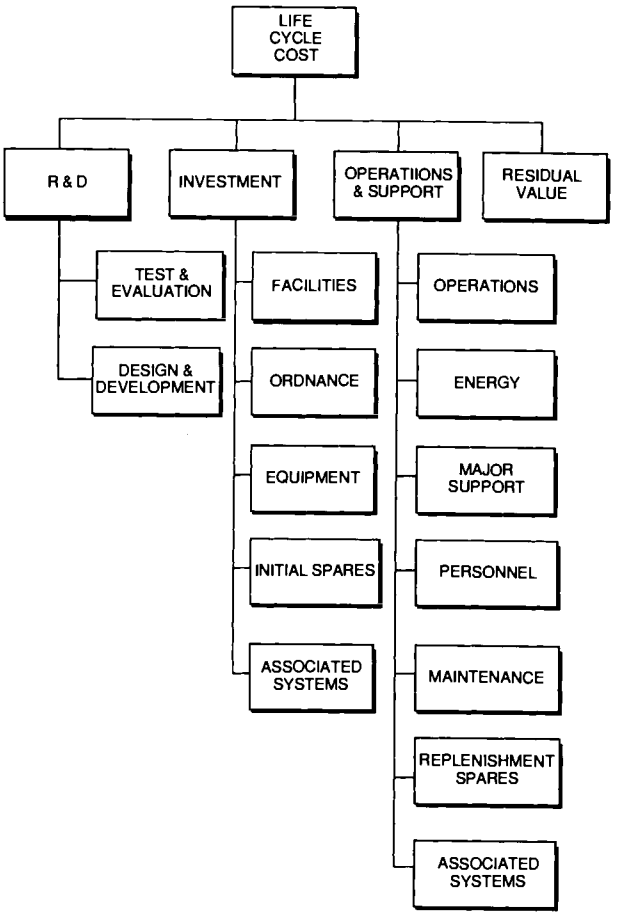

Fig. 5.10 Lifecycle cost tree.

major support costs such as training logistics and indirect personnel costs. Associated systems costs such as fueling trucks or other vehicles would be included in this cost element.

(iv) Residual or scrap value, C_{RES}. This is the value of the hovercraft at the end of its useful life. It can be determined by any one of several accounting methods, such as the single or double declining balance method.

While there is no general rule that can be applied to all craft, it might be useful to know that, for military vehicles with a 15-year life cycle, R&D typically counts for approximately 5 percent of the life cycle cost, investment for approximately 50 percent, operations and support approximately 50 percent, and the residual value for approximately 5 percent. As can be seen from the above, the two main elements of cost are the investment (or acquisition) cost

C_{INV} and the operating cost C_{OPS}. A discussion of these two main cost elements forms the remainder of this section. General equations in simplified form will be given together with examples of available (or releasable) detailed cost data to provide credibility to the equations and general trend information as a guide to where the main *cost drivers* appear.

5.3.2 Investment Costs

The investment (or acquisition) cost C_{INV} of any hovercraft is a function of its size, speed or power installed, quantity built, and several other factors described in this section. Before providing a detailed development of the acquisition cost of a hovercraft, it is informative to provide some statistical costs of existing vehicles and show how they compare with other competitive vehicles in the transportation spectrum. Figure 5.11 shows a compilation of vehicle costs expressed as *cost* versus size (gross weight). The *cost* dollar amount is actually the advertized price (i.e., cost plus profit) of a unit recognizing that it is usually the average unit cost of a small number of units bought (of the order of 2 to 5 units). The vehicle prices have been taken from various sources and apply to craft built in different years. To normalize the data, the dollar amounts have been adjusted to 1987 dollars by use of the inflation index shown in Figure 5.12.

The data shown in Figure 5.11 includes commercial and military air cushion craft (hovercraft and surface effect ships), commercial hydrofoils and, for reference, military displacement ships. The military air cushion craft data was taken from Meeks and Mantle (ref. 5) as part of the U.S. Navy's Advanced Naval Vehicle Concepts Evaluation (ANVCE) Program. A synopsis of the ANVCE program can be found in ref. 6 by Rhea. A more detailed discussion of the design and construction variations that impact the cost of these craft is given in ref. 7. Figure 5.11 reveals a general trend toward increasing cost (and price) as a function of increasing size and speed.

Dix and Riddell (ref. 8) showed that there appears to be a general law normalizing many different types of vehicles, from tanks to aircraft carriers (including hovercraft), that relates cost to vehicle size W_E, installed power P, and number N produced. The normalized cost (in 1974 dollars) was given as:

$$\$_V = 1000\ W_E + 1200\ PN^{-0.33} \tag{5.2}$$

where $\$_V$ is the unit procurement cost. Because of the accuracy level of the data (within a factor of 2 according to the authors) it is academic whether the dollars quoted are for *cost* or *price*. Equation (5.2) can be modified to 1987 dollars:

$$\$_V = 1800\ W_E + 2160\ PN^{-0.33} \tag{5.3}$$

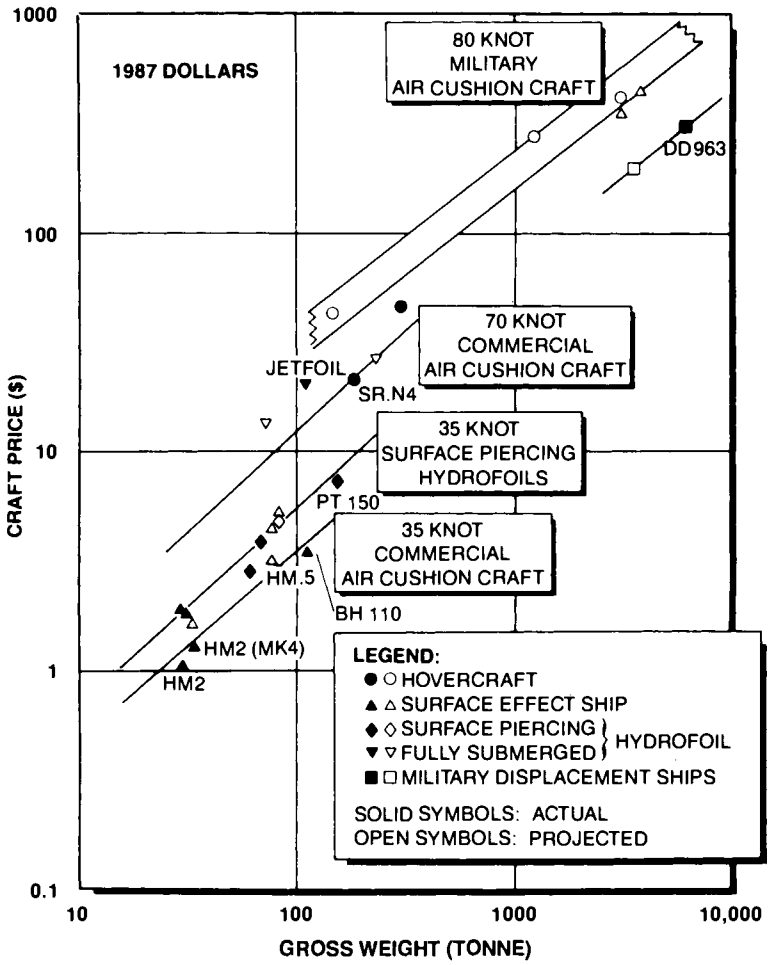

Fig. 5.11 Effect of size and speed on cost.

While it is understood that the accuracy of these two equations is insufficient to use in any particular case, they do provide trend information on the effect of size, power, and quantity built.

By way of example, consider a hypothetical military hovercraft with an empty weight W_E of 90 tonnes and an installed power of 11,180 kW (15,000 HP) similar to the U.S. Navy's LCAC. With this power, the speed will be in excess of 74.08 km/h (40 knots); with P = 7454 kW (10,000 HP) the speed will be approximately 37.04 km/h (20 knots). How does the cost vary with speed (or power installed) and number built? Using equation (5.3), a table such as Table 5.3 can be constructed.

The impact on cost of changing the speed or increasing the number built is

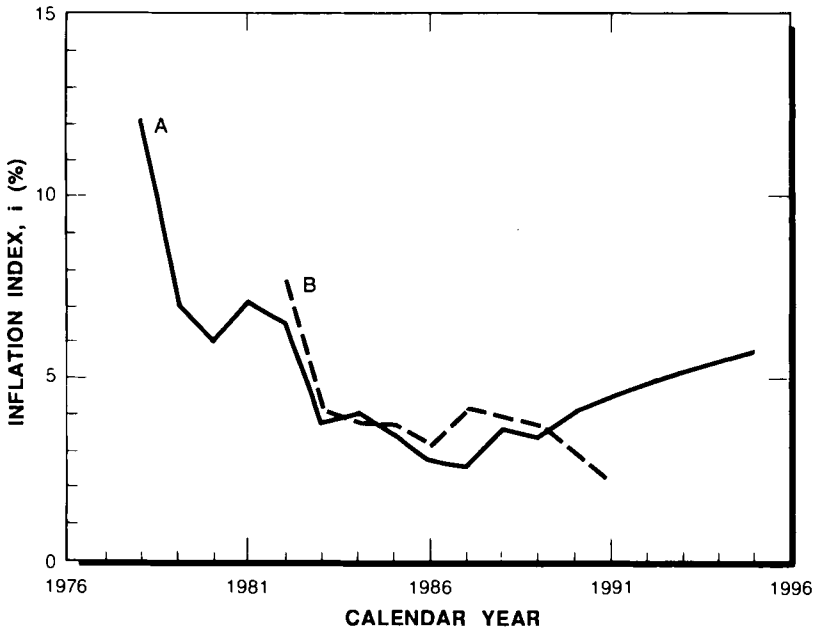

Fig. 5.12 Inflation indices. Curve A, defense procurement (source: U.S. Department of Defense); curve B, U.S. gross national product (source: Data Resources).

Table 5.3. Effect of speed and number built on cost of vehicle.

	Cost (Millions of 1987 U.S. dollars)	
Number of craft	74 km/h craft	37 km/h craft
Lead	32.56	21.76
2	25.76	17.23
3	22.52	15.07
4	20.57	13.77
5	18.95	12.69
6	17.98	12.04
7	17.01	11.39

clear. As has been discovered in many industries, mass production is a most effective way of reducing the cost of any vehicle. While such trend information is of some general interest, it does not provide information of sufficient accuracy or detail to predict the acquisition costs of any particular hovercraft. More detailed methods are required for such an analysis and will not be discussed.

The problem comes in determining a method of costing for rapid, early

design use, that is relatively simple to use with only a few parameters or craft details at the cost estimator's disposal. If the cost method is too general, it will of course provide a cost estimate of little use in guiding the designer. The method just discussed used only W_E, P and N as parameters and, while useful in a broad trend sense, gives insufficient detailed guidance to make design choices. Another alternative would be to do a *bottom-up* cost estimate using the craft parts list for material costs, engineering hours, production hours, inspection hours, etc., to determine the labour costs. This latter detailed cost estimating must be done for any particular design for which a bid is to be made and a narrow profit margin protected. This method could have 100 or more separate parameters. However, it suffers from being an *after-the-fact* cost estimating method of belated use to the designer attempting to make prudent economic decisions at the early stages.

In recent years, three cost estimating methods for the early design stages have been pursued and are still being refined. The first is the ANVCE method developed in 1977 to cover a wide range of air and surface vehicles, including hovercraft. The cost estimating relationships (CER) were basic to this method developed by Moy (ref. 9). They provide estimated costs for each of the major components or subsystems of a vehicle. These CERs required basic knowledge of the weights W_i of the seven subsystems, the power installed P, and about three to four complexity levels of each subsystem. This is not an unreasonable number of parameters for the designer to handle at the early design stage. The costs are then summed and applied in a systematic way to obtain the total cost of a vehicle developed for the ANVCE program, as described by Noah (ref. 10).

The second method, initiated in 1980, took the basic ANVCE CERs and incorporated them into an Advanced Surface Ship Evaluation Tool (ASSET). A description of the ASSET program can be found in refs. 11 and 12.

The third method was originally developed by RCA for costing systems in the electronics, avionics and aerospace fields. This has become known as the RCA PRICE model and the details of this method may be found in ref. 13. Like the ANVCE cost estimating method, the PRICE method also depends on the make-up of the components or subsystems and a set of complexity factors. In 1982, Salmon and Locke (ref. 14) applied the PRICE method to the cost of surface ships and found encouraging agreement with the available data. The parameters needed for PRICE were the subsystem weights, the enclosed volumes and the manufacturing complexities expected within each subsystem. In 1984, Jones, Mayo and Clark (ref. 15) applied the PRICE method to the costing of two hovercraft and found good agreement.

The reader is encouraged to pursue refs. 11-15 in refining the costing of hovercraft. Here, we will restrict ourselves to reviewing the original ANVCE CER method. The basic method is most applicable to military vehicles but, with

minor self-evident adaptations, is also applicable to commercial vehicles. The price of the vehicle is given as:

$$\$_V = \sum_{i=1}^{n=9} (CER)_i + \text{profit} \tag{5.4}$$

where n is the total number of CERs. The profit varies from supplier to supplier but, for estimating purposes, can be taken as 8-15 percent of the builder's cost. The CERs are the basic building blocks to determining the contractor's price. For military vehicles built for the Government, additional cost items must be added to determine *military budget* costs for any given vehicle. These additional items are for the payload or weapons system and for Government costs (such as Government management costs, change orders, and other items). For most military vehicles (including hovercraft) the Government costs typically add an additional 50 percent of the basic vehicle or platform cost. The cost of the payload varies markedly with the mission but typically can add a further 50-100 percent of the basic platform cost. In the following treatment, we will restrict ourselves to the hovercraft without payload.

The general form of the CER (ref. 9) is:

$$(CER)_i = F_i\ (W, P, \ldots, N) \tag{5.5}$$

This equation shows that each CER is expressed as some function of major determinants, such as weight W, installed power P and the number of craft built N. The form of the function varies with the type of system being installed, its complexity, and other known factors.

Specifically, from a wide range of vehicles, Moy (ref. 9) showed that the costs could be expressed as:

$$\$_V = \sum_{i=1}^{n=9} C_i + \text{profit} \tag{5.6}$$

where

$$C_i = K_i\ K_{i,j}\ X_i^{n_i} \tag{5.7}$$

in which C_i is the cost of *ship work breakdown structure*(SWBS) Group i, K_i is a constant associated with Group i, $K_{i,j}$ is a constant which reflects the scaling of the Group i cost according to the unique design features of vehicle j, X_i is an independent variable reflecting the group weight for Groups 1, 3, 4, 5, 6 and 7, the propulsion power for Group 2, and the sum of Groups 1 through 7 for Groups 8 and 9, and n_i is an exponent to which variable X_i is to be raised. The summation is over nine SWBS groups. The first seven of these groups correlate directly with the weight groups treated in Chapter 2. Groups 8 and 9 are solely cost groups pertaining to design, engineering and support costs as will be shown.

It is important to note that the ANVCE CERs provide no means for separating

labour and material costs. A similar situation exists for the ASSET and PRICE methods. This apparent shortcoming will be addressed where possible using available data. Curiously enough, while this methodology does not separate labour and material costs, it does nevertheless, predict fairly accurately the total cost of those vehicles that have been used to check the method. As a cautionary note in predicting the cost of military hovercraft (or any other military vehicle) one must be careful to account for any *government furnished equipment* (GFE) that may be included or excluded in the advertised price.

The price of the craft represented by equation (5.6) applies to the *lead craft* or first of a kind. As *follow craft* are built, a learning curve is usually experienced that reduces the unit cost of the subsequent vehicles. This was shown by the Dix and Riddell formulation (eqns. (5.2) and (5.3)) and the example provided in Table 5.3.

The existence of *learning curves* was first noted by T.P. Wright (ref. 16, in 1936, when the mass production of aircraft and other military hardware first occurred. It was found during the mass production programs that the cost of an article tended to decrease by a constant factor for each doubling of the number built. For example, an *85 percent learning curve* meant that craft number 4 cost 85 percent of craft number 2, and craft number 8 cost 85 percent of craft number 4, and so on.

For purposes of this discussion, if $\$_{VL}$ is the cost of the lead craft (or vehicle) and $\$_{VFF}$ is the cost of the first follow craft, then:

$$\$_{VFF} = \$_{VL} - \text{(initial design and support costs)} \tag{5.8}$$

Depending on how the builder chooses to write-off his initial design and support costs, this can cause a significant drop in costs from the lead craft. Once these costs have been accounted for, the learning curve provides the cumulative costs $\$_{VC}$ of the follow-on craft by the relationship:

$$\$_{VC} = \sum_{J=1}^{N} \$_{VJ} = \$_{VFF} N^{[(\ln 2r)/\ln 2]} \tag{5.9}$$

where $\$_{VJ}$ is the cost of the Jth vehicle, N is the total number of vehicles and r is the learning rate.

It should be noted that, in the normal calculation of learning rates, the *law* is applicable to labour improvements. However, equation (5.9) applies the learning curve to total vehicle costs. There is some justification for this simplication because material costs also tend to decrease with quantity purchased.

At this time, build rates of hovercraft of a common design have been insufficient to determine a typical learning rate. As a frame of reference, ships that typically are built in small batches experience cumulative learning rates r of approximately 97 percent. Aircraft structures which are usually built in

greater numbers can experience a cumulative learning rate of 75 percent. These adjustments to the determination of the cost of any particular hovercraft must be kept in mind when comparing data.

Returning now to the development of the CERs for each of the major subsystems of a *lead* hovercraft, the data will be presented for individual *ship work breakdown structures* (SWBS).

(i) Structural costs. Moy (ref. 9) gives the cost of the SWBS Group 100 (structure) as:

$$C_{100} = 40.85 \times 10^3 K_{i,j} W_1^{0.772} \tag{5.10}$$

where C_{100} is the cost of SWBS Group 100 in 1987 dollars. It should be noted that reference 9 provided different numerical values of K_i throughout, based on a 1977 data base. In the equations that follow and throughout this section, all cost (dollar) figures have been adjusted to 1987 dollars using the inflation indices provided in Figure 5.12.

In equation (5.10), W_1 is the structural weight (tonnes) of SWBS Group 100 and $K_{i,j}$ is a constant, within the 100 cost group, that reflects the type of material used in the construction. The materials considered include conventional steel hull (mild steel), high tensile (HT) strength steel, conventional aluminum and HT strength aluminum such as the 5000 and 6000 series of aluminum. The structural cost curves given by equation (5.10) and reflecting the variations in cost due to choice of material are shown in Figure 5.13. The actual values of the constants $K_{i,j}$ are provided in Table 5.4. The majority of the hovercraft built to date have used HT aluminum in their construction (curve 4 in Figure 5.13). As can be seen from the relative positioning in Figure 5.13, the use of such structures, while advantageous in reducing the craft weight, is disadvantageous in terms of cost. Some sporadic examples of hovercraft construction exist using the cheaper materials (including steel) and construction techniques.

Limited data is available for public release on the costs of particular hovercraft but some releasable data is provided here to lend credibility to the ANVCE CERs. Figure 5.14 shows some data on conventional ship steel hulls compared to the ANVCE CER for steel hulls. This data was also available with both labour and material breakdown. The comparison shows encouraging agreement and further shows where construction is labour intensive and where material costs become a significant factor. For the foreseeable future (with structural weights W_1 of the order of 100 tonnes) for hovercraft (if steel is used) the construction is still very manpower intensive unless new construction techniques can be developed. For aluminum construction, Figure 5.15 shows the CER together with two data points of the SES-100A and SES-100B which used similar construction methods and material to those used in hovercraft.

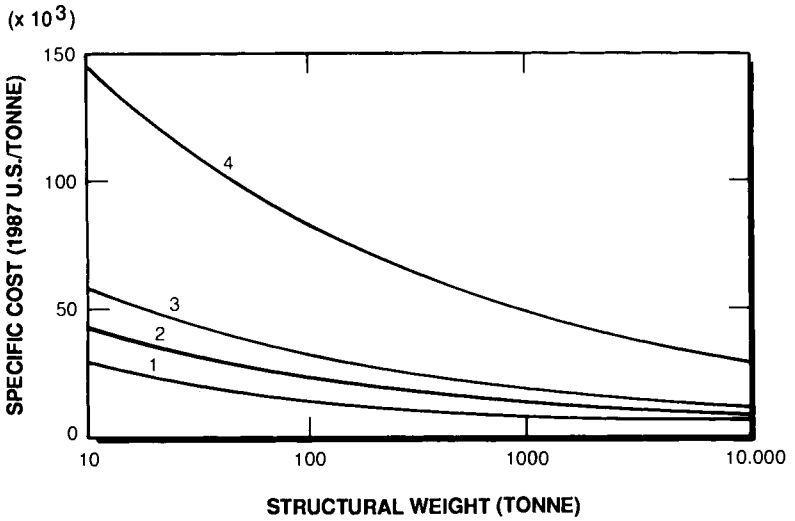

Fig. 5.13 Structural system costs for SWBS Group 100. Curve 1, conventional steel hull; curve 2, HT steel hull; curve 3, conventional aluminum hull; curve 4, HT aluminum hull.

Some early data by British Hovercraft Corporation on hovercraft construction is also shown in Figure 5.16. The data shows the impact of riveted aluminum (3-4 manhours/kg) and all-welded aluminum structure (1-2 manhours/kg) for hovercraft structure. Some data on the welded aluminum structure on hydrofoils (surface piercing and fully submerged) tend to substantiate these labour costs for hovercraft. The LCAC program datum is based on ten craft under construction or delivered. General learning and improvements in production techniques indicate that 1 manhour/kg is achievable with welded aluminum hovercraft structures. Accordingly, it is reasonable to assume that the cost C_{100} (1987 U.S. $/tonne) of aluminum structures for hovercraft, can be expressed, as:

$$C_{100} = 40.85 \times 10^3 \, K_{i,j}/W_1^{0.228} \tag{5.11}$$

where $K_{i,j}$ varies between 2.192 for conventional (low strength) marine aluminum and 5.587 for high strength (HT) marine aluminum. Insufficient generalized data for GRP structure in hovercraft use is available to draw trend information on the cost.

(ii) Propulsion system costs. In 1987 U.S. dollars, the ANVCE CER for SWBS Group 200 (propulsion system) is given as:

$$C_{200} = 2.24 \times 10^3 \, K_{2,j} \, P^{0.808} \tag{5.12}$$

where P is the total installed power (HP) including the lift power in the case of hovercraft. The constant $K_{2,j}$ reflects the impact of various types of

Table 5.4. Cost estimating relationship (CER) summary referring to the parameters of equation (5.7).

SWBS Group	10^{-3} K_i	Design feature		Variable and exponent
		$K_{i,j}$	Description	$X_i^{n_i}$
100: Structure	40.850	1.000	Conventional steel hull	$W_1^{0.772}$
		1.570	HT steel hull	
		2.192	Conventional alum. hull	
		5.587	HT alum. hull	
200: Propulsion	2.240	1.000	CODOG/CODAG power plant, high speed marine propulsors and straight drive train	$p^{0.808}$
		1.502	Gas turbines (GT/CODAG) power plant, high speed marine propulsors and right-angled drive train	
		1.979	Steam-turbine power plant, low speed, controllable pitch (CP) propeller and long shafts	
		2.346	GT power plant, low speed CP propeller and reduction gears	
		3.281	GT power plant with complex drives	
		3.437	Nuclear, steam-pressurized water reactor power plant, low speed fixed-pitch propellers, straight drive train	
300: Electrical	90.310	1.000	Conventional 60 Hz power, steam or diesel generator drive	$W_3^{0.910}$
		2.036	Conventional 60 Hz power, light diesel or GT generator drive	
		3.719	Very light 60 Hz or mixed 60/400 Hz, GT generator drive	
		12.685	All 400 Hz, GT generator drive	
400: Command and surveillance	130.630	1.000	Simple control system, minimal electronics	$W_4^{0.617}$
		3.154	Modest control systems, sophisticated electronics	
		6.907	Complex control systems, sophisticated electronics, weight critical ships	

Table 5.4. (Continued)

SWBS Group	10^{-3} K_i	Design feature $K_{i,j}$	Description	Variable and exponent $X_i^{n_i}$
500: Auxiliary system	114.150	1.000	Steam-propelled displacement ship	$W_5^{0.782}$
		1.528	GT propelled displacement ship	
		4.161	Fully submerged hydrofoils	
		5.370	Air cushion craft	
600: Outfit & furnishings	118.620	1.000	Conventional displacement ship	$W_6^{0.784}$
		1.857	Weight critical ship	
700: Armament	10.080	1.000	Conventional displacement ship	$W_7^{0.987}$
		3.401	Weight critical ship, light armament	
800: Design & engineering	0.019	1.000	Follow ship before 1970	(Sum of Grp 1-7)$^{1.099}$
		2.882	Follow ship 1970 and after	
		12.888	Lead ship, unsophisticated weapons	
		26.064	Lead ship, sophisticated weapons	
900: Construction services	0.385	1.000	Simple tooling, limited trials	(Sum of Grp 1-7)$^{0.839}$
		4.235	Complex tooling, extensive trials	

powerplants, power trains and propulsors.

Figure (5.17) displays the relationships for a range of vehicle types. Two curves are of particular interest for the hovercraft designer. Curve 2 was compiled from data on existing hydrofoils that employ combinations of diesel engines, gas turbine engines and right angle transmissions. While the data is taken from hydrofoil craft, it is directly applicable to hovercraft. Curve 5 applies to gas turbines and complex drive trains (e.g. right-angle drives with power take-offs for lift and propulsion systems). Data from both actual and projected hovercraft and SES form the basis for this relationship.

Accordingly, the cost of hovercraft propulsion systems can be written

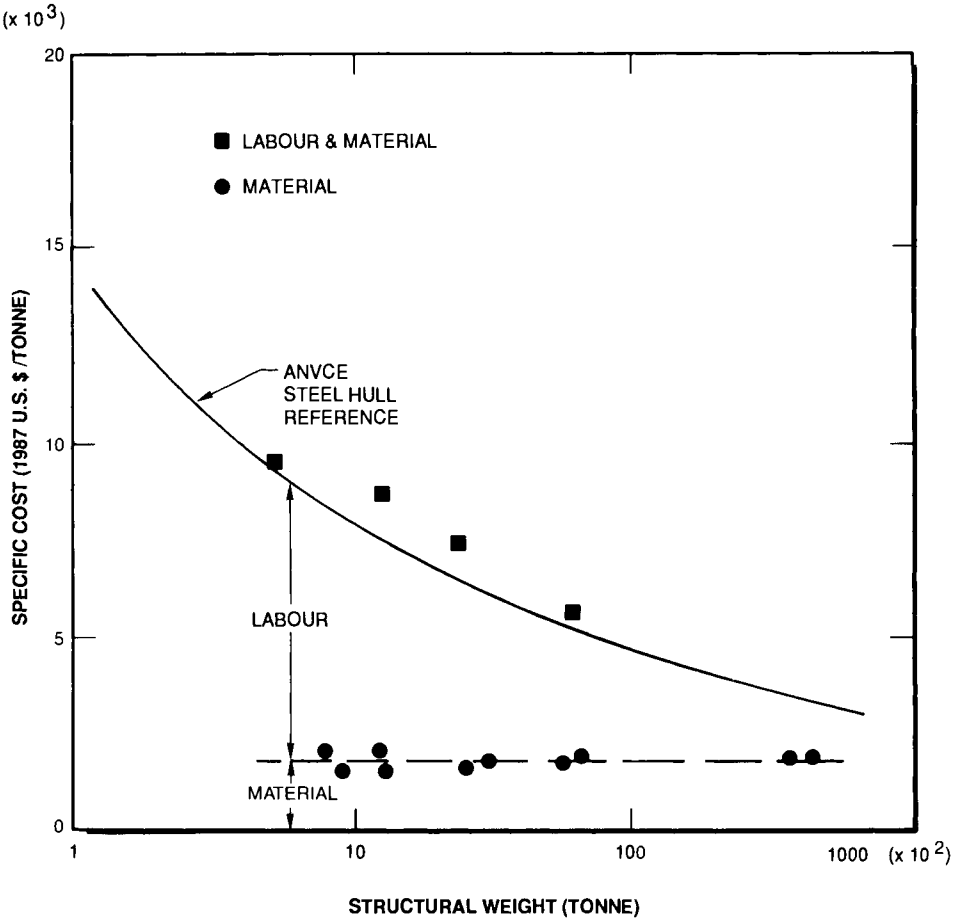

Fig. 5.14 Cost of conventional steel hulls for SWBS Group 100.

alternately as:

$$C_{200} = 2.24 \times 10^3 \, K_{2,j} \, P^{0.808}/W_2, \text{ 1987 U.S. \$/tonne} \tag{5.13}$$

where W_2 is the total weight (tonnes) and P is the total installed power (HP), or

$$C_{200} = 1.767 \times 10^3 \, K_{2,j}/P^{0.192}, \text{ 1987 U.S. \$/kW} \tag{5.14}$$

where P is the total installed power (kW), or

$$C_{200} = 2.24 \times 10^3 \, K_{2,j}/P^{0.192}, \text{ 1987 U.S. \$/HP} \tag{5.15}$$

where P is the total installed power (HP). Parameter $K_{2,j}$ varies between 1.502 and 3.281 depending on the type of propulsion system.

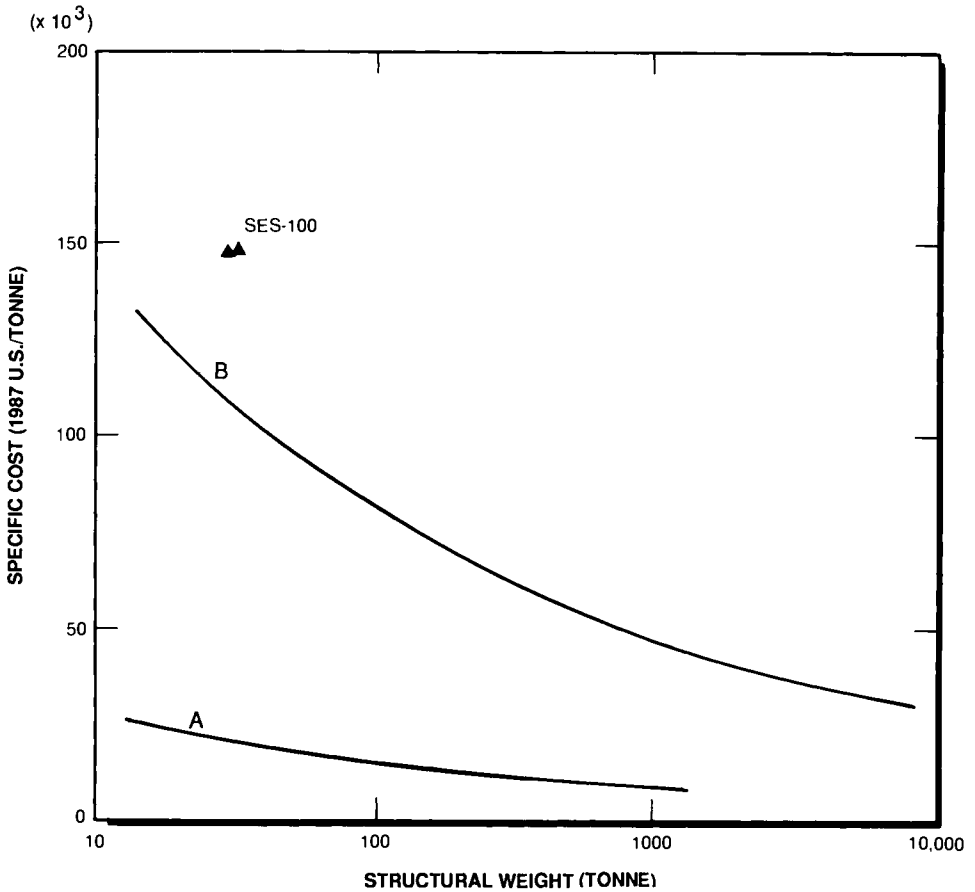

Fig. 5.15 Cost comparison of ANVCE conventional steel (curve A) and HT aluminum (curve B) hull references for SWBS Group 100.

(iii) Electrical system costs. In 1987 U.S. dollars, the ANVCE CER for SWBS Group 300 (electrical system) is given as:

$$C_{300} = 90.31 \times 10^3 \, K_{3,j} \, W_3^{0.910} \tag{5.16}$$

where W_3 is the weight of the electrical system. The constant $K_{3,j}$ reflects the type of electrical system (60 Hz, 400 Hz) and power generation such as diesel generator or gas turbine generator. Figure (5.18) shows the effect, on the specific cost ($/tonne), of these variations in choice of electrical system. All variations have been used in hovercraft. It is of interest to note the strong effect of using the light weight 400 Hz system on cost. The numerical values of $K_{3,j}$ are provided in Table 5.4. The specific cost of the electrical system is given by:

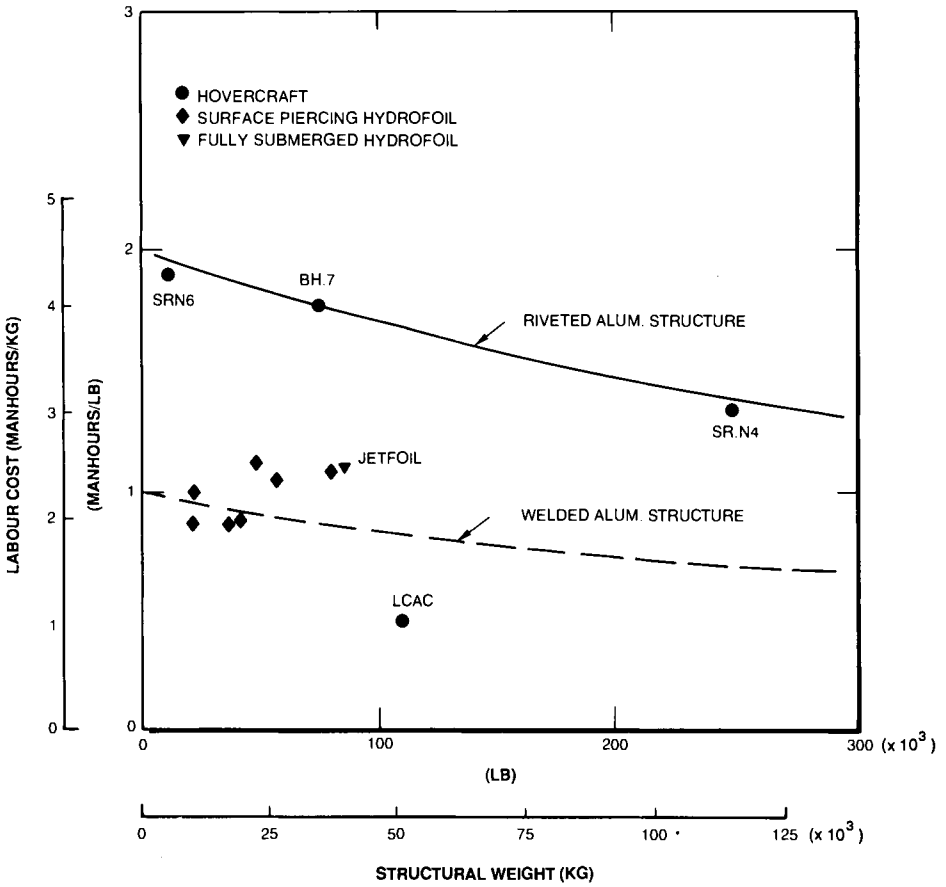

Fig. 5.16 Early data by British Hovercraft Corporation on labour costs.

$$C_{300} = 90.31 \times 10^3 \, K_{3,j}/W_3^{0.09} \tag{5.17}$$

(iv) Command and surveillance system costs. In 1987 U.S. dollars, the cost of SWBS Group 400 (command and surveillance system) is given as:

$$C_{400} = 130.63 \times 10^3 \, K_{4,j} \, W_4^{0.617} \tag{5.18}$$

where W_4 is the weight of the command and surveillance system in tonnes. The constant $K_{4,j}$ reflects the variation in command and surveillance system from simple control systems with minimal electronics, characteristic of small planing craft, to complex control systems with weight-critical components characteristic of many of the U.S. military hydrofoil and hovercraft designs. Figure 5.19 shows this variation. The constant $K_{4,j}$, summarized in Table 5.4, varies from 1.0 to 6.906. All variations have been used on hovercraft. In terms of specific cost (1987 U.S. $/tonne) the CER can be written:

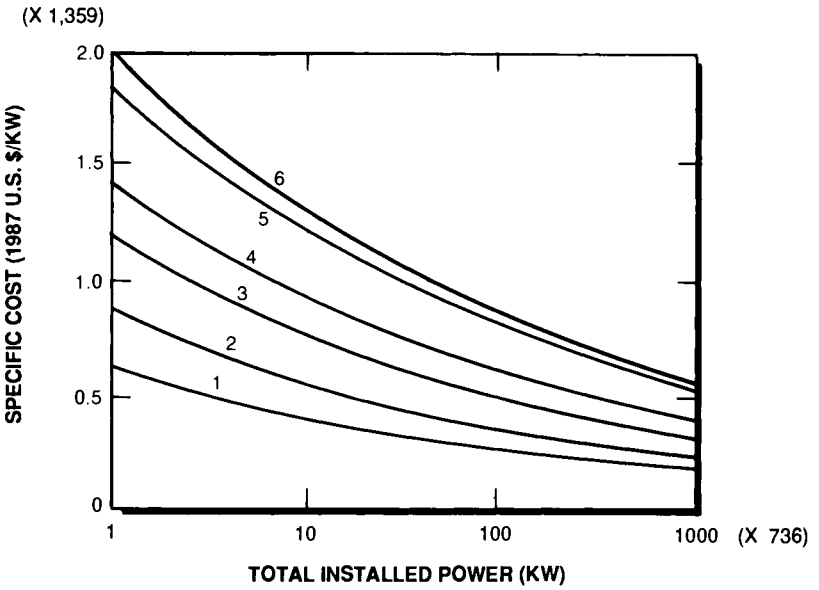

Fig. 5.17 Propulsion system costs for SWBS Group 200. Curve 1, CODOG/CODAG power plant, high-speed marine propulsors and straight drive train; curve 2, GT/CODAG power plant, high-speed marine propulsor and right-angled drive train; curve 3, steam turbine power plant, low-speed CP propeller and long shafts; curve 4, GT power plant, low-speed CP propeller and reduction gears with special arrangements as in swath; curve 5, GT power plant with complex drives; curve 6, nuclear steam pressurized water reactor power plant, low-speed FP propellers and straight drive train.

$$C_{400} = 130.63 \times 10^3 \, K_{4,j} \, W_4^{0.383} \tag{5.19}$$

(v) Auxiliary system costs. The auxiliary system in any hovercraft, as in other vehicles, is usually one of the high cost systems. In the case of hovercraft it is particularly difficult to isolate the costs because it includes the lift system (powerplant, life fans, ducting, and skirt systems) as well as the usual auxiliary systems of hydraulics, etc. In the case of those hovercraft that have integrated lift and propulsion systems, isolating the costs that are identifiable with the auxiliary system is particularly difficult. Despite these complications it has been possible to provide reasonable cost estimates for SWBS Group 500 (auxiliary systems). In 1987 U.S. dollars, the CER is given as:

$$C_{500} = 114.15 \times 10^3 \, K_{5,j} \, W_5^{0.782} \tag{5.20}$$

where W_5 is the weight of the auxiliary system (including the lift system). The constant $K_{5,j}$ varies according to the type of craft (displacement ship,

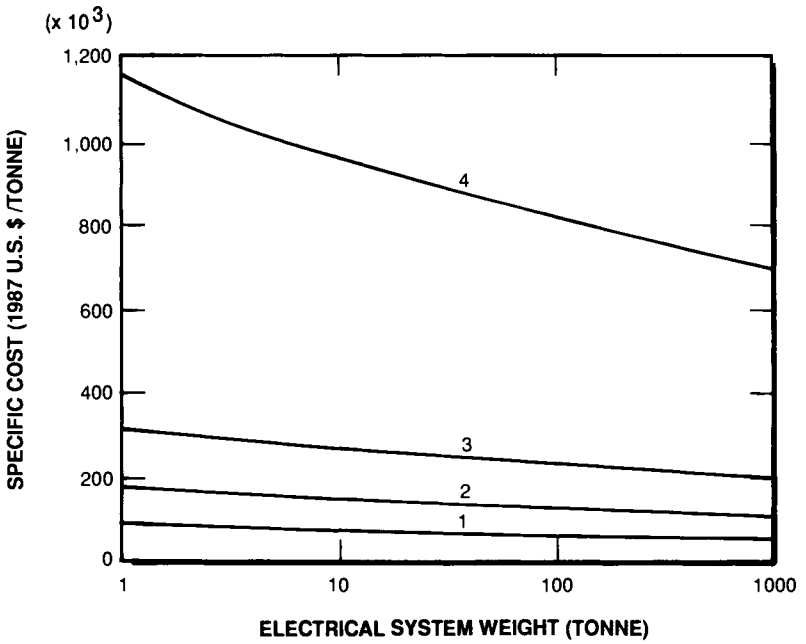

Fig. 5.18 Electrical system costs for SWBS Group 300, Curve 1, conventional 60 Hz power, steam or diesel generator drive; curve 2, conventional 60 Hz power, light diesel or GT generator drive; curve 3, very light 60 Hz or mixed 60/400 Hz GT generator drive; curve 4, all 400 Hz GT generator drive.

hydrofoil or air cushion craft). This variation is shown in Figure 5.20.

The top two curves (curve 3 for hydrofoils and curve 4 for air cushion craft) are the most directly applicable to hovercraft. The impact on cost of such additional components as lift fans and skirts can be visualized by comparing these curves. The values of constants $K_{5,j}$ are given in Table 5.4. For hovercraft use, the specific cost (1987 U.S. $/tonne) of the auxiliary system can be written:

$$C_{500} = 114.15 \times 10^3 \, K_{5,j} W_5^{0.218} \tag{5.21}$$

where the constant $K_{5,j}$ will typically vary between 4.161 and 5.370 depending on the complexity or sophistication of the lift system.

(vi) Outfitting and furnishing costs. In 1987 U.S. dollars, the ANVCE CER for SWBS Group 600 (outfit and furnishing) is:

$$C_{600} = 118.62 \times 10^3 \, K_{6,j} \, W_6^{0.784} \tag{5.22}$$

where W_6 is the weight of the outfit and furnishings system. The constant $K_{6,j}$ depends on the simplicity or the sophistication of lift weight systems. Figure 5.21 shows the variation. For conventional small ships and craft, $K_{6,j}$ = 1 and

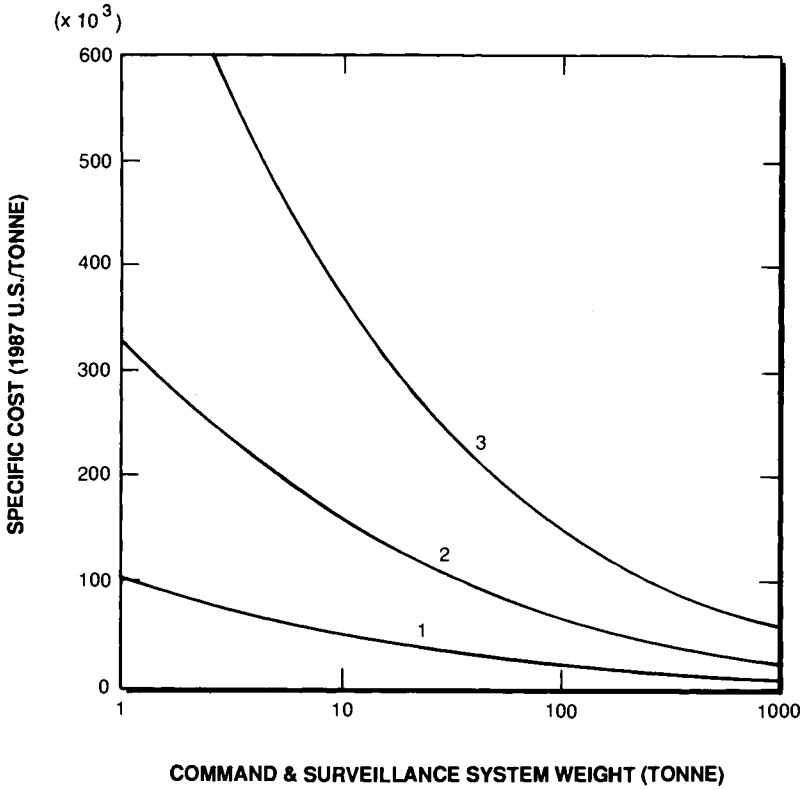

Fig. 5.19 Command and surveillance system costs for SWBS Group 400. Curve 1, simple control systems and minimal electronics; curve 2, modest control systems and sophisticated electronics; curve 3, complex control systems, sophisticated electronics and weight-critical ships.

for weight critical craft such as hovercraft, $K_{6,j} = 1.857$. Accordingly, the specific cost (1987 U.S. $/tonne) is given as:

$$C_{600} = 118.62 \times 10^3 \, K_{6,j}/W_6^{0.216} \tag{5.23}$$

The values and descriptions of parameter $K_{6,j}$ are provided in Table 5.4.

(vii) Armament costs. The cost of armament is one of the more difficult elements to determine because it depends on the mission for which the craft is designed. It should be noted that SWBS Group 700 (armament) includes only those items that are integrated with or attached to the craft; the payload or weapon systems are excluded. For example, the box launcher that is bolted to the deck is part of Group 700; the missile that goes into the launcher is part of the payload and is thus not included in SWBS Group 700.

Because of these complications, it is difficult to provide general rules for the cost of this system. However, the data base of conventional displacement ships and a few military hovercraft did support the following CER:

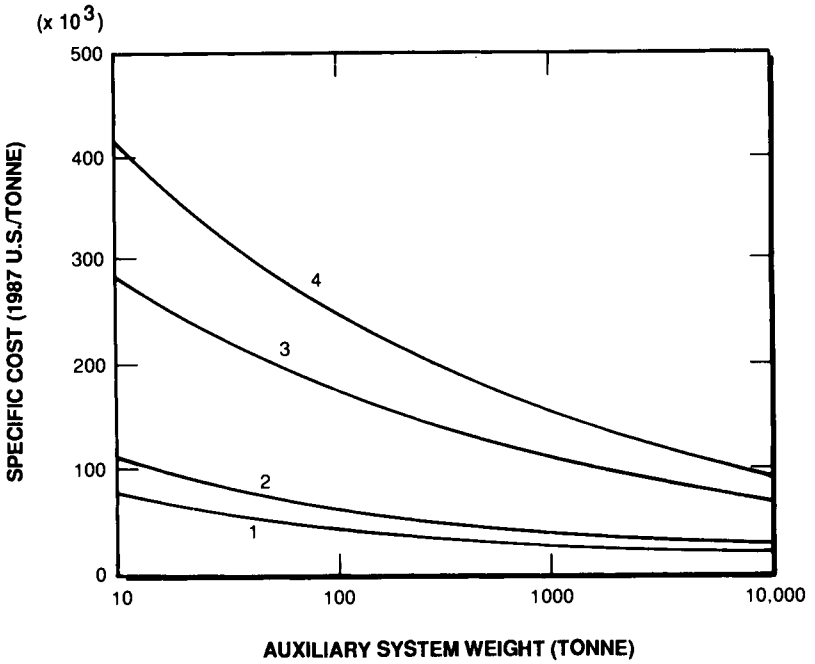

Fig. 5.20 Auxiliary system costs for SWBS Group 500. Curve 1, steam propelled displacement ship; curve 2, GT propelled displacement ship; curve 3, fully submerged hydrofoils; curve 4, air cushion craft.

$$C_{700} = 10.08 \times 10^3 \, K_{7,j} \, W_7^{0.987} \tag{5.24}$$

where C_{700} is the armament cost in 1987 U.S. dollars and W_7 is the weight of the armament group. Figure 5.22 displays this relationship, which can be expressed in terms of specific cost (1987 U.S. $/tonne) as:

$$C_{700} = 10.08 \times 10^3 \, K_{7,j}/W_7^{0.013} \tag{5.25}$$

where $K_{7,j}$ = 1 for conventional displacement craft such as patrol boats, *low mix* surface combatants and mine warfare craft, and $K_{7,j}$ = 3.401 for weight critical craft such as hydrofoils and air cushion craft.

(viii) Design and engineering costs. The cost estimating relationship (CER) for Group 800 (design and engineering) takes on a different form compared with subsystems Groups 1-7 that make up the craft. It is usually assumed that the design and engineering costs are best taken as a percentage of hardware or empty weight W_E costs for estimating purposes. The actual amount for any particular craft is strongly dependent on the uniqueness of the design and whether similar designs are available, thereby reducing the amount of design and engineering effort that needs to be accomplished.

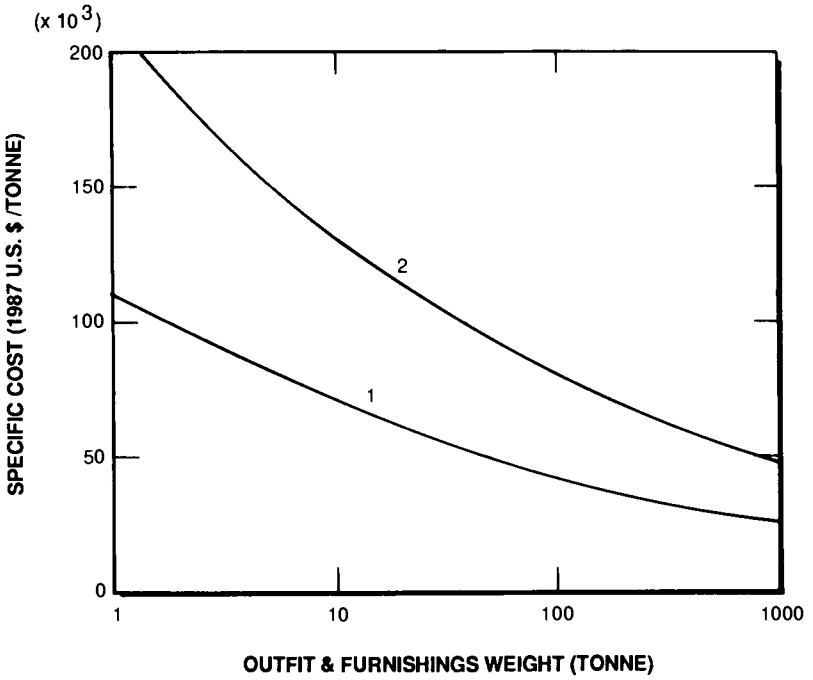

Fig. 5.21 Outfitting and furnishing costs for SWBS Group 600. Curve 1, conventional displacement ship; curve 2, weight critical ship.

From a large data base of various types of ships, small craft, hydrofoils and air cushion craft, Moy (ref. 9) showed that the cost of the SWBS Group 800 (design and engineering) could be expressed in 1987 U.S. dollars by the CER:

$$C_{800} = 0.019\ K_{8,j}\ \left[\sum_{i=1}^{7} C_i\right]^{1.099} \tag{5.26}$$

where C_i are the design and engineering costs of the individual systems and $K_{8,j}$ varies between 12.888 and 26.064, depending on the sophistication of the weapon systems (Table 5.4), for the lead craft. For follow-on craft, where most of the design and engineering effort has been accomplished, $K_{8,j}$ varies between 1.000 and 2.882 depending on the timeframe of the data base. Figure 5.23 shows these costs. It can be seen from this figure and equation (5.26) that the design and engineering costs of the lead craft can be significant (from between 30 percent to 100 percent of the initial hardware costs). For follow craft, the design and engineering costs drop rapidly to approximately 10 percent of the hardware costs.

(ix) Construction services costs. The cost of any hovercraft must also

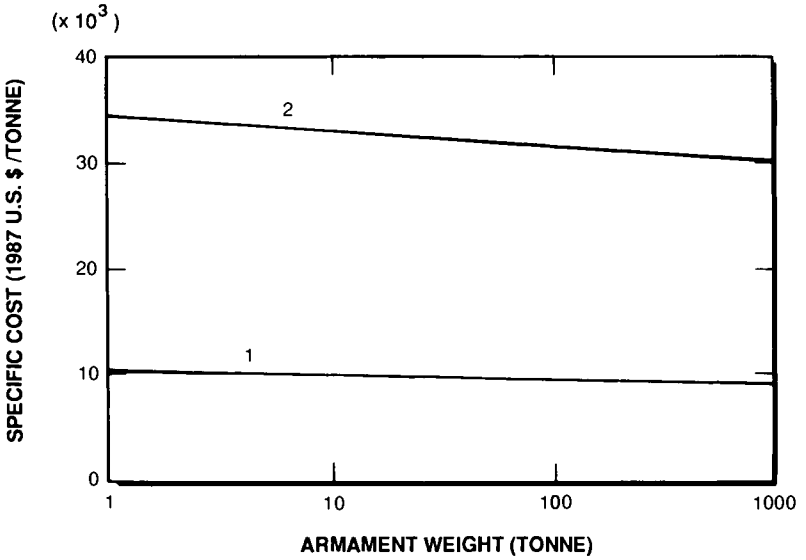

Fig. 5.22 Armament costs for SWBS Group 700. Curve 1, Conventional displacement ship; curve 2, weight critical ship and light armament.

include the costs of jigs, fixtures and other construction services. Also, items such as insurance and the cost of any builders trials prior to delivery of the craft to the customer are included in SWBS Group 900 (construction services). Similarly to the Group 800 costs, C_{900}(1987 U.S. dollars) is expressed as a function of the empty weight cost and takes the form:

$$C_{900} = 0.385\ K_{9,j} \left[\sum_{i=1}^{7} \right]^{0.839} \tag{5.27}$$

where C_i are the construction services costs of the individual system and $K_{9,j}$ varies between 1.000 for those craft that are built with simple tooling and are given modest or limited trials, and 4.255 for those craft that require complex tooling and more extensive trials. Figure 5.24 shows the likely costs based on a wide data base. As can be seen, these costs vary between 5 and 15 percent of the hardware or empty weight W_E costs.

5.3.3 Acquisition Cost of a Hypothetical Hovercraft

To place the above cost estimating relationships (CER) into perspective it is informative to cost an example hovercraft. For illustration purposes, consider the hovercraft discussed earlier with respect to the Dix and Riddell (ref. 8) formulation of cost. This hypothecial hovercraft has an empty weight W_E of 90 tonnes and an installed (GT engines) power of 11,180 kW (15,000 HP)

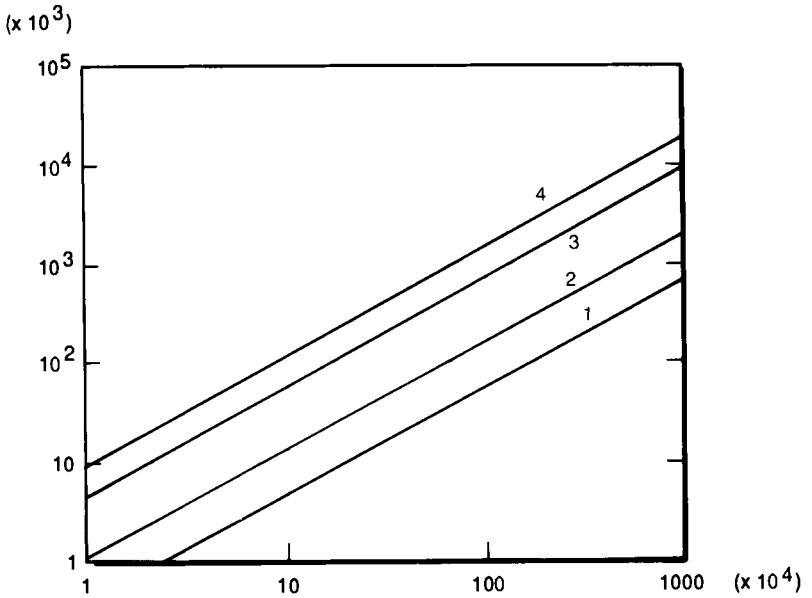

COMBINED COSTS: GROUP 100 THRU 700 (1987 U.S.$)

Fig. 5.23 Design and engineering costs for SWBS Group 800. Curve 1, follow ship, before 1970; curve 2, follow ship, 1970 and after; curve 3, lead ship and unsophisticated weapons; curve 4, lead ship and sophisticated weapons.

and a fairly straightforward drive train. It is constructed of all-welded, high-strength (HT) aluminum structure. Its design speed is in excess of 74.08 km/h (40 knots) with the associated control systems and auxiliary systems. It is for a military amphibious operation with only modest self-defense armament on-board, to be built in small numbers with simple (soft) tooling. What would the cost of the lead craft be and, assuming 94 and 90 percent learning curves, what would the follow craft cost for a production run of seven craft? There is no GFE supplied.

Using the weight algorithms of Chapter 2 and the cost estimating relationships (CER) presented here, one can prepare the pertinent costs as shown in Table 5.5 for the lead hovercraft ($\$_{VL}$) and the first follow craft ($\$_{VFF}$). Several points can be made from this table. The structure, while contributing to approximately 50 percent of the empty weight W_E, contributes only 10 percent to the craft cost. The propulsion system on the other hand is a major driver in both the weight (approximately 24 percent) and cost (approximately 30 percent). The auxiliary system is also a significant system in terms of both weight and cost (8 to 9 percent). As mentioned earlier, the design and engine-

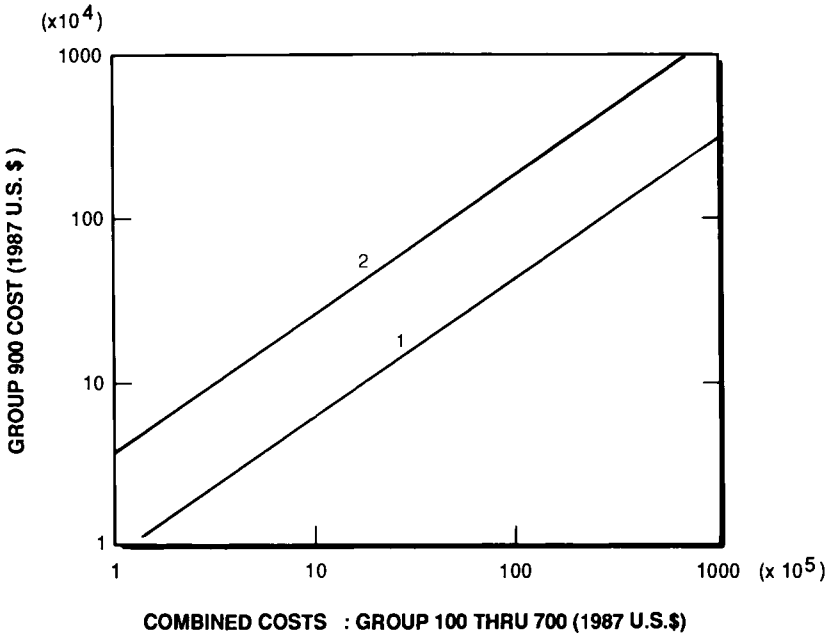

Fig. 5.24 Construction services costs for SWBS Group 900. Curve 1, simple tooling and limited trials; curve 2, complex tooling and extensive trials.

Table 5.5. Hovercraft cost example.

	Weight		Lead craft		First follow craft	
Group	(tonne)	% w_E	$c_i(\$_M)$	% $\$_{VL}$	$c_i(\$_M)$	% $\$_{VFF}$
100: Structure	46.3	51.4	4.4	10.8		
200: Propulsion	21.8	24.2	12.4	30.5		
300: Electrical	3.7	4.2	1.1	2.7		
400: C&S	2.4	2.7	1.5	3.7		
500: Auxiliary	8.2	9.1	3.2	7.9		
600: O&F	7.5	8.3	1.1	2.7		
700: Armament	0.1	0.1	--	--		
Subtotal	90.0	100%	$23.7M	58.3%	$22.3M	69.5%
800: Design & eng.			7.9	19.4	1.7	5.2
900: Const. services			5.4	13.3	5.2	16.2
Total cost			37.0	91.0	29.2	90.9
Profit (10%)			3.7	9.0	2.9	9.1
Total price			$40.7M	100%	$32.1M	100%

ering costs form a significant part of the lead hovercraft cost (approximately 19 percent) but only a minor part of follow-on craft costs (approximately 5

percent or less).

By using the learning rate relationship developed earlier, the costs of follow craft ($\$_{VN}$) to this hypothetical hovercraft example can be determined, as shown in Table 5.6. The costs are shown in millions of dollars. Figure 5.25 shows the costs of these follow-on ($\$_{VN}$) craft expressed as a ratio of the

Table 5.6. Example of hovercraft costs as functions of quantity and two learning rates.

Craft Number	Follow-on craft cost $\$_{VN}$ ($\$_M$) r = 94%	r = 90%
Lead	40.70	40.70
2	31.10	32.10
3	28.25	25.68
4	26.96	23.75
5	26.00	22.80
6	25.60	21.80
7	24.93	21.50

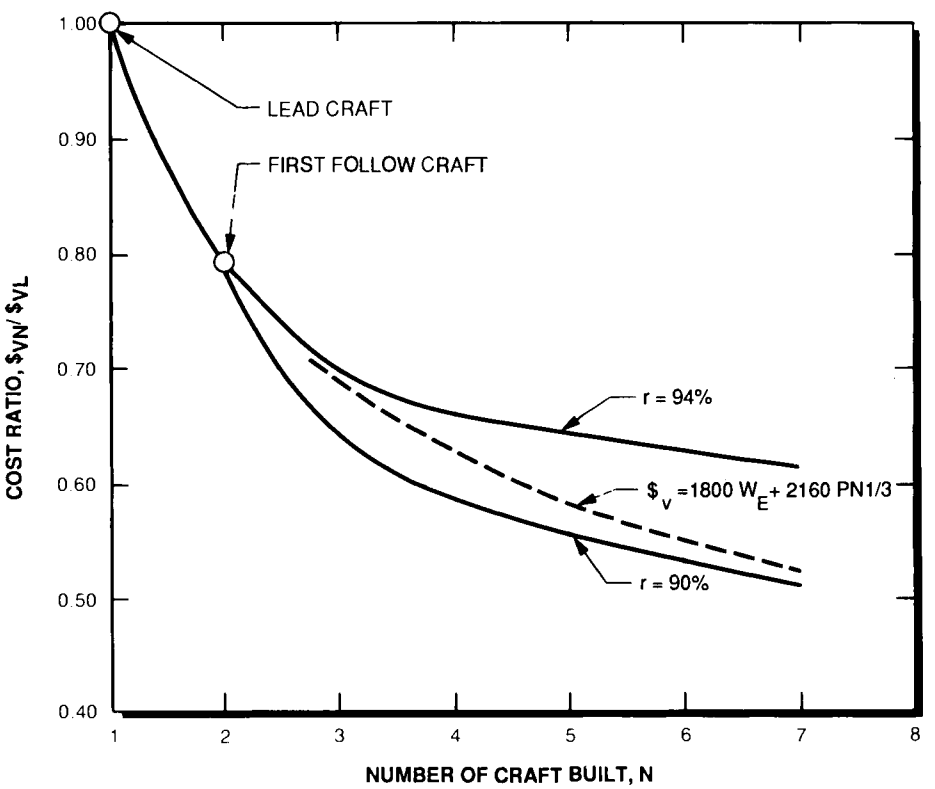

Fig. 5.25 Learning curves for hovercraft cost example (W_E = 90 tonnes, P = 11,180 kW (15,000 HP).

lead hovercraft cost ($\$_{VL}$). The Dix and Riddell formulation is also shown in this figure so as to compare the two different cost methods; i.e., the Dix and Riddell generalized method and the ANVCE CER detailed cost estimating method (ref. 9).

It should be noted that none of the methods presented here can substitute for the detailed cost accounting methods that must be employed in the costing of any particular design that a builder is planning. What these CER methods provide, however, are the identification of where the main cost drivers are and what tools are available to the designer to seek low cost alternatives to any particular design of the hovercraft.

5.3.4 Operating Costs

Various methods have been used to calculate the operating costs of hovercraft. Some of these methods are proprietary to the builders of the craft but the methods can usually be expressed in common terms for more general use. It has been found that, if one follows the basic methods outlined by the Air Transport Association (ATA) for commercial gas turbine powered aircraft (ref. 17), a fairly simple equation results that is directly applicable to hovercraft. It can be shown from an evaluation of the detailed ATA formulation for operating costs that they can be grouped as the sum of three terms in what can be called the economic equation for operating cost:

$$DOC = C_1 + C_2 W_F/R + C_3/V_b \tag{5.28}$$

where DOC is the direct operating cost in dollars per km (or mile), C_1 is the fixed crew cost and the public liability and property damage insurance costs in dollars per km (or mile), C_2 is the fuel and oil cost in dollars per liter (or gallon), C_3 is a variable cost factor in dollars per hour, W_F is the fuel consumed in liters (or gallons), R is the route length in km (or miles) and V_b is the block speed (including terminal time and maneuver time) in km/h (or mph). The variable cost factor C_3 is further decomposed:

$$C_3 = K_C + K_m + K_a/U \tag{5.29}$$

where K_c is the operating crew cost in dollars per block hour, K_m is the maintenance cost (including burden) in dollars per block hour, K_a is the amortization and craft insurance cost in dollars per annum, and U is the annual utilization in block hours per annum.

Normally, the second and third terms in equation (5.28) are by far the largest contributors to the direct operating costs. The total operating costs (TOC) are the sum of the direct operating costs (DOC) given above and the indirect operating costs (IOC) that account for such items as facilities, indirect personnel and general and administrative (G&A) costs. Hence, one can express these as:

$$TOC = DOC + IOC \tag{5.30}$$

or, as is more commonly treated,

$$TOC = DOC\ (1 + K_i) \tag{5.31}$$

where K_i is the indirect to direct cost ratio, or burden rate.

If w_p is the maximum allowable payload (say, in tonnes) then the TOC per available revenue earning capacity (in dollars/(tonne-mile)) is given by:

$$TOC/W_p = [(1 + K_i)/W_p]\ (C_1 + C_2\ W_F/R + C_3/V_b) \tag{5.32}$$

A variation on this equation can be used for passenger carrying hovercraft where payload (in tonnes) is replaced by seats, such that the economic measure becomes *dollars per seat km (or mile)*. Key design parameters that appear in this economic equation are the range R, fuel load W_F and block speed V_b of the craft. This relationship between the economic factors and the design parameters of the hovercraft provides an important guide on how to design the craft for the most advantageous return on investment.

Further insight into the impact of design parameters or hovercraft characteristics and the cost of operation of the hovercraft can be obtained by expanding on the range. It can be shown (ref. 7) that the range R (in nautical miles) of a hovercraft is given by the equation:

$$R = 325\ (\eta_p/sfc)\ (L/D)_{EFF} \ln\ (W_1/W_2) \tag{5.33}$$

where η_p is the propulsive system efficiency, sfc is the net specific fuel consumption of the lift and propulsion system (lb/HP-h), W_1/W_2 is the hovercraft weight ratio at beginning/end of the cruise, and $(L/D)_{EFF}$ is the effective lift-drag ratio.

The effective lift-drag ratio is a direct function of the performance parameters of the hovercraft:

$$(L/D)_{EFF} = W[D + (\eta_p/\eta_L)\ (p_c Q/V)]^{-1} \tag{5.34}$$

which is the familiar aerodynamic lift-drag ratio W/D (or hydrodynamic lift-drag ratio in the case of ships) modified by the hovercraft cushion effect $(\eta_p/\eta_L)(P_c Q/V)$, which has the dimensions of drag. In this equation, W is hovercraft weight, D is drag at cruise speed, η_L and η_p are lift and propulsion system efficiencies, p_c is cushion pressure, Q is cushion air flow, and V is cruise speed.

If P is the total power $(P_L + P_p)$, used to lift and propel the craft, then it can be shown (ref. 7) that:

$$\eta_p (L/D)_{EFF} = WV/P \tag{5.35}$$

where WV/P the *transport efficiency* of the hovercraft; i.e., the ratio of the the work done by the craft in moving its weight W at a speed V to the total

power P required to do the work. Because the weight, power, and fuel consumption vary along the route (as fuel is consumed) the actual calculation of the range is usually done best in a series of computational steps by standard methods of numerical integration.

The above equations provide the basic elements for calculating the operating costs of a hovercraft. It is useful to make some assumptions in order to simplify the equations and to provide insight into the relative importance of each of the terms in the cost equation. The relationships can be more easily assimilated if it is assumed that the weight of fuel is a small fraction of the total hovercraft weight. For a fuel fraction of 0.10, this approximation underestimates the range by 5 percent; for a 0.30 fuel fraction, it underestimates by 15 percent. By making this approximation, the logarithmic term in the range equation simplifies to a simple fraction and the range R in nautical miles can be approximated by:

$$R = 325\ (sfc)^{-1}\ (WV/P)\ (W_F/W) \tag{5.36}$$

With this expression for range, the total operating cost (in dollars/tonne-mile) of the hovercraft is given by:

$$TOC/W_p = (1 + K_i)\{(C_1/W_p) + C_2[325\ (sfc)^{-1}(WV/P)(W_p/W)]^{-1} + C_3/(W_pV_b)\} \tag{5.37}$$

where the term in square brackets is recognized as being proportional to the *payload ton miles per pound of fuel*. From calculations, it can be shown that the terms involving C_2 and C_3 in equation (5.37) are the dominant terms in controlling the operating costs and, therefore, are key factors in the design process of producing a well-balanced and economical hovercraft. For this reason, craft comparisons are sometimes based on the product $(WV/P)(W_p/W)$, which must be maximized in order to minimize the operating cost. This product can be considered as a product of the *performance efficiency* through WV/P and, for want of a better term, *design efficiency* through W_p/W. This latter efficiency tests the ability of the designer to design efficient structures and light weight craft subsystems to maximize space and weight for payload capability. The design challenge is to do this without increasing the craft and subsystem costs or reducing its reliability as characterized by the constants C_1, C_2, and C_3.

To place these various relationships into perspective, the operating costs of the British Hovercraft Corporation's (BHC) passenger carrying hovercraft AP.1-88 are provided. The data has been taken from ref. 8, which BHC provides to potential operators of the craft to guide their determination of fare structure. The data, as presented here, has been simplified and averaged for the purpose of indicating general trends without probing the detailed and proprietary cost data. Also, actual operating costs depend on the details of route length, operating speeds, turnaround times, number of personnel used, wages

paid, fuel costs, and many other variable factors. It is believed, however, that what follows is fairly representative of the costs over *typical routes*. More detailed discussion is given in Section 5.4 and reference 19.

The pertinent economic parameters are that the AP.1-88 is diesel powered with a total installed continuous power of 1277 kW (1712 HP). The all-up weight (AUW) is 38,500 kg (85,000 lb) with 101 passenger seats. The normal crew complement is 3 per craft plus a maintenance crew. With a block speed V_b of 55.56 km/h (30 knots) and a stage length of 18.52 km (10 nautical miles), the fuel consumption is approximately 317.94 litres/h (84 gallons/h). The annual utilization U is taken to be 2000 hours. With these *typical* values and the data from refs. 18 and 19, Table 5.7 can be constructed.

Table 5.7. AP.1-88 operating cost factors (typical).

Item	Cost
Fuel and oil (C_2)	\$94/h
Maintenance cost (K_m) Engines (\$10/h) Propeller (\$5/h) Skirt (\$32/h) Spares (\$17/h)	\$64/h
Operating cost	
Crew (K_c)	\$1.28/km (\$2.06/mile)
Maintenance (K_m)	\$0.50/km (\$0.81/mile)
Block speed (V_b)	55.56 km/h (30 knots)
Stage length (R)	18.52 km (10 n.m.)
Annual utilization (U)	2000 h

The operating cost shown is based on the assumption of two craft operating per year with a shared crew cost of 7 captains/radar operators and 4 lead men at typical salaries and benefits. The maintenance costs K_m include material and labour contributions.

For purposes of this illustration, the contribution to the *direct operating cost* (DOC) of the public liability and property damage insurance costs C_1 is negligible, such that the DOC can be written:

$$DOC = C_2(W_F/R) + (K_c + K_m + K_a/U)/V_b \tag{5.38}$$

Substituting the values of Table 5.7 into equation (5.38) and neglecting the K_a term that pertains to the costs incurred by amortizing the acquisition or investment cost of the craft over some period of time, a direct operating cost (DOC) of 4.37 \$/km is obtained. Reference 8 shows that the indirect costs (management, utilities, terminal costs, etc.) amount to 55 percent of the direct costs. Therefore, in this case, the *total operating costs* (TOC) are

6.77 $/km. For a 18.52 km route, this gives a total operating cost of $125.44 per trip. Thus, with 101 passenger seats and assuming a 100 percent load factor (all seats filled) the break-even fare is $1.24 per passenger. The actual break-even fare is larger than this if the amortization costs K_a are included and a less than 100 percent load factor is assumed (ref. 19 recommends 57 percent for the particular route discussed).

In this AP.1-88 example, the craft performance characteristics (C_2 term) contributed approximately 39 percent (1.69 $/km) to the direct operating costs, and the crew and maintenance costs (C_3 term) contributed approximately 61 percent (2.68 $/km) of the direct operating costs. This latter term would actually have been a larger percentage of the cost if the amortization term K_a had been included. While the details and actual costs vary in any particular case (see Section 5.4 for more details on the AP.1-88 economics), the essential elements of the operating costs of hovercraft are as described here (Section 5.3) with a set of basic equations that include the design, performance, and economic factors in any hovercraft.

5.4 BHC HOVERCRAFT

The British Hovercraft Corporation is the world's most experienced manufacturer of fully amphibious hovercraft. The company was originally a boat building business, but turned its attention to aviation, producing a series of amphibians and flying boats culminating in the Princess, which was the world's largest all-metal aircraft.

Hovercraft work began in 1958 with initial studies and tank tests. The company built the world's first successful man-carrying hovercraft, the SR.N1, in the following year. Since then, hovercraft have been developed for various roles. The civil SR.N2 was built in 1962 and went into passenger service. The first military craft was the SR.N3 which was constructed for the British armed forces. Production of a range of SR.N5 and SR.N6 craft for both civil and military operators was started in 1964. These craft were to be built in different variants until production ceased in 1982. The first of another military marque, the BH.7, was produced for the British Royal Navy in 1969, subsequent craft of this type being supplied to the Middle East.

Probably BHC's most remarkable achievement was to have the earliest version of the SR.N4 in scheduled passenger service across the English Channel between Britain and France in 1968. This was only ten years after starting its earliest work on the hovercraft principle; nine after construction of the first man-carrying machine. Five craft were built to the original SR.N4 Mk.1 standard, three being subsequently converted to Mk. 2 by having their accommodation widened on the original structural platform. This made a useful increase in carrying capacity at relatively low cost, and a further craft was built to the

Mk.2 standard.

5.4.1 The SR.N4 Mk.3 – Britain's Premier Fast Ferry

(i) General. By the time the SR.N4 Mk.3 (Super-4) was introduced into service in 1978 there was a large number of high speed hovercraft and hydrofoil ferries operating successfully. However, none of the craft in service carried vehicles, except that is, for the SR.N4 Mks 1 & 2 which may be considered as part of the Mk.3 development. All were limited by weather conditions to a greater or lesser extent when it came to year-round operations between England and France. What was required by British Rail (Seaspeed) was a passenger/vehicle carrying hover ferry which could be relied upon to be available for at least 98 - 99% of the year based on the statistical mean annual occurrence of wind/wave height for the English Channel. This meant a craft capable of operating in 3.5 m significant wave heights (5.6 m or 18.4 ft max. waves) and 40 knot winds, gusting 50 knots (see Fig. 5.26). Furthermore it was a requirement that the *worst weather* crossing should take no longer than 50 - 60 minutes. In order to meet these conditions, the craft's performance in rough water had to be improved by at least 25% compared with the Mark 1 and 2 versions and craft motion would need to be reduced by at least one third. Craft payload was to be increased by 75% in order to reduce direct operating costs by at least 25%.

After several years' study and very intensive R & D work on the performance, structural characteristics and safety of hovercraft flexible structures (skirts), the British Hovercraft Corporation was confident that the performance and economic targets could be met, even if, as proposed by Seaspeed, the existing engines and machinery were retained and the craft converted to the new standard. The changes proposed were extensive and involved:

a) Lengthening the craft by 16.8 m (55 ft).
b) Widening the side (passenger) cabins.
c) Fitting new side structures carrying a high-level outer skirt hinge line.
d) Fitting a completely new, deeper, tapered, low pressure ratio skirt.
e) Replacing the 5.8 m (19 ft) diameter propellers by 6.4 m (21 ft) diameter high activity propellers. This necessitated replacing the pylon supporting structure.
f) Completely redesigning and re-styling the passenger accommodation and services.
g) Lengthening and refurbishing the control cabin and fitting new radar systems.
h) Fitting improved heating and ventilating systems throughout.
i) Improving the engine air intake filtration and re-aligning and lengthening the drive to the forward fan/propeller units.
j) Increasing the capacity of the fuel system by 50% to give better range and improved fuel ballast shift capability.

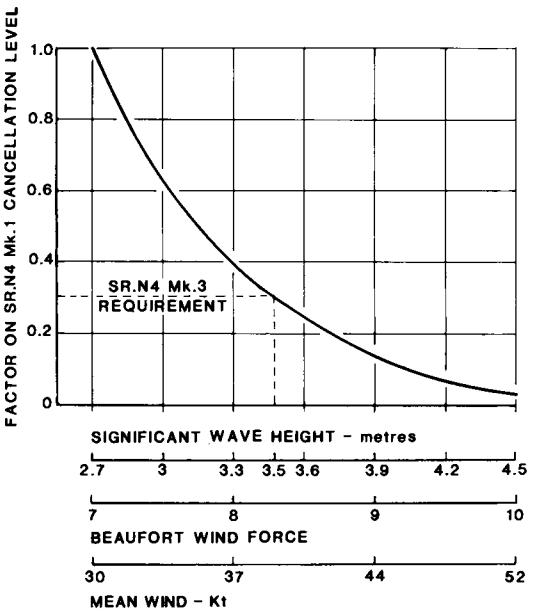

Fig. 5.26 Effect of improving craft operating limitations.

k) Revising and improving the safety equipment (e.g. more liferafts, larger anchors).

l) Strengthening and refurbishing the existing structure before being mated to the new centre section.

m) Improving and re-packing the hydraulic systems and re-wiring much of the electrics.

n) Repainting internally and externally with new house colours.

As shown in Fig. 5.27 the craft took on an improved longer, slimmer appearance with a much greater distance between the vectoring pylons which, together with the higher thrust levels available from the new propellers, meant that the directional control was as good as that for the earlier revisions in spite of its greater size and a 50% increase in weight.

The new *Super-4* was an immediate success and showed during trials and proving runs that all the Seaspeed targets had been met or exceeded, trials being conducted in seas from calm up to 5 - 7 metre (16.4 - 23 ft) significant waves. The larger, quieter, restyled and equipped passenger cabins were particularly liked and passenger comfort in large seas was much better due to less motion and a *softer* suspension. Performance was so good that Seaspeed decided to operate the craft using the Mk.1 cruise rating of 2535 kW/engine (3400 shp) for most of the time, reserving the Mk.3 rating of 2834 kW/engine (3800 shp) for

difficult or emergency conditions, thus reducing engine maintenance costs.

The *leading particulars* given in Fig. 5.27 show that the Super-4 has a payload capacity of 418 passengers and 55 cars, an increase of approximately 65% and 70% respectively over the Mk.1. Its increased speed capability of 5 - 10

Fig. 5.27 SR.N4 Mk. 3 craft description.

Dimensions: Overall length 56.4 m (185 ft)
Overall beam 25 m (82 ft)
Cushion area 1068 m^2(11500 ft^2)

Powerplant:
4 × Rolls-Royce Marine Proteus 15M/529 11,340 kW (15,200 HP) max. cont. rating
4 × 6.4 m (21 ft dia.) Hawker Siddely Dynamics propellers
4 × 3.5 m (11 ft 6 in) dia. BHC fans

Weights:
Max. laden weight 305 tonnes (300 tons)
Max. disposable load 117 tonnes (115 tons)
Typical fuel load 15.2 tonnes (15 tons)
Payload 55-60 cars and 418 passengers

Typical cruise waterspeeds:
Calm (0-0.6 m (0-2 ft) sign. waves 5 knots wind) 60-65 knots
Moderate (0.9-1.5 m (3-5 ft) sign. waves 20 knots wind) 50-55 knots
Rough (1.8-2.4 m (6-8 ft) sign. waves 27 knots wind) 40-45 knots

Endurance per tonne of fuel: 0.23 hours.

knots in most sea states has been used to maintain flight schedules in all weathers rather than in trying to squeeze in more flights. In spite of its greater capacity, improvements in passenger handling (e.g. larger doors and ground equipment) has meant that the turn-round time is only about 10% ($2\frac{1}{2}$ - 3 minutes) greater than for the earlier craft, thus still allowing an hourly schedule to be flown at peak times. A plan of the accommodation is shown on Fig. 5.28.

The other feature of the design of the SR.N4, and in particular the Super-4, which is not immediately apparent, is its very high safety. Not only are the four engine/fan/propeller units and their associated mechanical and control systems completely independent, but the structural layout of the craft ensures that, in the unlikely event of a serious skirt failure or a collision at sea, the craft will float without the car deck being flooded and with the passengers well above the waterline. This is because the large raft-like buoyancy tank and the bows have been divided into 32 water-tight compartments. The vehicles, which are carried directly on the top surface of the buoyancy tank, are always secured by lashings to prevent movement during flight. Tank tests and flight trials have demonstrated that it is impossible to turn the craft over, even in the critical beam-on hump speed case. All engines, including the auxiliary power units, are housed in fireproof compartments at the aft end of the craft.

Although they are largely constructed of aircraft grade light alloys, the high standard of painting and sealing used in their manufacture has ensured a remarkable life for these craft which have already been in service for almost 20 years and look set for many more yet (the first SR.N4 Mk.1 went into service in August 1968). By the end of 1986 both SR.N4 Mk.3s had accumulated approxi-

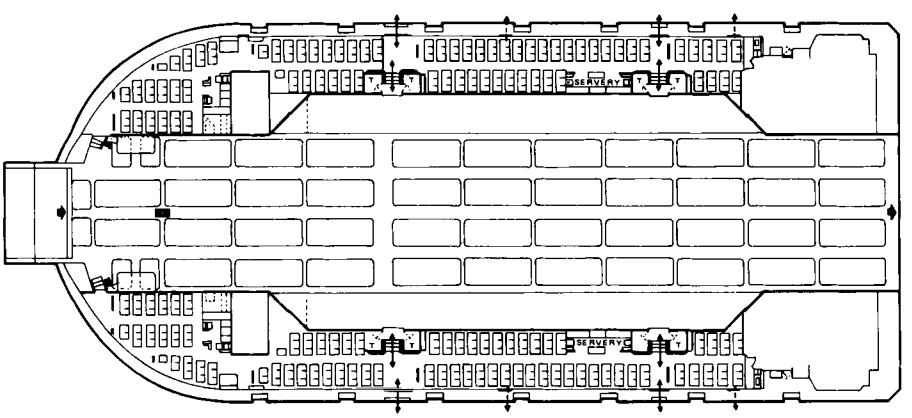

Fig. 5.28 SR.N4 Mk.3 accommodation.

mately 25,000 engine hours since their original build as Mk. 1s, half of which had been logged since their original build as Mk.1s, half of which had been logged since conversion. Operating (sea) hours would be about 10% less, which means that they had each travelled about 40 times round the earth or almost 1 million nautical miles, a very imposing record for the world's first high speed passenger/car ferry.

In many ways the development of the Super-4 is parallel to that of the *Concorde* supersonic aircraft but is far less known to the general public, possibly because it was developed at a fraction of the cost by a small but dedicated team of British engineers and because it has less environmental impact. Both craft raised the speed of travel in their respective fields by a factor of about 2½, both involved the application of state-of-the-art technology to the civil field, both came into service in the second half of the 1970s and look like continuing for many years yet. Neither is *fuel efficient* by comparison with their slower competitors but the gap could be closed in future designs. The Super-4 was indeed a very significant step forward in marine technology and still, 10 years after its construction, has no rival.

ii) SR.N4 design considerations.

a) Structure. The buoyancy tank is the major member of many hovercraft and, in a craft the size of the SN.N4, provides an interesting design problem. Provided there is sufficient volume to satisfy the requirements of floating and stability, the factors which determine the depth of the tank (0.75 m (2.46 ft)) are strength, weight, stiffness, and access. A structure of such size and uniformity obviously lends itself to some form of standardization to reduce production costs. The final solution reached was a basic grid of 2.4 m by 1.2 m (7.87 ft by 3.94 ft) cells made up, as shown in the inset of Fig. 5.29, with honeycomb panels for the top and bottom. Both longitudinal and lateral vertical webs were made up as sections bolted together at the corners of the cells. The advantages of assembly compared with, say, long-braced frames are obvious; but a further point was that the large numbers of relatively small and similar components made it possible to develop an adhesive technique (Redux) for the assembly of the stiffeners and edge members to the webs. The technique developed in conjunction with the production of the top and bottom honeycomb panels saved both weight and cost on a comparative riveted structure and was easier to protect from corrosion.

The next part of the structure that must be considered is the roof and here the designer is faced with a choice. He can let the buoyancy tank provide all the strength and construct a roof which is sufficiently flexible not to accept any load. Alternatively, he can make the roof part of the structure, in which case it must be strong enough to accept load; then, it effectively becomes the top flange of a beam subject to bending.

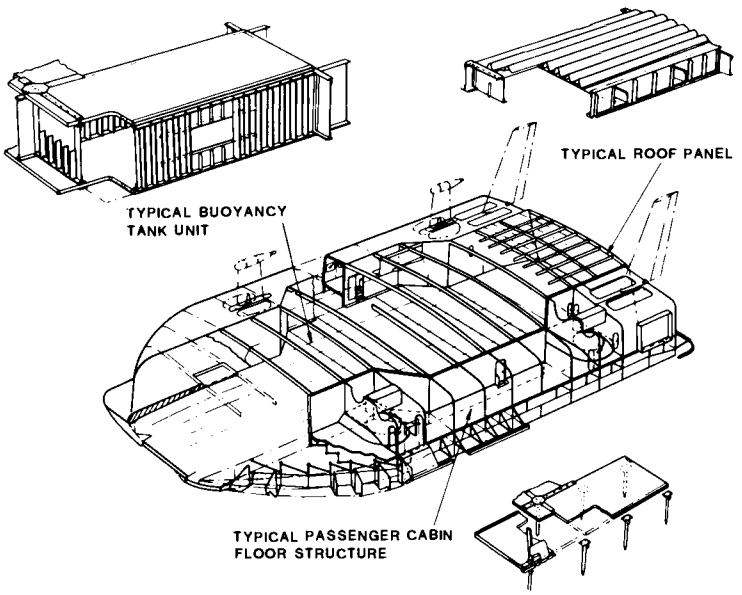

Fig. 5.29 SR.N4 structural layout.

The first solution can be achieved by using a material with a modulus of elasticity considerably lower than the tank structure material. In BHC's case this could well be GRP which has a modulus approximately a quarter that of aluminium alloys. The lighter, and generally more logical solution, is to make the roof load-bearing and this is the solution employed in the SR.N4. Because of the span required over the car bay, a fairly conventional structure of beams, stringers and panels is employed (Fig. 5.29). Again, advantage has been taken of the Redux process and the 2.4 m by 1.2 m (7.8 ft by 3.94 ft) panels are assembled with the external stringers using this method. There is the added advantage that the number of rivets, and therefore potential leaks, is drastically reduced.

The use of the roof as a structural member implies a shear connection to the buoyancy tank which is provided by the longitudinal car bay side walls (Fig. 5.29). Here again fairly conventional skin stringer construction was used with the maximum possible use of Redux.

The remaining parts of the primary structure involve the support of the machinery and, in particular, in the SR.N4, the mounting of the swivelling pylons. The use of integral lift and propulsion increases, to some extent, the structural problems, since the large air intakes and larger fan require the pylon loads to be carried well clear. At the same time, it is important not to waste possible passenger space. The basic solution employed in all our craft

with pylons is to use two transverse bulkheads supporting a fore and aft beam on which the pylon is mounted. The interference or airflow is thus reduced to a minimum and the loads are carried down into the buoyancy tank. The bevel gearbox which brings the power into the system can be hung very conveniently under the beam. Fig. 5.30 shows the arrangement in the SR.N4 (somewhat simplified) and shows that in this case the main fore and aft shear wall was used to complete the structure. In most cases the transverse bulkheads cannot be carried down to the buoyancy tank, since this would interfere with the airflow from the fan. A braced structure in the form of a series of struts is thus required.

The provision of access for vehicles means that large doors of some form or other are required. In deciding what form those doors should take, the following points must be considered: loading cases when closed (i.e., due to wave impact, wind loads, and so forth), craft turnaround time and weight. From the point of view of turnaround time, doors which form vehicle ramps when lowered

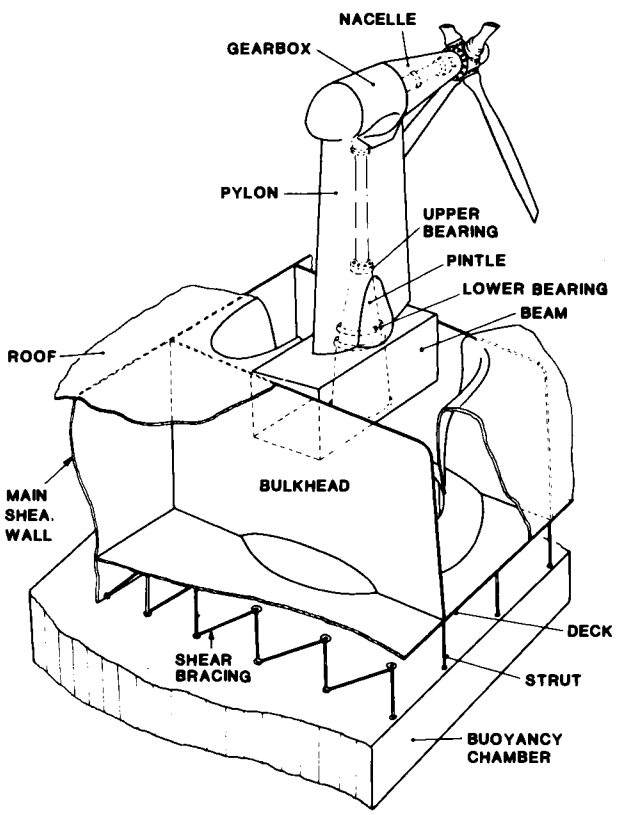

Fig. 5.30 Pylon support structure.

are desirable. However, these will be unnecessarily heavy for operational conditions, particularly if they are not required to take wave impacts.

In the SR.N4, the bow door will obviously suffer some impacts in rough conditions and the weight penalty in making this a vehicle ramp is not severe. On the other hand, the aft doors will not receive wave impacts when operating and can be lighter. For this reason a rear ramp is not used. Turnaround time is not affected since cars unload from the bow while a loading ramp is positioned at the stern.

The remaining structure is largely involved in ducting the lift air around the craft and supporting the skirt, the machinery and the passengers, and in keeping out the weather. Of interest here perhaps is the use of large numbers of struts, this being necessary to reduce interference in the air flow to a minimum. In areas of double curvature, such as the air intakes and corners of the roof extension, use if made of GRP. In fact, there is no panel beating required on the SR.N4.

Skirt bags are now assembled as far as possible by bonding techniques. These produce a lighter weight joint and reduce the damage to the craft structure which occurs due to solid fastenings in the skirt. In a craft the size of the SR.N4 it is inevitable that some breakdown joints must be provided and these are bolted. Attachment of the fingers is by huck-bolts and shackles to enable rapid changing, since these parts inevitably take the most wear.

b) Power plant and transmission. BHC has, from very early days, used what is known as an integrated system of lift and propulsion. The interchange of power is conveniently carried out by using a fixed bladed fan and a variable pitch propeller. Thus, for a given power, a small propeller pitch angle permits the system to run at high speed giving maximum lift. Large pitch angles cause the propeller to absorb more power and the speed of the system drops giving reduced lift and higher forward thrust. The system implies that the power output from the engine must be reasonably constant over a wide range of rpm. The choice of engines for a hovercraft is governed by three factors: weight, cost, (initial and operating), and power/rpm characteristics.

Taking the last item first, it can be seen that, for the integral system, a flat power/rpm curve is desirable. Fig. 5.31 compares the percent peak cruise power and percent peak rpm for a variety of engines. It is evident that the free turbine is superior on this basis.

In considering weight it is well-known that the gas turbine is best with a specific power-to-weight ratio of about 3.7 kW/kg compared with 0.2 kW/kg for a diesel. This is not the whole story, since the gas turbine consumes considerably greater weights of fuel. However, for engines in the 1500 - 2200 kW range, the breakeven point would only occur at endurances above 10 hours, which is an unrealistic duration for this size of vehicle.

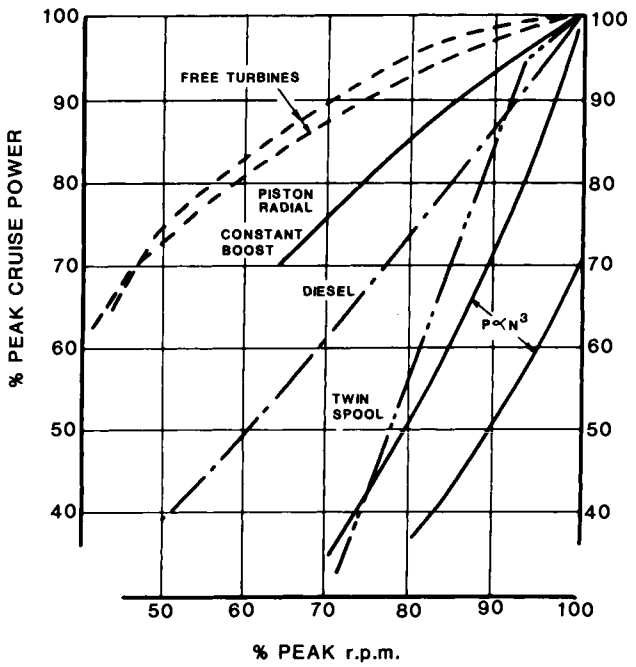

Fig. 5.31 Typical power/rpm curves.

In terms of cost, the diesel is at an advantage. However, if the additional specific weight of the diesel is assumed as a direct loss of payload then we find that, assuming 8900 kW cruise power for the SR.N4 and a duration of 2 hours, the additional weight using diesel engines is approximately 27 tonnes, which is 55 percent of the normal payload.

On the grounds of direct efficiency, the centrifugal fan is marginally better than the axial fan. A more important factor is that air must be drawn from the upper surface of the vehicle to prevent the entraining of too much water or dirt, and the flow must be turned through a right angle in order to distribute it to the periphery of the craft. The use of a centrifugal fan eliminates the duct losses which would otherwise be incurred in this flow change, making the centrifugal fan considerably more efficient than the axial. The third point in its favour is that rotational speeds are lower and the fan is thus inherently safer.

The requirements of high power absorption (up to 1100 kW on SR.N4) and light weight mean that there is no commercially available fan and it must be constructed by the hovercraft manufacturer. Although fibre glass fans of intermediate size have been constructed, BHC's experience at the time was that fans were best fabricated using normal aircraft methods. It is of interest to

note that the aerodynamic loads are of no significance, the loads coming entirely from the weight and inertia of the fan under acceleration and gyroscopic cases.

Since the disintegration of a fan would cause severe damage and possibly casualties to passengers and third parties, they are designed to high reserve factors (3.0 minimum). In addition, a prototype is usually oversped to approximately 20 percent above its normal maximum. Critical areas are examined as far as possible by strain gauge technique.

In contrast to the case of the fans, the manufacture of a propeller requires knowledge, experience, and skills outside the range of a normal aircraft manufacturer. The hovercraft designer must thus turn to specialist companies for these items and, since their development is a very expensive process, must use existing components as far as possible. This particularly applies to hubs. In the early days, this trend led to the use of propellers with a higher speed than was desirable and in turn gave the hovercraft the image of a noisy vehicle. On the SR.N4, however, with the cooperation of the propeller companies, it was possible to reduce tip speeds very significantly, despite the fact that the propellers are 5.8 m (19 ft) diameter.

We have seen that the basic machinery consists of engine, lift fans, and propellers. The disposal of these items around the craft is of interest. Important factors here are the consideration of safety and reliability. By using four fan/propeller units on the SR.N4, and by keeping them as completely uncoupled as possible, the change of immobilization of the craft due to power failure is very much reduced. Some coupling is inevitable, i.e., through the control and fuel systems, but mechanically at least they are quite separate. From the point of view of fans and propellers, it is efficient to establish the units at the corners of the craft since this gives the best lift distribution and least interference between propellers.

At first sight, it would seem logical to place each engine as close to its lift/propulsion unit as possible, to reduce transmission length and therefore weight. This was, in fact, projected at an early stage. Three factors militate against this arrangement. Firstly, the forward engines had to exhaust upwards, causing interference in the aft propellers and giving a downward thrust which would reduce payload or clearance. Secondly, there is a considerable saving in space if engines can be housed together. Thirdly, it is convenient to have all engine systems, and in particular fuel and fire extinguishing, grouped together; the provision for firewalls, and so forth, is also simplified. These advantages were deemed to outweigh the disadvantages of a long transmission run to the forward lift/propulsion units. Fig. 5.32 shows an aft transmission system. This consists of a direct drive from a reduction gearbox on the engine to a simple bevel box which splits the power to propeller and

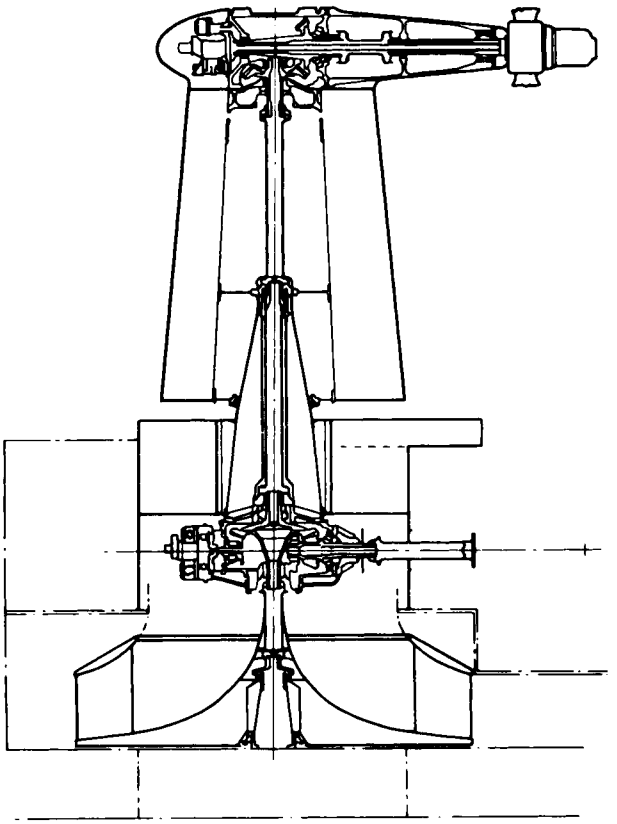

Fig. 5.32 Transmission layout.

fan. An auxiliary gearbox on the forward end of the main box provides power for the lubrication and hydraulic pumps. The lubrication pumps are simple gear pumps and serve their own primary gearbox only, thus maintaining the individuality of the units. The hydraulic systems will be discussed later. All bearing are ball or roller type.

A second bevel box at the top of the pylon drives the propeller. This box also carries the structural loads from the propeller. Power for lubrication and hydraulics is taken from the forward end of the box.

Shafts are of aluminium alloy, except for the propeller shaft, which carries severe bending loads, and the vertical pylon shafts, where space is a limitation. In order to allow for flexibility in the system, all shafts are coupled with gear couplings.

The forward system is identical except for the longer transmission. Here, allowance must be made for craft flexibility. The shaft is divided into approximately 2.5m (8.2 ft) lengths and supported by the units shown in Figure 5.33.

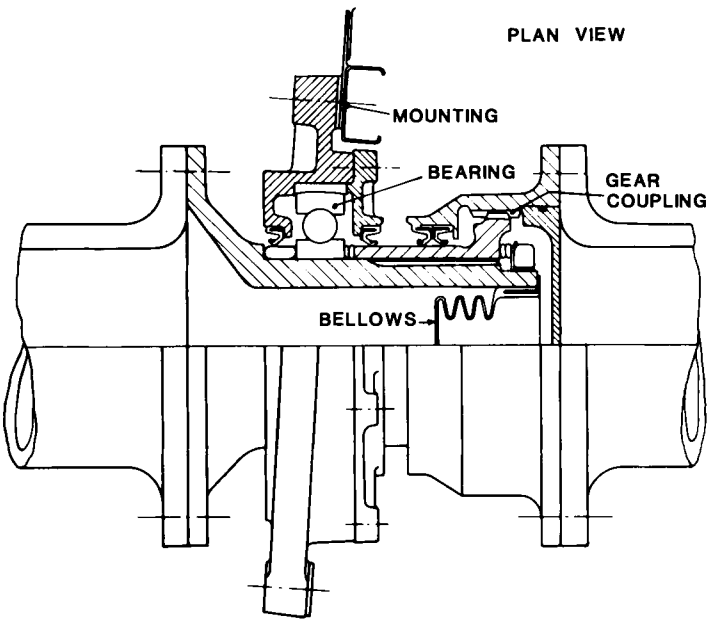

Fig. 5.33 Horizontal shaft combined bearing and gear coupling.

c) Systems. It has been BHC policy throughout to make each major component of the machinery provide its own lubrication. Thus each engine and gearbox has its own mechanically driven gear pump. This has the advantage that any contamination of one system leaves the other unaffected. Air for the cooler is provided by bleed from the cushion. Gear couplings run in sealed oil baths.

Hydraulic power is required for the operation of controls. These take the form of rotating pylons and fins and variable pitch propellers. In order to maintain the individuality of the fan/propeller units, the hydraulic pumps for each pylon are driven from their associated primary gearbox. Separate pumps on the aft units provide power for the fins.

In a similar fashion, power for propeller pitch control is taken from the pylon gearboxes. Because of the intermittent demand, servo pumps are used for the hydraulic systems. Auxiliary hydraulic systems are used for operating the main ramp and rear doors. These systems have electrically driven pumps.

Electrical power is required, among other things, for instrument, navigation equipment, radios, lighting and engine starting. In small craft, it is common to generate dc current directly from the main engine, using a battery for starting and other services required when not under way. In larger craft, this becomes impractical, if only from the engine starting point of view, and separate auxiliary power units are provided.

In the SR.N4 two Lucas 1S 90 gas turbines drive alternators. All the power

required for normal operation can be provided by one unit, the second providing main engine starting. Once the craft is under way, the loads are normally shared between the two units. Alternating current loads include fuel pumps, ventilation fans, auxiliary hydraulic power pumps, and lighting. A proportion of the output from each alternator is rectified. Direct current is required for the control system, APU fuel pumps, emergency lighting, and electronic equipment. A main battery is connected to the dc busbar and a reserve battery is kept constantly charged. The battery supplies essential services when the craft is *dead* and is used for starting the APUs.

The control of the pylons and fins is by means of a wheel and rudder bar in the control cabin. The signals from these are converted into electrical demand signals to operate the hydraulic servo valves by means of electronic equipment in the control cabin.

The hovercraft has shown itself to be particularly sensitive to fore and aft trim as far as optimum performance is concerned. In small craft, notably the SR.N6, some degree of control may be obtained using elevators, but a more powerful method uses the transfer of fuel between forward and aft tanks. In the SR.N6, this was provided as a separate system with provision to enable it to be used as an emergency reserve.

In the case of the SR.N4, however, the two functions have been combined in one system. The four groups of tanks are situated in the buoyancy tank, one at each corner of the craft, but clear of the machinery. A ring main provides a rapid means of transferring fuel for ballasting purposes and also serves as a refuelling line. Separate pumps feed the engines. By cross coupling the feed lines to each pair of engines, a duplication of pumps is achieved. This is one of the areas where there is, inevitably, some coupling between the separate propulsion units.

It is, of course, important that the buoyancy tank be kept free of water which may enter due to condensation or leakage. In small craft, bilging is normally by hand-pump which connects directly to pipes in the tanks. In the SR.N4, because of the large number of compartments, four electrically driven pumps are provided, each of which can drain one compartment at a time.

The use of gas turbines as a power plant has led to the adoption of the aircraft type of fire protection. The engine rooms are manned and each engine is contained in two separate fire zones: one containing the *cold* end of the engine, complete with fuel, lubrication, and electrical supplies; the other containing the *hot* part of the engine. In the SR.N4, these latter zones are formed by stainless steel cowls around the engine. The cold zone is also lined with stainless steel. Fire detection is by a fire wire which lights a warning lamp in the control cabin when the temperature in the zone reaches a preset value. The fire is extinguished by expelling an extinguishant (BCF) into the

affected zone.

d) Conversion. The first SR.N4 Mk.1 craft for conversion was withdrawn from cross-Channel service and arrived back at BHC's Columbine Works at Cowes in February 1977. Its skirt system and rotating components, including engines, gearboxes, transmission, fans, propellers, pylons, fins and rudders, were removed. At this point the craft was literally cut-in-two between frames 7 and 8 (see Fig. 5.34), slid apart and cleaned back to the adjacent frames. One structural bay (just under 2.4 m (8 ft) was therefore lost in this operation and the new centre section was close to 19.2 m (63 ft) (i.e. 8 structural bays) in length to provide the 16.8 m (55 ft) (7 bay) overall length increase. A view showing the new centre section inserted is given in Fig. 5.35. The box-like structure, seen in the foreground, is the beginning of the buoyancy tank for the second craft being prepared in advance.

Since, for the lengthened craft, the shear forces are substantially increased in the original fore and aft sections, and the bending moment is similarly larger over the new center sections, considerable reinforcement of the structure was necessary. In the main, this was achieved by reinforcement throughout the length of the two fore and aft bulkheads (just visible in Fig. 5.35), which are essentially the main shear walls. Over the new centre section, the additional bending moment was catered for by doubling the cross-

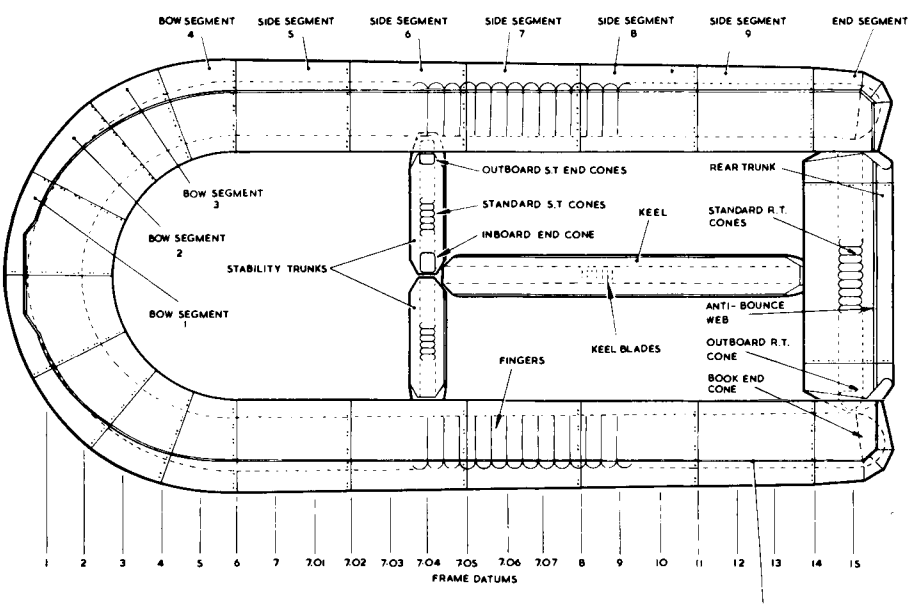

Fig. 5.34 SR.N4 skirt plan.

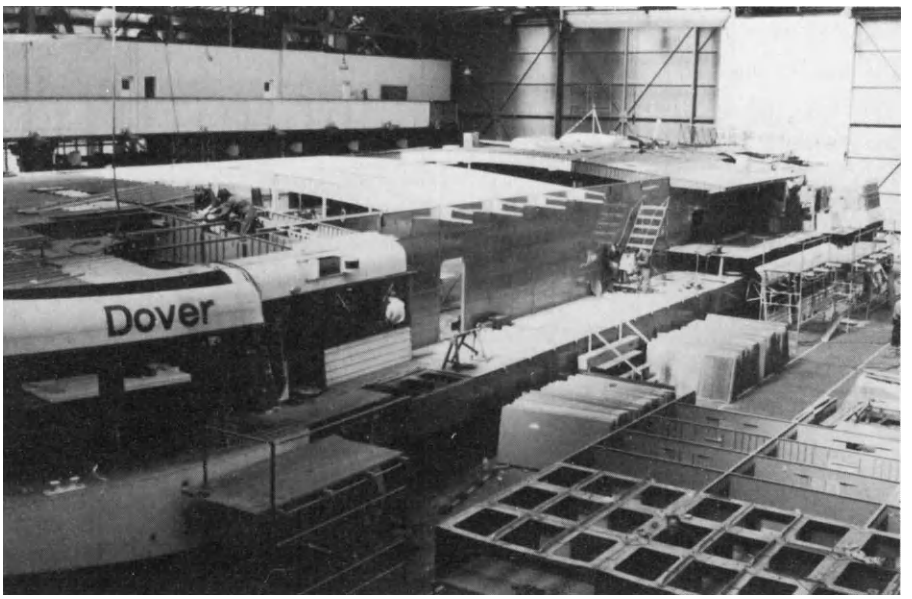

Fig. 5.35 SR.N4 Mk.3 during modification.

sectional areas of the roof skin and stringers adjacent to the bulkheads. This lengthened *strut* was stabilized by turning the transmission tunnel suspended beneath it into a structural member. Reinforcement of the transverse bulkheads, in both end sections, was also necessary and the area and load capability of each of the landing pads (now 7 instead of 5) was increased by about 50%.

iii) Performance. Subsequent to a comprehensive programme of ground running trials, the first craft conversion was launched from BHC's Columbine Slip on the 6th April 1978. It was then subjected to a series of sea trials and further tethered tests prior to acceptance by British Rail Seaspeed (now Hoverspeed (UK) Limited) on the 26th May 1978.

These acceptance trials (including some 70 hours at sea) demonstrated ample compliance with all the specification requirements for water speed, stopping distance and endurance. Craft handling and safety aspects were also shown to be very satisfactory over the full weight range from light (214 tonnes) up to overload starting weight at 325 tonnes, in sea conditions ranging from calm up to 3 metre significant wave height. Some particular points noted were:

a) Behaviour was very docile and easily controllable following simulated system failures. These covered propeller pitch, pylon and fin runaways, and engine cuts, over the water speed range up to 35 m/s (68 knots).

b) Manoeuvring control was good in boating and semi-boating modes and skirt

drainage times were acceptably brief (less than 2 minutes); base manoeuvring showed characteristics which were not significantly different from those of Mk.1 or Mk.2 craft, allowing for the extra craft length.

c) The skirt gave no plough-in tendencies in any of these conditions (with hemline attitudes down to negative values), or on ship's wake encounters; longitudinal decelerations were innocuous (i.e. less than 0.1g) and much less than noted on current Mk.1 or Mk.2 craft.

d) The combination of increased craft length and the deeper, low pressure ratio, 1.8 m fingered skirt, resulted in a marked improvement in ride comfort; bow vertical accelerations were typically half to two-thirds those experienced on the Mk.1 craft in similar conditions. These results, predicted from model testing, were confirmed qualitatively and by analysis of measured acceleration data.

For specification purposes, craft speed performance was related to the use of 2835 kW per engine and disposable loads up to 112 tonnes. Compliance was demonstrated at a nominal weight of 305 tonnes (115 tonnes disposable). The achieved beam wind waterspeeds, summarised in Fig. 5.36, are seen to be well in excess of the specification, particularly in the higher waves.

Figure 5.37 shows limited data obtained on into and down wind headings (not specification requirements), for the nominal 305 tonnes/2835 kW per engine condition. When corrected to the *standard* wind speed/wave height relationship, the worst into-wind speed results can be seen (Fig. 5.38) to be closely similar to the performance predicted using resistance derived from towing tank model data.

Vertical acceleration measurements (RMS 'g') obtained at bow, CG and stern stations on the first craft conversion are summarised in Fig. 5.39 for a range of sea states. Levels assessed by hand analysis of U/V trials records are indicated by white spots; the blank spots are computer spectral analysis of magnetic tape records obtained in-service. Acceleration levels are fairly constant (around 0.10 to 0.15 RMS 'g') with increasing sea state, due to decreasing craft speed (typically 30 - 33 m/s (58 - 64 knots) in 0 - 0.3m (0 - 1 ft) sea and 17 - 20 m/s (33 - 39 knots) in 2.1 - 2.4 m (7 - 8 ft) seas). For a given wave height, these accelerations are about 50% to 70% of levels experienced on SR.N4 Mk.1 and Mk.2 craft, whilst the craft speed is typically 5 m/s (9.7 knots) faster.

An example of vertical acceleration spectra, derived from computer analysis of FM tape records, is given in Fig. 5.40. The condition illustrated corresponds to 33 knots waterspeed in 1.2 - 1.5 metre seas.

(iv) Operating experience. Cross-Channel hovercraft operations commenced in the summer of 1968. The craft that inaugurated the service, the SR.N4 Mk.1, was considerably larger than any other craft, military or commercial, available

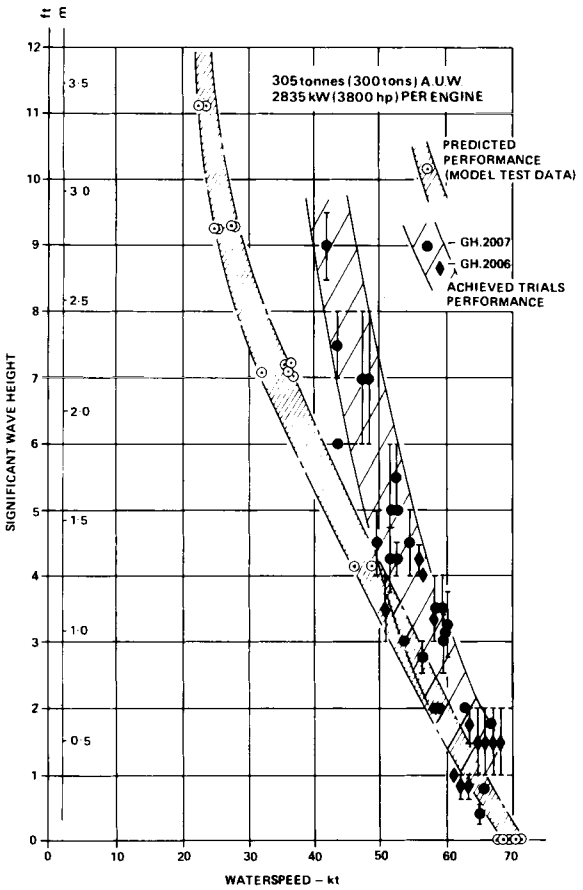

Fig. 5.36 SR.N4 Mk.3 beam-wind waterspeed performance.

at that time and represented a significant step forward in hovercraft technology.

Performance was not good in the first year, with over 20% of scheduled crossings cancelled owing to weather conditions, natural caution on the part of inexperienced crews and technical reasons. Most of the technical problems were caused by a weak finger attachment which was modified at the end of the first season. As crew experience increased and expertise improved, there was a significant reduction in the number of crossings cancelled because of inclement weather, and technical performance improved following various modifications to the craft. In the third year of operation, the 20% cancellation rate of the first summer was reduced to 10% over the whole year.

The popularity of the service was immediate, passengers were prepared to pay a premium fare for the faster crossing, even on a short 40 Km (25 mile)

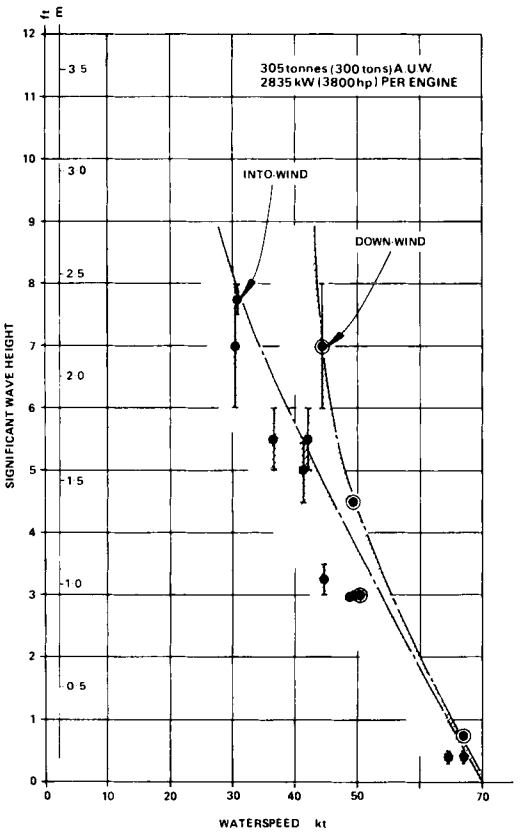

Fig. 5.37 SR.N4 Mk.3 waterspeed performance trials achievement.

route. Both operators, British Rail Hovercraft Limited and Hoverlloyd Limited, purchased additional craft until, in the 1973 season, hovercraft had captured 30% of the market to Calais and Boulogne with 8% of the ferry capacity available on these routes.

The early 1970s fuel crisis led to both Hoverlloyd limited and British Rail Hovercraft Limited modifying both their craft and their operations in different ways. Hoverlloyd Limited tackled the problem by widening their Mark 1 craft to the larger Mark 2 standard and, at the same time, another craft was ordered from the British Hovercraft Corporation. This gave a larger vehicle and passenger capacity and a greater flight departure frequency. British Rail Hovercraft Limited, on the other hand, decided to stretch their Mark 1 craft to the Mark 3 standard which would increase the carrying capacity by approximately 80% with a corresponding increase in operating costs of approximately 10%.

This project had to be shelved when it was announced that a Channel Tunnel

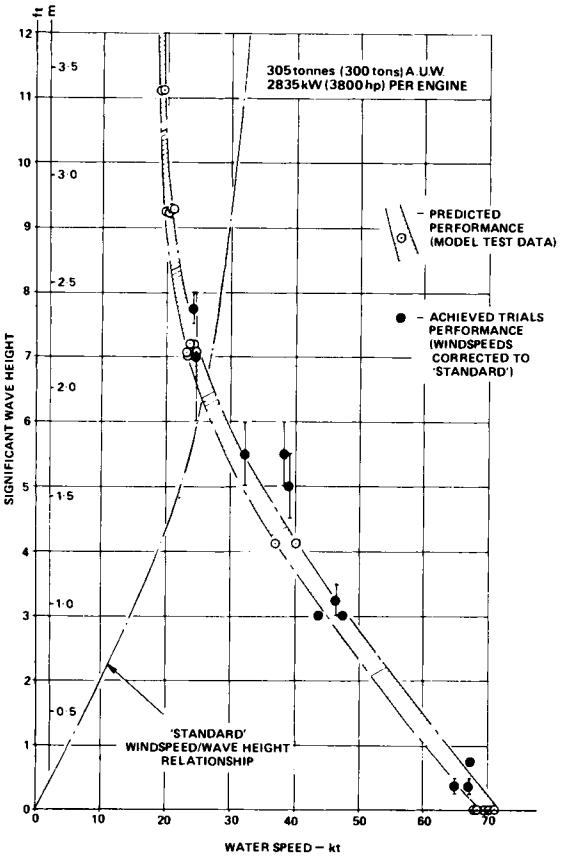

Fig. 5.38 SR.N4 Mk.3 into-wind waterspeed performance.

was to be built, but when the tunnel was cancelled by the Labour Government just after work had commenced in 1976, the British Railways Board authorised the stretching of their two craft and at the same time the company moved to a purpose-built hoverport in the Western Docks at Dover. The new hoverport was opened and operation with the first of the two Mark 3 craft commenced in July 1978.

There is no doubt that these changes made both companies more viable but, by the late 1970s, a further sharp increase in fuel prices had had an equally serious effect. At the same time, ferry competitors were continuing to increase the size of their fleets and the size of their ships to the extent that there was a doubling of ferry capacity on the English Channel in a matter of four years. This occurred at the time that the Government brought to an end the price fixing cartel exercised by all operators, which led directly to an

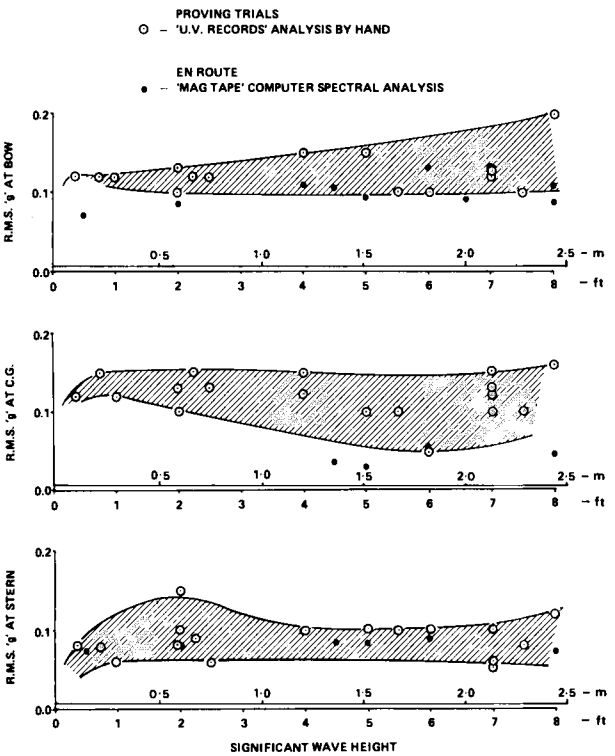

Fig. 5.39 SR.N4 Mk.3 sea-state induced craft accelerations (RMS).

acrimonious price war from 1979 to 1981. Whilst the price war generated large volumes of traffic, this was carried at considerably reduced fares and all operators incurred losses.

The hovercraft companies were more severely affected than the ferry competition during this period for several reasons, but mainly due to high fuel consumption. Once again, drastic action was necessary to avoid the closure of one or both companies. This took the form of a merger between Hoverlloyd Limited and British Rail Hovercraft Limited into Hoverspeed Limited, the company that is operating across the English Channel today.

The achievements of the SR.N4 on the English Channel have been significant. This craft, which was a prototype at the time of its design and construction, was a quantum leap forward in technology. It was expected to be outdated after 10 years, but is continuing to operate 20 years later and showing no signs of demise. It had carried 27 million passengers and today holds 16% of a highly competitive market with 7% of the available capacity.

The stretching of the SR.N4 Mark 1 was a milestone in the development of large amphibious hovercraft. It transformed the operating economics of the

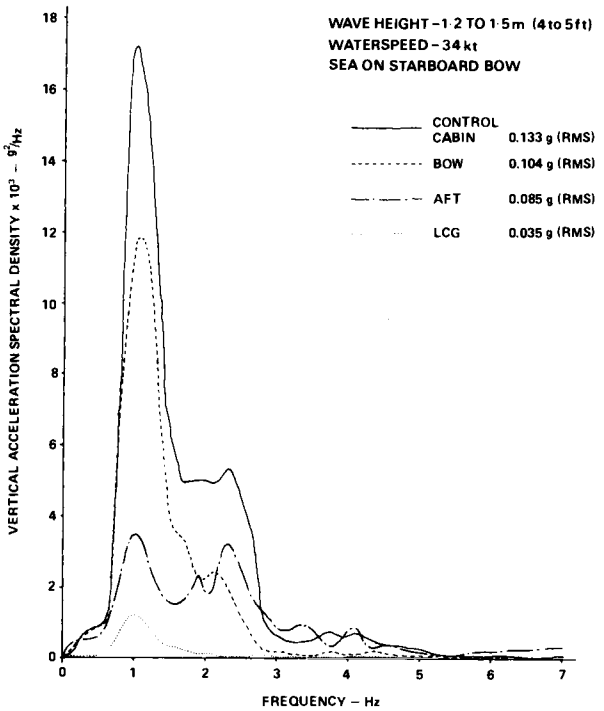

Fig. 5.40 SR.N4 Mk.3 vertical acceleration spectra.

craft and at the same time weather capability and passenger comfort was considerably improved. Technical reliability of the craft has improved over the years and, of all Mark 3 scheduled flights operated out of Dover, only half of one percent are now cancelled for problems associated with the craft. The annual cancellation rate of the Mark 3 craft now stands at 5%. The main area of technical advance has been in skirt maintenance. An indication of this is the fact that, in the early 1970s, it was considered necessary to provide one set of hydraulic jacks (used to lift the craft overnight to undertake skirt maintenance) for every two hovercraft. It is now considered feasible to maintain five craft on one set of hydraulic jacks. It is operating quite safely in much heavier weather than was originally intended, and it is carrying a much greater payload than the original design envisaged. In other words, as a concept and a technical achievement, large amphibious hovercraft in general, and SR.N4 Mark 3 in particular, have proved to be highly successful.

(v) SR.N4 Mk.3 operating costs. Based on operating experience on the English Channel, the following figures cover the direct variable operating costs, i.e., fuel plus spares and overhaul, as of August 1987.

	£ Sterling/Hour
1) Fuel: average consumption 4540 litres of kerosene (1100 gallons) per hour at £0.124 sterling/litre	560
2) Rotable items: engines, propellers, transmission gearboxes, APUs	200
3) Skirt and other spares and materials	495
Total direct variable operating cost	1255

5.4.2 The AP.1–88 Passenger/Utility Craft

(i) General. The SR.N6 hovercraft had proved itself to be an excellent workhorse. Civil versions had had a very successful operating history in scheduled passenger service within the UK. However, its success in the civil market had been limited by its relatively high costs. Being based on aircraft practice, it was expensive to build and required careful maintenance of its structure. More than that, the high overhaul costs and relatively high fuel consumption of its gas turbine engine were against it. In addition, there was some public objection to its considerable propeller noise. Against this background, it became necessary to produce a second generation machine that would be markedly cheaper in both first and operating costs and at the same time be environmentally more acceptable. Thus, the AP.1-88 was born.

The new craft is of welded, marine-type, construction, which is very much cheaper to build and also requires minimal maintenance in service. It is powered by diesel engines, which are lower in first cost, but, most importantly, are not subject to the very high overhaul costs associated with gas turbines. The transmission systems are straightforward, while the use of smaller, fixed pitch shrouded propellers saves on cost and reduces noise, thus making the craft environmentally acceptable. The structure and systems of the AP.1-88 are designed so that its maintenance in service generally requires the same skills as are necessary for the operation of any conventional ferry.

(ii) Description. The AP.1-88 has been produced in two versions, the prototype known as the AP.1-88/80, and the production craft called AP.1-88/100 (Fig. 5.41). The craft are very similar, the main differences being that the /100 is 3.4 m (11.2 ft) longer, has a more powerful lift system, and is fitted with a tapered skirt to improve its sea keeping capability.

The production craft is designed to carry up to 100 passengers together with their baggage. Alternatively the craft can transport between 10 and 12 tonnes of payload depending upon the amount of fuel needed for the particular voyage. The hull (Fig. 5.42) is manufactured from aluminium alloy using extrusions wherever possible to reduce manufacturing cost. The main structure component is a buoyancy tank constructed with 0.5 m (1.64 ft) deep "I" frames. Top and bottom are formed from 0.45 m (1.48 ft) wide aluminium alloy *planks*,

Fig. 5.41 AP.1-88/100 passenger craft.

complete with integral stiffeners. These are machine welded together to provide a continuous structure. The bow and side structures use tube for chines and gunwhales with plating and side frames welded in position. The cabin, control cabin and propulsion engine room are constructed from aluminium alloy material with welded frames and stiffeners as required. The roof of the main cabin is of light gauge material and is riveted to the roof frames.

The air cushion is contained by a *responsive* skirt which is the latest

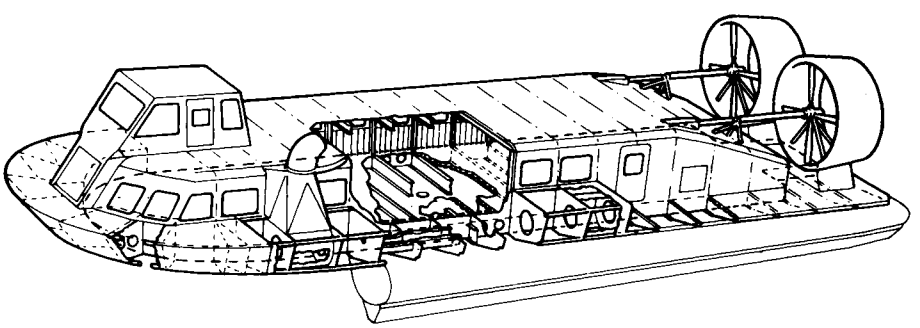

Fig. 5.42 AP.1-88 structure.

development of the BHC air cushion system. This has been designed to give the maximum cushion efficiency with minimum drag and to provide a comfortable ride in sea states in excess of 1.5m (4.9 ft). The skirt (Fig. 5.43) consists of a peripheral bag around the bow and along the sides of the craft. Below this are fingers which are sufficiently flexible to seal the cushion as the craft travels over waves; they produce very little drag and are easily replaced when worn. The cushion is contained at the rear by a separate bag with cones. This separation permits it to move backwards to allow waves to pass through the cushion with a minimum of drag. In order to provide stability the cushion is divided across the craft by stability trunks and the rear section of the cushion is divided longitudinally by a keel.

To supply air to the cushion, two pairs of centrifugal fans are mounted in each side structure aft of the engine, (Fig. 5.44). These are directly driven at a nominal 2200 rpm from 12 cylinder 373 kW (500 HP) Deutz turbo-charged air-cooled diesel engines, and deliver air into the bag of the side skirt. A further pair of fans, forward of the engine, supply air to the bow thruster which is described later. The transmission to the fans embodies flexible couplings and centrifugal clutches, to off-load the engine starting.

The craft is driven by two fixed pitch propellers mounted in ducts to increase their efficiency at low speed while maintaining relatively low tip speeds in the interests of noise reduction. Each propeller is driven at 1300 - 1400 rpm from a single 12 cylinder 373 kW (500 HP) Deutz turbo-charged air cooled engine through a toothed belt drive which gives a speed reduction of 0.6 - 1. A centrifugal clutch and flexible coupling are provided in the transmission forward of the engine.

The fuel system has the dual functions of fuel supply and craft attitude control (ballast system). Four tanks of approximately 1200 litres each are provided. Two of these are mounted in the bow and two at the stern of the craft. Each engine is supplied from one tank by means of a pump with filters, water separators, and shut-off valves in the fuel line.

Hovercraft performance is sensitive to the fore and aft trim of the craft and the correct trim angle varies depending upon the craft course in relation to wind and sea. Provision is made, therefore, to transfer fuel between forward and aft tanks at a rate of approximately 230 litres per minute. In this way, the craft centre of gravity can be adjusted to suit varying payloads and operational directions. For normal operations, the craft is fuelled to 3200 litres and re-fuelled when the contents have dropped to 1400 litres, so that there is always adequate tank space and fuel for trimming the running attitude of the craft. Warning devices and transfer cut-offs are provided to prevent an engine stopping due to an empty tank.

The craft has two directional control systems. Rudders mounted to the rear

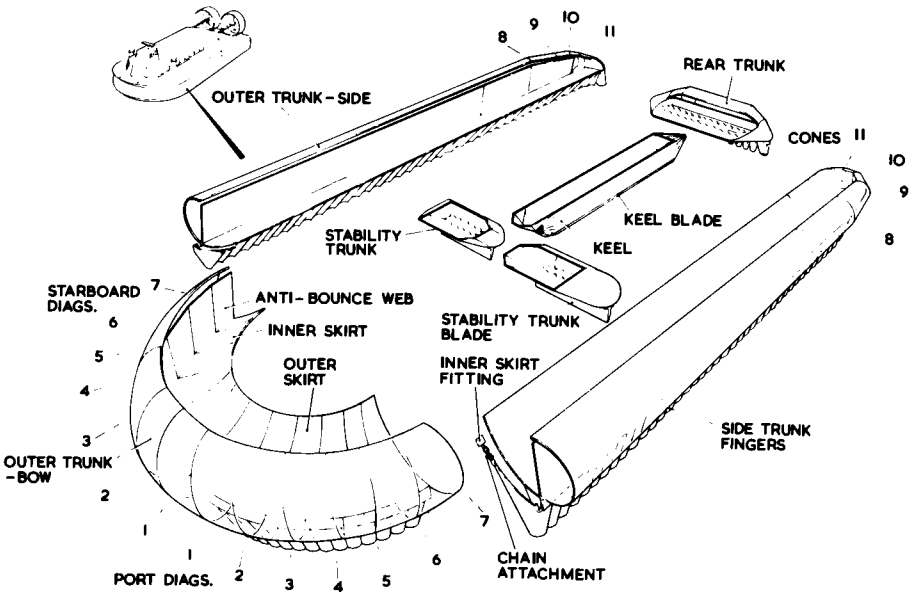

Fig. 5.43 AP.1-88 skirt.

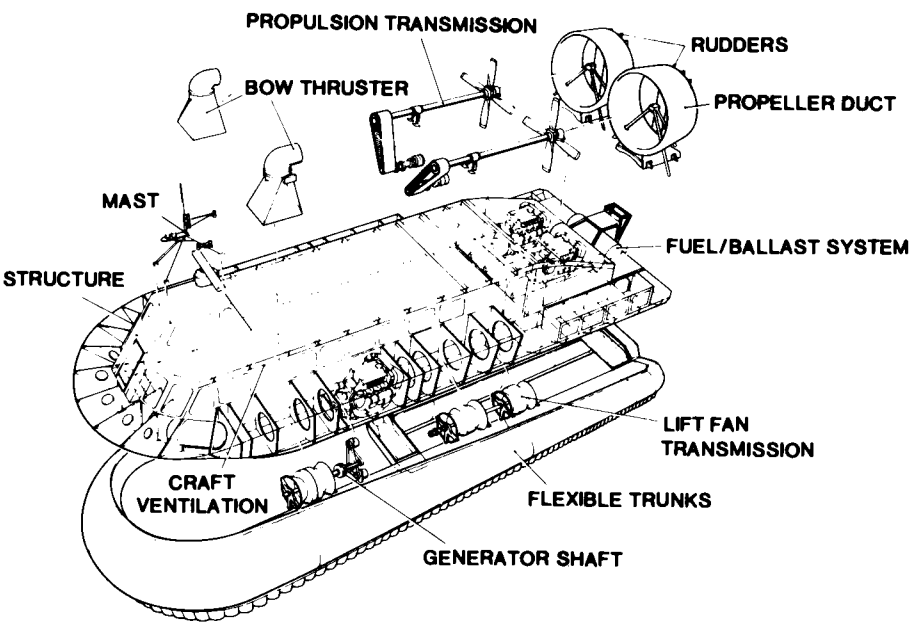

Fig. 5.44 AP.1-88 craft layout.

of the propeller ducts provide directional control at forward speed. They are controlled from a rudder bar in the control cabin (Fig. 5.45) and have a hydraulic power assisted system to give good response. Hydraulic power is provided from pumps on the two propulsion engines and the single jack acts directly on the control linkage.

The bow thrusters, fed from the forward pair of fans on the lift system, rotate about the vertical axis to provide side force and to roll the craft into the turn. The ducts are driven by electric motors which are controlled from a rotary selector in the control cabin. In normal operation, the ducts rotate between 90° outboard and 70° inboard of the fore and aft position. For decelerating in low speed manoeuvring, the sense can be reversed, so that the thrusters blow forwards while retaining their ability to move from side to side. Additional directional control is obtained at low speed by using differential propeller thrust.

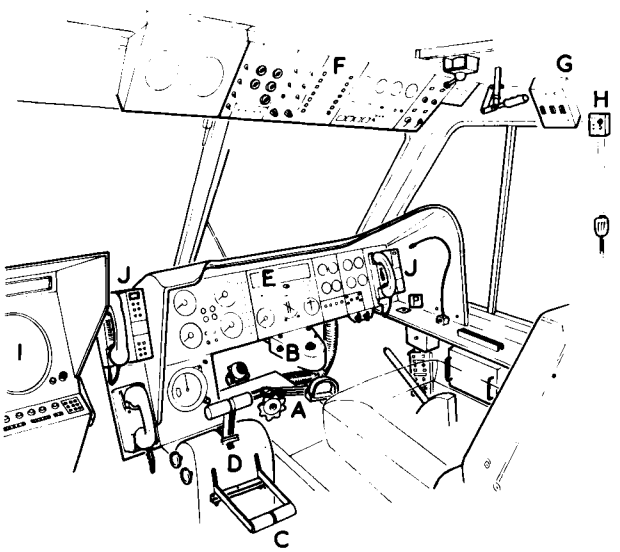

A RUDDER CONTROL PEDALS
B BOW THRUSTER CONTROL PANEL
C LIFT ENGINE THROTTLE LEVERS
D PROPULSION ENGINE THROTTLE LEVERS
E MAIN INSTRUMENT PANEL
F OVERHEAD INSTRUMENT PANEL
G FIRE CONTROL PANEL
H ELECTRICAL BAY SMOKE DETECTOR WARNING PANEL
I KELVIN HUGES 1600 RADAR DISPLAY
J VHF RADIO (2 SETS)

Fig. 5.45 AP.1-88 controls.

The craft has a 24V direct current system supplied with power from four generators driven by the lift engines. These supply a busbar from which all the electrical requirements for the craft are taken via fuses or circuit breakers. Batteries also feed the busbar to provide engine starting and will support the electrical system in the unlikely event of a complete generation failure. A separate busbar, normally supplied by the main busbar, but also equipped with its own batteries, supplies such essential circuits as engine and craft controls, radios, fire safety systems, navigation lights, etc. The main electrical bay housing the batteries and primary electrical systems, other than generators, is situated at the rear of the passenger cabin.

The craft is designed for operation by a single man with a second crew member as radar operator and navigator. The primary controls, as shown in Figure 5.45, are: rudder bar (A), bow thruster control selector (B), lift engine throttles (C), and propulsion throttles (D).

The main control panel (E) contains the speed, heading, and rate of turn indicators, with the engine rpm indicators, stop buttons and warning lights to the left and the engine oil temperatures to the right.

Fuel content indicators for the four tanks are to the extreme right. The overhead control panel (F) contains the main electrical generation and system state indication, and engine start switches. The engine fire warning and control panel (G) provides automatic warning of a fire in an engine bay and a push button to release fire extinguishant into the bay. (H) is the electrical bay smoke detector indicator. In the particular layout shown, the radar is to the far left (I); two VHF radio sets (J) are incorporated, but these depend upon customer requirement.

(iii) Performance. The waterspeed/waveheight performance is shown in Figure 5.46. The performance bands have been constructed on the basis of a large number of trials carried out by the company. The width of the bands shown for beam wind and into wind conditions represent: a) the variation between lightweight (32 tonnes) and maximum operating weight (41 tonnes), and b) variation in wave length to wave height ratio.

All hovercraft are sensitive to operating trim angle, a variation of 0.25° can affect the speed by as much as 4 to 5 knots under calm conditions. In rough conditions, the craft is less sensitive to trim. As noted earlier, the craft is provided with a ballast system which permits the captain to vary the craft operating trim to suit the conditions of a particular operation. Downwind performance is generally similar to that in the beam wind condition.

The curves illustrate achievement with the engines at a cruise power of 335 kW (450 HP). The use of maximum power (391 kW (525 HP)) will give speed improvements of the order of 2 to 4 knots, depending upon sea state. In the interest of engine life, this is normally restricted to 10% of the total

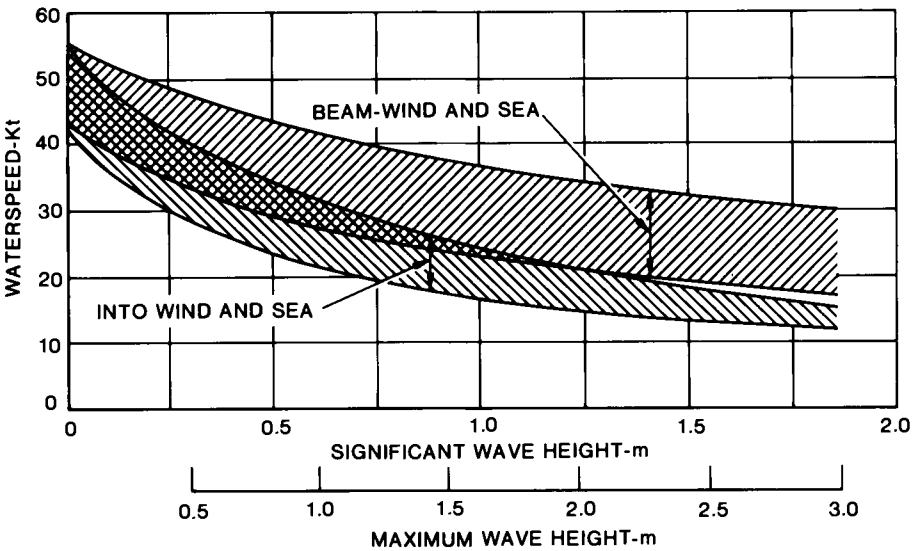

Fig. 5.46 AP.1-88 waterspeed/waveheight performance.

operating time.

The results shown in Figure 5.46 have been obtained over a temperature range 0 - 26°C. The use of turbo-charged diesels means that the craft are not sensitive to ambient temperature and the calm water performance does not vary more than 4 or 5 knots over the temperature range 0 - 35°C.

Craft fuel consumption varies between 360 litres per hour at cruise power to 410 litres per hour at maximum power. Overall fuel consumption will depend upon the proportion of idling and low speed operation involved. For short routes, values of 270 litres per service hour have been recorded.

(iv) Operations. Hovertravel Limited has operated a hovercraft passenger service between Ryde, in the Isle of Wight, and Southsea, on the English mainland, since 1965. This company was closely involved with BHC in the early design stages of the AP.1-88. The route is approximately 4½ nautical miles (Fig. 5.47) and the journey takes less than ten minutes.

The service runs in competition with Sealink, who operate fast catamarans on a parallel route between Ryde and Portsmouth. However, in addition to being considerably faster, the AP.1-88's amphibious capability eliminates the need for the half mile train journey along the pier at Ryde, which the Sealink passengers have to make. Ryde is a good example of how a hovercraft service can be integrated with the land transport system, the terminal being within yards of the main bus and rail services (Fig. 5.48).

Overnight maintenance is carried out at Ryde but the main maintenance effort is at a separate engineering base further along the coast of the Island.

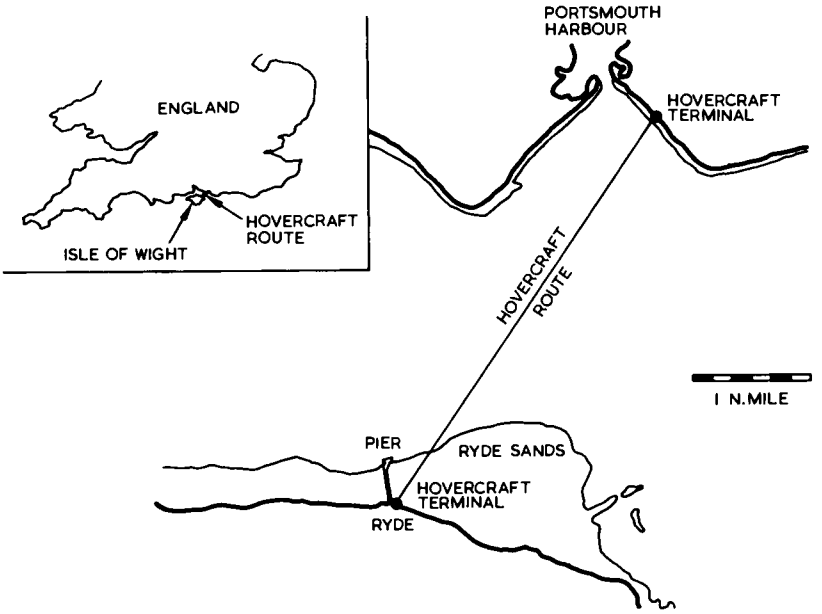

Fig. 5.47 Hovertravel route.

Fig. 5.48 Terminal at Ryde.

A major section of this maintenance is the replacing of the fingers on the flexible skirt with an average finger life of between 750 and 900 hours.

Since the introduction of the AP.1-88, Hovertravel has carried close to 2.25 million passengers with an average load factor in the region of 50%. Because much of the traffic is seasonal, the Isle of Wight being a holiday resort, factors nearer to 70% are achieved in the summer months. Overall service reliability of approximately 99% has been achieved throughout with each craft operating about 2000 hours a year.

A feature of the Hovertravel service was the need to keep the spray to a minimum, particularly at the bases, because of their closeness to the populated areas. The craft is therefore fitted with a spray skirt (Fig. 5.49), an additional apron outside the main skirt which very effectively deflects the spray downwards towards the water.

Damskibsselskabet Oresund A/S (DSO) opened a service in June 1984 using two production AP.1-88s to link Kastrup Airport (Copenhagen) in Denmark to Malmo in Sweden (Fig. 5.50). The route is across the 21 km (13 mile) wide Oresund Sound which separates the two cities and the crossing takes about 35 minutes. The service permits international airline passengers to book-in at Malmo and be delivered direct to the airfield. At the Malmo end of the route, no suitable land facilities were available for the hovercraft base; so the craft uses a

Fig. 5.49 AP.1-88/80 fitted with spray suppression skirt.

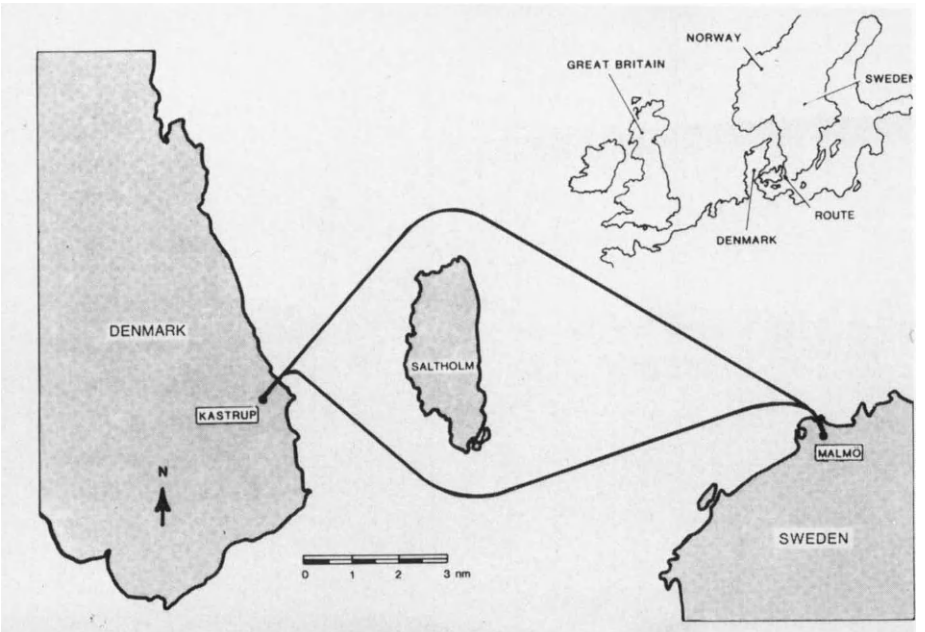

Fig. 5.50 DSO route.

floating pontoon (Fig. 5.51) moored alongside the quay.

An important feature of the service is that the craft can continue to operate throughout the winter months when the Oresund freezes up and normal services, such as hydrofoils or catamarans, are impossible. The three winters during which the craft have operated have been the severest experienced in 40 years and the combination of ice breakers keeping open the fairway and movement of the ice due to tidal flow and wind effect has resulted in pressure ridges in the ice over 2 metres high; furthermore, being newly broken, the ice is extremely sharp. This has created a need to develop improved protection for the skirt bag in order to prevent its life being reduced by the cutting action of the ice. Consideration is also being given to increasing the proportion of the lift power in icing conditions since model tests have shown that this gives a significant improvement (Fig. 5.52).

To the end of 1987, a total of about 420,000 passengers have been carried on the service, each of the two craft having operated for approximately 4250 hours. Service reliability has been in the region of 95% with a dip to 80 - 85% in the winter, due mainly to weather conditions. Reliability outside the winter period is governed more by craft availability, as the service requires both craft to be operational at peak times every day. Load factors are generally in the region of 34 - 50% but dip to 25% in the July/August period when there is a fall-off in business travel.

Fig. 5.51 Terminal at Malmo.

Fig. 5.52 DSO craft operating over ice.

The Hoverwest operation (Fig. 5.53) was set up to provide a fast ferry service between Victoria at the southern tip of Vancouver Island and the Expo '86 World Fair in the city of Vancouver, a distance of approximately 130 km (71 nautical miles) (Fig. 5.54). A single AP.1-88 hovercraft was leased from BHC for the six month period and started operations in mid-May 1986. The route length was considerably longer than anything previously operated by a hovercraft; the journey time was about two hours. However, the relatively sheltered aspect of large sections of the route, the provision of onboard refreshments and the general attractive route made the journey acceptable to the passengers. Two trips each way per day were scheduled. The service operated 7 days a week and, during the 120 day period of the lease, the craft totalled 1200 operating hours and carried 18,000 passengers. A service reliability of approximately 94% was achieved and, in view of the fact that this was a single craft operation with a very difficult schedule on a long operation, was considered to be very satisfactory.

In 1985, the North Queensland Engineers and Agents (NQEA) Limited shipbuilding company secured a lease from the British Hovercraft Corporation for the manufacture of the AP.1-88 hovercraft. The first craft (Fig. 5.55) was built in Cairns and was launched in November 1986. On completion of its trials, the craft then carried out a 4000 km (2500 mile) journey down the east

Fig. 5.53 Hoverwest craft at EXPO 86.

Fig. 5.54 Hoverwest route.

coast of Australia to the Port of Melbourne in Port Philip Bay. The journey took 11 days and sea states up to 3 m (10 ft) were encountered during the trip. Refuelling was carried out on suitable beaches and the trip was satisfactorily completed with no major problems. The craft entered service on 12th January 1987, providing a commuter service round Port Philip Bay (Fig. 5.56). The service attracted considerable attention but has been affected by a higher than expected weather cancellation rate. Apart from an unfortunate incident in which the failure of an hydraulic hose led to a propulsion bay fire, the craft has operated satisfactorily with no major problems. Two further craft have been built by NQEA and are now in service on the East Coast of Australia, providing rapid tourist transport from airport to hotel and also operating out to the Great Barrier Reef.

Hovertransport A/S leased an AP.1-88/100 from BHC to carry out a trials operation in Oslofjord (Fig. 5.57). This service, started in May 1988, provided a commuter service and an airport to city centre service. The region

Fig. 5.55 First AP.1-88 hovercraft built by North Queensland Engineers and Agents Limited, Australia, under lease from BHC.

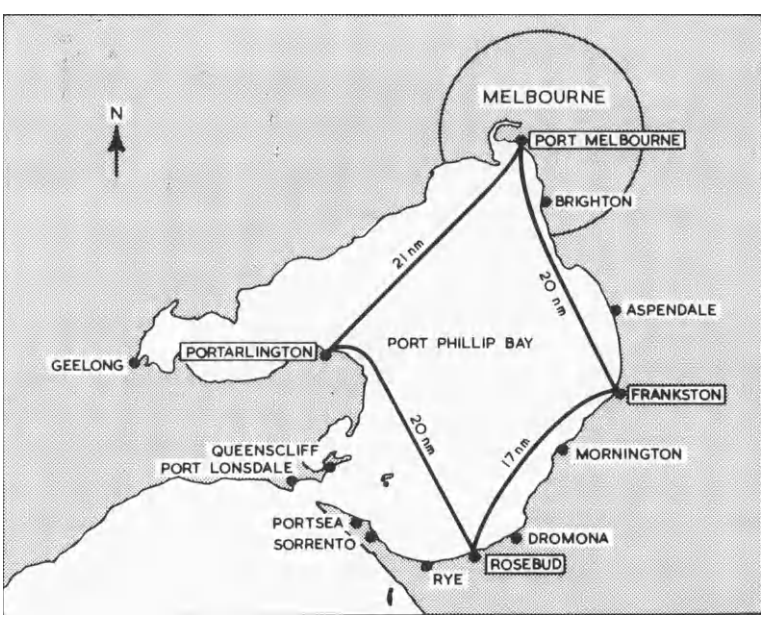

Fig. 5.56 Commuter service route round Port Philip Bay, Australia.

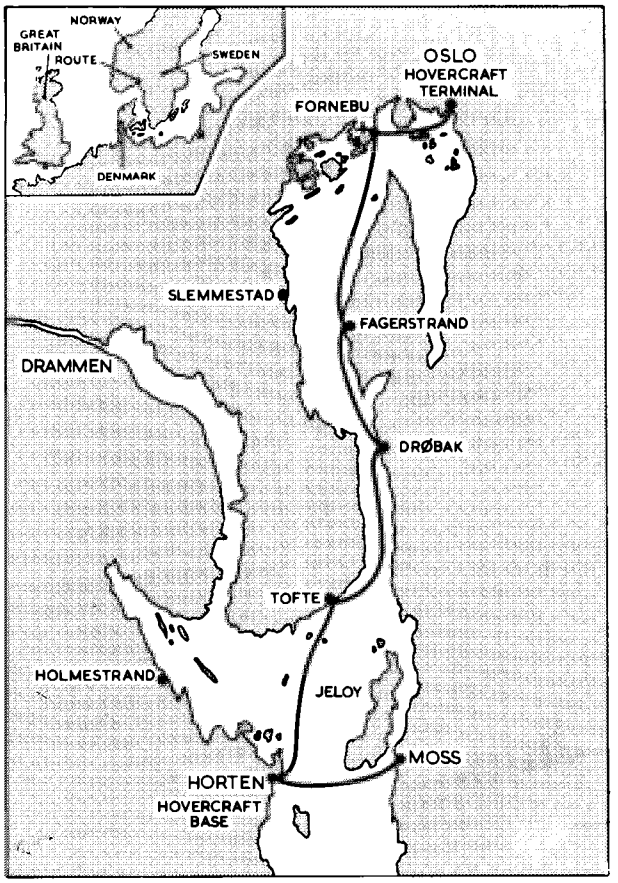

Fig. 5.57 Hovertransport routes in Oslofjord, Norway.

and nature of the terrain are such that road distances are long and extremely congested particularly close to Oslo. This route also had the potential to operate for the whole year, although the fjord usually freezes over and prevents the operation of normal waterborne traffic. The AP.1-88 operations to end of 1987 can be summarized: a) total number of craft built = 9, b) total cumulative operating hours = 24,000, c) total number of passengers carried = 2.7 million, and d) approximate distance covered = 1,325,000 km (720,000 nautical miles). These figures show that this craft is now well beyond the proving stage and is beginning to make its mark as a commercial ferry vehicle.

v) Operating costs. The total operating costs of any vehicle will depend on a large number of factors. They divide up into direct and indirect components and each of these in turn will be fixed or variable, i.e. independent or dependent on vehicle usage.

Since no two operations are the same, the following numbers quoted are limited to direct variable costs. These should be reasonably independent of local labour costs, finance charges and annual utilisation of craft; they relate purely to fuel consumption, use of spare parts and overhaul of machinery, i.e.; items that can be related reasonably to operating hours.

Even so, the following basic assumptions are made based on the practical experience of four different AP.1-88 operations:

a) The operation is predominately over water, with properly designed slipways to minimize skirt finger and cone wear. Under these conditions, skirt fingers should last about 750 hours and stern cones 500 hours.

b) Skirt finger and cone usage is the largest single component of maintenance cost. It is assumed that fingers are made by the operator using his maintenance staff who would otherwise be on waiting time.

c) Fuel consumption is very dependent on the nature of the route. Short routes usually produce lower hourly consumption than long ones due to a high proportion of time operating at low power settings associated with manoeuvring on the pads. This is well illustrated by comparing the 7.4 km (4 nautical miles) route across the Solent, which produces fuel consumptions as low as 195 litres (43 gallons) per hour, with the 145 km (78 nautical miles) Vancouver to Victoria operation, which produced consumptions up to 295 litres (65 gallons) per hour. For the purposes of this example, 65 gallons per hour is assumed.

d) The large majority of mechanical components on the AP.1-88 is maintained on an *on condition* basis. However, sufficient data is now available to include typical engine and transmission maintenance costs based on operator experience.

e) A contingency of 20% is allowed for repair of items not normally covered by regular maintenance (such as heaters, trim, paintwork and other unscheduled occurrences). This is again born out by experience.

Thus, typical direct variable operating costs of the AP.1-88, as of August 1987, can be summarized as follows:

		£ Sterling/Hour
1)	Fuel: 65 gallons (295 litres)/hour at £0.62/gallon	40.30
2)	Engines and transmission: scheduled maintenance plus mid-life overhaul, oil, propellers (renewal and repair of erosion strips and sealing)	10.32
3)	Shirt: regular renewal of fingers and cones, periodic replacement of stability and keel trunks. (Skirt bag is usually repairable on an indefinite basis)	23.89
4)	Allowance for unscheduled and other items: 20% of scheduled items	6.84
	Total direct variable hourly operating cost	£81.35

Other direct elements of cost need to be considered. The AP.1-88 normally operates with a crew of 4, i.e. captain, navigator and two cabin attendants. The navigator is usually also a captain as this enables effective use of captains whose hours in command are often limited by the regulatory authorities. The total number of crews employed will depend on service frequency and craft utilisation, typically 2½ crews will be needed to operate 2500 hours/year, 6 days/week. Maintenance requires around 2 man-hours per operating hour, although the requirement to have engineers on standby duty whilst the craft are operating will usually entail additional staff. A single craft operating 2500 hours/year will typically require 4 engineering staff. Hull insurance tends to run at 2 - 2½% of value per annum. Payload and third party insurance varies considerably according to the location, being as high as £1000/seat per annum in parts of the USA!

Based on the foregoing data, a figure of merit for the cost of operation of an AP.1-88 can be stated. Given a craft configured with 81 seats, toilets and galley operating 2500 - 3000 hours/year on a reasonably sheltered route, overall seat-mile costs (including financing and overheads) of £0.11 to £0.13 per seat mile should be achievable.

5.4.3 Craft for the Canadian Coast Guard

In 1983, the Canadian Coast Guard approached British Hovercraft Corporation for a hovercraft which could carry out a wide range of missions on the St. Lawrence Seaway. The Canadian Coast Guard is responsible to the Canadian Government for the control of the seaway, including the support and supply of navigation aids, pollution control, search and rescue, and flood control by means of ice breaking. The specification that the Canadian Coast Guard gave BHC included the following mission profiles.

(i) Re-supply of manned and unmanned navigation light stations (lighthouses). This involves the transport of large quantities of diesel fuel to unmanned stations and fuel, water and other supplies to manned stations. These stations are situated on islands, rocky cliffs, or free standing on the river bed and many are in remote areas. In addition, the hovercraft is to support the building of new fixed aids in inaccessible terrain by transport of personnel, equipment, material, tools, etc.

(ii) Floating aids positioning. Because the St. Lawrence Seaway freezes up during the winter months, conventional navigation buoys have to be removed in the autumn and replaced by spar buoys which can survive the movement of ice over them. The navigation buoys are replaced in the spring when the ice is clear. The craft has also to be capable of servicing the floating aids, checking position, etc.

(iii) Positioning of tide gauges. These are used to measure the height of the tide so that accurate water depth in the channel can be determined by

sounding vessels. The gauges are driven into the river bed in a series of predetermined positions and speed is required to move from site to site as quickly as possible.

(iv) Pollution control. The hovercraft is to carry a variety of pollution control equipment to the site of pollution and be able to deploy oil booms and provide a platform from which recovering equipment could be operated.

(v) Medical evacuation. The craft is required to be able to travel at high speed to a ship or shore site in order to transport a sick or injured person in speed and comfort to a suitable medical centre.

(vi) Search and rescue. The requirement is to locate and rescue or provide assistance to persons in distress in the marine environment with provision for a lengthy search day or night, if required.

(vii) Ice breaking. The St. Lawrence Seaway is kept open during the winter, as far up as Montreal, by means of ice breakers. However, in the spring thaw, ice jams, particularly in the tributary rivers, can result in severe flooding. It has been found that a hovercraft of about 40 tonnes can break ice up to a thickness of over one metre (3.3 ft) and the craft would be required to minimize flooding over the length of the St. Lawrence during the spring thaw.

The advantage of the AP.1-88 hovercraft is that the basic arrangement can be adapted to suit a range of different roles. To fulfill the requirements of the Canadian Coast Guard, the half well-deck version was chosen (Fig. 5.58). It can be seen that the lift and transmission systems remain the same as the basic craft but the cabin has been removed over the forward end of the craft, leaving a well-deck on which a variety of equipment can be carried. The craft has a bow ramp and a hydraulic crane, mounted on a wheeled chassis, which can be drawn up onto the craft and bolted into position. The crane has a lift capacity of 11 tonne metres. Together with a capstan on the port side foredeck and a winch on the starboard side foredeck, all driven from an auxiliary hydraulic system, it permits the craft to be used for the handling of navigation buoys, raising of the buoy sinkers, and loading and off-loading heavy items. Auxiliary power is drawn from a pump mounted on the forward end of the port lift system which can be clutched-in when hydraulic power is required. The lift system is then run at just above idle speed to provide the necessary power requirements. In the re-supply role, the crane is removed from the deck, and diesel fuel and drinking water are carried in large flexible bag tanks. Obviously a range of other materials and supplies can be carried on the well-deck. The cabin supplies day-time accommodation for up to 10 personnel, complete with galley and toilet, and 4 bunks are provided for long-range sorties. Stretcher facilities are also included to cover the medivac and search and rescue requirements.

Fig. 5.58 Canadian Coast Guard half well-deck craft.

The craft is required to operate at long distances from its base at Montreal and is therefore equipped with a fuel system capable of taking up to 6000 litres (1320 gallons) of fuel. The craft is required to operate from unprepared beaches and to be supplied by fuel trucked in to the nearest convenient point. To assist in maintaining the craft away from base, the craft jacking units can be carried either on the craft or by lorry to the operating site.

The craft is designed to operate in temperatures down to -40°C and is equipped with an anti-spray skirt for cold weather operation. This reduces the ice build-up on the craft considerably. In addition, electrical de-icing of the propeller ducts and the fan air intakes is provided. Because of the high power requirement, an auxiliary power unit is supplied. Heating is also provided in critical areas to prevent waxing of the fuel and ensure the operation of the craft in very cold conditions.

The control cabin is positioned above the main cabin and has been enlarged to include the necessary equipment for all the roles for which the craft is designed. The operational principles, however, remain the same as on the standard hovercraft. The craft is equipped with floodlights and with two Nightsun searchlights to assist in roles carried out during the night, particularly

search and rescue. Because of the wide range of equipment and roles, the craft weight has been increased to 44 tonnes and up-rated versions of the Deutz air cooled engines have been fitted to maintain performance.

The adaptation of the AP.1-88 for the specific requirements of the Canadian Coast Guard is typical of the way in which the craft can be altered to suit a particular role requirement. Other versions include the full well-deck craft (Fig. 5.59) which can carry vehicles or other payloads up to a total weight of 9.8 - 11.8 tonnes. The AP.1-88 has now demonstrated its capability as a fast passenger craft in many parts of the world. The advantage of its amphibious capabilities has been shown, not only in its operation over ice and in shallow waters, but also in its ability to operate in areas where floating debris provide a hazard for more conventional marine craft.

5.5 SUMMARY

In any good ship design, balance must be achieved through consideration of all of the factors affecting the design, as well as their interdependency. We have shown how lack of adequate resources, such as inability to make repairs at sea, causes a serious degradation of reliability and supportability. Similarly, lack of adequately trained personnel in the Fleet threatens both supportability and reliability. Conversely, growth in one factor, such as reliability, can reach a point where it is no longer commensurate with the resources applied. It becomes impractical at that point. If the ship's mission, operability, reliability, supportability and cost have all been assessed and balanced against each other, we shall have considered all of the factors required in good ship design. No single desired characteristic should be allowed to drive one of the factors to the point where it dominates the

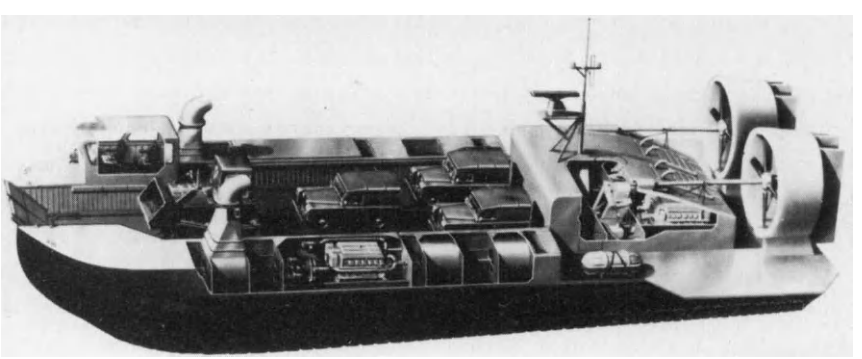

Fig. 5.59 Cut-away for well-deck craft.

design. Section 5.2 illustrated relationships between two of these factors which are often ignored: reliability and supportability.

The determination of the true cost of any vehicle is not a simple matter and many factors come into play to provide the final cost figure. This is true whether determining the acquisition cost or the operating cost of any particular vehicle. While the costing of a particular hovercraft requires the detailed knowledge of specific labour rates, overhead burdens, tooling costs, etc., of a particular builder, there are general trends that can be used to determine the likely cost of a new vehicle to a reasonable accuracy. The various equations that make up these trends were presented in Section 5.3, where they were grouped according to whether they pertained to the acquisition or operating costs of the hovercraft.

First there was the rather surprising relationship of equation (5.2) that showed the general acquisition cost equation applicable to any vehicle (ship, aircraft, tank, hovercraft, etc.) with a known empty weight W_E, installed power P and quantity built N. While clearly such a relationship is of insufficient accuracy to predict the cost of any particular vehicle, it does show the relative importance of those three key parameters. Because hovercraft rely on power for both lift and propulsion, one can see from this relationship why power (and indirectly, speed) plays such an important part in the cost of hovercraft. Any power-saving devices, such as high-efficiency lift fans and low hover gaps, should be considered in the design of hovercraft because of the direct impact on cost.

A more detailed method, the *cost estimating relationship* (CER) method, for determining the cost of a hovercraft was shown to be that which was developed for the ANVCE Program. It *built up* the vehicle cost from a detailed knowledge of its seven subsystems and two design and support functions, i.e., use of the U.S. Navy's Ship Work Breakdown Structure (SWBS). The cost of the lead or first craft was given by equations (5.6) and (5.7), in which the constants allowed for variations in the cost of each subsystem depending on the complexity or type of design being used in the hovercraft. For example, the cot of a propulsion system in a hovercraft would be different for a diesel engine powerplant than for a gas turbine powerplant installation even if each system was for the same power. Thus, the cost of hovercraft can be built up once the system characteristics are known or anticipated. This method is particularly useful if design changes are contemplated and the designer wishes to determine their impact on the cost of the hovercraft.

To determine the reduction in costs due to production of a number N of hovercraft, the learning curve method provides the basic information. The formulation used here was based on the cumulative average progress curve given by equation (5.9). There is disagreement among analysts as to the correct

shape and form of learning curves and usually each manufacturing firm keeps a set of data peculiar to its own operations on the effect of learning. Such data includes effects of manufacturing operations, tooling changes and other variables. It is sufficient to be aware of the effect. in the absence of detailed information of a particular manufacturing operation, the relationship summarized here provides an indication of what might be likely cost reductions in the production of a small number of hovercraft.

While there are several detailed methodologies available, usually in the office of operating companies, the adaptation of the Air Transport Association (ATA) method has been shown to be adaptable to hovercraft operating costs. The basic form for the *direct operating cost* (DOC) was given in equation (5.28). The DOC can be determined in dollars per mile or dollars per kilometer depending on the choice of units. For each particular route, the operating costs are determined by the key parameters of fuel consumed W_F, stage length (or range) R and block speed V_b. The coefficients in the equation reflect the operating costs peculiar to the vehicle, facilities and other functions. Specifically, they account for insurance, crew costs, maintenance costs and amortization. Also, through use of the range equation (5.36) for hovercraft, the effect of various design choices on the operating cost can be determined.

Costs are a difficult item to provide specific relationships for in either case of acquisition or operating. This is because they depend on the particular situations that exist at the manufacturing plant and at the operating company. Despite these difficulties, however, general methodologies for both acquisition and operating costs were presented. With care, they can be used to provide relatively accurate cost estimates and to determine where the main *cost drivers* lie. The cost relationships provided here offer rapid techniques for exploring cost reductions. However, references were given for more detailed treatments of hovercraft costs. This is important in that to become more widely accepted, hovercraft costs must be reduced to more competitive values in may application areas.

The operation, economics and technical features of the SR.N4 (called Super 4) series and the AP.1-88, two of British Hovercraft Corporation's (BHC) most successful craft, were described in Section 5.4. The design of the Super 4, the world's largest hovercraft, which continues to carry passengers and vehicles across the rough waters of the English Channel in all but very extreme weather conditions, incorporated features which made it a significant advance in the transport efficiency of hovercraft as a result of intensive research and development. The design earned the 1978 Award for Innovation in Transport of the Worshipful Company of Coach Builders and Coach Harness makers. The step in transport efficiency achieved with Super 4 was used to create the world's first diesel engined amphibious hovercraft, the AP.1-88, which is operating reliably

in the Solent, Scandinavia, Australia, the U.S.A., and Canada. This craft incorporates many design changes which have: a) halved capital and operating costs relative to previous amphibious hovercraft, b) given the craft much increased controllability in high winds, and c) significantly improved comfort in rough seas.

It is thought possible that the current AP.1-88 technology can be extended upward in size to craft of perhaps 150 tonnes all-up-weight. The technology may also be applicable, in part, to the design of a new generation of cross-Channel hovercraft. Although they may not necessarily follow the AP.1-88 in having diesel engines, they are perhaps more likely to have modern gas turbines which, while not as fuel efficient as the diesel, would be a major improvement on the turbines fitted to the SR.N4s.

5.6 REFERENCES

1. S.D. Judge and P. Leutjen, Determination of shipboard repair parts, level, Naval Engineers Journal, April 1979.
2. D.J. Vitale, Maintainable by design, High Speed Surface Craft Exhibition and Conference, Sussex, United Kingdom, June 25, 1980.
3. D.J. Vitale, A common sense approach to maintainable design, Fourteenth Canadian Symposium On Air Cushion Technology, Canadian Air Cushion Technology Society, Canadian Aeronautics and Space Institute, September 22-24, 1980.
4. Establishment of reliability and maintainability data base for shipboard machinery, Final Report, Vol. I, Publication OE13-01-1-1224, ARINC Research Corp., March 1973.
5. T.L. Meeks and P.J. Mantle, The Advanced Naval Vehicle Concepts Evaluation, American Institute of Aeronautics and Astronautics/Society of Naval Architects and Marine Engineers Advanced Marine Vehicles Conference, Paper 76-846, September 20, 1976.
6. J. Rhea, A Compass for the Crystal Ball, Sea Power Magazine, January 1978, pp. 31-35.
7. P.J. Mantle, Air Cushion Craft Development, US Government Printing Office, Stock Number 008-04700291-2, Report Number DTNSRDC 80/012, January 1980.
8. D.M. Dix and F.R. Riddell, Projecting Cost-Performance Trade-Offs for Military Vehicles, Astronautics & Aeronautics, September 1976.
9. J. Moy, Ship Construction Cost Estimating Relationships for Advanced Naval Vehicles Concept Evaluation (ANVCE) Study, Naval Ship Engineering Center Report 6112DE-045-77, August 1977.
10. J. Watson Noah, Inc., Cost Analysis of Advanced Naval Vehicles, Report FR-1220-USN, October 1977.
11. D.J. Clark., J. Fien., R. Jones and D. Sheridan, The ASSET Program - A Current Navy Initiative SNAME STAR Symposium, April 1984.
12. M.D. Devine, ASSET - A Computer Aided Engineering Tool for the Early Stage Design of Advanced Marine Vehicles, AIAA 8th Advanced Marine Systems Conference, Paper No. AIAA-86-2389, San Diego, California, September 22-24, 1986.
13. PRICE reference Manual, RCA PRICE Systems, Edition 3, March 1984.
14. C.L. Salmon and A.J. Locke, The Application of PRICE to Ships and Other

Large Structures, Paper presented at the PRICE Users Symposium, Munich, September 14-16, 1982.

15. R. Jones., D.L. Mayo and D.J. Clark, The Application of the RCA PRICE Parametric Cost Model to Air Cushion Vehicles, Paper presented to International Society of Parametric Analysts, Sixth Annual Conference, San Francisco, CA, May 16, 1984.

16. T.P. Wright, Factors Affecting the Cost of Airplanes, Journal of the Aeronautical Sciences, Vol. 3, February 1936, pp. 122-128.

17. Standard Method of Estimating Comparative Direct Operating Costs of Turbine Powered Transport Airplanes (Revised version), Air Transportation Association, October 1967.

18. AP.1-88 Operating Costs, British Hovercraft Corporation Document SP.5126, Issue 2, January 1984.

19. M.D. Mant, Operational Experience with the AP.1-88 Paper No. AIAA-86-2390, AIAA 8th Advanced Marine Systems Conference, San Diego, California, September 22-24, 1986.

20. A.D. Searle, Productivity Changes in Selected Wartime Ship Building Programs, Monthly Labor Review, Vol. 61, No. 6, December 1945.

21. W.Z. Hirsch, Manufacturing Progress Functions, The Review of Economics and Statistics, Vol. 34, May 1952.

Chapter 6

ICEBREAKING

6.1 INTRODUCTION

Traditionally, icebreaking to assist shipping in ice-covered waters has been accomplished by specially designed icebreaking ships. These icebreakers essentially operate on the principle of applying massive force, requiring very high installed power. Despite many years of concentrated effort there have been few revolutionary advances in icebreaking technology. Today's major icebreaking technique still consists of expending tremendous amounts of energy relentlessly pounding away at the ice with the traditional heavy, high-powered, conventional icebreakers. Although the development of more sophisticated, economical, conventional icebreakers should continue, there has been one discovery that offers significant potential, namely, that air cushion technology can be harnassed to break certain types of ice in a very effective and economical manner. This chapter sets out to review the theoretical studies and practical operational experiences relevant to the air cushion icebreaking phenomenon.

Since the early 1970's, the use of air cushion technology for breaking ice has gone from the purely experimental stage to the point where useful operations have been routinely performed. Many ice-interested nations have conducted experiments to evaluate the potential of air cushion icebreaking. Researchers in Canada, Finland, U.S.A. and the Soviet Union have carried out extensive model and full-scale testing aimed at understanding and harnessing the potential of this technology.

Recognition of the potential of air cushion icebreaking was probably first realized after the ACT-100 air cushion transporter trials conducted by Sunoco E&P Ltd. on the fresh water ice of the Great Slave Lake, Northwest Territories, Canada, during the winter of 1971-72. The 162 tonne air cushion transporter

was being used to evaluate the behaviour of the ice and transporter during traverse of the surface. These tests were part of a comprehensive program to develop an arctic drilling system, based on the adaptation of an air cushion vehicle to be an offshore drilling vessel.

Ice fracturing traverse tests were conducted with the ACT-100 to correlate loading and speed with ice properties and relate these data to vehicle behaviour. The ACT-100 continuously broke 68 cm of fresh water ice at speeds up to 6.4 km/h. As depicted in Fig. 6.1, the ACT-100 was secured fore and aft by cables from two shore-based winches and towed at various speeds and loadings. After witnessing these tests, officials of the Canadian Department of Transport became very interested in the air cushion icebreaking concept and have, since 1971, initiated several full-scale and model tests to better understand and evaluate this icebreaking method.

Further tests on the ACT-100's icebreaking performance were made by the Canadian Department of Transport at Tuktoyaktuk, Northwest Territories, during simulated ferry trials in the winter of 1972-73. The available 56 cm of ice was broken, and successive passes resulted in breaking the ice into considerably smaller floes.

Fig. 6.1 Air cushion transporter ACT-100. (Source: Arctic Systems Ltd.).

In order to determine whether craft size was a significant parameter, further tests using the smaller Terracross H-119 air cushion trailer were conducted in Montreal during the spring of 1973. Although these tests were abbreviated, the available 23 cm of ice cover was easily broken.

Following the Montreal tests the Canadian Government set up an interdepartmental ACV icebreaking working group to further evaluate this phenomenon. The group included representatives from the National Research Council of Canada (NRCC), Department of Environment, Canadian Coast Guard (CCG) and the Transportation Development Centre (TDC). Experiments up to this time had used vehicles which had no self-propulsion capability. Therefore, one of the first priorities was to attempt some trials which would not rely on winch/cable propulsion. Studies showed that it was not practical to give existing air cushion trailers self-propulsion for navigation in ice. Thus, it was decided to use a conventional tug to push an air cushion trailer secured across its bow. It was also decided to carry out trials using the self-propelled Bell Aerospace Voyageur ACV operated by the CCG. These trials would further investigate the potential of the low-speed (static) method (see Section 6.2.1), the only method known at the time; the self-propelled Voyageur would provide an opportunity to investigate the effect of cushion pressure, since it was much lower than on the towed craft.

Tests conducted in Toronto Harbour in the spring of 1974 with a tug pushing two different air cushion trailers, Terracross H-119 and Hover-Jak HJ-15 were beset by unseasonably warm weather, causing complications that did not allow the programme to be completed; nevertheless, the icebreaking capability was again demonstrated.

Also in the Spring 1974, the CCG conducted tests with the self-propelled Voyageur, which has a cushion pressure head in the order of 25 cm water, whereas all previous experiments had used cushion pressures in excess of 49 cm water. Using the approximation that the ice thickness which could be broken was slightly less than the cushion pressure head, it was therefore expected to break about 22-23 cm thick ice at speeds up to about 8 km/h. In fact, this was fully confirmed by operating over an ice sheet of gradually increasing thickness, with the breaking action stopping when the thickness exceeded about 24 cm. What had not been expected was the dramatically more powerful icebreaking action observed as the Voyageur accelerated through the speed range of about 20 to 30 km/h on its way to the low speed test area. A large standing wave appeared in the ice about half a craft length astern, and the ice sheet over the traversed areas was continually failing on the wave crest. A hastily arranged controlled experiment was organized, where the craft speed was accurately measured and the wave and ice characteristics recorded. This was the first recognized demonstration (in Canada, at least) of the high-speed

(dynamic) method (see Section 6.2.2); at this speed, 50 cm thick ice could be broken over a path about 30 m wide. In the low speed method, the width of the ice path broken by all of the vehicles previously tested had been about 3 m wider than the vehicle. It was therefore apparent that the high-speed method, which has been repeatedly demonstrated, broke ice which was twice as thick at twice the speed, and over a path almost three times as wide. There was no opportunity to further exploit this discovery at Parry Sound, but the potential was immediately recognized as being a breakthrough in icebreaking, at least for inland fresh-water first-year ice.

The spring of 1974 was really the point at which the potential of air cushion icebreaking gained significant attention. Not only had the Voyageur convincingly shown the potential of the high-speed method, but the interdepartmental ACV icebreaking working group recommended that the Department of Transport should investigate the effect of attaching an air cushion platform to the bow of a ship. To carry out this investigation a crude model of the ACT-100 was constructed and fitted to the bow of a model of the CCG icebreaker CCGS Norman Mcleod Rogers. Tests conducted in a towing tank through synthetic ice indicated a dramatic reduction in resistance to navigation, of the order of 30-40%, when the air cushion platform was attached; also, there was a significant clearance of the ice from the track astern (ref. 1).

As a direct result of these model tests, the CCG commissioned a design study for an air cushion platform attachment to the icebreaker CCGS Montcalm. The findings of the study, conducted by Bell Aerospace Canada (makers of the Voyageur self-propelled ACV) in early 1975, indicated a relatively sophisticated and expensive platform, due mainly to an overly ambitious specification. Construction of a prototype was not proceeded with, due to the expense and the need for further full-scale evidence.

The CCG's ACV Evaluation and Development Unit was moved from Parry Sound to Montreal; in the winter of 1974-75, the Voyageur was used to successfully develop the high-speed icebreaking method. Although primarily on an evaluation programme, much useful ice management and flood control work was accomplished in Lake St. Louis (St. Lawrence Seaway) and its adjacent rivers (ref. 2). Also, unseasonably cold weather in Vancouver enabled the CCG's Hovercraft Unit there to try its hand at air cushion icebreaking; its SRN-5 hovercraft broke ice and freed some fishing boats from a frozen harbour area.

In the spring of 1975, Bell Aerospace completed a Canadian Department of Transport commissioned study for a *heavy* Voyageur. The study called for increasing the all-up weight of the existing CCG Voyageur 002 from 40,000 kg to 59,000 kg and evaluating the effect on the craft's icebreaking capabilities. Although feasibility was proven, continuing with the study of the concept could not be justified at that time.

6.2 THEORY

Rupture of a floating ice cover is effected most efficiently by imposing a normal force on the ice surface. This creates bending stresses which ultimately result in failure. Applying a horizontal force to the surface would result in a buckling or crushing failure, but would be an order of magnitude greater. Consequently, the crushing mode is resorted to only in those rare cases where bending failure cannot be achieved, as, for example, in the case of grounded ice.

A conventional icebreaking ship applies the rupture force by riding up on the ice, and thus applying some of its weight. Unfortunately, in so doing, a resistance component, which is generally of the same order, is introduced because of the bow/ice contact angle, 15° to 25° for current icebreakers, and the friction between the ice and the hull. Rough steel on ice results in a friction coefficient of 0.2 or more, but present-day hull finishes can reduce this to 0.1 or less.

Calculation of ice rupture forces have been made in connection with the safe movement of vehicles over ice (ref. 3). However, for icebreakers, the icebreaking resistance is of greater interest because it dictates the power requirement. It was only when attempting to compare air cushion icebreakers with conventional icebreakers (ref. 4) that the ice rupture load became of interest. The ratio of the ice rupture load to the induced resistance, called the *Icebreaking Index*, has permitted direct comparison between icebreakers of any type. While not an absolute measure, use of this index (ref. 5) does provide an indication as to whether proposed hull designs are likely to be an advance on current forms.

In order to give an idea of the magnitude of the rupture load required, the following empirical relationship may be used:

$$M = 100h^2 \qquad (6.1)$$

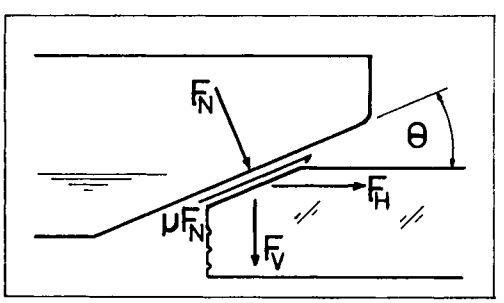

Fig. 6.2 Icebreaking forces relationship for a two-dimensional bow. (Source: TDC).

where M is the rupture load in tonnes, and h is the ice thickness in metres. For 1 m thick ice, this yields a 100 t load. However, since ice quality varies throughout the year, wide variations in this value can be expected. The relationship applies for a point load. For icebreakers, with beams of 15 to 25 m, about double the load would be required to break a path with the same thickness.

For a two-dimensional ramp bow, the relationship between the vertical force, F_V, and the induced (horizontal) resistance, F_H, can be expressed in terms of the normal force applied by the ramp on the ice, F_N, the angle between the ramp and the ice, θ, and the coefficient of friction between the ice and the bow, μ. A shear force is developed along the ramp equal to the product of the normal force and the coefficient of friction. Hence, as shown in Fig. 6.2:

$$F_V = F_N \cos\theta(1 - \mu\tan\theta) \tag{6.2}$$

$$F_H = F_N \cos\theta(\tan\theta + \mu) \tag{6.3}$$

whose ratio yields the Icebreaking Index, I_{IB}:

$$I_{IB} = F_V/F_H = (1 - \mu\tan\theta)/(\tan\theta + \mu) \tag{6.4}$$

A moving air cushion vehicle applies the rupture force by transferring its weight, or part of it, to the ice through the air cushion pressure. In so doing it will adopt a trim angle, θ, of the order of 3°, resulting in a small horizontal resultant from the cushion pressure, to which is added a drag component arising from skirt contact with the ice, of the order of 0.01 of the vehicle weight.

Hence, one finds an index of about 16 for an air cushion icebreaker whereas, for an icebreaker with a 20° ramp angle and a coefficient of friction of 0.2, the index is 1.6. As an icebreaker does not have a two-dimensional bow, this value is overly optimistic. Calculations taking into account the three-dimensional nature of a real bow yield values closer to 0.8 (ref. 5).

The following sections provide an analysis of the physical process of icebreaking with air cushion vehicles. However, a distinction must first be made between what have been termed the *static* and the *dynamic* modes of air cushion icebreaking. The static mode refers to the process occurring when an air cushion platform is pushed by a ship: ice break-up occurs quasi-statically. The dynamic mode involves creation of a wave train in the ice field, similar to that created when a hovercraft approaches hump speed; hence, the term *dynamic*.

The terms *low-speed* and *high-speed* are also used to describe these modes since the first takes place at a ship's speed (5 knots or so), while the other one takes place near the hovercraft hump speed, around 15 knots for the Canadian Coast Guard *Voyageur* (ref. 6). However, *static* operations

have taken place at up to 9 knots (ref. 7), at which speed the influence of dynamic action would certainly be contributory.

6.2.1 Static Icebreaking

An ice plate is ruptured through the imposition of a load sufficient to deflect the ice cover against the hydrostatic pressure of the water being pushed down to a point where the stresses created in the ice plate will exceed the ice bending resistance. Mathematical treatment of the case when the ice plate is unbroken has been done by Nevel (ref. 3) and others, with regard to the load-carrying capacity of an ice cover.

In a continuous ice cover the imposition of a point load results in a stress pattern that can be resolved into circumferential and radial components (Fig. 6.3). As the imposed load is increased, radial cracks will appear, followed by circumferential cracks. The appearance of radial cracks indicates that the practical load-carrying capacity of the ice sheet has been reached. This capacity depends on the thickness, elastic modulus and bending strength of the ice, as well as the manner in which the load is applied, that is, under what pressure and over what area. Since an ice cover is rarely homogeneous, mean values can be used; safe passage requires that some safety factor be applied, usually related to thickness and temperature of the ice cover (ref. 8).

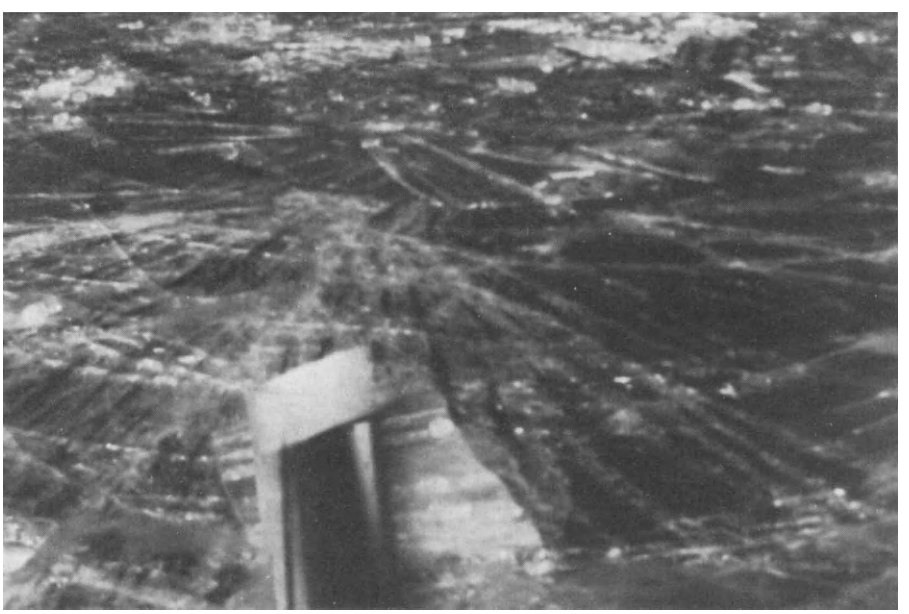

Fig. 6.3 Crack pattern after passage of CCG *Voyageur* at very low speed over 20 cm ice (Parry Sound, 1974). (Source: TDC).

When rupture is the objective, the applied load must be sufficient to produce circumferential cracks, thus transforming the ice sheet into ice blocks. At this stage, the ice cover has lost all tensile resistance. However, it is still supported by the water and by whatever compressive force may exist in the ice field. Since the ultimate objective of icebreaking is the passage of a ship, or the movement of broken ice with river current, the ice field must be disrupted so that the ice blocks will be separated and move more or less with the flow of the surrounding water.

With a conventional icebreaker, this disruption is effected by the ship's bow which, after applying the rupture load, pushes and aligns the ice blocks parallel to the prevailing water flow around the hull. Under an air cushion icebreaking bow (ACIB), disruption takes place quite differently, as differently as the method used to apply the rupture load.

(*i*) Rupture load. The ACIB hard structure does not contact the ice and its skirt is incapable of carrying out any significant load. Thus the ACIB weight is transmitted to the ice by the cushion pressure alone. When the ice field is unbroken, the approach used by Nevel for distributed loads is applicable. However, since the purpose is to break ice, that condition rarely applies, especially considering that a ship is usually pushing the ACIB. Thus the condition that applies is shown in Fig. 6.4, with the ACIB straddling the unbroken ice edge.

It can easily be seen that if the cushion pressure (expressed in terms of water column height) exceeds the ice thickness (or, to be more accurate, the ice thickness multiplied by the ice density), then the ice cover will be without support since the air pressure on both sides of the ice will be the same, namely, that of the cushion pressure. Hence, as a first approximation,

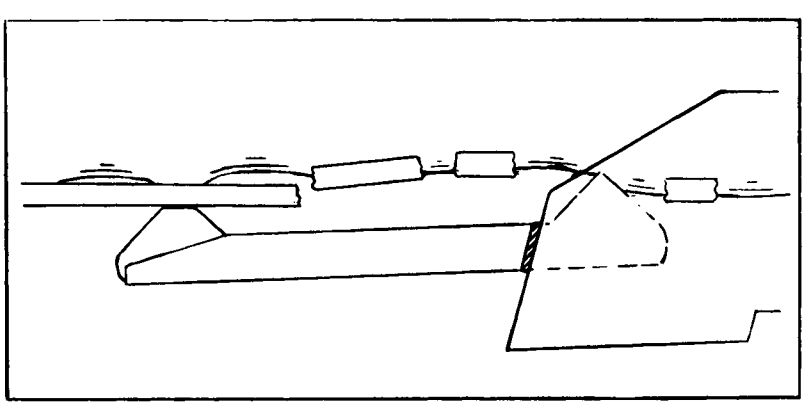

Fig. 6.4 ACIB in coupled operation. (Source: TDC).

the rupture load can be taken as that created by the weight of the straddled ice. When the cushion pressure is insufficient to depress the water level below the ice cover, the applied rupture load is that of the cushion pressure multiplied by the area of the ACIB that is straddling the unbroken ice.

(ii) Calculation of rupture conditions. If the ACIB is assumed to be circular in shape, one can calculate the rupture condition from the bending moment applied to the sector root by the sector weight (Fig. 6.5). The radius at rupture is thus:

$$R^2 = hs_r/P_I g \qquad (6.5)$$

where s_r is the ice tensile rupture strength, P_I is the ice density and g is the acceleration due to gravity, all in congruent units.

If the ACIB is wide, at least twice the ice rupture length, a two-dimensional approach may be used (Fig. 6.5). The length of the cantilevered ice piece at rupture is then given by:

$$L^2 = hs_r/3P_I g \qquad (6.6)$$

This simple approach does not take into account the ice deflection or the water support outside of the air cavity. Decker (ref. 9) used a cubic polynomial approximation for the depression created by the vehicle and assumed a radial crack pattern without an air cavity. He obtained results of the same order of magnitude as those obtained with the cantilever approximation. Carter (ref. 10) has applied the Nevel approach to the ice cover, extending the analysis from the cantilevered portion inside the cushion to the unbroken ice outside the cushion perimeter. Figure 6.6 relates the size of a circular ACIB to the thickness of the ice cover to be broken, calculated with the cantilever approach and with that of reference 10.

(iii) Disruption of the ice cover. After application of the rupture force, the broken ice drops into the cavity underneath the ACIB, where the

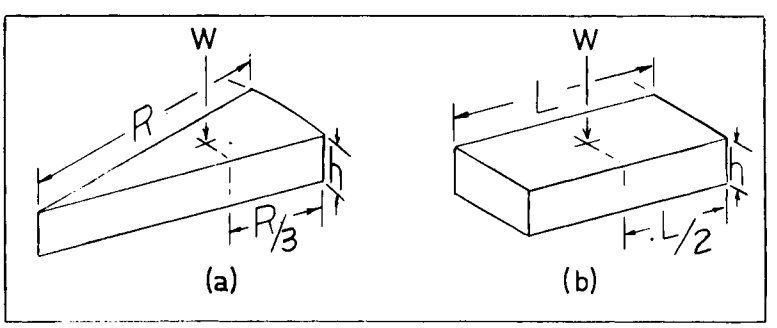

Fig. 6.5 Cantilever rupture assumption: (a) circular breaking pattern; (b) two-dimensional breaking pattern. (Source: TDC).

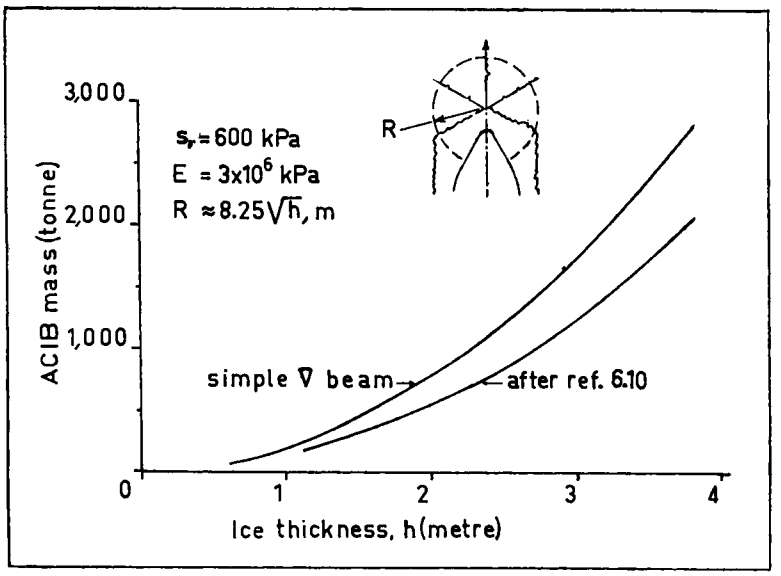

Fig. 6.6 Circular ACIB mass as a function of ice thickness to be broken. (Source: TDC).

pieces mix with the water being displaced by the bow of the pushing ship. A mixing length which permits the ice to return to the surface will minimize the possibility of the ice passing under the ship. Ideally the pieces should be displaced under the unbroken ice alongside the ship and stay trapped under it, leaving a clear track behind the ship/ACIB combination. However, at the relatively high speeds of operation, the passage of the ship induces a somewhat energetic back flow into the wake, drawing the ice floes back into the opened channel.

(iv) Effect of operational speed. The speeds attainable by the ACIB in actual operation, up to 9 knots in the 1976 operations (ref. 7), are sufficiently high (with Froude numbers of 0.15-0.25, based on ACIB length), to create wave trains within the cushion cavity. The troughs created within the cushion advance in phase with the ACIB. This explains why the cavity can move at the speeds observed in operation, without requiring an excessive cushion pressure. Such troughs help in maintaining a clearance between the bottom of the ice and the water when the cushion pressure is marginal, or when ice flexibility prevents the cushion cavity from moving underneath the ice cover.

If a bubble propagation mode is assumed the pressure in the cushion would to be sufficient to create a cavity depth, under the ice cover, equal to:

$$h' = V^2/2\,g \qquad (6.7)$$

where V is the ACIB speed. At 5 knots, the excess pressure would have to be equivalent to 0.3 m of water; at 9 knots, nearly 1 m. Such values were never observed, neither in the 1976/77 operations (ref. 7), nor during the 1982/84 operations (refs. 11 and 12). Furthermore, wave trains may not be stationary relative to the ACIB; under-ice air cavities radiating forward and laterally from the ACIB have been observed.

(v) Future developments. A number of points regarding ACIB technology still need to be resolved. Some of these, related to large ACV static and dynamic stability or to water/skirt interactions, are dealt with in other parts of this book. Air/water dynamics within the cavity, expansion of the air underneath the ice cover, and icebreaking patterns are typical of phenomena requiring further investigation.

6.2.2 Dynamic icebreaking

The phenomenon underlying dynamic icebreaking with hovercraft has been known for quite a number of years (ref. 8); it was previously encountered by truckers traveling over frozen lakes at speed. Its rediscovery at Parry Sound in 1974, when doing static icebreaking experiments with the Voyageur, led to the Canadian Coast Guard application of the technique.

The process studied here occurs when a vehicle, normally supported by the ice, starts to move forward. Following Decker's description (ref. 9), the depression created on the ice by the vehicle weight follows the vehicle, remaining centred relative to the vehicle, as long as the speed is low. As speed increases, the downward movement of the ice cover accelerates, entraining the underlying water mass until ice elasticity and water reaction stop the movement and start returning the ice toward its equilibrium position. As the vehicle is leading this movement, the return stroke is unrestrained, so the energy transferred to the ice cover by the vehicle is now dispersed through an oscillating motion. Further speed increase by the vehicle finally results in the vehicle weight being imposed too fleetingly for the ice cover to deflect locally by an appreciable amount.

(i) Analysis of ice rupture. As the hovercraft accelerates from rest, the ice deflection curve changes from its static value to a negligible value at high speed. However, at an intermediate speed, a resonance phenomenon takes place leading to large ice cover deflections and to curvatures in excess of the ice cover flexibility. The ensuing rupture occurs at a speed much in excess of that of conventional ice breakers and with much lighter vehicles.

The mathematical analysis of high-speed icebreaking has to define the resonant, or critical, speed as well as the relationship between vehicle weight, planform and ice cover characteristics. Mathematical analysis of a process is done in order to explain its behaviour in terms of known principles and, eventually, to permit extrapolation to conditions other than the ones

under which it was first observed. From a practical perspective, an analysis of dynamic icebreaking by a hovercraft should yield the following values: (a) the optimum operational speed, given the ice conditions and the hovercraft size, (b) the ice cover that can be overcome by a hovercraft of a given size, and (c) the induced drag during operation, so as to permit evaluation of power requirements.

(ii) Decker's theory. The development used by Decker in his treatment of static icebreaking (ref. 9) led to the calculation of a finite diameter for the depression created by an ACV. There are some mathematical limitations to Decker's approach (for instance, the deflection equation cannot be applied outside the calculated diameter) but, nevertheless, the theory provides a first approximation for the length of the wave imposed on the water by the depression under the ACV.

The speed of an open-water wave is calculated from (ref. 13):

$$V^2 = (gL/2\pi)\tanh v \tag{6.8}$$

where

$$v = 2\pi d/L \tag{6.9}$$

giving the wave velocity, V, for a wave of length L, over water of depth d. Decker assumed that, at resonant speed, L will be equal to the depression diameter, D, so that the water surface will have a free surface shape similar to that of the deflected ice cover, leading to a considerably diminished water upthrust. Hence, the support afforded by the water in the static case is not present anymore to counteract the weight of the ACV. This leads to an increase in the bending moment at the rim of the depression. Decker equated the energy fed into the ice sheet by an ACV riding on the forward slope of the depression to the work done on the water as the depression develops to its maximum depth.

The relation found by Decker for the weight of an ACV icebreaker is, after rearranging in terms of mass:

$$M = (13/21)10^{-3}s_r h^2/g[1-1.5(D_c/D)] \tag{6.10}$$

where M is the vehicle mass, D_c is the diameter of a circular cushion of surface equivalent to that of the ACV, and D is the ice depression diameter. This is calculated from a cubic polynomial approximation for the ice deflection, with the assumption that the displaced water weight is equal to that of the ACV. From ref. 9 the depression diameter is:

$$D^4 = 120(Eh^3)\rho_w g[1-1.5(D_c/D)] \tag{6.11}$$

where E is the ice elastic modulus and ρ_w is the water density. In solving eqns. (6.10) and (6.11), a few iterations are sufficient to yield results commensurate with the accuracy of this theory, and to the accuracy with which the values of E and s_r can be determined in practice.

The assumptions made by Decker in developing his equations are not perfectly valid. For example, when estimating the value of D, the bending moment acting at the depression periphery is neglected, although it could still support about 30% of the vehicle weight. However, in Decker's model, D and the maximum deflection are calculated by equating the displaced water weight to that of the vehicle.

Since the purpose of this calculation is to obtain a finite value of D, an approximation is nevertheless required. Fortunately, the Decker approach provides results which agreed fairly well with the results of icebreaking operations available at the time (1977) with data generally limited to ice thickness and atmospheric temperature. Results from Decker's analysis are shown in Fig. 6.7 (using the same ice characteristics as for Fig. 6.6). They are in close agreement with the icebreaking capability of the two known hovercraft that have been used in Canada for dynamic icebreaking, namely, the 7 tonne Air Trek 140 (ref. 14) and the 45 tonne CCG Voyageur (ref. 6).

The Decker analysis, which also looks into static icebreaking, yields a ratio of 3.8/1 for the weights required for static and dynamic icebreaking (in the static case, the constant 13/21 of eqn. (6.10) is replaced by 0.75π, yielding results in the range of those shown in Fig. 6.6 for the simple beam theory). Operational experience with the 260-tonne CCG ACIB and the 45-tonne

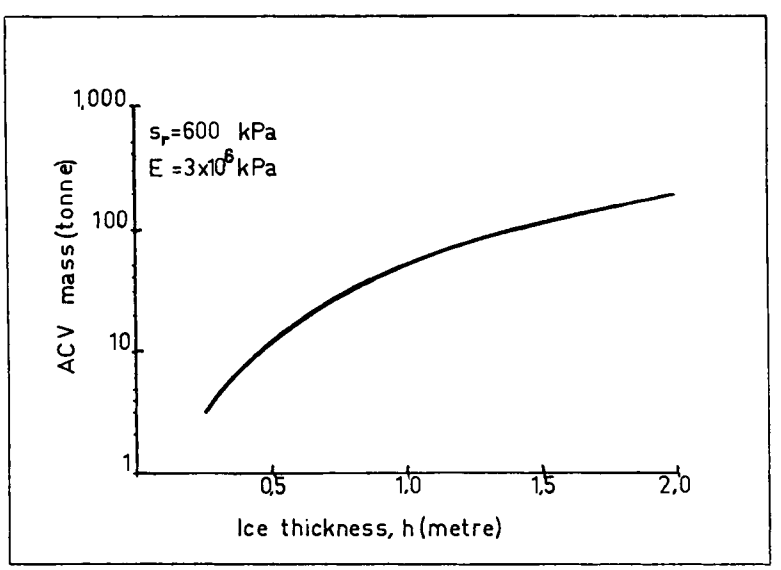

Fig. 6.7 Dynamic icebreaker mass as a function of ice thickness to be broken. (Source: TDC).

CCG Voyageur, whose icebreaking capacities are both in the 1 m range, would suggest a slightly higher ratio. However, one cannot be sure of similar ice conditions, nor of the respective efficiency of the two vehicles. It would therefore appear that Decker's ratio is a reasonable, conservative estimate.

(iii) Impulse theory. The theoretical limitation of Decker's assumption can only be eliminated if the physical process of dynamic icebreaking is analysed from first principles, or, at least, from the mechanics of a floating ice plate. This has been done by Nevel on a number of occasions, with regard to studies on over-ice transportation (ref. 3). The main difficulty encountered when applying Nevel's results to icebreaking is with the determination of the minimum weight required for rupture. Since rupture takes place at the resonant speed, with a theoretically infinite amplitude, one is faced with the so-called mouse paradox (ref. 15). That is, at resonance, a minute force would be sufficient to rupture any ice cover. In mathematical terms, the weight at resonance is indeterminate.

By assuming that the depression diameter is equal to an ice free wave of equal length, Decker was able to calculate the resonant speed. By equating the wave energy with that fed in by the ACV, he was able to determine the critical ice rupture weight without having to resolve any paradox, although by using a number of simplifying assumptions.

Shinbrot (ref. 15) reviewed Nevel's basic mathematical development and found that by introducing a damping term, prior to carrying out the Fourier transforms necessary for the solution of the problem, the paradox disappeared. Thus, by using a thin plate analogy for the floating ice, he was able to demonstrate the existence of a mathematical solution. Development of the solution was through the determination of the spatial response to a unit impulse, representing the action of an elementary portion of the air cushion. The response created by a finite air cushion was found by summation of unit impulse responses over the cushion area.

Hinchey (ref. 16) found that the wave pattern created by an air cushion depends only on the ice characteristics and on the speed of the vehicle. Hinchey used a small air jet to apply an impulse on a model ice sheet; the patterns observed can be used to verify the theoretical predictions.

(iv) Future developments. The early work by Nevel and the more recent studies by Hinchey tend to demonstrate the existence of a critical speed for dynamic icebreaking that is unrelated to the weight of the vehicle. Experimental work has validated these studies. However, there is still a need for an analysis, from first principles, that will relate the weight of a hovercraft to the ice cover that it can rupture. This will perhaps be achieved through a continuation of Shinbrot's work, or through an entirely original approach.

6.3 STATIC ICEBREAKING OPERATIONS

6.3.1 CCG Operational Experience

The possibility of using an air cushion vehicle as a means of breaking ice was perceived at Yellowknife, Northwest Territories, when, in the winter of 1971/72, the 100 t air cushion transporter, ACT-100, broke ice while being towed on Great Slave Lake. Later in 1972, further observations on the phenomenon were made in Tuktoyaktuk Harbour, when the mechanism of static, or better, low-speed icebreaking began to be understood. This understanding was reinforced by later tests at Montreal and Toronto with smaller towed air cushion barges, the Terracross H-119 and HoverJak HJ-15.

The Canadian Coast Guard also funded model tests, which, although limited in scope, indicated a reduction in resistance of about 30% when an air cushion barge was pushed ahead of a ship through model ice. Acknowledging the significance of these limited experiments, Transport Canada initiated a comprehensive program in which model and full scale testing was to be conducted over a three year period, 1975 through 1978. The ACT-100 was chartered and modified for the full scale trials.

The ACT-100 was conceived as a winch and cable driven prototype Arctic transporter for a 100 t payload. It was built for Arctic Systems Limited by the Dominion Bridge Company in 1971, and tested extensively in the Arctic. Although air cushion icebreaking had not been conceived at the time of its design and construction, it was, in 1975, the only vehicle available of suitable size and with the capability of developing an appropriate cushion pressure. It was moved from Inuvik, NWT, to Thunder Bay, Ontario where it was modified and instrumented for the program. The Canadian Coast Guard ship Alexander Henry, a twin-screw, 2648 kW diesel-powered icebreaker/buoy tender of 2240 t displacement and 13.25 m beam, was made available for the trials, and a pushing plate was added to its bow. A vee notch was incorporated in the stern of the ACT-100 to accommodate the bow of the ship, and there was no rigid attachment between the vessels. Modifications to provide the notch proved to be unexpectedly costly due to the complexity of the problem.

Because of its historic interest, some basic information on the ACT-100 notched configuration is given in Table 6.1. For the icebreaking trials, the ACT-100 normally carried a trial team of eight.

The first trials took place during the winter of 1975/76 in Lake Superior at Thunder Bay. During these trials the Alexander Henry/ACT-100 combination (Fig. 6.8) traversed level icefields ranging in thickness from 30 to 76 cm at essentially constant speeds ranging from 0.4 to 5.4 m/s (0.8 to 10.5 knots). As the ice thickness increased, the ACT-100 was ballasted to increase cushion pressure from a light condition of 51 cm of water to a maximum of 74 cm (5.0 to 7.3 kPa). The Alexander Henry was tested in one ice thickness only, 25 cm, in

Table 6.1. ACT-100 characteristics.

Length overall - structure	24.2 m
Width - structure	17.4 m
Notch depth - structure	4.0 m
Hull height - structure	2.0 m
Overall size - skirt inflated	25.4 m × 18.6 m
Maximum weight	276 t
Lightship displacement	172 t
Hover height (maximum)	1.2 m
Cushion pressure (maximum used during trials)	74.0 cm water (7.62 kPa)
Engines	2 Caterpillar D348 (each rated at 447 kW continuous at 1800 rpm)
Fans	2 Joy A-1670 Airfoil Centrifugal (each rated at 40 m^3/s at 1800 rpm and 86 cm static water pressure)

Fig. 6.8 CCGS Alexander Henry/ACT-100 combination at Thunder Bay, Winter 1976. (Source: CCG).

continuous motion at speeds ranging from 0 to 1.8 m/s (1.6 to 3.5 knots). The ship alone was brought to a halt by ice 25 to 30 cm thick, and could only proceed by ramming. The mean flexural strength of the ice varied from 400 to 900 kPa, and the depth of local snow cover varied between 0 and 38 cm. The meteorological conditions were consistent with normal winter conditions for the area. Temperatures ranged from -30°C to 6°C, wind speeds varied between 0 and 20.6 m/s (0 and 40 knots), and there were several heavy snowfalls.

Further trials were conducted in the same area during the winter of 1976/77, in which the ACT-100 was combined with three more host vessels of differing characteristics given in Table 6.2. The superior performance of the

Table 6.2. Host vessels.

	Displacement (t)	Power (kW)	Beam (m)
Thunder Cape: tug	400	1044	6.10
CCGS Griffon: light icebreaker/buoy tender	2793	2984	14.93
MV Imperial St. Clair: tanker	16450	4849	22.56

combination over the ship alone was again found to be impressive. The tug Thunder Cape, which could not normally operate in ice exceeding 12 cm, was able to break a solid ice cover 40 cm thick and with a strength of 650 kPa at a steady speed of 2.6 m/s (5.0 knots). The Griffon, which alone could not operate in ice over 35 cm thick without ramming, was able to break ice 80 cm thick and of 850 kPa strength at a steady rate of 4.0 m/s (7.8 knots). The beam of the Imperial St. Clair was some 3 m wider than the track broken by the ACT-100, and the constriction was sufficient to prohibit continuous motion in 80 cm of ice. However, ramming with the ship alone achieved an advance of only 60 m at each run, whereas, with the combination, advances of 365 m were attained.

The success of these trials prompted the Canadian Coast Guard to develop a performance specification for a purpose-built air cushion icebreaking bow (ACIB) which was the basis of a request for proposals and tenders from industry. The competition was won by Hoverlift Systems Limited of Calgary, in 1979, and subsequently a design was produced for an ACIB to be capable of breaking 0.91 m (36 in) ice. The craft was designated HSL-533, but subsequently became known simply as the ACIB. A general arrangement and leading particulars are to be found in Fig. 6.9. This is the original, as-completed configuration, which was not available until the end of March 1982, largely due to technical difficulties involved in providing a notch for the ACIB to fit the bow of the host ship. In spite of experience with the ACT-100, provision of this feature became an exercise in improvisation, and proved extremely costly. An acceptable notch seal was not achieved until preparation for the 1982/83 season, and, even then, the notching operation, which required mating afloat and then coming up to hover, was found to be awkward and occasionally hazardous.

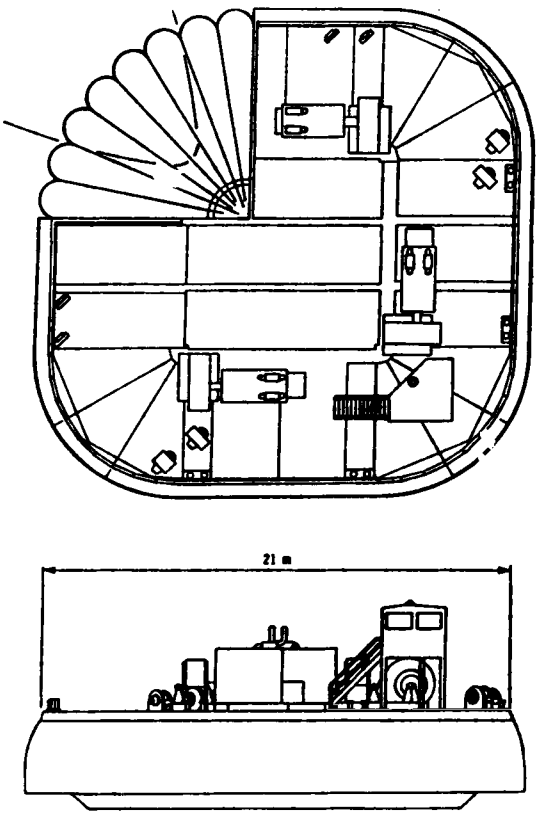

Fig. 6.9 Configuration of the air cushion icebreaking bow (ACIB): beam = 24.7 m; maximum weight = 270 t; maximum cushion pressure = 10 kPa. (Source: TDC).

Following the launch, there was only time for a brief evaluation of the icebreaking capability of the ACIB before the end of the 1981/82 season. The host ship was the CCGS Alexander Henry. Over the winters of 1982/83 and 1983/84 more extensive trials were carried out (refs. 6.11 and 6.12) and the Alexander Henry/ACIB combination was used exclusively for the ice management program in the Thunder Bay area (Fig. 6.10). On each occasion, repairs and modifications were made beforehand to rectify damage incurred and to incorporate improvements suggested by the previous season's operation.

The icebreaking capability of the combination was demonstrated to be greatly superior to that of the ship alone. When operating in essentially smooth, unbroken ice about 65 cm thick, the ship alone in the ramming mode was able to advance at an average speed of about 0.2 knot. Under the same condi-

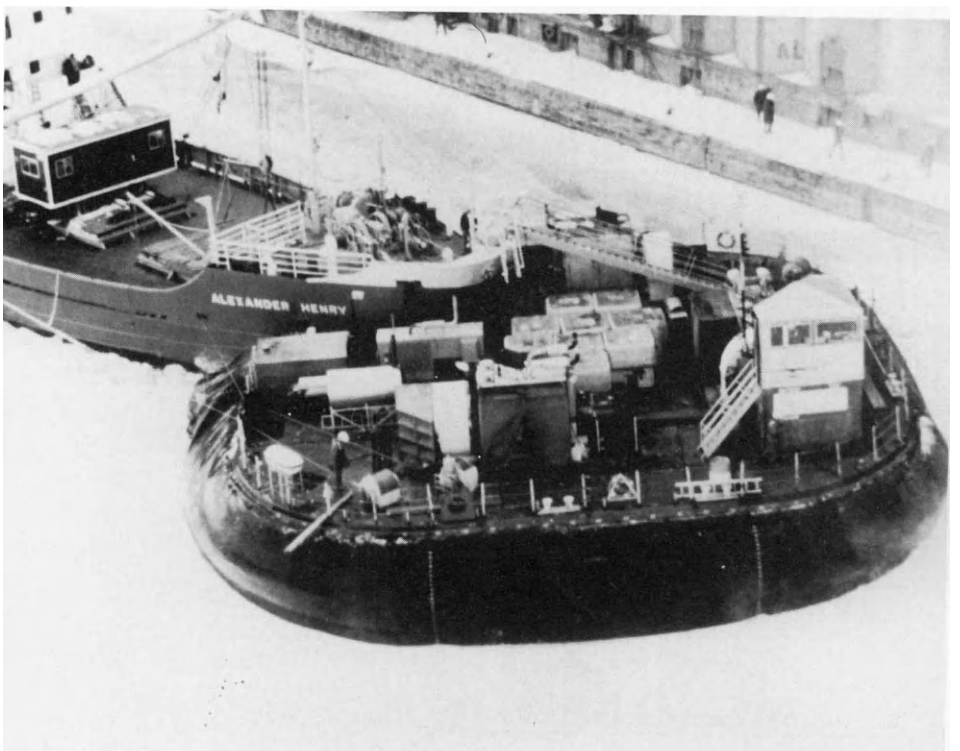

Fig. 6.10 CCGS Alexander Henry/ACIB combination in Manitoba Pool No. 1, Thunder Bay, March 1984; ice thickness to 0.95 cm. (Source: TEDC).

tions, the combination was able to proceed at a steady speed of over 4 knots, an improvement factor of 20. A general statement that the icebreaking performance of the Alexander Henry was improved by a factor of 10, an order of magnitude, when combined with the ACIB is considered very conservative. In addition, because the ship was only required to push the ACIB and clear a passage for itself through broken ice, damage to the hull structure was reduced, ice strikes on the propellers were virtually eliminated, and the power required was reduced and steady, resulting in a marked reduction in fuel consumption.

In spite of numerous problems caused by design deficiencies and the immediate operational use of an experimental craft, the ACIB was always available when required. In this connection, it is worth noting that the ACIB was operated and maintained by a crew of four contractor's personnel, a professional engineer, a design draughtsman and two technicians, none of whom had any previous experience with air cushion vehicles. Backup was obtained from local resources in Thunder Bay.

The trials were an evident success, and it was abundantly clear that ice management in and around ports such as Thunder Bay could be handled without the services of a specialized icebreaking ship being assigned for the winter. The economic implication is self-evident. Unfortunately for ACIB development, the Canadian Coast Guard was already committed to a re-equipment program which included a Type 1050 light icebreaker/navaids tender to replace Alexander Henry at Thunder Bay. It was decided to proceed no further with air cushion icebreaking, and the ACIB was disposed of as scrap.

6.3.2 USCG Operational Experience

During the winter ice season, November 1977 through March 1978, the United States Coast Guard (USCG) Research and Development Centre, Avery Point, Connecticut, conducted an operational test program. The objective was to evaluate two air cushion vehicles, one a barge and the other self-propelled, as river icebreakers for flood control and the facilitation of commerce on the Illinois and Mississippi Rivers (refs. 17 and 18).

The ACV barge was leased from Mackley Ace Incorporated (USA). Named the River Guardian (Fig. 6.11), it was a non-self-propelled steel barge type of ACV, simply designed and built according to conventional boat construction practice. Lift was obtained from two General Motors diesel engines of 447 kW each, driving two Allday and Peacock single inlet centrifugal fans with a flow rate of 22.6 m^3/s at 2,000 rpm. The hover height was 1.4 to 1.7 m and the cushion pressure was 6.5 to 8.9 kPa, depending on ballast. The platform was rectangular, with a length overall of 19.1 m and a beam of 15.7 m. A simple, flat pushing pad was fitted to the port and aft sides of the plenum structure. Because the River Guardian was not self-propelled, it had to be pushed through the ice; for this purpose, the river buoy tender CGC Sumac (WLR-311) of 354 t displacement was assigned to the project. The beam of the Sumac was 10.5 m. It was powered by three diesel engines of 596 kW maximum shaft power. Its hull

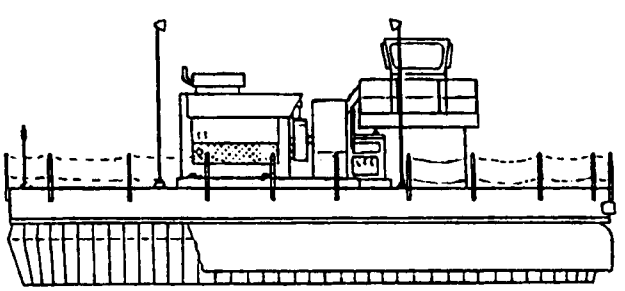

Fig. 6.11 River Guardian profile, with spray skirt cut back to reveal segments: length = 19.1 m; beam = 15.7 m; gross weight = 200 t. (Source: ref. 17).

was specially ice strengthened for the project, and fitted with ice deflectors to protect the keel coolers, rudders and propellers. Pushing knees were added at the bow. The Sumac was capable of operating at speeds up to 8.7 knots, but this was drastically reduced in ice clogged waters.

The self-propelled ACV was made available by the US Army in a joint Army/Coast Guard effort, together with crew and support personnel. It was a standard LACV-30 (Lighter, Amphibious, Air Cushion Vehicle, with 30 t payload) (Fig. 6.12). The LACV-30 has a length of 26.6 m, a beam of 12.8 m and a main deck of 156 m^2. It is powered by two Pratt and Whitney Twin-Pac gas turbine engines rated at 1,341 kW maximum shaft power. Lift capability is provided by two 2.4 m centrifugal, 12-blade, fixed pitch fans, and propulsion by two 3.1 m, 3-blade, variable pitch propellers. It has a cushion pressure of 3.4 kPa, and can attain speeds in excess of 40 knots. The LACV-30 is a lengthened version of the Bell Textron Voyageur used by the CCG.

Conditions in the area chosen for the evaluation are far from ideal for any icebreaking operation because of the shallowness of the water in the river/lake system. Navigation by towboat traffic is essentially confined to a dredged channel. In winter the extremely powerful towboats break ice and churn it up until the whole channel becomes full of slush and heavy brash ice to within a few feet of the bottom. Plates of ice from the sides of the channel break away and freeze into the slush on the surface, modules of ice being as much as 1.8 m thick. The icebreaker is therefore breaking a frozen combination of brash and

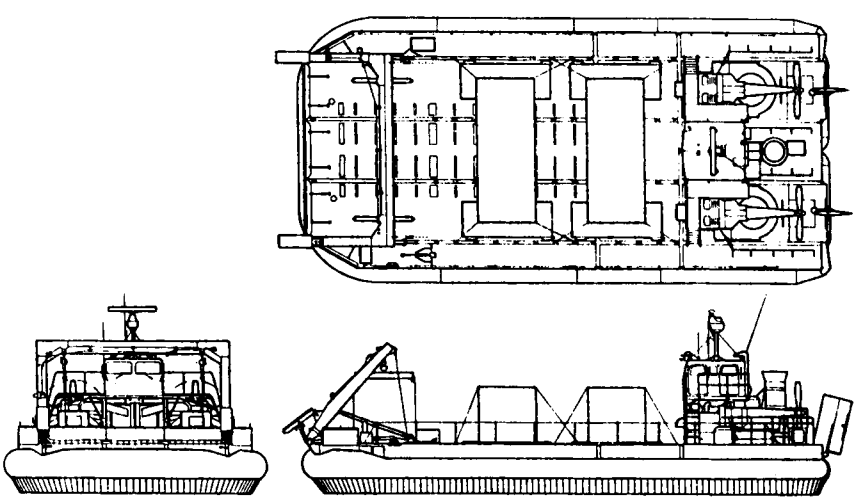

Fig. 6.12 LACV-30 profile: length = 26.6 m, beam = 12.8 m, groww weight = 52 t. (Source: Bell Aerospace Textron).

plate ice pieces over as much as fifteen feet of slush. In addition, the river current is too slow to make a significant contribution to clearing the broken ice. However, towboat operators were unanimous in claiming that, when the Sumac/River Guardian broke the channel directly ahead of them, their vessels required less power to achieve and maintain operating speed. The LACV-30 was used successfully over plate ice to assist in freeing vessels which were frozen in, and to carry out icebreaking as a flood control measure on rivers.

Both ACVs experienced maintenance difficulties, but these were mainly due to design deficiencies, inadequate support facilities and inexperience of personnel, all of which are to be expected in an operation conducted in a harsh environment for the first time. American and Canadian experience, conclusions and recommendations in this area were virtually identical. The major problem concerned the prevention, or at least the reduction, of skirt damage.

It is interesting that both the United States and Canadian Coast Guards commented on the poor ice clearing performance of the air cushion icebreaking bow, when, in fact, it does not clear ice at all, but is a pure icebreaker. The ACIB creates a situation in which the ice breaks as a cantilever under its own weight, and has no other influence on the motion of the ice, which falls into the depressed water area under the ACIB and rises to the surface at its stern. There is no hull to deflect the ice sideways, and any clearing is entirely dependent on the form of the pushing vessel.

Since one of the requirements for an ACIB is that its beam should be greater than that of its pushing vessel in order to prevent jamming in the broken channel, it follows that the ability of this vessel to displace ice under the ice sheet at the sides of the channel will be limited. Thus, the combination of ACIB and pushing vessel is not likely to have good ice clearing characteristics.

However, even a conventional displacement hull icebreaker will not provide a clear channel, because, as it moves forward, water will flow in behind it, carrying broken ice. Only specially designed hulls, such as a vessel with a Waas bow, have the potential to provide a clear channel, albeit at 2 knots or so. Thus far, pushing vessels have been assigned primarily on the basis of availability rather than suitability for the clearing role.

6.3.3 Second Generation Designs

Although the Canadian Coast Guard decided in 1985 to discontinue operations with the original ACIB, a contract had been placed earlier by the Transportation Development Centre for preliminary designs of two new air cushion icebreaking bows, designated as the Inland Waters ACIB and the Mid-Arctic ACIB, the requirements for which had been determined by survey. The design concepts for these two vessels were prepared by the personnel who had

been responsible for and directly involved in the operation of the ACIB at Thunder Bay (ref. 19).

(i) Inland Waters ACIB. The Inland Waters ACIB (Fig. 6.13) was designed for use on inland waterways or coastal areas, which would include the St. Lawrence Seaway, the Great Lakes and the East Coast of Canada as far north as Lake Melville. This craft was intended for ice management in harbours and along relatively short sea lanes, using a tug or light icebreaker as host ship. Salt and fresh water ice would be encountered, rarely exceeding 1 m in thickness and with flexural strengths up to 600 kPa. Ridge sail heights typically would be equal to ice thickness.

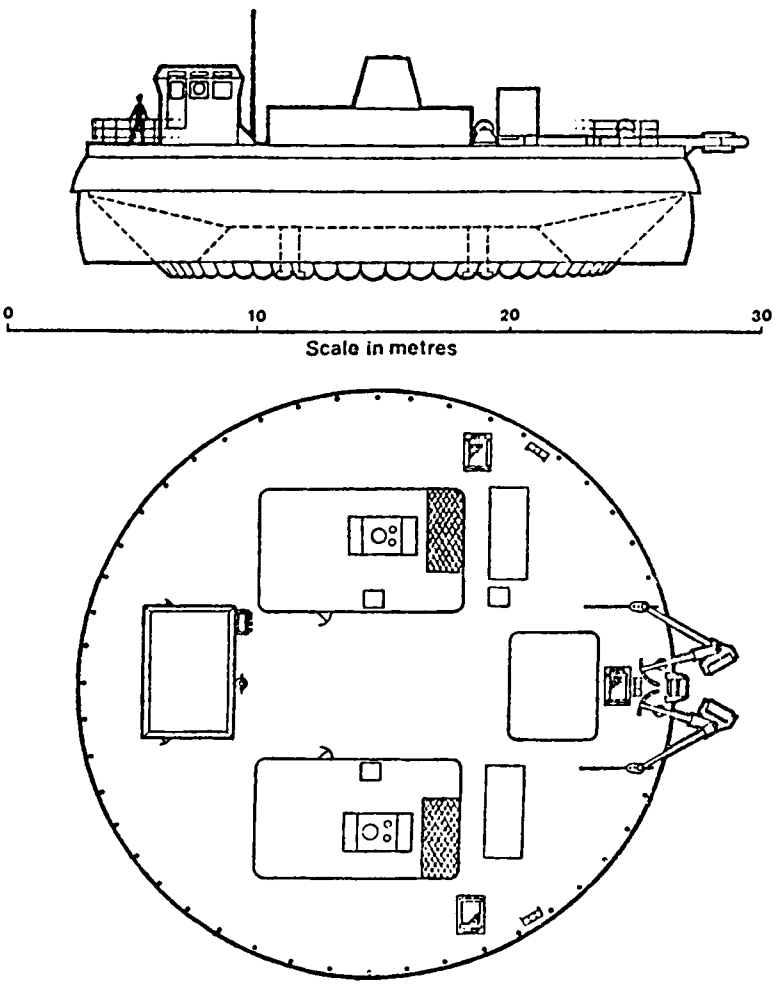

Fig. 6.13 General arrangement of the Inland Waters ACIB. (Source: TDC).

Specified to operate in ice up to 1.1 m in thickness, no new technological problems were foreseen, and, as a result, the craft was designed with the lessons of the ACIB firmly in mind and the objectives of simplicity and reliability.

The circular platform was chosen for a number of reasons. Experience has shown that ice under an ACIB fails in the classical pattern of radial and circumferential cracks, and consequently an advancing ACIB encounters a more or less circular ice edge. A circular platform also offers the best ratio of lifting area to periphery, which results in the most efficient use of lift air power and the shortest periphery. The uniform periphery permits the use of a single skirt segment type, which reduces production and maintenance costs.

A notch for host vessel attachment was not included in the design since no evidence could be found in the available literature or in the ACT-100 and ACIB trials to indicate any benefit. Furthermore, the adverse effect on design, manufacture, maintenance, operation and especially cost, was clearly demonstrated. An adjustable pushing yoke external to the cushion was provided. It was designed to allow freedom in pitch and heave, while restraining yaw, sway and surge motions.

The skirt segment design was kept as simple as possible. Its knuckleless form resulted in a small, light segment which could be stored flat or rolled. The skirt was mounted on rails along its top edges, and could be slid on and off tracks attached to the craft bottom. When installed, they were entirely underneath the craft, which would reduce the possibility of collision damage. During the ACIB trials a two-piece spray skirt was developed which virtually eliminated the spray problem; therefore, this design was selected.

Air feed to the cushion was through a peripheral duct which opened into the top of the skirt segments, providing low velocity air for the cushion and positive skirt inflation. Undercraft spray would be minimized by this system and a uniformly depressed water surface would result. The plenum was provided with an airlock and catwalk to permit inpsection during operation. The jacking system would permit the craft to lift itself while on solid, dry land to a point where the skirts would hang free for inspection or maintenance.

(ii) Mid-Arctic ACIB. The development of an air cushion icebreaker for 2 m ice thickness presents a number of technological challenges which have not yet been addressed. The requirement is well beyond any operating experience to date, and the required cushion pressure of 20 kPa is greatly in excess of anything currently in use. The high pressure and consequent high specific weight of the craft presents problems in the areas of stability, skirt material deformation and lift powering. These factors led to the concept of a rigid sidewall craft with flexible skirts at the fore and aft ends only (Fig. 6.14).

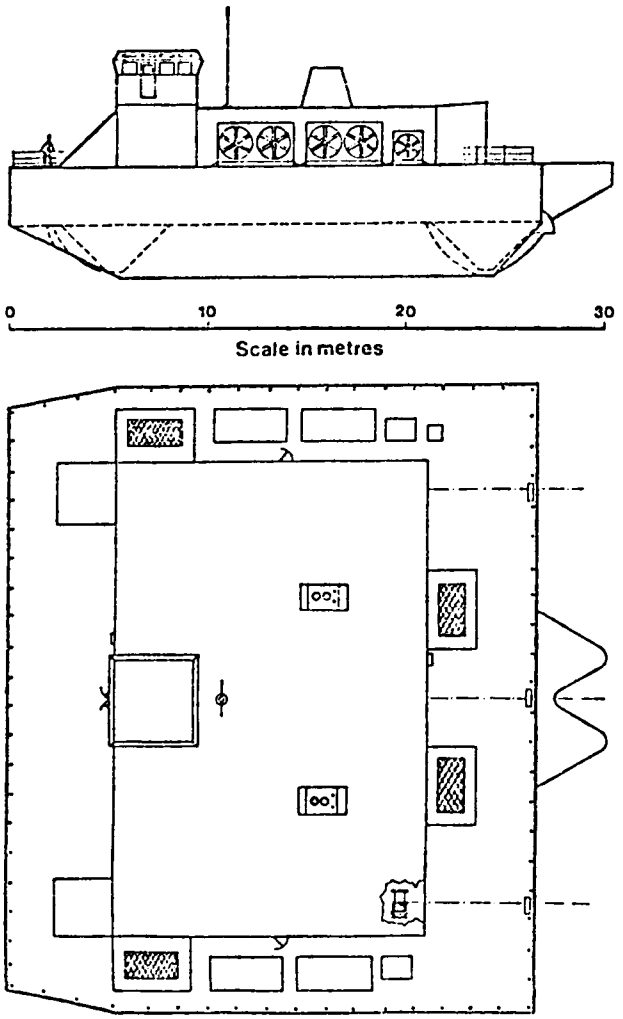

Fig. 6.14 General arrangement of the Mid-Arctic ACIB. (Source: TDC).

The partial immersion of the sidewalls of this conceptual design offers improvement in stability due to the hydrostatic forces on the structure. The solid sides could readily contain the high cushion pressure without distortion, and would minimize air leakage, thus reducing the lift power requirement. Being reduced to the lengths of the fore and aft ends, the flexible skirt periphery would permit the use of a single segment of the same simple knuckleless design employed in the smaller craft, with consequent minimal maintenance requirement. The high specific weight of the craft and the size of

the skirt segments would probably preclude over-water skirt maintenance, which would therefore best be achieved with the craft beached.

The rigid sidewall concept dictates a rectangular platform, but, by designing the leading edges of the sidewalls to provide cutting edges, it is believed that the rigid sidewalls and straight skirt runs would produce ice failure more in keeping with the prediction of two-dimensional theory. It is anticipated that the ice would fracture in a straight line, rather than the cusped pattern of three-dimensional theory which has been observed with soft-cushioned craft.

6.3.4 Observations and Conclusions

The ACIB is an accessory with which ice can be broken by any vessel capable of providing motive power. Since it does not clear ice, its host vessel must clear its own path, and its hull should be compatible with the ice through which it will pass. To minimize ice contact with propellers, rudders or any hull projections, a deep draught is desirable as well as a shear bow, unless the bow is specifically designed for ice clearing, as, for example, the Waas bow.

With the advantage of hindsight, it is clear that the American river operations were concerned primarily with clearing and not with breaking, and that an air cushion icebreaker was not the solution. The shallow, sluggish river was a special problem, which might possibly be solved by maintaining a very wide channel from the beginning of the season with an ACV, but possibly smaller and more economical than the LACV-30.

The notch of the Canadian ACIB caused considerable difficulties in mating the ACIB with the host ship. This was because mating had to be achieved with the ACIB afloat and the skirt deflated. Handling was difficult, and coming up on hover subsequently was distinctly hazardous on occasion. The American experience without a notch reduced the handling problems considerably.

The vulnerability of the skirt system must be kept in mind at all times. The ACIB should not be used when the ice can be broken by the host or other vessel alone; the thin, hard ice often encountered in such conditions can cause severe and unnecessary damage. Breaking a new track is less likely to cause damage than opening up a previously broken track with a jumble of ice pieces refrozen into it. And there is an optimum speed for a particular condition at which the tumbling motions of the ice pieces passing through the plenum are minimized. Hover height also affects the efficiency of the icebreaking process. Trim adjustments, which would be possible with a liquid ballast system, could have an appreciable effect on skirt wear and damage reduction.

To achieve reliability, rugged simplicity is needed in the design. Weight is not a critical factor when high cushion pressures are required. Particular attention must be paid to spray suppression, to protecting winches and other

handling equipment from ice, and to providing safe and convenient walkways for any deck requirements. The skirt system must be kept as simple and standard as possible, and the bottom of the hull designed to minimize ice accumulation. The Inland Waters ACIB design addressed both these features.

Because environmental conditions can be severe during the operational season, it is desirable for maintenance purposes to have as much equipment as possible under deck or under cover. Where this is not possible, as, for example, in the case of skirt segments, consideration must be given to the problems of handling and carrying out repairs in low temperatures, darkness and high winds by personnel in arctic clothing. The possibility of replacing damaged skirt segments during operation should be given a high priority.

6.4 DYNAMIC ICEBREAKING OPERATIONS

6.4.1 CCG Voyageur Operations

The Canadian Coast Guard (CCG) has been operating the Bell Textron *Voyageur* hovercraft for flood control in the lower St-Laurent River system, since 1976 (see Section 8.3). In 1987, after more than 15 years of service, the Voyageur was replaced by a BHC AP.1-88 of nearly similar all-up weight (40 tonne). The new craft is much less spartan in accommodation and uses diesel engines instead of gas turbines, resulting in quite reduced operating costs. Early reports is that it has slightly better icebreaking ability, so that the Voyageur experience reported here will be continued with the new craft.

Springtime flooding can be disastrous and repair to the damage caused can be expensive. Many springtime floods are caused by insufficient drainage for the amount of water that must be disposed of at that time of the year. Frequently, a flood is the result of a plugged drain which often takes the form of an ice jam. In these cases, damage is not only caused by water but also by the moving ice which can uproot trees and carry buildings away before it jams.

The solution to the flood problem caused by ice jams is to prevent its formation. This can be achieved by breaking the ice into small pieces and allowing it to be carried down the river by the current before it starts to move on its own due to increased temperature and water flow. Since 1976, this has been done along the St-Laurent River and on nine of its tributaries by using a hovercraft to break the ice.

Because of their low footprint pressure (about 2.3 kPa, or 50 lb/ft^2, for CCG hovercraft), hovercraft generally leave very little evidence, if any, of having passed over a surface. As discussed earlier, the following mechanisms can be invoked to break ice with a hovercraft:

(a) An air cavity is created under the ice by the air cushion which replaces the water supporting the ice, thus allowing the ice to break and fall into the void by its own weight.

(b) A relatively large amplitude wave is created by the hovercraft at near hump speed which, when directed into the ice, causes it to break.

(c) The wave-making effect of the hovercraft travelling over the ice at the so-called *resonance speed* (specific to a given ice thickness, ice strength and water depth) causes the ice to flex and break.

The CCG hovercraft can break about 25 cm of ice using mechanism (a). However, up to one metre can be broken using mechanisms (b) or (c). Furthermore, focusing the wave through certain astute manoeuvres can sometimes produce powerful action against thicker ice accumulations. In all cases, solid ice pieces will definitely not break if resting on the bottom. Mechanisms (b) and (c), termed *dynamic icebreaking*, are usually employed by the CCG since, when its services are required, the ice has generally grown well past half a metre in thickness.

To prevent flooding in the lowlands along the St-Laurent River and its tributaries, between Montreal and Trois-Rivières, a definite sequence of events occurs.

As spring approaches, the ice in Lake St-Pierre (about 25 km long by 10 km wide), a widening of the St-Laurent River upstream of Trois-Rivières, is broken into pieces small enough to be flushed down the river at a rate determined by the water flow. This prevents jamming at the outlet of the lake. The ice at the mouth of the tributaries is then cleared away. Meanwhile, Environnement Québec monitors the flow and water level in each tributary. When these approach their peak, but before the ice starts to move, the hovercraft is sent in to break up the ice, allowing it to flow out of the rivers without jamming. Thus, the excess spring water can escape without flooding the banks. The timing of icebreaking is very critical. If the hovercraft is sent in too early, the ice is difficult to break because of frazil (ice particulates) accumulating under the river ice; if too late, the ice will move and jam before a clear path has been opened in the river.

In a report prepared by Environnement Québec in 1984, it was stated that a minimum of half a million dollars per year is saved in flood damage through deicing with the CCG hovercraft. Its use also reduces the amount of dynamite that would be needed otherwise to break up the ice on these shallow rivers. Furthermore, the hovercraft is kind to the environment, since it does not damage the banks, surrounding vegetation and aquatic fauna.

Since 1976, there has been no flooding in the areas of operation of the CCG hovercraft. However, its size prevents it from going very far upstream in the smaller rivers. A smaller hovercraft (in the 5 to 10 tonne weight range) could be of use as an ice mover, helping dynamiters to perform more efficiently and with lesser explosive charges. It would not be very useful to break ice itself, since it would be limited to thicknesses of about 40 cm.

6.4.2 Air Trek 140 Operations

The Air Trek 140 (Fig. 6.15), a 7 t hovercraft designed by Jones, Kirwan & Associates, Hamilton, Ontario was used in the early 1980's as a personnel carrier to support forestry operations on Vancouver Island. In 1985, it was acquired by ICE Control Enterprises Incorporated for use as a light icebreaker. The icebreaking capability of this craft has been evaluated at 40 cm based on the assumption that the required vehicle weight is proportional to the square of the ice thickness to be broken, in accordance with Decker's theory (Section 6.2.2). The reference vehicle for this estimation is the CCG Voyageur, at a weight of 45 tonnes, and with a nominal icebreaking capability of 1 m.

ICE Control Enterprises operated the Air Trek 140 in the spring of 1986 on the Rideau River in Ottawa, where it complemented de-icing work done with explosives. In 1987, it was operated in the Chicoutimi, Quebec, harbour where it was used to clear ice around a petroleum terminal. Ice thicknesses varied from 30 to 45 cm, with occasional layers of 60 cm. The craft was able to overcome such thicknesses, but perhaps only because of local ice weaknesses. An ice knife was used at times with the Air Trek 140, so that excessive ice thicknesses could be weakened prior to icebreaking. However, this technique is still experimental and needs further refinements.

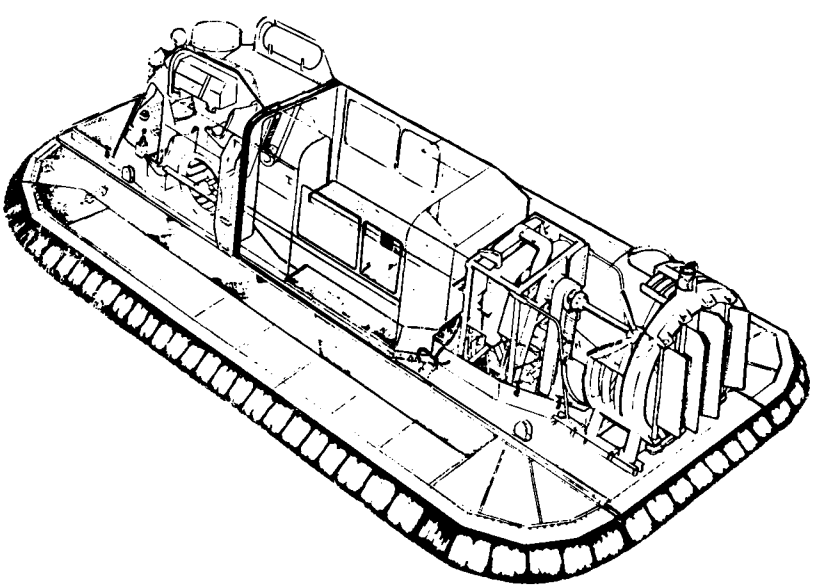

Fig. 6.15 Cut-away of the Air Trek 140 hovercraft: payload = 1.5 t; gross weight = 7 t; length = 11.2 m; width = 5.8 m. (Source: Jones, Kirwan and Associates).

6.5 SUMMARY

The ability of air cushion vehicles to overcome ice has been demonastrated repeatedly in both the so-called static and dynamic modes. ACIB's have been operated in Canada, the United States, and also in the U.S.S.R. (ref. 20), in fresh water ice covers exceeding 90 cm for the Canadian operations (ref. 12). The Canadian Coast Guard has operated the *Voyageur* hovercraaft as a high-speed icebreaker for more than 12 years in the St. Lawrence River system around Montreal.

Operational experience has led to a number of *hardware* improvements so that the reliability and maintainability of these vehicles can be tailored to the needs. A number of studies have been made to predict the behaviour of air cushion vehicles. Satisfactory predictions can be made for the performance of ACIB's, but the same cannot yet be said for high-speed icebreaking.

The future of ACV icebreaking in Canada depends on the manner in which these vehicles can be integrated into the mission of the Canadian Coast Guard. The evolution of this mission over the years has been partly determined by the capabilities and limitations of icebreaking ships. Presently no role has been defined for ACIB's by the Canadian Coast Guard. However, the *Voyageur* operation has created a type of service that cannot be denied. Its use in clearing small rivers of ice-jams has reduced considerably the flood damages that used to occur in the Montreal region every springtime. Thus the aging Voyageur has been replaced by a modern hovercraft, the AP.1-88 manufactured by Westland Aerospace (British Hovercraft Corporation), named ***Waban-Aki***.

6.6 REFERENCES

1. Wade, Edwards & Kim. 1975
2. Robertson 1976
3. D. Nevel, Moving Loads on a Floating Ice Sheet, CRREL Report No. 261, Cold Regions Research and Engineering Laboratory, Hanover, New Hampshire, 1968.
4. J.E. Laframboise, Comparative Analysis of Ice-Breaking: Conventional versus Air-Cushion, 13th Symposium on Air Cushion Technology, Montreal, September 1979.
5. D. Carter, Mathematical Model for Predicting Icebreaker Performance, Report TP 8531E, Transportation Development Centre, Transport Canada, Montreal, 1987.
6. B.W. Robertson, The High-Speed Method of Air Cushion Icebreaking, 10th Canadian Symposium on Air Cushion Technology, Ottawa, September 1976.
7. M. Ball, ACV Icebreaking Bow Platform Development Program - Phase I, Report TP 903, Canadian Coast Guard, Transport Canada, Ottawa, 1976.
8. A. Clayton, and H. Cohen, Research on Transport Aspects of Ice Sheets, Report TP 377BE, Transportation Development Centre, Transport Canada, Montreal, 1982.
9. J.L. Decker, The Application of Air Cushion Configurations to Icebreaking, Report MA-RD-940-78058, Maritime Administration, U.S. Department of Commerce, Washington, DC, July 1978.

10. D. Carter, Mathematical Analysis of Icebreaking by Air Cushion Platforms, Report TP 1238, Transportation Development Centre, Transport Canada, Montreal, 1977.

11. J.A. Tarzwell, P. Markham and C.W. Carter, Air Cushion Icebreaking Bow (ACIB) Trials Report, 1982/83, Report TP 4445E*, Transportation Development Centre, Transport Canada, Montreal, July 1983.

12. J.A. Tarzwell, P. Markham and T. Anderson, Air Cushion Icebreaking Bow (ACIB) Operations Report, 1983/84, Report TP 5497E, Transportation Development Centre, Transport Canada, Montreal, June 1984.

13. H. Lamb, Hydrodynamics, Cambridge University Press, 6th edition, 1975, p. 367.

14. D. Jones, Project FRIGONAV-Hovercraft Type 140 Operating Experience - February/March 1987, Report TP 8432E, Transportation Development Centre, Transport Canada, Montreal, 1987.

15. M. Shinbrot, A Mathematical Analysis of Dynamic Ice Rupture by Hovercraft, Report TP 4235E, Transportation Development Centre, Transport Canada, Montreal, 1983.

16. M.J. Hinchey and J. Whitten, Critical Speed Data for an Artificial Floating Ice Sheet, 1987 CACTS International Conference on Air Cushion Technology, Montreal, September 1987.

17. J. Buck and C.W. Pritchett, Air Cushion Icebreaking Test and Evaluation Program, Vol. I: Executive Summary; USCG Report No. CG-D-21-79, July 1978.

18. J. Buck, et al., Air Cushion Icebreaking Test and Evaluation Program, Vol. 2: Operational and Engineering Analysis; USCG Report No. CG-D-22-79, August 1978.

19. B. Colbourne, Advanced ACIB Concepts: Design Study, Report No. TP 5653E, Transportation Development Centre, Transport Canada, Montreal, July 1984.

20. V. Zuev, et al., An ACV Type Icebreaking Bow Attachment, RECHNOI TRANSPORT, Journal of the RSFSR Inland Waterways Shipping Ministry, No. 4, 1986, p. 37.

Chapter 7

ARCTIC TRANSPORTATION

7.1 INTRODUCTION

Although hovercraft have been used in the North American Arctic since 1966, there is a basic lack of familiarity with hovercraft as transport vehicles within Canada. Opportunity for direct public experience with hovercraft has been limited to short term special events, such as Expo 67 in Montreal and Expo 86 in Vancouver. Europeans are familiar with the successful cross channel SR.N4 hovercraft ferries carrying up to 60 cars and over 400 passengers between England and France; there has never been an equivalent commercial hovercraft operation in North America.

There are reports that hovercraft without self-propulsion are used extensively in the Siberian Arctic. Air cushion platforms with payload capacities in excess of 907 tonnes are said to be under development, while 181 tonnes payload platforms are in regular service. Photographs have been published showing a Soviet oil rig mounted on an air cushion platform (ref. 1).

Non-Soviet experiences with hovercraft in the arctic involve a small number of vehicles operated primarily in the Canadian and American Beaufort Sea since 1976. In spite of many problems with skirts and systems which were never designed for the arctic environment, the early operations proved that hovercraft have a definite role to play in offshore arctic transportation.

This chapter reviews the history of arctic hovercraft tests, demonstration programs and commercial operations to date. Future prospects for regular hovercraft operations in the arctic offshore are discussed in light of recent trends in air cushion technology development. For an earlier more general appraisal of air cushion vehicle potential in northern regions, the reader is referred to reference 2.

7.2 OPERATIONAL AND DESIGN CONSTRAINTS

The historical record of arctic hovercraft successes and failures should be viewed with the realization that most of the vehicles were originally designed for open water operations in temperate climates. The crews and maintenance engineers overcame numerous operational and technical problems. Their pioneering efforts proved the hovercraft concept in the arctic and provided the foundation on which to base future commercial operations.

The dominant arctic environmental feature affecting hovercraft design and operation is the ice cover. Depending on its thickness, ice can present either a flexible breaking surface or a solid base for hovercraft operation.

Although representing only about 10% of the year, the 4 to 6 week period from freeze-up to establishment of a stable ice cover nearshore can present the most severe arctic operating condition. Freezing spray while breaking ice can lead to heavy ice accumulation on the deck and exposed surfaces. Limited experiences with hovercraft under severe structural icing conditions have shown that operations can continue with regular inspection and removal. Operations further offshore can encounter freezing spray conditions in mid-winter, particularly in the Canadian Beaufort where wide expanses of thin ice are common during winter months. Careful route selection will direct the hovercraft over solid ice for most of the journey from a shore staging base, thereby avoiding the worst icing situations.

The hovercraft icebreaking phenomenon is examined in Chapter 6. Slow speed air cushion icebreaking was investigated in numerous trials (notably with the ACT-100 hoverbarge). The Bell Voyageur and Jeff(A) have demonstrated the quite different phenomenon of high speed icebreaking. Here the vehicle is deliberately held at the exact speed for maximum wavemaking to flex and crack the ice sheet. Once the vehicle either speeds up or slows down, this icebreaking effect disappears.

From December to June, the most important ice characteristic affecting offshore hovercraft operations is the distribution of ice roughness features, either as isolated ridges or extensive rubble fields. In this environment, a hovercraft requires accurate route marking and positioning systems, combined with suitable obstacle avoidance capability. The hovercraft must maintain sufficient speed for traversing obstacles within the clearance limits of the skirt system, while still being able to maneuver safely around critical ice features that may cause structural damage.

Ice roughness in the Beaufort Sea peaks in the water depth range 9 - 21 m (30 - 70 ft). Relatively large hovercraft will be required to achieve the 2.4 - 3 m (8 - 10 ft) obstacle clearances necessary to reliably service deep water locations. The ideal hovercraft for mid-winter offshore arctic operations combines a deep cushion with thrust vectoring for control. The skirt

system should be simple in geometry without inflated keels within the cushion periphery. Early hovercraft in the arctic employed the BHC skirt system developed for high-speed open water applications. Continual problems were encountered with ice damage to the internal inflated keels. Simple loop segment skirt systems such as used on the Wartsila Larus, and specified for the SOHIO ACV-300 design, offer greatly improved reliability over rough ice.

The arctic environment places a premium on overall design simplicity, and ease of maintenance. Early hovercraft designs used in the Beaufort area up to 1977 (principally the Bell Voyageur and SR.N6) relied heavily on aeronautical technology, with its associated demands for frequent inspection and a high level of technical training. The original 1960's concept of a rivetted aluminum alloy hull propelled by expensive gas turbines has evolved in the 80's to favour the marine-oriented approach, to high speed vehicles with welded aluminum hulls and diesel power plants. The British Hovercraft Corporation AP.1-88 and Wartsila *Larus* are two examples of this recent trend towards more practical, economical hovercraft.

Many of the systems problems experienced with early hovercraft were eliminated through the selection of materials more suited to -40°C temperatures and rough ice terrain. For example, heavier natural rubber skirts have dramatically improved skirt life, while maintaining flexibility in the most extreme temperatures; seals and lubricating fluids are available for extended cold temperature operation.

Appropriate insulation and built-in preheaters can solve the excessive warm-up times for lube oil, hydraulics and electronics systems mentioned in past trials reports. Properly designed heating and ventilating systems provide a sharp contrast to the harsh operating environment endured by crews in the seventies.

Local networks of microwave offshore positioning systems solve many of the navigational difficulties experienced by early craft, forced to rely on marine radar, gyrocompass and ADF position fixing.

Early hovercraft were not designed for an arctic ice covered environment. They were made to work through an often painful process of modification and repair under harsh conditions. In spite of the many problems, an impressive record of operational achievements with arctic hovercraft now exists as described in this chapter.

7.3 REVIEW OF HOVERCRAFT OPERATIONS IN FROZEN ENVIRONMENTS

It is important to review past experiences. Firstly, the past achievements in the arctic with craft designed for temperate climates confirm the potential of specially designed arctic hovercraft to solve future year-round transportation problems in ice covered areas. Secondly, the problems encountered in past arctic operations point to design areas requiring particular attention in the

future. Observations of craft handling over ice and descriptions of maintenance procedures provide an invaluable record to guide future designers and operators concerned with northern applications.

This section provides a chronological history of notable arctic hovercraft operations and a brief description of the vehicles involved. The historical record is divided according to the two main air cushion vehicle categories: the self-propelled airscrew-driven hovercraft and the externally-propelled hoverbarge. One exception, Hoversystems's D-PAAC, is a hoverbarge with a self-contained surface contact propulsion system.

The emphasis in this chapter is on self-propelled hovercraft. Hoverbarges have limitations in operating outside of the smooth landfast ice zone which provides a safe platform for tow vehicles. Similarly, small hovercraft lacking the necessary cushion depth to operate offshore within ridged ice are not considered here. A small hovercraft for the purposes of this chapter is considered to be less than 9 tonnes gross weight, equivalent to an SR.N6. Vehicles such as the Cushioncraft CC-7 in 1969 and, more recently, the Air Cushion Technologies Corsair have demonstrated potential applications in arctic nearshore areas.

7.3.1 Self-Propelled Hovercraft

The earliest known test of a self-propelled hovercraft in the North American Arctic involved an SR.N5 at Tuktoyaktuk, Northwest Territories, (ref. 6). This successful five week program included a 500 mile trip up the Mackenzie River during the initial stages of ice break-up. Figure 7.1 shows the SR.N5 clearing an ice pressure ridge in April 1966. Ridges up to 1.7 m (5.5 ft) were successfully negotiated by utilizing drifted snow on the approach side. Cruising speeds of 45 knots were sustained over smooth ice. The major operational problem was embrittlement of the PVC skirt material at temperatures below -20°C.

The pioneering N5 trial was followed two years later by an intensive test program at Churchill, Manitoba using the larger SR.N6 fitted with a neoprene coated nylon skirt (ref. 3). The Churchill trials involved 129 hours of operation, covering 2,200 km over a wide variety of land and ice surfaces. The tests involved a unique series of observations and measurements of ice accretion over open leads at air temperatures down to -37°C. Ice up to 1.9 cm thick had no noticeable effect on stability or handling during 14 to 62 minute exposures. There were no problems with propeller icing. Figure 7.2 shows an SR.N6 (similar to the one used at Churchill) over thin ice during cold weather trials in Finland.

These early trials proved that self-propelled hovercraft were an effective and safe means of arctic transport, and led to the first commercial arctic hovercraft operations in the summer of 1969. SR.N6 craft, owned by Pacific

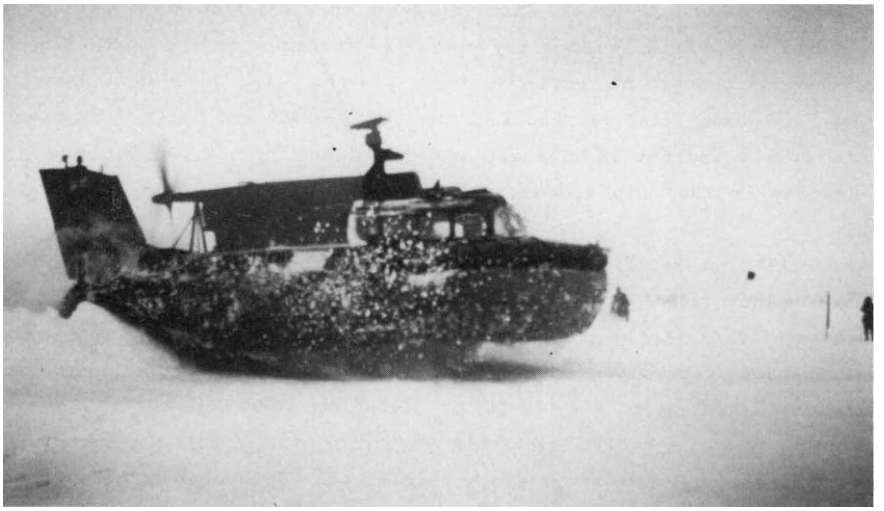

Fig. 7.1 SR.N5 *leaping* a pressure ridge during the 1966 Tuktoyaktuk trials. (Photo courtesy of British Hovercraft Corporation.)

Fig. 7.2 Prototype SR.N6 during trials in Finland. (Photo courtesy of British Hovercraft Corporation.)

Hovercraft Ltd., were used for hydrographic surveys, in the Canadian Beaufort Sea, and for logistics, in Alaska. The following year, Pacific Hovercraft used a modified flat-decked SR.N6 to carry oversized payloads on the North Slope. These pioneering commercial ventures were plagued with problems, largely related to inadequate financial backing, poor management and lack of maintenance. One of the Pacific SR.N6 craft was demolished in a freak accident in Alaska, leading to the only known fatality resulting from arctic hovercraft operations.

In April 1971, a Pacific Hovercraft SR.N6 carried out a field survey of multi-year pressure ridges in the Canadian Beaufort Sea (Fig. 7.3). The hovercraft successfully traversed ice rubble with 1.2 m (4 ft) blocks spaced about 3 m (10 ft) apart. In many cases, a tortuous path was followed at less than 5 knots between ridges up to 6 m (20 ft) in elevation. The client's account of this operation was extremely favourable regarding the future potential of Hovercraft in support of arctic field parties (refs. 7,8), but comments were made about the general rundown and dilapidated craft condition (related to a lack of reasonable maintenance facilities). The low speed maneuverability of the SR.N6 was rated as marginal during this operation.

The first serious commercial utilization of hovercraft over ice commenced during the winter of 1973/74 when Northern Transportation Company Ltd. (NTCL)

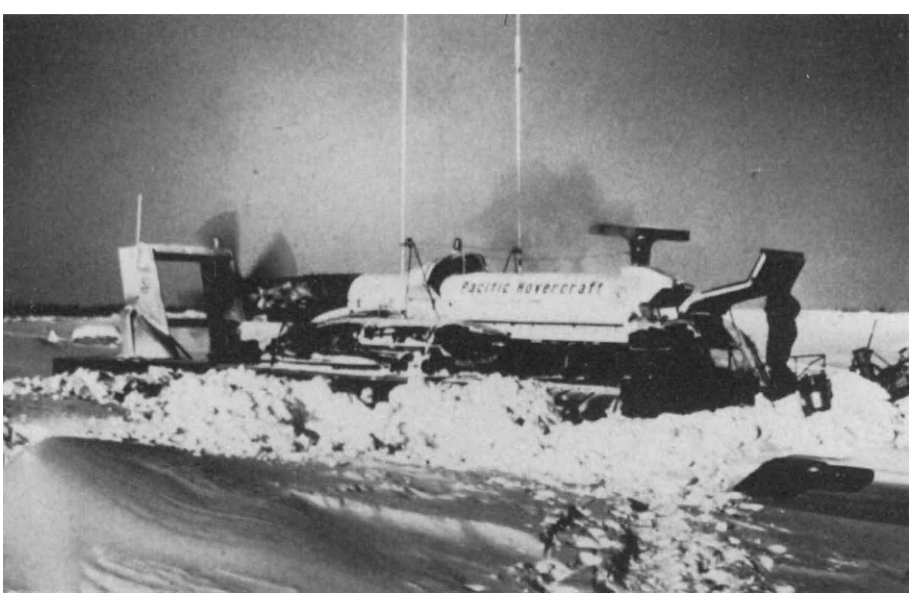

Fig. 7.3 Pacific Hovercraft SR.N6 in the Canadian Beaufort Sea, April 1971. (Photo courtesy of J. Hnatiuk.)

began operations with the SR.N6's purchased after liquidation of Pacific Hovercraft's assets in Vancouver. Figure 7.4 shows CH-NTA operating on the Mackenzie River near Inuvik. The two modules mounted on the side decks were used by NTCL as portable workshops to service the hovercraft at offshore drilling islands. As well as the passenger craft shown below, NTCL operated a specially modified SR.N6 with a portion of the cabin cut away to create a flat cargo area across the full beam. This vehicle carried awkward oversized cargoes up to 6.4 tonnes.

No other arctic hovercraft operation approaches NTCL's four-year operating record, achieved with two well-worn vehicles. In 1974, the first full year of operation, the two SR.N6 craft carried over 1,179 tonnes of cargo and 7,000 passengers, while covering 38,400 km in 950 hours (an average speed of 40 km/h). During four years of intensive operation, the NTCL craft experienced only one major accident. In November 1976, while returning from an oil drilling rig in darkness, an SR.N6 struck a projecting pinnacle of multi-year ice at approximately 93 km/h (50 knots). There were no injuries, but the craft was extensively damaged. This hovercraft was eventually salvaged and completely rebuilt to operate with the Canadian Coast Guard in Vancouver. In another incident, the NTCL hovercraft returned four miles back to base with a ripped skirt connected to the craft structure by a network of *herc* straps

Fig. 7.4 Northern Transportation Company Limited's SR.N6 over ice on the Mackenzie River. (Photo courtesy of B. Meade.)

(colloquial expression derived from the straps used to secure cargoes onboard a C-130 Hercules aircraft). Many other hovercraft have proven their ability to return home safely after suffering extensive skirt damage (e.g., SR.N4 in the English Channel.

The best documented description of NTCL's operation from a pilot's point of view is contained in reference 9. The often-humorous account of typical operating hazards makes entertaining reading. For example, *"At times with light load, only an increase in power and speed would turn CH-NTB (the flat decked N6) downwind. In between the pressure ridges, one developed a game of 'Arctic Chicken'. This entailed blasting at excessive speed through the darkness and blown snow just to maintain heading, while waiting for the searchlights to pick up barriers of ice ahead..."* Fortunately with rotating thrust vectoring used by hovercraft such as Larus and Jeff(A), this dangerous game is no longer necessary. The NTCL operation ran successfully until 1977, when oil industry contracts within the safe operating range of the SR.N6 declined below profitable levels.

During the same time period that the NTCL SR.N6's were active, a much larger hovercraft, the Bell Canada Voyageur, with up to 18 tonnes payload was introduced to the Canadian and Alaskan Beaufort. The second prototype (002) was used in a series of trials and commercial demonstrations sponsored by the Canadian Government on Great Slave Lake and the Mackenzie River System (Fig. 7.5). NTCL operated the Voyageur on behalf of the Ministry of Transport.

A cold weather evaluation was carried out over 157 operating hours from February to April 1973 (Transportation Development Agency, 1974). During this time, Voyageur (002) travelled between Tuktoyaktuk and Norman Wells carrying payloads up to 18 tonnes (refs. 10 and 11). The average speed over rough river ice was 53 km/h. The minimum operating temperature was -43°C. Major technical problems involved skirt damage and snow ingestion into the engine cowlings, thereby freezing the engine controls. Skirt finger life over ice was estimated at 450 hours. (Subsequent Canadian Coast Guard experience with Voyageur indicated that finger life could be doubled with the use of heavier materials.) Numerous incidents of damage to the internal stability bags and keels were reported. These problems continue to plague BHC-skirted craft in a rough ice environment (ref. 12). Skirt hinge attachment failures, a common form of skirt damage associated with the Voyageur trials, were eventually solved by fitting protective strips.

Eventually, the Voyageur (002) was developed into a successful hovercraft, operating with the Canadian Coast Guard out of Montreal from 1974 to 1987 on routine icebreaking and logistics missions. The Voyageur reached 155 km/h over smooth river ice (ref. 13). Figure 7.6 shows the Coast Guard Voyageur breaking ice in the St. Lawrence River. This craft was replaced in 1987 by an AP.1-88

Fig. 7.5 Bell Voyageur (002) operating over ridged ice near Tuktoyaktuk. (Photo courtesy of Transport Canada.)

designed to Canadian Coast Guard specifications. Initial experiences with the new craft are favourable, with the AP.1-88 proving to be even more effective in the icebreaking role than its predecessor. A stretched military derivative of the Voyageur, the LACV-30, carried out 150 hours of ice-breaking demonstrations on the Illinois River in 1978.

The British Hovercraft Corporation BH.7 was the largest self-propelled hovercraft to have operated over ice, until the introduction of the Wartsila Larus in 1981. A BH.7, operated by the Interservice Hovercraft Unit of the Royal Navy, completed a successful 6,400 km round trip from Finland to the Gulf of Bothnia north of Stockholm in 1972 (Fig. 7.7). Over 1,800 km of this trip consisted of solid and broken ice which was traversed at speeds up to 130 km/h. Little trouble was experienced crossing 3.7 to 4.6 m ridges at 37 km/h. Skirt damage was minor. Interestingly, the BH.7 had much deeper fingers as a proportion of the total skirt depth than other BHC-skirted craft (73% compared to less than 50%).

A complete series of engineering and operational reports are available on the BH.7 Swedish exercise (ref. 14). These reports contain the first accounts of hovercraft control characteristics over different ice surfaces with a

Fig. 7.6 Bell Voyageur operated by the Canadian Coast Guard. (Photo courtesy of Canadian Coast Guard.)

vehicle employing a swivelling propeller pylon. Given the level of air cushion technology in 1972, the BH.7 Swedish expedition was a milestone achievement in proving the offshore capabilities of a large powerful hovercraft. Radar was used effectively to route BH.7 around rough ice areas. Discrimination between minor and critical obstacles was poor, a problem which remains up to the present day. Landings were made with BH.7 on ice of various thicknesses. At 15 cm, the landing pads simply punched holes without usually breaking the main sheet, while the craft was fully supported on 25.4 to 30.5 cm of ice.

After the completion of the Voyageur trials in 1974, ten years passed before a large hovercraft was used in the Beaufort Sea. Subarctic experience continued with the Voyageur over ice in the St. Lawrence River, and the Wartsila Larus in the Finnish Archipelago from 1981 to 1984.

In November 1983, the Jeff(A) under contract to SOHIO Petroleum Company became the heaviest self-propelled hovercraft to operate in the Arctic (Fig. 7.8). Although bearing a striking resemblance to the Larus, Jeff(A) has double

Fig. 7.7 British Hovercraft Corporation BH.7 with rough pack ice in the Gulf of Bothnia. (Photo courtesy of P. Reynolds.)

the loaded weight, three times the payload and over six times the installed power of the Finnish craft. The Jeff(A) was designed to meet a military requirement to carry a tank from the well deck of a mother ship in rough seas and tropical conditions. To meet this stringent specification, Jeff(A) incorporates a unique pericell skirt system which results in an extremely stiff cushion. The pericell skirt is not well-suited for rough ice operations. The complex geometry and circular hoops lead to many potential ice snagging occurrences. SOHIO brought the Jeff(A) to Prudhoe Bay for two reasons: firstly, as a demonstration vehicle for offshore oil rig support; secondly, as a scientific test vehicle to collect basic design information for the ACV-300 concept and future designs (refs. 5, 15, 16).

The Jeff(A) tests provided the first full scale measurements of hovercraft skirt drag under different conditions. Results confirmed the importance of providing the optimum cushion air flow to minimize required propulsion thrust over rough ice. Maneuvering trials fully demonstrated the advantages of rotating propulsors over ice, compared to the fixed propeller installations of Voyageur and the SR.N6. The Jeff(A) demonstration programs conclusively proved the value of a self-propelled hovercraft in transporting heavy loads over a wide variety of ice surfaces, from early winter to spring break-up.

Recent experience with a hovercraft over ice involves the commercial operation of two British Hovercraft Corporation AP.1-88's between Copenhagen's

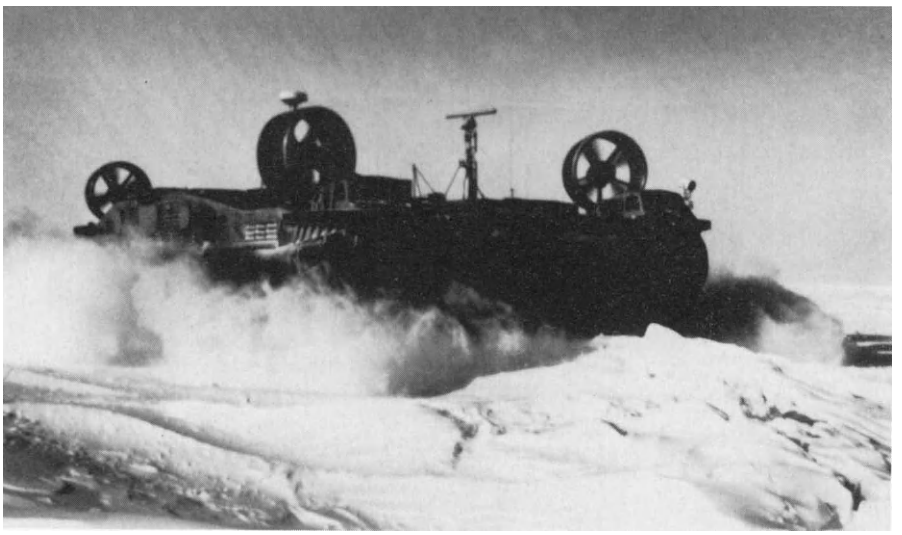

Fig. 7.8 Jeff(A) crossing a pressure ridge north of Prudhoe Bay, March 1984. (Photo courtesy of W. Bacon.)

Kastrup Airport and Malmo, Sweden (Fig. 7.9). Operated by DSO on behalf of Scandinavian Airlines System, this service carried 310,000 passengers between June 1984 and September 1986. Service reliability reached 95%, except during severe winters when ice-related problems reduced reliability to 80-85% (refs. 12, 17, 18).

The first winter of AP-1-88 operation (1984/85) was one of the coldest in 50 years. Temperatures reached -22°C in February and January, and the Oresund between Sweden and Denmark was completely ice covered. The AP.1-88's maintained scheduled services throughout the winter in spite of some problems with superstructure icing and torn skirts. The most serious difficulties were overcome by careful operating techniques and engineering modifications. For example: recommended procedures over broken, jagged ice included the use of maximum lift at speeds just over hump; the craft is operated at a lower lift setting over open water in below freezing conditions; care is taken to maintain forward speed well above hump once superstructure icing begins; sand ballast is sometimes carried up front to compensate for the weight of the antispray skirt; fewer passengers are booked when the risk of severe icing is predicted to be high; excessive ice building is removed with a hot water/glycol mixture; engine air intakes are kept clear by recirculating warm engine cooling. In spite of these precautions, there are times when, to quote one of DSO's senior hovercraft captains, "The craft have arrived looking more like an iceberg than a hovercraft" (ref. 12). After some initial mechanical teething problems, the

Fig. 7.9 SAS AP.1-88 over broken ice floes in the Oresund between Sweden and Denmark, during the winter of 1985. (Photo courtesy of British Hovercraft Corporation.)

SAS/DSO operation matured into a highly successful service. At the time of writing (Febraury 1989) a third craft was being introduced into Scandinavian service.

Additional arctic experience with another so called *new generation* style (welded aluminum, diesel power) hovercraft was gained with the commercial charter operations of the Wartsila *Larus* from September 1985 to September 1986. The *Larus* was operated in the Canadian Beaufort Sea from a base at Tuktoyaktuk, Northwest Territories, under lease from the Government of Finland by a Canadian joint venture (Arctic Transportation Limited and Wartsila Arctic Inc.). Originally completed in 1981, the *Larus* was used during four winter seasons of over-ice ferry service in the Baltic Sea before being refurbished and modified for Canadian operations.

The *Larus* Beaufort Sea operation was a qualified success in that the vehicle, as originally developed for Baltic Service, had insufficient skirt depth (0.8m) to operate over rough ice. This constraint limited the effective area of Canadian operation to a narrow band of smooth landfast ice near shore. Additional problems were encountered with snow ingestion into the machinery

spaces. Subsequent melting and refreezing led to a build-up of ice on the underside of the craft. This condition was eventually cured through modifications to the lift system. Loaded operations over breaking thin ice in the 15 to 30 cm range were avoided due to the greatly reduced speed, increased fuel consumption and possibility of skirt damage (ref. 19).

Undoubtedly, the *Larus* experience would have been much more positive if the craft had been fitted with a deeper skirt at the outset. Unfortunately, the sharp downturn in the offshore oil industry in 1986 effectively terminated the operation before the craft really had an opportunity to prove itself. Figure 7.10 and Table 7.1 compare the seven self-propelled hovercraft which have been used in a variety of ice environments from 1966 to 1989.

Table 7.1 Data on self-propelled hovercraft (>9 tonnes gross weight) used in arctic or ice operations from 1966 to 1989.

Hovercraft	Period	Gross weight (tonne)	Maximum payload (tonne)	Total power (kW)	Cushion depth (m)
SR.N6	1966-77	15	6	1 206	1.2
BH.7	1972	61	17	5 697	1.8
Voyageur	1973-87	47	24	3 485	1.2
Larus	1981-87	100	24	4 692	0.8
Jeff(A)	1983-84	177	77	30 161	1.2
AP.1-88	1984-89	41	11	2 295	1.4

7.3.2 Externally-Propelled Hovercraft

Externally-propelled hovercraft, commonly called hoverbarges, usually involve low-speed heavy-lift air cushion platforms with steel hulls and diesel engines for lift. Skirt systems are of simple geometry, reflecting the less stringent stability and control considerations of slow speed opereations. Propulsion is by a variety of means, including wheeled and tracked vehicles, cable winching, ice strengthened vessels, and even helicopters.

Five hoverbarge designs fabricated outside the U.S.S.R. played an important role in solving practical arctic logistics problems: the Mackace Yukon Princesses, the Global Marine ACT-100, Hoversystems D-PAAC and Warsila TAV40. The Yukon Princesses were assembled on site to bridge a critical transportation gap in the Trans Alaska Pipeline Project. During a 5 month period in 1975, these two vehicles carried over 634,900 tonnes of cargo by winch across the Yukon River. Although designed for a nominal 145 tonnes payload, overload situations were common. The largest single reported load was 234 tonnes (ref. 20).

The ACT-100, built in Canada, has a long history of successful arctic operation, beginning with the first documentation of air cushion icebreaking on

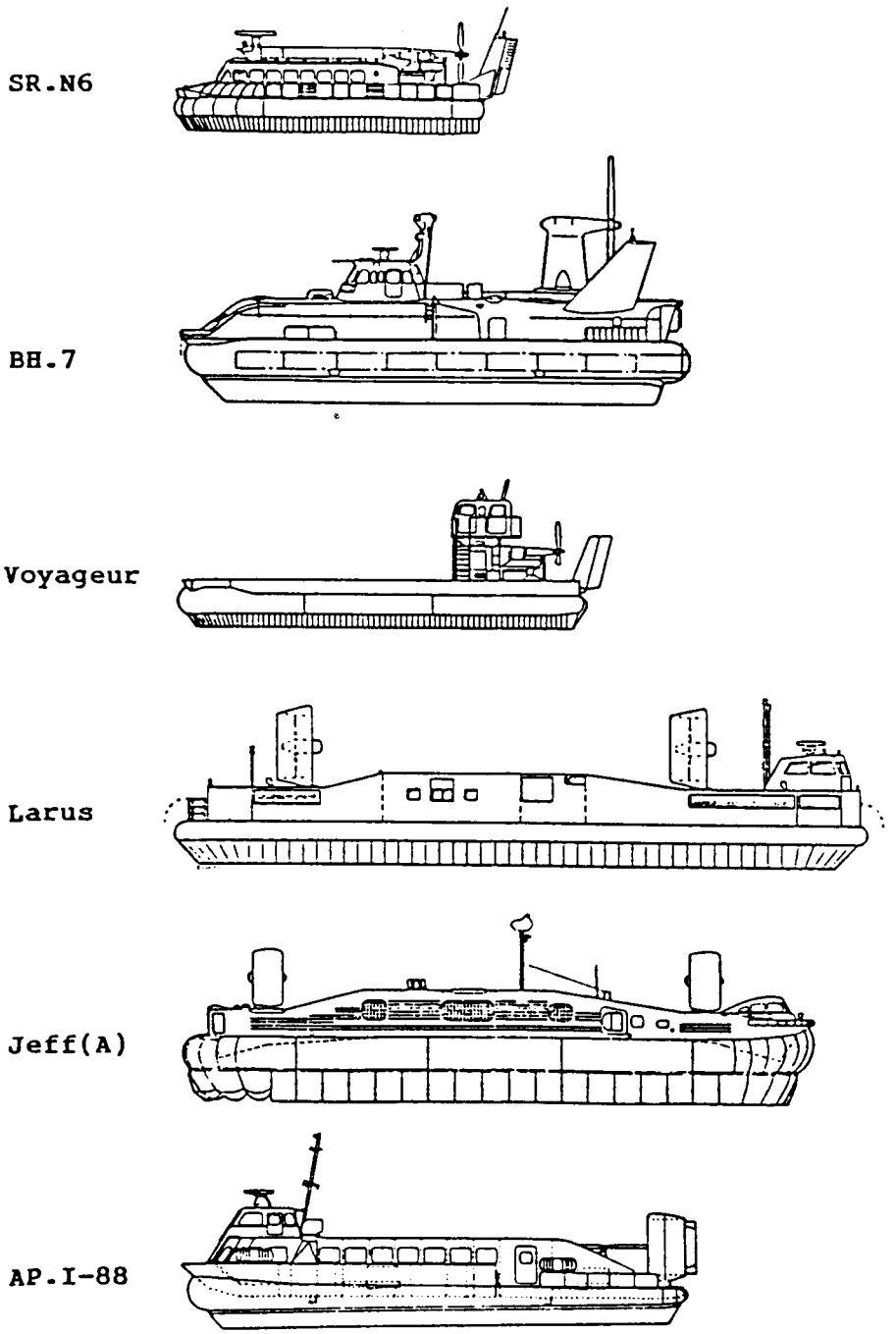

Fig. 7.10 Self-propelled hovercraft used in arctic or ice operations from 1966 to 1987 (relatively scaled). (See Table 7.1 for pertinent data.)

Great Slave Lake in 1971, and ending with the demobilization of the Mukluk offshore drilling island at Prudhoe Bay in 1984. Figures 7.11 and 7.12 show the ACT-100 during two arctic operations, separated by thirteen years. During the intervening years, the ACT-100 was winched while breaking ice at Tuktoyaktuk in 1972, and while moving a rig for Imperial Oil in 1973. From 1975 to 1977, the ACT-100 was successfully used to prove the air cushion icebreaking bow concept while attached to the bow of different vessels at Thunder Bay, Ontario (refer to Chapter 6).

In 1981, the ACT-100 began the third phase in its career, again as an independent hoverbarge, at Prudhoe Bay, Alaska (Figure 7.12). From November of that year until the Mukluk rig move in 1984, the ACT-100 was used in several demonstration projects sponsored by SOHIO Petroleum. These trials utilized a variety of propulsion techniques, including the ice strengthened tug *Arctic Fox*, Rolligons, and perhaps the most exotic form of tow vehicle, a Kawasaki-Vertol KV-107 tandem rotor helicopter (ref. 15).

The Hoversystems D-PAAC is a self-propelled hoverbarge employing four sets of hydraulically driven terra tyres mounted fore and aft. This craft successfully carried freight loads up to 71 tonnes between villages on the Kuskokwim River, Alaska, during the winter of 1980-81 (ref. 21). The Wartsila Vector 4 is a similar concept using steerable crawler tractor units instead of terra tyres (ref. 1).

Wartsila built fifteen 40-tonne payload hoverbarges during 1980-85 for use as ship to shore lighters on Soviet arctic cargo vessels. These craft have limited self-propulsion capability in water by venting lift fan air. They are

Fig. 7.11 ACT-100 breaking ice in Tuktoyaktuk Harbour, November 1972. (Photo courtesy of D. Dickins.)

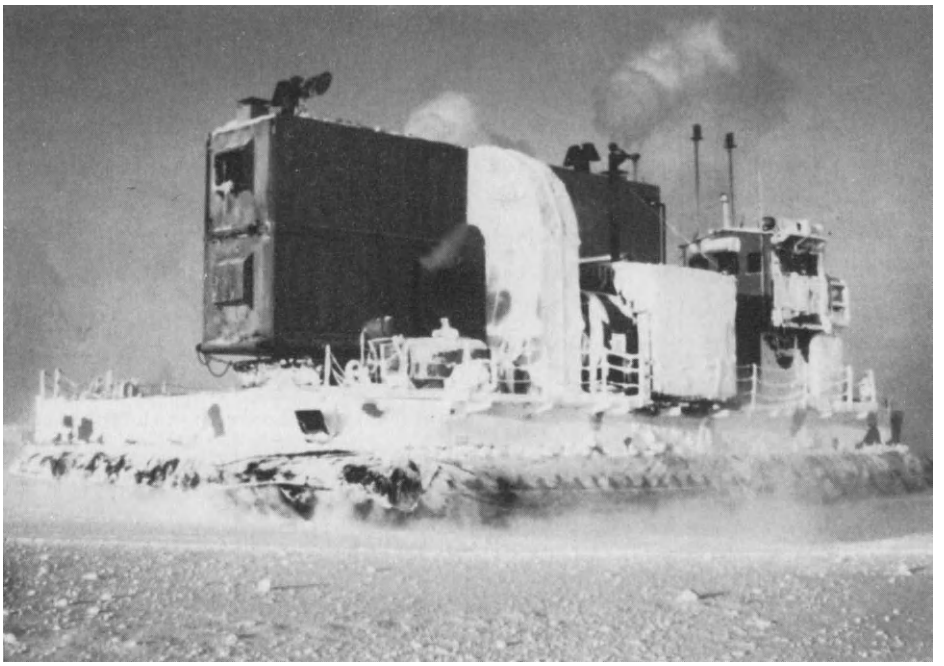

Fig. 7.12 Global Marine Development ACT-100 during the Mukluk rig move in February 1984. (Photo courtesy of H. Ramsden.)

intended for cable winching, or all-terrain tractor towing over ice (ref. 22).

7.4 FUTURE ARCTIC HOVERCRAFT DEVELOPMENTS

Future arctic hovercraft developments are closely tied to the needs of the offshore oil industry, during exploration and production development. Industry attention in the Arctic is currently focussed on deep water drilling concepts for the U.S. and Canadian Beaufort Sea and Chukchi Sea areas. The traditional nearshore roles perceived for hovercraft in the arctic are consequently shifting to favour larger vehicles with rougher ice capability.

The necessary cushion depths for offshore applications require vehicles in the 90-tonne plus weight category, and Jeff(A) or larger size range. Vehicles of this size operating at cushion pressures of 5 to 7 kPa will likely have payloads in excess of 70 tonnes. The maximum payload of new hovercraft designs is limited more by a willingness to operate outside the envelope of previous experience, rather than any basic limitation in air cushion technology. Slow speed hoverbarges have been constructed up to a gross weight of 680 tonnes (Mackace *Sea Pearl*). The SOHIO ACV-300 design was projected to have a gross weight of 907 tonnes and a maximum payload over 362 tonnes. This vehicle was considered well within the bounds of current technology in 1983 (ref. 15).

For nearshore operations over stable landfast ice, hoverbarges can be constructed economically with simple hulls and skirt systems. The efficient application of these vehicles depends on a need to move heavy loads in areas where an ice road is not practical or safe, or to significantly increase the loadbearing capacity of existing ice roads. Potential applications include winter rig moves to and from gravel islands, and winter pipeline installation and/or repair in smooth landfast ice areas. For offshore operations over broken ridged ice, hoverbarges have limited applications. Self-propelled vehicles are considered the most likely form of hovercraft to be built in the future to support offshore drilling and resupply of production facilities.

The Larus, Jeff(A) and AP.1-88 all incorporate design features which promise to improve the future capabilities, economics and reliability of arctic hovercraft. Key design features considered beneficial for arctic operations include: welded marine aluminum hull construction (compared with the light alloy aircraft hull construction of earlier designs); loop segment skirt systems (used successfully by the Larus, and considered to offer significant advantages over ice compared with the previous BHC bag/finger system); rotating propulsors or thrusters (considered essential for acceptable control over smooth ice and in maneuvering through ridges); diesel engines and industrial transmissions (offering reduced capital costs and longer overhaul lives). These four key design elements are expected to play a major part in directing the shape and form of future arctic hovercraft.

The single most important design variable affecting choice of lift and propulsion machinery, vehicle economics, vehicle configuration, and eventual payload is the total installed power requirement. The total power requirement of an arctic hovercraft optimized for over-ice operation can be substantially less than for an equivalent vehicle designed for high-speed open-water operation.

For example, the British SR.N4 MK.3 cross channel hovercraft weighing 341 tonnes fully loaded, requires 15,200 installed horsepower to carry 86 tonnes of payload at high speed in rough water. The SOHIO ACV-300 arctic hovercraft weighing 907 tonnes fully loaded, and using the SR.N4 propulsion units with similar total installed power, was designed to carry 349 tonnes of payload at low speed over rough ice. Figure 7.13 shows a general arrangement and artist's conception of the SOHIO ACV-300 design, as developed in December 1982 (refs. 5, 15, 23).

The Jeff(A) test results indicate that future arctic hovercraft can be designed with even lower power/weight ratios than the ACV-300. Skirt resistance reductions of 25% over rough ice are attainable by operating over ice at an optimum hovergap (ref. 5).

The SOHIO ACV-300 was designed with the specific purpose of moving complete rig modules to and from nearshore gravel islands at any time of the year. Future offshore hovercraft applications will likely call for smaller vehicles

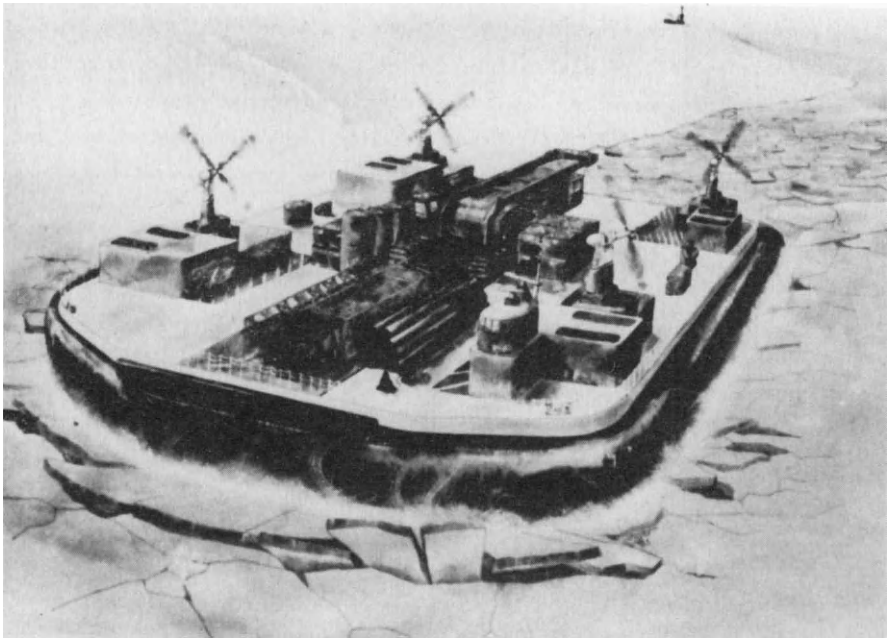

Fig. 7.13 SOHIO ACV-300 design for 1983 Alaskan Beaufort Sea operation. Principal characteristics: 2.4 m obstacle clearance; 492 tonnes empty weight; 66 tonnes fuel weight; 350 tonnes payload; 907 tonnes gross weight; 5.86 kPa maximum cushion pressure; four 2984 kW gas turbines; 4 centrifugal fans; 4 BH.7 type propulsors; 9.4 km/h speed when breaking 0.6 m ice in shallow water against a 42.6 km/h head-wind; speeds exceeding 27 km/h over solid ice with scattered ridges. (DF Dickins Associates Ltd.)

in the 70 to 180 tonne payload class. Such hovercraft will be capable of providing year-round heavy-lift support to a deep water exploration platform or production site in the Beaufort Sea and Chukchi Sea areas. Recent economic analysis shows that hovercraft can offer significant cost savings in arctic offshore resupply when compared with heavy lift helicopters (ref. 24).

7.5 DISCUSSION

Hovercraft are proven vehicles with known capabilities in the arctic near-shore area. They have now accumulated over 8,000 hours of operating experience in an ice covered environment. Vehicles with sufficient obstacle clearance to operate offshore in ridged pack ice have been in regular operation in the United Kingdom since 1969. Hovercraft in the Jeff(A) and Larus size range can be designed with sufficient cushion depth to clear 2.4 - 3 m ridges, allowing service to Beaufort and Chukchi drilling locations outside of the landfast ice zone. Less than 1 in 10 pressure ridges in first-year pack ice exceed 2.4 m in elevation.

Detours necessary to avoid extreme ice features are still practical when it is considered that a hovercraft's average transit speed over thick first-year ice will be more than five times that of a Class 6 ice-breaker. A hovercraft can carry heavy loads offshore with a fraction of the power required to achieve a year-round arctic transportation capability with traditional displacement ice breakers. Hovercraft are not restricted by water depth considerations and require no expensive dredging or channel maintenance to obtain access to a shore staging base.

A twenty year operating record has firmly proven the concept of arctic hovercraft. Recent advances in air cushion technology, through the adoption of a marine design philosophy, will enable the development of a new generation of more capable, cost effective arctic offshore hovercraft. Future commitments to construction of these large vehicles will require a stable economic climate of arctic offshore oil development.

7.6 SUMMARY

Since the first hovercraft trial in the North American Arctic twenty years ago, hovercraft capabilities in an ice-covered environment have been proven through thousands of hours of commercial and experimental programs. This chapter reviewed the history of arctic hovercraft operations and described the successes and failures leading up to the present day acceptance of air cushion technology. Recent advances in arctic air-cushion-vehicle design and performance prediction were discussed as they apply to future prospects of routine hovercraft operation in the arctic offshore area. Future applications were discussed in terms of the known advantages and estimated capabilities of new arctic hovercraft designs.

7.7 REFERENCES

1. R. McLeavy (ed.), Janes Surface Skimmers, Janes Publishing, London, U.K., 1985.
2. H.S. Fowler, The Air Cushion Vehicle: A Possible Answer to Some Arctic Transportation Problems, Polar Record, Vol. 18, No. 114, Cambridge, 1976.
3. O.G. Stoner, Report on SR.N6 Churchill Trials, Department of Transport, Ottawa, Canada, 1968.
4. D.F. Dickins, Ice Conditions Canadian Coast Guard Voyageur Ice-Breaking Trials, Parry Sound, Ontario, Environment Canada Internal Report, Ottawa, Canada, 1974.
5. D.F. Dickins, The Jeff(A) Arctic Test Program, Proceedings of the 1984 CACTS International Conference on Air Cushion Technology, Vancouver, Canada, September 1984.
6. Defence Research Board, Trials of an SR.N5 Hovercraft in Northern Canada - Spring 1966, Report DR182, Department of National Defence, Ottawa, Canada, 1966.
7. J. Hnatiuk, Report on Phase I of Pressure Ridge and Ice Island Study Evaluation of Hovercraft and Ice Reconnaissance, APOA Project No. 17, Gulf Oil Canada Limited, Calgary, Canada, 1971.

8. A. Kovacks and M. Mellor, Sea Ice Pressure Ridges and Ice Islands, Technical Note 122, Creare Inc. Hanover, N.H., U.S.A., 1971.

9. P. Lamb, Northern Transportation Company Ltd., Air Cushion Vehicle Operations, Hovering Craft and Hydrofoil, Vol. 14, No. 8, 1975.

10. Bell Voyageur 002: Cold Weather Evaluation, Transport Canada Report, August 1974.

11. Bell Voyageur 002: Engineering and Commercial Evaluation, Transportation Development Agency, Montreal, June 1975.

12. K. Rosquist, The AP.1-88 Hovercraft in Ice Operations, Proceedings of the International Polar Transportation Conference, Vancouver, Canada, 1986.

13. G.A. More, Achievements of Voyageur in the Canadian Coast Guard Laurentian Region, 13th Canadian Symposium on Air Cushion Technology, Montreal, Canada, September 1979.

14. Royal Navy Interservice Hovercraft Unit, Cold Weather Trials, 1972 - BH.7 Hovercraft XW255 - Trial Report, Lee on Solent, September 1972. (Unclassified September 1979.)

15. J.T. Walden and D.F. Dickins, Review of an Air Cushion Vehicle Program of Offshore Arctic Operations, 7th International Conference on Port and Ocean Engineering under Arctic Conditions, Helsinki, Finland, April 1983.

16. R.F. Tangren and D.F. Dickins, Design Studies for a Diesel Powered Heavy Lift Arctic Air Cushion Vehicle, 5th International Symposium on Offshore Mechanics and Arctic Engineering, Tokyo, Japan, March 1986.

17. M. Mant, Review of AP.1-88 Experience to Date, 8th American Institute Of Aeronautics and Astronautics Advanced Marine Systems Conference, San Diego, California, 1986.

18. AP.1-88 Over the Ice in Scandinavia, High Speed Surface Craft, Vol. 24, No. 2, March-April 1985.

19. J. Wainwright and E. Makinen, First Winter's Experience with the Air Cushion Vehicle "Larus" in the Beaufort Sea, International Polar Transportation Conference, Vancouver, Canada, 1986.

20. J.E. Ireland, The Yukon Ferry Operation, 10th Canadian Symposium on Air Cushion Technology, Ottawa, Canada, January 1979.

21. R.G. Longaker, A New Class ACV: Tanker Freighter, 15th Canadian Symposium on Air Cushion Technology, Toronto, Canada , September 1981.

22. S.V. Yakonovsky and V.I. Paresypkin, Design and Operation of ACV Lightering Barges, 1987 CACTS International Conference on Air Cushion Technology, Montreal, September 1987.

23. M. Bradner, Hovercraft Research May Solve Arctic Transportation Problems, Alaska Offshore, SOHIO Alaska Petroleum Company, Anchorage, Alaska, August 1983.

24. D.F. Dickins, An Economic Evaluation of Air Cushion Vehicles in Support of Offshore Oil Development, 1988 CACTS International Conference on Air Cushion Technology, Annapolis, Md, September 1988.

Chapter 8

COASTAL OPERATIONS

8.1 INTRODUCTION

The application of hovercraft in coastal regions is studied in this chapter by examining the Maryland Natural Resources Police (MNRP) and Canadian Coast Guard (CCG) operations. The CCG's experience with hovercraft dates back to 1968; the MNRP's, to 1984. Many of the functions of the two agencies are similar, e.g., search and rescue, law enforcement and ice-breaking. However, the CCG has additional responsibilities, particularly in the St. Lawrence River region, including laying, maintaining and position-checking of buoys, and construction, maintenance and supply of fixed navigational aids (lighthouses, beacons, radio towers and range markers). Of interest, also, is the similar resistance to change that both agencies encountered upon trying to insert *new* ACV technology in their operations.

8.2 MARYLAND NATURAL RESOURCES POLICE

From sailing vessels in 1868 to hovercraft in 1984 goes the saga of the Maryland Natural Resources Police (herein called the *force* or the *agency*). This saga shows the force to be the descendant of the oldest state law enforcement agency in Maryland, the State Oyster Police Force, which was created by legislative action in 1868 for conservation law enforcement. At that time, it was appropriated funds to acquire one suitable vessel and two tenders, to be propelled by sail, steam, oars or otherwise.

During the ensuing years, the force grew to be one of the largest marine law enforcement units in the United States, with varied duties ranging from conservation and boating law enforcement to investigating smuggling and other criminal activities. In addition, it is now responsible for search and rescue, boating accident investigations and emergency medical assistance to accident

victims on 6213 km^2 (2400 mi^2) of Maryland water ways. Since its creation, the agency has evolved through the era of sail, steam and gasoline power driven conventional vessels to today's modern fleet of one hundred fiberglass and aluminum craft.

This evolution has not been without its share of problems, especially since 1960. Legislative mandates established additional duties without funding to support them. Recreational use of Maryland's waterways increased many fold, creating demands for services without additional personnel and equipment. The commercial fisheries industry changed drastically due to court decisions and law changes. Criminal activities increased on Maryland waters due to the opportunities presented by the changing industries and society. Law enforcement demands and assistance to the public escalated, while the patrol fleet diminished. Federal funding for the agency dried up and State funds were cut so drastically in 1979 that routine patrols had to be curtailed. The energy crisis had depleted the fuel budget and supply; fuel was saved from emergency responses, such as search and rescue, emergency medical assists and evacuation during natural or man-made disasters.

At this time, the agency began to critically examine its patrol fleet and seek funding for replacement craft. Along with this replacement, it became apparent that the changes in demand for services necessitated changes in equipment used to perform the services. The agency realized there was a serious void in emergency response to accident victims on Maryland waters, especially during inclement weather conditions. Light aircraft would be grounded and the conventional patrol craft had very limited ice breaking capabilities. In light of these facts, it began to examine non-conventional water craft such as hydrofoils, inflatables, rigid hull inflatables, airboats and air cushion vehicles.

Due to their fully amphibious capability, air cushion vehicles (hovercraft) emerged as the most logical solution to fill the void in the agency's emergency response and law enforcement missions. Their capability to operate over critical environmental areas with minimal damage, to break ice, or to operate over shallow water or land were the deciding factors. However, these enhancements did not erase the problems, either internally or externally.

First, the history of the hovercraft industry had been quite dismal; many failures, slow growth and a very low profile in the United States were detriments. Acquisition and operation costs for available craft were prohibitive for the agency.

Second, there were no commercial or recreational hovercraft manufactured in the United States of a size to meet the agency's needs. This was not true of all the other types of craft, which were readily available, with a proven track record and competitive suppliers.

Third, all available hovercraft were foreign built hulls, which are subject to the Maritime Jones Act and precluded from use in U.S. commerce. This would not affect the agency's operation of such craft but would severely limit the agency's ability to dispose of the craft in accordance with the equipment replacement program.

Fourth, there were no hovercraft operated by a law enforcement agency in the United States at this time. Therefore, there were no available statistics from this type of operation to analyze and no craft available to examine.

Fifth, to change the agency's thinking from conventional to non-conventional craft was no small endeavour. A fear of the unknown prevailed. To many, the hovercraft was mysterious. By many, it was described as a detriment. To those who believed, it was seen as the solution to the problem.

Discussions with hovercraft manufacturers and operators, analysis of user cost, and potential demand resulted in efforts by the agency to seek funding for test and evaluation of a hovercraft. These efforts appeared to be in vain. After three years, no funds were forthcoming at either the State or Federal level and there was still a lack of interest for the program in the agency. Contacts continued to be made by those who believed in the project and persistence prevailed.

In the Spring of 1982, Frank W. Hake Inc., parent company of Hover Systems Inc., of Media, Pennsylvania, entered into an agreement with the agency to build a hovercraft capable of meeting the agency's needs, if the agency would test and evaluate the craft for at least one year. This agreement was very viable and served a dual role. It would allow the agency to evaluate the utilization of hovercraft in law enforcement and provide valid operational data for the manufacturer.

On April 27, 1984, the police took delivery of the Hake Husky Griffon Hovercraft, model 1000 TD. This craft was built by Griffon Hovercraft Ltd., Southampton, United Kingdom. Hull number one was a prototype, experimental craft, 8.45 m (27.8 ft) in length, capable of carrying ten passengers or a 1000 kg (2200 lb) payload.

Once the craft was accepted, the agency had to add the necessary equipment to make the craft compatible with the police role. This included the installation of a marine VHF/FM radio for contact with the maritime public, a low band FM police radio for operational activities and an electrified siren/public address system. Twin, flashing blue strobe lights were mounted on the windscreen top, one either side of the navigational radar. These lights are used for emergency response and the radar allows for high speed operation during periods of darkness or inclement weather. Also on the windscreen top were mounted three halogen lights, so arranged that one shines forward and one on each side of the forward bow quarters. These lights are used to illuminate landing sites, accident scenes, work areas or any other site as needed.

Additional equipment included a medical emergency kit, short back boards, clam shell stretcher, body recovery equipment for drowned victims, search and rescue equipment, portable fire pump, spare parts and a tool kit (ref. 1). The forementioned items are essential items only, items which must be considered in the cost of commissioning a hovercraft for law enforcement.

8.2.1 Selection and Training of Crew

The selection of personnel to form a hovercraft unit is critical to the unit's performance, both in efficiency and effectiveness of operation. Criteria must be established for the craft's missions, maintenance and operation. These criteria are based on the type of craft utilized and its capabilities. They should also weigh heavily toward establishing guidelines for crew selection. Without going into detail about the aforementioned criteria, consider the following example for clarification.

One of the missions assigned the hovercraft was emergency medical services. This assignment required the crew to be at least trained as Emergency Medical Technicians (EMT-A) or above. Prior training was required for selection to serve as crew members. In this case, maintenance was to be provided by the crew. The craft was powered by an air-cooled Deutz diesel engine, so the crew members were required to have a working knowledge of diesel engine operation and repair. The primary base of operation for the craft was set up in the mid-bay area near Annapolis. In order to have emergency response capabilities the crew members were required to live in the immediate area (within 30 minutes) of the base.

In this case, four officers were interviewed and selected to be reassigned from the field to the hovercraft unit. Problems immediately arose because the field commanders did not want to lose the highly qualified officers. But once again the problems were resolved and training began. This training program was conducted by two factory representatives and an agency officer for the first three weeks. Then the officers were allowed to continue training on their own for three months. This training period was interspersed with limited assignments which served as confidence builders for the crew.

On the other hand, this training period was not without mishaps; twice, the craft incurred considerable damage. On one occasion, it was from a collision with a piling, when the operator lost control while exiting the base; on another occasion, when the operator lost control while cruising and the craft side-plowed (ref. 2). Both of these accidents occurred as a result of operator error and adversely impacted the program. In addition to being time consuming and expensive, they provided arguments for critics of the program.

Training continued for three more months amid controversy, proficiency evolved from practice, and finally, the craft and crew were capable of accomplishing their assigned mission. Criticism began to erode, skeptics became converts and the program became operational.

8.2.2 Search and Rescue Missions (SAR)

Since 1959, the agency has been responsible for providing search and rescue service in Maryland waters. Demands for service continue to increase, with fiscal year 1986 showing that the patrol fleet responded to 1,677 emergency calls and 471 non-emergency calls. These emergency responses rescued or assisted 4,073 people and required 2,832 man-hours while the non-emergency responses assisted 744 people and required 1,408 man-hours to perform (ref. 3).

Primary examples of the aforementioned emergency responses include towing disabled vessels to port (764), freeing vessels from groundings (253), freeing vessels from ice (38), dewatering sinking vessels (34), fighting fires on board vessels (7), emergency medical services and transportation of victims (33 injured persons), search for overdue vessels (35), search for missing persons (28), and search for drowned victims (54).

These calls for emergency services generally occur during times of inclement weather, strong winds or at night, which stress both the equipment and the responding crews. This stress is further intensified by the fact that many search and rescue missions can only be performed by the use of navigational radar and Loran-C, due to limited visibility.

The addition of the hovercraft to the patrol fleet enhanced the emergency response capabilities of the agency and filled a void which existed in the immediate area of assignment. This void consisted of the inability to provide rapid response to emergencies by conventional patrol boats and light aircraft during freezing weather, snow storms and fog. The hovercraft, however, is capable of providing year-round rapid response in all weather conditions, even over ice-clogged rivers.

The hovercraft is capable of handling all emergency missions previously mentioned, including the towing of disabled vessels. However, towing is the least desirable mission for the hovercraft, since it can be accomplished by a conventional craft more expediently and efficiently. The hovercraft is generally capable of making a more rapid response than a conventional craft to the scene of an emergency in clear or inclement weather. This is due to the amphibious capabilities of the craft. Routes to the scenes can be shortened by transiting shallow water, sand bars, floating debris, etc. This is not possible by conventional craft without serious damage. The hovercraft crew keeps the agency communications center advised of the area that it is patrolling and responds to any call, or assists other patrol units as needed.

An example of search and rescue by the hovercraft involved a sinking vessel in heavy seas. A crew member was put aboard the sinking vessel, made temporary repairs and dewatered the vessel. The vessel was then escorted to a safe harbour.

On one occasion, the crew observed a sailboat strike the Chesapeake Bay Bridge and lose its mast. A crew member was put aboard the disabled vessel to assess damage and injuries to occupants. This maneuver with a conventional vessel would have been difficult due to the cables, ropes, sails and debris hanging overboard and capable of fouling propellers.

On another occasion, the hovercraft responded to a call of a vessel being aground in a tidal tributary. Two police boats were on the scene, but were unable to get within 0.6 km (0.5 mi) of the vessel which was aground. The hovercraft went alongside the vessel, removed the occupants and towed the vessel to deep water. This action saved approximately five hours of waiting for the tide to return.

These samples were given to show some types of emergency responses which can be handled by a hovercraft in a more efficient and effective manner than by conventional craft. The list can go on to include rapid shore-line searches for missing or injured persons, bodies of drowned victims and any other assignment in the shallow coastal waters.

8.2.3 Emergency Medical Services (EMS)

The investigation of boating and water related accidents is a primary mission of the Natural Resources Police. This includes providing emergency medical services to injured victims and their transportation to land based facilities. Therefore, since 1982, all officers graduating from the academy are trained as Emergency Medical Technicians. This training provides an increased level of care for accident victims and has enabled officers to save several lives since its inception.

The EMS mission is a primary mission assigned to the hovercraft since it is the most appropriate craft for the job. Its amphibious capabilities, structural design and smooth ride contribute toward enhancing the level of care provided to accident victims. This can be brought into perspective by citing the following examples which indicate that the hovercraft can out-perform conventional patrol craft in this type of mission.

The hovercraft responded to a call that a windsurfer was in trouble near the Chesapeake Bay Bridge. Upon arrival at the scene, the crew found an exhausted male subject, wearing a personal flotation device. Through conversation with the victim, it was learned that he had severely strained his back muscles and was unable to help himself. Even though seas were running 1.2 m (4 ft), the crew was able to retrieve the victim from the water and recover the sailboard. The victim and sailboard were transported to shore, across the beach to a waiting vehicle in the parking lot. This action saved valuable time and reduced handling of the victim. If a conventional patrol craft would have been used for the rescue, the injured person would have been taken ashore at another location due to the shallow water, and then transported overland to the waiting vehicle.

On another occasion, the hovercraft was on a routine law enforcement patrol at 11:30 p.m. when the crew monitored a *Mayday* call on VHF-FM channel 16. A tugboat Captain reported a pleasure boat with ten people on board had just collided with a barge, resulting in many serious injuries. The hovercraft responded to the scene, covering 32 km (20 mi) distance in 35 minutes. This quick response was possible by using navigational radar and transiting shallow water, not accessible to conventional patrol craft.

Emergency medical treatment was administered to the nine injured people at the scene. The three most seriously injured were placed on backboards and transported by hovercraft to the grounds of Fort Howard Hospital, which was the closest accessible land to the accident scene. The craft was driven up a boat launch ramp at Fort Howard, to land where a triage area had been set up in the parking lot.

This transport was accomplished in 6 minutes from the accident scene, while the less seriously injured victims were transported on two conventional patrol boats and required 26 minutes to reach the triage area. The amphibious capabilities of the hovercraft eliminated the problems associated with transferring patients from conventional patrol boats to docks, then into the ambulance, and reduced the victims' transport time by 20 minutes. Such a reduction in transport time and number of times the victim has to be handled is vital to serious trauma cases. It decreases the chance of aggravating the injury while enhancing the victim's chance of recovery (ref. 4).

These two examples of actual cases support the theory that today's mid-sized hovercraft are the most efficient and effective vehicles for handling waterborne EMS missions, especially in coastal and inland waters. These missions also include the transport of sick or injured people from isolated areas or ships to the closest land-based facility for treatment. Such cases can involve various conditions, from lacerations, to fractures, to heart attacks. Therefore, it is essential that the level of EMS training for the hovercraft crew be maintained, the trauma kit and equipment be upgraded periodically and communications be established with the land-based EMS organizations. If carried out, this will establish the basis for enhancement of the EMS program.

8.2.4 Emergency Evacuations (EE)

The evacuation of residents or users of Maryland's natural resources during natural or man-made disasters is a primary role of the Natural Resources Police. This role, as defined in the *Maryland Disaster Assistance Plan* and *Radiological Emergency Plan for Fixed Nuclear Facilities,* requires the agency to: 1) provide evacuation information to mariners and waterfront residents by public address systems from boats and/or motor vehicles, by personal contact, or by VHF-FM or citizen's band radios, 2) coordinate and evacuate pleasure boats from the waters which are affected by the disaster, 3) set up embarkation

and debarkation points to effectively handle waterborne traffic and evacuees, 4) provide boat transportation for evacuees from the area affected, and 5) provide monitoring of the affected area and monitor post re-entry of evacuees.

In the case of a disaster resulting from an accident at a fixed nuclear facility or a transportation accident involving radioactive material, the police will provide waterborne radiological monitoring of the perimeter. If the magnitude of the problem is beyond the capabilities of the officer's training and equipment, they will provide waterborne transportation for the monitoring teams from other agencies (refs. 5,6).

Since it is relatively impossible to predict when a waterborne accident may occur, the police must be constantly trained and equipped to respond in all types of climatic conditions, including ice covered waterways. Rapid response to the accident scene may only be possible by the use of hovercraft, especially if the waterway is ice covered, the water is shallow, or the weather is inclement. These are three geographic and climatic features which must be kept in mind when planning emergency response capabilities for all waterborne operations.

Natural disasters such as flooding create unique problems for emergency evacuation services. Respondents may find waterways and highways littered with debris and bridges washed away or damaged. In addition, highways and land masses are often covered with water to a depth which prevents vehicular traffic from transiting, while not deep enough to allow conventional patrol boats to operate.

When such conditions occur, the water movement over the land mass and waterways is often swift and turbulent. Therefore, operation of small conventional craft to effectuate a rescue or evacuation often becomes hazardous to the rescuer and the rescued. These craft (generally 4.2 m (14 ft) or less) are only capable of carrying two to four passengers per trip. This limited capacity increases the time required for mass evacuation while decreasing the chance for survival.

This method of evacuation is one of the most commonly used today because of the large number of small craft available to rescue organizations. However, this dependency on small conventional craft for evacuation missions may be eroded with the increase in small to mid-size modern hovercraft which are becoming available today.

These hovercraft (ranging in size from (5.9 m (20 ft) to 12.6 m (42 ft)) have been tested in swift turbulent water and found to be safe vehicles to operate, providing they are operated within the manufacturers' safe operating parameters. Not only do they perform well, they are capable of transporting five to thirty evacuees to safety per trip. These transports can generally be accomplished more expediently and efficiently by hovercraft than by

conventional craft. The hovercraft's completely amphibious capability should eventually make it the ideal vehicle for mass evacuations and ice operations.

8.2.5 Ice Operations

Ice operations are a major concern and a top priority for the hovercraft, due to the fact that the agency's response capabilities are at their lowest during periods of ice coverage on the waterways of Maryland. The conventional patrol craft have very limited ice breaking capabilities and attempt to break ice only in life threatening situations. The hovercraft, however, is capable of breaking ice or providing high speed transportation over it.

Ice-breaking experience with the Hake Husky Griffon, Model 1000 TD, hovercraft will be described briefly. Operational experience has shown that the hovercraft is capable of high speed icebreaking with the maximum icebreaking capability being directly related to load, open water hump speed and wave patterns generated in the floating ice sheet by the moving load. At or near hump speed (19.2-25.6 km/h (12-16 mph)), the wavelength is approximately equal to twice the length of the vehicle, radiating outward until the work energy is dissipated through cracks propagated in the ice sheet. This distance varies depending on ice conditions and load, but generally is at least three times the width of the craft on either side. These cracks are propagated by the heave and deflection of the ice as the load moves over it, thus causing smaller ice sheets to break away from the main sheet in the path of the craft.

The operator may then retrace his entrance path with subsequent paths or do a series of pirouettes to break the ice sheets even smaller. These small sheets of ice are then carried from the path by tidal movement or wave action. This opens a relatively clear path through the ice sheet and allows conventional craft to operate without damage. The Model 1000 TD hovercraft has been used consistently to break salt water ice up to 12.5 cm (5 in) thick. With a light load, this can be accomplished expediently, effectively and efficiently.

Some examples of ice operations include high speed patrols over the ice for law enforcement, search and rescue, damage assessment and service to aids to navigation. Speeds attained on these patrols have reached 101 km/h (60 mph) with the trips completed safely.

On one occasion, the hovercraft transported U.S. Coast Guard personnel to the upper Chesapeake Bay to assess ice problems. Approximately 40 km (15 mi) of this trip was over ice pack, with the area ninety percent ice covered. This trip was completed very expediently due to an average cruise speed of 73 km/h (45 mph).

On another occasion, the U.S. Coast Guard requested assistance from the unit to make emergency repairs on a major channel range light. Ice conditions and shallow water prevented any unit except the hovercraft or helicopter from

approaching the light. By using the hovercraft, valuable time, resources and operational expenses were saved.

On numerous occasions, the hovercraft was contacted to break ice in various small boat harbors so the commercial fishermen could get out to the fishing grounds. Ice coverage in the harbors ranged up to 15 cm (6 in) in thickness and was quickly and easily broken, without damage to the hovercraft or those craft receiving assistance.

In addition to the aforementioned, ice can be broken quickly and efficiently around piers, bulkheads and launch ramps, without being restricted by water depths and without causing damage. This is a capability inherent only to hovercraft and a tremendous plus when compared to conventional ice breaking craft.

Today's hovercraft can fill a void which may exist in an agency's overall operation and enhance its capabilities. This is true for waterborne law enforcement agencies as well as other service agencies.

8.2.6 Patrol and Law Enforcement

The hovercraft is assigned routine law enforcement patrols, especially during times of peak activity, darkness and limited visibility, if not on special assignment. One must remember that the hovercraft is a special purpose vehicle which supplements the patrol fleet. If used in the day-to-day routine patrol, it does not perform as well as conventional patrol craft. However, if properly used, it is more efficient, effective and expedient than conventional patrol craft. Examples of proper use of the hovercraft include law enforcement patrols during times when conventional craft are unable to operate and in those areas not accessible to them.

On one occasion, the hovercraft was used to provide security for the President of the United States. Security personnel were transported over a marshy area to set up a perimeter. This area was only accessible to hovercraft or helicopters.

On many occasions, the hovercraft is used to patrol the shallow water areas and coastal marshes not easily accessible by conventional patrol craft. This extension of the patrol area prevents violations, and allows apprehension of violators and seizure of contraband. It also allows the officers to check for pollution sources and take samples, which previously could only be accomplished by aircraft.

The hovercraft can also be used effectively as a surveillance platform from which to observe activities in the area. Its amphibious capabilities allows the craft to be hidden on the beach, in the reeds and elsewhere. From this vantage point, officers can conduct electronic or optical surveillance. Such action has been used successfully in cases involving larceny of commercial fishing gear and distribution of controlled dangerous substances.

Today's modern hovercraft are on the threshold of rapidly expanding applications. Modern technology and product reliability have made the hovercraft economically comparable to other types of watercraft, including purchasing and operating costs.

8.2.7 Hake Husky Griffon Model 1000 TD Hovercraft

The model 1000 TD is an amphibious hovercraft powered by an industrial air-cooled diesel engine driving a fixed-pitch ducted propeller and a centrifugal lift fan. The hull is made from marine grade aluminum, bonded and riveted, and consists of three separate compartments: the passenger and crew accommodation, the fan bay and the engine compartment.

The commander is seated on the left (port) side, at the forward end of the cabin. The crew chief's (radar operator's) seat is directly opposite on the right (starboard) side. Behind the crews' seats and running longitudinally aft along each side are seats for four passengers each. Engine speed is controlled by means of a throttle lever and a clutch pedal enabling the propeller to be disengaged to facilitate engine operation. The craft is steered by a steering yoke which operates twin air rudders mounted behind the propulsion duct. Quick changes in longitudinal trim may be achieved by using the four elevators mounted in the propulsion duct and changes in lateral trim are made by skirt shift. Longer term longitudinal changes may be achieved by fuel ballast transfer, while lateral trim is achieved by weight distribution as needed.

Full engine instrumentation is fitted to the dash panel, which also carries the fuel contents gauge, roll/ballast indicator compass and electrical switches. Rigid side bodies, which may be hinged upwards for transport, are fitted to the sides of the aluminum hull. The skirt is of the loop and segment type and is made from neoprene coated nylon. When not hovering, the craft rests on four, replaceable, heavy duty, rubber landing pads.

(i) Craft dimensions. The overall dimensions of the craft are as follows:

(a) External dimensions:

Over-all length, power off	8.45m	(27.8 ft)
Over-all length, power on	8.52m	(28.1 ft)
Beam	3.94m	(13.0 ft)
Beam with skirt inflated	4.80m	(15.8 ft)
Height over-all on landing pads	2.70m	(8.9 ft)
Height over-all skit inflated	3.19m	(10.5 ft)
Draught afloat:		
- to bottom of main structure	0.20m	(0.66 ft)
- to bottom of landing pads	0.26m	(0.85 ft)
Cushion area	$25.1m^2$	($271.8\ ft^2$)
Skirt depth	0.48m	(1.58 ft)

(b) Internal dimensions:

Length	3.20m	(10.56 ft)
Maximum width	2.20m	(7.26 ft)
Maximum height with hood fitted	1.42m	(4.68 ft)

(c) Weights:

Payload	1000 kg	(2200 lb)
Unladen weight	2000 kg	(4400 lb)

(ii) Engine. The craft is powered by a Deutz BF 6L913C six-cylinder, in-line, air-cooled, direct-injection diesel engine, producing 178 bhp at 2500 rpm. Fuel consumption, according to the manufacturer, ranges from 18.9 ℓ/h (4.9 gal/h) at 2100 rpm to 31.5 ℓ/h (8.2 gal/h) at 2500 rpm. Fuel capacity is 190ℓ (50 gal), which provides for an 8 hour, 400 km (250 mi) cruising range under average operating conditions.

The lift fan, which is driven off the front of the engine, is constructed of marine aluminum. It is a centrifugal type, measures 0.835 m (2.75 ft) in diameter, and runs at 1875 rpm with the engine at 2500 rpm.

The propeller, which is driven off the rear of the engine through a standard automotive type clutch, is constructed of wood, contains 4 blades and measures 1.37 m (4.52 ft) in diameter. The propeller operates within an aerofoil duct, with duct/propeller clearance of 6 mm (0.2 in).

(iii) Craft structure. The central structure of the Griffon is punt shaped and constructed of flat sheets of marine grade aluminum. A four-panel wind screen in an aluminum frame, with side windows in toughened glass, is provided. A flexible PVC hood, with side windows, covers the passenger/cargo area. Structural loads are carried by two longitudinal beams, running fore and aft. These beams are the only points suitable for lifting or jacking the craft. The hull is fitted with four lifting points, two in the forward area of the cockpit and two in the engine compartment on the rear of the engine frame. Two towing cleats are provided on the front deck with four more cleats fitted around the perimeter of the craft.

(iv) Air cushion and lift system. The craft is supported during operation on a cushion of low pressure air, contained under the craft by a loop and segment flexible fabric skirt. The skirt allows the craft to lift clear of the ground, and allows obstacles to pass through and under it with a minimum drag. By containing the lift air in this fashion, the craft uses less power for lift and the spray generated when the craft is running over water is minimized. The skirt also provides stability when the craft is hovering.

The lift fan is mounted behind the cockpit and driven from the front engine shaft via a powder coupling to minimize snatch in the transmission when starting and stopping the engine. This fan, of the centrifugal type, with backward facing blades, is mounted vertically in a casing. The casing serves

to collect and distribute the lift air and to give the fan protection from spray and debris damage.

(v) Craft power and transmission systems. The engine, the propulsion system and the lift fan may be removed simply and as separate units. Power for the lift system is taken from the front of the engine crank shaft. The fan shaft is mounted horizontally in two plummer block bearings, one on either side of the fan, and is driven by an HTD tooth belt. The propeller is driven from the rear of the engine via an extension from the engine bell housing. A pulley is mounted on the extension drive and power is transmitted by an HTD tooth belt to the fixed pitch propeller. Both tooth belts may be changed without the removal of any major component, and this can be achieved any time it may be required.

The engine is fitted with a standard automotive clutch which engages/disengages the propeller. This innovation in hovercraft technology, while certainly not new, is a welcomed addition. It provides for ease in starting the engine, and allows the craft to be hovered without forward thrust and to be easily manhandled when necessary. In addition, it enables the propulsion system to be rotated by hand for inspection, which should be performed daily, prior to going into service.

(vi) Craft control systems. The craft control systems may be divided into four groups: electrical, engine control, maneuvering and trim. The electrical systems are standard type, powered by a 12 V, 65 A engine-driven alternator, which charges one 12 V, 108 ampere-hour battery. The systems are protected by circuit breakers and fuses, with a battery isolation switch located under the operator's seat, which breaks all the electrical circuits, if needed.

The engine controls consist of a right-foot operated clutch, pedal and a left-hand operated, morse type, throttle lever, both adjacent to the commander's seat. There is also an engine shut down switch, cable operated, mounted on the throttle console. These three items provide the commander with complete control over the power train.

The craft is maneuvered by twin aerodynamic rudders mounted in the propeller duct outlet. These rudders are activated by a morse type cable from a hand-operated steering yoke mounted on the dash panel. Maneuvering may also be assisted by actuating the skirt shift.

The craft is trimmed by elevators mounted inside the propeller duct, a skirt shift system and a fuel ballast system. The four elevators are operated by a morse type cable from a lever operated by the left hand. They are used to alter longitudinal trim, to counteract wind forces or balance payload distribution. They may also be used to blank off the propeller efflux and push the craft stern down for speed reduction.

Skirt shift is achieved by an electric winch operated by switches mounted on the dash panel. Skirt shift causes the craft to bank to left (port) or right (starboard) and may be used to assist in maneuvering, adjust lateral trim, counteract a side wind, or inspect the skirt and finger system while up on hover and at a stand-still.

The fuel ballast system consists of three tanks, a 190 ℓ (50 gal) tank in the bow, a 114 ℓ (30 gal) tank in the stern, and a 22.8 ℓ (6 gal) service tank in the engine bay. Fuel may be transferred from one tank to another by means of electrically driven pumps, operated by a toggle switch on the dash panel. This transfer is used to provide longitudinal trim as needed. As the fuel is transferred fore to aft, the service tank from which the engine operates is always topped off, thus insuring an adequate fuel supply for the engine (refs. 2-7).

8.2.8 Test and Evaluation of Model 1000 TD Hovercraft

The Natural Resources Police have conducted tests and evaluations of the hovercraft over every type of accessible terrain and in every climatic condition found in the Chesapeake Bay and Coastal tributaries of Maryland. This terrain includes water, marsh, mud flats, sand beaches, grass fields, barren land, launch ramps, parking areas and public highways. The climatic conditions have included temperature variations from -11°C (12°F) to 44°C (112°F). Tests have been conducted during periods of fog, rain, snow and in winds up to 72 km/h (45 mph) during a two-year period.

(i) Water. The craft was operated over surf, ocean swells, short choppy seas and swift moving water. These tests were performed both fully laden and unladen.

Operations were conducted from the beach, through surf running 1.5 m (5 ft) without difficulty, then returning to the beach from the ocean. Ocean swells of the same height posed no problems when transited.

Short, choppy seas of 1.5 m (5 ft) posed no problem for the craft when unladen and operated routinely on patrol in the coastal waters. When the craft was heavily laden, problems with sustaining hump speed were sometimes encountered. This could be surmounted by altering course (tack) off wind at a 45° angle in order to maintain speed.

Swift moving water up to 17.6 km/h (11 mph) velocity posed no problem with operation and maneuvering. The craft was operated in both the displacement and hover mode without difficulty. Operating speeds were varied from no headway to 46 km/h (28 mph) during the swift water tests.

(ii) Marshy area. These tests were conducted over dry and wet marsh grasses, water-lillies and tall reeds. Heavy saw-toothed grass less than 12 cm (5 in) in height, on a dry marsh bed, can be transited with an unladen craft, both from moving and take-off positions. With a laden craft, the grass had a tendency to allow air to escape from the skirt system. This reduced hover height and created enough drag to hold the craft.

This same grass protruding above 2.5 cm (1 in) of water could be transited relatively easily, whether laden or unladen. The water helped create a seal to allow full hover height, while reducing friction and drag on the skirt, thus allowing the craft to move freely.

Areas heavily infested with water-lillies and other aquatic vegetation protruding 15 cm (6 in) above the water's surface could be transited easily, whether laden or unladen. Marshy areas with heavy reeds protruding 0.9 m (3 ft) or more could not be transited at slow speed. Distances of less than 50 m (55 yd) could be transited if penetrated at hump speed or above.

(iii) Mud flats and sand beaches. Mud flats and sand beaches posed no problems for the hovercraft. Transit was easy and could be accomplished with the craft laden or unladen, at speeds up to 64 km/h (40 mph).

(iv) Grassy fields and barren lands. Operation over grassy fields posed no problem when grass height did not exceed 12 cm (5 in). Grass heights above 12 cm (5 in) caused loss of cushion air and resulted in skirt drag, which hampered operations. Barren land posed no problem with operations, either laden or unladen, provided its surface was relatively smooth and level.

(v) Launch ramps and parking areas. Numerous tests were performed on various sloped ramps. Most ramps posed no problem for the craft, eight-degree slopes being climbed from take-off with an unladen craft. These steep ramps posed no problem even for a laden craft provided they could be approached at or near hump speed. Launch ramps with slopes of 5° to 8° were the most desirable and could be transited easily.

Parking areas were generally easy to transit. However, operators had to be constantly aware of wind angle, slopes, vehicles and patrons in order to transit these areas safely. Prop wash could carry debris which could cause property damage or injury to vehicles and patrons. Therefore, operations on this type of terrain should only be performed when necessary.

(vi) Public highways. Operation over public highways could be accomplished in the event of an emergency situation. The craft was tested in this environment, both laden and unladen. This was a tricky operation due to road bed crown, since the craft would tend to drift towards the lowest point of the slope. The key to success was to seek a road surface that was flat. When the road surface was completely covered with water, the operational problems were reduced or eliminated.

(vii) Ice. The ice breaking capability of this craft exceeded expectations. Some problems were encountered during the first ice breaking trials, when spray generated while transiting open water froze on the craft and in the propeller-duct structure. This ice build-up reduced the clearance between the propeller tip and duct wall, causing damage to the propeller. This problem was eliminated by the addition of a spray skirt and by redirecting exhaust manifold heat, such that the exhaust was drawn through the propeller duct.

8.2.9 Evaluation of the Hovercraft Program

The overall program is very successful. The model 1000 TD hovercraft exceeded every maximum performance limit established by the manufacturer. This performance was accomplished at an actual operational cost of approximately 28% less than projected for the trial period.

The patrol missions assigned to the hovercraft include all missions assigned to the conventional patrol craft. In addition, the hovercraft carries out those missions unique to its capabilities. These include patrolling areas not accessible to the conventional patrol craft, such as shallow waters and ice patrols. These functions cannot be performed as well by any other type of surface craft.

The excellent public relations received from the implementation of this program have surpassed any program operated by this agency. Coverage by newspapers, national magazines and television has attracted inquiries from around the world.

The most significant shortcoming of the program was the lack of personnel to provide for a 24-hour operation of the craft. This shortage adversely impacted the program by preventing it from reaching its maximum potential. Shortcomings of the craft itself have been relatively minor and appear to be the direct result of it being a prototype and a learning experience for both the manufacturer and the operator.

The hull structure remains tight and shows only a minor amount of corrosion and deterioration, which can be corrected through normal maintenance. The flexible PVC hood which covers the passenger/cargo area deteriorated and had to be replaced. This problem is common to the marine environment and conventional craft also.

The instrumentation and electrical system produced some minor problems, originating from the method used and the mounting locations of instruments, fuses, and electrical connections. These problems were increased by the added electronic gear which the agency installed and were completely eliminated by reworking those areas.

The propulsion assembly produced some unexpected problems. Routine inspections revealed some rust and corrosion on the engine cooling fins, which was corrected by cleaning and treating the engine for marine use. This treatment corrected the problem and should eliminate future problems.

The original propeller fell short of the 600-hour life expectancy. However, the erosion problem has been corrected and the current propeller has exceeded expectations. Powder couplings, shaft assemblies and drive belts were monitored closely early in the program. This prevented problems from developing and allowed drive belts to exceed their expected life.

The skirt and finger system exhibited some minor problems with fasteners, and tie backs early in the program. These problems were corrected during routine maintenance by changing the types of materials and replacement parts used. Once these minor problems were corrected the skirt and finger system performed beyond expectations, with the original loop still in use after 1500 operating hours.

8.2.10 Cost Effectiveness

It is difficult to compare the cost effectiveness of the hovercraft with conventional patrol craft. The hovercraft should not be viewed as a replacement for conventional patrol craft, even though replacement can occur in some instances. It should be viewed as the craft best suited for selected assignments, with the capability of enhancing the agency's mission and broadening its horizons.

During a two-year period, the Model 1000 TD was operated over 1200 hours, with an average fuel consumption of slightly over 15.2 ℓ/h (4 gal/h), and a total hourly operational cost of $9.35/h. These operational costs are approximately 50% of the cost of operating a conventional patrol craft. This is an impressive figure which was not anticipated.

Without an accurate method of predicting the durability and longevity of the hovercraft and its components, one can only project on the basis of experience. It is felt that the life of the hovercraft will compare favorably with the established life of conventional patrol craft, which is a 10-year serviceable life. Furthermore, it is felt that new technology in construction, skirt and propulsion design will continue to decrease production and operational costs as the market becomes more competitive. This technology will become more aligned with the marine industry, which should make parts more readily available and maintenance easier. Therefore, the cost effectiveness of operating hovercraft should continue to improve.

8.2.11 Trends for the Future

Interest in hovercraft is being shown by the public and private sectors, not only in Maryland but elsewhere. The U.S. Coast Guard is now proceeding with certification of hovercraft for use in commercial applications such as water taxis, sightseeing cruises and ferries. A demand for various sizes of hovercraft is growing for craft ranging from two to thirty passengers. To exploit this demand, several new companies have begun production of various sizes of craft in the United States. New dealers have established themselves on the East Coast to market these craft, with at least six dealers now operating in Maryland.

Hunters, fishermen and recreational boaters are now finding hovercraft technology fascinating, intriguing, or just a necessity to complement their other recreational interests. As this interest escalates and suppliers meet the demand, the requirement for services from law enforcement, search and rescue and emergency medical units will also increase.

8.3 CANADIAN COAST GUARD

By 1968, the potential of amphibious hovercraft had been sufficiently demonstrated, including three significant operations in Canada, to attract the attention of Canadian Coast Guard (CCG) to the concept of using it as a Search and Rescue resource. An SRN-5 hovercraft was therefore purchased from British Hovercraft Corporation, equipped to meet a CCG specification.

The waters between Vancouver and Vancouver Island contain some of the most dense and diverse population of marine craft (and aircraft) in the world. Therefore, Vancouver was selected as the base, specifically Vancouver International Airport - itself on an island whose shoreline is largely tidal and mud-flats.

The SRN-5 021 craft (Fig. 8.1) arrived at Vancouver, in July 1968, and shortly after performed her first rescue, while still engaged in crew training. In 1985, after a long eventful career, it was retired as the last remaining operational SRN-5.

In 1972, CCG expressed interest in the wider use of hovercraft in a number of

Fig. 8.1 SRN-5 (right) and SRN-6 (left) hovercraft of the Canadian Coast Guard at Vancouver base.

CCG roles. It participated in development trials of the Bell Aerospace Canada Voyageur, whose flat deck and 20-tonne payload capacity made it well suited to multi-tasking. The trials took place in 1972 and 1973 on the Great Lakes and in the northern reaches of the Mackenzie River and the Beaufort Sea. As a result, Voyageur 002 was purchased and entered CCG service in 1974. Initially based at Parry Sound on Lake Huron, it was moved to a base at Montreal in 1975. Again, after a long and varied career, it has now been retired, finally being sold as scrap in 1988.

By 1976, increased marine activity and additional tasking of 021 at Vancouver prompted consideration of additional craft. Experience with 021 indicated the need for a larger cabin but little other change; the SRN-6, essentially a lengthened SRN-5, met the requirement (Fig. 8.1). Accordingly, a new SRN-6-039 was purchased and then delivered to Vancouver in July 1977. The operational equipment was installed at Vancouver, and the craft entered service in September.

In 1979, two badly damaged SRN-6 craft, and a large quantity of spares were purchased at a very reasonable price from a defunct operator in Northern Canada, as a long-term source of spares for the SRN-5 and 6. But by 1980, increased fishing fleet activity was stretching the geographic coverage, resulting in extensive unproductive transit times. It was therefore decided to form a detachment of one craft, and deploy it to Parkesville, on Vancouver Island, some 100 km north of the main base. The advantage of the larger cabin of the SRN-6 and signs of old age on 021 focussed attention on the possibility of rebuilding one of the damaged craft. This was successfully carried out, entirely by CCG personnel at the Hovercraft Unit, and SRN-6 031 took on a new lease of life in late 1981. The SRN-5 then reverted to training and back-up, and when retirement became inevitable, the remaining damaged SRN-6, 030, was rebuilt; it was commissioned in 1986, proudly bearing the registration letters of its illustrious predecessor, CH.CCG.

By this time, Voyageur was also becoming very difficult and expensive to maintain and operate, being the only Voyageur still in operation. Experience with this craft was extensive and this was used to clearly define the specification for a replacement. British Hovercraft Corporation, now Westland Aerospace, responded with a variant of the AP.1-88 passenger ferry. A contract was negotiated in early 1986, and after acceptance trials in England, *Waban-Aki* (Fig. 8.2) entered service in Montreal in September 1987.

By the usual commercial yardstick of operating hours to measure experience, CCG hovercraft utilization is not very impressive - a cumulative total of about 30,000 hours using 6 craft over a period of almost 21 years. But many of the rescue missions, now totalling about 6000, have been dramatic and courageous, and the variety of roles and tasks performed by both CCG units are without

Fig. 8.2 Canadian Coast Guard *Waban-Aki* (BHC AP.1-88) hovercraft based at Montreal.

parallel. The more significant features of the two units and their operations, described in the following paragraphs and refs. 8-18, clearly illustrate how the potential of amphibious hovercraft can be realized by skillful and intelligent appreciation of that potential and application of experience.

8.3.1 Canadian Coast Guard Organization

In order to place the CCG hovercraft in the correct perspective, a very brief overview of the CCG organization will assist the reader. The CCG is a component of the Marine Administration within the Department of Transport, headquartered in Ottawa.

With a broadly stated mandate to assist safe navigation of shipping in Canadian waters, there is a large variety of tasks to be performed. Many of these are at the water-land interface; others involve operation in hazardous locations. The more major tasks include: a) laying, maintaining and position-checking of buoys, b) construction, maintenance and supply of fixed navigation aids (lighthouses, beacons, radio towers, range markers), c) ice-breaking and management, d) sounding and dredging, e) pollution control, f) search and rescue g) vessel traffic control, h) regulatory inspection of vessels, and

i) assistance in law enforcement.

To administer its mandate over all Canadian waters, CCG is organized into geographic regions, each of which is autonomous, responsible for utilizing and maintaining its designated resources and carrying out its share of the mandate. Each region must also justify any requirements for new or additional resources. Therefore, the introduction of an entirely new type of resource such as a hovercraft must overcome traditional experience and skepticism, and requires perception and imagination.

This resistance to change is by no means unique to CCG, even after 15 years of successful CCG operation of hovercraft. The Maryland Natural Resources Police, who have many similar tasks, found this resistance to be a daunting challenge. But the two regions in CCG with experience of hovercraft utilization have learned to appreciate their potential, and the initial skepticism has changed to increased application in many tasks. This change in perception was vividly demonstrated in both of the Regions in which CCG hovercraft operate, when proposals made to re-locate them were met with such resistance that they were dropped. The two Regions are: a) the Western Region, where the CCGHU (Canadian Coast Guard Hovercraft Unit) is based at Vancouver and Vancouver Island, and b) the Laurentian Region, where the E&D (Evaluation and Development) Unit was based at Montreal (1974-1980) and the Laurentian ACV Unit is also based at Montreal since 1980.

8.3.2 CCGHU Operations

The ACV's in CCGHU are primary Search and Rescue (SAR) resources, and as such are at instant readiness to respond to an emergency 24 hours/day, 7 days/week. This state of readiness has been possible since the first SRN-6 was commissioned in 1977. Whereas SAR is the primary and, therefore, pre-emptive role, the craft are also utilized on a wide variety of other tasks, such as:

a) Servicing navigation aids, by transporting technicians to service beacons in difficult locations, checking buoy positions, and servicing buoys;
b) Law enforcement, by high speed transportation of inspectors or law enforcement officers to inspect ships, fishing equipment or marine traffic violators;
c) Pollution control. In numerous exercises, Unit craft have demonstrated their ability to deploy a variety of pollution control equipment rapidly, including deployment of 300 m of boom direct from a road trailer on the beach (Fig. 8.3). With their very comprehensive communications equipment, the craft lend themselves admirably to serving as an on-scene command and coordination centre;
d) Shore-line patrols and surveys, carried out for a variety of agencies, including environmental studies, wild-life surveys, and anti-narcotics;
e) Ice breaking. Every four or five years (1989 was an example), low tempera-

Fig. 8.3 SRN-6 hovercraft of CCGHU streaming 300 m of oil boom directly from a road trailer.

tures cause the harbours and rivers used by fishing fleets to freeze over to a depth of up to 10 cm, and the Unit craft are readily capable of breaking and managing the ice to permit the fishing fleets to continue operations.

However it is the SAR role which is the Unit's prime function, and by their 20th anniversary since official dedication to this role, they have responded to approximately 6000 emergency calls. The average response time is under five minutes.

Emergencies can run from a simple daylight assistance to a pleasure boat which has run aground, run out of fuel, lost a propeller, etc., to a night cliff rescue in gale force winds. Towing has figured prominently in incidents, including retrieving floatplanes from the tidal mud-flats which surround much of Vancouver Airport; vessels up to 16 m in length have been towed. One of the more dramatic rescues occurred in late 1968, before the Unit was officially assigned to SAR duties, when 5 persons were removed from a 20 m pleasure boat aground on a rocky island. This operation was carried out in 35 knot winds, with an air temperature of -12°C and the sea 50% pan ice. Another incident demonstrated the speed and coordination capabilities when two large ships collided, resulting in several injuries. A craft was on patrol nearby; within minutes, the survivors were being transported at speed to ambulances which the craft had alerted by radio.

With the radar and searchlights, neither low visibility nor night-time conditions restrict operational capability; one of the floatplanes towed off the mud-banks had lost its way in fog, and was retrieved within 15 minutes.

The most dramatic incident amongst many in the Unit's 20-year history was probably the night in 1975 when the SRN-5, responding to one of a multitude of

emergency calls caused by a 65-knot gale, collided at 25 knots with an unlit dismasted yacht. Heavily damaged, taking on water and inoperative, the craft was barely kept afloat; but, after a long struggle, it was eventually towed in and lifted ashore to present a long and challenging task to the maintenance engineers.

8.3.3 CCGHU Equipment 1989

The three SRN-6's now in operation have been developed in the light of experience to the point where they are identical in all essentials. This development started in 1977 when the first N-6 arrived. Now, the process continues, but only insofar as equipment is being upgraded.

Externally, the two striking features are the large side decks, and the cluster of antennae sprouting from a mast above the cabin. The large decks provide good working surfaces for transferring equipment or personnel to another vessel, or for recovery of persons from the water. They also incorporate long range fuel tanks, extending endurance to about 8 hours at cruise power. The large cluster of antennae provides the N-6's with an extremely comprehensive navigation and communication capability in both marine and aircraft frequencies. Radios carried include HF-SSB, VHF, C.B., and telephone, while navigation is provided by P.P.I. Radar, Loran, Plotter, ADF and doppler speedmeter. Several of the aids are duplicated, of necessity. Since accurate recording of SAR incidents or law enforcement missions is required, the electronic plotter is highly sophisticated, state of the art, and a tape recorder is carried for the same purpose.

Also, on the mast with the antennae are two Nite-sun search lights, fully controlled from the crew compartment and providing excellent variable illumination for either long-range searching or lighting an incident scene. Also, on the outside of the craft, a heavy towing hawser is permanently shackled to the stern, and is stowed and secured on the port side deck, accessible and ready for passing to a vessel requiring towing.

Internally, the operator's position to starboard is relatively standard, as is the crewman's position in the port bow. Immediately behind the operator is the navigator's station or more correctly, the operation's centre. It is here that all the navigation and communication equipment is located, together with navigation charts, listings of all radio frequencies, and call signs or telephone numbers of all SAR resources and emergency agencies in the operating area.

The remainder of the cabin, some 5 m long, 2.8 m wide, is given up to storage of rescue and first-aid equipment, and limited seating. Rescue gear includes scuba diving suits, pump, swimming gear, heavy duty clothing, and large tool kit. Medical equipment includes stretchers, a body splint, oxygen, splints, cervical collars, saline, and kits for burns, hypothermia, obstetrics,

and body recovery.

The Vancouver base is provided with normal and emergency telephones, and land-based radio links. At Parkesville, the base has normal telephones and land-based radio.

8.3.4 CCGHU Personnel and Organization

The task of developing an organization which will provide instant response to emergency calls throughout 8700 hours/year (8784 in a leap year), and also maintain, refit and overhaul the craft and their engines, is not simple; various systems have been tried and discarded at Vancouver. In Parkesville, the situation is relatively simple in that the one craft has two complete crews, with the off-watch crew on an instant-call pager. Parkesville is neither manned nor equipped to carry out maintenance other than routine servicing.

The watch system put in place in Vancouver in early 1989 had five complete craft crews to man the two craft, although only one crew was on duty at the base under normal conditions, with a working day split into a 10-hour day shift and a 14-hour night shift. Two crews work a 4-day cycle: one on the day shift; the other, on the night shift. They then have 4 days stand down. When stood down, each crew is on a priorized stand-by status; in the event that one craft is deployed on an emergency, the priority one stand-by crew is called in by phone or pager.

Also in 1989, a long-standing need for a fourth craft crew member, which had previously been met on an opportunity basis, was satisfied by including the Unit maintenance engineers in crews. Many times in the past, crews had difficulties at rescue sites due to the need for a person at the controls, plus one monitoring and coordinating communications, while the rescue needed more than one person outside. Introducing an engineer filled another previously undetected gap, identified almost immediately when an on-board engineer alerted the craft captain to gasoline leaking from a simulated rescue site. The crew engineer is now responsible, in case of need, for ensuring site security by making certain that craft actions do not escalate an emergency.

A craft crew in 1989, therefore, consists of: a) a Craft Commander and a First Officer, whose qualifications permit them to be fully interchangeable at the craft controls or at the navigation/communications station, b) an engineer, and c) a rescue specialist, who is trained in rescue procedures, advanced first aid, swimming, diving, and use of all the on-board equipment. One noteworthy feature of the Unit's operational crews is the inclusion of two ladies: one qualified as a First Officer in the early 1980's; the other, as a Rescue Specialist.

Since 1968-1989 is quite a long period, the reader may question why the Unit organization is still fluid. There is no simple answer because the reasons include a number of factors. One big factor which must be recognized

in any organization where the work is of an emergency response nature is the need to relieve boredom and avoid the morale problems which it can so easily breed. Another factor is the need for continuation training, both in craft operation and navigation. Evaluation of new equipments and procedures is also necessary. Over the years, demands for the Unit's assistance from different agencies have affected internal organization. One craft was deployed to Prince Rupert, 600 km north, for an extended period, the Parkesville detachment was formed, and the two old SRN-6's were rebuilt. All these were factors which put different demands upon Unit personnel, and it is only in the late 1980's that the Unit has taken on, at least temporarily, a stable fleet of craft with a reasonably stable workload. Each Craft Commander and First Officer has some extraneous duty or project to provide variety. Training is a major internal commitment; one of the senior Commanders is responsible for training new candidates and refresher training for Unit crews. The Unit is continually evaluating equipment, night vision devices and radars being prime and continuing candidates; an officer is assigned to each evaluation project. Also, the Unit is an integral part of virtually any marine emergency in the immediate area. In recognition of this, the various and numerous agencies (at Federal, Provincial, Municipal and even private levels) devise exercises or simulated emergencies. Each of these involves pre-planning and post-evaluation, for which one or more Unit officers are assigned.

The 1989 Unit organization is not necessarily final. It appears to meet the current Unit roles and tasks, but may yet require further fine tuning. This is possibly a lesson which may be learned, that the organization set up to operate a Unit has to be as flexible as the tasking which is given to the Unit.

8.3.5 CCGHU Maintenance

From the outset, CCGHU was envisaged as a self-contained Unit carrying out all maintenance and, with some minimal external assistance, repairs. A nucleus of experienced engineers started the maintenance organization which, by internal on-the-job training, has now proven itself almost totally self- sufficient. The only exceptions are: a) the sharing of specialized electronic technicians with the airport to maintain the craft communications and navigation equipment, and b) full engine overhauls, which are contracted out. Engine maintenance was an initial problem with long lead-times and supply lines to England; in 1981, however, the base was equipped with full overhaul tooling and one engineer was trained. This enabled the Unit to perform all engine maintenance, but experience and changes in engine overhaul policy showed that more productive utilization of manpower and tooling would result from relocating this activity to a nearby commercial engine overhaul facility. This has proved itself to be totally successful; the Unit now has spare overhauled engines available at all times.

Unit personnel can point with pride to their achievements in craft repair and re-build. Very heavily damaged and lucky to survive a night collision during a storm rescue in 1975, the SRN-5 was successfully repaired, including a complete replacement of the electrical system and much of the bow and port side structure, in 4 months. Both of the two SRN-6's purchased in 1978 were completely rebuilt by the Unit; one had heavy damage to the hull near the lift fan, the other was damaged on one side. The side structures, incorporating the long-range fuel tanks, were constructed and completely new electrical systems were installed; contracted assistance installed the electronic equipment, to Unit specifications, and the furnishing of the first-aid and rescue stations. Including the initial purchase price (which included a comprehensive array of spares) Unit personnel provided CCG with two fully operational up-dated craft for a cost of under $1.5 M in 1987 dollars.

Craft on instant readiness for emergency response are parked on the ramp with cabins continually heated and ventilated. Experience has shown that, even with careful routine maintenance, the continual exposure to the salt atmosphere, and rescues in all weathers, causing the cabin interior to receive more than its fair share of salt water, requires the craft to undergo a thorough structural inspection after about 10 years. Given this, both the SRN-5 and 039 were given new leases of life, but with all 3 current craft now approaching 20 years, and specialized spares becoming difficult to find (the only remaining SRN-6's are in military service in the Middle East and in Belgium), refits involving more than commonly available material will become a challenge.

8.3.6 Evaluation and Development Unit (1974–1980)

As previously mentioned, Voyageur 002 entered CCG service in 1974 following a period of evaluation and development. Everything about the early years of Voyageur operation in CCG was unique. At that time, all hovercraft expertise in CCG Headquarters was concentrated in the ACV Division of the Ship Safety Branch, with only a tenuous link to the Branch and Regions who were responsible for acquisition and operation of Fleet resources. The Division developed the concept of acquiring a number of different hovercraft and placing them in the various regions to demonstrate how the unique features of hovercraft could assist in Coast Guard tasks. In the early 1970's, the Canadian Government had funded a number of projects to develop Arctic oil and gas exploration, included in which was the Voyageur, originally conceived as a 20-tonne arctic transport. Due to the vagaries of oil exploration, the Voyageur did not go into full production, and the second prototype belonged to the Government. It became the first, and as it turned out, the only hovercraft in the Coast Guard Evaluation and Development Unit (E & D Unit). The ACV Division in Headquarters now owned a hovercraft, but had no base from which it could operate, and no clearly defined task. Regional staff had no experience of, or perceived requirement

for, hovercraft, and the ACV Division staff had an uphill battle against the traditional resistance to change. The only attraction to a Region was that Headquarters would provide some facilities, which would be Regional assets if and when the Unit moved.

The first base was at Parry Sound, in the middle of the summer resort area of Georgian Bay on Lake Huron. It was not an auspicious choice, but it was the scene of the first recorded dynamic icebreaking by hovercraft.

A test programme had been planned in which Voyageur was to provide further data in the on-going low-speed icebreaking project which had been initiated previously by ACT-100 discoveries (see Chapter 6). To reach the test site, Voyageur had to travel some 20 km across the frozen Sound at cruising speed, and the crew was astonished to see 35 cm thick ice breaking astern. This discovery completely overshadowed the planned testing, in which some 22 cm was broken at about 10 km/h. Controlled tests to measure the high-speed icebreaking showed that up to 40 cm thickness was continuously broken at 24 km/h. The significance of this in the context of Canadian winter navigation and CCG icebreaking tasks was immediately appreciated, and was instrumental in the Unit being moved to Montreal in late 1974. It was later learned that similar icebreaking had been observed, but not seriously reported, during previous operations in the Baltic.

There was little potential for utilizing the capabilities of Voyageur at Parry Sound, and minimal requirement for icebreaking. By comparison, the Laurentian Region, covering the lower St. Lawrence River and its tributaries eastward from Cornwall, Ontario, to the Gaspé Peninsula, had a wide variety of tasks, including the vital maintenance of navigational safety throughout the winter as far upstream as Montreal. It was therefore decided to move the Unit, and a base was found at the maintenance depot of the ice control structure just upstream of the commercial docks in Montreal.

Again, it was an uphill battle to persuade Regional officials to assign tasks to the Unit. Although the Unit was totally self-supporting for maintenance and funded from Headquarters, legitimate claims of how the amphibious capabilities and speed could be utilized were received with skepticism; requests to demonstrate the potential were not enthusiastically received. Even the unprecedented icebreaking capability was used sparingly, and the very high rate of breaking initially caused problems by creating potential ice jams. Breaking ice at the rate of up to 15 km^2/h was unprecedented; the Region was not prepared to deal with the large quantities of ice released into the river. Therefore, they were not able to use Voyageur to its full potential in the first season. It fell to civilian agencies to create the demand for icebreaking, by clearing ice from the downstream reaches of the shallow tributaries in order to prevent upstream flooding, an annual hazard on a dozen tributaries

between Montreal and Quebec City.

Two of the more dramatic icebreaking operations in the early winters at Montreal illustrate the unique capabilities. In the winter of 1975, a large shore generating station in Montreal was threatened with a shut-down, due to heavy ice cover with hanging ice-dams threatening the water intakes. Voyageur successfully broke the 50 cm thick ice along each river bank (Fig. 8.4), but the ice cover in the centre remained fast, anchored to the bottom by the hanging dams, over a 4 km stretch of river. Over a period of 5 days, this ice was finally cleared by cracking and eroding it with waves created by constant operating and pirouetting at hump speed. One piece was captured for measurement and with the hanging dam attached, was just under 4.5 m (15 ft) thick.

Later that winter, a town on one of the tributaries was being inundated with floodwater, the river rising at 30 cm/h. After some 6 hours of operation (Fig. 8.5), Voyageur had completely cleared the downstream ice, and by the next morning, the river level had dropped by 2 metres. It is rumoured that the refuelling truck could only be reached by driving Voyageur along the main street to dry land. Certainly, during the month of March each year, every night was spent on a different river bank or in a different car park.

Breaking with chronology, to complete the icebreaking story, the St. Lawrence provides extremely favourable opportunities to utilize the craft's

Fig. 8.4 CCG Voyageur hovercraft breaking approximately 50 cm thick ice in Lake St. Louis at Montreal.

Fig. 8.5 CCG Voyageur hovercraft providing flood relief on the Chateauguay River.

speed and shallow-draft capabilities:

a) Downstream from Montreal, CCG is charged with keeping the shipping channel open. Immediately downstream, it is a narrow dredged channel for some 40 km through the length of Lac St. Pierre, which is otherwise too shallow to permit navigation. At its downstream end, which is also to leeward of prevailing winds, the lake abruptly narrows to normal river width. With a strong westerly wind, there is the constant danger of the ice cover, typically 60 cm thick, breaking up and jamming the narrow exit with heavy ridging. Conventional icebreakers were virtually powerless to keep all the ice flowing, and artificial islands had been built in efforts to stabilize the ice. With the advent of Voyageur, the ice covering the shallows could be broken at will, in advance of forecast winds, in controlled quantities to safely pass through the exit. Jams, and the need to hold icebreakers in instant readiness are now a thing of the past.

b) Summer navigation of the St. Lawrence upstream of Montreal is by way of the St. Lawrence Seaway, formed by a locked canal through Montreal to Lac St. Louis, bypassing the Lachine Rapids. Navigation beacons on Lac St. Louis are deactivated for the winter, and buoys are lifted. The only conventional vessel approach is through the Seaway canal, which is frozen. Reactivation and laying of the Lac St. Louis navaids necessary for upstream Seaway navigation, therefore, had to await icebreakers transiting the Canal and breaking the lake open. Again, Voyageur had access to Lac St. Louis at

any time over the Lachine Rapids; it could rapidly break the ice cover, allowing the icebreaker easy access, and also assist in early reactivation of the navaids and opening of the Seaway (Fig. 8.6).

c) Apart from the annual flooding of the tributaries, the ice jams in those tributaries broke in a random manner subject to natural forces releasing masses of ice into the main river channel and posing threats of jams with no warning. Now, the ice jams can be broken and released in a controlled fashion and potential jams in the shipping channel are minimized and predictable.

Returning to the narrative of general utilization of the Unit at Montreal, very few tasks were assigned to the Voyageur during the summer of 1975. On completion of the 1975-76 ice-breaking season, it was decided to use the summer of 1976 to carry out some major structural modifications, replacing the original prototype power modules with production standard modules, installing improved skirts, and incorporating a number of detailed improvements that included an up-rated electrical system and new crane and winches for buoy handling. Again, very little work was assigned to the Unit in 1977; therefore, plans were made to move to Sault-Ste Marie, on Lake Superior, where a useful programme of work had been identified. There was an immediate powerful reaction from the Quebec emergency organizations, which had come to rely upon Voyageur as the primary means of flood control in the major flood zone.

Fig. 8.6 CCG Voyageur laying buoys early to promote opening the Seaway through Lake St. Louis.

Pressure was such that Voyageur remained in Montreal, and the Region agreed to assign a meaningful work programme to the Unit in 1978 and 1979.

The 1978 programme was devoted to navigation aid work, commencing with activating lights in Lac St. Louis in March and April. Floating aids were checked for position and, where required, repairs and maintenance were carried out. Shore beacons and ranges were checked, repaired and maintained; in a number of cases, major equipment exchanges were made, such as generators at beacons. Speed was a major factor in buoy checking. In all tasks, the amphibious capabilities and provision of a large stable platform of adjustable height were particular advantages. One major task, which vividly demonstrated the single-resource capability of an ACV to complete a large amphibious construction project, was in October 1978. The task was to construct a generating station on top of a light-tower in the middle of the St. Lawrence River. A 4-metre tide provided working conditions varying from 2-metre deep water to a rock-strewn muddy island. Work crews were ferried daily. The craft transported and lifted all building supplies, tools and two generator sets weighing 500 kg each to the work site 8 m above the island. The on-board crane and, sometimes, the cushion, were used to accomplish this (Fig. 8.7). The task was

Fig. 8.7 CCG Voyageur involved in construction of a generating station on Richelieu Island.

completed in a fraction of the time anticipated by the Region. Also in 1978, trials were carried out to evaluate Voyageur for oil pollution control. Using all types of equipment then available, tests showed that the large working deck close to the water, together with high speed amphibious capability, made the ACV an ideal vehicle for rapid deployment of oil pollution equipment (Fig. 8.8).

In 1979, a major task assigned was the re-supply of lightstations in the lower reaches of the St. Lawrence, primarily between 200 and 300 km downstream of Quebec City, and 400 km from the Montreal base. Some of the stations are manned, some unmanned; all are either on islands (Fig. 8.9), shoals or cliffs (Fig. 8.10). All required diesel fuel, and the manned stations also required water and other supplies. Tanks and pumps were carried on deck, one 11,000 ℓ fuel tank, or four 2,000 ℓ water tanks. In 12 days, Voyageur visited 8 stations, operating from a beach, and supplied 86,000 ℓ of fuel, 45,000 ℓ of water, and 2 tonnes of supplies. Previously, island stations were supplied by a ship sending a boat ashore to manhandle supply hoses, while stations on cliffs were supplied by helicopter, slinging drummed fuel in.

This impressive demonstration was followed by a number of navigation aid tasks, including two deployments up the Ottawa River: the first, to activate and service 20 shore beacons and ranges; the second, to check and service 180

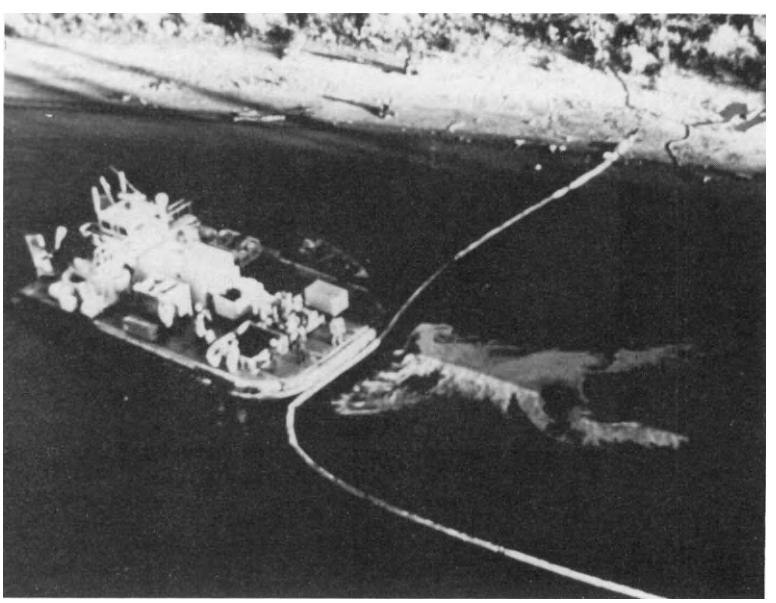

Fig. 8.8 CCG Voyageur deploying oil containment booms.

Fig. 8.9 CCG Voyageur refuelling an island lightstation.

Fig. 8.10 CCG Voyageur re-supplying a cliff lightstation.

buoys, which was completed in 5 days. Previously, this had taken up to 3 weeks. Many other diversified tasks involving construction and maintenance of beacons along the St. Lawrence shoreline were successfully accomplished during the 1979 summer season.

Having rapidly and successfully completed all tasks assigned during 1978 and 1979, Laurentian Region acknowledged that an ACV with Voyageur's capabilities could effectively be utilized. Therefore, in early 1980, the E & D Unit was handed over to Regional control, and was renamed the Laurentian ACV Unit.

In summary, the main characteristics of hovercraft that are pertinent to a CCG Regional work programme are:

a) High transit speed, reducing unproductive transit time. This is useful in all tasks, but highlighted by cases such as when a technician may be required to change a light bulb in a buoy 100 km distant.

b) Amphibious capability. A very large percentage of tasks are in shallow water or on the shore. Using conventional resources, a task may involve a ship, small boats, trucks and a helicopter. With an ACV, only the one resource is usually required, and provides dry transportation and working conditions for work crews and equipment.

c) The ACV is totally self-contained. The only need for outside support is fuel. No port or docking facilities are required.

8.3.7 Laurentian ACV Unit

Since its integration into the Region, the Laurentian ACV Unit has built upon the demonstration tasks of 1979 and 1980, expanding both its utilization and its geographic coverage. For instance, in 1984, Voyageur was deployed some 800 km to the Miramichi River in the Gulf of St. Lawrence to transport work crews and construction equipment to build two large towers on islands.

Over the years, the Unit's annual programme has evolved into a general pattern, which has the ACV at its Montreal base only for 2 months of the year, plus irregular other short periods. For most of the time, it is deployed downriver. In recognition of this, a facility is available within the CCG base at Quebec City, and a small sub-base has been built at Cacouna, some 200 km downstream of Quebec City. For ice-breaking operations, a rough ramp has been built at Trois Rivières at the downstream end of Lac St. Pierre, central to the ice management and flood relief operational area.

The annual pattern generally is: a) December-January, craft maintenance at Montreal, b) February-March, ice management and flood relief, deployed to Trois Rivières, c) April, ice breaking and activating navigation aids, Lac St. Louis, based at Montreal; on completion, deployed to Cacouna and Quebec City for Spring lightstation re-supply, d) May-September, installation of tide gauges, buoy and beacon maintenance and construction as required, based at Quebec City, Cacouna or Montreal, and e) October/November, fall lightstation re-supply, based at Cacouna; on completion, return to Montreal.

By 1985, Voyageur was 15 years old, the only one of its kind in service, and was becoming increasingly difficult and expensive to operate. With the operational tasking defined, and the experience gained, the specification for a

replacement was developed. The two major changes were the provision of on-board accommodation, which was a major shortcoming of Voyageur, and the use of diesel power, to reduce the maintenance and fuel costs associated with gas turbines. Drive-on and drive-off access to the working deck, which should be more sheltered, were also desirable features. In response to this, Westland Aerospace (British Hovercraft Corporation) offered a variant of their AP.1-88 passenger ferry; in early 1986, a construction contract was negotiated. Upon completion in the summer of 1987, Unit personnel conducted trials of the craft in England and accepted it. It arrived at Montreal in August 1987, named *Waban-Aki*, and took over Voyageur's duties in October. The very informal transfer actually occurred at Portneuf in October, where the two craft operated for the only time together as they passed, transiting between Montreal and Quebec City.

Voyageur was deactivated and was disposed of in 1988. Its successor was officially christened at a colourful ceremony attended by Indian chiefs in full native costume, in June 1988. *Waban-Aki* translates to *People of the Dawn*, and is the first of a series of tribal names selected for future CCG ACV's. For the Region, the main effect of the new craft has been a significant reduction in the fuel bill; for the Unit, the greater comfort, reduction of noise and improved directional control are the more noticeable changes.

8.3.8 Laurentian Unit Organization

The Unit personnel consists of a Commanding Officer, who is also a Craft Commander, one Craft Commander, two First Officers, a Chief Engineer and three Engineers. Seamen and deck hands are assigned by the Region according to the tasking. Unit personnel maintain and operate the craft and its equipment.

The main base at Montreal has a paved ramp and hardstanding leading to a hangar in which the craft is maintained, and which contains offices, stores and basic machine tools. Unit personnel make skirt fingers, and are generally self-sufficient for craft maintenance and repair. Light alloy welding repair work is one of the few jobs for which outside assistance is required.

The craft is normally operated with a Craft Commander and First Officer, both certificated operators, and an engineer. When on deployment, an additional engineer drives a Unit truck to the local base to provide logistic support. Crews change over usually every two weeks; the crew at Montreal carries on the administrative chores and arranges maintenance support, such as making skirt components and ensuring that adequate spares are held.

8.3.9 Waban-Aki Description

Primary requirements dictated by the Laurentian Region tasking include: a) a working/cargo deck for buoy work, construction and re-supply, b) a crane for handling cargo and buoys, readily transportable, c) winches for buoy work and for holding craft on station, d) precise control for accurate positioning and

station-holding in tideway, e) living, cooking and toilet facilities for crew and work parties, f) storage for craft spares and task equipment, g) fuel for at least 10 hours cruise, h) capable of operating in 1.5 m waves, 35 knot wind and temperatures as low as at least -30°C, from unprepared sites, by day and night, and i) comprehensive navigation and communication equipment.

To meet these requirements, Waban-Aki has a forward well deck 9.5 m long and 4.6 m wide, with securing points for a wheeled hydraulic crane which can be moved on and off through the bow ramp/door. It has a capacity, typically, of 2200 kg at 5.8 m radius and a maximum reach of 6.8 m. One winch and one capstan, also hydraulically powered, are fitted on the bow, power being provided from a pump driven by the port lift engine. Immediately aft of the well deck is the superstructure and accommodation, at the forward end of which are two rooms for role equipment, ready-use spares and tools, together with seating for 10 persons in reasonable comfort. The galley has 110 V power points, a microwave and a refrigerator, plus limited cupboard space.

Fuel is used for longitudinal trim as well as supplying the engines; therefore, while internal tankage is 5900 ℓ, normally about 5000 ℓ would be the maximum carried; this, with an average fuel consumption of 360 ℓ/h, provides a 10-hour endurance with substantial reserve. The precise manoeuvring and control is provided by powerful rotating thrusters either side of the bow, controllable pitch ducted propellers, and rudders.

Communications equipment consists of VHF/FM, VHF/AM, HF, mobile telephone, and full intercom throughout the craft. For navigation, a Decca radar, Loran C with plotter, a doppler speedmeter and two ADF sets are fitted, together with a G-M compass. Night operation is assisted by deck floodlights and two powerful searchlights.

For maintenance at unprepared sites and for overnight craft heating requirements, a diesel APU is fitted; it powers a 12 kW alternator providing 110/230 V AC power, which is also available to the 28 V DC system through transformer-rectifiers. The craft can be lifted by portable powered hydraulic jacks.

8.3.10 Economics

Comparison of costs of a wide variety of resources performing a very diversified assortment of tasks can only be valid if the criteria are correctly selected; even then, they can be distorted by peripheral factors. One very significant factor is the extent to which the potential capability of a resource is utilized on a given task. Therefore, rather than quote comparative operating costs per hour, or per km, or per tonne-km, the work content and resource requirements of some typical tasks are described here for the reader's judgement. The examples quoted are all based on actual events:

a) A light is reported extinguished. This requires a light technician with a

handbag of tools and a light bulb to fix. This is normally carried out either by a ship, which possibly has to lower a boat to reach the light, or, if the light is ashore, by a helicopter landing as close as possible. It has been known for a ship with a crew of some 30 men to steam 290 km (180 mi) at 12 knots to change a bulb. Discounting the fuel cost, the unproductive return mission time would be 900 man-hours. Using Waban-Aki, with a crew of three, the unproductive time would be 36 man-hours.

b) Refuelling a cliff-top lightstation with 15,000 ℓ by ship would involve the ship being loaded with barrels of fuel, steaming to the locale and anchoring while a helicopter made 40 return trips with 2 slung barrels each trip. The light keepers, or work crew then would have to pump the fuel into storage tanks. The lightstation is 242 km (150 mi) from base, giving the ship a transit time of about 12 hours, and a day at anchor during refuelling. Using Voyageur or Waban-Aki operating from a local beach, the transit time would be about 5 hours. The only logistic requirement is that a fuel truck can replenish the ACV's cargo tanks; two return trips to the lightstation, with total transit time of 2 hours, would enable the fuel to be pumped directly into the storage tanks.

c) Amphibious cable-laying through swamp and shallow water using conventional means requires trucks, ditching and dredging equipment, and work-boats. It involves working in very difficult conditions. This presents problems of logistically planning the integration of a wide variety of resources and sizeable work force. An ACV equipped with a back-hoe or digger would perform the task with no other resource required, at the same time providing a dry stable platform.

d) In flood relief operations, the Quebec government, after the first full year of Voyageur icebreaking, estimated that at least $400,000 had been saved by municipal governments alone; this took no account of personal damage or insurance settlements to individuals.

8.4 SUMMARY

The Maryland Natural Resource Police Hovercraft program has been the most thoroughly tested program in the history of the agency. The successful operation of the Hake Husky Griffon Model 1000 TD hovercraft has proven the viability of hovercraft technology in marine law enforcement. This program has also proven that hovercraft today, unlike bygone eras, are affordable to acquire and operate. This change in technology will now allow agencies to fill the voids which exist in their waterborne patrol capability and substantially enhance their service to the public. The hovercraft is not the cure for all problems to all agencies, but it is the solution to many problems encountered in a coastal environment by law enforcement agencies.

From the early faltering attempts in 1968-69 and 1977-79 to achieve recog-

nition in the Western and Laurentian Regions, ACV's in the Canadian Coast Guard (CCG) have, through perseverance and dedication, won their spurs and are now fully accepted and integrated resources with the Regional Fleets. One cannot help but be reminded that Hovertravel Ltd. are the world's oldest continuous operators of ACV's, and their three first AP.1-88's were aptly named *Tenacity, Resolution* and *Perseverance*. The CCG is the oldest non-commercial operator in the world; both they and Hovertravel relied very much on those three characteristics to win through to their respected status.

The traditional resistance to change which challenges the introduction of novel resources was short-lived in the face of early and continued successful SAR (Search and Rescue) missions. Now, with over 20 years of experience which is continually being built upon to develop new equipment and techniques, the CCG Hovercraft Unit (Western Region) has established itself firmly as a leading example of intelligent utilization of the potential of air cushion technology.

Likewise, the ACV is now a fully accepted and integrated resource within the Laurentian Region. Its capabilities and limitations are understood. Now that the ACV is utilized with these in mind, other resources are released to perform tasks more related to their capabilities. The overall effect is not highly visible since work programmes in the Region, as a whole, vary from year to year, but the ACV is utilized as a highly mobile, high-speed amphibious resource for a wide variety of tasks. The original skepticism and resistance has now given way to assigning appropriate and challenging tasks. Failures of equipment, such as the crane, once readily described by "the ACV has broken down again!", are now recognized for what they are.

8.5 REFERENCES

1. Maryland Natural Resources Police, Operational and Maintenance Reports.
2. H. Cook, Hovercraft in Law Enforcement, International Conference on Air Cushion Technology, Rockville, Maryland, September 23-25, 1985.
3. Maryland Natural Resources Police Annual Report, Fiscal Year 1986.
4. H. Cook, Hovercraft in Law Enforcement - Part II, International Conference on Air Cushion Technology, Toronto, Canada, September 15-17, 1986.
5. Maryland Disaster Assistance Plan, Maryland Emergency Management and Civil Defense Agency Publication.
6. Maryland Radiological Emergency Plan for Fixed Nuclear Facilities, Maryland Emergency Management and Civil Defense Agency Publication.
7. Type Operating Manual, produced by Griffon Hovercraft Limited, Carlton House, Ringwood Road, Southampton, SO42HT, England.
8. Operational Development of CCG Voyageur ACV, Report TP 1894, Vols. 1 and 2, Canadian Government Department of Transport, April 1980.
9. Utilization of an ACV in Construction of the Ile Richelieu Light Generating Station, Report TP 1858, Canadian Government Department of Transport, Sept-Oct 1978.
10. Winter and Icebreaking Evaluation of CCG Voyageur, Spring 1975, Report TP 297, Canadian Government Department of Transport.

11. Winter and Icebreaking Evaluation of CCG Voyageur, Spring 1976, Report TP 358, Canadian Government Department of Transport.

12. River Icebreaking for Flood Control Conducted by CCG Voyageur, March-April 1976, Report TP 406, Canadian Government Department of Transport.

13. Impact économique de l'aéroglisseur pour certaines municipalités, Ministère du Québec des Richesses Naturelle, 1979.

14. T.F. Melhuish, Hovercraft in the Canadian Coast Guard, High Speed Surface Craft Conference, Brighton, U.K., 1980.

15. T.F. Melhuish, Specification and Acquisition of AP.1-88 by CCG, CACTS International Conference on Air Cushion Technology, Montreal, 1987.

16. J.C. Leonard, Design of CCG AP.1-88, CACTS International Conference on Air Cushion Technology, Montreal, 1987.

17. G.A. More, Initial Operating Experience with CCG AP.1-88, CACTS International Conference on Air Cushion Technology, Montreal, 1987.

18. R.G. Wade, Ten Years of Operational Experience of Hovercraft in the Canadian Coast Guard, Advanced Marine Conference, AIAA/SNAME, Baltimore, 1979.

Chapter 9

INLAND APPLICATIONS

9.1 INTRODUCTION

The more spectacular applications of hovercraft have, to a degree, obscured other activities where air cushions have been used with success, and may yet be the subject of interesting developments. The applications discussed here are low visibility operations taking place in remote locations, generally inaccessible to other modes of transportation. Hence, they might be called *last resort* operations, when nothing else will work and the job must be done, or, sometimes, applications identified because somebody found that available air cushion vehicles could be used. The activities reviewed in this chapter cover application of the ACV for use in estuaries or as ferries, for overland transportation in remote areas, and in agricultural applications.

9.2 WORK PLATFORMS

Wherever civil engineering work takes place in estuaries or on river banks, one is faced with the task of providing a firm footing for the equipment and a safe base of operation for the workers. For instance, when working on a beach, approach to the work site can be made from the shore or from the water. In the first case, unstable banks may be met; in the second, water depth may be insufficient to float pontoons. If the pontoons are supported with an air cushion, the work site can be approached without concern as to available water depth. When working on tidal flats movement can be effected without regard to the tide.

J.T. Mackley & Sons, a British civil engineering firm involved in off-shore work, in collaboration with Air Cushion Equipment Ltd. (ACE), has developed a range of amphibious air cushion platforms based on commercial modular pontoon units (Fig. 9.1). These platforms can be built in sizes of 200 tonnes or more,

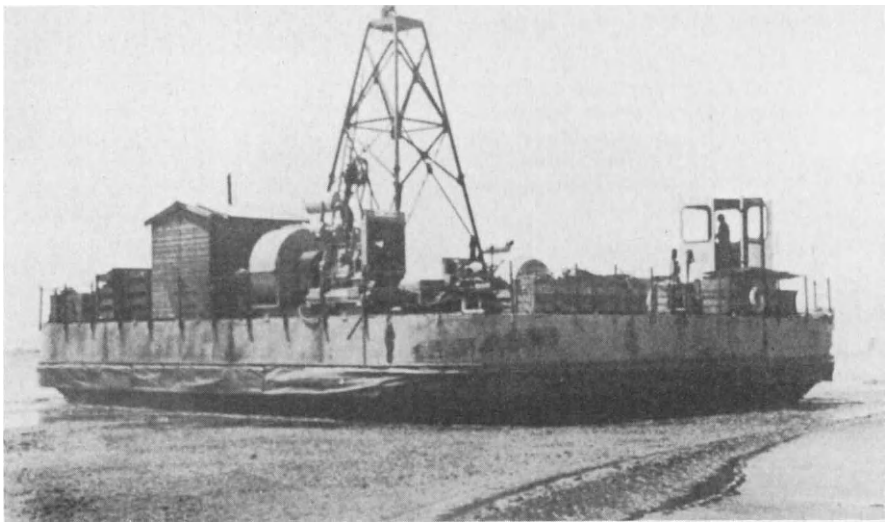

Fig. 9.1 A 30 tonne payload Mackley-ACE air cushion work platform operating on tidal mud. (Source: Jane's).

and can be assembled from the modular units at any convenient place near the work site. Special peripheral modules support the skirt segments, with Diesel powered fans providing the air pressure. The air pressure used may reach 10 kPa or more, but in any case, it must be greater than that at the draught depth of the loaded pontoon assembly when floating. As the segment tips are usually in mud, the required air flow is small, with cushion power requirements for the larger platforms of the order of 1 to 2 kW/tonne.

Air cushion platforms can be moved to the working location by any convenient means. Towing or winching are usual, a tractor or a boat providing the motive power, depending on the state of the tide. Mackley have experimented with self-powered platforms fitted both with outboard propellers and with hydraulically powered wheels.

The modular-built work platform has given rise to a number of air cushion applications, because of the possibility of assembling on site a vehicle that is too ponderous for road transportation. Mackley-ACE have used it for ferries and for heavy transporters. This design approach has also been used by Hoverlift Systems, Calgary, for their air cushion ferries and in their ACIB design, HL-533 (Section 6.3.1).

9.3 FERRIES

In this section the situation is one in which the traffic along a particular route is insufficient to warrant construction of a bridge, with distances to be covered not exceeding a few hundred metres.

Air cushion ferries would not be the most economic solutions when the proposed crossing is over a body of water of uniform depth with fairly consistent banks. A displacement hull, self propelled by water propellers, or cable towed, would usually be the cheapest system. However, the air cushion should be considered when the following situations arise:

a) Non-uniform water crossing, with segments too shallow for a displacement hull.
b) Fluctuation of the water level so that multiple docking facilities are required or that operations are curtailed at certain times during the day (in tidal regions), or at certain periods of the year.
c) Soft and unstable banks, preventing construction of docking facilities. With an ACV ferry the dock is built on dry land, above the high water mark.
d) Presence of an ice cover during part of the year.
e) Temporary traffic as, for instance, to support local construction work.

A complete economic justification should be done prior to committing to an air cushion solution. This should compare infrastructure and vehicle acquisition costs, operating expenses, personnel requirement, expected traffic, duration of operation, if temporary, and local social environment. For a temporary operation, recovery and further use of the equipment should be considered.

An air cushion ferry will usually operate below hump speed, the distances involved resulting in optimal speed of the order of 5-10 km/h. Thus a high cushion pressure is acceptable, and the skirts and air cushion fans will be similar to those of work platforms. Because such ferry operations will usually take place in remote areas, the vehicle should be as simple as possible, with conservative cushion characteristics, as follows:

a) A simple HDL type segment, maintainable without lifting the vehicle, will normally provide sufficient stability for the ferry.
b) Wear will not be a problem at low speed and in the liquid environment of a ferry. However, protective flaps may be considered for those segments where the inner side is facing the movement.
c) A spray skirt, as used in air cushion icebreakers (see chapter 6), is recommended for the comfort of users and operators, particularly if freezing is encountered.
d) Modular construction is almost a must for air cushion ferries since operating sites will be difficult to reach and will require local assembly. Most ferries built to date were assembled from standardised welded steel pontoons with special peripheral sections supporting the skirts, and with Diesel powered fans on deck.
e) Propulsion and guidance of these ferries is normally with cables, the simplest way to deal with the variety of surface traversed. Winch drives have been used, operated from the ferry or from the land. However, capstan

drives are lighter, and are not length limited.

A number of hover ferries operations have taken place in the past years, the better known one being the Yukon River crossing in Alaska. Two ferries were also built and operated in Canada in the western provinces.

9.3.1 Yukon Princesses

These Yukon Princess ferries were built to supply the Aleyeska pipeline construction in the mid 1970's and were operated for two seasons until a bridge across the Yukon River in Alaska became available (Fig. 9.2).

Two ferries were designed and built by Mackace Hoversystems, England. Both had 160 tonnes nominal payload, though with slightly different all-up weights, 375 tonnes and 418 tonnes, due to differences in the pontoon modules which had to be procured in Alaska and elsewhere in the U.S.A. With a 38 m by 25 m planform the cushion pressure would have been about 5 kPa. At this size, and with a fan providing up to 7 kPa (ref. 1), there appears to have been plenty of reserve for overload. This is a prudent design feature since one would not readily find a weight scale to control payload of this magnitude.

9.3.2 Hoverlift Systems Ferries

Two ferries were designed and built by Hoverlift Systems Ltd., Calgary. The first, HL-104, was 20 m by 11 m with a payload of 45 tonnes. It was operated on the Peace River in Alberta at a location called La Crete, where widely varying water level and broken ice cover prevented normal ferry operation. A characteristic of the operation was that the crossing was done broadside, limiting drag in mid-stream. This also permitted loading trucks parallel to the river banks, which made access to the ferry safer in view of the steepness

Fig. 9.2 Yukon Princess on ferry service, Alaska. (Source: Jane's).

of the banks.

The second ferry, HL-105, was built for the British Columbia Ministry of Transportation, Communications and Highways, and was operated on a river crossing at Fort Nelson in 1979. This ferry was a widened version of the Alberta ferry, being 20 m by 15 m, with a payload of 75 tonnes (Fig. 9.3).

Both these ferry services have been discontinued. The main difficulty for the ferry authorities in both these cases was to find, and keep, competent mechanics to maintain the ferries.

9.4 OVERLAND TRANSPORTATION

The use of the air cushion in overland transportation has been somewhat sporadic since, in general, land should give firm footing. However, in the northern areas of Canada, or Siberia, there are vast expanses of organic soils, such as muskeg and permafrost, where one meets active layers of thawing soils in the summer, not to mention the temporary *liquefaction* of the surface during spring thaw. In the absence of adequate vehicles to deal with such situations, prudence dictates that critical terrains be avoided. In fact, when required, overland transportation will take place in the winter season with three or, possibly, four months of operation, using trucks over snow roads or frozen rivers and lakes. Limited access is possible in summer months using

Fig. 9.3 Hoverlift Systems HL-105 at Fort Nelson. (Source: Hoverlift Systems).

tracked vehicles, but only over trails that eventually turn into muddy mire, thanks to the high humidity of organic soils.

The practice, therefore, has been to avoid traveling over certain areas at certain times of the year, and planners tend to organize their operations in this way. Hence, there is little demand for vehicles that will travel over muskeg or thawing soils. Wide-footed tracked vehicles can usually cope with the situation in the summer months, but at a walking pace (Fig. 9.4).

An air cushion provides a method to overcome low bearing strength terrains; its low pressure will also reduce surface destruction. With vehicles designed to provide year round transportation, or at least to operate when the temperature exceeds freezing, a number of economic gains can be made:

a) Local transportation on a work site can be maintained, whether the surface is firm or not.
b) Year round transportation removes the need for stockpiling, and makes construction schedules less dependant on weather.
c) Construction of all-weather roads may be postponed until the traffic attains economically viable values.

For long distance transportation, that is, exceeding one hour duration, a *practical* vehicle would be one that can provide speed in the same range as that of a truck, with acceptable comfort, over an unimproved trail surface. Air cushion vehicles proposed for overland transportation use higher air

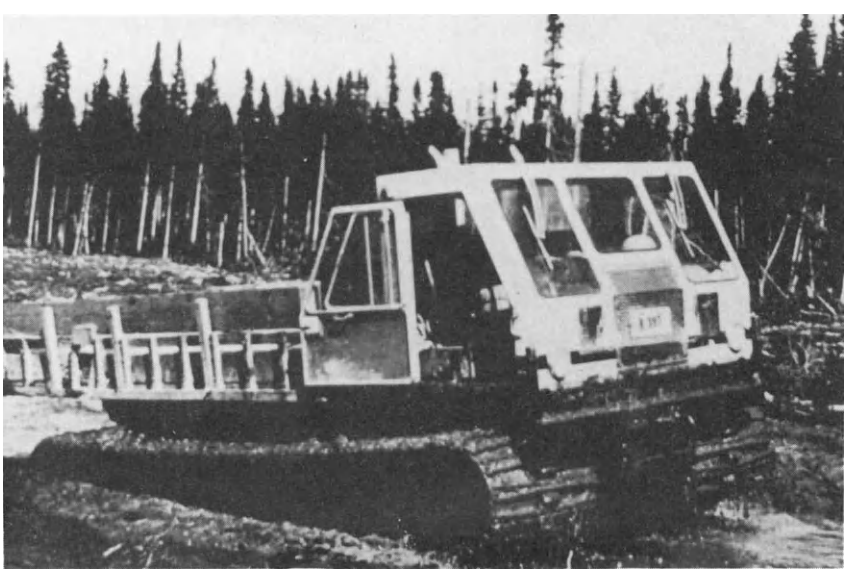

Fig. 9.4 Bombardier B-15 muskeg transporter. (Source: TDC).

cushion pressures than conventional hovercraft, more than double, in fact. The pressure is limited here by ground erosion, not by the hump speed drag, since over water use is sporadic and usually done at low speed when the transportation is nominally overland.

The first overland air cushion barges, such as the Hovertrailers International Ltd. H-119 (Fig. 9.5) were wholly air supported, provided with a towing bar, and equipped with guiding wheels at the back. The guiding wheels were loaded by means of air cylinders. Such vehicles are entirely satisfactory as long as they operate over flat areas that can provide a good seal, such as afforded by water or mud. Self-propelled versions have been developed, such as the Hoverlift Systems *Salamander* (Fig. 9.6).

The Bertin *Terraplane* BC7 (Fig. 9.7) is an original design of what a *practical* vehicle would be. While only a demonstrator, it was meant to operate over unimproved trails and was able to cross rivers and small lakes. Its purpose was to provide relatively fast transportation in areas where roads development were planned. If traffic increased during use of this vehicle a hard surfaced road could eventually be built. Preparation of a Terraplane trail was estimated at less than 5% of the cost of a normal road. Hence, considerable savings could be effected by holding off construction until needed, while transportation would still take place to the area of interest.

Fig. 9.5 Hovertrailer International HT-119, modified by Terracross for operation in Canada. (Source: TDC).

Fig. 9.6 Hoverlift Systems *Salamander* HL-115, a 5-tonne payload, self-propelled amphibious transporter. (Source: Hoverlift Systems).

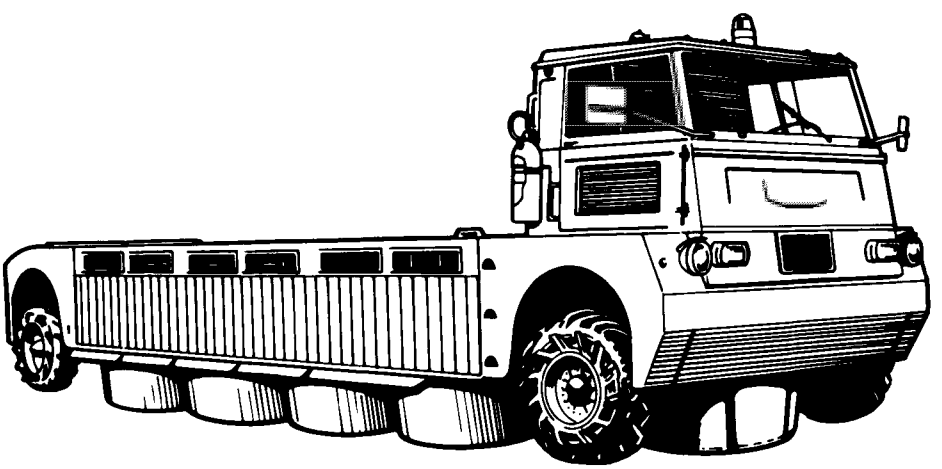

Fig. 9.7 Bertin/SEDAM BC-7 ACV for trail operation. (Source: Bertin et Cie, adapted by TDC).

A developed version, the T3S, was designed as a hybrid, being able to operate with or without the air cushion. Hence it could operate as a conventional vehicle over roads or over terrain with sufficient strength to support its

weight.

These vehicles were not developed beyond the demonstrator stage. Like the Salamander, they fulfilled a theoretical need which has always been carefully avoided by transporters or planners. When accidentally faced with situations where the air cushion would be helpful, transporters use what they have at hand, and cannot wait for a vehicle that promises all sorts of performance, but is still a year away.

There are a number of historical situations where new modes of transportation have matured to provide us with systems that are now looked on as indispensable. These have also taken a fair number of years to attain their present present status. In the process, there were a number of experimental designs of varying qualities, which eventally evolved into the vehicles that we now know. In the following sections, characteristics of off-road air cushion vehicles will be discussed, with descriptions of concepts and applications that appear pertinent in the long term.

9.4.1 Air Cushion Trailers

In 1973, the Transportation Development Centre (TDC), Transport Canada, in collaboration with the National Research Council, Ottawa, and Hydro-Quebec carried out a comparative evaluation of two air cushion trailers on a hydro-power line construction site in the Baie-Comeau area of Quebec. One of the trailers was the Terracross vehicle shown in Fig. 9.5, designed to carry a 12-tonne payload, and using an HDL skirt with loop. The second vehicle was the Hover-JaK HJ-15, designed by Jones, Kirwan and Associates and using the Bertin multicellular jupes (Fig. 9.8). Both these vehicles had lightly-loaded rear guidance wheels and a simple tow bar, so that nearly all the vehicle weight was carried by the air cushion. Wide track caterpillar *muskeg* tractors were used as towing vehicles.

The terrain in the test area was far from uniform, and certainly not flat. The test operation consisted in carrying construction supplies from a depot, which could be reached by conventional vehicles, to the transmission line route, over a cleared path. There were a number of locations where the air cushion showed its value, e.g., in marshes and, particularly, at any point where the trail crossed a small stream. Repeated passage by heavy vehicles quickly transformed such points into quagmire (Fig. 9.10). In between, however, the terrain could be firm, with low brush, and with noticeable slopes and side-slopes. The lack of lateral control was sorely felt, as well as the excessive porosity due to vegetation.

The Baie Comeau trials resulted in a number of observations concerning the use of air cushion lift in off-road trail vehicles:

a) Hybrids are a necessity whenever slopes and very low bearing strength terrains are encountered on the same route. Lateral stability can be con-

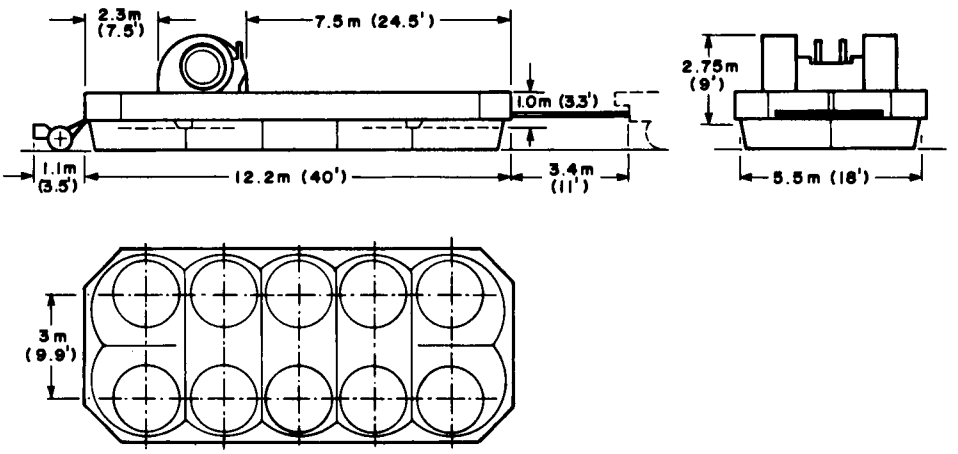

Fig. 9.8 Hover-JaK HJ-15 characteristics. (Source: TDC).

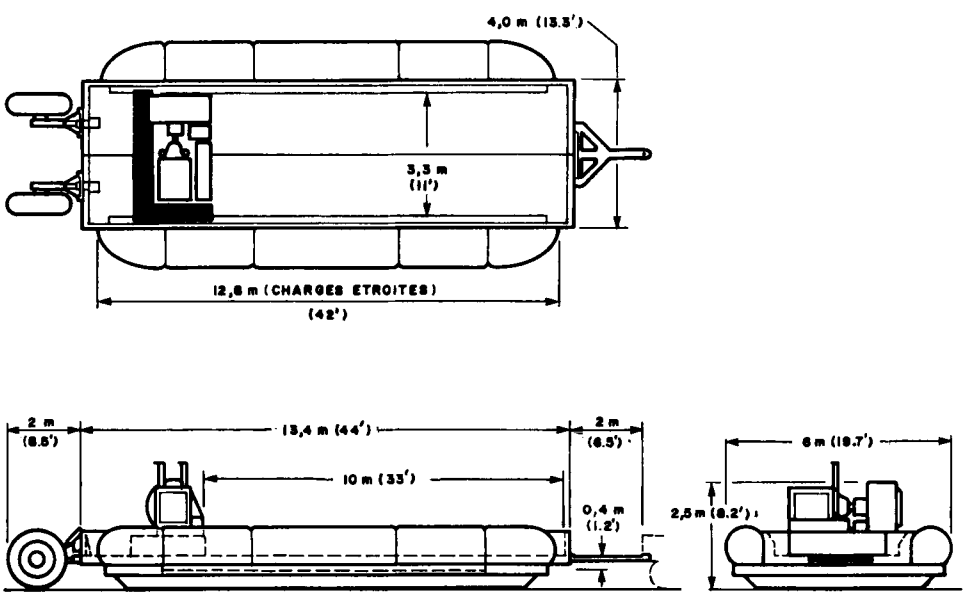

Fig. 9.9 Terracross HT-119 characteristics. (Source: TDC).

trolled by transferring weight onto wheels, or tracks, as necessary, with full load on the wheels when traversing hills or surfaces of sufficient firmness.

b) Muskeg towing vehicles, such as the B-15 (Fig. 9.4), have a payload capa-

Fig. 9.10 Surface destruction after multiple passes by heavy tractors and wheeled trailers. (Source: TDC).

bility equal to their empty weight. Hence, if the payload is carried on an ACV trailer, these vehicles operate at half their usual ground pressure, which results in improved performance over marginal terrain.

c) Traction on slopes will suffer since the payload, plus trailer, must now be pulled. A proposed solution is to use a goose neck towing system that would allow transfer of some of the trailer weight to the tractor, thus improving traction.

These observations result in an ACV trailer, as shown in Fig. 9.11, which uses similar components to those of conventional road trailers and tractors. This type of trailer could be operated on normal highways, if necessary, to reach its operational site. Such movement would be facilitated if the trailer had removable side-bodies to meet road width restrictions.

The air cushion trailer operates at pressures around 5 kPa, with up to 7 kPa (1 psi) for larger off-road transporters. The choice is a compromise between (a) low pressure and a large unwieldy vehicle, and (b) higher cushion power, increased erosion and a smaller, cheaper structure. Erosion will be minimized if load is transferred to the wheels whenever a dry, harder terrain is met.

The need for a hybrid ACV trailer to be amphibious depends on both the mission and the tractor. Since the trailer will usually have the required

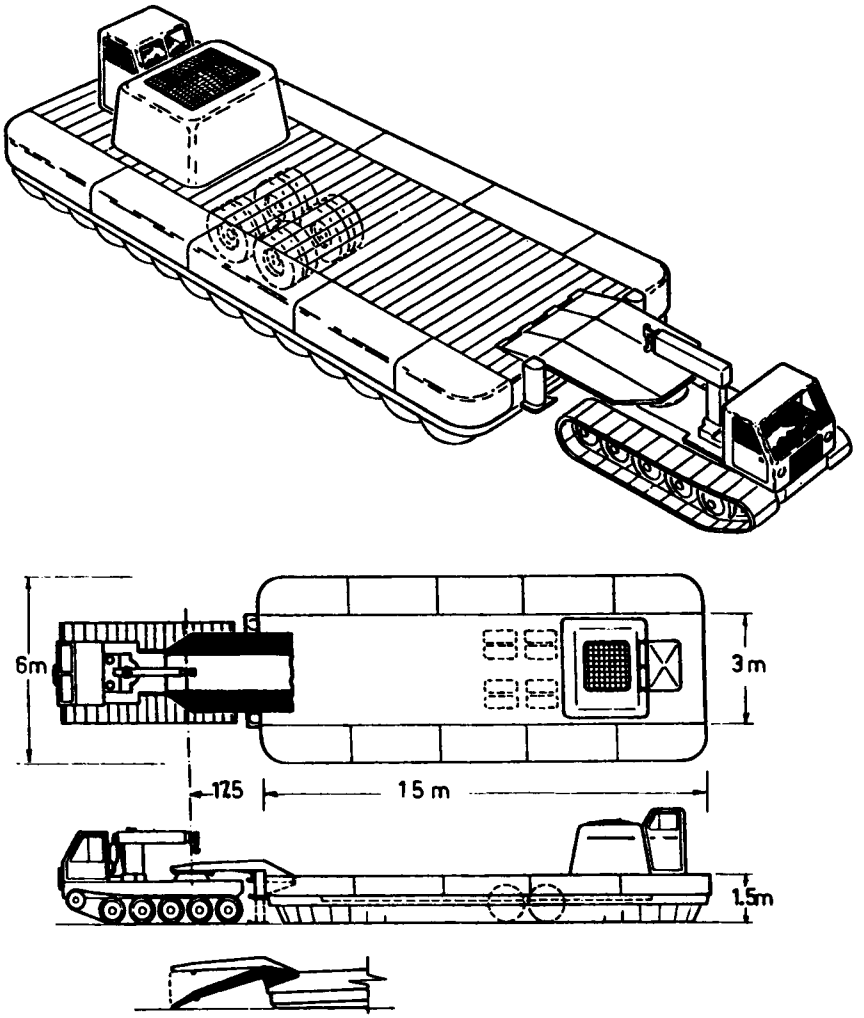

Fig. 9.11 Hybrid air cushion trailer concept with a payload of 20 tonnes. (Source: TDC).

displacement volume, this characteristic can easily be included in the design. Safety requires that the amphibious air cushion trailer floats when fully laden, since the air cushion fan could be accidentally stopped.

The payload of hybrid trailers will depend on the task at hand, and should correspond to that of equivalent road trailers. Hence a range of 5 to 20 tonnes is foreseen. Anything lighter probably does not need an air cushion to attain the required mobility. Heavier hybrid air cushion trailers could lose too much load efficiency because of the weight of the wheels and associated gear. As with road trailers, multiple ACV trailer units may be used with a tractor.

Cushion systems can be HDL type segments, attached to the platform periphery and easily replaced in case of mishaps. A multicellular skirt system can be advantageous on the lighter trailers because of its superior stability characteristics. In cooperation with a variable rate suspension, relatively higher speeds can be maintained over rough surfaces. The presence of wheels simplifies access to the underside of the trailer for repairs.

9.4.2 Air Cushion Transporters

The Terracross HT-119 (Fig. 9.9) and the Hover-JaK HJ-15 (Fig. 9.8), air cushion trailers were built without auxiliary support, and are at the low- payload end of a class of very large and heavy units that must remain *pure* air cushion vehicles. Such units are the Arctic Systems ACT-100 (Fig. 9.12) and the Mackace *Sea Pearl*, with 100 tonnes and 250 tonnes payload respectively. The girth of such transporters (up to 25 m for the Sea Pearl) limits their overland use to areas that can provide hoverways with grades not exceeding a few percent. The lighter vehicles are more easily operated because of the availability of muskeg tractors, which can handle their weight over steeper hills.

Air cushion transporters, as mentioned previously, will be most efficient over uniformly weak terrains such as the organic soils of the North-West Territories of Canada, where permafrost is prevalent. Various methods of traction are available for air cushion transporters, in addition to muskeg tractors. Some of them are described in a) to d) below; economics will influence the user's preference.

a) Muskeg vehicles provide the most flexible type of traction for air cushion transporters. Attachment is usually through a rigid tow bar attached to a hitch. This provides reasonable control of the load by the tractor, with lateral drift countered by wheels at the rear of the transporter. When insufficient force is available on these wheels, they can be replaced by metal discs which will sink in the soft soil, providing the required restraint. Very large transporters can be handled by a number of tractors

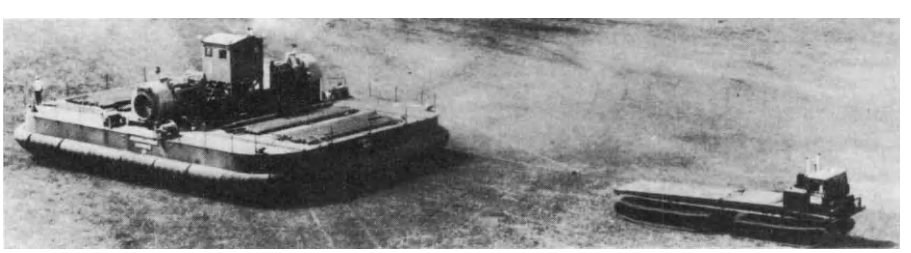

Fig. 9.12 The ACT-100 transporter towed by a Foremost *Husky* muskeg vehicle. (Source: Jane's).

hitched with cables. A restraining vehicle must be provided in order to prevent load overrun, cushion dumping by the transporter being too slow for safety.

b) Wheels have been fitted to air cushion transporters in order to provide lateral guidance. Powered wheels can provide sufficient forces to propel the vehicle, even with a fraction of the vehicle weight resting on them since, generally, the operation takes place over almost flat land and the vehicle itself has little drag. However, this is not to say that any tire will do. The nature of the soil, the tire pressure and sinkage must be considered when calculating the limiting shear forces that can be applied to the surface and, therefore, the resulting propulsion force (ref. 9.2). Figure 9.6 shows the use of low pressure Terra-tires on an air cushion transporter. Such tires also provide over-water mobility. The HL-115, moving at 5 knots across ponds, corresponds to the maximum infra-hump speed attainable by this vehicle (Froude Number = 0.25).

c) A spectacular traction method for ACV transporters is the use of helicopters. A test was done with the HJ-15 which indicated that, with little training, a helicopter pilot could handle the craft quite precisely. Later, the ACT-100 was also towed over ice in the Beaufort Sea. Technically these experiments were successful. The economy of the operation is directly related to the speed that the crew will dare to maintain.

d) Self-propulsion with a capstan drive has been discussed previously with regard to ferries. One could consider laying a cable along a trail over which a transporter pulls itself. A slight hollow ensures guidance of the craft; turns are negotiated by providing posts on the inner side of the turn, with a reverse slope keeping the vehicle away (Fig. 9.13). The path length is immaterial as the cable, or chain, would be self-anchored by its own weight. Hoverlift Systems has demonstrated the feasibility of the turning procedure.

9.4.3 Aerobac Hybrid Vehicles

The word *Aerobac* was used by TDC to denote a specific breed of air cushion transporters, self-propelled and able to operate with or without the use of air cushion lift. The concept evolved from the TDC cushion trailers trials referred to in Section 9.4.1. Figure 9.14 illustrates the concept; it results from the mating of a muskeg tractor (Fig. 9.4) with a trailer using a multicellular air cushion (Fig. 9.8). The combination of air cushion with caterpillar tracks has been proposed previously in the B3 built by E.N.B.E., The Netherlands, and in the MVP series of ACV built by the Oil Machinery Research Institute, Tyumen, USSR.

Its development came about with the realisation that the trailer concept shown in Fig. 9.11 would always be limited by the performance of its tractor.

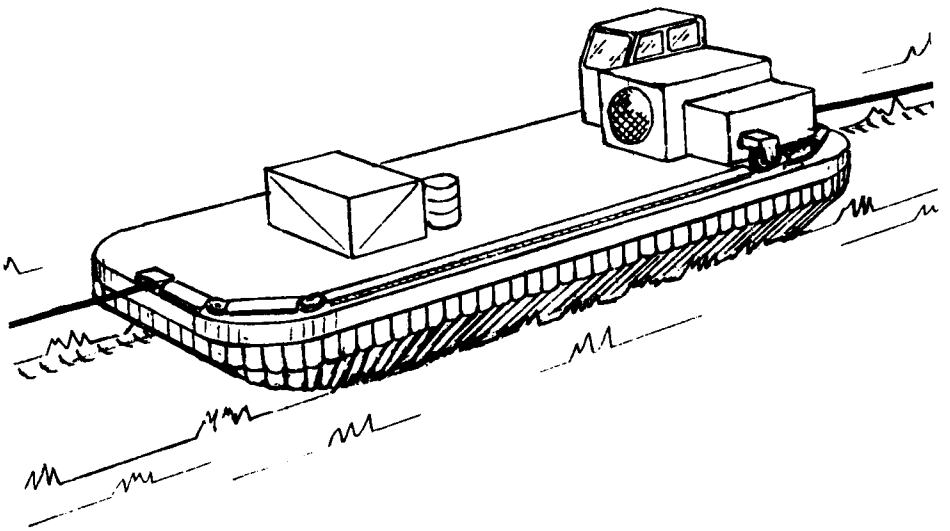

Fig. 9.13 Overland capstan cable towing. (Source: TDC).

Aerobac is amphibious, and its tracks provide sufficient traction to propel the craft over mud and in water. The size of the original design came from a requirement by Hydro-Quebec for a transporter able to carry a cable reel, the largest indivisible load carried on its transmission line construction sites.

As with other overland air cushion vehicles, the cushion pressure of Aerobac is in the order of 5 kPa, when operating with 15% of the weight on the tracks. An optimum payload range for this type of vehicle appears to be from 5 to 10 tonnes. As with the hybrid trailers (Section 9.4.1), a lower payload vehicle may not need air cushion load relief to have an acceptable mobility. Heavier versions would be too cumbersome to use over trails. However, for carrying heavier payloads, Aerobac can be coupled to air cushion trailers.

The use of tracks for a vehicle like the Aerobac (which would be tried, as a prototype, over the worst possible terrains) ensures maximum mobility. For many applications, tracks may not be warranted. New developments in off-road technology, proper concern for the physical nature of the terrain over which the vehicle will operate, and acceptance of some limitations could result in acceptable performance for a wheeled version of the Aerobac concept. One could then return to a vehicle format such as the BC-7 (Fig. 9.7), that is, with wheels at both ends instead of tracks. Use of wheels, together with side-bodies removable for over road movement, could result in a lighter vehicle, with speed performance equivalent to that of conventional trucks. Figure 9.15 illustrates such a wheeled version, that could also be configured as a passenger vehicle.

Apart from its use in support of construction work in marginal terrain, the

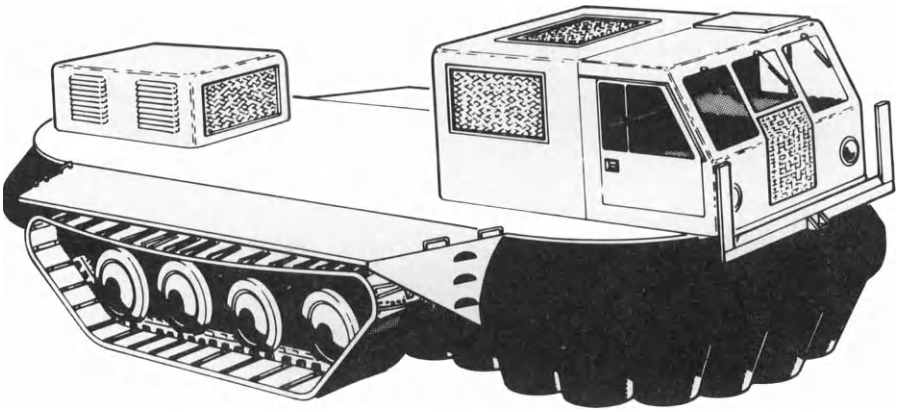

Fig. 9.14 Aerobac AB-7 hybrid air cushion transporter; payload = 7 t, gross weight = 21 t, length = 11.5 m, width = 6.2 m. (Source: TDC).

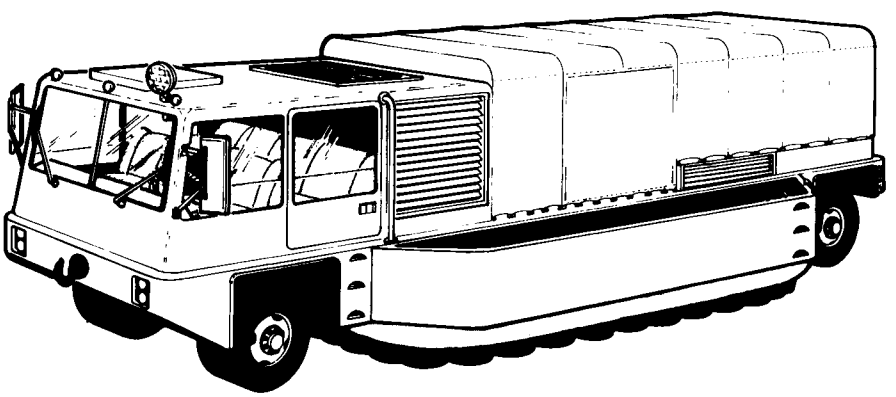

Fig. 9.15 Aerobac AB-5 hybrid ACV, wheeled version; payload = 5 t, gross weight = 12 t, length = 12.2 m, width = 4 m. (Source: TDC).

Aerobac concept (in tracked or in wheeled versions) has been evaluated for airport rescue vehicles and for general transportation in the Northern regions of Canada. Some results of this evaluation are presented here.

(i) Airport rescue. ICAO statistics for the last fifteen years show that in airport accidents, aircraft will come to rest within a 300 m wide area centered on the active runway, and stretching one kilometre at either end of the runway. Approximately half of accident locations are on the runway itself. It is desirable that rescue vehicles be able to reach any point of the area within 2 to 3 minutes. Such a service can only be done at present on the paved areas of airports, because vehicles presently in use are unable to move at high speed over non-paved areas. In the presence of deep snow, most would be unable

to move. In Canada some airports are provided with off-road vehicles that can crawl through deep snow to reach an off-runway site, but not within the 2-3 minute requirement. Local environments, such as tidal flats that are impassable except by hovercraft, may also present difficulties.

A study of the interaction of the Aerobac tracks with various summer and winter surface conditions at two Canadian airports (Vancouver, British Columbia, and Baie Comeau, Quebec) concluded that the combined air cushion/ muskeg tracks allowed passage of the vehicle at speed over all conditions observed (ref. 9.2). It remains to be seen if a wheeled version could be as successful. If so, its higher speed capability would ensure that the 2-3 minute objective would be met readily.

(ii) Northern transportation. As first proposed by Bertin, air cushion vehicles, such as the BC-7 and Aerobac, operating over trails can provide a transportation service at a fairly low cost, provided the cost of operation of the vehicle and the cost of the road way are both taken into account. When comparing with the cost of providing a road for the use of conventional trucks, one can determine a traffic volume below which ACV plus trail maintenance costs are less than truck plus road costs. Although costs fluctuate wildly, the break-even point is in the region of 100,000 tonnes per year. Hence, Aerobac type vehicles can provide a reasonable level of service in many isolated regions, without investment in costly road construction.

The concept can be extended to the exploitation of low-yield resources, either forestry or mines. By reducing the cost of transportation, overland ACV's may reduce the critical size of an industry thereby allowing locally based developments.

9.5 AGRICULTURAL APPLICATIONS

Farming is dependent on the weather. Long periods of rain, or a late thaw, may soften the ground to the point where conventional vehicles cannot operate. Usually these conditions are not encountered on a regular basis, and the cost of special machinery to cover such eventuality is not commercially justifiable. Any improvement in the performance of agricultural implements would best come from *add-on* equipment, that can be temporarily fitted to existing vehicles when the need arises. Double rear wheels and auxiliary track attachments on farm tractors are typical of such devices.

An air cushion assist unit may be used to move loads and heavy equipment on the farm in marginal soil conditions, in a manner similar to that discussed in Section 9.4. However, use of air cushion application on the farm must be reviewed in terms of those parts of the production cycle involving seeding, spraying and harvesting. Ploughing and tillage are operations requiring much tractive effort, and are done in periods when the soil is sufficiently dried to obtain the proper soil compaction. Hence, load relief with an air cushion

would be counter-productive at a time when the soil is firm enough for normal tractor operation. Therefore, the following sections are limited to examples of the use of air cushion technology for seeding, spraying and harvesting; other farming applications may evolve in the future.

9.5.1 Seeding

Conventional seeders are pulled by a tractor and have hollow spikes that pierce the surface, and through which the seed is dropped. The resistance of these spikes is high and may be greater than the draw-bar pull of the tractor in wet ground. Relieving the load on the wheels will not resolve the problem, because the spike resistance must still be counteracted and that can only be done if the tractor wheels can develop the required draw-bar pull.

A pneumatic seeder overcomes this problem because the seeds are propelled into the ground by a high pressure air jet, without involving high moving resistance. Load relief can now be considered if the soil humidity, or the need to reduce soil compaction, makes the use of a conventional tractor objectionable. The seeding system can be mounted on an air cushion platform and self-propelled with terra-tires, or with flexible paddle wheels in extreme conditions.

9.5.2 Spraying

A herbicide is sprayed on most emerging crops in the spring, followed by pesticides and fungicides during the growing season. The operation can be done by aircraft when the danger of drifting is minimal. Aircraft are normally used for large areas, and for dispersing materials which are not environmentally hazardous. Otherwise, spraying is done with tractor-pulled equipment, under controlled weather conditions, so that the spray particles (aerosols) will be deposited mainly where required.

The standard Canadian equipment consists of a tank, mounted on the rear of the tractor or on a separate chassis, with the spray boom extending on either side. In the case of long booms that cover swaths of 12-15 m, the boom is hinged at the midspan and supported at the ends with outrigger wheels. A pump, driven from the tractor power take-off, supplies the spray liquid to a number of nozzles spaced along the boom. The nozzles emit a fine mist that settles on the surface and is absorbed by the plants.

For the most efficient application, the nozzles are set at a height determined by the plants to be treated; operation takes place when the sky is clouded and there is no wind. On a sunny and windy day, much of the liquid can be evaporated or blown down-wind before it reaches the target. Drift poses a serious problem since it can destroy adjacent crops. In some locations, spraying is prohibited when the wind reaches a certain value.

The initial utilization of air cushion technology in spraying was to support part of the tank load and the loads on the outrigger wheels. The

pressure required in the cushion, though reasonably low, created an escape velocity under the skirt that was sufficient to blow the soil away from the roots of the crop, causing considerable damage. A series of experiments determined that, for most soils, the upper cushion pressure limit was 100 Pa (2 lb/ft^2). It was realised that in order to obtain such a low pressure the cushion had to encompass the full length of the spray boom. This led the developers (Jones, Kirwan and Associates Ltd., Hamilton, Ontario, Canada) to the integration of the air cushion with the spray function of the boom.

Figure 9.16 shows the cross-section of the spray boom, with the cushion defined by two bag skirts supported on a light frame. The bag configuration was chosen because its smooth line would be less damaging to the plants than the inner face of a segment or the near vertical wall of a jupe. The light frame allows the cushion to follow the ground contour, but provides rigidity in the horizontal plane. The nozzles are maintained at a fixed height over the surface, and the air flow within the cushion and out of the gap ensures that all droplets are put in intimate contact with the plants.

An in-depth development program was initiated by Agriculture Canada to evaluate the concept on a number of crops. The field trials were conducted by the University of Guelph, with a small 3.6 m boom, and by the Saskatchewan Research Council, with a 25 m boom.

The Guelph trials confirmed that there was virtually no droplet drift, even at wind speeds up to 9 m/s (20 mph). Furthermore, the top canopy of the cushion prevented the sun from vapourizing the spray droplets and the cushion kept the nozzles at the optimum distance from the ground. The towing speed could be greatly increased because the cushion was not subjected to boom whip. The air flow within the cushion deposited some of the chemical on the tender

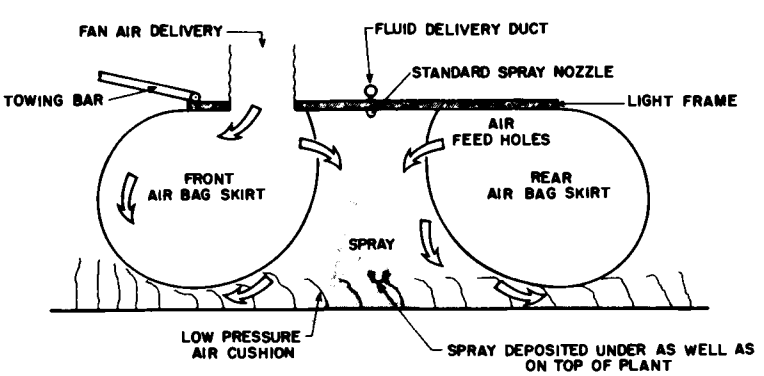

Fig. 9.16 Typical cross-section of the spray boom. (Source: Jones, Kirwan & Associates).

underside of the leaves, which resulted in greater absorption. The results showed that a good weed kill could be obtained with as little as 1/3 of the recommended chemical concentration value, a considerable saving to the farmer and a reduced stress on the ecology.

Tests at the Saskatchewan Research Council confirmed the previous results and showed that the bag skirt was the correct choice for wheat type crops, where the ground is relatively flat. For ridged crops, such as potatoes, the bag was not so successful, and was replaced by a segmented skirt, which operated satisfactorily in spite of earlier reservations.

The air cushion spray boom is evidently not an *add-on* device and should be considered as a new piece of equipment that replaces the conventional rig. As now designed, the boom consists of a chassis supported by the tractor and containing spray tank, spray pump and air cushion fan, both of these driven by the tractor power take-off (or hydraulic pump). The boom is slung from the chassis and allowed to follow the ground without restriction from the chassis. Figure 9.17 shows the major components of the spray boom, which may be folded for transportation.

9.5.3 Harvesting

Harvesting of expansive crops, such as wheat, is usually carried out by a machine that stores the produce in a bin and then discharges it into trucks that pull alongside when the hopper is full. Problems may arise when the ground will not support the fully-loaded harvester or truck. In such cases, both vehicles may be equipped with an air cushion assist package.

Jones, Kirwan and Associates have done a number of tests on a Massey-Ferguson combine to determine the amount of weight that should be taken by the air cushion and how much should remain on the wheels to provide traction. The

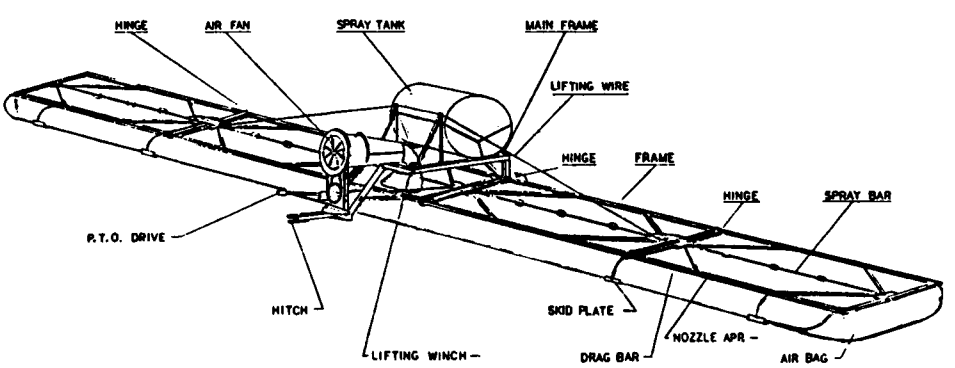

Fig. 9.17 Diagram of spray boom, showing major components. (Source: Jones, Kirwan & Associates).

results showed that if the harvester could not move empty it was probable that the crops were not in a condition to be harvested. Hence, the air cushion package would only have to provide a lift force equal to the weight of the crop in the bin.

9.5 SUMMARY

Many inland applications of air cushion technology can be identified. A number have taken place, usually in a sporadic manner, linked to specific construction projects, such as the work platforms of Mackley-ACE, or the Yukon ferries used during construction of the Aleyeska pipeline. The Hoverlift Systems ferries operated in Canada were discontinued because of a lack of suitable operators, or of servicing facilities, in the remote locations where such ferries are most likely to be used.

Attempts at overland transportation have not progressed beyond a small number of demonstration projects. Generally, the worth of the air cushion was demonstrated, but with prototypes that were less than adequate. While prospective customers could well be impressed by the promises, they were principally interested in specific transportation tasks with reliable vehicles. Hence, after a demonstrator had been taken to a remote site at great expense, the promotor was usually hard-pressed financially to rebuild his prototype. A second chance was rarely possible. Nevertheless, the experience gained has permitted the definition of vehicle concepts that could be successful, provided their physical realisation would have the sturdiness and reliability expected of off-road vehicles.

Agricultural applications have the same requirement for sturdiness. This very conservative market does not permit experimentation at the farm level. To be successful, the systems (such as the highly effective spray boom) must be produced and sold by well-known farm machinery manufacturers.

9.7 REFERENCES

1. J.Y. Wong, Theory of Ground Vehicles, John Wiley & Sons, Inc., Toronto, 1978.

2. R. Yong, B. Gauthier, and P. Alepin, Study of AEROBAC AB-7 Vehicle for Airport Rescue in Difficult Terrain, Report TP 5116E, Transportation Development Centre, Transport Canada, Montreal, 1983.

Chapter 10

SKIRT DURABILITY

10.1 INTRODUCTION

Surface Effect Ships and Vehicles require a flexible seal or skirt structure to contain the cushion of air on which the craft is supported to minimize drag between the cushion structure and the surface being traversed. Typically, the flexible skirt or seal consists of an upper bag supporting flexible fingers that are in contact with the local terrain. The fingers provide cushion retention with flexibility to permit their contouring to a continually changing three-dimensional surface with very low drag by minimum surface contact, but with excellent reinflation response when displaced by contact on the terrain. The bag functions similarly but with greater drag than the fingers because the bag presents a large contact area, or footprint. The bag reinflates more positively since it is directly inflated by fan air flow. In the presence of complete loss of cushion from terrain contact, however, the fingers must first rely on gravity to initiate their descent, before sufficient cushion air builds up to produce a more positive inflation.

Good cushion retention is achieved by complete flexibility in the seal or skirt and by selection of the proper configuration to maintain shape and stability. Since the seal or skirt is pressurized membrane structure, numerous constraints are placed on the shapes which can be used. Within these constraints, the seal or skirt must achieve the required shape with an acceptable accuracy, and must not collapse in one of numerous instability modes when loads are applied.

The seals and skirts serve two other purposes besides the principal function of retaining the cushion. The first of these is to contribute to the

stability of the craft; pitch stability in the case of the SES and pitch and roll stability in the case of the ACV. This contribution is obtained by arranging the geometry of the seal or skirt so that as the craft pitches or rolls a change in cushion geometry occurs. This results in a movement of the cushion center of pressure which in turn produces appropriate restoring moments. Secondly, the skirt or seal contributes to ride characteristics, as a consequence of its effect on the pitch, roll and heave stiffness of the craft. These contributions arise partly from seal or skirt geometry and the changes in geometry due to craft motion, and also from the pressures built up in the bags when these motions occur relatively rapidly. These contributions to ride are dependent not only on seal or skirt geometry but also on the selected pressure ratio between bag and cushion, and on the pressure and flow characteristics of the lift fans. Some alleviation is also provided by the seals or skirts to the loads and pressures which arise during slamming in high sea states, so that some reduction in hull structure weight is possible.

These overall loads establish design requirements for strength, the definition of which is complicated by the difficulties of predicting craft motions and the nonlinear interaction between seal or skirt system loads and the instantaneous seal or skirt shape. Also, it is important to design for life, both in the usual sense of life under repeated loadings and life under the dynamic flexing and flagellating, and erosive and abrasive conditions of high-speed craft operation over various types of surfaces. Presently this is largely empirical, with laboratory and operational testing being required to develop an adequate design.

The essential seal characteristics are achieved in the current designs of ACVs by using a low-pressure inflated structure constructed from an elastomer-coated woven fabric material. Seal or skirt structures represent a relatively new application for elastomer-coated fabric materials which were originally developed for other types of flexible structures such as conveyor belts and liquid storage containers. Air cushion seals are exposed to harsh environments which have different and more demanding requirements than existed for the previous applications for rubber coated fabrics.

10.2 GENERAL SKIRT-MATERIAL REQUIREMENTS

The material requirements for air cushion seals are dictated by the type of material and its response to the variety of applied static and superimposed dynamic loads, the calculated and inferred mechanical and environmental properties, the structural efficiency necessary for aircraft type structures and the damage processes deduced and observed from in-service failures. The known factors which influence the behavior of a coated fabric system are discussed in the following paragraphs.

10.2.1 Description of Fabric/Elastomer Materials

The rubber-coated fabric materials used for seals are composed of three constituents: the rubber covering, the woven fabric reinforcement, and the tie-coat which bonds the rubber and fabric together. The material is a three constituent laminant materials system with the woven fabric in the middle and the rubber covering on both sides of the fabric; the tie-coat is an almost imperceptible layer on both faces of the woven fabric.

The factors which influence the dynamic behavior and life of rubber-coated fabrics in seal/skirt applications are numerous and their relationships are sufficiently complex to have defied clear definition. The characteristics of coated fabrics are influenced by the nature of each constituent, but, in addition, there are behavioral aspects which are unique responses of the combined material system. The viscoelastic stress-strain response of the highly nonlinear rubber coating is modified by the presence of the woven fabric with its nonlinear viscoelastic directionally dependent characteristics which are modified by the macroscopic locking action of the tie-coat and rubber cover. The fabric behavior can be complicated by the presence of the tie-coat which can change the stiffness characteristics of the outer filaments in the yarn bundles, thereby modifying the internal load distribution among the filaments in the yarn. Although each constituent in a rubber-coated fabric contributes to the properties, it is important to keep in mind the large number of parameters involved and their complex interactions.

A summary of the various property - constituent relationships identified, to date, is presented in Table 10.1. The reinforcement determines the maximum tensile and tear strength, elongation and probably fatigue life of the laminant and may determine the stress relaxation properties, at least for certain fabric constructions. The reinforcement also contributes to both chemical and physical adhesion of the tie-coat/rubber as well as to flexibility, abrasion resistance and the response to dynamic loads such as flutter, flagellation, and bending fatigue. The tie-coat can reduce the maximum tensile and tear strength of the fabrics, can be a major contribution to coating adhesion, helps to maintain reinforcement geometry, contributes to flexibility, response to dynamic loads, dominates bonded-seam joint failure modes, may dominate environmental resistance to moisture, and contributes to fatigue life. The rubber coating contributes strongly to coating adhesion, maintains the reinforcement geometry, can dominate flexibility, can lower the maximum tear and tensile strength, contributes to response to dynamic loads, contributes to bonded seam joint failure modes, dominates crack growth resistance and crack initiation, can dominate abrasion resistance; dominates the temperature rise in specimen during dynamic flexing, dominates environmental resistance particularly with regard to ozone cracking and oxidation, and protects the oxidation, and protects the fabric

from ultraviolet radiation in the case of nylon.

Table 10.1. Summary of property constituent relationships.

Reinforcement	Tie Coat Adhesive	Rubber Coating
Tensile strength	Coating adhesion	Coating adhesion
Coating adhesion	Reinforcement geometry	Reinforcement geometry
Flexibility	Tensile strength Flexibility-bending modulus	Permeability Flexibility-bending modulus
Elongation	Response to dynamic loads	Tensile strength Abrasion resistance
Response to dynamic loads (flutter/flagel-lation/bending fatigue)	Bonded seam joint failure mode	Tear strength Crack growth resistance Crack initiation resistance Temperature rise during dynamic flexing
Tear strength	Environmental resistance	Response to dynamic loads
Stress relaxation	Fatigue life	Bonded seam joint failure mode
Fatigue life		Environmental resistance protects reinforcement from uv radiation

10.2.2 Current Limitations of Skirt Systems

One design/material limitation is the trade-off between life, weight of material, performance of a skirt system and cost. Because an aircushion vehicle is an aircraft type structure, low weight is a premium and the skirt system is designed to be as light as possible. Typically, rubber coated fabrics become heavier, thicker, and less flexible as they are made stronger with current nylon and polyester woven fabrics available today. Materials such as Kevlar, which have twice the specific strength of nylon and polyester, self-abrade in woven structures during flexing and weaken quickly. Also, the fabric weave geometry affects its thickness and strength and the thickness of rubber required to coat the fabric completely.

Commercial coated fabrics are limited in the width of material which is available (52 inches). As a consequence, almost all bags are constructed from neoprene coated nylon fabric because neoprene forms high strength, low cost bond joints with adhesives which do not require pressure cures. Bonded joints are required to fabricate bags because of their size versus the size and strength of available material. In fact, the larger the vehicle, the larger the bags and the larger the number of joints required.

Neoprene coated nylon bag materials exhibit an approximately 30% reduction in tear and tensile strength with age. The strength reduction may be caused by

repeated (fatigue) tensile, compressive, and flexural loadings of the material along a line of attachment or by an aging process which results in loss of strength of the nylon fabric.

Other factors also limit the life of a skirt system: the components of the system itself (bags, fingers, and cones), location on the craft (bow, stern, side, underneath), dominant damage modes, type of operating terrain, vehicle size, vehicle operational attitude (bow up) and velocity, material and material properties. Many of the factors are interrelated: craft operated in a bow up attitude will exhibit much sorter lives on components near and at the stern than near and at the bow; craft operated at high velocity will exhibit a shorter skirt life than craft operated at lower velocity; a craft operated over land, concrete, and jagged ice will exhibit shorter finger and cone life than a craft operated over water because the damage mode changes.

A typical skirt system consists of bags, fingers and cones and is illustrated in Figure 10.1. Bags attach to the hull or hard structure; outer

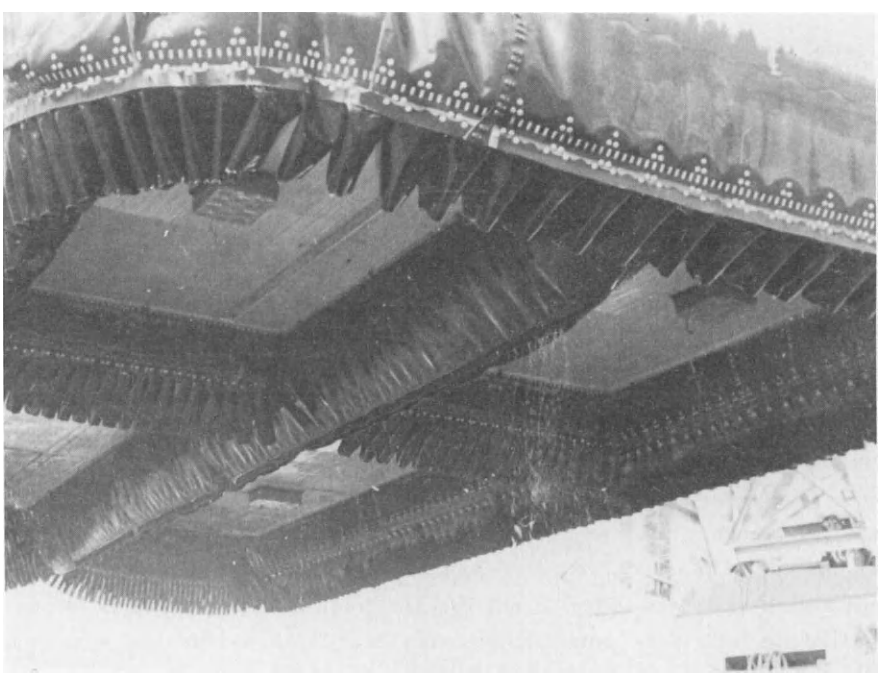

Fig. 10.1 Air cushion vehicle flexible skirt system (U.S. Army LACV-30) viewing from bow to stern. Fingers hang from the bow and side bags; cones hang from the stern bag and the stability bags (athwartship). Also shown is the keel bag extending from the bow to the stern. The fingers are inflated through feed holes in the bags.

bags are located around the entire edge of the craft and stability bags are located under the craft to impart pitch and yaw stability. Fingers attach to the bow and side bags and cones attach to the stern bag and the stability bags; the fingers and cones contact the terrain.

Typical operating life ranges are summarized for the various components in Table 10.2. As would be expected, fingers and cones exhibit the shortest lives of all the components and those at the stern of the craft may be a factor of 4 to 20 shorter than at the bow depending on the dominant terrain and craft operating attitude. Lives of fingers and cones over land appear to be 4 to 6 times shorter than over water and lives of these components over concrete or macadam may be 10 to 20 times shorter than over water.

Table 10.2. Life limitations for skirt systems.

Component of skirt system	Life limitation (hours)
Bow, side, stern bags	2000 - 4000
Stability bags	1000 - 3000
Bow fingers - small vehicles*	500 - 1200
Bow fingers - large vehicles	200 - 450
Side fingers - small vehicles	50 - 800
Side fingers - large vehicles	50 - 300
Stern cones - small vehicles	50 - 200
Stern cones - large vehicles	75 - 150

*Vehicles 27 tonnes or less gross weight.

Choice of materials can affect the life of fingers and cones by a factor of 1.5 to 2. Natural rubber - natural rubber polybutadiene blend, polyisoprene polybutadiene blend (provided they contain sufficient antiozonant and anti-oxidant) coated fabrics have longer lives than neoprene, hydrin, polypropylene, or PVC-nitrile coated fabrics with the fabric being essentially the same. The fabric design also can affect finger life by up to a factor of 2. Life improvement over the years has resulted from both design and materials improvements as more understanding of the damage modes was obtained.

10.2.3 Damage Processes

The bag and finger seal system is subject to various damage modes in operation and extensive data are available on the damage modes from operating vehicles such as the SR.N4, BH-7, Sr.N6, Voyageur, LACV-30, SES-100B and the LCAC. Knowledge of these failure modes establishes many key requirements for the material. The observations are summarized in Table 10-3 for a number of the vehicles. As is evident in the table, damage to bags and fingers differ because different damage mechanisms prevail for the two components. Usually different strength and weight materials are involved with the heavier and stronger material used for fingers. The dominant damage modes for fingers also differs for amphibious vehicles and for water-only vehicles such as SES.

After the bag-finger skirt concept evolved, initial damage processes to

bags consisted of tearing at joints and air feed holes. These damage processes were alleviated by redesigning the shape of the air feed holes, eliminating stress points and redesigning attachment areas for better load distribution. Consequently, these failure modes are not evident in more recently designed bags. The SES-100B, LACV-30 and LCAC vehicles exhibited no bow or stern bag failures.

The current dominant mode of failure for bags on amphibious vehicles is tear that propagates quickly through an entire bag section. The bottoms of stability bags on amphibious vehicles also exhibit abrasive wear which is caused by contact with and dragging on solid terrain.

Dominant damage modes to fingers and cones varies with terrain and material. For an SES type vehicle PVC-nitrile rubber coating develops flex cracks in the severely flexed regions near the bottom edges of the bow fingers. Gradually the isolated fragments of rubber delaminate and the remaining fabric develops holes, frays and unravels.

On amphibious vehicles which operate largely over water, such as the SR.N4, the bow fingers gradually wear by a slow peeling of the rubber coating immediately ahead of the bottom edge; once exposed, the fabric unravels and frays.

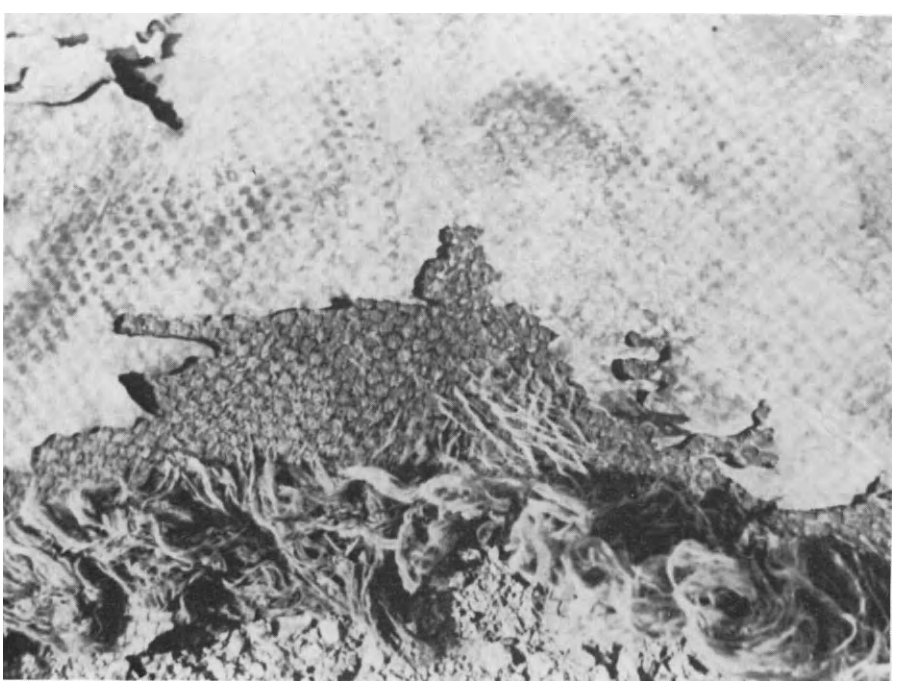

Fig. 10.2 Extensive delamination of rubber coating and fabric fraying on finger.

On other vehicles other types of damage modes have been observed which appear to initiate as rubber delamination (bond failure at high flex and bend regions in the fingers); this is shown in Figure 10.2 for a bow finger. Side fingers exhibit delamination of the rubber at buckle nodes which form at one-half to 90% of the finger height. Once delamination occurs, the rubber is lost and the fabric frays forming a hole. Eventually, wear from the tip meets the propagating elongated hole and the finger has the appearance of a tear.

Table 10.3. Dominant skirt failure processes for various vehicles.

Item	Vehicle	Outer bags	Stability bags
(a)	SR.N4 Cross channel ferry	Infrequent tears	Infrequent tears
(b)	Voyageur Canadian Coast Guard ice breaking	Tears	Abrasion, tears
(c)	Voyageur Arctic operations	Tears, rubber cracking	Tears
(d)	LACV-30	Nothing observed	Abrasion, one tear
(e)	LACV-30 vehicle trimmed bow-up		Abrasion of cones, replaced @ 375 hours
(f)	SES-100B	Some fastener abrasion, seam delamination, rubber cracking	Not applicable

	Bow fingers	Side fingers	Rear cones
(a)	Delamination crease line flex, fabric fray, abrasion	Abrasion, delamination, tearing, fabric fray, node flex	Abrasion, fabric fray
(b)	Abrasion, tearing, delamination, fabric fray	Abrasion, tearing, node flex, fabric fray	Abrasion, fabric fray
(c)	Abrasion, tearing, fabric fray, fingers torn off	Abrasion, tearing, node flex, fingers torn off	Abrasion, fabric fray cones torn off
(d)	Light abrasion	Light to heavy abrasion and tears (front to rear)	Abrasion
		Two rear side fingers replaced @ 500 hours	Abrasion, two rear cones replaced @ 500 hours
(e)	Light abrasion but fingers replaced @ 375 hours	All fingers and cones replaced @ 375 hours. Some replaced @ 50 hours	Very heavy abrasion, tears, replaced @ 375 hours
(f)	Flagellation, rubber cracking, fabric fray	Not applicable	Not applicable

On amphibious vehicles which operate over land, concrete, and ice, abrasive wear of the tips of the fingers and other areas of contact is a dominant damage mode. This is illustrated in Figure 10.3. If the craft is operated on a very low cushion, so that much of the finger is under the craft, abrasion occurs along the line of contact extending up the finger 50 to 75% of its length; the finger soon appears to have torn.

A number of approaches have been made to simulate in-service damage mechanisms at an accelerated rate in laboratory tests and correlate data with service life. The tests differentiate acceptable material from nonacceptable material but do not necessarily rank the acceptable materials successfully.

The laboratory tests included various types of flagellation tests and a de Mattia flexural fatigue test. The simple flagellation tests pass air over a flat sheet specimen or impact a flap in a flat sheet specimen with a high velocity jet of water. A more complicated water jet test impinges a high-speed jet of water on a specimen configured as a finger and supported by a cushion of air; specimens were tested with 12 or 24 inches in frontal width and about two feet long (ref. 1). Cushion pressures of both 85 and 200 lb/ft^2 were used.

These tests reproduce failure modes of rubber delamination, fabric fraying

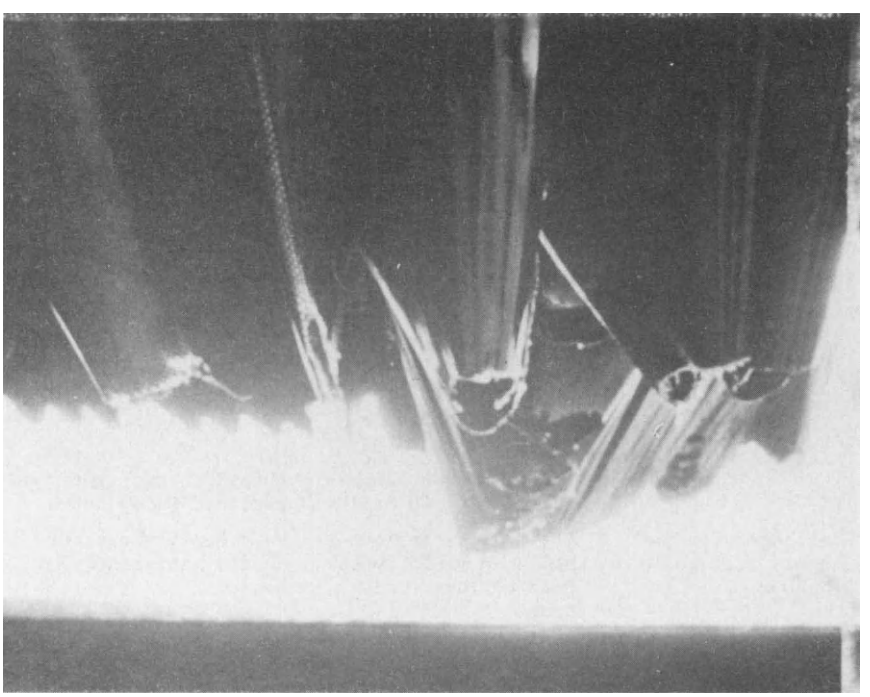

Fig. 10.3 Abrasive wear of fingers on LACV-30-2.

and unraveling and rubber flex cracking. The more complicated water jet test also yields body holes (perhaps comparable to the holes which develop at bend nodes in service). The body holes exhibit relatively high erosion rates relative to edge delamination; this failure mode was reported to increase in incidence as the stiffness of the finger material increased and as the frontal area increased. Specimens in the simple flagellator tests undergo a large amplitude, high frequency (6 to 10 Hz) flutter and exhibit high accelerations in the materials. High speed photographs show that the tips sometimes have a higher frequency flutter superimposed on the flap flutter. In the more complicated water jet test, the edges of the fingers at the cushion air, finger tip, and water jet interface fluttered at 100 to 300 Hz. These results were similar to results obtained at Naval Ship Research and Development Center in tow tests at lower speeds and cushion pressures (ref. 2).

Water jet flagellation tests have been used to evaluate the response of coated fabrics with different fabric geometries using specimens which were fabricated with the same rubber formulations to the same total weight (ref. 3). A significant difference in response was obtained for a 3 × 4 closed-basket construction which exhibited little damage and a 3 × 4 open-basket which exhibited extensive cracks in the rubber coating in the flagellating flap as shown in Figure 10.4. The edges of the flaps were inspected microscopically to identify the location of cracks with respect to the fabric reinforcement. The cracks in the rubber matrix extend from the edges of the yarns closest to the rubber surface and also from the juncture of two overlapping yarns. Two cracks had not propagated to the surface of the rubber, indicating that the rubber cracks initiated at the interface and propagated to the outer surface of the rubber.

Similar crack initiation and propagation was observed in de Mattia bend fatigue samples of rubber-coated fabrics, i.e., the cracks initiated at the fabric rubber interface and propagated outward to the free rubber surface. Hundreds of de Mattia flexural fatigue samples were evaluated and in every sample the cracks initiated at the rubber-fabric interface and propagated outward just as observed on the flagellation test specimens (ref. 4). It seems probable that rubber cracking in high-flex regions exhibited by fingers in service initiates in the same manner as observed in flagellation and flexural fatigue tests.

Currently, finger material specifications used by operators of the SR.N4, SR.N6 and LACV-30 require air flagellation acceptance tests on each roll of commercial, rubber coated fabrics. Materials up to 2.88 kg/m^2 (85 oz/yd^2) are evaluated in an air flagellator at an air velocity of 85.3 m/s (280 ft/s); materials from 2.88 kg/m^2 to 6.78 kg/m^2 (85 to 200 oz/yd^2) are evaluated in an air flagellator at an air velocity of 121.9 m/s (400 ft/s) (ref. 5).

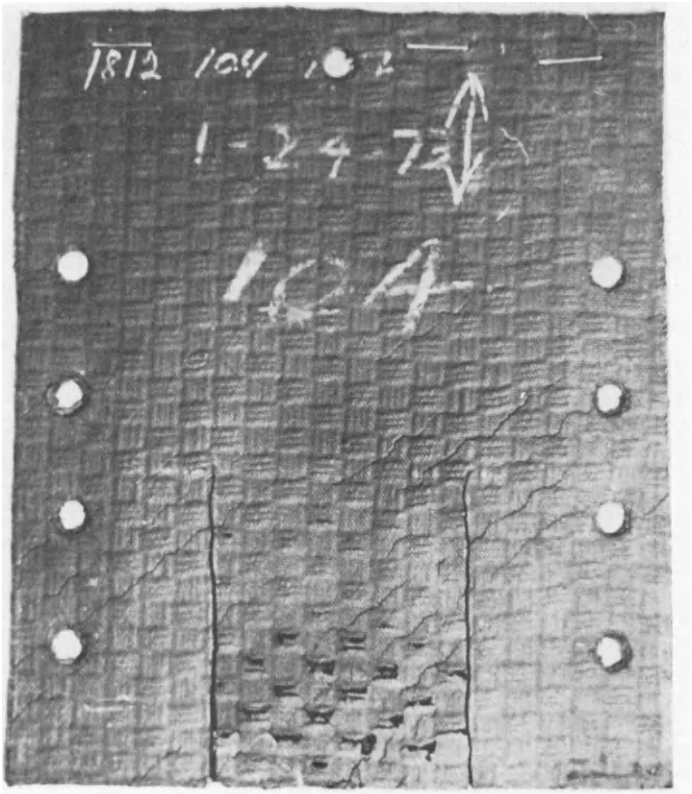

Fig. 10.4 Typical flagellation damage and macrostructure after testing. (BF Goodrich 1812-104; flagellation time = 16 hours).

10.2.4 Required Properties

To be resistant to the damage mechanisms and modes described, rubber coated fabric material has to sustain rapid strain rates and rapid strain recovery rates from tensile and compressive loads. At high rates of flexing, heat buildup may occur so that properties at 60°C to 150°C (150-300°F) may be important in small areas. Among the required properties are: high strength-to-weight; low flexural modulus; high flexural, compressive, and tensile fatigue resistance; and sufficient tensile and tear strength to carry the mechanical loads (static and superimposed dynamic) within the skirt system. The required tensile and tear strength increase with vehicle size and are approximately 214.5 kg/cm (1200 lb/in) of width and 227 kg (500 lb), respectively, for fingers for a 181 tonnes vehicle. For fingers for a 2721 tonne vehicle the tensile strength requirement was determined to be approximately 893.7 kg/cm (5000 lb/inch) of width.

In addition, the polymer coatings and the tie coat adhesive have to have high flex crack and crack growth resistance, high impact resistance, low

flexural modulus, high abrasion resistance, low hysteresis or excellent high temperature properties; outstanding environmental resistance (water, sunlight, ozone, fuel); and exhibit good coating adhesion.

10.3 DESIGN CONSIDERATIONS

As described earlier, the mechanical properties of rubber coated fabrics can be changed in a variety of ways. The goal is to identify the best combination of rubber coating, fabric weave geometry, and tie coat to obtain the best balance of properties for the application. An excellent state-of-art summary was published by the United States National Materials Advisory Board in 1978 (ref. 6).

10.3.1 Elastomer Type and Formulation

Elastomer coated fabrics have been fabricated and evaluated using a variety of gum rubber elastomers, blends of elastomers and varying the ingredients in the same elastomer to obtain the desired properties. Elastomer formulations have included natural, natural/butadiene blend, polyisoprene/butadiene blends, hydrin, gum polyurethane, castable liquid polyurethane, propylene oxide, neoprene, PVC-nitrile, and EPDM (ethylene propylene dieneterpolymer). The many varieties of elastomeric polymers and the multitude of compounding ingredients and cure states which are available introduce a large number of potential variables.

No one elastomer has all the best properties for seal application; e.g., natural rubber has excellent fatigue resistance, cut resistance, and abrasion resistance but only poor to fair ozone and oxidation resistance; butadiene has excellent abrasion resistance but only poor to fair ozone and oxidation resistance; EPDM has excellent resistance to ozone and air oxidation but has fair cut resistance and does not bond readily to reinforcements; polyurethanes have the highest specific strength and excellent resistance to abrasion but only fair to good fatigue resistance; cast polyurethane is an elastomer that can be formulated for room temperature cure and liquid castings without using solvents; neoprene has excellent resistance to ozone and oxidation, and is easy to bond to reinforcements with excellent bond strength but is only fair in cut and fatigue resistance; epichlorohydrin has excellent resistance to hydrocarbon fuels and oils but is only fair in abrasion and fatigue resistance; and propylene oxide rubber has excellent fatigue resistance and excellent resistance to ozone, sunlight, and oxidation but is difficult to bond to reinforcement.

Gum rubbers are combined into blends to obtain a better balance of properties: e.g. natural rubber has superior fatigue resistance at comparatively high elongations (>50%) whereas styrene-butadiene copolymer rubber (SBR) has excellent fatigue resistance at low elongations (0 to 50%) or when flexed under compression. The enhancement that is obtained by blending natural and styrene-butadiene rubber is shown by the data in Figures 10.5 (ref. 7) and 10.6 (ref.

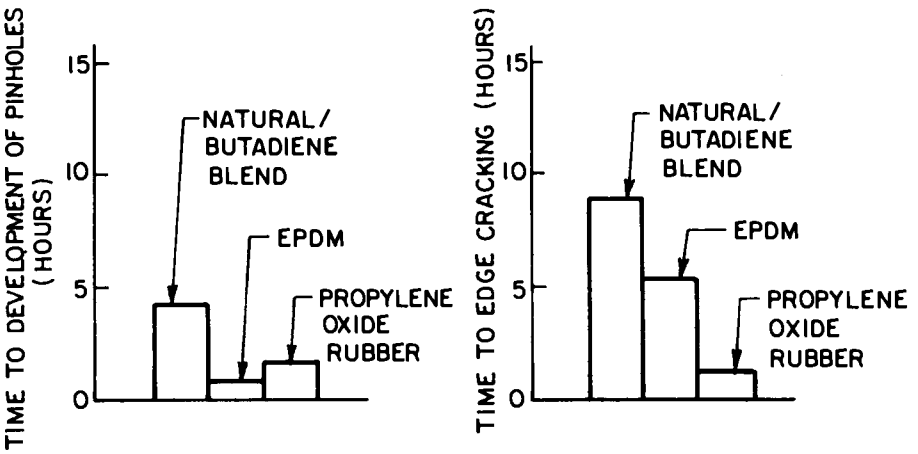

Fig. 10.5 Results from water jet flagellator test on rubber-coated fabric samples coated with natural/butadiene blend, propylene oxide rubber, and EPDM rubber.

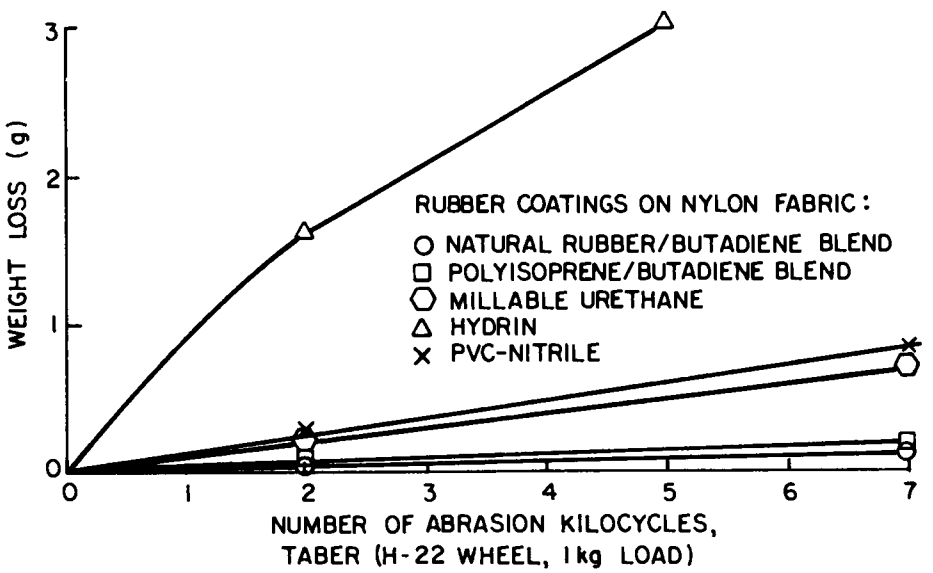

Fig. 10.6 Abrasion resistance of rubber-coated fabric materials.

3). The data in Figure 10.5 on water jet flagellation resistance reflect the relatively high strain (elongation and compression) as well as rapid recovery

from strain in the specimens during a water jet flagellation test; the three polymers were coated on the same fabric. The data in Figure 10.6 reflect the superior abrasion resistance of a natural/butadiene blend as illustrated by the weight loss versus thousands of cycles on a Taber abrasion tester; these data were obtained on the polymers coated on the same fabric.

Even for gum stocks with excellent fatigue, abrasion, and cut resistance properties, the type and amount of filler is crucial to maximize these properties together with good processibility, bondability to fabric reinforcements, and environmental resistance. In some instances, the fillers are synergistic and produce maxima in mechanical property data; determining the optimum amount of each is a trial and error process. Antidegradants must be selected carefully and be of the non-bleeding variety so as not to interfere with bonding to reinforcement.

In a series of studies by Goodyear Aerospace (ref. 7), B.F. Goodrich (ref. 3), and Bell Aerospace Textron (refs. 3, 8), formulations were chosen initially of 50/50 polyisoprene/butadiene and, subsequently, natural/butadiene blends in the range of 50/50 to 70/30. The polymer reinforcing filler level also was selected about 50 parts per hundred parts of rubber (pphr). Since an improvement in the adhesion of the rubber formulations to nylon was desirable, hydrated silica was included as a filler together with carbon black.

One series of formulations was evaluated for mechanical properties and adhesion to nylon; the results are summarized in ref. 8. The formulas were prepared and evaluated to determine the best ratio of polymers, the total amount of reinforcing filler, the ratio of carbon black to silica, the type of carbon black and silica, the type and amount of processing aids and the degree of cross linking. Carbon blacks generally promote scorch tendencies (premature curing) and accelerate cure rate, while hydrated silicas retard cure. Further, small particles and high structure blacks are used for improved abrasion and wear resistance but also cause greater scorch tendency than other blacks. Consequently, the formulations were a trial and error process tempered with experience in rubber formulating. From the results four formulations were identified as the best in terms of tear strength and peel adhesion.

The rubber formulations then were applied to the same nylon fabric of a weight and strength suitable for SR.N4 fingers using various tie coats, and the mechanical properties and flagellation resistance determined. Three of the formulation tie coat combinations generally exhibited little damage in the waterjet flagellator test. Using the three combinations, new rubber coated fabric specimens were prepared and evaluated including both waterjet flagellation testing and air flagellation testing at 122 m/s (400 ft/s) air velocity. All the materials except one exhibited little to no damage in the waterjet flagellation test consistent with the initial test results, and two combinations, exhibited less damage than an SR.N4 finger in the air flagellation test

(ref. 9).

Environmental factors such as temperature, aging and moisture affect the mechanical properties of rubber and rubber coated fabrics. High temperature affects the strength of the viscoelastic rubber and the greater the time at temperature the greater may be the effect. If the temperature is lowered through the glass transition temperature, then a drastic change in mechanical properties will occur as the behavior changes from ductile to brittle or vice versa. Most rubber formulations do exhibit strengthening and increase in tensile modulus as the temperature is decreased.

The effects of temperature on rubber-coated fabrics depend on the modulus changes of the rubber coating, the tie coat, and the fabric and the complex manner in which the coating, tie coat, and fabric interact. The data in Fig. 10.7 (ref. 3) illustrate the complex manner in which the properties of the individual constituents can interact to yield the properties of the composite; flexibility decreases with decreasing temperature whereas coating adhesion increases with decreasing temperature, although in a different temperature range.

Water wicking by nylon fabrics can lower the stiffness and the tear strength of the rubber-coated nylon fabric as illustrated by the results in Figure 10.8. In the figure, the percent change in stiffness, tear strength and coating adhesion are plotted versus days of water immersion of a natural rubber-butadiene blend coated nylon fabric. The loss in stiffness (20%) is surprisingly high but may reflect the effect of water on the glass transition temperature of nylon. The tensile fatigue resistance was determined on specimens that had been immersed for 3 months. Although a 230 percent reduction in tensile strength occurred after water immersion, little change was evident in the tensile fatigue.

Nylon coated with neoprene and other chlorine containing rubber exhibits aging effects under temperature and humidity conditions typical of the tropics. Neoprene rubber may decompose very slowly in these conditions and release chlorine which could attack nylon chemically and lower the tensile and tear strength. A deterioration of tear and adhesive properties of neoprene coated nylon fabric after service has been noted but attributed to water absorption and fatigue.

Temperature can affect the properties of nylon (and polyester) in two different ways. On first heating to an elevated temperature, the fiber or yarns exhibit shrinkage so to avoid this dimensional change, the fibers or yarns are previously heat set at the highest anticipated use temperature. Also, the breaking tenacity of the fibers or yarns decrease with increasing temperature; an increase from 21°C (70°F) to 93°C (200°F) reduces the breaking tenacity 20 to 22%.

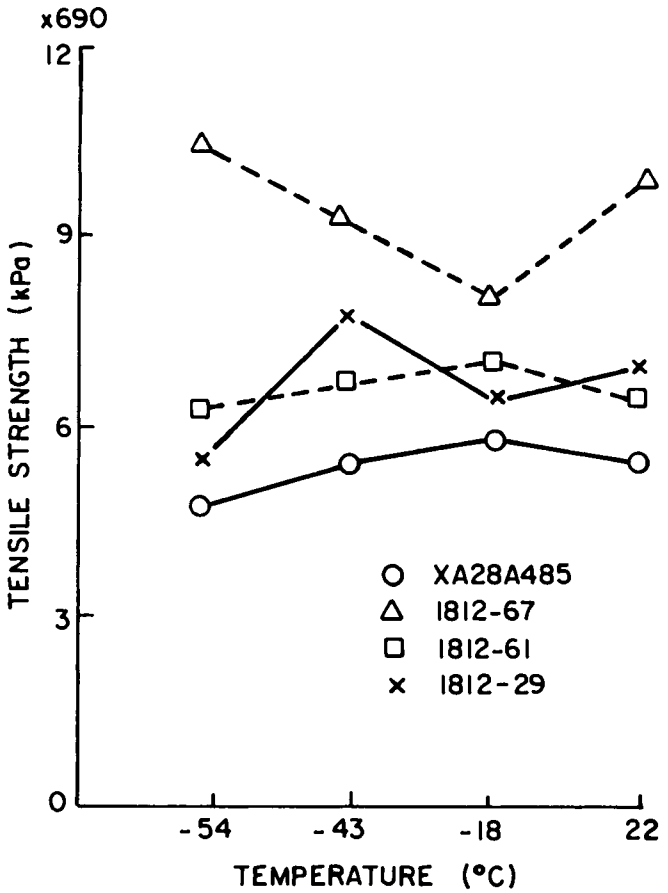

Fig. 10.7 Tensile strength of four different rubber coated fabrics at four different temperatures.

10.3.2 Fabric Substrate

The function of the woven layer of skirt materials is to provide strength without severely diminishing the flexibility of the protective elastomer layers. Fabrics are strong because of the strength of the individual filaments from which they are constructed and flexible because of the fine diameter of these filaments. Although the geometric arrangement of filaments in the yarn and of the yarns in the fabric can significantly influence fabric properties, fabric tensile strength ultimately depends on the type of filament from which the fabric is woven.

High-tenacity nylon filaments have traditionally been used in skirt fabrics for several of the same reasons that they have been successful as reinforcement reinforcement in automobile tires: they are strong, tough and elastic, bond

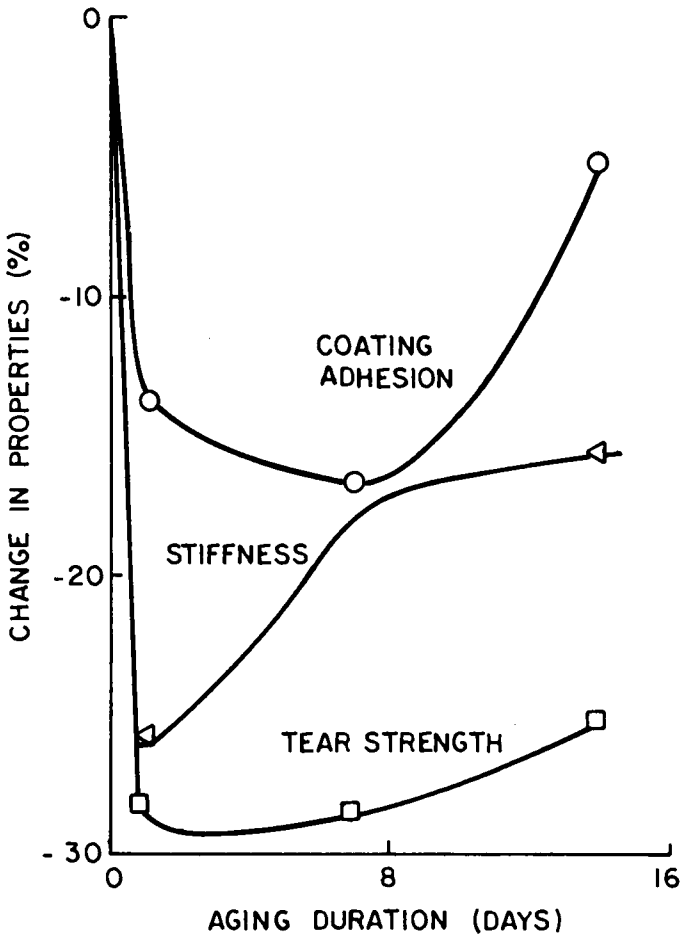

Fig. 10.8 Percent change of properties during water immersion of rubber coated nylon fabric.

well to rubber, resist fatigue and are cost effective. Tire-cord grade nylon yarns are available with tenacities to about 9 gpd (grams per denier). Polyester yarns, also available in tenacities to 9 gpd, have some properties, such as lower moisture absorption and lower creep rate, that might make polyester a more attractive material than nylon in this application, but polyester does not bond as well to rubber. In addition, high-tenacity polyester generally has a lower elongation to failure than nylon, exhibits poor dynamic fatigue performance and has a tendency to hydrolyze. Kevlar aramid fiber with a yarn tenacity of about 20 gpd has found considerable application in radial tires but early use of this material in skirt panels has shown it suffers from a tendency

to fibrillate and self-abrade. The extended chain polyethylene materials such as Allied-Signal's Spectra fiber with a tenacity in excess of 30 gpd, moisture insensitivity and good fatigue resistance is a promising new candidate for skirt reinforcement if good bonding with rubber can be achieved.

Higher strength fibers are particularly interesting for use as reinforcement in skirt fabrics because the fabric weight required to achieve a given level of tensile strength is inversely proportional to the tenacity of the yarns in the fabric. For example, the weight of a nylon fabric with a tensile strength of 5000 pli is on the order of 60-80 oz/yd^2 whereas a Kevlar fabric with the same strength would weigh less than half that amount and a similar Spectra fabric, less than a third. Yarn denier and, hence, fabric thickness would also be less for the stronger filament types with the result that less elastomer would be required to cover the fabric and fill the pores and the laminate would be less rigid.

The yarn and fabric construction parameters that must be specified in a fabric design include: yarn linear density (denier), yarn twist (singles and ply), yarn count in the fabric and fabric weave pattern. The total yarn denier per unit width of fabric is determined by the fabric tensile strength needed in the two principal directions and by the yarn tenacity. How this total yarn denier is divided among individual yarns will be specified by the count, or ends and picks per unit of fabric width. The count, in turn, is determined, within limits, by the degree of fabric openness desired and by the need to maximize tearing strength. Fabrics woven from fewer, larger denier yarns will be more open, thicker, and generally have a higher tearing strength than fabrics of the same tensile strength woven from a grater number of lower denier yarns.

Bundles of filaments are commonly consolidated in the yarn structure by the insertion of twist which causes the filaments to assume helical paths around the yarn axis. The higher the denier of the yarn being twisted (larger diameter), the greater the helix angle of the filaments at the yarn surface for a given number of turns per inch. Low-to-moderate levels of twist generally improve the strength of the yarn by redistributing length differences between filaments in the bundle so that applied tensile loads are more equally shared. At high levels of twist the strength of the bundle declines because of angulation of the filaments with the loading axis. Nevertheless, high twist levels may still be desirable in order to maintain an open weave: a high twist will more effectively constrain the filaments within a round cross-sectional shape whereas, if the twist is low, the yarn will spread in the fabric structure to fill the space available. Twisted singles yarns may be further combined by twisting them together to form plied or cabled structures called cords.

The choice of fabric weave pattern, whether a plain-weave or a longer float basket or twill weave, in combination with the fabric end count will influence such properties as elongation, tearing strength, free open area, weight, thick-

ness, flexural rigidity and to some extent, tensile strength. Various weave patterns and associated yarn configurations are illustrated in Fig. 10.9.

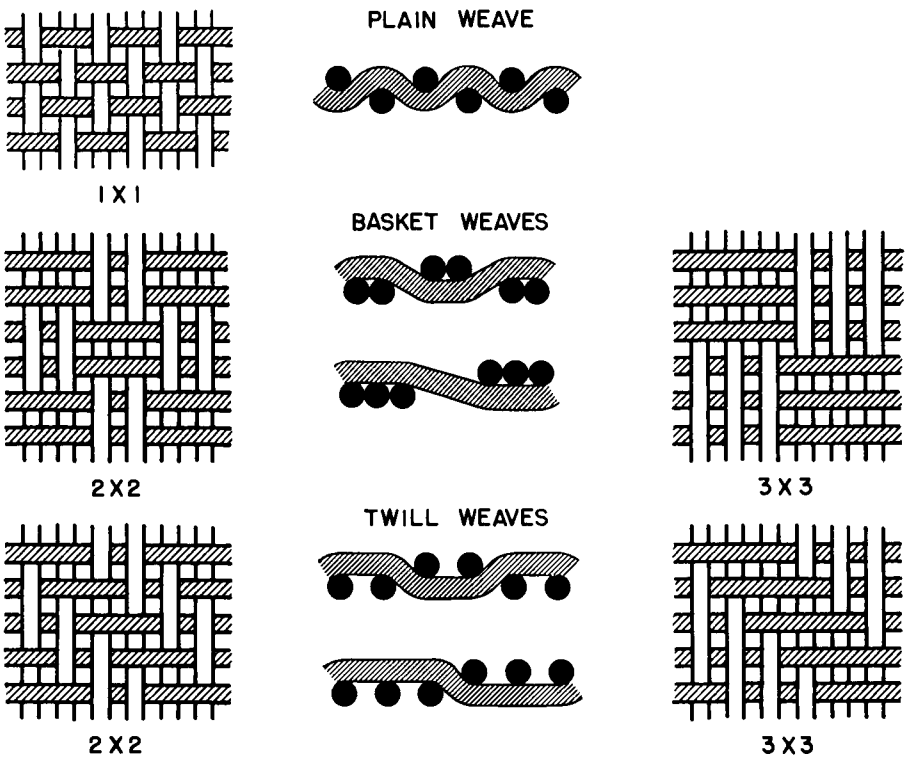

Fig. 10.9 Fabric weave patterns.

For fabrics of the same count, the plain weave, or 1 × 1 construction, will generally elongate more than the longer float weaves because of the greater length of yarn per unit length of fabric (yarn crimp) contained in their greater number of yarn interlacings per unit area. The larger number of interlacings may also restrict shearing in the plane and, as a result, lessen the tearing strength. However, the tearing strength of the plain weave could be improved by employing fewer, larger denier yarns to achieve the same nominal tensile strength. In such a structure, yarn crimp would increase as would the fabric thickness, elongation, and free open area while the shearing rigidity would decrease.

To illustrate some of these considerations in the design of a woven substrate for a skirt fabric, it is useful to consider a hypothetical fabric design. Suppose the requirements are a square, open fabric with a nominal

tensile strength of 1200 pli in both directions to be woven from highly twisted nylon yarns with a tenacity of 8 gpd. The first quantity to be determined is the total yarn denier per inch, De, needed to achieve the tensile strength specified. This is given by the expression:

$$\text{De (per inch width)} = \frac{453.6\ \text{(fabric strength in pli)}}{\text{(yarn tenacity in gpd)}}$$

$$= 68{,}040 \qquad (10.1)$$

For round yarns (high twist) the fractional free open area OA is related to the yarn diameter d_y and yarn count N (ends and picks per inch as follows: $OA = (1 - Nd_y)^2$.

For a round yarn, the diameter d_y can be calculated from the total yarn denier De and the count N by the following expression

$$d_y(\text{inch}) = \frac{1}{2.54}\left[\frac{(4/\pi)(De/N)}{(9 \times 10^5)\ \rho_f\ (\text{p.f.})}\right]^{1/2}$$

$$= 5.7 \times 10^{-4}\ [De/N]^{1/2} \qquad (10.2)$$

where ρ_f is the density of nylon fiber (1.14 g/cm^3) and p.f. is the volume packing factor of fiber in the yarn ($\cong$ 0.60). Therefore, substituting the above expression into the equation for free yarn area OA and rearranging terms gives the following relationship between yarn count N, free open area OA and total yarn denier De:

$$N = \frac{(1 - \sqrt{OA})^2}{(3.3 \times 10^{-7})\ De} \qquad (10.3)$$

For a free open area of 30, 9 ends and picks per inch would be needed with an individual yarn denier de of 7560 to achieve a tensile strength of 1200 pli. This number is less than the maximum number of ends that can be jammed into a plain weave and is, therefore, a weavable construction (see ref. 10 and Table 10.8).

Minimum thickness for this fabric would be achieved with balanced yarn crimp (same in both directions). For balanced crimp the fabric thickness would be approximately equal to two yarn diameters (if the yarns remain round in the fabric) or, 0.10 inch in the design under consideration. (In practice, even highly twisted yarns rarely remain round under coating pressures unless they are plied or cabled.)

Fabric weight W may be calculated from the number of ends and picks per inch N and individual yarn denier de with the inclusion of a factor for yarn crimp c. Thus,

$$W\ (\text{oz/yd}^2) = \left(\frac{2\ V\ 36^2 \times 2.54}{9 \times 10^5 \times 28.4}\right)(de)\ (N)\ (1 + c)$$

$$= (2.6 \times 10^{-4})\ (de)\ (N)\ (1 + c) \qquad (10.4)$$

For a plain-weave fabric woven from round yarns with 30% free open area, it can be shown that yarn crimp is approximately 13% and for a 3 × 3 basket or twill weave, about 4%, giving a fabric weight in the vicinity of 0.61-0.68 kg/m^2 (18-20 oz/yd^2). The choice of weave, whether plain or longer float, would be governed principally by the need to maximize tear strength (long float), maximize stability (plain-weave) or minimize weight (long float).

If 14 rather than 9 ends and picks per inch were specified for the above fabric, the individual yarn denier needed would be 4860, the round-yarn diameter would be 0.22 mm (0.04 in), fabric thickness for balanced crimp, 0.08 inch, free open area, 20%, crimp for a plain-weave, 18%, and the fabric weight, 0.64-0.71 kg/m^2 (19-21 oz/yd^2).

As seen above, the various fabric design parameters interact in complicated ways. These interrelationships often preclude exact calculation of the fabric properties although reasonable approximations can be made when simplifying assumptions are used.

10.3.3 Adhesive Tie-Coat

The adhesive or tie coat bonds the rubber coating to the woven fabric. The principal adhesive systems used in commercial rubber coated fabrics are resorcinol-formaldehyde-latex (RFL) or isocyanate systems. A comprehensive review was published of the influence of rubber composition, RFL formulation, type of curing process, and other variables on adhesion between rubber and tire cord (nylon, polyester, steel) (ref. 11). Also, the dependence of tire cord adhesion on elastomer properties was documented (ref. 12); higher values of adhesion occurred with elastomers that exhibited high elongation and high strength. With RFL adhesives, the ratio of the three principal ingredients can be changed to a considerable degree, the rubber latex can be varied among a number of different elastomers, and the reaction time and temperature can be varied. Each step and the order of each step is important in preparing an RFL adhesive to the degree of adhesion that can be obtained. Also the choice of latex will depend on the rubber coating to be bonded.

Isocyanate adhesives are less complex chemically than RFL adhesives. Isocyanate adhesives are a mix of rubber formulation, solvents, and an isocyanate. The adhesive level is dependent primarily on the isocyanate content but at low isocyanate contents (less than 1%) the rubber formulation can be a contributing factor. Rubber formulations usually are based on neoprene GNA rubber. Since isocyanates are sensitive to moisture, care must be exercised to exclude moisture from the system, to use fresh isocyanate, or to use a blocked isocyanate which will not react with moisture.

While the degree of coating adhesion is dependent on the constituents in an RFL system or the isocyanate content in an isocyanate based system, a large selectivity still exists for a particular adhesion system with various rubber

coatings. This is illustrated by the data in Table 10.4 for four rubber formulations and four commercial adhesive formulations bonded to the same woven fabric. These data also illustrate the ease with which neoprene can be bonded to nylon and the difficulty in bonding natural rubber to nylon.

Table 10.4. Coating adhesion dependent on rubber formulation and adhesive.

Adhesive system	Coating adhesion, kg/cm (lb/in) of width			
	Neoprene-1	Neoprene-2	EPDM	Natural Rubber
DuPont IPD-22 and D-5C (RFL)	9.7(54)	2.5(14)	-	-
Zamal Z-675A (RFL)	9.3(52)	9.0(50)	-	2.1(12)
Isocyanate 698B	35.8(200)	18.8(105)	0.5(3)	2.1(12)
Chemlok 402 (Isocyanate)	16.3(91)	10.9(61)	1.6(9)	1.1(6)

The chief problem with isocyanate based adhesives is to control the isocyanate level so that the modulus of the filaments is not changed appreciably after coating with the adhesive. Too much isocyanate increases the modulus of those filaments which are coated. Since the adhesive is applied to the surface of the yarns of the woven fabric, increasing the modulus of the outer filaments of the yarn bundle induces unequal load sharing among filaments in response to a tensile load; this results in sequential fracture of the filaments in the yarn and a loss in strength as shown by the data in Table 10.5. This table exhibits data from a 5000 pli fabric evaluated with two tie-coats each containing a different isocyanate quantity. Three of the four formulations reduced the tensile strength of the fabric by 20 to 40%. This was shown to be a modulus effect rather than a chemical reaction by treating individual filaments of nylon with the Chemlok tie-coat and measuring the tensile strength before and after treatment. No loss in strength was observed and in fact, the treated filaments were somewhat stronger after treatment (Table 10.6). Substantial processing experience is required to fabricate rubber coated fabric with both high coating adhesion and greater than 90% woven fabric strength efficiency.

Some isocyanate based adhesives react with moisture even after cure. Water environments are common for air cushion vehicles so resistance to moisture and high initial adhesion are both important properties. Water immersion test periods of one day to 6 months have been used to evaluate isocyanate based tie coats. Generally, a 7-day test at 65.6°C (150°F) was as effective as 4 months water immersion. The rate limiting step for reaction with water in rubber coated fabric is believed to be the time required to wick water through the fabric rather than reaction time of the isocyanate with water. After immersion in water, a rubber coated fabric exhibits approximately 50% of the total weight gain in 5 to 14 days; after 45 to 90 days no additional weight gain is

exhibited.

10.4 FABRICATION METHODS

The fabrication of skirt/seal components may require two distinct steps: (1) fabrication of the rubber coated fabric, and (2) fabrication of the skirt/seal component. Doublers (a second layer of material) are attached to skirt components in high stress attachment areas; the choice of the rubber coating usually determines whether the doubler is bonded after cure of the rubber coated fabric or is co-cured in a single operation where the rubber coated fabric and the skirt component are assembled in a single cure step. Components fabricated from neoprene or PVC-nitrile rubber coated fabrics are fabricated with the two step approach because these elastomers can be hot bonded to themselves with bond strengths that are as strong as the rubber. Components fabricated from natural rubber/butadiene or natural rubber/SBR are co-cured in a mold in a single curing operation because these elastomers do not form strong bonds to themselves once cured. Whichever method is employed to fabricate skirt components, the steps required to fabricate the rubber coated fabric are the same. These steps are woven fabric preparation, application of the tie

Table 10.5. Tensile strength of nylon woven fabric and tie-coat adhesive treated nylon woven fabric.

Sample no.	Tensile strength pli	Adhesive used	Comments
SEV 282	5,200	None	
SEV 276B	5,100	BAC 214	Isocyanate based adhesive
SEV 287	4,000	BAC 215	Twice as much isocyanate component as BAC 214
SEV 278B	4,000	Chemlok 402[1]	Isocyanate based adhesive diluted 1:1
SEV 279	3,100	Chemlok 402	Undiluted isocyanate based adhesive

[1]Adhesive Chemlok 402 is a product of the Hughson Chemical Company; Division of the Lord Manufacturing Company, Erie, Pennsylvania.

Table 10.6. Chemlok 402 adhesive is chemically compatible with nylon.

Direction of filament	Denier G per 9000 meters	Nylon filament breaking strength[1]	
		As received kg(lb)	After coating with adhesive[2], kg(lb)
Warp	885	7.4(16.4)	8.2(18.0)
Fill	3400	28.5(62.7)	32.4(71.4)

[1]Average of 4 or 5 values.

[2]Filaments were coated with Chemlok 402 adhesive and heated for seven minutes at 121.2°C (250°F).

coat, application of the elastomer and the curing and bonding the elastomer to the fabric in a final step.

10.4.1 Fabric Preparation

A size or lubricant may be coated on the yarns prior to weaving to reduce the amount of energy required to weave the fill yarns through the warp yarns. The sizing must be removed from the fabric prior to coating with the tie coat so as not to interfere with adhesion of the tie coat to the fabric. The sizing is washed free by passing the fabric through a soap solution. The fabric is then dried and heated under tension to some predetermined temperature of 121-177°C (250-350°F) in an oven in a continuous process to preshrink and stabilize the fabric thermally so that subsequent heating causes little further shrinkage.

10.4.2 Adhesive Application

The adhesive is in liquid form whether it is an RFL suspension in water or an isocyanate-rubber formulation suspended in a mixture of organic solvents. For small pieces of fabric, the adhesive is either painted on or applied with a paint roller to obtain an even layer over the surface. For automatic application to rolls of woven fabric, the fabric is drawn through continuously wetted rollers or through a bath of the adhesive and then through squeeze rollers to remove the excess. After application of the adhesive, the fabric is drawn through a large oven where the adhesive is heatset at a temperature up to 177°C (350°F) for 2 to 10 minutes to evaporate the solvent and adhere the adhesive to the fabric with a partial cure of the rubber elastomer. The selection of temperature and time at temperature is determined based on the elastomer used in the adhesive and the elastomer to which the adhesive is to bond. Natural rubber is not heated as high or as long as a neoprene rubber would be.

10.4.3 Elastomer Application

The elastomer coating formulation is mixed together in a Banbury mixer and dumped onto a calender where a succession of calendering steps is used to reduce the rubber coating to the desired thickness of 0.51 to 1.27 mm (0.020 to 0.050 in) and a width of typically 137 cm (54 in). In automatic processing, sheets of the uncured rubber and the adhesive coated fabric are passed through another calender to apply the rubber onto both sides of the fabric. From this calender, the coated fabric is drawn onto a rotocure drum where the rubber is heated under pressure and cured and the rubber is bonded to the fabric.

In a hand layup operation in a mold, a sheet of uncured rubber is cut to fit the mold, a section of adhesive coated fabric also cut to fit the mold is layed on top of the rubber sheet and then another rubber sheet is layed on top of the fabric. If doublers are to be attached, they are built up in the same manner on whichever side of the rubber coated fabric is desired. The mold is closed and placed in a press for cure.

10.4.4 Vulcanization

For rubber to develop its optimum properties, it must be cured under both temperature and pressure for 20 minutes to approximately one hour. Pressures range from 7 to 21.1 kg/cm^2 (100 to 300 lb/in^2) and temperature range from 138 to 177°C (280 to 350°F) depending on the elastomer. Neoprenes are cured at the higher temperature and natural rubber/butadiene or natural rubber/SBR are cured at the lower temperature of the range.

The exact time-temperature cure cycle is determined with a rheometer in which the change in viscosity of the rubber is plotted versus time at a particular temperature. A series of curves are developed at several different temperatures so the optimum time-temperature combination can be selected. Typically, the cure is selected based on the time required to obtain 90-95% of the maximum viscosity.

10.5 ELASTOMER/FORMULATION EFFECTS ON MECHANICAL PROPERTIES

Part of the work summarized to this point was from a U.S. Navy funded program in which strong, flexible rubber coated fabrics were developed for seals on large SES (1814-2721 tonnes) as part of a larger technology development program for such a large vehicle (refs. 1,8,13-16). This program explored natural rubber/cis-butadiene blend rubber formulations as well as investigating tie coat formulations and methodology for weaving nylon fabric in basket constructions with tensile strengths up to 893 kg/cm (5000 lb/in) of width. Several promising rubber coated fabrics were identified in testing (each coated with a natural rubber/butadiene blend) and one was fabricated into fingers and evaluated successfully on the SR-N4 cross channel ferry and the U.S. Army LACV-30 air cushion vehicle.

As a follow-on to this work the David W. Taylor Naval Research and Development Center (DWTNSRDC) funded additional programs on elastomer and fabric geometry development (refs. 4 and 17). Because of the extensive work completed on the earlier Navy program, the follow-on program concentrated on elastomers other than natural rubber/cis-butadiene blends. To identify promising candidates, the results from measured properties were compared to results from the natural rubber/cis-butadiene blend which had successful service evaluation. The best of the new elastomers were used subsequently to fabricate rubber coated fabric samples with the same fabric and tie coat and the results from testing these materials were compared to results from the rubber coated fabric material which had been evaluated successfully in service.

10.5.1 Elastomer/Formulation Screening and Characterization

Twenty formulations were developed and prepared by the customer service organizations or with the assistance of the customer service organizations which specialized in each of ten gum rubber polymers or polymer blends.

Generally, the variables in the gum rubber formulations were the type and amount of carbon black, the substitution of some silica for carbon black, the type and amount of plasticizer, the type of antiozonant/antioxidant, the use of polymer blends, and the type of cure system. Molybdenum disulfide was added to two polymer systems (propylene oxide and chlorinated polyethylene) to evaluate the effect of this additive on crack growth and flexural fatigue life (ref. 16).

In addition, castable liquid polyurethanes were prepared by reacting high molecular weight hydroxy terminated polyethers, polycarbonates or polybutadienes with one of several diisocyanates; the prepolymers resulting from these reactions were reacted subsequently with either a low molecular weight hydroxy terminated hydrocarbon or a diamine to gel at room temperature. In several instances, a reactive silane also was added to the polymer.

Molded specimens were evaluated for flexural properties, as initial screening tests. Some formulations exhibited superior crack growth resistance and flexural fatigue resistance compared to the control formulation. Two polymer types, propylene oxide and butyl rubber, did not yield formulations which were as good as the control in either property. The use of molybdenum disulfide was detrimental to crack growth and flexural fatigue life of propylene oxide polymer and yielded only slight improvement with chlorinated polyethylene polymer contrary to published results for a natural rubber/SBR/butadiene blend; it may be that the concentration used was not optimum for the particular polymers.

The polyurethane results were compared to a polyurethane control which had been evaluated as side fingers on the U.S. Army LACV-30. All polyurethane formulations had poor crack growth resistance but four had comparable or better fatigue resistance (including the control) than the gum rubber control. Consistent with this, the limited operational life data suggested that crack resistance could be a problem with polyurethanes. Six gum rubber formulations and four castable liquid polyurethane formulations were selected for characterization tests of hardness, tensile properties, tear properties, pico abrasion index, coating adhesion, hysteresis and resilience.

The various properties for the polymers including the control formulation exhibited a broad combination of properties. Examples are as follows:

(1) The tear strength and elongation at tear of the polymer formulations were not as good as the control formulation of 490 pounds and 610% although two gum rubber formulations had elongations at tear in excess of 500%.

(2) One gum rubber and two polyurethanes had abrasion indices greater than the control formulation.

(3) One gum rubber formulation had a coating adhesion level close to the value obtained for the control using the same woven nylon fabric and tie coat.

(4) Hysteresis results were particularly poor for one gum rubber and two polyurethanes.

In comparing the results, no formulation was better than the control.

10.5.2 Elastomer Formulation/Fabric Characterization

The polymers/formulations which were selected for evaluation as rubber coated fabrics were a chlorinated polyethylene, a SB block copolymer/natural blend, a bromobutyl/PDM/natural blend, and two polyurethanes. A bromobutyl/EPOM/natural blend was selected to include representative material from both ends of the results so that the usefulness of the polymer characterization tests could be judged.

The gum rubber coated fabrics were fabricated with the same procedures, nylon fabric, and tie coat except for variations in the polymer cure temperatures.

The polyurethane polymers were applied using liquid casting techniques. Each side of the fabric was coated separately; the polyurethane gelled and air cured overnight at room temperature and then was post cured.

The coated fabrics were evaluated for tensile and tear strength, ultimate elongation, tensile fatigue at constant jaw displacement and water wicking. The tensile strength, ultimate elongation and tensile fatigue were approximately the same for all the coated fabric materials indicating that the fabric reinforcement dominated these properties.

Significant variations in tear strength were measured. The control and the bromobutyl/EPOM/natural blend exhibited lower tear strengths at -1°C (30°F) than at room temperature. The effect is more pronounced when it is remembered that the tensile strength of nylon increases 15 to 20% as the temperature is decreased from 49°C (120°F) to -1°C (30°F).

Examination of the test specimens verified that the failure mode of the fabric changed for the tear specimens between 49°C (120°F) and -1°C (30°F). At the lower temperature, the modulus of the coating increased sufficiently to alter the yarn behavior in the coated fabric as discussed in Sections 10.3.1 and 10.3.3. This is caused by the coating and not the tie coat because a similar effect was not observed for the SB block copolymer/nataural blend. The tear strength results for the SB block copolymer/natural rubber blend was lower at 49°C (120°F) than at 24°C (75°F) or -1°C (30°F).

Differences also were observed in water wicking results as a consequence of the degree of penetration of the coating or tie coat into the fabric. The liquid coat polyurethanes penetrated into the fabric prior to gellation and very little wicking occurred as a result.

10.5.3 Reinforcement Alternatives to Woven Fabrics

Two approaches were evaluated as reinforcement alternatives to woven fabrics: 1) a reinforcing filler added to castable polyurethanes and 2) a knit nonwoven structure infiltrated with castable polyurethane. Polyurethane formulations were modified by mixing the neat resin with carbon black and fumed

silica. These additions had a very detrimental effect on flexural fatigue and crack growth resistance which was decreased by a factor of 30 to 1000 and a factor of 5 to 30 respectively; no other mechanical properties were measured.

Polyester and nylon knits were examined that were prepared by Rochelle knitting (which featured a lock stitch to prevent unraveling). A polyester of 0.498 kg/m^2 (14.7 oz/yd^2) was selected because it had the best strength-to-weight ratio of the specimens.

The mechanical properties were evaluated for the knit reinforcement after infiltration with polyurethane. The polyurethane coated knit had approximately a factor of 3 lower tensile strength and a factor of 4 lower tear strength than the woven fabric similar to the results for the uncoated reinforcement. The elongation of the knit was approximately three times greater than the woven fabric reinforced material. A knit reinforcement structure does not yield as efficient a reinforcement as a woven fabric on a strength-to-weight basis.

10.5.4 Conclusions

Elastomeric polymers were formulated which, at a flexural rate of 5 cycles per second, had crack growth and fatigue resistance better than a control formulation of natural rubber/cis-butadiene blend; this latter blend was the coating on a rubber coated fabric which exhibited improved seal life on an air cushion vehicle. As coatings on coated fabrics, little difference was found between bromobutyl/natural rubber/EPDM blend, SB block copolymer/natural rubber blend, chlorinated polyethylene, and the natural rubber/cis-butadiene blend coated fabric laminates because the fabric dominated the properties which were evaluated. On the other hand, unreinforced cast polyurethanes exhibited better flex fatigue resistance than as a coating on a woven fabric reinforcement.

Two nylon coated fabric laminates (nataural rubber/cis-butadiene blend and bromobutyl/EPDM/natural rubber blend) exhibited marked reductions in tear strength at -1°C (30°F) compared to tear strength at room temperature. The reduction in tear strength was a direct result of the lower strain to failure at low temperature of the yarns in the structure which reduced the number of yarn bundles involved in load-sharing at the apex of the tear.

Results from tensile fatigue evaluation at 5 cycles per second indicated that the fabric controlled the cyclic life for the polymer coated fabrics which were evaluated.

Cast liquid polyurethanes reinforced with dispersions of carbon black or fumed silica, and cast polyurethanes infiltrated into mat and knit reinforcements exhibited inferior flexure and tensile properties compared to elastomers reinforced with woven fabric.

10.6 FABRIC STRUCTURE EFFECTS ON FLEX-FATIGUE BEHAVIOR

Flex-cracking and delamination of the rubber layers of skirt fabrics are well-documented modes of failure for these materials. On the premise that this

type of failure is engendered by the high-speed, repetitive flexing that the tips of the skirt panels see during marine service, a study was undertaken to evaluate the effect of the structure of the woven fabric substrate on the flex-fatigue behavior of skirt materials (ref. 17). This investigation was designed to complement the evaluation of elastomer formulations described in Section 10.5.

10.6.1 Fabric Construction

In the fabric design study, one elastomer type was specified as the coating material for a variety of experimental nylon woven fabric constructions, all of approximately the same weight. The following factors were kept constant for all fabrics prepared:

(a) fiber material: high tenacity nylon 6,6;

(b) fabric tensile strength: 214.5 kg/cm (1200 lb/in) of width in the two principal directions;

(c) elastomeric coating:
- composition: natural rubber/cis-butadiene blend
- amount: 0.030 in calendered sheet applied to each side
- method of application: platen press, 300°F, 30 min, 440 psi.

The six principal construction features that were varied were fiber linear density (denier), yarn linear density (denier), yarn twist, fabric float length, weave pattern and yarn crimp level. The levels of these variables that were employed in factorial subsets of the experimental design are described in Table 10.7.

The yarn deniers chosen for the experiment were determined by the fabric design criterion of 214.5 kg per lineal cm (1200 pounds per lineal inch). The number of fabric ends per inch necessary to achieve this level of tensile strength with 8 gpd yarns and various yarn deniers is compared in Table 10.8 with the maximum number of ends weavable in a square, plain-woven fabric (ref. 10). As seen from the table, only yarn deniers above 5040 are suitable for such constructions. Fabrics were constructed from nominally 5040 and 10,080 denier yarns only since fabric woven from 15,000 denier yarns at the required density would be too sleazy and difficult to handle. Actual yarn tenacities ranged from 6 gpd to 9 gpd for the various fiber types employed.

Fabrics were either plain woven or 3 × 3 twill or basket weaves. Emphasis was placed on the twill construction with only a few basket weaves produced. An attempt was made to control yarn crimp during fabric production and subsequent finishing by the application of tension in the warp direction in order to maintain most of the crimp in the filling direction yarns.

Six fabric warps were produced as described in Table 10.9. From these six warps more than 30 different fabric structures were woven in approximately 10 yard lengths by varying the weave pattern as the fabrics were woven out. The

Table 10.7. Fabric construction variables.

FIBER:	Denier	Type	
	6	DuPont 728 (7140)	
	6,12	DuPont 704	
	2,6	Monsanto CO2	
YARN:	Denier	Twist	
	5,040	Low - 0.8 tpi (5°) High - 4.1 tpi (25°)	
	10,080	Low - 0.5 tpi (5°) High - 3.1 tpi (25°)	
FABRIC:	Float Length	Weave Pattern	Yarn Crimp
	1×1	Twill	Low
	3×3	Basket	High

Table 10.8. Determination of yarn denier from fabric strength criterion of 214.5 kg per lineal cm (1,200 pounds per lineal inch).

	Number of fabric ends per inch per yarn denier of: (multiples of 840)					
Criterion	2,520	3,360	5,040	7,560	10,080	15,120
To achieve 214.5 kg/cm (1,200 lb/in) (at 8 gpd)	27	20	14	9	7	5
Maximum weavable in square plain weave (ref. 10)	20	18	14	12	10	8

Table 10.9. Experimental fabric warp construction.

Warp no.	Fiber denier	Yarn denier	Ends/inch	Warp Yarn Twist Level
I	6	5,050	14	Low
III	6	10,080	7	Low
IV	12	5,040	14	High
V	12	10,080	7	Low
VI	2	5,040	14	Low
VII	2	10,080	7	High

various fabrics were produced in general by weaving with the same type of filling yarn as warp yarn except that the twist of the filling yarn was varied. The detailed construction of each of the fabrics produced and evaluated for flex behavior is given in Table 10.10.

The effect of yarn twist changes in one or both directions of the fabric on fabric openness is illustrated in Fig. 10.10 and 10.11 for the plain and 3 × 3 twill weaves, respectively. Obviously, consolidation of the yarn structure by insertion of high levels of twist results in a much more open fabric structure with greater opportunity for rubber strike-through during subsequent coating.

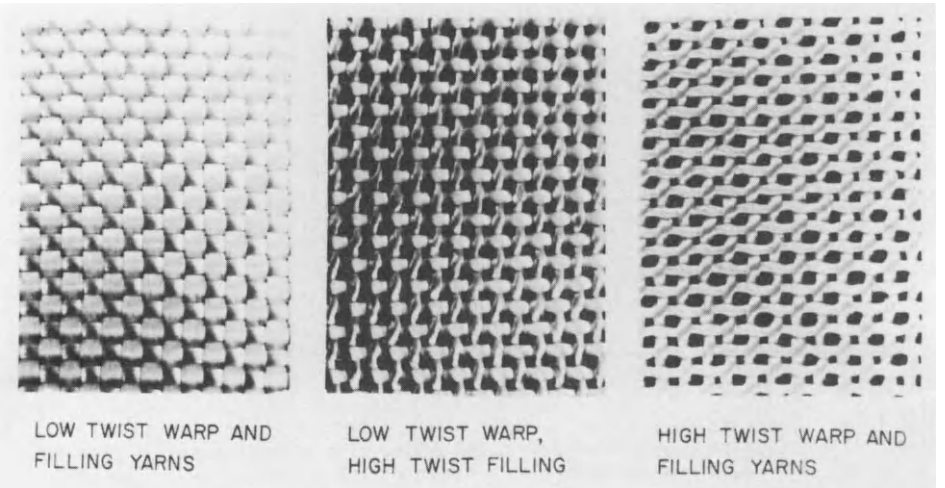

Fig. 10.10 Plain-weave fabrics from 10,080 denier yarn with different twist levels.

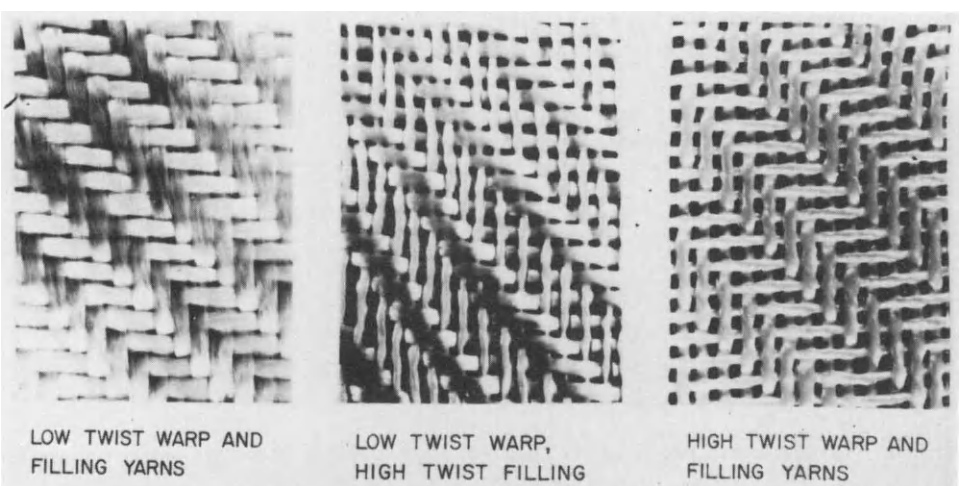

Fig. 10.11 3 × 3 Twill weave fabrics from 10,080 denier yarn with different twist levels.

10.6.2 Properties of Fabric/Elastomer Composites

The various woven fabrics prepared for the experimental study were finished and coated as follows:

(a) beam scoured to remove spinning oils and lubricants:

Table 10.10. Details of experimental fabric constructions.

Warp no.	Warp yarn twist level	Fiber Denier	Warp and Filling Construction: Nominal yarn denier	Warp and Filling Construction: Yarn count (yarns/inch)	Weave pattern	Filling yarn twist level
I	low	6 (type 728)	5,040	14×14	plain	low high
					3×3 twill	low high
					3×3 basket	high
In addition, Warp I contained the following four fabric constructions designed to provide a basis of comparison between yarn types:						
Filling Direction Fiber Denier and type		6 (type 704)	5,040	14×14	plain	low
		12 (type 704)	5,040	14×14	plain	low
		2 (type CO2)	5,040	14×14	plain	low
		6 (type CO2)	5,040	14×14	plain	low
III	low	6 (type 714)	10,080	7×7	plain	low high
					3×3 twill	low high
					3×3 basket	low high
IV	high	12 (type 704)	5,040	14×14	plain	low high
					3×3 twill	low high
V	low	12 (type 704)	10,080	7×7	plain	low high
					3×3 twill	low high
					3×3 basket	low
VI	low	2 (type CO2)	5,040	14×14	plain	low high
					3×3 twill	low high
VII	high	2 (type CO2)	10,080	7×7	plain	low
					3×3 twill	low high

160°F solution of 0.25% TSPP and 1% Triton X-100;

(b) heat-set to stabilize the fabric structure and prevent shrinkage during subsequent processing:
350°F circulating hot air under sufficient warp tension to maintain length in warp direction, no filling tension;

(c) adhesive application:
spray coated with neoprene-based adhesive tie-coat with PAPI isocyanate curing agent, dried, sealed against moisture;

(d) rubber lamination:
one, 0.76 cm (0.30 in) thick layer of natural rubber/cis-butadiene blend front and back, cured in hot-press at 149°C (300°F), 3.033 kPa (440 psi) for 30 minutes.

The properties of the resulting rubber coated fabrics are summarized in Table 10.11a. Measurements of tensile and tearing strength were made on 10,080 denier fabrics only; these individual properties are listed in Table 10.11b. Those fabrics with fewer yarn intersections per unit area, namely, the 3×3 twills and 3×3 basket weaves, generally exhibited the higher tearing strengths. (Tear strengths of the 5,040 denier fabrics would be expected to be less but tensile strengths should be slightly higher.)

Table 10.11a Composite fabric properties.

Weight:	
Substrate	0.68 to 0.91 kg/m^2 (20 to 27 oz/yd^2)
Coated fabric	2.37 to 2.71 kg/m^2 (70 to 80 oz/yd^2)
Thickness:	
Substrate	0.13 to 0.23 cm (0.05 to 0.09 in)
Coated fabric	0.23 to 0.28 cm (0.09 to 0.11 in)
Strength:	
Tensile	161.1 to 232.7 kg/cm (900 to 1300 lb/in)
Tear	227 to 454 kg (500 to 1000 lb)
Flexural rigidity: (at average curvature radius of 0.64 cm (0.25 in)	0.035 to 0.093 kg-cm^2/cm (0.03 to 0.08 lb-in^2/in)

Cross-sections of many of the coated fabrics produced illustrated the level of success in attaining straight warp yarns and highly crimped filling yarns. In the plain-woven, 5,040 denier fabrics, yarn crimp was nearly balanced. Among the 10,080 denier plain-woven constructions, a greater difference in crimp level between warp and filling yarns was observed. In the longer float fabrics, the warp tended also to lie straighter than the filling. The high tensions applied in the warp direction were insufficient in some cases to overcome the high transverse pressures applied by the press during rubber coating.

The fabric cross-sections also illustrated another important difference among the finished fabrics, namely, the variation in thickness of the rubber

Table 10.11b. Properties of experimental coated fabrics (10,080 denier only).

Item	Weave pattern	Yarn twist warp	Yarn twist fill	Weight Kg/m^2(oz/yd^2)	Thickness cm (in)
	Warp III, Type 714 nylon, 6 dpf:				
(a)	plain	low	low	2.71(80)	0.26 (0.103)
		low	high	2.78(82)	0.27 (0.108)
(b)	3×3 twill	low	low	2.51(74)	0.25 (0.098)
		low	high	2.74(81)	0.27 (0.106)
(c)	3×3 basket	low	high	2.57(76)	0.27 (0.106)
	Warp V, Type 704 nylon, 12 dpf:				
(d)	plain	low	low	2.34(69)	0.25 (0.099)
		low	high	2.54(75)	0.26 (0.102)
(e)	3×3 twill	low	low	2.64(78)	0.27 (0.105)
		low	high	2.68(79)	0.26 (0.101)

	Tensile strength kg/cm (lb/in)		Bird-wing tear strength kg (lb)		Flexural rigidity kg-cm^2/cm (lb-in^2/in)	
	Warp	Fill	Warp	Fill	Warp	Fill
(a)	226 (1260)	197(1070)	286(630)	268(590)	0.084(0.073)	0.082(0.071)
	204 (1140)	186(1040)	275(605)	322(710)	0.082(0.071)	0.069(0.060)
(b)	227 (1270)	236(1320)	427(940)	440(970)	0.065(0.056)	0.048(0.042)
	213 (1190)	190(1060)	361(795)	422(930)	0.076(0.066)	0.071(0.062)
(c)	211 (1180)	168(940)	415(915)	522(1150)	0.054(0.047)	0.050(0.043)
(d)	224 (1250)	208(1160)	241(530)	241(530)	0.061(0.053)	0.048(0.042)
	220 (1230)	202(1130)	238(525)	325(715)	0.055(0.048)	0.065(0.056)
(e)	238 (1330)	183(1020)	481(1060)	411(905)	0.061(0.043)	0.038(0.033)
	209 (1170)	161(900)	284(625)	381(840)	0.046(0.040)	0.035(0.030)

covering over the fabric knuckles. In fabrics woven from low denier, low twist yarns, the minimum thickness of the covering layer was much greater than in the high denier, high twist fabrics where the bulk of the rubber sheet was pressed into the fabric pores.

The peel strengths of those experimental fabrics with little or no open area to permit bridging of the rubber through the woven matrix was generally low (3.6-4.5 kg/cm (20-25 lb/in)). However, some of the more open weaves reached acceptable levels of adhesive bonding (7.2 kg/cm (40 lb/in)). Some of the experimental fabrics were also coated by Goodyear in order to evaluate the bonding achieved with their commercial process and proprietary adhesive. The results, given in Table 10.12, show no consistent or dramatic increase in peel strength with the Goodyear process.

10.6.3 Flex Tests

To determine the relative performance of the various experimental fabric constructions during flexing, a flex tester was designed and built from a four-

Table 10.12. Comparison of peel strengths of experimental fabrics coated by Goodyear and Albany International (filling direction).

Fabric Construction	Peel Strength kg/cm (lb/in) width	
	Coated by Goodyear	Coated by AI
Warp V: (10,080 denier)		
plain weave		
low twist filling	4.8 (27)	6.3 (35)
high twist filling	6.8 (38)	4.1 (23)
3×3 twill		
low twist filling	5.9 (33)	4.7,8.6 (26,48)
Warp VI: (5,040 denier)		
plain weave		
low twist filling	5.7 (32)	4.5 (25)
Warp VII: (10,080 denier)		
plain weave		
high twist filling	6.4 (36)	7.5 (42)

cylinder automobile engine. The tester imposes a high-speed, high-curvature rolling bend on fabric strips inserted in special fixtures attached to the pistons. The high-speed reciprocating motion is driven by an electric motor. Each of the four pistons is equipped to hold four separate test specimens, each attached at one end to a stationary center post and at the other to a movable platform connected to the piston. The specimens are subjected to the rolling high-curvature deformation illustrated in Figure 10.12. The engine block is water-cooled to keep the temperature uniform in all the specimens. The essence of the imposed deformation is that each element in the 2.4-inch central portion of the strip, which measures 5.0 inches in total length, undergoes a high-frequency cycle of curvature from no curvature to maximum curvature and back to no curvature in one cycle of reciprocating motion. Minimum radius of curvature, i.e., maximum curvature, undergone by each element is given by the expression (refs. 18,19):

$$r = 2.54(D-t)/2.4 \cong 0.43 \text{ cm}(0.17 \text{ in}) \tag{10.5}$$

where D, the distance between parallel supports, was set at 1.27 cm (0.5 in) and t is the fabric thickness. Mean radius of curvature for the 1.27 cm (0.5 in) spacing is given by:

$$r = 2.54(D-t)/1.4 \cong 0.71 \text{ cm}(0.28 \text{ in}). \tag{10.6}$$

With each of the 16 positions on the flex-tester filled with a standard Goodyear fabric XA28A504-2A, described in Table 10.13, the number of cycles to first failure was documented by visual inspection of each specimen. The results, listed in Table 10.14, illustrate the close agreement between the average value of the group of four specimens at each test station with the overall average for all sixteen specimens. They also show the wide range of values obtained, leading to a coefficient of variation in the test data of

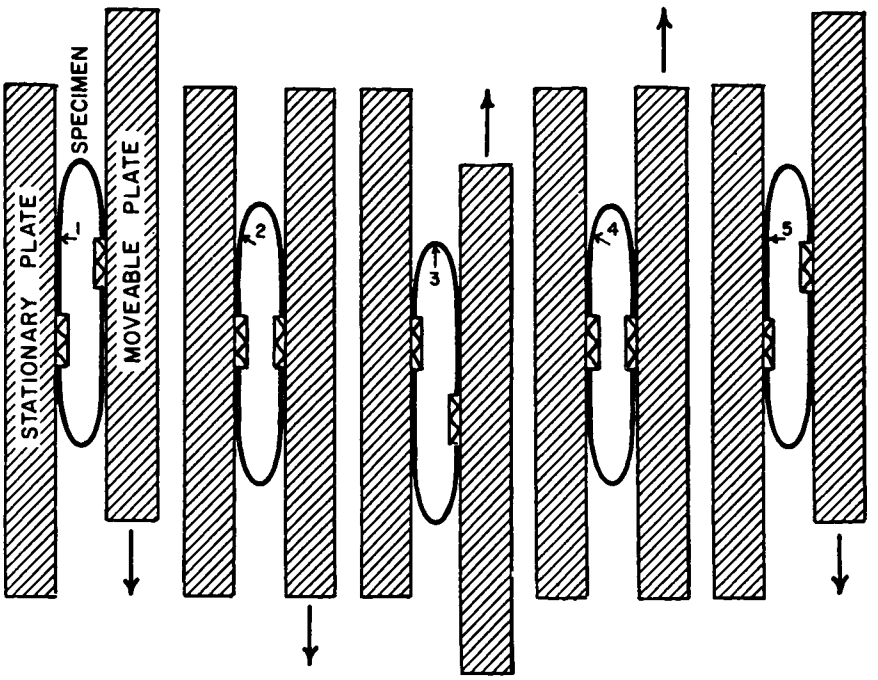

Fig. 10.12 Cycle of curvature for specimen in flex tester: Element at arrow, positions 1 and 5 - no curvature; positions 2 and 4 - intermediate curvature; position 3 - maximum curvature.

approximately 50%. Such large variations are common in fatigue data.

Table 10.13. Construction of Goodyear fabric XA28A504-2A.

Fabric substrate construction:	6 dpf nylon 4/2/840/12S/7Z 10×10 plain weave 0.91 kg/m^2 (27 oz/yd^2)
Fabric weight:	2.79 kg/m^2 (82 oz/yd^2)
Fabric thickness:	0.28 cm (0.110 in)
Fabric tensile strength:	214.8 kg/cm (1200 lb/in) nominal

On the basis of these measurements, the average number of cycles to the first appearance of a centrally located flex crack among four test specimens mounted at a single test station was taken as the indicator of the fabric flex fatigue. Cycling was continued after the first instance of flex cracking until more extensive damage was sustained, generally to 10 or 20 million cycles. Complete delamination of the rubber layers in the flexed region was eventually achieved when flexing was allowed to continue long enough.

Table 10.14. Number of cycles to first evidence of flex cracking in Goodyear fabric XA28A504-2A.

Test station	Initial flex cracking (millions of cycles)	Average (millions of cycles)
1	3.9, 1.5, 1.9, 2.7	2.5
2	2.2, 5.2, 1.5, 1.5	2.6
3	1.9, 2.4, 2.2, 3.9	2.6
4	0.2, 3.9, 1.7, 2.4	2.1
	Overall Mean	2.4
	Range	0.2 to 5.2
	Coefficient of Variation	50%

10.6.4 Flex–fatigue results

The average lifetime of the experimental fabrics fatigued to the occurrence of a flex crack (other than an edge crack) on the flex-cycling apparatus described in the previous section ranged from a low of 140,000 cycles for a 3×3 twill construction with high-twist, 10,080 denier yarns to a high of 21.7 million cycles for a plain-weave construction from low-twist, 5,040 denier yarns. Initial cracking almost always occurred on the outside, or tension side of the flexed specimen. The extent of ultimate damage for these two fabric types ranged from extensive after 300,000 cycles to not severe after about 30 million cycles.

The large effect of fabric construction on the flex-fatigue behavior of the rubber coated fabrics was well illustrated by the test results for twill weaves. Flex lifetimes spanned over two orders of magnitude for materials differing only in fabric substrate construction. The task of sorting out those differences in fabric construction that result in significant differences in the ability of the composite to withstand high-curvature, high-frequency flexing has required use of the statistical technique of analysis of variance, or factorial analysis (refs. 20–22). Limitations on the experimental design arising from the manner of varying fabric weave pattern and filling yarn twist level within a few specifically-constructed warps, combined with contractual restrictions, precluded attaining either a full or a balanced fractional design involving all of the principal fabric construction variables. Although the significance of the principal construction variables and their interactions could not be examined directly by an analysis of variance of the entire set of data, smaller full-factorial blocks involving only three or four of the variables in various combinations were analyzed separately. In addition, the effects of fiber type, fiber denier for the same fiber type, and weave pattern (twill or basket) were examined by direct comparison of the flex lifetime of structures between which only these variables changed level.

(i) Effect of fiber denier and type. Sections of the low-twist Warp I were plain-woven with low-twist filling yarns of the different fiber types in

those fiber deniers available. Fiber type at the same fiber denier (6 dpf) was determined to have an insignificant effect on flex lifetime. Similarly, in this group of fabrics the average flex lifetime was unaffected by fiber denier, as shown in Table 10.15.

Table 10.15. Effect of fiber denier for fibers of same type.

	Average flex lifetime (million cycles)			
	Type CO2 (Monsanto)		Type 704 (DuPont)	
	2 dpf	6 dpf	6 dpf	12 dpf
Warp I, 5,040 denier, low twist, plain weave, low crimp (filling direction only)	17	19	22	26

(ii) Effect of weave pattern. Flex lifetimes are compared in Table 10.16 for three distinct fabric categories woven in both the 3×3 twill and the 3×3 basket weave patterns. The differences between the three pairs of results are not significant at the 90% confidence level on the basis of the Student's t-test. The twills are preferred, however, for their greater stability and ease of handling before adhesive and rubber coating.

Table 10.16. Effect of weave pattern.

	Flex lifetime (million cycles)	
Fabric construction	3×3 twill	3×3 basket
Warp I, 6 dpf, 5,040 denier, high twist yarn, low crimp	3.4	2.8
Warp V, 12 dpf, 10,080 denier, low twist yarn, low crimp	1.6	1.3
Warp III, 6 dpf, 20,080 denier, high twist yarn, low crimp	0.4	0.3

(iii) Analysis of variance. Three full-factorial subsets of the body of flex data were analyzed statistically for the significance of main and interactive effects of the fabric construction variables. The subsets were formed by comparing: a) filling direction (low crimp) data only; b) data for plain weave (1×1) only; and c) data for plain weave only but with no distinction between different fiber deniers. Yarn crimp has a confounding effect on the results of the analysis of variance, as judged from the significance of its interaction with yarn denier, not only because it was not precisely controlled during fabric manufacture, but also because it was included in the experimental design at relative rather than absolute levels (low, high). The absolute level of yarn crimp, i.e., angulation of the yarns with the plane of the fabric, is, of course, dependent on the diameter of the yarns that are crossed. However, in

spite of this difficulty, the following factors emerge from the analysis of variance of the three data subsets as significantly (99%) affecting the flex-lifetimes of the experimental fabrics:

(a) yarn denier - lower denier preferred

(b) float length - plain weave (1×1) preferred

(c) yarn crimp - low level preferred.

(iv) Effect of fabric substrate thickness. The relationship between the thickness of the fabric substrate as it lies in the coated fabric and flex lifetime is graphed in Fig. 10.13. Flex lifetime is seen to be significantly higher among those fabrics with a lower substrate thickness. Examination of failed specimens that were flexed until extensive damage had been done showed that the rubber tends to crack in the thin regions covering the knuckles, or floats, of the yarns running in the opposite direction to those being flexed. As a result, the pattern of flex cracks takes on the image of the underlying

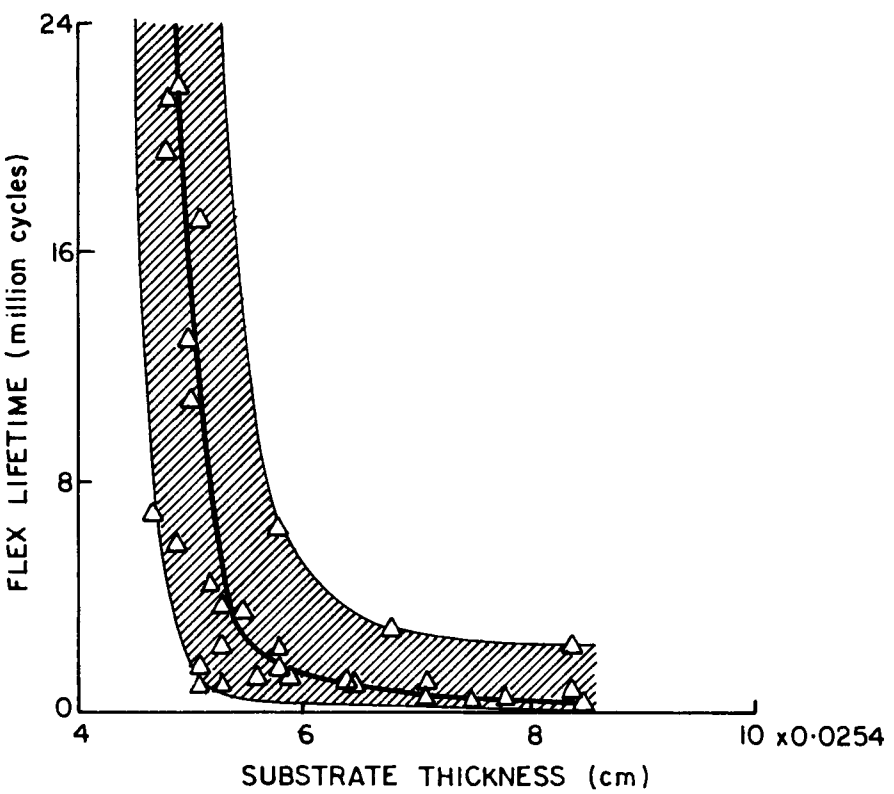

Fig. 10.13 Variation of the flex lifetime of rubber coated fabrics with substrate thickness.

fabric weave pattern in the damaged specimens, as illustrated in Fig. 10.14.

The contours of the rubber layers of several fabric constructions representing a wide range of flex lifetimes are presented in Fig. 10.15; these profiles were prepared from photographs of fabric cross-sections. Although the amount of rubber applied to each fabric was the same and the total thickness of each fabric after coating was about the same, the thickness of the rubber layer varies locally within the structure according to the pattern of the underlying weave. Obviously, from Fig. 10.15, the rubber layer is thinner over the fabric knuckles and thicker between yarn crossovers. Lower yarn denier, lower yarn twist, and lower yarn crimp all result in lower knuckle height and lower knuckle height results in a more uniformly thick rubber layer. In general, those fabrics with a more uniformly thick rubber layer were the most resistant

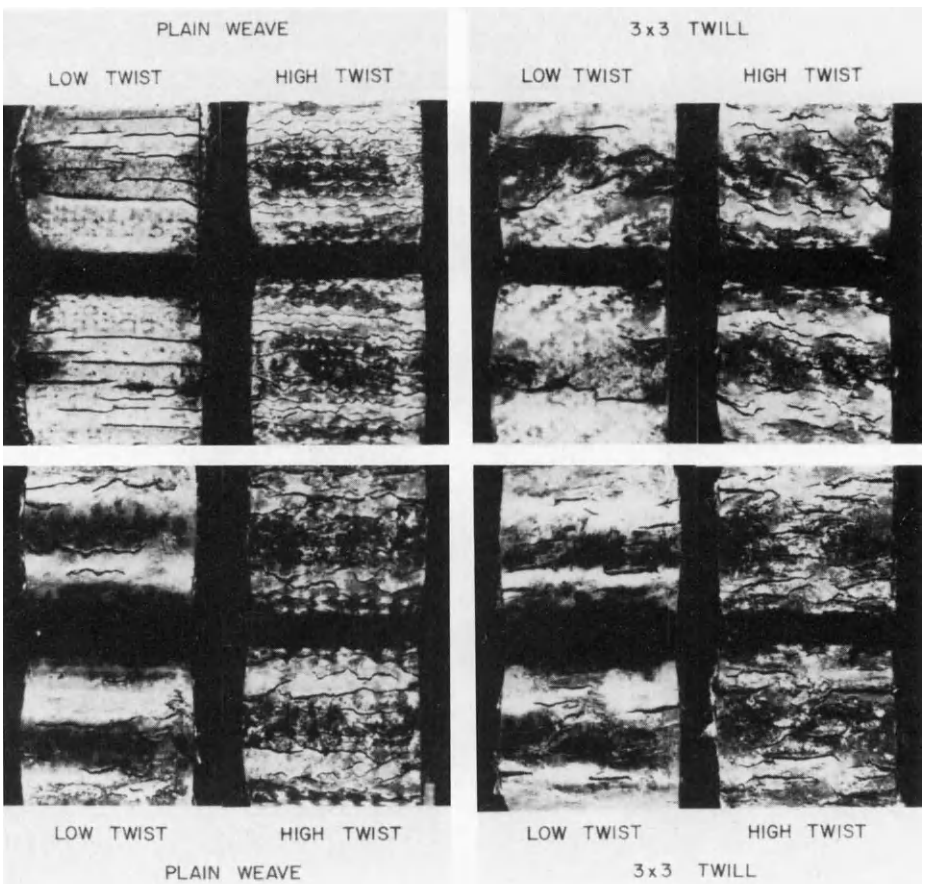

Fig. 10.14 Flex crack patterns in rubber coated fabrics with different substrate constructions.

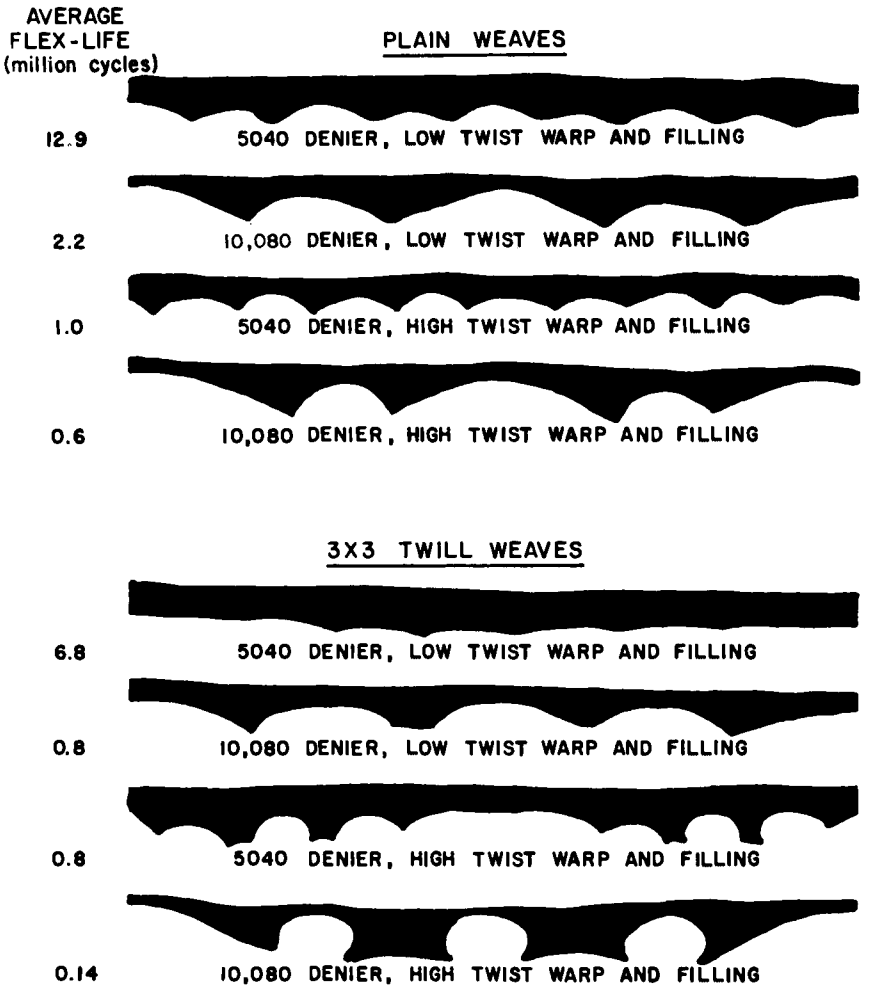

Fig. 10.15 Profiles of the rubber layer from several rubber coated fabrics.

to flex-cracking. It is interesting to speculate that the large effect of some of the fabric construction variables on flex lifetime springs ultimately from their geometric effect on rubber distribution with the coated structure.

(v) Effect of adhesive bonding. No correlation was found between lifetime in flex and the level of adhesive bonding either among experimental fabrics or those coated by Goodyear.

(vi) Effect of flexural rigidity. The ability to withstand many cycles of high-curvature flexing is also unrelated to the bending stiffness of the coated fabric construction.

10.6.5 Conclusions

Among a group of experimental skirt fabrics designed to be identical except for the structure of the fabric substrate - same fabric weight and strength, same type and amount of elastomer and adhesive system applied, same manufacturing procedure - the lifetime during high-speed, high-curvature flexing in the laboratory ranged over two orders of magnitude. Of the construction variables studied, yarn denier, yarn crimp and float length of the weave were found to significantly affect the resistance to flex-fatigue. Fabrics with lower yarn denier, lower yarn crimp and shorter float lengths (plain weaves) survived the longest. Since flex-cracking of the elastomer layer occurs initially in its thinnest regions, the effect of fabric structure may be an indirect one related principally to the effect of the underlying substrate geometry on local thickness variations in the rubber layer. Fabrics plain-woven from low denier yarns with little crimp are the most uniform in cross-sectional thickness as is the rubber layer applied to them. Unfortunately, however, such fabrics offer no opportunity for rubber strike-through during coating and high bond strengths between elastomer and fabric layers are less likely to be developed with them.

10.7 EVALUATION OF IMPACT RESISTANCE

A drum impact tester designed to simulate in-service damage modes of skirt materials at an accelerated rate was developed at DWTNSRDC. It was intended to replace flagellation testers which for a given water or air velocity yielded results dependent on the weight of the rubber coated skirt fabric. In the drum impact tester, specimens of rubber coated fabric bent into the shape of a U on its side and attached along the top edge are impacted along the bottom edge with a nylon blade at 70 knots and 3 impacts per second. The bottom edge of the sample remains free to deform on impact and fold back on itself. The impacted surface is cooled by a continuous spray of water. The impact tester was used to evaluate materials which had undergone or were undergoing craft trials together with the selected materials from the polymer formulation and fabric design studies. The impact test results which were obtained correlated fairly well with the craft trials but did not correlate as well with the results from the laboratory evaluations.

For experimental materials which were selected from the fabric design study, results from the impact test were the opposite of results from the rolling-fold flex test apparatus described in Section 10.6. The impact test caused less damage in plain and basket weaves with high twist yarn than in plain weave materials with low twist yarns, whereas results from the flex test were just the opposite. To perform well in the impact test, a minimum adhesive bond strength between the elastomer layers and the fabric substrate of 7.2 to 10 kg/cm (40 to 50 lb/in) width seems to be required. Those fabrics that performed reasonably well (survival time greater than 1.5 hrs) were generally

the more open fabric constructions containing at least one set of highly twisted yearns. Such constructions permit bridging of the rubber through the woven substrate and, as a result, higher bond strengths are developed. Although the more open fabric structures, constructed from heavy highly twisted yarns, are the most prone to flex-cracking, this effect seems to be completely overpowered during impact by the huge amounts of energy transmitted to the coated fabric. This energy is sufficient in some cases to disrupt the adhesive bond directly, causing delamination without the intermediate stage of rubber flex-cracking.

Another fundamental difference in material response exists between an impact or flagellation type of test and a flexural or rolling fold test which relates to the test specimen configuration. In the impact or flagellation test, the specimen has a free edge which can flutter at very high frequency following impact even though the impact frequency per se may be as low as 3 Hz. Similar motions occur at the bottom of a finger in service following impact with a wave or solid object. As discussed in Section 10.2.3, these frequencies can be as high as 100 to 200 Hz with high accelerations. However, since specimens used in flexural or rolling fold flexural tests do not have a free edge which can flutter, high frequencies and accelerations do not occur, and the specimen deformations are more simple and less severe.

The results of the drum impact tests suggest that the most important factor affecting the ability of rubber coated skirt fabrics to withstand the combination of high impact velocities and high-curvature high-speed flexing is the strength of the adhesive bond between elastomer and woven substrate. At present, the strongest bonds between layers are achieved by promoting bridging of the elastomer through the structure of the reinforcing fabric. However, whatever means can be taken in the design of the skirt fabric to combine bridging of suitable elastomer formulations with those fabric construction features that enhance flex-fatigue resistance should ultimately lead to coated fabrics better able to withstand the rigors of marine service.

10.8 FINGER PANEL TRIALS ON HOVERCRAFT SR.N4

The results from laboratory evaluation of elastomeric coatings are difficult to interpret in terms of service life because none of the laboratory tests reproduce all types or conditions of service failure. Consequently, the final test has to be an in-service evaluation. A number of rubber coated fabric combinations have been evaluated as fingers on various operating air cushion vehicles in the last 15 years building up to evaluation on SR.N4 cross channel ferries; these vehicles were selected because of their large size (fingers are larger but tend to wear out more quickly) and because service time is accumulated quickly from the frequent operations.

The in-service evaluation has been an American exercise with comparison to

standard British materials. On the Canadian Coast Guard Voyageur, fingers fabricated from a Goodyear material (natural rubber/polybutadiene blend on high twist, open, plain nylon fabric) designated XA28A504 and a Goodrich material (polyisoprene/polybutadiene blend on closed 2 × 2 nylon fabric) designated 1812-141 were found to have approximately 50% longer life than the *standard* neoprene coated nylon fabric fingers, (neoprene on 23 × 2 nylon) designated Northern Rubber C11184. Fingers fabricated from hydrin coated nylon fabric and natural rubber/polyisoprene blend on other weaves of nylon fabric were found to have less or approximately the same life as the neoprene coated fingers.

In-service evaluations of fingers also were performed on the U.S. Army, LACV-30 and the U.S. Navy AALC. Again the Goodyear and Goodrich materials exhibited a service life 50 to 60% greater than the neoprene fingers. In addition, a Bell Aerospace Textron material (natural rubber/polybutadiene blend on closed 3 × 4 nylon) designated BAT-502, and an Avon material (natural rubber/SBR blend on low twist 2 × 2 nylon) designated 4275-280HN also exhibited service lives 50 to 60% greater than the neoprene fingers. Goodyear materials consisting of natural rubber/polybutadiene blend coated on 2 × 2 and 4 × 4 nylon fabrics exhibit service lives of approximately the same duration as the neoprene fingers while both propylene oxide and cast liquid polyurethane coated on 3 × 4 nylon exhibited shorter service lives.

In one service trial on an SR.N4, BAT-502 (65/35 natural rubber/polybutadiene ratio) exhibited approximately one-half the wear rate and BAT-520 (70/30 natural rubber/polybutadiene ratio) exhibited the same wear rate as the *standard* finger (natural rubber/SBR blend) after 342 hours of craft operation, at which time the fingers were removed.

In another service trial on an SR.N4 the Goodyear XA28A504 and Goodyear XA28A578 (same coating and fabric as -504 material but with twice the weight of coating on one side of the fabric as on the other side) were evaluated with the Avon 280-HN. The -504 material was at a weight of 93 oz/yd^2 while the -578 material was 175 oz/yd^2 and the 280-HN material was 150 oz/yd^2. The -504 material exhibited the same service life as the 280-HN; the -578 material exhibited a shorter service life than the 280-HN.

A third service trial on an SR.N4 took place in 1983. Two types of weaves were used, each with two rubber formulations. The weaves were a construction similar to that used in the Goodyear-504 material but with less twist and a greater tensile strength and a unidirectional yarn held together with a spiral wrap. The coatings were the same as on the Goodyear -504 except with more antiozonant and the same as on the Goodrich 1812-141. In addition, fingers were fabricated from Goodrich rubber coated fabric 1812-140. These materials were evaluated with fingers fabricated from Avon 280-HN. All four of the materials exhibited similar service lives.

Conclusions from the service trials are that an open weave with high twist is preferred so that rubber strike through occurs to aid in adhesion to the fabric. Of course, the fabric must have sufficient tensile and tear strength to resist the tensile and tear loads encountered. Behavior of fingers is governed largely by the rubber coating and its adhesion. The rubber coating has to stay in place to protect the fabric and maintain its geometry for good service life.

10.9 SKIRT-FABRIC DESIGN RECOMMENDATIONS

10.9.1 Choice of Elastomer/Formulation

Neoprene coated fabrics have been used extensively in service for bags in the finger-bag seal configuration. Long life generally is being obtained from the materials which, with current designs, appear to be adequate for the application.

Finger life, however, has been unsatisfactory and a variety of polymers have been evaluated as the rubber coating. High velocity air and water jet flagellation tests, a new high velocity impact test developed at NSRDC, and in-service evaluation tests all yielded results that point to similar elastomer selections for use in fingers. The best results have been obtained from blends of natural and polybutadiene, polyisoprene and polybutadiene, and natural and styrene butadiene copolymer rubber. These blends may vary between 65:35 to 50:50 natural to butadiene rubber with typically 40 to 60 pphr (parts per hundred parts of rubber) carbon black plus silica. These ingredients have to be combined with the correct curing systems and long lasting, antibleeding antioxidants and antiozonants as well as a choice of plasticizer to obtain the desirable characteristics.

10.9.2 Fabric Substrate Design

The principal design criterion for the substrate of a skirt fabric is its tensile strength. The high strength usually required mandates a woven, rather than a non-woven, substrate structure. The inherent tenacity of the fibre chosen, together with the specified tensile strength of the fabric, predetermines the total load-bearing cross-sectional area of fiber needed per unit width of fabric in each of its two principal directions. Tire-cord grade nylon 6,6 has been the preferred fiber material, but polyesters also appear to be satisfactory, and other higher-strength fibers such as extended-chain polyethylenes may find increasing use if good adhesion to the elastomer can be achieved.

The geometric structure of the woven substrate can have a dramatic influence on both the resistance of the elastomer to flex-cracking and on the ability of the bond between elastomer and substrate to withstand high-speed, high-energy impact without delaminating.

To resist delamination during impact, an open-structure is required to

promote bridging of the elastomer through the substrate and the attainment of high adhesive bond strength between layers. To resist flex-cracking, as thin a fabric substrate as possible consistent with the tensile strength requirements is preferred. Unfortunately, these design requirements conflict. However, the need to prevent delamination during impact must take precedence until better adhesives are developed that do not require interlocking of the elastomer through the pores of the woven substrate for the development of high interfacial bond strength.

An open-weave fabric is achieved by employing a smaller number of larger denier yarns per unit width to reach the required tensile strength. High twist yarns are needed to consolidate the yarn and prevent its spreading. Thin fabrics, on the other hand, are achieved by using a larger number of smaller denier, low-twist yarns per unit width and by maintaining a balanced yarn crimp. The only way that a fabric that is both open and thin can be achieved is by the use of higher strength fibers that allow attainment of the specified tensile strength with a minimum number of low denier yarns.

At present, the best approach to designing a woven fabric substrate for skirt materials may be summarized as follows:

(1) Choose a fiber of as high a tenacity as possible;
(2) Specify the yarn denier and number of yarns per unit width to attain both the required tensile strength and a minimum free open area between yarns of no less than 10-12% (based on the round-yarn diameter, see Section 10.3.2);
(3) Prepare yarns with high twist;
(4) Weave in plain weave pattern with balanced yarn crimp.

10.9.3 Fabrication Method

Prior to coating, the woven fabric substrate should be scoured to remove spin finish and other lubricants and heat-set to relax residual stresses and stabilize the fabric geometry.

Rubber coated fabric is fabricated most economically using calender coating and rotocuring methods to obtain continuous rolls of material usually of 137 cm (54 in) width. The seal components are fabricated from the rolls of material. However, this may not be the best way to fabricate fingers with natural rubber coatings. As indicated previously, cured natural rubber is difficult to bond to itself. Fingers have doubler reinforcements bonded at the attachment areas to resist tearing.

To obtain the highest quality finger, fabrication should be by layup of uncured rubber and fabric cut to the desired shape. Doublers should be added to the layup at this time. The finger layups should be cured in an autoclave or a mold in a press at high pressure. Molding at high pressure is preferred because this insures flow of the rubber into the openings of the fabric and

yields good rubber bonding to itself.

10.10 SUMMARY

The flexible skirt system that contains the cushion of supporting air for SES and ACV's and which is an important contributor to craft stability and ride is generally constructed from elastomer coated woven fabric. The skirt panels are exposed to harsh environments in which they must survive a complicated and severe combination of static and dynamic loads over many hours of craft service without failure by tearing, flex-cracking, fraying, delamination or abrasion. Typical operating lifetimes for some components of the skirt system can be as short as 50 to 200 hours. The choice of elastomer type and fabric construction can have a dramatic effect in extending that lifetime.

The principal requirements of the skirt fabrics that must be met by the woven substrate are flexibility combined with high tensile and tearing strength, low weight and fatigue resistance. The elastomeric coating must also be flexible and lightweight, and resist abrasion, flex-cracking, impact loading, and the effects of water, sunlight, ozone and fuel as well as the degrading effects of high internal temperatures generated during high frequency flexing and the tendency to become stiff and brittle at low environmental temperatures. The effectiveness of the adhesive tie-coat in binding these two skirt fabric components together is critical to the skirt's ability to resist delamination and to its performance in general since neither fabric nor elastomer can serve as a useful skirt material separately. The goal of skirt fabric design is to identify the best combination of elastomeric coating, fabric material and geometry, and tie-coat chemistry to obtain the best balance of properties for the application.

No one polymer has the best properties for the task. Neoprene coated fabric bags, in the finger/bag seal configuration, have adequate in-service lifetimes but finger life has been unsatisfactory. Extensive laboratory evaluations of a wide variety of polymers and polymer blends, both separately and as coating on woven fabrics, have failed to identify an elastomer with better overall performance than a natural rubber/cis-butadiene blend. The best results in both laboratory tests and in-service trials have been obtained with blends of natural rubber and polybutadiene, polyisoprene and polybutadiene, and natural rubber/styrene/butadiene copolymers. For optimum performance, appropriate amounts of carbon black, silica, anti-oxidant, anti-ozonant, curing systems, and plasticizers must be incorporated in the elastomer blend and proper curing procedures followed.

Since the characteristics of the woven fabric substrate almost completely dominate the mechanical behavior of the skirt material, the choice of fiber type is critical not only to the ability of the fabric to meet strength specifications but also, to a large extent, in determining the fabric thickness and

openness. Tire-cord grade, high tenacity nylon is currently the material of choice although inherently stronger materials such as the para-aramid fibers and extended chain polyethylenes may find increasing use if problems of self-abrasion and poor bonding can be overcome. Laboratory evaluation of the flex-fatigue resistance of a variety of nylon fabric constructions designed with the same tensile strength and coated with the same elastomer has shown that fabric design can affect flex lifetime by over two orders of magnitude. Resistance to flex-fatigue is greatest in thinner, closed fabrics that are plain-woven from a greater number of smaller yarns since such a structure provides a thinner, uniform substrate layer and, as a result, a locally more uniformly thick coating layer. Avoidance of very thin regions in the rubber layer over the fabric knuckles, where flex cracks initiate, helps to promote good flex-fatigue resistance. Such a closed, fabric substrate is unfortunately the antithesis of what is needed to prevent delamination during the repeated high-energy impact that skirt fabrics must endure in use. Under these service conditions, the strength of the coating-to-fabric bond is overwhelmingly important to good fabric performance. The achievement of an adequate bond, at the present level of adhesion technology, dictates an open fabric weave so that mechanical interlocking of the elastomer through the pores of the fabric can occur. The obvious advantage of a higher strength fiber in this application is that fabric strength requirements could be met with a fabric construction that is both thinner, to promote a longer flex lifetime, and more open, to provide pathways for strike-through of the elastomer for better adhesion.

10.11 REFERENCES

1. Finger materials test data analysis and correlation report, CDRL No. 500G(H-9)C, Rohr Industries Inc., April 6, 1976.
2. Test data analysis and correlation report, SES-100B, Finger motions and finger drag, Report No. 7.593-925003, Bell Aerospace Textron (Navy Contract N00024-75-C-5034 Mod P00022, Sept. 1978.
3. Arctic surface effect vehicle program, Report No. 7416-960001, Vol. 3, (Task 2.1.2(b) Arctic SEV Skirt Materials Development), Bell Aerospace Textron, Feb. 1973.
4. P.K. Conn, I.C. Snell, and W. Klemens, Finger materials for air cushion vehicles, Vol. I: Flexible coatings for finger materials, David Taylor Naval Ship Research and Development Center, DTNSRDC 85/003.
5. Skirt material specifications for hovercraft vehicles, British Hovercraft Corporation.
6. Skirts and seals for surface effect vehicles, NMAB-340, National Materials Advisory Board, National Academy of Sciences, Washington, D.C., 1978.
7. Research and development of new seal materials for surface effect ships, GER 15460, Goodyear Aerospace Corp., Akron, Ohio, June 1972.
8. Test report bag and finger materials (L-9), Report No. 7446-928133, Bell Aerospace Textron, Contract No. N00024-74-C-0922 CDRL Sequence No. 500F, March 30, 1976.
9. Test report operational evaluation of finger materials (L-9), Bell

Aerospace Textron, May 17, 1976.

10. L.I. Weiner, Textile fabric design tables, Technomic Publ. Co., Stamford, CT, 1971.

11. K.D. Albrecht, Rubber Chemistry and Technology 46(4), Sept. 1973, p.981.

12. E.D. Erickson, Rubber Chemistry and Technology 47 , 1974, p.213.

13. Test report operational evaluation of finger materials (L-9), Bell Aerospace Textron, March 30, 1976.

14. Seals development summary report, CDRL No. 5007(L-6,L-7,L-8, and H-9), Rohr Industries, Inc., May 28, 1976.

15. J.J. Kelly, W. Klemens, and H.S. Preiser, Development and evaluation of skirt/seal materials for surface effect vehicles, Second International Hovering Craft, Hydrofoil and Advanced Transit Systems Conference, Amsterdam, The Netherlands, May 17-20, 1976.

16. G.G. Smith, R.D. Loban, Effects of molybdenum disulfide on elastomer flex life and other properties, Rubber Division, American Chemical Society, New Orleans, La. Oct. 7-10, 1975.

17. M.M. Schoppee, J. Skelton, M.M. Toney, and W. Klemens, Finger materials for air cushion vehicles, Vol. II: Base fabrics for finger materials, Ship Materials Engineering Dept. Research and Development Report DTNSRDC 85/004, Dec. 1984.

18. J. Skelton, The measurement of the bending elastic recovery of filaments, J. Textile Institute, Vol. 56, T454-T464, 1965.

19. J. Skelton, The effect of heat-setting on the bending behavior of woven fabrics, TRJ, Vol. 40, No. 12, December 1970.

20. K.A. Brownlee, Industrial experimentation, Chem. Publ. Co., New York, NY, 1953.

21. M.G. Natrella, Experimental statistics, NBS Handbook 91, August 1963.

22. W.G. Cochran and G.M. Cox, Experimental designs, J. Wiley and Sons, Inc., NY, 1957.

Chapter 11

OVERLAND DRAG

11.1 INTRODUCTION

The peripheral-jet hovercraft, as originally conceived by Cockerell, was virtually a low-flying aeroplane, and *flew* with a visible air gap under its hard hull. It has evolved into a skirted machine operating at such a relatively low airflow that it often drags its skirt along the ground with no visible air gap at all. The modern hovercraft, or air cushion vehicle (ACV), therefore uses far less lift air than the original version, with consequent economy of fuel and machinery. However, whereas the drag of the original hovercraft due to vehicle/ground interaction was extremely low, the overland ACV pays for its lift-air economy with a considerable drag due to the skirt/terrain interaction. It is the purpose of this chapter to examine this trade-off between lift economy and drag, and suggest a rationale for optimizing it. Since the drag of the low-speed overland ACV is largely determined by the interaction between vehicle and terrain, the terrain will be discussed as much as the vehicle.

To set the matter in perspective, the lift-air requirement, and total installed power of a peripheral-jet hovercraft with a total weight of 100 kN (about 10 tons), capable of traversing 30 cm obstacles at 25 km/h, can be six to eight times greater than for a comparable skirted craft; however, the drag is approximately five times greater with the latter. To further clarify the position, Figure 11.1 shows the relative magnitudes of the various sources of drag for the same 100 kN modern craft moving at 25 km/h over 30 cm vegetation on level ground, at typical lift airflow, based on NRC (National Research Council of Canada) test data.

Of the two configurations, the skirted ACV is economically preferable for low-speed overland use. The skirt/terrain interaction is the main cause of

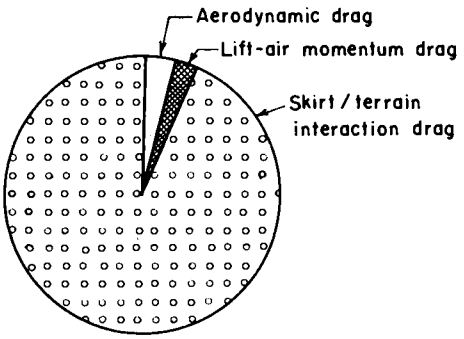

Fig. 11.1 Drag components of skirted hovercraft. Based on NRC test data for a 100 kN craft moving at 25 km/h, with typical lift airflows, over 30 cm vegetation on level ground.

drag. Evidence will be presented to show that, for a given vehicle, skirt/terrain interaction drag is primarily a function of lift airflow and terrain qualities. Thus, it is important for the vehicle designer to have an effective method of determining the optimum lift airflow for a given vehicle and operational requirement.

11.2 DESCRIPTION OF DRAG-STUDY VEHICLES

11.2.1 Hovercraft HEX-1B

Research vehicle HEX-1B consisted essentially of a girder frame on which were mounted a lift system, an auxiliary thrust system, a ballast system, and a cabin for the crew and instrumentation. All systems were heavily instrumented. The vehicle was mounted on a windbox, which was particular to the skirt being tested. The windbox contained the duct system to distribute lift air from the blowers to the skirt elements, and mounted the skirt attachment points. The flexible skirt was attached to these. Both the skirt and windbox were considered together as the experiment under test.

The whole assembly is shown, in Figures 11.2 and 11.3, mounted on an experimental skirt, an H.D.L. segmented design. In this case there was no windbox as such, the blowers delivering air straight downwards into the cushion area. The skirt was mounted on a girder framework and extended outwards from the sides of the girder chassis. Specifications for the vehicle are given below.

(i) Hard structure.

Length	-	8.10 m
Width	-	5.05 m
All-up mass (2nd expt.)	-	4850 kg
All-up weight	-	47.5 kN

(including 680 N of fuel, and a crew of two, weighing 1600 N

(ii) Lift system.

Engine	-	Deutz air-cooled diesel V-8, type F8L413
Fans	-	2 × 1.0 m diameter centrifugal
Maximum flow	-	38 m^3/s
Maximum shaft power to fan at 2300 engine RPM	-	149 kW (200 HP) approx.

(iii) Thrust system (auxiliary, for manoeuvering only).

Engines	-	2 × Volkswagen 1500
Fans	-	2 × 0.92 m diameter axial, 12-blade ducted units
Maximum thrust	-	3.2 kN approximtely (7% of total weight)
Maximum shaft power at 3800 engine RPM	-	30 kW (40 HP) approximately, each

(iv) Ballast system.

4 tanks, each 1.42 m × 0.46 m × 0.405 m = 0.263 m^3

Capacity of each tank = 2560 N weight of water

11.2.2 Hovercraft HEX-5

Research vehicle HEX-5 consisted essentially of a buoyant fibreglass hull, on which was mounted a lift system, a thrust system, a position for the pilot/observer, minimal fixed instrumentation, and detachable pods containing additional instrumentation when required. The skirt system, similar to the HEX-1B skirt, was mounted directly on the underside of the hull.

The vehicle, mounted on an H.D.L. segmented-type experimental skirt is shown in Figures 11.4 and 11.5. Specifications are given below.

(i) Hard structure.

Length	-	4.15 m
Width	-	2.44 m
All-up mass (1st expt.)	-	680 kg
All-up weight	-	6.68 kN

(including 270 N of fuel and one driver/observer, weighing 800 N)

(ii) Lift system.

Engine	-	2 cylinder, 2-stroke Kohler air-cooled
Fans	-	2 × 0.40 m diameter centrifugal
Maximum flow	-	3 m^3/s
Maximum power	-	40 kW at 5500 engine RPM (rated)

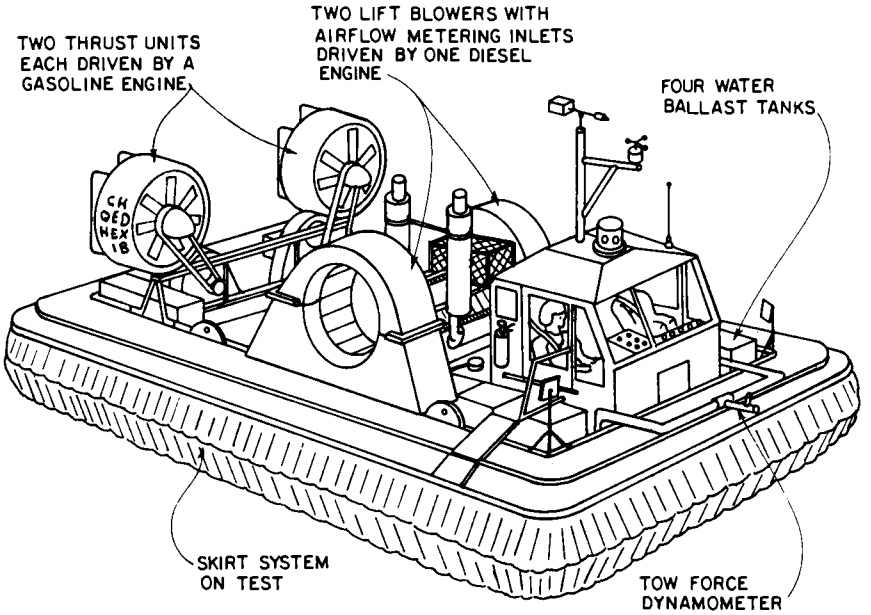

Fig. 11.2 Sketch of research hovercraft HEX-1B.

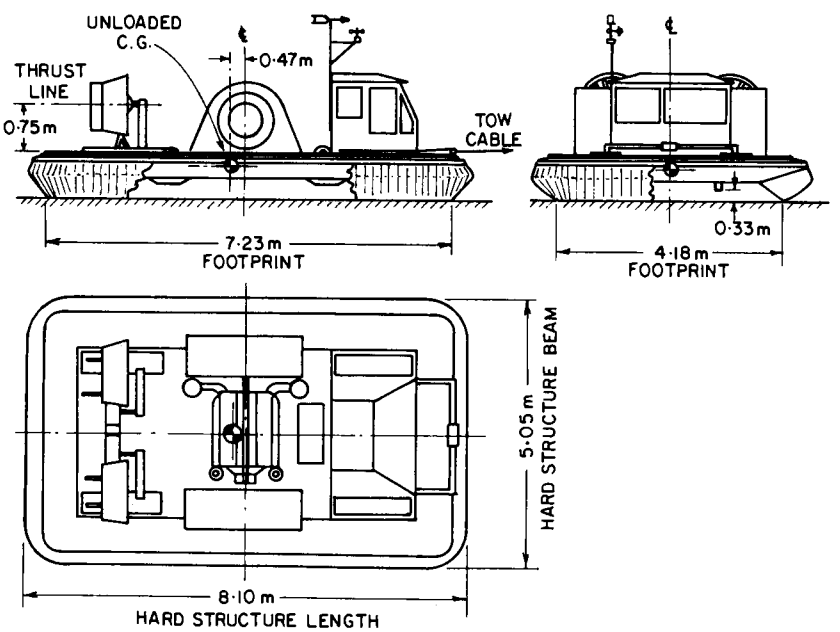

Fig. 11.3 Views of research hovercraft HEX-1B.

(iii) Thrust system.

Engine	-	2 cylinder, 2-stroke Kohler air-cooled
Propeller	-	4 blades, 0.915 m diameter, in duct
Maximum thrust	-	2 kN approximately
Maximum power	-	40 kW at 5500 engine RPM (rated)

(iv) Other data.

Footprint area (calculated) at 815 Pa cushion pressure = 8.04 m^2

(3.6 m × 2.23 m) at 6.55 kN total weight

Frontal area = 2.9 m^2; corresponding drag coefficient C_D = 0.37

Aspect ratio of cushion = 1.65:1

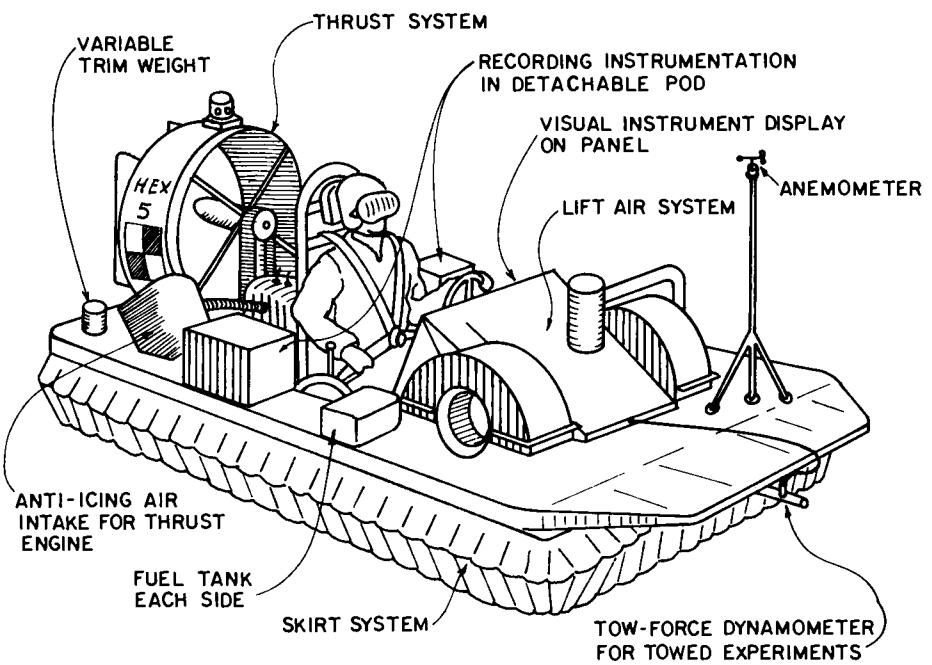

Fig. 11.4 Sketch of research hovercraft HEX-5.

11.3 HOVER REGIMES

It has been proposed that the lift-drag characteristic of a low speed ACV over land is of the general form shown in Figure 11.6 (ref. 1).

The characteristic is divided into four distinct regimes described below.

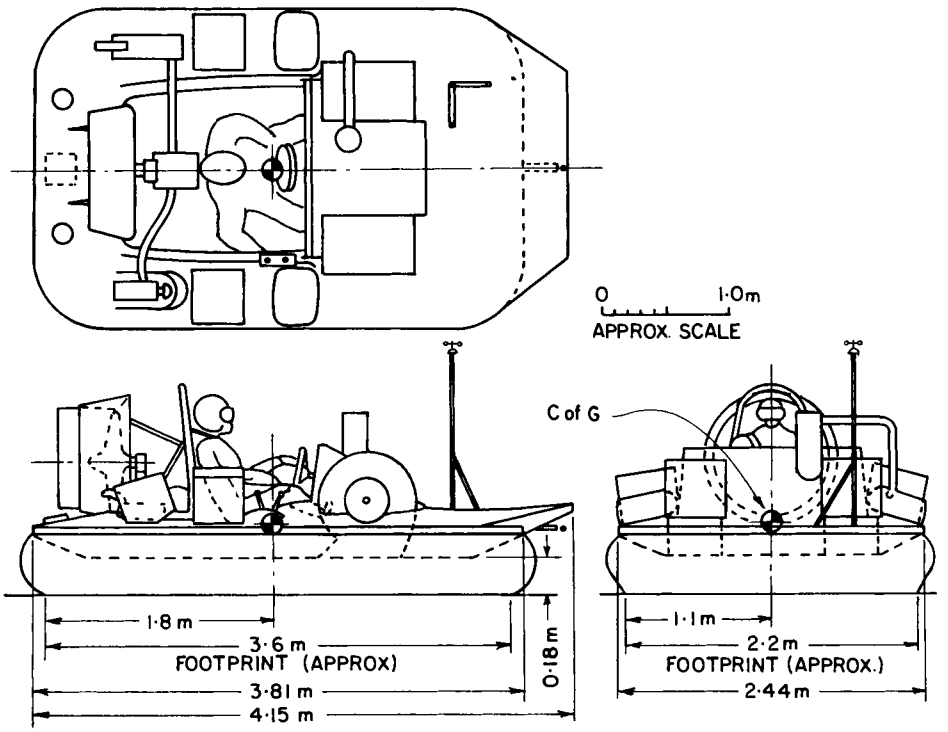

Fig. 11.5 Views of research hovercraft HEX-5.

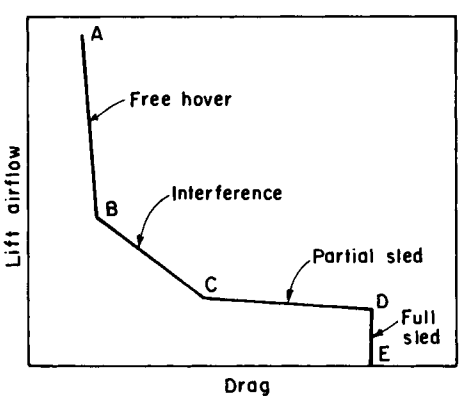

Fig. 11.6 General relation between lift airflow and skirt/terrain interaction drag.

11.3.1 Free-hover regime

In the free-hover regime (A-B) the lift-air supply is so great that the vehicle's skirt is held substantially clear of interference with terrain or vegetation. This region represents the minimum practical drag for the vehicle. A considerable increase of lift airflow leads only to very slight decrease of drag, and accurate level trimming of the craft to prevent local contact is essential. It is unusual for low speed overland ACVs to operate in this regime, as the price in lift airflow is high and the lack of interface drag makes directional control difficult. However, if high speed in unobstructed areas is required, considerations of skirt wear may force operation into this regime. As will be discussed in Section 11.9, abrasive skirt wear increases extremely rapidly with speed. If higher speeds are required it appears necessary to hover higher, with the skirt free of ground contact.

11.3.2 Interference regime

The interference region (B-C) of Figure 11.6 represents the normal operational condition of a low-speed overland ACV. The vehicle is still wholly supported by its air cushion, but the skirt is folded under to some extent and dragging against terrain or vegetation. This dragging naturally creates frictional drag, and further work is needed to push back the skirt to pass stiff terrain obstacles, or to bend vegetation over as the skirt passes. This suggests a division of the interference drag into two components, which might be crudely referred to as *scrubbing drag* and *bush-bashing drag* respectively. It might be suspected that the bush-bashing fraction would diminish greatly during a series of passes over the same track, and some evidence to this effect will be presented later. This component will not be affected by lift airflow, but the scrubbing drag certainly will, and will also be affected by the porosity of the terrain, and its vegetation cover. Again, quantitative evidence will follow.

From the above, it is reasonable to expect the drag in this regime to increase considerably as lift airflow is reduced and the vehicle sinks low onto the ground, folding its skirt under to a greater extent. Increased terrain porosity will show the same effect, by reducing the effective airflow. This is indeed the case in operation.

11.3.3 Partial-sled regime

In the partial-sled regime, the airflow is insufficient to maintain a cushion pressure high enough to support the vehicle fully, and an increasing proportion of the vehicle weight is supported by physical contact; the vehicle begins to act as a sled. Over some types of vegetation this mode of operation may be quite satisfactory, but either the vegetation or the vehicle will certainly show traces of the passage. Moreover, as the figure shows, region

C-D covers a dramatic rise of drag, caused by a small decrease of lift airflow or local increase of terrain porosity. This may be severe enough to be quite unacceptable.

11.3.4 Full-sled regime

Finally, when lift air is reduced to zero, we have the full-sled regime. Here the weight of the ACV is fully supported by mechanical contact between the hard structure and the terrain. The vehicle has become a pure sled, and the drag is that due to simple friction of its full weight plus bush-bashing. The lift airflow may be reduced to zero without further change, as shown in region D-E of Figure 11.6. This type of operation is usually very destructive of the vehicle and terrain, and is unacceptable. A real sled with proper runners would be more effective under these circumstances. It is conceivable that this regime might be exploited over some terrains, such as level ice or ice trails, by vehicles having air-lubricated sled runners.

11.4 MATHEMATICAL MODELS OF LIFT AIRFLOW AND DRAG

In order to study the lift airflow versus drag relationship in generalized terms, it is necessary to develop suitable quantitative expressions for both lift airflow and drag whereby experimental data from different vehicles operating at various conditions may be compared. The lift airflow must be rendered independent of vehicle dimensions and characteristics, and atmospheric conditions. A number of expressions for lift airflow have been proposed, including simple calculated hoverheight, flow rate per unit length of skirt perimeter, etc. Most of them have not fully satisfied the requirements stated above, although each has been suitable for a particular purpose. A notable exception involves the use of a parameter called *Efflux Gap Height (EGH)* which is a standard-day virtual hovergap, expressed in metres, and has an important physical relation to the terrain roughness, independent of vehicle size (ref. 2). The EGH concept is developed presently.

The fact that a craft *hovering* at low lift airflow with its skirts dragging on the ground (and hence a *negative hovergap* in practical terms) still has a positive airflow is accounted for largely by leakage between skirt segments or fingers. In such a case, the airflow calculation still demands an efflux area. This can be conveniently expressed as the product of skirt hem perimeter and a fictitious EGH. The preceding Section 11.3, and subsequent experimental evidence presented and discussed in Sections 11.5 and 11.6 suggest that the EGH is a helpful concept in practice, rather than a mere analytical abstraction.

Treating the efflux gap as a sharp-edged orifice, it can be shown (Chapter 12) that the airflow Q (m^3/s) is given by:

$$Q = C_D A(2P_c/\rho)^{1/2} \tag{11.1}$$

where C_D is a discharge coefficient (=0.61), P_c is cushion gauge-pressure (Pa), ρ is air density (kg/m^3), and A is the orifice cross-sectional area (m^2).

It is assumed that the efflux gap area can be approximated by:

$$A = Lh \tag{11.2}$$

where L is the skirt perimeter (m) and h is the efflux gap height (m). The EGH is decomposed further, as follows:

$$h = h_f K \tag{11.3}$$

where h_f is the gap height over smooth, flat and non-porous ground at low speed, and K represents the increase of h_f due to terrain porosity, unevenness, high-speed operation, wave-pumping, and other surface conditions.

The cushion pressure must be large enough to support the weight of the vehicle, i.e.,

$$P_c = w/S_c \tag{11.4}$$

where w is the total vehicle weight (N) and S_c is the footprint area (m^2).

Substitution of eqns. (11.2) to (11.4) into eqn. (11.1) yields:

$$Q = \beta(h_f K) \tag{11.5a}$$

where

$$\beta = C_D(L/S_c)(2/\rho)^{1/2}[w/(P_c)^{1/2}] \tag{11.5b}$$

The term (L/S_c) is related to vehicle planform, or aspect ratio. The term $(2/\rho)^{1/2}$ describes the atmospheric conditions. It is of surprising importance in designing and testing a vehicle for use in the Arctic, or on a high-altitude plateau, where temperature and altitude cause appreciable changes in air density. The term $[w/(P_c)^{1/2}]$ shows both the cushion pressure and total weight of the vehicle, and might be called a *loading* term. The convenience of eqn. (11.5b) to a designer is therefore apparent. It enables him to see at a glance the effect of juggling the several variables open to him in meeting a particular requirement. By using a value of $h_f K$ appropriate to the terrain and operational mode specified, he will produce a vehicle with adequate hovering performance.

For given craft dimensions, total weight and atmospheric conditions, it is seen that the lift airflow Q is proportional to the efflux gap height $h_f K$ by a constant factor β. Therefore, the EGH can be used as a measure of airflow. The bar chart of Fig. 11.7, for several hovercraft, gives values of $h_f K$ which have been found to give satisfactory performance. It is clear from this chart that different classes of hovercraft operate at considerably different values of EGH. To determine the corresponding airflows, we would require the applicable value of β in each case.

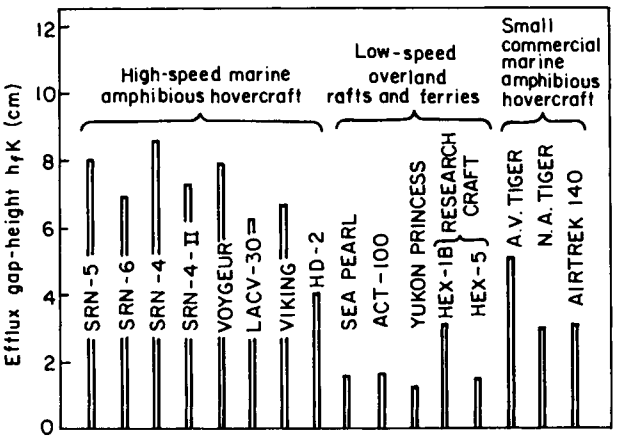

Fig. 11.7 Bar chart of efflux gap height for various hovercraft.

The description of drag appears to be much simpler. It appears that the function 100(Drag force)/(Vehicle total weight) gives a percentage non-dimensional description which is valid in practice.

Referring to the high speed marine hovercraft, Figure 11.7, the high value of h_fK is intended partly to reduce skirt drag and wear, by minimizing skirt/wave contact, and partly to offset the results of *wave-pumping*. The low speed overwater/mud-flat air-cushion ferry barges operate at low values of h_fK since they have only small frictional demands to contend with, and potentially excellent sealing as the skirt drags in mud or water with good lubricant properties. Experiments with the HEX vehicles and other scattered clues lead us to believe that operation over notably rough ground or porous vegetation at low speed, or high speed operation over flat ground, will require larger values of h_fK but still not up into the marine hovercraft range, since the *wave-pumping* requirement is eliminated.

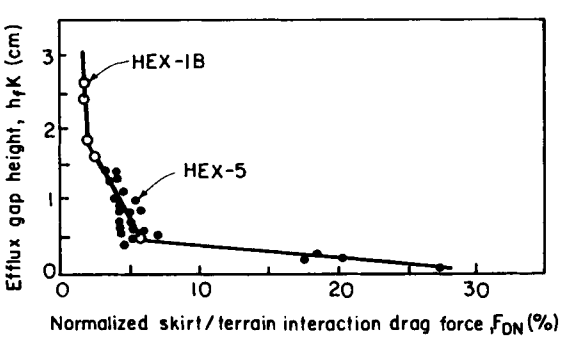

Fig. 11.8 Relation between EGH and skirt/terrain interaction drag for hovercraft HEX-1B and HEX-5. Data obtained with various weights, at 2 m/s speed on short grass.

A practical nondimensional characterization of the skirt/terrain interaction drag is achieved by:

$$F_{DN} = F_D/w \tag{11.6}$$

where F_D is the skirt/terrain interaction drag-force (N), F_{DN} is its normalized value, and w is the total vehicle-weight (N). Multiplication of eqn. (11.6) by 100 yields percentage values of F_{DN}.

11.5 EXPERIMENTAL VALIDATION

Using the lift airflow and drag expressions in eqns. (11.5) and (11.6), the data measured in field tests on the NRC research vehicles HEX-1B and HEX-5 over the same terrain is shown in Figure 11.8, which is a *real-life* version of the previous Figure 11.6. The terrain was the *short-grass* described in Section 11.6. The two vehicles weighed 47,500 N and 6,700 N respectively, with cushion pressures of 1,570 Pa and 850 Pa, and were tested at whatever atmospheric conditions came along. The only constant factors apart from the terrain were towing speed of 2 m/s, and the fact that the two vehicles had geometrically similar (scaled) skirts).

Looking at Figure 11.8, it is clear that although the two machines were operated at very different ranges of airflows, the EGH versus drag description discussed above puts these two experiments onto a single line of analyzed data. Moreover, the curve does in essence conform to the general proposal shown in Figure 11.6, with the free-hover, interference, and partial-sled regimes clearly recognizable.

11.6 TERRAIN AND VEGETATION EFFECTS ON LIFT AND DRAG

So far, discussion has dealt with the influence of changing lift airflow on vehicle drag, over some typical surfaces. Attention will now be shifted to the influence of different types of surface on the airflow required to hold drag to an acceptable level. Although the primary question before us is the minimum airflow to achieve acceptable drag, the data produced will show very clearly the different values of drag characteristic for various terrains and vegetation surfaces. Tentative explanations of these differences will be given.

The research hovercraft HEX-1B and HEX-5 were towed at a standard 2 m/s speed over a considerable range of surfaces, with on-board chart recorders connected to strain gauges between the vehicle and the tow-line. Motive power was supplied by a heavy 4-wheel drive truck driving on flat ground beyond the test track, with a steel cable tow-line. The truck speed was measured by a specially calibrated speedometer driven off the rear wheels. By moving the test track sideways for each run, measurements were made on undisturbed terrain each time, and care was taken to see that there was no perceptable difference in terrain between the whole series of test tracks. The levelness of the

ground was accurately surveyed. Any slope was interpreted as an equivalent drag force and the test data corrected accordingly. Calibrated instruments on board the vehicles measured the cushion pressure and lift airflow before and during the test runs.

Some of the results of this program of experiments are shown in Figure 11.9. The terrains and vegetation covered are described below.

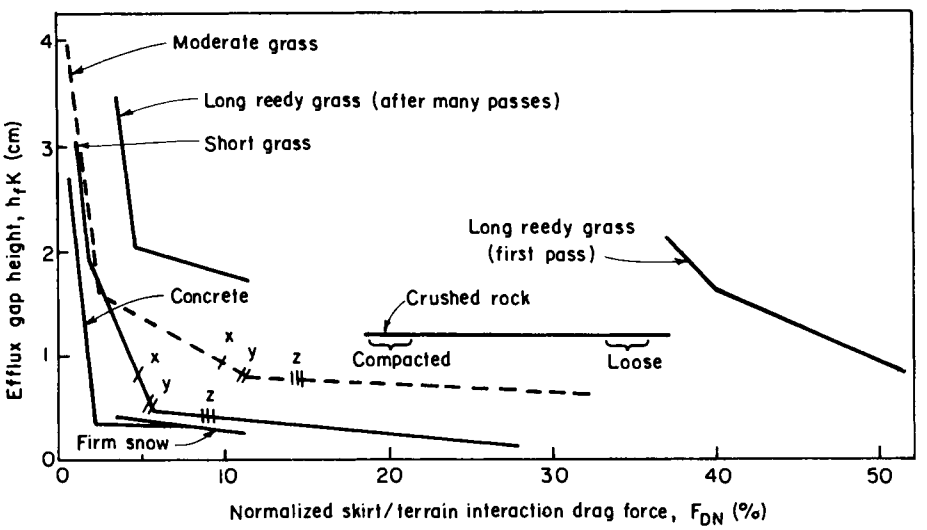

Fig. 11.9 Normalized skirt/terrain interaction drag force, F_{DN} (%).

a) Concrete runway. For a hard, flat, non-porous surface used as datum, the vehicles were tested on an airfield runway. In the lift airflow equation proposed above, the results on this surface could probably be taken to represent the efflux gap height $h_f K$, with $K = 1.0$.

b) Short grass. This was used to describe an area that had been a lawn. It was based on flat hard loam, and the grass/clover mix was frequently mowed, including a cutting shortly before the experiments. The growth was somewhat bristly, and averaged about 2.1 cm. While a gardener would call it *flat*, measurements showed that this flatness was not within ±1 cm over a 1 m × 2 m area.

c) Moderate grass. This description covers a test area on the edge of an airfield where heavy grass and weed had been roughly cut to a height of about 28 cm over rough meadow ground. The test runs were sited to avoid discontinuities such as slight drainage depressions, small rocks, ground-hog holes, and other hazards. The vegetation consisted of the bristly stubble of tall reedy grass, clover, dandelions, an underlayer of old dead cut grass, and dense short new growth.

d) Long grass. This area bordered on the above moderate-grass test area, and represented the same soil and vegetation but had never been cut. The vegetation was dense and uniformly 1.0/1.5 m high, and was quite difficult to push through on foot. It showed a very different resistance to progress between the first pass and subsequent passes; this is commented on in a later section.

e) Crushed rock. A sandy approach ramp to a pond had been surfaced with crushed rock, and tests were made on this before it was compacted. The rock layer was 10 cm thick, and covered the size range from 2 cm cubes to 8 cm cubes, in a fairly well-distributed mixture. The rock was laid on hard sand, which was not eroded during the experiments. In some places compaction had already been started, driving the rock into the sand. The roughness was not unduly decreased, but the porosity of the layer was noticeably reduced by this process.

Inspection of Figure 11.9 takes us some distance beyond the single *short grass* curve of Figure 11.8, and enables us to see the influence of terrain on vehicle performance, and on the lift air requirement. The curve for concrete on this figure shows a clearly marked minimum flow over hard non-porous surface, which could perhaps be taken as h_f for this skirt configuration. Further, it shows that by selecting a fairly well-defined corresponding point on the curves for other terrain surfaces, values of K could be found by which the lift airflow corresponding to h_f must be increased to operate at a reasonably optimum EGH/drag setting. Moreover, it suggests what the drag values are likely to be on each type of surface.

11.7 TERRAIN POROSITY MEASUREMENTS

At this point it is opportune to discuss a series of experiments on the porosity to lift-air of the ground surface and vegetation mat. A small ACV (HEX-5 in this case) was used to measured the airflow lost under a given skirt perimeter at a range of cushion pressures, either with the test vehicle locked at a fixed rise height, or allowed to rise naturally to measured rise heights. Under these conditions, air is lost through: 1) unsealed ground unevenness or actual ground porosity, 2) the vegetation mat above the ground, and 3) the inter-segment gaps and leaks in the vehicle's skirt. The basic purpose of the program was to discover and ultimately predict the lift airflow needed to hover an ACV over any particular vegetation. Since the degree of hovering and vehicle drag are apparently connected, drag measurements must of course be taken into account. The lift airflow measurements were therefore made with an actual skirted hovercraft.

Vehicle HEX-5 already had instrumentation installed to measure cushion pressure and lift airflow, as well as tow/drag force, so it was placed over the

sample terrain surfaces described, and both the lift and drag experiments carried out. In this case, the skirt perimeter was assumed to be constant at the nominal design figure, or was modified to agree with the vehicle total weight and measured cushion pressure once the vehicle had reached hover. Once the vehicle had started to hover, the exit area began to increase above that due to the squashed height alone, thereby terminating the validity of the experiment. The height of the vehicle above ground was therefore also measured, and showed clearly: a) to what point the vehicle was supported by the vegetation and blowing all its lift-air out through the vegetation, and b) where it then lifted off and gained a larger exit area through which to lose lift-air.

If the vehicle is capable of hovering over a given terrain, then the data generated will be of the general form shown in Figure 11.10, where lift airflow and rise height are both plotted against cushion pressure. Up to the lift-off region α the vehicle would be sitting on the vegetation mat, and losing air through it, without being able to build up enough cushion pressure to support the weight of the vehicle. Air flow q_α represents the flow needed to lift and hover the vehicle. This point could be transferred to the curves of Figure 11.9. For example, points x, y and z on the moderate- and short-grass curves show how a relatively small decrease of EGH (hence, flow) can bring the craft from an interference regime of operation to a partial-sled regime.

Operating in this manner, tests were carried out over the same terrains and vegetation previously described. Curves of rise height and EGH against cushion pressure are shown in Figures 11.11 and 11.12, respectively. The experiment

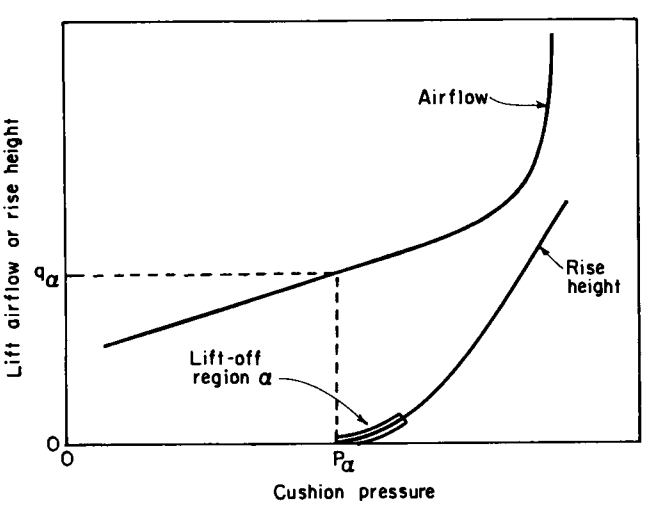

Fig. 11.10 General form of lift airflow (or EGH) and rise height relationships as functions of cushion pressure.

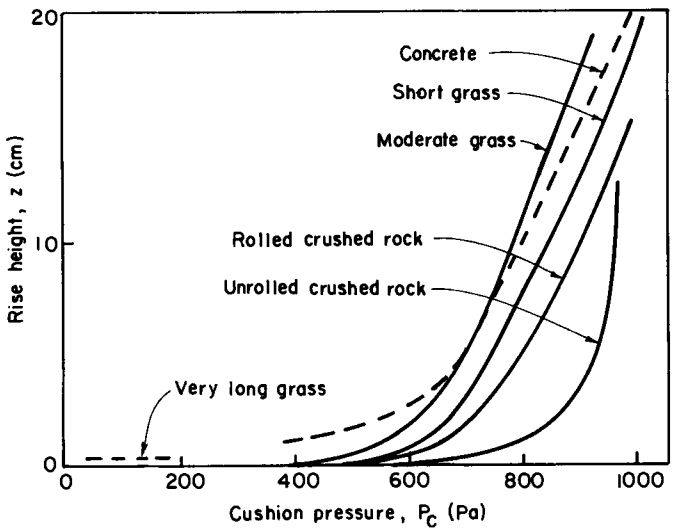

Fig. 11.11 Relation between rise height and cushion pressure for hovercraft HEX-5. Data obtained with constant 6.6 kN weight, at standstill on various terrains.

was considered valid as a terrain/vegetation porosity measurement until the vehicle had lifted over 20 cm, as the skirt should seal to more than this height if it were deployed over smooth flat ground.

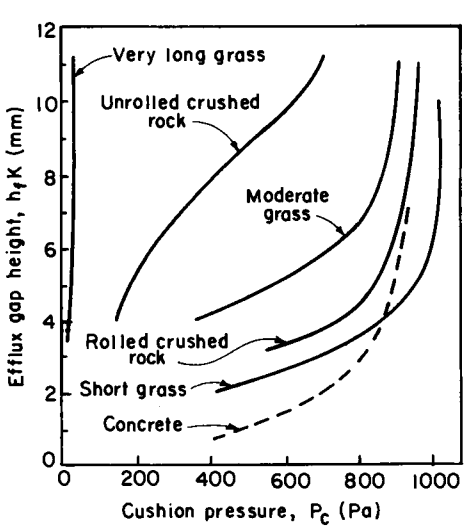

Fig. 11.12 Relation between EGH and cushion pressure for hovercraft HEX-5. Data obtained with constant 6.6 kN weight, at standstill on various terrains.

Measurements of pressure and airflow were made at the point of rising of hovercraft HEX-5. It was found that rising began at a cushion pressure of 840 Pa. Given the 6.6 kN weight of the craft during the experiment, the effective footprint under these conditions was 6600/840 = 7.86 m^2, which would be given by 3.56 m length and 2.21 m width dimensions. Therefore, by substitution C_D = 0.61, L = 11.54 m, S_c = 7.86 m, ρ = 1.218 kg/m^3, w = 6600 N and P_c = 840 Pa into eqn. (11.5b), the value of ß is 261.4. A calibrated bell-mouthed inlet to the fans was used to determine lift-off values of airflow with various terrains and vegetation. Corresponding values of h_fK were obtained by dividing the airflows by the above value of ß. However, the results given in Table 11.1 cannot be obtained accurately from the curves in Figure 11.12, since the latter are only rough smoothing approximations drawn through many experimental data points, all excluded from the figure.

Table 11.1. Lift-off values of lift airflow and EGH. Experimental results obtained with hovercraft HEX-5 at 6.6 kN weight over various terrains and vegetation. Lift-off pressure was 840 Pa.

Surface	Airflow, Q (m^3/s)	Efflux gap heights, h_fK (mm)
Concrete	0.8	3.06
Short Grass	1.25	4.78
Moderate Grass	1.80	6.89
Long Reedy Grass	No hover	No value
Rolled Crushed Rock	>1.4	>5.36
Unrolled Crushed Rock	>3.0	>11.48

These EGH values may be plotted onto curves of h_fK versus F_{DN} obtained in *drag tests, and should indicate closely the transition point between interference drag* and *partial sled drag*. This is done in Figure 11.13, and the cases in which positive rise to full hover were within the air capacity of the test vehicle are seen to agree with the (F_{DN}, h_fK) curves. It is therefore suggested that in future a small ACV with the appropriate skirt type should be tested over any particular terrain, and the airflow needed to generate the cushion pressure required to hover it be measured. This will indicate the minimum lift airflow, or generally applicable EGH, needed to hover an ACV over that terrain or vegetation.

Based on the above results and others, such as given in Figures 11.14 and 11.15, it seems possible to go further and make a tentative estimate of the values of K pertinent to various terrain and operational situations. In the

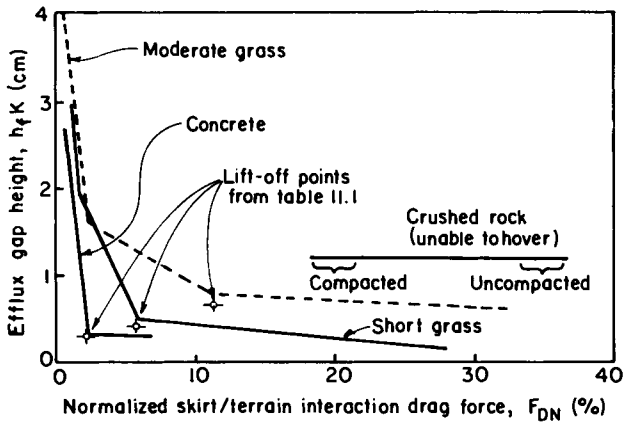

Fig. 11.13 Addition of lift-off points to selected (F_{DN}, $h_f K$) curves from Fig. 11.9.

Table 11.2. Tentative estimate of K values pertinent to various terrain and operational conditions.

Terrain and operational conditions	Operating point value of $h_f K$ (m)	K	Normalized drag force, F_{DN} (%)	Remarks
Smooth Concrete, Low Speed	0.0035	1.0	2	Basic value
Firm Snow	0.0055	1.5	2.5	
Short Grass	0.020	6	2	
Moderate Grass	0.020	6	2	
Long Reedy Grass 1st Pass	0.022	6	40	
Long Reedy Grass 10th Pass	0.022	6	5	
Crushed Rock	0.020	6	15–30	
Mud Flats	0.016	5	2–5?	U.K. data
Concrete, High Speed	0.013	4	2	Fig. 11.12*
Open Sea, High Speed	0.075	20	**	U.K. data

* The skirt wear factor is not yet established, and may demand a higher K value to achieve reasonable skirt life.

** The drag in this case is mainly controlled by sea and air states, and no set figure for skirt drag can be given.

case of smooth concrete, there is no visible *interference regime* between free hover and partial sled, but in most other cases the interference regime

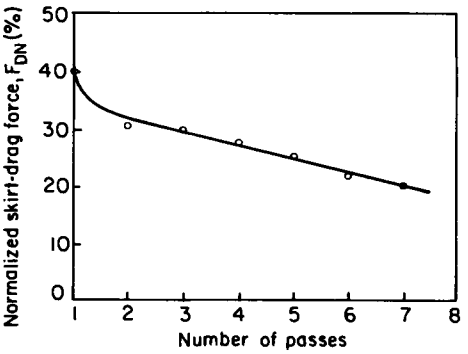

Fig. 11.14 Effect of repeated passes in long reedy grass. Vehicle HEX-5 over long (1.0-1.5 m) grass, with $h_f K$ = 1.26 cm; passes over same trail at 5 minute intervals.

becomes apparent. As a purely arbitrary decision on the grounds of practical experience, the *operating point* EGH value will be defined here as 10% above the EGH value at the transition between free hover and interference regimes. Therefore, for smooth concrete we have k = 1 (by definition), $h_f \simeq 0.0035$ m and $F_{DN} \simeq 2\%$ from Fig. 11.9 or Fig. 11.13. A table may then be prepared under these assumptions, setting out the operating point values of $h_f K$ and F_{DN} over various surfaces, and by relating the efflux gap heights to that over smooth concrete at low speed, the values of K may be estimated. The numbers given in Table 11.2 are tentative only, and should not be regarded as definitive.

11.8 THE BUSH-BASHING PHENOMENA

The drag of a hovercraft over vegetation can be somewhat arbitrarily divided into the interference drag (*friction*) of the skirt dragging over the plant surface, and the *bush-bashing* drag due to knocking down the vegetation in front of it as it passes. Two important points arise out of this. Firstly, if several passes are made before the vegetation rises back to its undisturbed position (which it may or may not do) then the bush-bashing fraction will decrease with the number of passes, while the friction part will remain roughly constant. This is illustrated by the data shown in Fig. 11.15, derived from an experiment in which HEX-5 was towed repeatedly over the same track through the 1.5 m high grass discussed in Section 11.6. Although the experiment was not carried to its conclusion, it is seen that some 25% of the drag is lost after the first pass, and it would appear that about 11 passes might reduce the drag to 1/4 of the initial value. Further experimental work is needed, but data gathered to date in long reedy grass, using vehicles HEX-1B and HEX-5, appear to confirm these ideas.

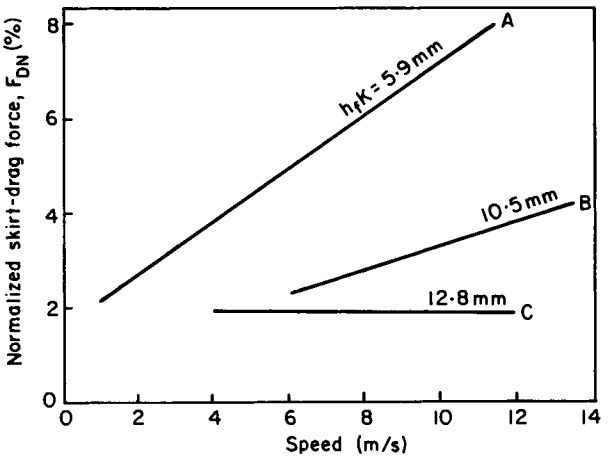

Fig. 11.15 Normalized skirt-drag force as a function of speed and EGH for hovercraft HEX-5 on concrete.

The second point is that the limit in traversing reedy-grass vegetation is usually imposed by the high thrust needed to knock down the vegetation, rather than by a high lift airflow requirement. However, in muskeg there is frequently considerable growth of much springier vegetation with less leaf and woodier stems, such as Spirea, and this statement may be much less valid in such cases. Here, the vegetation mat will be springier, thicker and less covered by leafage, so that its greater porosity may increase the loss of lift air so that this also becomes a major factor. In other words, there may indeed be an increase in the bush-bashing drag, but at the same time the loss of lift air will rise so drastically that this will greatly increase the frictional resistance at any given lift airflow. The coefficient of vegetation/skirt friction is also likely to increase, owing to the *rougher and snaggier* nature of the woody vegetation as opposed to the relatively smooth surface of a mat of pushed-over grass leaves.

11.9 VEHICLE SPEED EFFECTS

The investigation of the effect of vehicle speed on lift-air requirements for satisfactory operation is difficult. At relatively low lift airflows, skirt wear rises drastically with speed, thereby severely limiting the amount of testing possible. As an example, a skirt had survived 25 hours of operation at 2 m/s over a concrete runway, without much damage. When it was then operated in the 10-15 m/s range for less than 0.5 hour, it became so badly damaged as to be unusable for further performance testing. This represents only 20% of the distance travelled at the lower speed.

It seems clear that this damage is due to abrasion of the skirt material by hard particles protruding from the ground surface, whether fixed or lying loose

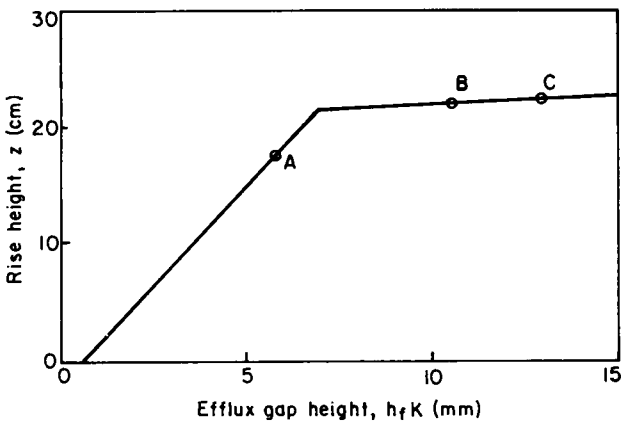

Fig. 11.16 Rise height versus EGH curve for hovercraft HEX-5 on concrete.

on it. This is made obvious by the shape of the worn patches on the skirt, which follow the crumpled segment-tip areas in contact with the ground when the craft has not lifted into the full-hover mode. Close examination of the worn patches confirms the abrasive nature of the damage. It varies in severity through the following stages: a) roughening of the outer rubber surface, b) complete loss of rubber and attack on the exposed nylon mid-layer, c) destruction of the nylon whose torn ends surround the worn patches, and d) complete destruction of the worn areas, leaving actual holes in the segments. Ultimately, the bottom of the skirt is reduced to a shredded and tattered fringe, making it impossible for the skirt to retain enough air to lift the craft off the ground. Qualitative observations indicate that the rate of skirt wear, for a given terrain is not merely proportional to velocity. It is more likely to be a function of a higher power of velocity, perhaps even as high as the cubic power.

At 2m/s it is easy to measure drag as the tension in a strain-gauged tow bar. At this speed, unwanted drag components such as aerodynamic and lift-air momentum drag are negligible compared with skirt interference drag. At higher speeds, these unwanted components may exceed the interference drag, and while they are calculable and can be subtracted from the total drag, the resulting accuracy of measurement of the interference drag is decreased.

When the drag is measured by tow-bar pull, the aerodynamic wake of the towing vehicle reduces the aerodynamic drag of the towed ACV by an undetermined but possibly large amount, depending on velocity. This could be minimized by towing with a long (30 m) nylon rope, but the effect would still be present to some extent and deceleration could become hazardous, owing to the ACV over-running the tow truck. Thus, this towing procedure was abandoned at over 6 m/s.

Higher speed measurements were made by self-propelling the hovercraft up to maximum speed, and then measuring its free deceleration along a course with markers at 5 m intervals. Analysis of 16 mm film shot from a distant point yielded a velocity/time history from which the total drag at any speed could be deduced, given the mass of the vehicle. Wind tunnel tests on an accurate scale model of the hovercraft and pilot defined the drag coefficient, so that aerodynamic drag could be calculated. The momentum drag was found from calibrated values of lift airflow. Slope drag was known from an accurate survey of the track. The remaining skirt/terrain interference drag was then found by subtraction. This method was not sufficiently accurate at low speeds, but this and the towed method showed good agreement of about 6 m/s. Data from the towed method were therefore used below this speed, and from the deceleration experiments at above 6 m/s.

The results of a series of experiments with hovercraft HEX-5 over a concrete runway, as presented in Figure 11.15, are related to the rise height versus EGH curve of Figure 11.16, which was extracted from Figures 11.11 and 11.13. Figure 11.16 shows the rise of the vehicle above the concrete surface as a function of increasing EGH (or airflow, which is proportional to EGH). The rise was rapid as the skirt unfolded up to 22 cm, at which point the skirt hem was just touching the ground. After this, the rise was slow because an actual gap opened to allow air to blow out freely. Points A, B and C in this figure correspond to the three runs of Figure 11.15, making it possible to gain some insight into the speed/drag characteristics.

On run A, where there were some 4 centimeters of skirt in contact with the concrete, the skirt interference drag rose steeply with speed. On run C, where there was a definite air gap of some 2-3 mm, the skirt drag appeared to be independent of speed, and was in fact probably not due to actual interference at all. Run B, with a gap of 1.2 mm, was an intermediate case. It must be realized that, with gaps of this order, the slightest pitch (even if only 1/10 degree or so), causes skirt contact at bow or stern. Therefore, before very large gaps were attained at considerable lift airflows, there was likely to be some interference and consequent rise of drag with speed. It must be noted that these experiments took place over bare concrete, so that the bush-bashing component of drag could be neglected. If this component were present, it is suggested that a characteristic more like A would be observed.

11.10 SUMMARY

Two research vehicles used for drag studies were described. Four general hover regimes were defined and experimentally verified: free hover, interference, partial sled and full sled. A mathematical model of lift airflow showed that it is proportional to a parameter called *efflux gap height* (EGH), which contains a factor representing terrain porosity. The skirt/terrain

interaction drag-force was expressed as a percentage of vehicle weight. Experimental results were presented to determine the effects of various terrains and vegetation on the EGH and skirt drag. The experimental surfaces included concrete, snow, crushed rock, and various grass types and lengths. An attempt was made to determine the porosity of these surfaces. The so-called *bush-bashing* phenomenon was examined. It was found that skirt drag is reduced as a function of the number of passes over a given path. Observations indicated that skirt drag and wear are strongly dependent on vehicle speed whenever the skirt is in contact with the terrain.

Thus, in this chapter, an account was given of a study of the lift air requirements of low-speed hovercraft operating over various terrains and vegetation. The approach was essentially empirical and there is room for further work in this area. However, the results presented can serve as a guide to development engineers, designers and specification writers in determining a vehicle's required lift-air capacity as a function of the intended speeds and terrains of operation.

11.11 REFERENCES

1. H.S. Fowler, The ACV as a load spreading device, Journal of Terramechanics, Vol. 12, No. 2, 1975, pp. 43-53.
2. H.S. Fowler, On the lift-air requirement of air cushion vehicles and its relation to the terrain and operational mode, Report ME-246 (NRC No. 17492), Division of Mechanical Engineering, National Research Council Canada, Ottawa, Canada, May 1979.

Chapter 12

SKIRT MATERIAL PROPERTIES AND THEIR EFFECTS ON DYNAMICS

12.1 INTRODUCTION

The choice of material to be used in the skirt system of an air cushion vehicle (ACV) can play a large role in determining the craft dynamics. This is graphically illustrated in Figs. 12.1 and 12.2, which give the angular response history of a 1.22 m by 2.44 m planform laboratory model (ref. 1) to the removal of an applied moment. In both cases the model was equipped with an uncompartmented segmented skirt air cushion, Fig. 12.3(c). However, the materials used in skirt construction were different. One was a thin polyethylene film; the other was a light-weight tent fabric made of urethane-coated nylon. The angular motion histories for the polyethylene skirt, given in Fig. 12.1, show oscillations which decrease in amplitude with time. In contrast, the angular motion histories for the nylon-urethane skirt, Fig. 12.2, show a more slowly decaying oscillation for the small initial angle test and a growing oscillation for the large initial angle test. Figure 12.4 shows the static stiffness relations for the same model and the same two skirts. These curves show that when surface contact occurs an increased moment is required during the load increasing portion of the curve over the load decreasing portion of the curve, i.e., there is hysteresis in the stiffness characteristic. This hysteresis represents an energy loss which is proportional to the enclosed area. Since the area enclosed by the polyethylene characteristic is much larger than that enclosed by the nylon-urethane, much more energy is dissipated with the polyethylene skirt. Hysteresis is also present in the static stiffness relations recorded for models with different skirt systems and for full scale vehicles (refs. 2-8). Full-scale dynamic hysteresis effects have not been documented in the open literature. In addition to hysteresis effects, dynamic response is

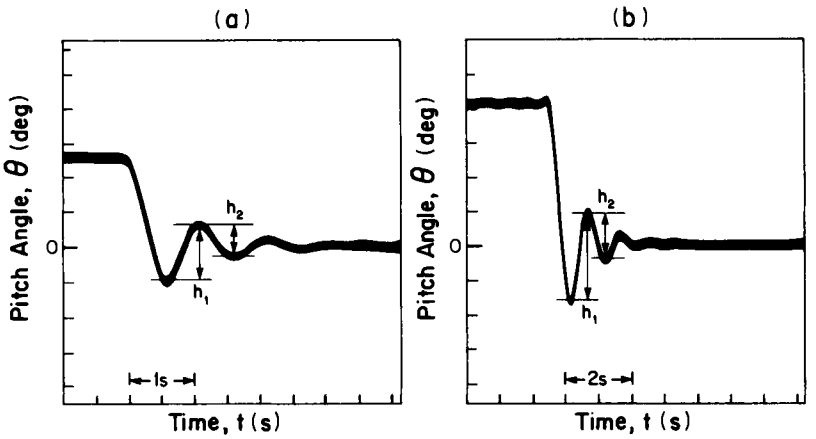

Fig. 12.1 Pitch response to initial disturbance of UTIAS 2.44 m × 1.22 m laboratory model with 0.13 mm polyethylene segmented skirt, W = 416N and θ_e = 0.0°: (a) C_{QC} = 0.01335, θ_0 = 2.6°, h_2/h_1 = 0.54; (b) C_{QC} = 0.011 θ_0 = 4.0°, h_2/h_1 = 0.53. (Adapted from ref. 5.)

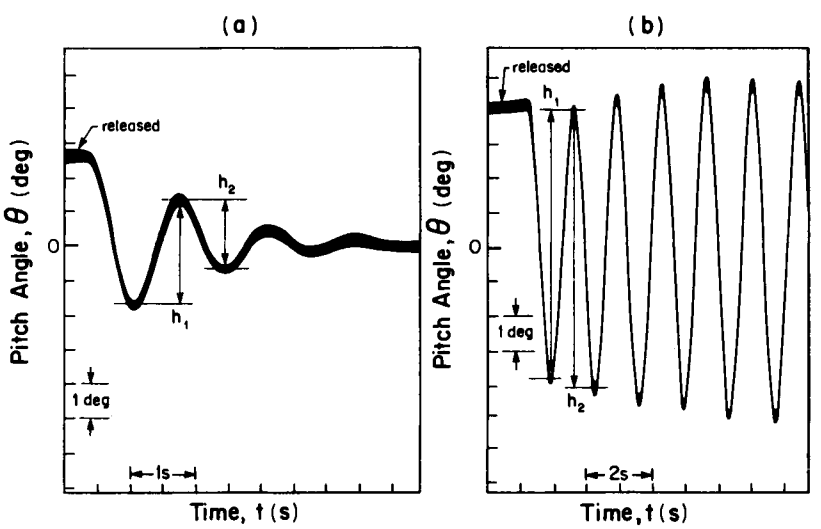

Fig. 12.2 Pitch response to initial disturbance of UTIAS 2.44 m × 1.22 m laboratory model with 0.10 mm nylon-urethane segmented skirt, W = 416N and θ_e = 0.0°: (a) C_{QC} = 0.01335, θ_0 = 2.6°, h_2/h_1 = 0.66; (b) C_{QC} = 0.01164, θ_0 = 4.0°, h_2/h_1 = 1.05. (Adapted from ref.5.)

affected by skirt-material extensibility (refs. 9-11). Because of their potential for producing large effects on vehicle dynamics, skirt-material properties must be understood insofar as they affect the action of the skirt as a suspension-system element.

The ACV flexible skirt may be viewed as a leaky container for the cushion of air which supports the craft. The skirt deforms to allow the craft to pass over surface irregularities but keeps the cushion's exit-airflow area small, so that lift-power requirements are minimized. This interaction with the lift-system airflow, and additional forces which arise from skirt-surface contact, provide the vehicle stiffness and stability mechanisms which determine the craft response to static and dynamic disturbances. The relationship between the skirt system and craft dynamics is shown in the block diagram of Fig. 12.5. It indicates that the skirt system is a feedback mechanism through which changes in the vehicle response vector are converted to changes in skirt shape and restoring forces. Three mechanisms cause these changes: (1) geometric shape changes resulting from pressure changes or ground contact; here distances on the skirt material surface remain the same but the relative positions of points on the surface are different, (2) changes due to skirt material extensibility, and (3) skirt structural forces arising from contact with the surface.

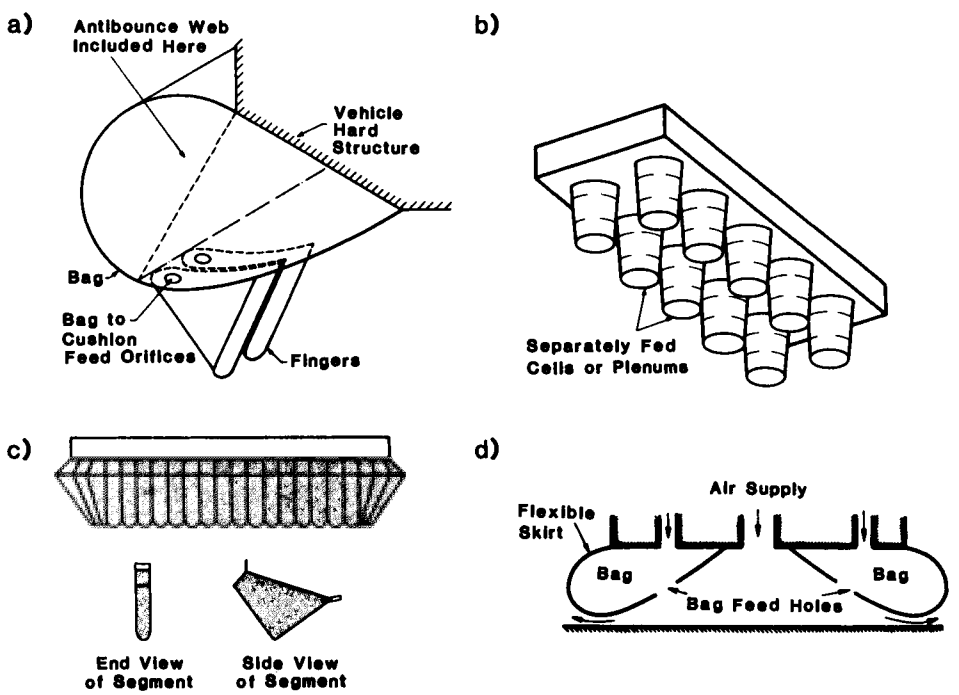

Fig. 12.3 Skirt designs: (a) bag and finger; (b) multicell; (c) segmented skirt; (d) bag or trunk skirt. (Reproduced from refs. 12, 5 and 45 with permission of AIAA, CASI and UTIAS.)

The first two mechanisms produce force changes indirectly by modifying the cushion volume, the projection of this volume on the surface or "footprint" area, the cushion-exit-airflow or "leakage" area, and the centre of pressure location which is a factor in the restoring moment. The third mechanism directly produces forces and moments which can cause hysteresis and thereby influence system damping (ref. 1, Chapter 4). These mechanisms are present to varying degrees in the dynamics of any given ACV.

Analyses of skirt systems often use an "ideal" skirt material assumption. This ideal material is a massless, inextensible, and perfectly flexible membrane. A skirt system made from this ideal material influences the dynamics

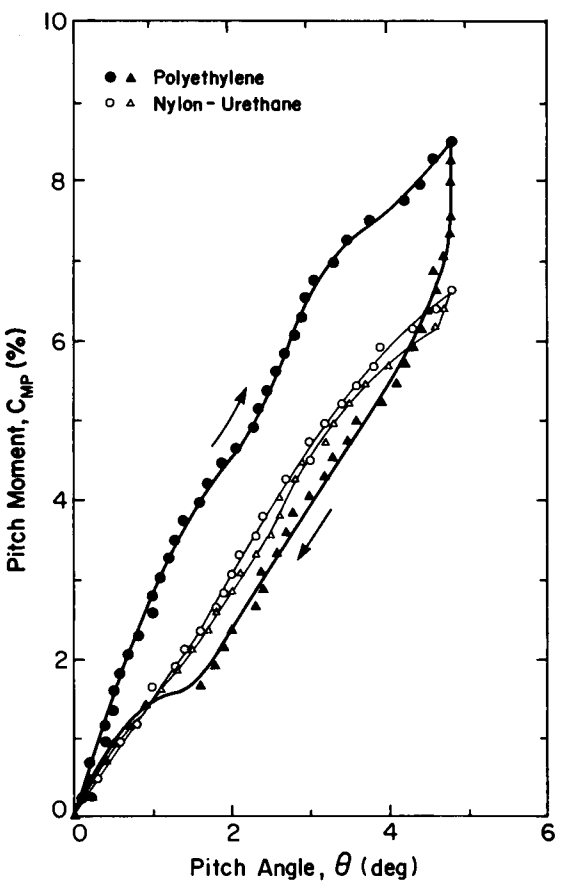

Fig. 12.4 Experimental static pitch stiffness characteristics for 0.13 mm polyethylene and 0.10 mm nylon-urethane segmented skirt systems on the UTIAS 2.44 m × 1.22 m laboratory model. Operating conditions: W = 511.7N, C_{QC} = 0.0075, C_{PC} = 0.012, C_{SC} = ∞, C_{SW} = 0.0067 (polyethylene), C_{SW} = 0.0043 (nylon-urethane). (Adapted from ref. 2.)

only through the geometric shape change mechanism cited earlier. The ideal skirt material does not stretch or shrink in response to pressure fluctuations and cannot sustain compressive structural loads since it is perfectly flexible. Analyses of cushion systems based on the ideal skirt material assumption are presented by various authors (refs. 1, 8, 12-14). In refs. 1 and 8, the analyses are compared with static stiffness experiments. It is found that in the absence of skirt surface contact reasonable agreement is obtained whereas, when contact occurs, material dependent differences occur. Ma and Sullivan investigated the linearized dynamic response of the bag and finger skirt system shown in Fig. 12.3(a) (Chapter 13 and ref. 12). They concluded that skirt system mass is an important parameter at higher frequencies, near the skirt bounce frequency, and that the extensibility of the bag is not an important factor in determining skirt system and skirt-cushion system response. Other authors (refs. 2, 9, 10) have used linearized models to study conical cell and tracked air cushion skirt designs and found the material extensibility to be an important factor affecting vehicle stability and damping. Investigations of nonlinear cushion dynamics invariably include skirt-surface contact and, although full-scale data is limited and mainly confined to statics (refs. 2-5), model results indicate that skirt structural forces and frictional forces can be important factors in vehicle response (refs. 1, 2, 5-7). Thus the applicability of the ideal skirt material assumption depends on several factors: the

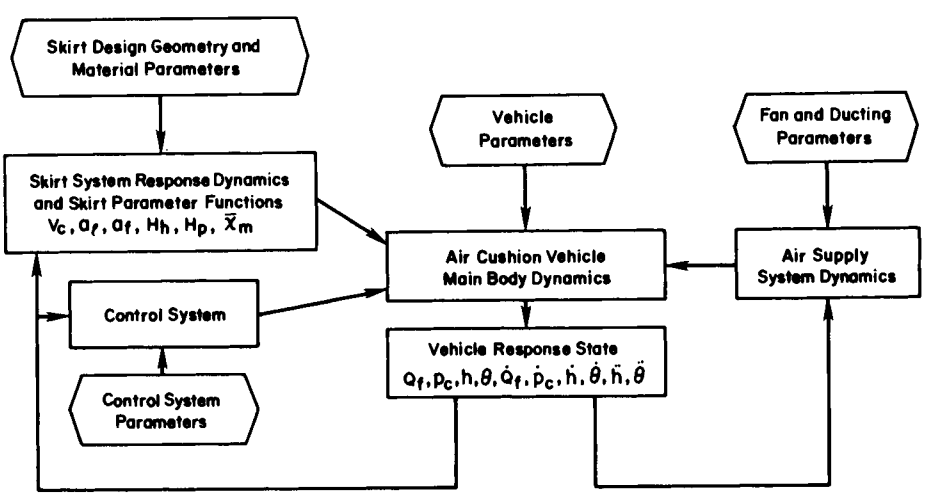

Fig. 12.5 Block diagram for pitch-heave motion of an ACV over a fixed-position surface.

type of dynamics problem being studied, for example static or dynamic, linear or nonlinear, the frequency and amplitude range of inputs, the skirt system design geometry, and the design and construction of the skirt material itself. In practice certain aspects of the skirt behaviour may be modelled using the ideal material concept while others require real material properties. For example, Boghani et al. (ref. 15) used the ideal material model to account for geometric shape changes along the side portions of an air cushion landing-system trunk, but included material damping due to the skirt material's flexural energy dissipation during skirt-surface contact.

The skirt is a structure which is inflated to deployed shape by the action of cushion and bag pressures. Its constituent materials operate at the surface-air interface and are subject to complex static and dynamic loading by high speed operation over water, land, marsh or ice. The skirt material experiences static and dynamic pressure forces and internal forces resulting from vibrations induced by air flow and constant beating against the surface, as well as contact forces from abrasion, drag and impact with unexpected obstructions (refs. 3, 15). These factors pose tremendous problems for material designers and combine to determine most of the design parameters of practical skirt materials, as discussed in Chapter 10. Under these conditions, the dynamicist is left with little say in skirt material design and must work to determine the implications of "real" skirt-material properties on the dynamics.

The properties of real skirt materials can differ significantly from the ideal. In particular these materials have mass, and are usually viscoelastic; that is, they exhibit tensile strength and stiffness properties which depend on time, stress and strain rate, and temperature. This implies that in addition to stored elastic energy the materials dissipate energy when subjected to time varying loads, even those of very low frequency. From the vehicle dynamics point of view this energy loss represents damping, which is usually manifested as hysteresis in vehicle stiffness curves.

Skirt materials usually consist of a woven fabric scrim coated on both sides with an elastomer, as shown in Fig. 12.6. The scrim provides most of the strength and stiffness of the material and consequently the material exhibits anisotropic stiffness properties. The anisotropic stiffness implies that the amount the material stretches under a given load depends on the direction in which it is stretched. For example, a regular rectangular weave fabric might have different size (denier) fibres in the warp and fill directions, thereby causing the stiffness in these directions to be different. In the 45° direction, between warp and fill directions, very little stiffness is provided by the scrim; the weaker elastomer coating provides most of the resisting force. These differences in stiffness can have a large influence on the dynamics (refs. 2, 9). Figure 12.7 gives heave stability results for a duct-plenum

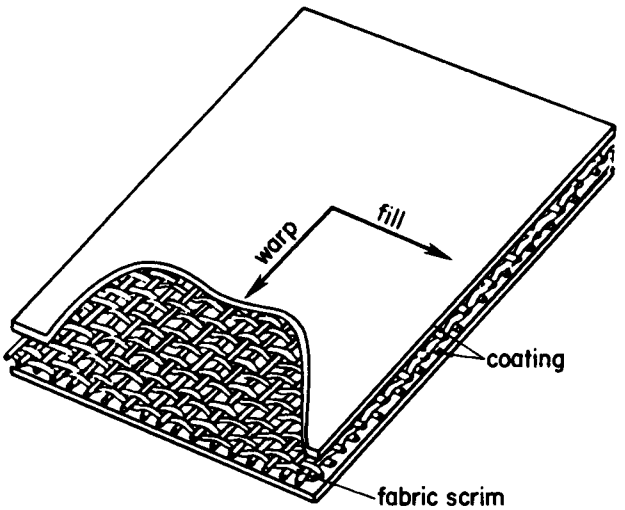

Fig. 12.6 Coated woven fabric. (Adapted from ref. 26.)

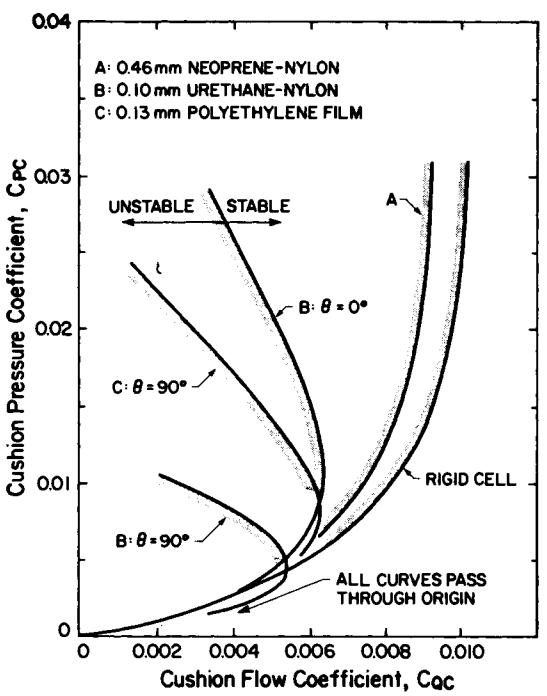

Fig. 12.7 Predicted dynamic heave stability boundaries for duct plenum system with single conical cell skirt and several materials. θ = material orientation relative to hoop direction, D_p = 0.467 m, L_D = 1.7 m and $h_e/D_p \simeq C_{QC}/2.4$. (Adapted from ref. 9.)

system equipped with conical cell skirts of various materials. The results are presented in terms of two parameters of operational importance: the cushion pressure as a fraction of atmospheric pressure, C_{PC}, and a nondimensional cushion flow coefficient, C_{QC}. Notice the curves in which the warp (0°) and fill (90°) directions on material B are aligned with the cone hoop direction.

The foregoing has indicated that, at least at model scale, the type of skirt material used can influence vehicle statics and dynamics strongly. Very little data from full scale craft is available to assess the importance of these effects as most skirt materials in use at any given time tend to be of similar weights and strengths. An assessment of the extent of these effects at full scale can be made only when the mechanisms are understood and suitable material tests defined. This chapter explains some of the physical mechanisms involved in models of up to approximately 2 m by 4 m planform, but with regard to full scale implications where possible.

12.2 MECHANICAL PROPERTIES OF SKIRT MATERIALS

When the ideal material model is not adequate the dynamics engineer is presented with the task of obtaining the simplest characterization of the material which will give the required accuracy in the simulations. The polymer and rubber materials used have stiffness and strength properties which can be temperature, rate and time dependent, anisotropic or orthotropic, highly nonlinear, and load-history dependent (refs. 17-20). The study of these materials comes under the branch of rheology known as viscoelasticity. As the name suggests, their mechanical behaviour can be modelled using elastic and viscous elements, i.e., springs and dashpots, which may or may not behave linearly. These concepts can be used to explain observed behaviour.

12.2.1 Viscoelastic Behaviour and Modelling Techniques

Viscoelastic material properties are complex functions of time, temperature, and the average state of stress and strain. These dependencies can be manifested as: (1) creep, an increase in strain following initial loading, (2) stress relaxation, a decrease in load levels following a strain input, (3) dynamic moduli, stiffnesses which are a function of loading frequency or rate, and (4) the presence of at least one transition involving a large change in stiffness over a narrow temperature range.

One way to understand viscoelastic behaviour is through the material response to various tests. Several methods exist and they may be broadly characterized as either static or dynamic. Static tests are either of the creep or stress relaxation type and are performed at constant temperature. Considering tensile tests for the moment, the simplest version of a creep test is a sample hung from a support with a weight on the lower end. The extension of the sample is then measured against time. An illustration of a simple apparatus and a

representative output are shown in Fig. 12.8. In stress relaxation experiments a given fixed strain is quickly imposed on the sample and the resulting stress history is measured. A simple apparatus for this type of test and a typical output are illustrated in Fig. 12.9. Note that the apparatus depicted in Figs. 12.8 and 12.9 are very crude and will give imprecise results.

In the simple creep test outlined above the output which is obtained is the creep compliance:

$$D(t) = \epsilon(t)/\sigma_0 \tag{12.1}$$

where $\epsilon(t)$ is the measured strain and σ_0 is the imposed constant stress. In the stress relaxation experiment the output is the tensile stress relaxation modulus

$$E(t) = \sigma(t)/\epsilon_0 \tag{12.2}$$

where $\sigma(t)$ is the measured stress and ϵ_0 is the constant strain input.

Unlike the elastic case the compliance and modulus are not reciprocals of one another, i.e.,

$$E(t) = \sigma(t)/\epsilon_0 \neq \sigma_0/\epsilon(t) = 1/D(t) \tag{12.3}$$

Consider two identical samples; one is subjected to creep test with a constant uniaxial stress, σ_a, for a time interval, t_p. The resulting strain, $\epsilon(t_p)$, is measured and applied as a step input to the second sample for a stress relaxation test. The stress is monitored and its value, $\sigma_b(t_p)$, is recorded at time

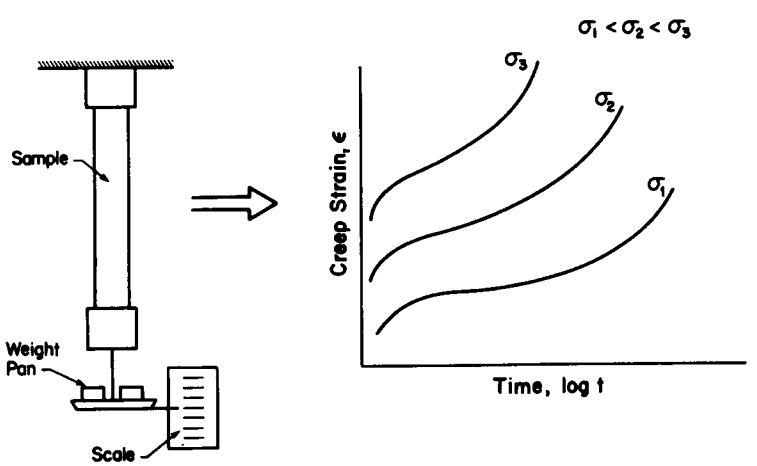

Fig. 12.8 Simple creep test apparatus and typical strain variation with time.

t_p. In general σ_a and $\sigma_b(t_p)$ will be different with the stress from the stress relaxation test, $\sigma_b(t_p)$, being lower (ref. 12.18). Since the strains are identical the modulus values, $E_a = \sigma_a/\epsilon(t_p)$ and $E_b = \sigma_b(t_p)/\epsilon(t_p)$, are different. Thus the test method must be stated so that parameter values such as modulus or compliance can be correctly interpreted. Stress relaxation and creep compliance data can be related to each other using Laplace transform techniques (refs. 18, 19).

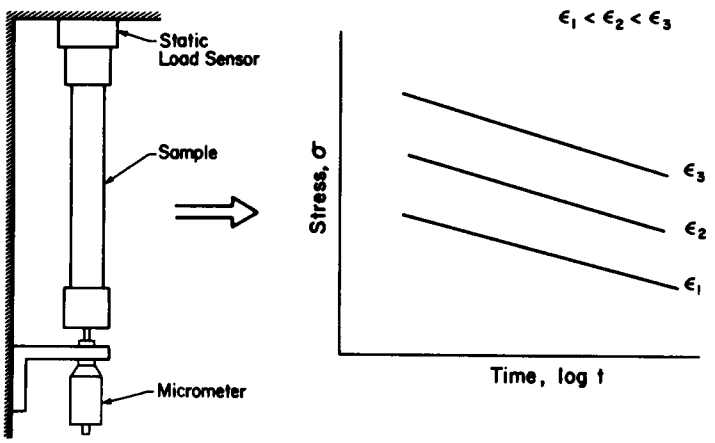

Fig. 12.9 Simple stress relaxation test apparatus and typical stress variation with time.

The general shape of the stress relaxation modulus versus temperature curve is shown in Fig. 12.10. Note the existence of a high modulus region referred to as the "glassy" region, a region where the modulus changes rapidly or

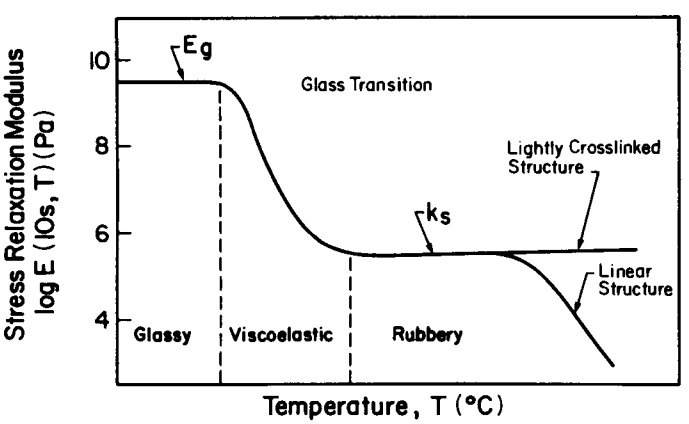

Fig. 12.10 Idealized stress relaxation modulus variation with temperature at 10s elapsed time. (Adapted from ref. 18.)

"transition" region, and a region of low modulus called the "rubbery" region. Some texts refer to a flow region at higher temperatures where the behaviour differs with chemical structure; however, the ultimate result in both cases is a decrease in modulus due to chemical degradation or melting of the material. For present purposes only three temperature regions of behaviour are discussed because it is sufficient here to combine the rubbery and high temperature regions mentioned above into a single "rubbery" region.

The modulus of a polymer at a constant temperature varies widely with the testing time elapsed before the modulus measurement is taken. This is illustrated in Fig. 12.11. Note again the presence of a glassy region, a transition region which may cover several decades of time, and a rubbery region as seen in the modulus-temperature relationship. It is possible to arrive at a time-temperature correspondence relationship when obtaining a full characterization of a material. This is called time-temperature superposition and is described in most texts on the subject (refs. 18, 19).

If an oscillatory stress or strain function with angular frequency ω is used as the input, a dynamic modulus is obtained which is a function of frequency as opposed to time. To understand this more fully consider three specimens which undergo a sinusoidal tensile strain input. The first is an elastic rod, the second a purely viscous element, and the third a viscoelastic element. In the elastic element the modulus, E, is constant and we have

$$\epsilon(t) = \epsilon_0 \sin\omega t = \sigma(t)/E \tag{12.4}$$

In the pure viscous case we have

$$\dot{\epsilon}(t) = \sigma(t)/\eta \tag{12.5}$$

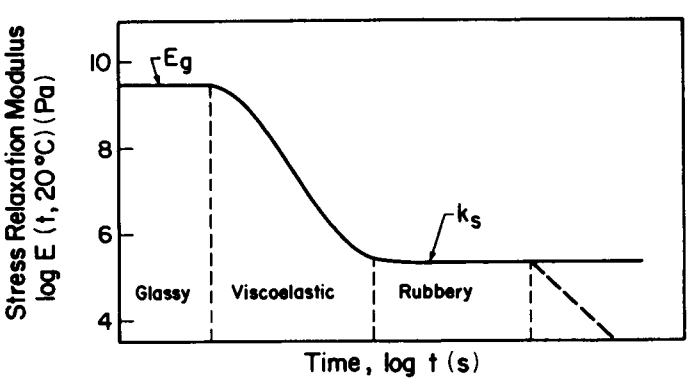

Fig. 12.11 Idealized stress relaxation modulus variation with time at 20°C. (Adapted from ref. 19.)

where η is the viscous constant. For the same sinusoidal input this gives

$$\omega\eta\epsilon_0\cos\omega t = \sigma(t) \tag{12.6}$$

which shows that the viscous stress leads the strain by 90°. For the visco-elastic material the stress will lead the strain by some angle between 0° and 90°. It is often convenient to decompose the stress into its "in-phase" and "out-of-phase" components. This is shown in Fig. 12.12. If the modulus value obtained from the in-phase stress component is referred to as E_1 and that obtained from the out-of-phase component is referred to as E_2 we have

$$E_1 = \sigma_1/\epsilon_0 \tag{12.7a}$$
$$E_2 = \sigma_2/\epsilon_0 \tag{12.7b}$$

where σ_1 and σ_2 are the in-phase and out-of-phase components of the stress vector. Similarly the strain decomposes to give the compliance components

$$D_1 = \epsilon_1/\sigma_0 \tag{12.8a}$$
$$D_2 = \epsilon_2/\sigma_0 \tag{12.8b}$$

If the angle between the stress and strain is δ then, from Fig. 12.12,

$$\tan\delta = \sigma_2/\sigma_1 = \epsilon_2/\epsilon_1 = E_2/E_1 = D_2/D_1 \tag{12.9}$$

where $\tan\delta$ is called the loss tangent and δ the loss angle. This is because the out-of-phase components are associated with the viscous action of the material and are hence related to the energy loss. The in-phase components are associated with the elastic or stored energy. This leads in a straight-forward

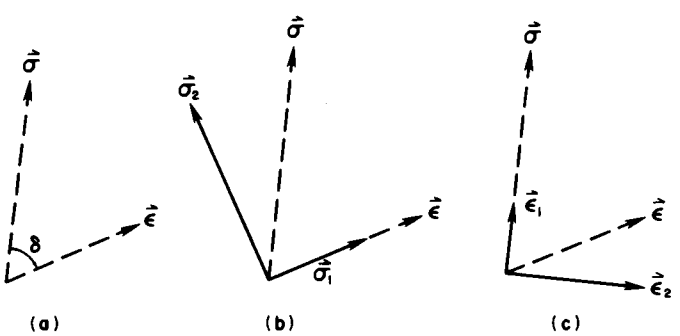

Fig. 12.12 Dynamic test stress-strain relationships. (a) Stress and strain vectors in a dynamic test. (b) Stress decomposed. (c) Strain decomposed. (Adapted from ref. 19.)

manner to the introduction of such terms as loss modulus and the elastic or storage modulus.

The two-component nature of the modulus lends itself to complex variable formulation. Thus, the complex modulus is

$$E^* = E_1 + iE_2 \tag{12.10}$$

and the complex compliance is

$$D^* = D_1 + iD_2 \tag{12.11}$$

Similar relations to the above are found for the complex shear modulus and shear compliance. Representative frequency dependence for the complex modulus is given in Fig. 12.13.

Static and dynamic testing is performed at constant temperatures and the tests are often repeated at different temperatures in order to produce a time-temperature master curve. General methods for producing such a curve are given in refs. 19 and 20. Both static and dynamic tests are necessary to produce such a plot. The dynamic tests provide the data for short time periods, less than 100s, or equivalently the higher frequency ranges; the static tests provide the data for time periods greater than 1s and the equivalent low frequency range.

Two methods of approach have been used to model and study viscoelastic behaviour. The first is the phenomenological approach which treats the material as a continuum and uses combinations of springs and dashpots to model the

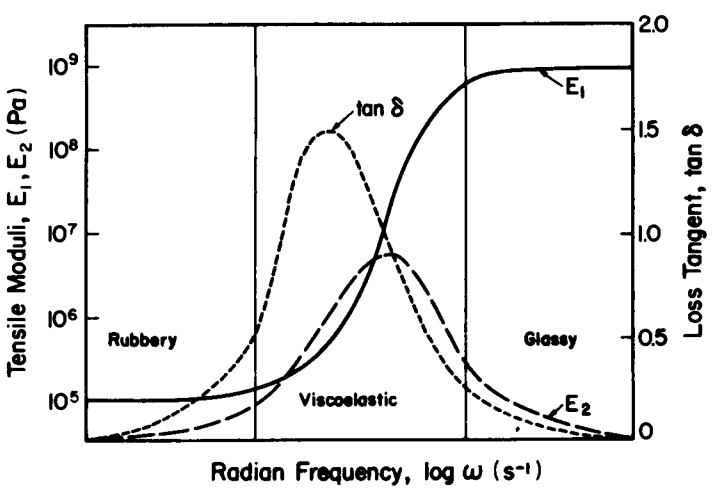

Fig. 12.13 Typical dynamic tensile moduli variations with frequency. (Adapted from ref. 18.)

macroscopic behaviour. The springs may be Hookean or nonlinear and the dashpots may be Newtonian or activated, that is, rate dependent. The second approach is from a chemical structure point of view. In this method the interactions of long chain molecules are studied and the macroscopic behaviour is predicted from a knowledge of the underlying chemical structures. Being concerned with macroscopic effects in air cushion skirt systems, the dynamics engineer uses the phenomenological approach. In keeping with the introductory nature of this work only linear models will be elucidated. Nonlinear viscoelasticity modelling is discussed by Ward (ref. 18).

The simplest models of viscoelastic behaviour contain only two elements, a massless Hookean spring and a Newtonian dashpot. These may be arranged in series as in the Maxwell model of Fig. 12.14(a), or in parallel as in the Voigt model of Fig. 12.14(b). The equation of motion of a Voigt element is

$$\sigma(t) = \epsilon(t)\, E + \eta\dot{\epsilon}(t) \tag{12.12}$$

which can be integrated in the case of a constant stress, i.e., creep test, to give

$$\epsilon(t) = (\sigma_0/E)(1 - e^{-(t/\tau)}) \tag{12.13}$$

where

$$\tau = \eta/E \tag{12.14}$$

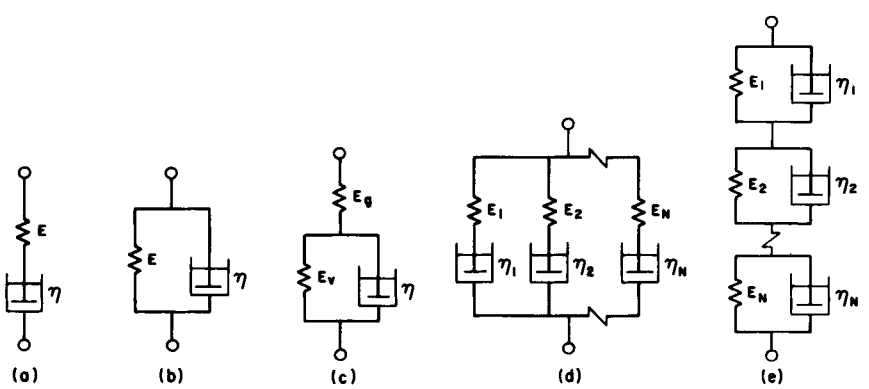

Fig. 12.14 Phenomenological models of viscoelastic behaviour; (a) Maxwell element; (b) Voigt element; (c) standard linear model; (d) Maxwell-Weichert model; (e) Voigt-Kelvin model.

is the relaxation time constant of the material. For long time periods the strain approaches a constant value

$$\epsilon(\infty) = \sigma_0/E \tag{12.15}$$

and a steady-state modulus may be obtained. It is apparent that the stress relaxation experiment could not be performed on a Voigt model since this would require infinite stress during the initial step input in strain. A sinusoidal strain loading can be expressed as

$$\epsilon(t) = \epsilon_0 e^{i\omega t} \tag{12.16}$$

Substituting this into the equation of motion gives

$$\sigma(t) = (E + i\omega\eta)\ \epsilon_0 e^{i\omega t} \tag{12.17}$$

This shows that the complex modulus is

$$E^* = E + i\omega\eta \tag{12.18}$$

and the loss tangent is

$$\tan\delta = E_2/E_1 = \omega\eta/E \tag{12.19}$$

There are obvious deficiencies present in the model. First the loss tangent is a linearly increasing function of frequency and, second, the elastic modulus is constant with frequency. The complex compliance of the Voigt model is evaluated as

$$D^* = \left[(1 + \omega^2\tau^2)E\right]^{-1} - i\omega\tau\left[(1 + \omega^2\tau^2)E\right]^{-1} \tag{12.20}$$

which is seen to give one transition when plotted against $\log\omega\tau$. Similarly the Maxwell model gives

$$\dot{\sigma}(t) + (E/\eta)\ \sigma(t) = E\dot{\epsilon}(t) \tag{12.21}$$

$$E^* = E\omega^2\eta^2/(E + \omega^2\eta^2) + iE\omega\eta/(E^2 + \omega^2\eta^2) \tag{12.22}$$

$$\tan\delta = 1/\omega\eta \tag{12.23}$$

and

$$D^* = (1/E) - (i/\eta\omega) \tag{12.24}$$

Thus the Maxwell model gives one transition in the modulus, shows a loss angle that decreases with frequency and has infinite compliance at zero frequency.

In general, materials will exhibit a number of minor transitions in addition to the major transition depicted in Figs. 12.8, 12.9 and 12.13. Thus, in order to fully describe a viscoelastic material at a given temperature, it is necessary to use series and parallel combinations of Voigt and Maxwell models, as shown in Fig. 12.14(d) and (e). An exact representation is possible only for an infinite number of components (refs. 18, 19). However, engineering accuracy can be obtained with a finite number of components, in which case the governing differential equation is of the form

$$\sum_{j=0}^{N} a_j \frac{d^j\sigma}{dt^j} = \sum_{j=0}^{N} b_j \frac{d^j\epsilon}{dt^j}, \qquad N < \infty \tag{12.25}$$

where a_j and b_j are combinations of the E_j and η_j.

If the material does not flow at long creep times the qualitative behaviour can be represented most simply by the standard linear model of Fig. 12.14(c). The governing equation of this model is

$$k_s\epsilon(t) + E_g\tau\dot{\epsilon}(t) = \sigma(t) + \tau\dot{\sigma}(t) \tag{12.26a}$$

where the static stiffness k_s and time constant τ are given by:

$$k_s = \frac{E_v E_g}{(E_v + E_g)} \tag{12.26b}$$

and

$$\tau = \frac{\eta}{E_v + E_g} \tag{12.26c}$$

The complex modulus is found by applying the Fourier transform to eqn. (12.26a), yielding:

$$(k_s + i\omega\tau E_g)\bar{\epsilon}(i\omega) = (1 + i\omega\tau)\bar{\sigma}(i\omega) \tag{12.27}$$

Thus, the complex modulus and loss tangent are given respectively by:

$$E^* = \bar{\sigma}(i\omega)/\bar{\epsilon}(i\omega) = \frac{k_s + E_g\omega^2\tau^2}{1 + \omega^2\tau^2} + i\,\frac{(E_g - k_s)\omega\tau}{1 + \omega^2\tau^2} \tag{12.28}$$

and

$$\tan\delta = \frac{(E_g - k_s)\omega\tau}{k_s + E_g\omega^2\tau^2} = \frac{E_g\omega\eta}{E_v(E_v + E_g) + \omega^2\eta^2} \tag{12.29}$$

The variation of the standard linear model's complex modulus with frequency is shown in Fig. 12.15. Comparing with Fig. 12.13, it is seen that the standard linear solid exhibits the two main transitions associated with viscoelastic behaviour.

A different perspective of viscoelastic behaviour can be obtained by using a series of stress relaxation times or creep retardation times. The analysis leading to these descriptions uses the Boltzmann superposition principle. The relaxation and retardation times can be calculated from the measured moduli and compliances using Fourier or Laplace transform techniques. An important point which arises from this type of description is that the current state of stress and strain in a sample is dependent upon the entire prior loading history. Since this can affect test results, it is necessary to allow sufficient time for the prior stresses and strains to decay to an insignificant level before proceeding with the next set of tests on a specimen. The techniques involved with this type of description are presented in refs. 17-20.

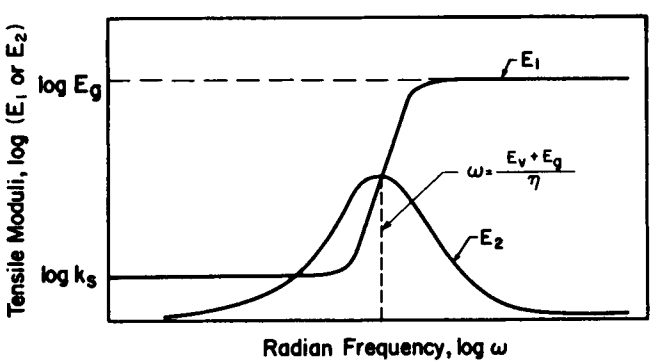

Fig. 12.15 Dynamic modulus variation with frequency for the standard linear model.

12.2.2 Additional Mechanical Properties

The typical skirt material is a composite construction of a woven fabric scrim coated with an elastomer. The fabric scrim is usually rectangularly woven although some materials have been developed using a triaxial weave (refs. 6, 21). The function of the scrim fibres is to provide strength and stiffness in tension. Therefore, the materials are much stiffer in the fibre

directions. This directional or anisotropic stiffness also affects the Poisson's ratio of the composite.

Consider the simple rectangular weave fabric shown in Fig. 12.6. Typical analysis assumes that the material is homogeneous with orthotropic properties. If the material is in a state of plane stress, the stiffness relationship is given by (refs. 22-24):

$$\begin{matrix} \sigma_1 \\ \sigma_2 \\ \tau_{12} \end{matrix} = \begin{matrix} Q_{11} & Q_{12} & 0 \\ Q_{21} & Q_{22} & 0 \\ 0 & 0 & 2Q_{66} \end{matrix} \begin{matrix} \epsilon_1 \\ \epsilon_2 \\ \gamma_{12}/2 \end{matrix} \tag{12.30}$$

where

$Q_{11} = E_{11}/(1 - \nu_{12}\nu_{21})$
$Q_{22} = E_{22}/(1 - \nu_{12}\nu_{21})$
$Q_{12} = \nu_{21}E_{11}/(1 - \nu_{21}\nu_{12}) = \nu_{12}E_{22}/(1 - \nu_{21}\nu_{12}) = Q_{21}$
$Q_{66} = G_{12}$
σ_1, σ_2 = tensile stress along fibre directions
τ_{12} = shear stress
ϵ_1, ϵ_2 = strain along fibre directions
γ_{12} = shear strain
ν_{12} = major Poisson's ratio
G_{12} = shear modulus
E_{11}, E_{22} = tensile modulus in fibre directions.

Note that ν_{21} may be determined from the symmetry of the stiffness matrix Q to be:

$$\nu_{21} = \nu_{12}E_{22}/E_{11} \tag{12.31}$$

This shows that, for orthotropic materials, the ratio of the Poisson's ratios corresponding to the fibre axis directions equals the ratio of the corresponding moduli. Thus, the $\nu < 0.5$ restriction of isotropic materials does not apply. In fact, for anisotropic materials, the sole restriction on Poisson's ratio is that the strain energy be positive (ref. 18). Also, the relation between the moduli and the major and minor Poisson's ratios shows that the Poisson's ratios remain constant with frequency if the moduli maintain a constant ratio. In this case, a static measurement of Poisson's ratio is sufficient.

The results of eqns. (12.30) and (12.31) were obtained assuming constant parameters but apply when moduli are time dependent as well (ref. 18). The matrix elements can also be strain dependent. Figure 12.6 shows that the fibres are bent over and under one another. Because of this, the material

properties are not as indicated by a straight fibre. Homogeneous polymer materials and straight fibre composites usually exhibit a decrease in their tensile moduli with an increase in mean stress (ref. 24), although subsequent hardening sometimes occurs at large strain values (ref. 20). This modulus decrease is illustrated in the stress relaxation data for polyethylene sheeting presented in Fig. 12.16. The tensile response of coated woven fabrics is usually characterized by a high initial stiffness at low stress levels, followed by a decrease in modulus as stress is increased, and then by a major section of increasing modulus as stress is increased further. The extent of the high initial stiffness region and its magnitude are determined by inelastic processes occurring during the initial loading (ref. 25) whereas the subsequent stiffening is due to fibres straightening under load (refs. 25, 26). The amount of subsequent stiffening in the warp direction can be markedly different from the fill direction as there may be a difference in the amount of bending of the fibres in the two directions. The stiffening observed with increasing stress is peculiar to woven materials. Texts devoted to conventional fibre layup composites (refs. 22-24) make no mention of this phenomenon. The oscillating test data of Fig. 12.17 show the modulus increase behaviour of a urethane-coated nylon fabric used in model tests. Data presented in ref. 27 shows typical nonlinear stiffness behaviour in the warp and fill directions of a full-scale material.

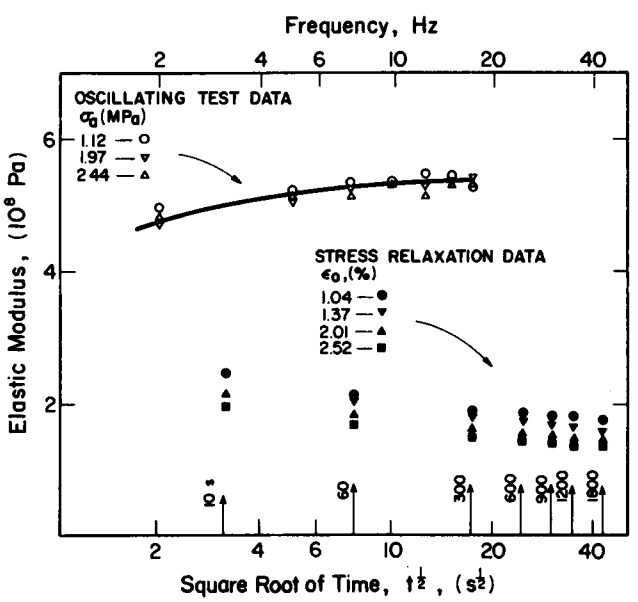

Fig. 12.16 Dynamic stiffness and stress relaxation data for 0.13 mm extruded polyethylene. (Adapted from ref. 9.)

Several other factors may influence skirt material mechanical properties. Included are interfibre friction, yarn debonding and slippage at the yarn/coating interface (refs. 25, 28, 29); they all produce hysteresis. Many composite materials exhibit a different modulus in tension from that in compression. The magnitude of the difference depends on the degree to which the reinforcing the reinforcing fibres can support compression. Although this does not affect most of the skirt, which is in tension due to internal pressure, it does affect it where local bending occurs during ground contact. Reference 30 shows that assuming similar modulus levels can lead to significant under-estimation of stress levels in the material. For typical full-scale skirt materials the modulus in tension can be tension 10 times that in compression because the fibres are very flexible and the compressive load is supported mainly by the coating. Lee et al. (ref. 6, p. 27) presented data for flexural damping constants obtained by observing decay rates of a material pendulum in a vacuum jar. This data showed that, for the coated fabrics tested, flexural damping factors were proportional to the thickness of the material. The material thickness was altered by increasing the amount of coating on the fabric, the fabric itself remained unchanged from one test to another. A dependence on the fabric material used for the scrim was observed also.

The mechanical properties of skirt materials are very complex and the task of modelling all the material properties in a simulation of ACV dynamics is

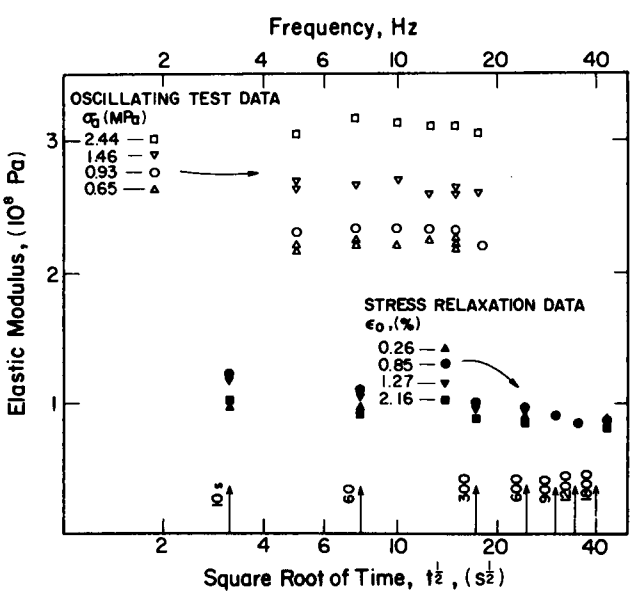

Fig. 12.17. Dynamic stiffness and stress relaxation data in fill direction for 0.10 mm urethane-coated nylon fabric. (Adapted from ref. 9.)

daunting. Complete models would require extensive material test programs to get the data. Furthermore, the large range of time constants involved in frequency effects, together with nonlinearities and temperature dependence, could result in the material properties taking up a major part of the simulation's computational load. Therefore, it is not feasible to include complete material models. Fortunately, the errors produced by simplified models which neglect some of the material structural effects may be negligible. The task of the dynamicist is to determine what material properties are important for the simulation desired. The following sections briefly introduce dynamic modelling and discuss materials-related dynamical effects and ways of obtaining simplified models.

12.3 VEHICLE PITCH–HEAVE DYNAMICS

12.3.1 Simplified Equations of Motion of a Single–Plenum Air Cushion

The hover equations of pitch-heave motion are derived for a single-plenum air cushion fed directly from a fan and operating over a hard surface as shown in Fig. 12.18. The fan is assumed to follow a quasisteady relationship of the form

$$p_f = p_0 + p_1 Q_f + p_2 Q_f^2 \tag{12.32}$$

where p_f is the fan pressure rise, Q_f is the volume flow through the fan, and p_0, p_1 and p_2 are the fan characteristic coefficients. It has been found that, except for large cushions, wave propagation effects inside the cushion are small and the pressure can be assumed uniform throughout (ref. 2, Appendix D, and ref. 31). Therefore, the unsteady compressible continuity equation for the cushion can be written:

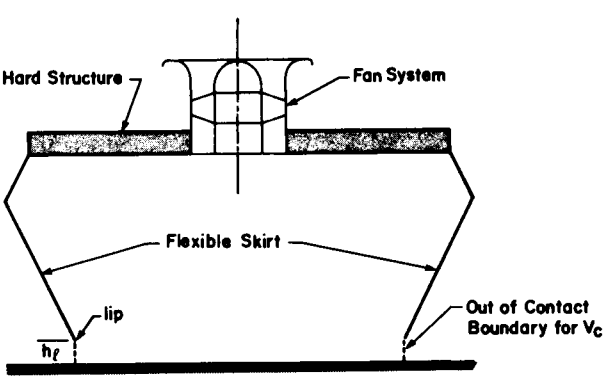

Fig. 12.18 Single-plenum air cushion.

$$\frac{d}{dt}(\rho_c V_c) = \dot{\rho}_c V_c + \rho_c \dot{V}_c = \rho_c Q_f - \rho_c Q_c \tag{12.33}$$

where ρ_c is the air density in the cushion, V_c is the cushion volume, and Q_c is the volume flow from the cushion to atmosphere. The air within the cushion is assumed to be compressible according to the polytropic equation of state:

$$P_c = K\rho_c^n \tag{12.34}$$

where P_c is the absolute pressure in the cushion, K is a constant and n is the polytropic constant describing the expansion process. Differentiating with respect to time:

$$\dot{\rho}_c = \dot{P}_c \rho_c / (nP_c) \tag{12.35}$$

Usually, isentropic compression is assumed so that $n = \gamma = 1.4$. Combining eqn. (12.35) with the perfect gas law, $P_c = \rho_c RT$, and noting that $\dot{P}_c = \dot{p}_c$ gives:

$$\dot{P}_c = \gamma RT\dot{\rho}_c = \dot{p}_c \tag{12.36}$$

where p_c is cushion gauge pressure, R is the gas constant for air and T is the absolute temperature of the cushion air. Since the actual changes in cushion pressure remain small relative to the absolute pressure the changes in absolute temperature are small and the temperature T is essentially constant. Substituting the expressions for ρ_c and $\dot{\rho}_c$ obtained from the perfect gas law and eqn. (12.36), respectively, into eqn. (12.33), we obtain:

$$\frac{V_c}{\rho_c \gamma RT}\dot{p}_c = Q_f - Q_c - \dot{V}_c \tag{12.37}$$

where $V_c/\rho_c\gamma RT = C_c$ is the lumped pneumatic capacitance of the cushion. In terms of the mass flow rates through the fan and from cushion to atmosphere, w_f and w_c respectively, eqn. (12.37) can be rewritten:

$$\dot{p}_c = \frac{\gamma RT}{V_c}(w_f - w_c) - \left[\frac{\gamma \dot{V}_c}{V_c}\right]p_c \tag{12.38}$$

The cushion volume depends on the craft's position relative to the surface and the pressure-dependent skirt-shape changes, including extensibility related and purely geometric changes. The surface compliance may also modify the volume.

The heave motion is described by newton,s law of motion,

$$m\ddot{h} = p_c a_f - mg + H_h - \xi_h \dot{h} \tag{12.39}$$

where m is the craft mass, h is the height of the craft centre of mass above datum, taken as positive upwards, a_f is the footprint area, g is the gravitational constant, H_h the heave hysteresis force resulting from skirt-surface contact, and ξ_h is a usually-negligible aerodynamic damping coefficient. In the absence of surface contact, H_h is zero. The footprint area a_f depends on the craft's position relative to surface and the cushion pressure.

The pitch motion of the craft is described by:

$$I_{yy}\ddot{\theta} = -p_c a_f \bar{x}_M - H_p - \xi_\theta \dot{\theta} + M_Q \tag{12.40}$$

where I_{yy} is the pitch moment of inertia, θ is the pitch angle, $\bar{x}_M$ is the horizontal distance from the centre of mass to the centre of pressure, that is, the moment arm, H_p is the pitch torque resulting from hysteresis forces produced during skirt-surface contact, ξ_θ is a damping coefficient which includes aerodynamic torque, and M_Q is a moment term arising from the momentum of escaping air. The ξ_θ and M_Q terms are usually small relative to the other terms and are normally ignored.

The cushion leakage flow Q_c is usually described by the quasisteady orifice-flow law:

$$Q_c = C_D a_\ell (2p_c/\rho_c)^{1/2} \tag{12.41}$$

where C_D is the flow discharge coefficient and a_ℓ is the leakage area for cushion exit flow. Results presented by Sullivan et al. (refs. 1, 11) indicate that this is a reasonable assumption, at least over a hard surface at vehicle motion frequencies.

In the preceding analysis, the flow system model has been greatly simplified over that which is often required. For example, the fan often discharges through a duct and/or a volume; therefore, equations describing the additional inertia and/or compressibility of the fluid may be required. Also, orifice losses, such as those from the bag to the cushion in a bag-and-finger skirt, may have to be described. The quasisteady fan law assumption is only adequate for steady flow or very low frequency dynamics since effects of air inertia in the fan, unsteady blade aerodynamics, and blade stall can lead to hysteresis in the fan characteristic, particularly during large pressure excursions where reverse flow can result. As indicated by Moran (ref. 32), these effects can be significant sources of system damping. Although several methods have been advanced to describe them (refs. 2, 15, 33-36), this is an area of current research.

These flow-related complexities have been left out of the model presented here since we are concentrating on skirt effects. The skirt design and material selection have an effect on the cushion volume, the footprint area, the

moment arm, the leakage area, the hysteresis functions in pitch and heave, and the flow discharge coefficient. Since the discharge coefficient is assumed constant for a given skirt design, it is not examined further here.

12.3.2 Relationship Between Material Properties and Skirt Parameter Functions

The skirt parameter functions are those elements of the system dynamics equations which are determined by the skirt response and geometry. They include V_c, a_f, a_ℓ, $\bar{x}_M$, H_h and H_p in the dynamics model described above. Each of these depends on the parameters of the skirt geometry description, e.g., the skirt length at the lip, L_s, the skirt width at the lip, B_s, the corner radii, R_s, the segment or finger angle to the plane of the skirt lip, ß, the trunk radius, R_t, etc. The nominal values of geometry parameters describe the skirt in its fully-deployed design shape but, because of the viscoelasticity of most skirt materials these parameters can be functions of skirt loads and loading rates. These loads and loading rates are defined by p_c, $\dot{p}_c$, h, $\dot{h}$, θ, and $\dot{\theta}$. However, when there is no surface contact, the skirt is fully deployed and the dependence of the loads on h, θ, $\dot{h}$ and $\dot{\theta}$ vanishes. Once the skirt is fully deployed, the additional loads which occur during slight contact are usually small, so that the overall change in geometry outside the contact area is small relative to the deployed geometry. The usual assumption made for skirt analysis is that outside the contact region the skirt retains its fully-deployed geometry, whereas in the contact region, the shape is determined by the condition that the skirt lies flat on the surface (refs. 1, 2, 13, 15, 37, 38). Thus, the overall geometry of the skirt is assumed to depend on p_c, $\dot{p}_c$ and the craft position relative to the surface, as defined by h and θ. A notable exception, analyzed in Chapter 13, is the tuck-under phenomenon in which contact forces are assumed large.

Under the above assumptions, the cushion volume function depends explicitly on h, θ, p_c and $\dot{p}_c$. If, in addition, the skirt material is assumed to be elastic and not viscoelastic, the $\dot{p}_c$ dependence drops out. Then eqn. (12.37) can be written as:

$$\left[\frac{V_c(h,\theta,p_c)}{\gamma RT p_c} + V_{c,p_c}(h,\theta,p_c)\right]\dot{p}_c = Q_f - C_D a_\ell(h,\theta,p_c)\left[\frac{2p_c}{\rho_c}\right]^{1/2} - V_{c,h}(h,\theta,p_c)\dot{h}$$

$$- V_{c,\theta}(h,\theta,p_c)\dot{\theta} \qquad (12.42)$$

where the notation $(\ )_{,x}$ is used for $\frac{\partial}{\partial x}(\ )$. The pressure dependence of the volume function is seen to be an addi;tional extensibility capacitance term. This has implications for the heave stability of a vehicle aqs discussed in the following section. Also note that the rate of change of volume with respect to heave, $V_{c,h}(h,\theta,p_c)$, is the footprint area function, $a_f(h,\theta,p_c)$. With a visco-

elastic material model it depends on $\dot{p}_c$ also. The moment arm function for this simple cushion depends on p_c and $\dot{p}_c$ to determine the undeformed shape and h and θ to determine area shape changes resulting from contact. The moment-arm function for a compartmented cushion would include extra pressure and pressure-rate terms for each compartment.

The leakage-area function depends on p_c and $\dot{p}_c$ to determine the deployed shape of the skirt and h and θ to determine the contact areas. Most analyses assume that cushion exit-flow is shut off in areas of skirt-surface contact. The leakage area thus determined consists of the area bounded by the surface and the lip of the cushion in areas where it is not touching the surface, and additional leakage areas which are not affected by skirt-surface contact, e.g., between fingers or segments, or in the plenum box. Christopher and Osburn (ref. 7) have suggested that a source of the observed heave hysteresis may be in gaps which form between fingers during decreasing heave and which do not close until a considerably larger heave height is attained on the return cycle. This mechanism would depend on the structural response of the fingers and on skirt material stiffness. Therefore, for a viscoelastic material, the heave and pitch rates would influence the response and the leakage area functional dependence would be $a_\ell = a_\ell(h, \theta, p_c, \dot{h}, \dot{\theta}, \dot{p}_c)$.

The heave and pitch hysteresis forces are direct structural forces arising from skirt-surface friction and the ability of the skirt to sustain compressive structural loads (refs. 2, 5, 6, 15). They are zero when there is no contact. Consider a portion of the skirt which is approaching a solid surface. Upon contact, the skirt must deform since it cannot pass through the surface. The deformation can take place through global phenomena such as bending, wrinkling, or buckling of the in-contact portion of the skirt, and/or through local bending phenomena initiated as a result of portions of the material bending through a large angle in the contact region. Because the skirt structure is thin-walled, its global bending stiffness depends on the product $E_c t_s$, where E_c is the elastic modulus of the material in compression and t_s is the thickness. The local deformation is essentially a plate-bending phemomenon in which the loads per unit length of material are proportional to Et_s^3 (refs. 2, 5, 39). Since the elastic modulus is usually rate-dependent, the hysteresis functions can also be expected to be rate-dependent, so that the functional dependence of the heave and pitch hysteresis functions is given by $H_h = H_h(h, \theta, p_c \dot{h}, \dot{\theta}, \dot{p}_c)$ and $H_p = H_p(h, \theta, p_c, \dot{h}, \dot{\theta}, \dot{p}_c)$, respectively. Friction can be an important component of pitch hysteresis (ref. 2, Appendix E), as seen in Fig. 12.19 where approximately 40% of the observed hysteresis for the polyethylene skirt is friction-related. The direct comparison was possible through the use of a low-friction rolling board, which could be either fixed or allowed to move freely with the craft during pitch or roll manoeuvres. The curve presented for the

nylon-urethane skirt in the same figure shows that friction had little or no effect on the stiffness hysteresis for that material. When friction is significant, the functional dependence of H_h and H_p includes a friction coefficient, k_f.

The previous paragraphs have discussed mechanisms which can cause hysteresis in ACV stiffness curves. Unfortunately very little information is available about the proportions which may be attributed to leakage area hysteresis, global bending or buckling hysteresis, local bending hysteresis, and friction related hysteresis. However recent work by Milligan, on a simple conical cell cushion with a polyethylene skirt (ref. 40), showed that the hysteresis force due solely to internal material losses is proportional to t_s. This supports the ideal of a global phenomenon governing the hysteresis.

When his results are scaled by $\lambda^{-1} = t_s(\text{full-scale})/t_s(\text{model})$ to the thickness and perimeter of material used on a 25 m diameter craft the skirt hysteresis force obtained is about 3% of the weight of the craft. This is comparable to results obtained from a full-scale craft equipped with a segmented skirt where, as seen in Fig. 12.20, hysteresis in the cushion pressure varies

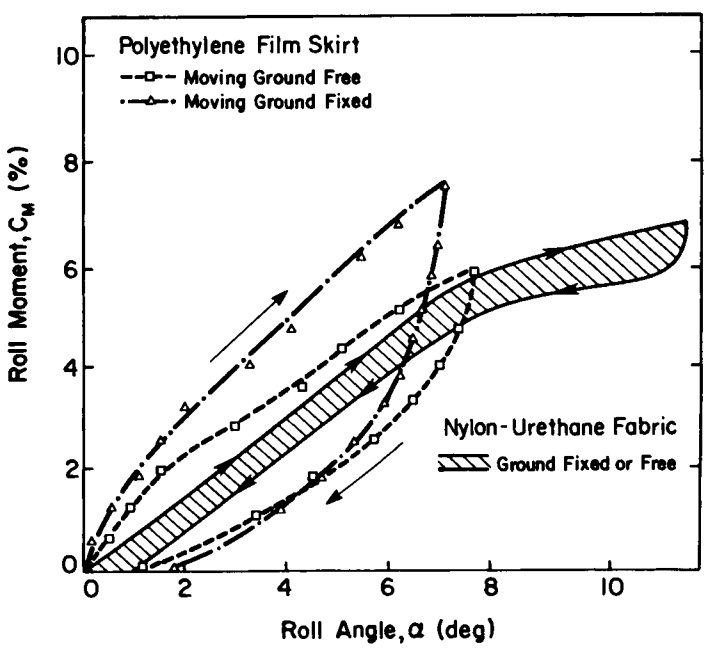

Fig. 12.19 Experimental roll stiffness characteristic for 0.13 mm polyethylene and 0.10 mm nylon-urethane segmented skirt systems on the UTIAS 2.44 m × 1.22 m laboratory model, showing the effect of skirt-table friction. W = 863N (194 lb), C_{QC} = 0.0082. Polyethylene: $C_{ST} = 9.57\times10^{-5}$, C_{SW} = 0.0040. Nylon-urethane: $C_{ST} = 8.32\times10^{-5}$, C_{SW} = 0.0026. (Adapted from ref. 5.)

from 1% to 4% during a heave cycle. However, the evidence is not yet conclusive that the internal material losses are the sole contributor to the cushion pressure hysteresis since the skirt materials are different and geometry differences between the cushions may have caused different mechanisms to be activated. For example, the leak-area hysteresis which may be present in the segmented skirt results of Fig. 12.20 was carefully eliminated from the conical skirt measurements.

12.4 SKIRT MATERIAL EFFECTS ON VEHICLE DYNAMICS

The ideas presented so far have been mainly conceptual in nature. The complex properties of skirt materials have been discussed together with their influence on some of the skirt's dynamical parameter functions. However, these functions would be difficult to implement if all the material and geometric properties of the skirt were to be taken into account. Consequently simplification is desirable and, fortunately usually possible.

The skirt effects can often be attributed to either the elastic or damping properties of the material. This separation is possible because the damping

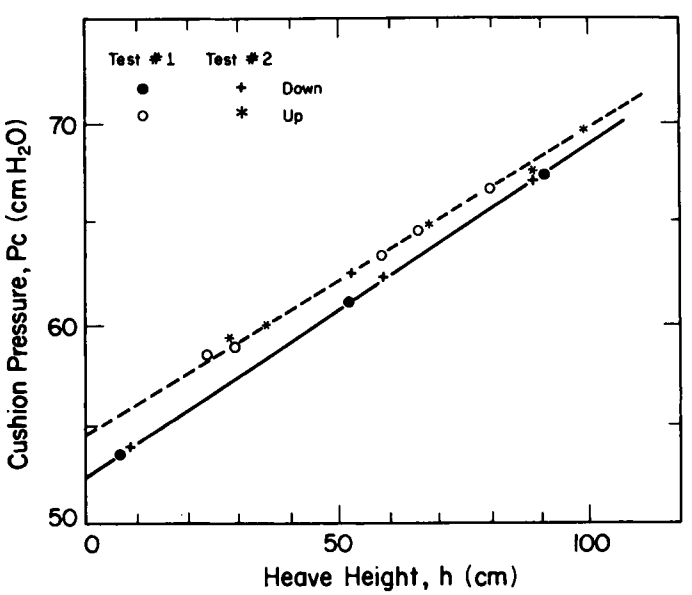

Fig. 12.20 Heave stiffness for the air cushion ice-breaking bow (ACIB) equipped with a segmented skirt. C_{SW} = 0.0056. (Adapted from ref. 5.)

effects due to losses associated with material extension are often small when there is no ground contact. The dynamicist can then etart asking questions such as: Are extension effects large or small relative to the skirt geometric response? Is the input frequency range small enough to treat the material storage modulus as a constant? Are pressure disturbances large enough to warrant a nonlinear stiffness model? Are the directional stiffness properties important? Similarly the damping aspects of the problem may be addressed by assessing the relative importance of hysteresis forces, pressure-related forces, and flow-system damping mechanisms to the modelling problem under study.

If the project is part of a development program which includes scale model testing, the above concerns must be applied to both the model and full-scale craft. The difficulties inherent in scaling criteria may dictate the need for a model-validated simulation which can then be run with full-scale parameters. Thus the simulation may have to include model-scale effects which could be unimportant at full-scale and vice versa.

The remainder of this section deals with some specific modelling challenges and the simplifications used. The focus is primarily on uncompartmented skirts with small geometric response. In this case, the importance of material extensibility and skirt-surface contact on stiffness characteristics is relatively large.

12.4.1 Extensibility Effects

The effects of material extensibility on cushion heave stability have been studied both theoretically and experimentally by Graham et al. (ref. 9). The University of Toronto Institute for Aerospace Studies' (UTIAS) sphere facility, described in Table 12.1, was used for the tests. The skirt system used was a single conical-cell element of a multicell cushion: a type which was used on an early version of the Bell Aerospace air-cushion equipment transporter (ref. 41). As shown in Fig. 12.21, air was supplied to the cushion through a duct connected to the cushion via a flexible bellows, which allows the cushion to move in heave. The duct inlet was in a large sphere which served to isolate the experiment from the fan so that the air supply dynamics of this system could be accurately modelled as a constant pressure source in series with an inlet loss and a lumped-inertance duct flow (ref. 36). A lumped-inertance duct model assumes that within the duct wave propagation effects are small and that the fluid acts as a single incompressible slug. The equation of motion is determined by balancing forces on the air slug:

$$\dot{Q}_d = \frac{A_d}{\rho_d L_d} \left[p_{di} - p_c\right] \tag{12.43}$$

where Q_d is the duct flow, A_d is the duct cross-sectional area, L_d is the duct

length and ρ_d is the air density in the duct. The pressure at the inlet, p_{di}, is determined from the quasisteady orifice law with inlet coefficient, C_{mi},

$$Q_d = C_{mi}A_d[2(p_s - p_{di})/\rho_d]^{1/2} \tag{12.44}$$

where p_s is the sphere pressure.

Hinchey had noted the existence of a flexibility effect on stability and found that static stiffness data for his material predicted a much larger boundary shift than obtained experimentally (ref. 36). For concial cells with the small taper angles studied, longitudinal stresses are typically 5% of the hoop stress value, or less. Based on this, a hoop-stress model of the skirt's radial deformation was developed. The longitudinal stress was assumed to be small enough for the skirt to remain conical in shape, except for a small region near the top (Fig. 12.22b). In the top region the material shape was approximated by a circular arc of radius $r_c = (D_{st}-D_{sto})/2$, where D_{st} and D_{sto} are the pressurized and unpressurized diameters of the top of the skirt respectively. The change in skirt height resulting from the longitudinal stress was expressed as an effective contraction ratio, ν_e, which multiplied the hoop length change (ref. 9). The contraction ratio is composed of the sum of three terms: the

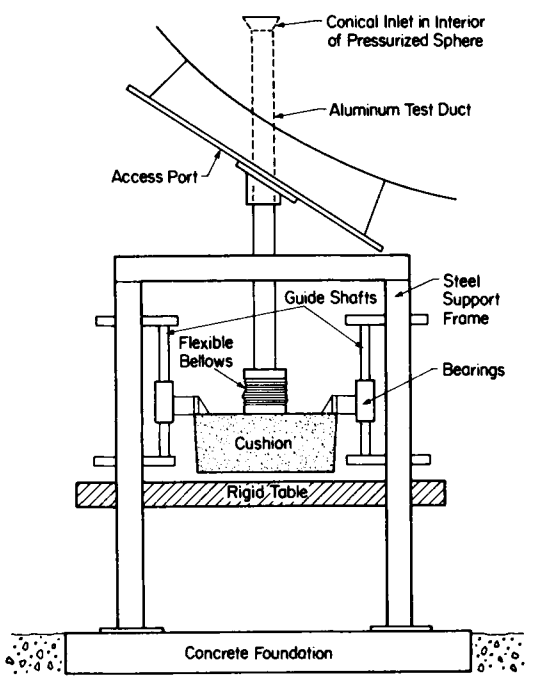

Fig. 12.21 Details of the UTIAS sphere facility experiment. (Reproduced from ref. 11 with permission of HBJ London Inc.)

normal material Poisson's ratio effect, ν_h, the effect due to the curvature at the top of the skirt, ν_c, and the effect of longitudinal stress, ν_ℓ, which is opposite in sign. With this deformation model three of the skirt parameter functions are affected: V_c, a_f and a_ℓ. The others, H_h and H_p, are zero since there is no skirt-surface contact.

The skirt parameter functions can be written in terms of the mean skirt diameter, D_{sm}, and the mean diameter to lip diameter ratio d_r. Then, the footprint and leak areas are respectively given by:

$$a_f(h, p_c) = \pi D_{sm}^2 d_r^2/4 \tag{12.45}$$

and

$$a_\ell(h, p_c) = \pi D_{sm} d_r (h - h_s) \tag{12.46}$$

where h is the height of the hard structure above the surface and h_s is the vertical height of the skirt. The volume is:

$$V_c(h, p_c) = \pi D_{sm}^2 \left[\left(h_s + \frac{h}{2}\right) \frac{d_r^2}{2} - h_s d_r + 2h_s\right] \tag{12.47}$$

which accounts for the conical shape. The two material-related factors, h_s and D_{sm}, remain; the former is determined from the unpressurized skirt height h_{so} and the hoop strain,

$$h_s = h_{so}(1 - \nu_e \epsilon^*) \tag{12.48}$$

where

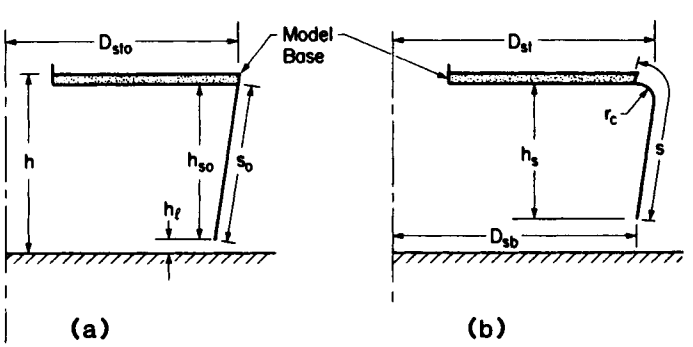

Fig. 12.22 Conical-cell skirt geometry: (a) unpressurized and undeformed; (b) pressurized and deformed. (Reproduced from ref. 9 with permission of AIAA.)

$$\epsilon^* = (D_{sm} - D_{smo})/D_{smo} \tag{12.49}$$

and the latter is determined from the material model and the mean hoop stress, neglecting end effects. The hoop stress

$$\sigma^* = p_c D_{sm}/(2t_s) \tag{12.50}$$

can be incorporated into the Voigt model, eqn. (12.12), to give, after some rearrangement:

$$\dot{D}_{sm}\eta = D_{sm}\left[\frac{p_c D_{smo}}{2t_s} - E\right] + ED_{smo} \tag{12.51}$$

If the standard linear model is used, substitution of eqns. (12.49) and (12.50) into eqns. (12.26) yields:

$$\eta \frac{d}{dt}\left[\frac{p_c D_{sm}}{2t_s E_g} - \epsilon^*\right] = E_v\epsilon^* - \left[1 + \frac{E_v}{E_g}\right]\frac{p_c D_{sm}}{2t_s} \tag{12.52}$$

The system formed from eqns. (12.37), (12.39), (12.41), (12.43)-(12.48) and the appropriate material model, i.e., eqn. (12.51) or (12.52), is linearized using a small perturbation analysis and grouped in matrix form $A\dot{\underset{\sim}{x}} = B\underset{\sim}{x}$. The stability of the system is determined directly from a computation of its eigenvalues.

The dynamic tensile properties of three skirt materials were characterized using stress relaxation and oscillatory tension tests. The materials were: (a) the polyethylene sheeting corresponding to the results of Fig. 12.16, (b) the nylon-urethane material for which results appear in Fig. 12.17, and (c) a 0.48 mm thick nylon-neoprene material. All these materials were much stiffer at the heave-instability frequencies than in static tests. The two coated woven-fabrics, i.e., nylon-urethane and nylon-neoprene, exhibited nonlinear stiffness characteristics in the stress range of interest. The loss angles were measured for the nylon-urethane and polyethylene materials over the frequency range of interest. For the nylon-urethane the loss angle was less than 1.5° throughout while for the polyethylene the loss angle decreased linearly from 7.5° at 2 Hz to 2° at 17 Hz. The stiffness and loss angle data for these materials are summarized in Table 12.2.

Experimental and theoretical results using two different duct lengths are shown for the nylon-urethane skirt in Fig. 12.23 and for the polyethylene skirt in Fig. 12.24. The cushion weight was fixed and the duct flow was adjusted experimentally by changing the sphere pressure, p_s. The stability or instability of a given operating point was determined by disturbing the cushion

slightly in heave and noting the decay or growth of the resulting oscillation. The duct flow was varied to find unstable and stable operating points in close proximity. The stability boundary was then found by interpolation. A standard linear model, fitted to the average of the tensile test data, was used for the polyethylene. The theoretical results for the nylon-urethane used: (a) a polynomial curve, fit to the static stress-strain data, to determine the equilibrium hoop-strain and skirt-deformation, and (b) a Voigt model with a variable E_v, again a function of stress, to represent the local dynamic stiffness. The experimental results for the nylon-urethane were found to be sensitive to the loading history and, therefore, the creep properties of the skirt. Good results were obtained with a test series which imitated the loading history used to determine the tensile properties. The discharge coefficient and ν_e were determined in a separate experiment.

The flexible skirt results of Figs. 12.23 and 12.24 include effects of skirt extensibility related changes in volume, footprint area, and leak area. The ideal skirt results, denoted as rigid skirt in Fig. 12.23, have none of these effects and show a marked difference in the qualitative nature of the boundary. In particular, the boundary does not curve back towards zero flow at higher pressures. The results of Fig. 12.25 show that the tendency to curve

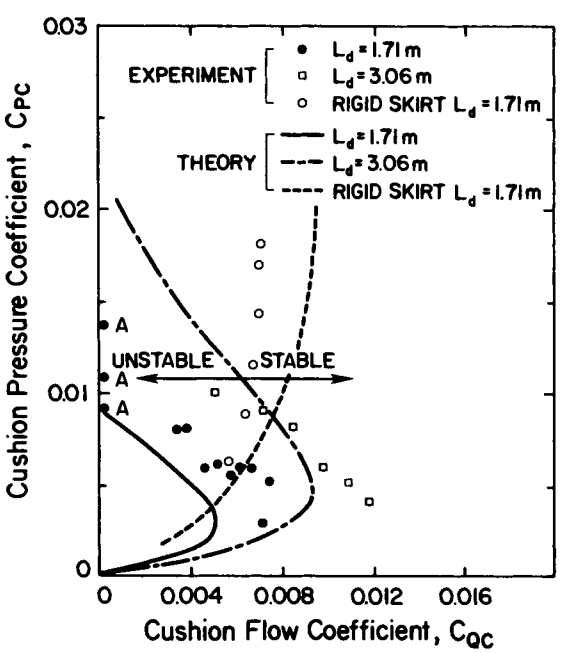

Fig. 12.23 Theoretical and experimental heave stability results for the nylon-urethane conical skirt and two duct lengths. Hoop direction aligned with the material fill-direction. (Adapted from ref. 9.)

back towards zero flow is primarily due to flow-area changes induced by large values of the effective Poisson's ratio. These results are for a modified experiment in which the skirt bottom could be clamped to a fixed rigid lip, thereby retaining only volume changes due to material extensibility. Note that the clamped results lie to the right of the ideal inextensible-cushion boundary. The results curve back towards the inextensible boundary at higher pressures. Presumably this is due to the material stress state changing from pure-hoop to biaxial as the skirt material stiffens with pressure. This explanation is supported by the fact that the high longitudinal-tension boundary approaches the inextensible boundary at a lower cushion pressure.

Some theoretical results obtained with the Voigt model are shown in Figs. 12.26 to 12.28. Figure 12.26 shows the results for various moduli of a skirt with very low contraction ratio, so that the main change is in the cushion volume. Perimeter-change flow-area effects and footprint-area effects are relatively small. These results show that the extensibility capacitance due to the volume change becomes more destabilizing as the material stiffness drops. Furthermore, the material used in the tests of Fig. 12.25 has a modulus which increases with stress. Figure 12.26 indicates that such a material would have stability boundaries similar in shape to the skirt-clamped boundaries of Fig. 12.25. Figure 12.27 shows the effect of the contraction ratio for a moderate-

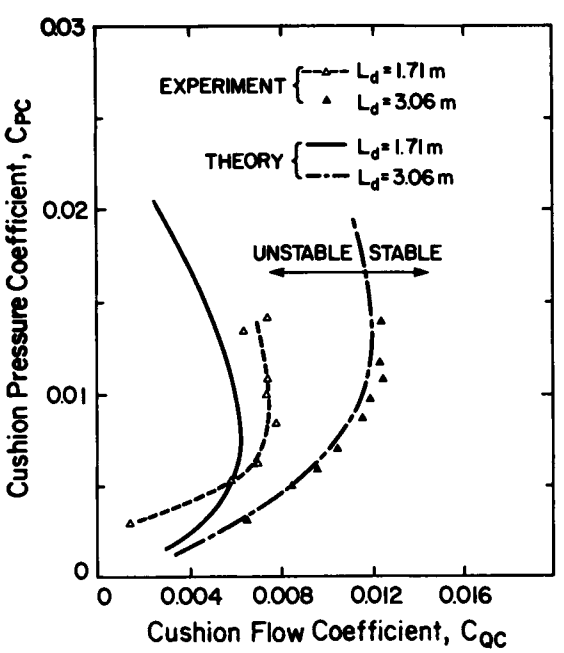

Fig. 12.24 Theoretical and experimental heave stability results for polyethylene skirt and two duct lengths. (Adapted from ref. 9.)

stiffness material. Notice the tendency to curve back towards zero flow and to increased stability as ν_e is increased. The reduction in h_s as a function of pressure is stabilizing since it corresponds to an increased hovergap and, hence, leak area. Similar effects can be produced by means of passive vent-valve control, as described in Chapter 14 and ref. 42. Figure 12.28 shows the effects of changing the material loss-angle for a cushion with very low contraction ratio. They are seen to be quite small for δ up to about 6°. Therefore, a purely elastic model should be adequate within this range. Stability boundaries were calculated for three skirt materials using a standard linear model for the materials. In all cases, the stress-related stiffness changes were averaged over the stress range of interest and the model coefficients were calculated from these averaged values. The predictions, seen in Fig. 12.7, indicate large material-type and orientation dependencies. They show that ignoring material extensibility would result in a theory which could not predict all the experimental trends.

Very little other work has been done on the dynamical effects of skirt material extensibility. An exception is Digges (ref. 43) who developed a model for the trunk of an air cushion landing system, in which the trunk was treated as a nonlinear elastic membrane. In this case, the trunk material stretched

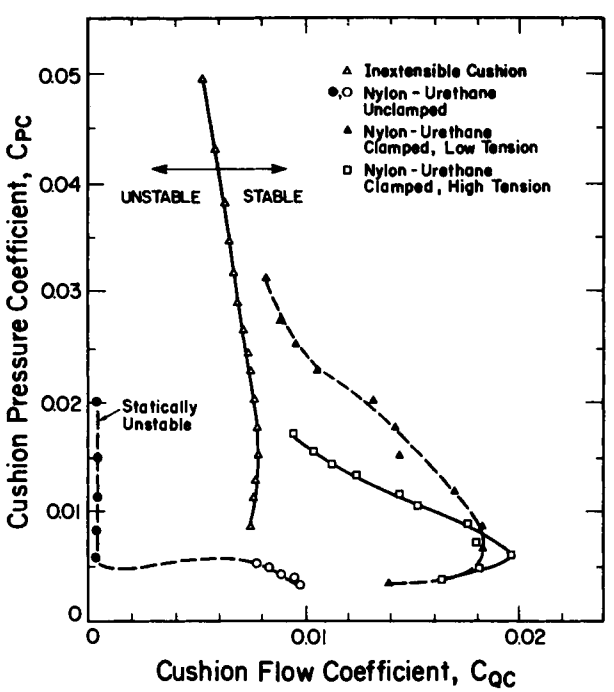

Fig. 12.25 Effect on heave stability of using a clamp to a rigid lip to prevent skirt contraction with the nylon-urethane skirt material. All curves unstable to left. (Adapted from ref. 9.)

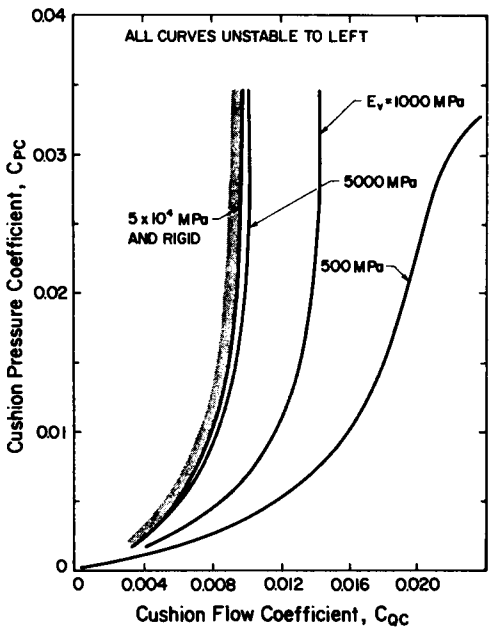

Fig. 12.26 Predicted effect of elastic modulus on dynamic heave stability with a low contraction-ratio skirt. Parameters: ν_e = 0.010, t_s = 0.150 mm, L_d = 1.71 m, η = 10 Pa·s. (Adapted from ref. 9.)

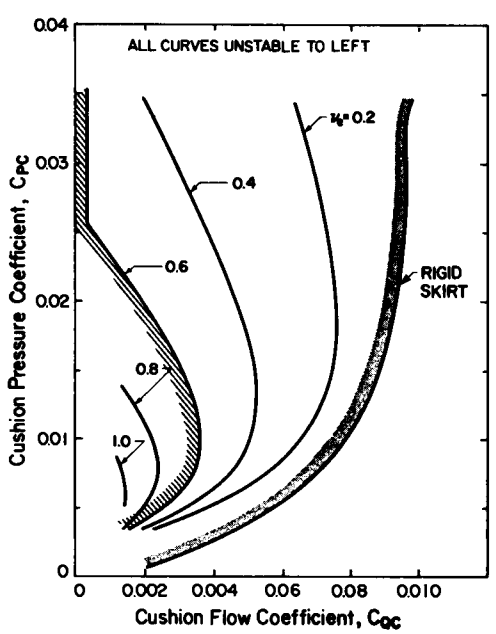

Fig. 12.27 Predicted effect of skirt contraction on dymamic heave stability. Parameters: E_v = 500 MPa, t_s = 0.150 mm, L_d = 1.71 m, η = 5 MPa·s. (Adapted from ref. 9.)

considerably under pressure since its elasticity was designed to assist retraction of the skirt during flight. The extensible trunk material was shown to allow large changes in trunk volume and cross-sectional area with pressure changes. However the extensible skirt model was used only to analyze the static condition for the stretched length of the trunk material. The dynamical analysis assumed that the skirt material was inextensible, so that there was no estimate of its effect on dynamics.

12.4.2 Damping Effects of Hysteresis

One of the characteristics of most experimental stiffness curves which have been published is the presence of hysteresis (refs. 1-8). The amount of hysteresis varies considerably from one case to another. In Fig. 12.20, which is for a 200 ton craft equipped with a segmented skirt, the hysteresis ranges from about 4% to 1% of the cushion pressure and represents about 2.5% of the energy input during a heave cycle. The static pitch curves for the 1.2 m × 2.4 m UTIAS laboratory model, equipped with segmented skirts made from polyethylene and nylon-urethane materials, are shown in Fig. 12.4. With the polyethylene skirt, the energy absorbed in the hysteresis is about 37% of the

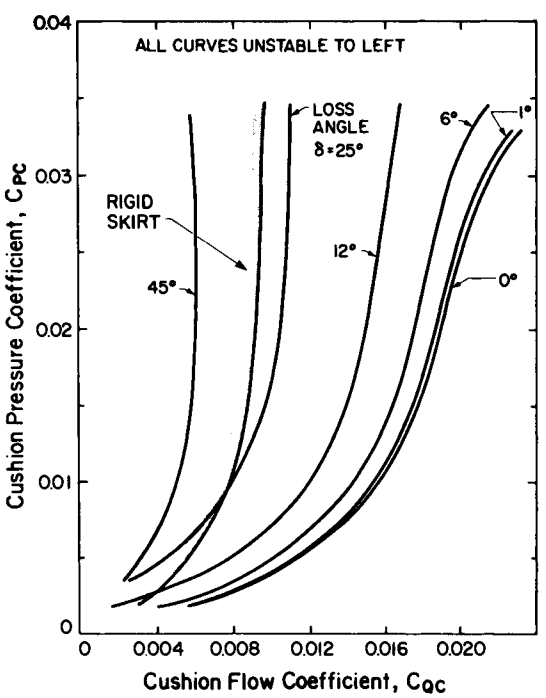

Fig. 12.28 Predicted effect of material loss-angle on dynamic heave stability. Parameters: E_v = 500 MPa, ν_e = 0.010, t_s = 0.150 mm, L_d = 1.71 m. (Adapted from ref. 9.)

total; with the nylon-urethane skirt, the hysteresis represents about 5.5% of the total energy in a pitch cycle. Christopher and Osbourn (ref. 7) also present model scale heave characteritics which show a 7% hysteresis in the heave cycle, with a bag and finger skirt.

If it occurs in the dynamics, the energy represented by hysteresis is a source of damping. Initial condition response tests were performed on the 2.4 m × 1.2 m UTIAS laboratory model equipped with the segmented skirts of Fig. 12.4. The tests consisted of applying a force to one end of the model and observing the pitch-heave response upon release from this equilibrium. The pitch response traces for the two skirts are shown in Figs. 12.1 and 12.2. The response with the polyethylene skirt is more damped. This is most dramatically shown in the larger input test. There the cushion exhibited a limit cycle response when the nylon-urethane skirt was installed, but remained well damped with the polyethylene skirt. Sullivan et al. (ref. 2, Appendix E) noted that the dynamical responses of Figs. 12.1 and 12.2 might be affected by extensibility effects similar to those discussed in Section 12.4.2, but they concluded that the improved damping with the polyethylene skirt mainly results from its larger hysteresis. It was shown by Hinchey et al. (ref. 31) that a hysteretic force of 5% of the vehicle weight can have an important stabilizing effect on the normally lightly-damped heave dynamics of large ACV's. Figure 12.29(a) shows the typical nonlinear limit-cycle heave response at an unstable operating point, omitting hysteresis, and Fig. 12.29(b) shows the well-damped response obtained at the same operating point when the 5% hysteresis force acts during downward motion.

Measurements of the hysteresis forces in polyethylene conical skirts of the same dimensions as those used in the UTIAS sphere facility were made by Milligan (ref. 40). The cushion was fixed in position and subjected to dynamic loading from a heaving table. Dynamic and static hysteresis were found to be similar in magnitude. For a 0.13 mm skirt thickness, the hysteresis force attributable solely to energy dissipation in the material was about 4% of the equilibrium pressure force during oscillations in which the lowest point of the table motion was below the fully-deployed skirt-lip position. The hysteresis was about 2% of the equilibrium pressure force when the skirt lip was always displaced from its fully-deployed position. The hysteresis was found to be frequency-independent up to about 5 Hz. Further experiments with 0.05 mm and 0.08 mm skirt thicknesses indicated that the hysteresis force is proportional to skirt thickness. This implies that the phenomenon is associated with global deformation of the skirt as discussed in Section 12.3.2.

Milligan also obtained a total force-hysteresis of about 9.5% of the equilibrium pressure at a measurement frequency of 0.01 Hz. About 2% was taken up in the material, leaving approximately 7.5% for other sources. This amount was

fairly constant at approximately 9.5% up to about 0.6 Hz, and began to increase with higher frequencies. In the low-frequency range 0.01-0.6 Hz, it is expected that the fan-system response was quasisteady, indicating a true leakage-area hysteresis effect. Observation of the cushion showed that the bottom-leakage area was increased during the table down-stroke because the bent portion of the skirt could not redeploy itself quickly enough. No estimate of the flow-area change was obtained, so that appropriate scaling parameters for area-change effects are not available.

Since tests of this type have not been performed for other cushion geometries, it would be hazardous to extrapolate the above results to them. Tests on a segmented skirt have shown that, although the cushion is shut off on the pitch-down side during a static pitch cycle, in the return motion there remains a small gap due to the material not returning to the deployed shape at the bottom of the segments (ref. 44). This produces an increased leak area during the return portion of the cycle. Boghani et al. (ref. 15), in their report on an oval-trunk-skirt system, make no mention of this type of hysteretic behaviour of the leak area.

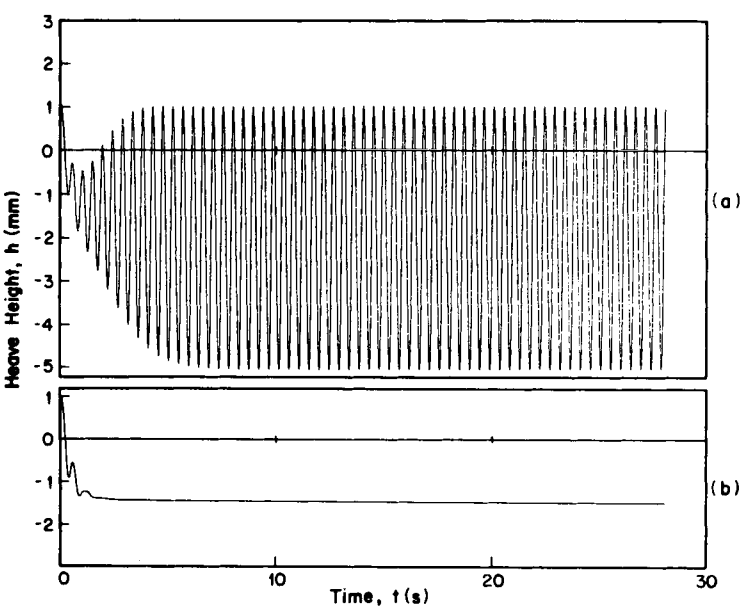

Fig. 12.29 Nonlinear simulation results showing the effect of a hysteresis force on heave motion of a large axisymmetric cushion, with cushion radius = 45.7 m and skirt height = 1.53 m. (a) No hysteresis; (b) hysteresis equivalent to 5% of vehicle weight. (Reproduced from ref. 31 with permission of HBJ London Inc.)

As discussed earlier, the hysteresis in stiffness curves represents damping. It has been shown to consist mainly of two components: one which appears to be caused by leak area differences and the other, by structural force action. Currently, methods of incorporating hysteresis in the dynamic models tend to be somewhat arbitrary. This is due to the difficulties involved in designing suitable experiments capable of isolating the individual hysteresis effects, and differentiating these effects from those of other cushion parameters. Authors concerned with this problem have usually assumed that the skirt deforms as an ideal membrane, so that the leak area exhibits no hysteresis. The work of Lee et al. (ref. 6) was an exception in which an empirical curve was fitted to account for leakage at the corners of a trunk cushion. The latter consisted of four sections fitted together with 45° angle corners, like a picture frame. Boghani et al. (ref. 15), analysing an oval trunk-skirt system, assumed the trunk was an inextensible membrane trunk and that all the damping losses were concentrated in the periphery of the contact region, where the high bending rates occur. The damping was assumed to be viscous, so that the forces depended on the local relative velocity between the surface and trunk during contact. In effect, they assumed $H_p = H_p(h, \theta, \dot{h}, \dot{\theta})$ and $H_h = H_h(h, \theta, \dot{h}, \dot{\theta})$. They obtained damping constants from the pitch-angle response's decay rate and the predicted contact periphery. It was found that, although most cushion response parameters were obtained with reasonable accuracy the angular accelerations were considerably overpredicted by this model. Therefore, they suggested that the damping aspect needed improvement. In the follow-up work by Lee et al. (ref. 6), the same damping model was used, but the damping constant was determined from the decay rates of a material pendulum, as described in Section 12.2.3. They also observed that the damping constant was proportional to material thickness.

Graham and Sullivan (ref. 12.36) have described a segmented-skirt model assuming a membrane behaviour which is ideal with respect to a_ℓ, a_f and V_c, but capable of supporting loads in skirt regions experiencing constant or increasing compressive forces during ground contact. Their method lumps all hysteresis effects into a skirt force which is proportional to the length of skirt material in contact. For a segmented skirt, this includes the portion of skirt along the contact periphery and the contact lengths along the sides of the segments. The hysteresis functions are then of the form

$$H_h(h, \theta, \dot{h}, \dot{\theta}) = \sum C_{FS}(\ell_{SP} + 2\ell_{SS}) \tag{12.53}$$

$$H_p(h, \theta, \dot{h}, \dot{\theta}) = \sum C_{FS}(\ell_{SP}\bar{x}_{SP} + 2\ell_{SS}\bar{x}_{SS}) \tag{12.54}$$

where the sums are over all segments which are in constant or increasing compression, C_{FS} is a constant equal to the amount of skirt force per unit

contact length, ℓ_{SP} and ℓ_{SS} are the contact lengths at the segment outer perimeter and along the sides, respectively, and $\bar{x}_{SP}$ and $\bar{x}_{SS}$ are the moment arms to the centre of ℓ_{SP} and ℓ_{SS}, respectively. Alternatively C_{FS} could be chosen to be proportional to the local segment velocity, v_{SS}, i.e., $C_{FS} = B_{FS}v_{SS}$, and the sum taken over all segments in contact. The force model would then be equivalent to that of Boghani et al. Errors are introduced if the leak-area change is significant. However, the skirt-force model of eqns. (12.53) and (12.54) agrees with the observations of refs. 40 and 44, where the skirt was at least partly out of contact with the surface while receding from it, so that the contact forces were greatly reduced. The model exhibits no frequency dependence in the amount of hysteresis and is compatible with the static hysteresis in the stiffness curves.

The model was used to predict the pitch response of the 2.44 m × 1.22 m UTIAS laboratory model to initial pitch disturbances of 4° and 2.6°. The pitch responses were obtained for two values of C_{FS}. No additional damping from other sources, e.g., skirt-ground friction, damping from connecting duct, or leak area effects was included. Curves were computed for C_{FS} = 4.3 N/m, which was obtained from the partial-contact results of ref. 40 for a 0.13 mm polyethylene skirt. Other curves corresponded to half of the measured skirt-force hysteresis, i.e., C_{FS} = 2.15 N/m. These curves could be compared with the traces of Figs. 12.1 and 12.2 since the computer model represents that physical model. The skirt-force hysteresis was seen to be a major source of damping. However, other sources of damping, possibly those mentioned earlier, were present in the physical model. This was especially apparent in the low-hysteresis curve, which did not exhibit the increased damping observed in the physical model at lower amplitudes.

The existence of significant damping effects related to skirt-force hysteresis introduces a parameter that requires interpretation in model tests and scaling. The material damping results noted earlier indicate that, over the ranges tested, the damping of a given material is approximately proportional to its thickness. However, only a few materials have been tested and no correlation with other material parameters, such as the loss modulus, has been published.

12.5 SYMBOLIC AND NUMERICAL SPECIFICATIONS

12.5.1 Nomenclature

(i) Roman

a_f	cushion footprint area
a_ℓ	cushion leak area
A	system matrix
A_d	duct diameter

A_{ref}	vehicle hard structure planform area
B	system matrix
B_b	vehicle hard structure width
B_s	skirt width at the lip
B_{FS}	viscous damping coefficient
C_{mi}	duct inlet mass flow coefficient
C_{pf}	nondimensional fan pressure coefficient = $p_f/(\rho N^2 D_f^2)$
C_{FS}	skirt force per unit length
C_{PC}	cushion pressure coefficient = p_{ce}/P_{atm}
C_{QC}	cushion flow coefficient = $Q_{ce}/(2mgA_{ref}/\rho_{ce})^{1/2}$
C_{Qf}	nondimensional fan flow coefficient = $Q_f/(ND_f^3)$
C_{SC}	fan slope coefficient = $\partial p_f/\partial Q_f$
C_{ST}	nondimensional skirt thickness = t_s/L_b
C_{SW}	nondimensional skirt weight per unit area = $\sigma_s/(W/A_{ref})$
d_r	ratio of mean diameter to bottom diameter in conical skirt
D	compliance
D_f	fan diameter
D_p	plenum diameter
D_{sm}, D_{smo}	deformed and undeformed mean diameter of conical skirt
D_{st}, D_{sto}	deformed and undeformed diameter at top of conical skirt respectively
E	Young's modulus
E_g, E_v	elastic constants in standard linear model
E^*	complex modulus = $E_1 + iE_2$
E_1	elastic modulus
E	loss modulus
G_{12}	shear modulus
h	heave height
h_ℓ	hovergap or leak height
h_s, h_{so}	skirt height from lip to hard structure - deformed and undeformed
H_b	vehicle hard structure height
H_h	skirt hysteresis function in heave
H_p	skirt hysteresis function in pitch, also vehicle pivot height
i	$(-1)^{1/2}$
I_{yy}	moment of inertia in pitch
k_f	coefficient of friction
k_s	static stiffness of standard linear model
ℓ_{SP}	segment contact length at periphery
ℓ_{SS}	segment contact length on sides

L_b	vehicle hard structure length
L_d	duct length
L_s	skirt length at lip
m	mass
M_Q	moment resulting from exit momentum
n	polytropic constant
N	fan speed
p_c	cushion pressure (gauge)
p_{di}	duct inlet pressure (gauge)
p_f	pressure rise across fan
p_s	sphere pressure (gauge)
p_0, p_1, p_2	fan characteristic coefficients
P_{atm}	atmospheric pressure
P_c	absolute pressure in cushion
Q_c	cushion exit volume flow
Q_d	duct volume flow
Q_f	fan volume flow
Q_{ij}	stiffness matrix elements
r_c	radius of curvature at top of conical cell
R	gas constant
R_s	skirt corner radius at lip
R_t	trunk radius
S, S_0	conical skirt slant height in deformed and undeformed state, respectively
t	time
t_p	time period
t_s	skirt thickness
T	temperature
v_{SS}	local segment velocity relative to surface
V_c	cushion volume
W	total vehicle weight
w_c	cushion exit mass flow
w_f	fan mass flow
$\bar{x}_M$	moment arm for cushion centre of pressure
$\bar{x}_{SP}$	moment arm to ℓ_{SP} centre
$\bar{x}_{SS}$	moment arm to ℓ_{SP} centre
$\underset{\sim}{x}$	state vector

(ii) Greek

β	segment angle
γ	ratio of specific heats = 1.4

γ_{12}	shear strain
δ	loss angle in viscoelastic material
ϵ	linear strain
ϵ^*	linear hoop strain
η	viscous constant in viscoelastic model
θ	pitch angle; also, material orientation relative to hoop direction
λ	geometric scale factor, model/full scale
ν	Poisson's ratio
ν_c	contraction ratio from curvature at skirt top
ν_e	effective contraction ratio, the sum of ν_c, ν_h, ν_ℓ
ν_h	normal Poisson's ratio for hoop strain
ν_ℓ	contraction ratio due to longitudinal stress (-ve)
ξ_h, ξ_θ	damping factors for heave and pitch respectively
π	3.14159...
ρ	air density
σ	stress
σ^*	hoop stress
σ_s	skirt material weight per unit area
τ	viscoelastic time constant
τ_{12}	shear stress
ω	radian frequency

(iii) Subscripts

c	cushion
e	equilibrium
o	unpressurized value; also, initial value

(iv) Acronyms

ACV	Air Cushion Vehicle
AIAA	American Institute of Aeronautics and Astronautics
CASI	Canadian Aeronautics and Space Institute
UTIAS	University of Toronto Institute for Aerospace Studies

12.5.2 Tables and Facility Descriptions

Table 12.1. Dimensions and parameters of sphere facility. (Adapted from ref. 11.)

Sphere diameter		=	12.2 m (40 ft)
Duct length:	Long	=	3.06 m (10.0 ft)
	Short	=	1.71 m (5.6 ft)
Duct diameter		=	0.0779 m (0.2576 ft)
Basic model weight:	Flexible	=	49.35 N (11.09 lb)
	Rigid	=	59.96 N (13.25 lb)
Duct flow friction factor		=	0.01656
Skirt diameter	Top	=	0.508 m (1.67 ft)
	Bottom	=	0.470 m (1.53 ft)
Skirt height		=	0.213 m (0.70 ft)
Lip discharge coefficient:	Nylon-neoprene	=	0.567
	Rigid	=	0.60
	Nylon-urethane	=	$0.591-0.147\times10^{-3}\times p_c$
	Polyethylene	=	0.53
Skirt contraction coefficient:	Nylon-urethane	=	1.9
	Polyethylene	=	0.9

Duct discharges directly into the cushion.

Table 12.2. Skirt material properties. (Adapted from ref. 9.)

Material	Thickness t_s (mm)	Static Modulus E (Pa) (1)	Dynamic Properties: Storage Modulus E_1 (2)	Dynamic Properties: Loss Angle δ (2)	Poisson's Ratio
Aluminum (Rigid Skirt)	1.58	6.9×10^{10}	-	-	0.33
Nylon-Neoprene (0° to warp)	0.483	$1.5\times10^{8}+271\sigma$	$5.2\times10^{8}+151\sigma$	-	-
Polyethylene (at 0° and 90°)	0.127	1.5×10^{8}	5.4×10^{8}	2°	0.3
Nylon-Urethlane (0° to wrap)	0.102	6.25×10^{8}	$6.52\times10^{8}+49.4\sigma$	<0.5°	-
Nylon-urethane (90° to warp)	0.102	No recovery:(3) 0.87×10^{8} Recovery:(3) $1.60\times10^{8}\times(1 + 10^{-7}\sigma + 10^{-14}\sigma^2)$	$1.84\times10^{8}+51.8\sigma$	<0.5°	0.75

Notes: (1) Moduli quoted are from stress relaxation tests at 20 minutes elapsed time and are functions of stress, σ, where appropriate.
(2) Values of E_1 and δ are quoted for a frequency of 15 Hz, which is the average of measured frequencies in test model.
(3) In the tests with recovery the material was released from tension between tests and for an extended period.

Table 12.3. UTIAS laboratory model description.

Hard structure:
- Length (L_b) = 2.489 m, Width (B_b) = 1.270 m, Height (H_b) = 0.305 m
- Pivot height (H_p) = 0.142 m

Skirt System:
- Length (L_s) = 2.214 m, Width (B_s) = 0.91 m, Height (H_s) = 0.240
- Corner radius (R_s) = 0.326 m
- Segment angle (ß) = 32.5 degrees

Fan System:
- Duct length (L_d) = 2.80 m, Duct cross-sectional area = 0.098 m^2
- Inlet flow coefficient = 0.127, Equivalent duct diameter = 0.313 m
- Fan diameter = 0.533 m
- Nondimensional fan characteristic: $C_{pf} = 6.878 + 5.343\, C_{Qf} - 26.71\, C_{Qf}^2$

Inertia properties:
- Mass (m) = 97.75 kg, Moment of inertia (I_{yy}) = 51.3 kg·m^2

Skirt symbols (L_s, B_s, H_s, R_s, ß) are defined in Fig. 12.30.

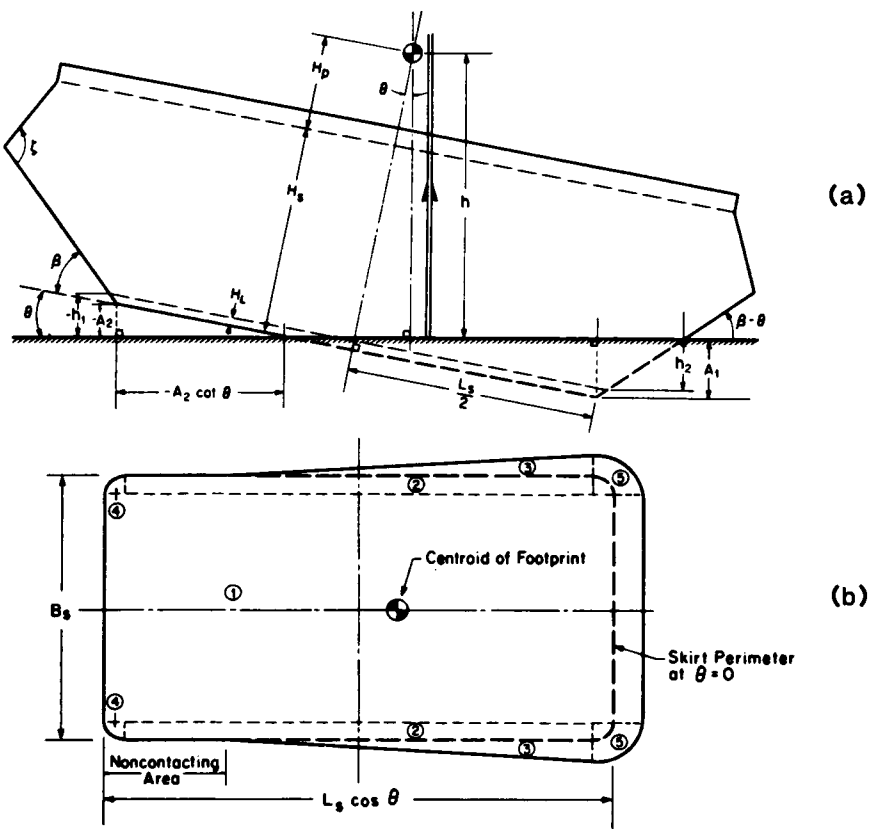

Fig. 12.30 Geometry and skirt parameter definition for a segmented skirt cushion: (a) profile view; (b) surface-intersection plane view. (From ref. 2.)

12.6 SUMMARY

The dynamic response of ACV skirts can be strongly influenced by the mechanical properties of the material used in the skirt. This has implications in analysis and scale model testing. Some of the mechanical properties of skirt materials can be explained through the use of linear viscoelastic theory. In particular, time-dependent extension or creep, and frequency- and temperature-dependent modulus properties can be modelled. Other properties, such as nonlinear stiffness, direction-dependent stiffness, and nonviscous internal energy dissipation can be described in terms of the structure of coated woven fabrics. The combination of these factors into a complete rheological model of a material would be very difficult and time consuming. It would require that a large number of variables be controlled independently during testing and then incorporated in the mathematical model. Fortunately, a complete material model is not usually necessary for vehicle- dynamics studies. The dynamic effects are primarily associated with the extensibility of the skirt material, its ability to sustain small compressive loads which induce hysteresis in the cushion's stiffness characteristics and skirt-surface friction. These effects can be separated and modelled independently within the various skirt-response parameter functions. This approach allows the dynamicist to include only those aspects of material behaviour which have a significant impact on vehicle dynamics.

The material extensibility influences the dynamics through three pressure-driven mechanisms: 1) the extensibility capacitance, which results from cushion volume modulation, 2) the modulation of the cushion leak-area, and 3) internal energy dissipation when there is no skirt-surface contact. For many materials, the latter has only a small influence. The discussion on extensibility effects illustrated the use of viscoelastic models to account for material dynamic-modulus effects and internal energy dissipation. The conical skirt geometry used in that discussion was quite simple. Application to more complicated geometries would require a biaxial stress model and specialized numerical modelling techniques such as finite element. Although difficult, extensibility models can be prepared for different skirt systems using current modelling techniques. The designer should be aware of the test method underlying any material stiffness data since creep may cause the material extension to vary significantly with stress time. Critical situations may require in-house testing of materials.

The hysteresis effects are caused by the skirt's direct load-carrying ability and resulting leak-area changes but, not being well-understood yet, they are the subject of ongoing research. Consequently, the methods used to describe this hysteretic behaviour tend to be heuristic. Nevertheless, they can provide reasonably good dynamic predictions. Some progress has been made

towards understanding the mechanisms. There has been recent verification that the direct skirt-force component of a given material scales in proportion to its thickness. The leak-area aspect has not yet been adequately quantified through experiment. At present, the hysteresis properties of each skirt system of different material must be measured individually, owing to a lack of appropriate composition related scaling factors for hysteresis.

12.7 REFERENCES

1. P.A. Sullivan, M.J. Hinchey, P.V. Hartmann, A. Dupuis, G.M. Green and T.A. Graham, Research into air cushion stability: 1979 report, Transportation Development Centre, Transport Canada, TP 3109E, TDC File No. D-500-431-1, January 1982.
2. P.A. Sullivan, M.J. Hinchey, T.A. Graham, J.E. Byrne, A. Dupuis, N. Milligan and C. Walsh, Investigations of the dynamics of large air cushions, Transportation Development Centre, Transport Canada, TP 7560E, TDC File No. D1460-125-2, August 1986.
3. P.J. Mantle, Air cushion craft development, U.S. Navy, David W. Taylor Naval Ship Research and Development Center, Bethesda, Md., DTNSRDC-80/012, Jan. 1980.
4. _____, Stability and control of hovercraft: notes for commanders, United Kingdom Department of Industry, Ship and Marine Technology Requirements Board BHC SP 4432, 1980.
5. T.A. Graham, P.A. Sullivan and M.J. Hinchey, Heave stiffness hysteresis measurements on a large scale air cushion, Seventeenth Canadian Symposium on Air Cushion Technology Preprints, Canadian Air Cushion Technology Society, Ottawa, Ontario, Oct. 1983, pp. 50-55.
6. E.G.S. Lee, A.B. Boghani, K.M. Captain, H.J. Rutishauser, H.L. Farley, R.B. Fish and R.L. Jeffcoat, Experimental and analytical studies of advanced air cushion loading systems, National Aeronautics and Space Administration, Contract Report NASA CR-3476, Aug. 1981.
7. P.A.T. Christopher and E.W. Osbourn, Hovercraft research and development on the Cranfield whirling arm facility, Cranfield College of Aeronautics Memo 8009, Dec. 1980.
8. P.A. Sullivan, M.J. Hinchey and R.G. Delaney, Static roll stiffness characteristics of two multicell type air cushion systems, Journal of Terramechanics, Vol. 15, No. 1, March 1978, pp. 15-41.
9. T.A. Graham, P.A. Sullivan and M.J. Hinchey, Skirt material effects on air cushion dynamic heave stability, Journal of Aircraft, Vol. 22, Feb. 1985, pp. 101-108.
10. W.A. Ribich and H.H. Richardson, Dynamic analysis of heave motion for a transport vehicle fluid suspension, Dept. of Mechanical Engineering, Massachusetts Institute of Techology, Boston, Mass., DSR-76110-3, Jan. 1967.
11. P.A. Sullivan, M.J. Hinchey and G.M. Green, A review and assessment of methods for prediction of the dynamic stability of air cushions, Journal of Sound and Vibration, Vol. 84, No. 3, 1982, pp. 337-358.
12. T. Ma and P.A. Sullivan, Linear analysis of the heave dynamics of a bag and finger air cushion vehicle skirt, presented at AIAA 8th Advanced Marine Systems Conference, AIAA Paper No. AIAA-86-2361, Sept. 1986.
13. R. Carrier, A.H. Magnuson, and M.R. Swift, Seakeepng dynamics of a single cushion peripheral cell-stabilized air cushion vehicle, Journal of Hydronautics, Vol. 12, No. 2, April 1978, pp. 49-54.

14. M.J. Hinchey and P.A. Sullivan, A theoretical study of limit cycle oscillations of plenum air cushions, Journal of Sound and Vibration, Vol. 79, No. 1, Nov. 1981, pp. 66-77

15. A.B. Boghani, K.M. Captain and D.N. Wormley, Heave-pitch-roll analysis and testing of air cushion landing systems, National Aeronautics and Space Administration NASA CR-2917, Feb. 1978.

16. National Materials Advisory Board (NMAB) Committee on Skirts and Seals for Surface Effect Vehicles, Skirts and seals for surface effect vehicles, NMAB National Academy of Sciences, Report No. NMAB-340, April 1978.

17. W.B. Graham, Material damping and its role in linear dynamic equations, University of Toronto Institute for Aerospace Studies Review No. 36, 1973.

18. I.M. Ward, Mechanical properties of solid polymers, Wiley, 1971.

19. J.J. Aklonis, W.J. MacKnight and M.C. Shen, Introduction to polymer viscoelasticity, Wiley-Interscience, 1972.

20. D.I.G. Jones and J.P. Henderson, Fundamentals of damping materials, section of notes from A Short Course on Vibrational Damping, University of Dayton Research Institute, Dayton, Ohio, Nov. 1979 (date).

21. C.R. Payne, Air cushion vehicle skirt systems, 1985 Joint International Conference on Air Cushion Technology, Rockville, Maryland, U.S.A., Sept. 1985.

22. J.E. Ashton, J.C. Halpin and P.H. Petit, Primer on composite materials analysis, Technomic Publishing Company Inc., 1969.

23. L.J. Brontman and R.H. Brock, Modern composite materials, Addison Wesley Publishing Co., 1967.

24. R.M. Jones, Mechanics of composite materials, Scripta Book Company, Washington, D.C., McGraw-Hill Book Company in other areas, 1975.

25. S. Thomas and N. Stubbs, An inelastic biaxial constitutive model for fabric-reinforced composites, Journal of Coated Fabrics, Vol. 13, Jan. 1984, pp. 144-160.

26. H. Minami and Y. Hakahara, An application of the finite element method to the deformation analysis of coated plain weave fabrics, Journal of Coated Fabrics, Vol. 11, April 1981, pp. 310-327.

27. T.A. Graham and M.J. Hinchey, Strength testing of ACIB skirt material, AERCOL Report for Canadian Coast Guard, March 1982.

28. P. Grosberg, The mechanical properties of woven fabrics, Part I: The initial load extension modulus of woven fabrics, Textile Research Journal, Vol. 36, No. 1, Jan. 1966, pp. 71-79.

29. P. Grosberg, The mechanical properties of woven fabrics, Part II: The bending of woven fabrics, Textile Research Journal, Vol. 36, No. 3, March 1966, pp. 205-211.

30. R.R. Nachlinger and J.R. Leininger, Bending of a beam made of a fibre-reinforced viscoelastic material, AIAA Journal, Vol. 7, No. 10, 1969, pp. 2016, 2017.

31. M.J. Hinchey, P.A. Sullivan and A.D. Dupuis, On the heave-dynamics of large air cushion platforms, Journal of Sound and Vibration, Vol. 96, No. 4, 1984, pp. 469-484.

32. D.D. Moran, Pitch and roll hydrodynamics of a pericell hovercraft, Canadian Aeronautics and Space Journal, Vol. 32, No. 4, Dec. 1986. pp. 314-330.

33. F.R. Goldschmied and D.N. Wormley, Frequency response of blower-duct-plenum systems, Journal of Hydronautics, Vol. 11, 1977, pp. 18-27.

34. H. Ohashi, Analytical and experimental study of the dynamic characteristics of turbopumps. NASA TN D-8413, 1968.

35. D.D. Moran and A.N. Jennings, Lift system and fan performance of air-cushion supported vehicles, David W. Taylor Naval Ship Research and Development Center Report DTNSRDC/SPD-0695-02, Feb. 1982.

36. M.J. Hinchey, Heave Instabilities of amphibious air cushion suspension systems, University of Toronto Institute for Aerospace Studies, Report No. 246, 1979.

37. T.A. Graham and P.A. Sullivan, Nonlinear dynamics of a segmented skirt air cushion, Preprints 1985 Joint International Conference on Air Cushion Technology, Rockville, Maryland, Sept. 1985, Canadian Aeronautics and Space Institute, Ottawa, 1985.

38. L.I. Doctors, Nonlinear motion of an air cushion vehicle over waves, Journal of Hydronautics, Vol. 9, No. 2, 1975, pp. 49-57.

39. E.P. Popov, Introduction to Mechanics of Solids, Prentice-Hall, Englewood Cliffs, New Jersey, U.S.A., 1968.

40. N.H. Milligan, An Investigation of air cushion vehicle skirt hysteresis, M.A.Sc. thesis, University of Toronto Institute for Aerospace Studies, June 1987.

41. R.W. Helm, Development of the air cushion equipment transportation, Late papers, 1985 Joint International Conference on Air Cushion Technology, Rockville, U.S.A., Sept. 24-26, 1985, Canadian Aeronautics and Space Institute.

42. J.R. Amyot, Passive control of air cushion heave dynamics, 1985 Joint International Conference on Air Cushion Technology, preprints, Rockville, U.S.A., Sept. 1985, Canadian Aeronautics and Space Institute, pp. 74-81.

43. K.H. Digges, Theory of an air cushion landing system for aircraft, Air Force Flight Dynamics Laboratory, Technical Report AFFDL-TR-71-50, June 1971.

44. P.V. Hartmann, Application of system parameter identificaton methods to the determination of dynamic pitch-heave characteristics of an ACV, M.A.Sc. Thesis, University of Toronto Institute for Aerospace Studies, June 1979.

45. P.A. Sullivan and R. Placek, A review of the status of air cushion technology, UTIAS Review No. 33, 1971.

Chapter 13

DYNAMICS OF RESPONSIVE SKIRTS

13.1 INTRODUCTION

The successful development of air cushion vehicles (ACV) is due in large part to the use of flexible skirts, which enable these vehicles to negotiate relatively large obstacles or waves while keeping lift air flow and power at moderate levels. A skirt is thus an integral part of an ACV's suspension system and, as such, it has a major effect on the dynamics and performance of the vehicle. During passage over waves or obstacles, the way it deflects in response to cushion pressure disturbances or to surface contact has a major effect on both stability and ride comfort or sea-keeping. The purpose of this chapter is to present a mathematical model of the dynamics of the bag-and-finger skirt and related systems, these being the most widely used systems on larger ACV's. It is intended that this will provide a rational basis for the improvement of existing designs. Some preliminary results from analyses based on this model are presented together with pertinent data obtained from laboratory models.

A key idea in skirt design is that of responsiveness (ref. 1). As an ACV passes over disturbances such as obstacles or waves the ideal skirt should respond by changing its geometry so that it minimizes the cushion pressure and hovergap fluctuations that occur in response to the disturbances. This both reduces dynamical inputs to the craft and keeps the loss of cushion air to a minimum. A skirt system which approaches this ideal may be said to be *responsive* or *surface-following*. Broadly speaking, existing skirt designs may be classified into two types: responsive and non-responsive. A characteristic feature of a *responsive skirt* is that, in response to input disturbances, even when the skirt material behaviour is inelastic, large changes of overall shape occur; that is, the skirt is said to undergo

geometric deformation. In contrast, for *non-responsive* skirts, except in the immediate neighbourhood of regions of surface contact, deformations occur mainly as a result of material strain, and are thus relatively small.

The most widely known responsive skirt is the *bag-and-finger skirt*. Developed in Britain (ref. 2), it is now used on craft built in that country, USA and China. A variant is the *bibag-finger* skirt developed in the USSR. A second less widely used responsive skirt is the *loop-and-segment* system, also developed in Britain. Examples of non-responsive skirts are the *multicell* system developed in France and the *uncompartmented segmented* skirt developed in Canada. The latter system is discussed in Chapter 12. This chapter considers the dynamics of skirts of the responsive type, especially that of the bag-and-finger.

Skirt responsiveness is obtained in two ways (ref. 1). In the first way, changes in hovergap cause changes in the pressure of the air in the cushion and other volumes. This in turn alters the pressure forces acting on the skirt, which responds by changing its shape. In the second way, surface contact forces changes in skirt geometry which in turn alter the pressure forces acting on the skirt, and thus its shape. The first way may be called pressure responsiveness, and the second, contact responsiveness. It is shown below that the loop-segment skirt has only contact responsiveness, whereas the bag-finger skirt has both types.

In general cushion systems are very sensitive to the surface over which they operate, and existing ACV's, including those that use skirts having some degree of responsiveness, are relatively stiff in heave, and thus have relatively poor ride quality. To circumvent this problem, three approaches have been proposed. One is to actively or passively control a cushion air vent valve (refs. 3-5); in general this considerably reduces heave acceleration, but there can be large increases in both lift power and the amount of surface contact, with the latter increasing drag. A second approach is to use some type of active fan control, such as by altering the blade angles of an axial fan (refs. 2, 6). However, although this reduces the air power loss, owing to increased time delays in the feedback mechanism, it is generally less effective than the vent valve, and surface contact drag is increased. The third approach is to increase skirt responsiveness. Responsiveness can reduce heave acceleration in the following way. When the vehicle passes over a disturbance such as a wave peak, the increased cushion pressure moves the skirt upwards relative to the craft, and thus increases the hovergap. The increased flow from the cushion tends to reduce or offset the pressure peak in a feedback sense. In a wave trough the opposite behaviour occurs. This surface-following capacity, although it is always out of phase with the surface motion to some extent, nevertheless can significantly improve

ride comfort, minimize lift air loss, and reduce surface contact drag. This concept of responsiveness has been accepted by many designers (refs. 7-9).

However increasing skirt responsiveness also tends to introduce stability problems. These are mainly of two types, a static instability of the bow skirt known as *tuck-under*, and a dynamic instability known as *skirt-bounce*. The first can occur in the following way. As craft speed increases, the forces generated by surface contact act on the bottom of the skirt, and increase rapidly. At a certain critical speed these forces become large enough to abruptly drag the bottom part of the skirt rearwards. The overall skirt geometry also changes from its intended shape to a new equilibrium; this is characteristic of a static instability. The leading edge of the cushion foot-print is also moved aft and, as a consequence, the craft may lose longitudinal stiffness and static stability, and then *plough-in*. Skirt-bounce is a self-excited limit cycle oscillation involving predominantly vertical motion of the entire skirt. It is caused by a dynamic instability involving an interaction between the motion of the skirt and the cushion flow processes. The oscillation frequency can be low enough to excite heave motion in the vehicle. Current bag-finger designs usually include a web known as the *anti-bounce web* or *anti-plough web* to prevent the onset of these instabilities (ref. 2) but, because they limit the downward motion of the skirt, responsiveness can be considerably impaired.

It is a major challenge to design a skirt to achieve maximum responsiveness while, at the same time, avoiding instability. Increasing skirt responsiveness also causes large changes in heave, pitch and roll stability through its effect on basic cushion heave stiffness, on compartmentation stiffness, and on surface contact forces. All of these aspects have to be considered by the designer; for example one must be particularly careful to evaluate the possibility of tuck-under, since a plough-in at high speeds can have disastrous consequences.

This chapter describes an analysis of the dynamics of responsive skirts of the bag-finger type. A nonlinear model of the skirt dynamics is formulated, and standard linear techniques are then used to obtain some basic insights into the factors that affect the response and stability of this system. The the approach is similar in many respects to the investigation of the aeroelastic behaviour of an aircraft.

Now although certain aspects of cushion dynamics can be highly nonlinear (refs. 10, 11), nevertheless a linear analysis seems to be an appropriate approach. In this respect it is worth noting that, although this skirt was introduced in 1966 (ref. 2), and has been developed extensively since then, very little information on its dynamical properties can be found in the open technical literature. Furthermore, as late as 1978, Wheeler (ref. 8) noted

that three major British manufacturers had conducted a joint experimental programme to elucidate the factors that affect skirt response, but that the results had been *less than satisfactory*. However he noted that the model response was found to be substantially linear over a moderate range of conditions.

The work described here has two distinct themes; the first is the statics and dynamics of the cushion in the absence of skirt contact. The second is the process of skirt-surface contact. The first provides insights into craft heave stiffness, ride comfort or seakeeping, and dynamic instabilities such as skirt bounce. The second is essentially static in behaviour, and addresses the tuck-under problem. However the two themes have many features in common so that they are developed simultaneously where appropriate.

Now it has been noted that the skirt motion generated by an ACV's passage over typical surfaces can be very complex (ref. 1), so that the analysis and ideas developed here necessarily involve considerable simplification. Nevertheless we believe that they can suggest ways of improving existing skirt designs. Also we believe that an adequate understanding of phenomena such as skirt bounce requires the use of the analytical techniques developed here.

13.2 A DYNAMICAL MODEL OF THE BAG-FINGER SKIRT

In this section the geometry and construction of the bag-and-finger skirt is described, the way in which it achieves responsiveness is discussed, some notation is introduced, and a basic block diagram conceptualization of the problem is presented. A measure of responsiveness is proposed, and the problems of analysis of skirt cushion dynamics are discussed. Finally, the mathematical model of the skirt adopted for the present study is developed.

13.2.1 Geometry and Construction of the Skirt

Figure 13.1 is a cross-section of the skirt depicting its major features. The *bag* ABO is attached to the craft base or *hard structure* through hinges or bolts at A and O, and is usually made from a single continuous sheet of elastomer-fabric. The *finger* BB'CD is usually attached at two locations: to the bag through a flap and bolts at B, and by means of chains or fabric straps DE to the vehicle base along a line which is very close to the bag inner attachment line O. The finger itself may be molded into its characteristic shape as depicted in the section I-I in Fig. 13.1, or it may be simply folded from a sheet of elastomer-fabric. The line passing through the bottom tips C of the fingers is called the skirt *hemline*. The angle B'CD is usually 90° but it can be larger. In some cases the outer profile of the finger BB'C may be a straight line, in others it may protrude as depicted.

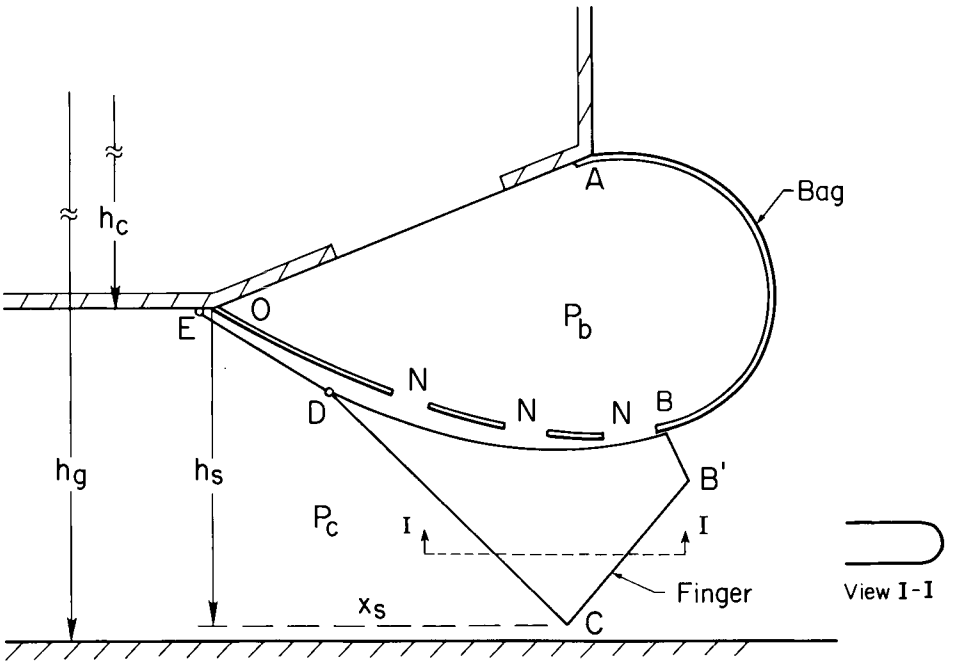

Fig. 13.1 Basic elements of bag-and-finger skirt.

This protrusion is included to offset the reduction of the cushion footprint area caused by the inward slope of the fingers. At equilibrium the upper edge of the fingers BD and the links DE may, in some designs, touch and even partially support the inner part of the bag BO, whereas in others there may be a clearance as depicted in Fig. 13.1. Because the tips C of the fingers tend to wear with use, in some designs these are cut off parallel to the line I-I.

The cushion air is usually supplied by centrifugal or mixed-flow fans, and the geometry of the bag air feed system can be one of two arrangements. In the first the fan rotor axes are vertical, and conventional outlet scrolls are not used. Instead the air spreads radially into a plenum chamber having a height equal to the width of the fan outlet annulus, and thence directly into the bags. In the second arrangement the fans may be mounted in conventional scroll housings which feed directly into the bags. In either case, except possibly for some diffusion in the first arrangement, the fans, in effect, deliver air directly into a plenum chamber of which the bag volumes form a part. In most craft the front and side bags comprise a single volume, with only the rear bag being separately fed. The air passes to the cushion through orifices N which may be distributed over the inner bag as depicted in Fig. 13.1, or may be concentrated close to the finger side BB'C.

The geometry of the rear skirt usually differs from that used on the front and sides. To prevent scooping of water, the rear fingers are usually replaced by cones, or in some cases a *bibag* system is used (ref. 2). The latter arrangement tends to be very responsive, but is prone to instability. We believe that the dynamics of the skirt system is not radically altered when fingers are replaced by cones, so that the latter geometry is not specifically considered here.

As in other cushion systems, the operating or equilibrium value of the cushion pressure p_c is determined primarily by the planform dimensions and weight of the craft, and the cushion equilibrium flow Q_e by the nature of the surface over which it operates. The equilibrium value of the bag pressure p_b is determined from considerations of responsiveness and stability, and the area of the feed orifices N is then chosen to obtain the required p_b/p_c.

The bag-and-finger skirt has pressure responsiveness because, as is shown below, the equilibrium shape of the bag and thus the skirt height depends mainly on the ratio p_b/p_c, and modulation of the cushion flow by vehicle motion changes this ratio. On the other hand it also possesses contact responsiveness because, even when p_b/p_c remains constant, surface contact forces partial collapse of the fingers, which in turn alters the pressure forces acting on them. Now from the point of view of the analytical development presented here, the loop-segment skirt is a special case of the bag-finger skirt in which the area of the orifices N is so large that p_b is always equal to p_c. Hence this skirt only has contact responsiveness.

13.2.2 Basic Notation

The simplest dynamics occurs when the vehicle moves at constant speed over surface disturbances having wavelengths which are much greater than the basic cushion length or width. In this case the surface disturbance is equivalent to a flat horizontal surface moving in pure heave under the cushion, and the resultant craft motion in the vertical plane can also be assumed to be pure heave. The basic motion variables required to describe the dynamics for this case are depicted in Fig. 13.1. All distances are measured vertically downwards from a datum, h_c being the *craft height*, h_s the *skirt height*, and h_g the *ground height*. Thus

$$h_g = h_c + h_s + h_e \tag{13.1}$$

where h_e, the distance between the skirt hemline and the ground, is called the *hovergap*.

When the motion is such that the skirt contacts the surface, be it solid or liquid, a significant portion of the finger is deformed. It is useful in

this case to introduce an *immersion* or *wetted height* h_w, which is the distance an undeformed finger would penetrate the surface. Thus

$$h_w = h_c + h_s - h_g \tag{13.2}$$

Comparison of eqns. (13.1) and (13.2) shows that, when $h_e < 0$, $h_w = - h_e$.

The lateral motion of the skirt in response to input disturbances can be important, since this modulates the cushion footprint area. Accordingly a craft-fixed coordinate system is located with origin at O, as shown in Fig. 13.1, and x_s is the lateral position of the skirt hemline.

With regard to notation, except where common usage dictates otherwise, constants and variables are denoted by upper and lower case symbols respectively, with Greek lettering reserved for angles. For the linear analysis, any quantity varying in time is assumed to be a small perturbation of a reference value, that is, for any variable $\phi(t)$, if ϕ_o and ϕ_r are, respectively, equilibrium and reference values, then

$$\phi(t) = \phi_o + \delta\phi(t), \qquad |\delta\phi| << |\phi_r| \tag{13.3}$$

where $\phi_r = \phi_o$ usually. With $s = \sigma + i\omega$ being the Laplace variable, the Laplace transform of $\delta\phi(t)$ is written $\Delta\phi(s)$. In a process in which $\phi(t)$ is the input and $\psi(t)$ is the output, the transfer function is written $\Delta\psi(s)/\Delta\phi(s)$, or more simply $\Delta\psi/\Delta\phi$. Certain particularly important transfer functions are given an appropriate notation. For example the disturbances in p_b caused by variations in p_c play a key role in the following development, and the corresponding transfer function $\Delta p_b/\Delta p_c$ is denoted P_{bc}. In linearized relationships in which equilibrium values of variables appear as coefficients, the subscript "o" is omitted. To facilitate further development of the ideas presented here, where appropriate, subscript and matrix notation is used. Thus the expression $y_i = y_i(x_j)$, $i = 1, 2, \ldots, N$, denotes a system of N equations depending on M variables, x_j, $j = 1, 2, \ldots, M$. The N×M matrix $[a_{ij}]$ is denoted by $\underset{\sim}{A}$ and, given the column vector $\underset{\sim}{x} = [x_1, x_2, \ldots]^T$, the operation $\partial y/\partial \underset{\sim}{x}$ creates the column vector $[\partial y/\partial x_i]^T$, and $\partial \underset{\sim}{x}/\partial y = [\partial x_i/\partial y]^T$.

13.2.3 Definition of Systems

In the present analytical development it is useful to consider the dynamics as the interaction of three systems (ref. 9). These are most easily introduced by considering the simplest dynamical case depicted in Fig. 13.1. Now in full-scale craft, the effect of lateral skirt deflection x_s usually has a negligible effect on cushion heave force, so that the linearized heave dynamics can be represented by the block diagram shown in Fig. 13.2.

Some combination of vehicle, ground and skirt motion alters h_e. Through the fluid flow processes, the change δh_e causes a change δp_c in p_c. This δp_c

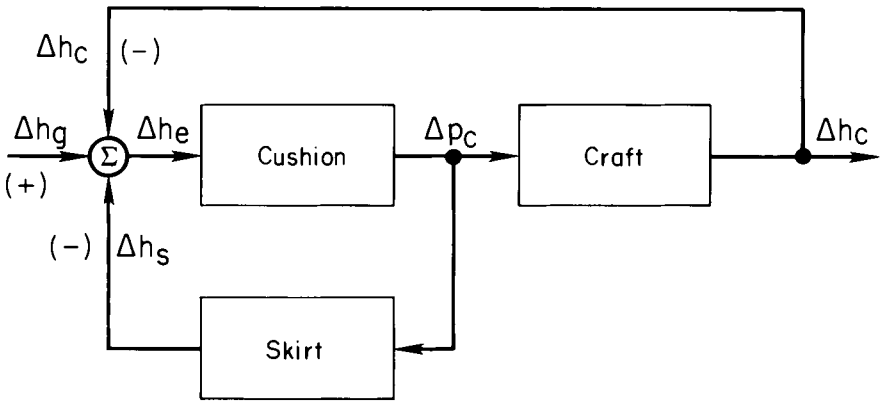

Fig. 13.2 Block diagram conceptualization of basic dynamics.

has two effects: first, by changing the forces on the skirt it alters h_s, and second, by acting on the base of the craft it causes craft motion $\delta h_c(t)$. Thus the *cushion lift system*, or *cushion system*, comprises the fluid flow processes from lift fan inlet to cushion exit, and in terms of the block diagram in Fig. 13.2, its input is Δh_e and output is Δp_c. The *skirt deformation system* or *skirt system* consists of the structural dynamics of the skirt, and its input is Δp_c, and output is the skirt deflection Δh_s. The *craft system* is the dynamics of the craft itself, so that its input and output are Δp_c and Δh_c respectively.

It is also useful to define two other subsystems. First, if the skirt is rigid so that the input δh_s to the cushion system is zero, then the overall system is called the *cushion-craft* system. If the craft does not move, the overall dynamics is that of the *skirt-cushion* system. The block diagram for the skirt-cushion system is depicted in Fig. 13.3a. The transfer function $\Delta p_c/\Delta h_e$ is called the *cushion pressure stiffness,* and $\Delta h_s/\Delta p_c$ is called the *skirt flexibility*.

For the tuck-under problem caused by skirt-surface contact, it is appropriate to introduce another subsystem equivalent to that of the skirt-cushion system. When a local surface perturbation Δh_g causes only part of the skirt perimeter to contact the surface, for simplicity it can be assumed that h_c and p_c do not vary significantly. However the immersion h_w generates a force f_w which acts to move the bottom of the skirt horizontally. As a result of skirt flexibility, h_s changes and a feedback occurs as depicted in Fig. 13.3b. The quantity $\Delta f_w/\Delta h_w$ is called the *hydro-stiffness* of the finger.

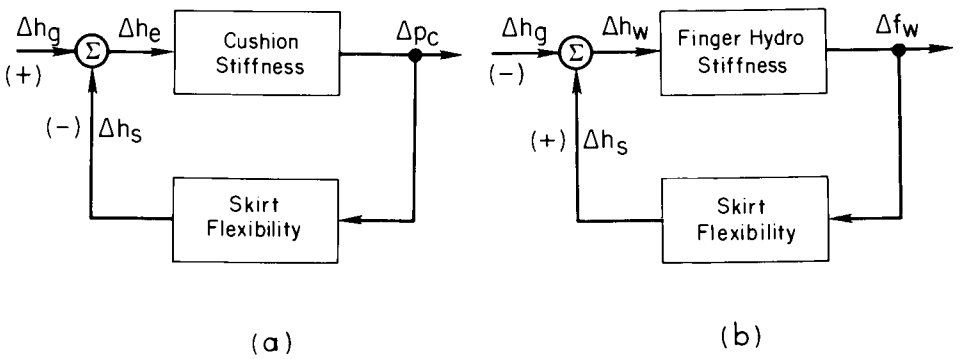

Fig. 13.3 Block diagram conceptualizations of skirt-cushion system: (a) in absence of contact; (b) with contact.

13.2.4 Classification of Skirt Responsiveness

In Section 13.1 it is noted that one of the major functions of a skirt is to minimize dynamical inputs into the craft. In terms of the block diagram in Fig. 13.2, to improve ride comfort, the craft heave motion Δh_c should be minimized. This in turn requires reduction of fluctuations in p_c, that is Δp_c. Since p_c is controlled through the cushion system by h_e, Δh_e has to be minimized. It follows that Δh_s should cancel the effect of Δh_g on Δh_e, so that the ideal skirt requires $\Delta h_s(s)/\Delta h_g(s) = 1$. Thus the extent to which the skirt approaches this ideal can be used as a measure or index of responsiveness.

To specify a simple numerical index, consider the static behaviour, that is $H_{sg}(0) \equiv \Delta h_s(0)/\Delta h_g(0)$, when $\Delta h_c = 0$. If $H_{sg}(0) < 0.5$ a skirt may be described as *non-responsive*. For $0.5 < H_{sg}(0) < 0.9$ the skirt is *responsive*, and if $H_{sg}(0) \geq 0.9$ it is *fully responsive*. In the following development it proves to be more useful to express the responsiveness in terms of $H_{se}(0) = \Delta h_s(0)/\Delta h_e(0)$. From eqn. 13.2, it follows that a skirt is non-responsive if $H_{se} < 1$, responsive if $1 \leq H_{se} < 9$, and fully responsive if $H_{se} \geq 9$. Figure 13.2a shows that H_{se} is the open loop gain of the skirt-cushion system.

An alternative approach to the measurement of skirt responsiveness is to define it in terms of fluctuations in p_c caused by ground and skirt motion respectively. In Section 13.4.3 it is shown that the two approaches are closely related.

13.2.5 Comments on Analytical Modelling of ACV Dynamics

Analysis of ACV dynamics can be very complex; it involves consideration of the basic craft dynamics, the air flow processes, the structural and dynamical behaviour of the skirt, together with the interaction of these processes.

Furthermore some aspects, such as the modulation of the cushion flow exit area, can be highly nonlinear, so that the problem is potentially much more complicated than its aeronautical counterpart, aeroelasticity. To make any progress it is essential to make major simplifying assumptions based on good physical insights. The assumptions used in the present analysis are discussed below.

Consider first those associated with the fluid mechanics. Sullivan, Hinchey and Green (ref. 12) have reviewed the assumptions used in basic cushion flow calculations. They observe that the flow from bag to cushion, and cushion to atmosphere can be assumed quasisteady and orifice-like. Only in certain special circumstances, one of which is discussed in Section 13.3.3, is the flow structure inside the cushion volumes significant, so that they can be usually modelled as plenum chambers. When the compressibility of the air in these volumes must be included, the thermodynamic process is effecively isentropic and can be modelled by a lumped pneumatic capacitance. If the cushion system contains any ducts, then they are usually so short that effects such as air inertia and frictional losses are negligible. However laboratory experiments may use moderately long ducting, in which case, except for very high frequencies, a lumped inertance is adequate (ref. 13). Perhaps the major area of uncertainty is the response of the lift fans to the fluctuating delivery pressures caused by vehicle motion. It has thus far been customary to assume that the fan flow is quasisteady, so that the steady state pressure-flow characteristic can be used. However available evidence suggests that, even at the relatively low frequencies characteristic of vehicle motion, significant departure from quasisteady behaviour can occur. It has been suggested that, for accurate calculations, a true dynamic characteristic should be used (refs. 8, 11); this point is discussed in more detail in Section 13.4.1.

Consider now the structural aspects of the skirt. All practical systems are constructed from elastomer-coated fabrics, and these materials can have both nonlinear orthotropic and viscoelastic properties. For some skirt geometries, cushion pressure fluctuations can generate small skirt deformations which, in turn, can significantly modulate hovergap and effective cushion capacitance (ref. 14), and thus the dynamics and stability may be affected considerably. This point is discussed in Chapter 12.

A second phenomenon is caused by the stress-relaxation or creep properties characteristic of many elastomers. When a portion of a skirt is forced towards a surface and contacts it, be it ground or water at planing speeds, small upward contact forces are generated (ref. 11). When the skirt moves away from the surface, owing to its creep properties, the original shape is not recovered immediately, so that the contact forces can be greatly reduced.

The resultant effect on the vehicle dynamics is a form of damping which, at model scale, can be very large; typically it appears as hysteresis in static stiffnesses. There is some evidence of its presence in full scale skirts of the type considered here (refs. 11, 15).

The present authors undertook a linear analysis of the heave dynamics of a bag-finger skirt in which the outer bag was modelled as a viscoelastic membrane; the computed effects on heave response were very small (ref. 16). It has been provisionally concluded that for responsive skirts, since geometric deformations are normally much larger than those associated with material strain, viscoelastic effects on geometry change can be ignored. However hysteretic effects on damping can still be important, and probably have to be included in a full nonlinear analysis.

Now observation of skirt motion suggests that, if surface contact does not occur, deformation is confined mainly to the bag, with the finger behaving essentially as a rigid body. Furthermore, in many cases, the motion of the inner bag tends to be confined mainly to a rotation about the inner attachment line O. This suggests that the simplest possible structural model of the skirt is a single degree of freedom system in which a rigid finger and inner bag assembly rotates about O in Fig. 13.1, with the outer bag modelled as an inelastic membrane. Furthermore, since for most skirts the ratio of cushion pressure p_c to material surface density μg is usually very large, at first sight it seems plausible to consider the outer bag as massless, with any required mass being lumped at the centre-of-mass of the finger. Thus the outer bag shape is always a circular arc. Ma (ref. 17) developed an analysis of skirt-cushion dynamics based on this concept. However this system is second order, and is always positively damped. It cannot predict static or dynamic instability of the skirt-cushion system, so that an adequate model requires additional degrees of freedom.

In this respect, the role of multiple degrees of freedom in generating both static and dynamic instability is well known in aeroelasticity. Furthermore, observations of model skirt motion in the neighbourhood of both static and dynamic instability indicates that significant motion of the point B in Fig. 13.1 along the chord OB can occur; and observation of outer bag motion during skirt bounce indicates that its geometry deviates considerably from a circular arc. This suggests that any model should have, at a minimum, two and possibly three degrees of freedom.

A two degree-of-freedom model proposed in the early literature assumes both inner and outer bags to be inelastic membranes subject only to air pressure loading (ref. 2) as depicted in Fig. 13.4. A potential difficulty with this model is that, even when the upper edges of the fingers are not attached to the inner bag, they usually contact it and provide partial support. A

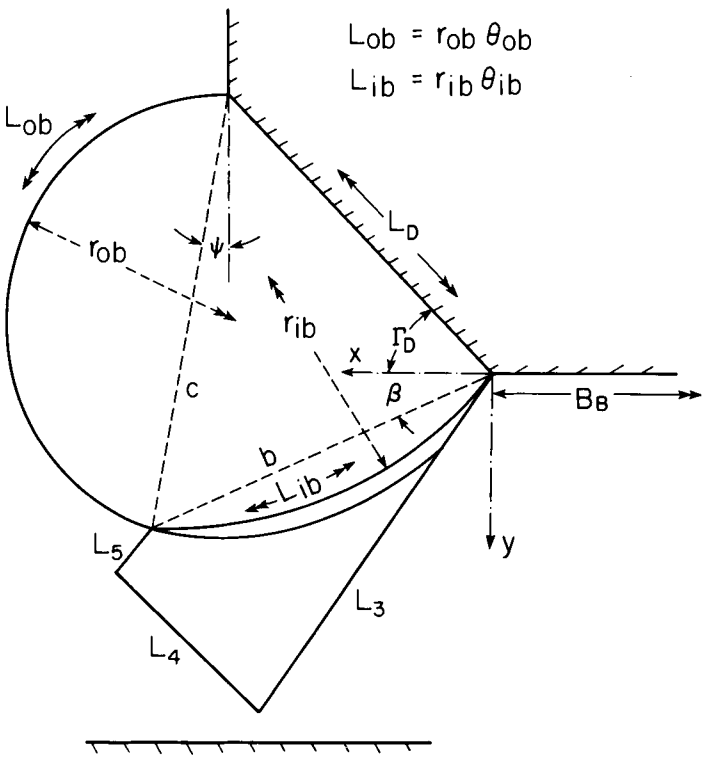

Fig. 13.4 Parameters used in skirt model defining base and bag geometry.

second approach is to model the fingers together with that part of the inner bag in contact with their upper edges as a single rigid body, with the remaining part of the inner bag, in this case OD in Fig. 13.5, as a rigid link (ref. 16). These two models thus might be viewed as limiting cases, with real skirt behaviour being somewhere between. In this respect, observation of model skirts at the authors' laboratories indicate that, even when the length ED is very small, significant variation of the chord length OB can occur during skirt motion. Results from both models are described in the following sections.

Finally, consider the modelling of the water surface contact forces and the resulting finger behaviour for tuck-under and other problems. Usually, at the craft speeds V_w for which these problems are significant, the ratios of the water hydrodynamic pressure to cushion pressure $[\frac{1}{2}\rho_w V_w^2]/p_c$ is very high, perhaps 50 or more. Thus one would not expect the finger to penetrate the water surface to any extent. Observation of both model and full scale

behaviour generally confirms this. However deformation of the finger is not confined to the immediate neighbourhood of the contact region; a considerable portion of the length B'C in Fig. 13.1 may be curved. This presents a significant modelling problem. Here we adopted highly simplified model first suggested by Plackett and Wade (ref. 18). Available evidence (ref. 19) suggests that it is at least qualitatively correct.

13.2.6 Formulation of Skirt Model

The equations for the model of the skirt are formulated by using a Lagrangian approach, and are then linearized. The analysis is developed for the general case of N degrees of freedom, with generalized coordinates $\underset{\sim}{q} = [q_1, q_2, \ldots, q_N]^T$. However at the time of writing, results have been obtained only for a two-degree of freedom model, $\underset{\sim}{q} = [\beta, b]^T$. Here β is the angle that the inner bag chord OB makes with respect to the horizontal, and b is the length of OB. Figures 13.4 and 13.5 define the geometry required for the latter case.

Now, for N degrees of freedom, Lagrange's equations for the skirt motion

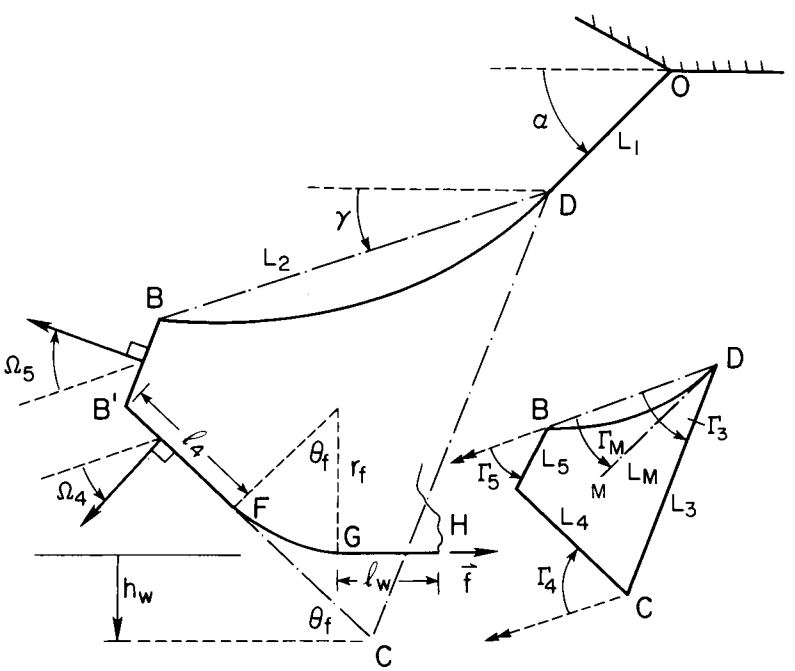

Fig. 13.5 Parameters used in skirt model defining finger geometry, including surface contact case. In the present model, the skirt mass M_s is lumped at M.

can be written in the form

$$\frac{d}{dt}\left\{\frac{\partial T}{\partial \dot{q}_i}\right\} - \frac{\partial T}{\partial q_i} + \frac{\partial P}{\partial q_i} = Q_i^{OB} + Q_i^{IB} + Q_i^{FP} + Q_i^{FW}, \qquad i = 1, 2, \ldots, N \tag{13.4}$$

Here $T(q_i, \dot{q}_i)$ is the kinetic energy of the skirt, $P(q_i)$ is the potential energy, containing terms due to gravity and possibly elasticity, and the terms on the right hand side are the non-conservative generalized forces. The first three non-conservative forces are generated by the pressures p_b and p_c, and the fourth, Q_i^{FW}, is that arising from surface contact. The first of the pressure force terms, Q_i^{OB}, is generated by p_b acting on the *outer bag,* AB in Fig. 13.1, the second, Q_i^{IB}, is generated by the difference $p_b - p_c$ acting on the *inner bag* BO, and the third, Q_i^{FP}, by p_c acting on the outer finger surface BC.

To calculate T, the skirt inertia is modelled as R discrete mass points each having mass M_i. If $x_i(q_1, q_2, \ldots, q_\alpha, \ldots, q_N)$, i = 1 to 3R are the cartesian coordinates of these mass points, measured with respect to any suitable inertial frame, then with $M_1' = M_2' = M_3' = M_1$, $M_4' = M_5' = M_6' = M_2$, ...,

$$T = \frac{1}{2}\sum_{i=1}^{3R} M_i' \dot{x}_i^{\,2} = \frac{1}{2}\sum_{i=1}^{3R} M_i'\left\{\sum_{\alpha=1}^{N} (\partial x_i/\partial q_\alpha)\dot{q}_\alpha\right\}^2 \tag{13.5}$$

These sums can be expanded and rearranged to give the form

$$T = \frac{1}{2}\sum_{\alpha=1}^{N}\sum_{\beta=1}^{N} m_{\alpha\beta}(q_i)\dot{q}_\alpha\,\dot{q}_\beta; \tag{13.6}$$

where

$$m_{\alpha\beta}(q_i) = \sum_{j=1}^{3R} M_j'\left\{\frac{\partial x_j}{\partial q_\alpha}\cdot\frac{\partial x_j}{\partial q_\beta}\right\} = m_{\beta\alpha} \tag{13.7}$$

The pressure force Q_i's are calculated by considering the work done by p_b and p_c associated with perturbations δq_i. Now it is a fundamental result of hydrostatics that, if a surface S moves and deforms under the action of a pressure p in such a way that it sweeps out a volume δV^S, then the work done δW^S by the resultant pressure force is simply $p\,\delta V^S$. Hence, since we can always write

$$\delta V^S = \sum_{i=1}^{N} \frac{\partial V^S}{\partial q_i}\,\delta q_i, \tag{13.8}$$

then

$$\delta W^S = \sum_{i=1}^{N} Q_i^S \, \delta q_i = p_i \sum_{i=1}^{N} \frac{\partial V^S}{\partial q_i} \, \delta q_i \tag{13.9}$$

The general form of the equations of motion can now be stated. If δV^{OB}, δV^{IB}, and δV^F are the volumes swept out by, respectively, the outer bag, the inner bag and the finger as a result of perturbations δq_i, and if

$$\lambda_{ijk} \equiv \{\frac{\partial m_{ik}}{\partial q_j} - \frac{1}{2} \frac{\partial m_{ij}}{\partial q_k}\} \tag{13.10}$$

then eqns. (13.4) become

$$\sum_{j=1}^{N} m_{ij} \, \ddot{q}_j + \sum_{j=1}^{N} \sum_{k=1}^{N} \lambda_{ijk} \, \dot{q}_j \, \dot{q}_k + \frac{\partial P}{\partial q_i}$$

$$= p_b \frac{\partial V^{OB}}{\partial q_i} + (p_b - p_c) \frac{\partial V^{IB}}{\partial q_i} + p_c \frac{\partial V^F}{\partial q_i} + Q_i^{FW}, \quad i = 1, 2, \ldots, N \tag{13.11}$$

In these equations, if $\underset{\sim}{R}_m = \{M_1, M_2, \ldots\}$ is a set of mass and other material property parameters, and $\underset{\sim}{R}_G = \{L_D, \Gamma_D, L_{ob}, \ldots\}$ is a set of geometrical parameters, then $m_{ij} = f(q_\alpha; \underset{\sim}{R}_m, \underset{\sim}{R}_G)$, $P = f(q_\alpha; \underset{\sim}{R}_m, \underset{\sim}{R}_g)$, and $\partial V^{OB}/\partial q_i = f(q_\alpha; \underset{\sim}{R}_G)$. Equations (13.11) also imply that, for a given skirt system, that is for given $\underset{\sim}{R}_m$ and $\underset{\sim}{R}_g$, in the absence of surface contact, the motion equations have the functional form

$$\underset{\sim}{F}(\underset{\sim}{q}, \dot{\underset{\sim}{q}}, \ddot{\underset{\sim}{q}}, p_b, p_c) = 0 \quad \text{or} \quad F_i(q_j, \dot{q}_j, \ddot{q}_j, p_b, p_c) = 0 \tag{13.12}$$

These equations can be linearized in the usual way and then converted to the Laplace domain. In the absence of surface contact, $Q_i^{FW} = 0$, and the system of equations so obtained can be expressed in the form

$$[s^2 \underset{\sim}{M}_s + \underset{\sim}{K}_s] \, \Delta \underset{\sim}{q} + \underset{\sim}{V}_p \begin{bmatrix} \Delta p_b \\ \Delta p_c \end{bmatrix} = \underset{\sim}{0} \tag{13.13}$$

In eqn. (13.13), $\underset{\sim}{M}_s$ is an inertia matrix with elements $[\underset{\sim}{M}_s]_{ij} = m_{ij}(\underset{\sim}{q}_o)$, $\underset{\sim}{K}_s$ is a stiffness matrix and, as discussed below, the matrix $\underset{\sim}{V}_p$ introduces exciting or input forces, damping and additional stiffness.

The matrix $\underset{\sim}{K}_s$ is called the *geometric stiffness matrix,* to distinguish it from the contributions to stiffness through $\underset{\sim}{V}_p$. It can be decomposed into

four submatrices:

$$\underset{\sim}{K}_s = \underset{\sim}{K}_{sg} + \underset{\sim}{K}_{ob} + \underset{\sim}{K}_{ib} + \underset{\sim}{K}_f \tag{13.14}$$

where the elements of the submatrices are:

$$[\underset{\sim}{K}_{sg}]_{ij} = \partial^2 P/\partial q_i \partial q_j \quad \ldots \text{ potential energy} \tag{13.15}$$

$$[\underset{\sim}{K}_{ob}]_{ij} = -p_b \partial^2 V^{OB}/\partial q_i \partial q_j \quad \ldots \text{ outer bag} \tag{13.16}$$

$$[\underset{\sim}{K}_{ib}]_{ij} = -(p_b - p_c)\, \partial^2 V^{IB}/\partial q_i \partial q_j \quad \ldots \text{ inner bag} \tag{13.17}$$

$$[\underset{\sim}{K}_f]_{ij} = -p_c \partial^2 V^F/\partial q_i \partial q_j \quad \ldots \text{ finger} \tag{13.18}$$

The identification of these contributions to $\underset{\sim}{K}_s$ is made because insights into the effect of the skirt system on the craft dynamics can be obtained by considering each in turn. As an example it is useful to think of the outer and inner bags as nonlinear or variable stiffness springs similar to a curved sheet of metal in which the stiffness decreases as the curvature increases. Figure 13.6 shows the relationship between the angle of a circular arc θ or semi-angle $\sigma = \theta/2$, and the ratio of chord to arc length c/L. For any given L, when r/L is large, θ is small, c/L is near unity, and a small change in c

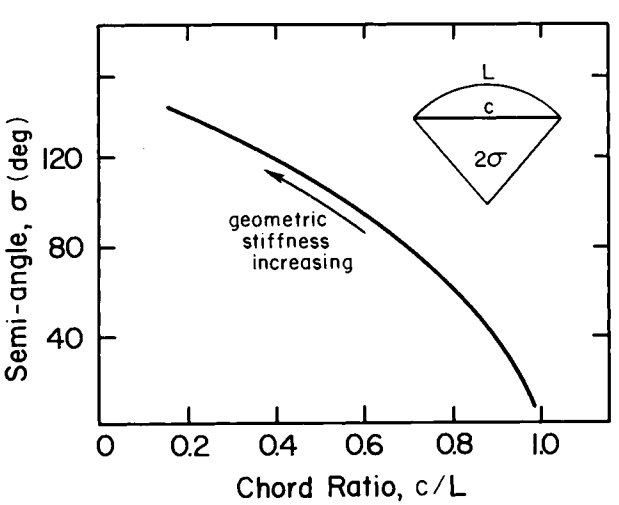

Fig. 13.6 Effect of inner and outer bag geometry on geometric stiffness.

causes large changes in θ and r. It follows from the equation for membrane tension, $t_m = pr = pL/\theta$, that a large change in t_m occurs and the *equivalent* spring is relatively stiff. Conversely, for large θ or small c/L the spring is much softer. Now, skirt responsiveness depends strongly on the stiffness of the outer bag. In general high responsiveness requires, for given inputs δp_c and δp_b, large δh_s and thus large vertical motion of the point B in Fig. 13.1. Hence the outer bag stiffness should be low, and a responsive skirt has a large arc angle θ_{ob}, perhaps as large as $\theta_{ob} = \pi$.

$\underset{\sim}{V}_p$ is an N×2 matrix, the i-th row of which is

$$[\underset{\sim}{V}_p]_i = -[[\partial V^{OB}/\partial q_i + \partial V^{IB}/\partial q_i],\ [\partial V^F/\partial q_i - \partial V^{IB}/\partial q_i]] \tag{13.19}$$

Note also that the elements of $\underset{\sim}{V}_p$ depend only on $\underset{\sim}{q}$ and the geometric parameters $\underset{\sim}{R}_g$.

It is useful to consider the perturbations in p_b and p_c as arising from two sources. The first source is motion of the skirt itself, which generates additional stiffness and damping, and the second source is motion of the craft and ground, which generates input or exciting forces. As is depicted in Fig. 13.2, stiffness forces are generated by interaction with the cushion system in the following way: changes in any of the q_i cause changes in h_e, which in turn modulates the cushion flow processes and, in particular, p_c and p_b. The idea is illustrated for a single degree-of-freedom system consisting of a rigid hinged lip and bag as depicted in Fig. 13.7. For fixed p_c and p_b, a change in ß alters the bag radius and thus the magnitude and direction of the tension force acting on the lip BO. On the other hand, changes in ß alter h_e and, through the fluid mechanics, p_c and p_b and thus the pressure force acting on BO. To distinguish this from the former contribution, it is called *pressure stiffness*. Contributions to the Q_α^S are generated by the velocities $\dot{q}_i$ because both the bag and cushion volumes V_b and V_c are functions of the q_i. The rate of variation of these volumes, $\dot{V}_b$ and $\dot{V}_c$, cause perturbations in the flows between the volumes which in turn generate fluid losses, and p_b and p_c which change the Q_i. The effect of $\dot{V}_b$ and $\dot{V}_c$ on p_b and p_c is essentially that of a dashpot. The development of the matrices describing the stiffness and damping generated by cushion feedback is given in Sections 13.3.3 and 13.4.3 respectively.

The skirt modulates both the cushion flow through the height h_s and the cushion lift force through the lateral displacement x_s. Since $h_s = h_s(q_i)$ and $x_s = x_s(q_i)$, define the 2×N geometric *transfer matrix* $\underset{\sim}{T}$ so that, with $\underset{\sim}{h}_s = [h_s, x_s]^T$,

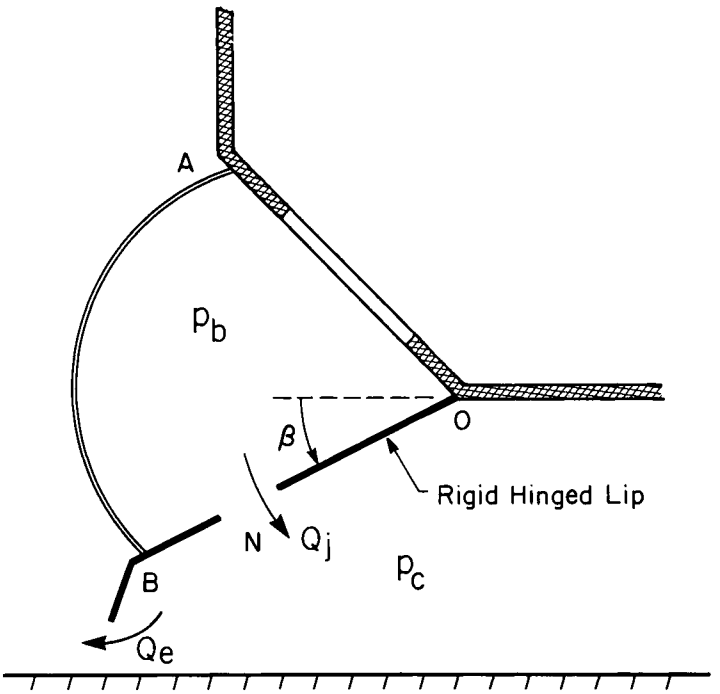

Fig. 13.7 Single degree-of-freedom model illustrating the difference between pressure and geometric stiffness.

$$\Delta \underset{\sim}{h} = \begin{bmatrix} \Delta h_s \\ \Delta x_s \end{bmatrix} = \underset{\sim}{T}\, \Delta \underset{\sim}{q}, \qquad \underset{\sim}{T} = \begin{bmatrix} \partial h_s/\partial q_i \\ \partial x_s/\partial q_i \end{bmatrix} \tag{13.20}$$

Also for each stiffness matrix $\underset{\sim}{K}_i$ we can define a corresponding flexibility matrix $\underset{\sim}{F}_i = \underset{\sim}{K}_i^{-1}$.

This completes the formulation of the mathematical model of the skirt dynamics. In the following sections it is shown that, within the context of linear theory, the effect of the skirt system on the dynamics occurs entirely through the matrices $\underset{\sim}{M}_s$, $\underset{\sim}{K}_s$ and $\underset{\sim}{V}_p$. However, to obtain specific results, in both nonlinear and linear analyses it is necessary to make additional assumptions that are consistent with the number of degrees of freedom adopted. In the following section these are developed for $\underset{\sim}{q} = [\beta, b]^T$.

13.2.7 Equations for the Two-Degree-of-Freedom Model

The simplest assumption about mass distribution that is consistent with $\underset{\sim}{q} = [\beta, b]^T$ is to lump it as a single mass M_s at an appropriate point in the

finger as shown in Fig. 13.5. Then with

$$\alpha = \beta + \arccos\,[(b^2 + L_1{}^2 - L_2{}^2)/2L_1 b] \tag{13.21}$$

and

$$\gamma = \beta - \arccos\,[(b^2 + L_2{}^2 - L_1{}^2)/2L_2 b] \tag{13.22}$$

and with M_c the total mass of the craft, including the skirt,

$$T = M_c \dot{h}_c{}^2/2 + M_s\{L_1{}^2\dot{\alpha}^2/2 + L_M{}^2\dot{\gamma}^2/2 + L_1 L_M \cos(\Gamma_M + \gamma - \alpha)\dot{\alpha}\dot{\gamma}$$

$$+ \dot{h}_c[\dot{\alpha}L_1\cos\alpha + \dot{\gamma}L_M\cos(\Gamma_M + \gamma)]\} \tag{13.23}$$

$$P = -M_c g h_c - M_s g\{L_1 \sin\alpha + L_M \sin(\Gamma_M + \gamma)\} \tag{13.24}$$

To calculate Q_β^{OB} and Q_b^{OB} with all the skirt mass lumped in the finger, it is consistent to assume that the outer bag is a massless membrane in which case, as depicted in Fig. 13.4, during motion it always remains a circular arc. Then, with L_s the length of skirt over which p_b and p_c act, with $\sigma_{ob} = \theta_{ob}/2$, and with $q_1 = \beta$ and $q_2 = b$, the outer bag generalized forces are:

$$Q_i^{OB} = p_b \frac{\partial V^{OB}}{\partial q_i} = p_b L_s\{\frac{c^2}{2}\frac{\partial\psi}{\partial q_i} - \frac{L_{ob}}{2}[\frac{\cos\sigma_{ob}}{\sigma_{ob}}]\frac{\partial c}{\partial q_i}\} \tag{13.25}$$

where

$$c^2 = L_D{}^2 + b^2 - 2L_D b\cos(\beta + \Gamma_D), \tag{13.26}$$

and

$$\tan\psi = (b\cos\beta - L_D\cos\Gamma)/(b\sin\beta + L_D\sin\Gamma_D) \tag{13.27}$$

and where

$$\frac{\sin\sigma_{ob}}{\sigma_{ob}} = \frac{c}{L_{ob}} \tag{13.28}$$

With the inner bag modelled as a membrane, the generalized forces are

$$Q_\beta^{IB} = (p_b - p_c)\frac{\partial V^{IB}}{\partial\beta} = (p_b - p_c)L_s b^2/2$$

$$Q_b^{IB} = (p_b - p_c)\frac{\partial V^{IB}}{\partial b} = -(p_b - p_c)(L_s L_{ib})\frac{\cos\sigma_{ib}}{\sigma_{ib}} \tag{13.29}$$

where

$$\frac{\sin \sigma_{ib}}{\sigma_{ib}} = \frac{b}{L_{ib}} \tag{13.30}$$

When the inner bag is modelled as two rigid links, then Q_{β}^{IB} is given by eqn. (13.29) and

$$Q_b^{IB} = (p_b - p_c)\frac{\partial V^{IB}}{\partial q_i} = (p_b - p_c)\frac{L_s L_1}{2}\left[\sin(\alpha-\beta) + b\cos(\alpha-\beta)\frac{\partial\alpha}{\partial b}\right] \tag{13.31}$$

In the absence of surface contact, the generalized forces caused by p_c acting on the finger are

$$Q_i^{FP} = p_c\frac{\partial V^F}{\partial q_i} = p_c L_s\{[L_1L_4\sin(\Omega_4 + \gamma - \alpha) - L_1L_5\sin(\Omega_5 + \alpha - \gamma)]\partial\alpha/\partial q_i$$

$$+ [L_4L_6 - L_4^2/2 - L_7]\partial\gamma/\partial q_i \tag{13.32}$$

where

$$L_6 = L_2\sin\Omega_4 - L_5\cos(\Omega_4+\Omega_5) \tag{13.33a}$$

$$L_7 = L_5(L_5/2 + L_2\sin\Omega_5) \tag{13.33b}$$

For the linear analysis, calculation of the matrices $\underset{\sim}{M}_s$, $\underset{\sim}{K}_s$ and $\underset{\sim}{V}_p$ is straightforward. Note that, in terms of the notation of eqn. (13.12), if $F_1 \equiv M$ and $F_2 \equiv F$, then

$$\underset{\sim}{K}_s = \begin{bmatrix} \partial M/\partial\beta & \partial M/\partial b \\ \partial F/\partial\beta & \partial F/\partial b \end{bmatrix} \tag{13.34}$$

and

$$\underset{\sim}{V}_p = \begin{bmatrix} \partial M/\partial p_b & \partial M/\partial p_c \\ \partial F/\partial p_b & \partial F/\partial p_c \end{bmatrix} \tag{13.35}$$

Because the $\underset{\sim}{q}$ frame of reference is not inertial, terms proportional to $\ddot{h}_c$ are present in the linearized formulation. However, insofar as the skirt dynamics is concerned, it has been found that these are usually small (ref. 16), and may be omitted.

13.2.8 Model of Skirt–surface Contact for Two Degrees of Freedom

Figure 13.5 depicts the model used by Plackett and Wade (ref. 18) to calculate the forces acting on a finger in contact with a water surface which is moving horizontally relative to the skirt. The finger is assumed to consist of two parts: a portion DBB'F which retains the shape that occurs in

the absence of contact, and the remainder FGHD which is in partial or total collapse. The part DBB'F is assumed to act as a rigid body. The front of the finger B'C of length L_4 is divided into three parts: the uncollapsed part B'F of length ℓ_4, a part GH of length ℓ_w which lies on the water surface, and a connecting length FG.

Now one would expect that the drag force f_w per unit width exerted on GH to depend on ℓ_w, and on the density ρ_w, viscosity μ_w and velocity V_w of the water, in which case dimensional considerations dictate:

$$f_w/[\tfrac{1}{2}\rho_w V_w^2 \ell_w] \triangleq C_D = f(Re_w), \qquad Re \triangleq (\rho_w V_w \ell_w)/\mu_w \tag{13.36}$$

Observations (ref. 18) suggest that the drag coefficient C_D may be taken as constant and having a value of about 0.01. Consequently f_w is expressed in terms of a *speed coefficient* K_D:

$$f_w = K_D p_c \ell_w, \qquad \text{where} \qquad K_D \equiv C_D \rho_w V_w^2/(2p_c) \tag{13.37}$$

To calculate the effect of f_w on the finger Plackett and Wade assumed that the part FG of the finger can be modelled as an inelastic massless membrane of radius r_f which is subject to the pressure loading p_c. Thus

$$\ell_4 + r_f\theta_f + \ell_w = L_4 \tag{13.38}$$

where

$$p_c r_f = f_w; \qquad \theta_f = \Gamma_4 - \gamma \tag{13.39}$$

and f_w is transmitted to the uncollapsed part of the finger only through this membrane. Also, from the assumed geometry

$$h_w = (L_4 - \ell_w)\sin\theta_f - r_f(1 - \cos\theta_f) \tag{13.40}$$

The quantities required for calculating the generalized forces acting on the finger are ℓ_w and ℓ_4; from eqns. (13.38 - 13.40) one obtains

$$\ell_w = g_{w1}(\theta_f)h_w \tag{13.41}$$

and

$$\ell_4 = L_4 - g_{w2}(\theta_f)h_w \tag{13.42}$$

where

$$g_{w1}(\theta_f) = \{K_D[(\theta_f \sin\theta_f + \cos\theta_f - 1] + \sin\theta_f\}^{-1} \tag{13.43}$$

$$g_{w2}(\theta_f) = [K_D\theta_f + 1]g_{w1}(\theta_f) \tag{13.44}$$

and where

$$h_w = h_c + h_s(q_i) - h_g \tag{13.45}$$

Thus, according to this model, the effect of surface contact on the forces acting on the finger is two-fold; first a force f_w acts along B'C and this increases as h_w increases, and second, the pressure force acting on the finger decreases as h_w increases.

For the two-degree-of-freedom system adopted here the generalized forces acting on the finger become

$$Q_i^{FP} = p_c L_s\{[L_1\ell_4\sin(\Omega_4 + \gamma - \alpha) - L_1L_5\sin(\Omega_4 + \alpha - \gamma)]\frac{\partial\alpha}{\partial q_i}$$

$$+ [L_6\ell_4 - \ell_4^2/2 - L_7]\partial\gamma/\partial q_i \tag{13.46}$$

and

$$Q_i^{FW} = p_c K_D L_s \ell_w\{L_1\cos(\Omega_4 + \gamma - \alpha)\partial\alpha/\partial q_i + L_8\partial\gamma/\partial q_i + \partial\ell_4/\partial q_i\} \tag{13.47}$$

where

$$L_8 = L_2\cos\Omega_4 + L_5\sin(\Omega_4 + \Omega_5) \tag{13.48a}$$

$$\partial\ell_4/\partial q_i \equiv \ell_{4,i} = g'_{w2}(\theta_f)\frac{\partial\gamma}{\partial q_i}h_w - g_{w2}\,\partial h_s/\partial q_i \tag{13.48b}$$

The linearization of these equations is discussed in Section 13.3.3.

13.3 HEAVE STATICS

In this section the static response of the skirt to its inputs p_b and p_c is discussed, the question of static stability and its relation to the tuck-under problem is investigated, and the equations for the pressure-flow characteristics for steady-state behaviour are developed. This is followed by derivation of the equations for the heave statics of the skirt-cushion system, and the heave stiffness of the overall system. The section concludes by presenting some experimental data on cushion response obtained from a small model.

13.3.1 Skirt System Statics

The static response and stability of the skirt is governed by the equations of static equilibrium. Consider first the behaviour when surface contact does not occur; then the nonlinear equations of equilibrium are

$$p_b \frac{\partial V^{OB}}{\partial q_i} + (p_b - p_c) \frac{\partial V^{IB}}{\partial q_i} + p_c \frac{\partial V^F}{\partial q_i} = \frac{\partial P}{\partial q_i}, \qquad i = 1, 2, \ldots, N \tag{13.49}$$

For $\underset{\sim}{q} = [\beta, b]^T$ and $\underset{\sim}{F} = [M, F]^T$ these equations have the functional form

$$q_1 = \beta: \qquad M(\beta, b, p_c, p_b; g, \underset{\sim}{R}_m, \underset{\sim}{R}_g) = 0 \tag{13.50}$$

$$q_2 = b: \qquad F(\beta, b, p_c, p_b; g, \underset{\sim}{R}_m, \underset{\sim}{R}_g) = 0 \tag{13.51}$$

We make two observations about the structure of these equations. The first is that eqns. (13.50-51) have a simple physical interpretation. The line BO in Fig. 13.1 may be considered a link hinged at o, free to rotate and telescope, but not to bend. Then static equilibrium requires, for all the forces acting at B, (a) the resultant acting along BO must be zero, and (b) the resultant moment about O must be zero. These give the equations for $q_2 = b$ and $q_1 = \beta$ respectively. Then the terms in eqns. (13.49) are generated respectively by the outer bag tension $t_{ob} = p_b r_{ob}$, the inner bag tension $t_{ib} = (p_b - p_c) r_{ib}$, the force due to p_c acting on the finger, and the skirt weight. The second observation is that, for a given skirt system, that is for given $\underset{\sim}{R}_m$ and $\underset{\sim}{R}_g$, if p_c and p_b are assigned fixed values, then eqns. (13.49) can be solved for the q_i:

$$q_i = f_i(p_c, p_b; g, \underset{\sim}{R}_m, \underset{\sim}{R}_g) \tag{13.52}$$

Equation (13.52) can be nondimensionalized. With L_D and Γ_D defined in Fig. 13.4, use $B_d = L_D \cos \Gamma_D$, p_b and g as reference quantities, and denote nondimensional quantities with an overbar ($\bar{\ }$), to obtain

$$\bar{q}_i = \bar{f}_i(\bar{p}_c, \bar{\underset{\sim}{R}}_m, \bar{\underset{\sim}{R}}_g) \tag{13.53}$$

In these equations $\bar{p}_c = p_c/p_b$ is a dimensionless input force. Furthermore, the magnitude of the mass elements of $\underset{\sim}{R}_m$, that is $\bar{M}_i = (M_i g)/p_b L_S B_d$, are usually very small so that, to investigate the statics, one can set $\bar{M}_i = 0$. Thus for a given family of skirts having the same set of nondimensional geometric parameters $\bar{\underset{\sim}{R}}_g$, the geometry of the inflated skirt depends only on $\bar{p}_c$. In particular, $\bar{h}_s = h_s/B_D = f(\bar{p}_c)$ and $\bar{x}_s = x_s/B_D = f(\bar{p}_c)$.

Figure 13.8 compares measured values of $\bar{h}_s$ and $\bar{x}_s$ obtained from a small two-dimensional model with predictions obtained by solving eqns. (13.49) and using the membrane model of the inner bag. In interpreting these results for the linear analysis, define a *pressure flexibility* $\bar{H}_{\bar{p}}$ as follows:

$$\bar{\underset{\sim}{H}}_p \equiv \begin{bmatrix} \bar{h}_{\bar{p}} \\ \bar{x}_{\bar{p}} \end{bmatrix} \equiv \begin{bmatrix} \Delta\bar{h}_s/\Delta\bar{p}_c \\ \Delta\bar{x}_s/\Delta\bar{p}_c \end{bmatrix} = \begin{bmatrix} \partial\bar{h}_s/\partial\bar{p}_c \\ \partial\bar{x}_s/\partial\bar{p}_c \end{bmatrix} \tag{13.54}$$

The results in Figs. 13.8 show that the skirt vertical response to $\bar{p}_c$ increases and lateral response decreases as $\bar{p}_c$ increases. This suggests that to obtain maximum responsiveness, $\bar{p}_c$ should be as close to 1 as possible.

The quantity of interest in the dynamics is the dimensional skirt response to p_c, that is, $\Delta h_s/\Delta p_c$ and $\Delta x_s/\Delta p_c$; and this depends on the characteristics of the cushion air supply system. Since $\bar{\underset{\sim}{H}}_{\bar{p}} = f(\bar{p}_c)$ then

$$\underset{\sim}{H}_c \equiv \begin{bmatrix} \Delta h_s/\Delta p_c \\ \Delta x_s/\Delta p_c \end{bmatrix} = \frac{B_d}{p_b}\{1 - \bar{p}_c P_{bc}\}\,\bar{\underset{\sim}{H}}_{\bar{p}} \tag{13.55}$$

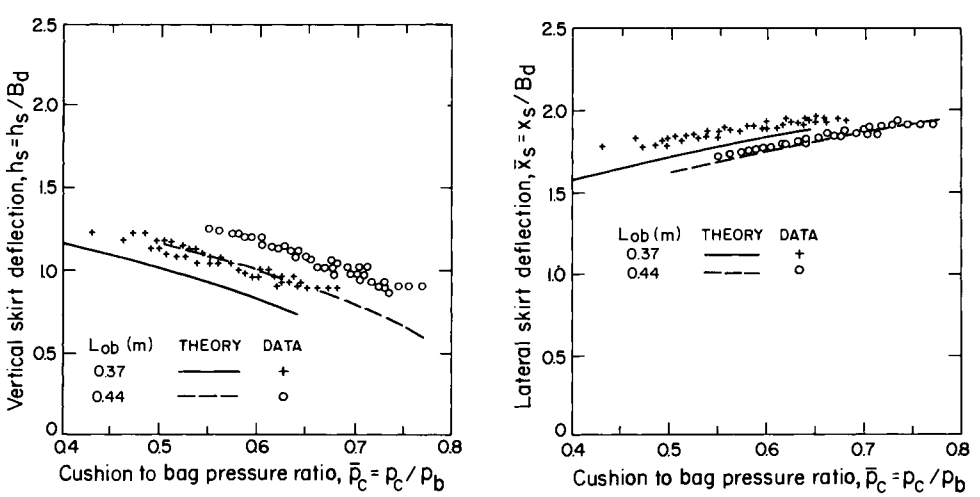

Fig. 13.8 Effect of cushion and bag pressure on static vertical and lateral response of a small model skirt. Parameters: $\Gamma_D = 41.64°$, $B_D = 0.1714$m, $L_{ib} = 0.395$m, $L_1 = 0.03$m, $N_f = 1300$–2300 rpm.

where $P_{bc} \equiv \Delta p_b/\Delta p_c$ is the *cushion-to-bag pressure response*. The latter quantity plays an important role in the subsequent development, and its static and dynamic forms are derived in the following sections.

13.3.2 Static Stability and the Tuck–Under Problem

Solutions to eqns. (13.49) are of no practical significance unless it can be shown that they are statically stable. Criteria for the stability of a particular equilibrium solution can be obtained in the usual way from the equations for a small perturbation about that equilibrium. Now, as discussed in Section 13.2.6, through its modulation of the hovergap, skirt motion contributes additional stiffness; that is, the static stability of the skirt system is in general influenced by the cushion system.

In the absence of contact, the combined skirt-cushion system is almost always statically stable. However when surface contact occurs, the Q_i^{FW} terms can contribute negative stiffness and a static instability can occur. In this case, since only a small part of the skirt contacts the surface, a relatively small fraction of the cushion flow is modulated, so that the assumption that p_b and p_c remain constant is believed to be acceptable.

In developing the linearized equations for the surface contact case, our aim is to use h_w as a feedback variable. Inspection of eqns. (13.46) and (13.47) shows that, if $\alpha_{,i} \equiv \partial\alpha/\partial q_i$ and $\gamma_{,i} = \partial\gamma/\partial q_i$, $Q_i^{FP} = Q_i^{FP}(p_c, \ell_4, \gamma, \alpha, \alpha_{,i}, \gamma_{,i})$ and $Q_i^{FW} = Q_i^{FW}(p_c, \ell_w, \gamma, \alpha, \alpha_{,i}, \gamma_i, \ell_{4,i})$, where $\alpha = \alpha(q_i)$ and $\gamma = \gamma(q_i)$. But $\ell_4 = \ell_4(\gamma, h_w)$, $\ell_w = \ell_w(\gamma, h_w)$ and $\partial\ell_4/\partial q_i = \ell_{4,i}(\gamma, q_i, h_w)$. Accordingly, define the following stiffness matrices, $\underset{\sim}{K}_{fp}$ and $\underset{\sim}{K}_{fw}$, and input vector $\underset{\sim}{F}_{hw}$ as follows:

$$[\underset{\sim}{K}_{fp}]_{ij} = \frac{\partial Q_i^{FP}}{\partial\alpha}\frac{\partial\alpha}{\partial q_j} + \frac{\partial Q_i^{FP}}{\partial\gamma}\frac{\partial\gamma}{\partial q_j} + \frac{\partial Q_i^{FP}}{\partial\alpha_i}\frac{\partial\alpha_{,i}}{\partial q_j} + \frac{\partial Q_i^{FP}}{\partial\gamma_i}\frac{\partial\gamma_{,i}}{\partial q_j} + \frac{\partial Q_i^{FP}}{\partial\ell_4}\frac{\partial\ell_4}{\partial\gamma}\frac{\partial\gamma}{\partial q_j} \tag{13.56}$$

$$[\underset{\sim}{K}_{fw}]_{ij} = \frac{\partial Q_i^{FW}}{\partial\alpha}\frac{\partial\alpha}{\partial q_j} + \frac{\partial Q_i^{FW}}{\partial\gamma}\frac{\partial\gamma}{\partial q_j} + \frac{\partial Q_i^{FW}}{\partial\alpha_i}\frac{\partial\alpha_{,i}}{\partial q_j} + \frac{\partial Q_i^{FW}}{\partial\gamma_i}\frac{\partial\gamma_{,i}}{\partial q_j} + \frac{\partial Q_i^{FW}}{\partial\ell_w}\cdot\frac{\partial\ell_w}{\partial\gamma}\frac{\partial\gamma}{\partial q_j}$$

$$+ \frac{\partial Q_i^{FW}}{\partial\ell_{4,i}}\cdot\left[\frac{\partial\ell_{4,i}}{\partial\gamma}\frac{\partial\gamma}{\partial q_j} + \frac{\partial\ell_{4,i}}{\partial q_j}\right] \tag{13.57}$$

$$[\underset{\sim}{F}_{hw}]_i = -\left\{\frac{\partial Q_i^{FP}}{\partial\ell_4}\frac{\partial\ell_4}{\partial h_w} + \frac{\partial Q_i^{FW}}{\partial\ell_w}\frac{\partial\ell_w}{\partial h_w} + \frac{\partial Q_i^{FW}}{\partial\ell_{4i}}\cdot\frac{\partial\ell_{4,i}}{\partial h_w}\right\} \tag{13.58}$$

Then, with $\underset{\sim}{K}_b \equiv \underset{\sim}{K}_{ob} + \underset{\sim}{K}_{ib}$ and $\underset{\sim}{K}_f \equiv \underset{\sim}{K}_{fp} + \underset{\sim}{K}_{fw}$, and with the contribution of skirt weight $\underset{\sim}{K}_{sg}$ neglected, the linearized and transformed equilibrium

equations become

$$[\underset{\sim}{K}_b + \underset{\sim}{K}_f]\Delta\underset{\sim}{q} = \underset{\sim}{F}_{hw}\Delta h_w \tag{13.59}$$

But since $\Delta h_w = \Delta h_c + \Delta h_s - \Delta h_g$, and since $\Delta h_s = (\partial h_s/\partial \underset{\sim}{q})^T\Delta\underset{\sim}{q}$, eqn. (13.59) can be rearranged to the form

$$[\underset{\sim}{K}_b + \underset{\sim}{K}_f]\Delta\underset{\sim}{q} = \underset{\sim}{F}_{hw}(\Delta h_g - \Delta h_c) + \underset{\sim}{F}_{hw}(\partial h_s/\partial \underset{\sim}{q})^T\Delta\underset{\sim}{q} \tag{13.60}$$

Define

$$\underset{\sim}{K}_w = -\underset{\sim}{F}_{hw}(\partial h_s/\partial \underset{\sim}{q})^T \tag{13.61}$$

so that eqn. (13.60) can be written

$$\underset{\sim}{K}_{ST}\Delta\underset{\sim}{q} \equiv (\underset{\sim}{K}_s + \underset{\sim}{K}_w)\Delta\underset{\sim}{q} = \underset{\sim}{F}_{hw}(\Delta h_g - \Delta h_c) \tag{13.62}$$

Here $\underset{\sim}{K}_w$ is a stiffness matrix arising from feedback through Δh_w; it is called the *water feedback stiffness matrix*. Figure 13.9 is a block diagram depicting the process governed by eqn. (13.62).

Stability criteria for this system can be determined in two ways. The first is that the overall stiffness matrix $\underset{\sim}{K}_{ST}$ must be positive-definite, which, for $\underset{\sim}{q} = [\beta, b]^T$ and $\underset{\sim}{F} = [M, F]$, reduces to the requirement that

$$E = \det \underset{\sim}{K}_{ST} \equiv \det \begin{bmatrix} \partial M/\partial\beta & \partial M/\partial b \\ \partial F/\partial\beta & \partial F/\partial b \end{bmatrix} > 0 \tag{13.63}$$

The second way is to exploit the role of h_w as a feedback variable as depicted in Fig. 13.9. Define the vector gain

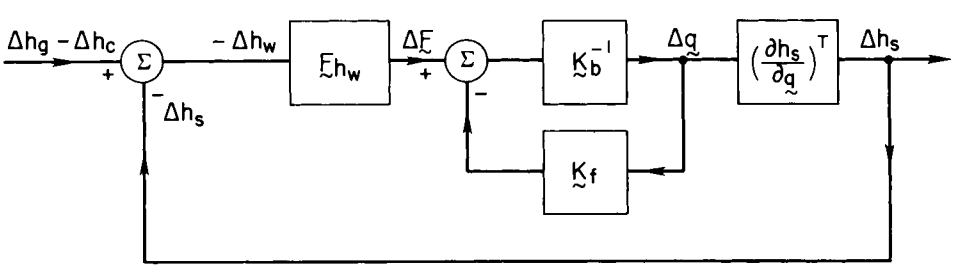

Fig. 13.9 Block diagram illustrating feedback mechanisms involved in tuck-under problem.

$$\underset{\sim}{G}_w = \begin{bmatrix} G_w \\ H_w \end{bmatrix} \begin{bmatrix} \Delta h_s/\Delta h_w \\ \Delta x_s/\Delta h_w \end{bmatrix} \tag{13.64}$$

Recalling eqn. (13.20), we have

$$\Delta \underset{\sim}{h}_s = \begin{bmatrix} \Delta h_s \\ \Delta x_s \end{bmatrix} = \underset{\sim}{T}\, \Delta \underset{\sim}{q} = \underset{\sim}{T}[\underset{\sim}{K}_b + \underset{\sim}{K}_f]^{-1}\, \underset{\sim}{F}_{hw}\, \Delta h_w \tag{13.65}$$

But, according to the chain rule of differentiation $(\partial h_s/\partial \underset{\sim}{q})^T(\partial \underset{\sim}{q}/\partial h_s) = 1$, so that from eqns. (13.61), (13.64) and (13.65)

$$\underset{\sim}{F}_{hw} = -\underset{\sim}{K}_w(\partial \underset{\sim}{q}/\partial h_s) \quad \text{and} \quad \underset{\sim}{G}_w = -\underset{\sim}{T}[\underset{\sim}{K}_b + \underset{\sim}{K}_f]^{-1}\underset{\sim}{K}_w(\partial \underset{\sim}{q}/\partial h_s) \tag{13.66}$$

Thus $\underset{\sim}{G}_w$ is related to the product of the inverse of the basic skirt contacting stiffness and the water feedback stiffness matrix. Now, as discussed below, as V_w increases from zero G_w is at first negative and then becomes positive. Thus from the block diagram in Fig. 13.3b, the system becomes unstable when $G_w = \Delta h_s/\Delta h_w = 1$.

In the absence of surface contact, then static stability requires det $\underset{\sim}{K}_s > 0$. Usually this occurs, although at high values of p_b/p_c it is possible for the coupling derivatives $\partial M/\partial b$ and $\partial F/\partial \beta$ to become large and thus create instability (ref. 16).

Figures 13.10 and 13.11 give computed values of the elements of E for a model skirt with $h_s = 0.25$m and $\bar{p}_c = 0.80$ (ref. 17). The elements are presented as functions of h_w with K_D as a parameter. These show that the magnitude of $\partial M/\partial \beta$ decreases rapidly as K_D increases because the force f_w increases rapidly with speed. On the other hand, for fixed K_D, as h_w increases, $\partial M/\partial \beta$ at first increases, reaches a maximum and then decreases. This occurs because immersion initially drags the skirt down and increases bag stiffnesses but eventually the loss of finger stiffness caused by reduction of the pressurized length ℓ_4 causes $\partial M/\partial \beta$ to decrease. Simultaneously, as K_D increases the component of f_w acting in the BO direction increases rapidly and causes the magnitude of the coupling derivative $\partial F/\partial \beta$ to increase rapidly. The element $\partial F/\partial b$ increases rapidly with both K_D and h_w because increases in b generate large forces along BO when at high K_D and h_w. Similarly, as K_D increases, the coupling derivative $\partial M/\partial b$ decreases rapidly. Static stability is thus controlled mainly by $\partial M/\partial \beta$ and $\partial F/\partial \beta$.

Figure 13.12 gives E as a function of h_w with K_D as a parameter for the skirt. It shows that E decreases rapidly as speed increases; and that as h_w increases, at first E increases and then it decreases. These variations are

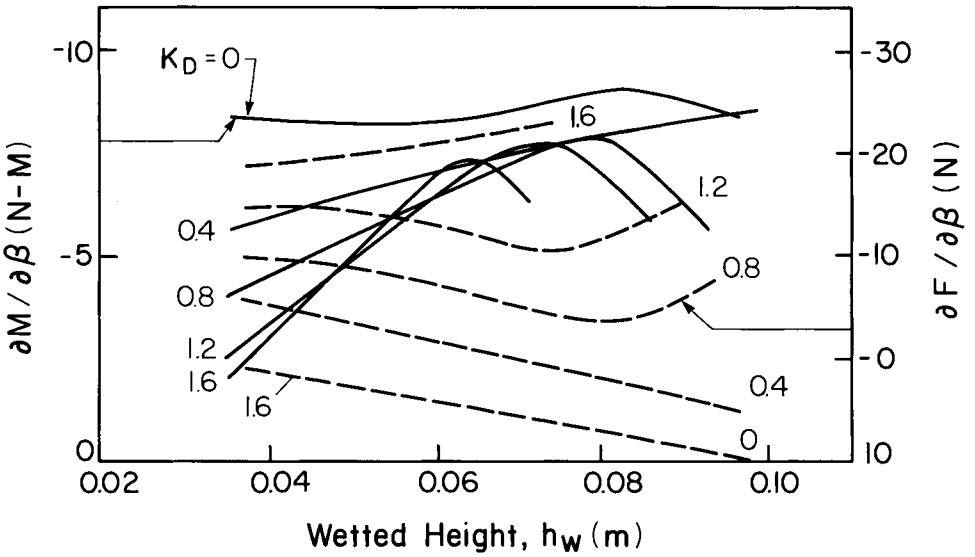

Fig. 13.10 Effect of wetted height h_w and water speed coefficient K_D on elements $\partial M/\partial \beta$ and $\partial F/\partial \beta$ of tuck-under stability matrix $\underline{K}_{ST}$ for a small laboratory model. Skirt height h_s = 0.25m.

caused by the opposing effects of outer and inner bag stiffnesses on the one hand, and the reduction of ℓ_4 and increase in f_w on the other. One concludes that, at high V_w and small h_w a skirt is much more prone to tuck-under than it is at low V_w and high h_w.

The geometry of the outer and inner bags, through their effect on $\bar{h}_{\bar{p}}$ in eqn. (13.54), has a large effect on static stability. Figure 13.13 shows some stability boundaries obtained from a model tested in a water channel (ref. 19). The hatched sides of the curves are stable, and the model dimensions are similar to those used for the computations discussed above. Case I is for a non-responsive skirt, and cases II to IV are for typical responsive skirts. The lengths of outer and inner bags of the responsive skirts is given relative to that of the non-responsive skirt. An anti-plough web was used for cases I, III and IV. For cases I and III the length of the anti-plough web was set to be just slack at equilibrium, while in case IV the web length was set at 0.87 of that for cases I and III. These results show that increasing $\bar{h}_{\bar{p}}$ makes the skirt more prone to tuck-under, with an anti-plough web clearly improving stability, although at the expense of reducing $\bar{h}_{\bar{p}}$. However even a slack anti-plough web increases the stability of a responsive skirt.

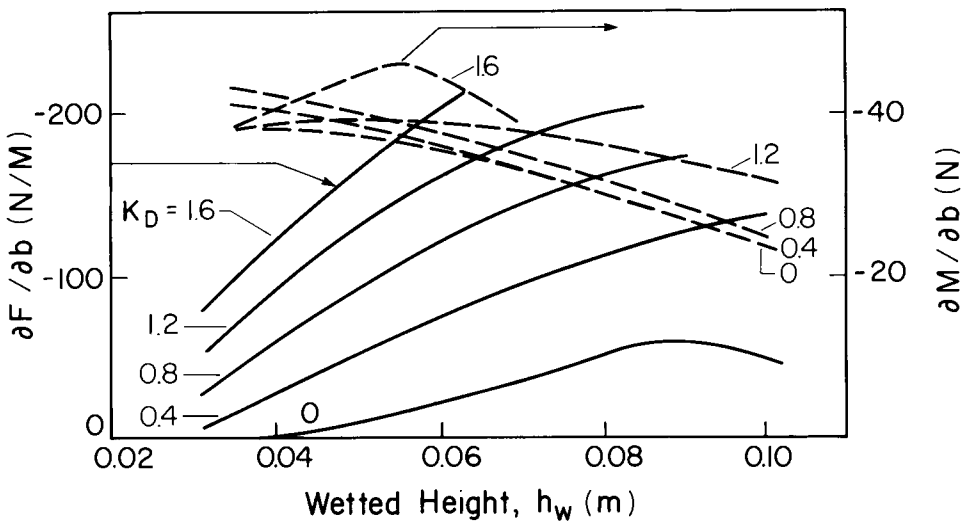

Fig. 13.11 Effect of wetted height h_w and water speed coefficient K_D on elements $\partial F/\partial b$ and $\partial M/\partial b$ of tuck-under stability matrix $\underset{\sim}{K}_{ST}$ of a small laboratory geometry. Skirt height h_s = 0.25m.

Now as discussed above, the skirt vertical response to immersion $G_w = \Delta h_s/\Delta h_w$, which is, in effect, the hydro-elastic open-loop gain of the skirt contacting system, has a large effect on the hydrodynamic drag on the skirt, on static stability and tuck-under, and on the craft pitch response to waves. If it is negative, that is, if skirt height decreases with increase of immersion, the hydrodynamic drag is reduced, the onset of tuck-under is delayed, and pitch stiffness is reduced. However this only happens at low speed and small immersion when the contributions of bag and finger stiffness outweigh that caused by f_w. However as K_D and h_w increase, G_w rapidly becomes positive, then f_w pulls the skirt downward. The lateral response $H_w = \Delta x_s/\Delta h_w$ is usually negative, and its magnitude increases rapidly as K_D increases causing reduced stability of the skirt, and loss of craft pitch stiffness.

13.3.3 Cushion System Fluid Mechanics

In this section the equations used to model the fluid mechanics for the statics are presented. The analysis includes two models of the basic cushion flow: a plenum chamber and a peripheral wall-jet.

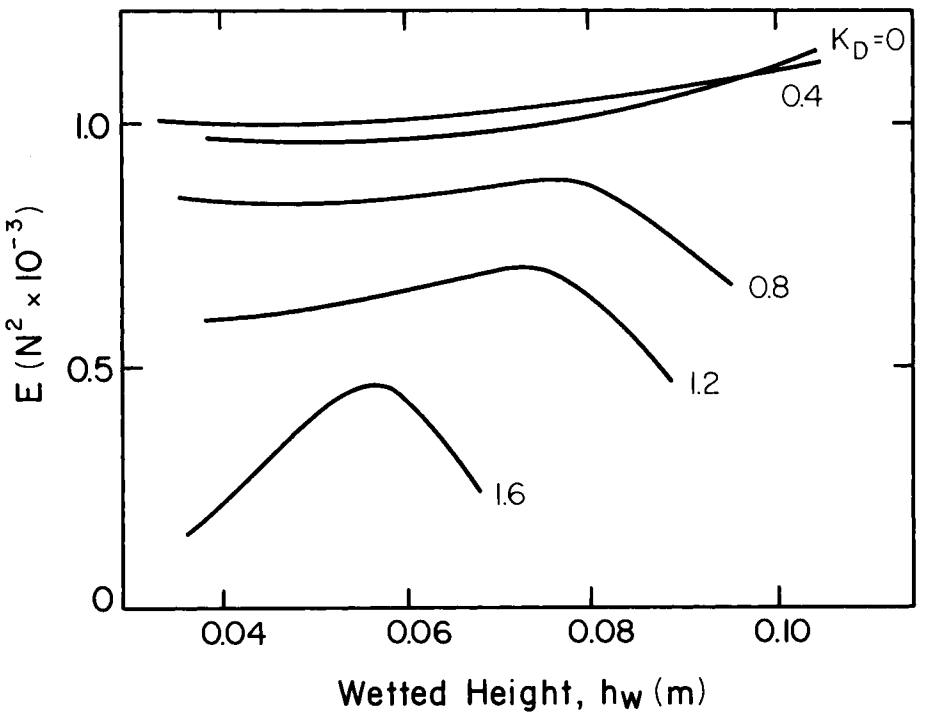

Fig. 13.12 Effect of wetted height, h_w, and water speed coefficient K_D on determinant of tuck-under stability matrix $\mathcal{K}_{ST}$ of a small laboratory geometry.

The relationship between the flow Q_f and pressure p_f delivered by the lift fan, that is, its *characteristic*, is determined from an empirical test, and a polynomial is usually fitted to the data:

$$p_f = \sum_{n=0}^{N} A_{fn} Q_f^n \tag{13.67}$$

where for a given fan the coefficients A_{fn} depend on both atmospheric density ρ_a and fan speed N. Usually a quadratic is sufficient, and this is assumed here. As noted in Sect. 13.2.1, the flow is usually delivered to the bag by a plenum chamber and, possibly, some ducting. Some of the air may be diverted for other purposes. In both cases the pressure-flow relationship for the volume flux Q_d of air entering the bag can be assumed to follow a polynomial

$$p_b = \sum_{n=0}^{N} A_{bn} Q_d^n \tag{13.68}$$

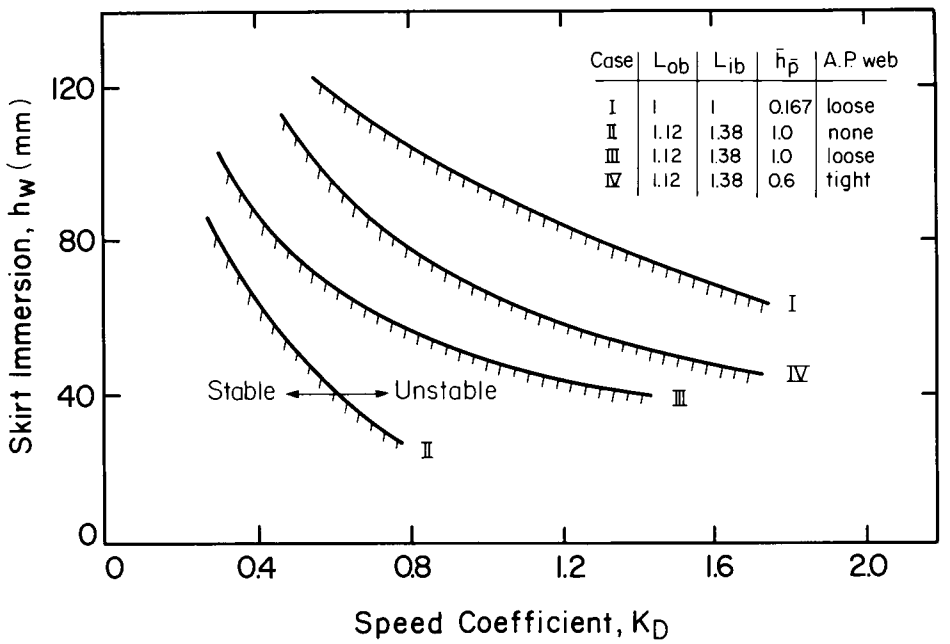

Fig. 13.13 Observed tuck-under stability boundaries for a model skirt tested in a water channel.

where again a quadratic is usually sufficient. Figure 13.14 shows the general shape of these two curves; head losses between fan outlet and bag steepen the bag pressure characteristic, while flow diversion flattens it.

The flow from bag to cushion is assumed to be governed by the usual orifice model based on Bernoulli's law and a discharge coefficient,

$$p_b = p_c + \frac{1}{2}\rho(Q_j/S_j)^2; \quad S_j = C_{mj}L_sB_j \tag{13.69}$$

where Q_j is the flow from bag to cushion, S_j is the effective flow area, C_{mj} a volume discharge coefficient, and B_j is the bag orifice area per unit perimeter of skirt. To test the validity of this assumption, the data obtained in Fig. 13.15 was obtained from a small model which consisted of a two-dimensional section of the skirt confined between end-plates. With measured Q_j, p_b, p_c and $A_j = L_sB_j$, eqn. (13.69) was used to calculate C_{mj}. In this case, considerable leakage occurred at the end-plates, so that C_{mj} based on A_j is considerably larger than the accepted orifice value of 0.61; but it is clear that the flow is orifice-like.

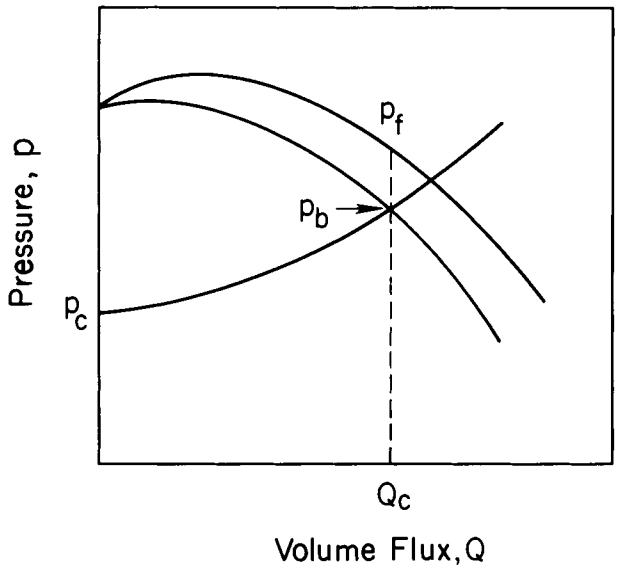

Fig. 13.14 Typical static pressure-flow characteristics of cushion air system.

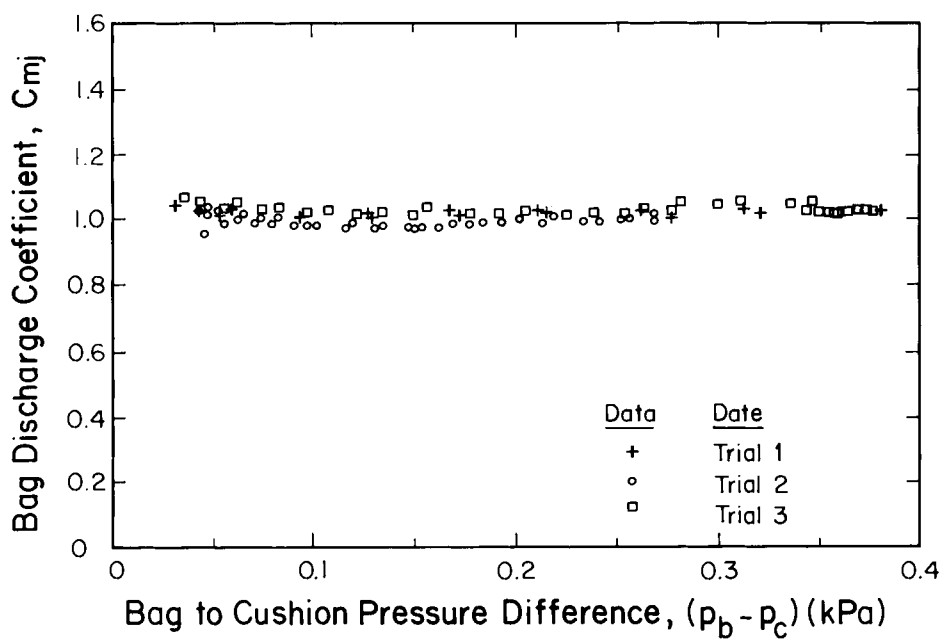

Fig. 13.15 Data from test of validity of orifice flow model for flow from bag to cushion.

In practice for complete skirts one can assume that $C_{mj} = 0.61$. Note that, in pure heave, $Q_j = Q_d$. Equation 13.69 is also drawn in Fig. 13.14; generally increasing B_j makes this curve less steep. Equations 13.68 and 13.69 together determine the operating point of the cushion air supply system.

The model to be used to calculate the air flow escaping from the cushion Q_e depends on the location of the bag orifices, and one must consider two cases. In the first case the bag orifices are distributed over the inner bag as depicted in Fig. 13.1; the cushion then behaves like a plenum chamber, and the air escape process is orifice-like. In this case one can use a law of the form

$$Q_e = h_f(h_e, \theta_f)L_s(2p_c/\rho_a)^{1/2} \tag{13.70}$$

In this expression h_f is an effective slot or leak height, which is a function of both h_e, and of θ_f. The dependence of h_f on h_e and θ_f can be calculated by using the geometry of the segments and known data about dicharge coefficients, but it may be more accurate to infer it from an experiment. Figure 13.16 gives h_f as a function of h_e with θ_f as a parameter, obtained from the model described above. Equation (13.70) was used to compute h_f from measured Q_e and p_c. The range of θ_f included in this data encompasses that observed during the heave motion of the model. For this data, at a given θ_f, as h_e increases from some negative value, h_f is at first constant, and then near $h_e = 0$ begins to make a transition to the linear dependence that is expected when the segment tips are well clear of the ground. The constant non-zero value of h_f for $h_e < 0$ is caused by air leaks between segments and, in the present model, at the model ends. For this model the segment tips were not cut off as depicted in Fig. 13.1. If the tips are removed, the transition to linear dependence that occurs as h_e increases is expected to become much more abrupt, but a significant dependence on θ_f should still be present.

Equations 13.69 and 13.70 can be combined to obtain the cushion pressure ratio $\bar{p}_c = p_c/p_b$; replace h_f by a discharge coefficient $C_{me} \equiv h_f/h_e$, and let $\bar{h}_e \equiv h_e/B_j$, then

$$\bar{p}_c = \{1 + [(C_{me}/C_{mj})(Q_e/Q_j)\bar{h}_e]^2\}^{-1} \tag{13.71}$$

Note that $C_{me} = C_{me}(h_e, \theta_f)$. Also, in general, owing to flow under stability bags between cushion compartments, only in pure heave motion is $Q_e = Q_j$. This expression is plotted in Fig. 13.17.

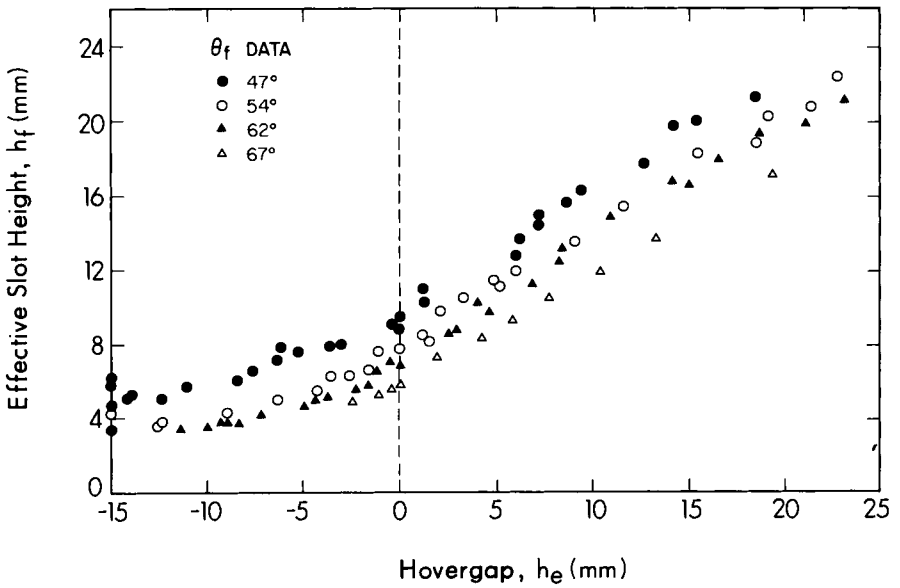

Fig. 13.16 Effective leak height as a function of hovergap for a small two-dimensional model.

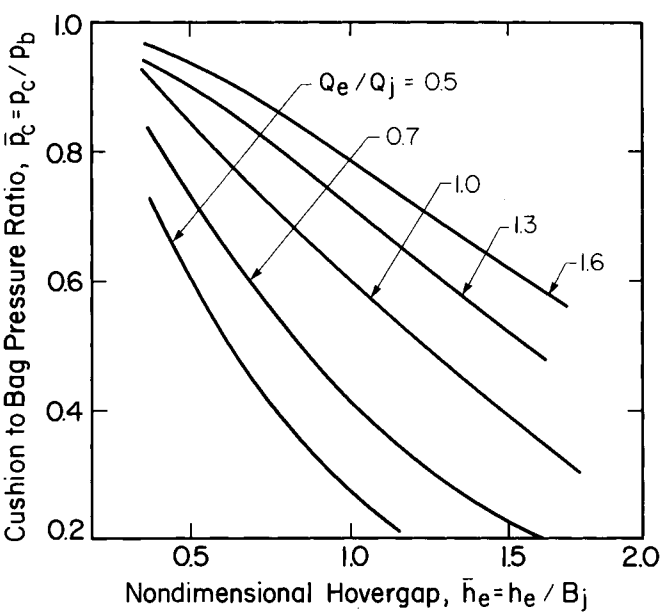

Fig. 13.17 Predicted pressure-flow characteristic for plenum chamber model of cushion flow processes.

In the second cushion feed case the orifices N in Fig. 13.1 are all located near the outer edge B of the finger so that, when $L_5 = 0$, the air flows down the inside of the finger and is attached to it; thus the flow is, in effect, a wall-jet. Ma et al (ref. 20) present an analysis of this flow; it uses available wall-jet analyses for the flow down the finger, and a momentum balance for an assumed peripheral jet escape flow. The analysis gives

$$\bar{p}_c = \{1 + 0.781\ \bar{h}_e[(M_e/M_j)[1 + 1.3(\bar{h}_e)^{-1/2}] + \cos\theta_f - 1]^{-1}\}^{-1} \tag{13.72}$$

where M_e and M_j are the magnitudes of the momentum fluxes escaping from the cushion and the bag orifices respectively. Now the theory of turbulent wall-jets shows that

$$M_e/M_j = f(Q_e/Q_j,\ L_4/B_j) \tag{13.73}$$

and typical values of M_e/M_j as obtained from this theory are given in Fig. 13.18. Figure 13.19 gives $\bar{p}_c$ as a function of $\bar{h}_e$ for a representative value of L_4/B_j as predicted by eqn. (13.72).

Now let $Q_c = Q_e - Q_j$ be the net rate of flow out of the cushion. Then eqns. 13.71 for the plenum chamber model, and (13.72-73) for the wall-jet model imply that, for a given skirt geometry,

$$\bar{Q}_c \equiv Q_c/Q_j = \bar{Q}_c(\bar{p}_c,\ \bar{h}_e,\ \theta_f) \tag{13.74}$$

Now $\theta_f = \theta_f(\underset{\sim}{q})$ and, according to eqn. (13.53), $\bar{\underset{\sim}{q}} = f(\bar{p}_c)$, so that eqn. (13.74) can be linearized and transformed to give

$$\Delta\bar{Q}_c = Q_h\Delta\bar{h}_e + Q_p\Delta\bar{p}_c \tag{13.75}$$

where $Q_h \equiv \partial\bar{Q}_c/\partial\bar{h}_e$, and $Q_p \equiv \partial\bar{Q}_c/\partial\bar{p}_c + (\partial\bar{Q}_c/\partial\theta_f)(d\theta_f/d\bar{p}_c)$.

Define a nondimensional cushion pressure stiffness $\Delta\bar{p}_c/\Delta\bar{h}_e$; since in pure heave $\Delta\bar{Q}_c = 0$, eqn. (13.75) gives

$$\Delta\bar{p}_c/\Delta\bar{h}_e = Q_h/Q_p \tag{13.76}$$

Equations (13.71-73) show that $\Delta\bar{p}_c/\Delta\bar{h}_e$ depends on the cushion and skirt configuration, and not the characteristics of the system supplying the air. Figure 13.20 is a plot of the predicted $\Delta\bar{p}_c/\Delta\bar{h}_e$ as a function of $\bar{h}_e$ for the two feed cases; it shows that both cases have comparable stiffness, with the plenum chamber case being somewhat stiffer for all but a small range of $\bar{h}_e$.

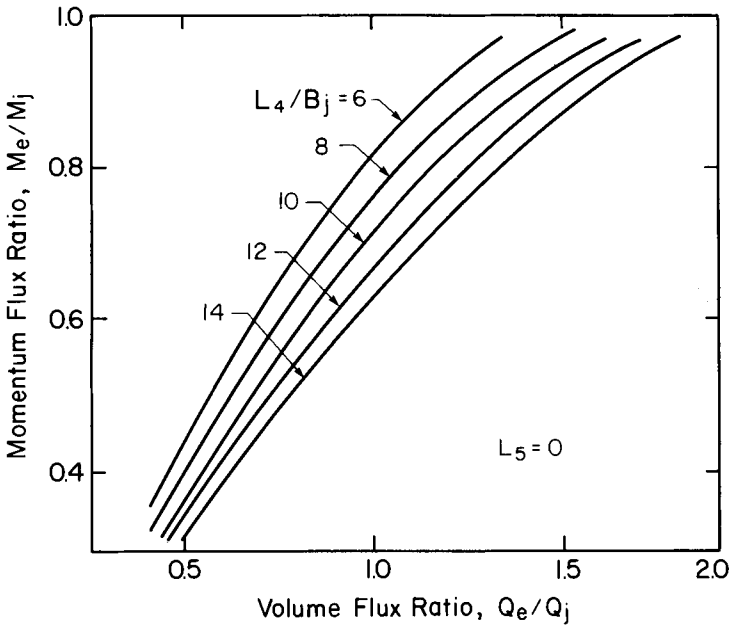

Fig. 13.18 Predicted momentum flux ratios for wall-jet model of cushion flow processes.

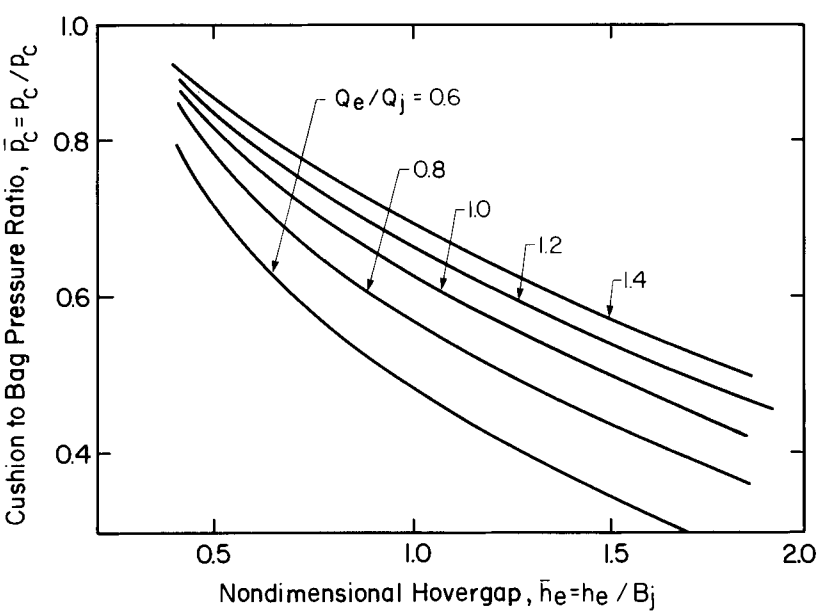

Fig. 13.19 Predicted pressure-flow characteristic for wall-jet model of cushion flow processes.

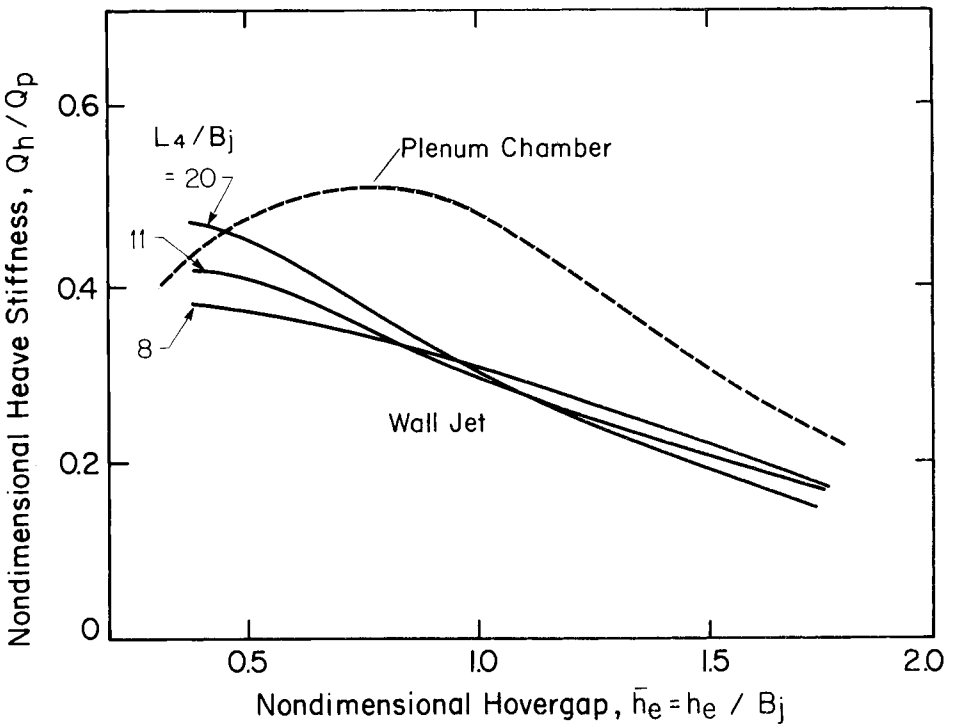

Fig. 13.20 Comparison of predictions of pressure-stiffness for plenum chamber and wall-jet models of cushion flow process.

Now let $P_{ch}(s) = \Delta p_c(s)/\Delta h_e(s)$; its static value $P_{ch}(0)$ is the cushion pressure stiffness. Since $\Delta\bar{p}_c/\Delta p_c = (1 - \bar{p}_c P_{bc})/p_b$,

$$P_{ch}(0) = -Q_h/Q_p(p_b/B_j)(1 - \bar{p}_c P_{bc})^{-1} \tag{13.77}$$

Now, as is shown in the following section, P_{bc} depends on the characteristics of the air supply system; hence in contrast to $\Delta\bar{p}_c/\Delta\bar{h}_e$, $P_{ch}(0)$ does depend on the air supply system behaviour. Also, for a given cushion geometry and $\bar{p}_c$, increasing P_{bc} increases cushion stiffness. This is opposite to the effect on the cushion to skirt pressure response, which is

$$\Delta h_s/\Delta p_c = (B_j/p_b)(1 - \bar{p}_b P_{bc})(\partial\bar{h}_s/\partial\bar{p}_c) \tag{13.78}$$

Now in order to ensure that the hovering process is as efficient as possible, energy losses associated with flow processes such as that from bag to cushion should be minimized. This requires that $\bar{p}_c$ be as close to unity as other considerations allow. Comparison of Figs. 13.17 and 13.19 suggests that the energy loss for the plenum chamber model is less than those for the wall-jet model if $\bar{h}_e < 0.7$ approximately or, equivalently, if $\bar{p}_c$ is greater than about 0.7. Since to minimize the air flow used to hover, most cushions operate with $\bar{h}_e$ less than 0.7, this suggests that the bag orifices should be distributed as shown in Fig. 13.1 rather than concentrated near the finger edge. Consequently in the following analysis the plenum chamber model of the cushion flow processes is used.

13.3.4 Impedance Analysis of Cushion System

The equations for the plenum chamber model of the cushion are now linearized. Equation (13.68) becomes

$$\Delta p_b = -R_{fd}\Delta Q_d \tag{13.79}$$

where R_{fd} is the combined fan-duct or *bag inlet resistance* given by

$$R_{fd} \equiv -\frac{dp_b}{dQ_d} = -(A_{b1} + 2A_{b2}Q_d), \tag{13.80}$$

and a minus sign is included because dp_b/dQ_d is usually negative at the equilibrium operating point. Similarly eqn. (13.69) becomes

$$\Delta p_b - \Delta p_c = R_j\Delta Q_j \tag{13.81}$$

where

$$R_j \equiv 2(p_b - p_c)/Q_j \tag{13.82}$$

is the *bag outlet resistance*. Finally eqn. (13.70) becomes

$$\Delta Q_e = C_e\Delta h_e + \Delta p_c/R_e \tag{13.83}$$

where

$$C_e = \frac{Q_e}{h_f}\frac{dh_f}{dh_e} = Q_e\{C_{me}^{-1}\, dC_{me}/dh_e + h_e^{-1}\} \tag{13.84}$$

and

$$R_e = 2p_c/Q_e \tag{13.85}$$

where R_e is the *cushion outlet resistance.*

For pure heave $\Delta Q_d = \Delta Q_j = \Delta Q_e$. Then eqns. (13.79, 81 and 83) is a system of three equations for the perturbations Δp_b, Δp_c and ΔQ_e in terms of the constants R_{fd}, R_j, R_e, C_e and the input Δh_e. However, for the development of the analysis, Δp_b, Δp_c and ΔQ_e are not used directly, it is the transfer functions $P_{ch} = \Delta p_c/\Delta h_e$ and $P_{bc} = \Delta p_b/\Delta p_c$ which are required. These are

$$P_{ch} = - C_e \frac{(R_{fd} + R_j)R_e}{(R_{fd} + R_j + R_e)} \tag{13.86}$$

$$P_{bc} = \frac{R_{fd}}{(R_{fd} + R_j)} \tag{13.87}$$

These formulae can be expressed more compactly by defining two equivalent resistances. The first is the *bag system resistance* R_b which is R_{fd} in parallel with R_j:

$$R_b^{-1} \equiv R_{fd}^{-1} + R_j^{-1} \tag{13.88}$$

The second is the *cushion system resistance* R_c. If $R_{fj} = R_{fd} + R_j$ is the *cushion upstream resistance* then R_c is R_e and R_{fj} in parallel,

$$R_c^{-1} = R_{fj}^{-1} + R_e^{-1} \tag{13.89}$$

Then

$$P_{ch} = -C_e R_c; \qquad P_{bc} = R_b/R_j \tag{13.90}$$

An alternative form for P_{ch} is

$$P_{ch} = \frac{2p_c}{h_e} \left[1 - (\bar{R}_{fd} + 1/\bar{p}_c)^{-1}\right] \tag{13.91}$$

where $\bar{R}_{fd} = R_{fd}/R_e$. These expressions for P_{ch} show that, as might be expected, increasing any of the basic cushion resistances R_{fd}, R_j and R_e increases cushion stiffness, but in particular, P_{ch} is proportional to R_c. Also, since P_{ch} is proportional to C_e, increasing the slope of the cushion flow function curve $h_f(h_e)$ increases stiffness.

13.3.5 Heave Stiffness of Skirt–Cushion System and Craft Response to Surface Inputs

If L_c is the total lift generated by the cushion, then the heave stiffness of the craft is given by

$$\frac{\Delta L_c}{\Delta h_c} = S_c \frac{\Delta p_c}{\Delta h_c} + p_c L_s \frac{\Delta x_s}{\Delta h_c} \tag{13.92}$$

The first term on the right hand side of this equation is the contribution from the change in p_c, and the second is the contribution from the change in footprint area. For full-scale craft, the second contribution is usually much smaller than the first, and can be ignored. However contributions from changes in x_s can be important for test model configurations in which h_s is comparable in magnitude to B_b, and for computation of pitch and roll stiffness at full scale.

To obtain an expression for $\Delta L_c/\Delta h_c$ using h_e as a feedback variable as depicted in Fig. 13.2, define the gain vector

$$\underset{\sim}{G} \equiv \begin{bmatrix} G \\ H \end{bmatrix} = \begin{bmatrix} \Delta h_s/\Delta h_e \\ \Delta x_s/\Delta h_e \end{bmatrix} \tag{13.93}$$

$\underset{\sim}{G}$ is related to the pressure stiffness by

$$\underset{\sim}{G} = P_{ch} \underset{\sim}{H}_c \tag{13.94}$$

where $\underset{\sim}{H}_c$ is defined in eqn. (13.55). The quantity G is the open-loop gain of the skirt-cushion system depicted in the block diagram in Fig. 13.2. It is called here the *skirt-cushion system gain*.

Now the static value of G(s), that is G(o), has a useful property: it depends only on the skirt geometry and $\bar{p}_c$ and not on the characteristics of the fan-duct system. This may seem surprising, but it may be demonstrated by considering its nondimensional equivalent, $\bar{G}(o)$, which is given by

$$\bar{G}(o) \equiv \frac{\Delta \bar{h}_s}{\Delta \bar{p}_c} \cdot \frac{\Delta \bar{p}_c}{\Delta \bar{h}_e} = \frac{B_j}{B_D} G(o) \tag{13.95}$$

Equations (13.53) and (13.76) show that both $\Delta \bar{h}_s/\Delta \bar{p}_c$ and $\Delta \bar{p}_c/\Delta \bar{h}_e$ depend only on the skirt geometric parameters, $\bar{\underset{\sim}{R}}_g$ and on $\bar{p}_c$. It follows that G(o) also depends only on these quantities. This behaviour occurs because the effects

of P_{bc}, which does depend on the characteristics of the air supply system, on $P_{ch}(0)$ is inversely proportional to that on $\Delta h_s/\Delta p_c$. The independence of G(o) of the characteristics of the air supply system thus makes it particularly suitable as an index of skirt responsiveness. Note also that eqn. (13.95) implies $G(o) \propto B_j^{-1}$, that is, reducing B_j increases G(o).

We now develop the linearized equations for the skirt-cushion system. On introducing the cushion to bag pressure response P_{bc}, the linearized skirt motion equation, eqn. (13.13) can, at equilibrium, be written in the form

$$\underset{\sim}{K}_s \Delta \underset{\sim}{q} + \underset{\sim}{A}_p \Delta p_c = 0 \tag{13.96}$$

where $\underset{\sim}{A}_p$ is a column vector transfer function given by

$$\underset{\sim}{A}_p \equiv \underset{\sim}{V}_p \begin{bmatrix} P_{bc} \\ 1 \end{bmatrix} \tag{13.97}$$

The vector $\underset{\sim}{A}_p$ plays a key role in the subsequent development. With $\underset{\sim}{q} = [\beta, b]^T$ and $\underset{\sim}{F} = [M, F]^F$, it has the form

$$\underset{\sim}{A}_p = \begin{bmatrix} \partial M/\partial p_c \\ \partial F/\partial p_c \end{bmatrix} + \begin{bmatrix} P_{bc} & \partial M/\partial p_b \\ & \partial F/\partial p_b \end{bmatrix} \tag{13.98}$$

To calculate G, rewrite eqn. (13.96) in the form

$$\underset{\sim}{K}_s \, \Delta \underset{\sim}{q} + P_{ch} \, \underset{\sim}{A}_p \, \Delta h_e = 0 \tag{13.99}$$

which gives

$$\Delta \underset{\sim}{q}/\Delta h_e = -P_{ch} \, \underset{\sim}{K}_s^{-1} \, \underset{\sim}{A}_p \tag{13.100}$$

Since $\Delta h_s = (\partial h_s/\partial \underset{\sim}{q})^T \Delta \underset{\sim}{q}$ we have immediately that the scalar gain is

$$G = -P_{ch}(\partial h_s/\partial \underset{\sim}{q})^T \, \underset{\sim}{K}_s^{-1} \, \underset{\sim}{A}_p = R_c C_e (\partial h_s/\partial \underset{\sim}{q})^T \, \underset{\sim}{K}_s^{-1} \, \underset{\sim}{A}_p \tag{13.101}$$

and its vector counterpart is

$$\underset{\sim}{G} = -P_{ch} \underset{\sim}{T} \, K_s^{-1} \, \underset{\sim}{A}_p \tag{13.102}$$

We now develop the equation of skirt motion in terms of inputs Δh_g and

Δh_c. With $\Delta h_e = \Delta h_g - \Delta h_c - \Delta h_s$ eqn. (13.96) can be rewritten as

$$\underset{\sim}{K}_s \, \Delta \underset{\sim}{q} = -P_{ch} \, \underset{\sim}{A}_p (\Delta h_g - \Delta h_c - (\partial h_s / \partial \underset{\sim}{q})^T \Delta \underset{\sim}{q}) \tag{13.103}$$

or

$$(\underset{\sim}{K}_s + \underset{\sim}{K}_p) \Delta \underset{\sim}{q} = \underset{\sim}{F}_{he} (\Delta h_g - \Delta h_c) \tag{13.104}$$

where $\underset{\sim}{K}_p$ is the *pressure stiffness matrix,* given by

$$\underset{\sim}{K}_p \equiv -R_c C_e \, \underset{\sim}{A}_p (\partial h_s / \partial \underset{\sim}{q})^T \tag{13.105}$$

and $\underset{\sim}{F}_{he}$ is an input vector given by

$$\underset{\sim}{F}_{he} = -P_{ch} \, \underset{\sim}{A}_p = R_c \, C_e \, \underset{\sim}{A}_p \tag{13.106}$$

The gain $\underset{\sim}{G}$ can be expressed in terms of $\underset{\sim}{K}_p$; since $(\partial h_s / \partial \underset{\sim}{q})^T (\partial \underset{\sim}{q} / \partial h_s) = 1$, from eqns. (13.102) and (13.105) it follows that

$$\underset{\sim}{G} = -\underset{\sim}{T} \, \underset{\sim}{K}_s^{-1} \, \underset{\sim}{K}_p (\partial \underset{\sim}{q} / \partial h_s) \tag{13.107}$$

Thus $\underset{\sim}{G}$ is related to the product of the skirt flexibility matrix and the pressure stiffness matrix. Comparison of this result with eqn. (13.66) shows that the form of the expression for $\underset{\sim}{G}$ is identical to that for $\underset{\sim}{G}_w$, with the matrix $\underset{\sim}{K}_w$ replaced by $\underset{\sim}{K}_p$.

With $\underset{\sim}{G}$ calculated from eqn. (13.102) we can now develop an expression for the overall craft stiffness $\Delta L_c / \Delta h_c$. Since $\Delta h_e = \Delta h_g - \Delta h_s - \Delta h_c$, and $\Delta h_s = G \Delta h_e$, then

$$\Delta \underset{\sim}{h}_s = \begin{bmatrix} \Delta h_s \\ \Delta x_s \end{bmatrix} = \frac{\underset{\sim}{G}}{1 + G} (\Delta h_g - \Delta h_c) \tag{13.108}$$

Also

$$\Delta p_c = \frac{P_{ch}}{(1 + G)} (\Delta h_g - \Delta h_c) \tag{13.109}$$

Thus on setting $\Delta h_g = 0$, eqn. (13.92) becomes

$$\frac{\Delta L_c}{\Delta h_c} = -\frac{1}{1 + G} (S_c P_{ch} + p_c L_s H) \tag{13.110}$$

Equation (13.110) illustrates clearly the effect of the skirt system on the craft heave stiffness. In the absence of a skirt G = H = 0 and, as noted above, for a full scale craft the contribution caused footprint area change through $\Delta x_s/\Delta h_e = H$ is very small, so that the predominant effect of the skirt is to reduce the heave stiffness by the factor (1+G). This suggests that improving the skirt's responsiveness, that is increasing $G = \Delta h_s/\Delta h_e$, can improve ride comfort considerably. Investigation of the dynamics confirms this.

13.3.6 Some Theoretical and Experimental Results

Figure 13.21 compares predictions and measurements of the static heave response of the model used to obtain the data presented in Figs. 13.15-16. The principal dimensions of the model are given in Table 13.1. The predictions were obtained by solving the nonlinear equations, that is, eqns. (13.68-70) for the fluid mechanics and eqns. (13.50-51) for the bag statics. Both models of the inner bag described in Section 13.2 were used, with the generalized forces given by eqns. (13.25-31). As can be seen, agreement between the predictions and measurements is good, with there being little

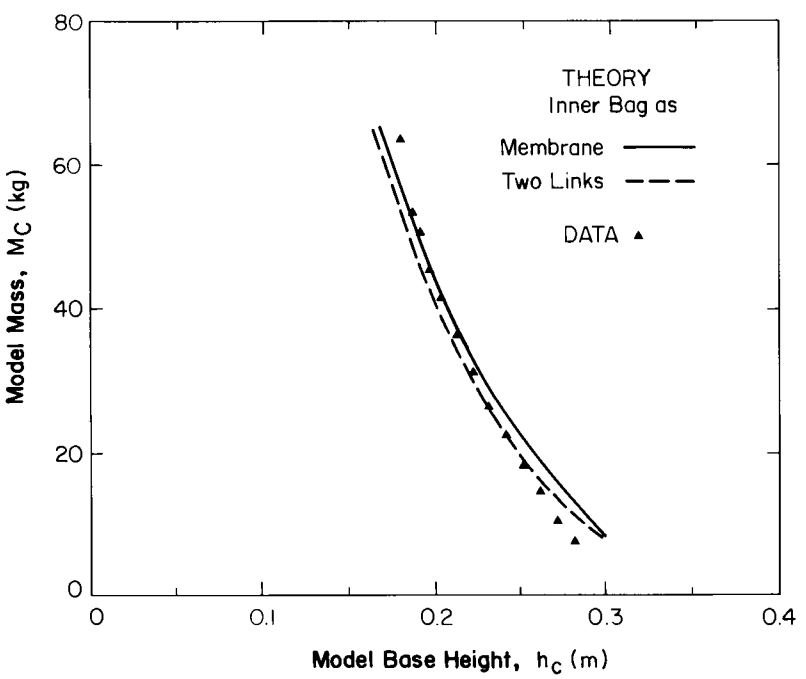

Fig. 13.21 Predicted and observed static heave response for a small two dimensional model. Skirt geometry, case C in Table 13.1; N_f = 2400 rpm.

Table 13.1. Geometry of Model Skirts Used in Calculations and Experiments.

	Base			Bag		Finger		
Skirt	L_m (m)	B_D (m)	Γ_D (deg)	L_{ob} (m)	L_{ib} (m)	L_4 (m)	L_5 (m)	Γ_4 (deg)
A	0.914	0.233	35	0.496	0.399	0.200	0.0	56
B	0.914	0.305	28	0.438	0.473	0.200	0.0	56
C	0.914	0.171	42	0.438	0.399	0.200	0.0	56

difference between the inner bag models. However other skirt configurations should cause the two models to give significantly different results.

Figures 13.22 and 13.23 are plots of measurements of p_c and an effective h_f, h_{fe}, as functions of h_c for skirt configuration A and for three values of A_j. The values of A_j are equivalent or nominal values computed by using eqn. (13.69), an assumed $C_{mj} = 0.61$ and measured Q_e, p_b and p_c; and h_{fe} was calculated using eqn. (13.70) and by setting $C_{me} = 0.61$. The values of A_j and other relevant parameters are given in Table 13.2. In Fig. 13.23, h_{fe} is nondimensionalized by a reference value of B_j, B_{jr}, corresponding to $A_j = 0.050\ m^2$, the maximum value used in these tests. The data in Figs. 13.22 and 13.23 shows that, over a moderate range of h_c used in the tests, the cushion response is effectively linear, so that it is appropriate to use the slopes of these curves to characterize the effect of the parameters of interest on cushion behaviour.

The results are summarized in Table 13.2, which gives $|\Delta p_c/\Delta h_c|$, $\Delta h_s/\Delta h_c$ and $\Delta h_{fe}/\Delta h_c$ for 7 cases. Attempts to calculate a value of $G = [(\Delta h_s/\Delta h_g)^{-1} - 1]^{-1}$ from the measured $\Delta h_s/\Delta h_g$ led to large errors, so that Table 13.2 presents a modified gain $G' \equiv (\Delta h_{fe}/\Delta h_g)^{-1}$. The data in Table 13.2 suggests that, of the four parameters, A_j, N_f, L_{ob} and L_{ib}, A_j has by far the largest effect on skirt responsiveness, and thus on overall heave stiffness. However, these results are only preliminary in nature, and it should be noted that, since the effect of varying A_j is to change the geometry of the inflated bag, other ranges of L_{ib}, L_{ob} and N_f will have a larger effect on responsiveness.

13.4 HEAVE DYNAMICS

In this section the equations governing the fluid flow processes for the skirt and cushion systems in the case of vehicle motion are developed and linearized, and the important concepts of cushion and bag impedance are introduced. The equations governing th dynamcis of the skirt system and its interaction with the cushion and craft systems are then developed. Finally some computed results for frequency resonse and stability are presented.

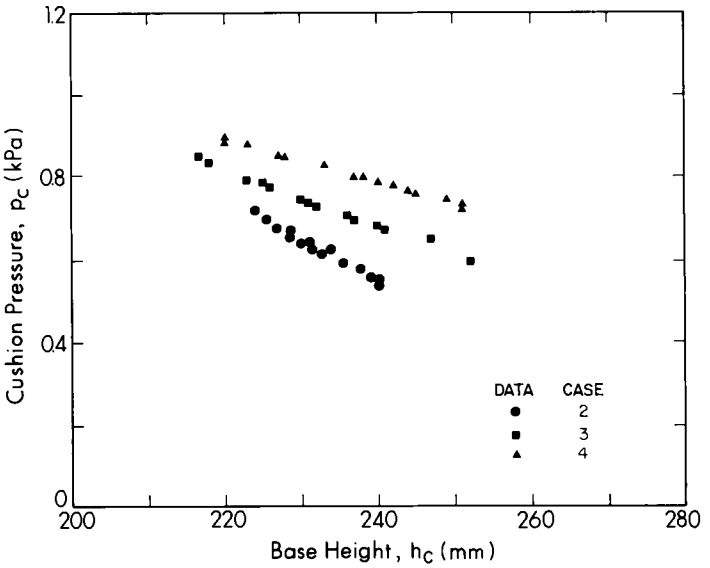

Fig. 13.22 Observed static pressure response of a small two dimensional model, with bag-to-cushion orifice area A_j as parameter. Cushion geometry and other parameters are given in Tables 13.1 and 13.2.

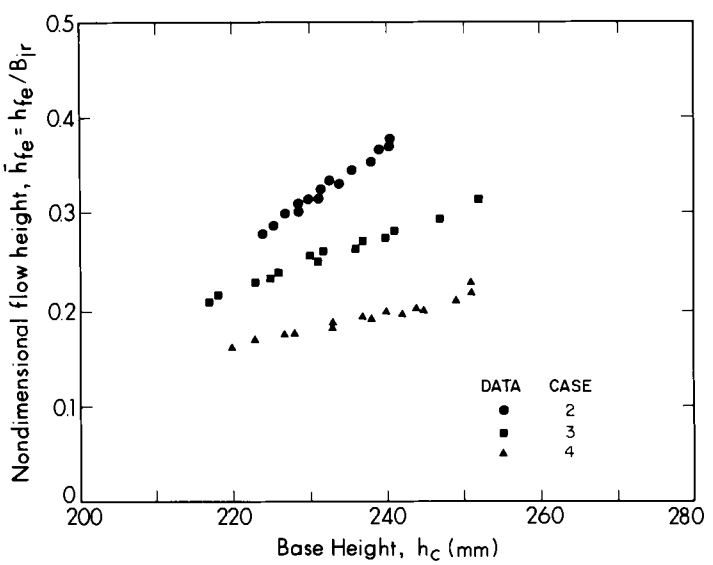

Fig. 13.23 Observed static hovergap response for a small two dimensional model, with bag-to-cushion orifice area A_j as parameter. Cushion geometry and other parameters are given in Tables 13.1 and 13.2.

Table 13.2. Effect of Skirt Geometry, Bag Feed Area, and Fan Speed on Cushion Response.

Case	Skirt	A_j (cm^2)	N_f (rpm)	$\lvert\Delta p_c/\Delta h_c\rvert$ (kPa/m)	$\Delta h_s/\Delta h_c$	$\Delta h_{fe}/\Delta h_c$	G'	p_b/p_c (1)
1	A	0.050	2723	11.2	0.78±0.05	0.136	6.35	1.15
2	A	0.049	2363	9.9	0.87±0.04	0.152	5.58	1.11
3	A	0.034	2373	7.0	0.73±0.04	0.0803	11.5	1.18
4	A	0.022	2374	5.2	0.78±0.02	0.0486	19.6	1.21
5	A	0.024	2722	7.1	0.87±0.03	0.0470	20.3	1.21
6	B	0.049	2368	6.9	---	0.110	8.0	1.15
7	B	0.025	2366	4.7	0.91±0.02	0.0413	23.2	1.18

Note (1) The quoted p_b/p_c is a mean value.

13.4.1 Equations of Fluid Flow Processes

As noted in Section 13.2.5, the major area of uncertainty in modelling the cushion flow processes is probably the dynamic behaviour of the fan. Possible effects include unsteady blade aerodynamics, and inertia and compressibility effects in the fan housing. To account for unsteady blade aerodynamics Ohashi (ref. 21) used cascade theory, and fitted his low frequency results with a simplified first order lag for the pressure p_f at the fan outlet:

$$\frac{\Delta p_f}{\Delta Q_f} \equiv -Z_f = -\frac{R_f}{1 + \tau_f s} \tag{13.111}$$

where the time constant τ_f depends on blade geometry and is inversely proportional to both flow coefficient and fan speed. Goldschmied and Wormley (ref. 22) noted that, at high frequencies, both the predictions of Ohashi's full theory and his experiments approached a phase lag of 45° so that, in place of eqn. (13.111), they used

$$Z_f = \frac{R_f}{\sqrt{1 + \tau_f s}} \tag{13.112}$$

Inertia and compressibility effects for the typical ACV fan housing may well be difficult to predict, so that the most effective approach is probably to determine unsteady fan response experimentally and to fit a suitable response model to the data. Methods of achieving this have been described in (refs. 23, 11), and the test results to date suggest that the predominant effect is the inertia of the air which causes the pressure to lead the flow (ref. 23). These observations suggest that the simplest model of dynamic fan behaviour should be a first order lead-lag

$$Z_f = R_f \frac{(1 + \tau_{f1}s)}{(1 + \tau_{f2}s)} \tag{13.113}$$

with higher order models being used for high frequency behaviour.

As noted in Section 13.2.1, the cushion air is either passed directly into the bag volumes or into a plenum chamber of which the bag volume forms a part. However, in some experimental apparatus, the fan may deliver the air to the skirt being tested through a moderately long duct. Duct air dynamics can have a major effect on cushion response (ref. 13). For very high frequencies wave propagation phenomena may have to be included (ref. 22); however in many cases of practical interest, with L_d the duct length and a the sound speed, if $\omega L_d/a_d << 1$ then a lumped parameter model can be used. With A_d the cross-sectional area of the duct, $C_d \equiv \rho A_d L_d/\rho a^2$ the pneumatic capacitance of the duct, $I_d = \rho L_d/A_d$ the inertance of the duct air, and R_d the duct resistance one can put

$$\frac{\Delta p_f - \Delta p_b}{\Delta Q_d} \equiv -Z_d = I_d s + \frac{R_d}{1 + \tau_d s}, \qquad \tau_d = R_d C_d \tag{13.114}$$

If, as is often the case, $I_d\omega >> R_d(1 + \tau_d^2\omega^2)^{-1/2}$ a simple lumped importance model is adequate (ref. 13).

When flow is not diverted from the fan for other purposes, $\Delta Q_d = \Delta Q_f$, then

$$\Delta p_b \triangleq -Z_{fd}\, \Delta Q_d \tag{13.115}$$

where $Z_{fd} = Z_f + Z_d$ is the *fan-duct impedance.*

As discussed in Section 13.2.5 the air flow processes from bag to cushion, and cushion to atmosphere can be assumed quasisteady, so that the flow equations are simply those used in the investigation of the statics; in the linearized-Laplace domain they are

$$\Delta Q_j = (\Delta p_b - \Delta p_c)/R_j \tag{13.116}$$

and

$$\Delta Q_e = C_e \Delta h_e + \Delta p_c/R_e \tag{13.117}$$

To complete the formulation of the dynamics of the cushion flow, equations of continuity for the bag and cushion volumes respectively are used. In the linearized-Laplace domain they are

$$C_b\Delta\dot{p}_b + \Delta\dot{V}_b = \Delta Q_d - \Delta Q_j \tag{13.118}$$

$$C_c\Delta\dot{p}_c + \Delta\dot{V}_c = \Delta Q_j - \Delta Q_e \tag{13.119}$$

In these equations $C_b = V_b/\rho a^2$ and $C_c = V_c/\rho a^2$ are the pneumatic capacitances of the bag and cushion volumes respectively.

13.4.2 Cushion System Impedance Analysis

The conservation equations for the bag and cushion volumes can be combined with the expressions for ΔQ_d, ΔQ_j and ΔQ_e to give

$$(C_b s + Z_{fd}^{-1} + R_j^{-1})\Delta p_b - \Delta p_c/R_j = -\Delta\dot{V}_b, \tag{13.120}$$

$$(C_c s + R_j^{-1} + R_e^{-1})\Delta p_c - \Delta p_b/R_j = -\Delta\dot{V}_c - C_e\Delta h_e, \tag{13.121}$$

In these equations, craft, ground and skirt motion generate $\Delta\dot{V}_b$, $\Delta\dot{V}_c$ and Δh_e which are the inputs to the skirt-cushion system controlling Δp_c and Δp_b. Now the term $C_e\Delta h_e$ is the perturbation of flow out of V_c generated by a perturbation in h_e. Similarly, positive $\Delta\dot{V}_b$ and $\Delta\dot{V}_c$ are equivalent to withdrawal of air from bag and cushion, that is they create virtual flows out of these volumes. Furthermore, positive $\Delta\dot{V}_c$ reduces Δp_c and thus increases the flow out of the bag, tending to further decrease Δp_b; and there is a corresponding effect of $\Delta\dot{V}_b$ on Δp_c.

Equations (13.120-121) are now solved for Δp_b and Δp_c. In the process we define certain equivalent impedances which play a central role in the dynamics. First, eqn. (13.120) suggests the definition of a *bag impedance* Z_b:

$$Z_b \equiv (C_b s + Z_{fd}^{-1} + R_j^{-1})^{-1} \tag{13.122}$$

Thus eqn. (13.120) becomes

$$\Delta p_b = -Z_b\Delta\dot{V}_b + (Z_b/R)_j\Delta p_c \tag{13.123}$$

One can associate with Z_b an equivalent *bag flow* ΔQ_b: $\Delta Q_b \equiv -\Delta p_b/Z_b$; then eqn. (13.123) shows that

$$\Delta Q_b = \Delta\dot{V}_b + \Delta Q_{jc} \tag{13.124}$$

where $\Delta Q_{jc} \equiv -\Delta p_c/R_j$ is the flow out of the bag caused by cushion pressure fluctuations. Equation (13.123) also gives the dynamic form of the cushion-to-bag pressure response: $P_{bc} = Z_b/R_j$.

Now introduce eqn. (13.123) into eqn. (13.121) to eliminate Δp_b:

$$\Delta p_c\{C_c s + R_j^{-1} + R_e^{-1} - Z_b/R_j^1\} = -\Delta\dot{V}_c - P_{bc}\,\Delta\dot{V}_b - C_e\Delta h_e \tag{13.125}$$

As for the bag conservation equation, this suggests the definition of a *cushion impedance* Z_c and an associated *cushion flow* ΔQ_c:

$$Z_c = (C_c s + R_j^{-1} + R_e^{-1} - Z_b/R_j^1)^{-1}; \quad \Delta Q_c \equiv -\Delta p_c/Z_c \tag{13.126}$$

so that

$$\Delta p_c = -Z_c\Delta Q_c = -Z_c(\Delta\dot{V}_c + P_{bc}\,\Delta\dot{V}_b + C_e\,\Delta h_e) \tag{13.127}$$

Finally

$$\Delta p_b = -Z_c[\{P_{bc}^2 + Z_b/Z_c\}\Delta\dot{V}_b + P_{bc}\,\Delta\dot{V}_c + C_e\,\Delta h_e] \tag{13.128}$$

Figure 13.24 is an equivalent circuit diagram for the fluid mechanical perturbations from equilibrium. Note that the energy sources for this system are $\Delta\dot{V}_b$, and $\Delta\dot{V}_c + C_e\Delta h_e$ induced by craft, skirt and ground motion.

13.4.3 Skirt–Cushion System Dynamics

To develop the linearized equations describing the interaction of skirt and cushion systems, eqn. (13.13) is our starting point; it is rewritten in the form

$$\underset{\sim}{A}_s\,\Delta\underset{\sim}{q} + \underset{\sim}{A}_p\,\Delta p_c = \underset{\sim}{0} \tag{13.129}$$

where we define the *skirt system matrix* $\underset{\sim}{A}_s$

$$\underset{\sim}{A}_s \equiv s^2\underset{\sim}{M}_s + \underset{\sim}{K}_s \tag{13.130}$$

and where $\underset{\sim}{A}_p$ is given by eqn. (13.97), $\underset{\sim}{A}_p = \underset{\sim}{V}_p[P_{bc}, 1]^T$, except that now $P_{bc} = Z_b/R_j$. The pressure disturbance Δp_c is calculated using eqn. (13.127), which includes contributions Δp_{ci} caused by craft and ground motion, and Δp_{cs} caused by skirt motion. That is

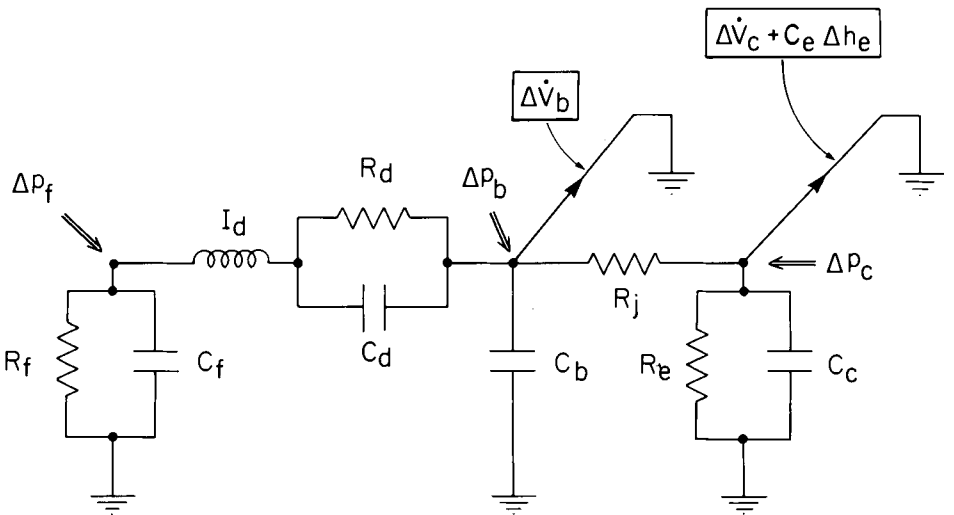

Fig. 13.24 Equivalent circuit diagram for cushion system fluid mechanics.

$$\Delta p_c = \Delta p_{ci} + \Delta p_{cs} \tag{13.131}$$

where $\Delta p_c = \Delta p_{ci}$ if $\Delta \underset{\sim}{q} = 0$, and $\Delta p_c = \Delta p_{cs}$ if $\Delta h_g = \Delta h_c = 0$.

Expressions for Δp_{ci} and Δp_{cs} can be derived from eqn. (13.127). First derive expressions for $\Delta\dot{V}_b$ and $\Delta\dot{V}_c$. Since the bag volume $V_b = V_b(q_i)$, then $\delta V_b = \Sigma(\partial V_b/\partial q_i)\delta q_i$ and

$$\Delta\dot{V}_b = (\partial V_b/\partial \underset{\sim}{q})^T \Delta\dot{\underset{\sim}{q}} \equiv s\underset{\sim}{V}_{bq}\,\Delta \underset{\sim}{q} \tag{13.132}$$

The cushion volume V_c can be expressed as

$$V_c = V_{cs}(q_i) + S_c h_e \tag{13.133}$$

where V_{cs} is that part of the cushion volume contained by the skirt. Thus

$$\delta V_c = \sum \frac{\partial V_{cs}}{\partial q_i}\,\delta q_i + S_c \delta h_e + h_e L_s \delta x_s, \tag{13.134}$$

so that

$$\Delta\dot{V}_c = s\{(\partial V_{cs}/\partial \underset{\sim}{q})^T + [-S_c,\ h_e L_s]\underset{\sim}{T}\}\Delta \underset{\sim}{q} + sS_c(\Delta h_g - \Delta h_c), \tag{13.135}$$

or, more compactly

$$\Delta\dot{V}_c = s\underset{\sim}{V}_{cq}\,\Delta\underset{\sim}{q} + sS_c(\Delta\dot{h}_g - \Delta\dot{h}_c) \tag{13.136}$$

where the row vector $\underset{\sim}{V}_{cq}$ is given by

$$\underset{\sim}{V}_{cq} = (\partial V_{cs}/\partial\underset{\sim}{q})^T + [-S_c,\ h_e L_s]\underset{\sim}{T} \tag{13.137}$$

Thus eqn. (13.127) becomes

$$\Delta p_c = -sZ_c[\underset{\sim}{V}_{cq}\,\Delta\underset{\sim}{q} + S_c(\Delta h_g - \Delta h_c)] - \frac{Z_b Z_c}{R_j}\,\underset{\sim}{V}_{bq}\,\Delta\underset{\sim}{q}$$

$$- Z_c C_e[(\Delta h_g - \Delta h_c) - (\partial h_s/\partial\underset{\sim}{q})^T\,\Delta\underset{\sim}{q}] \tag{13.138}$$

We have immediately that

$$\Delta p_{ci} = -Z_c[C_e + sS_c](\Delta h_g - \Delta h_c) \equiv P_{ch}(\Delta h_g - \Delta h_c) \tag{13.139}$$

and, with $Z_{bc} \equiv Z_b Z_c/R_j$,

$$\Delta p_{cs} = \{Z_c[C_e(\partial h_s/\partial\underset{\sim}{q})^T - s(\underset{\sim}{V}_{cq})] - sZ_{bc}\,\underset{\sim}{V}_{bq}\}\Delta\underset{\sim}{q} \equiv \underset{\sim}{P}_{cs}\,\Delta\underset{\sim}{q} \tag{13.140}$$

Given these definitions of P_{ch} and $\underset{\sim}{P}_{cs}$ we can write

$$\Delta p_c = \underset{\sim}{P}_{cs}\,\Delta\underset{\sim}{q} + P_{ch}(\Delta h_g - \Delta h_c) \tag{13.141}$$

and the skirt motion equation becomes

$$(\underset{\sim}{A}_s + \underset{\sim}{A}_p\,\underset{\sim}{P}_{cs})\Delta\underset{\sim}{q} + \underset{\sim}{A}_p\,P_{ch}(\Delta h_g - \Delta h_c) = 0 \tag{13.142}$$

A block diagram depicting the dynamics of the skirt-cushion system can be derived by rewriting the skirt motion equation in the form

$$\Delta\underset{\sim}{q} = -\underset{\sim}{A}_s^{-1}\,\underset{\sim}{A}_p(\Delta p_{cs} + \Delta p_{ci}) \tag{13.143}$$

and recalling that $\Delta p_{cs} = \underset{\sim}{P}_{cs}\,\Delta\underset{\sim}{q}$. This is given in Fig. 13.25. This block diagram immediately suggests the definition of the skirt-cushion system gain G(s) as

$$G(s) = \Delta p_{ci}/\Delta p_{ci} = \underset{\sim}{P}_{cs}\underset{\sim}{A}_s^{-1}\,\underset{\sim}{A}_{pm} \tag{13.144}$$

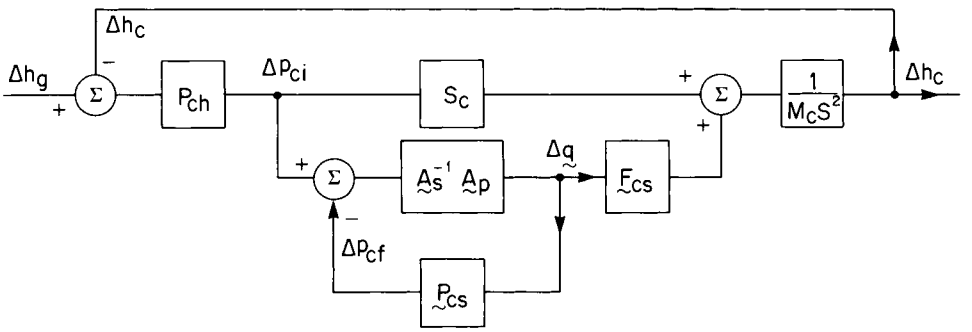

Fig. 13.25 Block diagram conceptualization of linearized heave dynamics.

so that

$$\Delta \underset{\sim}{q} = -\underset{\sim}{A}_s^{-1} \underset{\sim}{A}_p [1 + G(s)] \Delta p_{ci} \tag{13.145}$$

This definition is consistent with that given for the static behaviour of the skirt, $G(o) \equiv \Delta h_s / \Delta h_e$. That is, when $s = 0$ eqn. (13.144) reduces to eqn. (13.102).

Given this definition of G(s) it is now possible to develop simple expressions for Δp_c, $\Delta \underset{\sim}{q}$ and $\Delta \underset{\sim}{h}_s$. Using $\Delta \underset{\sim}{q} = -\underset{\sim}{A}_s^{-1} \underset{\sim}{A}_p \Delta p_c$ in eqn. (13.141) one obtains

$$\Delta p_c = \frac{P_{ch}}{1 + G} (\Delta h_g - \Delta h_c) \tag{13.146}$$

and

$$\Delta \underset{\sim}{q} = -\frac{\underset{\sim}{A}_s^{-1} \underset{\sim}{A}_p}{1 + G} P_{ch} (\Delta h_g - \Delta h_c) \tag{13.147}$$

and finally

$$\Delta \underset{\sim}{h}_s = -\frac{\underset{\sim}{T} \underset{\sim}{A}_s^{-1} \underset{\sim}{A}_p P_{ch}}{1 + G} (\Delta h_g - \Delta h_c) \tag{13.148}$$

Now the skirt motion eqn. (13.129) and eqn. (13.141) for Δp_c can be combined to give a form equivalent to eqn. (13.104) for the statics:

$$[\underset{\sim}{A}_s + \underset{\sim}{A}_p \underset{\sim}{P}_{cs}]\Delta \underset{\sim}{q} = \underset{\sim}{F}_{he}(\Delta h_g - \Delta h_c) \tag{13.149}$$

where $\underset{\sim}{F}_{he}(s)$ is now given by

$$\underset{\sim}{F}_{he} = -P_{ch} \underset{\sim}{A}_p = Z_c[C_e + sS_c]\underset{\sim}{A}_p \tag{13.150}$$

The term $\underset{\sim}{A}_p \underset{\sim}{P}_{cs} = \underset{\sim}{K}_p$ when $s = 0$, but in the dynamical case it also introduces both positive and negative damping. Thus

$$\underset{\sim}{A}_p \underset{\sim}{P}_{cs} = Z_c C_e \underset{\sim}{A}_p(\partial h_s/\partial \underset{\sim}{q})^T - sZ_{bc} \underset{\sim}{A}_p \underset{\sim}{V}_{bq} - sZ_c \underset{\sim}{A}_p \underset{\sim}{V}_{cq}. \tag{13.151}$$

Hence if, for the dynamics, we define

$$\underset{\sim}{K}_p = Z_c C_e \underset{\sim}{A}_p(\partial h_s/\partial q)^T; \quad \underset{\sim}{D}_b = -Z_{bc} \underset{\sim}{A}_p \underset{\sim}{V}_{bq}; \quad \underset{\sim}{D}_{sc} = -Z_c \underset{\sim}{A}_p \underset{\sim}{V}_{cq} \tag{13.152}$$

where $\underset{\sim}{D}_b$ is the *bag damping matrix* and $\underset{\sim}{D}_{sc}$ is *the skirt-cushion damping matrix*, the skirt motion equation becomes

$$[s^2\underset{\sim}{M}_s + s(\underset{\sim}{D}_b + \underset{\sim}{D}_{sc}) + (\underset{\sim}{K}_s + \underset{\sim}{K}_p)]\Delta \underset{\sim}{q} = \underset{\sim}{F}_{he}(\Delta h_g - \Delta h_c) \tag{13.153}$$

13.4.4 Equations of Craft Heave Dynamics

If M_c is the total mass of the craft, since h_c is positive downwards, the craft equation of motion is

$$M_c \ddot{h}_e = M_c g - S_c p_c \tag{13.154}$$

which, when linearized and transformed, becomes:

$$s^2 M_c \Delta h_c + S_c \Delta p_c + p_c L_s \Delta x_s = 0 \tag{13.155}$$

Introduce eqn. (13.141) for Δp_c, and define

$$\underset{\sim}{F}_{cs} \equiv S_c \underset{\sim}{P}_{cs} + p_c L_s \, \partial x_s/\partial \underset{\sim}{q} \tag{13.156}$$

to obtain

$$s^2 M_c \Delta h_c + \underset{\sim}{F}_{cs} \Delta \underset{\sim}{q} + S_c P_{ch}(\Delta h_g - \Delta h_c) = 0 \tag{13.157}$$

The dynamics embodied in eqn. (13.157) is depicted in Fig. 13.25.

To solve eqn. (13.157) for the craft heave response, $\Delta h_c/\Delta h_g$, introduce eqn. (13.147) for $\Delta \underset{\sim}{q}$ in terms of $(\Delta h_g - \Delta h_c)$. Also let

$$S_c G_F \equiv \underset{\sim}{F}_{cs} \underset{\sim}{A}_s^{-1} \underset{\sim}{A}_p \tag{13.158}$$

Then eqn. (13.157) can be cast into the form

$$\frac{\Delta h_c}{\Delta h_g} = \frac{-S_c P_{ch}(1 + G - G_F)}{s^2(1 + G)M_c - S_c P_{ch}(1 + G - G_F)} \tag{13.159}$$

Now in full scale craft the contribution $p_c L_s \Delta x_s$ to the cushion force is usually negligible, in which case $G_F = G$, and eqn. (13.159) reduces to

$$\frac{\Delta h_c}{\Delta h_g} = \frac{-S_c P_{ch}}{s^2[1 + G(s)]M_c - S_c P_{ch}} \tag{13.160}$$

and the effect of the skirt system on the craft heave dynamics enters only through the skirt-cushion system gain G(s).

13.4.5 Frequency Response Results

In this and the following section we present some computed frequency response and dynamic stability characteristics. These results, which were first reported in Ref. 16, used the two-link model of the skirt described in Section 13.2.7, but also included a distributed inertia model of the outer bag. Three configurations were used in the calculations, the first being a laboratory model similar to that described in Section 13.3.6, the second a 1.23 tonne test vehicle, and the third a 52 tonne craft.

The values of the parameters used in the calculations are given in Tables 13.3 to 13.5. For the 52 tonne craft, the parameters are representative of those used on high speed aerodynamically propelled vehicles. For these calculations, the cushion exit flow function $h_f(h_e)$ was estimated from the finger geometry. With B_f the width of a finger, this gave

$$\begin{aligned} h_f(h_e) &= h_e + 0.1073\, B_f, & h_e &> 0 \\ h_f(h_e) &= 0.1073\, B_f\{1 + 2h_e/[B_f \cos\theta_f]\}^2, & h_e &< 0 \end{aligned} \tag{13.161}$$

The data in Table 13.4 includes a nondimensional cushion flow coefficient, $C_{QC} = Q_e/(A_r V_r)$ where A_r is a reference base area, and V_r is a reference flow velocity. Here $A_r = L_M D_M$ and $V_r = (2p_r/\rho_a)^{1/2}$ where $p_r = M_c g/A_r$. In Table 13.4 the quantity μ is the skirt material surface density used in the calculations.

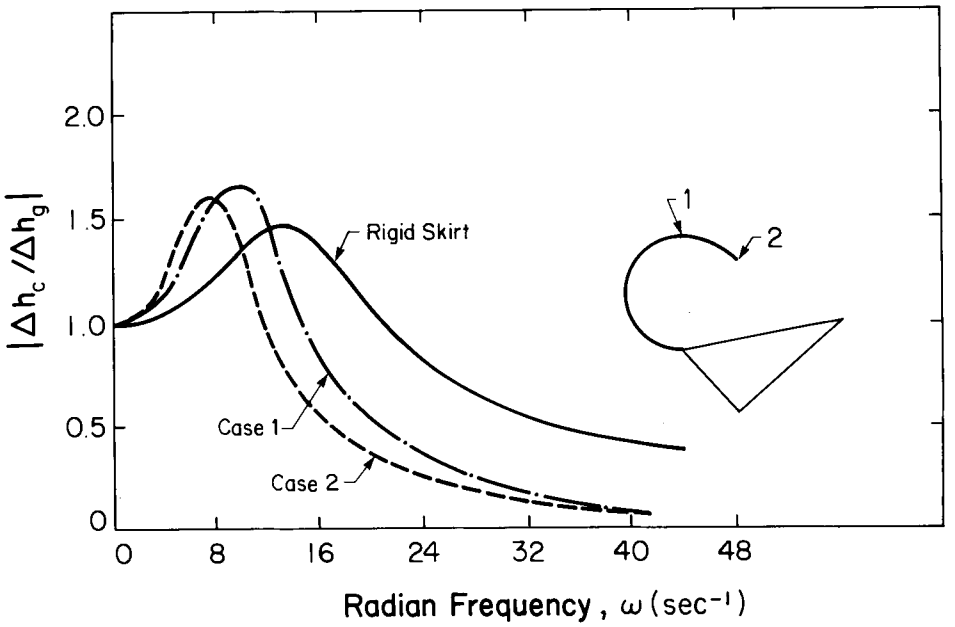

Fig. 13.26 Effect of outer bag length on heave amplitude response of laboratory model. Model parameters, cases 1 and 2 in Table 13.3.

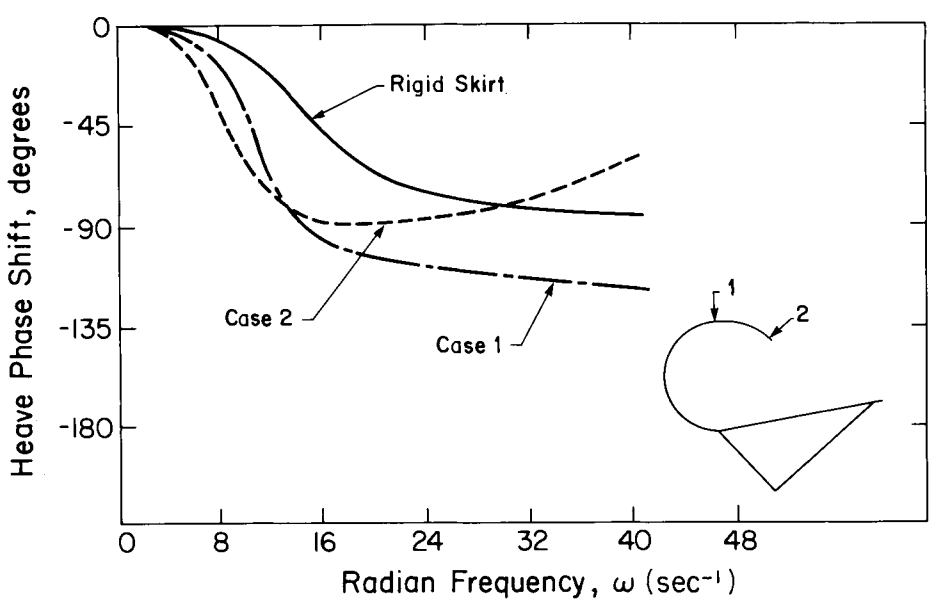

Fig. 13.27 Effect of outer bag length on heave phase response of laboratory model. Model parameters, cases 1 and 2.

Figures 13.26 to 13.29 give the effect of selected skirt geometry changes on the heave response for the laboratory model, with the corresponding basic cushion-craft system or *rigid-skirt* response given as a reference condition. Although, as depicted in these results, the responses appear to be similar to that of a second order system, they exhibit a second resonance at

Table 13.3. Major Craft Parameters Used in Frequency Response and Stability Calculations.

	Craft			Fan		
Case	L_m (m)	D_M (1) (m)	M_c (kg)	A_{f_0} (kPa)	A_{f_1} (kPa $m^{-3}s$)	A_{f_2} (kPa $m^{-6}s^2$)
1	0.965	0.9	69.4	0.762	1.198	-6.87
2	0.965	0.9	69.4	0.762	1.198	-6.87
3	0.965	0.9	83.3	0.985	1.364	-6.87
4	0.965	0.9	83.3	0.985	1.364	-6.87
5	6.0	2.7	122.9	0.762	1.236	-0.073
6	6.0	2.7	122.9	0.762	1.236	-0.073
7	0.965	0.9	69.4	1.292	1.560	-6.87
8	0.965	0.9	69.4	1.375	1.610	-6.87
9	0.965	0.9	69.4	1.292	1.560	-6.87
10	0.965	0.9	69.4	0.762	1.198	-6.87
11	19.80	9.87	52000	3.18	9.00×10^{-4}	1.57×10^{-5}

Note (1): $D_M = B_B + 2B_D$

Table 13.4. Cushion Parameters.

Case	Q_e (m^3s^{-1})	h_e (mm)	p_c (kPa)	p_b/p_c	C_{QC}
1	0.18	4.9	0.687	1.10	0.0057
2	0.18	4.9	0.687	1.10	0.0057
3	0.209	5.2	0.824	1.18	0.0061
4	0.209	5.2	0.824	1.18	0.0061
5	1.74	4.9	0.687	1.18	0.0030
6	1.74	4.9	0.687	1.18	0.0030
7	0.415	11.4	0.687	1.18	0.0131
8	0.415	11.4	0.687	1.25	0.0131
9	0.415	11.4	0.687	1.10	0.0131
10	0.18	4.9	0.687	1.10	0.0057
11	107.1	38.5	2.62	1.18	0.0083

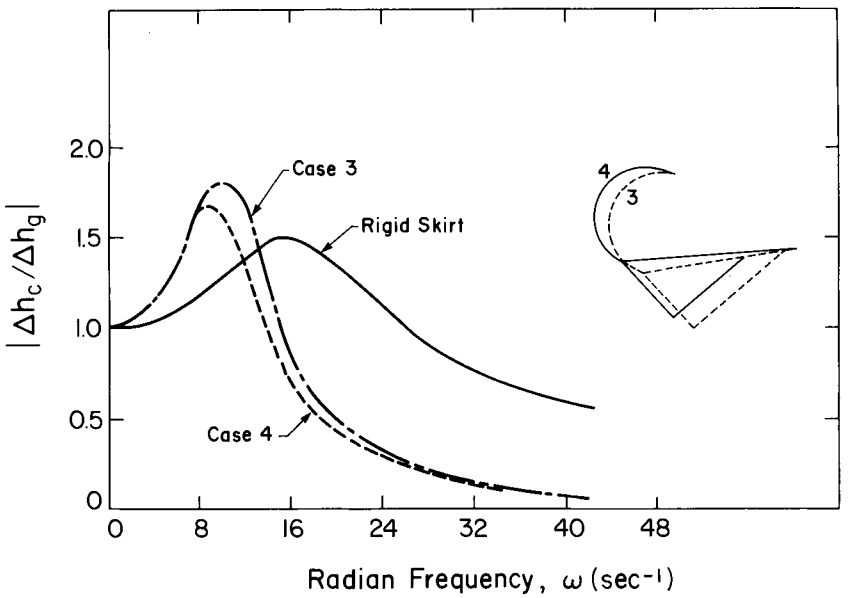

Fig. 13.28 Effect of inner attachment length on heave amplitude response of laboratory model. Model parameters, cases 3 and 4.

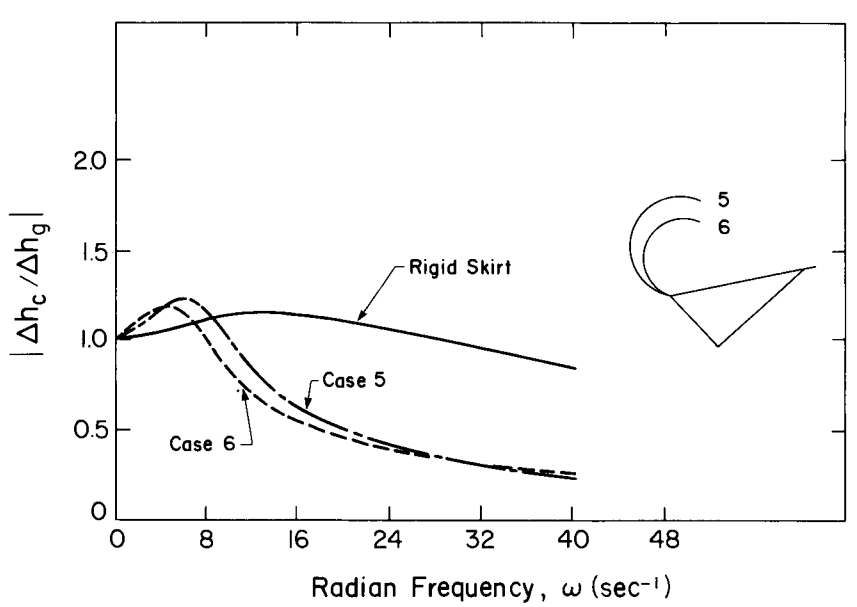

Fig. 13.29 Effect of outer bag radius on heave amplitude response for 1.23 tonne test vehicle. Model parameters, cases 5 and 6.

Table 13.5. Skirt Geometries.

Case	μ (kg/m^2)	L_1 (m)	L_2 (m)	L_4 (m)	Γ_4 (deg)	L_D (m)	α_o (deg)	x_{so} (m)	h_{so} (m)
1	0.335	0.069	0.360	0.230	50	0.375	35	0.258	0.223
2	0.335	0.069	0.360	0.230	50	0.280	35	0.257	0.224
3	0.335	0.009	0.360	0.200	57.5	0.280	35	0.213	0.230
4	0.335	0.029	0.360	0.200	57.5	0.280	35	0.249	0.222
5	0.335	0.069	0.360	0.230	54	0.280	35	0.285	0.217
6	0.335	0.069	0.360	0.230	54	0.255	26.5	0.287	0.214
7	0.335	0.029	0.360	0.200	57.5	0.280	35	0.260	0.212
8	0.335	0.029	0.360	0.200	57.5	0.280	35	0.245	0.230
9	0.335	0.029	0.360	0.200	57.5	0.280	35	0.260	0.212
10	0.335	0.029	0.360	0.200	57.5	0.280	35	0.260	0.212
11	4.28	0.18	2.02	1.10	57.0	1.70	35	1.378	1.261

about 80 rad/s. This resonance is associated with the dynamics of the skirt-cushion system, and its frequency is high enough to suggest that, in the case of the laboratory model, the inertial effects of the skirt are negligible in the neighbourhood of the first resonance.

The geometry changes investigated are: increase of outer bag length, extension of the inner bag, and decrease of the outer bag radius; the amplitude response for these three cases are given in Figs. 13.26, 13.28 and 13.29. Figure 13.27 gives the effect of increasing outer bag length on the phase response. All three geometry changes can affect the magnitude, frequency and bandwidth of the first cushion resonance. For example, increasing the outer bag length decreases the first natural frequency by 40% and significantly reduces the bandwidth. Extending the inner bag or reducing the outer bag radius has similar effects, although the first of these two tends to make the cushion more unstable.

Figures 13.30 and 13.31 give the effects of p_b/p_c and Q_e on heave response. Increasing p_b/p_c from 1.1 to 1.25 reduces the first natural frequency and increasing damping in this neighbourhood, but the system is more unstable. In Fig. 13.31 the C_{QC} for case 9 is representative of those currently used in practice; and reduction of Q_e to 43% of this value reduces the first natural frequency by 30%, although damping is also reduced.

For the 52 tonne craft, Figs. 13.32 and 13.33 give the effect of air compressibility on heave gain and phase response; for this craft the second natural frequency is about 3 to 4 Hz. Figures 13.32 and 13.33 show that, as one might expect, as frequency increases, compressibility effects become increasingly significant, being negligible at the first resonance, but highly significant for the second. This suggests that, for very low frequency

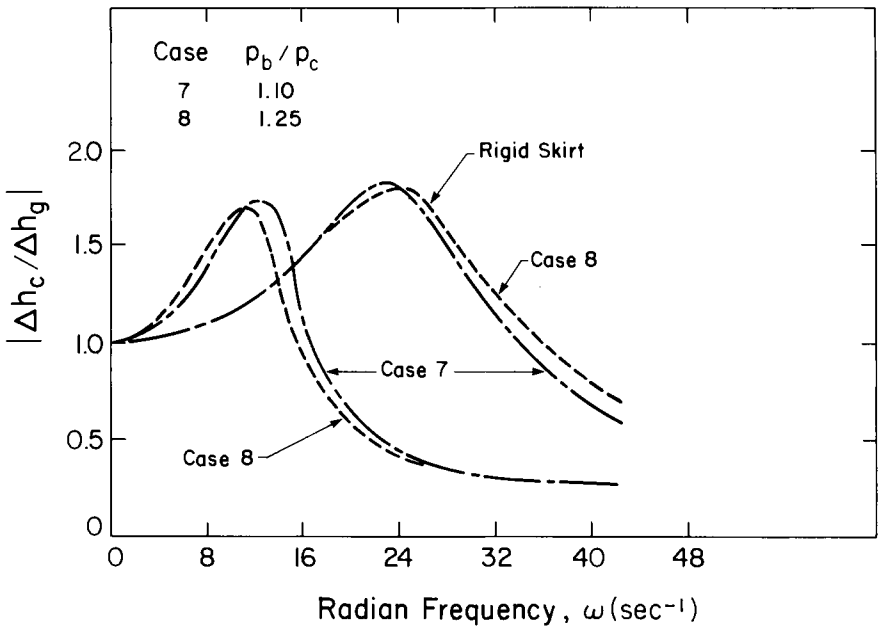

Fig. 13.30 Effect of ratio of bag to cushion pressure on heave amplitude response of laboratory model. Model parameters, cases 7 and 8.

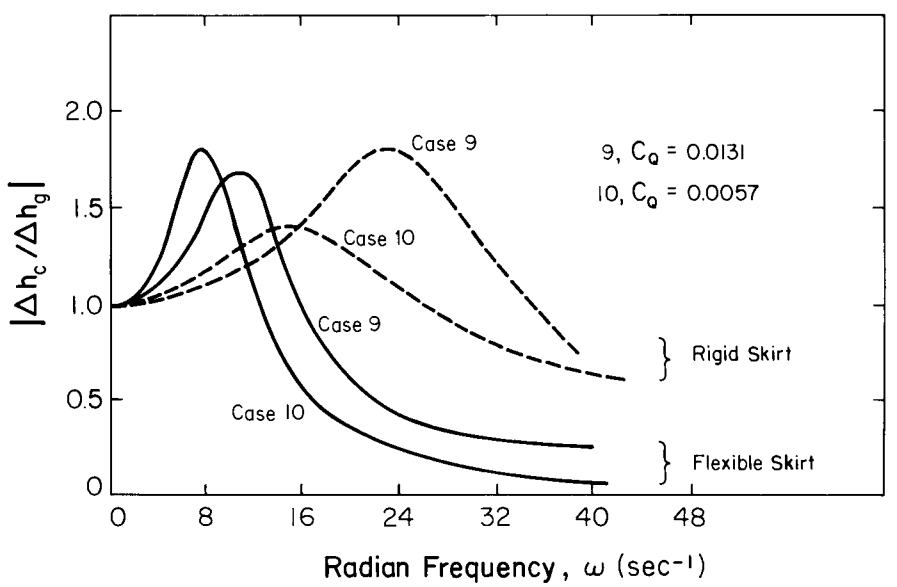

Fig. 13.31 Effect of equilibrium flow rate on heave amplitude response of the laboratory model.

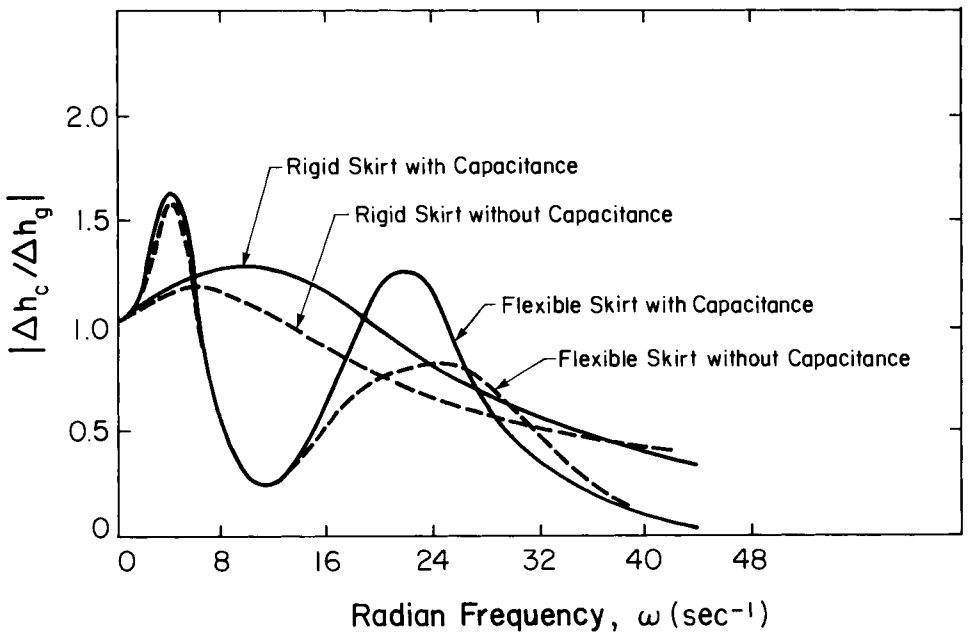

Fig. 13.32 Effect of cushion air compressibility on heave amplitude response of full scale vehicle. Parameters, case 11.

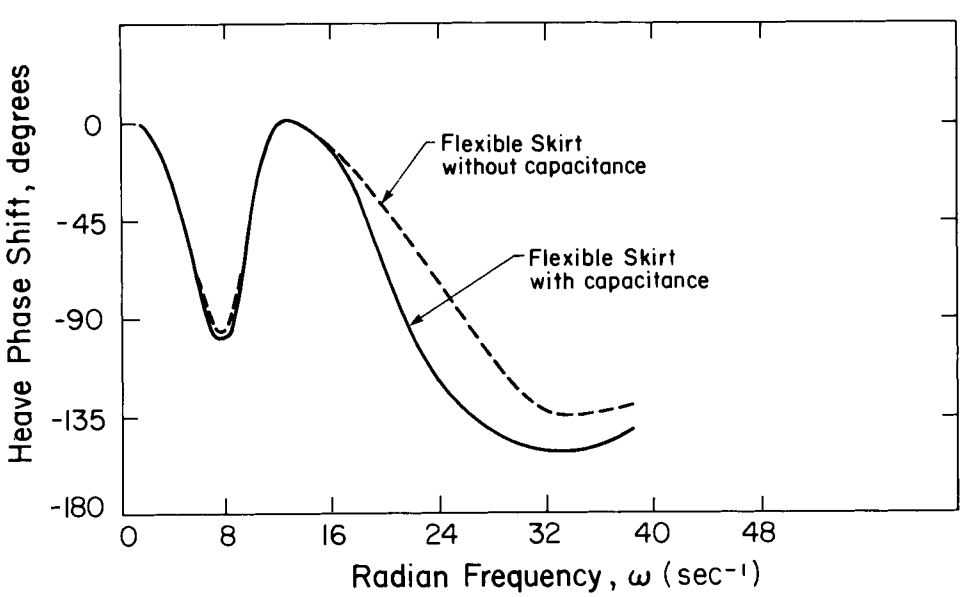

Fig. 13.33 Effect of cushion air compressibility on heave phase responses of full scale vehicle. Parameters, case 11.

response, the cushion capacitance might be omitted from the calculations; however for lower Q_e and for such problems as skirt bounce or high speed passage over short waves it should be included.

Figure 13.34 gives the effect of reducing the outer bag mass to one fifth of the value given in Table 13.5. The effect on the first natural frequency is negligible, thus implying, as for the laboratory model, that this skirt responds as if it is inertialess for frequencies in this neighbourhood. However, reducing outer bag mass has a signficant effect on the second natural frequency. This suggests that the two-degree-of-freedom model of the skirt described in Section 13.2.7, which lumps all of the skirt mass at a single point in the finger, is adequate for calculation of vehicle response at low frequencies. However for very high frequency response analysis, or for the skirt bounce problem, additional degrees of freedom including a distributed mass of the outer bag should be adopted.

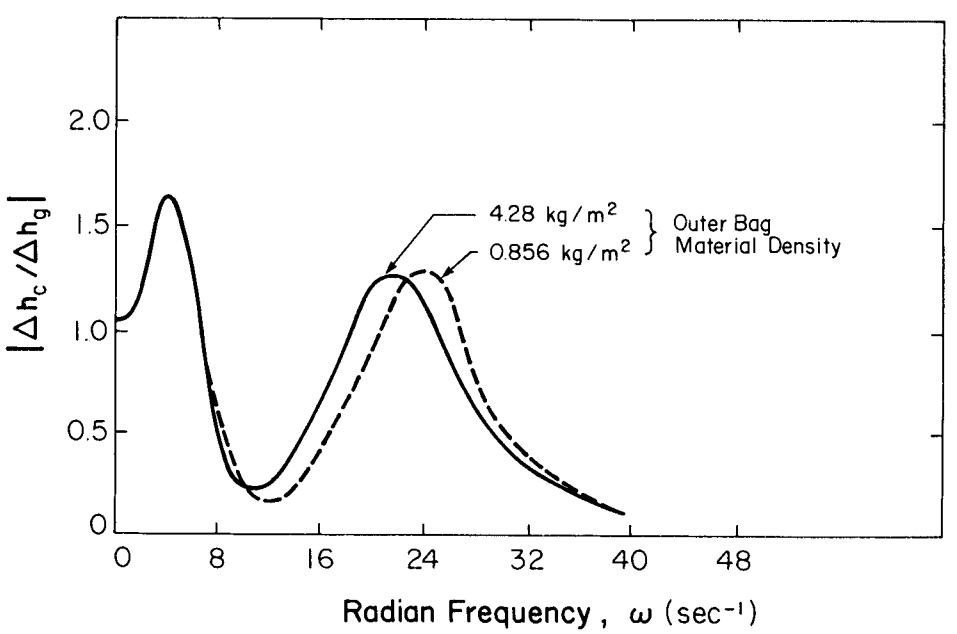

Fig. 13.34 Effect of mass of outer bag on heave amplitude response for full scale vehicle. Parameters, case 11.

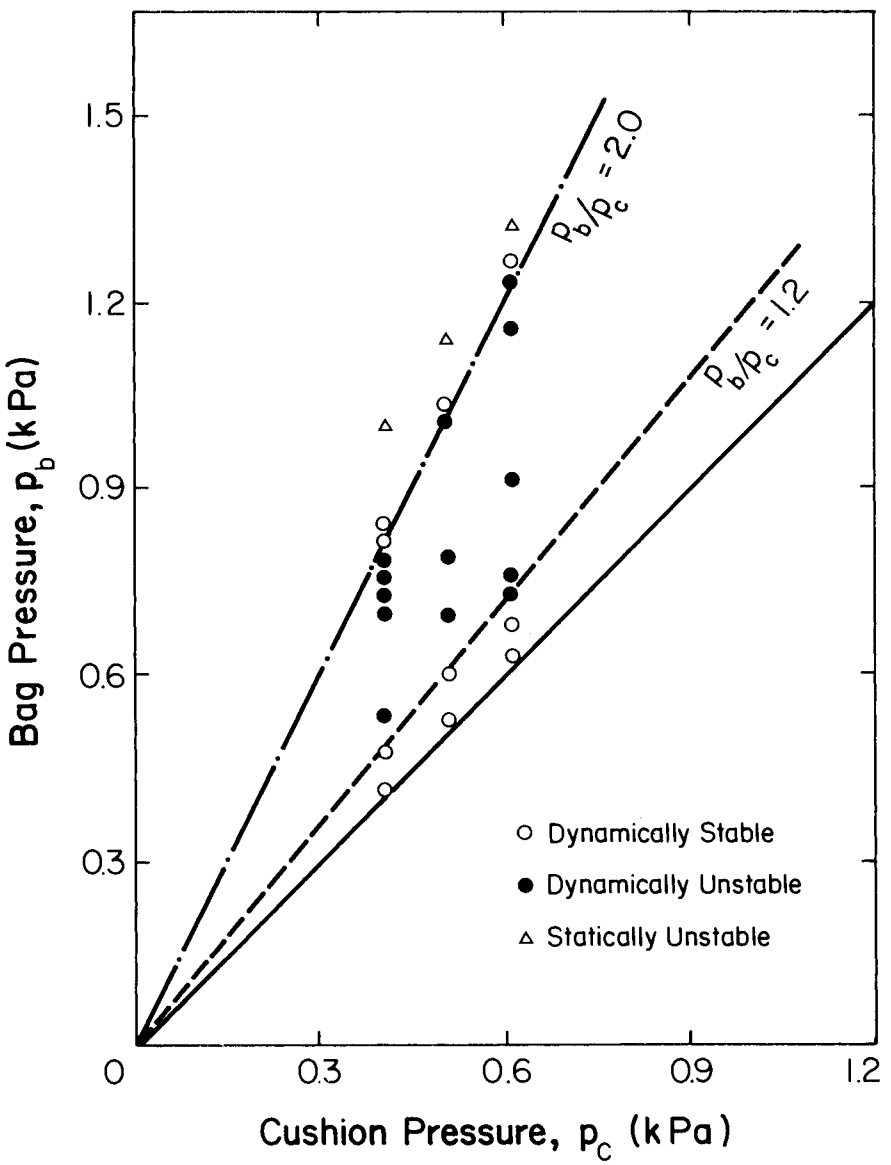

Fig. 13.35 Effect of bag and cushion pressures on dynamic stability as predicted for the laboratory model and various geometries.

13.4.6 Dynamic Stability Results

Figure 13.35 presents in the format used by Mantle (ref. 2) computed stability results for the laboratory model operating at various conditions. As noted above they include a distributed mass model of the outer bag. The results show that for $1.20 \leq p_b/p_c \leq 2.00$ the cushion is dynamically unstable; they are consistent with experimental data obtained from full scale craft reported by Mantle, and confirm that the dominant parameter indicating the onset of skirt bounce is the ratio p_b/p_c, with such other factors as fan characteristics and skirt geometry usually only having a secondary effect. Figures 13.36 to 13.38 give loci of the important roots of the characteristic equations of the overall system and the subsystems as computed for the laboratory model. In these plots the parameter being varied is p_b/p_c, either by changing bag orifice area A_j or fan speed N_f, and the arrow on the loci indicates the direction in which the roots move as p_b/p_c increases.

Figure 13.36 gives an example of the behaviour of the skirt system and skirt-cushion system roots. In Fig. 13.36 p_p/p_c is increased by reducing bag orifice area A_j, which forces the fan to operate closer to the maximum pressure it can deliver. For the skirt system, at $p_p/p_c = 1$ two roots are located on the imaginary axis, thus indicating that the system is marginally stable. As p_b/p_c increases, the roots at first move well into the $\sigma < 0$ region, and their frequency decreases. The lower frequency breaks into the real axis, and then both roots move towards $\sigma = 0$ and cross into the unstable region, $\sigma > 0$, simultaneously. Since one of these roots is real, the system is both statically and dynamically unstable, and this occurs because the effective fan slope dp_b/dQ_b becomes positive.

As shown in Fig. 13.36, the skirt-cushion system root behaviour differs from that of the skirt system in certain respects. As for the skirt system, at $p_p/p_c = 1$ the skirt-cushion system is marginally stable and, as p_b/p_c increases, the roots at first move into the stable region, and one breaks into the real axis before moving towards the unstable region. However the remaining complex root crosses into the $\sigma > 0$ region at a value of p_b/p_c which is lower than that for the skirt system alone, so that, well before the real root crosses into the $\sigma > 0$ region and static instability occurs, the cushion is dynamically unstable. Thus the feedback effect of the cushion pressure on the skirt system plays a role in generating instability.

Figure 13.37 gives the root loci for the complete system. There are three pairs of complex roots of interest, two of which behave similarly to those of the skirt-cushion system, and a low frequency root associated with the craft motion. Instability then occurs when one of the skirt-cushion system roots crosses $\sigma = 0$ at a value of p_b/p_c close to that in Fig. 13.36. However, at a slightly higher p_b/p_c the low frequency root also becomes unstable.

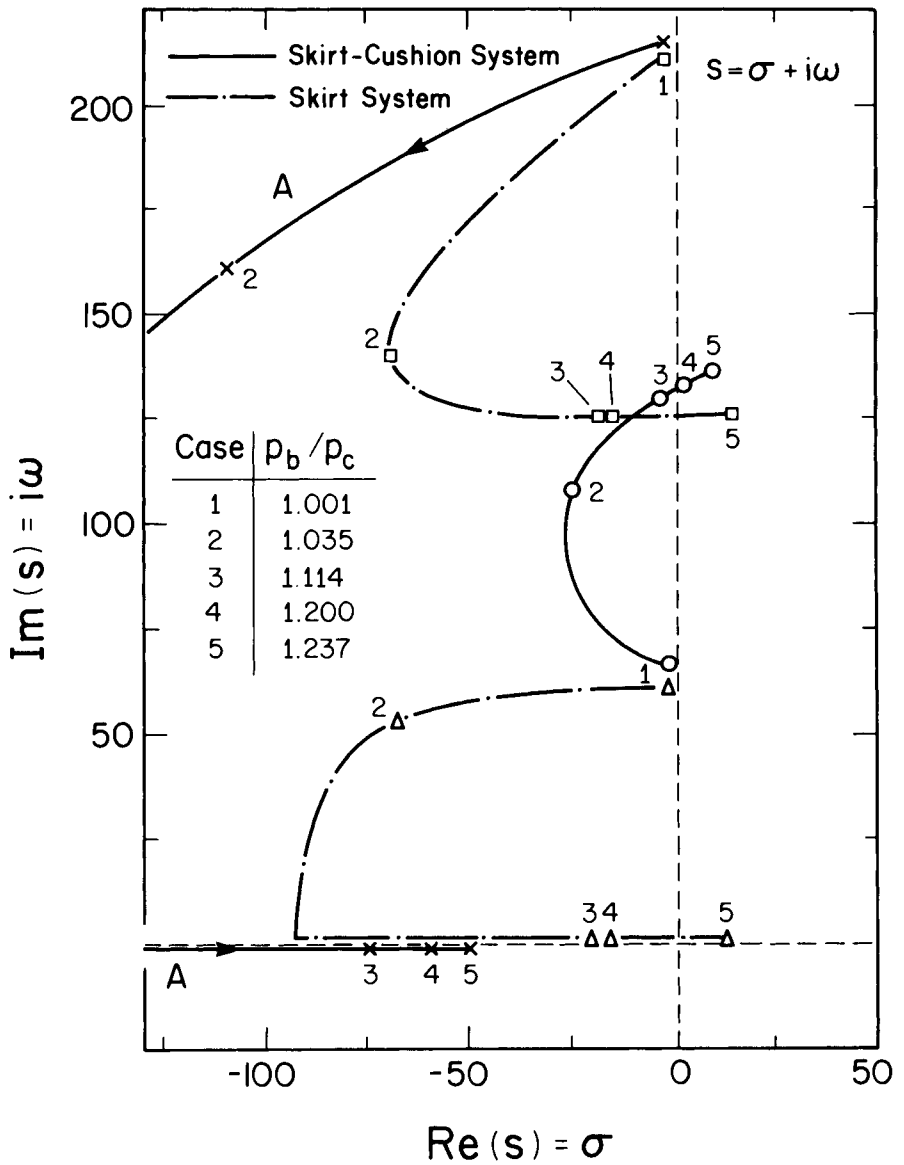

Fig. 13.36 Typical root-loci for laboratory model skirt-cushion system as a function of p_b/p_c, as obtained by changing A_j.

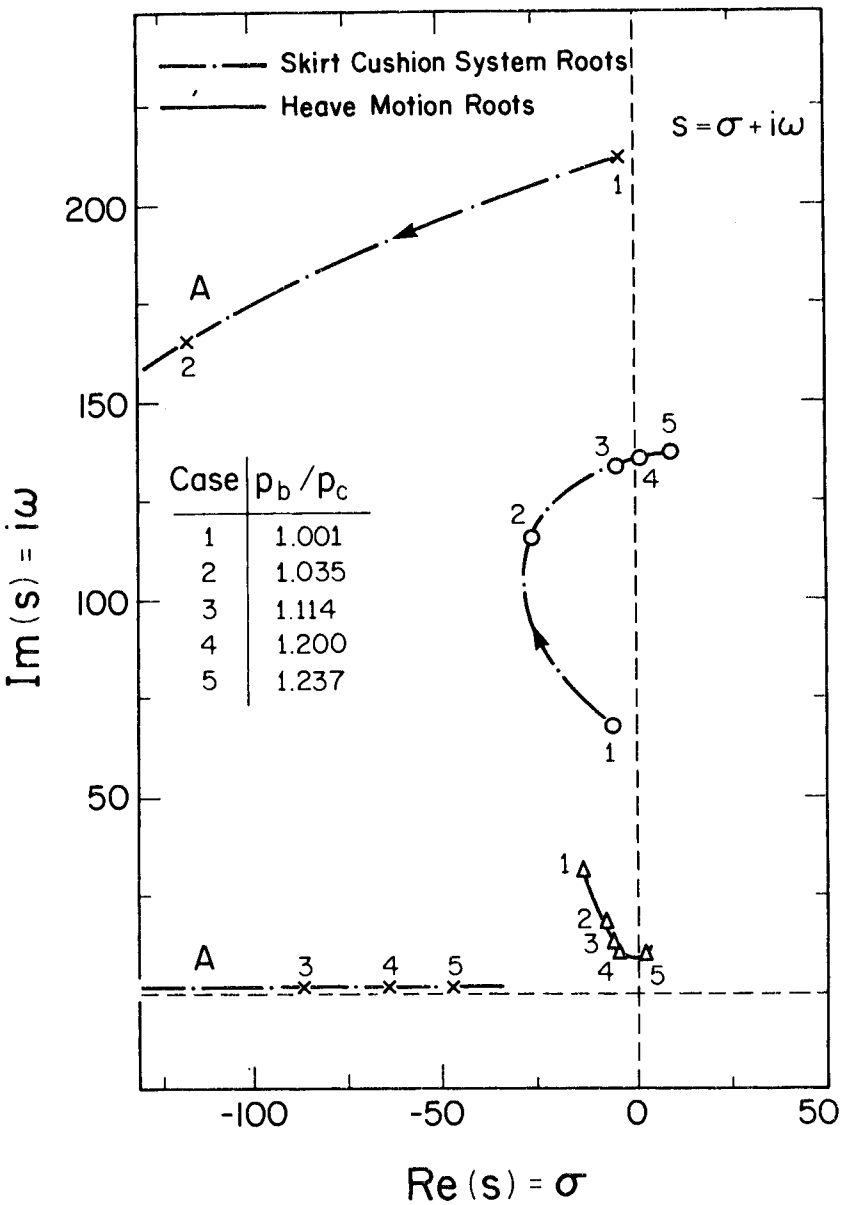

Fig. 13.37 Root loci for cushion system of Fig. 13.37 with heave motion dynamics included.

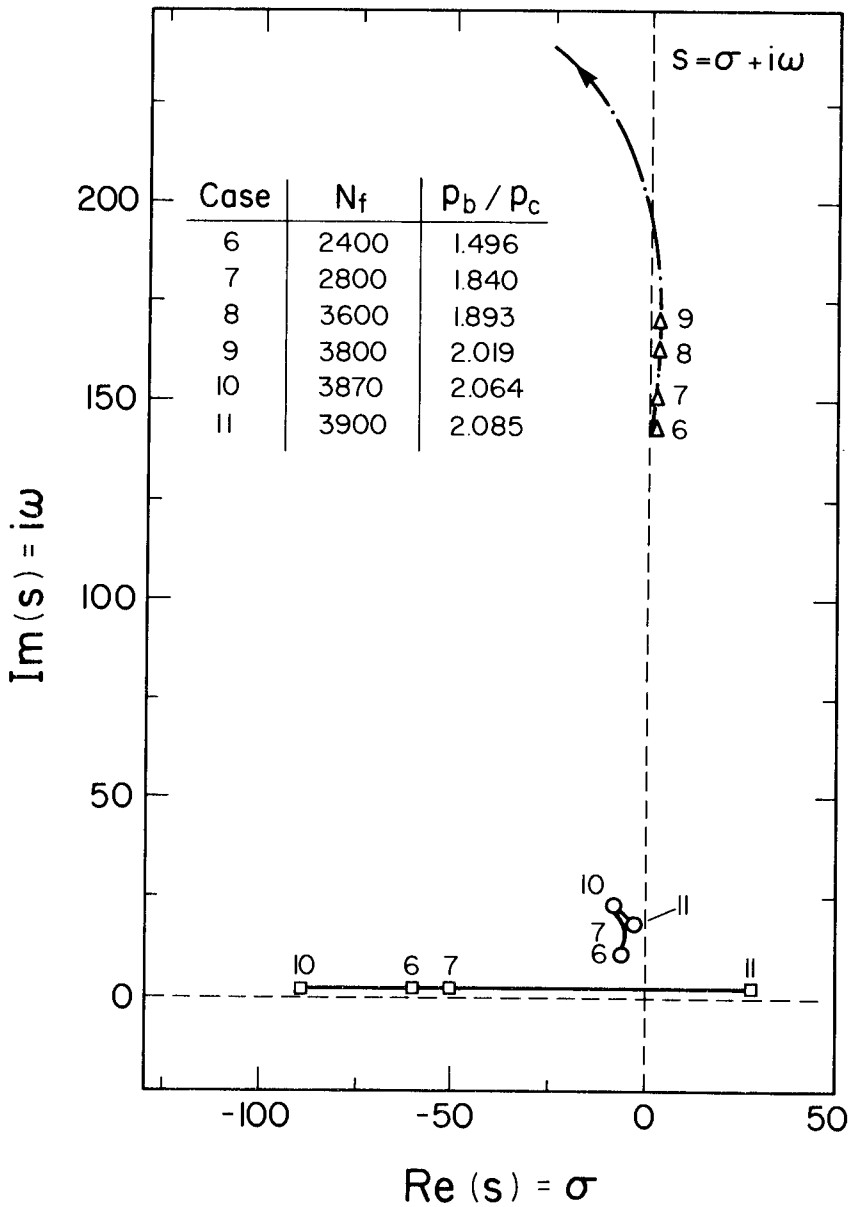

Fig. 13.38 Root loci for overall system for high values of p_b/p_c.

Figure 13.38 is a root locus plot for the complete system operating at very high values of p_b/p_c. In this case, to avoid static instability arising from a positive dp_b/dQ_b, the fan speed is increased to obtain the requisite p_b/p_c. Here the high frequency root becomes stable when $p_b/p_c > 2$ approximately, but at a slightly higher value the cushion becomes statically unstable. One possible explanation of this result is that, when p_b/p_c becomes sufficiently high, the resulting outer bag tension forces the segment angle γ close to the inner bag angle α, and the skirt to behave as if it were a single degree of freedom system and thus become dynamically stable. But being statically unstable it snaps through to a second equilibrium configuration.

13.5 NOMENCLATURE

(i) Roman

A_{bi}	Constants in polynomial fit to static pressure-flow characteristic for flow delivered by fan to bag
A_{fi}	Constants in polynomial fit to fan static pressure-flow characteristic
A_j	Total bag-to-cushion orifice area
$\underset{\sim}{A}_p$	Vector transfer function in skirt motion equation giving perturbations of generalized force inputs arising from perturbations in p_c, $\underset{\sim}{A}_p = \underset{\sim}{V}_p[P_{bc}, 1]^T$
$\underset{\sim}{A}_s$	Skirt system dynamics matrix, $\underset{\sim}{A}_s = s^2\underset{\sim}{M}_s + \underset{\sim}{K}_s$
b	Inner bag chord length, see Fig. 13.4
B_B	Width of vehicle base between inner attachment points of skirt
B_D	Reference length used to nondimensionalize skirt geometry, $B_D = L_D\cos\Gamma_D$ in Fig. 13.4
B_f	Width of one finger perpendicular to plane of Fig. 13.4
B_j	Equivalent slot width of bag-to-cushion orifice area, $B_j = A_j/L_s$
c	Outer bag chord length, see Fig. 13.4
C_D	Water surface drag force coefficient in tuck-under problem
C_e	Effective discharge coefficient in linearized cushion exit flow equation, defined in eqn. (13.84)
C_{me}	Cushion exit flow discharge coefficient, $C_{me} = h_f/h_e$
C_{mj}	Bag-to-cushion orifice discharge coefficient
C_{QC}	Nondimensional cushion flow coefficient, $C_{QC}=Q_e[\rho_a/(2M_c gL_M D_M)]^{1/2}$
$\underset{\sim}{D}_b$	Bag damping matrix, defined in eqn. (13.152)
$\underset{\sim}{D}_{sc}$	Skirt-cushion damping matrix, defined in eqn. (13.152)
E	Stability determinant for tuck-under problem, defined in eqn. (13.63)
$\underset{\sim}{F}_{cs}$	Vector transfer function in craft heave motion equation which

gives contribution to craft heave force caused by skirt motion, see eqn. (13.156)

$\underset{\sim}{F}_{he}$ Vector transfer function in skirt motion equation which gives force inputs caused by perturbations in h_g and h_c, see eqns. (13.106) and (13.150)

$\underset{\sim}{F}_{hw}$ Vector transfer function in skirt statics equation for tuck-under problem, which gives force inputs caused by perturbations in h_w, see eqn. (13.58)

f_w Magnitude of drag force per unit length of skirt exerted by water on skirt in tuck-under problem

g Acceleration due to gravity

$G(s)$ Skirt-cushion system open loop gain, $G(s) \equiv \Delta p_{cs}/\Delta p_{ci}$, see eqn. (13.144), also $G(0) = \Delta h_s/\Delta h_e$

$\underset{\sim}{G}$ Skirt-cushion system open loop gain vector, $\underset{\sim}{G} = [G, H]^T$

$\underset{\sim}{G}_w$ Surface contact feedback gain vector, $\underset{\sim}{G}_w = [G_w, H_w]^T = [\Delta h_s/\Delta h_w, \Delta x_s/\Delta h_w]^T$

H Skirt lateral deflection gain $= \Delta x_s/\Delta h_e$

$\underset{\sim}{H}_c$ Dimensional skirt pressure flexibility vector, $\underset{\sim}{H}_c = [\Delta h_s/\Delta p_c, \Delta x_s/\Delta p_c]^T$, see eqn. (13.55)

h_c Craft height measured downwards from a datum

h_e Hovergap or distance between bottom tips of skirt fingers and ground.

h_f Equivalent slot or leak height for cushion exit flow, defined in eqn. (13.70)

h_g Ground height, measured downwards from a datum

$\underset{\sim}{\bar{H}}_{\bar{p}}$ Nondimensional skirt pressure flexibility vector, $\underset{\sim}{\bar{H}}_{\bar{p}} = [\bar{h}_{\bar{p}}, \bar{x}_{\bar{p}}]^T$, see eqn. (13.54)

h_s Skirt height

$\underset{\sim}{h}_s$ $[h_s, x_s]^T$

h_w Equivalent depth of penetration of water surface by finger that would occur if the finger remained undeformed

I_d Duct inertance in cushion air feed system

$\underset{\sim}{K}_b$ Bag stiffness matrix, $\underset{\sim}{K}_b = \underset{\sim}{K}_{ob} + \underset{\sim}{K}_{ib}$

K_D Water speed coefficient in surface contact problem, $K_D = C_D \rho_w V_w^2/(2p_c)$

$\underset{\sim}{K}_f$ Contribution to $\underset{\sim}{K}_s$ generated by p_c acting on finger in absence of surface contact

$\underset{\sim}{K}_{fp}$ In surface contact problem, contribution to skirt stiffness matrix generated by p_c acting on uncollapsed part of finger

$\underset{\sim}{K}_{fw}$	In surface contact problem, contribution to skirt stiffness matrix generated by force f_w
$\underset{\sim}{K}_{ib}$	Contribution to $\underset{\sim}{K}_s$ generated by $(p_b - p_c)$ acting on inner bag
$\underset{\sim}{K}_{ob}$	Contribution to $\underset{\sim}{K}_s$ generated by p_b acting on outer bag
$\underset{\sim}{K}_p$	Skirt feedback stiffness matrix generated by effect of skirt motion on p_c, see eqns. (13.105) and (13.152)
$\underset{\sim}{K}_s$	Skirt geometric stiffness matrix, $\underset{\sim}{K}_s = \underset{\sim}{K}_b + \underset{\sim}{K}_f + \underset{\sim}{K}_{sg}$ in absence of contact and $\underset{\sim}{K}_s = \underset{\sim}{K}_b + \underset{\sim}{K}_{fp} + \underset{\sim}{K}_{fw}$ in presence of contact
$\underset{\sim}{K}_{sg}$	Contribution to skirt geometric stiffness matrix generated by skirt weight
$\underset{\sim}{K}_{ST}$	In surface contact problem, $\underset{\sim}{K}_{ST} = \underset{\sim}{K}_s + \underset{\sim}{K}_w$
$\underset{\sim}{K}_w$	Skirt feedback stiffness matrix generated by surface contact, see eqn. (13.61)
ℓ_w	Length of part of finger in contact with water surface, see Fig. 13.5
$L_1, L_2, \ldots$	Lengths of various parts of finger defined in Fig. 13.5
ℓ_4	Variable length of front face of finger in surface contact model, see Fig. 13.5
L_c	Total cushion lift force, see eqn. (13.92)
L_D	Length of line joining bag attachment points, see Fig. 13.4
L_{ib}	Length of inner bag
L_M	Length locating position of lumped mass of skirt in finger, see Fig. 13.5
L_{ob}	Length of outer bag
L_s	Total peripheral length of skirt
M_c	Mass of craft
M_e	Exit momentum flux in wall-jet model of cushion
M_j	Momentum flux of flow from bag to cushion
M_s	Lumped mass of skirt
N_f	Lift fan speed
$P(\underset{\sim}{q})$	Potential energy of skirt structure
p_b	Pressure of air in bag
P_{bc}	In linear analyisis, cushion-to-bag pressure transfer function; $P_{bc} = Z_b/R_j$
p_c	Pressure of air in cushion
P_{ch}	Transfer function relating cushion pressure response to craft and ground motion in absence of skirt motion; $P_{ch} = -Z_c[C_e + sS_c]$
$\underset{\sim}{P}_{cs}$	Vector transfer function given response of p_c to skirt deflection defined in eqn. (13.140)

p_f	Pressure of air delivered by fan
$\underset{\sim}{q}$, q_α	Generalized coordinates in Lagrangian formulation of skirt model
Q_c	Net flow out of cushion, $Q_c = Q_e - Q_j$ in statics
$\bar{Q}_c$	Q_c/Q_j
Q_e	Volume flux of air at cushion exit
Q_f	Volume flux out of fan
Q_i^{NC}	Nonconservative generalized forces acting on skirt
Q_h	$\partial\bar{Q}_c/\partial\bar{h}_e$, see eqn. (13.75)
Q_j	Volume flux through bag orifices
Q_p	$\partial\bar{Q}_c/\partial\bar{p}_c$, see eqn. (13.75)
R_b	Bag system resistance defined in eqn. (13.88)
R_c	Cushion system resistance defined in eqn. (13.89)
R_e	Cushion exit flow resistance, defined in eqn. (13.85)
R_{fd}	Effective combined fan-duct resistance defined in eqn. (13.79)
$\underset{\sim}{R}_G$	Set of geometric parameters in skirt model, $\underset{\sim}{R}_G = \{L_{ib}, L_{ob}, \ldots\}$
r_{ib}	Inner bag radius
$\underset{\sim}{R}_M$	Set of material property parameters in skirt model, $\underset{\sim}{R}_M = \{M_s, \ldots\}$
r_{ob}	Outer bag radius
s	Laplace variable, $s = \sigma + i\omega$
S_c	Cushion footprint area
S_j	Effective bag orifice area defined in eqn. (13.69)
T	Kinetic energy of skirt
$\underset{\sim}{T}$	Transfer matrix in linear analysis relating perturbations in h_s and x_s to the q_α
V_b	Bag volume
$\underset{\sim}{V}_{bq}$	Transfer function row vector giving perturbations in V_b caused by perturbations in $\underset{\sim}{q}$, see eqn. (13.132)
V_c	Cushion volume
$\underset{\sim}{V}_{cq}$	Transfer function row vector giving perturbations in that part of cushion volume contained by skirt caused by perturbations in $\underset{\sim}{q}$, see eqn. (13.137)
$\underset{\sim}{V}_p$	In skirt linearized motion equation, matrix giving generalized force inputs generated by bag and cushion pressure, see eqn. (13.19)
V_w	Craft speed over water
x, y	Craft-fixed coordinate system defined in Fig. 13.4
x_s	Lateral skirt deflection defined in Fig. 13.1
Z_b	Equivalent bag impedance giving perturbations in p_b caused by $\dot{V}_b$, and by perturbations in Q_j, see eqn. (13.123)

Z_{bc}	Equivalent impedance controlling bag damping, see eqns. (13.140) and (13.152)
Z_c	Equivalent cushion impedance giving perturbations in p_c caused by $\dot{V}_c$ and by perturbations in Q_e and Q_j, see eqn. (13.127)
Z_d	Duct impedance
Z_f	Equivalent fan impedance; see Section 13.4.1
Z_{fd}	Resultant impedance upstream of bag

(ii) Greek

α	Angle of link OD relative to horizontal, see Fig. 13.5
β	Angle of inner bag chord OB relative to horizontal, see Fig. 13.4
Δ	Laplace transform
γ	Angle of finger chord line BD relative to horizontal, see Fig. 13.5
Γ_D	Angle of line OA on vehicle between bag attachment points relative to horizontal, see Fig. 13.4
Γ_M	Angle specifying location of skirt mass in lumped finger, see Fig. 13.5
Γ_1, Γ_2, ...	Angles defining skirt geometry, see Fig. 13.5
θ_f	Angle of front face of finger relative to horizontal
θ_{ib}	Inner bag arc angle
θ_{ob}	Outer bag arc angle
μ	Skirt material surface density
ρ_a	Air density
ρ_w	Water density
σ	Real part of Laplace variable
τ	Time constant
ψ	Angle of outer bag chord line relative to vertical, see Fig. 13.4
ω	Imaginary part of Laplace variable, circular frequency
Ω_1, Ω_2, ...	Angles defining finger geometry, see Fig. 13.5

(iii) Subscripts

a	Atmosphere
b	Bag
c	Cushion
d	Duct
e	Exit
f	Fan
j	Bag orifice
o	Equilibrium

13.6 SUMMARY

A mathematical model of the dynamics of a bag and finger skirt and related systems is developed and applied to the heave dynamics of an air cushion vehicle. The aim is to obtain insights into the factors affecting frequency response and stabililty, with the ultimate intention of improving sea-keeping or ride comfort, and of reducing susceptibility to both the static stability known as tuck-under and the dynamic instability known as skirt bounce.

We discuss the idea of increasing skirt responsiveness, or surface-following ability, as a way of improving sea-keeping or ride comfort. We note that, although the bag-and-finger concept is capable of being highly responsive, current configurations do not fully achieve their potential. This is because improving responsiveness generally makes the skirt more susceptible to both tuck-under and skirt bounce. Furthermore, the web currently used to suppress skirt bounce inhibits the downward motion of the skirt considerably, and thus interferes with responsiveness.

To make the analysis tractable, the equations of the dynamics are formulated for a two-dimensional section of the skirt, and craft motion is confined to pure heave over a smooth, flat surface. A Lagrangian approach is used to simplify the formulation of the inputs to the skirt dynamics generated by bag and cushion pressures. Two very simple models of skirt structural behaviour are used to obtain quantitative results. Both are inelastic two-degree-of-freedom models, and both lump the entire skirt mass at a point in the finger. However, the Lagrangian formulation is stated for an arbitrary number of degrees-of-freedom, and the subsequent linear analysis uses matrix notation to allow straightforward inclusion of additional degrees-of-freedom required to consider such effects as distributed skirt mass or material viscoelastic behaviour.

Within the context of linear theory, the dynamics is considered in terms of the interaction of three sub-systems: the cushion system, the skirt system, and the craft system. The cushion system is essentially the fluid flow processes; its input and output are, respectively, the hovergap h_e, and the cushion pressure p_c. The skirt system is the skirt structural dynamics, with input being p_c, and output, the skirt height h_s. The craft system is the vehicle heave dynamics, with input and output being, respectively, p_c and craft vertical motion h_c. A key result of the linear analysis is the development of a general expression for the open loop gain of the combined skirt and cushion systems, G(s). This concept arises in the following way: craft and ground motion, in the absence of skirt motion, by modulating h_e, generate a cushion pressure perturbation $\delta p_{ci}(t)$. This perturbation generates skirt motion, which in turn, through its interaction with the cushion system, generates a further fluctuation in p_c, $\delta p_{cs}(t)$. The skirt-cushion system gain

is the open loop gain of δp_{cs} corresponding to the input δp_{ci}. It is shown that, for static behaviour, $G(o) = \delta h_s/\delta h_e$; and it is the magnitude of G(o) which is proposed as a measure of skirt responsiveness. Furthermore, for full size vehicles, the effect of the skirt system on the overall heave dynamics enters only through G(s). This gain includes the effects on the craft dynamics and stability of both the generalized skirt dynamics model and, through certain key equivalent circuit impedances, the cushion system fluid mechanics.

The nonlinear predictions of the static heave response are shown to be in good agreement with some measurements obtained from a small two-dimensional model. A limited amount of data obtained from this model shows the effect on skirt responsiveness of geometry, bag orifice feed area and lift fan speed. The data that is presented supports the idea that linear theory should, at the very least, give good qualitative insights into the factors that affect cushion response and stability. Computed results for linear frequency response, obtained by using one of the two proposed skirt structural models, are also presented. The dynamic stability problem is also explored by using root locus plots.

The analysis of the static stability of the skirt considers the destabilizing effect of the forces on the skirt generated by surface contact; this is the tuck-under problem. For this analysis, a previously proposed highly simplified model of finger deformation is used. One of the main results of the analysis is that this static stability is controlled by a scalar gain G_w which is very similar in form to G(o). Some computed results showing the effect of various parameters on the tuck-under instability are also presented, together with some stability boundaries obtained from a small model tested in a water channel.

13.7 REFERENCES

1. J. E. Rapson, Responsive hovercraft skirts, in: Proc. Third Int. Hovercraft Conference of Hovercraft Society, Southampton, England, November, 1981, Paper No. 1.

2. P. J. Mantle, Air cushion craft development, U.S. Navy, David W. Taylor Naval Ship Research and Development Center, Bethesda, Md., U.S.A., DTNSRDC-80/012, January, 1980.

3. J. J. Fee and F. H. Handler, The U.S. Navy's large surface effect ship, in: Proc. 10th Canadian Symposium on Air Cushion Technology, Canadian Aeronautics and Space Institute, Ottawa, Canada, January 1977.

4. J. R. Amyot, Computer studies of ACV performance as a function of vent valve proportional control parameters, Canadian Aeronautics and Space J., 29(1) (1983) 25-34.

5. T. Ma and W. L. Zhou, Control investigation of longitudinal motion of an SES with a cushion vent valve and a fan inlet valve, Marine Design and Research Institute of China, Shanghai, China, internal report, 1979.

6. P.A.T. Christopher, K. F. Man, E. W. Osbourn and Y. K. Chan, Heave control of amphibious hovercraft, in: V. Rembold, K. G. Kempf, D. R. Towill, G. Johannesen and M. Paul (Eds.), A Bridge Between Science and Technology, Vol. 5, Pergamon, Oxford, 1985.

7. A. J. Reynolds, The roles of skirt planform and deflection in hovercraft response, J. Mechanical Engineering Science, 19(1) (1977) 1-12.

8. R. L. Wheeler, Recent United Kingdom hovercraft development, J. Hydronautics, 12(1) (1978) 3-17.

9. X. Gu and T. Ma, Hovercraft skirt system, in: Proc. 14th Canadian Symposium on Air Cushion Technology, Canadian Aeronautics and Space Institute, Ottawa, Canada, September 1980.

10. P. A. Sullivan, J. E. Byrne and M. J. Hinchey, Nonlinear oscillations of a simple flexible skirt air cushion, J. Sound and Vibration, 102(2) (1985) 269-283.

11. P. A. Sullivan, M. J. Hinchey, T. A. Graham, J. E. Byrne, A. Dupuis, N. Milligan and C. Walsh, Investigations of the dynamics of large air cushions, Transportation Development Centre, Transport Canada, Montreal, Canada, Report TP 7560, August 1986.

12. P. A. Sullivan, M. J. Hinchey and G. M. Green, A review and assessment of methods for the prediction of the dynamic stability of air cushions, J. Sound and Vibration, 84(3) (1982) 337-358.

13. M. J. Hinchey and P. A. Sullivan, Duct effects on the heave stability of plenum air cushions, J. Sound and Vibration, 60(1) (1978) 87-99.

14. T. A. Graham, P. A. Sullivan and M. J. Hinchey, Skirt material effects on air cushion dynamic heave stability, J. Aircraft 22(2) (1985) 101-108.

15. ———, Stability and control of hovercraft: notes for commanders, United Kingdom Department of Industry, Ship and Marine Technology Requirements Board, London, Great Britain, Report BHC SP4432, 1980.

16. T. Ma and P. A. Sullivan, Linear analysis of the heave dynamics of a bag and finger air cushion vehicle skirt, in: Proc. Eighth Advanced Marine Systems Conference, San Diego, California, September 28-30, 1986, American Institute for Aeronautics and Astronautics, Washington, Paper No. 86-2361.

17. T. Ma, Design method and parameter analysis of low frequency responsive skirt, Marine Design and Research Institute of China, Shanghai, China, internal report, 1982.

18. M. J. Plackett and R. B. Wade, Design aspects of seal systems for air cushion vehicles, in: Proc. AIAA/SNAME Advanced Marine Vehicles Conference, San Diego, California, April 17-19, 1978. American Institute for Aeronautics and Astronautics Paper No. 78-755.

19. Y. N. Chen, S. H. Qiu and N. Zhen, Investigation of hydrodynamic performance of a responsive skirt, Marine Design and Research Institute of China, Shanghai, China, internal repport, 1979.

20. T. Ma, W. L. Zhou and X. Ghu, Theoretical and experimental investigation of non-equilibrium jet of air cushion vehicles, in: 13th Symposium on Naval Hydrodynamics, Shanghai, China, Oct. 1980.

21. H. Ohashi, Analytical and experimental study of the dynamic character istics of turbopumps, National Aeronautics and Space Administration, Washington, U.S.A., TN D-8413, 1968.

22. F. R. Goldschmied and D. N. Wormley, Frequency response of blower/duct/plenum fluid systems, J. Hydronautics 11(1) (1977) 18-27.

23. J. M. Durkin and L.W.H. Luehr, The dynamics response of lift fans subject to varying back pressure, in: Proc. AIAA/SNAME Advanced Marine Vehicles Conference, San Diego, California, April 17-19, 1978, American Institute of Aeronautics and Astronautics Paper, Washington, No. 78-756.

Chapter 14

HEAVE DYNAMICS CONTROL

14.1 INTRODUCTION

Regardless of whether a hovercraft carries passengers or cargo, it should not spontaneously develop self-excited vertical oscillations in the absence of surface disturbances. In other words, it should be stable in the heave direction of motion. The degree of heave stability is also important since ride quality and skirt wear are closely related to it.

A hovercraft can be underdamped in heave; that is, it can give a rough ride in response to water waves or ground irregularities. The degree of damping is usually related to system airflow in the sense that an increase in total lift-fan airflow tends to decrease damping, even to the extent of causing heave instability in some cases. However, reducing airflow to improve ride quality may not be acceptable in practice since this reduces elevation and results in skirt drag which, in turn, produces skirt wear and reduces vehicle speed, unless thrust is increased to maintain speed at the expense of fuel economy and accelerated skirt wear.

The stiffness of an air cushion is inversely related to its damping. A stiff cushion gives a rough ride because of the relatively large accelerations transmitted to the passengers or cargo when traveling over rough surfaces. In the practical operation of a craft, its cushion can be softened by decreasing lift airflow, possibly at the expense of a shortened skirt life. Thus, good ride quality and low skirt drag and wear are conflicting requirements in hovercraft design and operation.

Certain combinations of air ducting and cushion dimensions, skirt and lift-fan characteristics, cushion pressure, and lift airflow are conducive to heave instability (ref. 1). The complexity of practical craft often makes it

virtually impossible to predict their degree of stability or ultimate instability with meaningful accuracy. Furthermore, the heave dynamics of a vehicle depend on ageing and environmental conditions such as temperature, altitude, and terrain porosity and roughness. Thus, especially for craft which are only marginally stable, the availability of a tunable, on-board, heave-dynamics control system would be very useful.

The method of improving ride quality is to implement an automatic vent-valve control system. This approach was designed into the U.S. Navy's surface-effect ship SES-100A and tested in 1973 (ref. 2). It was then retrofitted to the SES-100B ship in 1974 so that comparisons could be made and the necessary data collected for evaluation. The venting system consisted of an overboard valve, at the stern, which dumped the cushion air that would otherwise impart vertical acceleration to the craft due to the piston-like action of the waves. The area of the venetian-blind type of valve was approximately 1.86 m^2, or 1% of the cushion area. Starting from a nominal open setting, its position was modulated about this setting according to the heave acceleration of the bow or, in later tests, pressure changes. One of the former tests can be described in three stages.

(1) At 41 knots in a 1 m average wave-height sea, with the valve closed and a cushion flow of approximately 161 m^3/s, the rms heave acceleration was 0.39 g.

(2) Upon opening and holding the valve at 25%, approximately 113 m^3/s, or 70.2% of the cushion flow, was diverted to the vent, causing immersion of the sidehulls and a reduction of craft speed to 35 knots. The rms acceleration fell to 0.19 g.

(3) The rms acceleration decreased further to 0.13 g when the control system was activated to modulate the position of the valve about its 25% setting according to heave acceleration of the bow.

In order to improve performance over a wide range of sea states, the above automatic vent-valve control system was integrated with control of fan-inlet guide vanes (IGVs). The resulting ride control system (RCS) has been successfully demonstrated on U.S. Navy surface effect ships (ref. 3).

The ride control problem in marine operation of air cushion craft is quite different from the stabilization problem of heavy-load air cushion craft operated at relatively low speeds over land. For such applications, experimental and analytical studies conducted at the National Research Council of Canada (NRCC) have shown (refs. 4-7) that vent valve control is not significantly detrimental to lift power requirements, provided the vent valves are controlled from a nominally-closed position. Here, the action of the valves is to regulate the net outflow of air following a disturbance. This is accomplished by reducing the net outflow variations about a nominal value corresponding to the

operating elevation. The purpose of this chapter is to present the essential features and results of the NRCC studies.

14.2 COMPUTATIONAL MODELS

The performance of various automatic vent-valve control systems was examined by means of computer models in which the heave dynamics were kept the same for comparison purposes. This section describes the air-cushion dynamics, the various control systems, and the computer implementation methods used.

14.2.1 Air Cushion Heave Dynamics

As a first step in studying the problem of ride quality and heave instability over land, the NRCC defined a conceptual model structure for hovercraft heave dynamics involving the interaction of measured fan and skirt characteristics with cushion and platform dynamical equations. The approach was applied to a small research hovercraft where some quantitative steady-state and qualitative dynamic validation was performed (ref. 8). Then, since the research hovercraft was stable on land and the objective was to improve unstable or marginally stable craft, a conceptual model was postulated, based on the above structure and experimental data from another physical model capable of heave instability, such that stability improvement by automatic vent-valve control could be studied (ref. 9).

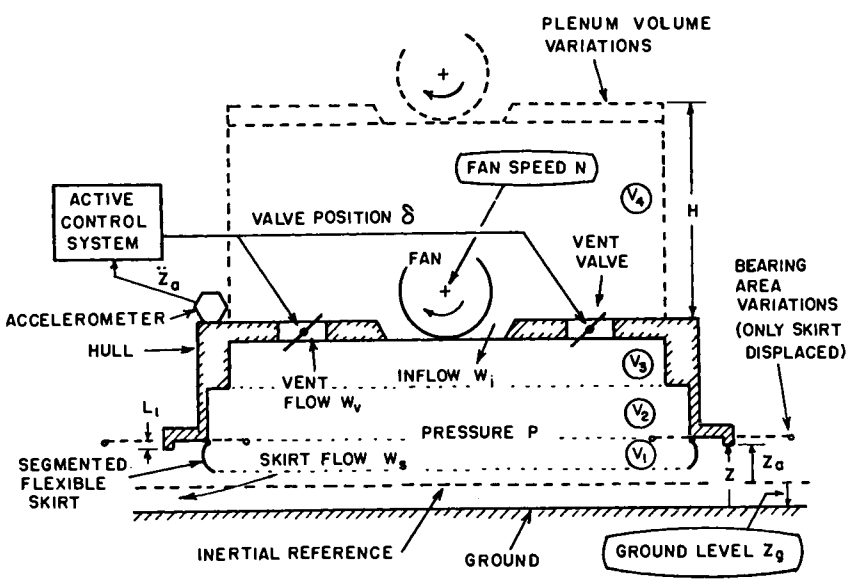

Fig. 14.1 Schematic diagram of conceptual model with active control.

The latter conceptual model was based on Fig. 14.1, which shows some of the main variables and dimensions. The reader is referred to Section 14.8.1 for definitions of symbols. The inertial reference frame is fixed in space to serve as reference for platform (hull) dynamics and the variable ground level. The bearing area is variable by displacing the skirt inwards or outwards whereas the fixed portion of cushion volume can be varied by changing plenum depth. For the active control scheme shown in this figure, symmetrically-located vent valves are controlled in unison by a control system which tries to reduce hull motion in a frequency band including the hovercraft's natural frequencies but excluding operational elevation-control frequencies. Velocity is determined by integration of an accelerometer's output. An active control system, unlike a passive one, requires: 1) measurements of the controlled variables, and 2) auxiliary power for its actuators. A passive control scheme will be described in Section 4.2.3.

Fan speed N is the control variable which determines airflow W_i into cushion volume V, which is variable depending on hull rise height z. An air mass-balance relationship involving inflow W_i, outflow W_o consisting of skirt flow W_s and vent flow W_v, and volume V establishes cushion pressure P, which is equal to the net vehicle weight divided by the footprint area under steady conditions at a constant rise height. Mass variations Δm, externally-applied force F and ground level z_g are possible disturbance variables for test purposes although only the latter was used in this study.

The information flow diagram of Fig. 14.2 gives an overview of the interaction between the air-cushion heave dynamics and the control system. In computer implementations (Section 14.2.5) of the conceptual model, values of cushion parameters such as volume and nominal bearing area can be set. Likewise, control parameter values, fan speed and ground level variations can be established.

The information flow diagram of Fig. 14.3 is a mathematical expression of a conceptual model of the air-cushion heave dynamics. Numerical values of constants, parameters and initial conditions are given in Section 14.8.2. The platform dynamics were derived with the positive-upwards convention and from the viewpoint of an inertial reference observer, by application of Newton's second law of motion:

$$F_T = \frac{d}{dt}(m_v \dot{z}_a) = m_v \ddot{z}_a + \dot{z}_a \dot{m}_v \tag{14.1}$$

where F_T is the total vertical force applied to vehicle mass m_v, including only the suspended portion of skirt mass, m_{vs}. Although this component of skirt mass was determined to be negligible, the $\dot{z}_a \dot{m}_v$ term in eq. (14.1) was retained because the dynamic addition or removal of mass was included as a possible disturbance.

The cushion air mass-balance equation was shown in Chapter 12 to be derived from:

$$W_i - W_o = \frac{d}{dt}(\rho V) = \rho\dot{V} + V\dot{\rho} \tag{14.2}$$

where $W_i - W_o$ is net air inflow, ρ is specific density and V is cushion volume. The derivation was carried out by substituting the ideal gas law

$$\rho = P^a/(RT^a) \tag{14.3}$$

and the relationship

$$\dot{\rho} = \dot{P}/(nRT^a) \tag{14.4}$$

into eq. (14.2). Equation (14.4) was obtained by differentiating the natural logarithm of the polytropic equation of state

$$P^a/\rho^n = \text{constant} \tag{14.5}$$

Assuming an isentropic compression-expansion process within the volume during transients, the value of n was set equal to the ratio of specific heats for air.

The fan and skirt characteristics of Fig. 14.4 include extrapolations of steady-state physical measurements. The extrapolations were required to cope with transients, especially those resulting form downward ground steps.

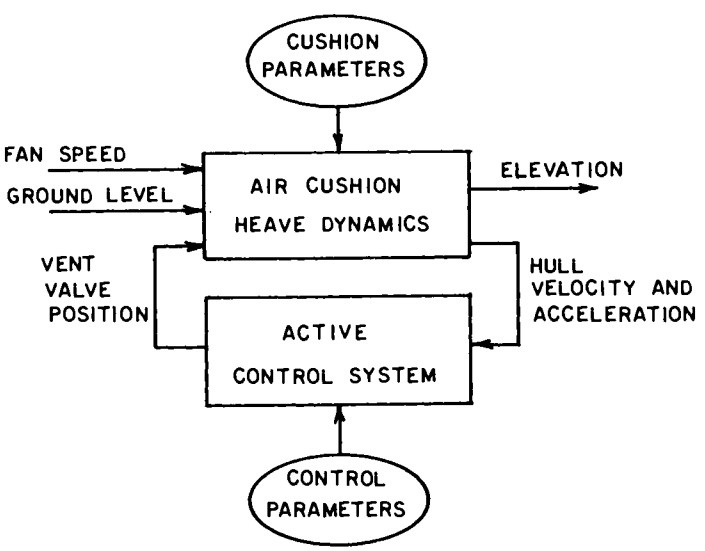

Fig. 14.2 Overview information flow diagram of conceptual model with active control.

Negative cushion pressures can occur during transients, but are usually small. They were limited to small values by letting back-flow under the skirt be proportional to negative pressure, with a constant of proportionality K adjusted by trial and error on the computer model. Duct resistances were included in the fan characteristics, but their dynamic effects were neglected on the assumption of relatively small duct lengths. The effect of unsteady fan aerodynamics was assumed to be negligible, although this may not always hold in practice, as discussed in Chapter 12. The quasi-steady orifice flow law presented there in conjunction with the cushion exit flow was also used in Fig. 14.3 to describe the valve airflow, based on similar reasoning. The skirt contribution to vehicle mass was assumed to be negligible and therefore set to zero.

Under steady operating conditions without an externally-applied force, vehicle weight is counter-balanced by the cushion force which is equal to pressure times the effective bearing area, A. It was found that calculations of the latter based on skirt geometry did not agree closely with experimental

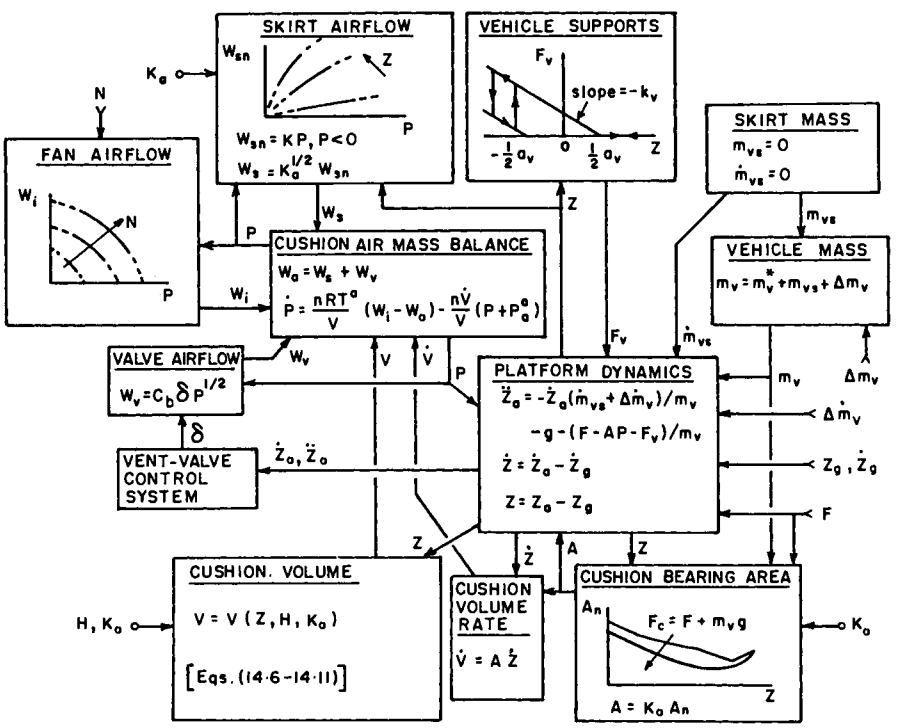

Fig. 14.3 Information flow diagram of air cushion heave dynamics and interaction with an active vent-valve control system.

results, a fact which was attributed to skirt flexibility. Indeed, it was found that the effective area at a given rise height was a function of vehicle weight (hence, mass) as shown in the cushion bearing area curves (Fig. 14.5). These curves were obtained by superimposing the experimental free-hover pressure-flow curves on the skirt characteristic curves (Fig 14.4), reading the pressure and rise height at each intersection, and calculating the effective area as the ratio of weight to pressure. For the constant vehicle-mass tests reported here, the need to interpolate between the bearing area curves was eliminated by choosing nominal vehicle masses corresponding to these curves. For example, with $m_v^* = 1068$ kg, we have $F_c = 1068 \text{ kg} \times 9.807 \text{ m/s}^2 = 10.47$ kN; therefore, the $F_c = 10.5$ kN curve would be used.

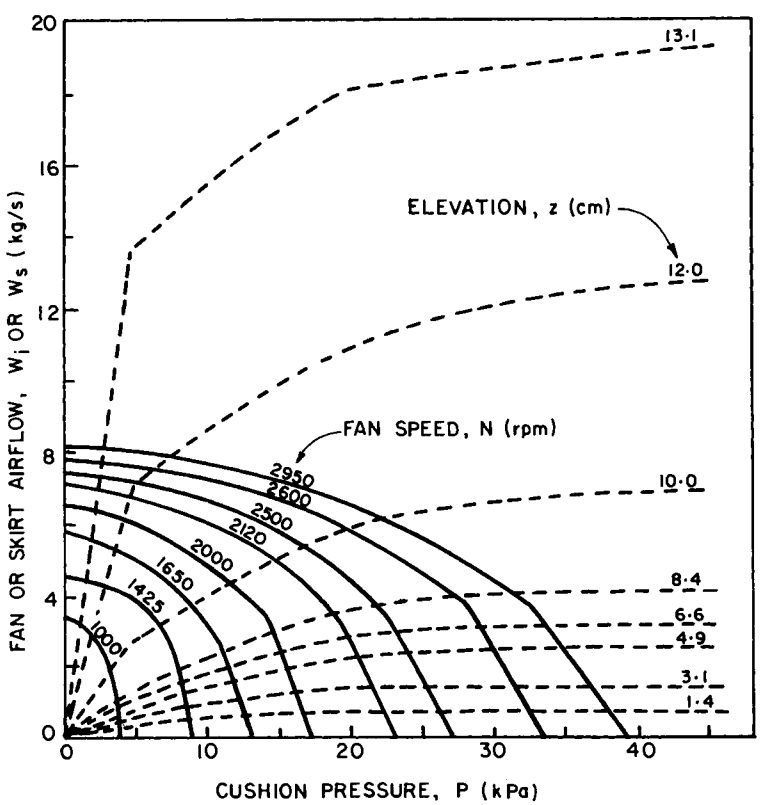

Fig. 14.4 Fan and skirt characteristics.

The cushion volume was a function of rise height z, plenum depth extension H and bearing area factor K_a, as follows:

$$V = V_F + V_1 \tag{14.6}$$

where

$$V_F = C_1 + C_2H_0 + C_3H \tag{14.7}$$

$$V_1 = \begin{cases} V_{1a}, & 0 \le z < z_1 \\ V_{1b}, & z_1 \le z < z_2 \\ V_{1c}, & z_2 \le z \end{cases} \tag{14.8a}$$

$$V_{1a} = B_0z + C_4z^2 \tag{14.8b}$$

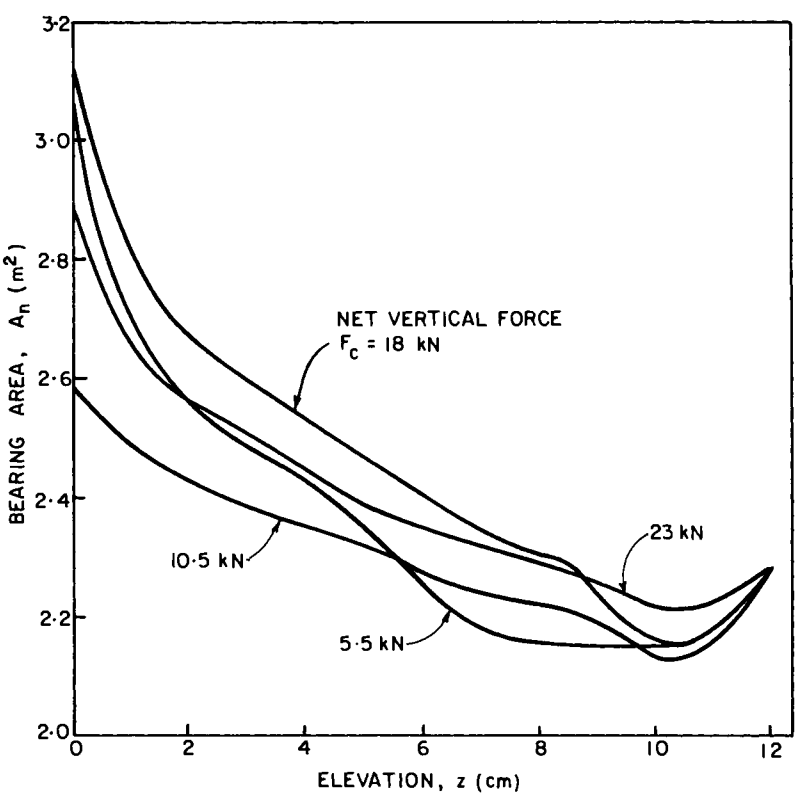

Fig. 14.5 Effective footprint area curves.

$$V_{1b} = C_5 + C_6 z + C_7 z^2 \tag{14.8c}$$

$$V_{1c} = C_8 + B_2 z \tag{14.8d}$$

and

$$C_4 = 0.5\ (B_1 - B_0)/z_1 \tag{14.9a}$$

$$C_5 = 0.5 z_1 (\alpha z_1 + B_0 - B_1) \tag{14.9b}$$

$$C_6 = B_1 - \alpha z_1 \tag{14.9c}$$

$$C_7 = \alpha/2 \tag{14.9d}$$

$$C_8 = C_5 + (C_6 - B_2) z_2 + C_7 z_2^{\ 2} \tag{14.9e}$$

and

$$B_0 = K_a B_{0n} \tag{14.10a}$$

$$B_1 = K_a B_{1n} \tag{14.10b}$$

$$B_2 = K_a B_{2n} \tag{14.10c}$$

$$\alpha = (B_2 - B_1)/(z_2 - z_1) \tag{14.11}$$

A model of vehicle supports was necessary only to permit operation over the full range of rise heights. Thus, modeling accuracy was not essential in this case and the supports were represented simply as a stiff spring with hysteresis losses as shown in the *vehicle supports* module of Fig. 14.3. When the vehicle was sitting on its supports with zero cushion pressure, the rise height was zero, the vertical force of the supports, F_v, was equal to the supported weight, and the support deformation was equal to $a_v/2$. The upper line was followed during compression; the lower, during expansion. The area inside a closed compression-expansion path represents loss of mechanical energy in the form of heat.

Moving the ground up and down in the model of Fig. 14.1 is not a good representation of what happens when the translating vehicle encounters a ground-step up and down since it produces compression and suction pressures which do not normally occur in practice. Thus, for the ground-step up, it was assumed that sufficient air escapes to keep the pressure constant in the process of moving from the lower to the higher ground level and $\dot{P}$ was set equal to zero, accordingly. On the other hand, in the process of stepping down, it was assumed that the plenum is essentially open to atmosphere, i.e., $W_o = W_i$ and $P = 0$. Whenever a ground step was simulated, the subsequent transients were obtained by solving the differential equations with the above initial conditions set appropriately.

This conceptual model of the heave dynamics of an air cushion is neither complete in all details nor meant to be representative of any specific hovercraft. However, it does contain the essential properties of an air cushion system since: a) it is based on an experimental system against which it has been qualitiatively validated (ref. 9), and b) it has been used as a guide in the design of active vent-valve control systems for physical experiments, yielding qualitative validation relative to stabilization performance trends as functions of control system parameters (refs. 5-7). This validation is partly attributed to the tendency of a feedback control system to reduce the overall sensitivity of some parameter variations in the controlled system (ref. 10). In other words, the system is more tolerant of modeling approximations. Thus, whereas the quantitative results are applicable only to the specific conceptual model postulated, they can be used as a qualitative guide for practical application.

14.2.2 Active Feedback

The active control systems consisted of a high-pass filter, a control algorithm, and actuator and valve dynamics, as shown in Fig. 14.6. The first-order high pass filter makes the control system less sensitive to low operating

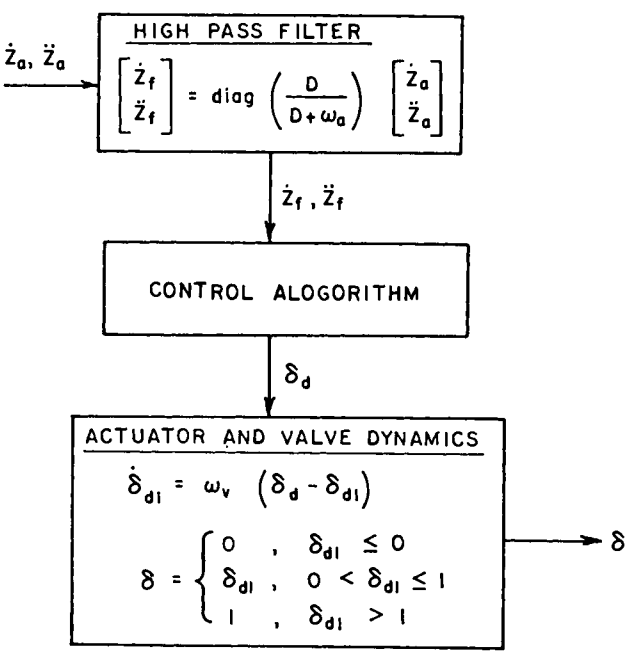

Fig. 14.6 Information flow diagram of active control systems.

frequencies below break frequency ω_a than to high transient frequencies above ω_a. This allows unwanted high frequency components of velocity and acceleration to be attenuated by the control system while permitting normal operation of the vehicle. The control system's performance depends especially on the control algorithm and its parameter values. The response δ of symmetrically-located valves to changes in desired valve position is limited by first-order dynamics and the fully-closed and fully-open scaled positions, i.e., $\delta = 0, 1$.

i) Relay feedback of velocity. The control algorithm was given by:

$$\delta_d = \begin{cases} 0, & \dot{z}_f < \epsilon_o \\ 1, & \dot{z}_f \geq \epsilon_o \end{cases} \tag{14.12}$$

where ϵ_o is an adjustable threshold velocity. In this case, the vent valves move from a closed to fully-open position as rapidly as the actuator and valve dynamics will allow whenever the hull's filtered velocity $\dot{z}_f$ exceeds an adjustable threshold velocity ϵ_o. Physically, when the hull reaches a low point in heave motion and starts to rise again with a positive velocity exceeding ϵ_o, the vent valves are opened to reduce the upward propelling force. When it approaches a high point with its velocity decreasing to less than ϵ_o, the vent valves are closed to establish a cushion pressure which will tend to prevent the falling hull from hitting the ground.

ii) Proportional feedback of velocity and acceleration. With this control algorithm (ref. 11), the desired valve position δ_d is equal to the sum of terms proportional to the filtered velocity $\dot{z}_f$ and acceleration $\ddot{z}_f$ by factors K_v and K_a, respectively; thus:

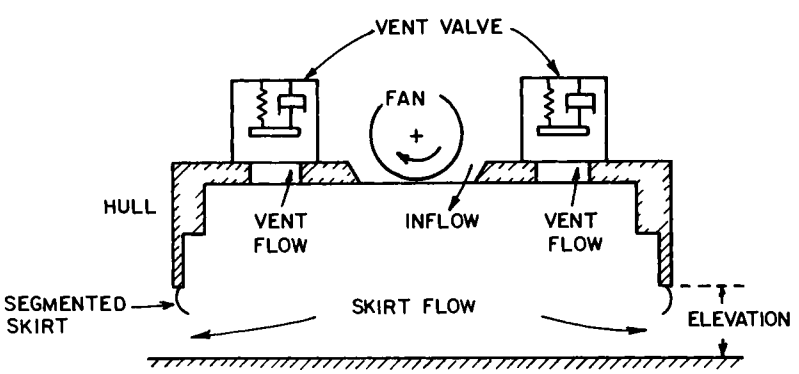

Fig. 14.7 Schematic diagram of an air cushion with passive vent-valve control.

$$\delta_d = K_v \dot{z}_f + K_a \ddot{z}_f \tag{14.13}$$

14.2.3 Passive Feedback

A passive vent-valve control system of the type described schematically in Fig. 14.7 was studied by computer modeling and simulation (ref. 12). Symmetrically-located vent valves were actuated by the cushion pressure and controlled passively by springs and dashpots. The same air-cushion heave dynamics model as employed in the active control studies was used here as a basis for comparison of results. The diagram of Fig. 14.8 gives an overveiw of the interaction between the air cushion, the vent valves, and the computer-model operator. The operator sets the cushion and valve parameters, and determines the fan speed and the occurrence of ground-level disturbances.

The vent-valve model is based on the schematic diagram of Fig. 14.9, which highlights the main parameters without intending to restrict the design to the configuration shown. The parameters are: diameter D_v, mass M, linear spring constant K and damper constant B. The valve displacement δ is constrained by hard limits to move within the range $[o, \delta_L]$. The cushion pressure P is assumed to act over the whole area, $A_V = \pi D_v^2/4$, for all valve positions in this range and a quasi-steady flow representation is used. As shown in the static characteristics of Fig. 14.10, the spring is pre-compressed to keep the valve

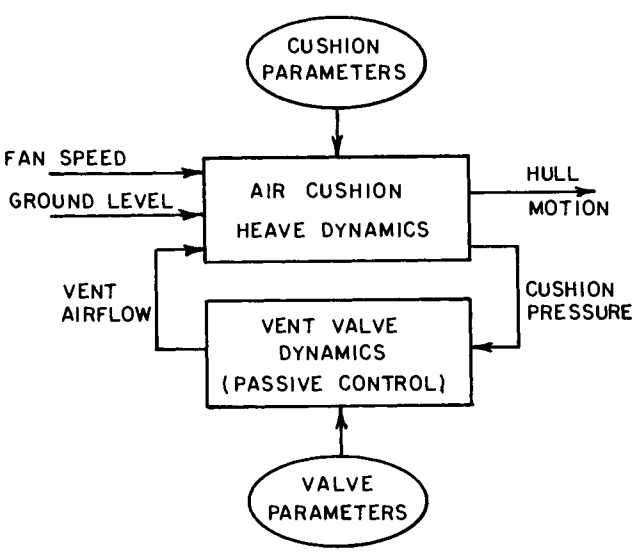

Fig. 14.8 Overview information flow diagram of conceptual model with passive control.

closed for all pressures less than the nominal pressure, $P_n = m_v^* g/A^*$, required to support a nominal vehicle mass m_v^*. Then, the valve displacement is proportional to pressure increases, $P - P_n$, by the factor A_v/K. If the vehilce's mass is increased by an amount Δm_v, the operating position δ_o of the valve is nonzero, i.e., $\delta_o = \Delta m_v g A_v/(A^* K)$.

A single circular valve, equivalent to any number of symmetrically-located valves, was asssumed for modeling purposes. The conceptual model of the valve is contained in the information flow diagram of Fig. 14.11. The valve dynamics are expressed in terms of variations (P_1, δ_1) about the operating point (P_o, δ_o) using canonical parameters: damping ratio ζ, natural undamped frequency ω_v and gain G. The fully-open constraint position δ_L is expressed as a factor α multiplied by a quarter of the valve diameter, $\delta_3 = D_v/4$. Thus, if α is unity, the maximum valve opening is equal to one-quarter of the valve diameter.

14.2.4 Computer Implementation

Two conceptual models, one with relay feedback of velocity and the other with proportional feedback of velocity (i.e., acceleration feedback equal to zero) were implemented on a hybrid computer consisting of a minicomputer, two analog consoles and a linkage console for high speed data communication between the analog and digital computers. Analog strip-chart recordings of variables as functions of time were the main form of output. However, specified print-outs were also available by operating a sense switch on the digital console.

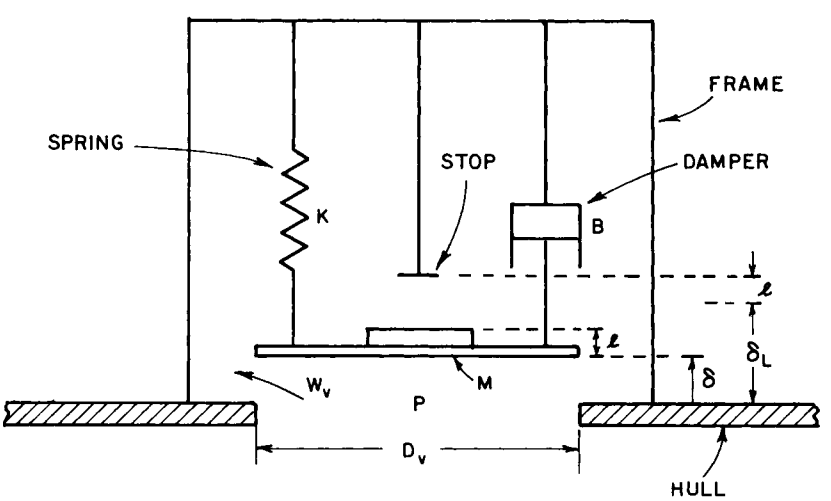

Fig. 14.9 Schematic diagram of vent-valve for passive control.

The computerized model was operated at one-twentieth of real time (ref. 13) for computational stability. It turned out that this was a good time scale factor from a human interaction point of view; therefore, no steps were taken to speed-up the solution.

Parameter values could be changed by operating a sense switch and typing-in new values. Engine speed was controllable continuously by knob from its minimum to maximum value, making it possible to *operate* the model as one would the physical hovercraft. Fan speed, applied force, incremental mass and ground-level step tests were available to the operator by pressing pushbuttons.

The other models were implemented in the Advanced Continuous Simulation Language (ACSL, ref. 14) on a minicomputer with a virtual memory operating system which supports multitasking. In these cases, all parameter values, and test conditions such as fan speed and ground disturbances, had to be established prior to each simulation run. A parameter optimization program called PAROPT (ref. 14), written in FORTRAN, was used in conjunction with the ACSL implementation of the proportional feedback of velocity and acceleration model. The method, described in ref. 15, was used to determine optimum values of control gains K_v and K_a to minimize various performance criteria defined in Section 14.4.

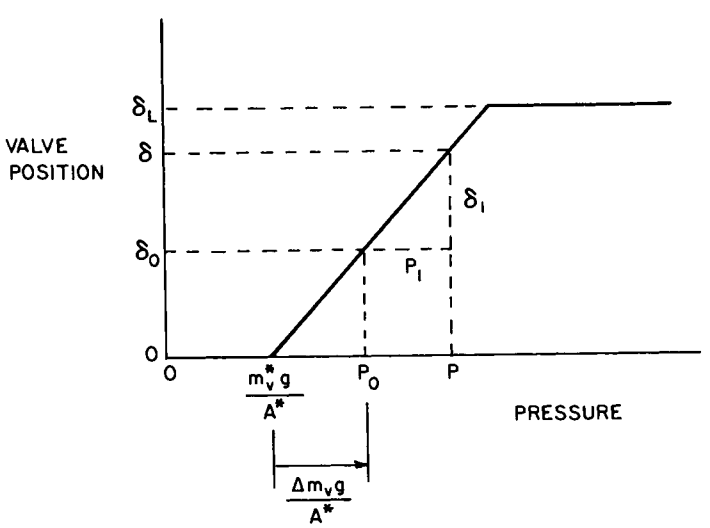

Fig. 14.10 Static characteristic of vent-valve for passive control.

14.3 PHYSICAL MODELS

Some of the vent-valve control schemes studied by computer modeling and simulation were later tested by physical experimentation. However, no attempt was made to reproduce exactly the air-cushion heave dynamics and feedback models used computationally. The computational results were employed only as a qualitative guide in the design of physical experiments. Conversely, a qualitative agreement between experimental and computer simulation results would provide a measure of validation of the computer models.

14.3.1 Air Cushion System

An actual hovercraft consists of a hull, on which is mounted a blower to provide air for lift, and propulsion machinery, cabin, etc. This hull is supported by the air cushion retained beneath it by a flexible *skirt* and the ground, and which is continually replenished with air by the blower. However, such an arrangement in a model for heave experiments poses difficulties, since the instrumentation, blower, etc., would be too heavy to mount on the model, which needs to be tested over a range of weights. If these components are

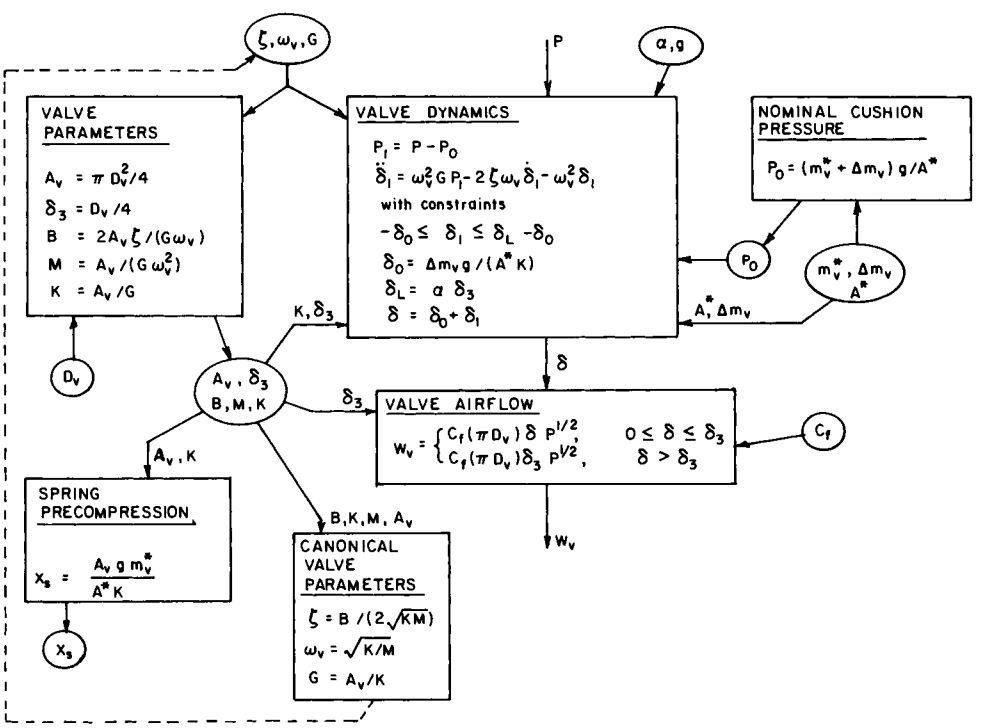

Fig. 14.11 Information flow diagram of vent-valve for passive control.

mounted on the ground and connected to the model by flexible lines, the mass and flexibility of these lines impose a very indeterminate restraint on the heave motion of the model.

It was therefore decided to invert and anchor the model hovercraft, whose air and instrument lines could then be made rigid, while the *ground* would be represented by a board supported above the model by the inverted air cushion. The 'ground' would then oscillate freely in heave, and weights placed on it would simulate the vehicle weight by controlling the cushion pressure. The assumption inherent in this inversion is that the gravitational forces on the inverted skirt are negligible compared to the aerodynamic forces on it. Since the skirt was made of 0.05 mm plastic sheet, this was considered justifiable.

The experiment was designed to (1) contain the essential components of a hovercraft, i.e., blower, plenum and flexible skirt, (2) exhibit underdamped stable, conditionally unstable and unconditionally unstable regimes of operation, and (3) demonstrate the feasibility of improving stability by means of automatic vent-valve control. Although the numerical results would not necessarily be applicable to any specific hovercraft, a strong demonstration of stabilization by active control might provide sufficient justification for the undertaking of a practical engineering design study.

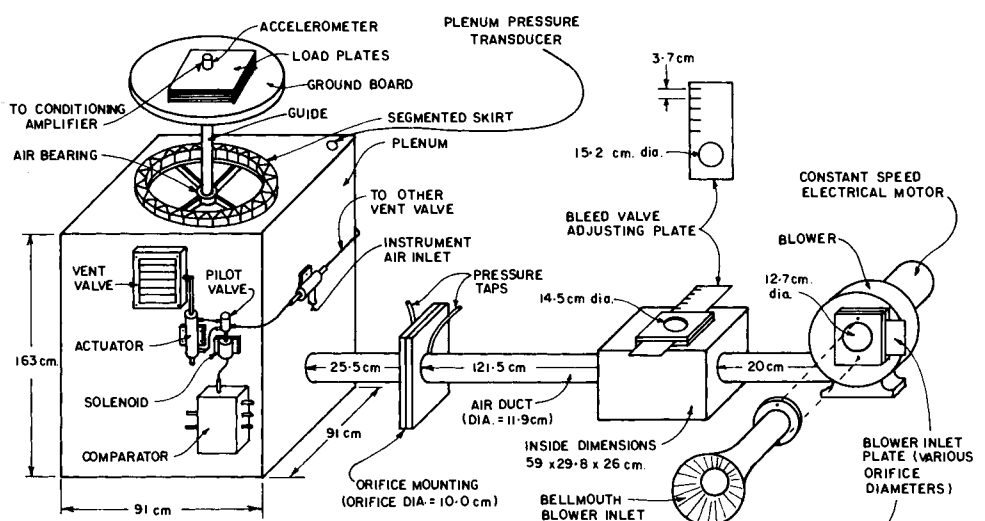

PLATE NUMBER	1	2	3	4	5	6	7
ORIFICE DIA. (cm.)	10·16	9·53	8·89	8·26	7·62	7·00	6·35

Fig. 14.12 Physical layout of air cushion system with relay velocity-feedback.

In the light of these considerations, a test rig was built as shown in the diagram of Fig. 14.12. The power unit was a centrifugal blower driven by a 1.1 kW electric motor. Since this was a constant speed machine, the airflow to the rig was controlled by throttling the blower inlet and opening or closing the bleed valve which was sited immediately downstream of the blower.

Since it was essential to measure the airflow entering the cushion, a long straight pipe was placed between the bleed valve and plenum, with a standard sharp-edged metering orifice in it. A pressure transducer enabled the pressure differential across this orifice to be used to calculate the lift airflow.

Although the presence of a relatively long duct compared with many hovercraft applications was known to be destabilizing (ref. 1), it was accepted as an experimental constraint which would tend to produce conservative estimates of the stabilizing ability of automatic vent-valve control. The air from the duct was discharged into the large plenum box which represented the hull of the inverted hovercraft. On the top of this box was the model skirt, and above this, supported on the cushion of air, was the *ground-board*. It was essential that this ground-board should be completely free to oscillate in heave, and at the same time not allowed to roll, pitch, or move sideways. It was therefore fitted with a vertical shaft on its centre, extending downward through an air bearing. This arrangement was essentially frictionless, and possessed no inertia other than that due to the mass of the board and rod. The cushion pressure could be varied by placing steel-sheet weights on the ground-board, whose total mass could thus be varied from 3.93 kg to 15.90 kg.

The skirt used a simple, segment-only HDL type, with a circular footprint of 42 cm diameter, a height from ground to upper hinge-point of 9 cm, and having 60 segments each of 1.6 cm width. It was made of extremely flexible 0.05 mm thick transparent polyethylene sheet.

Initially, it was not known how small the vent valves could be for satisfactory control system performance. Therefore, for the first experiments on relay feedback of velocity, a pair of conservatively-sized *venetian-blind* type of vent valves was constructed. Each one was operated by an air-jack actuator and consisted of five vanes, 20.5 cm long, pivoted on their centrelines and moved by cams connected to a common bar moved by the air jack. The full aperture when open was 20.5 × 25.5 cm, obstructed only by the five edge-on vanes, each of 8 mm thickness. During the early experiments this opening was masked by progressively smaller orifices, until an 8.9 cm diameter orifice was selected. Furthermore, it was found that a single vent valve was sufficient.

An improved venetian-blind type of vent valve was constructed for the second set of experiments on proportional feedback of acceleration. It was smaller, with less inertia and leakage, than its predecessors. This valve was operated by a linear electromechanical stepper actuator through a lever linkage

providing displacement amplification. It consisted of three vanes, 10.16 cm (4.0 in) long, pivoted on their centrelines and moved by radius arms connected to a common bar moved by the lever. The full aperture when open was 10.61 × 9.84 cm (4.0 × 3.87 in), obstructed only by the three edge-on vanes, each of 5.1 mm (0.2 in) thickness. During the experiments, this opening was masked immediately upstream by a circular orifice of selectable size; the sizes used were 2.54 cm (1.0 in), 3.18 cm (1.25 in) and 3.81 cm (1.5 in). Whereas the skirt diameter was only 42 cm (16.5 in), an analysis of orifice size requirements for larger skirts is given in Section 14.3.5.

14.3.2 Relay Velocity–Feedback System

The heave oscillation of the system was sensed by an accelerometer mounted on the ground-board. The signal from the accelerometer was filtered to remove unwanted high frequency trembling, and integrated to indicate inverted (i.e. negative of) velocity. When this inverted velocity exceeded a preset threshold level, the vent valve was actuated to reduce the oscillation. This was achieved by the circuit shown in detail in Fig. 14.13. After the accelerometer output passed through the band-pass filter to eliminate high-frequency noise it was integrated to give an inverted velocity signal which was amplified. This

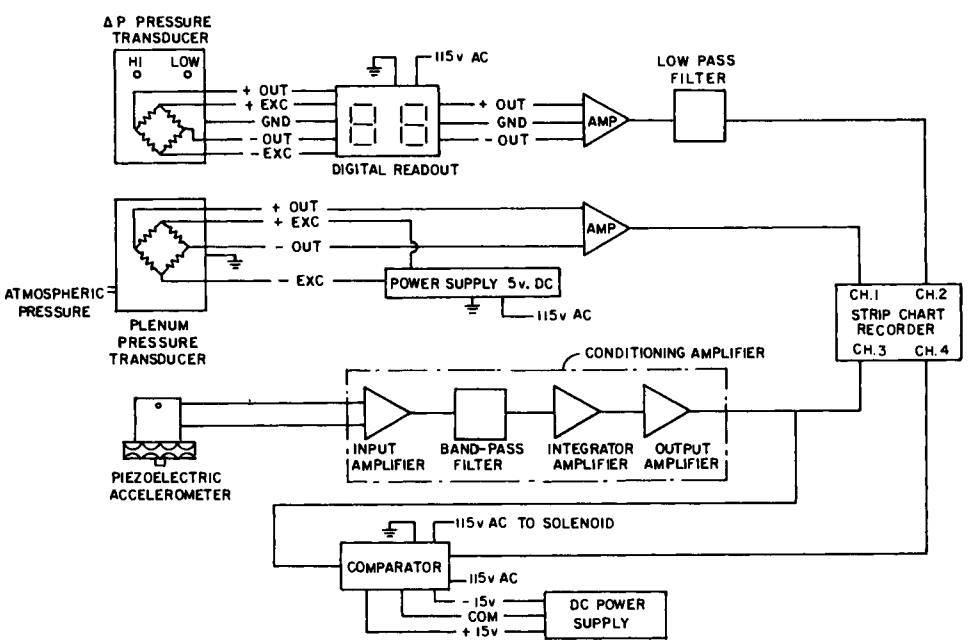

Fig. 14.13 Instrumentation for relay velocity-feedback experiments.

signal was applied to a comparator whose threshold value could be set over the full range of velocities [-1.5, 1.5] m/s. When the input signal exceeded the set threshold value, normally about +0.3 m/s, the solenoid valve was energized. This opened the heave-control vent valve. A similar chain of events closed the vent valve when the velocity fell below the threshold value again.

The threshold value, as noted above, was set at +0.3 m/s, where the positive sign indicates downward direction of the ground-board (or of the craft in the real-life case) since inverted velocity was connected to the comparator. However, assuming a vent-valve actuation delay of approximately 0.18 s, that is one half-period of a 2.78 Hz ground-board oscillation frequency, the above comparator action effectively synchronized actual valve motion with non-inverted

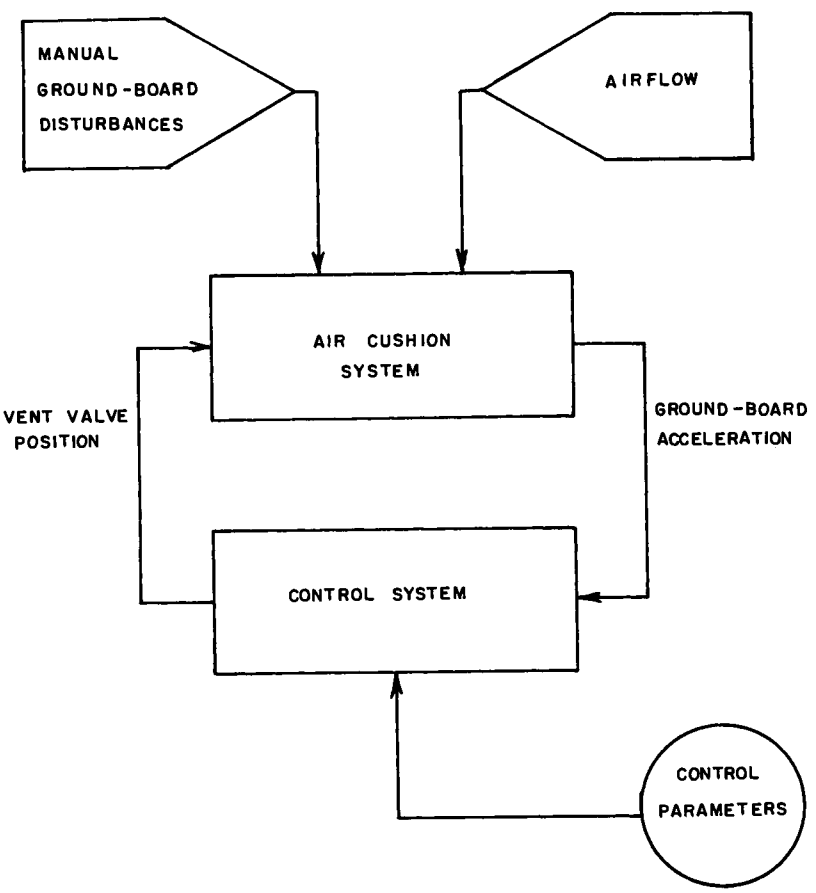

Fig. 14.14 Overview information flow diagram of physical model with proportional acceleration-feedback.

velocity. Therefore, after the craft had reached the lowest point in the heave cycle and was starting to move again, the vent valve opened to reduce the lifting force, thus allowing gravity to reduce the oscillation. The vent was not opened during the downward part of the oscillation, because at that time a high cushion pressure was needed to arrest the falling craft, and stop the heave.

14.3.3 Proportional Acceleration–Feedback System

The overview diagram of Fig. 14.14 shows that the cushion system acted on ground-board acceleration measurements to control vent-valve position. The dynamic behaviour of the air cushion could be influenced by varying the airflow into the plenum or disturbing the ground-board manually. On the other hand, the cushion system performance was subject to certain control-parameter settings.

An information flow diagram of the control system is shown in Fig. 14.15. The ground-board acceleration $\ddot{z}$ was transformed to a voltage $V_{\ddot{z}}$ by anaccelerometer and charge amplifier. The proportionality factor between these two

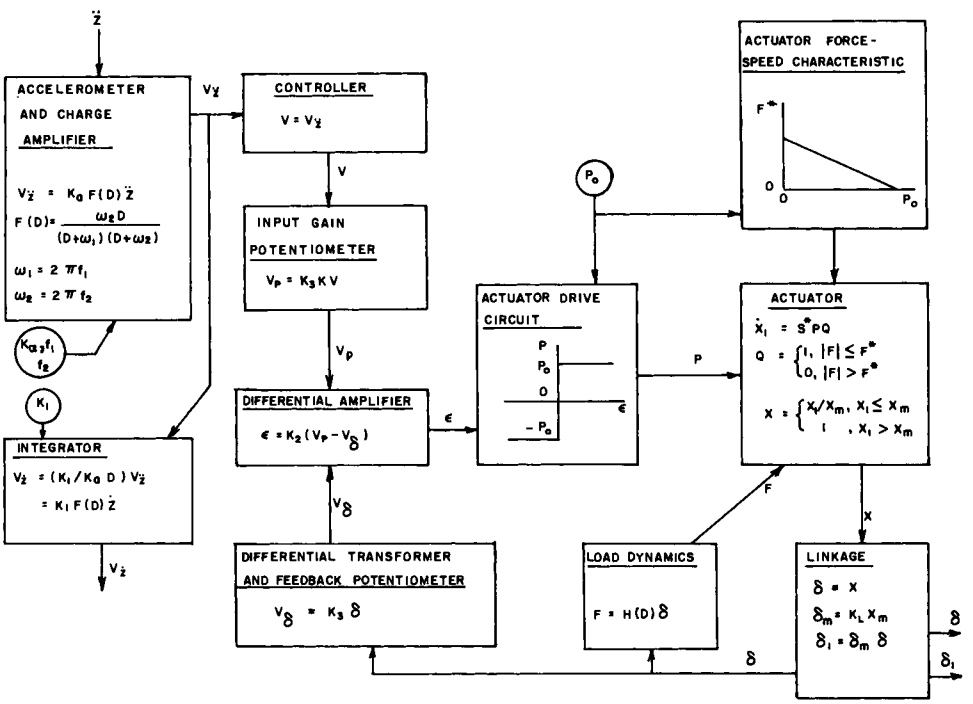

Fig. 14.15 Information flow diagram of physical system for proportional acceleration-feedback.

variables was K_a (0.1 V/m/s^2) in the pass-band of filter F(D), whose lower and upper frequencies respectively were f_1 (1.0 Hz) and f_2 (100 Hz), and where D is the time derivative operator d/dt. Thus, normal operating frequencies below f_1 and noise above f_2 were not acted upon by the control system. The acceleration voltage $V_{\ddot{z}}$ was integrated for purposes of monitoring the ground-board velocity $\dot{z}$, resulting in a velocity voltage $V_{\dot{z}}$ proportional to $\dot{z}$ by a factor K_1 (1.75 V/m/s).

The controller, in general, could have been a function of ground-board position, velocity and acceleration. However, only the acceleration voltage was used, and then attenuated to voltage V_p by an input potentiomenter factor K_3K, where K (0.57 to 6.86) was the input control gain. The factor K_3 (0.155 V/deg, nominally), a proportionality constant relating the normalized angular vent-valve position δ to a corresponding voltage V_δ, was determined by a differential transformer type of position transducer connected in series with a feedback potentiometer. Since the maximum angular vent-valve displacement for normalization was δ_m (= 50°), the angular vent-valve position δ_1 was given by the product of δ and δ_m. A differential amplifier determined the control error (V_p-V_δ) and amplified it by a gain K_2(= 10) to produce an analog voltage ϵ, which was converted to a pulse waveform of frequency P by an actuator drive circuit.

A fast actuator response was ensured by: (a) selecting, from its force-speed characteristic and experimentally, the largest pulse frequency P_0 (= 250 Hz) at which its force F* (= 11.3 N; 40 oz) would not be exceeded by the dynamic load force F, and (b) letting the actuator be driven at the linear speed $\dot{x}$ = S*P_0 (= 0.65 cm/s; 0.25 in/s), in a direction to open the valve when ϵ was positive, or to close it at x_1 = -S*P_0 when ϵ was negative, where S* (= 0.0254 mm; 0.001 in) was the actuator step-displacement per pulse. The normalized actuator displacement x was obtained by dividing x_1 by the displacement x_m (= 0.425 mm; 0.108 in), which was proportional to δ_m by the linkage factor K_L (= 182.6 deg/cm; 463.8 deg/in). The mechanical and aerodynamic load force F acting on the motor was related to δ by an undetermined transfer function H(D).

Frequency response tests indicated that there was a phase shift of approximately 90° through the control system. Therefore, since ground-board velocity oscillations lagged acceleration by approximately 90°, the action of the control system was to open the vent valve when the platform velocity was positive.

14.3.4 Data Acquisition and Reduction

The instrumentation scheme for the relay velocity-feedback experiment (Fig. 14.13) consisted of four channels, whose outputs were displayed by a

strip-chart recorder. One of the four channels, from the accelerometer mounted on the oscillating ground-board, also acted as the controller of the vent valve.

Channel 1 on the recorder was fed by signals from the plenum pressure transducer. This sensor was mounted inside the plenum in one of the top corners, where it would be close to the skirt but shielded from the dynamic effects of air movement.

Channel 2 was connected to a transducer measuring the pressure difference across a standard sharp-edged orifice in the straight pipe from blower to plenum. The signal from this sensor therefore gave an indication of the air-flow to the cushion. Its output was also displayed in digital form, to assist the operator in setting up required running conditions.

Channel 3 was connected to the output of the accelerometer on the ground-board, as already described. This enabled the inverted heave velocity of the ground-board to be recorded.

Channel 4 received a signal from the comparator in the same circuit, so that when the comparator found that the inverted velocity singal overpowered the preset threshold value and consequently triggered the solenoid valve, this event was recorded. This channel could therefore be regarded as showing the point at which the vent-valve actuation was triggered. The actual opening and closing of the valve occurred after an assumed delay described above.

Since all channels of data were recorded on the same chart, it was possible to relate the phasing of the heave motion itself, airflow, plenum pressure and vent-valve operation. By running the rig without the control operating, either with self-excited heave or by perturbing it by hand, the uncontrolled oscillation could be recorded. If the controlling circuit was then energized, the effectiveness could be assessed, and the number, extent, and phase of the vent valve operation could be measured.

Subsequently, for the proportional acceleration-feedback experiments, a simultaneous record of acceleration was implemented, a rotary potentiometer was connected to the ground-board via a light swinging arm, to give a direct record of board position instead of having to deduce this from the velocity trace, and a differential transformer type of position transducer was installed to measure vent-valve opening. Thus, the six-channel strip-chart recorder was used to record simultaneously ground-board acceleration, velocity and position, vent valve opening, plenum pressure and net airflow as functions of time.

Ground-board acceleration was recorded also on magnetic tape for subsequent data reduction by analog computation to: (a) determine the root mean square (rms) acceleration as a function of control gain and vent-valve orifice size, and (b) compare the performance with the International Standard Organization's (ISO) ride quality standards (ref. 16).

14.3.5 Vent Valve Dimensional Analysis

The purpose of this analysis is to obtain an approximate relationship for the required vent orifice diameter as a function of the skirt's peripheral length. This may be used to extrapolate the results of model-scale experiments as an aid in the design of practical hovercraft.

Consider two air cushion systems: (i) cushion 1 with a skirt of perpheral length L_{s1}, hovering at an airgap h_1, and a vent-valve orifice of diameter D_{v1}, and (ii) cushion 2 with a skirt of peripheral length L_{s2}, hovering at an airgap h_2, and a vent-valve orifice diameter D_{v2}. Furthermore, let P_1, Q_{s1} and Q_{v1}, respectively be the cushion pressure, skirt airflow and vent airflow of cushion 1, with P_2, Q_{s2} and Q_{v2} as the corresponding variables for cushion 2. Then, modeling the air escape past a skirt or vent-valve orifice as a quasi-steady orifice flow (ref. 17), the airflows out of cushion 1 are:

$$Q_{s1} = C_{s1}L_{s1}h_1(2P_1/\rho)^{\frac{1}{2}} \tag{14.14}$$

and

$$Q_{v1} = C_{v1}(\pi D_{v1}^2/4)(2P_1/\rho)^{\frac{1}{2}} \tag{14.15}$$

where C_{s1} and C_{v1} respectively are skirt and valve coefficients, and ρ is atmospheric density. It follows that the valve-to-skirt airflow ratio is:

$$R_1 = \frac{Q_{v1}}{Q_{s1}} = \frac{C_{s1}L_{s1}h_1}{C_{v1}(\pi D_{v1}^2/4)} \tag{14.16}$$

Similarly, for cushion 2:

$$R_2 = \frac{Q_{v2}}{Q_{s2}} = \frac{C_{s2}L_{s2}h_2}{C_{v2}(\pi D_{v2}^2/4)} \tag{14.17}$$

Assuming geometric similarity between the two air cushion systems, we have:

$$C_{s1} = C_{s2} \tag{14.18}$$

$$C_{v1} = C_{v2} \tag{14.19}$$

and

$$h_1/h_2 = L_{s1}/L_{s2} \tag{14.20}$$

Since the cushion air-mass balance equation for the rate of change of pressure P, neglecting distributed capacitance effects, involves the difference between net airflow into and out of the cushion, it is postulated that the valve-to-skirt airflow ratios should be approximately equal if the control system is to be equally effective with both cushions. Therefore, let the constraint

$$R_1 = R_2 \tag{14.21}$$

be applied.

Substituting eqs. (14.16) and (14.17) into eq. (14.21), and applying eqs. (14.18) to (14.20), yields

$$D_{v2} = D_{v1}(L_{s2}/L_{s1}) \tag{14.22}$$

or, for the special case of circular skirts,

$$D_{v2} = D_{v1}(D_{s2}/D_{s1}) \tag{14.23}$$

where D_{s1} and D_{s2} are the skirt diameters of cushions 1 and 2, respectively. For example, if the diameter of the circular skirt doubled, then the vent orifice needs to be doubled. However, until such time as practical data become available for their validation, these equations must be considered tentative and should be used with caution.

As an example of the use of eq. (14.23), suppose it would be required to determine the vent-orifice size needed to stabliize a cushion having a circular skirt 4.88 m (16 ft) in diameter. Given that, in the experiment, a 2.54 cm (1.0 in) diameter orifice was sufficient to stablize a cushion having a 42 cm (1.38 ft) diameter skirt, let the experimental system be cushion 1 and the proposed system, cushion 2. Then, solving Equation (10) with D_{v1} = 2.54 cm, D_{s1} = 42 cm and D_{s2} = 488 cm yields D_{v2} = 29.5 cm (11.62 in).

14.4 PERFORMANCE CRITERIA

The computational and experimental studies reported in this chapter were performed with the aid of various definitions of performance criteria, characterized as either *performance indices* or *optimization criteria*. The performance indices provided a quantitative measure of a system's response to given disturbances. The optimization criteria determined those parameters which were to be optimized for the minimization of specific performance indices. Although several performance criteria are defined below, and all were eventually used, only a few were selected as appropriate for any given study.

14.4.1 Performance Indices

i) Transient response indices. Seven indices were defined to characterize the transient heave response of a fast-moving vehicle traveling over a downward step in ground level. The speed was assumed to be large enough to render any step-induced pitch motion negligible insofar as its effect on heave motion is concerned. The first index consisted in counting the number of peaks (i.e., positive and negative-going extrema) N_p after which the hull's velocity response remained within ±10% of the magnitude of its first peak (Fig. 14.16). The second was response time T_s at which the hull's elevation returned to and

remained within a region defined by its nominal position ±10% of the disturbance's magnitude (Fig. 14.17). The first criterion was a measure of damping; the second, a measure of the tendency of the skirt to drag and wear during operation over large-scale ground irregularities.

All step response tests were performed with ground steps of the form:

$$z_g/z_{gm} = -b\ u(t) \tag{14.24}$$

where z_g is ground level, z_{gm} is a scale factor equal to the fully-extended skirt length as measured from vehicle supports, u(t) is the unit step function occurring at time t = 0, b is the absolute value of the scaled step magnitude, and the negative sign denotes the downward direction. Numerical values of constants such as z_{gm} are given in Section 14.8.2.

The rms value of a variable is popular in steady-state analysis, but can be used for transient analysis also. The rms acceleration is given by:

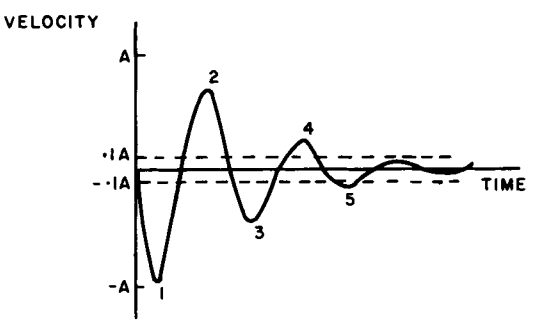

Fig. 14.16 Illustration of the number of peaks performance index, N_p.

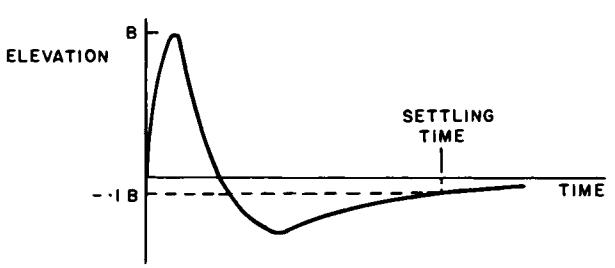

Fig. 14.17 Illustration of the settling time performance index, T_s.

$$E_a = [\frac{1}{\tau}\int_o^\tau \ddot{z}_a^2 dt]^{1/2} \tag{14.25}$$

where the time interval τ must be specified to suit the application.

The ride quality of a hovercraft is a function of the stiffness of its air cushion. The stiffer the cushion, the rougher the ride because of relatively large accelerations transmitted to the passengers or cargo when traveling over rough surfaces. On the other hand, skirt drag and wear due to surface contact are inverse functions of the cushion stiffness. Thus, good ride quality and low skirt drag and wear are conflicting requirements in hovercraft desgin. This conflict and its resolution were examined by means of acceleration and elevation indices respectively defined by:

$$\epsilon_a = [\frac{1}{T}\int_o^T (W\ddot{z}_a)^2 dt]^{1/2} \tag{14.26}$$

and

$$\epsilon_p = [\frac{1}{T}\int_o^T (WE)^2 dt]^{1/2} \tag{14.27}$$

where

$$W = 1 - e^{-4t/T} \tag{14.28}$$

is an exponential weighting function, and

$$E = \begin{cases} z - z_o, & z - z_o < 0 \\ 0 \quad , & z - z_o > 0 \end{cases} \tag{14.29}$$

is a measure of elevation variations in the direction of skirt contact; z_o is the nominal operating elevation. The weighting factor W reduced the large initial variation contributions which otherwise tended to dominate the results. The integration interval was set at T = 3.48 s, equivalent to 8.4 cycles of the uncontrolled cushion's limit cycle frequency f_c = 2.4 Hz. In most cases, a steady-state was either completely or approximately achieved within this interval.

A combined acceleration and elevation index was defined as:

$$\eta = \epsilon_a + C_p\epsilon_p \tag{14.30}$$

where the value of constant C_p determines the weight given to the latter relative to the former. The occurrence of solid contact between the vehicle and ground was expressed by:

$$C_s = \begin{cases} 0, & z(t) > 0 \\ 1, & z(t) \le 0 \end{cases} \quad ; t \in [0,T] \tag{14.31}$$

Thus, the seven transient response indices were: number of velocity peaks N_p, settling time T_s, rms acceleration E_a, modified rms acceleration ϵ_a and position ϵ_p, modified rms acceleration and position combination η, and solid contact occurence C_s. In addition the number of valve opening events following a ground step was given by index N_v.

ii) Steady-state indices. An unstable cushion is characterized by a limit cycle whose amplitude depends on the degree of instability. The residual motion due to noise in a marginally stable system is characterized by a trembling motion which is not necessarily cyclical. In either case, the rms acceleration E_a is useful as a measure of the motion and associated ride quality. This index is involved in the ISO ride quality standards. Other performance indices pertinent to this study are: (a) the limit cycle velocity amplitude without control, L_u, b) the relative limit cycle velocity amplitude,

$$L_{CR} = L_c/L_u, \tag{14.32}$$

where L_c is the limit cycle velocity amplitude with control, and c) the number of velocity cycles per valve opening, $N_{c/v}$, indicating the degree of valve activity required for control.

iii) Control-switching response indices. Index N_{CT} was a measure of the time taken by an unstable cushion to settle to a smaller limit cycle after the control system was switched on. It was given by the number of velocity cycles associated with the transition from uncontrolled to controlled steady-state limit cycles. The number of valve opening events occurring during the same interval gave the value of index N_{VT}.

14.4.2 Parameter Optimization Criteria

In the case of proportional velocity and acceleration feedback, there were two control parameters, K_a and K_v. Given that the performance indices ϵ_a and ϵ_p were functions of these parameters, the following criteria were defined for optimization purposes:

a) $$K^*_{ar} = \{K_a | \epsilon_a = \min \epsilon_a,\ K_v = 0,\ K_a \geq 0\} \tag{14.33}$$

Thus, K^*_{ar} is the value of K_a which minimizes ϵ_a with constraints $K_v = 0$ and $K_a \geq 0$. This is a ride quality optimization criterion since it minimizes the acceleration index.

b) $$K^*_{vr} = \{K_v | \epsilon_a = \min \epsilon_a,\ K_v \geq 0,\ K_a = 0\} \tag{14.34}$$

c) $$K^*_{ac} = \{K_a | \epsilon_p = \min \epsilon_p,\ K_v = 0,\ K_a \geq 0\} \tag{14.35}$$

This is a skirt contact minimization criterion since it minimizes the elevation index.

d) $K^*_{vc} = \{K_v | \epsilon_p = \min \epsilon_p,\ K_v \geq 0,\ K_a = 0\}$ (14.36)

e) $K^*_r = \{K_v, K_a | \epsilon_a = \min \epsilon_a,\ K_v \geq 0,\ K_a \geq 0\}$ (14.37)

f) $K^*_c = \{K_v, K_a | \epsilon_p = \min \epsilon_p,\ K_v \geq 0,\ K_a \geq 0\}$ (14.38)

g) $K^* = \{K_v, K_a | \eta = \min \eta,\ C_p > 0,\ K_v \geq 0,\ K_a \geq 0\}$ (14.39)

This is a combined acceleration and skirt contact minimization criterion.

By means of these criteria, it was therefore possible to optimize for ride quality or low skirt wear, or a combination thereof. Furthermore, the optimization could be carried out with respect to either one, or both, of the control parameters.

14.5 RELAY CONTROL PERFORMANCE

14.5.1 Computational Results

Computational results pertaining to the relay velocity-feedback model of Section 14.2.2 are presented here. Some comparisons with computer simulation results on proportional velocity-feedback are made. The results are discussed under three headings: i) limit cycle, ii) underdamped stable system, and iii) conditionally unstable system.

i) Limit cycle. Trajectories A, B and C in the phase plane (Z', $\dot{Z}$) of Fig. 14.18 were obtained by operating the system at a steady elevation Z_o = 12 cm and applying downward ground steps of 1 cm, 2 cm and 9.5 cm, respectively. Only a finite time portion of the trajectories are shown to avoid cluttering the figure unnecessarily. A complete presentation would show trajectory A eventually converging to (0,0) with increasing time, B diverging to the stable limit cycle (SLC), and C converging to the SLC. Somewhere between trajectories A and B, there exists an unstable limit cycle (ULC), which defines the stable region of the system in the phase plane. Thus, if a trajectory were to begin on the ULC, it could not remain on it. Depending on disturbances, however small, the trajectory would depart from the ULC and either converge to (0,0) with time or diverge to the SLC.

Fan speed is a dominant factor determining the existence and size of limit cycles. The stable region tends to diminish and the size of the SLC tends to increase with increase in fan speed. When the stable region is negligibly small, the system is *unconditionally unstable*. Conversely, when it encompasses the entire practical region of the phase plane, the system is *stable*. Between these two extremes, it is *conditionally unstable*. Within a stable region, the system may be *underdamped* or *well-damped* depending respectively on whether the number of encirclements of the origin is large or small.

ii) Underdamped stable system. Figure 14.19 presents velocity attenuation and valve activity as functions of threshold velocity for a downward step in ground level applied to a nominally underdamped stable system and Fig. 14.20 gives time response examples. It is seen in both that the number of velocity peaks (extrema) to ±10% of the magnitude of the first peak following a ground step disturbance without control is $N_p = 29$ whereas it is $N_p = 3$ with $\epsilon_o = 0.075$ m/s (i.e., $\epsilon_{SR} = \epsilon_o/E_V = 8.3$ %, where $E_V = 0.9$ m/s is the amplitude of the first positive velocity peak without control) and that the number of valve openings in the latter case is $N_V = 4$. The valve does not always reach its fully-open position due to its dynamical limitations. For relative threshold velocities ϵ_{SR} less than 8.3%, the number of valve openings increases rapidly

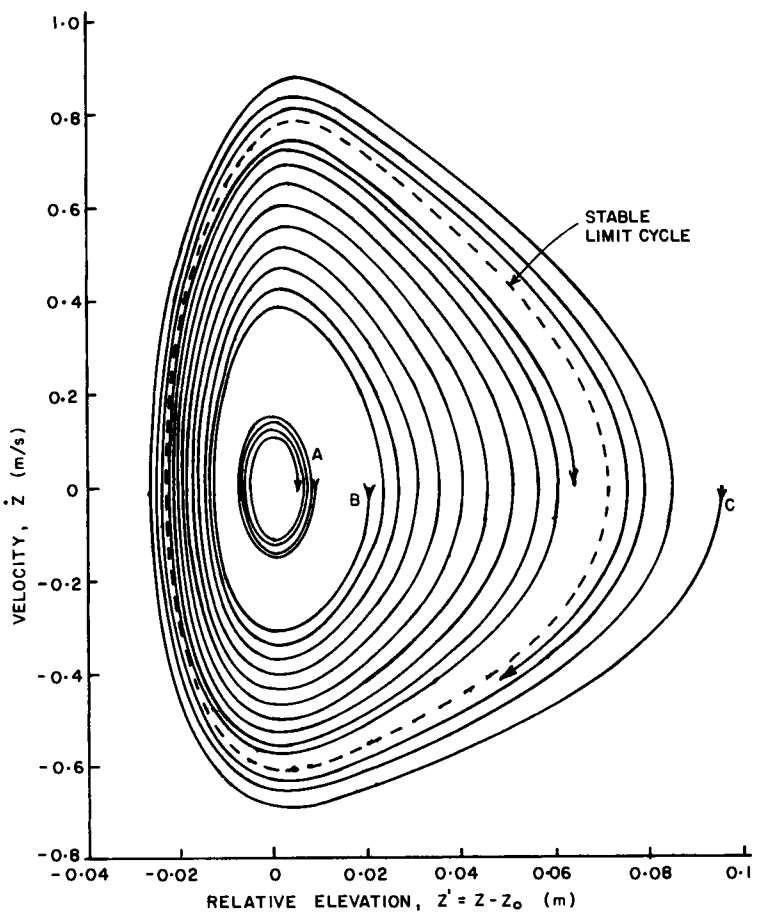

Fig. 14.18 Phase plane trajectories.

to infinity implying that the valve is continually activated by small velocity fluctuations. This excessive valve activity would be unacceptable in practice. On the other hand, N_V decreases to [1,2] and N_p increases to [6,9] for $\epsilon_{SR} \in$ [30%, 100%]. When $\epsilon_{SR} >$ 100%, the system operates essentially without control since the valve is not actuated. Thus, depending on the desired compromise between velocity attenuation and valve activity, an optimum setting would be in the interval $\epsilon_{SR} \in$ [8.3%, 30%].

iii) Conditionally unstable system. The results presented in this section were obtained with a fan speed N = 2050 rpm such that the uncontrolled system was conditionally unstable. Thus, since an unconditionally unstable system is a conditionally unstable system whose unstable limit cycle amplitude tends to zero, the discussion is qualitatively general for unstable operation. The results presented in Figs. 14.21-14.23 were obtained by first disturbing the system to establish a stable limit cycle without control and then activating the feedback control. The limit cycle velocity amplitude without control was L_U = 0.75 m/s and the effect of control was to reduce it to a controlled limit cycle velocity amplitude L_C. The relative limit cycle velocity amplitude is defined by eq. 14.32.

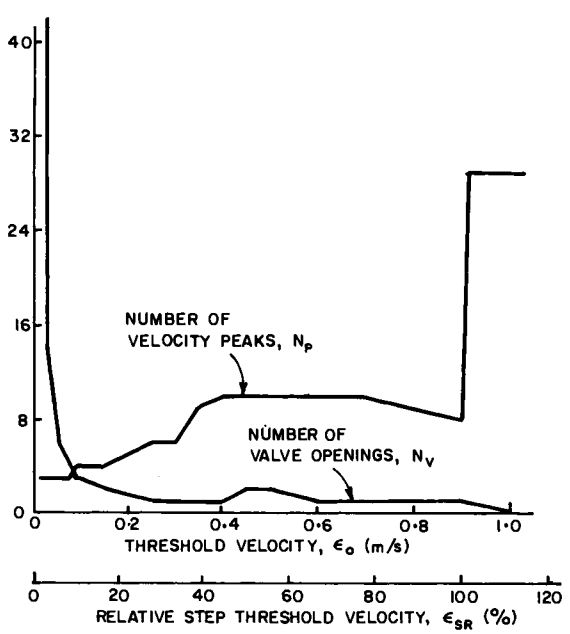

Fig. 14.19 Step response attenuation and valve activity as functions of threshold velocity.

Figure 14.21 shows that $L_{CR} = 0$ for $\epsilon_o \in [0.025, 0.125]$, i.e., the relative limit cycle threshold velocity $\epsilon_{LR} = \epsilon_o/L_U$ in the interval [3.33%, 16.6%]. In this same interval, the number of valve openings N_{VT} in transience from uncontrolled to controlled limit cycles decreases monotonically from 11 to 4 while the number of transience velocity cycles N_{CT} increases from 4 to 6. Therefore, the maximum threshold velocity capable of forcing the trajectory into the

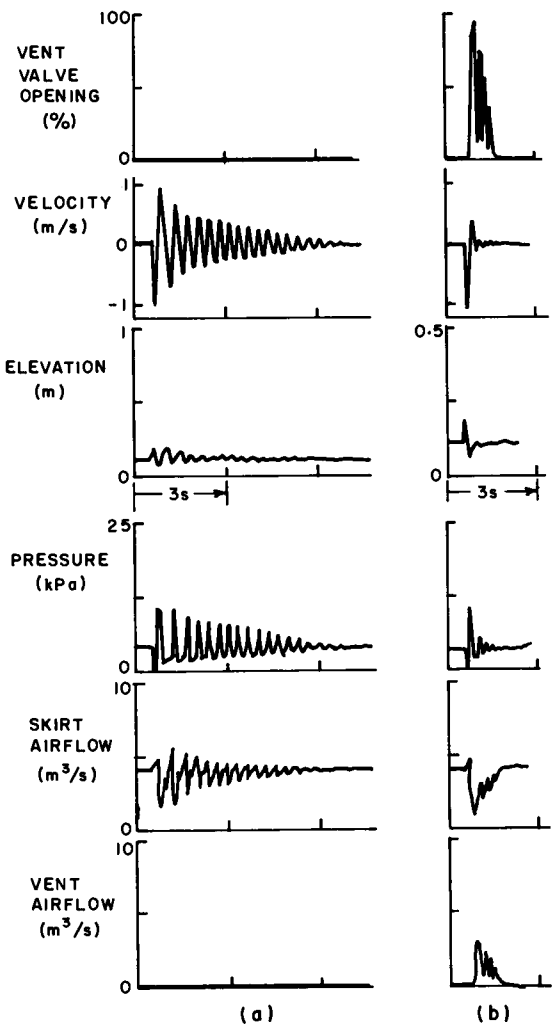

Fig. 14.20 Step disturbance time response; fan speed = 1625 rpm and hover elevation = 11 cm; (a) without control, (b) with relay control and $\epsilon_o = 0.075$ m/s.

stable region of the phase plane is ϵ_o = 0.125 m/s, or ϵ_{LR} = 6.67%, and this setting yields minimum valve action. The value of L_{CR} increases monotonically to 33% for $\epsilon_{LR} \in$ (16.67%, 40%), indicating that the threshold velocity is not small enough to force the system into its stable region but the stable limit cycle amplitude is reduced. The controlled limit cycle is maintained at a dimished amplitude by cyclical valve operation, the frequency of which can be characterized by the number of velocity cycles per valve opening $N_{C/V}$. It is seen that $N_{C/V}$ decreases monotonically from 3 to 1 in the interval $\epsilon_{LR} \in$ [20%, 40%]. Thus, the inverse relationship between L_{CR} and $N_{C/V}$ in this interval is fortunate since it indicates that valve activity is reduced as the controlled limit cycle amplitude is reduced. For ϵ_{LR} > 100%, the system is effectively uncontrolled; therefore, L_{CR} = 100% whereas $N_{CT} = N_{VT} = 0$, but $N_{C/V}$ is a meaningless quantity since the valve is not activated. The system was not tested in the interval $\epsilon_{LR} \in$ (40%, 100%).

For comparison purposes, simulations were conducted with proportional feedback of velocity by setting $K_a = 0$ in eq. (14.13) and defining $K_p = K_v$ for this special case. Also, the same filter and valve dynamics as in the relay feedback case were implemented. It is seen from Fig. 14.22 that proportional

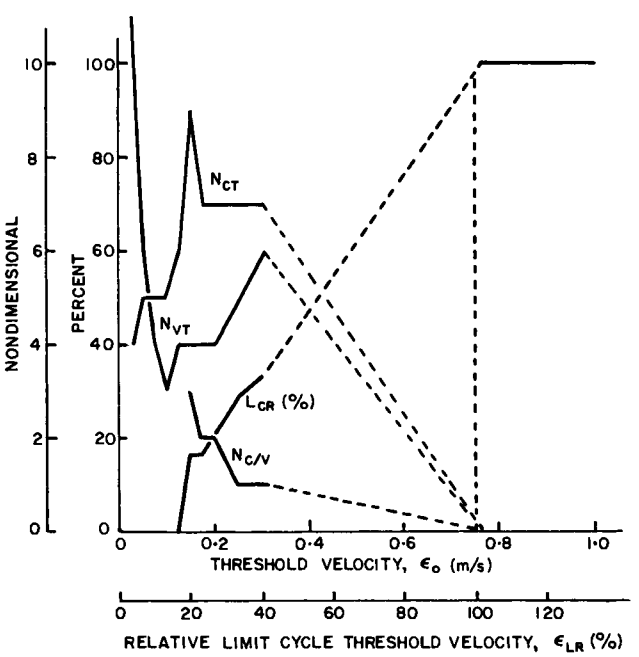

Fig. 14.21 Limit cycle attenuation and valve activity as functions of threshold velocity.

control stabilizes the system for a wide range of control gain values, i.e., $K_p \in [1, 10]$, and N_{CT} decreases monotonically in the corresponding interval $N_{CT} \in [18.5, 2.5]$; also, there is no residual limit cycle. Furthermore, with a nominally-underdamped stable cushion, the effect of varying the vent-valve set point from 0 to 40% of the fully-open position was found to be negligible for ground-step disturbances. Thus, there is no need to incur the additional power losses associated with a non-zero set point.

Limit cycle attenuation time responses are shown in Fig. 14.23 for (a) relay control with $\epsilon_o = 0.075$ m/s, or $\epsilon_{LR} = 10\%$, (b) relay control with $\epsilon_o = 0.175$ m/s, or $\epsilon_{LR} = 23.3\%$, and (c) proportional control with $K_p = 8$. The difference in valve activity between traces (a) and (c) is practically negligible but proportional control keeps the final velocity more steadily constant at a value of zero than relay control which is inactive in this region. Figure 14.23(b) illustrates the residual controlled limit cycle obtained with a larger threshold velocity and the two velocity cycles per valve actuation.

14.5.2 Experimental Results

The experimental results reported here pertain to the air-cushion system of Section 14.3.1, controlled by the relay velocity-feedback system of Section 14.3.2. The behaviour of the combined system in three stability regimes will

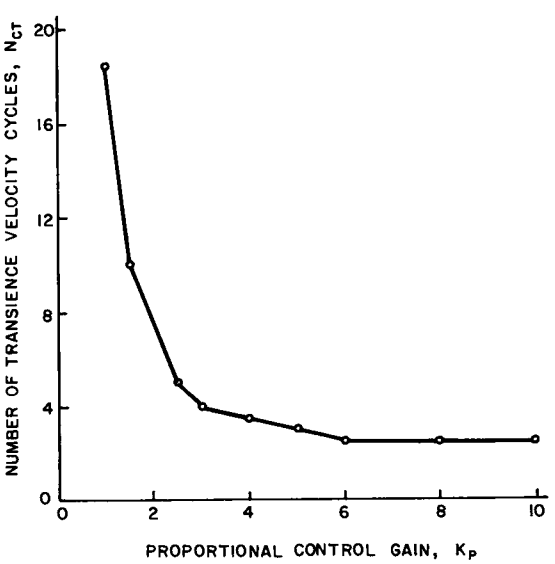

Fig. 14.22 Limit cycle attenuation as a function of proportional velocity-feedback gain.

be discussed, and the influence of the relay heave control system shown in each case.

In all three cases the threshold heave velocity was set at 0.3 m/s; one vent valve only, with an orifice of 8.9 cm diameter, was used. And the mass of the ground-board plus weights was 15.90 kg. The difference between the three cases was the airflow. It is well known in actual vehicle operation that heave

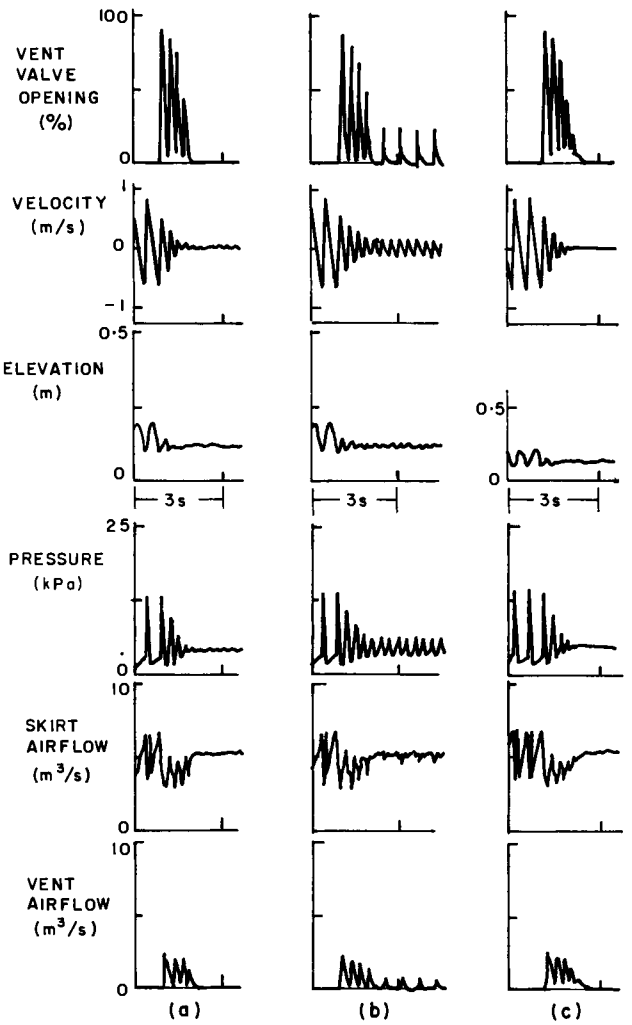

Fig. 14.23 Limit cycle attenuation time response; fan speed = 2050 rpm and hover elevation = 12 cm; (a) relay control with ϵ_o = 0.075 m/s; (b) ϵ_o = 0.175 m/s; (c) proportional velocity-feedback with K_p = 8.

can be induced by exceeding a critical lift airflow, and can be stopped either by reducing the lift airflow, by moving onto porous terrain, or by introducing a deliberate leak between skirt segments. The latter two actions do in fact reduce the effective lift airflow.

i) Conditionally unstable system (Fig. 14.24). In this case, the airflow was adjusted to make the system conditionally unstable. As explained previously, this is a condition where the magnitude of a disturbance determines the stability of the response. A sufficiently large disturbance will result in the system going unstable and reaching its limit oscillation.

Three sets of traces from the chart recorder are shown. Trace (a) shows, on an expanded time scale, the system oscillating in heave at its limit cycle. The three traces shown display the phase relation between plenum pressure (0.04

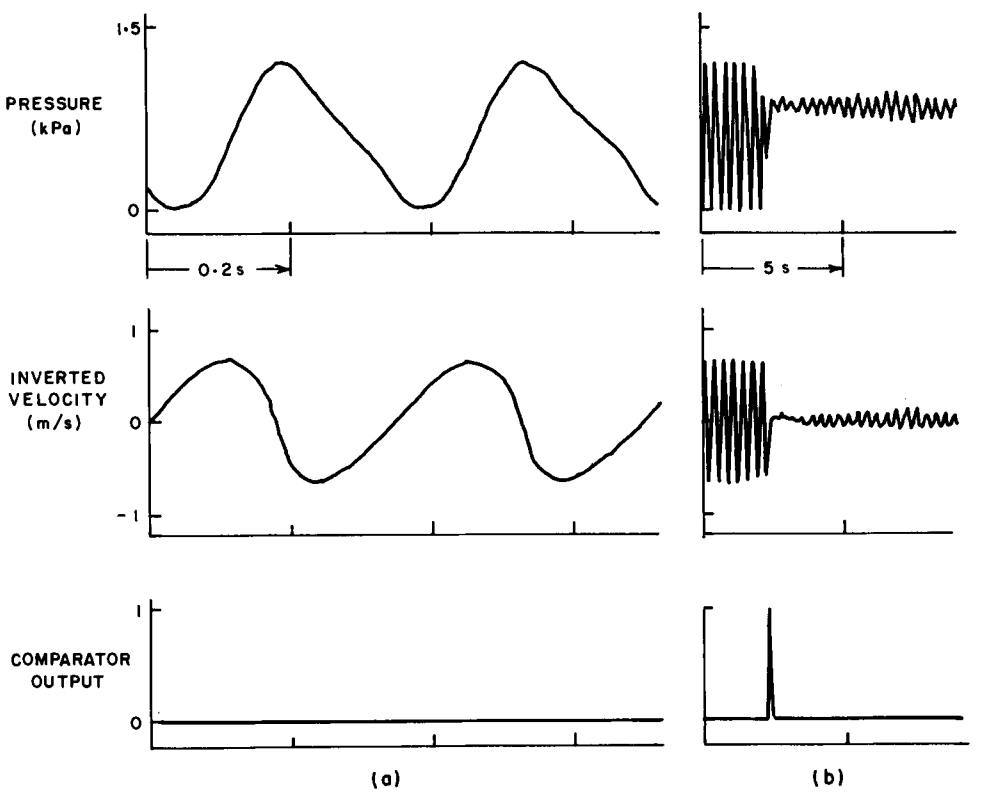

Fig. 14.24 Experimental time responses of conditionally unstable system using relay velocity-feedback: (a) uncontrolled stable limit cycle; (b) control applied during stable limit cycling.

to 1.24 kPa) and inverted velocity (-0.65 to +0.65 m/s). The fact that the vent valve did not operate was because the comparator output was zero. The frequency was approximately 2.78 Hz.

It is interesting to note that, since force (i.e. pressure multiplied by area) is equal to mass multiplied by acceleration, plenum pressure variations must be in phase with acceleration. Therefore, in the case of sinusoidal variations, velocity must lag pressure by 90°, or inverted velocity must lead by 90°. This is seen to be approximately the case in Fig. 14.24(a) where the waveforms are imperfect sinusoids. Furthermore, as expected, the cushion pressure peaks when the ground-board reaches its lowest position, which can be identified as the instant when the actual velocity passes through zero with a positive slope, or a negative slope in the case of inverted velocity.

Trace (b) shows, on a condensed time scale, the result of applying vent-valve control to the system in limit cycle oscillation. A single vent-valve

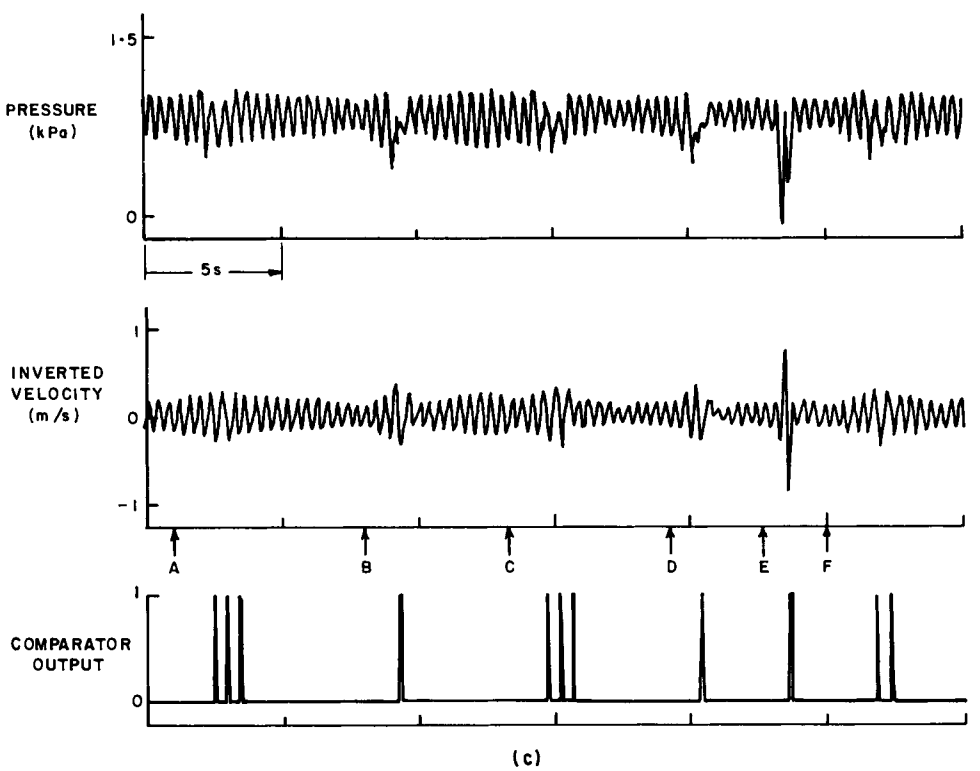

Fig. 14.24 (c) repeated downward manual impulses (A-F) on ground-board.

action was sufficient to bring the system into stable operation. The inverted velocity was reduced from ±0.70 m/s (far above the threshold triggering value of 0.3 m/s) to about ±0.1 m/s, and careful inspection shows that the triggering did take place in the downward (+0.3) motion. The computer simulation suggests that a proportional control would have reduced the final oscillation to an even lower level.

Trace (c) shows the result of a series of applied disturbances. These represent a series of sharp downward pushes, randomly delivered at different phases of the oscillation, at points A to F on the trace. It is seen that the system tended to destabilize, but that bursts of one, two or three valve actions brought the system back within bounds in every case.

ii) Unconditionally unstable system (Fig. 14.25). In this case, the airflow was high enough to make the system unconditionally unstable. As Fig. 14.25(a) shows, control was switched on after the limit cycle had been established, and momentarily reduced the oscillation. However, since the system was unstable, the oscillation built up again, requiring repeated operation of the vent valve. It is clear that while the vent valve was effective,

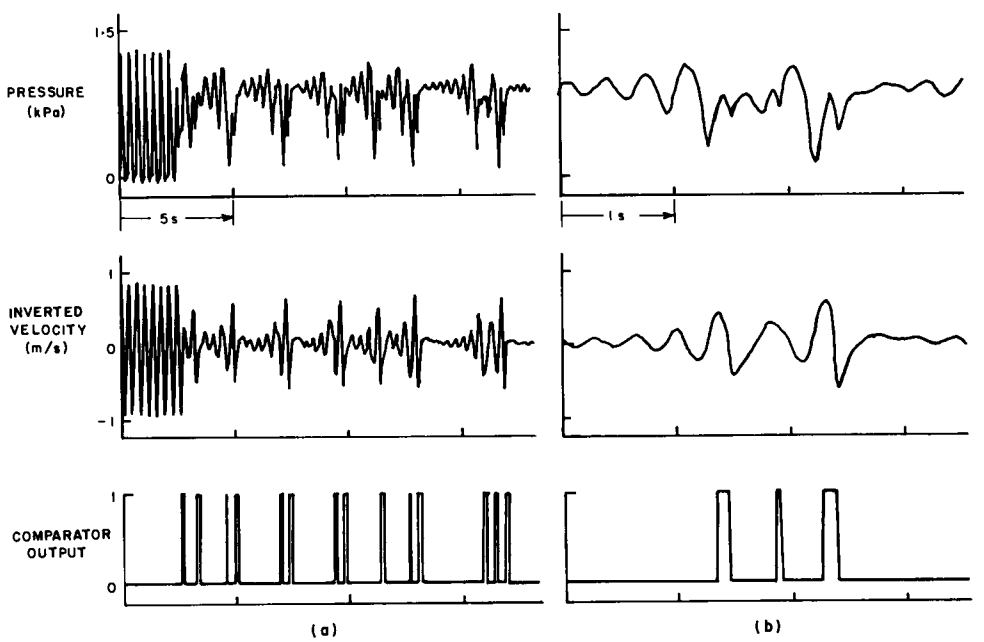

Fig. 14.25 Experimental time responses of unconditionally unstable system using relay velocity-feedback: (a) control applied during stable limit cycling; (b) continuation of (a) with expanded time scale.

the relay control system was not, and permitted repeated bursts of heave oscillation.

In trace (b), plotted on an expanded time scale, it is seen that by displacing the triggering actions to the right by an assumed 0.18 s delay, the actual open-valve periods correspond approximately to the negative inverted-velocity extrema, i.e., positive velocity extrema. Furthermore, the variations in magnitude of positive and negative inverted-velocity extrema tend to be consistent. Consequently, it is interesting to see that the length of the vent valve's open period appears to be proportional to the rate of increase of vertical velocity at the moment of exceeding the threshold value. A higher rate of velocity increase might well be expected to result in a bigger overshoot during the valve-opening moments, and hence require a longer period and consequent greater plenum pressure drop before the upward motion could be arrested. Indeed this state of affairs is shown in the first and third valve operations. The second operation, in response to a slower rate of velocity rise, was of much shorter duration.

iii) Underdamped stable system (Fig. 14.26). This case shows an underdamped stable system, which was excited into oscillation by lifting and dropping the ground-board. The board was lifted sufficiently high that the air escape area between skirt and ground-board was large enough to drop the plenum pressure to zero. Since the system was stable although underdamped, when the board was then dropped, it entered a damped oscillation which decayed to zero in a little over ten seconds. Trace (a) shows that it required 42 peaks of oscillation before the amplitude decayed to 10% of the level of the largest peak. Trace (b) shows the performance of the same system with the vent valve control switched on from the outset. The oscillation decayed to 10% in the much shorter time of 12 peaks in this case, showing the effectiveness of the relay control in dealing with strong perturbations of an underdamped stable system.

Trace (c) shows, on an expanded time scale, the reaction of the control system. The initial negative inverted velocity represents the manual lifting of the ground-board during which the pressure diminishes to zero. The subsequent positive portion of the inverted velocity trace corresponds to dropping the ground-board, and the first pressure peak occurs when the inverted velocity goes through zero with a negative slope, that is, the instant when the ground-board reaches its lowest position before rising again. Comparing trace (b) or (c) with trace (a), it is seen that the implementation of the control system had the effect of increasing the duration of zero pressure, hence free fall, upon dropping the ground-board, so that the amplitude of oscillation during the first cycle was actually increased by the control system. However, only two subsequent valve actuations in trace (c) were required to restore stable equilibrium almost completely.

14.6 PROPORTIONAL CONTROL PERFORMANCE

14.6.1 Computational Results

Some proportional velocity-feedback results have already been given in Section 14.5.1 for relay-control comparison purposes. In this section, computer results pertaining to the dual-feedback model (i.e., proportional velocity and acceleration feedback) of Section 14.2.2 are presented. However, in order to minimize effects due to filter and valve dynamics, these results were obtained with $(\omega_a, \omega_v) = (1.7, 170)$ instead of (3.14, 18.9) used in all the other active-control computer studies reported in this chapter.

Computer results for unit step tests (b = 1) are presented in Table 14.1 and Figs. 14.27 to 14.29. Figure 14.27 shows two curves: (1) ϵ_a as a function of K_a, with $K_v = 0$, and (2) ϵ_a as a function of K_v, with $K_a = 0$. The optimum value of K_a from the first curve is approximately 0.5, thus $K^*_{ar} = (0.5, 0)$; from the second, the optimum value of K_v is approximately 10, so that $K^*_{vr} = (0, 10)$. It is seen that K^*_{ar} yields a smaller value of ϵ_a than K^*_{vr}, namely 1.02

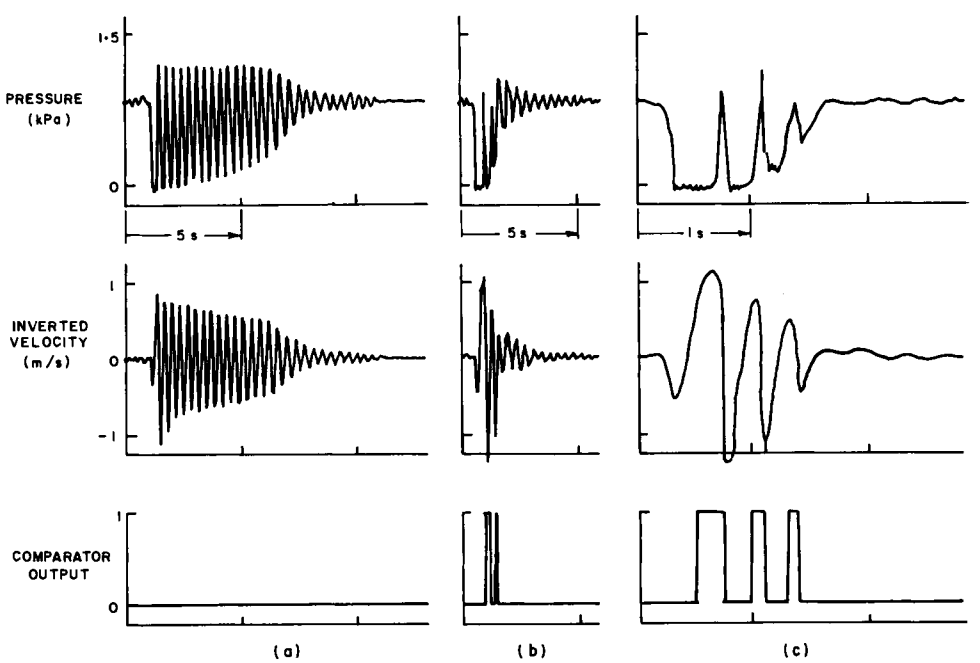

Fig. 14.26 Experimental time responses of underdamped stable system using relay velocity-feedback, upon dropping ground-board from a 25 cm elevation: (a) without control; (b) with control; (c) with control and expanded time-scale.

compared with 1.34. Corresponding curves of ϵ_v are shown in Fig. 14,28, where it is seen that K^*_{ac} = (0.05, 0) and K^*_{vc} = (0, 5) yield ϵ_p = 0.0033 and ϵ_p = 0.0024, respectively.

There is no optimum gain conflict between the K_a = 0 curves of Figs. 14.27 and 14.28 since both ϵ_a and ϵ_p are approximately minimized for $K_v \in [4, 10]$. However, this does not apply to the K_v = 0 curves since the range is approximately $K_a \in [0.15, 25]$ for minimum ϵ_a and $K_a \in [0.04, 0.1]$ for minimum ϵ_p.

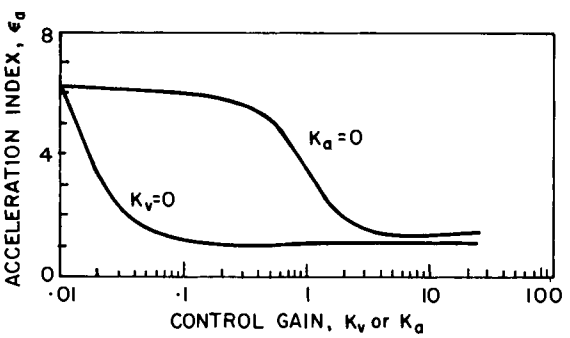

Fig. 14.27 Acceleration index as a function of individual proportional control gains in simulated dual-feedback system.

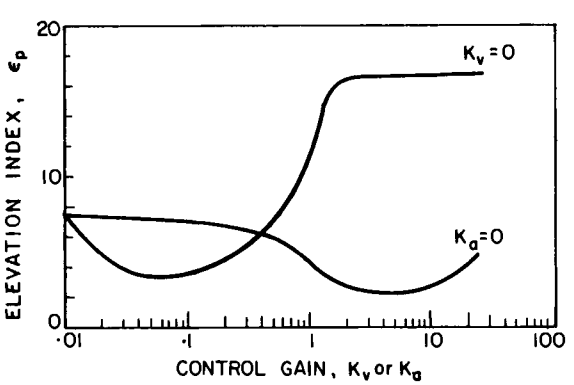

Fig. 14.28 Elevation index as a function of individual proportional control gains in simulated dual-feedback system.

If a choice were to be made between acceleration or velocity feedback, based on Table 14.1, the decision would depend on the predominant performance criterion. Should ride quality far outweigh skirt considerations, then acceleration feedback would be chosen since K^*_{ar} yields a smaller value of ϵ_a than K^*_{vr}, K^*_{ac} and K^*_{vc}. Otherwise, should both criteria be important, velocity feedback would be implemented since K^*_{vr} and K^*_{vc} yield smaller values of both criteria than K^*_{ac}, and K^*_{ar} produces a large ϵ_a value.

When acceleration and velocity feedback are combined such that both K_v and K_a are nonzero in the control algorithm of eq. (14.13), ride quality can be improved significantly without increasing skirt contact; for example, K^* yields $\epsilon_a = 0.55$ compared with $\epsilon_a = 1.02$ for K^*_{ar}. Alternatively, skirt contact can be reduced at the expense of less improvement in ride quality; comparing K^*_c with K^*, ϵ_p is reduced from 0.0027 to 0.0018 whereas ϵ_a is increased from 0.55 to 0.72.

Figure 14.29 illustrates the elevation and acceleration time responses corresponding to the gains of Table 14.1. The skirt contact performance index ϵ_p is the rms value of the negative portions of elevation response relative to the nominal elevation $z_o = 0.12$ m in the interval $t \in [0, 3.48]$, but modified by an exponential weighting factor reduction with a 0.835 s time constant. Although elevation trace (a) culminates in a relatively large limit cycle while trace (b) settles to a stable elevation, it is seen that the latter trace's downward excursions tend to be of longer duration; hence, the almost equal values of ϵ_p in Table 14.1 for these two cases.

Traces (f) and (h), which were obtained with gains K^*_r and K^*, respectively, are also interesting to compare since their ϵ_a values are identical while the ϵ_p value of the latter ($\epsilon_p = 0.0027$) is less than the former ($\epsilon_p = 0.004$). Indeed, whereas their acceleration traces are quite similar, the second downward excursion of the K^*_r elevation trace is somewhat greater and broader than the corresponding excursion of the K^* trace.

The results of ground step magnitude tests are depicted in Fig. 14.30. For gain K^*_{ar}, it is seen that the vehicle's supports strike the ground for the magnitude $b \geq 3.5$, i.e., $z_g = bz_{gm} \geq 0.35$ m. The other curves can be interpreted similarly; for example, K^*_c yields support contact with $b \geq 5.5$, or $z_g \geq 0.55$ m. From this figure, it can be concluded that the gains which favour ride quality at the expense of skirt drag yield softer cushions and a greater tendency for the vehicle to make solid contact with the ground. Gains K^*_{ar}, K^*_{ac}, K^*_r and K^* can be grouped in this category since they are distinctly lower than K^*_{vr}, K^*_{vc} and K^*_c on the abscissa. Thus, pure acceleration feedback, or an emphasis on ride quality control with both velocity and acceleration feedback, tends to produce a softer cushion. On the other hand, pure velocity feedback, or an emphasis on skirt drag reduction, tends to stiffen the cushion.

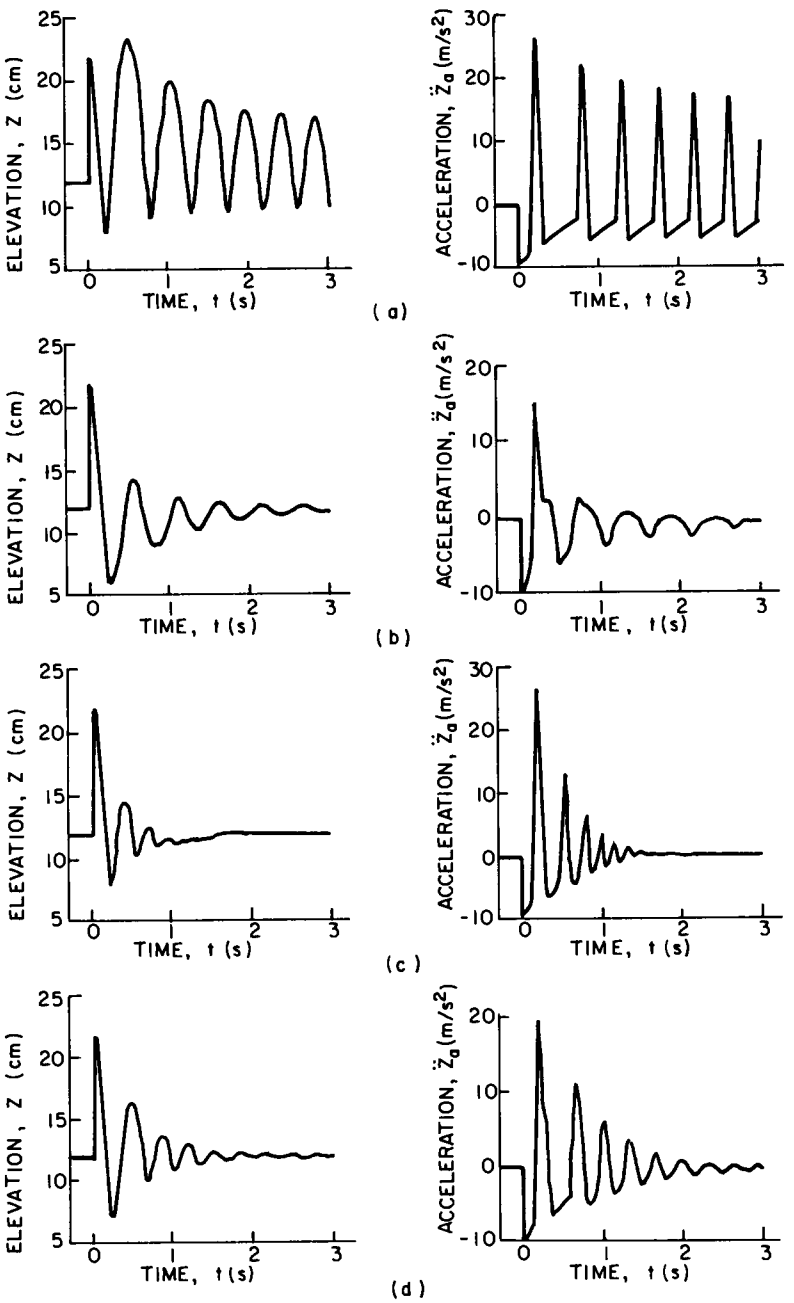

Fig. 14.29 Unit step responses corresponding to the gain values of Table 1: (a) $(K_a, K_v) = (0, 0)$; (b) $K^*_{\ddot{a}r} = (0.5, 0)$; (c) $K^*_{\dot{v}r} = (0, 10)$; (d) $K^*_{\ddot{a}c} = (0.05, 0)$.

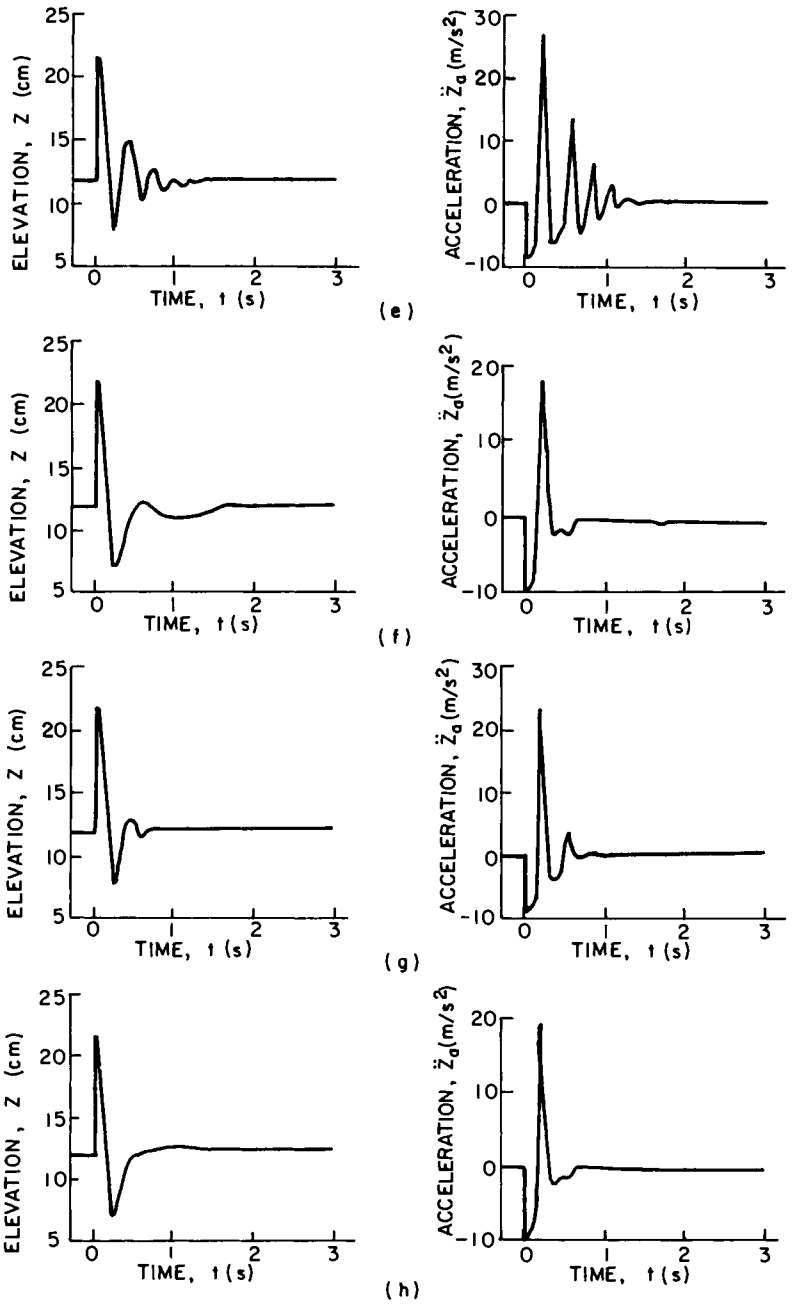

Fig. 14.29 (continued): (e) K^*_{vc} = (0, 5); (f) K^*_r = (1.8, 15); (g) K^*_c = (0.07, 1.8); (h) K^* = (0.7, 7).

Table 14.1. Optimum gains and performance indices.

CRITERIA	GAINS		PERFORMANCE INDICES	
	K_a (s^2/m)	K_v (s/m)	ϵ_a (m/s^2)	ϵ_p (m)
–	0	0	6.24	0.0074
K^*_{ar}	0.5	0	1.02	0.0073
K^*_{vr}	0	10	1.34	0.0029
K^*_{ac}	0.05	0	1.61	0.0033
K^*_{vc}	0	5	1.38	0.0024
K^*_r	1.8	15	0.55	0.0040
K^*_c	0.07	1.8	0.72	0.0018
K^*	0.7	7	0.55	0.0027

14.6.2 Experimental Results

The experimental results reported here pertain to the air-cushion system of Section 14.3.1, controlled by the proportional acceleration-feedback system of Section 14.3.3. Measurements were made to determine the influence of the vent-orifice diameter and control gain K on stability and ride quality.

Figure 14.31 gives rms acceleration curves as functions of control gain and vent-orifice diameter for a strongly unstable air cushion, as indicated by the A/g rms acceleration level of 0.67, where A is the rms acceleration with the control system switched off and g is the acceleration due to gravity. Without control, the limit cycle frequency was approximately 2.5 Hz. The ISO 1-minute FDP (fatigue decreased proficiency) level in a 1/3-octave band about this frequency is approximately 0.37 g. Therefore, with A = 0.67 g, a person could function effectively for less than one minute. With control, the frequency of

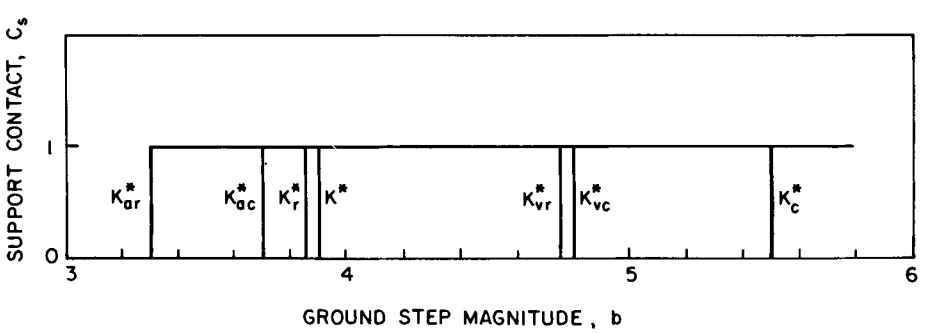

Fig. 14.30 Solid contact with ground as a function of step magnitude and control gain values in simulated dual-feedback system.

any residual motion tended to be approximately 3.3 Hz. At this frequency, the ISO 4-hour and 12-hour FDP levels in 1/3-octave band are approximately 0.06 g and 0.03 g, respectively. Therefore, it is seen from the A_c/g curves, where A_c is the rms acceleration level with the control system switched on, that a person could function effectively for a period of time between 4 hours and 12

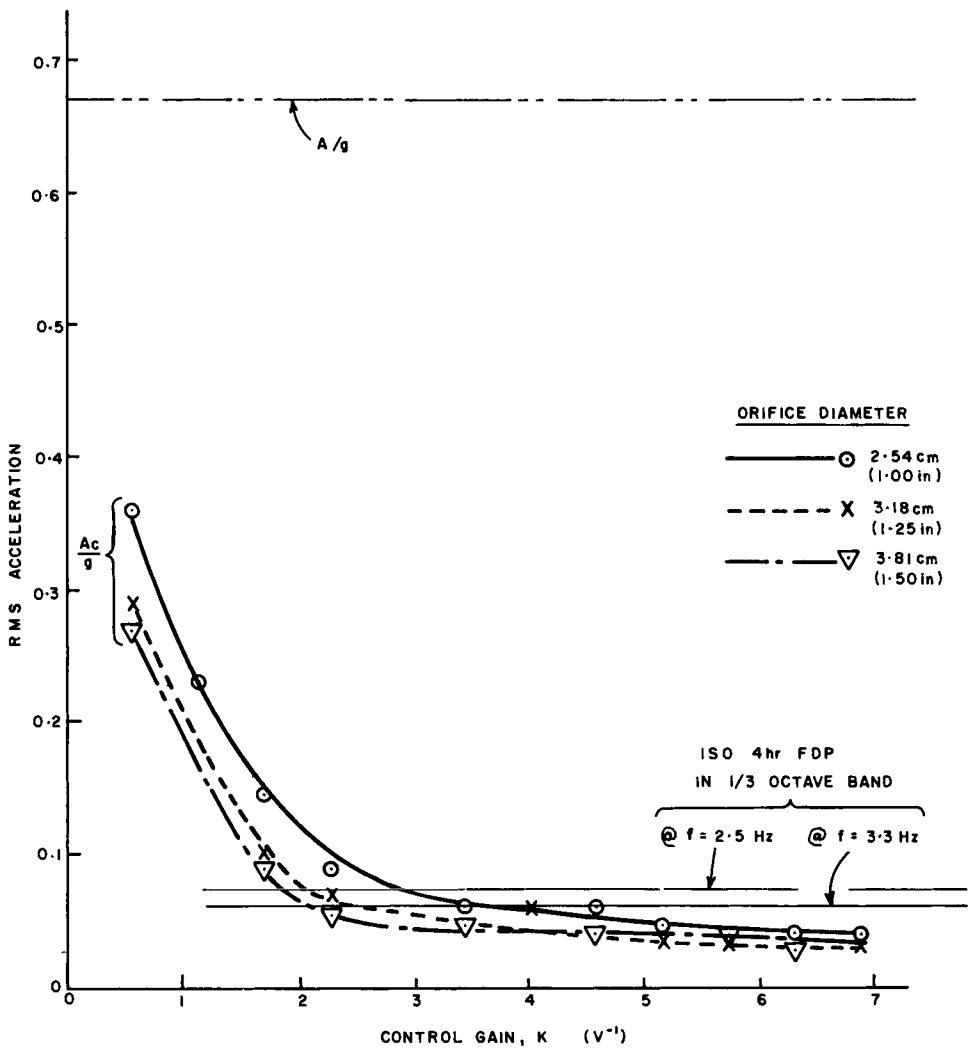

Fig. 14.31 Rms acceleration as a function of control gain and orifice size for a strongly unstable cushion.

hours, with a value of control gain in the range [4, 6.8] and a vent-orifice diameter equal to either 2.54 cm (1.0 in), 3.18 cm (1.25 in) or 3.18 cm (1.5 in), irrespectively. Also, for the larger values of K, these three orifice sizes do not yield much difference in performance.

A weaker instability was obtained by reducing the airflow, as seen by the A/g value of 0.23 in Fig. 14.32. In this case, the uncontrolled system would allow a person to function effectively for close to 25 minutes, but the controlled system, with K in the range [5, 6.8] would increase this time to close to 24 hours, the corresponding ISO level being approximately 0.015 g.

A deterministic view of the measured variables as functions of time is given in the strip-chart recordings of Figs. 14.33 and 14.34. Figure 14.33 shows the time response of a highly unstable cushion upon application of control, with K = 5.7 and a 2.54 cm (1.0 in) orifice diameter. It is seen that the oscillation is damped out within 3 or 4 cycles and the vent-valve opening peaks are in phase with the positive velocity peaks, thereby demonstrating the

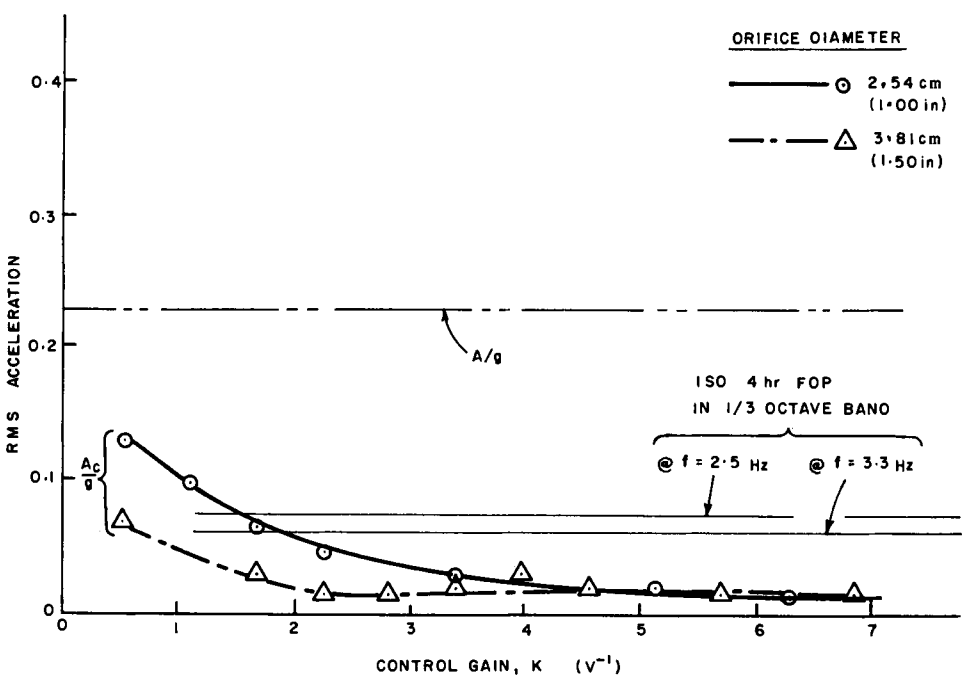

Fig. 14.32 Rms acceleration as a function of control gain and orifice size for a weakly unstable cushion.

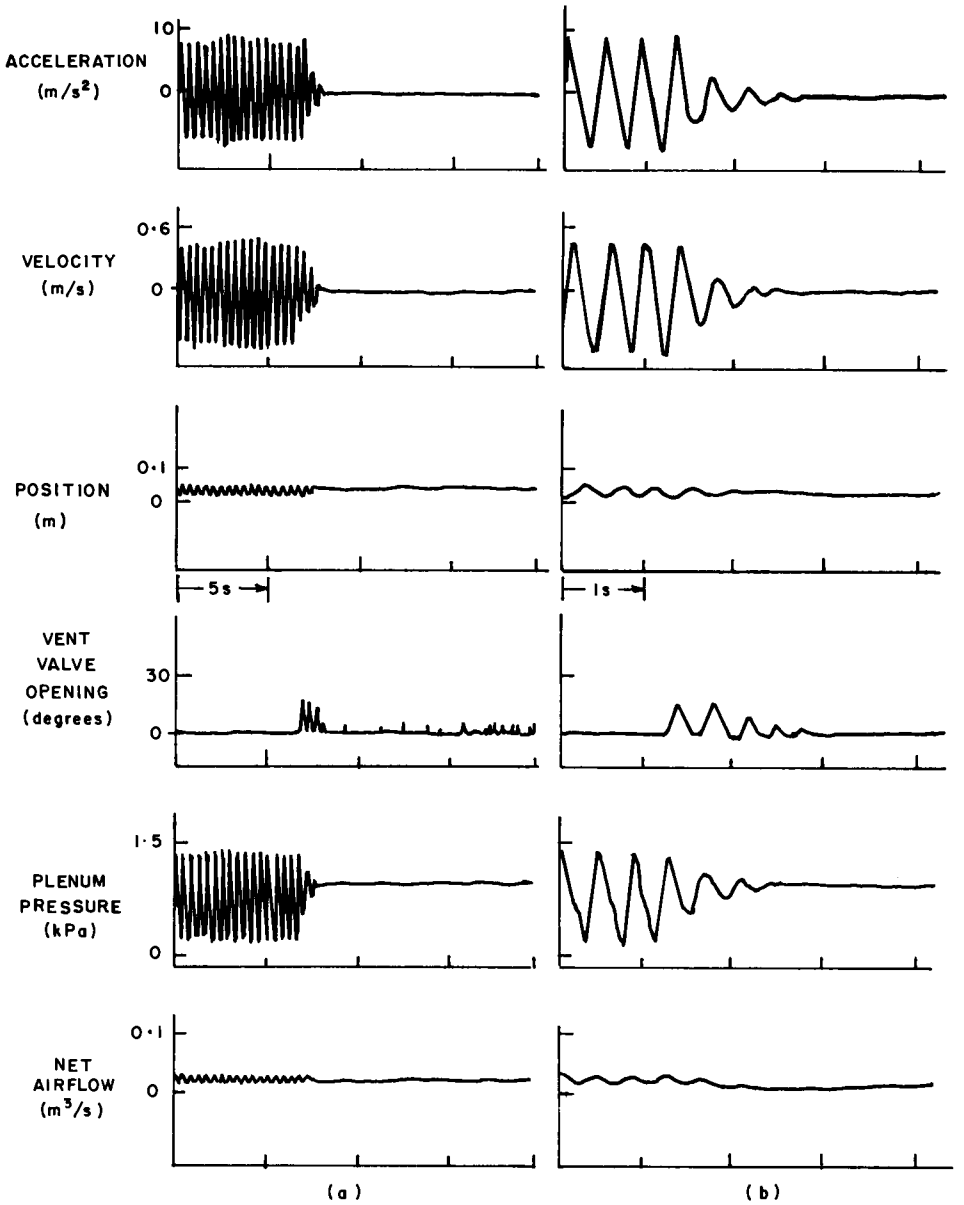

Fig. 14.33 (a) Time response of a highly unstable cushion upon application of control with K = 5.7 and a 1.0 inch orifice diameter; (b) Repeated with expanded time scale.

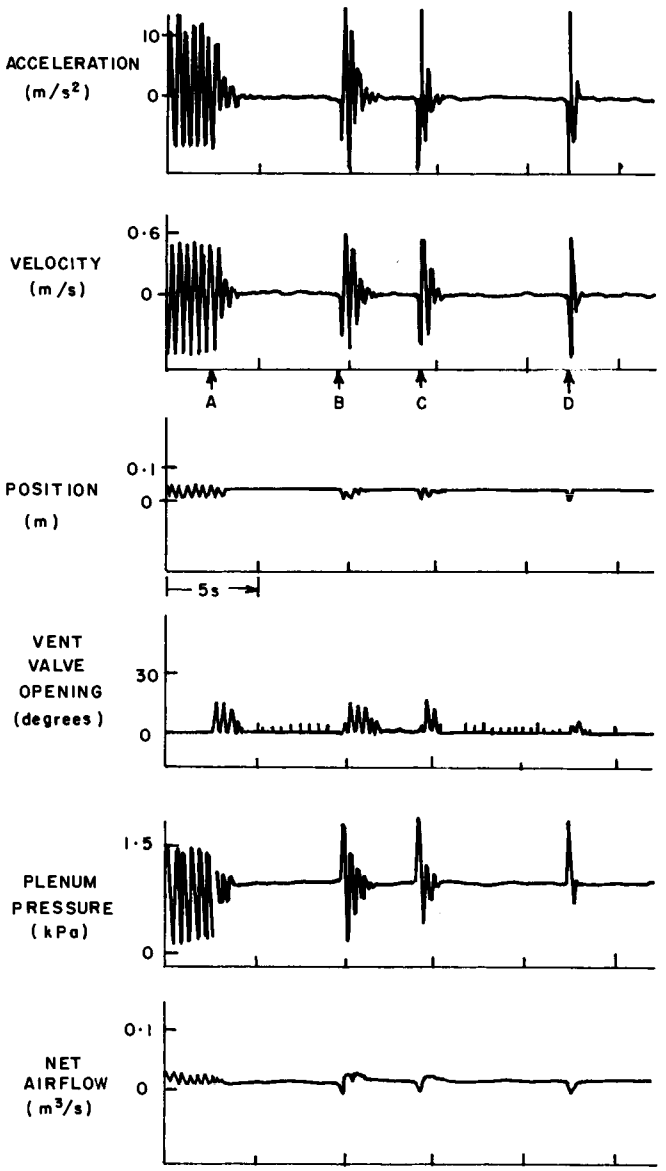

Fig. 14.34 Time response of a highly unstable cushion to repeated manual downward impulses (B, C, D) on the ground-board, while the system is controlled with K = 5.7 and a 1.0 inch orifice diameter.

phase shift of approximately 90°, from acceleration to valve position, through the control system. However, in traces (b) of the figure, it is seen that the magnitudes of the first two vent opening peaks are equal in spite of the fact that the magnitudes of the two corresponding velocity peaks differ by a factor of about 3. Since this was due to the speed limitation of the stepper actuator, it is felt that the performance of the control system could be improved by a faster-acting actuator. The speed limitation of the actuator prevented the control system from being fully *proportional*, except for relatively small oscillation amplitudes. Turning to phase relationships, it is seen that acceleration and plenum pressure are in phase, ground-board velocity lags these by 90°, and both ground-board position and net airflow lag velocity by 90°.

Again with a highly unstable cushion, Fig. 14.34 shows the response to application of control at time t = A, followed by a sequence of strong downward manual impulses, pushing the ground-board close to its supports, at t = B,C,D. In each case, the system returns to a stable equilibrium within 3 or 4 cycles. This test indicates that an ACV, controlled in this way, should be able to travel over terrain irregularities without losing stability. However, the ride quality would depend on the magnitude and frequency of the irregularities.

14.7 PASSIVE CONTROL PERFORMANCE

Computer simulation results pertinent to the passive feedback system of Section 14.2.3 are presented here. The fan speed was adjusted for unstable operation and a downward step in ground level was used as test condition to determine performance as a function of valve parameters. The step magnitude was 7.5 cm, i.e., 75% of the fully-extended skirt depth as measured from the vehicle supports. The performance index was rms acceleration E_a, calculated by eq. (14.25) over an interval τ which began at the instant of occurrence of the step and ended at time t = 2 s. This interval corresponded approximately to five oscillation cycles of the system with vent valves closed. On the other hand, with an optimum set of valve parameters, approximately two seconds were required for the transients to be reduced to negligible amplitudes.

The constants used to obtain the results presented here are:

$A^* = 2.2\ m^2$ $\qquad$ $m^*_v = 1068$ kg

$C_f = 0.75$ $\qquad$ $\Delta m_v = 0$

$D_v = 0.18$ m $\qquad$ $\alpha = 1.5$

$K = 9.807\ m/s^2$

The above value of D_v was chosen on the basis of simulation results which indicated that deviations from this value tended to reduce the stabilizing ability of the vent valves. This value gives a valve area $A_v = 0.0254\ m^2$ which

is 1.15% of the nominal skirt bearing area A*. It turns out that this is close to the 1% value used in the SES-100 ships mentioned in the introduction.

The simulation results are summarized in Fig. 14.35, where E_a is given as a function of the valve's damping ratio ζ and natural undamped frequency f_v. Practical values of primary parameters M, K and B were ensured by the following procedure:

(a) An upper limit X_{SM} was imposed on the spring pre-compression:

$$X_s = A_v g m_v^* / (A^* K) < X_{SM} \tag{14.40}$$

By the valve parameter equation (Fig. 14.11), we have:

$$K = M\,\omega_v^2 \tag{14.41}$$

Substitution of eq. (14.41) into (14.40) yields the constraint:

$$M > \beta/\omega_v^2 \tag{14.42}$$

$$\text{where} \quad \beta = A_v g m_v^* / (A^* X_{SM}) \tag{14.43}$$

$$\text{and} \quad \omega_v = 2\pi f_v \tag{14.44}$$

(b) A value of f_v was specified.

(c) The corresponding value of mass was calculated by eqs. (14.42) to (14.44) and a value was specified not to be less than a practical lower limit M_L, as follows:

If $M > M_L$, set $M = \beta/\omega_v^2$; otherwise, set $M = M_L$.

(d) With the above values of f_v and M, the spring stiffness K was calculated by eq. (14.41).

(e) The damping ratio ζ was varied in the range [0.05, 50]; the corresponding B ranges were calculated by:

$$B = 2\zeta(KM)^{1/2} \tag{14.45}$$

Table 14.2. Parameter data corresponding to the vent valve performance curves of Figure 14.35.

Curve	f_v (Hz)	X_s (m)	M (kg)	K (N/m)	ζ range	B range (N/m/s)
A	0.8	0.310	15.880	397	[.05, 50]	[7.9, 7940]
B	2.4	0.310	1.764	397	[.05, 50]	[2.7, 2647]
C	4.8	0.310	0.440	396	[.05, 50]	[1.3, 1320]
D	6.4	0.310	0.244	390	[.05, 50]	[1.0, 976]
E	9.6	0.135	0.244	878	[.05, 30]	[1.46, 878]

The curves in Fig. 14.35 and corresponding data in Table 14.2 were obtained with X_{SM} = 0.3 m and M_L = 0.244 kg.

Let (ζ, f_v, E_a) define a general point of the curves in Fig. 14.35 and let [f_c, Z_L, N_c] be properties associated with it, where f_c is cushion heave frequency (Hz), Z_L is the limit cycle amplitude (cm) and N_c is the number of cycles required for the elevation time-response to decrease and remain within 10% of the step-disturbance amplitude, i.e., 0.75 cm. Thus, a general point and its properties can be identified by:

Point = (ζ, f_v, E_a) : [f_c, Z_L, N_c]

The following points are highlighted in Fig. 14.35:

Point 1: (0.2, 0.8, 8.80) : [2.6, 5.5, ∞]
Point 2: (0.09, 2.4, 6.88) : [3.3, 1.4, ∞]
Point 3: (0.15, 2.4, 6.20) : [3.3, 0, 8]
Point 4: (0.3, 6.4, 4.75) : [2.6, 0, 3]
Point 5: (21, 6.4, 6.88) : [3.1, 0, 10]

In addition, [2.3, 7.2, ∞] are shown to be properties assoicated with the uncontrolled cushion i.e., where the valves are held in a closed position. Therefore, the uncontrolled cushion exhibits a 2.3 Hz limit cycle with a 5.5 cm amplitude; hence, N_c = ∞.

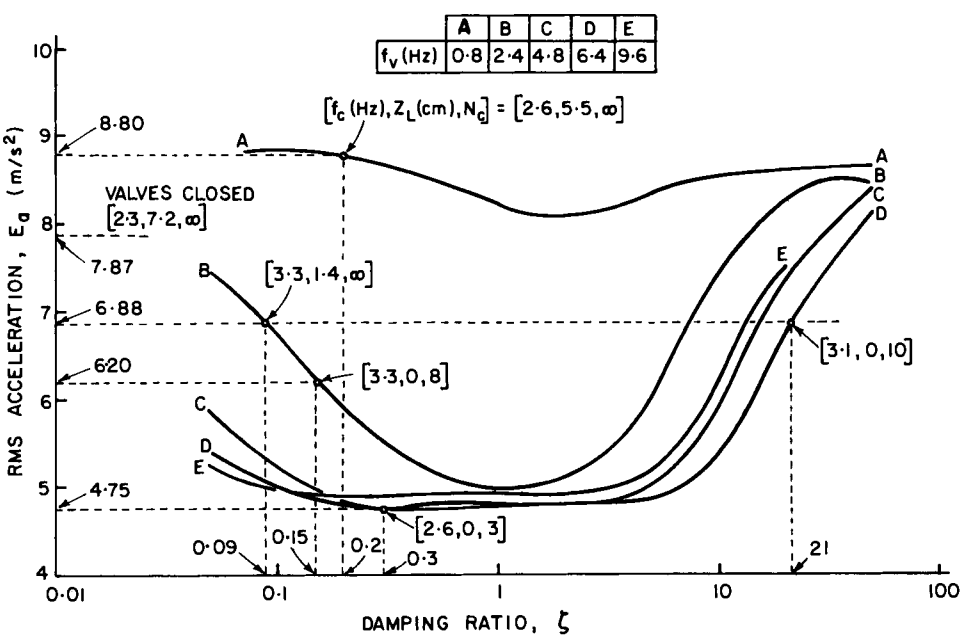

Fig. 14.35 Vent-valve performance curves.

The properties associated with the above points were determined from time responses. For example, the existence, amplitude and frequency of the uncontrolled cushion limit cycle can be observed in Fig. 14.36. Similarly, the properties associated with the optimum parameter values of Point 4 were determined from the time response of Fig. 14.37(a). The valve opening events are seen to be synchronized with the pressure peaks; the valve outflow peaks coincide with skirt flow troughs, so that the valve action tends to minimize variations in net cushion outflow.

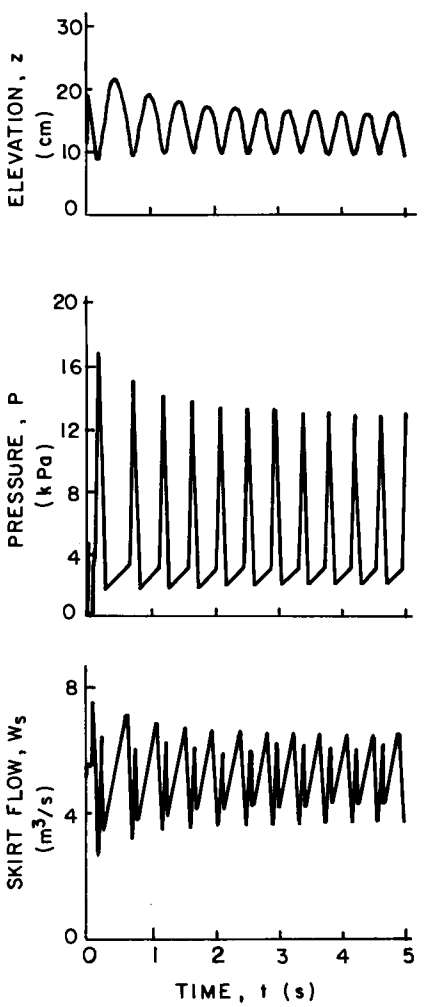

Fig. 14.36 Time response of uncontrolled cushion.

On the other hand, Fig. 14.37(b) corresponds to the poorly-tuned parameters of Point 1. Here, the system is not stabilizied, but the limit cycle amplitude is smaller than in the uncontrolled cushion case. The large E_a value can be attributed to a frequency increase, from 2.3 Hz to 2.6 Hz, which more than compensates for the reduction in oscillation amplitude. The poor tuning is reflected in the valve displacement which is out-of-phase with the pressure peaks. Since the pressure is low when the valves are open, the valve flow is small and the smoothing effect on net outflow is minimal. In this case, the valve sluggishness is due to its small natural frequency (f_v = 0.8 Hz) compared with the uncontrolled cushion's resonant frequency (f_c = 2.3 Hz).

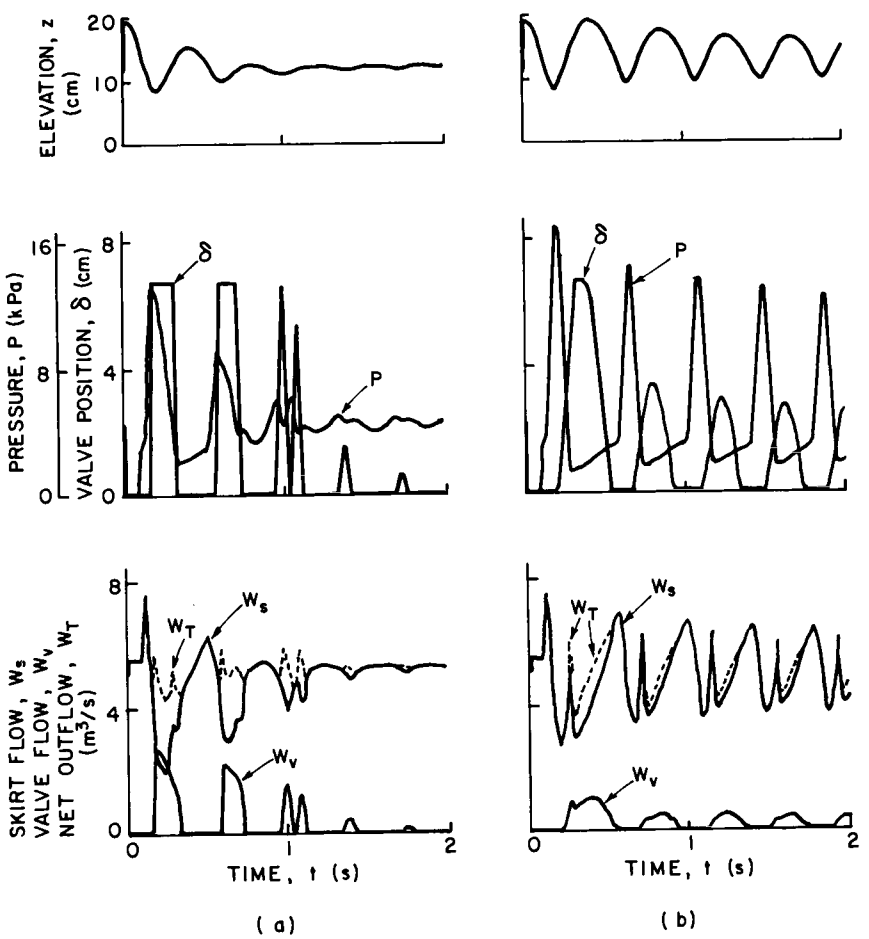

Fig. 14.37 Time responses of passively-controlled cushion: (a) optimally-tuned valve (point 4), f_v = 6.4 Hz and ζ = 0.3; (b) poorly-tuned valve (point 1), f_v = 0.8 Hz and ζ = 0.2.

Returning to Fig. 14.35, Points 2, 3 and 5 indicate that E_a in the range [6.20, 6.88] defines a transition region between stable and unstable systems. Since curve A never enters the stable region, a 0.8 Hz valve cannot stabilize a 2.3 Hz cushion. A 2.4 Hz valve (curve B) can stabilize the cushion for $\zeta \in [0.15, 5.4]$, but the best performance is restricted to a small range of approximately $\zeta \in [0.7, 2]$. On the other hand, for $\zeta \in [0.1, 5]$, curves C, D and E exceed the best performance of curve B. Furthermore, since curve E is higher than curves C and D with the latter two being approximately equal in this range of ζ, it can be concluded that there is no need to increase the valve's natural frequency beyond approximately twice the cushion's resonant frequency. Thus, a quasi-optimal set of valve parameters, from curve C in Table 14.2 is:

$M = 0.44$ kg

$K = 396$ N/m

$B \in [2.6, 132]$ N/m/s

This range of B corresponds to $\zeta \in [0.1, 5]$ and the required spring precompression is $X_s = 0.31$ m.

14.8 SYMBOLIC AND NUMERICAL SPECIFICATIONS

14.8.1 Nomenclature

A dot or double dot over a variable respectively denote the first or second derivative with respect to time. For simplicity, the symbols are defined below without these modifiers. The units apply to the conceptual models and other equations. However, derived or engineering units are sometimes used for convenience in the text, tables and figures.

Roman

A	Cushion bearing area, m^2
A^*	Nominal skirt bearing area, m^2
A_n	Nominal cushion bearing area, m^2
A_v	Valve area, m^2
a_v	Vehicle-support hysteresis width, m
B	Valve damping coefficient, Ns/m
b	Absolute value of scaled ground-step magnitude
B_0, B_1, B_2	Parameters in cushion volume equations
B_{0n}, B_{1n}, B_{2n}	Nominal parameters in cushion volume equations
C_f	Valve flow coefficient
C_p	Elevation index weighting factor in the combined performance index, s^{-2}
C_s	Vehicle-to-ground contact variable
$C_1, \ldots, C_8$	Vehicle-to-ground contact variable
D	Time differential operator

D_v	Valve diameter, m
E	Elevation variations in direction of skirt contact, m
E_a	Rms acceleration, m/s^2
E_v	Amplitude of first positive velocity peak during ground step down test without control, m/s
F	Vertical applied force, N
F_c	Net vertical force due to weight and applied force, N
f_c	Limit cycle frequency of uncontrolled cushion, Hz
F_v	Vehicle support force, N
f_v	Valve undamped natural frequency, Hz
G	Canonical gain of valve, m/Pa
g	Acceleration due to gravity, m/s^2
H	Vertical extension of air cushion, m
K	Proportionality constant in reverse skirt airflow; also, valve spring stiffness, N/m
K^*	Dual gain values which minimize the combined performance index
K_a	Factor by which bearing area is increased; also, acceleration feedback gain, s^2/m
K^*_{ac}	Pure acceleration feedback gain value which minimizes the elevation index, s^2/m
K^*_{ar}	Pure acceleration feedback gain value which minimizes the acceleration index, s^2/m
K^*_c	Dual gain values which minimize the elevation index
K_p	Velocity feedback gain with no acceleration feedback, s/m
K^*_r	Dual gain values which minimize the acceleration index
k_v	Vehicle support stiffness, N/m
K_v	Velocity feedback gain, s/m
K^*_{vc}	Pure velocity feedback gain value which minimzes the elevation index, s/m
K^*_{vr}	Pure velocity feedback gain value which minimizes the acceleration index, s/m
L_{CR}	Controlled relative to uncontrolled limit-cycle velocity-amplitude (peak-to-peak)
L_U	Uncontrolled stable limit-cycle velocity-amplitude (peak-to-peak), m/s
L_s	Fully extended skirt length, m
L_1	Height from top of skirt to bottom of support, m
M	Valve mass, kg
M_L	Lower limit of valve mass, kg
m_v	Vehicle mass, kg
m^*_v	Vehicle mass without skirt; also, nominal vehicle mass, kg

Δm_v	Incremental mass added to vehicle, kg
m_{vs}	Suspended portion of skirt mass, kg
N	Fan speed, rpm
n	Polytropic change of state exponent
N_c	Number of cycles required for the elevation time-response to decrease and remain within 10% of the step-disturbance amplitude
N_{CT}	Number of transience velocity cycles from uncontrolled to controlled limit cycle
$N_{C/V}$	Number of velocity cycles per valve opening with controlled limit cycle
N_p	Number of velocity peaks (extrema) to ± 10% of first peak following a ground step
N_V	Number of valve opening events following a ground step
N_{VT}	Number of valve opening events in transcience from uncontrolled to controlled limit cycle
p	Cushion gauge pressure, Pa
P_a^a	Atmospheric absolute pressure, Pa
p_n	Nominal cushion gauge pressure, Pa
p_o	Cushion operating gauge pressure, Pa
p_1	Cushion gauge pressure variations, Pa
R	Universal gas constant, $m^2/(s^2 \cdot K^0)$
T	Integration interval for performance indices, s
t	Time, s
T^a	Cushion absolute air temperature, K^o
u	Unit-step function
V	Net cushion volume, m^3
V_F	Parameter in cushion volume equation, m^3
V_1	Air-cushion volume segment enclosed by skirt and ground, m^3
V_{1a}, V_{1b}, V_{1c}	Intermediate cushion volume variables, m^3
V_2	Constant air-cushion segment shown in Fig. 14.1, m^3
V_3	Constant air-cushion segment shown in Fig. 14.1, m^3
V_4	Additional air-cushion volume segment determined by the vertical extension H, m^3
W	Exponential weighting function in performance indices
W_i	Net inflow into cushion, kg/s
W_o	Net outflow from cushion, kg/s
W_s	Skirt airflow, kg/s
W_T	Net outflow from cushion, kg/s
W_v	Valve airflow, kg/s
z	Elevation of vehicle supports above ground, m

Z'	Elevation of supports relative to z_o, m
z_a	Elevation of vehicle supports above an inertial reference, m
z_f	Filtered elevation of vehicle suppors above an inertial refrence, m
z_g	Elevation of ground above an inertial reference, m
z_{gm}	Scale factor equal to the fully-extened skirt length, measured from vehicle supports, m
Z_L	Limit cycle amplitude, m
Z_o	Constant value of Z during stable steady-state hover operation, m
z_1	Application range limit in cushion volume expressions, m
z_2	Application range limit in cushion volume expression, m

Greek

α	Constant factor relating δ_L to $D_v/4$; also, parameter in cushion volume equations
β	Constant factor relating M to ω_v^{-2}
δ	Scaled vent-valve setting; also, actual opening of passive valve, m
δ_d	Desired vent-valve setting
δ_{d1}	Vent-valve setting between fully-closed and fully-open positions
δ_L	Valve opening stop limit, m
δ_o	Valve operating position, m
δ_1	Valve opening variations, m
δ_3	Valve opening beyond which flow increases negigibly, m
ϵ	Parameter range symbol
ϵ_a	Acceleration index of performance, m/s^2
ϵ_{LR}	Threshold velocity relative to uncontrolled limit-cycle velocity amplitude
ϵ_o	Threshold velocity, m/s
ϵ_p	Elevation index of performance, m
ϵ_{SR}	Threshold velocity relative to E_V
η	Combined index of performance, m/s^2
ω_a	High-pass filter break radian frequency, s^{-1}
ω_c	Cushion resonant radian frequency, s^{-1}
ω_v	Actuator and valve break radian frequency, s^{-1}
ρ	Specific density of air, kg/m^3
τ	Integration interval for rms acceleration computation, s
ζ	Valve damping ratio

14.8.2 Numerical Data

(i) Constants

$a_v = 0.0002$ m	$g = 9.80665$ m/s^2	$V_2 = 0.5$ m^3
$B_{0n} = 2.78$ m^2	$K = 16$ m·s	$V_3 = 0.339$ m^3
$B_{1n} = 2.16$ m^2	$k_v = 6.68 \times 10^6$ N/m	$z_{fd} = 0$ m/s
$B_{2n} = 2.30$ m^2	$L_1 = 0.025$ m	$z_{gm} = 0.1$ m
$C_b = 0.066$	$L_s = 0.124$ m	$z_o = 0.12$ m
$C_p = 50$	$n = 1.396$	$z_1 = 0.10$ m
$C_1 = 0.839$	$P_a^a = 1.0133 \times 10^5$ Pa	$z_2 = 0.12$ m
$C_2 = 0.025$	$R = 288.87$ m$^2/(s^2 \cdot K^o)$	$\rho = 1.218$ kg/m^3
$C_3 = 1.672$	$T = 2.48$ s	
$f_c = 2.4$ Hz	$T^a = 288$ K^o	

(ii) Initial Values

$F(o) = 0$	$z_a(o) = 0$
$H = 0$	$\dot{z}_a(o) = 0$
$m_v^* = 1068$ kg	$z_g(o) = 0$
$\Delta m_v(o) = 0$	$\dot{z}_g(o) = 0$
$\Delta \dot{m}_v(o) = 0$	$\delta_{d1}(o) = 0$
$N(o) = 0$	$\omega_a = 3.14$ s^{-1}
$P(o) = 0$	$\omega_v = 18.9$ s^{-1}

14.9 SUMMARY

The concept of controlling the heave dynamics of air cushions by means of vent valves was introduced. Computer models were used to study active and passive feedback control. Included in the former were: 1) relay (bang-bang) velocity-feedback, 2) proportional velocity feedback, and 3) proportional velocity and acceleration feedback. Passive feedback consisted of a valve, with spring and dashpot, reacting to cushion pressure variations. Physical models were used to study relay velocity-feedback and proportional acceleration feedback. Although the computer and physcial models were not identical, they were conceptually similar and did contain the dynamic heave elements of many hovercraft. The control system properties discovered by the two approaches were mutually supportive and, as such, could be extended qualitatively to practical applications describable by conceptually-similar models.

Several performance indices were defined to describe the steady-state behaviour of the hull, and its transient response to step changes in ground level. Various criteria were defined for purposes of optimizing the control parameters of systems with proportional velocity and acceleration feedback. The objective functions took into consideration ride quality and the propensity for skirt wear, based on the amount of skirt contact with the ground after a disturbance.

It was found that the existence and amplitude of stable and unstable limit cycles of an air cushion is strongly dependent on airflow; hence, fan speed. The latter limit cycle is completely surrounded by the former and defines the region of stability in the phase plane. Relay control can improve dynamic performance significantly without excessive valve action, provided the system exhibits a sizable region of stability. On the other hand, proportional control tends to be easier on the valve, is less dependent on stability region size, and reduces the magnitude of residual motion.

The ride control problem in the marine operation of air cushion craft is quite different from the stabilization problem of heavy-load air cushion craft operated at relatively low speeds over land. For these latter applications, it was shown that vent-valve control is not significantly detrimental to lift power requirements, provided the vent valves are controlled from a nominally-closed position. Here, the action of the valves is to regulate the net outflow of air following a disturbance. This is accomplished by reducing the net outflow variations about a nominal value corresponding to the operating elevation. Based on step-response studies, a greater improvement of ride quality and skirt life is possible with a combination of proportional velocity and acceleration feedback than with either one alone. Further work would be required to determine the applicability of these results to other gorund disturbance, but a positive outcome could be expected.

It was shown that a highly unstable air cushion could be stabilized by passive control provided the vent-valve's natural frequency was approximately equal to or greater than the resonant frequency of the uncontrolled cushion. However, quasi-optimal performance over a wide range of valve damping could be obtained with a natural valve frequency twice as great as the cushion's resonant frequency. The action of such a valve was to reduce cushion pressure variations by minimizing net cushion outflow fluctuations. The presence of control tended to increase the resonant frequency of the cushion. The valve spring was pre-compressed to operate from a nominally-closed position, thereby eliminating steady losses. However, the nominal valve position would increase in proportion to ACV load increases unless compensating adjustments to the pre-compression would be made, which could be impractical. By comparison, an active control system operating from an accelerometer signal would not exhibit

this problem. Furthermore, control adjustments for ground irregularities, temperature variations and aging of components would be easier to include in vehicle operating procedures. Thus, whereas a passive control system could be adequate and cheaper for some applications, such as the stabilization of a fixed-load raft operated on a smooth hard surface, an active one tends to be more versatile.

A dimensional analysis, which remains to be verified physically, indicated that the ratio of required vent-orifice diameters of two air cushions is equal to the ratio of the cushions' peripheral lengths. Therefore, the extrapolation of the physical models to typical ACV sizes appears to be practical. The conclusion of the investigation reported in this chapter is that the vent-valve control concept is a promising approach for the stabilization of air cushion vehicles.

14.10 REFERENCES

1. M.J. Hinchey, An Overview of UTIAS Research on the Dynamic Stability of Air Cushion Vehicles, Canadian Aeronautics and Space Journal, Vol. 29, No. 4, Ottawa, Canada, 1983, pp. 371-390.
2. P.J. Mantle, Air Cushion Craft Development, Report DTNSRDC-80/012 (4727 Revised), David W. Taylor Naval Ship Research and Development Center, Bethesda, Maryland, January 1980, pp. 165-180.
3. E.A. Butler (Ed.), The Surface Effect Ship, in: Special Edition on Modern Ships and Craft, Naval Engineers Journal, American Society of Naval Engineers, February 1985, pp. 220-222.
4. J.R. Amyot, Computer Studies of ACV Heave Performance as a Function of Vent Valve Proportional Control Parameters, Canadian Aeronautics and Space Journal, Vol. 29, No. 1, Ottawa, Canada, 1983, pp. 25-34.
5. J.R. Amyot, Simulation of Air Cushion Heave Dynamics with Vent Valve Relay Control, Preprints of the Seventeenth Canadian Symposium on Air Cushion Technology, Ottawa, Canada, October 1983, pp. 27-32.
6. J.R. Amyot and H.S. Fowler, An Experiment on Active Control of Air Cushion Heave Dynamics, Canadian Aeronautics and Space Journal, Vol. 30, No. 3, Ottawa, Canada, 1984, pp. 240-248.
7. J.R. Amyot, A Proportional Control Experiment on Air Cushion Heave Stabilization, Canadian Aeronautics and Space Journal, Vol. 31, No. 4, Ottawa, Canada, 1985, pp. 315-324.
8. J.R. Amyot, Computer Model of Heave in Hovercraft HEX-5, Proceedings of the Fourteenth Canadian Symposium on Air Cushion Technology, Ottawa, Canada, September 1980, pp. 123-139.
9. J.R. Amyot, Computer Studies of ACV Heave Dynamics Stabilization, Proceedings of the Fifteenth Canadian Symposium on Air Cushion Technology, Toronto, Canada, September 1981, pp. 99-112.
10. R.C. Dorf, Modern Control Systems, Addison-Wesley, 1967, pp. 62-68.
11. J.R. Amyot, Performance Criteria for Air Cushion heave Dynamics, Preprints of the 1986 CACTS International Conference on Air Cushion Technology, Toronto, Canada, September 1986, pp. 31-37.

12. J.R. Amyot, Passive Control of Air Cushion Heave Dynamics, Canadian Aeronautics and Space Journal, Vol. 32, No. 2, Ottawa, Canada, 1986, pp. 122-130.

13. J.R. Amyot, Defining a Real-Time Model, Simulation, Vol. 38, No. 1, 1982, p. 27.

14. J.R. Amyot, PAROPT: A Parameter Optimization Program, Proceedings of the 1985 ASME International Computers in Engineering Conference and Exhibition, Boston, August 1985, pp. 451-456.

15. J.R. Amyot and G. van Blokland, Parameter Optimization with ACSL, Proceedings of the 1985 Summer Computer Simulation Conference, Chicago, July 1985, pp. 63-68.

16. Guide for Evaluation of Human Exposure to Whole-Body Vibration, International Standard Organization (ISO) Document ISO/DIS 2631, 1972.

17. V.L. Streeter, Fluid Mechanics, 5th Edition, McGraw-Hill, 1971, p. 472.

Chapter 15

EXTERNAL ACTION OF LIFT AIR

15.1 INTRODUCTION

The aerodynamic forces acting on a moving ACV are important not only for the estimation of the required power, but also for the understanding of the stability and the handling characteristics. The air ingested at the inlet of on ACV is forced into the cushion chamber and escapes under the skirt as a jet into the ambient fluid flow. The jet interacts with the ambient flow and the ground/water surface. The interaction with the ambient flow is very complex and has not yet been clarified in detail.

The operation of an ACV over water differs from that over land in one important aspect. The water surface is deformed from the horizontal by the action of the air cushion, resulting in a loss of useful hover height. It is necessary to understand the behaviour of an ACV hovering over water, in order to estimate the relation between the air flow rate, the hover height measured from the free water surface, the cushion lift and the corresponding power requirements of an ACV. For SES the hover height affects the hull bouyancy and cushion pressure. However, very little work on air-water interface theory has been done to date.

In the present chapter we first discuss the interference thrust of a moving ACV. The interference thrust is caused by the interaction of both the discharging flow under the rim of the vehicle and the ambient flow around the vehicle. Then, considering the case of an ACV without forward speed, the deformation of a free water surface at the lip is studied by means of a lip-flow model.

15.2 INTERACTION WITH ATMOSPHERE

The interaction of the outer ambient flow with the jet flows issuing from the front and rear edges of an air cushion vehicle (ACV) is very important to

the estimation of aerodynamic forces acting on the vehicle. The interaction of the outer flow with the jet flows, especially, causes the cushion pressure to reduce and affects the pressure distribution on the upper surface of the ACV. In the vehicle handling problem, therefore, this interaction is very important because the aerodynamic forces, lift, drag, crosswind force, pitching moment, and rolling moment play important roes.

In earlier works, two kinds of approach have been carried out: one, called *mound flow*, is aimed at determining the aerodynamic lift generated on the upper surface; the other deals with the interaction of the craft's peripheral flow with the atmosphere as a function of forward speed. The former, first analyzed by Strand et al. (ref. 1), was used to discuss the lift force, the position of separation, the effect of the intake position, etc. Cook et al. (ref. 2) applied this method by modifying Tulin's model of cavity flow to include a finite constant pressure wake at the rear of the ACV. Regarding the latter, wind tunnel experiments (ref. 3) have shown the interaction of the forward speed with the annular jet. Five flow regimes occurred as the forward speed was increased: 1) the subcritical regime, 2) the transition regime, 3) the Poisson-Quinton's critical regime, 4) the second critical regime, and 5) the supercritical or jet-flap regime, as sketched in Fig. 15.1. Cooke et al. (ref. 2) and Yasutomi (ref. 4) analyzed these flows by means of an iterative numerical method using one-dimensional momentum theory and conformal mapping.

With regards to the drag force, Ando et al. (ref. 5) pointed out the existence of the interference thrust. Assuming the drag due to the water spray and the frictional drag on the base surface of the ACV are negligibly small, they expressed the drag force D as:

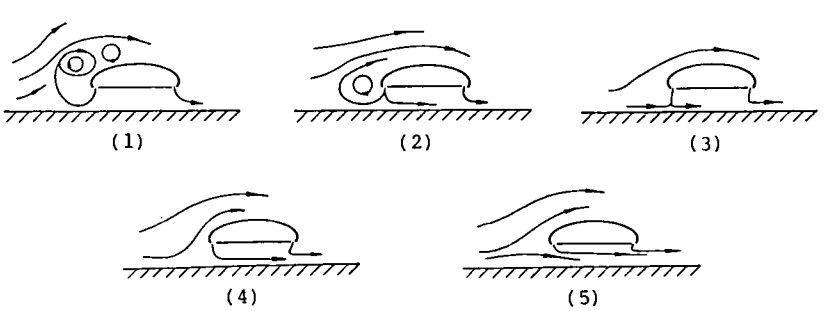

Fig. 15.1 Flow regimes for various forward speeds.

$$D = D_{p'} + D_{mom} - T_{int} + W \tan \alpha - \rho g T_j \qquad (15.1)$$

where $D_{p'}$ is the fictitious parasite drag which may be estimated by the above-mentioned *mound flow* analysis D_{mom} is momentum drag, T_{int} is the interference thrust, $W \tan \alpha$ is the drag due to the attitude α, and $\rho g T_j$ is the propulsive component of the jet momentum measured at the nozzle exit. They asserted that T_{int} was due to: 1) the ingested air at the inlet and the ejected air at the rear of the ACV preventing the ambient flow from separating, 2) the ejected air at its rear effectively causing propulsive work, and 3) the ejected air at its front having some propulsive effect via a standing vortex and the increase of the base pressure at rear surface of the ACV due to the horseshoe vortex of this standing vortex. Thus, T_{int} plays a very important role in the drag force. Therefore, it is important to examine the generating mechanism of the suction force at the front due to the interaction of the jet with the ambient flow.

The main purpose in subsections 15.2.1 to 15.2.3 is to determine the detailed mechanism of generating suction force at the front of the ACV. For this purpose we will treat the transient case of the abrupt starting of the two-dimensional ACV. The discrete vortex method will be applied to simulate this transient flow.

15.2.1 Transient Flow

(i) Conceptional model for compute studies. Let us consider the relative state with the fixed coordinate at the ACV. In the two-dimensional case, the jet emerging from the front edge is regarded as entering into the oncoming uniform flow and that from the rear edge is combined with the streaming uniform flow with same direction. In the transient low, there are many direct numerical methods of the Navier-Stokes equation for a jet issued into the rest of the ambient flow, such as MAC method (e.g., ref. 6); however, it is very hard to carry out the present problem even in the two-dimensional case. Thus, it may be very difficult to analyze exactly the interaction of the ambient flow with the jet flows issuing from the edge-line of the contour of the ACV by using the Navier-Stokes equation.

In the present subsection, we treat a two-dimensional flow around the ACV and use the discrete vortex method. The discrete vortex method has been used by many authors (e.g., refs. 8 and 9); it is especially powerful for the high Reynolds number flows with strong shear. In the present problem, the strong shear flows are formed at the edge of the jet flows issuing into the ambient flow from the front and rear edges of the ACV; so the discrete vortex method might be effective to determine the qualitative behavior of the interference. To examine the conceptional mechanism of generating the interference thrust, we treat a simple model of the ACV: the plenum chamber type with external cushion air supply, as shown in Fig. 15.2.

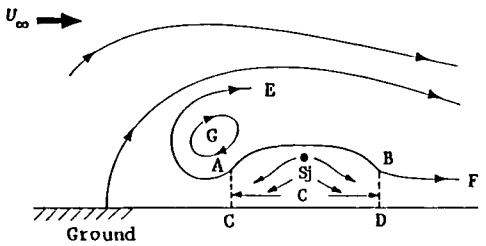

Fig. 15.2 Physical model.

The outline of the relative flow pattern with the fixed ACV is shown in this figure, where U_∞ is the forward speed, S_j is the air supply position, and AC and BD are the front and rear exits of the jet issuing to the ambient flow. ACBD becomes, therefore, the plenum chamber. The free shear flow of the jet emerged from A concentrates vortices and forms a cluster of the many concentrated vortices G, and the free shear flow from B flows downward and concentrates vortices far downstream just like the starting jet in the rest ambient flow. We assume that the Reynolds number is high enough to apply the discrete vortex method.

In the discrete vortex method, the fluid flow is assumed to be incompressible and inviscid, so that the governing equation is:

$$\Delta\phi = 0 \tag{15.2}$$

where Δ is the Laplacian and ϕ is the velocity potential. In the earlier works of the discrete vortex method, the conformal mapping technique has been used; however, it is very difficult to obtain the mapping function analytically in this problem due to the complexity of the shape of the ACV.

There are mainly two methods to determine the issuing vortex in the analysis of the discrete vortex method (e.g., ref. 10): 1) the rate of the circulation of the vortex sheet per unit length $\Gamma(t)$ with which a vortex sheet leaves the edge A or B is given by $d\Gamma(t)/dt = U(t)^2/2$, where t is time and U(t) is the tangential velocity at the edge of the contour of the ACV, so that the centroid of the vortex sheet shed in the small time interval Δt is located at $U(t)\Delta t$ extended tangentially from the edge point, and 2) the location of the centroid of the vortex sheet shed in the small interval is determined in advance and its strength is obtained by using the Kutta condition. In the former method, we need iteration to obtain the position and strength; on the other hand, the latter method does not need iteration, so that it does not use more CPU time than the former. In the present work, the latter method is used.

The last problem in constructing the governing equation is how to express

the air supply at S_j in this analytical method. If the gap clearance, AC and BD, are very small compared with the maximum height of the ACV, the cushion pressure in ACBD may be almost uniform, so that the velocity profile at AC and BD may be uniform. However, if the gap clearance is not so small, the velocity profile at the exits may be influenced remarkably by the interaction of the ambient flow. We therefore propose two models in this analysis. One is to give the velocity profiles at the nozzle exits, and another is to give the mass flux and the air supply position. We here call the former as *velocity-distribution model* and the latter as *concentrated source model*. The former is simulated by the source distribution across the nozzle exits, AC and BD, and the latter is done by the source distribution near S_j in the cushion chamber, as for simulation of the air supply.

In the following analysis, we take the typical length, velocity, and time as the chord length c, flight speed U_∞, and c/U_∞, respectively. The gap clearance normalized with c is defined also as h. The shedding circulations from A and B are denoted by γ_{Ak} and γ_{Bk} (k = 1,2,..), respectively. The locations of the circulation of the vortex sheet shed in the small interval from the edges A and B are assumed to the extended positions from edge points along the contour of the ACV, as shown in Fig. 15.3, whose extended length is defined as E.

Using the complex variable z (=x + iy), the complex potential F(z) ($=\phi + i\psi$), where ϕ and ψ are respectively the velocity potential and the stream function, is expressed as:

$$F(z) = z + \frac{i}{2\pi}\int_{AS_oB}\gamma(s)\ln\{\frac{z - z(s)}{z - z^*(s)}\}ds + \frac{i}{2\pi}\sum_{k=1}^{K_A}\gamma_{Ak}\ln\{\frac{z - z_{Ak}}{z - z^*_{Ak}}\}$$
$$+ \frac{i}{2\pi}\sum_{k=1}^{K_B}\gamma_{Bk}\ln\{\frac{z - z_{Bk}}{z - z^*_{Bk}}\} + \frac{1}{2\pi}\int_0^h m_A(\eta)\ln\{(z + 1/2 - i\eta)(z + 1/2 + i\eta)\}d\eta$$
$$+ \frac{1}{2\pi}\int_0^h m_B(\eta)\ln\{(z - 1/2 - i\eta)(z - 1/2 + i\eta)\}d\eta + \frac{1}{2\pi}\int_{S_j} m(s)\ln\{z - z(s))$$
$$(z - z^*(s))\}ds \qquad (15.2)$$

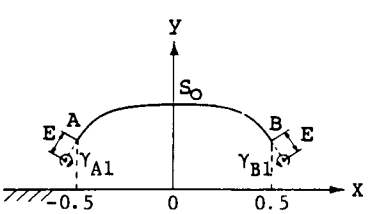

Fig. 15.3 Vortices shed from both edges, A and B.

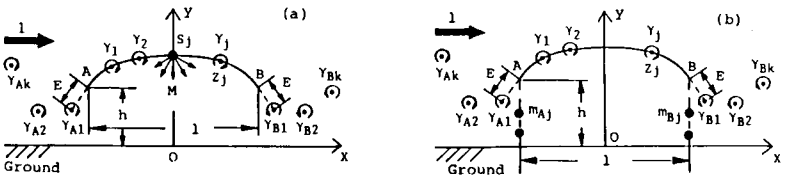

Fig. 15.4 Numerical models: (a) concentrated source model; (b) velocity-distribution model.

where S_j denotes the position of the air supply, $\gamma(s)$ is vorticity distribution, $m(s)$ and $m_{A,B}(\eta)$ are source distribution and z^* denotes the conjugate of z.

In the velocity-distribution model, we put $m(s) = 0$, and we put $m_A(\eta) = m_B(\eta) = 0$ in the concentrated source model. The shedding circulations, γ_{Ak} and γ_{Bk}, are flown with the induced velocity at their points:

$$\left.\begin{aligned} \frac{dz^*_{Ak}}{dt} &= \lim_{z \to z_{Ak}} \left[\frac{dF}{dz} - i\,\frac{\gamma_{Ak}}{2\pi}\ln(z - z_{Ak})\right] \\ \frac{dz^*_{Bk}}{dt} &= \lim_{z \to z_{Bk}} \left[\frac{dF}{dz} - i\,\frac{\gamma_{Bk}}{2\pi}\ln(z - z_{Bk})\right] \end{aligned}\right\} \tag{15.13}$$

Furthermore, the Kelvin Theorem is required in every interval:

$$\sum_{k=1}^{K_A} \gamma_{Ak} + \sum_{k=1}^{K_B} \gamma_{Bk} + \int_{AS_oB} \gamma(s)ds = 0 \tag{15.4}$$

The governing integral equation is obtained from eqn. (15.2) and the flow tangency condition at the upper surface of the contour of the ACV:

$$v = u \tan\theta \tag{15.5}$$

where θ is the gradient angle of the contour with respect to the x-axis, and

$u - iv = dF/dz$ at $z \epsilon AS_oB$.

The velocity components of x and y denoted by u and v are given:

$$\begin{aligned} u(x,y) = 1 &+ \frac{1}{2\pi}\int_{AS_oB} \gamma(s)[K_y(x,y;x(s),y(s)) - K_y(x,y;x(s),-y(s))]ds \\ &+ \frac{1}{2\pi}\sum_{k=1}^{K_A} \gamma_{Ak}[K_y(x,y;x_{Ak},y_{Ak}) - K_y(x,y;x_{Ak},-y_{Ak})] + \frac{1}{2\pi}\sum_{k=1}^{K_B} \gamma_{Bk}[K_y(x,y; \\ &x_{Bk},y_{Bk}) - K_y(x,y,;x_{Bk},-y_{Bk})] + \frac{1}{2\pi}\int_0^h m_A(\eta)[K_x(x,y;-1/2,\eta) + K_x(x,y; \\ &-1/2,-\eta)]d\eta + \frac{1}{2\pi}\int_0^h m_B(\eta)[K_x(x,y;1/2,\eta) + K_x(x,y;1/2,-\eta)]d\eta \\ &+ \frac{1}{2\pi}\int_{S_j} m(s)[K_x(x,y;x(s),y(s)) + K_x(x,y;x(s),-y(s))]ds \end{aligned} \tag{15.6}$$

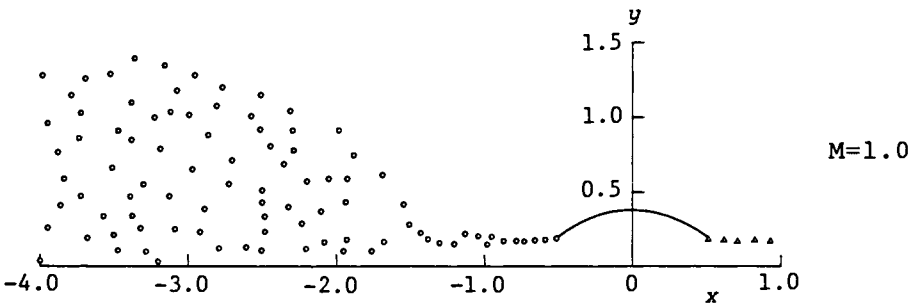

Fig. 15.5 Patterns of vortices (T = 9.0): 0, clockwise circulation from the front edge; •, anti-clockwise circulation from the front edge; Δ, anti-clockwise circulation from the rear edge.

$$v(x,y) = -\frac{1}{2\pi}\int_{AS_oB} \gamma(s)[K_x(x,y;x(s)),y(s)) - K_x(x,y;x(s),-y(s))]ds$$

$$-\frac{1}{2\pi}\sum_{k=1}^{K_A} \gamma_{Ak}[K_x(x,y;x_{Ak},y_{Ak}) - K_x(x,y;x_{Ak},-y_{Ak})] - \frac{1}{2\pi}\sum_{k=1}^{K_B} \gamma_{Bk}[K_x(x,y;x_{Bk},y_{Bk})$$

$$- K_x(x,y;x_{Bk},-y_{Bk})] + \frac{1}{2\pi}\int_0^h m_A(\eta)[K_y(x,y;-1/2,\eta) + K_y(x,y;-1/2,-\eta)]d\eta$$

$$+ \frac{1}{2\pi}\int_0^h m_B(\eta)[K_y(x,y;1/2,\eta) + K_y(x,y;1/2,-\eta)]d\eta + \frac{1}{2\pi}\int_{S_j} m(s)$$

$$\times [K_y(x,y;x(s),y(s)) + K_y(x,y;x(s),-y(s))]ds \tag{15.7}$$

where

$$K_x(x,y;x(s),y(s)) = (x - x(s))/\{(x - x(s))^2 + (y - y(s))^2\}$$

$$K_y(x,y;x(s),y(s)) = (y - y(s))/\{(x - x(s))^2 + (y - y(s))^2\}$$

If (x,y) approach to $(x(s_o),y(s_o))$ from the normal direction of the upper surface of the ACV, we have the following relations:

$$\frac{1}{2\pi}\int_{AS_oB} \gamma(s)K_y(x,y;x(s),y(s))ds = \frac{1}{2\pi}\fint_{AS_oB} \gamma(s)K_y(x,y;x(s),y(s))ds$$

$$+ \frac{1}{2}\gamma(s_o)\cos\theta \tag{15.8}$$

$$\frac{1}{2\pi}\int_{AS_oB} \gamma(s)K_x(x,y;x(s),y(s))ds = \frac{1}{2\pi}\fint_{AS_oB} \gamma(s)K_x(x,y;x(s),y(s))ds$$

$$+ \frac{1}{2}\gamma(s_o)\sin\theta$$

where integral sign $\fint$ means the Cauchy type integration. Similarly, we have the following relations:

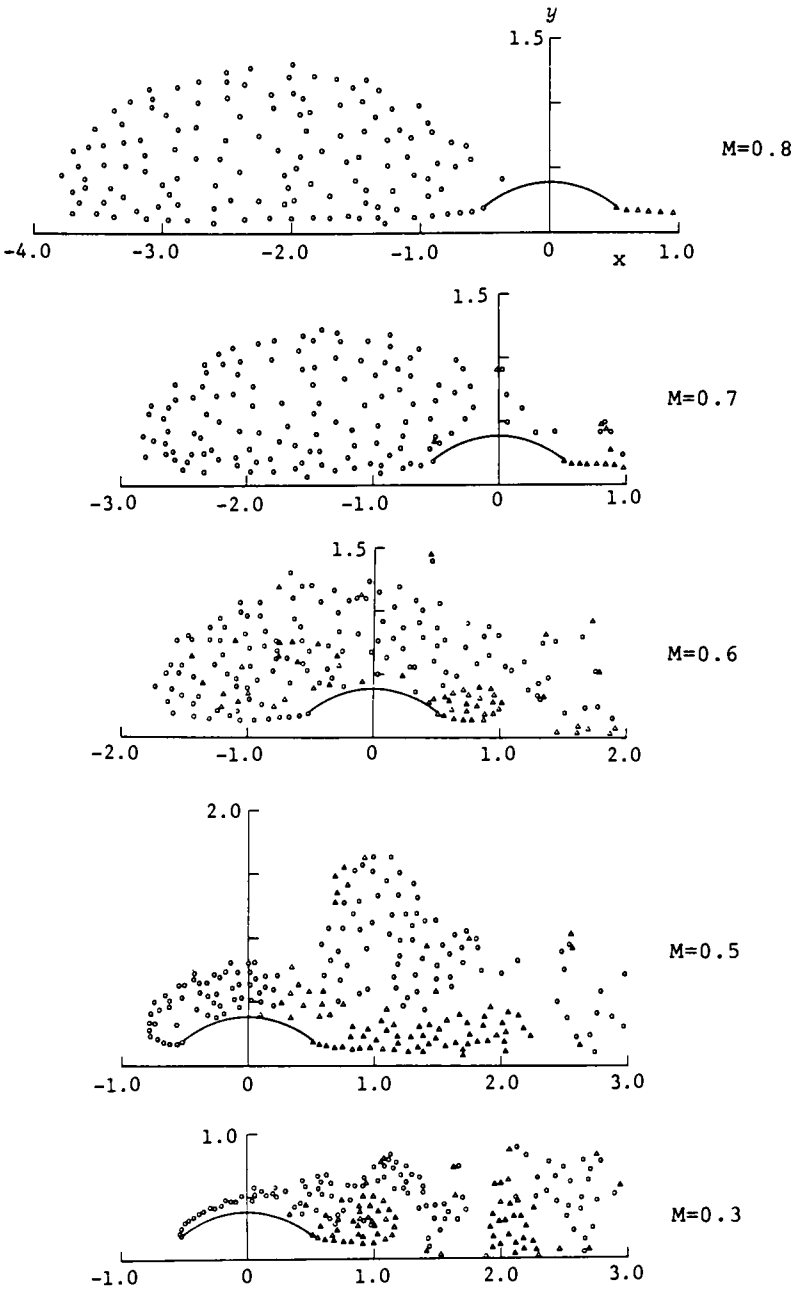

Fig. 15.5 (Continued - A).

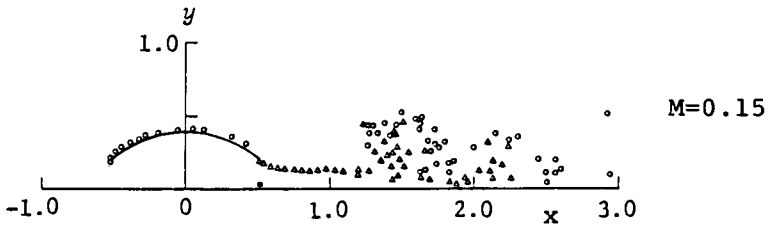

Fig. 15.5 (Continued - B).

$$\frac{1}{2\pi}\int_{S_j} m(s)K_y(x,y;x(s),y(s))ds = \frac{1}{2\pi}\fint_{S_j} m(s)K_y(x,y;x(s),y(s))ds + \frac{1}{2}m(s_o)\cos\theta \qquad \text{for } s_o\epsilon S_j \tag{15.9}$$

$$\frac{1}{2\pi}\int_0^h m_{A,B}(\eta)K_y(x,y;\pm 1/2,\eta)d\eta = \frac{1}{2\pi}\fint_0^h m_{A,B}(\eta)K_x(x,y;\pm 1/2,\eta)d\eta$$

$$\text{for } x \to -1/2-0 \text{ or } 1/2+0 \text{ and } 0<y<h \tag{15.10}$$

$$\frac{1}{2\pi}\int_0^h m_{A,B}(\eta)K_x(x,y;\mp 1/2,\eta)d\eta = \frac{1}{2\pi}\fint_0^h m_{A,B}(\eta)K_x(x,y;\mp 1/2,\eta)d\eta \mp \frac{1}{2}m_{A,B}(y)$$

$$\text{for } x \to -1/2-0 \text{ or } 1/2+0 \text{ and } 0<y<h \tag{15.11}$$

Using eqns. (15.10) and (15.11), we have the boundary conditions at the nozzle exits from eqn. (15.6) in the velocity-distribution model:

$$1 + \frac{1}{2\pi}\int_{AS_oB} \gamma(s)[K_y(x,y;x(s),y(s)) - K_y(x,y;x(s),-y(s))]ds$$

$$+ \frac{1}{2\pi}\sum_{k=1}^{K_A} \gamma_{Ak}[K_y(x,y;x_{Ak},y_{Ak}) - K_y(x,y;x_{Ak},-y_{Ak})] + \frac{1}{2\pi}\sum_{k=1}^{K_B} \gamma_{Bk}[K_y(x,y;$$

$$x_{Bk},y_{Bk}) - K_y(x,y,;x_{Bk},-y_{Bk})] + \frac{1}{2\pi}\fint_0^h m_A(\eta)[K_x(x,y;-1/2,\eta) + K_x(x,y;$$

$$-1/2,-\eta)]d\eta + \frac{1}{2\pi}\fint_0^h m_B(\eta)[K_x(x,y;1/2,\eta) + K_x(x,y;1/2,-\eta)]d\eta$$

$$\mp \frac{1}{2}m_{A,B}(y) = u_\mp(y) \qquad \text{for } x = \mp 1/2 \text{ and } 0<y<h \tag{15.12}$$

where $u_+(y)$ and $u_-(y)$ are the velocity distributions at the nozzle exits, BD and AC, respectively, which are given *a priori*. Thus the governing integral equations (15.4), (15.5) and (15.12) are given for unknown functions, $\gamma(s)$, $m(s)$, $m_A(\eta)$, and $m_B(\eta)$. The shedding circulations, γ_{Ak} and γ_{Bk}, are constant and are flown down by eqn. (15.3). The initial values, γ_{A1} and γ_{B1}, are determined by applying the Kutta condition. The flow tangency condition is also satisfied at both edges of the contour of the ACV.

(ii) Viscosity effect. In the above mentioned governing equation, the effect of viscosity is ignored. To estimate its effect, mainly two models have

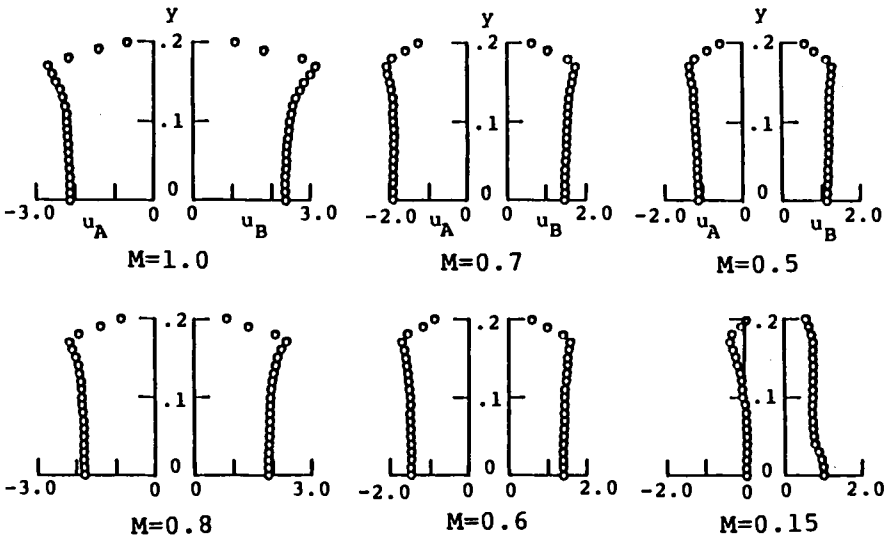

Fig. 15.6 Velocity profile at nozzle exits in the case of T = 9.0: u_A, front edge; u_B, rear edge.

been proposed: one estimates the dissipation of circulation due to the viscosity (e.g., ref. 10); the other estimates the diffusion effect of viscosity (ref. 7).

From the Navier-Stokes equation, we have:

$$D\omega/Dt = \Delta\omega/R_e \tag{15.13}$$

where R_e is the Reynolds number and ω is vorticity. We introduce relative coordinates (x',y'), given by $x' = x + \int^t u dt$ and $y' = y + \int^t v dt$, where (u,v) are the velocity components at the vortices. Then the Navier-Stokes equation (15.13) is given by:

$$\partial\omega/\partial t = \Delta'\omega/R_e \tag{15.14}$$

where $\Delta' = \partial^2/\partial x'^2 + \partial^2/\partial y'^2$. In the relative coordinates, $1/R_e$ is regarded as the diffusion factor D in the diffusion equation, so that we may model the above equation (15.14) as the random walk problem (ref. 7). Let us define τ as the time interval of random walk step $\pm a$. Then the probability of displacement ma at n-th step is given by:

$$P_n(m) = \frac{n!}{2^n} / \left(\frac{n+m}{2}!\ \frac{n-m}{2}!\right)$$

Using the Stirling formula in the above equation for $n \to \infty$, we may have the diffusion factor D as:

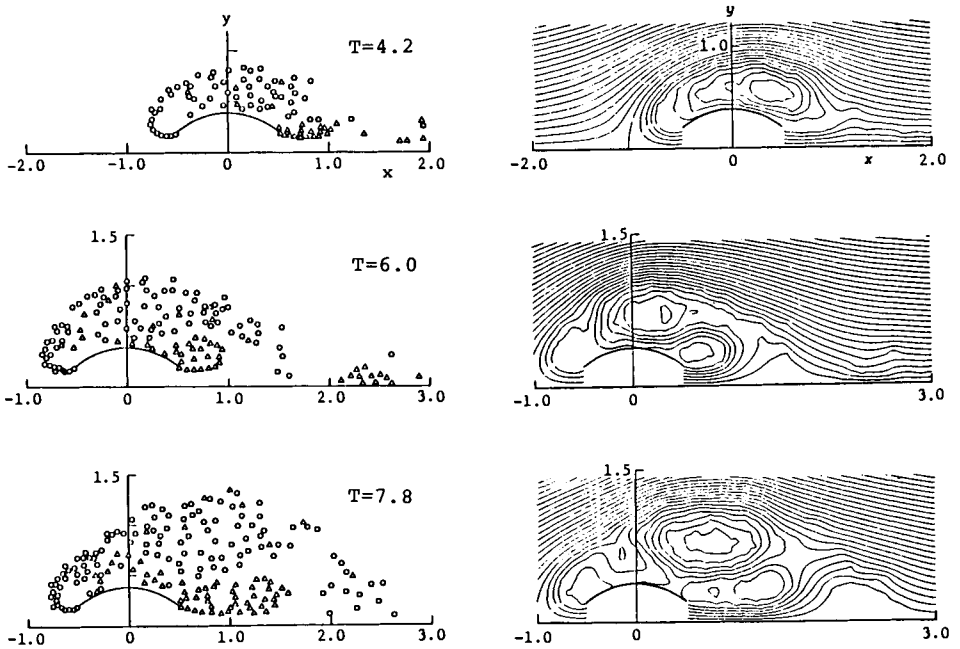

Fig. 15.7 Flow patterns and streamlines for M = 0.5 (see Fig. 5.5 for symbols).

$D = a^2/(2\tau)$

Therefore, the Reynolds number R_e is given by:

$$R_e = 2\tau/a^2 \tag{15.15}$$

This model proposed by Chorin (ref. 7) implies that the interior flow of the cluster of vortices is not necessarily expressed correctly by this method; however, the overall flow behavior obtained by this model may be correct statistically for high Reynolds number flow.

Let us consider the dissipation of the circulation due to the viscosity (e.g., ref. 10). In eqn. (15.14), we impose the following initial condition:

$$\omega = \omega_o \delta(x')\delta(y') \quad \text{at } t = 0 \tag{15.16}$$

where $\delta(x)$ is the Dirac delta function. When we use the Fourier transformation, the vorticity ω is expressed as:

$$\omega = \frac{1}{(2\pi)^2} \iint_{-\infty}^{\infty} \Omega(k_x, k_y; t)\exp(ik_x x' + ik_y y')dk_x dk_y$$

Taking eqn. (15.16) into account, we have from eqn. (15.14):

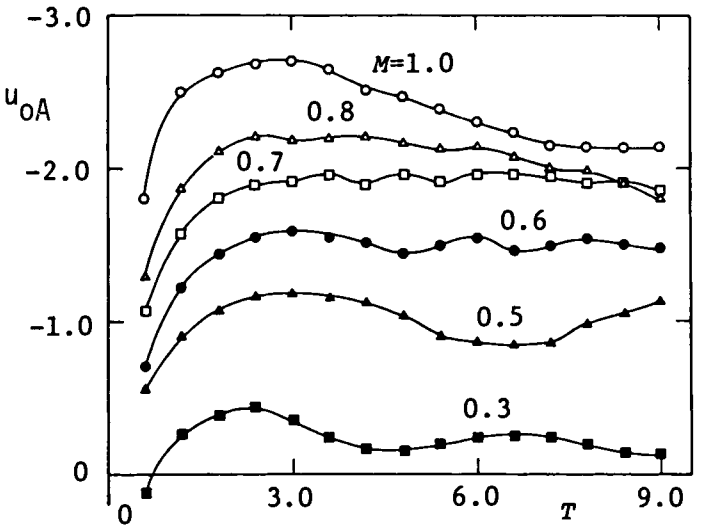

Fig. 15.8 Velocity u_{oA} on the ground just at the front edge.

$$\omega = \frac{\omega_o}{2}\frac{R_e}{2t}\exp\left(-\frac{R_e}{4t}r^2\right) \tag{15.17}$$

where $(x',y') = (r\cos\theta,\ r\sin\theta)$. The circulation Γ $(=2\pi\int_0^r \omega r dr)$ is given from eqn. (15.17):

$$\Gamma/\Gamma_o = 1 - \exp(-R_e r^2/(4t)) \tag{15.18}$$

where Γ_o is the initial circulation $(t = 0)$.

Another dissipation model is given by the following consideration (e.g., ref. 11). In eqn. (15.13), we assume that the vorticity ω is expressed as the separated form $\omega = H(t)f(x,y)$. Substituting this relation into eqn. (15.13), we have:

$$\frac{DH}{Dt}\frac{R_e}{H} = \frac{\Delta f}{f} = -1/\hat{a}^2$$

where $\hat{a}$ is a non-dimensional constant. From this equation, $H(t)$ is given by:

$$H(t) = H_o\exp(-t/(\hat{a}^2R_e)) \tag{15.19}$$

where H_o is vorticity at $t = 0$. The function $f(x,y)$ is related with:

$$\Delta f = -f/\hat{a}^2$$

Therefore, the stream function is governed by:

$$\Delta\psi = -\psi/\hat{a}^2$$

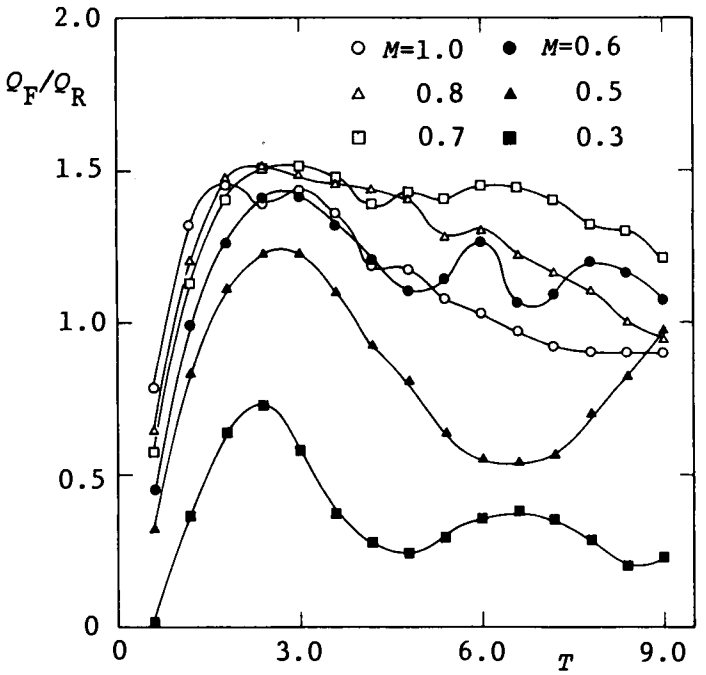

Fig. 15.9 Flow flux ratio.

As pointed out by Batchelor (ref. 11), it may be difficult to solve for the flow satisfying this equation. However, the solution is a simple one if it is expressible as a separated form. We note that â is not determined.

From these approaches, we may suppose that the random walk model might be valid for the case where the small vortices concentrate and become a cluster of vortices due to the diffusion. On the other hand, the dissipation model might be valid for the time-development of the large cluster of vortices due to the dissipation.

(iii) Numerical procedure. To solve numerically the unknowns, $\gamma(s)$, $m(s)$, $m_A(\eta)$, and $m_B(\eta)$, given in (i), we use here the panel method, which is called the *vortex-lattice method*. We divide the contour of the ACV to N and denote the coordinate of nodal points as z_j (j=1, 2, .. , N) as shown in Fig. 15.4. We approximate the integral as follows:

$$\int_{AS_oB} \gamma(s)\ln\left(\frac{z - z(s)}{z - z^*(s)}\right)ds = \sum_{j=1}^{N} \gamma_j \ln\left(\frac{z - z_j}{z - z_j^*}\right) \tag{15.20}$$

This approximation means that the vortex distribution $\gamma(s)$ is given by

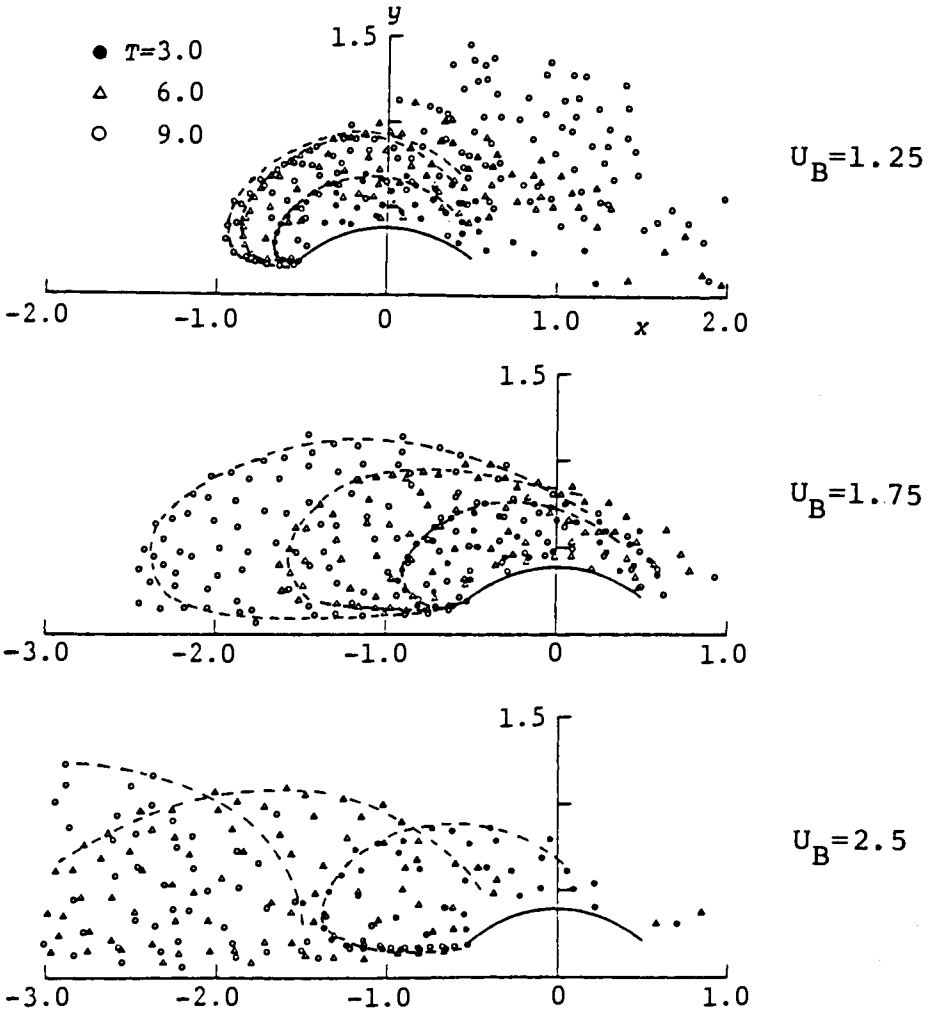

Fig. 15.10 Vortices history from the front edge ($u_+ = -u_- = U_B$).

$$\gamma(s) = \sum_{j=1}^{N} \gamma_j \delta(z - z_j)$$

In the concentrated source model, we suppose that the width of air supply to the cushion chamber is very small. Therefore, we approximate the following integral as:

$$\int_{S_j} m(s)\ln\{(z - z(s))(z - z^*(s))\}ds = M \ln\{(z - z_M)(z - z_M^*)\} \quad z\epsilon S_j \qquad (15.21)$$

where

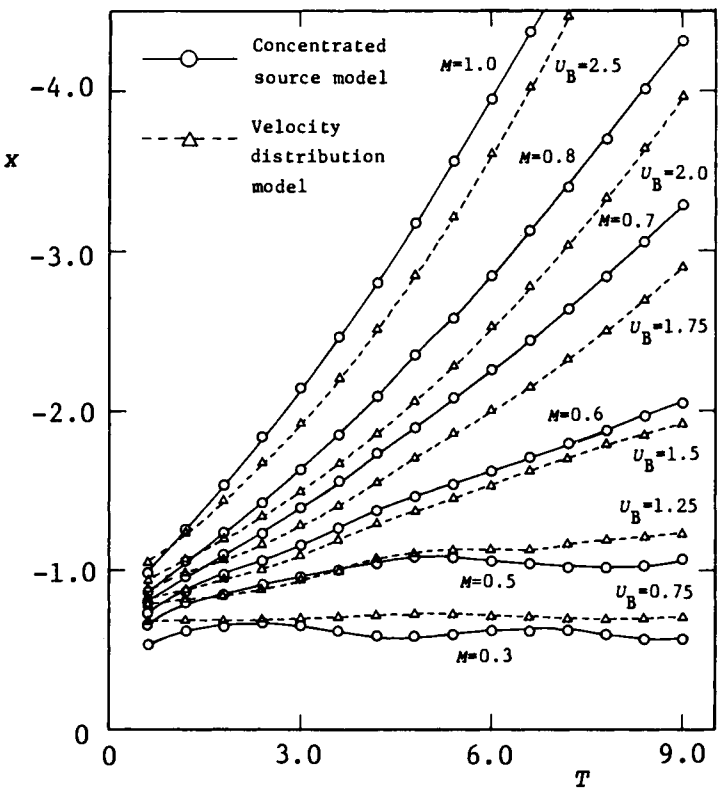

Fig. 15.11 Position of upward stagnation point on the ground ($u_+ = -u_- = U_B$).

$M = \int_{S_j} m(s)ds$

In the velocity-distribution model, we assume that $m_A(\eta)$ and $m_B(\eta)$ are given by:

$$m_{A,B}(\eta) = \sum_{j=1}^{L} m_{Aj,Bj}\, \delta(\eta - \eta_j) \tag{15.22}$$

The boundary condition (15.5) is satisfied at the mid-point of each panel:

$$\left.\begin{aligned} &z_{cj} = (z_{j-1} + z_j)/2, \quad (j=2, 3, .., N) \\ &z_{c0} = z_A, \quad z_{cN+1} = z_B \end{aligned}\right\} \tag{15.23}$$

where z_A and z_B are corresponding to the edges of the contour, A and B. Substituting eqns. (15.20), (15.21), and (15.22) into eqns. (15.6) and (15.7), respectively, and setting $z = z_{cj}$ (j=1, 2, .., N+1), we have (N+1) simultaneous algebraic equations with N unknowns γ_j and shedding unknown circulations γ_{A1},

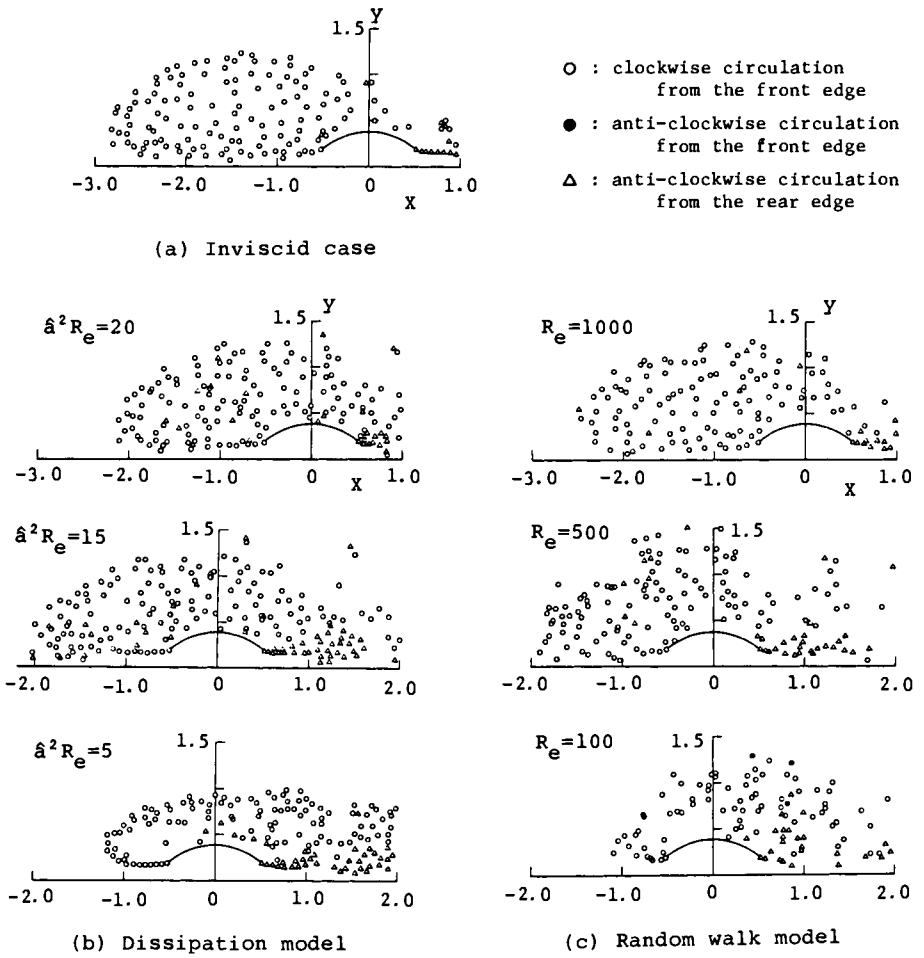

Fig. 15.12 Viscosity effect on vortices patterns (M = 0.7 and T = 9.0).

γ_{B1} in the concentrated source model from (15.5). To obtain the unique solution, we apply the Kelvin Theorem (15.4). Thus, we have (N+2) simultaneous equations with (N+2) unknowns. We must note in the concentrated source model that there is the case where the control point z_{cj} is equal to z_M. In this case, we need to apply (15.9).

In the vortex-distribution model, we may obtain similarly (N+2+2L) simultaneous equations by using eqns. (15.12) and (15.22).

The position of the shedding circulations is given by the condition that these vortices are flown down with induced velocity as given by eqn. (15.3). In numerical calculation, we use:

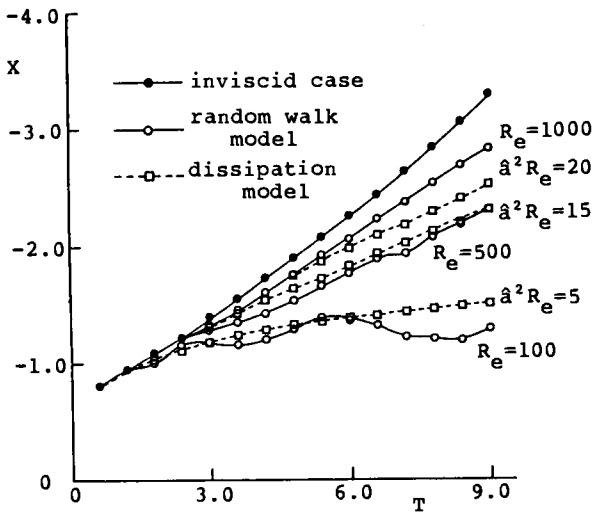

Fig. 15.13 Position of upward stagnation point on the ground (M = 0.7).

$$z_{Ak,Bk}(t + \Delta t) = z_{Ak,Bk}(t) + (dz^*_{Ak,Bk}/dt)^*\Delta t \tag{15.24}$$

where $dz^*_{Ak,Bk}/dt$ is obtained from eqn. (15.3) at t=t

In the present numerical calculation, new shedding circulations, γ_{A1} and γ_{B1}, from A and B are introduced at every twice travelling time, that is, $2\Delta t$. The position of the new shedding circulations is extended from both edges A and B along the line of the contour and its extended length is taken as E, as already mentioned (Fig. 15.3). In the actual calculation, various sets of E and Δt were determined beforehand, and we see that they depend somewhat on the flow pattern although the overall pattern is almost the same. We here set Δt = 0.03 to save computational time.

Brown et al. (ref. 12) show that, in the shear flow mixing two different uniform velocities, there is a coherent structure, and the vortices concentrate and form a large cluster of vortices. This cluster of vortices flows down with mean velocity of the different uniform flow. If the speed of the ACV is equal to half times of the exit velocity of the jet from the front edge, we may imagine that the cluster of concentrated vortices develops near the front edge. When we set $-u_-(y) = u_+(y) = 2$ and calculate several values of E, we see that the developing cluster of concentrated vortices is almost formed near the front edge at E = 0.02. For this reason, we choose here E as 0.02.

In the actual calculation, we furthermore assume: (1) if a shedding vortex approaches to the contour nearer than 0.01, or goes across it in the time interval Δt, its circulation is set as zero by the reason that the vortex

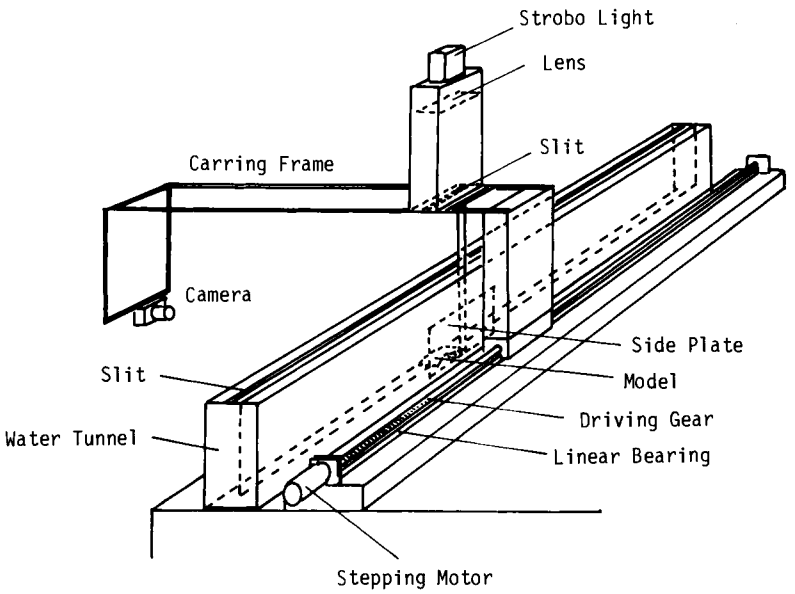

Fig. 15.14 Outline of experimental equipment.

decays by the dissipation of viscosity of the boundary layer at the surface, (2) if a shedding vortex approaches or goes across the ground surface, its circulation is also set as zero, and (3) if the distance between shedding vortices is remarkably small, the induced velocity due to the adjacent vortex becomes large unrealistically, so that the cut-off radius introduced by Chorin (ref. 7) is used and it is taken as 0.02.

15.2.2 Computer Results of Transition Flow

To show the power of the present method, we choose a simple ACV shape. The contour is an arc and its maximum height ratio is 0.18 with respect to the chord length; so there seems to be no separation on the upper surface of the ACV even without the emerged jet. Furthermore, we set N as 16, and gap clearance is taken as 0.2, to save computational time. The vortices flown down four times more from the center of the ACV are gathered as a single vortex with same total circulation. In the velocity-distribution model, the concentrated sources are set with equi-distance as shown in Fig. 15.4 and L is taken as 10.

(i) Large air gap clearance. If the hovering height becomes comparatively large, we suppose the interaction between the front jet and the ambient flow becomes strong, that is, the local pressure near the front edge may be assumed not to be constant. In this case, the velocity profile across the jet from the

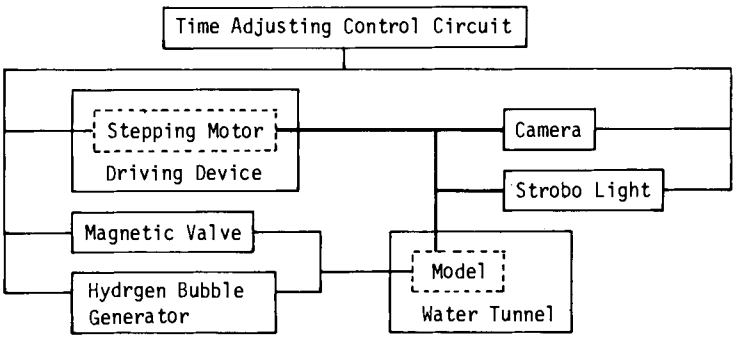

Fig. 15.15 Block diagram of flow visualization system.

front edge is not uniform and is influenced by the forward speed of the ACV. Therefore, we adopt here the concentrated source model to simulate this case. Fig. 15.5 shows the numerical calculated results at T = 9.0, where T is the total time from abrupt starting with uniform speed. This fixture shows the relative flow with the coordinate fixed at the ACV; M is the air supply flux to the cushion chamber. We see that there may be four regimes of flow pattern, depending on the value of M. For $M > 0.7 \sim 0.8$, the cluster of vortices is developing and flows upstream with time. The velocity profile of the jet at the front and rear edges is shown in Fig. 15.6. From this figure, we see in this case that the jet velocity at the front edge is larger than the forward speed. For $M \simeq 0.7 \sim 0.8$, the cluster of the concentrated vortices develops near the front edge and it is almost stationary. The vortices shed from the front edge are gathered in it and they scarcely flow downstream.

Let us define the mean jet velocity at the front edge by V. Then we guess from Brown et al. (ref. 12) that the flow velocity of vortices from the front edge is about V/2. If the forward speed U_∞ is almost V/2, the vortices shed from this edge are concentrated near the front. Fig. 15.6 shows that the jet velocity at the front edge is almost 2 for $M = 0.7 \sim 0.8$. For $M = 0.6 \sim 0.5$, the vortices shed from the front edge are concentrated partially near the front edge and flow downward partially. The vortices shed downstream interact with the vortices shed from the rear edge. The detailed flow pattern for M = 0.5 is shown in Fig. 15.7. The vortices are concentrated at T = 4.2 and form a cluster at rear part of the contour, then the pressure near the rear edge decreases so that the vortices from the rear are flown upward and the cluster is raised up by them and flown downward (see T = 7.8). Afterwards, a new cluster of vortices is formed by the shedding vortices from the front edge.

For $M = 0.2 \sim 0.15$, the concentrated vortices near the front edge are not formed, and the vortices from the front edge are flown downstream and interact

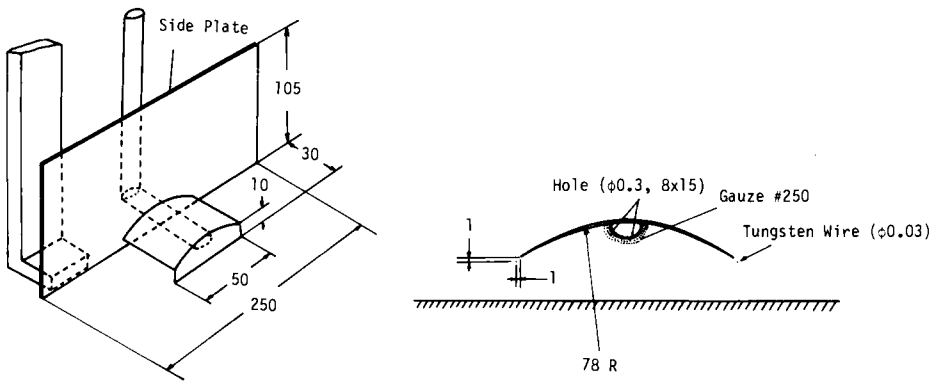

Fig. 15.16 Model geometry.

with rear vortices remarkably. M = 0.15 seems to be the limit at which the cushion chamber is maintained. Fig. 15.8 shows the relation between the jet velocity u_{oA} on the ground just at the front edge and time T. We note that u_{oA} is almost the mean velocity of the jet. For the case where M is less than 0.6, u_{oA} seems to oscillate as mentioned above. Fig. 15.9 shows the flow flux ratio Q_F/Q_R of the front edge against the rear edge and an oscillation.

(ii) Small air gap clearance. In this case, the ambient pressures at the front and rear edges are unknown and we suppose they are uniform at the nozzle exits. To determine them, it may be necessary to solve the flow within the cushion chamber just like Cook et al. (ref. 2). In the transient case treated here, it is very difficult to analyze the whole flow, so we here assume the velocity distribution at the nozzle exits, that is, we assume the uniform profile and the front jet velocity is equal to the rear one. Fig. 15.10 shows the vortices history from the front edge. The dotted lines in this figure show the contour of the cluster of concentrated vortices. We easily see from this figure that there are the first three patterns mentioned in the previous section (i).

Figure 15.11 shows the position of the upward stagnation on the ground. It is seen that the tendency is almost the same in both the velocity-distribution model and the concentrated source model.

(iii) Effect of viscosity. We here calculate the dissipation model given by eqn. (15.19) and the random walk model to determine the effect of viscosity. Fig. 15.12 shows the results of these viscosity models at the same condition. The overall pattern of the shedding vortex is not so remarkably influenced by the viscosity, but the penetration of the vortices shed from the front edge is smaller due to the viscosity; therefore, the upstream stagnation point on the

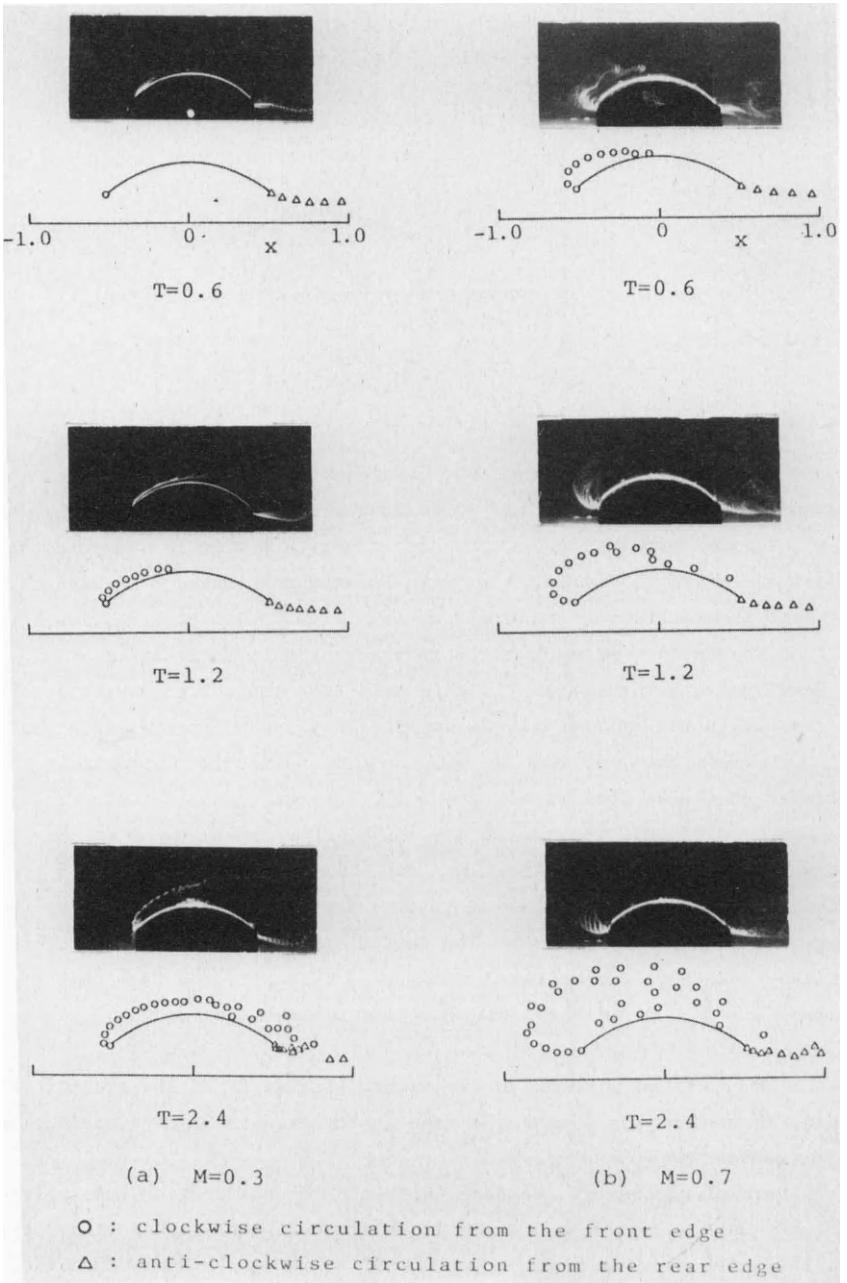

Fig. 15.17 Comparison of vortices patterns with numerical results.

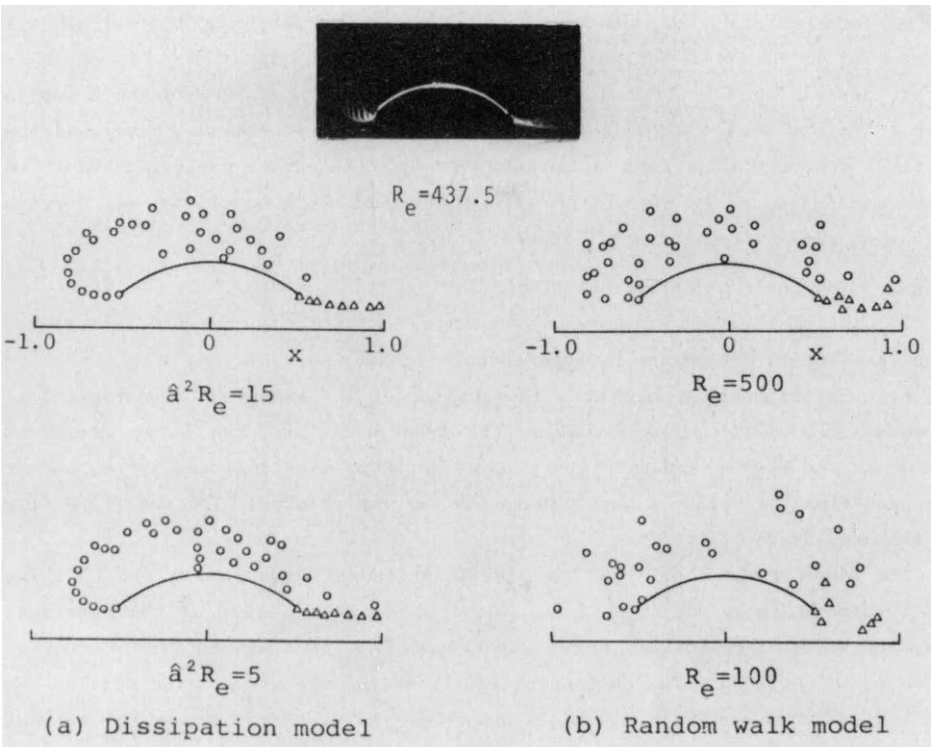

Fig. 15.18 Viscosity effect for M = 0.7 and T = 2.4; (see Fig. 15.17 for symbols).

ground is closer to the front edge, as shown in Fig. 15.13. This fact implies that the effect of viscosity corresponds to the decrease of the air supply flux M in the inviscid case. This figure further implies that the viscosity effect makes the time to the stationary flow shorter. Hence, we need to estimate the viscosity effect as accurately as possible to obtain the stationary flow. However, the present authors have not confirmed yet that we are able to arrive at the stationary flow by means of the present numerical method.

The absolute jet velocity at the front nozzle of the ACV is given by $V - U_\infty$, where V is the mean jet velocity nearly equal to M/(2h) for the given clearance h from the ground. Therefore, it might be necessary to take the Reynolds number as $R_e = (V - U_\infty)c/\nu$ for the front jet and $R_e = (V + U_\infty)c/\nu$ for the rear jet, respectively. It implies that the effect of the viscosity of the front jet is more important than that of the rear one. In the present calculation, however, the same factor in the viscosity models is assumed because the interaction of vortices shed from the front edge with ones from the rear edge

does not have a strong influence on the vortex pattern around the ACV.

The main difference between the random walk model and the dissipation model is the concentration of the vortices. In the former, the contour of the cluster of vortices is not so smooth; on the other hand, in the latter it is smooth especially for the small time T. In the former model, as the Reynolds number becomes small, the concentration of vortices is not so clear, and the vortices are partially flown downstream, so that the vortex pattern seems to be more oscillatory. By comparison with the random walk model, we may suppose that $\hat{a}$ in the dissipation model is nearly 0.2.

15.2.3 Flow Visualization of Transient Flow

To confirm the fact obtained by numerical calculation, the flow visualization was carried out by the hydrogen-bubble method.

(i) Experimental equipment. The outline of the experimental equipment is shown in Fig. 15.14. To visualize the transient flow, the water tunnel is fixed and the model with the camera moves abruptly with constant speed, and at the same time the water is supplied to the cushion chamber. The mass flow flux is measured by the flow meter.

The block diagram of the flow visualization is shown in Fig. 15.15. The model used is shown in Fig. 15.16, whose shape is the same as the numerical one, and is set vertically in the water tunnel. The tungsten wire is set as shown in this figure. The photograph is taken from the side of the model.

(ii) Comparison with numerical results. Figure 15.17 shows the typical comparison with the numerical results which neglected the viscosity effect. It is seen that the overall flow feature is the same as predicted by the numerical calculation. Especially, we can see that the cluster of vortices near the front edge is shown in these photos, although this fact was much clearer to the naked eye. The comparison with numerical results including viscosity effects is shown in Fig. 15.18. It is seen that the viscosity effect is not very significant in this short starting time and high Reynolds number flow.

15.2.4 Discussion of Results

Let us consider the total drag D in the present transient case. The aerodynamic drag is expressed as the sum of the pressure drag D_f due to the pressure distribution of the upper surface of the ACV, the momentum drag and thrust at both nozzle exits, and the pressure force across the front and rear jets at the nozzle exit. In the actual flow we must consider the friction drag of the upper surface of the ACV, the drag due to water spray, and the frictional drag of the skirt; however, these drags are beyond the present work. If the concentration of vortices is formed near the front edge, the pressure near this region decreases due to the vortices, so that D_f diminishes or becomes negative; that is, thrust appears. However, this low pressure induces the high jet

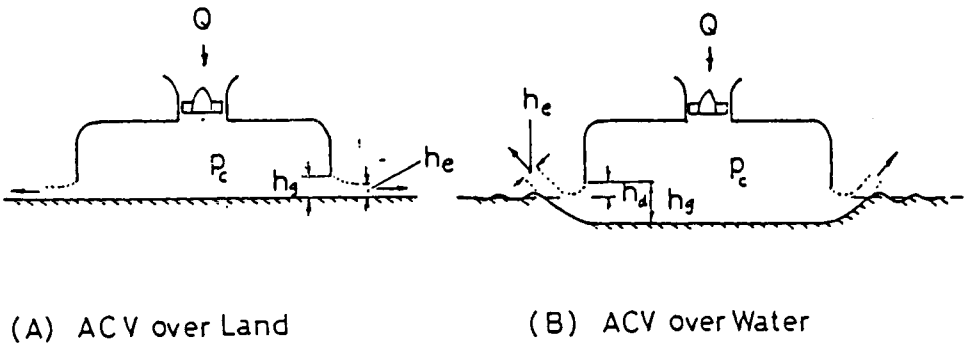

Fig. 15.19 Flow model of a plenum chamber type ACV over land and over water.

velocity at the front edge and makes the velocity low at the rear edge if the mass flux of the air supply is constant, so that the momentum drag of this flow becomes large. Thus, the concentration of vortices near the front edge increases the drag due to the momentum; on the other hand, the low pressure near the front edge decreases the drag, so it implies that w must take care of the shape of the contour of the ACV. Furthermore, the occurrence of separation on the upper surface of the ACV is scarce in the front part of the ACV. However, in the rear part, separation is likely to occur due to the interference of the front shedding vortices with the rear ones, as shown in Fig. 15.5. However, it may be considered that the viscosity makes this effect small and the entrainment effect of the rear jet prevents the separation in this region.

In the actual case where the air gap clearance is very small compared with the height of the ACV, that is, the height of the ACV is much larger than that of the present numerical model, the thrust component of the pressure force near the front part of the ACV due to the low pressure distribution on its surface becomes large. Therefore, we may consider that the decrease of the drag due to the low pressure distribution on the surface of the ACV near its front is dominant in the actual case, compared with the increase of the momentum drag due to the low pressure near the front nozzle exit.

These conclusions imply that we must further study the effect of the shape of the ACV on the interaction of the jet with the ambient flow.

15.3 WATER SURFACE DEFLECTION

15.3.1 General Aspects of Craft Hovering over Water

Consider a plenum chamber type ACV model over land (shown in Fig. 15.19A). High pressure is delivered by the fan to the cushion chamber. Discharge to the atmosphere occurs under the rim of the cushion chamber. If the rim is considered to be constructed with a sharp edge, the flow coefficient c = 0.61 can be

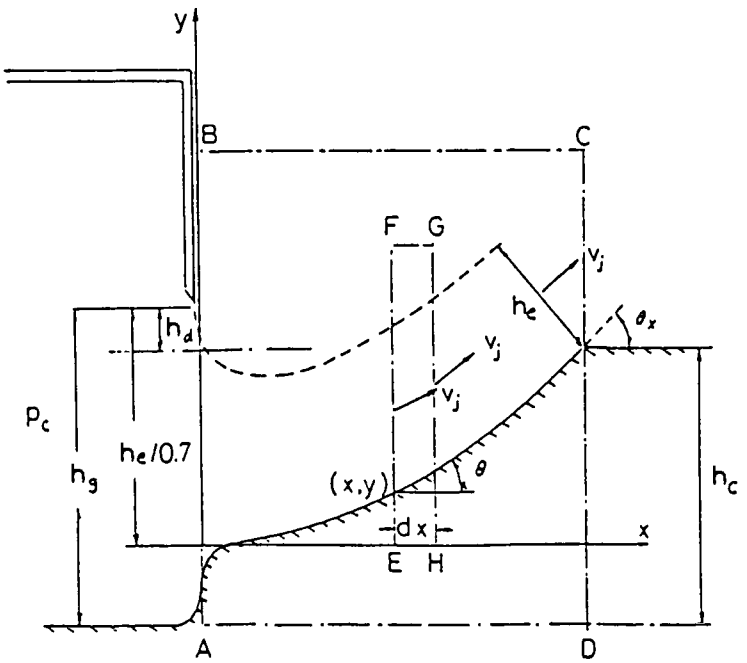

Fig. 15.20 Assumed path of air escaping from cushion (Jones' model).

given theoretically. However, in the case of an ACV over water the discharging flow under the rim of the cushion chamber curves along the water surface which is deformed due to cushion pressure (Fig. 15.19B). Usually the water surface deflections may be unsteady because of the air-water interference. The flow also consists of an air-water spray.

In this section, however, it is assumed that the lip flow is steady and the pressure in the water is hydrostatic. It is considered that the values of the flow coefficient c may not be the same as that over land. Some useful information concerning the deformed water surface has been found by the author. The problem of depressions in a liquid surface due to an impinging jet has been studied analytically by Olmstead & Raynor (ref. 13), and later by Tselnik (refs. 14-17). In the early stages, Mack proposed a simulation model where the water surface was deformed by a thin annular jet (ref. 18). Hogben reviewed the general aspects of ACV over water (ref. 19). Kida has discussed this problem on the basis of potential flow (ref. 20).

Jones developed a simple flow model for the prediction of the hovering performance of a plenum chamber ACV over water (ref. 21). Jones' model is shown in Fig. 15.20. His assumptions are as follows:

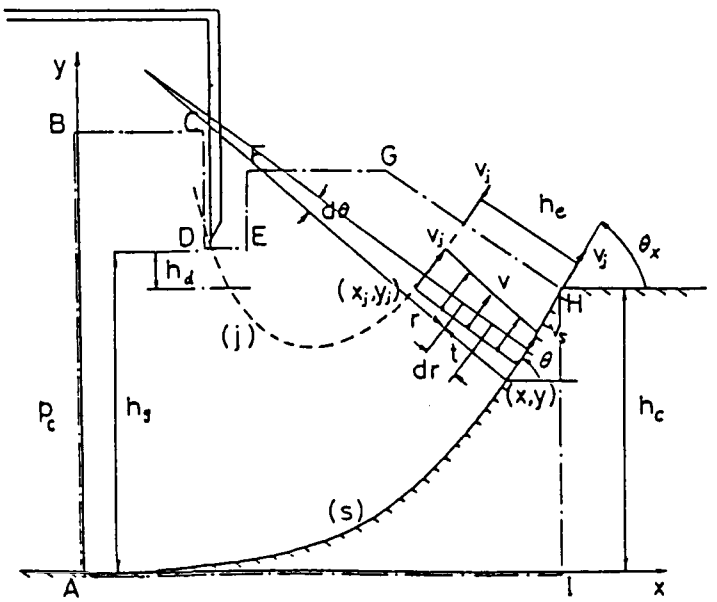

Fig. 15.21 Air flow model proposed by the author (wall jet type).

(1) The air flow leaving the cushion is inviscid,

(2) The momentum of the air leaving the cushion remains constant in the discharging process,

(3) The slope of the deflected water surface is small, and

(4) The escaping air causes a further depression near the rim of the plenum chamber because of the air momentum, and the static pressure of the air is atmospheric over the whole of the deformed discharge area.

His simulation model is reviewed and compared with the model proposed by the author. Considering the control surface ABCD and EFGHE, the momentum equations are expressed respectively by:

$$rv_j^2h_e(\cos q_x-1) = p_c[h_c-(h_e/0.7)]-(1/2)p_ch_c \tag{15.25}$$

for the x-direction, and

$$rv_j^2h_e[\sin q+\{d(\sin q)/dx\}dx]-rv_j^2h_e\sin q = r_wg[h_c-h_g+(h_e/0.7)-y]dx \tag{15.26}$$

for the y-direction, where v_j is the jet velocity; r and r_w are the density of air and water, respectively; $p_c = r_wgh_c$ is cushion pressure; g is the acceleration of gravity; h_d is the hover height above the free water; h_g is lip height above the water surface depressed by the air cushion; h_e is the equivalent air gap defined by $h_e = Q/v_j$, where Q is volume flow of jet per unit width of a

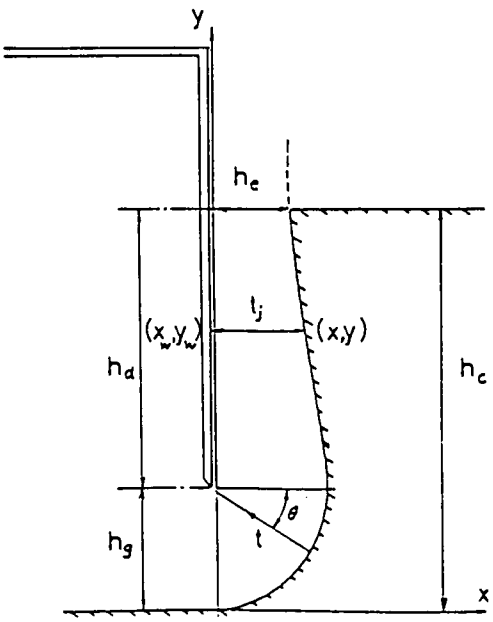

Fig. 15.22 Air flow model proposed by the author (overflow type).

two-dimensional plenum chamber; q is the angle of the water surface profile; q_x is the angle the escaping air makes with the free water surface; $c = h_e/h_g$ is discharge coefficient; x is the horizontal distance in an outward direction from the point where the escaping air first starts cutting a depression in the water (see Fig. 15.20); y is the vertical distance from the horizontal x-axis.

Assuming $\theta << 1$, then $\sin\theta \doteqdot \tan\theta = dy/dx$, and equation (15.26) becomes

$$d^2y/dx^2 + (1/2h\ h\ )\ y - (1/2h\ h\ )[h\ -h\ +(h\ /0.7)] = 0 \qquad (15.27)$$

Introducing the dimensionless variables $\bar{h} = h/h_c$, $\bar{x} = x/h_c$ and $\bar{y} = y/h_c$, the following equations are obtained:

$$2\bar{h}_e(\cos\ \theta_x - 1) = \bar{h}_g - (\bar{h}_e/0.7) - (1/2)\ , \qquad (15.28)$$

$$d^2\bar{y}/d\bar{x}^2 + (1/2\ \bar{h}_e)\ \bar{y} - (1/2\bar{h}_e)[1 - \bar{h}_g + (\bar{h}_e/0.7)] = 0 \qquad (15.29)$$

The equation (15.28) and the differential equation (15.29) with the initial conditions $\bar{y} = 0$ and $d\bar{y}/d\bar{x} = 0$ at $\bar{x} = 0$ define the problem, where

$$\theta_x = \tan^{-1}(d\bar{y}/d\bar{x}) \quad \text{at} \quad \bar{y} = 1.$$

By solving these equations the relation between the hover height and the flow rate can be obtained, and it is shown that the dimensionless parameter h_e/h_c

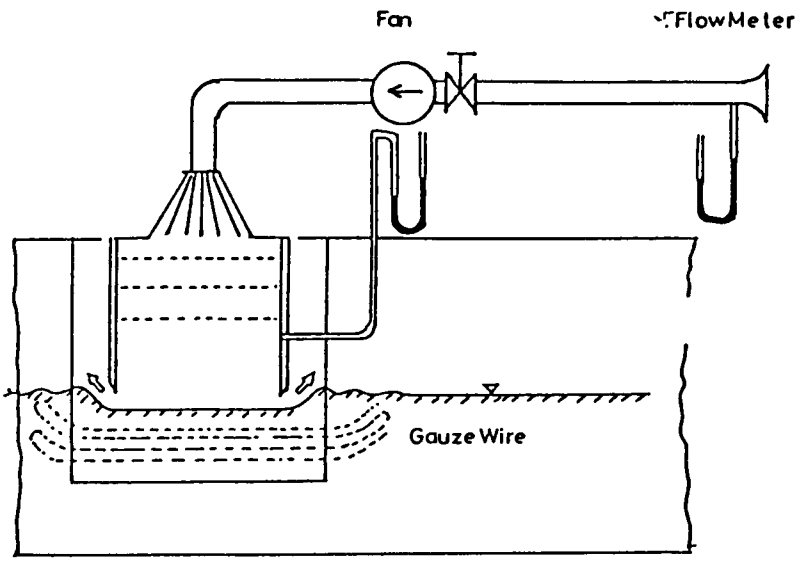

Fig. 15.23 Layout of the experimental apparatus.

controls the phenomena involved in this analysis. According to the experiments shown later, however, the step-like water surface profile shown in Fig. 15.20 does not actually appear.

The relation between the hover height and the equivalent air gap does not agree with the experiments except in the narrow range of h_e/h_c. This suggests that the assumptions used in Jones' simulation model were not valid.

15.3.2 Mathematical Model for the Water Surface Deflection

As it was found that the Jones model was inadequate, the author proposed a new simulation model for the discharge of an air flow over water. As shown in Fig. 15.21, the water surface is depressed by the pressure of the air cushion, and the air leaving the cushion at the lip forms a curved wall jet along the water surface. The flow is assumed to be inviscid. The centrifugal force acting on the jet element dr. rdθ is given by equating the force caused by the pressure difference dp, i.e.,

$$r\, d\theta\, dr\, v^2/r = dp\, r\, d\theta \tag{15.30}$$

Consequently,

$$\int_0^p dp = \int_{r_s-t_j}^{r_s-t} \rho v^2 dr/r \tag{15.31}$$

where v is the velocity and r is radius of curvature of the jet element path. The *jet thickness variable* t is the length measured from the deflected water

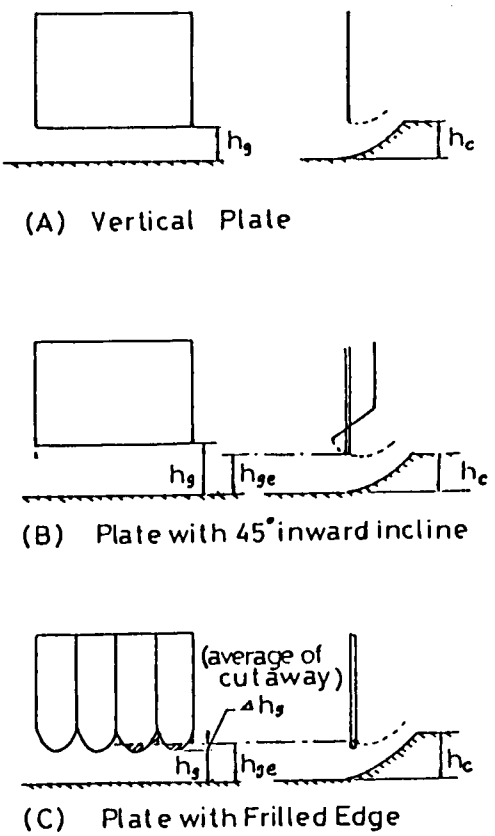

Fig. 15.24 Models of plate type nozzles.

surface. Subscripts s and j denote the deflected water surface and the jet boundary at the atmosphere side, respectively. Using the Bernoulli equation and the continuity equation, we have:

$$p_c = (\rho/2)v_s^2 + p_s = (\rho/2)v^2 + p = (\rho/2)v_j^2 \tag{15.32}$$

and

$$\int_{r_s-t_j}^{r_s} v\, dr = v_j\, h_e \tag{15.33}$$

where h_e is the equivalent air gap.

At the point (x,y) on the deflected water surface, the pressure p and the radius of curvature r are expressed as follows:

$$p_s = \rho_w g(h_c-y)\ , \tag{15.34}$$

$$r_s = [1-(dy/dx)^2]^{3/2}/(d^2y/dx^2) \tag{15.35}$$

Taking the control surface ABCDEFGHIA (shown in Fig. 15.21) the momentum

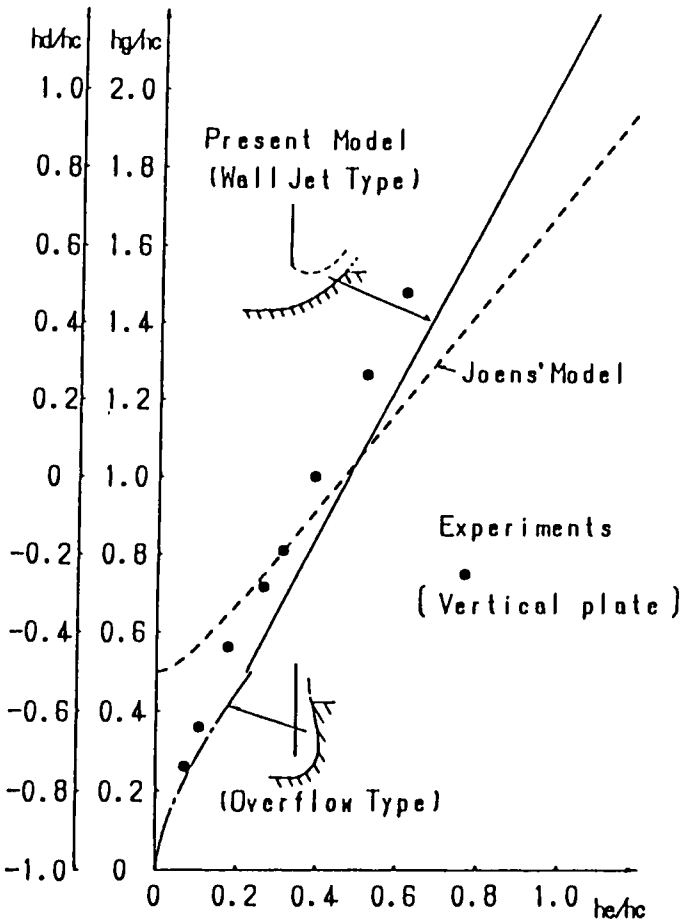

Fig. 15.25 Variation of lip height above depressed water surface or free water surface with equivalent air gap (vertical plate nozzle).

equation for the x-direction can be given by:

$$\rho v_j^2 h_e \cos\theta_x = p_c h_g - (1/2) p_c h_c \tag{15.36}$$

where h_g is height of the lip above the water surface depressed by the air cushion and θ_x is the angle the escaping air makes with the free water surface outside the cushion chamber (shown in Fig. 15.21), which is given by:

$$\theta_x = \tan^{-1}(dx/dy)_{y = h_c}$$

Introducing the dimensionless variables $\bar{h} = h/h_c$, $\bar{r} = r/h_c$, $\bar{t} = t/h_c$, $\bar{x} = x/h_c$, $\bar{y} = y/h_c$, $\bar{v} = v/v_j$, and $\bar{p} = p/p_c$ the basic equations (15.31) to (15.36) are expressed as follows:

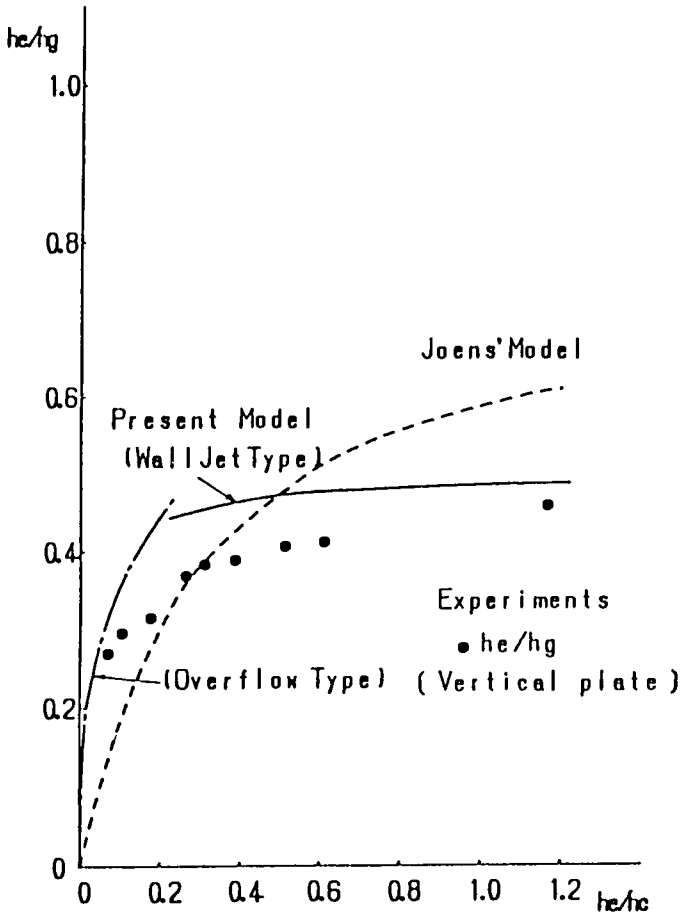

Fig. 15.26 Variation of flow coefficient with equivalent air gap (vertical plate nozzle).

$$\int_0^{\bar{p}} d\bar{p} + \int_{\bar{r}_s-\bar{t}_j}^{\bar{r}_s-\bar{t}} 2\,\bar{v}^2 d\bar{r}/\bar{r}, \tag{15.37}$$

$$1 = \bar{v}_s^2 + \bar{p}_s = \bar{v}^2 + \bar{p}, \tag{15.38}$$

$$\int_{\bar{r}_s-\bar{t}_j}^{\bar{r}_s} \bar{v}d\bar{r} = \bar{h}_e \tag{15.39}$$

$$p_s = 1 - y\ , \tag{15.40}$$

$$\bar{r}_s = [1-(d\bar{y}/d\bar{x})^2]^{3/2}/(d^2\bar{y}/d\bar{x}^2)\ , \tag{15.41}$$

$$\bar{h}_g = 2\bar{h}_e \cos\theta_x + (1/2)\ . \tag{15.42}$$

Using equations (15.38) and (15.40), equation (15.37) is integrated into the form:

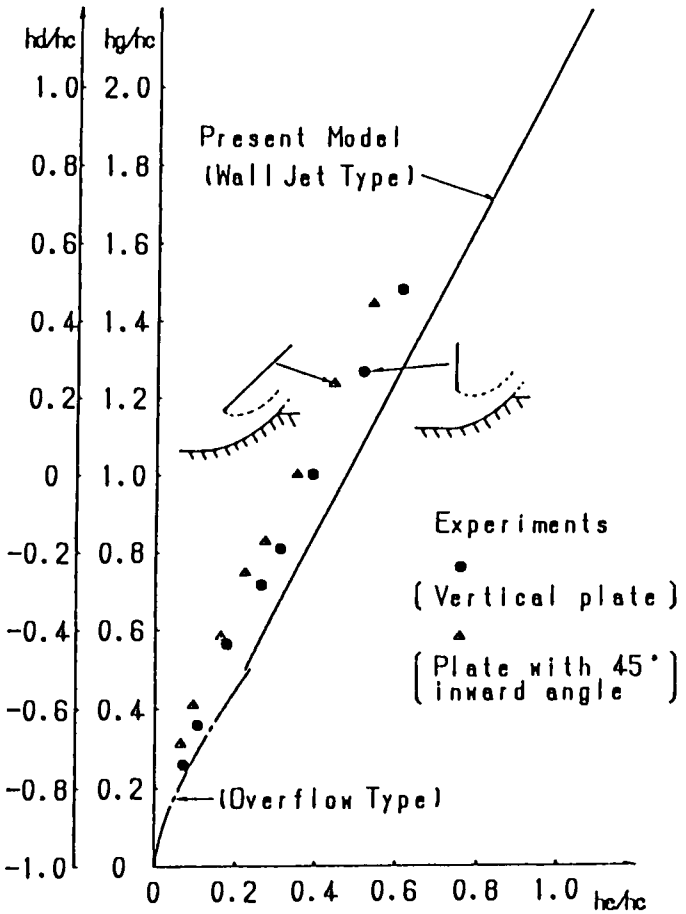

Fig. 15.27 Variation of lip height above depressed water surface with equivalent air gap (plate nozzle with a 45 degree inward incline).

$$(1-\bar{p}) = [(\bar{r}_s - \bar{t}_j)/(\bar{r}_s - \bar{t})]^2 \tag{15.43}$$

Consequently,

$$(1-\bar{p}_s) = [1-(\bar{t}_j/\bar{r}_s)]^2 = \bar{y} \tag{15.44}$$

is obtained.

Using equations (15.38) and (15.43), the continuity equation (15.39) is integrated into the form:

$$\ln[1/\{1-(\bar{t}_j/\bar{r}_s)\}] = (\bar{h}_e/\bar{r}_s)/[1-(\bar{t}_j/\bar{r}_s)] \tag{15.45}$$

Then the radius of curvature of the deflected water surface $\bar{r}_s$ is expressed by:

$$\bar{r}_s = -2\bar{h}_e/[\bar{y}^{1/2}\ln\bar{y}] \ . \tag{15.46}$$

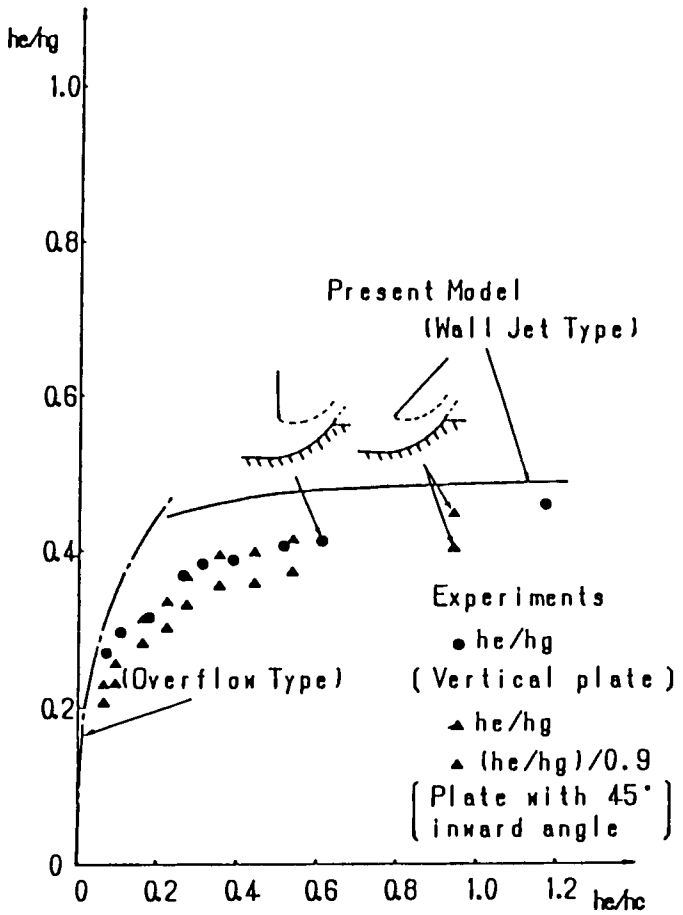

Fig. 15.28 Variation of flow coefficient with equivalent air gap (plate nozzle with a 45 degree inward incline).

Using (15.46) the differential equation (15.41) is rewritten into the form:

$$d^2\bar{y}/d\bar{x}^2 = -(1/2)\bar{y}^{1/2}\ln\bar{y}[1-(d\bar{y}/d\bar{x})^2]^{3/2}/\bar{h}_e \ , \tag{15.47}$$

and its solution with the initial conditions $\bar{y} = 0$ and $d\bar{y}/d\bar{x} = 0$ at $\bar{x} = 0$ are obtained numerically using the Runge-Kutta method. The jet boundary $(\bar{x}_j, \bar{y}_j)$ expressed by:

$$\bar{x}_j = \bar{x} - \bar{t}_j(d\bar{y}/d\bar{x})/[(d\bar{y}/d\bar{x})^2 + 1]^{1/2} \tag{15.48a}$$

$$\bar{y}_j = \bar{y} + \bar{y}_j/[(d\bar{y}/d\bar{x})^2 + 1]^{1/2} \tag{15.48b}$$

The height of the lip above the water surface depressed by the air cushion h_g is obtained from (15.42). The position of the lip on the jet boundary is finally defined from the results of calculations. According to various obser-

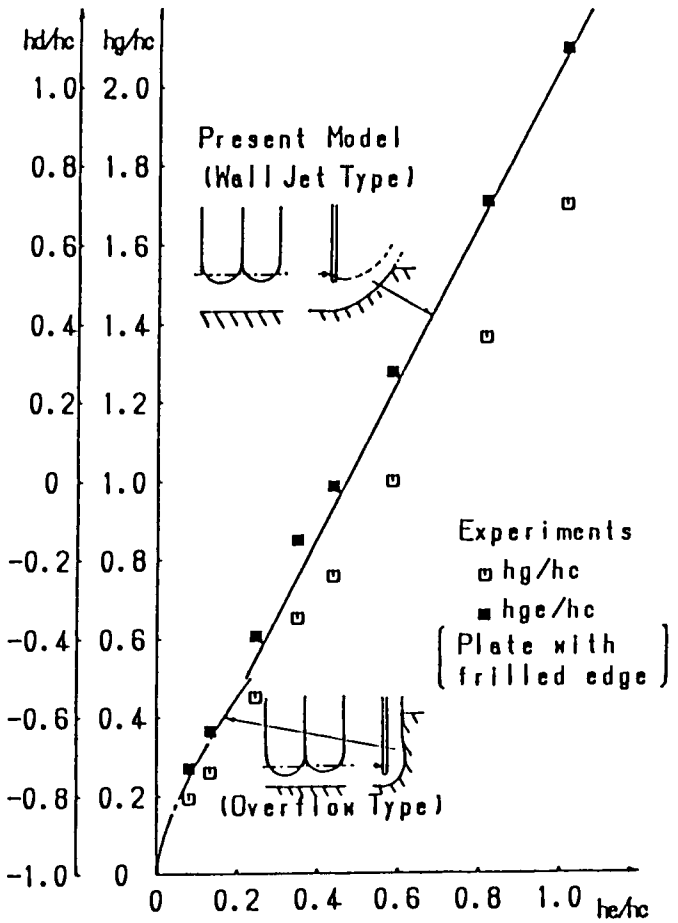

Fig. 15.29 Variation of lip height above depressed water surface with equivalent air gap (plate nozzle with a frilled edge).

vations of a jet escaping from an air cushion lip over water, the flow pattern of the jet changes when the equivalent air gap is small compared to the air cushion depth. As shown in Fig. 15.22, the jet flow attaches to the outer wall of the lip and a water surface forms a channel through which the air flows. Hinchey has pointed out this type of flow (ref. 22). The author also deals with the simulation model of this overflow type.

Using the Bernoulli equation and the continuity equation,

$$p_c = (\rho/2)v^2 + p = (\rho/2)v_j^2 \ , \tag{15.49}$$

$$\int_0^{h_g} v dy = \int_0^{t_j} v dt = h_e v_j \ , \tag{15.50}$$

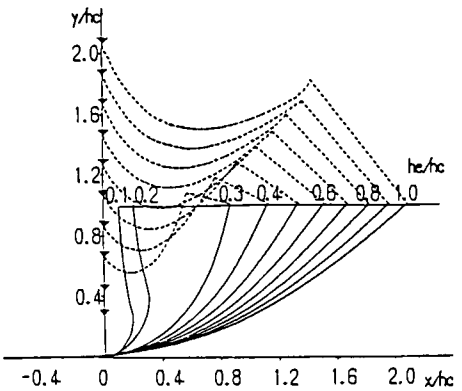

Fig. 15.30 Deflected water surface profiles and jet boundaries calculated by using the author's model.

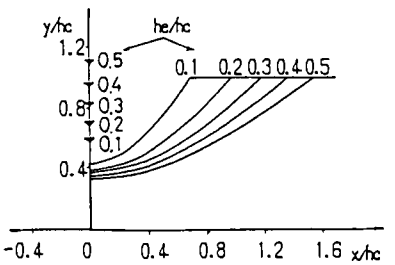

Fig. 15.31 Deflected water surface profiles calculated by using Jones' model.

where t_j is the air flow width. The pressure on the water surface profile is given by:

$$p_s = \rho_w g(h_c - y) \ . \tag{15.51}$$

The relation between (x,y) and the coordinates of the outer wall of the lip (x_w, y_w) are expressed by:

$$\left.\begin{aligned} x &= x_w + t_j \cos\theta \\ y &= y_w - t_j \sin\theta \end{aligned}\right\} \tag{15.52}$$

where θ is the angle of the air flow's cross section to the horizontal. In dimensionless form, equations (15.49) to (15.52) are as follows:

$$1 = \bar{v}^2 + \bar{p} \tag{15.53}$$

$$\int_0^{\bar{h}_g} \bar{v}d\bar{y} = \int_0^{\bar{t}_j} \bar{v}d\bar{t} = \bar{h}_e \tag{15.54}$$

$$\bar{P}_s = 1 - \bar{y} \tag{15.55}$$

$$\left.\begin{aligned} \bar{x} &= \bar{x}_w + \bar{t}_j \cos\theta \\ \bar{y} &= \bar{y}_w - \bar{t}_j \sin\theta \end{aligned}\right\} \tag{15.56}$$

If the p ressure in the discharging air flow can be assumed to be equal to the hydrostatic pressure of water of the same depth, the continuity equation

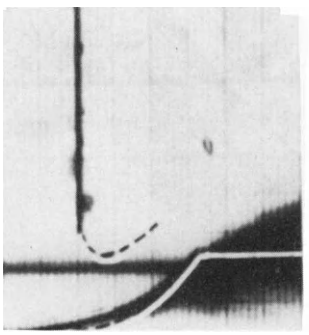

Fig. 15.32 Deflected water surface (h_e/h_c = 0.51 for vertical plate nozzle).

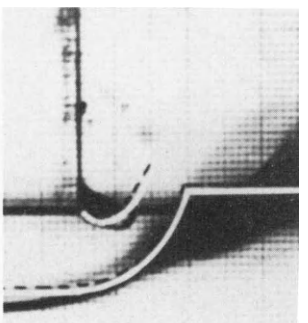

Fig. 15.33 Deflected water surface (h_e/h_c = 0.39 for vertical plate nozzle).

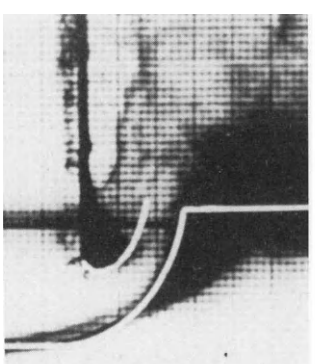

Fig. 15.34 Deflected water surface (h_e/h_c = 0.26 for vertical plate nozzle).

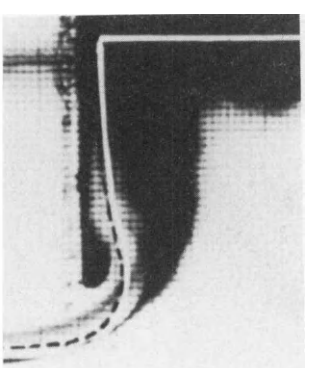

Fig. 15.35 Deflected water surface (h_e/h_c = 0.07 for vertical plate nozzle).

(15.54) is rewritten as:

$$\int_0^{\bar{t}_j} \bar{v} d\bar{t} = \int_0^{\bar{t}_j} [\bar{y}_w - \sin\theta\ (\bar{t}_j - \bar{t})]^{1/2} d\bar{t} = \bar{h}_e \qquad (15.57)$$

By integrating equation (15.57), the jet thickness t_j is obtained as:

$$\bar{t}_j = [\bar{y}_w - \{\bar{y}_w^{3/2} - (3/2)\bar{h}_e \sin\theta\}^{3/2}]/\sin\theta \qquad (15.58)$$

By substituting $\bar{y}_w = \bar{h}_g = \bar{t}_j$ and $\theta = \pi/2$ in equation (15.58), the height of the lip above the depressed water surface is obtained by:

$$\bar{h}_g = (3/2)^{2/3} \bar{h}_e^{\ 2/3} \ .$$

The water surface profile is obtained from equations (15.56) and (15.58).

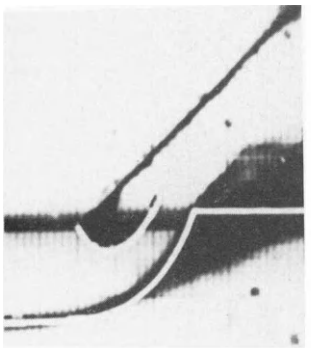

Fig. 15.36 Deflected water surface (h_e/h_c = 0.54 for plate nozzle with a 45 degree inward incline).

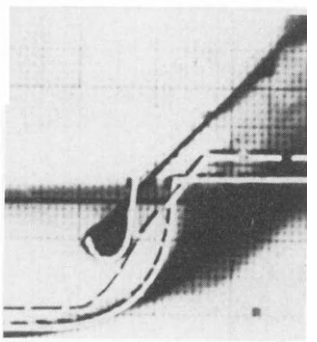

Fig. 15.37 Deflected water surface (h_e/h_c = 0.22 for plate nozzle with a 45 degree inward incline).

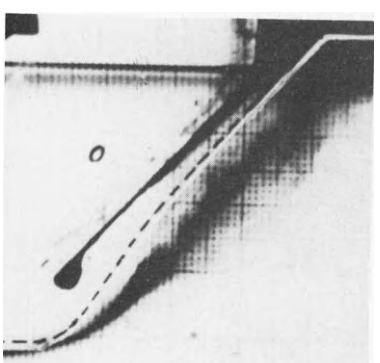

Fig. 15.38 Deflected water surface (h_e/h_c = 0.16 for plate nozzle with a 45 degree inward incline).

15.3.3 Physical Model for Experimental Studies

The following experiments are carried out to confirm the validity of this simulation model. The outline of the experimental apparatus is shown in Fig. 15.23. It consists of a plenum chamber type air cushion model, a radial blower, an inlet flow meter and a flow control valve provided between the flow meter and the blower. The air cushion model is made of acryl, and the dimensions are 320 mm length, 80 mm breadth, and 480 mm height. The rims and skirts of the air cushion model are detachable. The flow supplied to the air cushion chamber is equally distributed after the diffuser by means of guide vanes and three screens. A bell-mouth type inlet flow meter was calibrated by using a laminar flow meter.

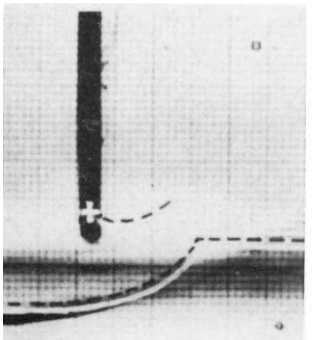

Fig. 15.39 Deflected water surface (h_e/h_c = 0.82 for plate nozzle with a frilled edge).

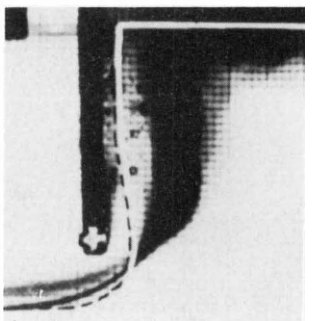

Fig. 15.40 Deflected water surface (h_e/h_c = 0.08 for plate nozzle with a frilled edge).

A free surface circulating water tank was used. The dimensions of the channel are 600 mm width, and approximately 500 mm depth and 4 m length. In order to adjust the hover height measured from the free water surface, the water level of the tank can be controlled.

In the preliminary tests, violent oscillations of the water surface occurred because of the complex interaction between the jet, the air cushion and the water. To dampen the hydrodynamic oscillation, numerous sheets of wire gauze were installed in the tank beneath the model (see Fig. 15.23). By this arrangement, the sloshing of water was considerably reduced, but the shorter waves caused by the lip flow continued.

15.3.4 Comparison of Simulation and Experimental Results

In this subsection, the predictions based on the proposed simulation model are shown and compared with the experiments. For standard outlet nozzles, a plate type vertical nozzle was chosen. An inward inclined plate, a frilled plate and a vertical plate were tested (Fig. 15.24).

(i) Hover height and flow rate. Concerning the vertical plate, Fig. 15.25 shows the relationship between the air flow rate, the hover height and cushion pressure. Three variables are presented nondimensionally using h_e/h_c, h_g/h_c or h_d/h_c, where h_e is the equivalent air gap, h_g is the lip height over the depressed water surface, and h_d is the hover height over the free water level.

The computable domain using a *wall jet type simulation model* must be larger than approximately 0.21 of the nondimensional equivalent air gap h_e/h_c. This is because the derivative of the deflected water surface reaches an extremely large value; q_x approaches 90 degrees in the process of computation by the Runge-Kutta method.

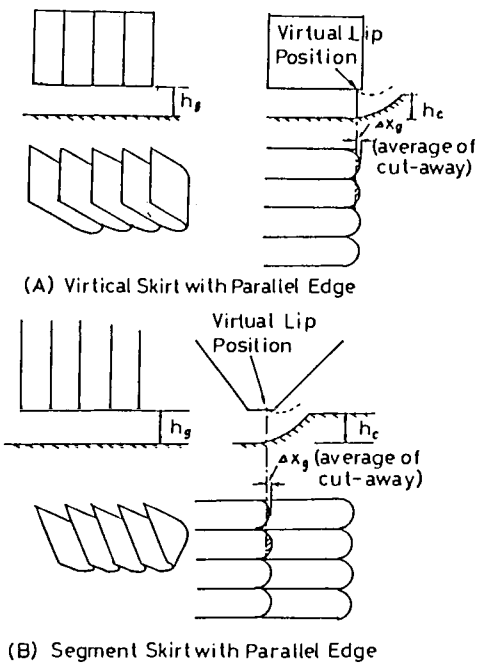

Fig. 15.41 Models of flexible skirt with parallel edge to the water surface.

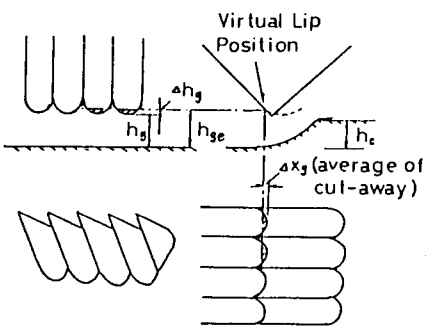

Fig. 15.42 Models of flexible skirt with frilled edge to the water surface.

For smaller values of h_e/h_c, calculations using an *overflow type simulation model* were carried out. The numerical results almost agree with the measured values of the vertical plate nozzle. The calculations based on Jones' model is also shown in Fig. 15.25. It does not agree with the previously mentioned experiments except in the narrow range of h_e/h_c. The variation of the flow coefficient with the equivalent air gap is shown in Fig. 15.26. The flow coefficients measured over water are smaller than the theoretical value of 0.61 that is usually applied over land. Although the experimental values are a little smaller than predicted, the experiments seem to support the validity of the assumptions.

The experimental results of a plate nozzle with a 45 degree inward angle are compared with those of a vertical plate (Fig. 15.27). It is recognized

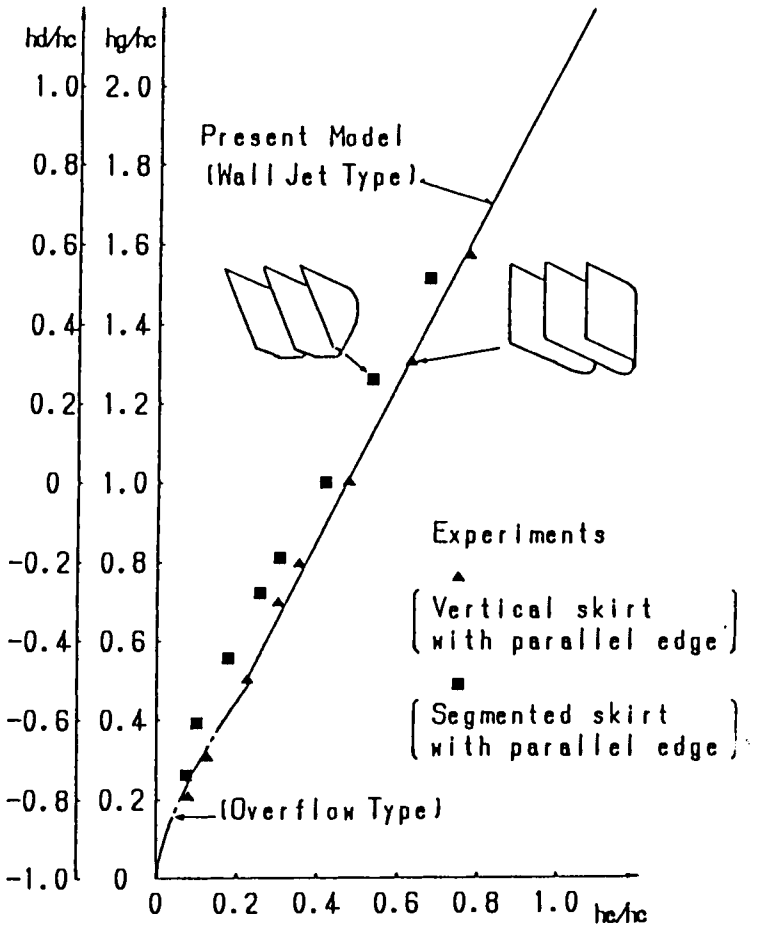

Fig. 15.43 Variation of lip height above depressed water surface or free water surface with equivalent air gap (for skirts with parallel edge).

that the flow coefficients of the inward inclined plate are about 10% smaller than for a vertical plate. By using the correction factor 0.9, the flow coefficients of the inward inclined plate can be predicted from those of the vertical nozzle (Fig. 15.28). The experimental results of the plate with a frilled edge, of course, indicate that a higher flow rate is required to keep the same lip height over the depressed water surface (Fig. 15.29). This is because of the increased escape area due to its shape. The increase of escaping area can be expressed by Δh_g in geometrical averages (see Fig. 15.24), and then the equivalent lip height over the depressed water surface h_{ge} is defined by $h_{ge} = h_g + \Delta h_g$. If equivalent lip height h_{ge} is used instead of h_g, the relation between h_e/h_c and h_{ge}/h_c is well predicted by using the above mentioned

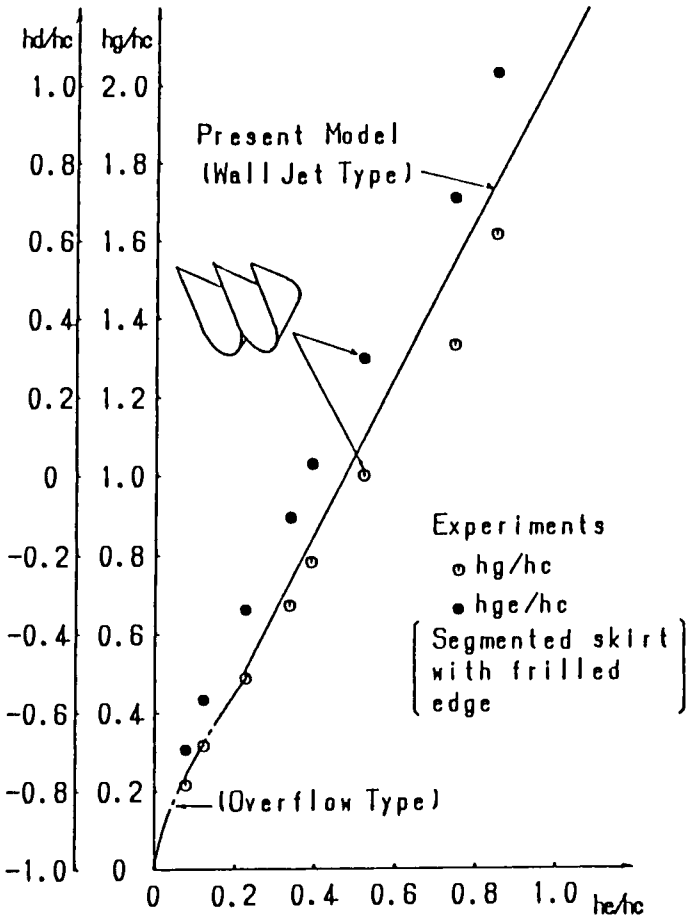

Fig. 15.44 Variation of lip height above depressed water surface or free water surface with equivalent air gap (for skirt with frilled edge).

simulation model, as shown in Fig. 15.29.

(ii) Deflected water surface profile. The calculated results of the deflected water surface profiles and the jet boundaries are shown in Fig. 15.30 with changing nondimensional equivalent air gap of h_e/h_c. As previously mentioned, the water surface profiles for lower equivalent air gap h_e/h_c are calculated by the overflow type model. The water surface profiles calculated by Jones' model are shown in Fig. 15.31. According to Jones' assumption, the deflected water profiles have a step-like water level elevation beneath the lip.

Figures 15.32 to 15.40 show photographs of the deflected water surface profiles. Using a long exposure of 1/8 second, the profiles of the shorter waves

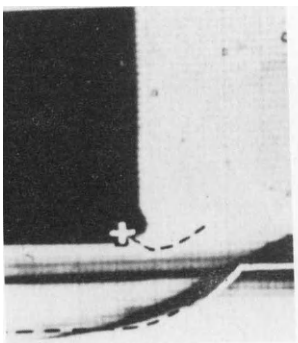

Fig. 15.45 Deflected water surface (h_e/h_c = 0.77 for vertical skirt with parallel edge to water surface).

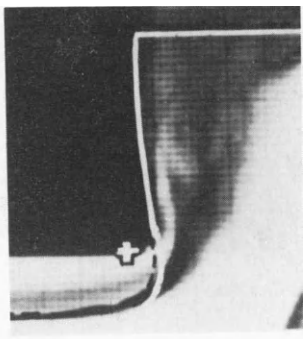

Fig. 15.46 Deflected water surface (h_e/h_c = 0.08 for vertical skirt with parallel edge to water surface.

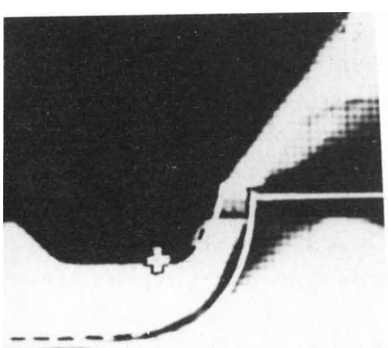

Fig. 15.47 Deflected water surface (h_e/h_c = 0.26 for inward incline skirt with parallel edge).

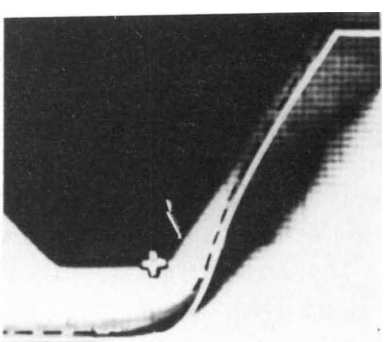

Fig. 15.48 Deflected water surface (h_e/h_c = 0.07 for inward incline skirt with parallel edge).

caused by the lip flow are superimposed. No step-like water level elevations assumed by Jones' model were observed. The calculated results by using the author's simulation model are drawn on the photographs. Although the slope of the calculated profiles seems to be steeper than that of the observations, the calculations express almost the same features as the actual water surface profiles. Figures 15.32 to 15.34 show the wall-jet flow. Figure 15.35 shows the overflow type for a vertical plate nozzle. The deflected water surface boundaries were not distinctly observed because of a heavy spray. The transition from the wall-jet type to the overflow type flow patterns seems to occur between 0.20 and 0.10 of h_e/h_c for the vertical plate. This transitional value of h_e/h_c is somewhat smaller than 0.21 predicted by the simulation method.

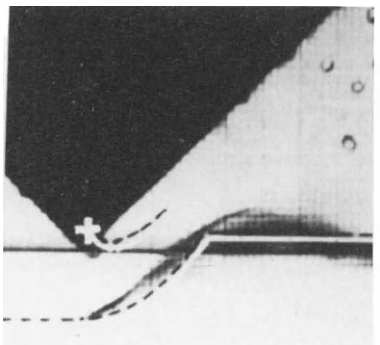

Fig. 15.49 Deflected water surface (h_e/h_c = 0.52 for inward incline skirt with frilled edge).

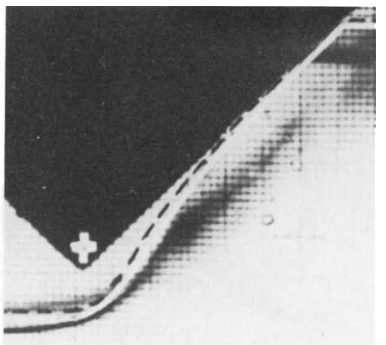

Fig. 15.50 Deflected water surface (h_e/h_c = 0.08 for inward incline skirt with frilled edge).

In the case of the inward inclined plate, the transition seems to occur at a larger value of h_e/h_c compared with the vertical nozzle, because the jet impinges on the inclined plate before the escaping jet angle approaches 90 degrees. Figures 15.36 to 15.38 show the water surface profiles for the plate with 45 degree inward inclined angle. According to observation, the transitional value of h_e/h_c seems to be smaller than the predicted value, as shown in Figure 15.37. In the case of the inward inclined plate, the calculated profiles are drawn corresponding to the *virtual lip position* which is defined by by the lip height of the equivalent vertical nozzle above the depressed water surface, h_{ge} (Fig. 15.24).

In the case of the plate with a frilled edge, the calculated profiles are drawn corresponding to the *virtual lip position*, which is defined by the equivalent lip height above the depressed water surface, h_{ge}(Figs. 15.39 and 15.40).

15.3.5 Practical Implications

(i) The effects of a skirt's shape on cushion sealing. In the previous subsection, the deformation of a free water surface due to an air cushion was discussed based on a two-dimensional lip-flow model. However, the shapes of the rim of practical ACVs with segmented skirts are much more complicated than those of a plate. As the flow escaping from the lips of a skirt is three-dimensional, it is not established that the simple two-dimensional model previously mentioned can be used to estimate the water surface profiles. In order to evaluate the effects of the skirt's shape on the sealing of an air cushion, three types of flexible skirts were tested (Figs. 15.41 and 15.42). Fig. 15.41(A) shows a vertical skirt with parallel edge, namely its edge is parallel

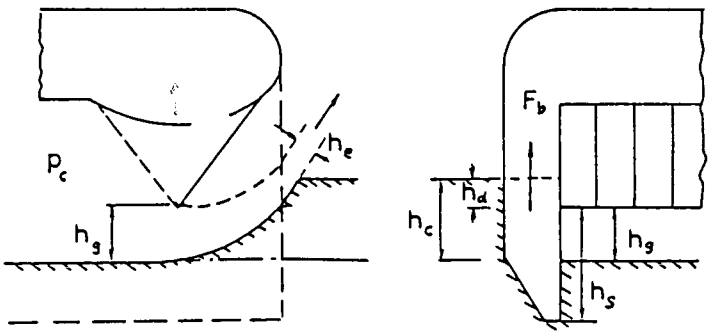

Fig. 15.51 Cushion sealing and hull buoyancy of SES in hover.

to the water surface in *side view* and is frilled in *plan*. Fig. 15.41(B) shows an inward inclined segment skirt with parallel edge. Fig. 14.42(C) shows an inward inclined segmented skirt with frilled edge, namely its edge is frilled to the water surface in *side view* and in *plan*. The equivalent horizontal and vertical adjustment of the lip position can be expressed by Δx_g in geometrical averages in *plan view* and Δh_g in geometrical averages in *side view*, respectively (see Figs. 15.41 and 15.42). By using Δx_g and Δh_g, the virtual lip position can be defined as shown in Figs. 15.41 and 15.42. The relationship of the lip height above the depressed water surface to the equivalent air gap is shown in Figs. 15.43 and 15.44. In the case of the edge that is parallel to the water surface, the air flow rate escaping from the skirt seems to agree with that of the vertical plate (Fig. 15.43). However, in the case of the edge that is frilled to the water surface, the air flow rate increases compared with the vertical plate. Figure 15.44 shows that the air flow rate escaping from the skirt with frilled edge is predictable by using the equivalent lip height h_{ge} defined by $h_{ge} = h_g + \Delta h_g$.

Figures 15.45 to 15.50 show the deflected water surface profiles for the three skirts. The calculated profiles are drawn according to the virtual lip positions. The prediction by the calculations seems to agree fairly well with the experiments, except for the deflected water surface profiles calculated by using the overflow type model. From a practical point of view, the concept of virtual lip position seems to be beneficial.

(ii) Hull buoyancy of SES. The lift force acting on a SES in hover consists of air cushion lift and hull buoyancy as shown in Figure 15.51. The hull buoyancy is decided by the hull depth under the free water surface; accordingly, it is affected by the flow rate escaping from the air cushion. The relationship between the all-up weight W, cushion pressure p_c and hull buoyancy F_b of SES is approximately expressed by $W = F_b + P_c S_c$. The F_b depends both on the sinkage of the side hull, z, and the side hull's geometry. The

sinkage of side hull z is expressed by h_d+h_s, consequently, $h_c-h_g+h_s$, where h_s is the side hull depth under skirt. Therefore, the relationship of h_c to the equivalent air gap h_e can be calculated if W, S_c, h_c and h_e are given as the design parameters.

15.4 SUMMARY

In Section 15.2, the mechanism of interference thrust was studied by numerical simulation. The shape of the ACV was an arc with 0.18 maximum height ratio to the chord length and the two-dimensional plenum chamber type was chosen. To determine the mechanism of the generation of the interference thrust, the transient flow and the abrupt starting flow were calculated. For the numerical simulation, the discrete vortex method was used and the effect of viscosity was further taken into account by both a dissipation model and a random work model. From the numerical results, it was shown that there are mainly four regimes of flow pattern by various mass fluxes of air supply to the cushion chamber. Especially, the vortices shed from the front edge of the contour of the ACV do not flow downstream or upstream if an appropriate mass flux is set. These flow patterns were examined by flow visualization using the hydrogen-bubble method.

The concentrated vortices result in a decrease of pressure near the front edge of the ACV, so that the pressure drag is reduced. On the other hand, this low pressure induces an increase in issuing velocity at the front exit, so that the momentum drag increases. In the actual case, however, the decrease in pressure drag due to the low pressure distribution on the surface of the ACV near its front may be dominant because the air gap clearance is very small compared with the height of the ACV.

In Section 15.3, the sealing of an air cushion over waters without forward speed was discussed, and the deformation of the free surface at the lip of an air cushion was studied based on a lip-flow model proposed by the author. This simulation model differs essentially in the underlying assumptions compared with Jones' model. The model of the discharging air flow under the rim of an air cushion is classified into two types: wall jet and over flow. For both flow types, mathematical models were derived in a dimensionless form. By solving the basic equations, it was shown that the nondimensional equivalent air gap, which corresponds to air flow rate, plays a dominant role in the phenomena involved in this analysis.

Experiments with several types of lip, including flexible skirts, were carried out. The deflected water surfaces were observed for various plate lips, and the relationship between air flow rate, the lip height over the depressed water surface and cushion pressure were found experimentally. The experiments seemed to support the validity of the simulation model. It was found that the

flow coefficient over water is smaller than the theoretical value of 0.61 usually applied over land, and it changes depending on the nondimensional equivalent air gap.

The numerical simulation model can be used to estimate the effects of skirts' shapes on cushion sealing, as well as the side hull's buoyancy for SES.

15.5 REFERENCES

1. T. Strand, W.W. Royce and T. Fujita, J. Aero. Space Sci., 29(1962) 702-711.
2. G.C. Cooke and R.E. Duffy, J. Aircraft, 9 (1972) 675-681.
3. N.K. Walker, Proc. National Meeting on Hydrofoils and Air Cushion Vehicles, Washington DC., Sep.17-18,1962, pp.65-80.
4. Z. Yasutomi, Experimental Study of Cushion Pressure Characteristics of Air Cushion Vehicle in Forward Speed, Ph.D. Thesis (University of Osaka Prefecture) 1977 (in Japanese).
5. S. Ando and J. Miyashita, Aero. Engr., (1960-10) 24-25 and 79-83.
6. A. Shimizu and T. Wada, Computers & Fluids, 13 (1985) 83-97.
7. A.J. Chorin, J. Fluid Mech., 57 (1975) 785-796.
8. W.T. Ashurst, in: F. Durst, B.E. Launder, F.W. Shmidt and J.H.Whitelaw (Ed.), Turbulent Shear Flow I, Springer-Verlag, Berlin, 1978, 402-413.
9. A.V.J. Edwards and C.L. Morfey, Computers & Fluids, 9 (1981) 205-221.
10. T. Nishiyama (Ed.), Report of Research Committee on Application of Computer to Fluids Engineering (in Japnese) JSME, 1983.
11. G.K. Batchelor, An Introduction to Fluid Dynamics, Cambridge, London,1967.
12. G.L. Brown and A. Rosko, J. Fluid Mech., 64(1975) 775-816.
13. W.E. Olmstead and S. Raynor, J. Fluid Mech., 19, Part 4,(1964) 561-576.
14. D.S. Tselnik, Stevens Inst. Tech. Technical Rept. ME-RT-80005,(1980) 1-13.
15. D.S. Tselnik, Stevens Inst. Tech. Technical Rept. ME-RT-80006,(1980) 1-23.
16. D.S. Tselnik, Stevens Inst. Tech. Technical Rept. ME-RT-80008,(1980) 1-11.
17. D.S. Tselnik, Stevens Inst. Tech. Technical Rept. ME-RT-80010,(1980) 1-20.
18. L.R. Mack, Proc. Symp. on Ground Effect Phenomena, Princeton Univ., (1959) 263-284.
19. N. Hogben, Advances in Hydroscience Vol. 4, in: V.T. Chow(Ed.), Academic Press, New York, 1967.
20. T. Kida and Z. Yasutomi, Studies on ACV, 15(1), (1982) 3-7(in Japanese).
21. D.I.G. Jones, J. Aircraft, 3(4) (1966) 333-338.
22. M.J. Hinchey, UTIAS Report No.246 (1980) 1-68.

Chapter 16

A PERSONAL PERSPECTIVE

16.1 FOREWORD

This chapter was written by Dr. William R. Bertelsen, an ACV pioneer who designed and built the first controllable man-carrying ACV, called the Bertelsen Aeromobile, and demonstrated it at the First Symposium on Ground Effect phenomena, Princeton University, October 1959. It is on display in the Permanent Collection of the National Air and Space Museum of the Smithsonian Institution, Washington, DC. Dr. Bertelsen's personal involvement in ACV development, his commitment to the ACV concept and his interest in the industry's evolution have withstood the test of time. Not surprisingly, he holds strong views on the subject. For these various reasons, it is fitting that Dr. Bertelsen's personal perspective on the history, status and potential of hovercraft or ACV's, as he prefers to call them, is one of the two concluding chapters of this book.

16.2 BACKGROUND

In the 1950's, serious research had begun on air cushion phenomena, first in models and, ultimately, on full-scale craft, then called *Ground Effect Machines (GEM's)* in the United States. The British called them *Hovercraft*, which is a slight misnomer since the objective is to *stop* hovering and travel at desired speeds over water and various terrains. The term *Air Cushion Vehicle*, or *ACV*, is now widely used in North America and preferred by this writer.

Bertelsen research on ground effect phenomena resulted from experiments, in 1957, with a vertical take-off aircraft model named the *Arcopter*. The model was characterized by a spanwise arc wing and deflected slipstream, as shown in Figure 16.1. With two nesting arc flaps extended, it demonstrated increased lift near the ground. A given weight would require less power to carry it near the surface than away from it. There was pressure rise under the craft, and

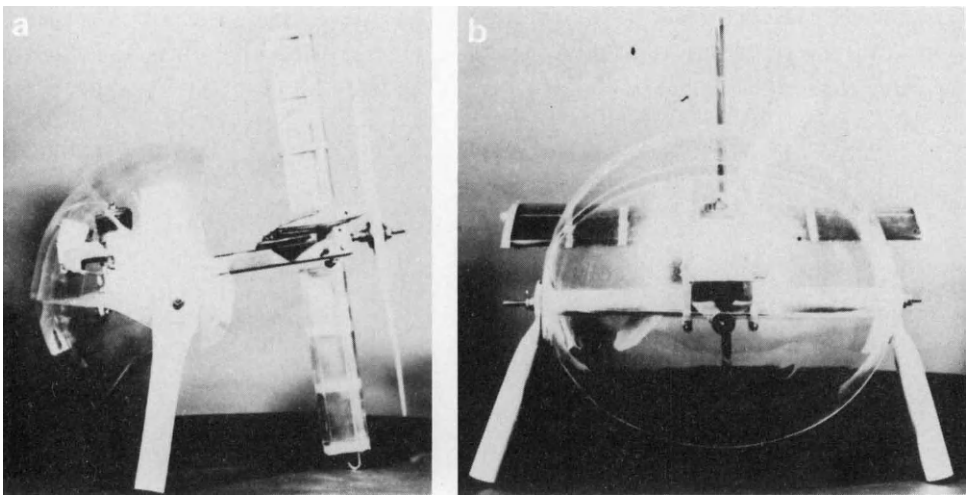

Fig. 16.1 Arcopter vertical take-off and landing (VTOL) aircraft model featuring an arc wing and canard controls. Arc flaps fully deployed for 70° downward deflection of slipstream: (a) Side view; (b) rear view.

therefore lift increase from ground effect. This phenomenon led to the concept of the *flying automobile* which, as far as was known at the time, had never been built. It was reasonable to experiment with configurations which would augment the ground effect and to think of vehicles traveling a few inches or feet from the ground over relatively level surfaces of various kinds. Such a craft would not need aircraft certification, pilot training, or licensing, and would be far less expensive than an aircraft to build and operate. The Arcopter was, and is, a successful deflected-slipstream VTOL concept. But since the GEM seemed more immediately attainable, it was chosen over the VTOL aircraft for research at that time.

No one could imagine how long it would be before a viable air cushion vehicle could be designed and built. After three decades, there are a few hundred homebuilt small ACV's throughout the world, a few dozen medium-sized four- to eight-passenger craft, and approximately 265 large to very large craft.

This chapter retraces the steps of a determined investigator moving from known to unknown, model to model, concept to concept, with a fixed objective: to design and build a successful vehicle in a totally new medium with no fixed idea of how to reach that objective. A series of diverse and, in retrospect, sometimes ridiculous vehicles were built, tested and abandoned until one configuration survived to provide adequate performance.

16.3 DESCRIPTION OF BERTELSEN ACV DEVELOPMENT WORK

16.3.1 Plenum Chamber ACV's

The first true Bertelsen ACV, built in 1958, was a model that used an electric vacuum cleaner blower (Fig. 16.2(a)). The blower was inserted in a square with a 1.9 cm (0.75 in) thickness and 33 cm (13 in) per side. This model would not *fly*, except on a surface plate, until a 3.81 cm (1.5 in) long by 0.318

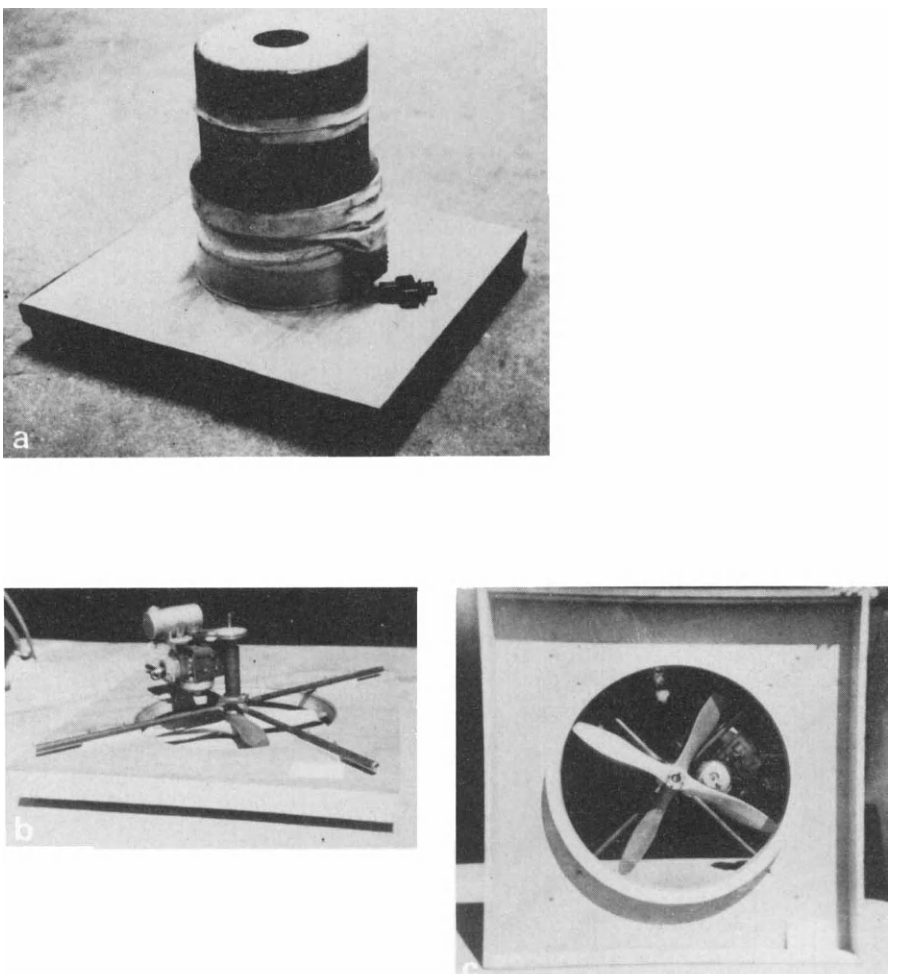

Fig. 16.2 Early ground effect machine (GEM) models: (a) electric vacuum cleaner blower and flexible rubber skirt; (b) gasoline powered axial-flow ducted fan and rigid side walls; (c) bottom view of (b).

cm (0.125 in) thick rubber dam was fitted around the base. The lift chamber was then 1.9 cm (0.75 in) high and the blower was adapted to allow the model to float on concrete, wood flooring, and similarly smooth surfaces. This may have been the first ACV to be fitted with a flexible skirt.

The next plenum chamber model of 1958 had a square plywood base, 1.9 cm (0.75 in) thick and 1.22 m (4 ft) on each side, with rigid sidewalls 10.16 cm (4 in) high (Fig. 16.2(b)). A two-cycle two-cylinder 1.87 kW (2.5 HP) engine drove a mandrel-mounted 76.2 cm (30 in) diameter four-bladed propeller via a 5:2 V-belt reduction. The power unit was set in a 76.52 cm (30.125 in) duct with a 7.62 cm (3 in) throat and a rounded intake lip. A bottom view is shown in Figure 16.2(c). This model flew well on concrete and relatively flat surfaces but would not move over grass, gravel, or other irregular surfaces.

16.3.2 Peripheral Jet ACV's

Interesting results were reported in NACA publications on research and development of vertical take-off aircraft, including research done at NACA Langley Field, now NASA Langley Research Center, on the very efficient deflected slipstream (ref. 1; 1955) and a Technical Note by von Glahn (ref. 2; 1957). After inserting a centerbody in a rocket nozzle, von Glahn found that, in ground effect, the centerbody received a significant pressure increase from the peripheral jet surrounding it. The thrust from the rocket was greatly increased within one jet diameter from the ground but greatly reduced at higher altitudes, away from ground effect, due to negative pressure on the centerbody.

This discovery dictated the configuration of the next Bertelsen model, called Aeromobile 35-1, shown at rest in (a) and (b) of Figure 16.3 and in *flight* (November, 1958) in Figure 16.3(c). it was a square peripheral jet model, 1.22 m (4 ft) per side, with a 26.1 kW (35 HP) twin-cylinder two-cycle engine and a six-bladed wooden propeller. Figure 16.3(d) shows the bottom view. Internal and external hinged flaps were connected with tie cables. The two top and two bottom jet flaps are shown deflected downward by gravity. Figure 16.3(e) shows the horizontal flaps in the same position, but the vertical internal and external flaps on the right and left are deflected to the left, which would direct the peripheral jet accordingly. This was an attempt to use the high-velocity jet sheets for propulsion. Undoubtedly the jet deflection produced some reaction force, but it also tilted the craft by shifting the center of lift to the left, effectively moving the centerbody (Fig. 16.3(e)). Tilting the main lift vector also produced a horizontal component.

On October 13, 1958, the author stood astride the duct on this machine, while it was hovering at full power, and rode it. This was perhaps the earliest man-carrying flight of a peripheral jet ACV. It was discovered that shifting weight produced the largest propulsive force. This was because it tilted the lift vector, the magnitude of which was the sum of the empty weight of

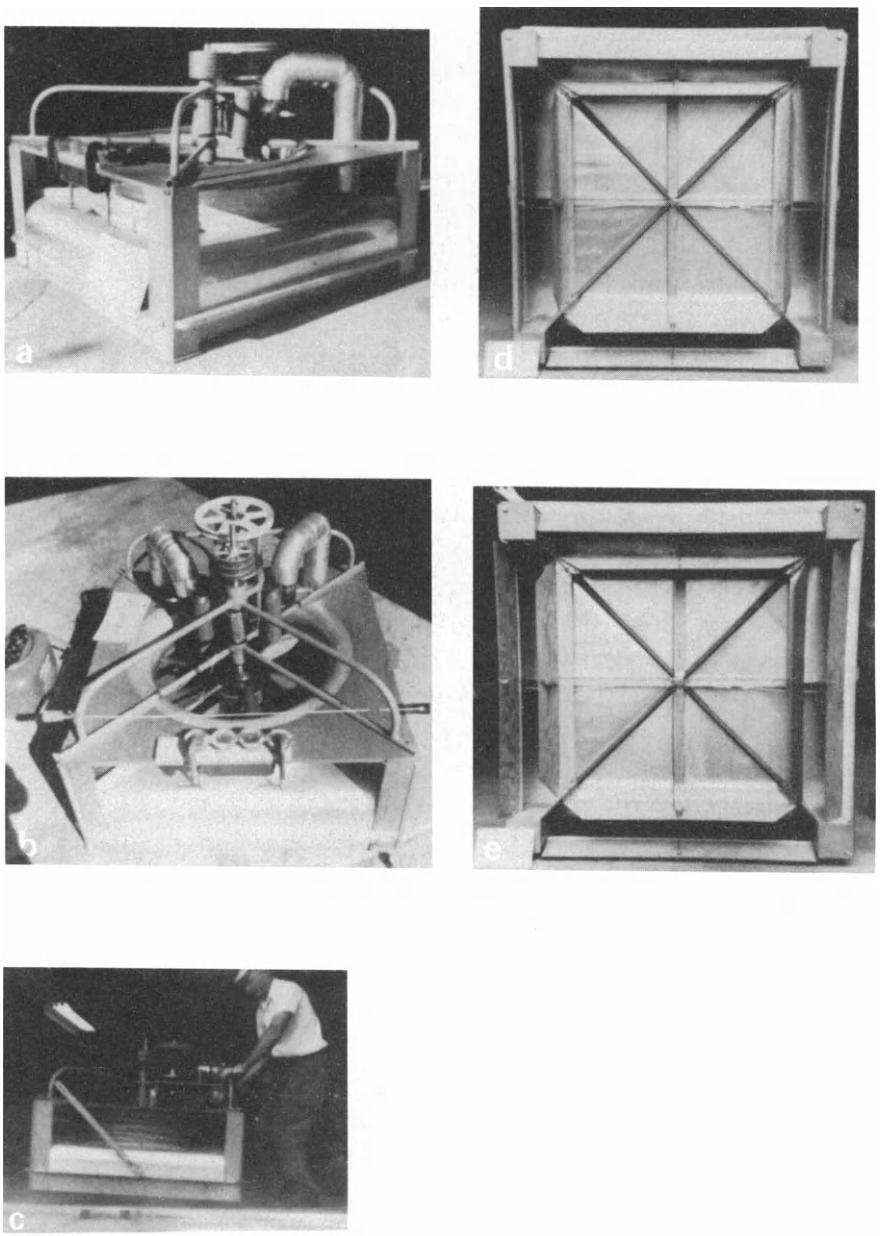

Fig. 16.3 Aeromobile 35-1: (a) side view; (b) top view; (c) in *flight*; (d) bottom view with top and bottom flaps deflected downward; (e) bottom view with all flaps deflected.

Aeromobile 35-1 and the pilot's weight, for a total of about 193 kg (425 lb). The horizontal component of that tilted vector was proportional to the tilt angle. The problem with this means of propulsion was two-fold: 1) there was no yaw control, and 2) the hovering height of the unloaded craft was only 10.3 cm (4 in) and, at gross weight with the *pilot* on board, the ground clearance was only 5 cm (2 in), which limited the degree of tilt and the corresponding horizontal force. A tilting ACV has marginal propulsive force on level surface. Furthermore, it has to *out-tilt* any hill it must climb. In Aeromobile 35-1, the maximum was about a 5% grade.

By working out a propulsion means with hinged flaps around the peripheral jet, a larger man-carrying craft with yaw control was built. Experiments on

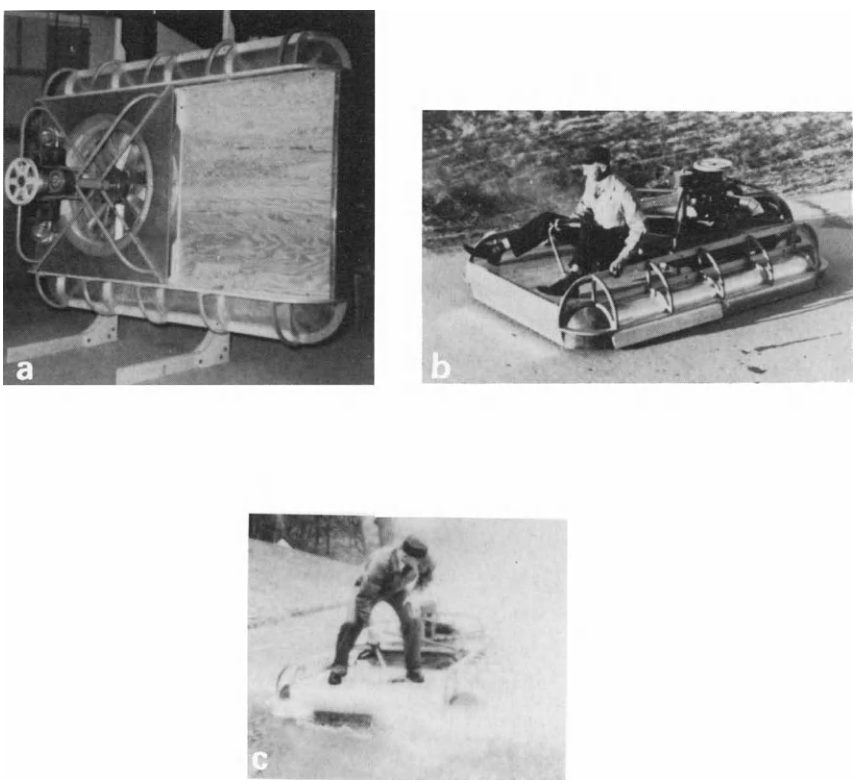

Fig. 16.4 Aeromobile 35-2: (a) top view of vehicle set on edge on stands; (b) on a road; (c) moving sideways on water. (Latter two photos courtesy of Popular Science Monthly.)

Aeromobile 35-1 proved that deflecting the inner row of flaps inside the peripheral jet contributed negligibly to the horizontal force; hence they were eliminated.

Aeromobile 35-2 (refs. 3-7), shown in Figure 16.4(a), was constructed by installing the engine and fan mounts of Aeromobile 35-1 in a larger 1.8 m (71 in) × 2.56 m (101 in) chassis. The rectangular planform allowed two flaps on each of the long sides which could be moved together to produce lateral motion, or differentially to produce yaw force for the first time. A bottom view of Aeromobile 72, the identical chassis of Aeromobile 35-2 with conversion to a 53.7 kW (72 HP) engine, is shown in Figure 16.5(a). The differential deflection of the longitudinal flaps is clearly evident, as is the central toggle which operates all the flaps remotely from the joy stick base on the right, or front, of the craft. Fore and aft motion of the joy stick moves the front and rear flaps back and forth. Lateral motion of the stick moves the side flaps collectively, and rotation of the stick deflects the flaps differentially to produce yaw force and control. To move forward, the pilot pushes the stick forward, which moves the fore and aft flaps rearward and tilts the craft bow-down. Similarly, to move backward, the pilot pulls the stick rearward causing forward deflection of the fore and aft flaps and tilting of the craft stern-down. To move to the right, the pilot moves the stick to the right resulting in the two right and two left side-flaps deflecting to the left, which rolls the craft clockwise and causes it to move to the right. Similarly, counter-clockwise roll and left propulsion are effected by a left deflection of the stick. The narrower lateral dimension allows greater tilt and, therefore, greater propulsive force sideways than either fore or aft. It was usual to yaw the craft 90° to the desired direction of travel, tilt it sideways for acceleration, and then yaw it forward to travel. On April 6, 1959, *Popular Science Monthly* (ref. 3) photographed Aeromobile 35-2 moving forward on a road (Fig. 16.4(b)) and, the following day, moving sideways on water (Fig. 16.4(c)).

The poor performance of Aeromobile 35-2 dictated an increase in installed power from 26.1 kW (35 HP) to 53.7 kW (72 HP), resulting in Aeromobile 72 (Fig. 16.5(b)). The larger engine was set vertically in an elongated duct. The intake scroll was raised and spaced with a sheet-aluminum cylinder to accommodate the direct-drive eight-bladed fan made of wood. The performance was somewhat improved. Figure 16.5(c) shows the Aeromobile 72 in forward flight, as indicated by the nose-down tilt.

However, the very low altitude achieved by all the above vehicles restricted their propulsive force, speed, and grade climbing ability. The logical solution seemed to be greater installed power, fan diameter, and increased base area to lift the craft higher and allow greater tilting and propulsive force in all directions. Aeromobile 200-1 (ref. 8), first flown on June 3, 1960, was the

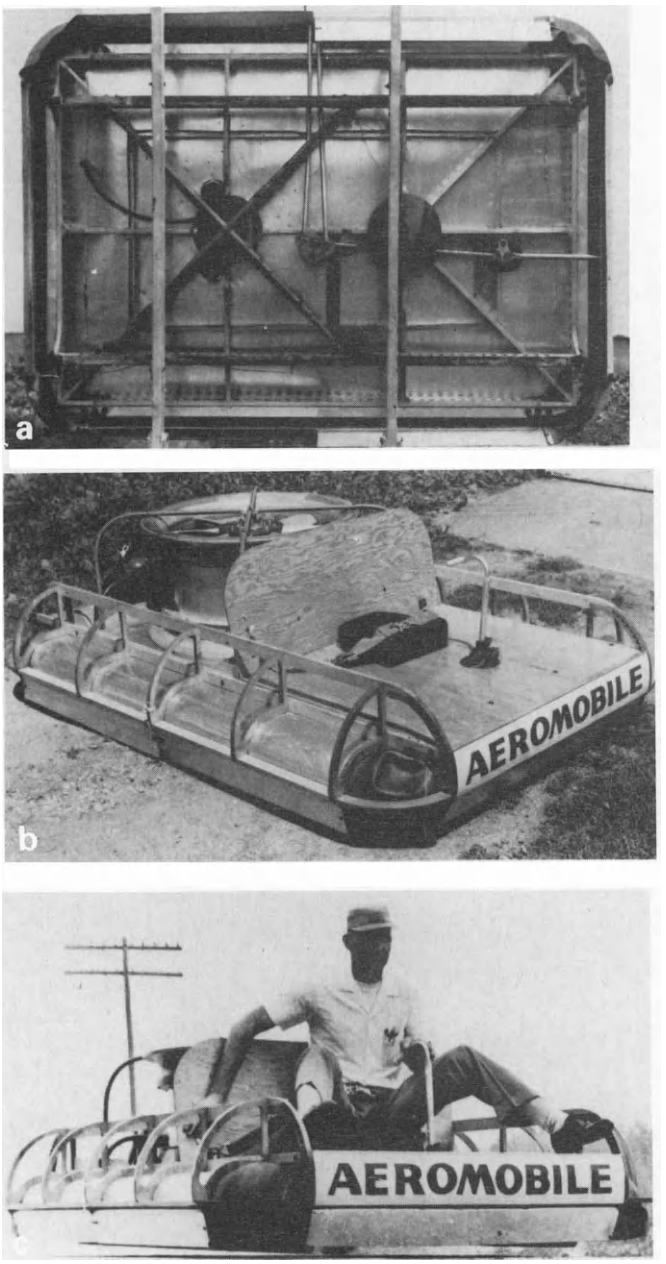

Fig. 16.5 Aeromobile 72: (a) bottom view; (b) right front view; (c) in *flight*.

fourth in the series of full-scale *ground effect machines*. The chassis of this craft is shown hovering in Figure 16.6(1). It was powered by an air-cooled 149.2 KW (200 HP) helicopter engine driving a 2.14 m (7 ft) diameter eight-bladed fan through a modified automobile differential, 90° bevel gear, speed-reduction unit. The lift air was directed to a 20.32 cm (8 in) wide

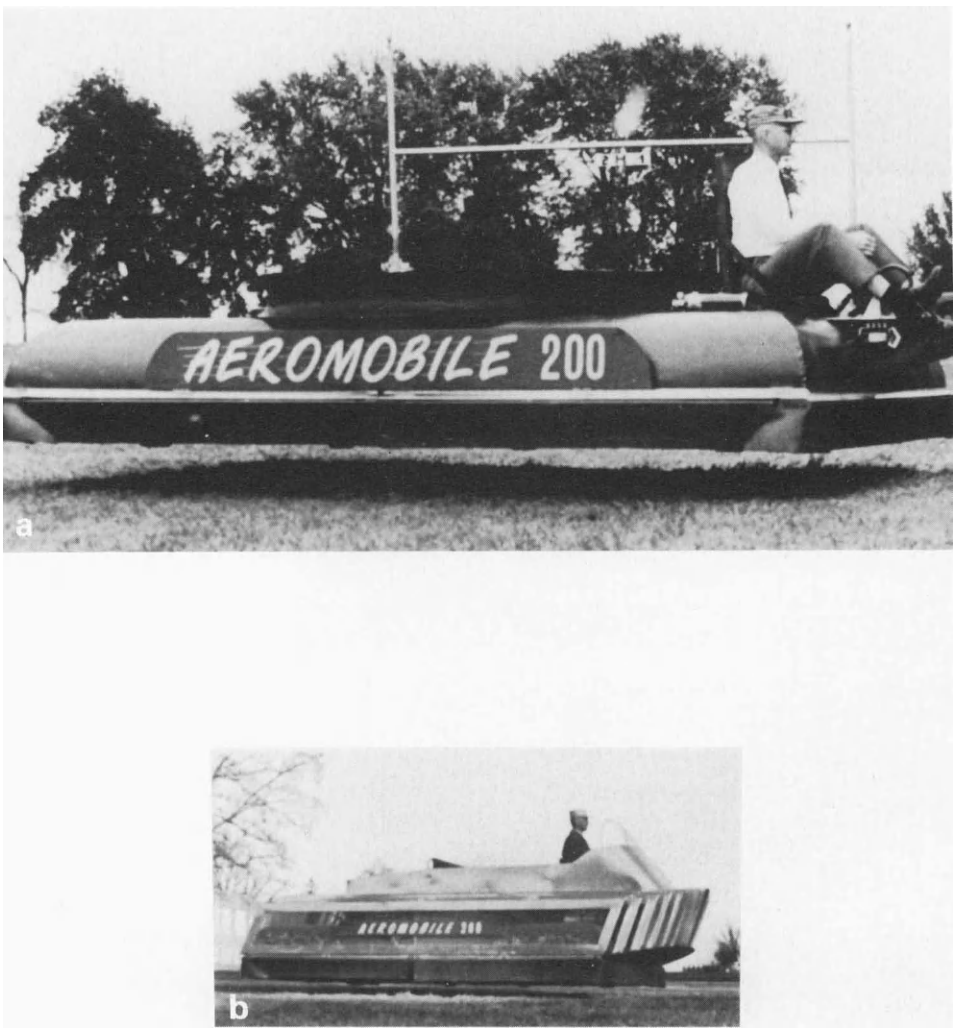

Fig. 16.6 Aeromobile 200-1: (a) chassis on cushion; (b) four-passenger body on cushion.

peripheral jet surrounded by six 30.49 cm (12 in) high flaps. The hinged flaps were operated as in the Aeromobile 35-2 and 72 craft, except that foot pedals actuated the differential motion of the side flaps for yaw control, more like an aircraft. The pitch and roll motions for longitudinal and lateral propulsion were activated by the control stick. Figure 16.6(b) shows the A-200-1 hovering with its four-passenger body installed.

In 1961, the Aeromobile 200-2 was built for the U.S. Department of Commerce, Office of International Trade Fairs (OITF). Its chassis was nearly identical to the Aeromobile 200-1 chassis, but was fitted with a highly-styled fiberglass body designed by OITF and manufactured by the Molded Fiberglas Body Company, the firm which built the Corvette automobile body. Figure 16.7 shows the Aeromobile 200-2 *flying* at the U.S. Pavilion of the Fourth Tokyo International Trade Fair in 1961. It was demonstrated through 1961 and 1962 at the U.S. pavilions in Tokyo (Japan), Zagreb (Yugoslavia), Turin (Italy), and New Delhi (India). Attendance would surge at the U.S.Pavilions when the noisy Aeromobile was fired up and performed its feats of levitation and frictionless motion from one circular arena to the other. The craft was eventually delivered to a U.S. Army research and development center for *human engineering* studies, and finally dismantled.

One more quasi-peripheral-jet craft, the ninth ACV, was built for Universal Pictures in 1964, as a *Magic Carpet* for promotion of their motion picture, *The Brass Bottle*. The chassis of the Aeromobile 250 is shown hovering in

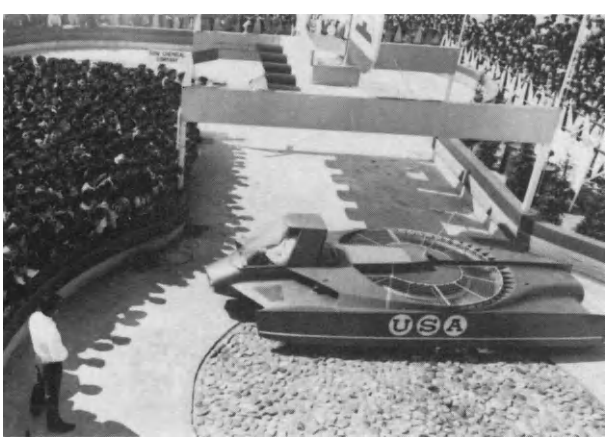

Fig. 16.7 Aeromobile 200-2 at Fourth International Trade Fair in Tokyo, Japan, 1961. (Photo courtesy of the Office of International Trade Fairs, United States Department of Commerce.)

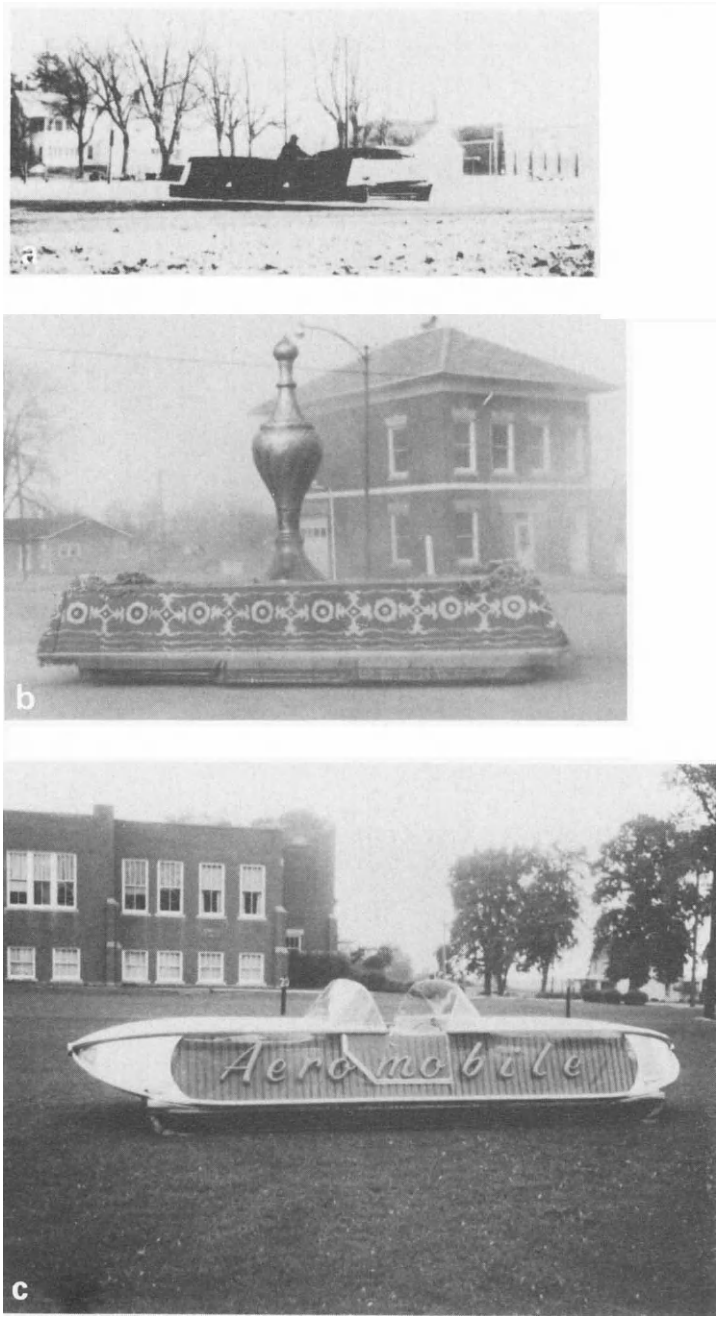

Fig. 16.8 Aeromobile 250: (a) chassis on cushion; (b) with *magic carpet* body for Universal Pictures; (c) with styled three-passenger body.

Figure 16.8(a). Although this craft was built after the Arcopter GEM series (ACV's 6, 7 and 8), it is discussed here as a member of the peripheral jet series. Two 48.5 kW (65 HP) aircraft engines, converted to vertical crankshaft operation, drove air boat propellers in two 1.52 m (60 in) ducts that directed the airflow into fore and aft plenum chambers through bilateral peripheral jets enclosed by three movable flaps on each side. The two right and left flaps on each end directed the high-velocity propeller slipstream left or right for yaw force. The fore and aft flaps directed the slipstream fore or aft and tilted the craft in the direction of travel. To move sideways, all six side-flaps were deflected to cause lateral tilt and propulsion. The Aeromobile 250 is shown with its magic carpet body in Figure 16.8(b). After repurchase from Universal Pictures, it was converted to a styled demonstrator which could seat three passengers side-by-side (Fig. 16.8(c)).

The peripheral jet configuration was tested extensively with six different full-scale vehicles. Although peripheral jet ACV's were good *show pieces*, they failed to give adequate performance in control, obstacle clearance, or speed in any direction. In operation, immense spray, dust and surface erosion from the massive lift air efflux were experienced. Clearly, a new approach was needed.

16.3.3 Arcopter GEM Series

In order to get sufficient thrust to drive the ACV at acceptable speeds, the next series of full-scale craft reverted to the original Arcopter concept, having a horizontal thrust axis with an aircraft engine and propeller. Three *Arcopter GEM* ACV's were built (refs. 9 and 10).

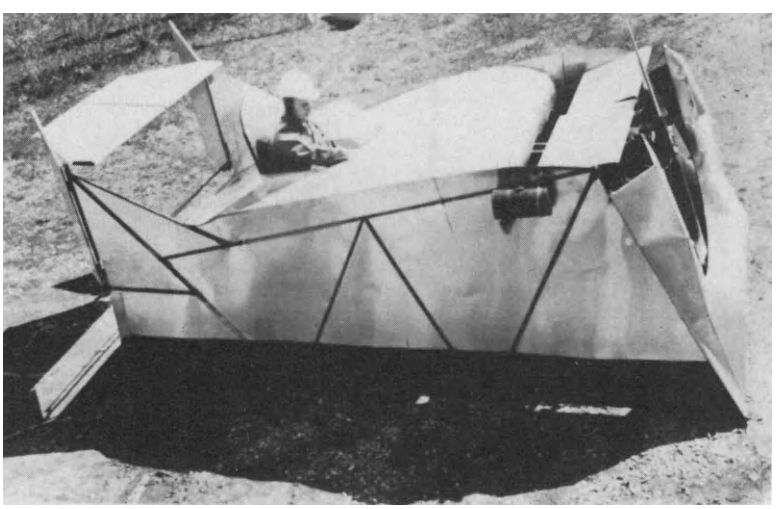

Fig. 16.9 Arcopter GEM-1.

Arcopter GEM-1, flown in 1961, is shown in Figure 16.9. It was a single-seater, powered by a 48.5 kW (65 HP) aircraft engine. About one-half of the propeller slipstream was diverted overhead for airfoil lift and yaw control by twin rudders. Some pitch and roll control was effected by a conventional elevator and two forward canard surfaces. The split canard surfaces in the slipstream were meant to yield roll control, but turned out to be very weak. This craft did achieve great forward speed and positive yaw control. It was, however, frightening to *fly* because of its high center of gravity, narrow beam, 2.44 m (8 ft) length and absence of any braking or reverse thrust.

Arcopter GEM-2, flown in 1962, was longer, but not wider, and was powered by a 85.8 kW (115 HP) engine. The craft is at rest on snow in Figure 16.10(a), and in flight in Figure 16.10(b). This more powerful *arc wing* ACV was even more scary to fly because of its great speed capability, estimated at 112,7 km (70 mph) but never achieved because of its treacherous pitch-up tendency. The latter figure shows a visible nose-high attitude. This is a so-called wing-in-ground (WIG) type of vehicle. At low speed, air cushion lift is centered at 50% chord (distance from bow to stern). However, the airfoil lift

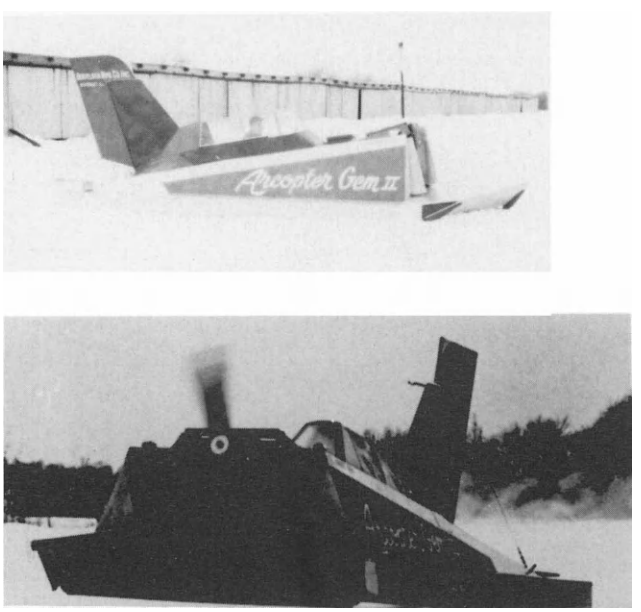

Fig. 16.10 Arcopter GEM-2: (a) at rest on snow; (b) in *flight* on snow.

at high speed is centered at about 25% chord, a significant forward shift of center of lift causing the pitch-up. There were several very dangerous moments, while proceeding down a field at 80.5 km/h (50 mph) air speed, when a gust would strike the craft and raise its nose nearly 45° in the air without roll control. From then on, the speed was limited to a maximum of 80.5 km/h (50 mph).

Arcopter GEM-2 was a very good amphibian capable of traveling on grass, snow, water, ice, and ice floe. On January 22, 1962, it became the first ACV to cross the Mississippi River, by traversing the completely ice-covered waters at Rock Island, Illinois. It did so with such great ease that it was difficult to keep below pitch-up speed. This adventure had an interesting sequel. The river was nearly evenly covered with about a 15.3 cm (6 in) layer of ice when the craft arrived. At the end of the day, after running repeatedly over it, the ice was seen to be broken up and moving downstream. The craft was in fact performing high-speed ice breaking, a phenomenon recognized and exploited in later years by the Canadian Coast Guard. ACV's are now used to keep water channels open in some cold regions. The performance of the Arcopter GEM-2 was far superior to any of the previous Bertelsen peripheral jet craft, but still had its pitch-up problem and lacked any braking, backing, and roll control capability. Forward visibility was limited by the high cowl and engine. It would also *hang up* on various projections, rocks, hummocks, etc.

The Arcopter GEM-3, flown in October, 1963, was designed to overcome the pitch-up and visibility problems. It had a 134.3 kW (180 HP) Lycoming engine and an air boat propeller mounted in the rear wing to avoid the cabin noise and vibration experienced with the previous two GEM's. This craft was effectively a negative-stagger biplane with sidewalls, the forward airfoil being under the cabin and including it. All of the ACV's so far were under 2.44 m (8 ft) wide to allow road travel without folding or dismantling parts of the craft. Adding folding stub wings to increase lift and much needed roll control was considered but not implemented. Figure 16.11(a) shows a front view of the Arcopter GEM-3, which had wheels for better handling and preventing *hang-up* on local surface elevations. A flexible membrane skirt was added to the sides to absorb surface roughness, without severe loss of lift, and to avoid high friction drag. There was a hinged forward gate to close the lift chamber at low speed, and a 15.2 cm (6 in) belting membrane at the bottom edge to take abrasion. This gate was meant to swing back up flush with the front wing when the dynamic pressure exceed the static pressure at high speed.

Figure 16.11(b) shows the rear gate/elevator which was closed at low speed to capture lift air pressure. At high speed, when the fore and aft air foils were lifting in ground effect, the rear surface was to become an elevator for pitch control. The rudder served for yaw control at all speeds. Although the Arcopter GEM-3, with its wheels and flexible skirts, was an improvement over its

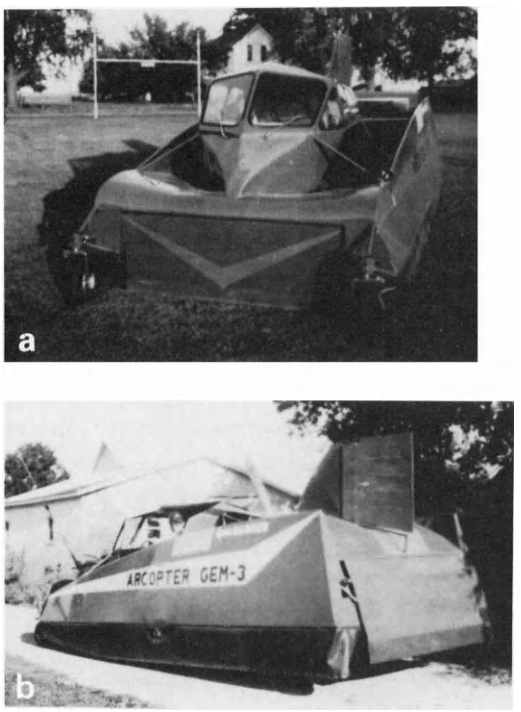

Fig. 16.11 Arcopter GEM-3: (a) front view; (b) left rear view.

two predecessors, it did not overcome the braking, backing and lateral control problems; so the concept was abandoned.

16.3.4 Tilting Fan ACV's

Several attempts were made in subsequent models and full-scale ACV's to direct the slipstream to provide both lift and propulsive force from a single ducted fan. A circular 2.44 m (8 ft) diameter craft (Fig. 16.12) with a 8.9 cm (3.5 in) flexible rubber skirt was flown on April 4, 1965. The ducted fan had fore and aft tilt-ability, and the slipstream was confined to the lift chamber by means of a flexible shroud. Multiple rudders were used for yaw control. This was the tenth in the series of full-scale ACV's. The object was to produce both thrust and lift forces by reaction of the slipstream exiting through the circular base.

The tiltable, shrouded and ducted fan, rudders and 6 kW (8 HP) direct-drive engine from Aeromobile 10 (i.e., the tenth ACV) were fitted onto a rectangular 1.22 m × 2.44 m (4 ft × 8 ft) chassis. With the addition of a 15.2 cm (6 in)

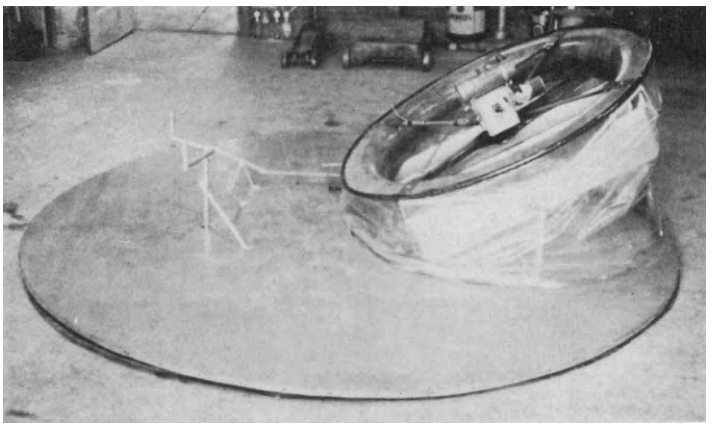

Fig. 16.12 Circular planform Aeromobile 10 with shrouded tilting duct.

segmented skirt, this craft became Aeromobile 11 (Fig. 16.13). Both vehicles achieved lift, but very weak thrust and yaw forces. It was then concluded that directing lift air for steering or propulsion was hopelessly inadequate, no matter how it was accomplished. Only free air slipstream over the deck would be adequate for propulsion, braking, steering, and bow and stern positioning.

Fig. 16.13 Rectangular planform Aeromobile 11 with shrouded tilting duct and segmented flexible skirt.

The first attempt to achieve this was to refit the Aeromobile 11 chassis with a tiltable drum in which a twin, 6 kW (8 HP), ducted fan was installed. The lift would be provided by part of the slipstream directed below at all times, and fore or aft thrust would be imparted by tilting the drum fore and aft to shoot free slipstream over the deck. This provided non-steered braking force in reverse (Fig. 16.14(a)). The rudders on the stern discharge provided yaw control for forward travel only, a less than optimal result (Fig. 16.14(b)). This was Aeromobile 12, flown in December, 1966.

The next concept was a model with a universal electric motor and 20.3 cm (8 in) propeller set in a duct within a cylindrical drum that rotated on a transverse tilting axis in the rear of a 61 cm (24 in) × 35.6 cm (14 in) aluminum chassis. The discharge end of the drum-mounted duct had rudders in the slipstream of the fan for steering or yaw control at all angles of fore and aft tilt of the drum. Figures 16.15(a) to (c) show the model with one side removed. When the fan shaft was vertical (Fig. 16.15(b)), the discharge was into the lift chamber only, but the rudders could direct the thrust right or left for yaw force. Figure 16.15(a) shows the drum tilted to discharge part of the slipstream over the tail for thrust, and the other part into the lift chamber.

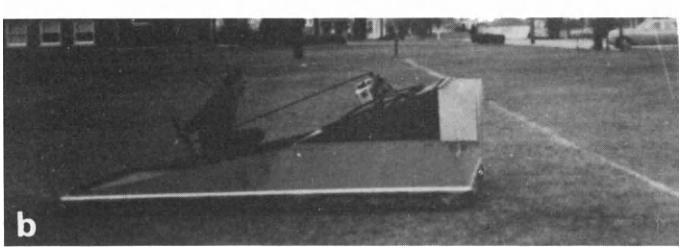

Fig. 16.14 Rectangular planform Aeromobile 12 with segmented skirt and ducted fan mounted in transverse axis tilting drum: (a) drum in reverse for braking thrust; (b) drum tilted for forward thrust and slipstream ejected through stern rudders for yaw control.

tilt of the drum. Figures 16.15(a) to (c) show the model with one side removed. When the fan shaft was vertical (Fig. 16.15(b)), the discharge was into the lift chamber only, but the rudders could direct the thrust right or left for yaw force. Figure 16.15(a) shows the drum tilted to discharge part of the slipstream over the tail for thrust, and the other part into the lift chamber. The rudders would be effective for yaw control. Figure 16.15(c) shows the drum tilted for reverse thrust with the top part of the slipstream ejected forward. The rudders would steer the craft in backing or braking. The bottom part of the slipstream would provide lift.

This was just before the dawn of the incredibly obvious (in retrospect) *Gimbal Fan* concept whereby the slipstream direction can be controlled arbitrarily in three-dimensional space. How much blundering was done before the ultimate, inevitable, free-tilting ducted fan was conceived! Ideally, there should have been a single leap from plenum chamber to gimbal fans instead of the many models and 13 full-scale machines. This concept, through its application to the Aeromobile 13 to 16 ACV's, is presented in Section 16.5.3 on improved controllability.

16.4 REASONS FOR SLOW GROWTH OF THE ACV INDUSTRY

16.4.1 Comparison with the Aircraft Industry

There is a sharp contrast between the time frame in the development of the aircraft industry and that of the ACV. The Wright brothers first flew a controllable, powered, man-carrying aircraft in 1903, and by the start of World War I in 1914, a mere eleven years later, every major nation had operational military aircraft. There were, by then, hundreds of airplanes world-wide. The exponential propagation of aircraft over the earth has continued relentlessly, and air travel is the principal national and international long-range mode of transportation. At the present time, relatively few people have seen, much less traveled on, an air cushion vehicle. Most people would not know where to find an ACV, with the exception of the English Channel hovercraft ferries which are often confused with hydrofoils.

Another contrast can be drawn between the development of the helicopter and that of the ACV. Igor Sikorsky flew his first successful helicopter in 1939, and helicopters were in limited use in Word War II. The American government spent more than one billion dollars over two decades to bring this awkward, vibration-generating, self-destructive and failure-prone aircraft to reasonable utility. Other governments as well (U.S.S.R., U.K., West Germany and France, for example) have invested heavily in helicopter research and development.

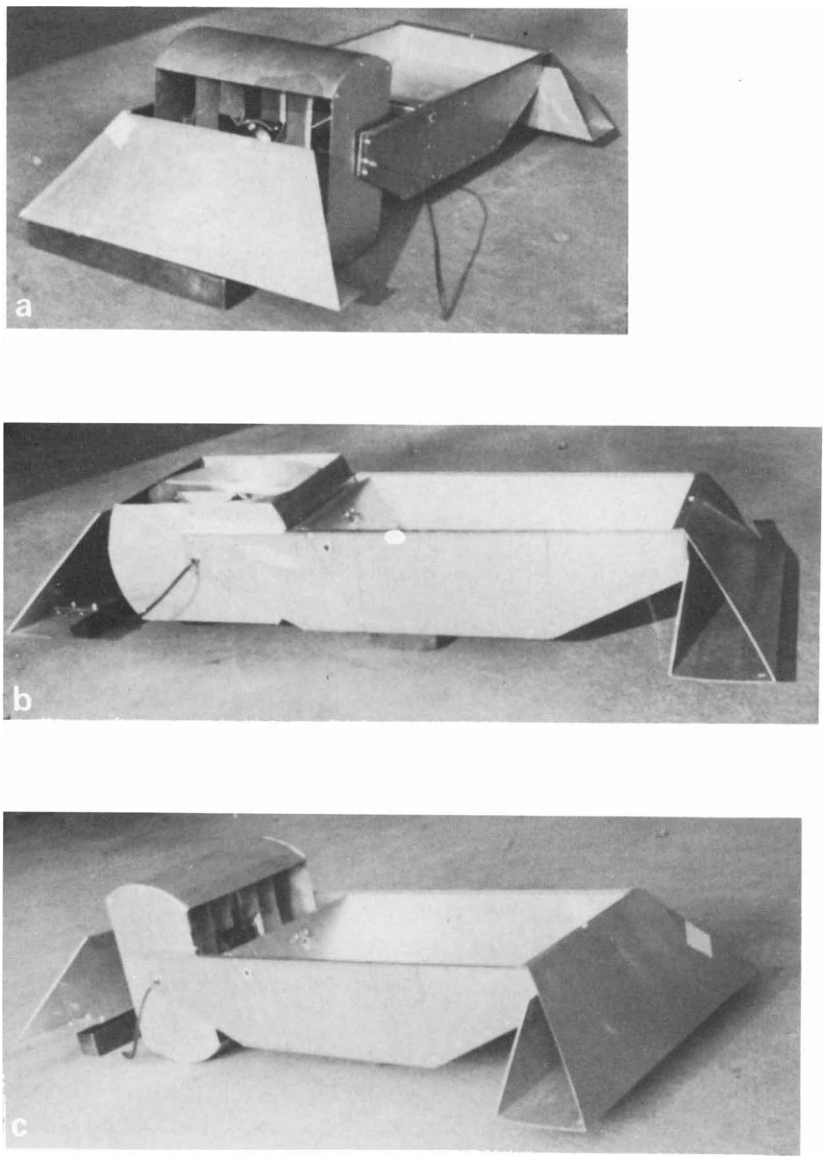

Fig. 16.15 Electrically-powered model with ducted fan mounted in transverse axis tilting drum and multiple rudders in fan slipstream: (a) fan oriented to provide forward thrust and lift, with rudders for yaw control; (b) fan oriented to provide lift air only, with rudders producing yaw force; (c) fan oriented to provide reverse, or braking, thrust and lift.

Despite the high fatality rate, and the exorbitant first cost and operating expense compared to fixed-wing aircraft, it has been almost the only VTOL available. The military branches of every government have helicopters. Helicopters are used for civilian transport, corporate travel and rescue, among other applications.

The multi-billions of dollars spent to overcome difficult technical problems associated with helicopters and to procure them in large numbers contrasts sharply with the paltry few millions spent by governments over three decades on research, development and purchase of ACV's. Many missions performed by costly and dangerous helicopters could be accomplished more quickly, cheaply and safely by ACV's. The failure of governments and corporations to recognize the capability of ACV's and to develop and purchase them for multiple uses, as they did with airplanes and helicopters, is one critical cause of the present state of ACV neglect.

16.4.2 Disappointments

The ACV concept was perhaps over-sold, especially in the early years, so that the potential buyer, investor or user expected more than it could provide. The ACV tended to be regarded as an *all-terrain vehicle* (ATV), which is impossible in its conventional form because it cannot climb significant grades or overcome large obstacles. The buying public and manufacturers were too slow in discovering that the *conventional* ACV was not an ATV, and that there were many early technical problems and inherent limitations. The overweening elegance and *magic* of the free air flotation of a vehicle led many investors and entrepreneurs to spend too much too soon on styling, tooling and marketing of unperfected and, as yet, impractical craft.

Poor product performance and insufficient sales led to multiple bankruptcies. Low research and development funding and purchase of ACV's by governments inhibited further private capital from being ventured. Thus, the evolution, optimization and production of practical craft stagnated.

16.4.3 Product Liability

To add to all the problems of new and old industries, product liability now rears its ugly head in the United States. A recent Hoverclub of America rally at Indianapolis had to be cancelled because the insurance premiums to cover the liabilities of such an event were prohibitive. When the price of every general aviation aircraft was increased by 30% for product liability coverage, it nearly sealed the doom of that industry. As a result, almost no single-engine private aircraft are now being manufactured in this country. In the future, unless the laws are changed drastically, it will require very brave people to invest in a new product with a limited safety record and high, or unknown, liability premiums.

16.4.4 Technological Stagnation

The development of the ACV came to a standstill about two decades ago. its configuration became *frozen* internationally from about the late sixties to the late seventies. The accepted design had unshrouded thrust propellers at the stern, with rudders and elevators in the slipstream, and separate lift fans. The performance limitations inherent to this configuration were recognized by the public and investors alike. The following shortcomings were highly detrimental to the success of these vehicles:

(a) They could not climb sustained grades in excess of 10% and were unable to negotiate a side hill since no side force was available to steer the bow.

(b) They could not be steered sharply like an automobile or a boat. Great skill was required from the driver to negotiate a high-speed turn, avoid obstacles, or resist wind gusts.

(c) Reverse thrust for braking or backing-up was minimal and there was essentially no control in reverse.

(d) The unshrouded thrust propellers produced excessive noise.

(e) The small craft that were available usually had two-cycle snowmobile engines: one for lift; the other for thrust and steering. Being air-cooled, these engines were subject to seizure. They were not designed for marine operation and often had other operating problems. A failure of either engine incapacitated the craft. There was often great consternation whenever it occurred in remote locations, where the craft was quite capable of traveling.

(f) The cost of large ACV's was high. Though quite reliable, they had costly turbine engines which used excessive fuel at sea level. The purchasing and operating costs of these craft were prohibitive for all but large operators and the military. Very few were sold privately, and the total worldwide market has been only a few hundred large craft.

(g) Most *conventional* ACV's continue to have high stern vertical surfaces to provide yaw stability at cruise speed, or rudders for yaw control. These vertical surfaces do provide those benefits but introduce *weathercocking* into the yaw dynamics. Any side wind creates a moment which tries to turn the craft into the relative wind, at an angle given by the resultant forward velocity and wind velocity. The *crab angle* is the angle between the latter resultant velocity and the forward velocity. An airplane encountering the same phenomenon is said to be *crabbing*. The crab angle adds a degree of roll instability since the ACV is partly heading with its side into the relative air velocity, and the beam is narrower than the length. Furthermore, the vertical tail surfaces with stern-pusher propellers make traveling downwind at low speeds almost impossible because

of weathercocking. The requirement of slipstream over the rudders to achieve yaw control while traveling downwind causes the pilot to increase thrust and make the craft go faster, not more slowly. Therefore, it is usually necessary to approach destinations upwind, if possible, which seriously restricts operating freedom and demands more pilot training and skill.

(h) High-speed turns on water, in the conventionally configured ACV with stern propulsion and no keel, result in large crab angles. The stern-only thrust force must be directed radially outward to overcome centrifugal force and hold the craft in a given radius of turn. The ACV is then proceeding at high speed nearly beam-on or sideways and even more prone to capsize than in crabbing.

(i) The usually high thrust line of the stern pusher propeller causes a nose-down pitching moment that can cause the ACV to *plow-in* or nose-dive into the water, especially at full throttle. This is a dangerous occurrence that can cause damage to the structure or capsizing of the craft.

(j) The typical medium-sized ACV has the rear half of its hull occupied with engine, transmission, lift fan, propulsion fan or propeller, with rudders and even elevators in the slipstream, thereby rendering it tail-heavy and limiting its cargo space.

(k) With only the forward half of the hull remaining for cargo or passengers, longitudinal trim can be a problem. It is often necessary to use ballast shifting, fuel transfer, skirt manipulation, or elevator deflection to offset changes in the static pitching moment due to cargo or passenger loading changes.

The new *breed* of medium-sized ACV's in the 1980's has an incremental performance improvement over the *frozen* design of the sixties and seventies. It persists in a technological *arrest* at another stage of development, well short of total adequacy. It remains to be seen if the public will share the producers' enthusiasm for this generation of ACV's any more than the first offerings. There are, and no doubt will be, some sales of these craft since there is now essentially only one configuration in production from all manufacturers, all with an obsession for duplicating nearly identical ACV's. Regrettably, these *new* ACV's do not eliminate many of the old problems and even *aggravate* some of them. The following are some of the improvements and shortcomings of mid-sized ACV's of the eighties:

(1) They all have ducted fans which reduce the noise, propeller diameter and thrust line, but *add to the weathercocking tendencies*.

(2) Some have reversible-pitch propellers which can produce braking and backing thrust, but, in the single-duct vehicles, there is with virtually *no yaw*

control since the rudders are on the intake side of the duct in this mode of operation.

(3) The elevators in the duct discharge *reduce the thrust force* by introducing drag and deflecting the thrust vector, notwithstanding the benefit of their straightening effect on the slipstream swirl of single-rotation propellers.

(4) The dependence on elevators for pitch-trim forces is *highly capricious* since these forces vary with thrust. When the thrust is reversed, elevator trim is negated.

(5) There is no improvement in the weight and space required for lift and propulsion at the stern of the *unstretched* craft, nor in the consequent *longitudinal trim problems*.

(6) In the *stretched* versions with single lift and propulsion power systems in the stern, the center of lift is less obstructed, and placing more payload there reduces the pitch-trim problem. However, elongation of the base *decreases yaw controllability* and the ability to operate sideways on hills.

(7) By installing dual lift and propulsion systems in the stern (usually with both length and width stretching), greater lift, thrust and payload are realized with twice the reliability of the single-power-system ACV's. However, the gain in yaw control and bow positioning ability with laterally-disposed stern thrusters is somewhat limited by the use of fixed-pitch propellers. By throttling down one power system and increasing power on the other, the yaw torque is increased over and above the effect of deflected rudders, but again the craft is thrusted forward, which may or may not be desired. *The ability to go slowly downwind has not been achieved. Weathercocking is even worse* with more rearward vertical surfaces on a longer lever arm from the center of gravity.

(8) There is no improvement in the ability to negotiate high-speed turns, avoid obstacles, or resist waves or gusts, since no universal thrust force is available to the pilot from either bow or stern.

16.4.5 Universal Thrust in Large Modern ACV's

The following are some of the large modern ACV's that have attempted to deal with the problem of producing universal thrust at both ends of the craft:

(a) The SRN-4 has four huge swivelling pylon-mounted propellers, one above each corner of the top deck. Each one is capable of directing thrust in any direction for much improvement in controllability. However, this configuration is limited to large craft with no people on the top deck who can enter the domain of the rotable propellers. It cannot be scaled down to medium or small ACV's because of personnel hazard and the pitch and roll effect from

the high thrust line. Also, even with controllable reversible-pitch propellers, such a system does not provide quick redirection of force in response to waves and winds.

(b) The BHC-7, with two top-deck pylon-mounted propellers, has similar advantages and limitations.

(c) The latest, most advanced, large craft include the AP.1-88 of the British Hovercraft Corporation. It has dual stern-mounted reversible-pitch ducted propellers with rudders in the slipstream. Two forward centrifugal lift fans on each side divide their discharge between the lift chamber and a vertical stack with a 360° pivoting, right angle nozzle for horizontal force from the bow. When directed rearward, it adds to the forward thrust and can be used for lateral force on the bow and for braking or backing. The total nozzle force is a fraction of the total stern-propeller force. Differential stern propulsor thrust adds to yaw control. The craft can be turned in its own length when hovering, but great skill is required of the pilot to use full reverse thrust for yaw control at cruise speed.

(d) Like the AP. 1-88, the U.S. Navy Landing Craft Air Cushion (LCAC) has a similar configuration with similar limitations. Neither one can produce 100% of thrust force rapidly in any azimuth direction, including forward, nor finely-metered force which can be cut off instantly or reversed as needed. Of course, these are very massive craft, less susceptible to wind and wave forces than small or medium ACV's.

(e) Some large ACV's, such as the Jeff A (unsuccessful contender in the competition for the U.S. Navy's LCAC contract), have four large universally-swivelling ducted fans, one on each corner of the top deck. A large ACV built by Wartsilla in Finland has similar propulsion and steering. Only very large craft can safely use this system because of the need for a clear top deck to avoid sucking or blowing materials or people into the ducts or off the vehicle. In smaller craft, the relatively high thrust line would impart unacceptably large pitch and roll moments.

Pilot training for operating the SRN-4, BHC-7, Jeff A, Wartsilla, and other such craft with high-mounted rotable multiple-thrusters must be very intensive. Pilot performance must be flawless in close quarters. The pilot has to contend with not only the direction of thrust from several points, but also thrust magnitude using throttles or pitch controls. To start and stop translational or rotational motion of such massive craft requires exactly the correct positioning of, and magnitude and duration of power to, thrusters despite much lag in the equipment. In open seas or on ice, the piloting is less difficult, but when approaching breakwaters, piers, other craft, etc., anticipation and quick, but accurate, responses are necessary. No sudden force is available to the hapless

operator in response to a high wave or strong wind gust. Time is required to wave or strong wind gust. Time is required to rotate and speed up or change pitch of the thrusters even if he chooses his actions correctly and quickly.

As a result, accidents are inevitable, such as that suffered by the large French Naviplane some years ago. It had mounted the ramp at its arrival base and, while still on its 2.44 m (8 ft) cushion, was blown over by a gust into a car parking lot. The only choice the pilot had was to throttle back on lift and thrust, causing the craft to settle on and crush several unoccupied automobiles. More recently, the Princess Margaret SRN-4 struck a breakwater while approaching the Dover base. Hull damage, injuries and several fatalities resulted. Both accidents might have been avoided if the pilot had had access to a quickly-available, universally-directable, maximum thrust force to counter divergent motions of the craft from any cause.

16.4.6 Inherent Problems

Certain problems are inherent to ACV technology. The objectionable spray or efflux of water, mud, sand or dust from the cushion region can be minimized, but never eliminated. To minimize the efflux and keep lift-air power-demand reasonable, the base pressure should be below approximately 1.72 kPa (0.25 psi) in small and medium ACV's. Therefore, in order to carry useful loads of people or cargo, the base area must be quite large. However, the craft cannot be merely increased in length to provide the required lifting base area because it can then become roll unstable. To make the craft stable in roll, the width should ideally be at least one-half the length. The resulting width for a medium-sized ACV of 2,268 kg (5,000 lb) gross mass (about eight passengers) necessarily becomes wider than the 3.05 m (10 ft) maximum *roadable* width. Thus, for highway, ship or air transport, it is often necessary to design detachable, or folding, skirt-carrying side-structures.

With the benefit of skirts comes yet another limitation, namely, the height, or vertical length, of the skirt. Experience shows that the maximum height to produce a stable ACV is about 10% of the narrowest base dimension. For example, a 3.05 m (10 ft) wide craft is limited to a skirt height of 30.5 cm (12 in). Such a craft will clear only a 30.5 cm (12 in) protrusion without *hangup* and it will have to do so at low speed to avoid skirt damage. To get a higher belly clearance, it is necessary to incorporate a wider base and either ignore roadability or design folding elements.

Finally, the skirt is vulnerable to damage from sharp projections, such as stumps, rocks and ice ridges, and is subject to wear from other surfaces. Notwithstanding possible improvements in skirt technology, skirt wear is a factor which will always limit the utility of ACV's and contribute to their cost of operation.

16.5 MEANS TO REVITALIZE THE ACV INDUSTRY

16.5.1 Innovation

The above critique makes the ACV sound like a hopeless proposition. Its relative lack of success to date indicates that the old machines were not very good, and the new ones are not much better. It appears that there has been far more engineering on production than innovation, although the engineering of medium and large modern ACV's is excellent. Still more discouraging is the fact that some ACV problems are inherent. However, none of the inherent shortcomings are sufficiently severe to eliminate the craft from contention. It has the potential of being accepted as a critically needed, truly successful amphibian which will go at twice the speed of boats, oblivious to climate, seasons, mud shallows, debris, ice, ice floe, sand bars, etc., *provided* it is affordable, safe, and acceptably controllable and maneuverable under all conditions.

The salvation of the industry, especially the small-craft industry, depends on fundamentally new concepts and their implementation. The best example of a brillant innovation that advanced ACV technology is the segmented skirt, invented by the late D. S. Bliss of Hovercraft Development Ltd., in England. This skirt made the ACV practical in performance and economical of lift-air power.

16.5.2 Advanced Structures

The ACV structure has to be capable of withstanding salt-water corrosion, water soaking, mold, vibration fatigue, impact damage, and other forms of deterioration over a long life-time. In the past, it has been built of wood, aluminum, steel, fiberglass (FRP) composites, or thermoplastics. New materials offer new possibilities.

One of the most promising materials for marine structures has been developed by Gougeon Brothers, Inc., of Bay City, Michigan. They are experienced boat builders who have evolved the Wood Epoxy Stabilization Technique, or WEST, System (Trade Mark). Douglas fir sheets of 0.254 cm (0.1 in) thickness are coated with epoxy resin and laminated one on another to the appropriate thickness for the required strength at any given point. The structure is then vacuum pressed, or pressed into a pre-formed mold, and cured for eight hours. Typically, each side of a boat hull can be constructed in this fashion. Then, after planar trim sawing, epoxy putty is used to cement the two halves and the transverse bulkheads. The end product is extremely resistant to corrosion, water, mold, fatigue and impact damage, and has a greater stiffness than FRP. It is also highly repairable in the field without welding or riveting. The empty weight and cost of a carefully designed chassis, large or small, would probably be less than one built with FRP, aluminum, or other wood techniques.

Very large structures have been constructed by the Gougeon WEST System: a) one 39.6 m (130 ft) diameter two-bladed wind generator for NASA, b) sixteen 42.7 m (140 ft) diameter two-bladed wind generators for Westinghouse, and c) over one thousand 15.2 m (50 ft) and 24.4 m (80 ft) blades for wind-farm operators. The wood epoxy laminates have withstood various forms of deterioration better than any other structural material, including Kevlar reinforced FRP and other metal or composite combinations.

The sidewall Vosper Hovermarine HM-2 is made of FRP and, upon stretching the craft, the limits of that composite material are being approached. The wood-laminate techinque using epoxy should be considered for large and small craft. For small and medium ACV's the Gougeon WEST System will certainly save weight, money, labor, and maintanence.

16.5.3 Improved Controllability

The solution to the problem of universal controllability, at least for small and medium-sized ACV's, is the Gimbal Fan System (refs. 11 and 12) introduced briefly at the end of Section 16.3.4. This invention has evolved and been exhaustively tested through four full-scale prototypes, namely the Bertelsen Aeromobile 13 to 16 ACV's (Figs. 16.16 to 16.19). The twelve-bladed fan used in Aeromobile 16 is shown on a test stand in Figure 16.20.

The gimbal-fan concept has been tested in ACV's of up to 2,268 kg (5,000 lb) gross mass. It was found that the horizontal force required to accelerate, turn, side-step, back-up, and brake while steering, or pivot in place on cushion, is available to the pilot at all times. The gimbal fans are kept at cruise throttle whenever the craft is on cushion, and sufficient air is always diverted to the lift chamber regardless of the maneuvre. But the maximum thrust, or any fraction of it, can be applied instantly in any direction by

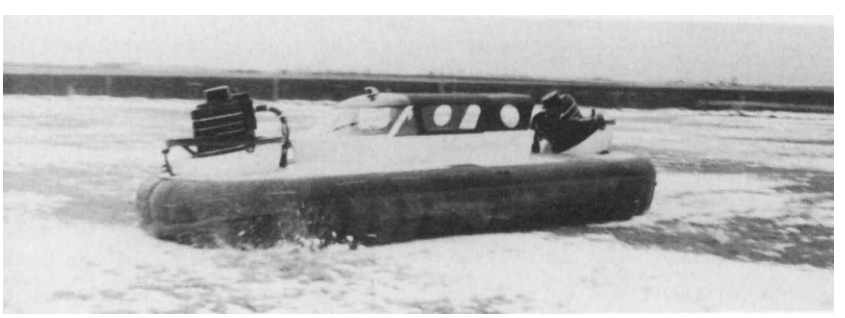

Fig. 16.16 Aeromobile 13. Two gimbal fans, each driven by a 93 kW (125 HP) engine, with front fan providing lift only and rear fan thrusting, lifting and steering the craft.

Fig. 16.17 Aeromobile 14. A single gimbal fan, driven by a 41 kW (55 HP) engine, providing lift for three persons, yaw control and sufficient thrust for a top speed of 20.6 m/s (40 knots).

tilting the gimbal to release slipstream over the deck. The pilot needs little training and makes few errors since he only needs to move the stick in the desired direction of travel. The control of the craft is natural in the sense that the pilot will instinctively take the appropriate action for the desired response.

The following controllability advantages of the gimbal-fan ACV have been demonstrated: a) 100% of thrust force available in any direction, in any intensity, and instantly cancellable and reversible, b) full forward propulsion, or reverse propulsion for braking or backing, with yaw control from each gimbal at any degree of tilt, c) full sideways, or diagonal, force available, or

Fig. 16.18 Aeromobile 15. The single gimbal fan is driven by a 93 kW (125 HP) engine.

rotational moment for pivotal motion, d) no weathercocking, e) low thrust line across the deck level, reducing pitch and roll moments, f) instant saving forces available against plow-in or overturning, g) up to 100% of power divertible for lift, if required to travel over porous, permeable substrates such as large gravel, brush vegetation, etc., h) 50% of total thrust available at each end of the craft for omnidirectional effort to control the bow or stern position for sideways hill negotiation, i) smaller turning circle using radial force inward by outward gimbal-fan thrust, allowing bow-forward turns without crabbing, j) full lift-thrust to *rock* the craft off a hang-up by tilting the gimbals back and forth while maintaining full throttle, and k) powerful and reliable control forces and natural operating mechanisms to reduce pilot training time.

The operational advantages are: 1) inherently quiet, efficient and safe, ducted fans, 2) low silhouette, 3) low center of gravity, 4) payload at center of gravity and center of lift, avoiding trim problems, 5) hold or deck relatively unobstructed by lift or propulsion machinery, providing an excellent work platform for agriculture, freight, etc., 6) self-sufficient gimbals, independent with respect to fuel, electrical, servo and ignition systems, thereby providing multiple engine reliability, 7) separate lift, thrust and control of each gimbal unit to operate the craft in the event of one engine failure, 8) minimal time, effort and labor to remove and replace gimbal units, 9) growth capacity by designing for several gimbal units on larger craft, and 10) worldwide availability of reliable, light weight, marine engines up to 164 kW (220 HP), with parts and service.

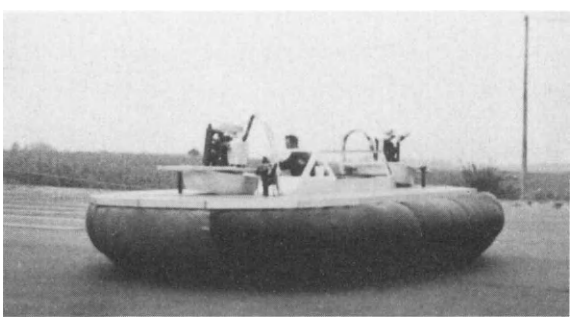

Fig. 16.19 Aeromobile 16. Two 91.5 cm (36 in) gimbal fans, each driven by a 93 kW (125 HP) engine. The fans are being replaced by 101.6 cm (40 in) diameter 12-blade fans (Fig. 16.20) to be driven by 112-164 kW (150-220 HP) engines.

The available gimbal fan technology can provide all the lift, thrust, steering and braking requirements of small- to medium-sized ACV's. However, the combined lift-thrust gimbal fans which could satisfy the performance

requirements of large ACV's have not yet been designed or tested. They would have to compete with the very efficient centrifugal blowers which are now the standard lift-air generators in heavy ACV's. Single rotation, unstatored fans would no doubt be stalled against the relatively high cushion pressures of large ACV's. It may be possible to design ducted fans with several stages of fans and stators, or dual rotation, to be efficient in both high-pressure lift generation and relatively low-pressure, but high-thrust, production. A combination of centrifugal and axial-flow gimbal fans may be possible. Research and development are required in this area. If such equipment were available, the operator of the very large ACV would also have access to a 360° thrust force from any corner of the craft to provide the same precise positioning and controllability available to the pilot of small and medium-sized gimbal fan vehicles.

Fig. 16.20 Twelve-bladed 101.6 cm (40 in) diameter fan on test stand without spinner.

In the author's experience, such strong and instantaneously directable forces as are available from gimbal fans are mandatory for good controllability and safety. Furthermore, it is his belief that wide public acceptance of ACV's is dependent on the implementation of such a technology. Therefore, in case others cannot share his enthusiasm for the gimbal-fan concept, he urges them to propose alternative innovations capable of giving new life to the ACV industry.

16.5.4 Funding and Publicity

All instances of superior performance by ACV's should be publicly demonstrated. Television offers the ideal medium for showing the world (not just the ACV community) that ACV's can perform better than other craft in appropriate applications worldwide.

Private capital should flow naturally into the industry, once a truly satisfactory machine has been demonstrated. The profit motive should inevitably draw investment into the ACV industry after the opprobrium of failures has been superseded by craft which will have finally lived up to their potential and justified their mass production and marketing. This is where government plays a crucial role. Money will not be attracted from investors until they see that ACV's are better than other vehicles at performing certain missions econcomically. Government must fund promising ACV prototypes as it did for airplanes and helicopters.

16.6 CONCLUSION

The challenge facing the ACV industry is the choice between stagnation and triumph. Triumph demands bold concepts, daring innovation, inventive genius; serious, practical business enterprise fuelled by courageous, enlightened investment; and persevering confidence in the stupendous principle of the Air Cushion Vehicle.

16.7 REFERENCES

1. R.E. Kuhn and J.W. Draper, Investigation of Effectiveness of Large-Chord Slotted Flaps in Deflecting Propeller Slipstreams Downward for Vertical Take-off and low Speed Flight, NACA TN 3364, 1955.
2. U.H. von Glahn, Exploratory Study of Ground Proximity Effects on Thrust of Annular and Circular Nozzles, NACA TN 3982, NACA Lewis Flight Propulsion Laboratory, Cleveland, Ohio, April 1957.
3. M. Mann, Here Come Cars without Wheels, Popular Science Monthly, July 1959.
4. W.R. Bertelsen, Experience with Several Man-Carrying Ground Effect Machines, Princeton Symposium on Ground Effect Phenomena, Princeton University, October 21-23, 1959.
5. W.R. Bertelsen, Aeromobile, Winter meeting, American Society of Agricultural Engineers, December 15-18, 1959.
6. W.R. Bertelsen, The Design of Ground Effect Vehicles, Canadian Aeronautical Journal, Vol. 6, No. 6, June 1960.
7. W.R. Bertelsen, 1,500 M.P.H. Family Cars?, Popular Science Monthly, August 1961.
8. W.R. Bertelsen, Aeromobile, Arcopter, Aeroplow, Airtrack, and Other Uses of Ground Effect, Winter Meeting, American Society of Agricultural Engineers, December 13-15, 1961.
9. W.R. Bertelsen, The Ultimate Vehicle, Initial Lecture to the Research Symposium on Air Cushion Craft, Department of Engineering, University College of Swansea, Great Britain, July 21-23, 1964.
10. W.R. Bertelsen, Aeromobile, National Safety Congress, Chicago, 1964.
11. W.R. Bertelsen, The Evolution of Integrated Lift, Propulsion and Control in the Aeromobile Air Cushion Vehicle, Third Symposium on Air Cushion Technology, Canadian Aeronautics and Space Institute, Montreal, Canada, 1969.
12. W.R. Bertelsen, The Gimbal Fan Air Cushion Vehicle, AIAA/SNAME Advanced Marine Vehicles Conference, San Diego, California, April 17-19, 1978.

Chapter 17

SAFETY CONSIDERATIONS

17.1 INTRODUCTION

Hovercraft are sufficiently different from other forms of transport that their special design and operational characteristics must be fully understood and recognized when attempting to develop safety requirements and when trying to operate them.

When the SRN-1 crossed the English Channel in July 1959, thus demonstrating the potential for international hovercraft service, two questions immediately and repeatedly arose: "What is it?" and "Is it a ship or an aircraft?" Even today, after over 20 years of service on that and other international routes, there are no clearly consistent answers amongst countries in which hovercraft operate. Why not? Furthermore, does it matter? To this last question, the answer is a very clear "Yes, it does matter". It matters because national authorities responsible for safety of transportation need to develop and apply appropriate safety measures. Under democratic forms of government, such measures require some form of legal power, such as an act of parliament, before they can be introduced. A government must therefore decide what form of transport it considers a hovercraft to be, and then either introduce new legislation or amend existing acts to provide the necessary legal power. It also matters because the safety of aircraft and ships is subject to international rules and codes upon which countries base their detailed safety regulations. It is therefore essential that the position of the hovercraft within the overall transportation scene be firmly established so that appropriate international safety measures can be adopted.

Initially, there were three options available to governments. Hovercraft could be treated as an entirely new breed of vehicle, or they could be regarded as either aircraft or ships. The fact that all three options have been

exercised, and the manner in which they have been treated clearly illustrates the dilemma and problems faced by governments. The United Kingdom elected to recognize hovercraft in their own right, and passed the Hovercraft Act providing power for their safety regulation. That power is administered, for the vehicle itself, by the agency responsible for aviation safety; for crew certification, passenger safety and operations, by the department responsible for marine safety. The United States elected to regard hovercraft as ships, so they are required to comply with regulations applicable to conventional ships. This would appear to require some broad interpretations and the need for exemptions of detail (ref. 1). The Canadian government has classified amphibious hovercraft as aircraft. This conflicts with international agreements (see below) and, possibly prior to publication of this work, legislation may be passed permitting them to be classed as ships.

International services between England and France grew from tentative experiments in 1966 to full service in 1968, and the dilemma had to be resolved. The solution was provided by ICAO (International Civil Aviation Organization), the international body responsible for aviation safety which, in 1967, re-defined an aircraft specifically to exclude hovercraft. Internationally, since hovercraft could not be aircraft, they were regarded as ships. IMCO (Inter-Governmental Marine Consultative Organization, now International Marine Organization), the marine equivalent of ICAO, attempted to grapple for a number of years with the novel problems posed by these craft, but the result was inconsistent levels of safety in different aspects. Recognizing this, IMCO charged an expert working group with the task of developing an international safety code for hovercraft (and hydrofoils). This task was completed between 1972 and 1977, and resulted in ref. 2. The background to this work is described in refs. 3 and 4.

What are these problems which caused so much concern and took so long to resolve? Any form of transport must have a body or hull designed to withstand the stresses of its operational environment and which contains all the necessary machinery and systems to enable it to move and navigate along its route, avoiding obstacles, and to communicate. It must also contain provisions, systems and equipment to deal with possible emergencies and to evacuate personnel if necessary. Finally, it must be provided with an appropriately trained and qualified crew. Let us now look at some of these in detail, and since it was attempts to relate hovercraft to marine safety which created difficulty, we will use marine concepts as a yardstick. However, it is absolutely fundamental to remember that the overall level of required safety can only be achieved by correlating the component aspects which combine to provide the required overall balance. Lack of opportunity to do this initially within IMCO was the cause of early problems.

17.2 DESIGN-BASED CHARACTERISTICS

A conventional ship is designed to float and operate in water of a minimum depth; consequently, it has immediate and constant access to water for cooling machinery and fighting fires. But it is restricted to deep-water channels and, if it runs aground, it can take on water and sink if it is not sufficiently compartmented and provided with a comprehensive bilge pumping system. Because ships require a minimum water depth, their choice of routes may be restricted regarding, for instance, approaches to harbours; this can lead to congestion and an increased risk of collision. Fire and sinking resulting from bottom damage or collision are probably the two most significant risks affecting the guiding principles of design. Associated with collision damage, which may result in capsizing, is the consideration of floating hydrostatic stability. A ship's hull form and buoyancy characteristics must meet clearly defined stability criteria, wherein the relative vertical positions of the centre of buoyancy and centre of gravity are predominant factors.

In a conventional ship, weight and space generally are not primary constraints which affect design or selection of machinery and systems components. The preferred structural material is steel, and this is followed through into machinery and systems. The components are designed to operate for days at a time over a period of many years, albeit with adequate space for routine monitoring and maintenance. In passenger ships, the passengers are free to walk about, sit in numerous saloons, and are generally unsupervised. This must be considered when providing not only fire safety measures, but also the evacuation facilities and procedures.

Taking the above points in the context of a hovercraft, we can perhaps begin to grasp the nature of the problems posed by these craft in providing at least a similar level of safety. Hovercraft are not designed to operate in the water, but over it. Certainly they must be designed to float in case the lift system fails or because they are used for operations requiring them to float. But in their primary mode of operation (excluding sidewall craft or SES), they do not have access to water for firefighting or machinery cooling. Fire safety must be self-contained, and machinery which does not rely upon water cooling alone must be selected. Since they operate above the water, the risk of bottom damage and taking on water is greatly reduced. For the same reason, hovercraft have freedom of movement outside deep-water channels and the risk of collision with other vessels is therefore minimized. But hovercraft are amphibious, and they can suffer bottom or side damage either by landing on rough surfaces or by colliding with structures or buildings. There is therefore a need for water-tight compartmentation and for a bilge pumping facility - but the latter, in view of the different nature and consequences of the risk of damage, can be simpler than in a ship. Floating hydrostatic stability has very little meaning

in hovercraft. By their very nature, the hull forms of hovercraft provide stability far in excess of any value which may cause concern when they are floating. Stability when operating in the cushion-borne mode *is* a problem indigenous to hovercraft, without parallel in ship technology, and one to which we shall return.

The ability of a hovercraft to realize its true potential is dependent to a large extent upon its light weight. Space is also generally at a premium. Hovercraft structures are generally made of aluminum alloys or fibre-reinforced plastics, and the machinery and systems components are frequently direct descendants from aviation technology. A marine engineer, expert in designing ship propulsion transmissions, expressed complete disbelief when shown a hovercraft main gearbox capable of transmitting 4,000 kW, weighing less than 1 tonne, and small enough to fit on his office desk. His version would have weighed at least twenty times as much and would have filled his office. The main machinery of hovercraft is installed in small unmanned spaces. System components, such as valves, pumps, etc., are generally selected such that they require little or no routine monitoring, and are remotely controlled.

The use of light alloy or plastics as structural materials does introduce a higher level of fire risk which influences design and safety philosophy, but the problem is alleviated to some extent by the fact that recognized danger zones are relatively small. The small engine spaces can be isolated by structural fire insulation with little sacrifice in weight, and the engines can be readily monitored by remote-indicating fire detectors. The small volume means that small quantities of total-flooding fire extinguishant are required.

Hovercraft passengers are accommodated in designated cabins with supervision. All furnishings must meet fire safety standards so that the risk of a fire is minimal. The supervised and discrete passenger accommodation, coupled with the lower structural fire resistance, has a marked impact upon evacuation philosophy. During a major emergency in a ship, the assembly and control of passengers can be a significant and time-consuming operation. Provided the passengers can be kept within safe bounds, evacuation is not necessarily of immediate priority. With hovercraft, passenger accommodation and supervision allow for rapid and controlled action as soon as an emergency situation fails to respond to remedial measures.

17.3 SYSTEMS AND EQUIPMENT

Mention has already been made of weight and space limitations of hovercraft, and a major effect of this in comparison with a ship is that any system or system component which affects safety must be managed and monitored from one central location. Unlike a ship, there is no space for crew members to physically monitor machinery or effect running repairs; the most that can be accomplished in a hovercraft is to diagnose a fault or breakdown and repair or

isolate minor leaks. Even these simple tasks involve removal of access hatches and working in very confined spaces.

Providing the necessary level of safety under these different ground rules is accomplished by: a) selection of components with proven reliability and/or acceptable overhaul lives, b) redundancy of components which are vital to safety, and c) comprehensive monitoring and warning systems remotely located at a crew station always occupied when the craft is operating - normally in the control cabin. These concepts are closely analogous to aeronautical solutions to similar problems, and it is easy to understand the difficulties facing a marine engineer when they are proposed to him. During one of its meetings, the IMCO expert working group had the opportunity to visit the assembly line of a modern airliner, and also to see a large ocean oil rig under construction. Delegates from both the marine and aircraft engineering disciplines rapidly gained a new appreciation of each other's problems and the constraints affecting the solutions.

We have already mentioned bilge pumping systems, and it can be appreciated that a ship designed to operate in water must be provided with a comprehensive and powerful pumping system to remove floodwater and adjust the ship's trim in the event of bottom damage. Two factors mitigate against the need for such a system in a hovercraft: 1) the risk of bottom damage is greatly reduced, and 2) so long as the hovercraft is capable of maintaining a cushion, there is no risk of flooding. The last thing a hovercraft commander wishes to do is to set a craft with bottom damage down in the water, and design should ensure that the damage will not destroy all lifting capability. Water-tight integrity and substantial sub-division, coupled with a large degree of reserve buoyancy, are required to counter a specified amount of damage. All water-tight compartments must be capable of being bilged by (frequently portable) pumps of specified minimum capacities.

Steering a ship is normally controlled by under-water rudders and possibly the use of differential thrust. Response is powerful and positive, and rarely is any other device normally required or provided. Generally, there is no need to restrict their use, since full deflection would have no effect on the safety of the ship. Hovercraft must rely upon other means of directional control, using air as the working medium. Controllability is therefore greatly reduced; with minimal surface friction and no hydrodynamic forces, response is anything but positive if rudders alone are used. The immediate response is that the craft will turn but continue to travel along the same track; the difference between the track and the angle at which the craft is pointing is called *yaw*, 90° of yaw representing full broadside travel. In order to provide more positive control and prevent this potentially dangerous situation (we will discuss this more later), other controls have been developed. It is unusual

for a hovercraft to have less than two means of directional control; three or more are frequently provided. Operational techniques and training play a vital role in making effective use of the controls. However, the controls, their use, the systems which activate them, and possible failures have significant effects upon safety. Therefore, the control systems must be carefully analyzed at the design stage and thoroughly tested operationally. As an example, a frequently used method is to vector the propulsive thrust of an air propeller. The propeller may be capable of developing 5 tonnes of thrust 4 metres above the craft's centre of gravity, and also capable of exerting that thrust at 90° to the craft's centre line. The induced rolling moment must be considered, and also the effects of a possible failure of the control when at full deflection. Safety considerations may dictate that use of full control may be limited in given conditions.

In the context of emergencies, we have already seen that the different passenger accommodation arrangements of ships and hovercraft have a strong influence on emergency evacuation. The evacuation equipment and its siting also reflect the different evacuation philosophies. A ship is provided with life-boats hanging from davits, frequently on a deck high above the waterline. Not only is embarkation and lowering a time-consuming operation requiring a number of crew members, but the difficulties are compounded if the ship has any serious roll motion. Of course, ships also have other forms of survival craft which are more easily launched but not affording the same degree of comfort.

In a hovercraft, inflatable liferafts are the only practical survival craft from weight and space considerations. Since passenger exits are normally 1 metre or less above the floating waterline, it is natural and expedient to locate the liferafts immediately outside the exits with sufficient space for passenger movement. The liferafts are secured with quick-release slips and a lanyard of length designed to activate the inflation as the raft enters the water. With the raft floating just outside the exit, embarkation is relatively simple and rapid. Because of the shape of a hovercraft, it is most unlikely to develop any significant roll angle (indeed, water-tight subdivision must be provided to limit this to 8°), thus simplifying evacuation in the most adverse conditions.

One uniquely nautical and frequently used piece of equipment in a ship is an anchor. A ship will drop an anchor to hold itself in a position for any one of a large number of reasons. Having completed its stay, it will hoist, or *weigh* the anchor before *proceeding on its lawful occasions*. A hovercraft will also carry an anchor for the same purpose, but will only use it, unless engaged on special operations, in dire emergency for one reason - to prevent drifting when floating powerless. It is essentially emergency equipment available for immediate dropping, but weight and space generally preclude

making provision to hoist it. When the emergency is over, the line can be buoyed and cut so that another vessel can retrieve the anchor.

Enormous navigational strides have been made with the development of both terrestrial and satellite electronic systems, but the traditional ship's navigator still requires a sextant, charts and chart table to fix and plot the ship's position and to provide back-up should the electronic systems fail. On the spacious bridge of a ship sedately cruising at 18 or 20 knots on a steady course, he has adequate facilities and plenty of time to practise his skills. Not so in a hovercraft. Due to high wind-induced drift or steering-induced yaw, the compass loses much of its significance as a navigation instrument. Furthermore, the craft's speed would make any position fix obsolete by the time it was calculated and plotted even if there would be room for a chart-table, and craft motion frequently makes any legible writing impossible. Hovercraft navigation must be either by means of electronic systems or, within sight of land, charts used purely for reference and identification of landmarks or buoys, not for plotting fixes. For specialized applications, conventional fixes may be required and appropriate facilities and space would be provided, but this would not apply to passenger craft.

The one system where comparison with a ship is not possible is, of course, the lift system, of which there are two major components: the lift air generation and distribution system, and the cushion containment system. Lift generation systems present no special safety considerations per se, although their arrangements do, and we will return to these shortly. Not only does the cushion containment system give hovercraft their unique capability, but it is also a major contributor to safety in determining the dynamic stability of the craft. Air is delivered from the hull to the cushion where it is contained by the bottom of the craft, the land or water surface, and a flexible skirt suspended all round from the periphery of the hull. In order to prevent total loss of air in case the craft rolls or pitches sufficiently to open up a gap at the bottom, the cushion may be subdivided by a longitudinal central keel and by athwartship stability bags, also made of flexible material. If the craft rolls or pitches, the differential pressure between the compartments provides a restoring moment. Some skirts are designed so as to deform and move the cushion centre of pressure and produce a restoring moment if the craft rolls or pitches, in which case compartmentation is not required. The only analogy to a ship is in the static case wherein a hovercraft is deliberately rolled and pitched in an experiment to establish its static hovering stability; this is very similar to a ship's inclining experiment, but conducted for a different reason. For a given type of skirt, values of static hover stability provide an empirical guide as to the dynamic roll and pitch characteristics and to the degree of ride comfort.

It is the cross-sectional geometry of the flexible skirt and the craft's peripheral structure that determines the safety of the craft's dynamics. In skirt designs where differential pressures are possible, pressure ratios may also have some effect. In 1965 and 1966, three commercial hovercraft capsized; one in Norway, one in California, and one in England. None were in passenger service at the time, and no serious injuries were incurred. All three accidents occurred in calm conditions, and all three occurred when the craft was yawed at speed. Extensive model tests showed that with a high (45° or more) angle of yaw, the leading section of skirt could deform downwards, allowing the side bow to dig into and scoop up the water over the craft to cause an overturn moment. Modifications to the skirt and restrictions of yaw angle at speed appeared to cure the problem. Then, in 1972 a hovercraft capsized in England while on passenger service. The accident occurred in very heavy weather conditions, which probably contributed to the loss of life incurred. It resulted from a combination of critical factors amongst which was possibly a reduction in lift power at a critical instant. Whilst craft stability was not a major consideration, the ensuing investigation provided valuable data for the future guidance of craft designers, operators and safety authorities, in the form of guidance relating to skirt and craft geometrical parameters. These data are contained in refs. 5 and 6, and we shall return to the operational safety discussion in the next section.

The arrangement of lift air generation systems has some operational safety connotations. Some hovercraft have multiple, independently powered fans all discharging into a common duct to the cushion. Should one fan fail or stop, discharge air from the others would escape through its intake instead of providing lift, and the craft would set down in the water or on the land. While in no immediate danger, it would move only with difficulty through the water, with the skirt hanging like a massive sea-anchor around it; overland, it would be immobilized. To overcome this, hovercraft with multiple fans are required to be able to fit plugs to blank off a fan intake. Lift fans may be powered by their own engine, or they may also be driven by an engine which also provides propulsion - an *integrated* system. This latter system may be varied by incorporating a clutch into the propulsion drive train. Both layouts have safety aspects which must be examined when considering the effects of an engine or transmission failure; these effects will differ depending upon whether the craft has single or multiple engines for lift. Unless independent thrust control is provided, integrated systems give forward thrust as soon as the throttle is opened, which is not desirable. Failure at speed removes lift (which can be disastrous), but it also removes thrust (which may alleviate the loss of lift hazard); if the thrust is also an effective directional control, that is also lost. In multi-engined craft, a frequently used layout has the

engines side by side. In this case, failure of one engine not only results in loss of lift air, but produces a powerful turning moment which requires immediate corrective action. Failure of a separate lift engine results in loss of lift air but no loss of thrust, and again appropriate corrective action is required.

Hovercraft safety is also affected by longitudinal trim, and some form of control must be provided to adjust trim. A convenient way to do this is to move ballast longitudinally. Since a hovercraft cannot afford the weight penalty of *dead* ballast, it is usual to make use of the fuel system for this purpose. Thus, powerful transfer pumps and a transfer system must be built in, and adequate volumetric capacity must be provided to permit movement of fuel to give the required trim authority.

17.4 OPERATIONAL SAFETY

It is by the manner in which it operates (its dynamic behaviour and response to controls and to equipment failures) that a hovercraft differs so much from all other forms of transport and poses unique problems of safety. Operating in its true medium, it is subject almost exclusively to aerodynamic forces generated either by the relative air velocity or by directional or trim control devices. The safety problems must be recognized and fully investigated.

The velocity-generated forces can be substantial and dictate the directional stability of the craft at speed, i.e., its natural tendency to either maintain or wander from a straight course. The amount of stability and its variation with direction of the relative airstream will influence the directional controls required. One early hovercraft showed a strong tendency, almost uncontrollable in strong winds, to head into wind. A simple and quick solution was to remove some vertical stabilizer area from the stern and replace it near the bow. This craft was also fitted with aerodynamic rudders, in the propeller slipstream, that were ineffective at low craft or propeller speed. Again, a simple quick remedy was found. Some air was ducted and directed over the rudders from the cushion to provide airflow at all speeds. Velocity-generated forces may also affect longitudinal trim; thus, a primary safety concern is the effect of hydrodynamic forces at high speed. For both performance and safety reasons, hovercraft are best operated with a slight bow-up trim, but changing course from up-wind to down-wind may cause a bow-down tendency. If a hovercraft is permitted to operate bow-down, the skirt at the bow may contact the water, generating high drag forces which create a powerful bow-down moment, resulting in a rapidly divergent bow-down attitude and the hovercraft coming to an abrupt halt. This is known as *plough-in*. Provided that the craft is travelling straight relative to the water it is a perfectly safe (if somewhat disconcerting) manoeuvre. A deliberate plough-in, induced by

reducing lift power, is a recognized and effective means of emergency stopping. By this method, a craft may be brought to rest from speed in two or three craft lengths. But with any appreciable yaw angle, a plough-in can rapidly develop into a capsize, as discussed earlier.

Course-keeping and manoeuvring characteristics are markedly different from those of conventional ships. When operating in a cross-wind, a hovercraft's bow may be pointing in a markedly different direction from that of its destination. This is not always understood by the captains of other vessels in the area, who may take unnecessary avoiding action and aggravate a collision situation. To identify this characteristic, all hovercraft are required to show a flashing amber light when cushion-borne. Turning a craft at speed frequently involves an appreciable yaw angle which must be taken into account when altering course, either deliberately or for collision avoidance. Because manoeuvring depends upon aerodynamic forces, and hovercraft are not provided with highly effective steering when water-borne, they are most controllable when operating at speed. Also, when waterborne, their hull shape creates a substantial wash even at low speeds. These facts are not readily appreciated by harbour authorities who may be unfamiliar with hovercraft and who may consequently insist upon speed limits being adhered to.

It is the effect of mechanical failures which is a primary safety consideration. Because of the random nature of these failures, each one must be considered in the worst operating scenario. Failures and their effects are investigated during the design phase, but it is only when the craft is operating that its safety can be truly established. With the multitude of possibilities of machinery layouts, and the wide variety of directional control devices and their configurations, it is impossible to adopt rigid safety criteria. Each design must be considered on its own merits and thoroughly analyzed.

17.5 FAULT ANALYSIS

Fault analysis constitutes a major part of safety considerations and is normally carried out on a system basis during the design. Having established safety requirements and designed a system to comply with those requirements, the possibility of failure of a system component which may affect safety must be considered and its effect analyzed. The number of systems is not insignificant, including engines, power transmission (possibly both lift and propulsion), engine controls, variable pitch propeller controls, controls of each (possibly 3 or 4) directional control device, fuel system, and electrical power generation and distribution systems. Each system may have a number of components which must be examined, and possibly more than one mode of failure must be considered. Each has to be analyzed with respect to its immediate effect upon safety. Can the craft continue to operate safely and, if so, with

what limitations or restrictions? Is the failure indicated or readily apparent? Does it affect other components of the system or other systems? Can its effect be corrected or neutralized? What corrective action or reaction should be taken? Since this is not necessarily a complete list of the questions which must be investigated, it can be seen that a complete fault analysis is not a simple undertaking.

Faults or failures are assumed to occur singly but, of course, their effect may spread to other systems, in which case duplication or isolation is required. Possibly the most evident illustration of this is the electrical system, upon which many other systems vital to safety rely. The IMCO safety code requires that such systems can be connected to alternate sources of electrical power. Nevertheless, not every eventuality can be covered. For example, a multi-engined hovercraft recently had a fire in an electrical panel. Using recommended procedures, the fire was rapidly isolated and extinguished, but the procedures also required that all engines should be stopped. Unfortunately, the fire occurred at such a position as to damage cables and switchgear so that no power was available to re-start the main engines. The craft had to be towed in to port, fortunately in calm sea conditions.

To the casual or uninformed observer, the need for analyses to these depths may appear questionable. A typical comment is; "Well, if it does fail, the craft will only drop a few feet and float safely". As a broad generalization, that is true; compared to an aircraft with a failure, a hovercraft certainly has altitude and speed in its favour when it has to descend abruptly. But the fault analysis performs a number of functions, each of which contributes to safety. It ensures that design engineers will emphasize the functional aspects of their work, leading to higher quality alternatives in design and component selection. It serves as a significant check on the design as a whole, ensuring that appropriate duplication of components, or isolation or preventive measures, have been provided where needed. It helps to recognize needs for either design revision or deeper investigation during trials. It also ensures that comprehensive guidance is available to crew members as to the effects of a failure upon craft safety and their subsequent actions. Apart from providing these benefits, the need for failure analysis must be viewed against the background of a hovercraft's unique operating characteristics and their influence upon safety in the event of a failure. The majority of faulty components cannot be replaced until the hovercraft reaches port.

Two obvious characteristics of hovercraft have safety connotations which are not always appreciated. They can operate over surfaces where no other form of surface transport can, and they have large dimensions (relative to their mass) and no wheels. A *dead* hovercraft lying on a surface of low load-bearing capacity is inaccessible by anything other than a helicopter, or

another hovercraft, and is virtually impossible to move until it is repaired.

17.6 SAFETY TRIALS

Returning briefly to our analogy with a ship, initial safety trials of a hovercraft will follow a very similar pattern, with identical objectives. All water-tight spaces will be tested, all fluid systems will be filled, tested and functioned, the electrical systems will be fully tested and functioned, and all warnings, safety systems and emergency systems will be functioned. Main engines will be run and monitored. Steering, navigation, lighting, heating, ventilation, etc., systems will all be functioned and adjusted. The ship will do an inclining experiment and a bollard pull test; the hovercraft will do a static stability test and a thrust test. But once these engineering trials have been completed at the builder's plant, there is very little similarity between the programme of a ship and a hovercraft for safety trials. The ship will perform some limited trials to verify adequacy of steering in normal and emergency conditions; lifeboat drills will be carried out, and further checks of safety and emergency systems under operating conditions will be performed. Machinery and systems will be checked and monitored under full-load operating conditions. But these are virtually all systems engineering checks, and the dynamic behaviour and response of the ship requires little, if any, attention from a safety aspect.

By contrast, the sea trials programme of a new hovercraft must thoroughly explore the safety of its dynamic behaviour, beginning with its handling and directional control and longitudinal trim. Do the primary directional controls have sufficient authority, with appropriate sensitivity, to give safe and effective manoeuvring? Does wind direction have any significant effect on this? Does the craft tend to *plough-in*? Is the craft directionally stable during a straight *plough-in*? Is low-speed handling and control adequate? These questions and many others form the basis for a trials programme. Trials will be repeated in varying weather conditions, at various weights and with various longitudinal centre-of-gravity positions, with the craft behaviour and trials parameters being carefully monitored and documented. An air propeller will be strain-gauged for sea trials to establish that it has no unsafe vibratory stresses, or to indicate the need for operational restrictions. As the trials progress, failures will be investigated, possibly the most significant being engine failures during a turn at speed in order to establish a safe relationship between speed and yaw angle. The engines, both lift and propulsion, on both the inside and outside of a turn, should be investigated. Again, these tests will be carried out, at least in a random *spot check* fashion, in varying conditions of weather and craft loading. Other failures will include those of: a) steering devices, i.e., failure to operate at all or

to return from full deflection, and b) system components considered during the fault analysis as being in need of further investigation.

A unique operational characteristic of hovercraft which has an engineering safety connotation is the spray generation. Aerosol salt water or fine dust spray can wreak havoc with the established reliability of components. Major engineering efforts have to be made to minimize spray ingestion into engines and trials must be carried out to establish the results of these efforts.

Another feature which will be qualititatively checked at this time is the layout of the operating control cabin and instrument panels, and its impact on the work-load of crew members required to control and manage the craft and its systems. While this will have been the subject of intensive study during design, the actual work-load can of course only be truly assessed under operational conditions. It is normal for a hovercraft safety trials programme to include some night operation to check that both internal and external lighting conditions do not impair safety. Visibility of all essential instruments and warnings and immediate access to all emergency controls are essential criteria.

Safety trials of a hovercraft will also include a *live*, though simulated, emergency evacuation, in which a representative selection of the liferafts will be launched, and *survivors* will be embarked. This will establish the efficacy of the proposed evacuation drill or highlight the need for changes. It will also establish that evacuation is possible within a pre-determined time, which is related to the structural fire protection provided for the recognized fire zones.

Since the trials' primary objective is to establish safety of the craft's dynamic behaviour, and since that behaviour is affected (sometimes unexpectedly or disproportionately) by changes to the skirt, the trials programme can become protracted - especially if skirt changes have to be made. That is not to say that skirt changes are necessarily required or numerous. It is just another factor that does not enter into the evaluation of a ship's safety.

It is not unusual for the trials of a new hovercraft type to take a month before all required safety considerations can be fully demonstrated. Even then, some work may be outstanding if all weather or environmental conditions for which the craft was designed have not been encountered. Safety trials will determine an *operational envelope* within which adequate safety has been demonstrated and within which the craft is permitted to operate. The primary parameters are weight, speed, longitudinal centre-of-gravity limits, wind speed, wave or obstacle height, and ambient temperature (especially in countries where icing may present problems). The envelope will also include the safe limits of yaw angle at various speeds, usually in the form of a graph, and may include other restrictions or limitations.

17.7 CREWING

So far, we have been discussing how the characteristics of hovercraft themselves affect safety considerations. However, the best efforts of designers and safety authorities can be neutralized if the crew is not also fully versed in these characteristics. Continuing with our previous analogies with a ship, the crew's duties and responsibilities will now be discussed.

What is a ship's Captain, and what are his duties? The Captain of a ship is master of all he surveys and his powers extend far beyond being responsible for the safety of his ship and all that is in it. He may conduct marriage ceremonies and burial services, he can punish members of his crew and engage or discharge them, he attends to the wishes of passengers both professionally and socially, and he has a wide range of legal and administrative responsibilities.

The ship is his home (possibly for many years), which he leaves only for brief periods (when in port), but he can transfer to another vessel of very different service (unless it is of a special nature) on short notice. He will have reached this pinnacle of his career after many years at sea in lesser capacities, and after passing many examinations on a wide variety of topics.

Except when entering or leaving port, steaming in adverse weather or in close proximity to other shipping, or in emergencies, he may be rarely on the bridge. When he is there, he issues commands and takes responsibility for them. But the response to his commands is in the hands of others, who are frequently out of sight in the depths of the vessel.

In a similar fashion, other officers and crew members make the ship their home, and their career is recorded in both the ship's documents and in personal records. Their training, duties, responsibilities, privileges, punishments and career structure have evolved over centuries, and are heavily guided by tradition.

The severity of the break with tradition enforced by the arrival of hovercraft on the scene is well illustrated by the reaction of a ship's Captain during a discussion in 1967 on the qualifying time required for a hovercraft commander candidate to be awarded a command certificate. The concensus of a number of hovercraft operational experts at the meeting was converging on about 200 hours at the controls when the Captain, his salt-encrusted beard bristling, exploded "200 hours - gad, that isn't even 10 days at sea!" To digress a little further, even the title is not fully agreed on to this day. *Captain*, *Pilot*, *Operator*, *Pilot-in-Command*, even *Hovernaut*, are some of the titles that have been used, but *Craft Commander* is now becoming generally accepted, and will be used here.

The prime responsibility of the craft commander for the safety of his hovercraft and all that is in it is probably the only direct similarity with the duties and responsibilities of a ship's captain. While he is not

necessarily at the controls, he will spend a good proportion of his time aboard at the controls, particularly in difficult conditions. When at the controls, he is physically steering the craft, adjusting speed, controlling lift power, adjusting trim, and monitoring and responding to indications of machinery or system conditions and warnings or emergency indicators. As mentioned earlier, all hovercraft systems are monitored in the control cabin, and there may be 30 or 40 indicators, each of which must be recognized and appropriately responded to. When at the controls, he is performing duties requiring constant attention and co-ordination, usually in a relatively small control cabin and a high noise environment. The combination of workload and environment is such that safety concerns of fatigue are very real, and on-board duties are generally limited to a number of hours or voyages (depending on the route) per day. Thus, a craft commander does not have a particular craft of which he is commander. Conversely, any one craft does not have a particular commander or crew.

What are the qualifications required to enter the hovercraft sphere with aspirations of becoming a craft commander? This is one question to which the answer, when given unequivocally, is guided by tradition and is related to the qualifications for ships' officers. But the answer cannot necessarily be given unequivocally since (by their very nature) hovercraft can be (and are) used in areas of water where no existing qualifications would be of any benefit, and we have seen that hovercraft operating characteristics have little in common with those of a ship. Perhaps the question should rather be: What makes a good hovercraft commander? The answer is not necessarily "A good ship's Captain". There have been numerous instances where ship captains with many years of experience have quickly shown during hovercraft familiarization that they do not possess, or cannot assimilate, the aptitude or co-ordination to master the totally new techniques. The vast majority of the earlier hovercraft commanders were aircraft pilots, with a few others from many walks of life - including an army officer whose previous duties had included a pack of mules in Hong Kong! Ships' officers were very much in the minority, but this was a haphazard and completely unintentional development. Many of the early hovercraft commanders are still employed as such, over 20 years later. Crew qualifications and certification requirements have not yet fully evolved, certainly in countries where hovercraft are still rare. The only qualification upon which there is unambiguous agreement is that the person at the controls of a hovercraft must demonstrate that he has the ability to safely operate that type of hovercraft and respond correctly to emergencies, and has a thorough knowledge of that type of craft. Since no two types of craft are alike in controls, systems, or operating characteristics, certification is required for each type.

In a similar fashion to the craft commander or person at the controls, the navigator of a hovercraft must also adapt to the peculiar operating character-

istics and different approach to navigation. Visual navigation is similar, but navigation by radar in restricted visibility is very different because of the difference in available space for chartwork and the higher speed. A qualified ship's radar observer could quickly become disoriented by the picture presented on the screen of a hovercraft undergoing a high rate of yaw, and his collision avoidance interpretation of the picture would probably need to be very different from that of a ship's radar picture. Again, a hovercraft navigator must receive appropriate training and be capable of assimilating it.

17.8 SAFETY CONTROLS

How is the safety of hovercraft controlled and enforced? The IMCO safety code provides guidance to national agencies charged with safety regulation, as determined by their governments. As a frame of reference, the guidelines are based upon the premises that hovercraft operations will be controlled with respect to weather conditions, the proximity of safe refuges, and the availability of emergency, communication and weather forecasting services in the operating area.

The national agency develops detailed safety requirements (as exemplified by refs. 7 and 8), and works closely with designers and manufacturers to monitor and approve a new hovercraft through design and construction. Operational safety will be demonstrated to the agency following an agreed trials programme, the result of which will be: a) the imposing of any limits or restrictions, and b) confirming the effects of failures or emergencies on safety and the necessary subsequent action. These will be detailed in an *operations manual* produced by the manufacturer for guidance of craft commanders and crew members. To ensure safety when in service, both the owner and the hovercaft itself must comply with safety requirements. The owner must satisfy the agency that he has: 1) adequate safety facilities, by way of communications with safety and weather services, 2) safe passenger handling facilities, and 3) appropriately qualified operating and maintenance personnel. He must show that the hovercraft he intends to operate is, in fact, adequately safe for the service. The hovercraft will be inspected to ensure that it has all required safety and emergency equipment on board in a serviceable condition, and that the craft itself is also serviceable with all systems functioning. This inspection will normally be carried out annually, and include maintenance procedures and records. Fair wear and tear can make substantial inroads on safety; to combat it, the craft manufacturer develops a schedule of preventive maintenance, which the agency approves. Maintenance is therefore a vital constituent of continued safety, so that its recording is an essential part of safety inspections.

The national agency is also responsible for developing the standards for operating and maintenance personnel certification. Candidates must pass exami-

nations and tests on basic hovercraft knowledge, general skills, and the specific type of hovercraft for which they are seeking certification.

Reference has frequently been made to *the national agency*, meaning the authority empowered by a national government to regulate safety. This authority may be vested in different types of agencies by different countries. A substantial list is provided in ref. 9.

17.9 THE SAFETY OF SMALL HOVERCRAFT

This discussion on safety has so far been concerned with hovercraft designed for and in commercial service. The IMCO Code does not apply to hovercraft designed to carry less than 12 passengers. This is consistent with a similar treatment of conventional ships, but also takes note of previous practical experience of some countries. National agencies may thus adopt their own criteria for small hovercraft, including privately owned hovercraft. Safety standards developed under the guidance of the IMCO Code can and should apply, possibly in simplified form, to all hovercraft in commercial service, and also to all hovercraft above some arbitrarily defined limit. The form of that limit, and it's value, is clearly very debatable. Should it be length? weight? engine size? Is a craft 6 m in length or weighing 1,500 kg any more or less safe than one which is 6.5 m long or which weighs 1,475 kg? This is discussed in a narrower context in ref. 1. Without debating the point here, the general safety concerns of the small recreational type of hovercraft need to be considered, for they are important. There is a very real possibility that they: i) will have been designed by persons with less than a full appreciation of the hovercraft breed, ii) will be operated by persons with inadequate knowledge or skill, and iii) will be used in very remote areas with no communications.

To design and build a small hovercraft is very simple - but to design and build a successful and safe one is a very different story. The chief designer of a large hovercraft manufacturer was once asked, when future prospects for his company's products were looking bleak, whether the company had considered entering the recreational craft field. The answer was "Yes, we have and it's too difficult!" There is a great deal more behind that brief response than meets the eye, but its truth has been borne out many times by companies who have made the attempt and failed.

Small hovercraft are designed and built either by entrepreneurs or by private owners. Of the former, many have tried but to date none have survived. Of the latter, a number have succeeded to the point where their craft, or their design, is marketable. The difference lies in their approach. Given the simplicity of a small hovercraft with the added attractions of novelty and versatility, the entrepreneur possibly views it more from an economic stand-

point than from a practical one. He must become aware of the need to consider the practical consequences of producing a craft which may sacrifice good engineering design and safety in favour of aesthetics, economics or other marketing pressures. A craft destined for quantity production may also succumb to market pressures by being released before sufficient development and testing to reveal the need for changes (possibly of a safety nature) have been completed. In such instances, unfavourable customer reaction is a powerful force as has been shown several times. Market reaction and the degree of responsible approach on the part of the manufacturer and his marketting appear to be the influencing factors on all aspects (including safety) of small hovercraft at present.

The year 1986 saw a marked and sustained increase in interest of recreational hovercraft in Canada, and some unsatisfactory features gave cause for concerns over safety. An abbreviated safety standard was developed, but for legal reasons it can only be applied on a voluntary basis with the cooperation of the manufacturer. Response from manufacturers has been instrumental in a number of cases in resolving safety concerns, although the voluntary nature cannot provide 100% coverage.

But above all else, regardless of the application of safety standards, the prime need on the part of all persons engaged in manufacturing and selling small hovercraft, and the novice new owner, is to appreciate the need for adequate instruction. It cannot be stressed too strongly that this lack of appreciation is probably the biggest single factor which has led to accidents (usually capsizes) or to creating danger to other water users, the prime cause of which is innocent mishandling born out of ignorance. Accidents generally are not fatal, but several fatalities have resulted from casual comments, such as: "That looks like fun, I'd like to try it". To which the response has been: "Go ahead. That's the throttle, and there's the steering wheel". Such situations are clearly not amenable to safety regulation.

Because it contains so many departures from safety, it is worth reviewing the known facts relating to a fatal accident which occurred in Canada late in 1987. A new craft (not of Canadian manufacture) was sold to an owner with no previous hovercraft knowledge by a dealer who not only had no training himself, but who saw no need to give any instruction other than a video which was a marketting aid. The instruction handbook for the machine contained minimal information on operating. Shortly afterwards, the victim experienced mechanical problems with the engine which he diagnosed as ice in the fuel lines but in all probability was air intake filter icing. The next day, while operating over a partially frozen lake, alone and many kilometres from the nearest habitation in sub-freezing temperature, he capsized. He was not wearing a lifejacket. The capsized craft and his body were recovered some 30 hours later;

the craft was virtually undamaged, and he had been alive after capsizing as shown by a knife in his hand and marks in nearby ice. This was therefore probably a static capsize resulting from the victim being on one side at the stern for some time, either trying to clear ice or to re-start the engine (it had no electric start), and either slipping on an ice surface, or causing the craft to take on water in one corner. But, given the lack of training and experience, it could easily have been a dynamic capsize, which is more normal and results from an instinctive reaction to close the throttle when turning and travelling broadside at high speed towards an obstacle.

Even extensive training may not be *adequate*. A new owner received several hours of good instruction from the manufacturer one winter, and spent several months enjoying his new toy. But then, the river changed from ice to water, over which he had never operated, and on his first trip, he capsized.

The Coroner Jury's verdict on the 1987 fatality included recommendations that all hovercraft sold in Canada should be approved, and that dealers should be trained and should train customers. The impact of this fatality was immediate; the manufacturer made several significant changes to the design, and greatly expanded the instruction handbook, concentrating on operational safety.

To maintain a balanced perspective, it must be immediately noted that a similar machine produced by the same manufacturer is operated most effectively and safely by a unit of the Canadian Coast Guard Auxiliary. During the winter of 1987-88, it was responsible for recovery of many stranded persons and their equipment while operating over partially frozen waters from their base near Montreal. The difference is that these operators were trained by, and maintain close liaison with, the manufacturer. Other machines of similar size are being used in various parts of Canada for similar operations by municipal emergency agencies. Reference 10 provides an illustrated account of these operations, and also discusses the 1987 fatality.

There are several hoverclubs and associations to which private owners belong. At least a partial listing is provided in Chapter 3 and ref. 9. These clubs have developed safety standards (frequently with advice from the national agency) which are strictly applied to craft participating in rallies and competitions. It is through such activities that craft built (possibly designed) by private owners have in some instances been developed to the point where they are marketable. Sufficiently comprehensive guides to design, construction and safety have been published to permit a person to gain adequate knowledge to design and construct a craft and understand at least the rudiments of operation before venturing out for the first time. References 11 to 16 provide a partial list of such guides. Experience gained in rallies will indicate the need for any changes and will provide opportunities for practical evaluation to a

greater extent than may be given to a craft intended for quantity production.

This discussion on the safety of small hovercraft is merely an attempt to place in perspective the priorities and considerations which must be addressed in the context of safety. Small hovercraft, like anything else which involves an element of risk, are safe until it is forgotten that they can be dangerous. Designers, manufacturers and owners alike must appreciate their peculiarities and make due provision to prevent them from becoming unsafe.

17.10 SUMMARY

In this Chapter, an attempt has been made to indicate that hovercraft *do* possess certain features and characteristics which present novel, sometimes unprecedented problems requiring solution when considering safety. The first fundamental problem was to resolve how to classify them, and it was agreed that international safety standards should be administered by the agency responsible for maritime safety. That does not mean they are ships (early attempts to treat them as such failed) and different countries administer the international standard that has been developed according to their own domestic legislative interpretation.

Since their primary operation is in the marine environment, the novel problems of hovercraft, and their solutions, are illustrated by direct comparisons with ships. Fire and collision are two emergency situations of major concern for which totally different treatments are required. These, coupled with differences in passenger accommodation and life saving equipment, result in a totally different evacuation philosophy.

Directional control, and the means by which it is achieved, is totally different, and manoeuvring characteristics of a hovercraft are such that entirely new skills are required for control and navigation. Multiple means of directional control are frequently used, and hence a new type of hovercraft must be subjected to a very comprehensive trials programme to demonstrate, amongst other unique features, that it can be safely operated in the event of a failure of any one of many components which affect safety of handling.

The status and duties of a hovercraft commander are very different from those of a ship's captain, and he is in direct control of the craft and all its systems during his relatively short period of duty, which is measured in hours rather than weeks. Similarly, the duties and responsibilities of the owner are administered in a different fashion in order that the level of safety of his service is adequate.

The amphibious capability of hovercraft makes them very attractive as recreational vehicles, but domestic legislation does not always provide the power to impose appropriate safety measures. Even if such measures are adopted by manufacturers, the safety of operation is then in the hands of novices who

may not appreciate the need for special knowledge and skills. At the same time, such small craft, when operated by skilled and responsible persons, can perform valuable rescue missions.

17.11 REFERENCES

1. D.F. Bobeck, Regulations for advanced marine vehicles - the next step. AIAA/SNAME Marine Systems Conference, New Orleans, February 1983.
2. Intergovernmental Maritime Consultative Organization, Code of safety for dynamically supported craft, IMCO Resolution A.373(X), November 1977.
3. D.F. Bobeck and T.E. Thompson, the IMCO code for dynamically supported craft, AIAA/SNAME Advanced Marine Vehicles Conference, San Diego, April 1978.
4. R.G. Wade, Marine safety standards for air cushion vehicles - the development of a new approach, AIAA/SNAME Advanced Marine Vehicles Conference, San Diego, April 1978.
5. Civil Aviation Authority, London, CAA Paper 75017 - Report of the special committee on hovercraft stability and control, June 1975.
6. Department of Industry, London, Stability and control of hovercraft - notes for commanders, 1980.
7. Civil Aviation Authority, London, British hovercraft safety requirements, Issue 5, August 1983.
8. Canadian Coast Guard, Standards relating to design, construction and operational safety of dynamically supported craft - Vol. 1, Air Cushion Vehicles, Transport Canada, Ottawa, December 1985.
9. Jane's high speed marine craft and air cushion vehicles, published annually by Jane's Publishing Company, London.
10. Hovercraft Bulletin, September 1988. Published monthly by the Hovercraft Society of Great Britain.
11. H.S. Fowler, The design, construction and operation of light air cushion vehicles, Canadian Aeronautics and Space Institute, Ottawa.
12. G.H. Williams, Home-built hovercraft, a plain man's guide to ACV design and construction, Iliffe Transport Publications Ltd., London, 1967.
13. D.M. Waters, Light hovercraft design handbook, Report TT 6902, Loughborough University of Technology, 1969.
14. R.J. Windt, Hovercraft construction and operation, Universal Hovercraft, Cordova, Illinois.
15. Hoverclub of Great Britain, Ltd., Light hovercraft handbook, published annually by Hoverclub of Great Britain, Ltd.
16. Hoverclub of Great Britain, Ltd., Light hovercraft design, construction and safety requirements, Hoverclub of Great Britain Ltd.

APPENDIX A

AUTHOR INDEX

Tables A.1 and A.2 can be used to determine the author(s) of each chapter and the contributions (down to the section level) of each author, all in alphabetical order. This information coupled with the biographical data in Appendix B defines the competence of authorship of this book.

Table A.1. Index of chapters and contributing authors.

CHAPTER	AUTHOR(S)
1	Mantle
2	Mantle
3	Fitzgerald
4	Fowler
5	Heizmann, Mandel, Mantle, Vitale, Wheeler
6	Laframboise, Markham
7	Dickins
8	Cook, Wade
9	Laframboise, Markham
10	Conn, Schoppee
11	Fowler
12	Graham
13	Ma, Sullivan
14	Amyot
15	Hayashi, Kida, Murao, Yasutomi
16	Bertelsen
17	Wade

Table A.2. Index of authors and contributed chapter(s) and/or section(s).

AUTHOR	CHAPTER(S)/SECTION(S)
Amyot, J.R.	Ch. 14
Bertelsen, W.R.	Ch. 16
Cook, H.C.	Sect. 8.2
Conn, P.K.	Sects. 10.1-2, 10.3.1, 10.3.3, 10.4-5, 10.8
Dickins, D.F.	Ch. 7
Fitzgerald, C.J.	Ch. 3
Fowler, H.S.	Chs. 4, 11
Graham, T.A.	Ch. 12
Hayashi, R. (with Kida and Yasutomi)	Sect. 15.2
Heizmann, J.R. (with Mantle and Vitale)	Sect. 5.2
Kida, T. (with Hayashi and Yasutomi)	Sect. 15.2
Laframboise, J.E. (with Markham)	Chs. 6, 9
Ma, T. (with Sullivan)	Ch. 13
Mandel, D.B. (with Heizmann and Vitale)	Sect. 5.2
Mantle, P.J.	Chs. 1, 2, Sect. 5.3
Markham, P. (with Laframboise)	Chs. 6, 9
Murao, R.	Sects. 15.1, 15.3
Schoppee, M.M.	Sects. 10.3.2, 10.6-7, 10.9-10
Sullivan, P.A. (with Ma)	Ch. 13
Vitale, D.J. (with Mandel and Heizmann)	Sect. 5.2
Wade, R.G.	Sect. 8.3, Ch. 17
Wheeler, R.L.	Sect. 5.4
Yasutomi, Z. (with Hayashi and Kida)	Sect. 15.2

APPENDIX B

AUTHOR BIOGRAPHIES

JOSEPH R. AMYOT

Division of Mechanical Engineering
National Research Council of Canada
Ottawa, Ontario, Canada K1A 0R6

Joseph R. Amyot earned the B.A.Sc. (Ottawa 1960), M.Sc. (Manitoaba, 1963) and Ph.D. (West Indies 1978) degrees in electrical engineering. His career includes four years of industrial design and development, five years teaching and sixteen years of research in the Division of Mechanical Engineering, National Research Council of Canada. There, he has been involved mainly in mathematical modeling and computer simulation of dynamical systems, with emphasis on methodology, analysis, design, control and optimization. He is an author of over thirty-five technical papers, including several on air-cushion heave dynamics control, and co-author of a book entitled *Computer-Aided Simulation in Railway Dynamics*.

Dr. Amyot has served the Canadian Air Cushion Technology Society (CACTS) as its Vice-Chairman (1981-3) and Chairman (1983-6). He was Program Chairman (1982/3/5) and Conference Chairman (1984-6) of the annually-held CACTS International Conference on Air Cushion Technology. In addition to membership in several scientific organizations, he is a Senior Member of both the Institute of Electrical and Electronics Engineers and the Society for Computer Simulation, and an Associate Fellow of the Canadian Aeronautics and Space Institute.

WILLIAM R. BERTELSEN

Bertelsen, Inc.
113 Commercial Street
Neponset, Illinois 61345, U.S.A.

William R. Bertelsen earned the B.S. (Illinois 1945) and M.D. (Illinois 1947) degrees and is a licensed pilot of single and multi- engine aircraft. He has been practicing various forms of medicine, including general practice, chest medicine and emergency care, since 1948. Also, through Bertelsen, Inc. founded in 1960, he has been engaged in technical research and development. He is an author of over a dozen papers on air cushion craft.

Dr. Bertelsen is a hovercraft pioneer, having demonstrated the first controllable man-carrying hovercraft, called the Bertelsen Aeromobile, at the

First Symposium on Ground Effect Phenomena, Princeton University, October 1959. It is on display in the Permanent Collection of the National Air and Space Museum, Smithsonian Institute. In addition to membership in several scientific organizations, he is a Fellow of both The Hovercraft Society and the Canadian Aeronautics and Space Institute.

HARVEY C. COOK

Hover Systems, Inc.
Eddystone, Pennsylvania 19013, U.S.A.

Harvey C. Cook earned the B.S. (Maryland) degree in business and management, and the Associate of Arts (Charles County College) in police administration; he is a graduate of the Federal Bureau of Investigation National Academy. Since the beginning of his career as a police officer, in 1958, he advanced through grades to Lieutenant Colonel, recently retiring as Deputy Superintendent of the Maryland Natural Resources Police Force. He has received various awards for boating safety, highway safety and drug law enforcement. He was chosen Officer of the Year by the Force in both 1973 and 1974.

As hovercraft project manager for over six years, beginning in 1980, Lieutenant Colonel Cook has been a highly successful promoter of hovercraft for use in the Force. He presented papers on the subject at the 1985/6/7/8 International Conferences on Air Cushion Technology. He is currently serving as Director, Hovercraft Training and Operations, Hover Systems, Inc.

PAUL K. CONN

Bell Aerospace Textron
P.O. Box 1
Buffalo, New York 14240, U.S.A.

Paul K. Conn earned the A.B. (Kenyon College), M.S. (Kansas State) and Ph.D. (Kansas State); the latter two degrees were in physical chemistry. While with the General Electric Company for over thirteen years, Dr. Conn managed various research and development groups specializing in high temperature materials, testing and radio-active materials. He spent the following seventeen years with Bell Aerospace Textron, where he is Director of the Engineering Laboratories and Test Directorate with responsibility for material, metallurgy and chemistry research and development, and environmental, vibration, shock and structure testing. Among many other responsible positions held, he was Program Manager/Technical Director for research and development on flexible composites, including hovercraft skirt/seal materials, impact and biofouling resistant coatings, oxidation resistant coatings, gaseous hydrogen embrittlement, carbon composites and materials characterization.

Dr. Conn is a member of several scientific organizations and listed in American Men and Women of Science.

DAVID F. DICKINS

DF Dickins Associates Ltd.
503A, 21 Water Street
Vancouver, British Columbia, Canada V6B 1A1

David F. Dickins earned the B.A.Sc. (University of British Columbia, 1971) degree in mechanical engineering. He has seventeen years of arctic research experience, beginning with Environment Canada and progressing through four years of consulting in Yellowknife, N.W.T., to a partnership in a new engineering consulting firm. D F Dickins Associates Ltd. now has a ten year record of worldwide engineering projects. From 1969 to 1974, Mr. Dickins participated in a variety of arctic air cushion vehicle test programs and demonstration projects: the CC.7 in the Mackenzie Delta (1969), the ACT-100 at Tuktoyaktuk (1972), and the Bell Voyageur at Parry Sound (1974). Beginning in

1981, he became the prime contractor responsible for the technical direction of SOHIO Petroleum Company's arctic hovercraft research program. He assembled an international design team to develop a 1000 ton (gross weight) heavy-lift air cushion vehicle capable of carrying drilling modules over the ice to offshore exploration sites in the Beaufort Sea. During the winter of 1983/84, he directed the testing of the heaviest self-propelled air cushion vehicle to have operated over sea ice, the Jeff (A).

Mr. Dickins is actively working with industry clients to evaluate the potential applications of hovercraft in support of arctic offshore oil development. He is the author of 17 technical reports and papers on arctic hovercraft design and operation. One of these received the Peter Heron Winter award for best conference paper at the 1984 CACTS International Conference on Air Cushion Technolgoy, held in Vancouver. He is a member of the Hovercraft Society (UK), the International Glaciological Society, the Association of Professional Engineers of British Columbia, and the Canadian Institute of Marine Engineering.

CHRISTOPHER J. FITZGERALD

Neoteric Hovercraft Inc.
1649 Tippecanoe Street
Terre Haute, Indiana 47807, U.S.A.

Christopher J. Fitzgerald earned a Diploma (Footscray Institute of Technology, Australia) in mechanical engineering and studied aeronautical engineering at Farnborough Technical College, England. During the early sixties, he organized a group of Australian talent and supervised the design and construction of a styled leisure hovercraft, which entered the world's first hovercraft race, held in Canberra, 1964. In 1969/70, he travelled to several countries on a Rotary Foundation award, a two-year worldwide study of air cushion vehicle developments. As part of this study, he worked and trained in many areas within the British Hovercraft Corporation, England. He is currently a part-time lecturer in engineering design and business at the Rose-Hulman Institute of Technology and President of Neoteric Hovercraft Incorporated, a manufacturer of light hovercraft.

Mr. Fitzgerald received the O'Shannessy Award from the Society of Automotive Engineers (Australia), in 1968, for one of his technical papers on hovercraft. In addition to membership in various technical organizations, he is founder and past President of the Hoverclub of America, Inc.

HOWARD S. FOWLER

76 Elliot Avenue
Ottawa, Ontario, Canada K1S 0M5

Howard S. Fowler earned a B.Sc. (London 1942) degree in mechanical engineering. From 1942 to 1950, he worked for D. Napier and Son Aeroengine Manufacturers, where he became Head of the Internal Aerodynamics Laboratory, developing superchargers and early gas turbines. The next couple of years were spent at the Pametrada Marine Turbine Research Station, Newcastle, as Head of the Aerodynamics and Heat Transfer Laboratory, working on steam and gas turbines, including the world's first marine gas turbine.

Mr. Fowler was a research engineer in the Engine Laboratory, Mechanical Engineering Division, National Research Council of Canada (NRC), from 1952 to 1980, and Principal Research Officer and Head of this laboratory from 1980 to 1985. He carried out research on jet engine anti-icing and afterburning, and centrifugal compressor aerodynamics. From 1970 to 1982, he was in charge of the CASPAR research program on air cushion technology. During this period, his research was directed almost exclusively to air cushion technology, with special emphasis on skirt-terrain interaction. He has set up and operated field-testing facilities in swampy wooded areas, open grass areas and runways, has designed and driven the HEX series of man-carrying research hovercraft,

and has driven some twenty-three other types for manufacturers and the Department of National Defence. He has advised or worked on several other projects, including a 100-ton peat-digging raft, two 120-ton all-season air cushion ferries, and an airbed for burn patients. He retired from NRC in 1985.

Mr. Fowler has published approximately fifty papers and reports, including many on hovercraft technology. He is a Fellow of the Canadian Aeronautics and Space Institute and three times Past-Chairman of the Canadian Air Cushion Technology Society.

TERENCE A. GRAHAM

Sunwell Engineering Company Limited
180 Caster Avenue
Woodbridge, Ontario L4L 5Y7

Terence A. Graham earned the B.Sc. (Queen's 1976) degree in mathematics and engineering, the M.A.Sc. (Toronto 1980) in aerospace studies, and the Ph.D. (Toronto (1989) also in aeorspace studies. From 1976 to 1979, he worked as an engineer in the nuclear generation division of Ontario Hydro. From there, he joined the University of Toronto Institute for Aerospace Studies, where he worked in the air cushion technology group as a masters student, research engineer and doctoral candidate. His work there centered mainly on the dynamics and stability of hovercraft but also included aspects of compliant surface air bearing technology. His research interests are in the area of dynamics and stability of vehicles and other fluid-mechanical systems.

Dr. Graham is an author of over ten papers and reports on hovercraft dynamics air bearing technolgoy. He has served on the executive committee of the Canadian Air Cushion Technology Society for over six years. He is currently manager of research and development at Sunwell Engineering.

RYUICHI HAYASHI

Faculty of Education, Technology
Shimane University
Nishikawatu, Matue, Shimane, Japan

Ryuichi Hayashi earned the B.E. (Osaka Prefecture 1966) and M.S. (Osaka Prefecture 1968) degrees in mechanical engineering. Since then, he has been at Shimane University as Assistant Professor (1968-72), Lecturer (1972-77), Associate Professor (19778-87) and Professor (1988-present). His research has been directed towards educational technology, with special emphasis on the educational applications of computers. His present interest is in computer simulation of fluid dynamics associated with hovercraft, especially the interactions of jet flows with outer ambient flows and water surface.

Mr. Hayashi is an author of several papers on hovercraft and jet curtain.

JOHN R. HEIZMANN

1004 Downs Drive
Silver Spring, Maryland 20904, U.S.A.

John R. Heizmann, now retired, was a Design Workstudy Engineer in the manpower analysis unit of the Manning and Controls Integration Section. He supervised development of the ships' complements for USS Nimitz and a variety of other ships. Mr. Heizmann received a B.S. degree from the University of Detroit. Following that, he worked as a steel mill metallurgist and then spent 3½ years in the Army Air Force during World War II, most of that period as a metallurgist in charge, on a Base Air Depot in England. He then spent 17 years in engineering and management for a variety of manufacturing firms. In 1969 he left DCAS Baltimore to join the Naval Ship Engineering Center.

Mr. Heizmann is a registered professional engineer in Maryland

(mechanical) and in Pennsylvania (industrial). He is a member of the American Society of Naval Engineers, the Association of Scientists and Engineers, and the American Institute of Industrial Engineering.

TERUHIKO KIDA

Department of Mechanical Engineering
University of Osaka Prefecture
Mozu, Sakai, Osaka, Japan

Teruhiko Kida earned the B.E. (Osaka Prefecture 1963) and Dr. (Osaka Prefecture 1973) degrees in mechanical engineering. He was a researcher with Hitachi Ship Building Company from 1963 to 1965. Since then, he has been at University of Osaka Prefecture as Assistant Professor (1965-70), Lecturer (1970-73), Associate Professor (1973-86) and Full Professor (1986-present). His research has been directed towards the aerodynamics of the ground effect wing, supercavitating hydrofoil, and fluid machinery. His present interest is in computer simulation of the fluid dynamics associated with hovercraft and in fundamental problems of fluid dynamics, especially the asymptotic analysis of an integral equation containing a small parameter.

Dr. Kida is an author of several papers on ground effect wing, hydrofoil and jet curtain.

JACQUES E. LAFRAMBOISE

Transportation Development Centre
Transport Canada
200 René-Lévesque Blvd. West, 601 West Tower
Montréal, Québec, Canada H2Z 1X4

Jacques E. Laframboise obtained his Engineering degree in 1951 from Ecole Polytechnique, Montréal. He received an Athlone Fellowship in 1956 and obtained an M.Sc. from City and Guilds College, London (1961). Prior to joining the Transportation Development Centre in 1972, he worked in a defence laboratory (DREV), an engineering firm (SNC Inc.) and with Société Bertin, at their Montréal office. He is now Modal Coordinator for off-road transportation and air cushion technology developments at the Transportation Development Centre of Transport Canada. He has been extensively involved with conventional and air cushion icebreaking, in collaboration with the Canadian Coast Guard, and with air cushion applications to overland transportation.

Mr. Laframboise is an Associate Fellow of the Canadian Aeronautics and Space Institute. He was a member of the Canadian Air Cushion Technology Society's executive committee for several years and its Chairman in 1988. He is a member of the Ordre des Ingénieurs du Québec, the Engineering Institute of Canada, and the Canadian Society for Terrain-Vehicles Systems

TAO MA

Marine Design and Research Institute of China
346 Sichuan Road, Central
P.O. Box 3053
Shanghai, China

Tao Ma earned the B.Sc. (Jiao Tuong 1967) degree in naval architecture. Since then, he has been with the hovercraft division of the Marine Design and Research Institute of China, working mainly in research and development of air cushion craft, with emphasis on skirt and cushion system dynamics. He has done analytical and experimental research on drag, longitudinal and heave instability, seakeeping and ride quality control. He established a laboratory for experimental studies on skirt dynamic characteristics. As a visiting scholar at the Institute for Aerospace Studies of the University of Toronto, he continued his investigations into the effect of skirt responsiveness on air cushion heave dynamics. He then developed a theory on skirt/cushion aeroelastic and hydroelastic dynamics.

Mr. Ma is an author of over ten papers and reports on air cushion craft.

DAVID B. MANDEL

Naval Sea Systems Command
Code 05M5
Washington, DC 20362-5101, U.S.A,.

David B. Mandel is an Operations Research Analyst in the Reliability Branch, Systems Engineering Division, Ship Design Integration Directorate, Naval Sea Systems Command. He is responsible for reliability analysis of new ship designs. He received his B.S. degree in Applied Mathematics from the University of Michigan.

Mr. Mandel is a member of the Society of Reliability Engineers.

PETER J. MANTLE

Lockheed Marine Systems
3385 Scott Blvd.
Santa Clara, California 9505, U.S.A.

Peter J. Mantle earned advanced degrees in aeronautical engineering and mathematics from Cranfield College of Aeronautics, England (D.C.Ae., 1958), Laval University, Canada (M.Sc. 1960) and California Institute of Technology (Ae.E., 1964). He has been closely involved in hovercraft development since Sir Christopher Cockerell first developed the hovercraft with British Hovercraft Corporation (then Saunders-Roe) in England, in 1959. Mr. Mantle started his career at British Hovercraft Corporation in 1951, emigrated to Canada, then to the United States of America. In 1964, he designed, built and test flew a Wing-in-Ground Effect (WIG) craft for the Maritime Administration. He continued his career in hovercraft and Surface Effect Ship (SES) development at Bell Aerospace and pioneered the U.S. Navy's SES-100B, which set the world's speed record for Navy warships in 1972. In 1973-1975, he was Director of Engineering for Aerojet General's development of SES-100A and the JEFF(A) hovercraft. He spent six years (1978-1984) in the Pentagon, first on the Secretary of the Navy's staff, then as Director of Technology Assessment for the Chief of Naval Operations prior to his joining Lockheed Marine Systems Group as Director, Strategic Planning, and is now Director, Business Development.

Mr. Mantle is an author of many technical papers, a patentee in the field of hovercraft and other marine vehicles, and author of the 1980 (second edition) compendium on Air Cushion Craft Development published by the United States Government Printing Office. In addition to being a member of the American Institute for Aeronautics and Astronautics (AIAA) and American Society of Naval Engineers (ASNE), he is Founder Chairman and Founder President of the U.S. Hovercraft Society.

PHILIP de LACEY MARKHAM

85 Avenue Road
Ottawa, Ontario, Canada K1S 0P1

Philip Markham served an engineering apprenticeship in the British aircraft industry and received further education at the Royal Air Force School of Aeronautical Engineering and United States Air Force Institute of Technology (1952). He served for twenty-six years in the RAF and RCAF as an engineer and pilot and then for thirteen years with the National Research Council of Canada. Latterly he was with German & Milne Inc. naval architects and marine engineers, where he was responsible for trials conducted with the Canadian Coast Guard Air Cushion Icebreaking Bow and for the concepts for two advanced designs. He is now semi-retired.

Mr. Markham is a Professional Engineer (Ontario), Chartered Engineer (UK), Fellow of the Canadian Aeronautics and Space Institute, and Member of the Royal Aeronautical Society.

RINICHI MURAO

College of Science and Engineering
Aoyama Gakuin University
Chitosedai, Setagaya, Tokyo 157, Japan

Rinichi Murao earned the B.E. (Tokyo Institute of Technology 1952) and Dr. (Nagoya University 1976) degrees in mechanical engineering. He joined the Transportation Technical Research Institute, Ministry of Transport, Japan in 1952, where he eventually became Director of the Engine Development Division, Ship Research Institute. He is now Professor in the Mechanical Engineering Department of Aoyama Gakuin University. He has been involved in fluid dynamics studies of air cushion vehicles since 1960. His main interests in the post-sixties have been directed towards the performance estimation of side-wall surface effect ships using towing tanks and computer simulation.

Since 1978, Dr. Murao has been Chairman, Hovercraft Section of the Logistics Committee, National Institute of Polar Research.

MEREDITH M. SCHOPPEE

Albany International Research Company
777 West Street
Mansfield, Massachussetts 02048, U.S.A.

Meredith M. Schoppee studied mathematics at Massachussetts Institute of Technology and Utah State University. She has been involved in the physical and mechanical characterization of fibrous materials for government agencies and industrial clients for twenty-five years at Albany International Research Company (formerly Fabric Research Laboratories, Inc.), where she is a Senior Research Engineer. Her particular interests center on the combined effects of fiber properties and geometrical structure on the response of fibrous assemblies to mechanical and thermal loading. She has had published over thirty journal articles and government reports related to the properties and structure of fibrous materials.

Mrs. Schoppee was President of the Fiber Society in 1985 and one of its academic lecturers in 1983-4.

PHILIP A. SULLIVAN

Institute of Aerospace Studies
University of Toronto
4925 Dufferin Street
Downsview, Ontario, Canada M3H 5T6

Philip A. Sullivan grew up in Australia, and took his undergraduate education in mechanical engineering at the University of New South Wales, located in Sydney. After graduating in 1959, he conducted research in theoretical aerodynamics at the same university, and for this work he was awarded a Master's degree in 1961. He then traveled to England to undertake theoretical and experimental research towards a Ph.D. degree at the Imperial College of Science and Technology in London, in the field of hypersonic aerodynamics. He was awarded the degree in 1964, and subsequently spent a post-doctoral year at Princeton University in the U.S.A. In 1965, he joined the academic staff of the Institute for Aerospace Studies at the University of Toronto, where he has since remained. Initially he continued his research interests in hypersonics, but in 1968, in response to a perceived Canadian industrial need, he initiated a research programme in air cushion technology. This programme has since made significant contributions towards an understanding of cushion dynamics. Currently he holds the rank of Professor and is actively involved in research in hypersonics, collapsible tube flows, as well as in air cushion dynamics.

Professor Sullivan is a Fellow of the Canadian Aeronautics and Space Institute (CASI), and an Associate Fellow of the American Institute for

Aeronautics and Astronautics. He was Chairman of the Air Cushion Technology Section of CASI during 1973-75, has been a member of the Canadian Air Cushion Technology Society since its foundation, and served as Chairman in 1980-81. He is an author of 44 journal publications and technical reports, 35 of which are on various aspects of air cushion technology.

DONALD J. VITALE

12701 Chilton Circle
Silver Spring, Maryland 20904, U.S.A.

Donald J. Vitale earned a B.S. (University of Maryland 1956) degree in mechanical engineering. As an employee of the Naval Sea Systems Command, Department of the Navy, U.S.A., he has been a Quality Assuance Engineer for ship systems and equipment, Supportability Engineer for several ships and hovercraft, Aviation Systems Engineer for aircraft carrier designs, Ship Design Manager for three ships, Ship Integration Engineer for two aircraft programs, and Design Engineer for various ship-borne missiles. He has been a staff member of the Applied Physics Laboratory of Johns Hopkins University, the White Oak Laboratory of the Naval Surface Weapons Center, and the National Security Agency. He has published several papers on hovercraft.

Mr. Vitale is a member of the U.S. Hovercraft Society, in addition to other engineering societies.

RONALD G. WADE

Canadian Coast Guard Transport Canada
344 Slater Street
Ottawa, Ontario, Canada K1A 0N7

Ronald G. Wade obtained a B.Sc. (Eng) at the Royal Naval Engineering College, Manadon, and an M.Sc. in aeronautical engineering at the College of Aeronautics, Cranfield, while serving as an air engineer officer in the Royal Navy Fleet Air Arm. After 4 years associated with development of the Sea Vixen all-weather naval fighter aircraft and 2 years exchange service in the RCN at Shearwater, Nova Scotia, he was appointed to the Interservice Hovercraft Trials Unit in 1964. He was among the first British military personnel to operate hovercraft for evaluation, and in the next 2 years he conducted trials on SRN-5 craft in Borneo, Aden and Tuktoyaktuk, together with a number of other craft in the United Kingdom. In 1966, he was appointed as project engineer for the Naval BH-7 and was resident at the British Hovercraft Corporation during its design. He resigned from the Navy in 1968, joined Hovermarine and emigrated to Canada. In 1969, he joined the Department of Transport, in Ottawa, as an engineer responsible for development of hovercraft in the Canadian Coast Guard and for safety regulation of all Canadian hovercraft. He served on a number of Canadian government committees and participated in most of the initial experiments which led to the successful use of hovercraft for ice-breaking. From 1972 to 1977 he was the Canadian delegate to the international working group which developed the *Code of Safety for Dynamically Supported Craft*. In 1984, he was appointed Superintendent, Special Ships, in which capacity he is responsible for development and administration of safety regulations in Canada for hovercraft, hydrofoils, bulk chemical carriers, liquefied gas carriers, and sail training vessels.

Mr. Wade is the author of several technical papers on hovercraft ice-breaking and safety, and has served on the Canadian Aeronautics and Space Institute Journal Editorial Committee and on the Canadian Air Cushion Technology Section Committee. He has built a 2-seat sports hovercraft.

RAYMOND L. WHEELER

British Hovercraft Corporation Limited
East Cowes, Isle of Wight, England

Raymond L. Wheeler earned a B.Sc. (University College, Southampton 1949) degree in aeronautical engineering and M.Sc.(Eng.) (Imperial College 1952) in mechanical engineering. His full-time studies at Southampton were undertaken upon receipt of a Spitfire-Mitchell Memorial Scholarship in 1948 after having commenced an apprenticeship with Saunders-Roe Limited in 1945. He joined the Stress Office at Saunders-Roe in 1952, was eventually associated with development of the Princess Flying Boat, the SR.53, Black Knight, Black Arrow, SR.N1, SR.N2, SR.N3 and SR.N5/N6 hovercraft, and progressed to Chief Stress Engineer. As Project Engineer for the SR.N4 hovercraft, he was responsible for all aspects of the craft's design. He was appointed Chief Structural Engineer, in 1965, and Chief Designer the following year, when the British Hovercraft Corporation was formed. In 1972, he became Technical Director whilst retaining the responsibilities of Chief Designer. Upon reorganization of the Westland Group, in 1985, Westland Aerospace Limited was formed from the British Hovercraft Corportion, with three subsidiary companies: British Hovercraft Corportion Limited, Westland Aerostructures Limited and EEL Limited. Mr. Wheeler was appointed Business Development Director for Westland Aerospace Limited.

Mr. Wheeler is an author of several technical articles and reports on hovercraft and was Keynote Speaker at the Sixteenth Canadian Symposium on Air Cushion Technology, held in Charlottetown, Canada, October 1982.

ZENSABURO YASUTOMI

Department of Mechanical Engineering
University of Osaka Prefecture
Mozu, Sakai, Osaka, Japan

Zensaburo Yasutomi earned the B.E. (Osaka Institute of Technology 1963) and Dr. (Osaka Prefecture 1977) degrees in mechanical engineering. He has been at University of Osaka Prefecture as Assistant Professor (1966-81) and Lecturer (1981-88), and at Kinki University as Associate Professor (1988-present). His research has been directed to the fluid dynamic problems of hovercraft and his present interest is in the application of the concept of the air cushion to various new fields, such as a floating system of extremely thin sheet and a vertical suction system.

Dr. Yasutomi is an author of many papers on hovercraft, especially aerodynamics of hovercraft with forward speed.